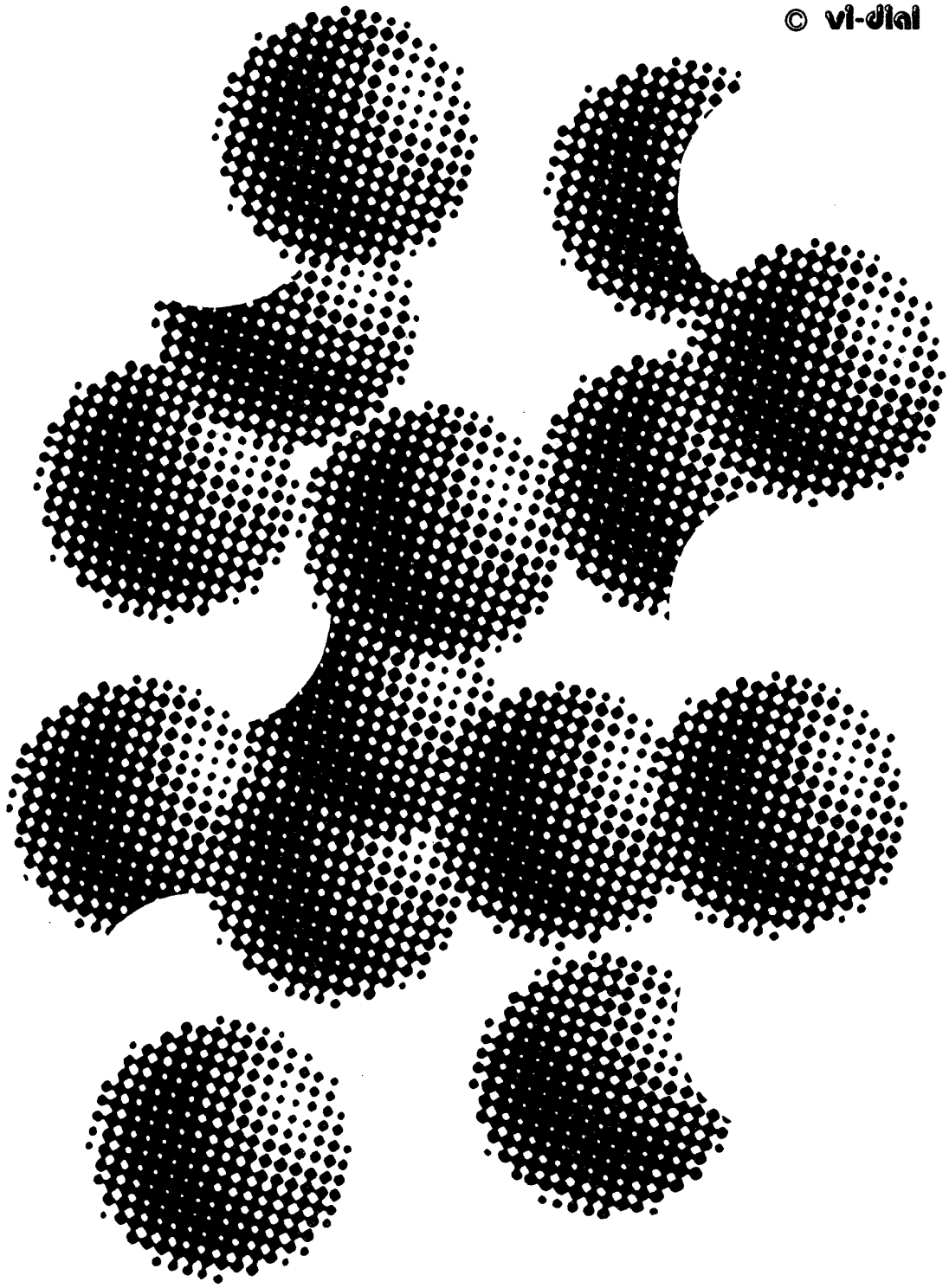
# electromagnetic compatibility

part —1

© vi-dial



DISTRIBUTION STATEMENT A
Approved for Public Release
Distribution Unlimited

/2000

**Fifteenth
International Wrocław
Symposium and Exhibition
on Electromagnetic Compatibility
June 27-30. 2000**

## The Symposium organizers gratefully acknowledge the following organization and firms for their assistance to and support of this Symposium:

**NATIONAL RADIOCOMMUNICATIONS AGENCY**
Kasprzaka 18/20, 01-211 Warsaw, Poland

**TELEKOMUNIKACJA POLSKA S.A.**
Nowy Swiat 6/12, 00-400 Warsaw, Poland

**PLUS GSM**
**DIGITAL MOBILE TELECOMMUNICATION NETWORK**
Al.Jerozolimskie 81, 02-001 Warsaw, Poland

**PTK CENTERTEL Sp. z o.o.**
Panska 57/61, 00-830 Warsaw, Poland

**RADIO ESKA S.A.**
Senatorska 13/15, 00-075 Warsaw, Poland

## We also wish to thank the following for their contribution to the success of this Symposium:

**European Office of**
**Aerospace Research and Development**
**Air Force Office of Scientific Research**
**United States Air Force Research Laboratory**
223/231 Old Marylebone Rd, London NW1 5TH, UK

# REPORT DOCUMENTATION PAGE

Form Approved OMB No. 0704-0188

Public reporting burden for this collection of information is estimated to average 1 hour per response, including the time for reviewing instructions, searching existing data sources, gathering and maintaining the data needed, and completing and reviewing the collection of information. Send comments regarding this burden estimate or any other aspect of this collection of information, including suggestions for reducing this burden to Washington Headquarters Services, Directorate for Information Operations and Reports, 1215 Jefferson Davis Highway, Suite 1204, Arlington, VA 22202-4302, and to the Office of Management and Budget, Paperwork Reduction Project (0704-0188), Washington, DC 20503.

| 1. AGENCY USE ONLY (Leave blank) | 2. REPORT DATE | 3. REPORT TYPE AND DATES COVERED |
|---|---|---|
| | 24 July 2000 | Conference Proceedings |

4. TITLE AND SUBTITLE

Emc - 15TH International Wroclaw Symposium And Exhibition On Emc , Part 1

5. FUNDING NUMBERS

F61775-00-WF074

6. AUTHOR(S)

M.M. Janiszewski, W. Moron, W. Sega (Editors)

7. PERFORMING ORGANIZATION NAME(S) AND ADDRESS(ES)

Institute of Telecommunications
ul. Swojczycka 38
Wroclaw 51-501
Poland

8. PERFORMING ORGANIZATION REPORT NUMBER

N/A

9. SPONSORING/MONITORING AGENCY NAME(S) AND ADDRESS(ES)

EOARD
PSC 802 BOX 14
FPO 09499-0200

10. SPONSORING/MONITORING AGENCY REPORT NUMBER

CSP 00-5074

11. SUPPLEMENTARY NOTES

Two volumes. Part 2

12a. DISTRIBUTION/AVAILABILITY STATEMENT

Approved for public release; distribution is unlimited.

12b. DISTRIBUTION CODE

A

13. ABSTRACT (Maximum 200 words)

The Final Proceedings for 15th INTERNATIONAL WROCLAW SYMPOSIUM AND EXHIBITION ON EMC, 27 June 2000 - 30 June 2000

This is an interdisciplinary conference. Subject matter will include all aspects of Electromagnetic Compatibility (EMC) theory and practice as seen in this partial list of topics for planned sessions: EMC on Component and PCB Level; Lightning and ESD; EMC in Communication and Power Systems; Modeling and Simulation Theory and Practice. NATO EMC issues: Military vs Civil EMC Standards - Comparisons and Problems, Standard Procedures for Simulation, Prediction and Modeling Antennas and Propagation, Biological Effects of EM Radiation - Technical Aspects, Spectrum Management and Monitoring, EM Hazards and Terrorism, EMC Matters and Satellite-based Systems I, Computational EM Technique in Mobile Wireless Communications

14. SUBJECT TERMS

EOARD, Modelling & Simulation, Electromagnetics, Electromagnetic Compatibility

15. NUMBER OF PAGES
924 + cover matter
(two volumes)

16. PRICE CODE

N/A

| 17. SECURITY CLASSIFICATION OF REPORT | 18. SECURITY CLASSIFICATION OF THIS PAGE | 19. SECURITY CLASSIFICATION OF ABSTRACT | 20. LIMITATION OF ABSTRACT |
|---|---|---|---|
| UNCLASSIFIED | UNCLASSIFIED | UNCLASSIFIED | UL |

NSN 7540-01-280-5500

Standard Form 298 (Rev. 2-89)
Prescribed by ANSI Std. 239-18
298-102

20000913 038

DTIC QUALITY INSPECTED 4

FIFTEENTH INTERNATIONAL
WROCŁAW SYMPOSIUM AND EXHIBITION

# ELECTROMAGNETIC COMPATIBILITY 2000

## PART I

EDITORS:

J.M. JANISZEWSKI W. MORON W. SĘGA

Published by the National Institute of Telecommunications

AQ F00-12-3817

All papers are published on responsibility of the authors

©Copyright by Wrocław Symposium on EMC

Applications for reproduction of this book or parts thereof should be directed to EMC Proceedings Editor

Organizers address:

EMC Symposium, Box 2141
51-625 Wrocław 12, Poland
fax: +4871 3728878
e-mail: emc@il.wroc.pl
www.emc.wroc.pl

**ISBN 83-901999-8-X**

**Patron:**

T. Szyszko
Minister of Posts and Telecommunications of
the Republic of Poland

**Under the auspices of:**

Polish Academy of Sciences (PAN)
Committee of Electronics and Telecommunication

**Organizers:**

The Association of Polish Electrical Engineers
The Wroclaw University of Technology
The National Institute of Telecommunications

**Cosponsor:**

International Union of Radio Science

**Cooperating:**

**International organizations**

International Union of Radio Science (URSI); International Telecommunication Union: Radiocommunication Bureau (ITU-R), Telecommunication Standardization Bureau (ITU-T) and Telecommunication Developement Bureau (ITU-D); International Electrotechnical Commission (IEC): International Special Committee on Radio Interference (CISPR) and TC 77 Electromagnetic Compatibility (IEC TC77); UNESCO International Centre for Theoretical Physics (ICTP); European Broadcasting Union (EBU); European Telecommunications Standards Institute (ETSI); Pacific Telecommunication Council (PTC); Region 8 (Europe) and Poland Section of the Institute of Electrical and Electronics Engineers (IEEE); International Amateur Radio Union (IARU) – Region 1

**Convention of National Societies of Electrical Engineers of Europe – EUREL**

Austrian Electrotechnical Association – ÖVE *(Austria)*; Association of Electrical Engineers Graduated from the Montefiore Institute – AIM *(Belgium)*; Royal Flemish Society of Engineers – TI-KVIV *(Belgium)*; Royal Belgium Society of Electrical Engineers *(Belgium)*; The Association of Electrical, Electronics and Automation Societies in Finland – FINEL *(Finland)*; Association of Electrical and Electronics Engineers – SEE *(France)*; Association for Electrical, Electronic & Information Technologies – VDE *(Germany)*; Hungarian Electrotechnical Association – MEE *(Hungary)*; Institution of Engineers of Ireland – IEI *(Ireland)*; Italian Electrotechnic and Electronic Association – AEI *(Italy)*; Association of Polish Electrical Engineers – SEP *(Poland)*; Portugese Association of Engineers – OE *(Portugal)*; Slovak Electrotechnic Society – *SES (Slovakia)*; Swedish Society of Electrical and Computer Engineers – SER *(Sweden)*; Swiss Electrotechnical Association – SEV *(Switzerland)*; Institution of Electrical Engineers – IEE *(United Kingdom)*

**Other Associations**

Scientific Technical Society for Radio Technology, Electronics and Electrocommunications – BORES *(Belarus)*; Union of Electronics, Electrotechnics and Telecommunications – UEEEC *(Bulgaria)*; Association for the Protection against Electromagnetic Interference – EMCAS *(Czech Republic)*; Estonian Electronics Society – EES *(Estonia)*; Association of Electrical Engineers – AEE *(Finland)*; Scientific Society for Telecommunication – HTE *(Hungary)*; The Institute of Electronics, Information and Communication Engineers – IECE *(Japan)*; Latvian Society of Radioelectronic and Communication Engineers – AERE *(Latvia)*; Lithuanian Society of Informatics, Communications and Electronics – LIREB *(Lithuania)*; Association of Electronics and Radio Engineers – NERG *(The Netherlands)*; Pakistan Institute of Telecom Engineers – PITE *(Pakistan)*; A.S. Popov Scientific Technical Society for Radio Technology, Electronics and Electrocommunications – RORES *(Russian Federation)*; Chamber of Turkish Electrical Engineers – EMO *(Turkey)*; Ukrainian Scientific and Engineering Radio, Electronics and Communication Society – UORES *(Ukraine)*; Institute of Electrical and Electronics Engineers, EMC Society – IEEE EMCS *(USA)*

**Symposium Council:**

*Chairman:*
Prof. W. Majewski, *Poland*

*V-chairmen:*
Prof. A. Pilatowicz, *Poland*; Dr M. Rusin, *Poland*

Prof. M. Amanowicz, *Poland*; Prof. G. Balodis (AERE), *Latvia*; V. Bulavas (LIREB), *Lithuania*; Prof. K. Feser (VDE), *Germany*; G. Goldberg (SEV), *Switzerland*; W. Grabowski, *Poland*; S. Grela (PAR), *Poland*; J. Grzybowski (SEP), *Poland*; Prof. S. Hahn (URSI-Nat. Com.), *Poland*; Prof. V. Heinrichsen (EES), *Estonia*; M. Javed (PITE), *Pakistan*; Dr E. Joffe (IEEE-EMCS), *Israel*; R. Jones, *ITU-R*; P.J. Kerry, *IEC-CISPR*; Dr W. Kromolowski, *Poland*; A. Kornatowski (PAR), *Poland*; P. Laven, *EBU*; Prof. P.E. Leuthold (EMC Symp.), *Switzerland*; W. Nietyksza, *IARU-Region 1*; A. Peurala (AEE), *Finland*; Prof. V.V. Pilinsky (UORES), *Ukraine*; Dr A. Radasky, *IEC-ACEC*; Prof. S.M. Radicella, *UNESCO-ICTP*; K.H. Rosenbrock, *ETSI*; P. Rzepka (TP S.A.), *Poland*; Prof. H.R. Schmeer (EMC Congress), *Germany*; Prof. B. Smólski, *Poland*; Dr M. Suchanski, *Poland*; Dr J. Svoboda (EMCAS), *Czech Republic*; Dr B. Szentkuti, *IEC - TC77*; Prof. A. Wierzbicki (IL), *Poland*; B. Wojtynski (POLKOMTEL), *Poland*; Prof. W. Wolinski (PAN), *Poland*; Prof. T. Yoshino (IEICE), *Japan*; H. Zhao *ITU-T*; Prof. M. Zientalski, *Poland*; Dr Yu.B. Zubarev (RORES), *Russian Federation*; Dr E. Zernicki, *Poland*

**Scientific Program Committee:**

*Honorary Chairman:*
Prof. F.L. Stumpers, *The Netherlands*

*Chairman:*
Prof. R.G. Struzak, *Poland*

Prof. J. Bach Andersen, *Denmark*; T. Boe, *Norway*; Prof. J.A. Catrysse, *Belgium*; Prof. P. Degauque, *France*; G. Goldberg, *Switzerland*; Prof. E. Habiger, *Germany*; Prof. M. Hayakawa, *Japan*; G. Hurt, *USA*; Prof. M. Ianoz, *Switzerland*; Prof. A. Karwowski, *Poland*; W. Luther, *USA*; Prof. A. Marvin, *United Kingdom*; Prof. H. Mikolajczyk, *Poland*; Prof. E. Nano, *Italy*; Dr. A. Pavliouk, *Russian Federation*; Dr. A. Schiavoni, *Italy*; Dr. J. Shapira, *Israel*; Prof. G. Varju, *Hungary*; M.C. Vrolijk, *The Netherlands*; Prof. T. Yoshino, *Japan*

**Symposium Organization:**

Prof. D.J. Bem *(Symposium Chairman)*

J. Rutkowski *(Co-chairman)*

W. Moroń *(Organizing Chairman)*

Dr M.J. Grzybkowski, Dr J.M. Janiszewski, H. Ługowska, Prof. J. Malko, Dr T. Niewodniczański *(Public Relations)*, Dr M. Pietranik, Z. Rabiej, Dr W. Sęga *(Program Coordinator)*, Prof. T.W. Więckowski, Dr R.J. Zieliński *(Exhibition Coordinator)*, Dr R. Żarko

# Author's index


## A

Aboaba O. 624
Agostinelli M. 825
Aizawa T. 59
Akino T. 566
Allahverdiev A. 397
Alter L. 679
Altman Z. 240
Amemiya F. 346
Aniserowicz K. 144
Aporovitch V. 605
Araz I. 841
Augustyniak L. 159
Aust D. 865
Azaro R. 309, 341
Azoulay M. 79, 441
Azzarone R. 16

## B

Baker S. 294
Ball R. 294
Bandinelli M. 807
Batueva E. 626
Baum C. 898
Baumann J. 410
Beletsky A. 637
Bellan D. 260, 265
Bem D. 829
Benamar A. 884
Benedetti A. 807
Bertotto P. 245
Bielli P. 245
Blaunstein N. 479
Bliksrud E. 868
Blocher T. 314
Bochkov K. 444, 453
Boscovic D. 884
Bose R. 84
Boudreau D. 703
Brunello F. 250
Budai A. 683

## C

Can M. 397
Caorsi S. 309, 341
Cerri G. 168
Cesky T. 721
Chan G. 657
Charalampakis I. 448
Charrere M. 250
Chavka G. 609
Cheparin V. 571
Chernikova L. 587
Chiarandini S. 168
Chiti S. 807
Christodoulopoulos C. 448
Cioni R. 807, 812
Cooray V. 173
Czajkowski J. 687

## D

Daguillon O. 280
Darizhapov D. 626
Davydenko S. 483
De Brito G. 872
De Leo R. 168
Despres B. 441
Dhamrait M. 661
Di Laura S. 816
Dikmarova L. 583
Dimitrov D. 791
Dinan U. 502
Disco D. 250
Doebbelin R. 89
Dole C. 208
Donelli M. 309
Dostert K. 98
Drozd A. 314
Dub P. 383
Dufour M. 703
Dymarkowski K. 846

## E

Eged B. 64
Egorova N. 319

## F

Faizoulaev B. 457
Fei Xikang 137
Feix N. 194
Felic G. 94
Filcev J. 724
Fiori F. 41
Floreani M. 270
Foster K. 413
Fujiwara O. 255

## G

Galvan A. 173
Gambin D. 250
Garbe H. 289
Gardner R. 178, 466, 889, 896, 898
Gattoufi L. 240
Gavan J. 921
Gazizov T. 45, 469
Gelencser I. 64
Gianola P. 250
Goldberg G. 31, 103, 410, 418, 427
Gonschorek K. 216, 336
Gorisch A. 230
Gorobets N. 630
Gouliaev A. 691
Gragnani G. 309
Griese E. 70

## H

Habiger E. 304
Haehner T. 198
Haga A. 149
Halme L. 203
Hamid E. 902
Hansen D. 107, 361
Harms H. 284
Harms R. 850
Hattori K. 546
Hayakawa M. 275, 523, 536, 546, 561, 915
Heidemann M. 289
Heyder D. 89
Hiroshima Y. 346

## I

Ianoz M. 183, 908
Ishibashi N. 275
Itoh T. 546
Iudin D. 523, 528

## J

Jakobus U. 221, 642
Jecko B. 194, 575
Jennings P. 294
Joskiewicz Z. 829

## K

Kaluski M. 436
Kanzaki H. 536
Karwowski A. 240
Katulski R. 121
Katz M. 125
Kawamata K. 149
Kawasaki Z. 902
Kazama S. 50
Kazik J. 854
Kebel R. 289
Kharkovsky S. 397
Kharlap S. 453
Kho K. 749
Kikuchi H. 488, 493, 910
Kincaid J. 208
Kinsht N. 125
Kitaytsev A. 571
Klima J. 728
Klok H. 794
Klosok W. 646
Kogan V. 708
Kolakowski J. 128
Kolchigin N. 319
Koledintseva M. 571
Kolodziej H. 579
Korovkin N. 523
Kosinski A. 121
Kostenko M. 188
Kourennyi E. 322, 587
Kovalev K. 683
Kowalczyk P. 370
Kozel V. 683
Krzysztofik W. 401, 614
Kuleshova V. 473
Kurby C. 736
Kurgan E. 326
Kurowski T. 591
Kus A. 770
Kuwabara N. 346
Kuznetsova-Tadjibaeva O. 45

## L

Lalande-Guionie M. 194
Larkin V. 551
Larkina V. 506, 551, 556
Lascu D. 75
Lascu M. 75
Lavell-Smith A. 799
Laven P. 8
Lee S. 275
Leenders H. 420
Lenivenko V. 596
Leontiev N. 45
Lever P. 294
Lodge J. 703
Logatchev V. 457
Loginov N. 708

Loyka S. 132
Luszcz J. 601
Luther W. 713
Lyubimov V. 379

## M

Macdonald-Bradley C. 294
Macher M. 436
Makita K. 561
Mamtchenkov P. 691
Manara G. 820
Mandzij B. 55
Mardiana R. 902
Mareev E. 498
Mariani Primiani V. 168
Martinod E. 194
Masada E. 406, 432
Maslowski G. 154
Mazzetti C. 183
Mecke H. 89
Medeisis A. 619
Meidan R. 741
Michalak M. 366
Mikhailovsky L. 571
Mikolajczyk H. 475
Minegishi S. 149
Missala T. 299
Misuri G. 836
Mizuma T. 406
Monorchio A. 820
Moorut P. 884
Mordachev V. 331, 683
Mund B. 198

## N

Nadeau P. 575
Nalbandian A. 666
Nichoga V. 383, 583
Nickolaenko A. 528, 532
Nikonov V. 683
Nitsch J. 225
Nomicos C. 512
Nucci C. 183

## O

Ohta K. 536, 561
Ohtsuka M. 517
Okyere P. 304
Oraevsky K. 457
Oraevsky V. 508

## P

Paskovich D. 703
Patenaude F. 703
Pavelka C. 733
Pavliouk A. 670, 708
Pawlowski W. 121, 633
Pazar S. 841
Pesta A. 314
Petropavlovsky Y. 125
Petrosov V. 322, 587
Pietranik M. 695
Pignari S. 260, 265
Pilinsky V. 591
Pirjola R. 915
Pivnenko S. 319, 387
Podgorski A. 366
Podgorski E. 366
Pogrebnyak N. 322
Preobragenskaya O. 125
Procacci V. 836
Pulinets S. 473

## R

Rabinowicz L. 532
Rachidi F. 183
Radasky W. 3, 893, 896
Radulescu M. 448
Raffetto M. 309
Reineix A. 575
Repacholi M. 413
Revermann L. 850
Richiardi G. 245
Ristau D. 361
Rodionova M. 591
Rozycki S. 436
Rucinschi D. 448
Russo P. 168
Ruzhin Y. 506, 508, 512
Ryazantseva N. 444
Rybin A. 591

## S

Sadowski M. 609
Sato R. 50, 59, 566
Schiavoni A. 245
Schwarz H. 424
Sega W. 695, 699, 718
Selivanov M. 691
Semenikhina D. 637
Senin B. 556
Sergeeva N. 556

Shagimuratov I. 508
Sharpe M. 876
Shihab S. 94
Shinohara S. 50, 59, 566
Shvets A. 541
Siebert P. 753
Silin N. 125
Siwiak K. 744
Smirnov N. 691
Sowa A. 159, 370, 579
Spoelstra T. 758, 775
Sroka J. 374
Stecher M. 351
Steinmetz T. 225
Stewart F. 804, 859
Stoudt D. 466, 898
Struzak R. 21, 890

## T

Tarafi R. 280
Teti F. 812
Tiedemann R. 336
Trakhtengerts V. 523
Trigubovich V. 461
Trzaska H. 646
Tyczynski W. 699, 718

## U

Uczciwek J. 846
Ustuner F. 841

## V

Vaananen A. 356, 650
Vallianatos F. 512
Van Driel W. 779
Varshney P. 314
Vasiltsov I. 55
Vercellotti G. 163
Verduijn J. 675
Verholt C. 655
Vick R. 111
Villien P. 213
Vogt A. 579

## W

Wang J. 255
Weiner D. 314
Wheaton O. 881
Wiart J. 240
Wieckowski T. 391, 829
Wik M. 893, 896
Wilhelmsen P. 116
Winkler T. 89
Winnberg A. 784
Wolfsperger H. 235
Wollenberg G. 230
Wong M. 240
Wu Yunxi 137

## Y

Yamamoto H. 59
Yang Shiwu 137
Yazici M. 841
Yeliseyeva N. 630
Yoshino T. 502, 517
Yumoto K. 546

## Z

Zagoskin V. 708
Zajac R. 846
Zarko R. 695
Zawadzki P. 280
Zeddam A. 280
Zich R. 163, 235, 270
Zielinski R. 763
Zivic T. 140
Zlahtic F. 140
Zorman M. 140

# CONTENTS

## PART I


## I PLENARY SESSIONS

### PLENARY SESSION I

Chairman: PROF. R. STRUZAK, *Co-Chair, URSI WG on SM, Member ITU RRB, Poland*

- W. RADASKY, *Metatech Corporation, Goleta, USA:* **Electromagnetic Compatibility Strategy for the Future** ..... 3
- P. LAVEN, *European Broadcasting Union, Geneva, Switzerland:* **The Future of Broadcasting** ..... 8

### PLENARY SESSION II

Chairman: PROF. D.J. BEM, *University of Technology, Wroclaw, Poland*

- R. AZZARONE, *General Directorate TELEDIFE, Rome, Italy:* **Civilian vs Military EMC Standardization - View of NATO Special Working Group 10 on Electromagnetic Environment Effects** ..... 16
- R. STRUZAK, *Co-Chair, URSI WG, ITU RRB, Poland:* **Noise Interference in Radiocommunication Networks: Shannon's Formula Revisited** ..... 21

### PLENARY SESSION III

Chairman: DR W.A. RADASKY, *IEC-ACEC Chairman, Metatech Corporation, Goleta, USA*

- G. GOLDBERG, *Past chairman IEC-ACEC, Zurich, Switzerland:* **EM Phenomena and Implications for Standardization. EMC - Safety - Human Exposure** ..... 31

## II SECTIONAL SESSIONS

### EMC ON COMPONENT AND PCB LEVEL - PART I

Chairman: DR E. GRIESE, *Siemens AG IC, Paderborn, Germany*

- F. FIORI, *Technical University, Torino, Italy:* **ICs Susceptibility: A Critical Assessment of the Test Procedures** ..... 41
- T. GAZIZOV, N.A. LEONTIEV, *State University of Control Systems and Radioelectronics,* O.M. KUZNETSOVA-TADJIBAEVA, *Research and Design Center "Polus", Tomsk, Russian Federation:* **Far-End Crosstalk Reduction in Coupled Microstrip Lines with Covering Dielectric Layer** ..... 45
- S. KAZAMA, S. SHINOHARA, R. SATO, *EMC Research Laboratories Co Ltd, Sendai, Japan:* **Estimation of Current and Voltage Distributions in a Digital IC Package** ..... 50
- I. VASILTSOV, *Academy of National Economy, Ternopil,* B.A. MANDZIJ, *State University "Lvivska Politechnika", Lviv, Ukraine:* **New 3D Model of Internal Electromagnetic Noises in VLSI Chip** ..... 55

## EMC ON COMPONENT AND PCB LEVEL - PART II

Chairman: PROF. T.R. GAZIZOV, *State University of Control Systems and Radioelectronics, Tomsk, Russian Federation*


- T. AIZAWA, H. YAMAMOTO, S. SHINOHARA, R. SATO, *EMC Research Laboratories Co Ltd, Sendai, Japan:* **Evaluation of the Radiated and Immunity Characteristics of Optical Transceiver Modules** ..... 59
- B. EGED, I. GELENCSER, *Technical University, Budapest, Hungary:* **The Effect of Discontinuities on Ground/Power Planes of High-Speed Printed Circuit Boards** ..... 64
- E. GRIESE, *Siemens AG, Paderborn, Germany:* **A Hybrid Electrical/Optical Interconnection Technology for Printed Circuit Boards** ..... 70
- M. LASCU, D. LASCU, *Technical University, Timisoara, Romania:* **Finite Element Method Applied in Modelling Perturbations on Printed Circuit Boards** ..... 75


## EMC IN COMMUNICATION AND POWER SYSTEMS

Chairman: DR R. VICK, *EMC Consulting and Management, Dresden, Germany*


- M. AZOULAY, *TDF, Saint Quentin en Yvelines, France:* **Radio Interference Cases on Broadcasting Sites** ..... 79
- R. BOSE, *Indian Institute of Technology, Delhi, India:* **Optimally Placing Base Stations in a Microcellular Urban Environment** ..... 84
- R. DOEBBELIN, D. HEYDER, H. MECKE, T. WINKLER, *Otto-von-Guericke University, Magdeburg, Germany:* **Resistance Welding Machines - a Critical Power Supply Network Load Concerning Power Quality and Electromagnetic Emissions** ..... 89
- S. SHIHAB, G. FELIC, *Royal Melbourne Inst of Technology, Melbourne, Australia:* **Monitoring of Electromagnetic Interference in High Voltage Substations** ..... 94


## POWER-LINE COMMUNICATION - EMC PROBLEMS

Invited session

Organizer/Chairman: DR R. VICK, *EMC Consulting and Management, Dresden, Germany*


- K. DOSTERT, *University of Karlsruhe, Karlsruhe, Germany:* **EMC Aspects of High Speed Power Line Communications** ..... 98
- G. GOLDBERG, *Past chairman IEC-ACEC, Zurich, Switzerland:* **Evaluation of Power Line Communication Systems** ..... 103
- D. HANSEN, *EURO EMC SERVICE (EES), Berikon, Switzerland:* **Megabits per Second on 50 Hz Power Lines?** ..... 107
- R. VICK, *EMC Consulting and Management, Dresden, Germany:* **Radiated Emission of Domestic Main Wiring Caused by Power-Line Communication Systems** ..... 111
- P. WILHELMSEN, *Norwegian Post and Telecommunications Authority, Oslo, Norway:* **A Regulatory Authority's Evaluation of PLC and EMC** ..... 116

## EMC IN COMMUNICATION, POWER AND TRANSPORT SYSTEMS


- R. KATULSKI, *Technical University, Gdansk,* A. KOSINSKI, *Naval Academy, Gdynia,* W. PAWLOWSKI, *Technical University, Gdansk, Poland:* **Radiocommunication Aspects of EMC Analysis and Measurements on a Ship** ..... 121

- N. KINSHT, M.A. KATZ, N.V. SILIN, O.V. PREOBRAGENSKAY A, Y.B. PETROPAVLOVSKY, *State Far-Eastern Technical University, Vladivostok, Russian Federation:* **Application of Electromagnetic Radiation of High-Voltage Equipment for Diagnostic of its Technical State** ..... 125

- J. KOLAKOWSKI, *University of Technology, Warsaw, Poland:* **Application of Wavelet Transform for Adjacent Channel Transient Power Measurements** ..... 128

- S. LOYKA, *Belarusian State University of Informatics & Radioelectronics, Minsk, Belarus:* **Numerical Modeling of Nonlinear Interference and Distortions for Wireless Communications** ..... 132

- YANG SHIWU, FEI XIKANG, WU YUNXI, *Northern Jiaotong University, Beijing, China:* **New Approach to Suppress Impulsive Interference on Track Circuit of Electrified Railways** ..... 137

- F. ZLAHTIC, M. ZORMAN, T. ZIVIC, *Elektroinstitut Milan Vidmar, Ljubljana, Slovenia:* **Electromagnetic Compatibility Assurance in Electric Power Substations** ..... 140


## LIGHTNING AND ESD

Chairman: PROF. R.E. ZICH, *Technical University, Milano, Italy*


- K. ANISEROWICZ, *Technical University, Bialystok, Poland:* **Comparison of the Lumped- and Distributed-Circuit Model of the Lightning Protection System** ..... 144

- K. KAWAMATA, *Hachinohe Institute of Technology, Aomori,* S. MINEGISHI, A. HAGA, *Tohoku Gakuin University, Tohoku, Japan:* **Time Domain Measurement of Very Fast Transition Durations Due to Gap Discharge in Air as a Simulation of the CDM ESD** ..... 149

- G. MASLOWSKI, *University of Technology, Rzeszow, Poland:* **Modeling of the Lightning Electric Field for Different Models of the Channel-Base Current with Standard Parameters** ..... 154

- A. SOWA, L. AUGUSTYNIAK, *Technical University, Bialystok, Poland:* **Lightning Overvoltages in Structural Cabling Systems** ..... 159

- G. VERCELLOTTI, R.E. ZICH, *Technical University, Milano, Italy:* **LEMP-Like Effects on Railways Systems** ..... 163


## LIGHTNING EFFECTS AND COUPLING MODELS

Invited session (sponsored by URSI Commission E)

Organizer/Chairman: PROF. M.V. IANOZ, *Swiss Federal Institute of Technology, Lausanne, Switzerland*


- R. DE LEO, G. CERRI, S. CHIARANDINI, V. MARIANI PRIMIANI, P. RUSSO, *University of Ancona, Ancona, Italy:* **A Hybrid Method for the Analysis of Transients in EMC Problems** ..... 168

- A. GALVAN, V. COORAY, *Uppsala University, Uppsala, Sweden:* **On the Maximum Overvoltages Inducted in Low Voltage Power Installation Networks Due to Indirect Lightning Flashes** ..... 173

- R. GARDNER, *Spectral Synthesis Labs, Alexandria, USA:* **Modeling of the Base of a Lightning Return Stroke** ..... 178

- M. IANOZ, *Swiss Federal Institute of Technology, Lausanne, Switzerland,* C. MAZZETTI, *University of Rome "La Sapienza", Rome,* C.A. NUCCI, *University of Bologna, Bologna, Italy,* F. RACHIDI, *Swiss Federal Institute of Technology, Lausanne, Switzerland:* **Lightning Indirect Effects Modeling Applied to Protection Design and Evaluation** ..... 183

- M. KOSTENKO, *State Technical University, St Petersburg, Russian Federation:* **Associative Modeling of Incoming and Reflected Waves in Lightning Channel and in Stroked Overhead Line** ..... 188

- E. MARTINOD, N. FEIX, M. LALANDE-GUIONIE, *IRCOM, Brive la Gaillarde,* B. JECKO, *IRCOM, Limoges, France:* **Analysis of Connectors Behaviour in Term of Electromagnetic Compatibility** ..... 194


## EMC PERFORMANCE OF SYMMETRICAL AND COAXIAL CABLINGS

Invited session

Organizer/Chairman: DR L. HALME, *University of Technology, Helsinki, Finland*


- T. HAEHNER, *Alcatel Cable France, Paillart, France,* B. MUND, *bedea Berkenhoff & Drebes GmbH, Asslar, Germany:* **Background, Content and Future of the EMC Measurement Standard prEN 50289-1-6 - Open/Shielded Test Methods** ..... 198

- L. HALME, *University of Technology, Hut, Finland:* **Primary and Secondary Electro-Magnetic Screening (Shielding) Parameters** ..... 203

- J. KINCAID, C. DOLE, *Belden Electronics Division, Richmond, USA:* **Shielded Screening Attenuation Test Method Down to 5 MHz** ..... 208

- P. VILLIEN, *3P Third Party Testing, Hoersholm, Denmark:* **Future Development of Standardisation of Coupling Attenuation** ..... 213


## EMC MODELLING AND ANALYSIS

Invited session

Organizer: PROF. K. GONSCHOREK, *University of Technology, Dresden, Germany*

Chairman: DR H. HARMS, *Thyssen Nordseewerke GmbH, Emden, Germany*


- K. GONSCHOREK, *University of Technology, Dresden, Germany:* **Introduction to MOM, GTD/UTD and Their Combination** ..... 216

- U. JAKOBUS, *University of Stuttgart, Stuttgart, Germany:* **Latest Developments in the Method of Moments for an Efficient Numerical Solution of Complicated and Large Scale EMC Problems** ..... 221

- T. STEINMETZ, J. NITSCH, *Otto-von-Guericke University, Magdeburg, Germany:* **Analysis of Complex Systems with Cables Using Electromagnetic Topology** ..... 225

- G. WOLLENBERG, A. GORISCH, *Otto-von-Guericke University Magdeburg, Germany:* **Using Hybrid PEEC-MTL Models for the Analysis of Interconnection Structures** ..... 230

- R. ZICH, *Technical University, Milano, Italy,* H.A. WOLFSPERGER, *Karlsruhe University, Karlsruhe, Germany:* **Analysis of the Shielding Performances of Loaded Perforated Shields** ..... 235

## COMPUTATIONAL EM TECHNIQUES IN MOBILE WIRELESS COMMUNICATIONS

Invited session

Organizer/Chairman: PROF. A. KARWOWSKI, *Silesian Technical University, Gliwice, Poland*


- Z. ALTMAN, *CNET, Issy les Moulineaux, France,* A. KARWOWSKI, *Silesian Technical University, Gliwice, Poland,* M. WONG, J. WIART, *CNET, Issy les Moulineaux,* L. GATTOUFI, *Bouygues Telecom, Velizy, France:* **Dosimetric Analysis of Base Station Antennas via Simulation and Measurements** ..... 240

- P. BERTOTTO, A. SCHIAVONI, G. RICHIARDI, P. BIELLI, *CSELT, Torino, Italy:* **Directional Antennas for the Reduction of SAR Inside the Human Head** ..... 245

- F. BRUNELLO, M. CHARRERE, D. DISCO, D. GAMBIN, P. GIANOLA, *CSELT, Torino, Italy:* **Electromagnetic Fields in Proximity of GSM Base Stations** ..... 250

- J. WANG, O. FUJIWARA, *Institute of Technology, Nagoya, Japan:* **The Role of Head Tissue Complexity in the Peak SAR Assessment for Mobile Phones** ..... 255


## EMC MODELLING - PART I

Chairman: DR E.B. JOFFE, *KTM Project Eng. Ltd, Ramat Hasharon, Israel*


- D. BELLAN, S. PIGNARI, *Technical University, Milano, Italy:* **A Probabilistic Model for Transmission Line Voltages Inducted by an External Field** ..... 260

- D. BELLAN, S. PIGNARI, *Technical University, Milano, Italy:* **A Prediction Model for Crosstalk in Large and Densely-Packed Random Wire-Bundles** ..... 265

- M. FLOREANI, R.E. ZICH, *Technical University, Milano, Italy:* **Analysis of the Shielding Effectiveness of a Truncated Chiral Cylinder** ..... 270

- N. ISHIBASHI, S. LEE, M. HAYAKAWA, *University of Electro-Communications, Tokyo, Japan:* **Theory and Experiment on Radiation from a Bent Transmission Line** ..... 275

- P. ZAWADZKI, *Silesian Technical University, Gliwice, Poland,* R. TARAFI, O. DAGUILLON, A. ZEDDAM, *CNET Technopole Anticipa, Lannion Cedex, France:* **An Efficient Method for Calculation of the Radiation from Copper Installations with Wideband Transmission Systems** ..... 280


## EMC MODELLING - PART II

Chairman: PROF. D.J. BEM, *University of Technology, Wroclaw, Poland*


- H. HARMS, *Thyssen Nordseewerke GmbH, Emden, Germany:* **EMC Analysis for Frequencies Above 1 GHz in Naval Shipbuilding** ..... 284

- M. HEIDEMANN, H. GARBE, *University of Hannover, Hannover,* R. KEBEL, *Daimler-Chrysler Aerospace AG, Bremen, Germany:* **Calculation of Electromagnetically and Thermally Coupled Fields in Real Soil Decontamination** ..... 289

- C. MACDONALD-BRADLEY, P.A. JENNINGS, R.J. BALL, P.H. LEVER, S. BAKER, *University of Warwick, Coventry, UK:* **A Statistical Approach for Computational Electromagnetics** ..... 294

- T. MISSALA, *Industrial Research Institute for Automation and Measurements, Warsaw, Poland:* **Models for Simulation of Fieldbus Transmission Line EMC Testing** ..... 299

- P. OKYERE, E. HABIGER, *University of Technology, Dresden, Germany:* **Cost-Effective EMC-Conforming Design of Switched-Mode Power Supplies** ..... 304


## EMC MODELLING - PART III


- R. AZARO, *University of Genoa, Genoa,* S. CAORSI, *University of Pavia, Pavia,* M. DONELLI, G.L. GRAGNANI, M. RAFFETTO, *University of Genoa, Genoa, Italy:* **A Software for the Evaluation of Field Penetration Inside Shielding Box with Apertures** ..... 309

- A. DROZD, *ANDRO Consulting Services, Rome, NY,* T.W. BLOCHER, A.J. PESTA, *Air Force Research Laboratory, Rome NY,* D.D. WEINER, P.K. VARSHNEY, *Syracuse University, Syracuse, NY, USA:* **Predicting EMI Rejection Requirements Using Expert System Based Modeling & Simulation Techniques** ..... 314

- N. KOLCHIGIN, N.P. EGOROVA, S.N. PIVNENKO, *State University, Kharkov, Ukraine:* **Modeling the Measurement of the Transient Wave from the Object Located over Earth Surface** ..... 319

- E. KOURENNYI, *State Technical University, Donetsk,* V.A. PETROSOV, *The Priasovsk State Technical University, Mariupol,* N.M. POGREBNYAK, *State Technical University, Donetsk, Ukraine:* **Squaring and Smoothing in EMC Models: A Statistical Solution** ..... 322

- E. KURGAN, *University of Mining and Metallurgy, Krakow, Poland:* **Magnetic Analysis of Inhomogeneous Double-Layer Shields at Low Frequencies** ..... 326

- V. MORDACHEV, *Belarusian State University of Informatics & Radioelectronics, Minsk, Belarus:* **Radiosignals Dynamic Range in Space-Scattered Mobile Radiocommunication Networks** ..... 331

- R. TIEDEMANN, K. GONSCHOREK, *University of Technology, Dresden, Germany:* **Rebuilding the Screen of a Cable by a Double Layer of Parallel Wires** ..... 336


## EM INTERFERENCE MEASUREMENTS

Chairman: DR D. HANSEN, *EURO EM Service, Berikon 2, Switzerland*


- R. AZARO, *University of Genoa, Genoa,* S. CAORSI, *University of Pavia, Pavia, Italy:* **Determination of the Field Reduction Properties of Shielding Devices by Modulated Scattering Measurements** ..... 341

- N. KUWABARA, Y. HIROSHIMA, F. AMEMIYA, *NTT Corp., Tokyo, Japan:* **An Investigation on Measurement Method of Disturbances at Telecommunication Ports by Using Both Voltage and Current Probe** ..... 346

- M. STECHER, *Rohde & Schwarz GmbH & Co KG, Munchen, Germany:* **Weighting of Interference for its Effect on Digital Radiocommunication Services** ..... 351

- A. VAANANEN, *Polytechnic University, Vaasa, Finland:* **Screening Effectiveness of CATV Networks - Field Measurements** ..... 356


## EMC MEASUREMENT TECHNIQUES

Chairman: DR A.S. PODGORSKI, *ASR Technologies, Ottawa, Canada*


- D. HANSEN, D. RISTAU, *EURO EMC SERVICE (EES), Berikon, Switzerland:* **Antenna Factors of the New EUROTEM Cell for Fully Compliant Emission and Immunity Testing** ..... 361

- A. PODGORSKI, E. PODGORSKI, *ASR Technologies, Ottawa, Canada,* M.P. MICHALAK, *National Institute of Telecom, Wroclaw, Poland:* **Semi-Anechoic Chamber BGF Facility for Measurements of Emission and Immunity - Latest Advancements** ..... 366

- A. SOWA, P. KOWALCZYK, *University of Technology, Wroclaw, Poland:* **Test Chamber Characteristics - Important Factor Determining Required RF Power of Amplifier in Radiated Immunity Tests** ..... 370

- J. SROKA, *Schaffner EMV AG, Luterbach, Switzerland:* **On the Proper Use of the Injection Clamps in IEC/EN 61000-4-6 Test** ..... 374


## EMC MEASUREMENTS


- V. LYUBIMOV, *IZMIRAN, Troitsk, Russian Federation:* **Instruments for the Natural Magnetic Fields Registration in the City Conditions: The Magnetic Storm Indicators** ..... 379

- V. NICHOGA, P. DUB, *National Academy of Sciences of Ukraine, Lviv, Ukraine:* **Analysis of Noise Parameters of Highly Sensitive Induction Sensors for Measurement of Very Weak Electromagnetic Fields** ..... 383

- S. PIVNENKO, *State University, Kharkov, Ukraine:* **Slotline Sensor for Pulse Measurements** ..... 387

- T. WIECKOWSKI, *University of Technology, Wroclaw, Poland:* **Loop Antenna in the Emission Measurements** ..... 391


## BIOLOGICAL EFFECTS OF EM RADIATION - TECHNICAL ASPECTS


- S. KHARKOVSKY, A. ALLAHVERDIEV, M. CAN, *Cukurova University, Balcali, Turkey:* **Calibration of the Microwave Oven for Studies of Microwave Electromagnetic Radiation Effects on Cell Cultures** ..... 397

- W. KRZYSZTOFIK, *University of Technology, Wroclaw, Poland:* **The Near-Field of GSM 900/1800 Handset Terminals with Build-in Antennas** ..... 401

- E. MASADA, *Science University of Tokyo, Noda,* T. MIZUMA, *Traffic Safety and Nuissance Research Institute, Mitaka-city Tokyo, Japan:* **Electromagnetic Environment in Railway Systems** ..... 406


## REGULATIONS FOR THE LIMITATION OF HUMAN EXPOSURE TO EM FIELDS - PART I

Invited session

Organizer/Chairman: G. GOLDBERG, *Past Chairman IEC ACEC, Zurich, Switzerland*


- J. BAUMANN, *Swiss Agency for the Environment, Forest and Landscape, Bern,* G. GOLDBERG, *Past chairman IEC-ACEC, Zurich, Switzerland:* **Regulations for the Protection of the General Population in Switzerland** ..... 410

- K. FOSTER, *University of Pennsylvania, Philadelphia, USA,* M. REPACHOLI, *WHO, Geneva, Switzerland:* **Biological Effects of Electromagnetic Fields with Emphasis on Health and Safety** ..... 413

- G. GOLDBERG, *Past chairman IEC-ACEC, Zurich, Switzerland:* **The Different Kinds of EMF Standards** ..... 418

- H. LEENDERS, *Philips Corporate Standardization Dept., Eindhoven, Netherlands:* **European EMF Legislation - Turning the Thread of Trade Barriers into an Opportunity by Means of Standardization** ..... 420

- H. SCHWARZ, *Safety Test Solutions, Eningen, Germany:* **Standardisation and Regulation in Germany** ..... 424


## REGULATIONS FOR THE LIMITATION OF HUMAN EXPOSURE TO EM FIELDS - PART II

Invited session

Organizer/Chairman: G. GOLDBERG, *Past Chairman IEC ACEC, Zurich, Switzerland*


- G. GOLDBERG, *Past chairman IEC-ACEC, Zurich, Switzerland:* **Regulations for the Limitation of Human Exposure to EM Fields - An Overview** ..... 427

- E. MASADA, *Science University of Tokyo, Noda, Japan:* **Regulations for the Limitation of Human Exposure to EM Fields in Japan** ..... 432

- S. ROZYCKI, *Institute of Power Engineering, Warsaw,* M. KALUSKI, M. MACHER, *National Institute of Telecom, Wroclaw, Poland:* **Regulations for the Limitation of Human Exposure to EM Fields in Poland** ..... 436


## EMC REGULATIONS

Chairman: DR N.V. RYAZANTSEVA, *State University of Transport, Gomel, Belarus*


- M. AZOULAY, *TDF, Saint Quentin en Yvelines,* B. DESPRES, *France Telecom Research and Development, Issy les Moulineaux, France:* **Presentation of CISPR/H Activities** ..... 441

- K. BOCHKOV, N.V. RYAZANTSEVA, *State University of Transport, Gomel, Belarus:* **Determination of Rated EMC Parameters Based on the Probabilistic Approach and Consideration of Actual Conditions** ..... 444

- M. RADULESCU, *INSCC,* D.C. RUCINSCHI, *University "Politehnica", Bucharest, Romania,* C. CHRISTODOULOPOULOS, *INTRACOM S.A., Peania Attika,* I. CHARALAMPAKIS, *INTRACOM S.A., Athens, Greece:* **Technical EMC Specifications for Telecommunications Products** ..... 448


## IMMUNITY


- K. BOCHKOV, S.N. KHARLAP, *State University of Transport, Gomel, Belarus:* **Computer Analysis of the Performance of Essential Microelectronic Circuits in Intricate Electromagnetic Environment** ..... 453

- B. FAIZOULAEV, V.V. LOGATCHEV, K.S. ORAEVSKY, *EMC Scientific & Test Center "IMPULS", Moscow, Russian Federation:* **Immunity Investigation of Electronic Equipment Under Simulation of Indirect Electrostatic Discharge** ..... 457

- V. TRIGUBOVICH, *Belarusian State University of Informatics and Radioelectronics, Minsk, Belarus:* **Multi-Signal Method to Receiver's Selectivity Estimation** ..... 461

## EM HAZARDS AND TERRORISM

Chairman: R.L. GARDNER, *URSI Com. E Chairman, USA*


- R. GARDNER, *Spectral Synthesis Labs, Alexandria,* D.C. STOUDT, *Naval Surface Warfare Center, Dahlgren, USA:* **Requirements for Mitigation in Intentional Electromagnetic Interference** ..... 466
- T. GAZIZOV, *State University of Control Systems and Radioelectronics, Tomsk, Russian Federation:* **Design of Electronic Systems Protected from Electromagnetic Terrorism** ..... 469
- V. KULESHOVA, S.A. PULINETS, *IZMIRAN, Troitsk, Russian Federation:* **The Human Health Dependence on the Geomagnetic Activity** ..... 473
- H. MIKOLAJCZYK, *Prof. emeritus of Occupational Hygiene, Lodz, Poland:* **ELF EM Radiations and Intrinsic EM Phenomena in Human Organism Need for a Convention** ..... 475


# PART II

## GRAVITO-ELECTRODYNAMICS, EHD, SELF-ORGANIZATION, AND PRE-EARTHQUAKE EFFECTS IN THE ATMOSPHERE, IONOSPHERE AND MAGNETOSPHERE

Invited session (sponsored by URSI Commission E)

Organizer: PROF. H. KIKUCHI, *Institute for Environmental Electromagnetics, Tokyo, Japan*

Chairman: PROF. S.A. PULINETS, *IZMIRAN, Troitsk, Russian Federation*


- N. BLAUNSTEIN, *Ben-Gurion University of the Negev, Beer Sheva, Israel:* **Modulation of AGW-Inducted Plasma Inhomogeneities in the Disturbed Ionosphere in Period of Earthquake Preparation** ..... 479
- S. DAVYDENKO, *Russian Academy of Science, Nizhny Novgorod, Russian Federation:* **On the Calculation of the Quasistatic Atmospheric Electric Field and Current** ..... 483
- H. KIKUCHI, *Institute for Environmental Electromagnetics, Tokyo, Japan:* **Gravito-Electrodynamics of Dust in Electric Cusps and Electric Mirrors with Electric Reconnection and Its Applications to Diffuse Dust Layer in the Troposphere and Pre-Earthquake Atmospheric and Ionospheric Effects** ..... 488
- H. KIKUCHI, *Institute for Environmental Electromagnetics, Tokyo, Japan:* **A Model of Fireball or Plasmoid Produced by a Supersonic Gas Flow in the Laboratory and by Inter-Cloud and Airplane Discharges in the Atmosphere Based on Concept of Critical Ionization Velocity and Electric Reconnection** ..... 493
- E. MAREEV, *Russian Academy of Science, Nizhny Novgorod, Russian Federation:* **Dusty Particles Effects on Terrestrial Electromagnetic Environment and their EHD Description** ..... 498


## ENERGY TRANSMISSION FROM EARTHQUAKE FOCUS AND EM EMISSION WAVE GENERATED ON THE GROUND SURFACE AND IN THE IONOSPHERE

Invited session (sponsored by URSI Commission E)

Organizer/Chairman: PROF. T. YOSHINO, *University of Technology, Fukui, Japan*


- U. DINAN, *University of Ankara, Ankara, Turkey,* T. YOSHINO, *Fukui University of Technology, Tokyo, Japan:* **The Anomaly Unstable Polarization Fading of HF Wave Propagation Appeared at the Earthquake in Turkey of 1999** ..... 502

- V. LARKINA, Y.Y. RUZHIN, *IZMIRAN, Troitsk, Russian Federation:* **Plasmaspheric Low-Frequency Emission Intensity and Spectrum Variations over Preparation Zones of Quick (Seismogenous) and Slow Geodynamic Processes in the Earth Crust** ..... 506

- V. ORAEVSKY, Y.Y. RUZHIN, I.I. SHAGIMURATOV, *IZMIRAN, Troitsk, Russian Federation:* **Anomalies of Ionospheric TEC Above the Turkey Before Two Strong Earthquake at 1999** ..... 508

- Y. RUZHIN, *IZMIRAN, Troitsk, Russian Federation,* C. NOMICOS, *TEI, Athens,* F. VALLIANATOS, *TEI Chania Branch, Crete, Greece:* **High Frequency Seismoprecursor Emissions** ..... 512

- T. YOSHINO, M. OHTSUKA, *Fukui University of Technology, Tokyo, Japan:* **The Study of the Energy Correspondence Between Bottom Ionosphere and Earthquake Focus for Seismogenic EM Emission** ..... 517


## TERRESTRIAL EM NOISE ENVIRONMENT - PART I

Invited session (sponsored by URSI Commission E)

Organizer/Chairman: PROF. M. HAYAKAWA, *University of Electro-Communications, Tokyo, Japan*


- M. HAYAKAWA, D. IUDIN, N.V. KOROVKIN, *University of Electro-Communications, Tokyo, Japan,* V. TRAKHTENGERTS, *Russian Academy of Science, Nizhny Novgorod, Russian Federation:* **Cellular Automaton Model of Lightning Discharge Preliminary Stage** ..... 523

- A. NICKOLAENKO, *National Academy of Sciences of Ukraine, Kharkov, Ukraine,* D. IUDIN, *University of Electro-Communications, Tokyo, Japan:* **Hurst Exponent Derived for Natural ELF Electromagnetic Noise** ..... 528

- A. NICKOLAENKO, L. RABINOWICZ, *National Academy of Sciences of Ukraine, Kharkov, Ukraine:* **A Compact Solution for Natural ELF Pulse in Time Domain** ..... 532

- K. OHTA, H. KANZAKI, *Chubu University, Kasugai Aichi,* M. HAYAKAWA, *University of Electro-Communications, Tokyo, Japan:* **Three Dimensional Ray-Tracing for Very Low Latitude Whistlers with Considering the Latitudinal and Longitudinal Gradients of the Ionosphere** ..... 536

- A. SHVETS, *National Academy of Sciences of Ukraine, Kharkov, Ukraine:* **Worldwide Lightning Mapping with ELF Tomography** ..... 541


## TERRESTRIAL EM NOISE ENVIRONMENT - PART II

Invited session (sponsored by URSI Commission E)

Organizer/Chairman: PROF. M. HAYAKAWA, *University of Electro-Communications, Tokyo, Japan*


- M. HAYAKAWA, T. ITOH, *University of Electro-Communications, Tokyo,* K. HATTORI, *Institute of Physical and Chemical Research, Shizuoka,* K. YUMOTO, *Kyushu University, Fukuoka, Japan:* **ULF Electromagnetic Precursors for an Earthquake at Biak, Indonesia on February 17, 1996** ..... 546

- V. LARKIN, V.I. LARKINA, *IZMIRAN, Troitsk, Russian Federation:* **Natural Low-Frequency Emissions as a Tool of Research of Processes Occurring in the Plasmasphere** ..... 551

- V. LARKINA, *IZMIRAN, Troitsk,* N.G. SERGEEVA, *Polar Geophysical Institute, Murmansk,* B.V. SENIN, *SoyuzMorGeo, Gelendzhik, Russian Federation:* **Ionospheric Electromagnetic Effects Above Various Eurasia Arctic Tectonic Areas** ..... 556

- K. OHTA, K. MAKITA, *Chubu University, Kasugai Aichi,* M. HAYAKAWA, *University of Electro-Communications, Tokyo, Japan:* **On the Association of Anomalies in Subionospheric VLF Propagation at Kasugai with Earthquakes at the Center of Japan** ..... 561

## EMI REDUCTION TECHNIQUES

Chairman: PROF. B. JECKO, *IRCOM, Limoges Cedex, France*


- T. AKINO, S. SHINOHARA, R. SATO, *EMC Research Laboratories Co Ltd, Sendai, Japan:* **Estimation of Attenuation Characteristics of Feed-Through Type EMI Filters Using Fe-Si Alloy Flake-Polymer Composite** ..... 566

- L. MIKHAILOVSKY, A.A. KITAYTSEV, M.Y. KOLEDINTSEVA, V. CHEPARIN, *Power Engineering Institute, Moscow, Russian Federation:* **Research and Design of Gyromagnetic Media and Devices on Their Base for EMC and Ecology Problems** ..... 571

- P. NADEAU, A. REINEIX, *IRCOM, Limoges Cedex,* B. JECKO, *IRCOM, Limoges, France:* **Transmission Link Radiation And Common Current Generation by 15 Pin D Connector** ..... 575

- A. VOGT, H.A. KOLODZIEJ, *University of Wroclaw,* A.E. SOWA, *University of Technology, Wroclaw, Poland:* **New Generation of Absorbing Materials** ..... 579


## EMI SOURCES, COUPLING PATH TO VICTIMS AND REDUCTION TECHNIQUES


- L. DIKMAROVA, V. NICHOGA, *National Academy of Sciences of Ukraine, Lviv, Ukraine:* **Electromagnetic Radiation of Multipair Balanced Cables with Double Twisted Conductors** ..... 583

- E. KOURENNYI, *State Technical University, Donetsk,* V.A. PETROSOV, *The Priasovsk State Technical University, Mariupol,* L.V. CHERNIKOVA, *State Technical University, Donetsk, Ukraine:* **Linear Filtration of Random Processes in EMC Models: The "Partials Reactions" Method** ..... 587

- T. KUROWSKI, *Technical University, Zielona Gora, Poland,* V.V. PILINSKY, M.V. RODIONOVA, A.I. RYBIN, *National Technical University of Ukraine, Kiev, Ukraine:* **Mains RFI-Filters Design Methodology** ..... 591

- V. LENIVENKO, *EM Solutions, Yeerongpilly, Australia:* **High Frequency Spurious Response of Rectangular Waveguide Components** ..... 596

- J. LUSZCZ, *Technical University, Gdansk, Poland:* **Conducted Electromagnetic Interference Propagation through the Power Transformer** ..... 601


## ANTENNAS AND PROPAGATION

Chairman: A. MEDEISIS, *State Radiofrequency Service, Vilnius, Lithuania*


- V. APOROVITCH, *Research Institute of Automation Facilities, Minsk, Belarus:* **Multiple-Knife-Edge Diffraction Loss Estimation by the Logarithmic-Cell- Simulation Method** ..... 605

- G. CHAVKA, M. SADOWSKI, *Technical University, Bialystok, Poland:* **Frequency-Domain and Pulse Radiation of Broadband Matched Antenna Array** ..... 609

- W. KRZYSZTOFIK, *University of Technology, Wroclaw, Poland:* **Reception Conditions of Communication Satellites in Poland** ..... 614

- A. MEDEISIS, *State Radiofrequency Service, Vilnius, Lithuania:* **Fine Tuning of the Okumura-Hata Propagation Prediction Model Using the Minimum Squares Method and Fuzzy Logic Approach** ..... 619

## ANTENNAS AND PROPAGATION


- O. ABOABA, *Obafemi Awolowo University, Ile-Ife, Nigeria:* **Interference Due to Superrefraction and Ducting in the VHF Band in a Tropical Location in Nigeria** ..... 624
- E. BATUEVA, D.D. DARIZHAPOV, *Siberian Branch of RAS, Ulan-Ude, Russian Federation:* **Fluctuations of VHF/UHF Signal Level in Distant Tropospheric Propagation over the Far-Eastern Region of Russia** ..... 626
- N. GOROBETS, N.P. YELISEYEVA, *State University, Kharkov, Ukraine:* **Reducing Level of Side Radiation of Vibrator and Microstrip Antennas in Definite Direction** ..... 630
- W. PAWLOWSKI, *Technical University, Gdansk, Poland:* **Statistical Studies of VHF and UHF Radio Waves Propagation in the South Baltic Area** ..... 633
- D. SEMENIKHINA, A.A. BELETSKY, *State Radio Engineering University, Taganrog, Russian Federation:* **Excitation of the Infinite Perfect Conducting Nonlinear Loaded Circular Cylinder Coated with the Dielectric** ..... 637


## EMC IN AMATEUR RADIO SERVICE

Invited session (sponsored by IARU Region 1 WG EMC)
Organizer: PROF. H. TRZASKA, *University of Technology, Wroclaw, Poland*
Chairman: C.M. VERHOLT, *IARU Region 1 EMC WG, Copenhagen, Denmark*


- U. JAKOBUS, *University of Stuttgart, Stuttgart, Germany:* **Numerical Computation of the Near-Field of Typical Amateur Radio Antennas and Comparison with Approximate Result of Far-Field Formulas Applied in the Near- Field Region** ..... 642
- W. KLOSOK, *Polish Amateur Radio Union, Leszno,* H. TRZASKA, *University of Technology, Wroclaw, Poland:* **EM Radiation Hazard in Residential Areas** ..... 646
- A. VAANANEN, *Polytechnic University, Vaasa, Finland:* **Very High Power Scientific Radio Emissions as EMI Sources to Radio Amateur Service** ..... 650
- C. VERHOLT, *Danish Standards Association, Charlottenlund, Denmark:* **EMC Work in IARU** ..... 655


## RADIO SPECTRUM ISSUES IN 2000

Invited session
Organizer/Chairman: R.J. MAYHER, *SMILE Associates, Edgewater, USA*


- G. CHAN, *Industry Canada, Ottawa, Canada:* **The Determination of the Coordination Area Around Earth Stations** ..... 657
- M. DHAMRAIT, *Radiocommunication Agency, London, UK:* **Work of the ITU-R Task Group 1/5: Unwanted Emissions** ..... 661
- A. NALBANDIAN, *ITU BR, Geneva, Switzerland:* **ITU Spectrum Management Process and Results of WRC 2000** ..... 666
- A. PAVLIOUK, *Radio Research and Development Institute - NIIR, Moscow, Russian Federation:* **Spectrum Sharing and Spectrum Fees in 2000** ..... 670
- J. VERDUIJN, *Radiocommunications Agency, Nederhorst den Berg, Netherlands:* **The Changing Role of Monitoring in the Spectrum Management Process** ..... 675

## SPECTRUM ENGINEERING


- L. ALTER, *LONIIR, St Petersburg, Russian Federation:* **Probability of Intermodulation Interference of Land Mobile Cellular Radio Systems** ..... 679

- A. BUDAI, *Belarus Ministry of Post and Telecommunications,* K. KOVALEV, V. KOZEL, V.I. MORDACHEV, *Belarusian State University of Informatics & Radioelectronics,* V. NIKONOV, *Belarus State Supervisory Dept for Telecommunications, Minsk, Belarus:* **Generalized EMC Analysis of Air Navigation and GSM Networks in Belarus** ..... 683

- J. CZAJKOWSKI, *Merchant Marine Academy, Gdynia, Poland:* **The Problem of Generating False Alert Signals with Help of Digital Selective Calling - DSC in the GMDSS System** ..... 687

- A. GOULIAEV, P.N. MAMTCHENKOV, M. SELIVANOV, N. SMIRNOV, *NIIR, Moscow, Russian Federation:* **Problems of UMTS Networks EMC with Radio Relay Systems of the Fixed Service in Russia** ..... 691

- M. PIETRANIK, W. SEGA, *National Institute of Telecom,* R. ZARKO, *University of Technology, Wroclaw, Poland:* **Compatibility Between Mobile Services and TV Broadcasting in VHF Band. Practical Experiences** ..... 695

- W. SEGA, W. TYCZYNSKI, *National Institute of Telecom, Wroclaw, Poland:* **Assessment of the International Coordination Necessity of Microwave Radio Relay Links** ..... 699


## SPECTRUM MANAGEMENT AND MONITORING

Chairman: W.A. LUTHER, *Federal Communications Commission, Washington, USA*


- D. BOUDREAU, M. DUFOUR, J. LODGE, *Communications Research Centre,* D.H. PASKOVICH, *Directorate of Automated Spectrum Monitoring,* F. PATENAUDE, *Communications Research Centre, Ottawa, Canada:* **Monitoring of the Radio-Frequency Spectrum with a Digital Analysis System** ..... 703

- V. KOGAN, *NIIRDAR,* N. LOGINOV, *GOSSVIAZNADZOR of the RF,* A.P. PAVLIOUK, *Radio Research and Development Institute - NIIR,* V. ZAGOSKIN, *GOSSVIAZNADZOR of the RF, Moscow, Russian Federation:* **Accuracy Analysis of the HF Transmitter Location Procedure by the Single Station Location (SSL) Method** ..... 708

- W. LUTHER, *Federal Communications Commission, Washington, USA:* **Interferometric System Direction Finding Improvements on Circularly-Disposed Wide-Aperture Direction Finding System Accuracy** ..... 713

- W. SEGA, W. TYCZYNSKI, *National Institute of Telecom, Wroclaw, Poland:* **Compatibility Criteria of Microwave Links Used in International Coordination** ..... 718


## COMPUTER SUPPORT OF INTERNATIONAL FREQUENCY MANAGEMENT ACTIVITIES

Invited session

Organizer/Chairman: T. CESKY, *SES Astra, Luxemburg, Luxemburg*


- T. CESKY, *SES Astra, Chateau de Betzdorf, Luxemburg:* **Support of Introduction of Digital Broadcasting in Europe** ..... 721

- J. FILCEV, *CRC Data, Prague, Czech Republic:* **Implementation of Component-based Frequency Spectrum Management Software** ..... 724

- J. KLIMA, *University of Mathias Bel & PTT Research Institute, Banska Bystrica, Slovak Republic:* **Vienna Agreement '99 - Harmonized Calculation Method Activities** ..... 728

- C. PAVELKA, *TESTCOM, Praha, Czech Republic:* **Exchange of Data for Frequency Spectrum Management** ..... 733


## EMC MATTERS AND SATELLITE-BASED SYSTEMS - PART I

Invited session

Organizer/Chairman: DR R. MEIDAN, *MOTOROLA, Tel-Aviv, Israel*


- C. KURBY, *Motorola Inc, Libertyville, USA:* **Emissions Control Techniques for MSS Handset Transmitters** ..... 736

- R. MEIDAN, *Motorola, Tel-Aviv, Israel:* **Out-of-Band Emission Limits for Mobile Satellite Earth Terminals** ..... 741

- K. SIWIAK, *Motorola Inc, Boynton Beach, USA:* **Polarization Cross-Coupling in LEO and MEO Satellite Links** ..... 744


## EMC MATTERS AND SATELLITE-BASED SYSTEMS - PART II

Invited session

Organizer/Chairman: DR R. MEIDAN, *Motorola, Tel-Aviv, Israel*


- K. KHO, *NATO HQ C3 Staff, Brussels, Belgium:* **Sharing Properties of Mobile Satellite Service (MSS) Below 1 GHz and NATO Military Terrestrial Communications Systems** ..... 749

- P. SIEBERT, *Societe Europeenne des Satellites, Chateau de Betzdorf, Luxemburg:* **Standardization of Ka-band Satellite Terminals** ..... 753

- T. SPOELSTRA, *ESF Committee on Radio Astronomy Frequencies, Dwingeloo, Netherlands:* **Oh Satellite, Oh Satellite!** ..... 758

- R. ZIELINSKI, *University of Technology, Wroclaw, Poland:* **Risk of Interference to Aircraft from VSAT, SNG and SIT Terminals** ..... 763


## SCIENTIFIC USE OF RADIO - REGULATIONS AND FACTS

Invited session (sponsored by ESF-CRAF)

Organizer/Chairman: DR T.A. SPOELSTRA, *Committee on Radio Astronomy Frequencies, Dwingeloo, Netherlands*


- A. KUS, *Nicholas Copernicus University, Torun, Poland:* **Radio Astronomy in Poland** ..... 770

- T. SPOELSTRA, *ESF Committee on Radio Astronomy Frequencies, Dwingeloo, Netherlands:* **Regulations and Scientific Use of Radio Frequencies** ..... 775

- W. VAN DRIEL, *Unite Scientifique Nancay, Observatoire de Paris, Section de Meudon, Meudon, France:* **The Need for Radio Astronomical Line Observations: From Hydrogen to Alcohol** ..... 779

- A. WINNBERG, *Space Observatory, Onsala, Sweden:* **Scientific Use of Radio - Challenges from Space** ..... 784

## NATO/1: MILITARY VS CIVIL EMC STANDARDS - COMPARISONS AND PROBLEMS

Chairman: CAPT. R. AZZARONE, *General Directorate TELEDIFE, Rome, Italy*


- D. DIMITROV, *Head Quarter Bulgarian Navy, Varna, Bulgaria:* **Provision of EMC in Bulgarian Navy and Harmonization of Naval and Civil E3 Standards** ..... 791
- H. KLOK, *Royal Netherlands Navy, Oestgeest, Netherlands:* **Risk Analysis by the Use of Commercial Equipment in a Military Environment** ..... 794
- A. LAVELL-SMITH, *Defence Evaluation and Research Agency, Portsdown West, UK:* **Harmonization of EMC Standards for the Naval Environment - a United Kingdom Approach** ..... 799
- F. STEWART, *U.S. Space and Naval Warfare Systems Command, San Diego, California, USA:* **Harmonization of E3 Standards** ..... 804


## NATO/2: STANDARD PROCEDURES FOR SIMULATION, PREDICTION AND MODELLING

Chairman: A. LAVELL-SMITH, *Defence Evaluation and Research Agency, Portsdown West, UK*


- M. BANDINELLI, A. BENEDETTI, S. CHITI, R. CIONI, *IDS Company, Pisa, Italy:* **Numerical Prediction of Ship Antenna Performance in the Radar Band** ..... 807
- R. CIONI, F. TETI, *IDS Company, Pisa, Italy:* **Prediction of E.M. Field Levels Inside Closed Structures by a Statistical Approach** ..... 812
- S. DI LAURA, *Defence Evaluation and Research Agency, Portsdown West, UK:* **Modelling of Microwave Electromagnetic Interference in a Complex Coupling Environment** ..... 816
- G. MANARA, A. MONORCHIO, *University of Pisa, Pisa, Italy:* **Validation of a Time Domain MoM Simulator for EMC Standards Guidelines** ..... 820


## NATO/3: APPLICATIONS OF EXISTING STANDARDS IN EMC TESTING AND MEASUREMENTS

Chairman: DR M. KUKULKA, *Polish Navy HQ, Gdynia, Poland*


- M. AGOSTINELLI, *CISAM Center, Pisa, Italy:* **Applications of Civilian and Military Standards to Carry out Transient Electromagnetic Field Measurement at CISAM EMP Facilities** ..... 825
- D. BEM, Z.M. JOSKIEWICZ, T.W. WIECKOWSKI, *University of Technology, Wroclaw, Poland:* **Alternative Methods for Radiated Emission Measurements** ..... 829
- G. MISURI, V. PROCACCI, *Mariteleradar Institute, Livorno, Italy:* **Applications of NATO Standards for Evaluating Bulkhead Shielding in the Operational Rooms on Board of Ships** ..... 836
- F. USTUNER, I. ARAZ, M. YAZICI, *TUBITAK National Research Institute of Electronics and Cryptology, Kocaeli,* S. PAZAR, *TUBITAK National Research Institute of Electronic and Cryptology, Gebze, Turkey:* **Testing the EMP Effect on an Ordnance System** ..... 841

## NATO/4: ASPECTS, METHODS AND AWARENESS IN EMC STANDARDS IMPLEMENTATION

Chairman: F.M. STEWART, *U.S. Space and Naval Warfare Systems Command, San Diego, USA*


- K. DYMARKOWSKI, J.M. UCZCIWEK, R.P. ZAJAC, *R&D Marine Technology Centre, Gdynia, Poland:* **Implementation of Standardised EMC Criteria During the Warship Design Process in Poland** ..... 846

- R. HARMS, *Daimler-Benz Aerospace AG, Bremen,* L. REVERMANN, *WTD 71 Dept. Communication-Navigation EMC, Eckernfoerde, Germany:* **Costs and Time Effective EMC Testing of Equipment Used in Safety Critical Environments** ..... 850

- J. KAZIK, *Defence Evaluation Research Agency, Portsdown West, UK:* **EMC Assesment Using the Transmission Line Matrix Method (TLM)** ..... 854

- F. STEWART, *U.S. Space and Naval Warfare Systems Command, San Diego, California, USA:* **Electromagnetic Environmental Effects (E3) Awareness in the US Navy** ..... 859


# III WORKSHOPS

## EUROPEAN TELECOMMUNICATIONS STANDARDS INSTITUTE ACTIVITIES IN EMC AND RADIO SPECTRUM MATTERS

Chairman: O.J. WHEATON, *Radiocommunications Agency, London, UK*


- D. AUST, *NOKIA GmbH, Bochum, Germany:* **Automotive EMC Directive and the Use of Radio Products in Vehicles** ..... 865

- E. BLIKSRUD, *Norwegian Post and Telecommunications Authority, Oslo, Norway:* **Maritime EMC and the International Community** ..... 868

- G. DE BRITO, *CNET, ISSY-LES-MOULINEAUX, France:* **The Interface Between ETSI and the Spectrum Managers in the European Radiocommunications Committee (ERC) of the European Conference of Postal and Telecommunications Administration (CEPT)** ..... 872

- M. SHARPE, *ETSI, Sophia Antipolis, France:* **Overview of ETSI Activities** ..... 876

- O. WHEATON, *Radiocommunication Agency, DTI, London, UK:* **European Legislation Initiatives: the R&TTE Directive and SLIM Initiative** ..... 881


## THE SPECTRUM ENGINEERING ADVANCED MONTE CARLO TOOL (SEAMCAT)

Chairman: A. BENAMAR, *Centre de Recherche de Motorola, Paris, France*


- A. BENAMAR, P. MOORUT, D. BOSCOVIC, *Motorola Labs, Gif-sur-Yvette Cedex, France:* **The Spectrum Engineering Advanced Monte Carlo Analysis Tool (SEAMCAT)** ..... 884

# IV OPEN MEETING OF URSI COMMISION E "EM NOISE AND INTERFERENCE"

Organizer/Chairman: R.L. GARDNER, *Comm. E Chairman, USA*


- R. GARDNER, *Spectral Synthesis Labs, Alexandria, USA:* **Commission E Open Meeting** ..... 889
- R. STRUZAK, *Co-Chair, URSI WG, ITU RRB, Poland:* **URSI WG E1: Spectrum Management/Utilization and Wireless Telecommunications** (WG E1 Report) ..... 890
- W. RADASKY, *Metatech Corporation, Goleta, USA,* M.W. WIK, *Defence Materiel Administration, Stockholm, Sweden:* **The Standardisation of High Power Electromagnetic Transient Phenomena in the IEC** (WG E2 Report) ..... 893
- M. WIK, *Defence Materiel Administration, Stockholm, Sweden,* W.A. RADASKY, *Metatech Corporation, Goleta,* R.L. GARDNER, *Spectral Synthesis Labs, Alexandria, USA:* **Intentional Electromagnetic Interference - What is the Threat and What Can We Do about it?** (WG E2 Report) ..... 896
- R. GARDNER, *Spectral Synthesis Labs, Alexandria,* D.C. STOUDT, *Naval Surface Warfare Center, Dahlgren,* C.E. BAUM, *Air Force Research Laboratory, Albuquerque, USA:* **Testing Strategies for Susceptibility Testing in High Power Electromagnetics** (WG E3 Report) ..... 898
- E. HAMID, Z. KAWASAKI, R. MARDIANA, *Osaka University, Osaka, Japan:* **Impact of the 1997-98 El Nino Event on Lightning Activity over Indonesia** (WG E4 Report) ..... 902
- M. IANOZ, *Swiss Federal Institute of Technology, Lausanne, Switzerland:* **EMC Problems Connected to the Use of the Low Voltage Power Network for Information Transmission** (WG E5 Report) ..... 908
- H. KIKUCHI, *Institute for Environmental Electromagnetics, Tokyo, Japan:* **Gravito--Electrodynamics of Dust and its Applications to Pre-Earthquake Effects and Tornadoes** (WG E7 Report) ..... 910
- M. HAYAKAWA, *University of Electro-Communications, Tokyo, Japan,* R. PIRJOLA, *Finnish Meteorological Institute, Helsinki, Finland:* **Geoelectromagnetic Disturbances and Their Effects on Technological Systems** (WG E8 Report) ..... 915
- J. GAVAN, *Academic Institute of Technology, Holon, Israel:* **Radio Noise and Interference above 30 MHz** (WG E9 Report) ..... 921



# EMC 2000

## Patron's Address

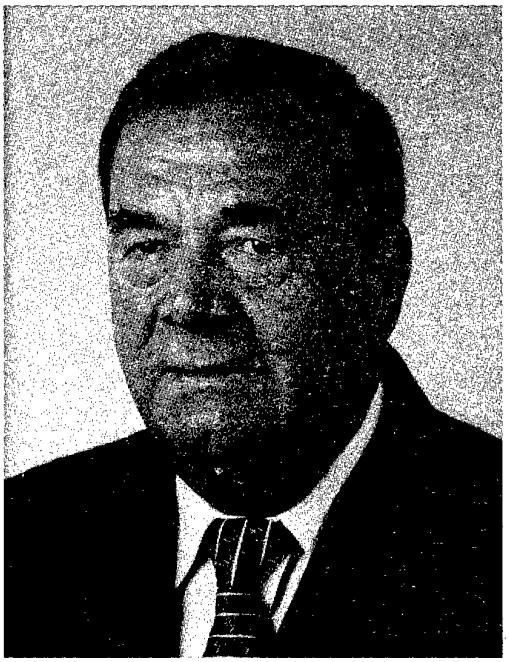
It is my great pleasure to greet the participants of the 15th Wroclaw Symposium on Electromagnetic Compatibility which takes place on the verge of the new millennium.

The coming age will be, do we want it or not, the age of Information Society for which the converging telecommunication, computing, and media are the cornerstones. Their proper and fast development is a prerequisite for the society's progress and welfare.

This development depends on favourable regulatory environment but to a great extent also on your ability to solve the growing EMC problems stemming from the convergence process, and from the ever-growing demand for new services and systems.

I sincerely appreciate your efforts to make all the elements compatible, and I wish you success in finding the most effective solutions.

*Tomasz Szyszko*
Minister of Posts and Telecommunications
of the Republic of Poland



# EMC 2000

## CHAIRMAN'S MESSAGE

**Ladies and Gentlemen, dear Guest and Friends,**

I have the honour to welcome you cordially to the 15th International Wrocław Symposium and Exhibition on Electromagnetic Compatibility being held in the Jubilee Year 2000. As our electromagnetic environment keeps growing and becomes more complex, EMC is becoming more and more essential for the whole society. The future of our technical civilization depends on the ability of solving growing EMC problems.

The well reputed position of the Wrocław EMC Symposium is to a great extent the merit of numerous individuals around the world, and of many international organizations and associations of electrical and electronic engineers from many countries. They are quoted in these Proceedings, and we extend our gratitude to all of them. We owe our reputation also to the Scientific Program Committee with Professor Frans Louis Stumpers, Member of the Royal Netherlands Academy of Arts and Sciences, and Doctor Honoris Causa of the Wrocław University of Technology, who chaired it successfully for many years and now is the Honorary Chairman, and to Professor Ryszard Strużak – its present Chairman. Professor Strużak was the Chairman of the Wrocław EMC Symposium in the years 1980 - 1984. I would like also to bring out the role of the Symposium Council with its Chairman Professor Władysław Majewski. The international flavour of the Symposium has been gained with the support offered by the International Union of Radio Science URSI. The auspices granted by the Committee of Electronics and Telecommunications of the Polish Academy of Sciences add to the scientific atmosphere of the event.

The Symposium would not be possible without the authors of the papers presented here who always play the most important role in such events, and I should specially mention the eminent specialists who have organized and chair

the invited sessions. Thank them all very much indeed for their contribution to the success of the Symposium.

The Symposium owes very much to the eminent patronage of Mr. Tomasz Szyszko, the Minister of Posts and Telecommunications of the Republic of Poland, and his kind personal support. From the very beginning the Symposium has enjoyed the patronage of the consecutive Ministers of Posts and Telecommunications, and this tradition is most valuable for us.

We are very grateful to our sponsors who are quoted in these Proceedings. Their financial support helped greatly to organize the Symposium.

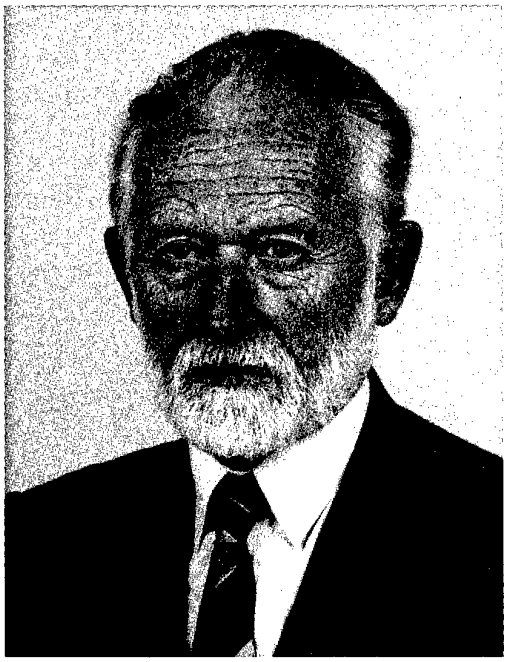
The objective of the Symposium is to bring together engineers and scientists who are interested in a better understanding of electromagnetic phenomena, and their influences on technical and biological systems. Our purpose in doing so is to become better mutually informed about our current work, to appraise the status of the field, to stimulate the future work, and, of course, to become better acquainted with each other.

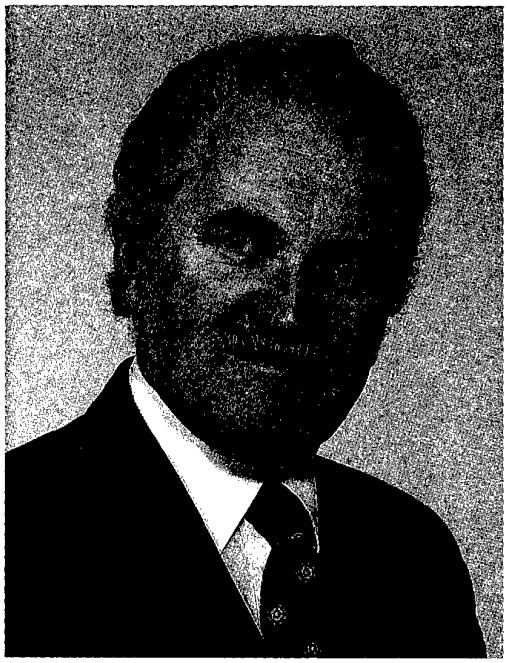
It is up to you to decide to what extent this event and the information presented, will contribute to those aims.

Most of the preparation work we owe, traditionally, to Mr. Władysław Moroń, the Organizing Chairman, and to all the members of the Organizing Committee. Their endless efforts to make the Symposium a scientific and organizational successes, are appreciated.

I hope that the 15th Wrocław EMC Symposium will mark a new important step in promoting the development of EMC technology. I wish all the participants fruitful discussions and pleasant stay in beautiful Wrocław.

*Prof. Daniel Józef Bem*
Symposium Chairman





**Welcome to EMC Wroclaw 2000**

Almost thirty years ago, a few enthusiasts from the Wroclaw University of Technology and from the National Institute of Telecommunications (Wroclaw Branch) decided to organize a conference on electromagnetic compatibility (EMC), and the Wroclaw Symposium on EMC was born in 1972.

At that time, the concept of electromagnetic compatibility was already established in the United States, and EMC conferences were regularly being held there, but in Europe, divided by the cold-war iron curtain, there was no such event organized on a regular basis. Starting, we did not know whether we would have any support but the idea found wide appreciation, creating an international fraternity interested in the development of art and science of EMC.

At the beginning, the majority of participants came from Central and Eastern Europe, and the symposium proceedings were a chronicle of major achievements in EMC field in that region, but that pattern has changed with time. Every two years, Wroclaw has been gathering a number of individuals from around the world involved in research of electromagnetic interactions among natural and man-made systems. Thus, the Wroclaw Symposium proved to be the oldest regular European Conference in its field, with the Proceedings totalling more than 10'000 pages published until now.

During these years, we always tried to bring together individuals interested in various aspects of EMC, theory and practical applications, to enable their interaction, in the belief that new bright ideas often sparkle on the borders of different fields of activity.

As a result, Wroclaw became a meeting place of people involved in research of earth natural electromagnetic (EM) phenomena: people working in spectrum

engineering, management and monitoring; radioastronomers fighting for a clear spectrum for their observations people involved in the EMC measurements; people working in radio wave propagation and antenna theory; people involved in technical side of research of biological hazards of EM radiation; and people interested in counteracting the EM terrorism. Looking at the continuing interest evidenced by a wide participation, we believe that this approach has been welcomed by all.

The International Wroclaw Symposium on Electromagnetic Compatibility is a cooperative not-for-profit project that would not be possible without the support of numerous individuals and organizations. Having the privilege to be among the symposium founders, we would like to take this opportunity to express our deep gratitude to all of them.

Three persons deserve special tribute here. The late Professor Wilhelm Rotkiewicz created in fifties the Wroclaw Branch of the National Institute of Telecommunications that become later the national centre of EMC research and organisational base for the symposium. The late Professor Jan Holownia, first chairman of this symposium, was the main initiator of the symposium concept. Professor Frans Louis Stumpers played, as a Program Chairman, a crucial role in coordination with EMC initiatives in Western Europe and with the International Union of Radio Science (URSI), where he served as President and then Honorary President.

The years that have passed since the origination of the symposium witnessed many changes. About fifteen generations of electronic technologies appeared, according to the Moore's Law. Thirty generations of engineers/scientists left universities to start professional careers. The iron curtain has disappeared and European Union was born. The old millennium comes to the end, and the new millennium opens a new era marked by concepts of Global Information Society. All that reminds us that it is a time of change, and a time for change.

*W. Moroń*
Organizing Chairman

*Prof. R. Strużak*
Program Chairman

# I
# PLENARY SESSIONS

EMC 2000 INTERNATIONAL WROCŁAW SYMPOSIUM ON ELECTROMAGNETIC COMPATIBILITY

# ELECTROMAGNETIC COMPATIBILITY STRATEGY FOR THE FUTURE

William A. Radasky
Metatech Corporation
358 S. Fairview Ave., Suite E
Goleta, CA 93117 USA
Fax: +1-805-683-3023
Email: wradasky@aol.com

*The ability to design and achieve electromagnetic compatibility is becoming more challenging with the rapid development of new electronic products and technologies. This paper reviews the definition and status of EMC today, discusses the near term trends that have appeared, and proposes strategies to solve the EMC problems of the future.*

## 1. INTRODUCTION

This paper addresses four questions of importance today and in the future with respect to the problem of Electromagnetic Compatibility (EMC) of electronic systems:

- What is EMC?
- What is the status of EMC today?
- What are the EMC problems of the (near) future?
- What is our strategy to solve these EMC problems?

As the author is the Chairman of the International Electrotechnical Commission (IEC) advisory committee on electromagnetic compatibility (ACEC), most of this paper will focus on the activities of the IEC. The IEC has been very active in developing new and improved EMC standards over the past 10 years.

## 2. WHAT IS ELECTROMAGNETIC COMPATIBILITY (EMC)?

As most workers in the field understand, electromagnetic compatibility describes a state when the electromagnetic environments produced by natural phenomena and other electrical and electronic devices do not cause interference in electronic equipment and systems. Of course to reach this state, it is necessary to reduce the emissions from sources that are controllable, to increase the immunity of equipment that may be affected, or to do both.

It is important to understand that EMC as defined does not absolutely prevent interference from occurring. Rather, it is recognized that emissions from various sources are variable (e.g. lightning impulses on power lines vary with the level of lightning current and its distance from a home or office). In addition, the immunity of a particular piece of equipment can vary (e.g. induced voltages on a circuit board are strong functions of the angle of incidence and polarization of the incident EM field). This variability results in a situation where a balance is found between immunity and emissions for a particular type of disturbance to prevent problems in a large percentage (but not all) of the cases of interest. To try to eliminate all problems (by decreasing emissions and increasing immunity further) could create a high cost to industry and could prevent new technologies from emerging.

For example a restriction to lower the transmitting power of cell phones so that consumers could lay their cell phones on top of any piece of electronic equipment could compromise the performance and economic viability of cell phone systems. On the other hand, a requirement that all commercial electronic equipment perform without malfunction at levels of 50 V/m, would place a financial burden on a large range of equipment. A good compromise is to warn consumers of reasonable restrictions, although special actions may be necessary when malfunctions could cause a threat to human safety.

## 3. WHAT IS THE STATUS OF EMC TODAY?

### 3.1. Overview

The focus of today's work in EMC is clearly on standardization -- especially in international organizations. The requirements of the World Trade Organization and the desire to reduce worldwide trade

barriers have resulted in a strong emphasis on international standards. Of course it is clear that regional developments, such as the European Directive on EMC, has had a strong influence on the pace of work.

In terms of the international standards bodies, the majority of the EMC standardization work is occurring in the International Electrotechnical Commission (IEC), while significant segments of work are also occurring in the International Standards Organization (ISO), and the International Telecommunications Union (ITU).

The IEC and its two principal horizontal EMC committees, CISPR and TC 77, have developed, and are continuing to develop, a significant range of basic EMC standards that define the measurement and test methods necessary for repeatable standards. In the area of emissions, CISPR and SC 77A are also developing emission limits for high–frequency electromagnetic fields and low-frequency power line disturbances, respectively. Within the IEC, ACEC coordinates the EMC work and also coordinates with other standards bodies to reduce duplication in the marketplace.

The ISO and the ITU are working in their respective areas to develop standards dealing mainly with moving vehicles and communication systems, respectively. In particular, the ISO is actively working with automotive, aircraft and space EMC standards. ITU deals with the EMC aspects of emerging telecommunications equipment including both radio and "wired" technologies. Both organizations are coordinating their work with the IEC in the hopes of minimizing the number of basic EMC standards that are developed so that industry will not be required to test and certify their equipment to conflicting standards.

One important aspect of the development of international standards is that they are voluntary in nature, although they may be applied in commercial contracts or by regional standards organizations in a mandatory fashion.

### 3.2. The IEC EMC Approach

As alluded to above, the IEC has focused its EMC standardization work into four main categories. These include the development of:

- -- emission limits for all products;
- -- basic EMC standards that include test and measurement methods for emissions and immunity;
- -- generic EMC standards that specify a set of "essential" disturbances, test methods and test levels appropriate for an environment class (e.g. residential) for both emissions and immunity; and
- -- product EMC standards that are tailored either to a class of equipment in a product family standard or to a specific type of equipment in a product standard (these standards usually include both emissions and immunity clauses).

Within the IEC, the EMC work is coordinated in the Advisory Committee on Electromagnetic Compatibility (ACEC). In addition, IEC Guide 107 [1], which has been developed by ACEC, provides guidance to IEC committees on how to properly develop EMC standards and reports. To accomplish its work, ACEC meets two to three times a year to consider new developments in EMC standardization within and outside of the IEC. The committee consists of technical experts in the field of EMC and representatives of the major participants in the development of basic and product EMC standards. ACEC provides its recommendations to the IEC Committee of Action for their consideration after every meeting.

### 3.3. Status of Important EMC Issues

One of the major problems today within the standardization process is the translation of emission limits and basic standards into product standards. Although considerable effort has been made to establish high–frequency emission limits by CISPR, there have been several cases in product standards were the limits were ignored or improperly applied. Unfortunately these errors are not always found until after a product standard is published, and it may take years to correct the error. ACEC is developing a new procedure to solve this problem by tracking the development of product standards to try to improve the accuracy of EMC clauses.

A relatively new area of concern involves the generation of power frequency harmonics by electronic equipment. Due to the large number of new electronic equipment with switched-mode power supplies, these harmonics can be significant enough to propagate within the power network and cause interference to other consumer-owned equipment. Work is ongoing to develop standards that balance the needs of electronic manufacturers and the power utilities; however, progress has been slow.

Another area of concern involves the need to develop basic test methods that are applicable to test frequencies above 1 GHz. This is a real concern due to the development of more and more commercial products operating at higher frequencies. New test methods such as the reverberation chamber have advantages at higher frequencies in terms of better coverage of angles of incidence and polarization while reducing test time. The IEC is working to develop a basic standard, 61000-4-21 [2], that will provide an option to those interested in an alternative test method.

## 4. WHAT ARE THE EMC PROBLEMS OF THE (NEAR) FUTURE?

Several important trends in technology are underway today that are likely to continue in the future. The most obvious is the increase in the density of microprocessors in homes, businesses, factories and vehicles. For the sake of clarity, this discussion will be separated into two parts -- fixed and mobile microprocessors.

In the area of fixed microprocessors, it is clear that many of our electrical appliances are becoming "smart" with the addition of microprocessors. It is now possible to buy a refrigerator that has a built in computer. There are plans to develop this appliance to the point that it will know when the last bottle of mustard has been used, and it will order a replacement for you through the Internet. Although this may not seem to be a problem, if one considers that EMC is based, in part, on physical distances between emitters and "victims", the fact that there will be many more emitters and "victims" in the same space, raises a concern. Will the consumer know that separating installed equipment can reduce interference problems?

Although the problem of fixed microprocessors may be solvable, what happens when a large number of mobile transmitters are introduced into a fixed space? Of course there is the cell phone which will continue to develop as it passes from one generation to the next. However, there is now the possibility of a new set of transmitters that could be placed in nearly every piece of electronics -- Bluetooth technology. Bluetooth is a specification for a frequency-hopping radio technology that uses the unregulated 2.4 GHz ISM band to communicate automatically between electronic devices within a range of approximately 30 meters. The operational specification for Bluetooth has now been accepted by over 1200 companies worldwide, and it is projected that 400 million devices will be using Bluetooth by 2004 [3]. While it is apparent that devices designed to use Bluetooth should work properly when exposed to the incident radio signal, it is unclear whether other devices not designed for Bluetooth will operate without interference.

Another aspect of future problems is the continual increase in the frequency of operation of new products. While cell phone technology has extended above 1 GHz and Bluetooth will operate at 2.4 GHz, there are other products involving satellite communication near 10 GHz and automobile radars operating above 40 GHz. While new frequencies in themselves are not necessarily a concern, one particular aspect of this increase could be a problem. In particular, higher frequencies have smaller wavelengths and are able to penetrate equipment enclosure seams and apertures more easily than lower frequencies. For instance, the wavelength of 100 MHz is 3 meters, 1 GHz is 30 cm and 10 GHz is 3 cm. For a 2-cm long seam 1-mm wide in a metal enclosure, the attenuation of each these fields 3 cm behind the aperture is 79, 59, and 39 dB, respectively. In addition to this increase in the disturbing environment with increasing frequency, the development of new microprocessors operating at clock speeds of 1 GHz today allows the possibility of more direct interference in the operation of electronic systems from both an immunity and an emissions point of view.

The EMC standardization process has been very good in producing test methods to evaluate the acceptability of equipment and small systems built by manufacturers. On the other hand, it has been difficult to develop standard methods to evaluate the immunity of large equipment or systems that are installed together for the first time. Size is a very important factor since test facilities are expensive to build, and immunity testing in the open field requires large test generators and produces "threats" to other equipment that are not under test. Even in the case of emissions testing, it can be difficult to establish the level of emissions from a particular piece of equipment after it has been installed in an operating factory.

Another new area of concern deals with safety aspects of electromagnetic fields; there are at least two areas in which this applies. The first is the so-called area of EMF (a very poor acronym for electromagnetic fields, which in this case implies the concern of EM fields on the health of humans). Most recently, EMF activities at ICNIRP (International Commission on Non-Ionizing Radiation Policy) and the WHO (World Health Organization) have resulted in an initiative in the IEC to support those organizations by developing measurement standards. Mr. Goldberg was the chairman of these IEC coordination activities and will review this work in this conference and proceedings [4]. A second related area of interest is the possibility of electromagnetic disturbances causing electronic systems to malfunction and cause a safety risk (for example a cell phone in a factory causing an industrial robot to injure a worker). Again the IEC is active in this area, and Mr. Goldberg also treats this subject in his paper [4].

In terms of the "structural" aspects of EMC standardization, several issues warrant mention. In the EMC standardization process, as noted earlier in this paper, the balancing of the work to obtain EMC between the emitters (by reducing the emission limits) and the potential victims (by increasing the immunity levels), is a continual problem. This process has been made more difficult due to the rapid change of technology and the very short time from product concept, to development, to production, and to the end of the product lifetime. This results in a very short period of time for EMC standardization bodies to evaluate the impact of new technologies in order to maintain EMC. When product cycles become shorter than the time required to develop a standard, a problem may occur. In addition, when companies developing

new electronic products and technologies do not participate in the standardization process, there is an increased likelihood of EMC conflict.

Finally, there are structural problems in the standardization process itself that are likely to create difficulties in the near future. First there is the problem of the availability of EMC experts in all areas from product development to standardization. Those involved in the discipline of electromagnetics know that fewer engineers are graduating with these credentials. The competition and rewards in industry are for computer programmers and Internet experts. Many who have worked in the field are nearing retirement, and some do not have the support of their management to work in the standardization field. The second problem lies with the standardization bodies themselves. With the digital revolution, everyone wants a digital copy of the latest standard. Because of financial considerations, the IEC and their national committees need the funds from the sale of standards to keep their organizations operating. The alternative is to charge the national committees a higher annual fee for the operation, but there is significant resistance to this idea. In fact in the United States, reviewers of standards were recently asked to pay an annual fee to participate in the USNC; this resulted in a loss of participants who were volunteering their personal time to review EMC standards that are under development.

## 5. WHAT IS OUR STRATEGY TO SOLVE THESE EMC PROBLEMS?

One major strategy to solve the EMC problems of the future is to continue and even expand the focus of EMC standards within the IEC. This effort should involve even closer cooperation with the ISO and the ITU in order to utilize limited EMC expert resources in the most efficient manner. The major effort should be to develop a single set of emission and basic EMC test standards that can be used by manufacturers. In addition, the application of the IEC Guide 107 within the ISO and ITU would improve the consistency of EMC standards in all three organizations.

A second strategy is for EMC engineers and scientists to evaluate emerging technologies that may have EMC impacts. This includes the review of popular and scientific literature as new ideas are formulated. When necessary, review groups such as ACEC in the IEC or other standardization bodies should organize meetings or seminars to learn of potential conflicts of operation. Also companies involved in the development of new technologies should be encouraged to contact standards bodies for advice on how to minimize interference to other systems.

Another area for active work is the development of standardized test methods for higher frequency disturbances (above 1 GHz). Work should proceed rapidly to fully develop the reverberation test method, the TEM test cell method and ancillary standards for sensor calibrations. The current work in the IEC needs to be accelerated to respond to the rapid development in new products.

More attention should be focused on the complex functional problems caused by EM disturbances that may lead to a loss of safe operation. While this may appear to be a classical safety problem, the ability of electromagnetic fields to interact in a complex way, with systems that are exchanging electronic data in real time, requires the attention of EMC experts. One of the difficulties is that the points of entry of an EM disturbance may be widely distributed throughout a system. For this reason a classical approach of shielding external influences and a reliance on a strong EMC test program are necessary. Mr. Goldberg is the working group convenor on the IEC draft specification 61000–1–2 [5] that addresses many of these issues.

With regard to the problem of testing large systems and pieces of equipment, the IEC and other standards organizations need to expend more resources to develop standardized procedures for the future. There has been some effort in this direction by those working with testing to the high-altitude electromagnetic pulse (HEMP) environment. Because many military systems in the past were often very large, big TEM and radiating simulators were built (see the draft IEC 61000-4-32 [6] for examples). Many of these simulators throughout the world are available for testing objects that are transportable. Also many of these simulators can be adapted to other waveforms and frequencies. Another option used by the HEMP community is to illuminate systems with low-level swept CW signals in order to measure transfer functions to potentially vulnerable points within a system. These types of testing options are described in IEC 61000–4–23 [7].

Another strategy is needed with regard to the translation of emission limits and basic EMC test standards into product EMC standards. One approach being planned within the IEC is to organize a group of reviewers to check the consistency of all product standards with regard to their treatment of EMC. The objective is to find problems at an early stage in the document development so that improvements can be made without slowing down the development of the standards. Another proposal is to develop additional generic standards that will minimize the need for product committees to translate the EMC basic standards to specific applications. This approach could be successful if the product committees feel that the generic standard environments are appropriate for their equipment.

While most of the standardization effort in the IEC and other standard organizations is focused on test

methods, substantial gains could be made if more effort was applied to EM protection methods. Proper EM shielding and cable filtering could go a long way to solving many EMI problems. One strategy would be to develop a general set of EM protection guides and a second set that is tailored to specific types of equipment. Of course one difficulty is that this approach would require significant effort by EMC experts who are already in short supply, especially in the standardization arena.

Another strategy for advancing understanding of this problem is through technical and standards workshops and seminars. The IEEE EMC society is very active in this area and has done an excellent job in educating its membership with regard to the complexity of EMC compliance. The IEC has recently initiated a series of workshops aimed at educating industry regarding the status and plans of EMC standardization within the IEC. It is hoped that these workshops will continue in the future. Also universities should be encouraged to offer courses in the EMC discipline, to include instructors from industry.

Another strategy of importance is to educate industry of the importance of participating in the development of international standards. It is clear that international trade is here to stay and will continue to expand in the future. Companies that are able to help develop new EMC standards will have an advantage with regard to their competition in that they will have a "head start" to develop compliant products. Without the participation of industry, there is a possibility that the standards developed will not be practical with regard to the test methods and the costs of compliance. The IEC and its national committees are always trying to educate industry to the advantages of standardization. There are also new ways to develop "pre–standards" in a rapid way beginning with industry specifications.

Finally, new approaches must be found to finance the development of standards that will allow the low-cost (or free) distribution of standards throughout the world. It is clear that a qualified staff is needed to produce consistent and high-quality standards. It is therefore left to the national committees of the IEC to decide how these changes can be accomplished without sacrificing the quality of the work.

## 6. REFERENCES

6.1. "Electromagnetic Compatibility -- Guide to the Drafting of Electromagnetic Compatibility Publications," IEC Guide 107, 1997.

6.2. "Electromagnetic Compatibility (EMC) -- Part 4–21: Testing and Measurement Techniques -- Reverberation Chambers," Draft IEC 61000-4-21, 1999.

6.3. R. Schneiderman, "Bluetooth Projections Push Product Development," Wireless Systems Design Supplement, Winter Issue, 1999, pp. 9-14.

6.4. G. Goldberg, "EM Phenomena and Implications for Standardization: EMC -- Safety -- Human Exposure," Proceedings of the 15th International Wroclaw Symposium on EMC, 2000.

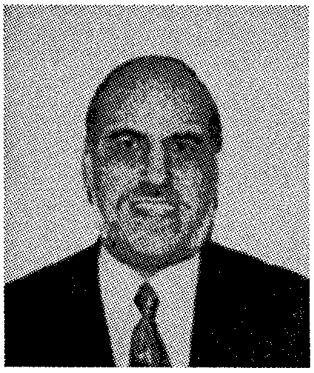
6.5. "Electromagnetic Compatibility (EMC) -- Part 1-2: General -- Methodology for the Achievement of Functional Safety of Electrical and Electronic Equipment with Regard to Electromagnetic Phenomena," Draft IEC 61000-1-2, 1999.

6.6. "Electromagnetic Compatibility (EMC) -- Part 4–32: Testing and Measurement Techniques -- HEMP Simulator Compendium," Draft IEC 61000-4-32, 2000.

6.7. "Electromagnetic Compatibility (EMC) -- Part 4–23: Testing and Measurement Techniques -- Test Methods for Protective Devices for HEMP and Other Radiated Disturbance," Draft IEC 61000-4-23, 1999.

## BIOGRAPHICAL NOTES

Dr. Radasky graduated from the U.S. Air Force Academy with a B.S. in Electrical Engineering and in Engineering Science in 1968, an M.S.E.E. from the University of New Mexico in 1971, and a Ph.D. in Electrical Engineering from UC Santa Barbara in 1981. He is the President and founder of Metatech Corporation in Goleta, California. He is also very active in the International Electrotechnical Commission where he is Chairman of ACEC and SC 77C, which is developing standards dealing with High Power EM transients. Dr. Radasky has published over 200 technical papers and reports dealing with electromagnetic interference and protection.



EMC 2000 INTERNATIONAL WROCLAW SYMPOSIUM ON ELECTROMAGNETIC COMPATIBILITY

# THE FUTURE OF BROADCASTING

Philip Laven
European Broadcasting Union
Geneva, Switzerland

*The speed of progress in the world of telecommunications and broadcasting has become breathtaking. The future of broadcasting is obviously digital, but which of the broadcast delivery systems (terrestrial, satellite or cable) will become dominant for digital TV? When will analogue broadcasting stop? Is there a long-term need for broadcasting? Will broadcasting be supplanted either by the Internet or by other telecommunications systems? Will "convergence" lead to a single delivery system for multimedia services?*

## 1 INTRODUCTION

Fig.1 shows the approximate dates of introduction of various technologies in broadcasting and related sectors. It is clear that the pace of technology is accelerating. Although Fig.1 indicates that some technologies (such as AM radio) have lasted a very long time, rapid changes in technology mean that there is little prospect of such stability in the future.

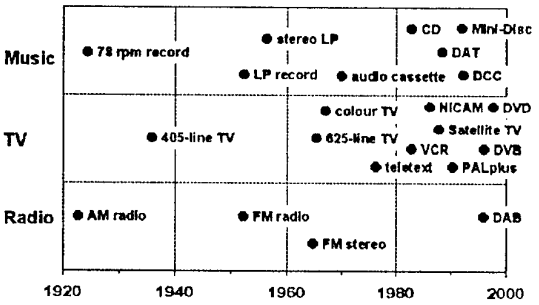



*Fig. 1 Approximate dates for the introduction of various technologies*

It is obvious that the future of broadcasting is digital. Digital transmission delivers numerous benefits for broadcasting. Compared with analogue broadcasting, spectrum efficiency can be improved dramatically – for example, by a factor of 4:1 for terrestrial TV or 10:1 for satellite TV. This improvement in spectrum efficiency permits a much greater choice of programming. Digital satellite TV services often include "near-video-on-demand" services where, say, 6 copies of several films are transmitted simultaneously. As their starting times are staggered by multiples of 15 minutes, viewers have to wait no more than 15 minutes to see their choice of film.

Digital transmission offers rugged and reliable reception - even under difficult conditions, such as multipath propagation that is often encountered on portable or mobile receivers. It also offers lower transmission costs per programme, together with the opportunity to deliver added-value data services.

The transition to digital broadcasting provides the opportunity for broadcasters to trade quantity for quality. For example, a digital multiplex of about 20 Mb/s can accommodate one high-definition TV service or four standard-definition TV services – or even more services if the source material is undemanding in terms of bit rate (such as most films). Even more important is that digital broadcasting permits this flexibility to be used dynamically on a second-by-second basis to meet programming needs.

## 2 DIGITAL RADIO

Despite intense competition from TV, radio is a vibrant and expanding medium – which will also benefit from the transition to digital broadcasting.

What will consumers expect from the next generation of radio services? They certainly will not expect digital radio services to be inferior in any respect to the existing analogue radio services. Although this principle may seem very obvious, the designers of some digital radio systems seem to have forgotten it.

In the analogue world, much radio listening is either "mobile" (e.g. in cars, buses or trains – or whilst walking or jogging) or "portable" (e.g.

moving a radio from room to room or having several radios scattered throughout your home). Radio listening has evolved from the time when listeners gathered around their only radio to listen attentively to the programme of their choice. Nowadays, radio listening is usually done whilst doing something else, such as driving a car, reading or doing household chores – in the computer world, this is known as "multi-tasking"! One of the great strengths of analogue radio broadcasting is that it can accommodate these diverse patterns of use.

Mobility and portability are essential requirements for any system aiming to replace analogue radio broadcasts. Those digital radio systems requiring a fixed satellite dish inevitably require the listener to be stationary or, at least, to stay in earshot of a fixed radio. Even worse, some system designers expect viewers to listen to audio services through a TV set! The Eureka-147 DAB system was expressly designed from the outset to provide perfect reception on mobile and portable receivers.

Arguably even more important in driving consumer demand for digital audio broadcasting is the range of services offered by the new technology. Some people will be keen to obtain digital simulcasts of analogue services, but even more would be attracted by additional "digital-only" services.

In summary, digital radio services must replicate the mobility/portability of existing analogue services, as well as allowing enhanced services, either more audio services or multimedia services.

### 2.1 DAB (Digital Audio Broadcasting)

The developers of the Eureka-147 DAB system recognised the importance of delivering high-quality audio (and data) services to mobile and portable users. It is interesting to reflect that their original plans envisaged the use of satellites, rather than terrestrial delivery. However, satellites cannot meet all the needs of radio broadcasters. Apart from the difficulties of achieving adequate reception within buildings, satellite delivery was not a sensible proposition for the growing number of local radio stations.

A key feature of DAB is its immunity to multipath propagation. Due to the use of COFDM, delayed signals can actually improve reception because they constructively contribute more power to the wanted signal. An additional benefit is that this feature permits the use of single-frequency networks, even to the extent where national DAB networks have been built using just one frequency. In areas where the DAB signals are received from two or more transmitters in a single-frequency network, the DAB receiver effectively regards one signal as a delayed version of the other signal – thus providing unprecedented continuity of reception, as well as unrivalled spectrum efficiency.

DAB services (see http://www.worlddab.org) are currently on the air in more than 20 countries around the world. To date, there has been a problem with availability of cheap DAB radios, but there are signs that this problem will be overcome in the near future.

### 2.2 DRM (Digital Radio Mondiale)

As with DAB and digital terrestrial TV, the combination of advanced digital modulation schemes with new algorithms for the digital compression of audio signals offers tremendous potential – even within 9 kHz or 10 kHz RF channels currently used for AM broadcasting.

Digital systems within a 9 kHz or 10 kHz channel can probably give performance equivalent to monophonic FM services – whilst being much less fragile than AM in terms of immunity to interference and selective fading.

Despite the rapid advances in technology, many people are still dependent on HF broadcasting for impartial news and information. In recent years, international broadcasters (such as the BBC, Deutsche Welle and Voice of America) have increasingly re-broadcast their signals via local MF or VHF-FM transmitters. Although such transmitters increase the potential audience, they are vulnerable in times of domestic crisis. For example, one of the first actions in many civil wars has been to seize control of radio and TV stations. In such circumstances, HF broadcasting becomes a vital source of impartial information.

Nevertheless, audiences now expect higher quality (and reliability) than can be delivered by AM broadcasting in the HF bands.

Digital Radio Mondiale (http://www.drm.org) has the objective of agreeing a single standard for digital radio in the AM bands. This could be used as the long-term replacement for AM broadcasting in the HF bands, as well as in the LF and MF bands.

Ideally, the DRM solution will be applicable to existing AM transmitters with only minor modifications. Broadcasters are naturally attracted by the potential re-use of expensive hardware, such as high power transmitters and transmitting antennas.

## 3 DIGITAL TV

The DVB Project (http://www.dvb.org) was established in 1993 to provide specifications for digital TV systems. It has been very successful not only in defining technical specifications for the complete range of broadcast delivery systems – but also for many other related specifications, such as for "return" channels to permit interactive TV services.

Digital satellite TV transmissions permit the rapid introduction of digital services across an entire country (or countries). They are ideal for covering large sparsely populated areas, where digital cable TV networks would be uneconomic.

Digital terrestrial TV transmissions offer reception on existing roof-top antennas. This may not seem to be very important, but DVB-T set-top boxes are being sold "ready for use" in the UK. In the vast majority of cases, the average member of the public needs no professional assistance in setting up such equipment.

DVB-T reception is also possible using the set-top antennas used by many "second" TV sets. This is particularly important because, in many homes, only the "main" TV set is connected to a roof-top antenna, satellite dish or cable TV network. In the analogue world, "second" or "third" TV sets are unable to deliver adequate quality pictures because they are connected to a "set-top" antenna.

In the near future, we can expect portable digital TV receivers, similar to the fully-functioning Nokia "Media Screen" DVB-T receiver shown in Fig. 2.



*Fig.2 Nokia Media Screen DVB-T receiver*

DVB-T even offers the possibility of *mobile* TV reception. This prospect is especially important in countries (such as Germany and the Netherlands) with high penetration of cable and satellite TV – where the demand for multi-channel TV has already been satisfied. There have been numerous impressive demonstrations of mobile reception of DVB-T transmissions.

For historical reasons, terrestrial transmission has been the dominant form of delivery for analogue TV services.

Which broadcast delivery system will be dominant in the digital era?

It is important to recognise the different environments of different countries. For example, cable TV systems have very high penetration in the Netherlands and in Belgium. On the other hand, cable TV systems have limited penetration in France, whilst in the UK, satellite TV is more popular than cable TV.

Each broadcast delivery system has its own particular strengths and weaknesses. Broadcasters will need to choose the most appropriate mix of digital delivery mechanisms for their country. There will be no universal solution for digital broadcasting.

## 4 THE INTERNET

The rapid growth of the Internet has surprised almost everybody. It is often quoted as an example of the sheer unpredictability of our technological age.

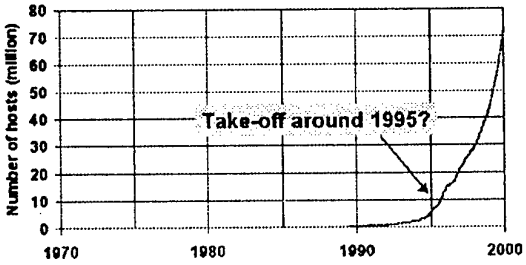



*Fig. 3 Growth of the Internet*

Fig. 3 appears to indicate that the growth of the Internet "exploded" around 1995, coinciding roughly with the establishment of the World Wide Web. Looking at this graph, it is hard to believe that anybody could have predicted this sudden "take-off".

However, if exactly the same data is plotted on a logarithmic scale, as in Fig. 4, it is clear that there was no sudden change around 1995. In fact the Internet has had a long history of sustained exponential growth. Although there are limits to exponential growth, ultimately set by the population of the world, it is obvious that the use of graphs with a logarithmic scale would have given

us "early warning" about the phenomenal growth of the Internet.

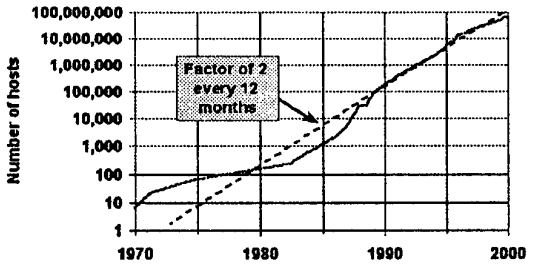



*Fig. 4 Growth of the Internet (logarithmic scale)*

Although the Internet has shown impressive growth, it is important to put this growth into perspective. Fig. 5 shows the speed at which households in the USA adopted various technologies. These curves are very similar despite a separation of 60 years between the introduction of radios and VCRs. It has often been claimed that the Internet is the fastest growing consumer product, but Fig. 5 illustrates that, even if it reaches the predicted 50% take-up in the USA by 2003, it will simply be matching the success of the video-recorder!

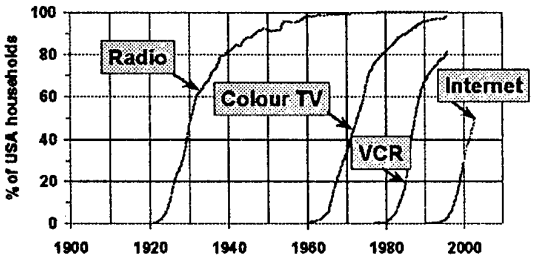



*Fig. 5 Penetration curves for the USA*

What is the relationship between broadcasting and the Internet?

It is obvious that the Internet has great long-term potential for broadcasters. Many broadcasters use the Web to offer programme-related information, as well as limited audio and video services. Broadcasters already operate some of Europe's most popular web sites.

Audio via the Internet has now become a practical reality. More than 1600 broadcasters are already providing such services. More than 40 million copies of RealAudio® software have been downloaded over the Internet. Nevertheless, it is not clear whether audio broadcasting via the Internet makes sense either for broadcasters or for listeners.

Although there are millions of potential listeners on the Internet, typical audio servers can support only a maximum of 100 or 200 simultaneous listeners. Audio servers capable of handling up to 500 simultaneous listeners are available, but they are expensive and require broadband connections from the broadcaster to the Internet.

As each listener requires a continuous dedicated stream of data at 20 kbit/s, a 2 Mbit/s connection from the broadcaster to the Internet is needed for every 100 listeners. Not many broadcasters would spend $50,000 or more on a new radio transmitter that would serve a maximum of 200 people. But they do on the Internet!

To accommodate additional listeners, broadcasters have to pay for extra hardware (e.g. servers) and extra bandwidth. In practice, the cost of bandwidth can be exorbitant. In other words, broadcasters pay for every additional listener on the Internet.

If a web site becomes very successful, its operator must pay for more hardware (e.g. servers) and for greater bandwidth connections. As there are very few proven models of financial success on the Internet, this can lead to vicious spiral in which successful operators become "victims of their own success".

This contrasts sharply with the concept of broadcasting. One of the remarkable characteristics of broadcasting is that, in the language of economists, it is a "public good" because the costs of programme production and distribution remain constant whether a particular programme attracts 1 million or 2 million viewers.

Video over the Internet is some way from reality. At present, video pictures are typically not that much larger than a postage stamp. The video quality usually leaves a lot to be desired, but we must remember that the Internet is still in its infancy.

Despite numerous high-profile attempts to organise large scale "live broadcasts" via the Internet, the reality is that traditional broadcasting remains the only sensible method of delivering video and audio simultaneously to millions of people.

The Internet is not yet suitable for one-to-many services (e.g. broadcasting), but it is ideal for one-to-one services (e.g. audio-on-demand). As the capabilities of the Internet improve, it will undoubtedly become even more important for broadcasters as a new delivery mechanism, especially for on-demand services (including video) – as well as for international audiences.

## 5 BROADCASTING & TELECOMS

Will there be convergence between broadcasting and telecommunications? It is important to understand the differences between these separate industries. Telecoms is mainly "one-to-one", whereas broadcasting is mainly "one-to-many"

From the all-important perspective of users, both models have advantages and disadvantages. Both models will continue to be needed for different types of services and applications.

Until recently, there was a significant gap between the data rates needed for broadcasting and the data rates available on most telecommunications systems. However, this is now changing with the emergence of broad-band delivery systems, such as cable modems and ADSL. These technologies, aimed at domestic users, will probably deliver up to 2 Mb/s. This falls slightly short of the 4 – 6 Mb/s needed for delivery of good quality television programmes. However, 2 Mb/s is dramatically better than that offered by the 56 kb/s modems used to access the Internet!

The development of UMTS is particularly interesting to broadcasters – as it offers "up to 2 Mb/s". In practice, this data rate will almost certainly not be available on a sustained basis – nor will it be available on a wide-area basis. In practice, 2 Mb/s on UMTS will be restricted to very small cells – and probably to fixed (rather than mobile) users. As shown in Fig. 6, UMTS will probably offer data rates of 128 kb/s for mobile users and 384 kb/s for pedestrian users.

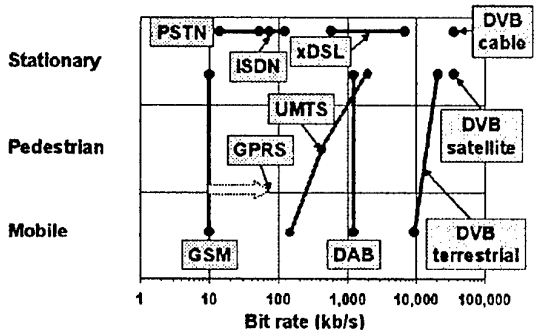



*Fig. 6 The relationship between UMTS and other digital technologies*

It is clear from Fig. 6 that UMTS is just one of many technologies that can be considered for the delivery of multimedia signals.

Although it has been suggested that UMTS could be used to deliver audio services, there seems to be uncertainty about the costs that each user would have to pay for such services. From the perspective of the operator, any business is good, particularly if the call lasts a long time! However, it seems improbable that listeners would move from radio broadcasting (which is essentially free) to telecoms-delivered audio services (which will be expensive).

UMTS may not be competitive in delivering 2 Mb/s broadcast services to static users, but UMTS could find an important role in providing enhanced multimedia and interactive services or return channels for interactive broadcasting (e.g. in conjunction with DAB).

## 6 WITHDRAWAL OF ANALOGUE BROADCASTING

When digital broadcasting becomes universal, it will be possible to withdraw the analogue transmissions. This will allow the release of large amounts of spectrum, which could be used for additional digital broadcasting and/or for other services. This is an important objective, but when will it happen?

In order to answer this question, it is instructive to examine some precedents.

### 6.1 AM radio

The introduction in the 1950s and 1960s of FM broadcasting sounded the death-knell for AM broadcasting. As FM was so much better than AM, it seemed obvious that AM would disappear within 10 years - or 20 years at the most. In fact, AM is still with us.

*Why has it refused to lay down and die?*

From a technical perspective, there should be no contest between AM and FM. The 9 kHz RF channels in the LF and MF bands set the maximum audio bandwidth for AM at 4.5 kHz. In practice, the frequency response of most AM radios is typically -3 dB at 3.5 kHz, whereas FM offers 15 kHz bandwidth as well as stereo.

Although ground-wave reception of LF and MF stations can be reasonably good during the day, reception at night is often ruined by interference from sky-wave signals, either from the wanted transmitter or from distant co-channel transmitters.

Despite the clear technical benefits of FM, AM did not quickly replace FM. In countries (such as the UK) where the FM transmissions simply duplicated the existing AM services, admittedly in higher quality, there was little incentive for listeners to buy relatively expensive new FM radios. Conversely, in countries (such as Germany) where the LF/MF

assignments were insufficient to meet the programming requirements, many services were available only on the FM band – and hence FM listening became popular more quickly.

Until the late 1960s or early 1970s, most portable radios and car radios could only receive AM services. By the 1980s, most new radios included FM, but AM radios were not discarded in favour of the new FM radios. Some of the AM radios remained in use - with the consequence that many listeners continued to listen for part of the time to AM services, because their old radios could not receive FM services.

However, this was only part of the problem. Not everybody accepted the technical arguments in favour of FM. Perversely, some people preferred the "mellow" sound of AM, rather than the "tinny" sound of FM. There is little doubt that such complaints were justified: some cheap portable radios sounded terrible. Furthermore, even within the last few years, some FM radios are so insensitive that they are essentially "deaf", since they cannot receive any weak FM signals.

More substantially, some listeners acknowledged the superiority of FM reception on a hi-fi system with a good antenna but, rightly, observed that FM reception on portable or car radios was often unsatisfactory.

Whereas AM reception is relatively stable, the use of VHF transmissions means that moving an FM radio by, say, one metre can cause dramatic variations in reception quality. In a car, such variations can cause temporary "drop-outs" which might be acceptable if they are infrequent. However, the variability of reception with location is judged by many to be completely unacceptable on a portable radio at home.

Unfortunately, adequate reception of a specific FM transmission can require a portable radio to be physically moved from its "natural" position on a table or kitchen shelf to a less satisfactory location – only to be moved back to receive a different FM transmission.

AM reception cannot match the best quality obtainable on FM, but AM might be more reliable - at least during the day!

At long last, at the end of the 1990s, AM listening is showing signs of decline. FM seems to have won the long battle. AM remains viable for news and sports services, but is less likely to be successful for music formats. New broadcasters are reluctant to build AM transmitters because FM transmitters are cheaper to build and operate. Furthermore, some AM services have already been closed down. This trend is likely to continue as broadcasters examine their high-power AM services in terms of cost per listener.

### 6.2 Withdrawal of TV services

Various Governments and regulators have suggested dates by which the existing analogue TV services might be withdrawn. The Federal Communications Commission (FCC) in the USA has announced that all analogue TV services will be switched off in 2006. In Europe, similar proposals have been made but in the timeframe 2009 – 2015.

Broadcasters who are introducing digital TV services would probably welcome such initiatives. Announcing a date for the closure of analogue TV would emphasise to consumers that digital TV will eventually replace analogue TV. This would have the immediate effect of depressing the sales of analogue TV sets and accelerating the take-up of digital services. This would benefit broadcasters by increasing the availability of their new digital services and, hence, reducing the cost-per-head of such services. By reducing the period of "simulcasting" (i.e. parallel operation of analogue and digital transmitter networks), it would also help to reduce the costs for broadcasters.

However, given the uncertainties about the speed at which consumers will adopt digital TV and the fact that few digital terrestrial TV services are yet on the air, it seems premature to announce precise timetables for the replacement of analogue TV by digital TV.

Market research in the USA suggests that only about 50% of homes will have digital TV by 2006, which is the proposed date for withdrawal of the analogue TV services. This implies that about 50% of homes will still be dependent on analogue TV. Clearly, there is a problem here: either the analogue TV services will have to be maintained much longer than the FCC expects, or the market researchers have seriously under-estimated the impact of digital TV.

It is important to be realistic about the prospects for rapid take-up of digital TV. Few consumer electronics products achieve penetration of 3% of households within 3 years and only the most successful, such as the audio CD, have reached 50% within 10 years. In the case of digital TV, there will inevitably be resistance from some members of the public who will not be able to afford digital TV equipment, or who see no reason why they should not continue to use their analogue TV sets. Even worse, it should also be noted that

an increasing number of households have more than one TV set. Every TV and every VCR must be replaced or equipped with a digital set-top box before the closure of analogue TV services.

There is not much experience to guide us in determining a realistic timetable for the withdrawal of analogue TV services. The nearest parallels are the withdrawal of the 819-line services in France and the 405-line services in the UK. The latter involved a 15-year period of simulcasting, ending in 1984.

It might be thought that the transition to digital TV could take place even more quickly. However, circumstances were very different then. The last 405-line TV sets were manufactured in the UK at the end of the 1960s and they used valves, rather than transistors. At that time, the "life expectancy" of such sets was about 8 years. In other words, it was surprising that there were any 405-line sets still operating in 1984. Modern television sets last much longer, with a life expectancy of 15-20 years and, hence, we cannot rely entirely on the natural replacement of TV sets as the catalyst in the transition to digital TV.

More recently, various broadcasters - especially in Eastern Europe - have made or plan to make the transition from SECAM to PAL. As most modern TV sets can receive PAL as well as SECAM, this transition should be relatively painless, except for those people with older colour TV sets.

In most countries, it is the politicians who will set the timetable for the withdrawal of the analogue TV services. Depriving the viewers of their TV services is unlikely to win many votes!

Although there are arguments in favour of setting a date for the closure of analogue TV services, this date will almost certainly need to be revised, depending on the take-up of digital TV. There is no value in setting an unrealistic date for the withdrawal of analogue TV services.

## 7 DEVELOPMENTS IN BROADCASTING

The transition to digital transmission is very important, but it does not change the essential nature of broadcasting. Traditional broadcasting is a one-to-many, one-way communications system. By its nature, it is consumed in a passive, linear manner – unlike the World Wide Web where users actively select "where" they wish to go at the click of a mouse.

The evolution of broadcasting will include new types of service – not just "more of the same".

Rapid technological changes in other areas could have substantial impact on broadcasting. For example, Fig. 7 shows that the cost of storage is falling rapidly: in the case of hard disks, the cost per MB of storage has fallen consistently by a factor of 2 every 12 months during the last 10 years. Industry experts expect this trend to be maintained for 5 – 10 years.

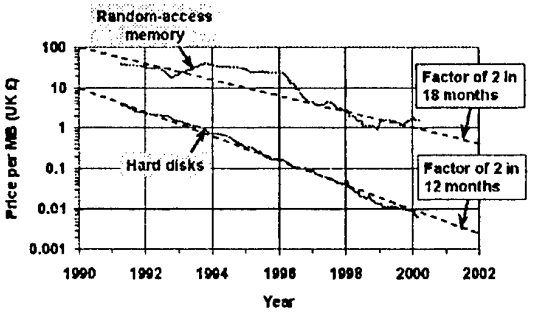



*Fig. 7 Cost of storage*

Hard disks are now becoming so cheap that they can be used as "intelligent" video recorders (e.g. TiVo, Replay Networks, some PCs). Unlike tape-based VCRs, hard disks can record and replay at the same time. This means that you can record a "live" programme but if the telephone rings, you can press "pause" to freeze the displayed picture. Whilst you are on the telephone, the broadcast will continue to be recorded on the hard disk. When convenient, you can resume watching the programme with full VCR-like controls - allowing you to "rewind" or "fast forward" whilst the programme is still being recorded. One notable feature is that you can also use this technology to "skip" the advertisements!

The availability of "local" storage will permit TV viewers to "order" a programme to be recorded by a single click during a trailer. Even better, intelligent software agents will record TV programmes that they "think" you might want to watch – on the basis of your previous viewing habits.

Recorded programmes will be automatically indexed, and retrieved with an easy-to-use electronic programme guide.

Linear programmes (e.g. a news bulletin) can be consumed in a non-linear manner. In other words, you will be able to select the items of interest to you – whilst skipping past those of no interest.

By using "intelligent" storage in the receiver, a modest amount of over-air data capacity can deliver sophisticated interactive multimedia information services. Stored information will be continuously up-dated and instantly available to users. In effect, you will have instant access to the latest news or

information – all of which will have been broadcast and stored locally.

The TV-Anytime Forum has been established to provide specifications for systems using local storage. Full information about the activities of this Forum is available at http://www.tv-anytime.org

## 8 CONCLUSIONS

Digital broadcasting will become ubiquitous in the next few years. The Internet is not yet able to compete with broadcasting in terms of quality and reliability, but broadcasters recognise that the Internet is important today and will be even more important in 5 years. However, the Internet will not "kill" broadcasting.

The future will see a proliferation of potential delivery methods for multimedia content – some of which are shown in Fig. 8. Not all of the new delivery methods will be successful, but the one certainty is that we will not converge on to a single delivery system!

Given the rapid changes in technology, broadcasting will not "stand still". Broadcasters will adopt and adapt any new technologies, such as local storage, that will offer benefits for them or for their consumers.

Broadcasters will almost certainly see themselves primarily as content providers and they will become neutral about delivery technologies.

It is important to note that many debates on the future of broadcasting concentrate on merits of different delivery systems. A few consumers are motivated by technology, but most are simply attracted by "content". We must not neglect the much more important issue of content provision.

**Technology is "everywhere" .....**
**but good content is "rare"**

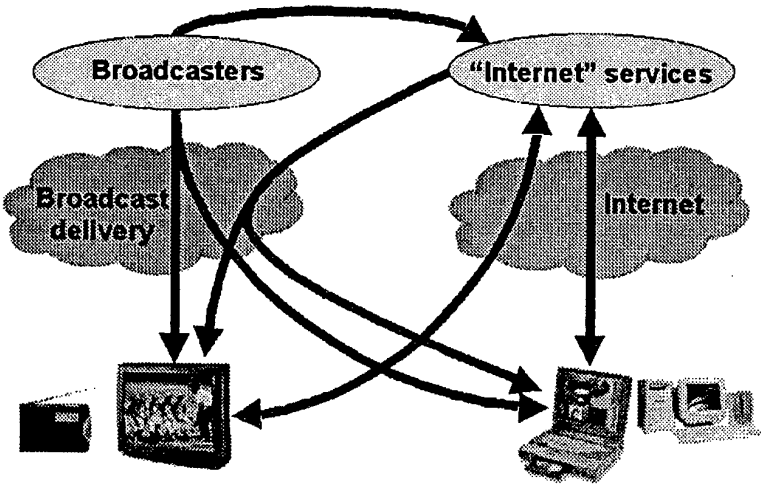



*Fig. 8 Convergence – or divergence?*

**EMC 2000** INTERNATIONAL WROCŁAW SYMPOSIUM ON ELECTROMAGNETIC COMPATIBILITY

# CIVILIAN VS. MILITARY EMC STANDARDIZATION
## - VIEW OF NATO SPECIAL WORKING GROUP 10 ON ELECTROMAGNETIC ENVIROMENT EFFECTS -

Captain (ITN) Raffaele Azzarone
General Directorate TELEDIFE – Viale dell'Università 4 – 00185 Roma, Italy
Tel. +30-06-49866617– fax +39 06- 49864257 - e-mail: teledife.infratlc@tiscalinet.it

*The aim of the present paper is to illustrate the point of view of the NATO Special Working Group 10, "Naval Electro-magnetic Environment Effects(E3)", on the Harmonisation of Military and Civilian Standards and the undertaken activities in this field.*

*This harmonisation will improve the effectiveness of single ships and task groups, by minimising system performance degradation caused by the E3 when installing both military and Commercial Off The Shelf (COTS) equipment on board a platform and co-locating them in the same reduced volumes, that are typical inside a ship, in presence of a highly E.M. polluted environment.*

*The first steps for achieving such a harmonisation are the comparison of the existing military and civilian standards and requirements, considering the particular naval environment, and the evaluation of the possible risk deriving from the coexistence of military and COTS apparatus, with respect to measurement methods, frequency range and limits, in order to define, when needed, additional rules or other additional limitations.*

## 1. NATO SWG-10 ACTIVITIES IN THE EMC FIELD

As is widely known, positive control of electromagnetic effects is of vital importance in an environment where equipment is ever more dependent on electricity and electronics, with consequent propagation of, and susceptibility to electromagnetic fields.

Therefore, if all the producers and users of electric and electronic equipment are affected by these problems, it is not surprising that a lot of specialists are working on the different matters in different fields, and among them the military specialists.

In NATO there are different groups which are pursuing, mainly, the following specific areas of concern associated with electromagnetic interference and compatibility:

- RADHAZ;
- Air Environment;
- Standardisation of Materiel;
- Safety ;
- etc.

And last but by no means least, this brings us to the NATO Special Working Group 10 on *Electro-Magnetic Environment Effect(E3)* dedicated to the naval environment.

The group is attended by 14 NATO Nations and is open to the Partners for Peace Countries, that are Bulgaria, Finland, Russia, Sweden, Lituania, Romania etc.

The most relevant characteristics of the group include long duration participation of the Representatives, with an average of 5 years, which makes it cohesive and strong, and the considerable contribution from technical experts and Centres.

The main aim of SWG –10 is to enhance the operational effectiveness of ships and naval task forces by means of the minimization of electromagnetic interference, both inside a single ship or amongst ships in a naval formation, through the identification, control and elimination of sources of electromagnetic interference or reduction of the undesired effects.

The naval environment is a very complex one due to the fact that the topside antenna arrangements of a modern warship are fitted with. a multitude of active and passive sensors, communication and weapon control emitters and receivers, operating across the whole frequency spectrum and at different levels of power, but occupying a very small space.

For this reason, NATO formed the SWG 10 to work towards ensuring that in this special and demanding environment, electromagnetic interference does not inhibit operational capability.

The SWG-10 Group addresses both the analysis and the remedy of EMI. This is done in a

productive way by measuring both near field and far off electromagnetic fields on board ships, and then assessing the incidents.

Special measurements can then be recommended and agreed upon as Standards.

Additionally, the mandate of the group extends to the remedy of EMI between ships in a multinational maritime force, including the impact on frequency planning and management.

The group uses information exchange as the fuel for the work that must be done to achieve minimised EMI, and the end products of this work are NATO Standardisation Agreements and Allied Naval Engineering Publications.

## 2. ADOPTION OF COTS EQUIPMENTS IN THE NAVIES

In recent years, due to the financial cuts exercised by all the Nations in the Defence Programs and due also to the exponential-law technological progress in commercial design and production in electronics field, the attention of Combat - Systems designers has been orientated also to the commercial market.

In particular the following apparatus can be indicated as products of normal employment on board ships:

- Navigation radar;
- GMDSS (Global Maritime Distress and Safety Systems), including radio equipment;
- Gyrocompass;
- Meteorological equipment, utilising both MF radio frequency band and satellite media;
- Personal Computers;
- Wire Telephones;
- Portable telephones (e.g. GSM);
- Facsimile equipment;
- Television and broadcast receivers;
- Navigation aids (e.g. Loran –c and GPS );
- Satellite communications (i.e. INMARSAT);
- Internal communications device;
- VHF–International Maritime communications;
- etc..

This situation has led us to keep in due consideration the coexistence, in the same internal spaces of a ship, both military and commercial equipment, that must operate respecting the required functional performance, without reciprocally interfering, even if designed and produced according to different standards.

In this context it is important to underline the importance of reaching the goal of the Harmonisation of commercial and military standards as a hot topic in the NATO Navies, and according to this policy the SWG –10 has started to investigate possible EMI problems arising from the insertion on board of COTS equipment.

## 3. MILITARY AND CIVILIAN STANDARDS

As a preliminary approach to the above mentioned harmonisation among standards, it is important to mention the historical origins and the following evolution of Documents and Regulations inherent to the EMI-EMC, both in the military and civil world [1].

The first military EMI documents were developed in the more industrialised Countries in the period immediately following the Second World War, with the aim of defining the main characteristics of EM emissions and susceptibility of the equipment, Systems and Sub/Systems.

As an example, let me mention the first Regulation published in the US, the JAN–I-225, regarding the test procedures EMI to be utilised for measuring the interference arising on board of vehicles. Later, this specification was substituted by the JAN-I-227 and then, in June 1950 by the MIL-I-6181.

The limits fixed in this specification were inclusive also of the emissions, without any differences between broad-band and narrow-band measurements, and were limited to the control of the interference of the telecommunication equipment up to 30 MHz.

Always in the USA, in 1953, the MIL-STD – 225 was proposed, with the aim of applying it to the three Services, but never adopted due to the incoming policy of separating the specifications for the Navy, The Air Force and the Army.

In these late documents the utilised limits and measurements units were different, and they could generate some misunderstanding in the application for certifying the same equipment employed in the three Services, with the consequent procurement problems. Thus it was decided to solve the problem through the promulgation of the MIL –STD –826, common to the three Services, never adopted for the heavy reserves expressed on it. Finally, the following Standards were agreed upon and widely adopted, not only in the USA, constituting also the basis, with some amendments, for the development of other military specifications in other Countries:

- MIL-STD-461 Electromagnetic Interference Characteristics, Requirements for Equipment;
- MIL-STD-462 Electromagnetic Interference Characteristics, Measurements of;
- MIL-STD-463 Definition and System of Units, Electromagnetic Interference and Technology.

A similar situation occurred in other industrialised Countries, with the same initial approach in developing different Standards for the three Services, and the following policy based on their unification.

Examples of military standards developed in national contexts or in International bodies are listed below:

- DEF-STAN 59-41 (UK),
- VG 95373 (Germany),
- STANG 3516 (NATO),
- GAM EG 13 (France),
- PMS (Poland),
- NO (Poland).

In the civilian field, the history has deeper roots, in fact, already in 1934 the first International Congress on Radio Interference(CISPR) was held.

Due to the war events, there was a long period of inactivity in the development of Regulations and limits, followed by an intense revival in the international context in the subsequent years.

In the '60s various Institutes were founded in many Countries with the aim of studying suitable methodology and identifying appropriate limits in order to satisfy the EMI/EMC requirements for the different equipment in commerce, that is: radio receivers, medical and scientific apparatus, domestic electrical appliances and so on.

It is important to note that the above mentioned Institutes have produced a great number of documents, some times in contrast with each other, generating difficulties in the diffusion of the equipment in Countries other than the one in which the product originated.

In order to solve this problem, many efforts are underway in order to identify a policy able to permit, in the short term, the unification of the Regulation, through qualified Committee as the CENELEC in European Community.

Among the major Organisations present in the World with the task of identifying, on an international scale, a common basis among the various documents, it is possible to list, mainly, the following:

- The Department of Defence of USA, which includes the Organisms that generated the above mentioned MIL STD 461-462-463;
- The Federal Communications Commission (FCC), created in the 1934 in the USA, with the aim of promulgating rules for construction of equipment that can cause interference with radio reception.
- The International Special Committee on radio Interference (CISPR), whose role is to develop the international EMC Standards;
- The Society of Automotive Engineers (SAE), founded in 1905, that operate in the field of terrestrial, aeronautic and naval vehicles;
- The American National Standard Institute (ANSI), a federation that includes industries, federal agencies and financial groups, with the aim of co-ordinating the development of Standards in the private sector;
- The Verband Deutdscher Elektrotechniker (VDE), a non-governmental German association that prepares the regulations for electrical systems, in co-operation with the German Institute for the Standardisation;
- The Economic European Community (CEE); whose role is to harmonise the regulations in the context of the Community;
- The CENELEC, that is an association of 17 technical national Committees in Europe with the aim of technical co-ordination among the Standards in order to achieve their unification for a free exportation of the equipment in the Countries inside the Community.

In addition to the above listed Organisation is also important to mention the existence of many others national bodies.

Among the numerous Documents produced is significant to mention the following:

- VDE Regulations (Germany),
- CISPR Specifications (Intern.Commitee),
- FCC Regulations (USA),
- CENELEC Regulations (EN) (Europe),
- CEI Regulations (Italy)
- IEC Specifications (Intern. Commitee)
- IEEE Standards (UK),
- ANSI Specifications (USA),
- DO-160D Procedures (USA),
- BS Standards (UK),
- etc.

In conclusion of this brief and clearly not exhaustive explanation of what is underway in the World, it is possible to underline that there are many differences between the military and civil EMC standards [2]. These differences concern the primary aims of the standards which address the principal problems arising from their respective operating environments.

Military EMC specifications primarily concentrate on intra-system compatibility of sub-assemblies, in order that complete system level compatibility is achieved in a potentially high packing density situation.

On the other hand, the civil standards are more concerned with the inter-system

compatibility and generally involve greater protection distances.

These guidelines have been drafted taking into consideration the differences between civil and military environments, test methods and procedures.

In this very complicated area, as far as the naval EM environment is concerned, the NATO SWG-10, with the support of other NATO bodies in order to achieve a unified methodology in solving the problem, is approaching the matter of the harmonisation of the civil and military standards, in consideration of the widely adopted use of COTS equipment in the Navies and their installation on board of a naval platform and of their co-location with military equipment in the reduced spaces typical on board of a ship, and is producing efforts in order to assure the EM compatibility among them in the way exposed at the next paragraph.

## 4. SWG-10 APPROACH TO THE HARMONIZATION

[3] Over these last ten years there has been a significant decline in many national Defence budgets and a need to rethink how equipment could be procured.

One of the easiest solutions is to procure "Commercial Off The Shelf" (COTS) equipment.

Consequently, COTS equipment has allowed the armed Services to obtain state-of-the-art technology faster and cheaper than before.

However, the problem with most COTS equipment is that it has been built to commercial standards and assessments, that may differ from the ones needed to ensure that the equipment will work in a harsh EM environment, where there are strict controls on the amount of EM emissions, and equipment is required to have a high level of immunity over a wide frequency band.

In particular the naval EM environment, that is being studied by the NATO SWG-10, is an extremely harsh workplace, where equipment must operate in close proximity to many high power emitters, such as HF transmitters and radars, which generate high field strength over different frequency band.

To begin with the naval environment can be categorised in two following main areas:

- The "Above Deck", typical of the outside of surface ship;
- The "Below deck", divided in three different environments: metallic hull, non-metallic hull and submarines.

Obviously the "Above Deck" is the harsher EM environment and, as a consequence, the "Above decks' " equipment must have the higher level of immunity and produce very low levels of unintentional emissions.

The "Below Deck' " environment, due to the metallic screening nature of metallic hull and its superstructure is less stressed and in some respects is more like the industrial/commercial environments, with more restrictions.

In such a context the urgent need to address the problem has been recognised inside the SWG-10.

Due to the fact that in these last forty years various technical Documents, Regulations, Specifications, Standards etc., have been produced inside Nations and in the International context, both for military and civil application, the SWG–10, considering the complexity of the matter, has recognised the need of understanding in advance the implications of choosing one standard over another, verifying the deriving advantages and the associated risks from the choice done.

In order to achieve this knowledge, it is deemed important to investigate the existing Standards of relevant interest, both military and civil, searching for evidence of the difference between them, and identifying application fields, limits, benefits and any other relevant aspects.

This policy emerges in the works prepared for the Special Session dedicated to the SWG-10 Group in the EMC Symposium 2000 in Wroclaw.

The presentations have been grouped in specialised Sub-Sessions, in compliance with the undertaken policy- lines explained in the following points.

*(1)* The comparison of existing EMC military standards with the civil Standards, by means of the analysis of limits, frequency bands and constrains;

*(2)* The definition of Standard procedures for simulation, prediction and modelling, with the double aim of verifying the existing Standards by means of software tools and laying the basis for future developments of standardised methods for modelling considered useful in ship design;

*(3)* The analysis of the out-coming results deriving from the application of the existing standards in EMC testing and measurements;

*(4)* The evaluation of the correlated aspects, like the costs, the lessons learned adopting some Standards, the necessity of appropriate training for the apposite personnel, in order to avoid or eventually solve the EMC problems arising on board, and so forth.

This approach represents, obviously, the first attempt to resolve a problem that requires intensive work in order to identify, or eventually develop, harmonised Standards to be applied in both a civilian and military context.

In this area SWG-10 will continue its work having given to the matter the highest importance and priority.

## 5. CONCLUSIONS

The military naval EM environment is recognised to be more severe than the residential, commercial and industrial environment.

Based upon a technical rationale, compliance with the appropriate class of military standards will ensure conformity with the protection requirements for COTS equipment.

The total set of requirements [2] for the apparatus to be used both for military and civilian purpose should comprise a core of EMC tests common to both the military and civil environment, to be used in the presence of common phenomena and additional conformity requirements to address specific typical military EM phenomena not covered by civil standards

Manufacturers of civilian equipment need to be aware that there are EMC requirements over and above those required by civil specifications, if the apparatus is also to have a military application.

In this way the apparatus intended for dual use (both civilian and military) placed on the market will satisfy the protection requirements of the basic directive, will be supplied with a valid declaration of conformity and instructions for installation and will be capable of being updated and modified, by a kit, in the case of application in a stressed military environment.

On the other hand, manufacturers of military apparatus should consider the likelihood of the apparatus causing electromagnetic disturbance on equipment not specifically designed to be compatible in the same reduced space of a naval environment.

Where that disturbance is liable to degrade the performances of other apparatus which might reasonably be expected to be present in the environment associated with the military apparatus' use, prudent measures should be taken "in loco" to reduce or eliminate that disturbance.

However, today, the task of harmonising military and civilian E3 standards appears very complicated, considering that the existing Standards have been written by different national or international Organisations with different purposes, but the significant benefits that can be achieved, in terms of parity of performance, cost reduction, comparable quality of the products, etc., are so desirable that it is important to continue as begun, through the selection of the most appropriate standards.

This being so, guidance to the correct choice of standards is important, when considering the acquisition of COTS equipment for use in a military environment.

Thus, there is a need to look more closely at the harmonisation of civil and military standards and the likely impact of choosing one over the other.

In order to achieve this goal, it is important to analyse each relevant standard, giving evidence of the differences between them, by means of comparison, tests and/or using modelling for simulation and prediction, evaluating risks and implication, before selecting or developing new standards suitable for the dual use.

According to this policy, in the last few years NATO SWG-10 is moving in co-operation with other NATO bodies involved, with the aim of achieving a unified approach to the problem, not only confined to the naval aspects but also embracing the complete area of EMC.

## 6. REFERENCES

6.1 - B. Audone "Compatibilità Elettromagnetica" (Italian)- Mc Graw Hill- Milano, Italy –Sept.1993, pagg. 221-230.

6.2 – "Guide to EMC Conformity of Apparatus Designed for Military and Other Purpose" CENELEC Report – January 1998- Ref No R210 – capt. 4 and 5 pagg. 4,5,6and 7.

6.3 – A.Lavell–Smith "Harmonisation of EMC Standards for the Naval Environment–A United Kingdom Approach"- Proc.of EMC Symposium and Exhibition – June 2000- Wroclaw –Poland.

## BIOGRAPHICAL NOTE

Captain Raffaele Azzarone is an Armament Officer of the Italian Navy. Today he is the Chief of the "Radio and Satellite Communications" Division in the MOD General Directorate for Telecommunications, Informatics and Advanced Technologies (TELEDIFE) of MOD in Rome.

He was awarded a degree in Electronic Engineering at the Polytechnic University in Torino, in 1974, and developed his experience mainly in telecommunication field, especially in HF frequency band and in Satellite communication.

In 1997 he was elected Chairman of the NATO SWG-10.

**EMC 2000** INTERNATIONAL WROCŁAW SYMPOSIUM ON ELECTROMAGNETIC COMPATIBILITY

# NOISE INTERFERENCE IN RADIOCOMMUNICATION NETWORKS: SHANNON'S FORMULA REVISITED

Ryszard Struzak
*Co-Chair, URSI WG on Spectrum Management/ Use and Wireless Telecommunications*
*Member, ITU Radio Regulations Board*
*ryszard.struzak@ties.itu.int*

*Problem of unintended interference noise in radiocommunication networks is discussed from information-theoretic perspective and placed into a context of congestion of the radio frequency spectrum. The congestion reduces the capacity of radiocommunication links, an aspect absent in Shannon's formula on channel capacity. The paper proposes a quantitative measure to deal with congestion issues and a correction to Shannon's formula.*

## INTRODUCTION

Technological progress, economical processes and social changes are making the Information Technology Sector one of the most important for modern society. Its significance relative to the other sectors of economy increases. Figure 1 illustrates the trend. The total amount of information offered to assure normal functioning of the society increases faster than the Gross Domestic Product does. That phenomenon, registered first in Japan, is shown in Figure 2. These trends lead us toward the Global Information Infrastructure and Global Information Society.

Within the Information Technology Sector, we witness the renaissance of radio. Radio waves as communication channel offer a number of benefits in comparison with wires and cables. Their unique characteristic is the ability to transmit information any time and any place, between any points, mobile or fixed, on the earth or even in the interplanetary space.

The benefits offered by radio waves have caused a phenomenal growth of radiocommunication services and applications during the recent years. For instance, the worldwide population of mobile phones reached roughly 285 million in 1998, and number of new mobile telephone subscribers increased from 4 million in 1990 to 75 million in 1998. Before you finish reading this page (which may take two minutes or so), about five hundred new wireless telephones will be put into operation within the limited frequency band available to that service. All other radio services and applications have also grown. That growth is expected to continue in the foreseeable future, leading to an unprecedented increase of congestion of the radio frequency spectrum.

How radio systems will operate under such congestion? A lot of work has been done on that problem. Only a few weeks ago the Radiocommunication Assembly and World Radio Conference of International Telecommunication Union (ITU), the WRC Istanbul 2000, discussed various aspects of the problem (although the term "congestion" did not appear explicitly in their agendas). The spectrum congestion problem was raised by R. Kirby and this author at the XXII URSI General Assembly in 1987 [6]. A special URSI working group on spectrum management/ utilization and wireless telecommunications was created that continues until now. Discussions within URSI culminated with a special lecture closing the XXVI Assembly in 1999 [1]. In that lecture, entitled "Spectrum Congestion", W. Baan and P. Delogne presented a comprehensive analysis of the current status-of-the-art.

***Note***: *The views expressed in the article are those of the author and do not engage any entity. The article develops ideas proposed in correspondence [9].*

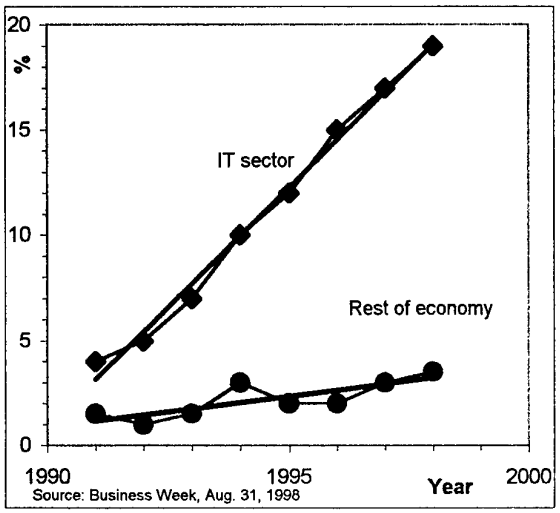



*Figure 1 Annual growth rate of Information Technology Sector over previous three years (%) compared with the rest of economy (USA, 1991 - 98).*

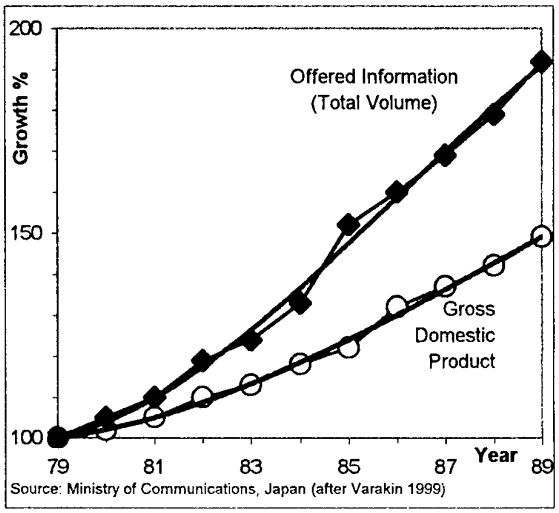



*Figure 2 Growth of the volume of information offered, compared with the growth of the Gross Domestic Product (Japan, 1979 - 89).*

This article extends further considerations offered in [1]. It approaches the problem from information-theoretical perspective and proposes:

- a quantitative measure of spectrum congestion, potentially applicable to system design and spectrum management problems
- a correction to Shannon's formula on capacity of radio channel.

The article is organized as follows. First, we discuss the channel capacity limit in conjunction with environmental interactions, and we introduce a concept of isolation of radio link. Then, a correction to Shannon's formula is proposed and a concept of capacity loss due to spectrum congestion is discussed, along with its consequences. Possible ways of reducing the loss are mentioned and illustrative examples are discussed. The examples idealize situations that may happen in practice. The last section summarizes our findings.

## ENVIRONMENT & SHANNON'S LIMIT

### *Shannon's Formula*

Claude Shannon showed [5] that the maximum amount of information ($C_0$) that a communication link can transport in unit time and unit bandwidth is limited:

$$C_0 = \log_2(1 + q) \qquad (1)$$

Here q is the power ratio (q = S/N) of wanted signal (S) to the total noise (N) at the receiver. For instance, if q = 1, then $C_0 = \log_2(1 + 1) = 1$ bit per Hertz per second. With constant q, the volume of information transmitted by a channel in unit time is proportional to the bandwidth. Shannon did not say how to design the communication channel to reach that limit. However, his formula has widely been accepted as useful reference to which various communication systems can be compared. Practical systems can only approximate this theoretical limit. The best systems can reach 0.1dB or so below the Shannon's limit, according to Rimoldi [4].

### *Environmental Influence*

The Shannon's limit was derived for an isolated communication link. However, no radiocommunication link can be isolated from its environment. Due to basic laws of physics, the non-guided radio waves used for radio communications cannot be confined to any specific volume.

When a number of neighbouring radio links operate at the same time and frequency, a part of power transported by radio waves penetrates from one link to another and adds to the link's noise power. The process involves the receiving end of the victim link and the radiating ends of the other links ("radiators").

This aspect, specific to radio channel, is absent in Shannon's general model of communication channel [5]. It is also absent in works of other authors (including Baan and Delogne [1]) who, following the Shannon's example, disregard environmental interactions (see eg [2]). In the following sections, we revisit the issue. We will see that environmental interactions play critical role in congested environment.

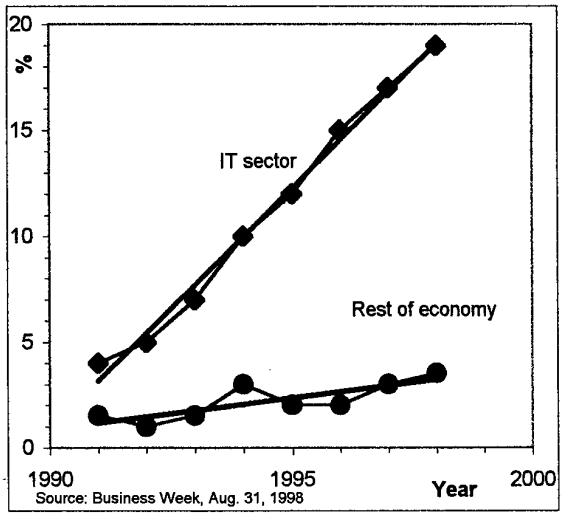



*Figure 1 Annual growth rate of Information Technology Sector over previous three years (%) compared with the rest of economy (USA, 1991 - 98).*

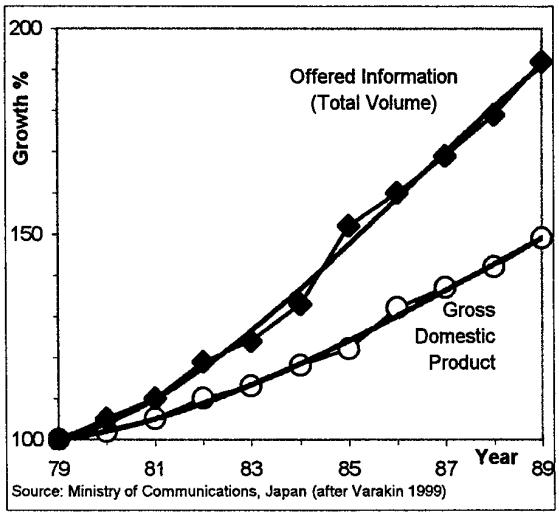



*Figure 2 Growth of the volume of information offered, compared with the growth of the Gross Domestic Product (Japan, 1979 - 89).*

This article extends further considerations offered in [1]. It approaches the problem from information-theoretical perspective and proposes:

- a quantitative measure of spectrum congestion, potentially applicable to system design and spectrum management problems
- a correction to Shannon's formula on capacity of radio channel.

The article is organized as follows. First, we discuss the channel capacity limit in conjunction with environmental interactions, and we introduce a concept of isolation of radio link. Then, a correction to Shannon's formula is proposed and a concept of capacity loss due to spectrum congestion is discussed, along with its consequences. Possible ways of reducing the loss are mentioned. Illustrative examples are discussed in the annex. The last section summarizes our findings.

## ENVIRONMENT & SHANNON'S LIMIT

### *Shannon's Formula*

Claude Shannon showed [5] that the maximum amount of information ($C_0$) that a communication link can transport in unit time and unit bandwidth is limited:

$$C_0 = \log_2(1 + q) \qquad (1)$$

Here q is the power ratio (q = S/N) of wanted signal (S) to the total noise (N) at the receiver. For instance, if q = 1, then $C_0 = \log_2(1 + 1) = 1$ bit per Hertz per second. With constant q, the volume of information transmitted by a channel in unit time is proportional to the bandwidth. Shannon did not say how to design the communication channel to reach that limit. However, his formula has widely been accepted as useful reference to which various communication systems can be compared. Practical systems can only approximate this theoretical limit. The best systems can reach 0.1dB or so below the Shannon's limit, according to Rimoldi [4].

### *Environmental Influence*

The Shannon's limit was derived for an isolated communication link. However, no radiocommunication link can be isolated from its environment. Due to basic laws of physics, the non-guided radio waves used for radio communications cannot be confined to any specific volume.

When a number of neighbouring radio links operate at the same time and frequency, a part of power transported by radio waves penetrates from one link to another and adds to the link's noise power. The process involves the receiving end of the victim link and the radiating ends of the other links ("radiators").

This aspect, specific to radio channel, is absent in Shannon's model [5]. It is also absent in works of other authors (including the review by Baan and Delogne [1]) who, following the Shannon's example, disregard environmental interactions (see eg [2]). In the following sections, we revisit the issue. We will see that environmental interactions play critical role in congested environment.

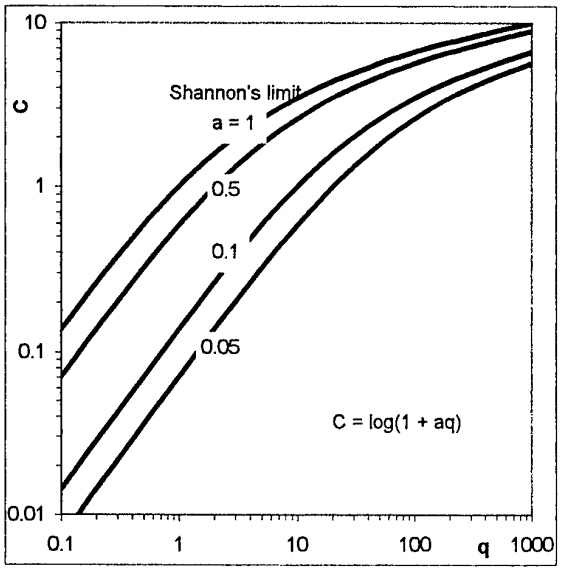



*Figure 3 Capacity of radio link (C) increases with isolation index (a) and signal-to-noise ration (q). The top line represents the Shannon's limit (1).*

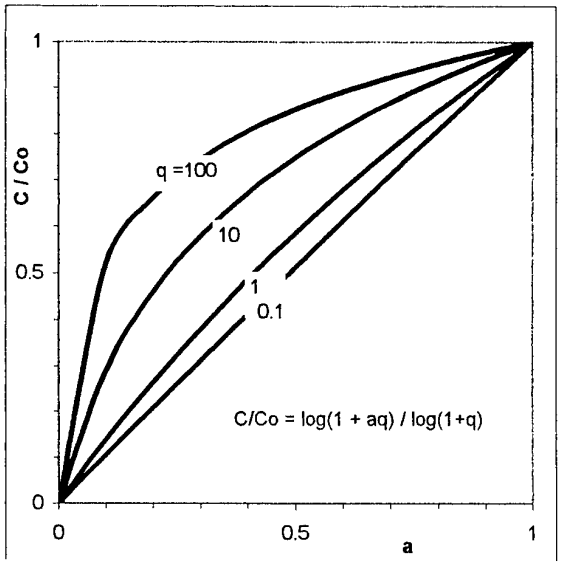



*Figure 4 Loss of radio link capacity decreases with the isolation index (a) and signal-to-noise ratio (q). Co is the Shannon's limit for isolated link.*

### *Isolation Factor*

To discuss spectrum congestion issues in an unambiguous way, we need an objective, quantitative measure. For that purpose, we propose the "*Coupling Index*" or "*Congestion Index*" (a*), and associated complementary "*Decoupling Factor*", "*Isolation Factor*", or "*Isolation Index*" (a). These are defined as the power ratio of "environmental" noise component (I), or "internal" noise component, to the total noise (N + I) at the receiver input:

$$a^* = I / (N + I) \qquad (2)$$

$$a = N / (N + I) \qquad (3)$$

The indexes are dimensionless and their numerical values are conveniently confined between one and zero. When there is no environmental noise component (I = 0), the coupling index equals zero and isolation index is one. When the environmental noise and internal noise are equal each other, the both indexes reach 1/2. Note that by definition there is always $a + a^* = 1$.

### *Correction to Shannon's Limit*

The Shannon's limit, when applied to radiocommunication links gives too optimistic estimates. For better estimation of the maximum capacity of a radio link operating in congested environment, his formula has to be modified.

As the link capacity is limited by the total noise, it is sufficient to replace the background link noise (N) in equation (1) by the total noise (N + I). After substitution, we receive corrected formula on maximum capacity of a radio link operating in congested environment:

$$C = \log_2[1 + S / (N + I)] = \log_2(1 + aq) \qquad (4)$$

In contrast to the original Shannon's formula (that involves only one variable), the equation above introduces additional parameter - isolation index (a). Figure 3 illustrates this relation.

### *Capacity Loss*

Equation (4) conveys a straightforward message: capacity of a radio link in congested environment is always less than it would be if the link were operating in isolation. That loss in the capacity depends on two parameters: the isolation index (a) and signal-to-noise power ratio (q) of isolated link. Could the difference be significant? Assume, for instance, a link with q = 1, as in the previous example. With a = 0.5 the link is theoretically capable to transmit $C = \log_2(1 + 0.5) = 0.58$ bit per Hertz per second. This contrasts with the potential link capacity, which is 1.7 times greater!

From equations (1) and (4) we obtain the relative link capacity ($C/C_0$)

$$C / C_0 = [\log_2(1 + aq)] / [\log_2(1 + q)] \qquad (5)$$

Figure 4 illustrates the relation.

Note that the capacity loss due to the environmental influences depends on two parameters only: a and q.

Relative Loss = $[(C_0 - C) / C_0] = = 1 - C/C_0$

Absolute Loss = $(C_0 - C) = \log_2[(1 + q) / (1 + aq)]$

## MULTIPLE-LINK INTERACTIONS

When there are many radio links (not necessarily belonging to any common network), each link can interact with all remaining links. If $I_{ij}$, denotes the noise component of *i-th* radio link due to radiation from *j-th* radio link, and K denotes the total number of links, then the noise power at *i-th* link coming from all other links is

$$I_i = \Sigma_j I_{ij}, \quad (6)$$

where i, j = 1, 2, ..., K, and $i \neq j$.
The isolation coefficient and capacity of *i-th* link are

$$a_i = 1 / [1 + I_i / N_i] \quad (7)$$

$$C_j = \log_2(1 + a_j q_j) \quad (8)$$

The total capacity of all interacting links together is simply the sum of capacities of individual links:

$$C_\Sigma = C_1 + C_2 + ... + C_K =$$

$$= \log_2\{\Pi_i(1 + a_i q_i)\}, i = 1, 2, ..., K \quad (9)$$

Note that it depends on the isolation indexes of each individual link $a_i$. As $a_i < 1$, that capacity is always smaller than the capacity of the same links operating in isolation, when $a_i = 1$:

$$C_{0\Sigma} = \log_2\{\Pi_i(1 + q_i)\}, i \backslash= 1, 2, ..., K. \quad (10),$$

The relative loss of transmission capacity due to environmental interactions equals $(1 - C_\Sigma / C_{0\Sigma})$.

### *Identical Contributions*

If all K links and their mutual interactions were identical ($a_i = a_1$, and $q_i = q_1$), then these equations simplify:

$$C_\Sigma = K \log_2(1 + a_1 q_1), \quad (11)$$

$$C_{0\Sigma} = K \log_2(1 + q_1) \quad (12)$$

$$C_\Sigma / C_{0\Sigma} = \log_2(1 + a_1 q_1) / \log_2(1 + q_1) \quad (13)$$

In this particular case, $C_\Sigma / C_{0\Sigma}$ would be the same as for any individual link, independently on the number of the links. Such a case is illustrated in Figure 4. However, in any limited set of radio links, receivers centrally located suffer more noise than those located at the perimeter, and the equation above is approximate.

### *Practical Cases*

The idealised examples discussed in the annex illustrate the dependence of the isolation index of a radio link on geometrical deployment and technical characteristics of equipment. Impact of such parameters as the number and disposition of neighbouring links, power radiated, and antenna directive patterns is analysed under simplifying assumptions.

Actually, the capacity loss depends on a number of additional variables, such as operating frequencies, signal processing gain, radio wave propagation and terrain obstacles effects, etc. In addition, spurious radio channels must be taken into account. The real-life systems may require sophisticated models, statistical approach, and simulation techniques (see eg [7]).

## CONGESTION CONSEQUENCES

A growing number of radio stations in operation increase noise component due to unwanted power penetrating from environment. This in turn deteriorates the capacity of the links involved. Consequently, a smaller volume of information can be transmitted in a given time and bandwidth, and smaller number of users can enjoy the benefits of radio. Additional bandwidth, or longer transmission time, (or both) is necessary to transmit a given amount of information. Note that increase of signal power by all radio links will not help, as signal-to-noise ratio would remain without change. All this means that additional communication means are necessary to keep the total transmission capacity at its original level. Ironically, if these additional communication means use radio waves, the spectrum congestion may not decrease!

### *Price to paid*

The congestion of the radio spectrum implies increased costs. It is evident when additional communication means have to be installed, or existing means modified. With no such changes involved, the cost increase can be evaluated basing on the capacity loss, as smaller volume of information can be transmitted in unit time, whereas the transmission costs remain unchanged. These increased costs will ultimately be transferred on the consumer shoulders, as otherwise the service providers would bankrupt. Thus, whole society will pay the price.

Moreover, there are losses that are difficult to translate into money. In some applications, the capacity loss might cause irreparable harm.

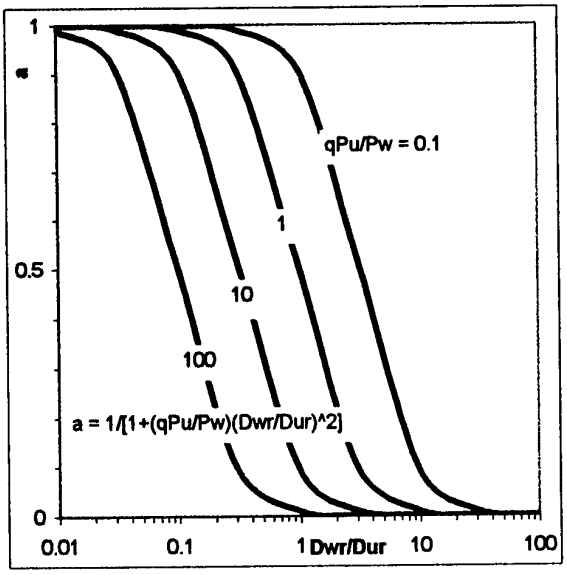



*Figure 5 Isolation index of isotropic links decreases with distance ratio ($D_{WR}/D_{UR}$) and power ratio ($qP_U/P_W$)*

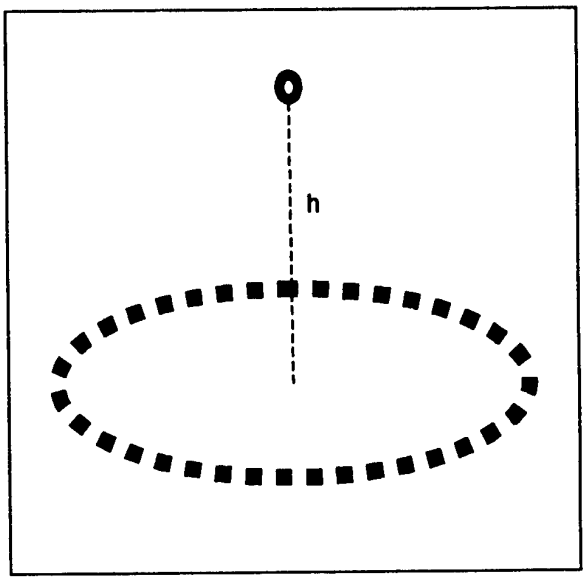



*Figure 6 Radiators create a circular ring. The victim receiver is located centrally on the disk, or at height h above it.*

We will begin with two fixed interacting radio links operating at the same time and at the same frequency in free space. Then, we will increase the number of discrete radiators. When the radiators are concentrated with great density one close to another, distributed models may be more convenient; we discuss two such models. We have to note that the ***radiators*** not necessarily must be transmitting radio stations; they may be also other radio frequency apparatuses such as microwave ovens, or other ISM equipment [12]. ISM stays for operation of equipment or appliances intended to generate and use locally radio frequency energy for industrial scientific, medical, domestic or similar purposes, excluding applications in the field of telecommunications [4].

### *Two Links, Isotropic Antennas*

With isotropic antennas, the power of wanted signal (S) at the receiver input is [2]

$$S = P_W [\lambda/(4\pi D_{WR})]^2. \quad (1)$$

Here, $\lambda$ is the wavelength, $P_W$ is power radiated by the wanted transmitter of the link, and $D_{WR}$ is the span of the link. Similarly, the environmental-noise power is

$$I = P_U [\lambda/(4\pi D_{UR})]^2. \quad (2)$$

$P_U$ is the power radiated from the unwanted radiator, and $D_{UR}$ is the distance from the victim receiver to the unwanted radiator. As the signal to noise ratio of the isolated link is q, thus its noise power is

$$N = S / q = (P_W / q) [\lambda/(4\pi D_{WR})]^2. \quad (3)$$

The isolation index of the radio link under consideration is therefore

$$a = 1 / (1 + I/N) =$$

$$= 1 / \{1 + q[(P_U / P_W) (D_{WR} / D_{UR})^2]\}, \quad (4)$$

### *Two Links, Directive Antennas*

When the links have directive antennas, the signal power and interference power are modified:

$$S = S^* (G_{RW} G_{WR}) \quad (5)$$

$$I = I^* (G_{RU} G_{UR}) \quad (6)$$

Here, S* and I* are the signal and noise with isotropic antennas. $G_{RU}$ and $G_{RW}$ are the receiving antenna gain in direction of the wanted (W) and unwanted (U) transmitters. Similarly, $G_{UR}$ and $G_{WR}$ are the transmitting antenna gain of the two links in direction of the receiver.

The isolation index of the link is now modified by the directive antenna gains

$$a = 1 / [1 + q (P_U / P_W) (D_{WR} / D_{UR})^2 \, Rat], \quad (7)$$

Rat is the ratio of the antenna gains:

$$Rat = (G_{UR} / G_{WR}) (G_{RU} / G_{RW}). \quad (8)$$

### *Multiple-Radiator Environment*

Figure 6 shows specific deployment of equipment in which the victim receiver receives identical portions of noise power ($I_1$) from each of K isotropic radiators from the neighbourhood.

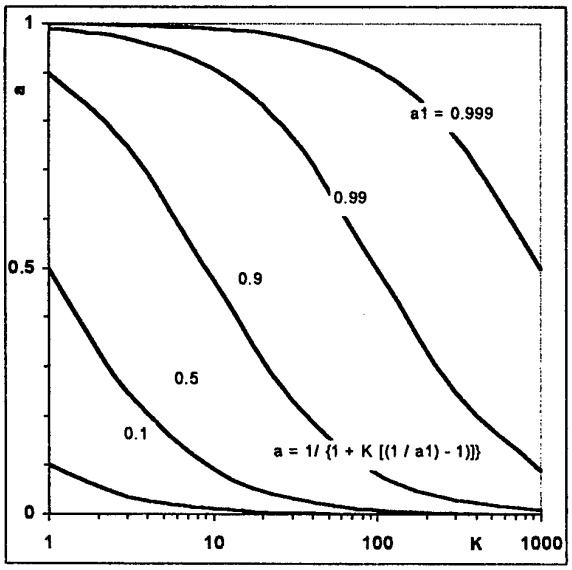



*Figure 7 Isolation index (a) of radio link decreases with the number of other links in the neighbourhood (K)*

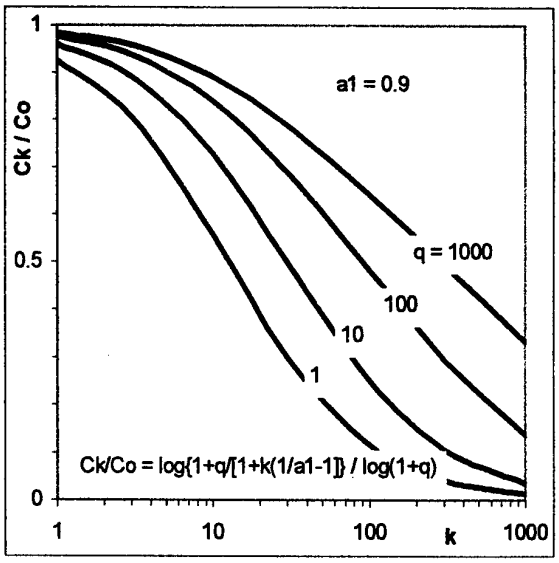



*Figure 8 Capacity of radio link Ck decreases with the number of other links (k). Co is the Shannon's capacity of isolated link.*

In such a case, the resultant environmental noise power I is K times the individual component, $I = K I_1$, and the isolation index of the victim link amounts

$$a = 1/ [1 + K I_1 / N] \quad (9)$$

Let $a = a_1$ for $K = 1$, that is $a_1 = 1 / [1 + I_1 / N]$. Then $I_1 / N = [(1 / a_1) - 1]$ and

$$a = 1/ \{1 + K [(1 / a_1) - 1)]\} \quad (10)$$

This relation is shown in Figure 7.

Therefore,

$$C = \log_2(1 + q / \{1 + K [(1 / a_1) - 1)]\}) \quad (11)$$

This relation is illustrated in Figure 8.

Note that these equations holds also when the radiators are located on a spherical surface around the victim receiver. They can also be used to more general case when the radiators are located on a number of concentric rings or concentric spheres.

### *Radiators Distributed on Line*

Figure 9 shows an example of spatial deployment of equipment, where identical isotropic radiators are distributed uniformly along a segment of straight line with the density of $k_o$ radiators per unit length. The victim receiver is located symmetrically at height h above the segment. Each emitter radiates power $p_o$. The contribution of the closest radiator to noise power at the victim receiver is

$$I_o = p_o(\lambda/4\pi h)^2. \quad (12)$$

The total length of the segment is $2R_{max}$, and there are $K = 2k_oR_{max}$ radiators on it, with the total power radiated

$$P_u = Kp_o = 2k_op_oR_{max} \quad (13)$$

If all of them were concentrated at the central point, the noise power at the victim receiver would be

$$I^* = P_u (\lambda/4\pi h)^2 \quad (14)$$

Actually, the noise contribution from distant radiators is smaller that that coming from radiators located at closer distances. Take a small line element *dr* at distance *r* from the central point. Its distance from the victim receiver is

$$d = (h^2 + r^2)^{(1/2)} \quad (15)$$

Noise power radiated by that element amounts

$$I_r = k_o\, p_o\, dr \quad (16)$$

With isotropic antennas, noise power at the receiver is

$$dI = dI_r(\lambda/4\pi d)^2 = k_op_o(\lambda/4\pi)^2[\, dr /(h^2+r^2)] \quad (17)$$

Noise received from the whole line segment is the sum, of $dI_r$ over all radiating elements, or integral

$$I = \int_{radiatinga\ \ rea} dI$$

Substituting for *dI* we receive

$$I = \frac{\lambda^2 k_0 p_0}{16\pi^2} \int_{-R\max}^{R\max} \frac{1}{\left(h^2 + r^2\right)} dr \quad (18)$$

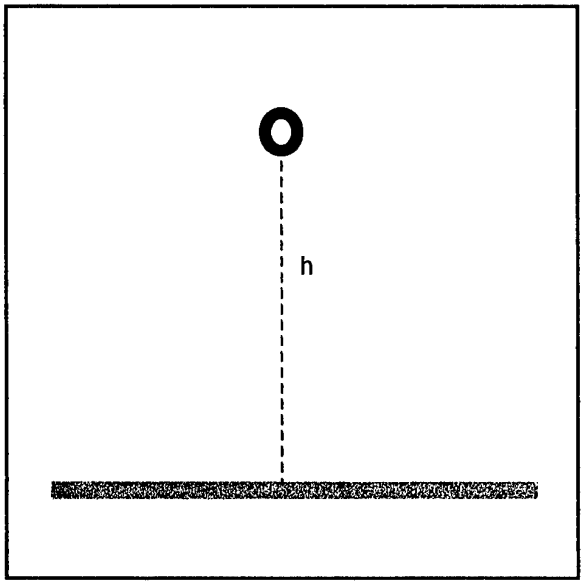



*Figure 9 Radiators are distributed uniformly on a line segment. The victim receiver is above the segment at height h.*

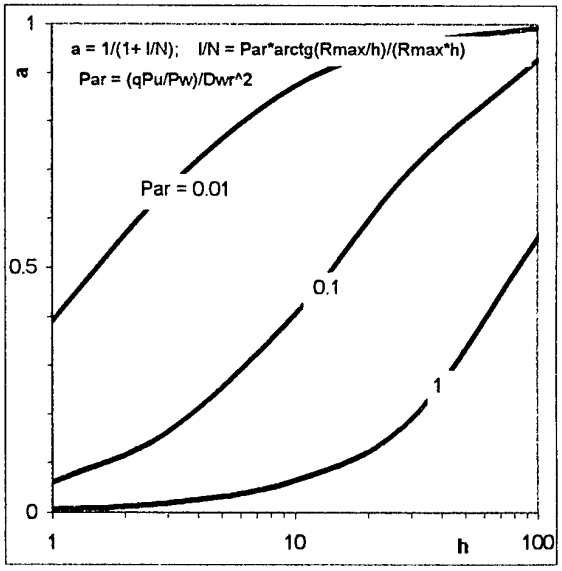



*Figure 10 Isolation index of radio link (a) increases with distance to linearly distributed radiators (h)*

The indefinite integral is

$$\int \frac{1}{\left(h^2 + r^2\right)} dr = \frac{1}{h} arctg\left(\frac{r}{h}\right) \qquad (19)$$

Substitution for the integration limits gives

$(1/h)arctg(R_{max}/h) - (1/h)arctg(-R_{max}/h) =$

$= (2/h)arctg(R_{max}/h)$ and

$$I = (\lambda/4\pi)^2 (k_o p_o/h)\, 2arctg(R_{max}/h) \qquad (20)$$

By multiplying and dividing this relation by $R_{max}$, we transform this equation to following form:

$$I = (\lambda/4\pi)^2 P_u [(1/(hR_{max})] arctg(R_{max}/h) \qquad (21)$$

At large heights,

$(R_{max}/h) << 1$, $arctg(R_{max}/h) \sim (R_{max}/h)$, and

$$I_{oo} \sim [(\lambda/4\pi)^2] P_u / h^2. \qquad (22)$$

It is as if all emitters were concentrated at the centre; noise power depends on the total power radiated and not on the radiator density. At low heights

$(R_{max}/h) >> 1$, $arctg(R_{max}/h) \sim (\pi/2)$,

and

$$I_o \sim (\lambda/4)^2 k_o p_o/\pi h \qquad (23)$$

It depends on the radiator density and does not depend on the total number of radiators. The ratio of the total power to the power from a single (closest) radiator is

$$I/I_o = 2(ko/h)\, arctg(R_{max}/h) \qquad (24)$$

As $N = (P_W/q)[\lambda/(4\pi D_{WR})]^2$, the ratio of environmental noise to internal noise is

$$I/N = (qP_u/P_W)[D_{WR}^2/(hR_{max})] arctg(R_{max}/h) \qquad (25)$$

and the isolation index of the link is $a = 1/(1 + I/N)$

Figures 10 and 11 illustrate the case.

### *Radiators Distributed on Disk*

Figure 12 shows another example of spatial deployment of equipment. Here, identical isotropic radiators are distributed uniformly on a plane circular disk and the victim receiver is located at height h above the disk centre. As previously, each radiator radiates power $p_o$. The total area (A) of the disk of $R_{max}$ is $A = pR_{max}^2$, and the total number of radiators is

$$K = Ak_o = k_o \pi R_{max}^2$$

and the total power radiated is

$$P_u = Kp_o = k_o p_o \pi R_{max}^2. \qquad (26)$$

If all emitters were concentrated at the disk centre, the noise power at the victim receiver would be

$$I^* = P_u (\lambda/4\pi h)^2 \qquad (27)$$

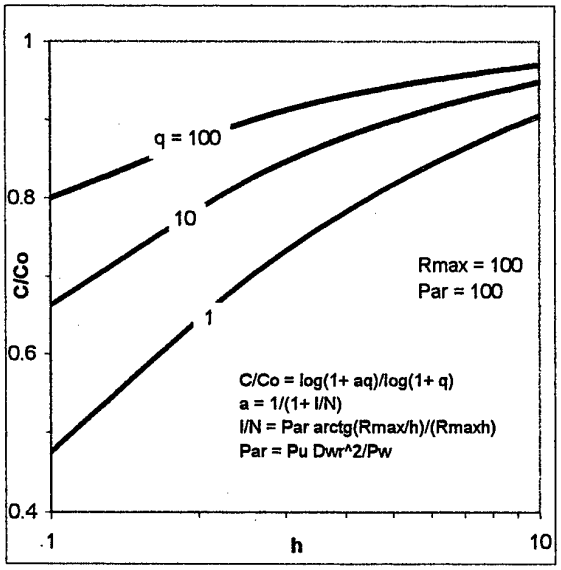



*Figure 11 Capacity loss of radio link (C) increases with distance from radiating line (h). Co is Shannon's capacity of isolated link*

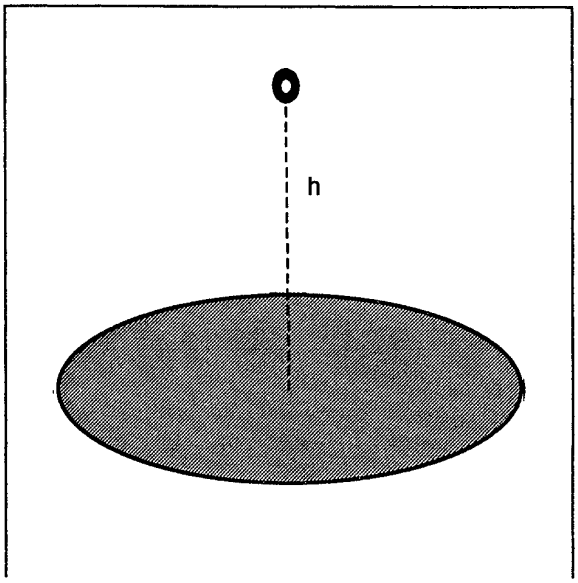



*Figure 12 Radiators are distributed on a disk. The victim receiver is located symmetrically above the disk at height h.*

Take a small element of the disk, at distance r from the disk centre. The distance (d) from the victim receiver to that element is

$$d = (h^2 + r^2)^{(1/2)} \quad (28)$$

In polar coordinates (r, φ), the elementary surface is dS = r dr dφ. Noise power radiated from it amounts

$$I_r = k_o\, p_o\, dS = k_o\, p_o\, r\, dr\, d\varphi \quad (29)$$

With isotropic antennas, noise power received from dS is

$$dI = dI_r(\lambda/4\pi d)^2 \quad (30)$$

After substitution for $dI_r$ there is

$$dI = k_o p_o(\lambda/4\pi)^2[r\, dr\, d\varphi /(h^2+r^2)] \quad (31)$$

Power received from the whole disk is sum, or surface integral, of dI:

$$I = \iint_{\substack{radiating \\ area}} dI$$

Substituting for dI we receive

$$I = \frac{\lambda^2 k_0 p_0}{16\pi^2} \int_0^{2\pi}\left[\int_0^{R\max} \frac{r}{\left(h^2+r^2\right)} dr\right] d\varphi \quad (32)$$

The first integral (within the square brackets) is

$$\int \frac{r}{\left(h^2+r^2\right)} dr = \frac{1}{2}\log_e\left(h^2+r^2\right) \quad (33)$$

Substitution for the integration limits gives

$(1/2)\,[\log_e (h^2 + R_{max}^2) - \log_e (h^2)] =$

$= (1/2)\log_e [1 + (R_{max}/h)^2]$.

In the second integral (involving φ), the function to be integrated does not depend on φ, and the integration results in multiplication by 2π. Finally,

$$I = (\lambda/4\pi)^2]\, k_o p_o(2\pi)\,(1/2)\log_e[1 + (R_{max}/h)^2] \quad (34)$$

At large heights above the disk,

$(R_{max}/h)^2 << 1$, $\log_e[1 + (R_{max}/h)^2] \sim (R_{max}/h)^2$ and

$I \sim (\lambda/4\pi)^2\pi k_o p_o (R_{max}/h)^2 = P_u\,(\lambda/4\pi h)^2$, as

$$P_u = k_o p_o \pi R_{max}^2 \quad (35)$$

At large heights, noise depends on the total power radiated, as if all emitters were concentrated at the disk centre. At low heights when $(R_{max}/h)^2 >> 1$,

$$I \sim [\lambda^2/(8\pi)]\, k_o\, p_o \log_e(R_{max}/h). \quad (36)$$

It means that at low heights, the total noise is proportional to the radiator density ($k_o$) and to power radiated by individual radiator ($p_o$), and does not depend on the total number of radiators.

As $N = (P_W / q)\,[\lambda/(4\pi D_{WR})]^2$, the ratio of environmental noise to internal noise is

$$I/N = q(D_{WR}/R_{max})^2(P_U/P_W)\log_e[1+(R_{max}/h)^2] \quad (37)$$

The isolation index of the link is a = 1 / (1 + I/N). Figure 13 illustrates the case.

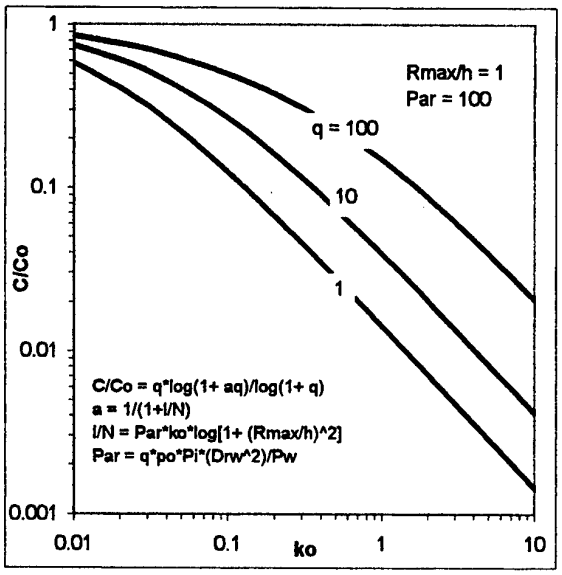



*Figure 13 Capacity of radio link (C) decreases with radiator density (ko). Co is the Shannon's capacity of isolated link*

## REFERENCES


[1]. Delogne P, Baan W: *Spectrum Congestion*; in Stuchly M A (ed.), *Modern Radio Science 1999*, Oxford University Press 1999, p. 309-327

[2]. Hall M, Barclay L, Hewitt M: *Propagation of Radiowaves*; The Institution of Electrical Engineers 1996, ISBN 0-85296-819-1

[3]. Pierce J R: *An Introduction to Information Theory*; Dover Publications 1998, ISBN 0-486-24061-4

*[4]. Radio Regulations*; International Telecommunication Union, Geneva 1998

[5]. Rimoldi B: *The Mobile Radio Interface*; Presentation at Journee de la Recherche EPFL 1999

[6]. Shannon C: *Communication in the Presence of Noise*; Proceedings of the IRE, January 1949, p. 10-21

[7]. Struzak R and Kirby R: *On Radio Spectrum Competition and Collaboration*; XXII General Assembly of the International Union of Radio Science, Tel Aviv, Israel, August 24 - September 2, 1987, Joint Session of Commissions C, E, F, J on Spectrum Management and Frequency Allocation

[8] Struzak R: *Simulation Model for Evaluating Interference Threat to Radiocommunication Systems*; Telecommunication Journal (ITU), Vol. 57 -XII/1990, p. 827 - 838

[9]. Struzak R: *Spectrum Congestion - a Voice in Discussion*; the Radio Science Bulletin No. 291, December 1999, p. 6-7

[10]. Struzak R: *Spectrum Management: Key Issues*, Pacific Telecommunications Review, Vol. 18, No. 1, September 1996, p. 2 - 11.

[11]. Struzak R: *Terrestrial Electromagnetic Environment*, in Rotkiewicz W (ed.): Electromagnetic Compatibility in Radio Engineering, Elsevier 1982, ISBN 0-444-99722-9, p. 3 - 56

[12]. Struzak R: *Vestigial Radiation from Industrial, Scientific, and Medical Radio-Frequency Equipment*; in Kikuchi H (ed.) *Nonlinear and Environmental Electromagnetics*, Elsevier 1985, ISBN 0-444-52571-3, p. 223 - 252

[13]. Struzak R: *Frequency Reuse and Power Control in Wireless Networks*; in Global Communications, 1999 (New Orleans)

[14] Varakin L (ed.): Telecommunications in Russia in the XXI Century; International Telecommunication Academy, 1999


*Ryszard STRUZAK is Co-Chairman, URSI WG on Spectrum Management/ Utilization and Wireless Telecommunications, Member, ITU Radio Regulations Board, and Co-founder of International Wroclaw Symposium on EMC.*



*During his academic carrier, he obtained his EE, MSc, PhD and DSc degrees and the title of Full University Professor. In recognition of his professional achievements, he was elected to leadership positions in national and international organizations and received numerous awards and decorations, including two international awards and the ITU Silver Medal. He was also elected to the grade of IEEE Fellow and Academician of International Telecommunication Academy, and was invited to lecture at all continents, except Australia.*

*Prof. Struzak has over thirty years of professional experience. His activities have been related mostly to strategic issues of development of radiocommunications on a national and international scale, and associated engineering, standardisation, and regulatory problems. As the head of national EMC laboratories, and professor at technical university for many years, and later as high ITU official for over ten years, he advised governmental agencies and private-sector entities in a number of countries. He participated in World Radiocommunication Conferences Geneva 1995 and Istanbul 2000 in advisory capacity. He continues as independent consultant.*

EMC 2000 INTERNATIONAL WROCŁAW SYMPOSIUM ON ELECTROMAGNETIC COMPATIBILITY

# EM PHENOMENA AND IMPLICATIONS FOR STANDARDISATION EMC – SAFETY – HUMAN EXPOSURE

G.Goldberg
Past Chairman IEC ACEC (Advisory Committee on Electromagnetic Compatibility)
Wannerstr. 43/61 8045 Switzerland Fax: +41 1 463 63 32 e-mail: gegegezurich@swissonline.ch

## ABSTRACT

*Caused by the tremendous development of the use of electric power, of electronic equipment and of telecommunication applications, we are now completely immersed in a wide and complex electromagnetic (EM) environment. This EM environment can affect all aspects of our life and one of the ways for mastering the situation is to develop appropriate regulations: standards, recommendations, guidelines, (...A great technical activity takes place presently in numerous technical organisations and in relevant regulatory authorities (National Authorities, EU commission, etc...). Aim of this paper is to give an overview on this activity. At a first stage it will characterise the EM environment and then look at three related domains of interest – or of concern: Electromagnetic Compatibility, Human Exposure to Electromagnetic Fields, Safety. Some general conclusions will be drown regarding the future standardisation work.*

The electromagnetic (EM) environment influences nowadays all aspects of our life: the equipment we use possibly our health, possibly our safety and a need arises to control it by regulations. The paper aims at giving an overview on the technical standardisation work involving Electromagnetic Fields: Electromagnetic Compatibility (EMC), Health effects of the fields (EMF), and Safety effects. To give a complete information in the limited framework of this report is not possible. The paper will deal only with the organisation of the work and the general rules, not with specific standards. It will refer mainly to the activity in IEC which is now the most important world wide electrotechnical standardisation body, to CENELEC which is of great importance for European countries (and the ones who want to deal with them), and more briefly to other organisations.

A further aim is to allow a reciprocal information of the three groups of experts that they know what happens in the other related domains.

## 1. The Electromagnetic Environment

Dealing with regulations concerning EM phenomena requires first a thorough knowledge of the EM environment. Since ever we are living in the earth magnetic field but with the development of the use of electricity, first for power applications, then for radiobroadcast, later for electronic industrial and domestic equipment, more recently for new telecommunication means, for medical applications, we are now embedded in an increasing and complex EM environment.

Regulations have to be established:
- for normal operational conditions: frequency, voltage, current,...
- against negative effects of disturbances.

IEC TC 77 has established for the EMC work a classification of the EM disturbances, which is largely applied and can be useful for other domains. It is based on the following features:
- two frequency domains: low frequency (LF) disturbances or high frequency (HF) disturbances whereby the boundary has been set conventionally at 9 kHz,
- line conducted disturbances or radiated disturbances,
- continuous disturbances or transient disturbances.

Not all the disturbances have the same weight and the ones listed below appear to be the most important (in brackets it has been indicated for which domain they are mostly to be considered). All these disturbance phenomena are relevant with regard to EMC and most of them with regard to Safety. However regarding EMF only the radiated phenomena are concerned, this as well under normal operational conditions as in the case of disturbances.

Some IEC publications (or from other organisations) specify standardised operational values. The TC 77 documents of the series IEC 61000 – x – y

or others give a comprehensive information about the actual operational levels or of the disturbance levels to consider:

LF conducted phenomena

- Harmonics of the mains voltage (EMC),
- Voltage dips and short interruptions (EMC; Safety),
- Voltage fluctuations (EMC).

LF radiated phenomena

- Power frequency magnetic fields (EMC; EMF; Safety),

HF conducted phenomena

- induced HF voltages or currents, continuous waves (EMC, Safety),
- induced HF voltages or currents, modulated waves (EMC, Safety),
- "slow"(μs) transients voltages- surges or damped oscillations (EMC, Safety),
- "fast" (ns) transients bursts (EMC, Safety).

HF radiated phenomena

- electromagnetic fields (EMC, EMF, Safety),
- continuous waves,
- modulated waves,
- transients.

Electrostatic discharges (EMC, Safety)

High power electromagnetic pulses, conducted or radiated (EMC; EMF; Safety)

## 2. Electromagnetic Compatibility

2.1. Electromagnetic Compatibility is defined "as the ability of an equipment or a system to function satisfactorily in its electromagnetic environment without introducing intolerable electromagnetic disturbances to anything in that environment" [IEV 161-01-02]

Four important features should be noted:

- EMC concerns only equipment (objects, not living beings),
- EMC concerns the correct functioning of these objects,
- EMC concerns as well immunity as emission aspects,
- EMC concerns only EM disturbances (not normal operation).

2.2. EMC concerns disturbance phenomena, and does not deal with normal operational values (or only when they exceed acceptable limits). In course of time several rules have been established for EMC regulations regarding EM disturbances:

IEC has issued a Guide 107 "Guide for the drafting of EMC publications", the rules of which are in principle also applied by CENELEC and many countries [1] [2]. The guide defines practically two main kinds of EMC publications (standards or technical specifications):

- "Basic EMC publications" which specify the fundamental and general rules for the achievement of EMC. They concern for example Terminology, Characterisation of the environment, Instrumentation, Procedures, this as well for Emission as for Immunity matters (requirements and tests).
- "Product EMC publications" which specify the requirements and test procedures relevant to a specific product to achieve EMC. Practically Guide 107 defines three categories of product standards: "Product Families Standards" (groups of similar products)," Product Standards" (for particular products), and "Generic Standards".
- The latter are general "default" product standards to be applied for product families or particular products for which no specific standard exists. They are related to particular environments, for the time being to domestic and industrial environments and are very useful to bridge the time until a specific standard is developed (or to be applied definitely for a particular product).

All product committees should consider immunity requirements and the limitation of emissions:

- particularly important is the rule that emission limits are set for all kinds of emissions by two responsible committees: TC 77 for LF phenomena and CISPR for HF phenomena and that in order to assure an overall co-ordination these limits should not be exceeded by individual sources( or in special cases only after consultation of these two committees),
- with regard immunity the product committees should follow the recommendations of the basic standards but a certain flexibility is allowed. A rising scale of compliance criteria has been established:
  a. normal performance within limits specified by the manufacturer,
  b. temporary loss of function or degradation of performance which ceases after the disturbance ceases,
  c. temporary loss of function or degradation of performance, the correction of which requires operator intervention or system reset,
  d. loss of function or degradation of performance which is not recoverable.

The compliance criterion for EMC is that the equipment after a disturbance or a test continues to operate as intended.

2.3. IEC has set up an efficient organisation to develop EMC standards (although somewhat influenced by history). The standardisation work started 1924 in CISPR for the protection of the radio transmission and was followed in IEC by the setting up of TC 77 in 1970 for Electromagnetic Compatibility in general.

TC 77- "Electromagnetic Compatibility" – has a quite large scope: it is responsible for a number of the general matters i.e. the basic standards related to LF emissions, measurement techniques, immunity testing, etc, and for the Generic Immunity Standards.

CISPR – "Comité International Special des Perturbations Radioélectriques" – is also responsible for some HF basic standards, for HF emission limits, for Information Technology Equipment and for the Generic Emission standards.

There is to note that these two committees are not directly in charge of safety or EMF matters

PRODUCT COMMITTEES, e.g. for domestic equipment, for high voltage equipment, etc, are directly responsible for the EMC problems of their products (in particular mitigation measures)

The work between these committees is co-ordinated by ACEC – Advisory Committee on Electromagnetic Compatibility – which ensure also the co-ordination with outside organisations like ISO, ITU, etc....

Further in more than 50 countries there exist National Committees of IEC which implement the IEC EMC standards in their countries.

Other international organisations deal also with EMC standards for products in specific areas e.g. ISO for automotive vehicles or ITU for Telecommunication matters.

An important factor with regard to the EMC standards of IEC is that their application is in principle voluntary. Their application becomes mandatory in a country if the responsible regulatory authorities decide this. They may also be specified in commercial contracts.

2.4. The situation is quite different in the European Union and in CENELEC. The Commission of the EU has recognised already several years ago the importance of EMC and has issued an EMC Directive 89/336/EEC "Council Directive of May 1989 on the Application of the Laws of the Member States Relating to Electromagnetic Compatibility" according to which, in principle, all the products put on the market must comply. For products the application of the relevant standards is therefore mandatory [5] [6].

The development of the standards for the implementation of the directive has been allocated to CENELEC and ETSI. For this task CENELEC has set up a committee TC210 /SC210A which covers more or less the responsibilities of IEC TC/77and CISPR. According to an IEC/CENELEC agreement, practically TC210 takes over most of the standards developed by IEC – sometimes with some amendments – so that a good co-ordination worldwide and Europe-wide is ensured for the profit of industry and the users.

2.5. With regard to the present state of the standardisation work, it can be said that practically all-important Basic Standards exist already and are now or will be updated. The most important Generic Standards for the Domestic and Industrial environments are also available. An important work remains to be done for the product standards.

The Chairman of ACEC has identified some important features and subjects for the future work [3]:
- the increase of the frequency range to consider, up in the GHz range,
- the immunity testing of large systems,
- the addition of microprocessor in numerous devices and an increase of their sensitivity,
- mobile communication (cellphone, bluetooth technology),
- power quality.

It has been criticised that too many EMC Standards have been developed and therefore that there application would put a great charge on industry. It shall be remembered that the application of the IEC standards is voluntary and that they become mandatory only when a responsible authority decides this. This complains has been raised in particular in CENELEC and special SLIM group ("Simpler Legislation for the Single Market") is studying how to simplify the requirements.

## 3. EMF – Exposure to Electromagnetic Fields

3.1. The effects of EM Fields on health are a quite old concern of the general public or workers. A considerable medical/biological research work has been and is still carried out in relevant institutions: Universities, Laboratories, etc. However the present stage of knowledge is such that if there is a very wide amount of results on specific partial subjects, there is still an insufficient overall view on certain

general subjects In particular, adverse effects on humans seems well established for short term exposure and immediate health consequences but long term effects have not yet been scientifically clearly established.

EMF deals with radiated phenomena but there is a difference with EMC:
- EMF is concerned by long time exposure,
- EMF is mostly concerned by normal operational conditions – e.g. magnetic fields from power lines – not by transient phenomena.

From the viewpoint of standardisation, there is to differentiate between two kinds of regulations (people working in this field prefer the term "standard" so that we shall use it also in the following, even if a document does not correspond to its formal definition):
- biological /medical regulations (they concern mainly exposure limits),
- technical standards .They concern mainly:
  - description of the environment (which fields frequency, magnitude,...),
  - measurement instrumentation,
  - measurement procedures,
  - calculation methods.

For scientific work no standardisation is envisaged, although common rules for epidemiological investigations would be appropriate in order to get comparable results.

3.2. The frame work for technical EMF standards is given:
- on one hand by the characteristics of the fields: frequency range, biological effects, effects on health,
- on the other hand by the kinds of the field sources.

A short overview:
- it is appropriate, depending on the health effects, to consider two – sometimes three - frequency ranges:
  - a low frequency (LF) range – apart from 0 Hz static fields – from 0 Hz to 3...10 kHz,
  - an intermediate frequency (MF) range from 3..10 kHz to 1..10 MHz,
  - a high frequency range (HF) from 1..10 MHz to the GHz range e.g. 300 GHz,
- the biological effects are caused In general by the current induced by the fields flowing in the body tissues:
  - low frequencies cause "non-thermal" effects like the stimulation of nerves and muscles, an effect on the hormonal production, an influence on the eyes, ....In particular LF field are suspected to initiate or to promote cancer,
  - high frequency fields are at the origin of thermal effects i.e. the heating of the tissues, which shall not exceed 1 C.

An important feature to consider is that it is not possible to measure directly the currents and the effects induced by the EM fields inside the body (at least in humans beings). For this reason, two different values are defined:
- "Basic Restrictions": exposure restrictions directly based on established health effects inside or at the surface of the body – as said often not directly accessible,
- "Reference levels": external field values, which actually induce the effects in the body and can be used for practical assessment purposes. They are derived from the Basic Restrictions by measurement or calculation techniques, or by biological investigations.

Basic Restriction would be the subject of "Biological Standards"; Reference levels the subject of "Technical standards".

Which are the sources of EM fields against which precaution may have to be taken:
- in the LF range in particular power lines, domestic devices, industrial installations,...
- in the HF range cellular phone – mobile devices and base stations-, broadcast transmitters, industrial installations, etc,...

A main subject of the technical standardisation is the measurement of the field distribution and field magnitude around these sources. Another important subject concerns calculation methods.

Compliance criteria is that the exposure criteria: field magnitudes, energy absorption (SAR) are not exceeded.

3.3. Which are the organisations involved in the development of EMF standards?

3.3.1. Organisations dealing with Biological Standards:

Three international organisations need to be mentioned:
- WHO, the " World Health Organisation", which has a scientific orientation and has started in 1996 an "International EMF Project". Aim of this Project is "to assess the scientific literature and reports on health effects, promote research in this field and provide a co-ordinated international response to concerns about possible heath effects of exposure to EMF". Actually WHO does not have a real standardisation task and will issue recommendations,
- ICNIRP, the "International Commission on Non-Ionizing Radiation Protection" issues Guide-

lines specifying recommended exposure limits, the application of which is in principle voluntary but which serve as world-wide reference, in particular for national regulations [8],
- IEEE has also issued several standards dealing with the limitation of exposure.

There exist of course in numerous countries national regulations issued by National Authorities (as for the EU see below) [9].
It shall be pointed out that IEC decided not to deal with Exposure limits.

3.3.2. International organisations dealing with "Technical Standards":

It does not exist yet "world-wide standards" but work is in progress or has just started:
- IEC started first with the measurement techniques for LF and HF Fields. In order to progress, ACEC established 1997 a Task Force which developed a comprehensive programme of work (see below) and by the end of 1999 a new Technical Committee TC106 has been set up to deal at large with the technical problems related to human exposure.
- IEEE has also issued several standards dealing with the measurement techniques.
- of course there exist national standards in several countries.

3.3.3. Like for EMC, it is for Europeans useful to be aware of the situation in the EU and CENELEC.

The Commission of the EU, after previous attempts, issued 1999 a "Council Recommendation of 12 July 1999 on the limitation of exposure of the general public to electromagnetic fields (0 Hz to 100GHz) – 1999/519/EC)". It specifies common definitions and exposure limits (basic restrictions, reference levels, SAR). There is to note that this document is not a directive whose application is mandatory but only a recommendation.

The implementation work has been allocated first to CENELEC .The tasks are defined by means of Mandates and carried out in a TC211 set up in 1992. TC211 had initially the task to define exposure limits, a task now superseded by the Council Recommendation, It shall deal in future with the field sources and will have a programme of work similar to the one of IEC (see below chapter 3.4) Implementation work is also allocated to ETSI for Telecommunication devices (however the problems on cellular phones remains with CENELEC). Some Directorates have also set up own "standardisation" bodies like Dir. V (COST) or Dir. XIII (CEPHOS).

3.4. The programme of work prepared by the ACEC TF EMF distinguishes between two types of standards with a structure somewhat similar to the EMC publications:
- Horizontal Standards related to general matters:
  - Measurement of LF fields with regard to Human Exposure,
  - Measurement of HF fields with regard to Human Exposure,
  - Calculation methods for induced currents.
- Vertical Standards related to specific sources of LF or HF fields:
  - LF fields from Power and Railways lines,
  - HV substations and MV/LV transformer stations,
  - Industrial equipment,
  - Handhold mobile telephones,
  - Base stations,
  - Household equipment,
  - Railways exposure of the workers,
  - Antitheft devices.

CENELEC TC 211 has a similar programme of work and a close co-ordination would be appropriate in order to have same standards World-wide and Europe-wide.

IEEE has developed mainly "horizontal" standards but collaboration of the IEC US National Committee in TC106 is expected.

## 4. Functional Safety

4.1. The "standardised" safety definitions may not be familiar to EMC or EMF experts so that they are reminded in the following list [ISO/IEC Guide51. 1990]:
- safety: freedom from unacceptable risk of harm,
- harm: physical injury and/or damage to health or property,
- hazard: a potential source of harm,
- risk: the probable rate of occurrence of a hazard and the degree of severity of the harm,
- functional safety: freedom from an unacceptable risk of harm due to the malfunctioning of an equipment or system including that resulting from reasonably foreseeable misuse.

"Safety" in a comprehensive understanding of the matter encompasses all kinds of hazards: electric shock, excessive temperature, mechanical stress, access to moving parts, etc, EM effects are only one of these factors. From a general viewpoint the

term " safety" concerns the two – fully different – aspects described in the previous chapters:
- the effects of EM Fields on health, a subject which is not the main subject of this paper,
- the effects of EM phenomena on Functional Safety which are somewhat related to EMC and will be examined in this chapter.

4.2. Which are the EM phenomena that can create a safety risk? In fact all the phenomena mentioned in the description of the EM environment in chapter 2 – also some other ones less important – if they reach an unacceptable level. The same faults may be considered than for EMC but from the viewpoint if they create a risk of harm e.g.:
- loss of function or degradation of performance, even if recoverable by operator intervention,
- damage to hardware or to software or loss of data.

Malfunctions involving safety risks shall be carefully evaluated:
- no operation when operation is required,
- unwanted operation when no operation is required,
- deviation from normal operation.

The equipment may be normally submitted to the same tests than for EMC but with higher test levels.

Compliance criterion is that no risk of harm to health or damage to property happens (sometimes it may be difficult to differentiate EMC compliance and safety assurance).

4.3.1. IEC has recognised years ago the importance of safety standards and has set up an "Advisory Committee on Safety" ACOS similar to ACEC to co-ordinate the work between the IEC committees and with t outside organisations. ACOS has published a Guide 104: "Guide to the drafting of safety standards and the role of Committees with safety functions". This Guide defines three types of safety standards: "Basic safety standards"," Group safety standards", "Product safety standards, ...a structure similar to the structure of the EMC standards.

With regard to the EM phenomena, the work is carried out in TC 77. IEC TC 77 has in course of completion a Technical Specification IEC 61000-1-2 "Methodology for the achievement of functional safety of electrical and electronic equipment with regard to electromagnetic phenomena". The document refers also to the general framework for safety considerations developed by SC 65A in the generic standards IEC 61508 – x – y. The proposed analysis method is based on a classical dependability method described in standard IEC 61025: "Fault tree analysis" which allows, starting from an unwanted event, to analyse step by step the sensibility to EM phenomena of the equipment. It recommends also testing the devices with higher test levels than for EMC purposes. This methodology applies as well to single apparatuses as to complex systems, to LF and to HF phenomena, mainly to immunity aspects but also to the limitation of emissions.

In the general framework of ACOS ca 30 committees deal directly or indirectly with safety matters and have developed ca 60 relevant standards. Most of them did not look yet at the effects of EM phenomena but the situation should change due to the importance the subject gains now.

4.3.2. In the EU several EC Directives such as the Low Voltage Directive refers also to Safety matters and CENELEC has – only recently – set up a special working group CLC/BTWG 99-2 "Functional Safety" to deal in a comprehensive manner with the problem. The WG has issued a report CLC/BT (Bxl/SG) 1053.Dec 1999 from which we draw some important conclusions:
- CENELEC should base / refer (?) to the work in IEC and adopt its standards,
- IEC 61508 (see above) should be considered as a basic generic standard.
- with regard to the effects of EM phenomena Publication IEC 6100-1-2 (see above) may be considered as very important.
- There is further to note that also ETSI has set up a n own TC Safety which should deal mainly with radiated phenomena, particularly with health effects.

On the activity on Functional Safety in other bodies (Regulatory Authorities, Technical Committees) specifically with regard to EM effects, no information seems available.

4.4. Future work in this field: implementation of the recently developed rules, implementation in product standards.

## 5. Summary and Conclusions

5.1. The EM environment in which we live may be considered from two viewpoints:
- normal operation of the networks and normal EM environment (frequency, voltage, current),
- electromagnetic disturbances (conducted, radiated, low frequency, high frequency),

They can have different kinds of effects:
- EMC Electromagnetic Compatibility effects,
- EMF Biological and Health effects,
- (Functional) Safety effects.

These three aspects have common sources and therefore they have some relationship which, even if their effects are different, may be considered in the standardisation work.

5.2. EMC is related to the behaviour of electrical or electronic equipment with regard to EM disturbances:
- it concerns equipment: apparatus and systems,
- it is particularly relevant when the EM disturbances take unacceptable high values,
- it concerns emission and immunity features,
- compliance criterion for EMC is that the equipment continues to operate as intended after testing or in operation.

5.3. EMF is related to biological/medical effects of EM fields:
- it concerns living beings, particularly Human Beings,
- it considers mostly the normal state of the EM environment, less EM disturbances,
- two kinds of standards should be considered:
  - biological/medical standards (e.g. exposure limits) for which relevant institutions are responsible,
  - technical standards (e.g. measurement techniques) which are in the province of technical organisations like IEC, CENELEC, IEEE.
- compliance criterion is that the recommended exposure limits are not exceeded.

5.4. Functional safety shall ensure that EM disturbances do not create a risk of harm to health or damage to property:
- in principle the equipment is submitted to the same tests than for EMC testing, however with higher test levels,
- compliance criterion is that no unacceptable risk of harm due to the malfunctioning of an equipment occurs (practically it happens that often it is difficult to make a distinction between an EMC and a Safety acceptance criterion).

5.5. From the viewpoint of standardisation it appear that three types of standards need to be developed in all three domains:
- description/specification of the environment,
- basic/horizontal standards (measurement techniques, etc, ..),
- specific product standards.

5.6. Then a question arises for the standardisation work, particularly with regard product standards: should three different standards be issued for the three domains or should all the requirements and test specifications be concentrated in one comprehensive document?

It appears that for EMC and Functional Safety, the EM phenomena to consider are the same, the test procedures are the same or very similar; only the acceptance criteria are different, more severe for Functional Safety. Further it seems advisable that product experts deal with in a comprehensive manner for their products. A common document seems to be the best solution.

However for EMF, the EM phenomena to consider are somewhat different from the ones relevant for EMC and Functional Safety – other phenomena or mostly under normal operational conditions, the experts may be different, and separate documents seem more appropriate.

However a subject is common to the three domains: the description and specification of the EM environment. Common documents would be useful.

5.7. A similar question arises for testing: should the three series of test be carried out in the same laboratory, possibly by the same experts, or should different people carry out the tests at three different places. A similar answer than for the standardisation work seems appropriate.

5.8. A short inquiry among standardisation experts showed that the opinions diverge:
- as for the development of standards, it is argued that there may be different experts for the three domains – in particular it should be considered that safety includes several other issues than EMC. This would support the view of different separate standards,
- on the other hand, for the development of the products, for the design engineer, it may be more convenient to have one comprehensive document,
- as for testing, some people argue that the task should be carried out by different specialised experts in specialised laboratories, however most of the EM tests can be carried out with the same testing equipment,
- for certification purposes, a comprehensive document may be more appropriate.

An answer may also depend on whether the three domains are treated by the same or by different committees.
A definite answer does not seem possible. A case by case issue!!

## 6. Bibliography

[1] IEC guide 107, "Electromagnetic Compatibility. Guide for the drafting of electromagnetic compatibility publications" – CEI/IEC, Geneva, 1998.

[2] IEC Brochure, "Electromagnetic Compatibility. The role and contribution of IEC standards"(with a list of the current EMC publications of IEC) - CEI/IEC, Geneva, 1997.

[3] W.A. Radasky, "Electromagnetic compatibility strategy for the future, Proceedings of the Wroclaw EMC Symposium 2000 – Wroclaw, Poland, June 2000.

[4] IEC guide 104, "Guide to the drafting of Safety Standards and the role of the committees with safety pilot functions and safety group functions" – CEI/IEC, Geneva 1980.

[5] Council of the European Communities, "Council directive of 3. May 1989 on the approximation of the laws of the Member States relating to Electromagnetic Compatibility" – Official Journal of the European Committees. L 139/19, 23.5.1989.

[6] European Parliament and Council, "Directive 1999/5/EC of March 1999 on radio equipment and telecommunications terminal equipment and the mutual recognition of their conformity" – Official Journal of the European Communities L 91/10, 07.04.1999.

[7] Council of the European Communities, "Recommendation of 12. July 1999 on the limitation of exposure of the General Public to Electromagnetic Fields (0 Hz to 300 GHz)" – Official Journal of the European Communities L.199/59-61, 30.07.1999.

[8] International Commission on Non-Ionizing Radiation Protection (ICNIRP), "Guidelines for limiting exposure to time-varying electric, magnetic and electromagnetic fields (up to 300 GHz)" – Health Physics, vol. 74, Nr.4, April 1998.

[9] G. Goldberg, "Regulations for the limitation of Human Exposure to EM-Fields – An Overview" – Proceedings of the Wroclaw EMC Symposium 2000, Wroclaw, Poland, June 2000.

***Biographical Note***

G. Goldberg graduated as Electrical Engineer at ETHZ - Federal School of Technology Zürich. He worked thereafter mainly in the field of Control Equipment for Power Systems and became there acquainted with the EMC problems. He was from 1985 to1994 Chairman of IEC TC 77 – Electromagnetic Compatibility - and from1990 to 1996 of ACEC – Advisory Committee on Electromagnetic Compatibility. He is presently still active member of ACEC where he initiated the IEC work on Human Exposure to EMF.

# II
# SECTIONAL SESSIONS

**EMC 2000** INTERNATIONAL WROCŁAW SYMPOSIUM ON ELECTROMAGNETIC COMPATIBILITY

# ICs susceptibility: a Critical Assessment of the Test Procedures

*Franco Fiori*

Dipartimento di Elettronica, Politecnico di Torino
C.so Duca degli Abruzzi 24, 10129 Torino (Italy)
ph. +390115644141, fax +390115644099, E-mail fiori@polito.it

***Abstract*** - In this paper some methods to perform integrated circuit (IC) susceptibility tests are described. The Work Bench Faraday Cage method allows the measurements of small PCBs or ICs immunity to common mode conducted RF interference, while the direct injection method makes it possible the evaluation of IC immunity to differential mode disturbance. The evaluation of ICs susceptibility to electromagnetic radiated field can be performed by the TEM cell method. Test benches related with methods summarized in this paper, were realized and used in order to verify experimentally the immunity of a micro-controller IC. In this work the different measurement procedures are compared and the test benches weak points are highlighted.

## I. INTRODUCTION

Analog and Digital integrated circuits are widely used in equipment that work in electromagnetic polluted environments as in automotive, aeronautics and industrials systems. The power supplies distribution and signal communications among electronic modules of these equipment are realized by cables that couple with environmental electromagnetic fields: cables behave as receiving antennas and collect interference that are superimposed on system signals.

In case of modules composed of a printed circuit boards (PCBs) with dimensions less then interference wavelength, it can be assumed that interference collected by a PCB traces and by integrated circuits package frames are negligible if compared with those collected by connecting cables.

Since actual electronic systems have to be compliant with normative in electric security matter, the connection of each module to ground is mandatory. For EMC purposes, the common mode impedance represents the connection between modules metal cases.

The experimental evaluation of interference induced into an electronic equipment by the coupling of a radiated electromagnetic field and an equipment shown that the amplitude of common mode interference collected by cables is higher then that of differential mode [1]. However, an IC susceptibility to conducted interference can be observed only if RF voltages are present among IC pins, while cables connected to the modules collect essentially common mode interference: the PCB translates the common mode interference in the differential mode one at the IC pins. In this work the immunity of a microcontroller IC to conducted interference has been evaluated. Measurements have been performed following three different test procedures, which are described in normative proposals and scientific paper [2][3][4]. The comparison of experimental results makes it possible to highlight some critical points of these measurement methods.

## II. MEASUREMENT METHODS

The evaluation of ICs immunity to conducted continuous wave RF interference can be performed by the measurement of interference amplitude at which DUT failures occur. Another criterion to perform ICs immunity test consists in the measurement of the frequency ranges in which DUT failures occur, if constant amplitude of the interfering signal is taken.

The last criterion comes from those usually adopted in verifying the compliance of electric and/or electronic equipment to EMC normative, while the first one makes it possible the evaluation of the DUT functional limits due to interference. In this work, the immunity measurements were performed referring to the first criterion enunciated, by using the test methods described below.

### *A. Workbench Faraday Cage Method*

The Workbench Faraday Cage (WBFC) method was proposed to perform immunity and emission tests of ICs or small electronic modules in the frequency range 150 kHz - 1GHz [1][5]. The basic concept of this method is taken from the European normative EN61000-4-6 that regards the immunity of electronic equipment to common mode conducted RF interference. The interference is coupled in the EUT via coupling de-coupling networks (CDNs) [6].

The WBFC method is based on the hypothesis that ICs are meanly reached from interference collected by cables that are directly connected to the PCB. A bundle of cables, i.e. a receiving antenna connected to the DUT, in the WBFC is replaced by the series of an interference source and a radiation resistance $R_g$=150 Ω. In actual equipment the radiation resistance depends on cables lengths and geometry but its average value is about 150 Ω with standard

deviation of 7 dB. A test board, with the DUT soldered on, is inserted into a Faraday cage.

There are some reasons to perform measurements into a Faraday cage: metal can that contains electronic modules prevents them from thermals and mechanical stress. The Faraday cage emulates a metal can and makes it possible immunity tests with interference in the DUT surrounding confined to the cage.

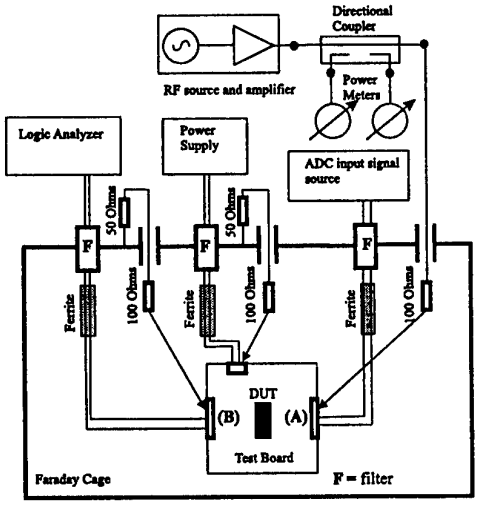



Fig. 1. The Workbench Faraday Cage

Common mode filters realize links among DUT, power supply and auxiliary instruments in the test bench. Each filter is composed of a $\pi$ cell that is inserted through a wall of the cage, in series with common mode inductance, that are realized by a couple of wires wrapped on a NiZn ferrite core ($\mu_r$>1000). The common mode resistances $R_{c1}=R_{c2}=150\ \Omega$, shown in Fig.2, represent the radiation resistances of two different bundles respectively connected to the node (A) and (B). Since bundles connected to each module come from different directions, the RF voltages induced to bundle terminals are different in amplitude.

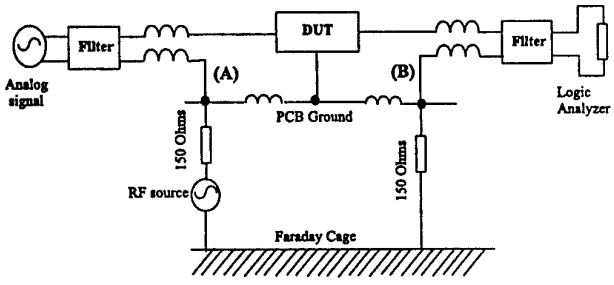



Fig. 2. Simplified circuit description of the tests bench in case of interference applied to the node (A) of common mode injection.

This is the reason to inject interference in one common mode node at time, as described in Fig.2 [5]. In this test bench, the immunity of IC to common mode conducted RF interference strongly depends from the PCB design.

Since PCB translates the injected common mode interference in voltages at the DUT pins, it is able to hide or highlight the DUT immunity to RF. Furthermore, the test setup of Fig.1 shows some weakness for interference frequencies higher then 300 MHz. In fact, the considerations in [5] are valid until the dimensions of the Faraday cage and those of objects placed into the metal cage are negligible if compared with interference wavelength $\lambda$. The Faraday cage, with dimensions *length*=0.5 m, *width*=0.35 m, *height*=0.15 m, behaves as resonant cavity at the frequencies $f_m=300*n$, $f_{rm}=430*m$ with $m,n\in$ N.

However, the WBFC method makes it possible to apply common mode interference to a PCB, that means interference to the DUT pins with spectral components superimposed on those of system signals.

### *B. Direct Injection method*

By this method the interference is directly applied between a DUT pin and the IC ground (Fig. 3). The device is soldered in a test board and a bias tee circuit gives, at the DUT pin, the interference superimposed on the system signal. The immunity of an IC evaluated by this method does not depend on the layout of PCB layers. Each pin of the DUT is characterized in terms of a receiving antenna equivalent circuit, that is composed by the series of a 50 $\Omega$ radiation resistance and a voltage source. The amplitude of this RF source is obtained by the measurement of the RF available power that induces failures in the DUT.

This method can be used successfully for narrow band interference and in case of the system signal spectral components separated from those of the disturbance. In other words, it does not allow the injection of interference on digital signals that show a wide band spectrum.

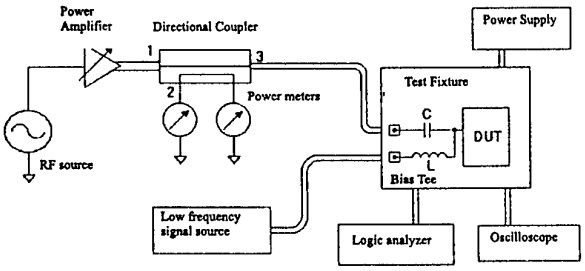



Fig.3. Test bench for direct injection.

### *C. TEM cell Method*

In previous methods CDNs superimposed interference on system signals. The TEM cell method makes it possible the evaluation of ICs immunity to radiated electromagnetic field. TEM cell characteristics and the PCB design rules are taken from the SAE 1752/3 normative that describes the test setup and procedure in the evaluation of ICs electromagnetic emission [7]. The TEM cell shows a lateral aperture with dimensions suitable for the PCB where the

DUT is inserted. The DUT is placed on the layer that works as a part of the TEM cell walls, and it is connected to the other layers by vias. The ground layer realizes a good contact to the TEM cell wall, all along the border of the aperture. In order to have the communication of the DUT with components and auxiliary instruments guaranteed, the connection cannot be filtered and the interference generated into the TEM cell will appear outside, in the TEM cell surrounding too. The immunity tests have to be performed by the test bench in Fig.4 in the frequency range 150kHz-1GHz. The amplitude of electric field is stepped till DUT failure occurs, while the interference amplitude, frequency and the DUT status are picked-up.

## III. The Device Under Test

The DUT is a microcontroller IC realized by an HCMOS process and inserted into SO28P package [8]. It is composed of a clock circuit generator, an 8 bit control unit (CPU) with a set of 63 instructions, 8kB of EPROM, 256 bytes of RAM, 22 bi-directional and multifunction Input-Output lines.

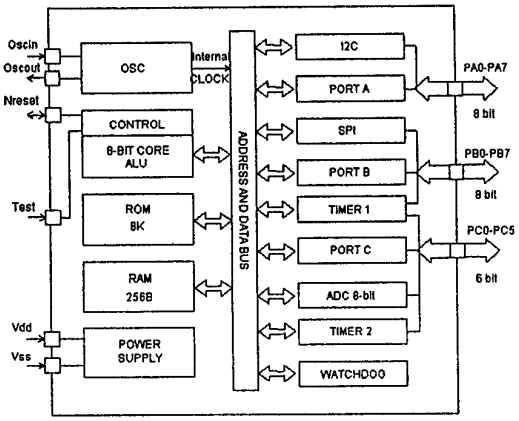



Fig.5. Microcontroller general description.

The following peripherals are also included: two independent 16 bit timers, an 8 bit Analog to Digital Converter (ADC), a watchdog circuit, an SPI interface and an I2C bus interface (see Fig.5).

### A. Test Code

A batch program composed of simple modules was charged in the EPROM of the device. The microcontroller executes each module and jump to the next one by an external interrupt signal. For instance, a program module controls the ADC conversion and gives the digital data available at one of the micro controller output ports.

## IV. Experimental Results

The microcontroller was soldered in a PCB that fits well the requirements of the three methods described in previous sections. The PCB is composed of two layers: one that works as ground plane and the other that gives connections among the DUT and the auxiliary components, required to have the DUT working.

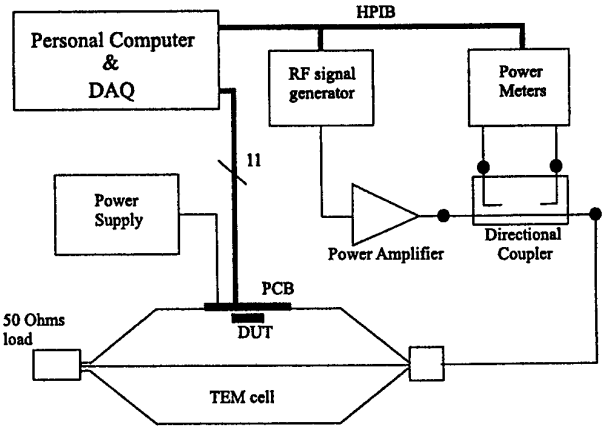



Fig. 4. Test setup of the TEM cell method.

The DUT is placed in the center of the ground plane and connected to the routing layer by vias. Its $V_{DD}$ and $V_{SS}$ pins are connected to a 5V power supply filtered in the routing layer by two capacitors of 100pF and 100nF in parallel. The immunity test was performed by the injection of RF interference, monitoring the DUT behavior when the ADC program module was running. Functional errors of the ADC were taken when data differed from what expected of 2 LSB.

### A. Measurements performed by the WBFC method

As required in the WBFC measurement procedure, two common mode injection points were identified in the test board: the node (A) close to the connector of digital interface and the node (B) near the ADC cable connector (see Fig.3).

Measurements were performed with interference applied at the node (A) and the node (B) connected to the Faraday cage by the $R_{c2}$=150 Ω. In the tests all over the frequency range of 150kHz-1GHz, neither ADC conversion errors or system failures were observed. The excellent behavior of the DUT is apparent because the test board was designed in order to avoid common mode impedance in the PCB ground layer. As a matter of fact, the method can be proposed as standard in the evaluation of IC susceptibility but it needs to be completed by detailed test board design guidelines. Otherwise, it is useful in the evaluation of small modules immunity to conducted RF interference.

### B. Measurements performed by the direct injection method

Differential mode interference was injected in microcontroller input and output pins, and experimental results show the high sensitivity of the ADC input pin and the RESET pin.

The ADC immunity was measured by the RF source available power required to induce conversion errors higher

then 2 LSB. With RF injected in the RESET pin, the available power required to put the DUT in the RESET state was measured. Figs.7, 8 show the experimental results obtained by the interference direct injection [9].

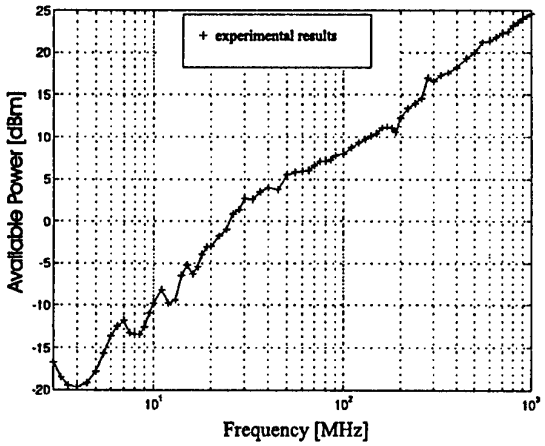



Fig.7. Microcontroller immunity in case of interference applied to the ADC input port.

### C. *Measurements performed by the TEM cell method*

The immunity tests were performed in the frequency range 10MHz-1GHz, by the evaluation of the electric field amplitude by which DUT failure occurs. The electric field amplitude, data converted and microcontroller status were picked up with 500 different interference frequencies [10].
The experiment of immunity test was performed for each program module and it was found that the microcontroller was susceptible during the analog to digital conversion. However, conversion errors were observed for electric field higher then $400 V/m$. In fact, the DUT seems robust to the radiated fields and errors appear with high intensity fields, because the antenna efficiency of the DUT package frame to the die is really poor.

## V. CONCLUSIONS

The susceptibility of a microcontroller to conducted RF interference was verified by three different test methods. Since the test board, where the DUT is soldered, was designed and realized in order to reduce the ground layer common mode impedance, the DUT did not show functional errors during the WBFC tests. This method can be proposed as standard for the immunity measurements, but it has to be completed by detailed test board design guidelines.
Measurements performed by the direct injection method shown that ADC and RESET pin are the most susceptible to differential mode interference, while investigations performed by the TEM cell method shown that high intensity of the electromagnetic field is required to observe DUT functional errors.

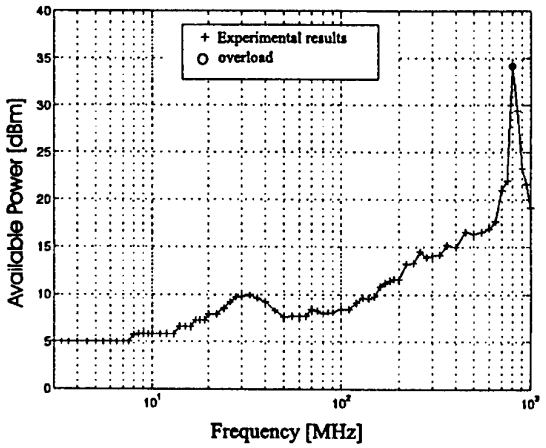



Fig.8. Microcontroller immunity in case of interference applied to the RESET pin.

## VI. REFERENCES

[1] M.J. Coenen, "Common mode impedance measurements on cables in the frequency range 30MHz-1GHz", EIE92004}, Philips Semiconductor, 1994.
[2] "Measurement of electromagnetic emission and immunity of integrated circuits in the range of 150kHz to 1GHz", IEC 47A/netherlands/NP, {\em IEC TC47A/WG2}, Sept. 1997.
[3] A. Engel, H. Astrain, J. Cagle, S. Ledford, M. Mahalingam, "A TEM cell based method for radiative susceptibility characterization of Low-Power Microcontroller", IEEE Internat. Symp. on EMC, Santa Clara (CA), August 1996, pp. 76-81.
[4] "Integrated circuit Electromagnetic Susceptibility investigation - Phase III", McDonnel Douglas Astronautics Company internal report MDC E1929, San Louis, Missouri, 1978.
[5] M.J. Coenen, "EMC workbench: testing methodology, module level testing and standardization", Philips Journal Research, 1994, Vol.48, pp. 83,116.
[6] "Immunity to conducted disturbances, induced by radio frequency fields", EN61000-4-6, Cenelec, Bruxelles (Belgium), 1996.
[7] "Electromagnetic compatibility measurement procedures for integrated circuits radiated emissions measurements procedure 150kHz to 1GHz, TEM cell", SAE 1752/3, Society of Automotive Engineers, Warrendale, PA, 1995.
[8] "ST72E25 User Manual", STMicroelectronics, Agrate Brianza (Italy), 1997.
[9] C. Esposito, L.Martino,"Confronto tra metodi di caratterizzazione di circuiti integrati e schede ai fini della compatibilita' elettromagnetica", Tesi di Laurea, Politecnico di Torino, Torino (Italy), Dic. 1998.
[10] S. Caprioli, "Gestione Automatica di un banco per misure di immunita' Irradiata", Tesi di Diploma, Politecnico di Torino, Torino (Italy), Dic. 1998.

EMC 2000 INTERNATIONAL WROCŁAW SYMPOSIUM ON ELECTROMAGNETIC COMPATIBILITY

# FAR-END CROSSTALK REDUCTION IN COUPLED MICROSTRIP LINES WITH COVERING DIELECTRIC LAYER

T.R.Gazizov*, N.A.Leontiev*, O.M.Kuznetsova-Tadjibaeva**

*Tomsk State University of Control Systems and Radioelectronics, Lenin Ave., 40, Tomsk, Russia, 634050, phone/fax:+7 3822 223262, E-mail: talgat@tu.tusur.ru, leon@tu.tusur.ru

**Research and Design Center "Polus", Kirova 2, Tomsk, Russia, 634050, phone/fax:+7 3822 557766/+7 3822 555191, E-mail: POLUS@ONLINE.TOMSK.NET

*The method of far-end crosstalk reduction in coupled microstrip lines by covering dielectric layer has been presented. Influence of all main parameters of covering layer (relative permittivity, height, length and position) on far-end crosstalk, near-end crosstalk and active line waveforms has been investigated by modeling the parameters of lines and simulation of waveforms.*

## 1. INTRODUCTION

The crosstalk reduction problem becomes one of the most important signal integrity problems being an obstruction for development of high-speed and high-density digital electronic equipment. Particularly, the problem is actual for PCBs with long interconnects in nonhomogeneous dielectric filling. In this case, the magnitude of crosstalk at the far end of passive line may be much more than at the near end, as it is shown, for example, in well known paper [1].

The far-end crosstalk may be reduced by wider separation of coupled interconnects. However, it is often impossible in case of high-density interconnects. Another way consists in placing the additional grounded traces between coupled interconnects, but it has the same drawback and as it is shown in [1], sometimes has the negative effect. In [2] a double-layered dielectric PCB with interconnects formed by suspended and inverted microstrip lines is described. A number of useful possibilities for reduction of high-speed signal distortions in high-density interconnects of the board are shown in [3] and investigated in detail in [4]. Moreover, some additional possibilities for reduction of far-end crosstalk in cascaded sections of the board's interconnects have been presented recently [5, 6]. Particularly, the property of capacitive coupling coefficient of two coupled suspended or inverted microstrip lines to be more than inductive coupling coefficient is used in these improvements properly. Unfortunately, this property is not inherent to usual microstrip lines used widely for high-speed signals' transmission in various applications.

Recently [7], a possibility of far-end crosstalk reduction in two coupled microstrip lines by covering dielectric layer has been shown. An influence of all main parameters of the covering layer (relative permittivity, height, length and position) on far-end crosstalk compensation has been investigated by modeling the parameters of lines and simulation of waveforms. The method has been found simple and low-cost, however more detailed investigation of the method is necessary for proper usage of the method in practice. Particularly, an influence of far-end crosstalk compensation on near-end crosstalk and on waveforms of signal at near and far ends of active line may be very important and will be investigated in this paper.

## 2. THE PROPOSED METHOD

We consider here a case of two coupled lines only, assuming for simplicity that the influence of other conductors is negligible. First, the main idea of the method will be described briefly. The method is very simple and consists in the following.

As shown in [8, 9], the capacitive coupling of suspended or inverted microstrip lines may be more than, less than or equal to the inductive coupling in accordance with parameters of the lines. Therefore, the far-end crosstalk being approximately proportional to the difference of capacitive and inductive couplings will have positive or negative polarity or will be canceled in accordance with parameters and type of the lines. It is well known that the capacitive coupling of usual microstrip line is always less than the inductive coupling for any parameters of the line. However, a simple addition of covering dielectric layer over the usual microstrips transforms the ones to lines similar to inverted microstrip lines (Fig.1). Therefore, some new properties absent in usual microstrip lines may appear in the covered microstrip lines and may be used in single section or cascaded sections of the coupled lines. Particularly, if the difference of capacitive and inductive couplings in one section has a sign, which is opposite to the difference of capacitive and inductive couplings in other section, the partial or complete compensation of far-end crosstalk is possible. To test this assumption the calculation of lines' parameters and simulation of waveforms would be done.

## 3. CALCULATION OF CAPACITIVE AND INDUCTIVE COUPLINGS

Per unit length matrixes of capacitive coefficients [C] and inductive coefficients [L] are calculated for two coupled microstrip lines with covering dielectric layer by program based on two-dimensional method of moments and described in [8,9]. Then, using the calculated elements of matrixes [C] and [L] a capacitive coupling ($K_C=-C_{2,1}/C_{1,1}$) and an inductive coupling ($K_L=L_{2,1}/L_{1,1}$) are obtained.

The calculated difference of capacitive and inductive couplings ($K_C-K_L$) as a function of $H_{d2}/W$ is shown in Fig.2. Note that the possibility of ($K_C-K_L$) to be equal to zero or more than zero is seen clearly for coupled microstrip lines with covering dielectric layer (while it is impossible for coupled microstrip lines without covering dielectric layer, when $H_{d2}/W=0$). Moreover, it is seen that condition $\varepsilon_{r2}>\varepsilon_{r1}$ is necessary for this phenomenon.

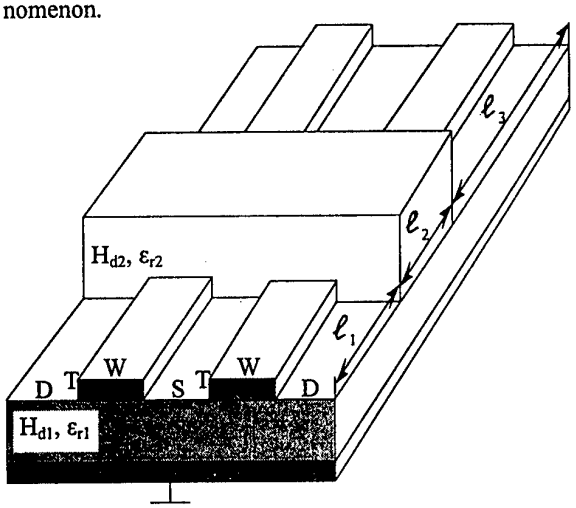



Fig.1. Two coupled microstrip lines with covering dielectric layer

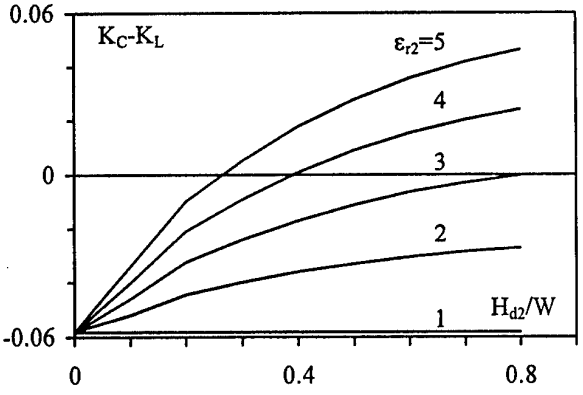



Fig.2. Dependence of difference of capacitive and inductive couplings ($K_C-K_L$) of two coupled microstrip lines with covering dielectric layer on height of the layer $H_{d2}/W$ for various relative permittivities of the layer $\varepsilon_{r2}=1...5$. $H_{d1}/W=0.5$, $\varepsilon_{r1}=3$, D/W=3, S/W=1, T/W=0.1

## 4. SIMULATION OF WAVEFORMS ON NEAR AND FAR ENDS OF ACTIVE AND PASSIVE LINES

All calculated waveforms are presented in two-column Tables 1-3. In each of the tables the active line waveforms are shown in left column and the passive line (crosstalk) waveforms are shown in right column.

First, the near-end and far-end crosstalk and active line waveforms have been calculated (assuming the lines to be without loss and without dispersion) for structure consisting of one section of two coupled microstrip lines with covering dielectric layer ($\ell_1=0$, $\ell_2=20$ cm, $\ell_3=0$). Parameters of the lines are according to Fig.2 for $\varepsilon_{r2}=5$. All terminations of lines are equal to 50 Ohms. Ramp input signal with magnitude $V_{in0}=10$ V and rise time $t_r=100$ ps is applied at beginning of active line. Three examples of all four waveforms calculated for $H_{d2}/W=0$, 0.4, 0.8 are shown in three rows of Table 1, accordingly. It is seen clearly that far-end crosstalk changes significantly when increasing the height of covering dielectric layer. Particularly, far-end crosstalk polarity may be changed and far-end crosstalk magnitude may be reduced considerably. It is seen also that for given value of $\varepsilon_{r2}$ (when $\varepsilon_{r2}>\varepsilon_{r1}$) the according value $H_{d2}$ may be chosen to minimize the far-end crosstalk. Some increasing the near-end crosstalk because of increasing the capacitive coupling are observed. Moreover, the results of mismatching are observed clearly on active line's waveforms.

For more detailed investigation of the possibility of far-end crosstalk reduction a dependence of the waveforms on the length of covering dielectric layer was considered. For this aim the two-section structure ($\ell_1=0$) consisting of a section of coupled microstrip lines with covering dielectric layer and a section of coupled microstrip lines without the layer was analyzed. Analytical formulae used for calculation of far-end crosstalk waveforms in two-section structure with capacitance at junction of the sections have been presented in [5] and are omitted here. A detailed derivation of the formulae is given in [10]. Strict accounting for the value of capacitive discontinuity at junction demands a comprehensive three-dimensional electrostatic field calculations, for example, by method of moments presented in detail in [11, 12], but it is not in scope of this paper. Nine examples of all four waveforms calculated for cases when the length of the section of lines with covering dielectric layer was increasing ($\ell_2=2,4...18$ cm), while the total length of two-section structure was constant ($\ell_2+\ell_3=20$ cm) are shown in nine rows of Table 2, accordingly. Parameters of section with covering layer are according to Fig.2 for $\varepsilon_{r2}=5$ and $H_{d2}/W=0.8$. It is seen that far-end crosstalk magnitude may be reduced in this case similarly to the previous case. However, it is achieved by means of compensation of the negative far-end crosstalk of the second section by the positive far-end crosstalk of the first section. Thus, in case of very thick covered dielectric layer the length of the layer would not be very long for complete compensation of far-end crosstalk.

Table 1. Active (left column) and passive (right column) lines' waveforms (V, ns) calculated for $H_{d2}/W=0$, 0.4, 0.8 (in rows from above down)

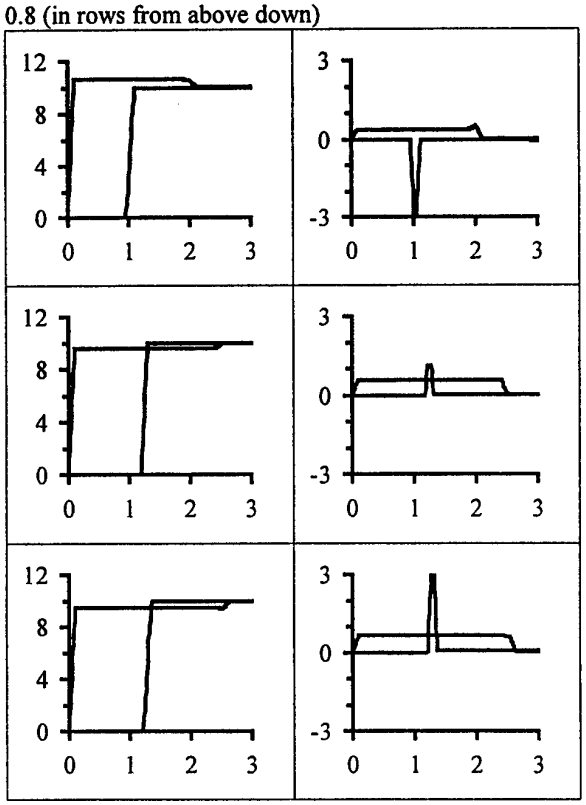


Table 2. Active (left column) and passive (right column) lines' waveforms (V, ns) calculated for increasing length ($\ell_2$=2,4...18 cm) of section with covering dielectric layer, while $\ell_1$=0 and $\ell_2+\ell_3$=20 cm. $H_{d2}/W=0.8$, $\varepsilon_{r2}=5$.

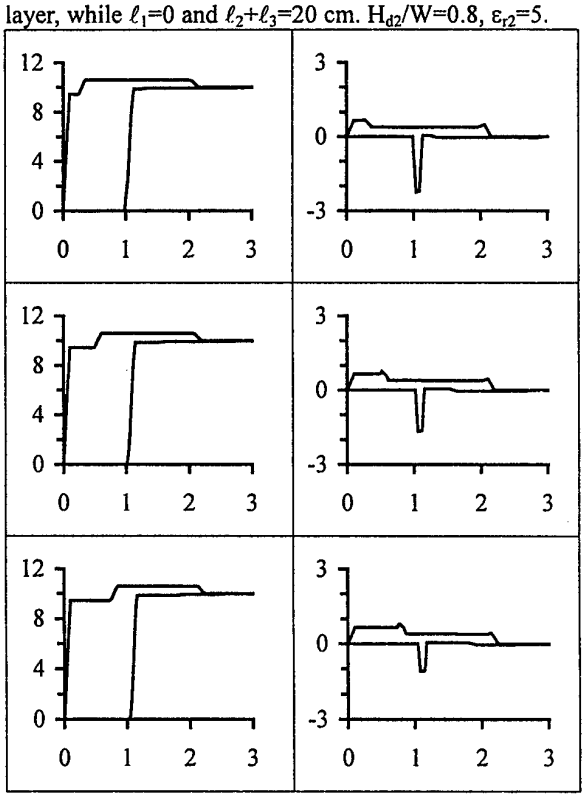


Table 2 (continued)

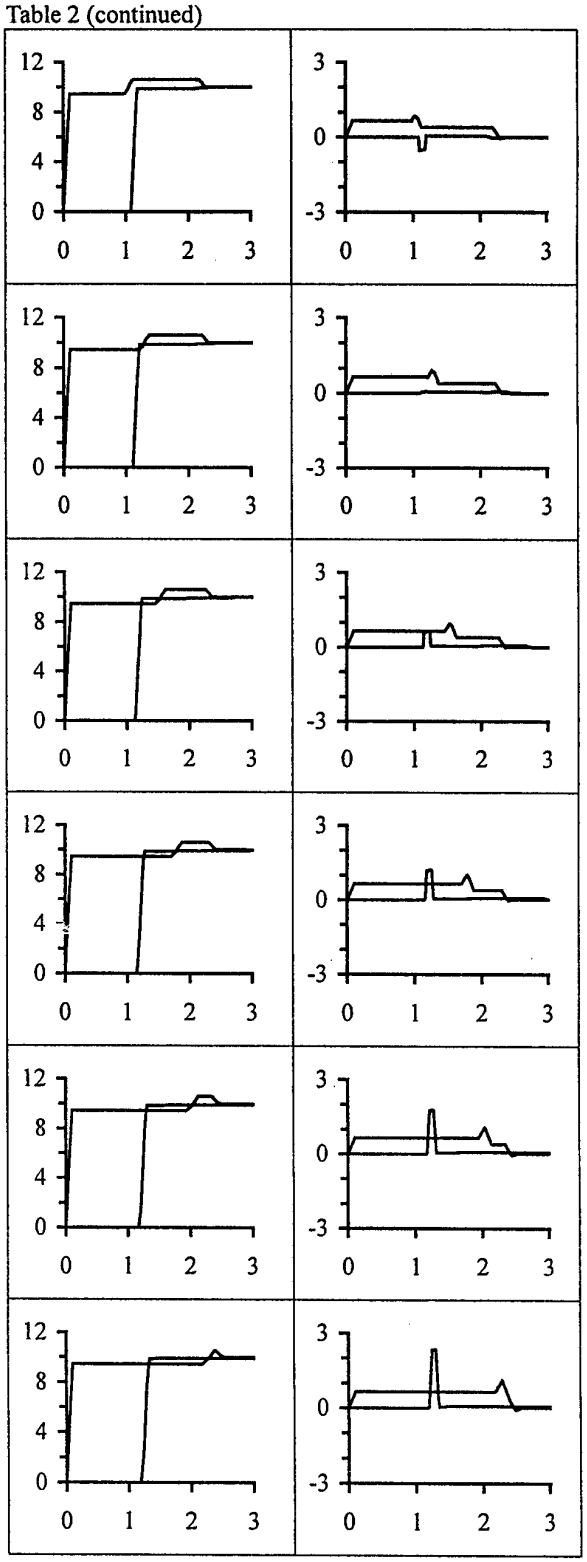
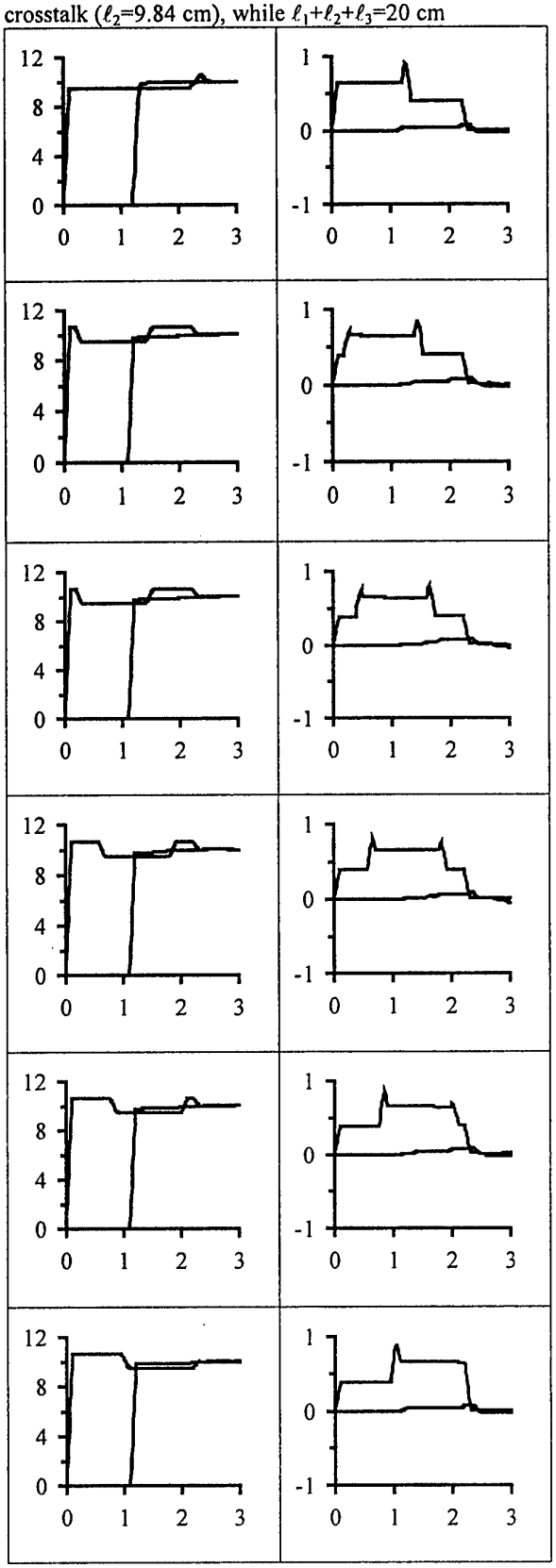


Table 3. Active (left column) and passive (right column) lines' waveforms (V, ns) calculated for increasing position ($\ell_1$=0,2...10 cm) of section with covering dielectric layer according to complete compensation of far-end crosstalk ($\ell_2$=9.84 cm), while $\ell_1+\ell_2+\ell_3$=20 cm




At last, an influence of covering dielectric layer's position on complete far-end crosstalk compensation was considered. For this aim, the length of covering dielectric layer according to complete compensation of far-end crosstalk for structure of Table 2 has been found ($\ell_2$=9.84 cm). Then, the position $\ell_1$ of this covering dielectric layer from lines' beginning was increased ($\ell_1$=0,2...10 cm), while the total length of three-section structure was constant ($\ell_1+\ell_2+\ell_3$=20 cm) and according waveforms have been calculated by analytic formulae proposed in [13] and extended by authors for lines of arbitrary lengths [14].

All four waveforms calculated for considered cases are shown in six rows of Table 3, accordingly. It is seen that phenomenon of complete far-end crosstalk compensation is observed also in structure consisting of three sections of lines. Moreover, an influence of position of covering dielectric layer on this phenomenon is negligible.

Behavior of near-end crosstalk waveforms both in Table 2 and Table 3 is quiet interesting. It is seen that upper part of near-end crosstalk waveforms is some image of covering dielectric layer. Particularly, the durability of the upper part is proportional to length of covering dielectric layer, while the start time of the upper part is according to position of covering dielectric layer from lines' beginning. The phenomena may be used properly in some applications.

## 5. CONCLUSIONS

5.1. The method of far-end crosstalk reduction in coupled microstrip lines by covering dielectric layer has been presented.

5.2. The method is very simple and low-cost because the covering dielectric layer may be implemented, for example, manually by attaching the layer of glue or dielectric plate.

5.3. The method may be used for improving the directional couplers' directivity.

5.4. Moreover, the method may be useful, for example, for quick reduction of large far-end crosstalk detected suddenly in circuit boards having been traced and manufactured without proper modeling of interconnects.

5.5. Influence of all main parameters of covering layer (relative permittivity, height, length and position) on far-end crosstalk, near-end crosstalk and active line waveforms have been investigated by modeling the parameters of lines and simulation of waveforms.

5.6. Very small influence of the covering dielectric layer's position on complete far-end compensation may simplify considerably the usage of the method in practice.

5.7. All four waveforms calculated for various parameters of the covering dielectric layer show clearly the phenomenon of far-end crosstalk compensation and its influence on near-end crosstalk and active line waveforms. The influence is found to be, as a rule, insignificant and quiet controllable for proper usage of far-end crosstalk compensation in practice.

## 6. ACKNOWLEDGMENT

T.R.Gazizov thanks N.I.Bazenkov for enthusiasm on scientific work and A.V.Gazizova for great support.

## 7. REFERENCES

7.1. A.R.Djordjevic, T.K.Sarkar, and R.F.Harrington, "Time-domain Response of Multiconductor Transmission Lines," IEEE Proceedings, vol.75, no.6, June 1987, pp.743-764.

7.2. T.R.Gazizov, "Low-cost PCB with high-speed and high-density interconnects", XXVI-th General Assembly of International Union of Radio Science, Toronto, Ontario, Canada, August 13-21, 1999, p.264.

7.3. T.R.Gazizov and N.A.Leontiev, "Reduction of high-speed signal distortions in double-layered dielectric PCB interconnects", Digest of 6-th Topical Meeting on Electrical Performance of Electronic Packaging, October 27-29, 1997, San Jose, California, pp.67-69.

7.4. T.R.Gazizov, "Improving the interconnects of circuit boards" (Russian), Ph.D. thesis, Tomsk State University of Control Systems and Radioelectronics, Tomsk, 1998.

7.5. T.R.Gazizov and N.A.Leontiev, "An effect of far-end crosstalk compensation in double-layered dielectric PCB interconnects", Proceedings of the 14-th Int. Wroclaw Symposium on EMC, Wroclaw, Poland, June 23-25, 1998, pp.353-356.

7.6. T.R.Gazizov and N.A.Leontiev, "Compensation of far-end crosstalk in interconnects of a double-layered dielectric PCB", Proc. of the 13-th Int. Zurich Symp. on EMC, Zurich, Switzerland, February 16-18, 1999, pp.645-648.

7.7. T.R.Gazizov, N.A.Leontiev, O.M.Kuznetsova-Tadjibaeva, "Simple and low-cost method of far-end crosstalk reduction in coupled microstrip lines", Presented at the 2000 Int. Symp. on Antennas and Propagation, Fukuoka, Japan, August 22-25.

7.8. T.R.Gazizov, "Computer simulation of electromagnetic coupling in interconnects of a double-layered dielectric PCB: parallel lines on one side of the layer", Proc. of the 13-th Int. Wroclaw Symposium on EMC, Wroclaw, Poland, June 25-29, 1996, pp.230-234.

7.9. T.R.Gazizov, "Computer simulation of electromagnetic coupling in interconnects of a double-layered dielectric PCB: parallel lines on opposite sides of the layer", Proc. of the 6-th Int. Symposium on Antennas and Propagation, Chiba, Japan, September 24-27, 1996, pp.681-684.

7.10. T.R.Gazizov and N.A.Leontiev, "Analytical expressions for transient response of two cascaded transmission line sections" (Russian), Trudy TUSUR, vol.1, 1997, pp.63-67.

7.11. T.R.Gazizov, "Capacitance matrix of three dimensional system of conductors and dielectrics", (Russian), Izvestya vuzov. Fizika, no.3, 1998, pp.123-125

7.12. T.R.Gazizov, "Calculation of Capacitance Matrix of Three Dimensional Multiconductor System in Multiple Dielectric Media", Record of International Symposium on Electromagnetic Compatibility (ISBN: 3-929757-25-7), Magdeburg, Germany, October 5-7, 1999, pp.31-36.

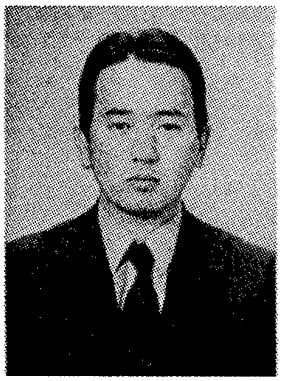
7.13. Q.Gu and J.A.Kong, "Transient analysis of single and coupled lines with capacitively-loaded junctions", IEEE Trans. Microwave Theory Tech., vol.MTT-34, pp.952-964, Sept.1986.

7.14. N.A.Leontiev, "Time-domain response analysis in interconnects of high-speed electronic circuits" (Russian), Ph.D. thesis, Tomsk State University of Control Systems and Radioelectronics, Tomsk, 2000.

## BIOGRAFICAL NOTES



Gazizov Talgat Rashitovich was born in 1963. He got his higher professional education on radioengineering in 1985 in the Tomsk Institute of Automatic Control Systems and Radioelectronics and Ph.D degree in 1999. His research interest is signal integrity problem. Now he is working toward Doctor of Sciences degree.



Leontiev Nyurgun Anatolievich was born in 1974. He got his higher professional education on radiophysics and electronics in 1996 in Yakutsk State University. His research interest is calculation of time-domain response in transmission line structures. He has finished his research and presented Ph.D. thesis in 2000.



Kuznetsova-Tadjibaeva Olga Mihailovna was born in 1975. He got his higher professional education on design and technology of radioelectronic systems in 1997 in Tomsk State University of Control Systems and Radioelectronics. His research interest is EMC-adequate system design. Now he is working toward Ph.D. degree.

EMC 2000 INTERNATIONAL WROCŁAW SYMPOSIUM ON ELECTROMAGNETIC COMPATIBILITY

# ESTIMATION OF CURRENT AND VOLTAGE DISTRIBUTIONS IN A DIGITAL IC PACKAGE

Satoshi KAZAMA, Shinich SHINOHARA and Risaburo SATO
Electromagnetic Compatibility Research Laboratories Co., Ltd.
6-6-3, Minami-Yoshinari, Aoba-ku, Sendai, 989-3204 JAPAN
Telephone: +81-22-279-3781 Fax: +81-22-279-3640 e-mail: kaze@emc-l.co.jp

***Abstract*** *This paper describes a method for estimating current and voltage distributions by scanning with a probe. The method takes advantage of the phenomenon that the coupling between the current and the probe varies with the direction of the probe. The current and voltage are estimated by calculating the probe vector output for each of four directions. Both the current and voltage vector distributions can thus be estimated at the same time by using a single probe. The simple structure of the probe should make it easy to reduce its size. The estimated distributions in a digital IC package showed that this method produces reliable results.*

## 1. INTRODUCTION

To identify the source of electromagnetic radiation emanating from electronic equipment, it is helpful to know the current and voltage distributions in the equipment. This information can then be used to eliminate or reduce electromagnetic interference. The current and voltage distributions in IC packages and on printed circuit boards have thus been investigated. Magnetic probes such as shielded loops[1] and electric probes[2] have been used to measure the near electromagnetic field. The current distribution is estimated from the near magnetic field, and the voltage distribution is estimated from the near electric field. Therefore, both magnetic and electric probe scanning are necessary to determine the current and voltage distributions.

Shielded loops, which are used for estimating the current distribution, have a shielded structure to prevent electric coupling. This structure makes it difficult to reduce the size of the probe. Furthermore, in some cases, the shield structure is ineffective against high-frequency radiation.

In this paper we describe a method for estimating both the current and voltage distributions simultaneously by scanning with a single probe. The probe has a simple structure, so it should be easy to reduce its size. The method takes advantage of the difference between electric coupling with the voltage and magnetic coupling with the current. The coupling current and voltage are estimated by measuring the vector outputs from the probe when the orientation of the probe is changed. By scanning with this probe, the current and voltage distributions can be calculated. We also describe the measurement system using this method and our estimation of the current and voltage distributions in a digital IC.

## 2. ESTIMATING METHOD

### 2.1 Couplings with current and voltage

Figure 1 shows the probe coupling with voltage V and current I, which is parallel with the probe. The voltage and current are given by

$$V=A\sin\left(\omega t+\theta_{v}\right). \quad (1)$$

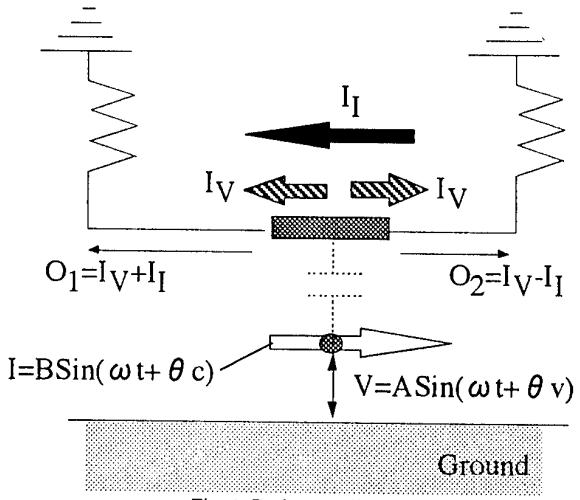



Fig. 1. Probe couplings.

$$I=BSin\left(\omega t+\theta_{c}\right). \quad (2)$$

where A and B are the magnitude of voltage and current, and $\theta_{v}$ and $\theta_{c}$ are phase angles.

The probe is a metal line that is smaller than the wavelength. It is coupled with the current and voltage, and each end is terminated by the same impedance. The current resulting from the magnetic coupling with current ($I_I$) and that resulting from electric coupling with voltage ($I_V$) flow in the probe. The directions of the current resulting from the magnetic coupling ($I_I$) are different at the two ends of the probe, but the directions of the current resulting from the electric coupling ($I_V$) are the same at the two ends. Therefore, the outputs at the two ends of the probe are different. The current and the voltage are estimated from this difference.

The outputs at the two ends of the probe are given by

$$O_{1}=\alpha_{1}V+\beta_{1}I. \quad (3)$$

$$O_{2}=\alpha_{1}V-\beta_{1}I. \quad (4)$$

where $\alpha_{1}$ and $\beta_{1}$ are the coupling coefficients, which vary with the position of the ground and probe.

From these relationships, the current I and voltage V are derived as

$$V=\frac{O_{1}+O_{2}}{2\alpha_{1}}. \quad (5)$$

$$I=\frac{O_{1}-O_{2}}{2\beta_{1}}. \quad (6)$$

2.2 Current and voltage distributions

Figure 2 illustrates our method for estimating the current and voltage distributions. It shows current I with current angle $\phi$ and voltage V at point (x, y) on the measurement plane. The probe outputs for the four rectangular directions ($O_{xf}$, $O_{xr}$, $O_{yf}$, $O_{yr}$) are given by

$$O_{xf}=\alpha_{2}A_{(x,y)}Sin\left(\omega t+\theta_{v(x,y)}\right)$$

$$-Cos\,\phi\beta_{2}B_{(x,y)}Sin\left(\omega t+\theta_{c(x,y)}\right). \quad (7)$$

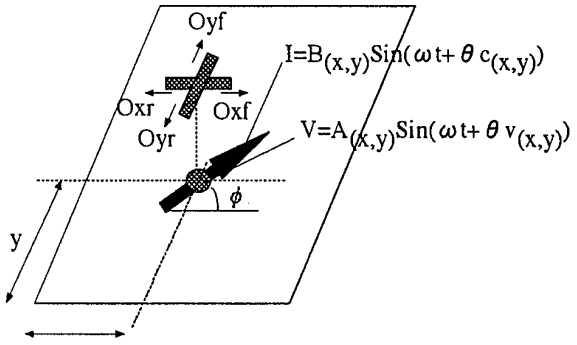


Fig. 2. Estimation of current and voltage distributions.

$$O_{xr}=\alpha_{2}A_{(x,y)}Sin\left(\omega t+\theta_{v(x,y)}\right)$$

$$+Cos\phi\beta_{2}B_{(x,y)}Sin\left(\omega t+\theta_{c(x,y)}\right). \quad (8)$$

$$O_{yf}=\alpha_{2}A_{(x,y)}Sin\left(\omega t+\theta_{v(x,y)}\right)$$

$$-Sin\,\phi\beta_{2}B_{(x,y)}Sin\left(\omega t+\theta_{c(x,y)}\right). \quad (9)$$

$$O_{yr}=\alpha_{2}A_{(x,y)}Sin\left(\omega t+\theta_{v(x,y)}\right)$$

$$+Sin\,\phi\beta_{2}B_{(x,y)}Sin\left(\omega t+\theta_{c(x,y)}\right). \quad (10)$$

where $\alpha_{2}$ and $\beta_{2}$ are coupling coefficients, $A_{(x,y)}$ and $B_{(x,y)}$ are the magnitudes of the voltage and current, and $\theta_{v(x,y)}$ and $\theta_{c(x,y)}$ are the phase angles.

From these relationships, we derive the X direction voltage (Eq. 11), the Y direction voltage (Eq. 12), the X direction current (Eq. 13), and the Y direction current (Eq. 14).

$$A_{(x,y)}Sin\left(\omega t+\theta_{v(x,y)}\right)=\frac{O_{xf}+O_{xr}}{2\alpha_{2}}. \quad (11)$$

$$A_{(x,y)}Sin\left(\omega t+\theta_{v(x,y)}\right)=\frac{O_{yf}+O_{yr}}{2\alpha_{2}}. \quad (12)$$

$$Cos\phi B_{(x,y)}Sin\left(\omega t+\theta_{v(x,y)}\right)=\frac{O_{xf}-O_{xr}}{-2\beta_{2}}. \quad (13)$$

$$Sin\,\phi B_{(x,y)}Sin\left(\omega t+\theta_{v(x,y)}\right)=\frac{O_{yf}-O_{yr}}{-2\beta_{2}}. \quad (14)$$

If these relations are correct, the X and Y direction voltages must be the same.

## 3. MEASUREMENT SYSTEM FOR ESTIMATION

### 3.1 Probe

Figure 3 shows the structure of the probe used for this estimation system. It is composed of a sensing component and two 50-ohm strip lines made in a multilayer printed circuit board. The sensing component consists of a 0.2-mm width line and is about 0.4 by 0.6 mm. The current and voltage of the measurement plane couple with the 0.2-mm line. One end of the 50-ohm strip lines is connected to a measuring instrument, and the other is terminated by an impedance of 50 ohms.

### 3.2 Measurement system

Figure 4 shows the setup of the estimation system for testing a digital IC device. The probe scanning is driven by a 3-dimensional actuator controlled by a personal computer. The vector outputs from the probe are measured using a vector-signal analyzer (HP89441A), which measures both the magnitude and phase of the high-frequency signals. The signal generator used to run the device being tested uses a standard signal from the vector-signal analyzer to maintain the accuracy of its signal frequency, which is necessary to measure the phase of the signal.

The probe is shifted between four rectangular orientations while it is continuously scanning above the device being tested. The vector outputs at each of these probe positions are measured, then used to calculate the current and voltage distributions.

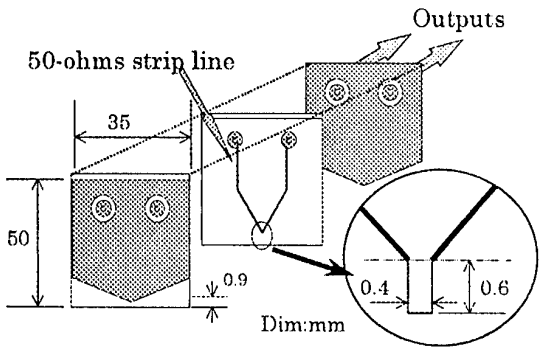



Fig. 3. Structure of the probe.

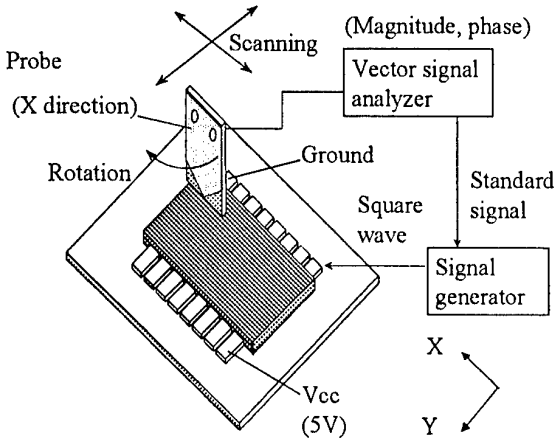



Fig. 4. Estimation system.

## 4. DISTRIBUTIONS IN A DIGITAL IC

The current and voltage distributions of the 300-mil small-outline-package CMOS digital IC (74AC04) shown in Figure 5 were estimated using this method. The IC was mounted on a printed circuit board. Six inverters in the IC were connected as shown in Fig. 5 and driven by a 20-MHz wave. The source voltage was 5 V. The probe scanned in 0.2-mm steps on a plane about 0.5 mm above the IC package.

Figure 6 shows the estimated X direction current and voltage distributions in the IC at the 5th harmonics (100 MHz) of the signal wave. Because the coupling coefficients are unknown, the magnitude scales are relative. Figure 7 shows the estimated Y direction distributions at the 5th harmonics.

To verify these estimated results, we compared the voltage distributions (magnitude and phase) in the X and Y directions. Both the magnitudes and phase angles showed good agreement, indicating that this measurement

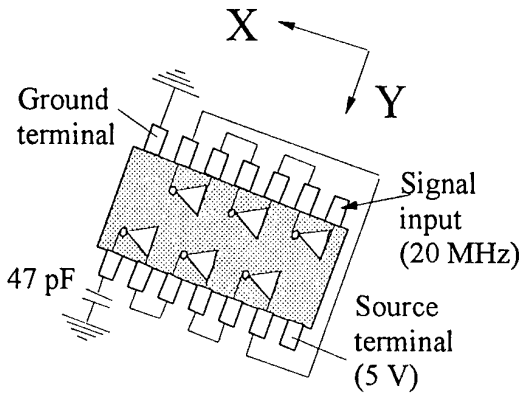
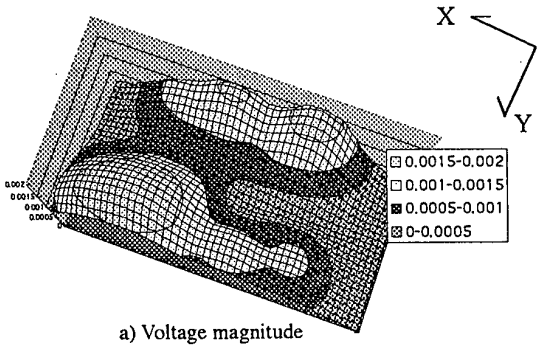
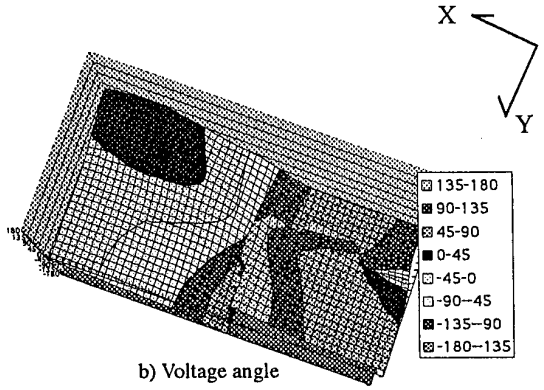


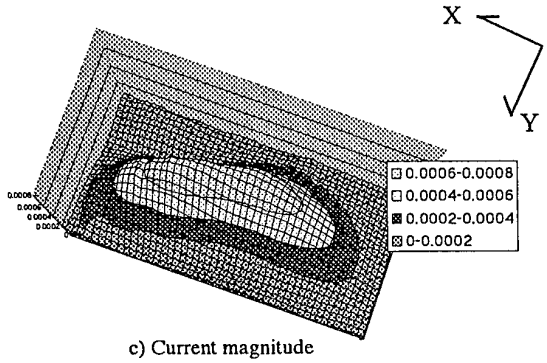

Fig. 5. Measured IC.



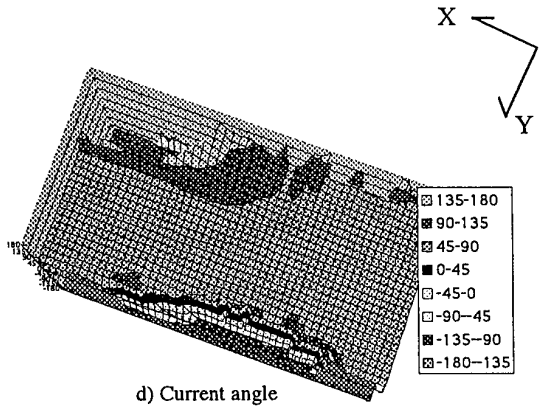

a) Voltage magnitude




b) Voltage angle

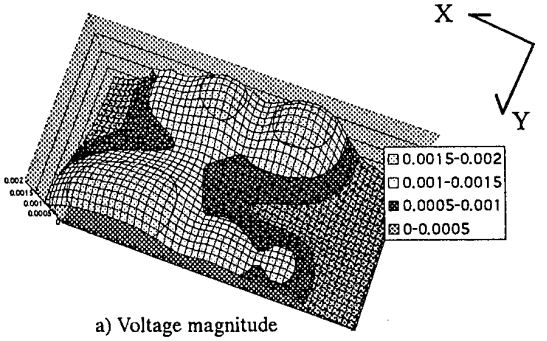



c) Current magnitude

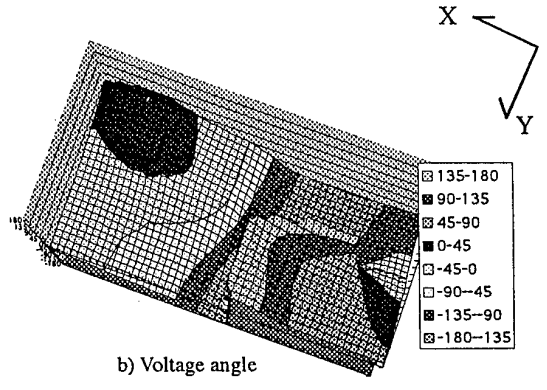



d) Current angle

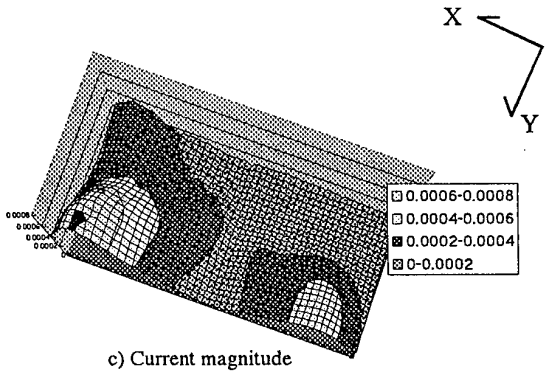
Fig. 6. X direction current and voltage distribution in a IC (100MHz: 5th harmonics).



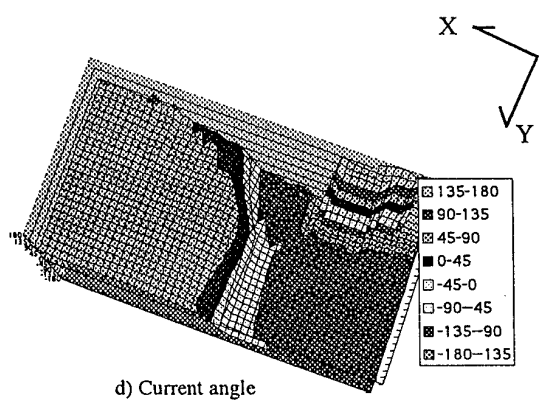

a) Voltage magnitude




b) Voltage angle




c) Current magnitude




d) Current angle

Fig. 7. Ydirection current and voltage distribution in a IC (100MHz: 5th harmonics).

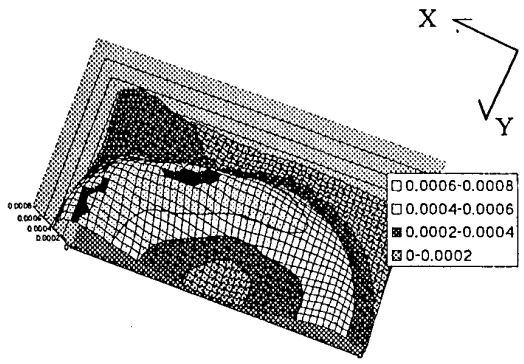



Fig. 8. Current distribution in a IC (100MHz: 5th harmonics).

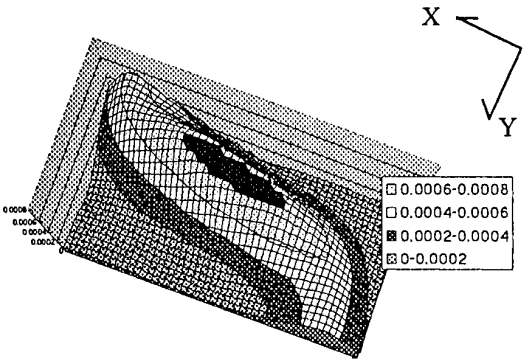



Fig. 9. Current distribution in a IC (120MHz: 6th harmonics).

system gives reliable estimations.

We calculated the current magnitude ($I_m$) distributions by using

$$I_m=\sqrt{I_x^2+I_y^2}. \quad (15)$$

where $I_x$ is the current magnitude in the X direction and $I_Y$ is that in the Y direction. Figure 8 shows the current magnitude distributions at the 5th harmonics (100 MHz). Figure 9 shows the current magnitude distributions at the 6th harmonics (120 MHz).

As shown in Figure 8, the 5th harmonics current flowed in the last inverter lead-frame, which had a load of 47 pF and in the source and ground lead-frame. A similar pattern was seen at odd harmonics. As shown in Figure 9, the 6th harmonics current mainly flowed in the source and ground lead-frame. A similar pattern was seen at even harmonics.

The waveform in the output lead-frame is thus trapezoidal and consists mainly of odd harmonics, while the current in the source and ground lead-frame contains even harmonics.

## 5. CONCLUSIONS

We described a method for estimating current and voltage distributions by using a simple probe. This method takes advantage of the phenomenon that the coupling between the current and the probe varies with the direction of the probe. Both the current and voltage vector distributions can be estimated at the same time by using a single probe. The probe has a simple structure, so it should be easy to reduce its size.

We set up an estimation system using this method and estimated the current and voltage distributions in a digital IC.

Our experimental results showed that our method is effective for estimating current and voltage distributions, which will be useful information for EMC.

## 6. REFERENCES

[1] H. Wakuba, N. Masada, N. Tamaki, H. Tohya, T. Watanabe, M. Yamaguchi, and K. Arai, "Estimation of the RF Current at IC Power Terminal Using Magnetic Probe with Multilayer Structure.", Technicalreport of IECE. EMCJ 98-6, pp. 39-43, April 1998.

[2] A. Namba, O. Wada, and R. Koga, "Measurement of Near-Field Emission from Printed Circuit Board Using Miniature E-Field Probe.", Technical report of IECE. EMCJ 98-46, pp. 41-46, Sept. 1998

## BIOGRAPHICAL NOTES

**Satoshi Kazama** received his B.E. degree from Niigata University, Niigata, Japan, in 1986. He joined Taiyo Yuden Company in 1986. Since 1996, he has worked at the Electromagnetic Compatibility Research Laboratories. His research interests include electromagnetic compatibility and microwave components.

**Shinichi Shinohara** received his B.E. and M.E. degrees from University of Electro-Communications, Chofu, Japan, in 1970 and 1972, respectively. From 1972 to 1998, he worked in the NTT's Laboratories. He joined Sony Corporation in 1998. Since 1996, he has been a general manager at Electromagnetic Compatibility Research Laboratories. Presently he is engaged in research on countermeasures technology on EMC.

**Risaburo Sato** received his B.E. and Ph.D. degrees from Tohoku University, Sendai, Japan, in 1944 and 1952, respectively. From 1961 to 1984, he was a professor at Tohoku University. From 1984 to 1999, he was dean of the faculty of engineering of Tohoku Gakuin University, Tagajo, Japan. His research activities include studies on distributed transmission circuits as multi-conductor systems, antennas, computer networks and EMC. He is the president of Electromagnetic Compatibility Research Laboratories.

EMC 2000 INTERNATIONAL WROCŁAW SYMPOSIUM ON ELECTROMAGNETIC COMPATIBILITY

# NEW 3D MODEL OF INTERNAL ELECTROMAGNETIC NOISES IN VLSI CHIP

Igor V. Vasiltsov
Institute of Computer Informational Technology, Ternopil Academy of National Economy,
Lvivska street, 11, Ternopil, 48004, UKRAINE, E-mail: iv@tanet.edu.te.ua; igorvasiltsov@mail.ru
Bogdan A. Mandzij,
State University "Lvivska polytechnika", Bandery street, 12, Lviv, 290646,UKRAINE

*In this paper a problem of constructing a new three-dimensional calculation model for evaluating the parasitic electromagnetic noise is considered.*

*The mathematical model of internal electromagnetic conductive noise for matrix VLSI with complanar topology of power supply feeding have been obtained.*

*Obtained model have to be used when calculating the reliability parameters of designed digital devices constructed on programmable VLSI chip.*

## 1. INTRODUCTION

The main reasons of false functioning of modern digital devices are short-timed self-repairing failures, intensity of which is some level above intensity of the steady faults. These failures appearance is a result of internal electromagnetic parasitic noises in VLSI chip during simultaneous switching of logic gates. That is why the determine of failures occurrence risk at the early stages of designing as well as making requested correction into the structure of device is the especially actual task.

The method of evaluation of digital devices functional reliability, which is based on the accounting approach to constructing of internal noise mathematical models and estimation of their characteristics together with taking into account the constructive and technological parameters of VLSI chips has been discussed in [1]. Using of this method request to determine the estimation of the internal noise characteristics with taking into account the constructive and technological parameters of VLSI chips as well as determine appropriate confidence intervals. The analysis of the electromagnetic noises shows [2, 5], that the main reason for decreasing noise immunity margin of a logic element is a conductive noise. It arises according to current value during simultaneous switching of logic gates (LG) and causes the decreasing of voltage value applied at LG. This decrease the noise immunity margin of LG.

So, according to mentioned above it is necessary to develop the mathematical models (MM) for evaluation consistently the parameters of internal electromagnetic noises for different types of topology layout.

In this paper the MM of internal conductive noise in matrix VLSI with complanar topology has been considered.

## 2. MODEL OF POWER SUPPLY FEEDING

For the evaluation of internal noises parameters it is requested to analyse their appearance process on the basis of corresponding equivalence circuits.

Earlier, the equivalent calculation circuits of internal noises have been obtained [3]. They have been used to build the appropriate mathematical models of internal noises. On to the basis of obtained relations the models of mathematical expectation and dispersion of conductive noise have been developed.

But obtained relations describe only single situation, using 2D models of internal electromagnetic noises. Sometimes it is important for developer to have the estimation of the electromagnetic field distribution of the whole chip. Such data can be compared with others (for example with the chip temperature distribution) to define the critical area of the chip from the viewpoint of complex influence of temperature and internal electromagnetic noises as well.

On the Fig.1 a simplify variant of matrix VLSI with a complanar topology of power supply feeding has been shown. There are next marks on the Fig.1: $R_0$ describes the resistance between power supply and feed/ground lines; $\Delta R_1$ describes resistance of horizontal part of feed/ground lines; $\Delta R$ describes resistance of vertical part of feed/ground lines. In general case these three resistance can be different. It depends on the particulars of specific technological process and requested constructional layout.

Supposed that probability of all LG state combinations are equal, we can find the dispersion and mathematical expectation of variables $x_{ij}$, $x_{il}$ :

$$M(x_{ij})=M(x_{il})=0,5; \quad D(x_{il})=D(x_{il})=0,25.$$

According to this the mathematical expectation of internal conductive noise in matrix VLSI with orthogonal topology of power supply feeding will defined as follows:

$$M[U_{k,l}] = 2I_1R_0\sum_{i=1}^{N}\sum_{j=1}^{M}M[x_{ij}] + 2I_1\Delta R_1 \times$$
$$\times\left[\sum_{i=1}^{N}\sum_{j=s}^{S}|\alpha-j|M[x_{ij}]+\sum_{i=1}^{N}\sum_{j=p}^{P}|\alpha-l|M[x_{ij}]\right]+$$
$$+I_1\Delta R\cdot\left[\sum_{i=1}^{k}i\cdot M[x_{il}]+k\sum_{i=k+1}^{N}M[x_{il}]+\right.$$
$$\left.+(N-k+1)\sum_{i=1}^{k}M[x_{il}]+\sum_{i=k+1}^{N}(N-i+1)M[x_{il}]\right] = \quad (6)$$
$$= I_1R_0\cdot N\cdot M + I_1\Delta R_1\left[\sum_{i=1}^{N}\sum_{j=s}^{S}|\alpha-j|\right]+$$
$$+I_1\Delta R_1\cdot N(P-p+1)|\alpha-l|+I_1\Delta R\times$$
$$\times\frac{2k(N-k+1)+N^2+3N+2}{4}$$

and dispersion respectively:

$$D[U_{k,l}] = (2I_1R_0)^2\sum_{i=1}^{N}\sum_{j=1}^{M}D[x_{ij}]+(2I_1\Delta R_1)^2\times$$
$$\times\left[\sum_{i=1}^{N}\sum_{j=s}^{S}|\alpha-j|^2D[x_{ij}]+\sum_{i=1}^{N}\sum_{j=p}^{P}|\alpha-l|^2D[x_{ij}]\right]+$$
$$+(I_1\Delta R)^2\cdot\left[\sum_{i=1}^{k}i^2\cdot D[x_{il}]+k^2\sum_{i=k+1}^{N}D[x_{il}]+\right.$$
$$\left.+(N-k+1)^2\sum_{i=1}^{k}D[x_{il}]+\sum_{i=k+1}^{N}(N-i+1)^2D[x_{il}]\right] =$$
$$= (I_1R_0)^2\cdot N\cdot M+(I_1\Delta R_1)^2\left[\sum_{i=1}^{N}\sum_{j=s}^{S}|\alpha-j|^2\right]+$$
$$+(I_1\Delta R_1)^2\cdot N(P-p+1)|\alpha-l|^2+\left(\frac{I_1\Delta R}{2}\right)^2\times$$
$$\times\left[k(k-N-1)+1+\frac{2N^3+9N^2+13N}{6}\right] \quad (7)$$

The simulation of obtained 3D models were made. It permits to determine the logic gates which are in the worst-case situation from the viewpoint of internal electromagnetic noises influence (see Fig.2, 3). For the simulation the next parameters were used: N=M=21; E=5 V; $I_1$=1 mA; $R_0$=0.005 Ohm. $\Delta R_1$=0.002 Ohm.$\Delta$R=0.01 Ohm. In the worst-case situation is LG situated farthest from the connect point of power supply feeding. In the given example these are gates situated at the middle of the outside columns. For used parameters the calculated maximum value of internal conductive noise is equal 6.847 mV.

## 4. CONCLUSION

Obtained relations allow to evaluate consistently the influence of the electromagnetic noises, caused by simultaneous switching of LG. These models have been used for the evaluation of the digital device reliability. The obtained equations take into account the properties of the chip constructive realisation. This increases efectivity and shorts terms of the designing process.

## 5. REFERENCES


[1] Bogdan A. Mandziy, Igor V. Vasiltsov. Problem of Reliability at Designing of Signals Processing Digital Devices. *In Proc. of Intern. Conference TELSIKS'97, 8-10 October*, 1997, Nis, Yugoslavia, pp.245-248.

[2] High-speed matrix LSI and VLSI. Theory and design / B.N.Fajzulaev, I.I. Shagurin, A.N.Karmazinski and others. Moscov.: *Radio and communications*, 1989 - 304p. (in Russian).

[3] Bogdan Mandzij, Igor Vasiltsov. Simulation of Simultaneous Switching Noise of Logic Gates in VLSI. In *Proc. of XV Symposium on Electromagnetic Phenomena in Nonlinear Circuits.*, 22-24 September, 1998, Liege, Belgium, pp.224-226.

[4] B.A.Mandzij, I.V.Vasiltsov, R.I.Gelyakl. Estimation of the functional reliability parameters of digital devices of data processing systems // *"Telecommunication" Regular Scientific and research Journal on Telecommunication, Radio and Television* №2/1997, pp. 12-15. (in Russian).

[5] Michael Gutzmann. Modellirung des Simultaneous Switching Noise von MOS-Ausgans Treibern. *Facta Universitatis. Series: Electronics and Energetics*. Vol.10, No. 1(1997), University of Nis, pp.75-90. (in Duetch).

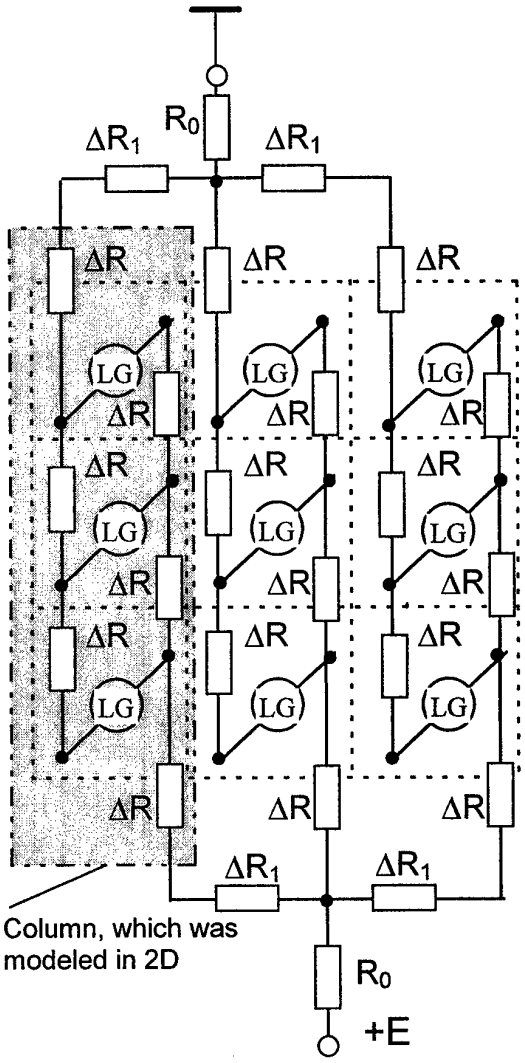



Fig.1. Variant of matrix VLSI with a complanar topology of power supply feeding

## 3. MATHEMATICAL MODELS OF INTERNAL CONDUCTIVE NOISE

For constructing of mathematical models of internal conductive noise the second law the classical laws were used. According to it the noise voltage at any logic gate in the matrix chip with complanar topology of power supply feeding will defined as follows:

$$U_{k,l} = 2U_{R_0} + 2U_{\Sigma\Delta R_1} + U_{\Sigma\Delta R} = \\ = 2i_{R_0} \cdot R_0 + 2i_{\Sigma\Delta R_1} \cdot \Delta R_1 + i_{\Sigma\Delta R} \cdot \Delta R \quad (1)$$

where $E$ – means the nominal value of power supply feeding; $U_{R0}$ – means the voltage drop at the $R_0$ resistance; $U_{\Sigma\Delta R1}$ – means the voltage drop at the all $\Delta R_1$ resistance, which are included in the calculated closed loop; $U_{\Sigma\Delta R}$ – means the voltage drop at the all $\Delta R$ resistance, which are included in the calculated closed loop (see Fig.1).

All resistance value can defined on to the basis of constructional and technology parameters of the chip as shown in [1, 4]. So, to obtain a noise voltage it requested to calculate the currents which flow through each part of feed/ground lines. The noise voltage at any gate will be determined as follows:

$$U_{k,l} = 2I_1 R_0 \sum_{i=1}^{N}\sum_{j=1}^{M} x_{ij} + 2I_1 \Delta R_1 \times \\ \times \left[ \sum_{i=1}^{N}\sum_{j=s}^{S} |\alpha - j| x_{ij} + \sum_{i=1}^{N}\sum_{j=p}^{P} |\alpha - l| x_{ij} \right] + \\ + I_1 \Delta R \cdot \left[ \sum_{i=1}^{k} i \cdot x_{il} + k \sum_{i=k+1}^{N} x_{il} + \right. \\ \left. + (N-k+1)\sum_{i=1}^{k} x_{il} + \sum_{i=k+1}^{N} (N-i+1) x_{il} \right] \quad (2)$$

where $I_1$ – means a nominal current of LG at the high output level; $N$ – means the number of LG in the column; $M$ – means the number of LG in the row; $k$, $l$ – determine the ordinal number of LG in the column and row respectively; $x_{ij}$, $x_{il}$ – means the logical state of LG, it can take the value one or zero accordingly to logic state of LG;

$\alpha$ – means the ordinal number of middle column:

$$\alpha = \frac{M+1}{2} \quad ; \quad (3)$$

$s$, $S$ – mean number of first and last row between *l-th* row and middle row respectively:

$$s = \begin{cases} l, & \alpha > l \\ \alpha, & \alpha \le l \end{cases} \\ S = \begin{cases} \alpha - 1, & \alpha > l \\ l, & \alpha \le l \end{cases} \quad ; \quad (4)$$

$p$, $P$ – mean number of first and last row between *l-th* row and edge row respectively:

$$p = \begin{cases} 1, & \alpha > l \\ l, & \alpha \le l \end{cases} \\ S = \begin{cases} l-1, & \alpha > l \\ M, & \alpha \le l \end{cases} \quad (5)$$

Supposed that probability of all LG state combinations are equal, we can find the dispersion and mathematical expectation of variables $x_{ij}$, $x_{il}$:

$$M(x_{ij})=M(x_{il})=0,5; \quad D(x_{ij})=D(x_{il})=0,25.$$

According to this the mathematical expectation of internal conductive noise in matrix VLSI with orthogonal topology of power supply feeding will defined as follows:

$$M[U_{k,l}] = 2I_1R_0\sum_{i=1}^{N}\sum_{j=1}^{M}M[x_{ij}] + 2I_1\Delta R_1 \times$$
$$\times\left[\sum_{i=1}^{N}\sum_{j=s}^{S}|\alpha-j|M[x_{ij}] + \sum_{i=1}^{N}\sum_{j=p}^{P}|\alpha-l|M[x_{ij}]\right] +$$
$$+ I_1\Delta R\cdot\left[\sum_{i=1}^{k} i\cdot M[x_{il}] + k\sum_{i=k+1}^{N}M[x_{il}] + \right.$$
$$\left. + (N-k+1)\sum_{i=1}^{k}M[x_{il}] + \sum_{i=k+1}^{N}(N-i+1)M[x_{il}]\right] = \quad (6)$$
$$= I_1R_0\cdot N\cdot M + I_1\Delta R_1\left[\sum_{i=1}^{N}\sum_{j=s}^{S}|\alpha-j|\right] +$$
$$+ I_1\Delta R_1\cdot N(P-p+1)|\alpha-l| + I_1\Delta R\times$$
$$\times\frac{2k(N-k+1)+N^2+3N+2}{4}$$

and dispersion respectively:

$$D[U_{k,l}] = (2I_1R_0)^2\sum_{i=1}^{N}\sum_{j=1}^{M}D[x_{ij}] + (2I_1\Delta R_1)^2\times$$
$$\times\left[\sum_{i=1}^{N}\sum_{j=s}^{S}|\alpha-j|^2D[x_{ij}] + \sum_{i=1}^{N}\sum_{j=p}^{P}|\alpha-l|^2D[x_{ij}]\right] +$$
$$+ (I_1\Delta R)^2\cdot\left[\sum_{i=1}^{k}i^2\cdot D[x_{il}] + k^2\sum_{i=k+1}^{N}D[x_{il}] + \right.$$
$$\left. + (N-k+1)^2\sum_{i=1}^{k}D[x_{il}] + \sum_{i=k+1}^{N}(N-i+1)^2D[x_{il}]\right] =$$
$$= (I_1R_0)^2\cdot N\cdot M + (I_1\Delta R_1)^2\left[\sum_{i=1}^{N}\sum_{j=s}^{S}|\alpha-j|^2\right] +$$
$$+ (I_1\Delta R_1)^2\cdot N(P-p+1)|\alpha-l|^2 + \left(\frac{I_1\Delta R}{2}\right)^2\times$$
$$\times\left[k(k-N-1)+1+\frac{2N^3+9N^2+13N}{6}\right] \quad (7)$$

The simulation of obtained 3D models were made. It permits to determine the logic gates which are in the worst-case situation from the viewpoint of internal electromagnetic noises influence (see Fig.2, 3). For the simulation the next parameters were used: N=M=21; E=5 V; $I_1$=1 mA; $R_0$=0.005 Ohm. $\Delta R_1$=0.002 Ohm.$\Delta R$=0.01 Ohm. In the worst-case situation is LG situated farthest from the connect point of power supply feeding. In the given example these are gates situated at the middle of the outside columns. For used parameters the calculated maximum value of internal conductive noise is equal 6.847 mV.

## 4. CONCLUSION

Obtained relations allow to evaluate consistently the influence of the electromagnetic noises, caused by simultaneous switching of LG. These models have been used for the evaluation of the digital device reliability. The obtained equations take into account the properties of the chip constructive realisation. This increases efectivity and shorts terms of the designing process.

## 5. REFERENCES


[1] Bogdan A. Mandziy, Igor V. Vasiltsov. Problem of Reliability at Designing of Signals Processing Digital Devices. *In Proc. of Intern. Conference TELSIKS'97, 8-10 October*, 1997, Nis, Yugoslavia, pp.245-248.

[2] High-speed matrix LSI and VLSI. Theory and design / B.N.Fajzulaev, I.I. Shagurin, A.N.Karmazinski and others. Moscov.: *Radio and communications*, 1989 - 304p. (in Russian).

[3] Bogdan Mandzij, Igor Vasiltsov. Simulation of Simultaneous Switching Noise of Logic Gates in VLSI. In *Proc. of XV Symposium on Electromagnetic Phenomena in Nonlinear Circuits.*, 22-24 September, 1998, Liege, Belgium, pp.224-226.

[4] B.A.Mandzij, I.V.Vasiltsov, R.I.Gelyakl. Estimation of the functional reliability parameters of digital devices of data processing systems // *"Telecommunication" Regular Scientific and research Journal on Telecommunication, Radio and Television* №2/1997, pp. 12-15. (in Russian).

[5] Michael Gutzmann. Modellirung des Simultaneous Switching Noise von MOS-Ausgans Treibern. *Facta Universitatis. Series: Electronics and Energetics.* Vol.10, No. 1(1997), University of Nis, pp.75-90. (in Duetch).

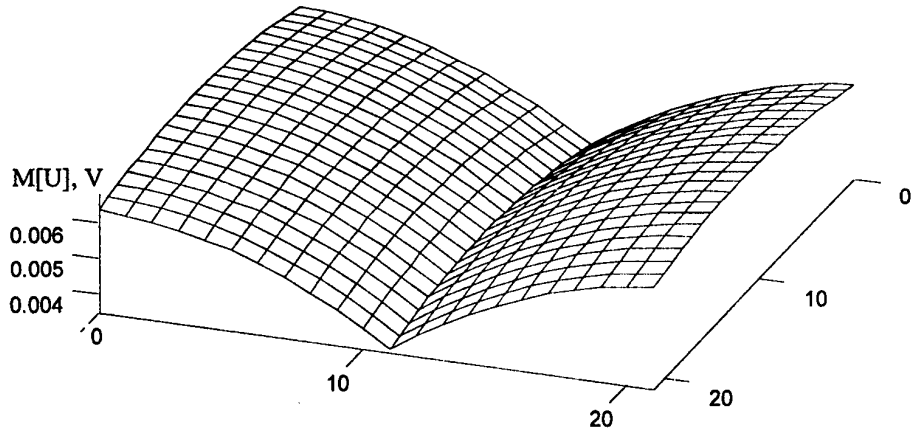



Fig.2. Distribution of the mathematical expectation of internal conductive noise accordingly to ordinal number of LG in the VLSI chip

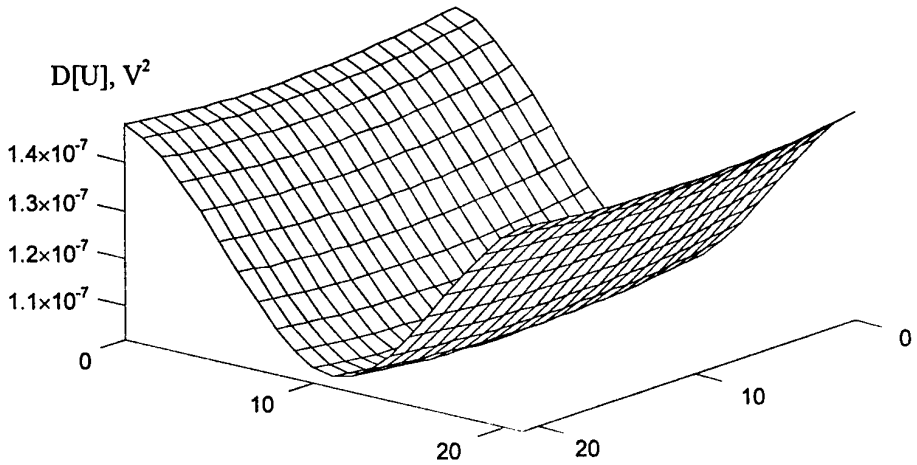
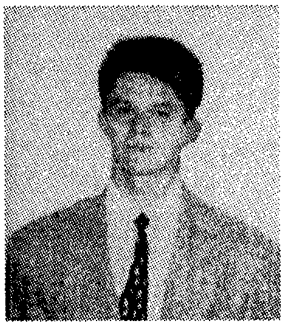



Fig.3. Distribution of the dispersion of internal conductive noise accordingly to ordinal number of LG in the VLSI chip

BIOGRAPHICAL NOTES



Igor V. Vasiltsov was born in 1971 in Ukraine. Receive Ph.D. degree from State university "Lvivska Polytechnika" in 1999. Since 1999 he is with the Specialized Computer System Chair, Computer Information Technology Institute in Ternopil Academy of National Economy as Assistant Professor. Area of research interest is microelectronics reliability, digital devices design., applied cryptology, developing applied specialized CAD/CAM systems.



Bogdan A. Mandzij was born in 1932 in Ukraine. Since 1990 he is Full Professor with the Radioengineering Department of State University "Lvivska Polytechnika". Since 1985 he is Head of Scientific and Research Laboratory at State University "Lvivska Polytechnika". Since 1996 he is a Chairmen of Theoretical Radioengineering and Radio measurements Chair. Area of research interest is microelectronics reliability, analog and digital devices design, system design, applied CAD.

EMC 2000 INTERNATIONAL WROCŁAW SYMPOSIUM ON ELECTROMAGNETIC COMPATIBILITY

# Evaluation of the Radiated Emission and Immunity Characteristics of Optical Transceiver Modules

Takeshi AIZAWA, Hidetoshi YAMAMOTO, Shinichi SHINOHARA, Risaburo SATO
Electromagnetic Compatibility Research Laboratories Co., Ltd.
6-6-3, Minami-yoshinari, Aoba-ku, Sendai, 989-3204, Japan

*Experiments have been conducted to investigate the characteristics of radiated emission from optical transceiver modules, and its radiated immunity. The experimental results reveals that in order to suppress radiated emission, it is necessary to reduce the antenna efficiency between the light emitting diode (LED) and the LED driver. In order to increase the immunity to radiated noise, we need to reduce antenna efficiency by shielding the optical/electro (O/E) converter.*

## 1.INTRODUCTION

Since long distance transmission of large capacity media such as video, audio are currently required, optical fiber transmission networks, with its characteristic wide band and low loss, have been improved and implemented. Until recent, the EMC in optical fiber transmission systems has not been considered a problem [1][2], such that there are only a few reports on the immunity of the O/E converter [3][4] and optical modulator [5] at short wavelengths. However, in optical fiber transmission systems, various electric circuits are used, and both the electro/optical (E/O) converter and optical transmission equipment may radiate electromagnetic noise [6]. Additionally, they may possibly be affected by electromagnetic interference waves. It is important therefore, to comprehend this in design procedures and to apply countermeasures against them.

In this study, we report on the experimental investigation into the characteristics of radiated emission and radiated immunity of optical transceiver modules. With regard to the radiated electromagnetic noise characteristic, we measured the strength of the radiated electric field and the distribution of the near magnetic field. Concerning radiated immunity, we measured the radiated impulse noise immunity and searched the lowest electric/magnetic immunity points.

## 2.EXPERIMENT

In this experiment we used seven types of commercially available optical transceiver module, which are currently used for high speed computer communication systems based on the Fiber Distribution Digital Interface (FDDI) standard. Optical fibers with a connector designated for FDDI are connected to each module. The connecting pins are 13PIN-DIP, and the package is plastic molded. The module size is 64 mm x 44 mm x 13mm. The optical center wavelength for fiber optic transmission via multi-mode fibers is 1300nm. The data transmitting speed is 125Mbps. The power voltage is 5V, supplied from batteries. The module is a transceiver with an optical transmitter/receiver, configured in a single package.

Fig. 1 shows a block diagram of the circuit. The optical receiving unit employs a photo diode (PD) as the receiving device. A digital circuit is also incorporated into the optical receiving circuit. On the other hand, the optical transmission circuit incorporates an LED as a light-emitting device in the 1300 nm band. The optical transceiver is composed of the LED and LED driver. Table 1 shows both O/E and E/O configurations of each module.

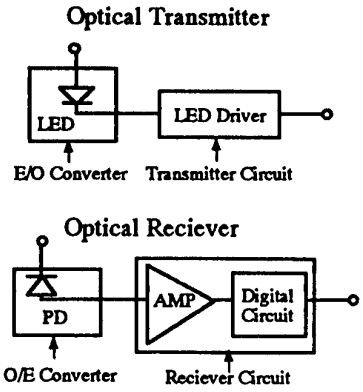



Fig. 1 Block diagram of the circuit

Table 1 List of evaluation samples

| Sample | O/E structure | E/O structure |
|---|---|---|
| No.1 | PD bare chip | LED bare chip |
| No.2 | PD bare chip | LED bare chip |
| No.3 | PD module | LED module |
| No.4 | PD-AMP module | LED module |
| No.5 | PD-AMP module | LED module |
| No.6 | PD-AMP module | LED module |
| No.7 | PD-AMP module | LED module |

### 2.1 Measurement of radiated electric field strength characteristics

Fig. 2 shows a radiated electric field strength measuring system. The 3m method was adopted with an optical transceiver module mounted in an anechoic chamber, and both biconical and log-periodic antennas were employed. To eliminate the influences from electric cables, signals were passed through optical fibers originating from outside of the anechoic chamber. Output signals were transmitted to a bit error rate tester (BERT) installed outside the anechoic chamber and the rate was measured for confirmation of the error free state. The power voltage of +5V was supplied using batteries.

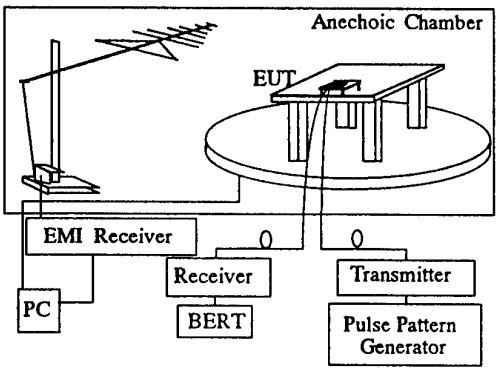



Fig. 2 Radiated electric field strength measuring system

### 2.2 Measurement of near magnetic field distribution

Fig. 3 shows a near magnetic field distribution measuring system. An interference source detecting unit based on an antenna scanning method was mounted on a desk in a shielded chamber, with an optical transceiver module mounted in a reversed manner on the measuring surface of the unit. The input and output digital transmission signals were passes through optical fibers. Output signals were transmitted to the BERT and the BER was measured for confirmation of the error free state. The near magnetic field distribution was measured in this state to identify points with high magnetic strength as interference sources. Power was supplied from a stabilized DC power supply.

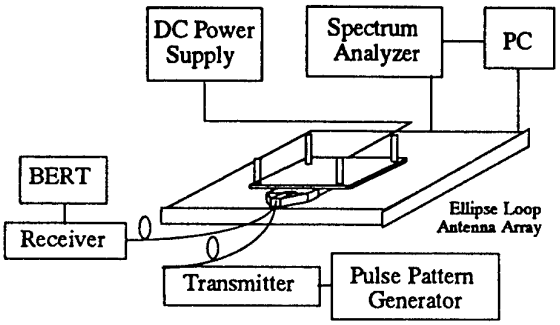



Fig. 3 Near magnetic field distribution measuring system

### 2.3 Measurement of radiated impulse noise immunity

Fig. 4 shows a radiated impulse noise immunity measuring system. An optical transceiver module was mounted within a G-TEM cell. To eliminate influences from coaxial cables, the input and output signals were passed through optical fibers outside the G-TEM cell. Output signals were transmitted to the BERT installed outside the cell, and the rate was measured. The impulse noise that entered the G-TEM cell had a rise time of 1 ns or less, a pulse width of 1 ms, and a pulse cycle of 20 ms. When the optical input power was set to -31 dBm, the maximum applied voltage at which BER of 2.5E-10 was sustained was identified as the immunity level.

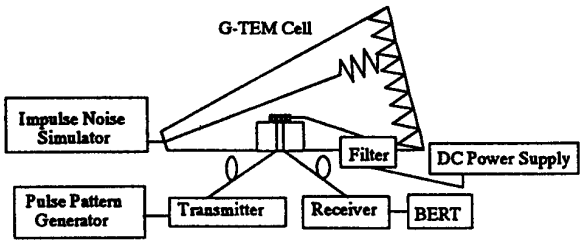



Fig. 4 Radiated impulse noise immunity measuring system

### 2.4 Measurement of the lowest electric/magnetic immunity points

Fig. 5 shows a lowest electric/magnetic immunity point measuring system. An optical transceiver module was mounted on a desk in a shielded chamber, and the input and output signals were passed through optical fibers. Output signals were transmitted to the BERT for confirmation of the error-free state. Electric and magnetic fields were applied under these conditions through a probe. The optical input power was set to -31dBm and the applied voltage of noise generator was gradually increased. The immunity level was identified as the applied voltage at which the data failed. The applied noise was made from dampened oscillations of 10 ms period.

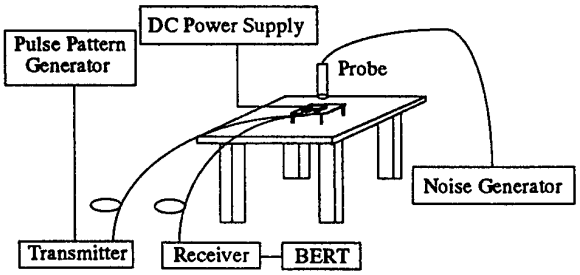



Fig. 5 Electric/magnetic immunity point measuring system

## 3. RESULTS

### 3.1 Characteristics of the radiated emission

Fig. 6 shows a typical example of the measured radiated electric field. A strong peak of radiation was observed at the 8th high harmonic of 500 MHz in the clock frequency of 62.5 MHz.

To estimate the interference source at the frequency at which the above peak was observed, the near magnetic field distribution was measured at 500 MHz. Fig. 7 shows the results of this measurement. Since a strong magnetic field distribution was observed in the section between the LED and the LED driver, this section was estimated to be the interference source. It is presumed that this section acted as the interference source since digital modulation signals with large amplitude were transmitted between the LED and the LED driver, with the wiring acting as an antenna.

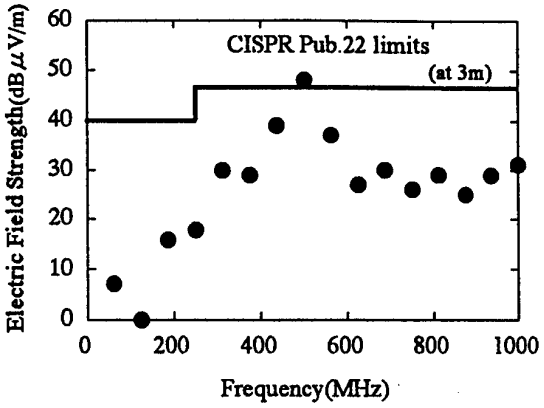



Fig. 6 Far electric field strength measurements

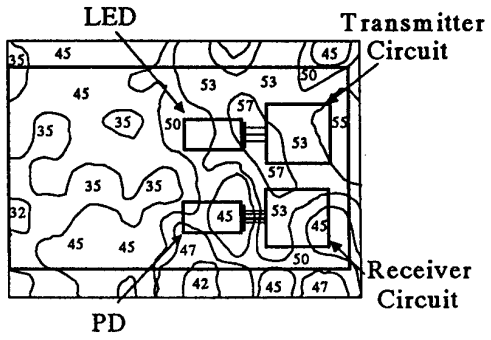



Fig. 7 Near magnetic field distribution measurements

Table 2 shows the measured near magnetic field distributions of all the test samples. The distribution of strong magnetic fields, between the LED and the LED driver of the E/O structures of all the samples, was observed, and it is presumed that these sections acted as the interference sources. However, no distribution of strong magnetic fields was observed in the O/E structure of any of the samples, allowing us to assume that they did not act as interference sources.

Reports [6] have already shown that the peaking effects from deformed pulse waveforms entered into the LED to increase its speed and the radiation characteristics of the optical transmission circuit act as factors that increase the radiated electric field strength of the specific frequencies in the optical transceiver mod-

ules. However, any attempt to change the digital signal waveforms transmitted between the LED and the LED driver is difficult to drive them at high speeds. Therefore, to suppress the radiated electric field strength, it is necessary to reduce the antenna efficiency between the LED and the LED driver.

Table 2 Radiated emission and interference source measurements

| Sample | CISPR limits margin | Interference source |
|---|---|---|
| No.1 | -3.5~-0.5dB | LED~LED driver |
| No.2 | +5.0~+6.0dB | LED~LED driver |
| No.3 | -4.5~-2.5dB | LED~LED driver |
| No.4 | -2.5~-1.5dB | LED~LED driver |
| No.5 | +7.0~+12.0dB | LED driver |
| No.6 | +11.0~+13.0dB | LED |
| No.7 | 0~+2.0dB | LED driver |

### 3.2 Characteristics of the radiated immunity

Fig. 8 shows the measured radiated impulse noise immunity and the lowest electric/magnetic immunity points. The radiated impulse noise immunity level increased as the O/E structure was gradually changed from the bare PD chips to the PD modules and then to the PD-AMP modules. The PD is usually used with reverse bias applied to achieve higher-speed, the impedance being increased in this state, and therefore the PD becomes more noise-sensitive. Moreover, it becomes more noise-sensitive, because the PD output signal current, from the PD to subsequent circuits, is very small and the voltage is amplified by a high-impedance amplifier. It is therefore suggested that the influences of noise are the strongest in the bare PD chips, in which the noise affects the PD more than in the case of the PD modules. The noise is the most suppressed in the PD-AMP modules in which an amplifier and the PD output signal are shielded by a module package. This means that the section from the PD, or the PD-AMP module, to the subsequent circuits acted as an antenna, its influence being observed in the differences in the radiated impulse noise immunity levels.

The immunity at the lowest electric/magnetic noise points was measured using a probe to directly apply noise to an optical transceiver module. Table 3 shows the measured results, for which the same trend was observed that had been obtained in the measurement of the radiated impulse noise immunity. All of the results indicate that the immunity level is the lowest in the section from the PD, or the PD-AMP module, to the subsequent circuits, suggesting that this portion acts as an antenna and is the most affected by the noise. These observations also indicate that the reduction of antenna effects for external electromagnetic field, including the shielding of the O/E structure, are needed to increase the radiated immunity.

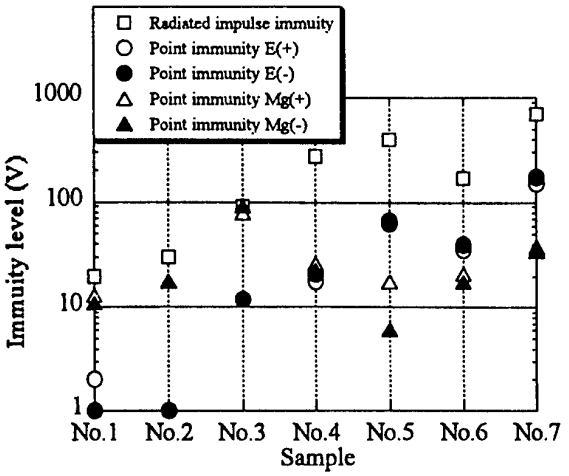



Fig. 8 Radiated impulse and point immunity measurements

Table 3 Lowest magnetic/electric immunity points measurements

| Sample | lowest magnetic immunity point | lowest electric immunity point |
|---|---|---|
| No.1 | PD~AMP | PD~AMP |
| No.2 | PD~AMP | PD~AMP |
| No.3 | PD、Receiver Circuit | all |
| No.4 | PD-AMP | PD-AMP |
| No.5 | PD-AMP~Receiver Circuit | PD-AMP~Receiver Circuit |
| No.6 | PD-AMP、Receiver Circuit | PD-AMP、Receiver Circuit |
| No.7 | PD-AMP~Receiver Circuit | PD-AMP~Receiver Circuit |

## 4. CONCLUSION

We have conducted experimental evaluations of the radiated emission and immunity characteristics of optical transceiver modules. It is found that the section from the LED to the LED driver often acts as a interference source of the radiated electromagnetic noise characteristics while the section from the O/E converter to subsequent circuits acts as an antenna of the radiated immunity. Hence, it is necessary to take appropriate measures against these phenomena.

## 5.REFERENCES

[1] Alina Karwowska-Lamparska, "EMC IN CABLE TELEVISION SYSTEMS", International Wroclaw Symposium on Electromagnetic Compatibility, 1992, pp.181-183.

[2] Hisao-Chang Chu and Chun Hsiung Chen, "Shield ing and Reflection Properties of Periodic Fiber Matrix Composite Structures", IEEE transactions on Electromagnetic Compatibility, vol.38, No.1, 1996, pp.1-6.

[3] Cheng-Kuang Liu and Cheng-Yie Chou, " RF Interference Effects of PIN Photodiodes", IEEE transactions on Electromagnetic Compatibility, vol.37, No.4, 1995, pp.589-593.

[4] Cheng-Kuang,Han-Chang Tsai and Jine-Tine Liou " Effects of AC Interference on Photovoltages of Junction Diodes ", IEEE transactions on Electromagnetic Compatibility, vol.37, No.3, 1995, pp.452-457.

[5] John K Daher, " Measured and Modeled Conducted Susceptibility Characteristics of a Lithium Niobate Electrooptic Modulator", IEEE transactions on Electromagnetic Compatibility, vol.36, No.4, 1994, pp.283-293.

[6] Takeshi Aizawa, Hidetoshi Yamamoto, Shinichi Shinohara, Risaburo Sato, "A Study on Mechanism of Radiated Emissions from Fiber Optical Module", International Symposium on Electromagnetic Compatibility, EMC'99TOKYO, 1999, pp.98-101.

## BIOGRAPHICAL NOTES

**Takeshi Aizawa** received the M.E. degrees from Tokai University, Hiratsuka, Japan, in 1990. He joined Sumitomo Electric Industries, Ltd., and was engaged in development of the optical transmission circuit. Since 1996, he has been engaged in research on EMC of an optical transmission module at the Electromagnetic Compatibility Research Laboratories Co., Ltd.

**Hidetoshi Yamamoto** received the B.E. degree from Osaka University, Osaka, Japan, in 1982. He joined Murata man. co., Ltd., and was engaged in the development of EMI suppression filter. Since 1998, he has been a senior researcher at Electromagnetic Compatibility Research Laboratories Co., Ltd. Presently he is engaged in research on countermeasures technology on EMC.

**Shinichi Shinohara** received the M.E. degrees from University of Electro-Communications, Chofu, Japan, in 1972. He worked in the NTT's Laboratories, and was engaged in development of telephone System. He joined Sony Corporation in 1998. Since 1996, he has been a general manager at Electromagnetic Compatibility Research Laboratories Co., Ltd. Presently he is engaged in research on countermeasures technology on EMC.

**Risaburo Sato** received the Ph.D. degrees from Tohoku University, Sendai, Japan, in 1952. From 1961 to 1984, he was a Professor at Tohoku University. From 1984 to 1999, he was Dean of the Faculty of Engineering of Tohoku Gakuin University, Tagajo, Japan. He is a life member of IEEE of USA and the president of Electromagnetic Compatibility Research Laboratories Co., Ltd.

EMC 2000 INTERNATIONAL WROCŁAW SYMPOSIUM ON ELECTROMAGNETIC COMPATIBILITY

# THE EFFECT OF DISCONTINUITIES ON GROUND/POWER PLANES OF HIGH-SPEED PRINTED CIRCUIT BOARDS

Bertalan Eged, István Gelencsér
Technical University of Budapest, Department of Microwave Telecommunications
Goldmann tér 3. 1111 Budapest Hungary
Phone: +36-1-463-3614 FAX: +36-1-463-3289 e-mail: beged@nov.mht.bme.hu

***Abstract*** *- Power and ground planes are required to have low impedance over a wide range of frequencies. Parallel ground and power planes in multilayer printed-circuit boards exhibit multiple resonances which increase the impedance. When rectangular shape of printed circuit board is not allowed for optimal using of the available physical dimensions the cutted area can be seen as a discontinuity of the plane. This kind of discontinuity can decrease a frequency of resonancies and increase the impedance of the plane pair. Simulation based on transmission line grid model and measurements results are presented for some typical configurations.*

## I. Introduction

For many years of digital electronic designs, a +5V supply voltage for TTL and CMOS logic, and/or a -5.2V supply for an ECL logic was common. With the constant need to decrease power dissipation by reducing supply voltage, and due to submicron silicon feature sizes which limits the breakdown voltage of the silicon at below 5V both in the core and in the I/O area, the supply voltages are on the fall. At the same time, the growing demand for higher data throughputs results in wider buses and higher clock rates. To avoid the runaway of total current requirements of the wider buses, and to reduce the potential EMI risk, too, the signaling voltage drops steadily from generation to generation. Because in every new generation new functionality is added, the growth of the number of I/O lines usually outweighs the decrease of current in one I/O, therefore the net supply current demand is still on the rise. The lower signaling voltage calls for a lower value of tolerable noise on the supply rails, which together with the higher current consumption dramatically reduces the impedance that should be provided by the power-distribution network. [1]

The faster bus signaling also comes with faster edges and transients, requiring a proportionally wider bandwidth in the power-distribution network. A high-end system today with single-ended signaling may have 10A total transient current in the signal-return path of buses, and may require 50mV maximum ripple on the power-distribution network. This converts into 5 milliohms of required power-distribution impedance. With a 0.3...0.6nsec signal transition time, the necessary bandwidth for the power-distribution impedance is 0.5-1GHz. To avoid excessive simultaneous switching noise, the power-distribution network (the power-distribution planes) must exhibit low enough impedance over the full bandwidth of signals.

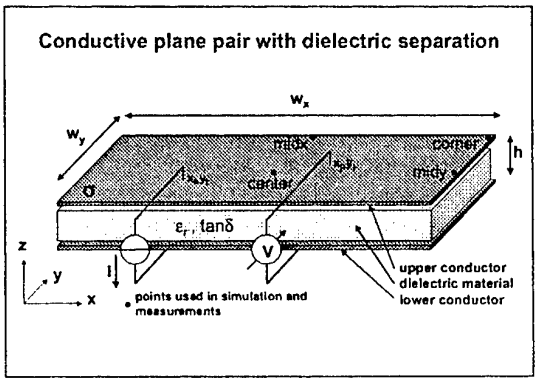



Figure 1. A pair of parallel planes in the Power Distribution System (PDS).

## II. Characterization of power-ground distribution system

For digital electronics below the MHz clock-frequency range, individual traces or metal bus bars were sufficient to distribute ground and power. In the MHz range, the ground traces were gradually replaced with a solid copper layer in the multilayer board, while the power distribution many times still relied on individual traces rather than solid planes. With a solid ground plane, impedance-matched traces also became common.

A solid ground plane serves to distribute power and to carry the return currents of signal traces. With low trace density, the ground plane behaves like an ideal ground. With increasing speeds and trace densities, the inductive and resistive drops along the ground plane have to be considered [2]. In recent years, signal speeds and trace densities reached values such that the return current required solid power planes as well, forming a pair of parallel planes in the Power Distribution System (PDS). (Figure 1)

If the two planes are placed closer, the static capacitance between them is increased, which helps local bypassing, at the same time the return current travels a shorter distance from one plane to the other, such reducing the inductive voltage drop in the PDS. As for signal traces as well, the above lumped approximations, which start out with the static capacitance and loop inductance, are accurate only as long as the dimensions are much shorter (say ten times smaller) than the shortest wavelength of the signals. Signal transition times in high-speed digital systems today are one nsec or less. In FR4 dielectric, the bandwidth of a one nsec transition time signal corresponds to an approximate wavelength of 50 cm. Therefore boards bigger than 5cm in size, with digital signals faster than a nanosecond, the distributed nature of power-ground planes taken in consideration.

Power and ground planes in a multilayer PCB may be considered as two-dimensional transmission lines, where both the x and y dimensions are longer than one tenth of the shortest wavelength of interest. Throughout this paper we assume that the h separation of the planes along the Z axis is still negligible compared to the shortest wavelength.

### II.1. Analytical expression of power-ground plane impedances

In contrast to signal traces where the signal travels along the axis of signal conductor, the wave generated by an injected signal between the planes launches a radially expanding wave. Two-dimensional transmission lines are therefore also referred to as radial transmission lines. The self and transfer impedances of radial transmission lines with rectangular or circular shapes can be analytically calculated. Impedances of square-shaped parallel planes are widely analyzed in the literature for planar microwave circuits and printed antennas. Analytical formulation is given, e.g. in [3], [4]. Assuming infinitesimally small port sizes, and open boundaries at the edges, the generalized transfer impedance between ports i and j (at coordinates $x_i$,$y_i$ and $x_j$,$y_j$ respectively) of a pair of parallel, rectangular planes with side dimensions $w_x$ and $w_y$ along the x and y axes, with plane separation (dielectric height) of h along the z axis, can be written as.

$$Z_{i,j} = \frac{\mu h \chi_{mn}^2}{w_x w_y} \sum_{m=1}^{\infty} \sum_{n=1}^{\infty} \frac{j\omega}{k_m^2 + k_n^2 - k^2} C \qquad (1)$$

$$C = \cos k_x x_i \cos k_y y_i \cos k_x x_j \cos k_y y_j \qquad (2)$$

where $m$ represents the $m$th mode associated with the x-dimensions, $n$ represents the $n$th mode associated with y-dimensions, k represents the real wavenumber for lossless case, $k = \omega\sqrt{\mu\varepsilon}$, $k_m = m\pi/w_x$, $k_n = n\pi/w_y$. The constant $\chi_{mn}$ =1 for $m$=0 and $n$=0, $\sqrt{2}$ for $m$=0 or $n$=0, 2 for $m \neq 0$ ,$n \neq 0$. When considering a low-loss case $k$ is complex: $k = k_r - jk_i$ where $k_r$=$k$ above and $k_i = (k_r/2)(\tan(\delta) + (r/h))$, where $\tan(\delta)$ is the loss tangent of the dielectric, $r$ is the skin depth in the metal plane.

The analytical expression is not limited by finite spatial granularity like transmission line grid model, but is has a double infinite series, which for practical calculations must be truncated which leads to introducing error in calculation [5]. The above $Z_{(j\omega)}$ expression is good for numerical calculation, but not well suited for circuit simulation where the planes have to be simulated with the whole part of electronics. For circuit simulations, either a macromodel can be generated [6], or an electrical equivalent circuit of the pair of planes is formed.

### II. 2. Transmission line grid equivalent circuit model of power-ground plane

A pair of parallel planes can be simulated by an equivalent circuit of a grid of transmission lines, as described in e.g., [7], [8]. The low-frequency equivalent components of the planes can be derived from a quasi-static model. We assume a pair of rectangular planes with dimensions of $w_x$ and $w_y$. First we define the $u$ size of the square unit grid cell, which should be equal to more or less than 10% of the shortest wavelength of interest. The $u$ cell size is selected such that we have an integer $N_x$ and $N_y$ number of cells along the x and y axes, respectively. For every unit square of the planes with side dimensions of $u$, plane separation (dielectric height) of $h$, the $t_{pd}$ propagation delay along the edge of the unit cell and the $C$ static plane capacitance can be calculated.

$$t_{pd} = u\frac{1}{c}\sqrt{\varepsilon_r} = u\sqrt{\varepsilon_r}\sqrt{\varepsilon_o \mu_o} \qquad (3)$$

$$C = \frac{u^2}{h}\varepsilon_r \varepsilon_o \qquad (4)$$

From the capacitance and delay, an equivalent $L$ inductance and $Zo$ characteristic impedance of the unit cell can be calculated.

$$L = \frac{t_{pd}^2}{C} = h\mu_o \qquad (5)$$

$$Zo = \sqrt{\frac{L}{C}} = \frac{h}{u}\frac{1}{\sqrt{\varepsilon_r}}\sqrt{\frac{\mu_o}{\varepsilon_o}} \qquad (6)$$

In the above expressions, all input and output parameters are in SI units, $\varepsilon_o = 8.86*10^{-12}$ [As/Vm] the dielectric constant in Vacuum, $\mu o = 4*10^{-7}$ [H/m] is the permeability of Vacuum.

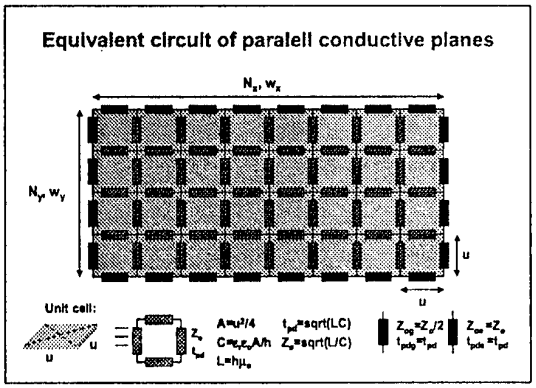



Figure 2. Equivalent circuit representation of parallel conductive planes with a rectangular grid of transmission lines.

The unit cells are replaced by four transmission lines along the edges of unit cells, (Figure 2), each transmission line representing the same delay but only one quarter of the area, thus having an impedance of 2Zo. Inside the equivalent grid, where the sides of unit cells touch, the capacitance of transmission lines are doubled, reducing the characteristic impedance to 2Zo/sqrt(2). Along the outer edges, the unit-cell transmission lines are standing alone. The parameters for the edge (Zoe, tpde) and grid (Zog, tpdg) transmission lines are.

$$Zog = \sqrt{2}Zo \quad tpdg = tpd/\sqrt{2} \qquad (7)$$

$$Zoe = 2Zo \quad tpde = tpd/\sqrt{2} \qquad (8)$$

The sqrt(2) correction factor in delays are used to match the equivalent circuit's delay along the x and y axes [10]. Alternative equivalent circuits may use lossless LC ladder [9] or lossy transmission lines [10], [11] representation of each transmission-line segment. For all simulations presented in this paper, lossless transmission line grids were used.

Note that the grid takes the effect of edge discontinuity into account to some extent by using twice the characteristic impedance of transmission lines along the edges. The transmission line model can be used easily for simulation of power planes and the other components of the circuit including the dissipative edge termination [11] used for reducing the effect of the resonance behaviour. The price of this feature of the model is the spatial granularity of the transmission line grid.

### III. Simulation of the truncated power-ground plane pairs

In some applications the rectangular shape of printed circuit board is not allowed for optimal using of the available physical dimensions. Typical case when the power supply units are placed in one corner of the box and the rectangular PCB should be truncated. This can be seen as a discontinuity of the rectangular PCB. In our simulation and measurements we examined two basic discontinuity configurations with two different size of cutting area. These basic shapes are the corner cutted and center cutted shapes. (Figure 3) The impedance of the full rectangular plane was calculated and simulated too, as a reference.

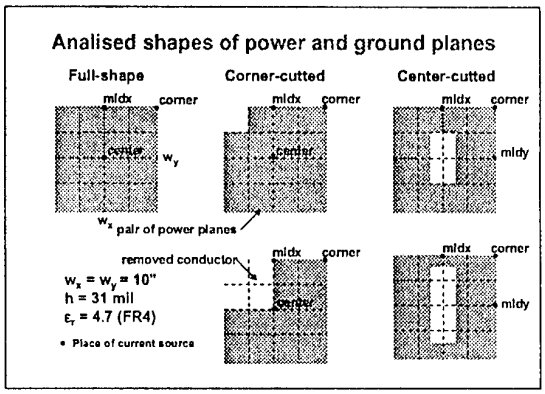



Figure 3. Cutted shapes of power-ground planes

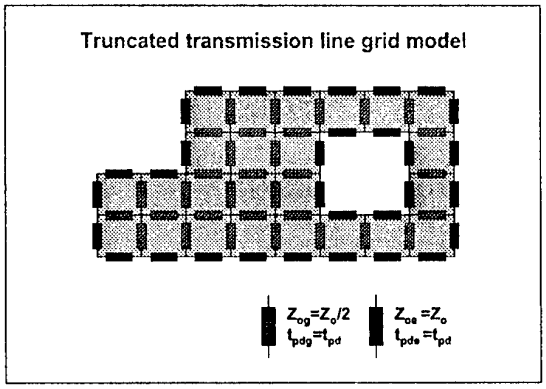



Figure 4. Transmission line grid model used in the simulation of the discontinuity of planes

Three representative points were defined on all kind of shapes for simulation and measurements called 'midx', 'corner' and 'center'. Instead of 'center' on the center cutted shape the 'midy' was used. (Figure 3) The self impedances eg. $Z_{(midx,midx)}$ of these points were simulated and measured, so it

means 3 different results for all of the analysed shapes.

The full transfer impedance profile of the planes at a given frequency was not determined like in [11]. In the high-speed digital applications when a driver pulls current from the power and ground planes, the current creates a voltage drop according to the impedance of the plane at that point and the noise voltage is propagate along the plane to the other places. This effect is known as delta-I noise. [12] So instead of plotting the transfer impedance of the pair of power planes at a given frequency, it is more effective plotting the maximum amplitude of the noise voltage as a function of phisical dimensions with a given place of current pulse source. The noise voltage can be simulated by a simple transient simulation of the transmission line grid model or can be calculated using FFT from the frequency domain impedance data.

In our simulation instead of the full transfer impedance profile the time-domain response was computed using FFT. The resonance nature of the impedance leads to ringing in time-domain. We can sign the maximum amplitude (positive or negative peak) of the time domain ringing and draw the 'noise map' of the analysed plane. The simulated and measurements results are presented in the following sessions.

The truncated transmission line grid was used for simulating the cutted plane pairs, which is equivalent to the model described above, but the effect of open terminated nature of the cutting edge is modelled with a double impedance of the transmission lines. (Figure 4)

### III. 1. Impedances of the reference shape

The impedances of the full-shaped power plane was calculated by analytical expression and simulated using the transmission line grid model by SPICE circuit simulator for using as a reference. Three self impedance profiles as a function of frequency were calculated by the analytical expression using N=10 and M=10 summation limit. (Figure 5)

The reference plane was simulated by SPICE simulator using the transmission line grid model using u=0.5 inch grid spacing, and lossless T lines models were used. The impedance profiles near exactly same as from the calculation. (Figure 6)

In Fig. 7 we can see a typical time-domain response of the power plane for a 1A current step which shows its ringing nature. We can generate the noise map of the entry plane by measuring the maximum of the ringing of noise voltage in the grid points. (Figure 7 and 8)

As we can see from the calculated and simulated impedance profiles the low-frequency response is a capacitive downslope to the first serial resonant of the static capacitance and the whole spreading inductance

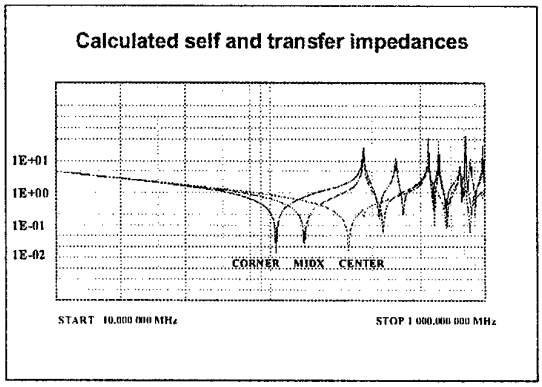



Figure 5. Calculated impedances of the reference plane using N=M=10 summation limit

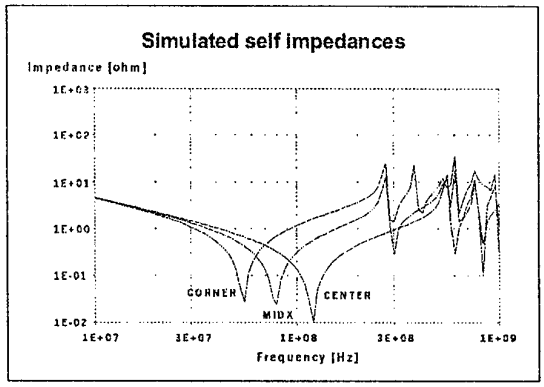



Figure 6. Simulated impedances of the reference plane using u=0.5 inch grid size by SPICE

On the other hand we can see the first resonant as the frequency where the length of the radial transmission line from the open terminated edge to the point of the current source is one quarter of the wavelength. This nature of the first serial resonant can be seen in the pictures where the lowest frequency produced at the corner and the resonant frequency is increased as we move the observing points to the midx and center respectively.

The effects of the discontinuity of the planes like cutting of the corner or center lies in this nature. When the length of the first reflection points of the radial transmission line decreased the resonant frequencies is increased. On the other hand the total static capacitance of the shape is decreased with the decreased area of the planes and it leads to the increased resonance too

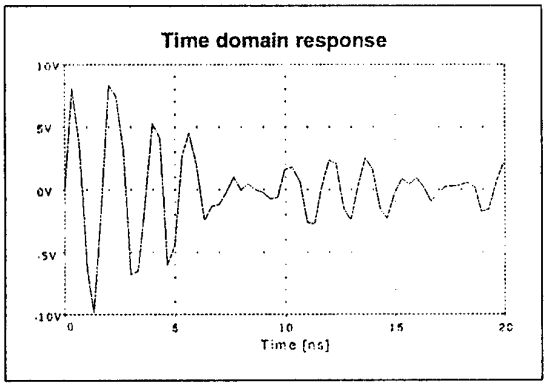



Figure 7. Typical time-domain voltage waveform response to the 1A current step

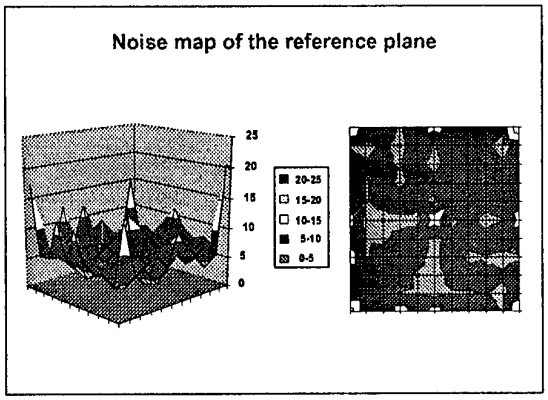



Figure 8. Noise map of the plane by signing of the peak noise voltage as the function of dimension

### III. 2. Simulation of the truncated shapes

For the analysis of the effects of discontinuity the truncated transmission line grid model was used in the simulation. (Figure 4) In this model at the open edge of the plane the higher characteristic impedance of the line should be used.

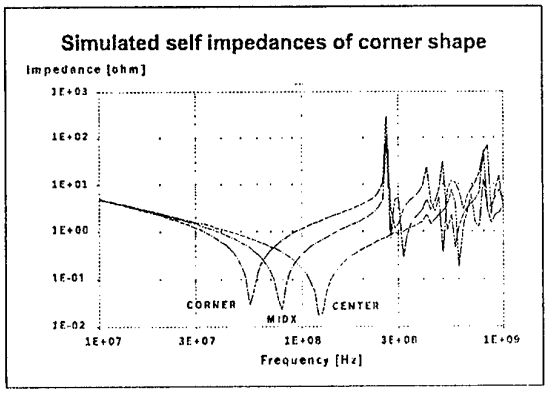



Figure 9. Simulated impedances of the corner cutted shape

The u=0.5 inch grid size was used for simulation as in the reference case. This grid size limited the possible place of cutting of PCB. This is one of the limitations of this kind of modelling the power planes. The simulation was done at three places of the current source midx, corner and center on corner cutted shape and midx, corner and midy on the center cutted shape. (center point is not useable on the center cutted shape)

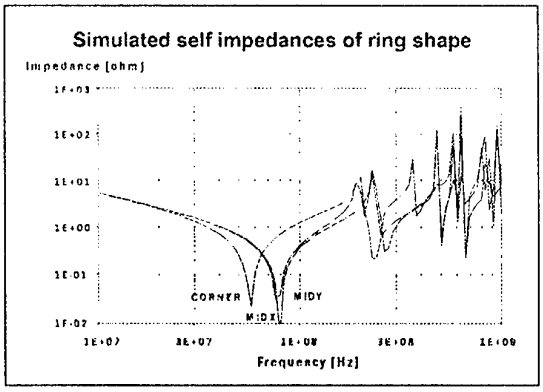



Figure 10. Simulated impedances of the center cutted shape

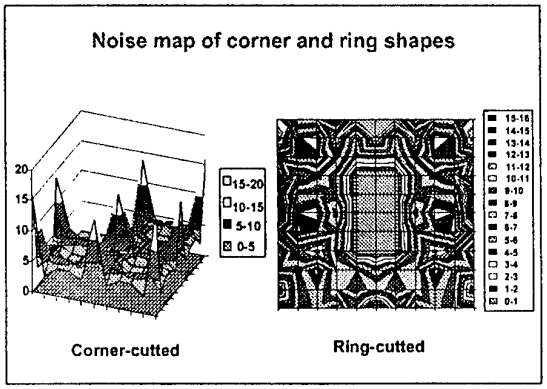



Figure 11. The noise map of the cutted shapes

### IV. Measurement results

To correlate simulated and measured impedances, a 10 by 10 inch square pair of planes was selected with 31 mil FR4 dielectric material.

Self and transfer impedances were measured with HP8720 vector-network analyzers in the 300kHz-3GHz range, respectively. The probe connections, calibrations, conversions from S parameters to impedances were according to [13].

To improve the measurement accuracy at low impedance readings, two-port S21-based self-impedance measurement was used. The S21 parameter readings were converted to self impedance values by the Z=25*S21 approximate formula [13].

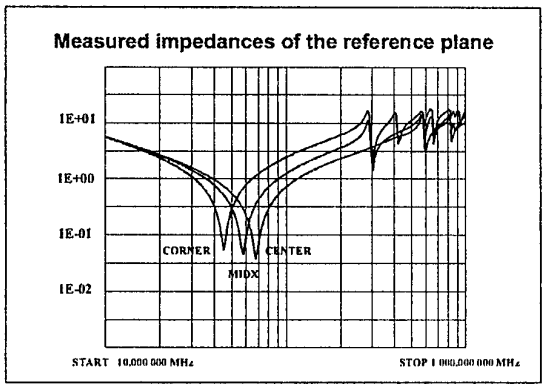



Figure 12. Measured impedances of the reference plane at the representation points

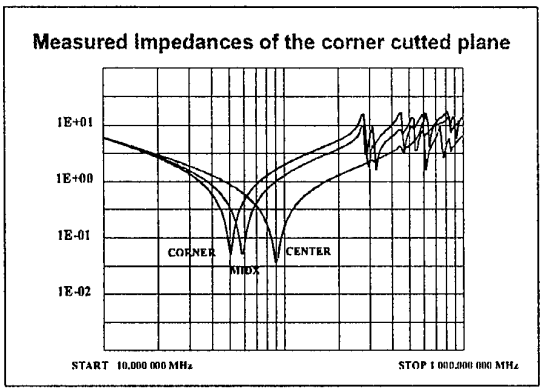



Figure 13. Measured impedances of the corner cutted plane in midx, corner and center points

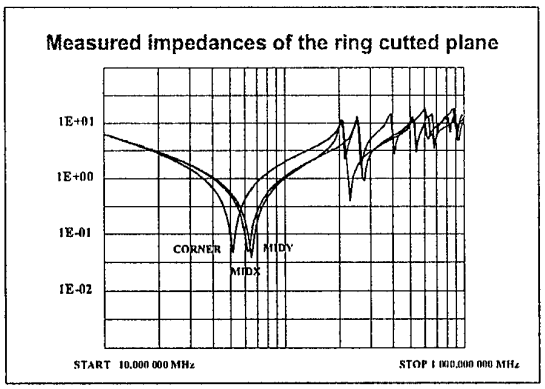



Figure 14. Measured impedances of the ring cutted plane in midx, midy and center points

## V. Conclusions

Power-ground planes in multilayer printed-circuit boards with open edges behave like radial transmission lines, and exhibit multiple resonance frequencies.

The self impedances plots exhibit the first minimum at a frequency where the distance from the probe location to the open boundary corresponds to one quarter of the wavelength. The resonance frequency shifts higher when the shape of the board is not rectangular and the lowest distance of the open boundary less than the original dimensions of the planes. The whole static capacitance of the plane is reduced by the cutting which leads to the shifting of the first resonance higher

## References

[1] Larry D. Smith, "Packaging and Power Distribution Design Considerations for a SUN Microsystems Desktop Workstation," in Proceedings of the 6th Topical Meeting on Electrical Performance of Electronic Packaging, October 27-29, 1997, pp.19-22.

[2] R. Senthinathan, A. C. Cangellaris, J. L. Prince, "Reference Plane Parasitics Modeling and Their Contribution to the Power and Ground Path "Effective" Inductance as Seen by the Output Drivers," IEEE Transaction on Microwave Theory and Techniques, Vol. 42, No. 9, September 1994, pp. 1765-1773.

[3] T. Okoshi, T. Miyoshi, "The Planar Circuit – An Approach to Microwave Integrated Circuit," IEEE Transaction on Microwave Theory and Techniques, Vol. 20, No. 4, April 1972, pp. 245-252.

[4] K. R. Carver, J. W. Mink, "Microstrip antenna technology," IEEE Transactions on Antennas and Propagation, AP-29, pp. 2-24, January 1981.

[5] I. Novak, "Accuracy Considerations of Power-Ground Plane Models," in Proceedings of the 8th Topical Meeting on Electrical Performance of Electronic Packaging October 25-27, 1999, San Diego, CA, pp. 153-156.

[6] Nanju Na, Madhavan Swaminathan, "Modeling and Simulation of Planes in Electronic Packages for GHz Systems," in Proceedings of the International Conference on Computer Design, October 1999, pp. 149-152.

[7] E. Leroux, P. Bajor, "Modeling of Power Planes for Electrical Simulations," Proceedings of the 1996 Wroclaw EMC Symposium, pp. 664-668.

[8] K. Lee, A. Barber, "Modeling and Analysis of Multichip Module Power Supply Planes," IEEE Transactions on Components, Packaging, and Manufacturing Technology - Part B, Vol. 18, No. 4, Nov. 1995, pp. 628-639.

[9] C. B. O'Sullivan, L. D. Smith, D. W. Forehand, "Developing a Decoupling Methodology with SPICE for Multilayer Printed Circuit Boards," in Proceedings of the 1998 International Symposium on Electromagnetic Compatibility, Aug 1998, Denver, CO, pp. 562-565.

[10] H. H. Wu, J. W. Meyer, K. Lee, A. Barber, "Accurate Power Supply and Ground Plane Pair Models," in Proceedings of the 7 th Topical Meeting on Electrical Performance of Electronic Packaging, October 26-28, 1998, pp.163-166.

[11] I. Novak, "Reducing Simultaneous Switching Noise and EMI on Ground/Power Planes by Dissipative Edge Termination," IEEE Tr. CPMT, Vol.22, No.3, August 1999, pp.274-283.

[12] Y. Chen, Z. Chen, J. Fang, "Optimum Placement of Decoupling Capacitors on Packages and Printed Circuit Boards Under the Guidance of Electromagnetic Field Simulation," in Proceedings 46th Electronic Components & Technology Conference, May 28-31, 1999, Orlando, FL, pp.756-760.

[13] I. Novak, "Probes and Setup for Measuring Power-Plane Impedances with Vector Network Analyzer," in Proceedings DesignCon99, High-Performance System Design Conference, February 1-4, 1999, Santa Clara, CA, pp.201-215.

EMC 2000 INTERNATIONAL WROCŁAW SYMPOSIUM ON ELECTROMAGNETIC COMPATIBILITY

# A Hybrid Electrical-Optical Interconnection Technology for Printed Circuit Boards

Elmar Griese
Siemens AG IC C-LAB
Fürstenallee 11 · 33094 Paderborn · Germany
Email: eg@c-lab.de

***Abstract*** *— A new interconnection technology for printed circuit board applications is presented which is able to meet the high performance requirements of future electronic equipment while at the same time the electromagnetic compatibility (EMC) is improved significantly. Moreover, this technology has a far-reaching compatibility with the conventional pc board technology, which means that the existing design and manufacturing processes of the electrical part do not need significant modifications. The application of this hybrid technology enables completely new and highly capable architectures for computers and other information and communication equipment. After a description of the most important basic technologies for its realization first engineering samples are presented. In the second part the paper focuses on the modeling of electrical-optical interconnects. Especially the transient analysis is addressed. The developed overall modeling strategy is explained and available results are presented. Apart from a time domain simulation model for optical multimode waveguides the corresponding modeling approaches for laser- and photo diodes are presented.*

## 1. INTRODUCTION

Microprocessors of the next generation provide on-chip clock frequencies above 1 GHz. The theoretically resulting system performance can be obtained only if the off-chip interconnection technology provides a sufficiently high bandwidth. This need for off-chip bandwidth will become even stronger in the near future because in the next 10 to 12 years the further development of the semiconductor technology will not be limited by fundamental physical effects and microprocessors operating at on-chip clocks of about 10 Ghz are expected to be available in 2011 [9]. Due to this technology innovation the challenge of getting signals in the GHz frequency range off-chip and into the system after packaging is even greater than the challenge of on-chip performance at this frequency [8]. As the performance of electrical interconnects is limited due to dispersion, emission of and susceptibility against electromagnetic radiation, optical solutions for intra-system interconnects can be used in order to provide the required high-bandwidth interconnects. Moreover, optical interconnects do not radiate themselves and they are completely insensible against electromagnetic radiation.

## 2. OPTICAL INTERCONNECTION TECHNOLOGY

Since printed circuit boards will continue to be among the most important components of electronic equipment, advanced concepts and technologies are necessary in order to provide these components with the required high-bandwidth properties. Taking into account that not every interconnect has to be designed for high-bandwidth data transmission, approaches are necessary which provide easy, robust, as well as cost efficient solutions.

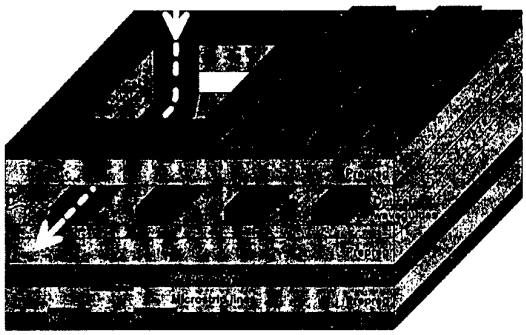


**Fig. 1:** Concept of a pc board with integrated optical waveguides

This means that furtheron conventional pc board technology is sufficient for a lot of low-bandwidth interconnects. Therefore, the only practical and acceptable solution is the extension of conventional multilayer pc boards by optical interconnects (figure 1). This can be realized by the integration of passive optical layers. This solution is able to combine the advantages of microelectronics and optics and it avoids most disadvantages of both technologies. Furthermore, the EMC behaviour of pc boards based on this technology can be improved significantly.

### 2.1. Requirements

There are a lot of requirements which have to be taken into account during the development of this new hybrid technology. The overall one is to guarantee compatibility with the existing processes for designing and manufacturing pc boards. The manufacturing tolerances of the optical interconnects or optical layers, respectively, have to be comparable to the existing tolerances acceptable for electrical layers and transmission lines. This in turn determines the cross sectional sizes of the optical waveguides, which have to be in the range of those of microstrip lines (approx. $100 \times 100\,\mu m^2$). Another very important demand is to guarantee surface mounting and pick and place assembly of the optical transmitter and receiver modules with the exiting assembly and placement equipment used for electrical pc boards. Both above mentioned requirements can only be fulfilled using optical multimode technology. Taking into account practicable optical transmitters (e. g. vertical cavity surface emitting lasers) emitting at a wavelength of 850 nm, the optical interconnects are highly multimodal, which means the waveguides are guiding more than 1000 propagating modes.

Within the standard lamination process of pc boards the optical layers have to withstand during a time period of 50 to 70 minutes high temperatures of about 180°C at a pressure of about

150 N/cm$^2$ and more. Furthermore, the soldering of pc boards has to be taken into account where the temperature reaches during the reflow process 230°C. This temperature will still increase taking into account the unleaded soldering, to be introduced in only a few years.

Apart from these technological demands there are also functional demands. The most important one is, that the wiring of optical waveguides requires those degrees of freedom obvious for wiring electrical lines. This means, not only straight point–to–point interconnects are needed but also arbitrary multi–point interconnects, e. g. necessary for bus interconnects. The realization of multi–point interconnects requires passive optical structures (e. g. splitters, combiners, etc.). The need for these passive optical components excludes a fiber-in-board approach, where optical multimode fibers are integrated into a pc board [10]. A practical solution can only be based on processes which allow the manufacturing of all needed interconnection types within separate optical layers. Due to the temperature and pressure conditions mentioned above, these optical layers should be integrated *into* the pc board, where they can be protected against these unfavourable conditions.

### 2.2. Manufacturing and integration of optical layers

To be compatible with the multilayer pc board manufacturing process the optical interconnects are realized within one or more separate optical layers which are manufactured by a hot embossing process [5]. This optical layer is a foil consisting of a cladding–core–cladding combination and its fabrication is compatible to standard lamination processes. One possible way of fabrication is based on the structuring of a polymer foil, filling the resulting grooves with prepolymeric core material, and curing. Finally, a second polymer foil is laminated on the first one (figure 2) [2].

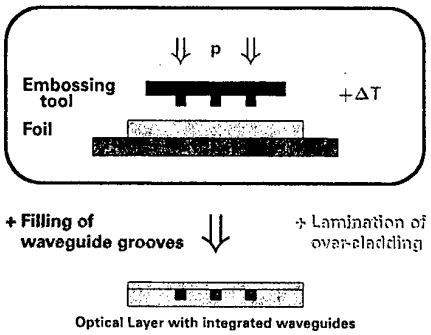



**Fig. 2:** Manufacturing of optical layers by means of hot embossing

This approach provides the degrees of freedom necessary for wiring the *optical* signals and the capability to realize optical multi-point interconnects. The required embossing tool can be manufactured by realizing a primary structure — the master — by UV deep lithography and a following electro-forming process in order for instance to get a Nickel stamping die [5]. Depending on the tool manufacturing process and the hot embossing process itself very accurate surface qualities can be obtained. The remaining surface roughness can be investigated experimentally, e. g. by the atomic force microscopy. The maximum depth was measured as far below 100 nm but it has to be taken into account that it depends strongly on the manufacturing of the embossing tool.

The next step is to integrate the optical layers into pc boards without a significant modification of the established pc board lamination process. First experimental results (figures 3 and 4) show that there seem to be no major problems which could not be solved. Of course the limited resistance against heat and pressure of the polymeric material used for the optical layer has to be taken into account and an improvement of these properties could be helpful.

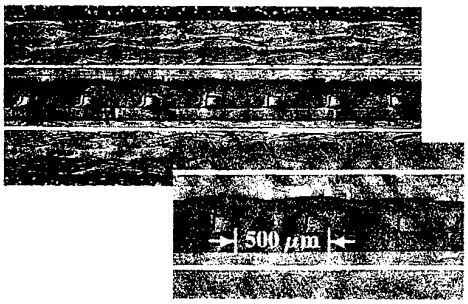



**Fig. 3:** Cross section of a pc board with 4 electrical layers and integrated optical waveguides

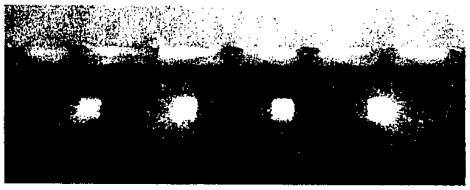


**Fig. 4:** Printed circuit board with integrated optical waveguides, illuminated by VCSELs

Moreover, different coupling concepts based on direct and indirect coupling using 45° mirrors have been investigated and successfully demonstrated. The corresponding modules providing the coupling of the optical transmitters (VCSELs) and receivers (photo diodes) to the waveguides are currently under development.

## 3. MODELING OF MULTIMODE INTERCONNECTS

With the drastically increasing clock speed of computing hardware modeling and simulation of interconnects is of rapidly growing importance. Optimization and prediction of timing behaviour and signal integrity of all interconnects of a system during the design phase is a very expendable task taking into account the complexity of todays electronic equipment.

First applications of this new optical interconnection technology will contain separate coupling modules and the timing and signal integrity analysis has to be applied to hybrid electrical-optical interconnects depicted in figure 3. Simulation models and algorithms to predict timing and signal integrity of electrical interconnects became established for many years [7]. Comparable models allowing time domain analysis of highly multimode waveguides are not available which means that a transient analysis of interconnects depicted in figure 3cannot be performed with available simulation algorithms and tools, respectively.

### 3.1. Modeling of waveguides

The modeling of optical interconnects for a transient analysis is very closely related to the capabilities for modeling highly

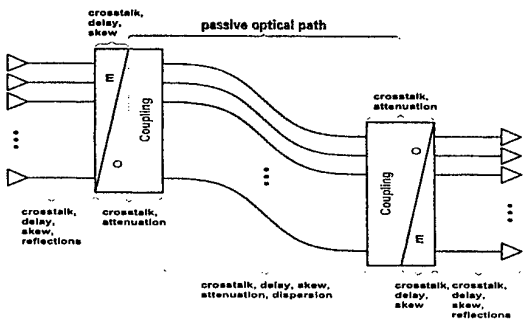



**Fig. 5:** Parallel electrical-optical interconnects and the physical effects to be considered

multimodal waveguides which is a challenging task. Due to the large transversal dimensions of the waveguides, compared to the wavelength of light, there are more than 1000 propagating modes [4]. Furthermore, the boundaries of waveguides manufactured by hot embossing show a non-negligible roughness leading to additional losses and to crosstalk. Another problem is to find an appropriate and practicable way to describe the surface roughness by a limited set of parameters or functions, respectively, which can be determined very precisely. Due to these waveguide properties conventional numerical methods for the analysis of optical waveguides like BPM and FEM are not applicable for practical algorithms and tools. Even if the numerical complexity leads to trustworthy results, the acceptance of tools based on such an analysis approach is very low, taking into account the huge need of computer memory and the expected huge numerical effort leading to extremely high computation times.

As the geometrical dimensions of the waveguides are much larger than the emission wavelength of laser diodes, geometrical optics can be applied in order to model and to simulate signal propagation within these optical multimode waveguides. This wellknown analysis method, called ray tracing, has to be extended for being able to consider the influence of surface roughness on electromagnetic wave propagation. As the local scattering behaviour of a ray is approximately equivalent to the scattering of a plane wave by a rough surface the required new *ray tracing boundary conditions* can be derived from the general scattering problem of a plane wave by a rough surface separating two dielectric media. Assuming slight roughness depths (compared to the wavelength) a first order pertubation theory was applied and explicite, polarization dependent formulas could be derived describing the scattered reflected and scattered transmitted optical power [1]. In these representations the surface roughness is described by its autocorrelation function which can be approximated very well by a declining exponential function [3] characterized by only three parameters, being the root mean square $B$ of the roughness depth and the correlation lengths $D_y$ and $D_z$, respectively. Examples of a calculated reflected and transmitted spectrum are given in figures 6 and 7.

In a second step these *ray tracing boundary conditions* were integrated into a ray tracing formalism, where the following described problem had to be solved. At the rough interface every incident ray is divided into continuous spectra of reflected and transmitted plane waves or rays, respectively. This means that the number of rays to be observed is increasing drastically and even the largest super computer would not be able to provide enough memory and acceptably short computation times following the conventional ray tracing methodology.

A more efficient approach is a Monte Carlo based ray tracing where every scattering event generates only one new ray. The properties of this new ray, which are the polarization, the

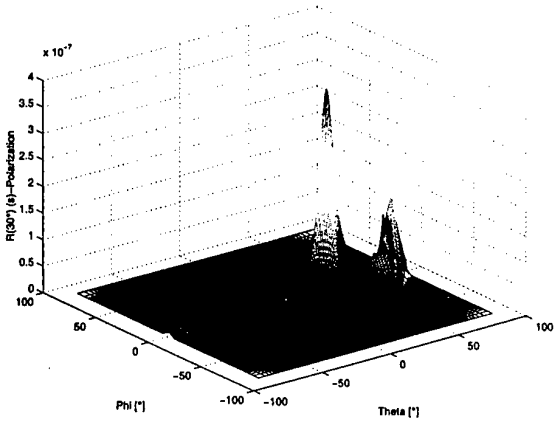



**Fig. 6:** Reflected scattering spectrum of a rough surface ($\theta_i$=30°, $n_1$=1.5, $n_2$=1.45, $D_y$=$D_z$=1.0 $\mu$m, $B$=70.7nm)

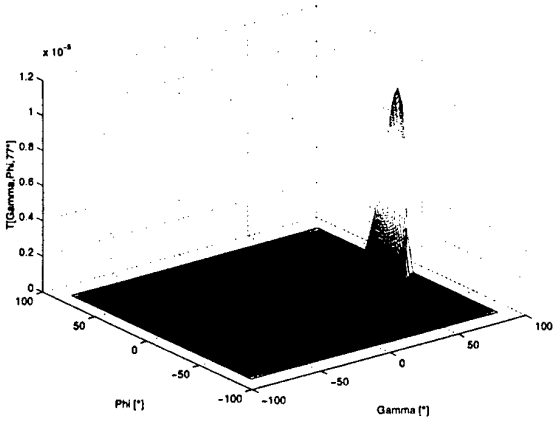



**Fig. 7:** Transmitted scattering spectrum of a rough surface illuminated by a plane $s$-polarized wave ($\theta_i$=77°, critical angle of total reflection: $\theta_c$=75.16°)

propagation direction, and of course the decision whether it is a reflected or transmitted one, are determined by a random process where the required probability density functions are derived from the reflection and transmission spectra computed before. After a large number of very simple and therefore fast calculations the real propagation behaviour can be approximated in an acceptable way. This new method was verified by analyzing a slab waveguide which was chosen because its modes can be determined very easy and very accurately . In case of highly multimodal waveguides with arbitrary cross sections the determination of the modes is in general nearly impossible. Results of this new method were compared with results obtained by the Coupled Power Theory [6]. This method is based on wave optics and it describes the power of the propagating waveguide modes versus the axial coordinate of the waveguide. The ray tracing results were transformed into an equivalent power distribution of the waveguide modes. The comparison shows a very good agreement (figure 8).

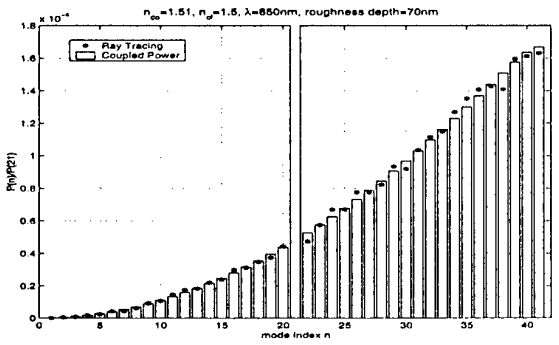



**Fig. 8:** Normalized power of all 41 guided modes of a slab waveguide excited by the 21st guided mode calculated by the Coupled Power Theory and the Monte Carlo based ray tracing

### 3.2. Modeling of optical transmitters and receivers

The approach to model the optical behaviour of the optical transmitters (VCSELs) and receivers (photo diodes) has to be compatible with the ray tracing modeling approach for the multimode waveguides. This means, that the optical output and input behaviour of these active components has to be modeled by rays as depicted in figure 9. In order to minimize the number of model parameters a macro modeling approach was chosen. This approach is based on the description of the input and output behaviour solely and does not describe the internal physical effects of the components.

**Modeling of vertical cavity surface emitting lasers:** A laser diode can be modeled very effectively by a macro model which

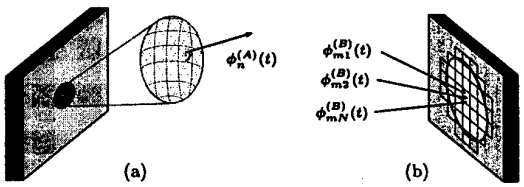



**Fig. 9:** Ray tracing compatible modeling of the optical output behaviour of VCSELs (a.) and the optical input behaviour of photo diodes (b.)

consists of two circuits, each describing the static and dynamical input and output behaviour. Both circuits are coupled by an appropriate control quantity of the input circuit which controls a voltage or a current source being part of the output circuit. The physical output quantity of a laser diode is the optical power which will be represented in the following by an appropriate voltage. This proceeding enables the modeling of the optical part through active and passive *electrical* components which is a precondition for an easy integration of the models into existing simulation tools for pc board analysis.

As the passive optical path is analyzed by ray tracing, the optical output behaviour of a laser diode has to be modeled by a finite number of rays. Each ray describes the optical power emitted into a finite steradian element and is characterized by its starting point, its direction, and its carried power. This results in a multiport representation with one electrical input and $N$ optical outputs each representing the dynamical behaviour of the optical power of one initial ray (figure 10).

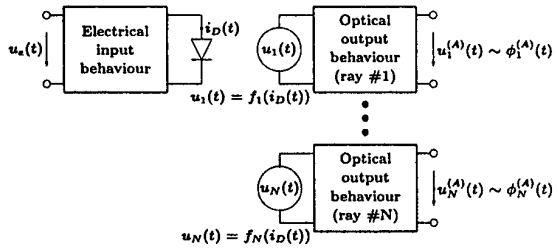



**Fig. 10:** Structure of a macro model of a laser diode to consider the spatial distribution of the emitted optical power

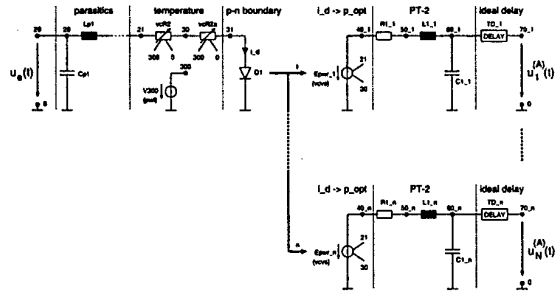



**Fig. 11:** Ray tracing compatible equivalent circuit of a laser diode

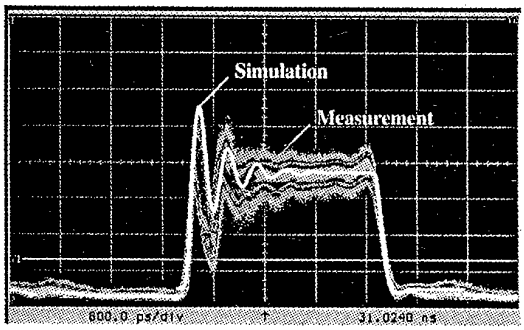



**Fig. 12:** Optical output power of a VCSEL

A HSPICE implementation of this model is shown in figure 11. In a first step the total optical output power of a VCSEL was modelled and compared with measurements (figure 12). Although the rising edge shows a completely different behaviour as the sloping edge, the simply structured circuit is able to model this effect very accurately.

**Modeling of photo diodes:** The ray tracing equivalent modeling of photo diodes can be realized by a model structure depicted in figure 13. Again a macro modeling approach was chosen in order to limit the number of model parameters. The depicted model is able to take into account a location- and angular dependent sensitivity of the photo diodes active area. The most important elements of this model are the voltage controlled current sources $Q_{mn}$, the circuits $N_{mn}$, and the output network $N_D$. In this model each node $m$ is the root of a sub-tree which represents the $m$th discrete element of the photo diodes active area. With the $n$ branches of each sub-tree the angular dependent sensitivity of each element can be modeled. The optical power of each incident ray is described by an equivalent voltage $u_{mn}(t)$ which yields through the current source $Q_{mn}$ to a partial photo current, where the dependence of $Q_{mn}$ on the voltage $u_{mn}(t)$ is given by the corresponding angular dependence. With the circuits $N_{mn}$ the dependence of the sensitivity on the location — including special delays — can be modeled. The output circuit $N_D$ contains elements to describe the intrinsic resistance and capacitance as well as the parasitic effects of packaging. This model was implemented into HSPICE and in a first step it was parameterized for the dc-behaviour. The comparison of simulation results with measurement results shows a very good agreement.

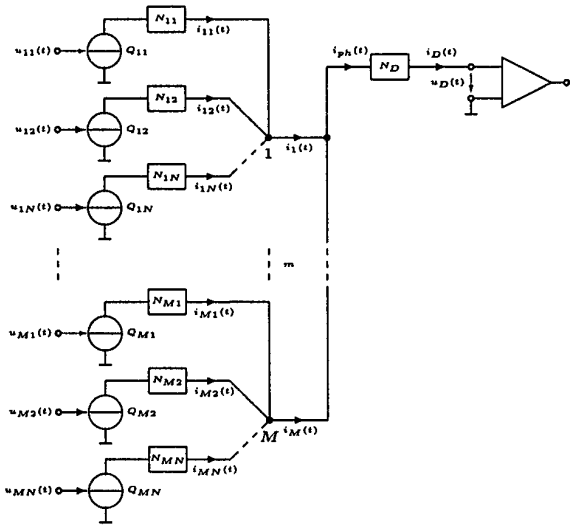


**Fig. 13:** Structure of a macro model of a photo diode considering the location- and angular dependent sensitivity

### 3.3. Approach to model the optical multimode path

In the following a modeling approach is described which enables a time domain analysis of multimode waveguides where the characterization of the passive optical path is performed by ray tracing. For simplification, but without loss of generality, the angular dependent sensitivity of the photo diode is omitted in the following. A later extension of the modeling approach for being able to consider this photo diode property do not pose any problem, solely an increasing complexity will be the result. With this pre-conditions a multiport (figure 14) with $N$ inputs representing the discrete ray directions of the laser diode model and $M$ outputs representing the discrete elements $A_m$ of the

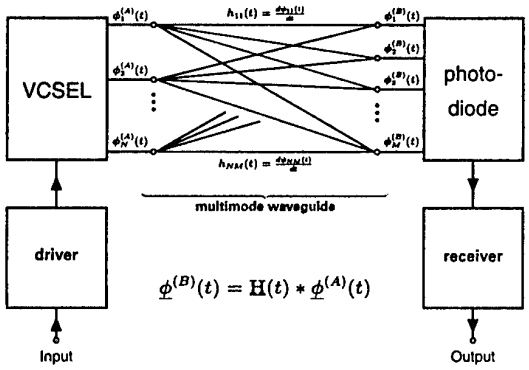



**Fig. 14:** Multiport representation of the optical path

photo diode can be defined. Assuming non-reactiveness, transfer functions $\psi_{nm}(t)$ can be computed [3]. They describe the transfer behaviour of the entire passive optical path excited by the $n$th ray and can be computed by the ray tracing algorithm described above. This characterization of the waveguide is done by the excitation with rays carrying each a constant power (normalized to 1) in order to compute the step response $\psi_{nm}(t)$ regarding the $n$th excitation direction. The time dependence is derived from the total length of the propagation path of each ray.

From the physical properties of optical multimode waveguides some fundamental properties of the functions $\psi_{nm}(t)$ can be derived. Due to the finite velocity of light they will be zero for $t < T_0$ where $T_0$ is determined by the fastest mode or the rays with the shortest propagation paths, respectively. Furthermore, there will be a time $T_1$ with $T_1 > T_0$ which defines a steady state power distribution in the reference plane at the end of optical path. $T_1$ is mainly determined by the slowest mode or the rays with the longest propagation paths. Strictly speaking, this assumption is valid only for the total optical power at the end of the optical path if there is no modal noise. But if the elements of the photo diode are chosen to be sufficient large compared to the granularity of the speckle pattern, this assumption is also approximately valid for the sub-areas $A_m$. For the time in between ($T_0 \leq t \leq T_1$) the functions $\psi_{nm}(t)$ show a monotonously increasing behaviour. As $\psi_{nm}(t)$ are not given explicitly they have to approximated appropriately in order to be able to determine on the one hand the impulse response $h_{nm}(t) = d\psi_{nm}(t)/dt$ and on the other hand to allow an efficient numerical convolution, necessary for time domain simulation. More efficient than an approximation through step-functions [3] seems to be an approximation by exponential functions which enables the application of very fast recursive convolution procedures [7].

After the determination of the transfer functions $h_{nm}(t)$ they can be combined to a matrix $\underline{\mathbf{H}}(t)$ and optical power received by the photo diode can be determined by a convolution product (figure 14).

## 4. CONCLUSION

A novel hybrid electrical-optical interconnection technology providing optical interconnects on pc boards and being able to guarantee the performance properties of next generation printed circuit boards was presented. Besides a short description of the technology itself a general modeling strategy for a transient analysis of parallel hybrid electrical-optical interconnects was presented which easily allows the extension of existing transmission line simulators.

The approach considers unavoidable roughness of waveguides as well as the emission and sensitivity properties of the optical transmitters and receivers, respectively. The propagation of light within and between multimode waveguides is described by transfer matrices which are computed by means of the geometrical optics with the aid of a Monte Carlo technique. A complete analysis is divided into the characterization of the multimode waveguide in order to determine its dynamical behaviour and the following transient simulation which can be executed with arbitrary stimuli. This concept is already known from transmission line theory and requires the characterization of the passive optical path only once.

## REFERENCES


[1] Th. Bierhoff, A. Wallrabenstein, A. Himmler, E. Griese, and G. Mrozynski: An Approach to Model Wave Propagation in Highly Multimodal Optical Waveguides with Rough Surfaces, Proc. *X. Int. Symp. on Theoretical Electrical Engineering (ISTET '99)*, pp. 515–520, Magdeburg (Germany), September 1999.

[2] E. Griese, D. Krabe, and E. Strake: Electrical/Optical Circuit Boards: Technology – Design – Modelling. presented at *3. Int. IEEE Workshop on "Signal Propagation on Interconnects"*, Titisee-Neustadt (Germany), May 19–21, 1999.

[3] E. Griese: Parallel Optical Interconnects for High Performance Printed Circuit Boards. *Proceedings of 6th International Conference on Parallel Interconnects (PI '99)*, pp. 173–183, Anchorage/Alaska (USA), 1999.

[4] E. Griese: Reducing EMC Problems Through an Electrical/Optical Interconnection Technology. *IEEE Trans. on EMC*, Vol. 41, No. 4, pp. 502–509, Nov. 1999.

[5] D. Krabe and W. Scheel: "Optical Interconnects by Hot Embossing for Module and PCB Technology — The EOCB Approach —", *Proc. 49th Electr. Comp. and Techn. Conf.*, pp. 1164–1166, San Diego/California (USA), 1999.

[6] D. Marcuse: *Theory of Dielectric Optical Waveguides*, Academic Press, New York, 1972.

[7] M. Ramme, E. Griese, and M. Kurten: Fast Simulation Method for a Transient Analysis of Lossy Coupled Transmission Lines Using a Semi-Analytical Recursive Convolution Procedure, *Proc. 1997 IEEE Int. Symp. on EMC*, pp. 277–282, Austin/Texas (USA), 1997.

[8] Semiconductor Industry Association: *The National Technology Roadmap for Semiconductors — Technology Needs*, 1997 Edition and 1998 Update, SIA (USA).

[9] Semiconductor Industry Association: *The National Technology Roadmap for Semiconductors — Technology Needs*, 1999 Edition, SIA (USA).

[10] Q. Tan and J. Vandewege, 2.5 gb/s/mm Optical Fiber Interconnections, *Proc. 1996 ECOC*, pp. 2.55–2.58, Oslo, Norway, 1996.


This work is part of the German projects 'Electrical/Optical Circuit Board' and 'OptoSys' which are supported by the German Government, Department of Education, Science, Research, and Technology (BMBF) under grants 16 SV 802/6, 16 SV 803/7, and 01 BP 801/01. The responsibility for this publication is held by the author only.

## BIOGRAPHICAL NOTE



**Elmar Griese** was born in Delbrück, Germany, in 1960. He received his diploma and his Ph. D. degree in electrical engineering from the University of Paderborn in 1987 and 1993, respectively.

From 1987 to 1992, he was employed with the University of Paderborn, department of electrical engineering, where he worked as a research and teaching assistent engaged in electromagnetic field theory and its application to the development of numerical algorithms for analyzing the diffraction behaviour of conducting and dielectric gratings. In 1992 he joined Siemens Nixdorf Informationssysteme AG (Siemens AG since October 1, 1998), where he had been head of the Analog System Engineering Group at C-LAB, a joint R&D institute of the University of Paderborn and Siemens Nixdorf Informationssysteme AG from January 1995 until March 1997. During this time he was responsible for the development of methodologies, numerical algorithms, and simulation tools for supporting the EMC-compliant pc board and system design. Since April 1997 he has been responsible for the development of a new hybrid electrical-optical interconnection technology applicable for high-performance computer equipment and telecommunication switches and routers. His scientific research activities are focused on the development of the corresponding design methodologies which include the development of design-, analysis-, and simulation algorithms and tools for electrical-optical interconnections on pc board level.

Dr. Griese is lecturing at the University of Paderborn on 'Numerical Methods for Calculating Electromagnetic Fields'. His current position is Vice Director of C-LAB and head of C-LABs department 'Optical Interconnection Technology'.

EMC 2000 INTERNATIONAL WROCŁAW SYMPOSIUM ON ELECTROMAGNETIC COMPATIBILITY

# FINITE ELEMENT METHOD APPLIED IN MODELLING PERTURBATIONS ON PRINTED CIRCUIT BOARDS

Mihaela Lascu, Dan Lascu

Politehnica University of Timişoara Faculty of Electronics and Telecommunications MEO Departament
B-dul Vasile Pârvan, no. 2, 1900 Timişoara, Phone: 40-56-19.06.08, Fax: 40-56-19.06.08, E-mail: mihaela@ee.utt.ro

*Abstract:This paper is concerned with predicting the electrical behaviour of metallisation patterns printed onto dielectric substrates. The method described was initially aimed at the modelling of PCB layouts, but is just as applicable to VLSI layouts. It involves the generation of an equivalent circuit to model the electrical properties of the layout. This can be obtained efficiently and provided directly to a circuit simulation program. Predictions can then be made of how the performance of a circuit implemented on a PCB is modified by its physical layout, or of the performance of printed components such as spiral inductors.*

## 1. INTRODUCTION

Miniaturisation has been the one of the key driving forces behind the electronics industry for over thirty years now. Component technology has progressed from valves to transistors to integrated circuits to very large scale integrated circuits (VLSI), with features well under a micron in size. As the components have reduced in size, so the methods used to connect them together have changed, principally through the introduction and evolution of the printed circuit board (PCB).

However, as circuit design became more complex and constraints on space increased, problems began to be seen, particularly in high-frequency design. The cause of these was that the PCB in fact behaves in a complex manner, with various electrical-loss and internal-coupling mechanisms.

## 2. ELECTROMAGNETIC MODELLING

Electromagnetic modelling has a long history: some of the basic techniques were developed more than a century ago, by Maxwell and others. However, before the widespread use of computers, only a very limited range of problems could be tackled, such as isolated conducting objects of symmetrical shape.

The development of the digital computer changed all that. There is now a large set of numerical techniques that can be applied and a vast associated literature describing both methods and particular applications.

All of the methods work by transforming the continuum set of integro-differential equations into a set of purely algebraic equations which can be solved on a computer using standard numerical techniques. For electromagnetic modelling, there is a fairly natural subdivision of the techniques into differential and integral methods.

## 3. GOVERNING EQUATIONS OF TWO COUPLED LINES

The problem of two coupling transmission lines (TL) is essential in the design of PCB and VLSI.

The basic definitions of capacitance and inductance are explained [10], and used as the starting point for a detailed analysis wich demonstrates that the equivalent-circuit model for the PCB provides an approximate solution to Maxwell's equations. The principal approximations are:

- the assumption that the dominant coupling effects take place over electrically short distances, and
- the forms of charge and current distribution assumed in the conductors.

Both of these approximations are well founded for the application areas envisaged, namely electrically small but geometrically complex structures, and their validity is borne out by accuracy of the results obtained.

The aim of this analysis is to produce an equivalent-circuit model for the PCB. The flows of current in the inductors and charge in the capacitors give an approximation to the real charge and current distributions, while the resistors represent both dielectric and resistive losses.

The equivalent circuit model of a part $dx$ belonging to two TL, lossless, coupled, with comun returning is represented in Fig.1. It is neccesary to take into account the mutual inductivity, which appears

between line 1 and the ground, as well as that which is appearing between line 2 and the ground.

Taking into account the presented figure, we may write the following relationships:

$$-\frac{\partial u_1}{\partial x} = L_{11}\frac{\partial i_1}{\partial t} + L_{12}\frac{\partial i_2}{\partial t} + L_{10}\frac{\partial i_0}{\partial t} \quad (1)$$

$$-\frac{\partial u_2}{\partial x} = L_{21}\frac{\partial i_1}{\partial t} + L_{22}\frac{\partial i_2}{\partial t} + L_{20}\frac{\partial i_0}{\partial t} \quad (2)$$

$$-\frac{\partial i_1}{\partial x} = (C_{11} + C_{12} + C_{10})\frac{\partial u_1}{\partial t} - C_{12}\frac{\partial u_2}{\partial t} \quad (3)$$

$$-\frac{\partial i_2}{\partial x} = -C_{12}\frac{\partial u_1}{\partial t} + (C_{22} + C_{12} + C_{20})\frac{\partial u_2}{\partial t}. \quad (4)$$

The previous relations (1)÷(4) can be rewritten in matrix form as follows:

$$-\frac{\partial}{\partial x}[u] = [L]\frac{\partial}{\partial t}[i] \quad (5)$$

$$-\frac{\partial}{\partial x}[i] = [C]\frac{\partial}{\partial t}[u]. \quad (6)$$

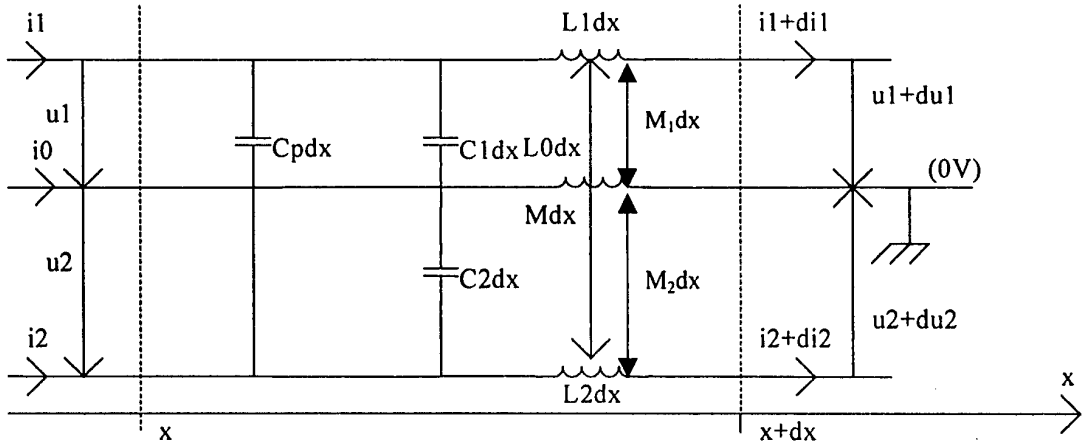



Fig.1. Equivalent circuit model of a part dx belonging to two TL, lossless, coupled, with commun returning.

The derivative with respect $x$ of (5) and (6) and replacing them in (5), respectively (6) we obtain :

$$\frac{\partial^2}{\partial x^2}[u] = [L][C]\frac{\partial^2}{\partial t^2}[u][A_u] = [L][C] \quad (7)$$

$$\frac{\partial^2}{\partial x^2}[i] = [C][L]\frac{\partial^2}{\partial t^2}[i][A_i] = [C][L] \quad (8)$$

where :

$$[u] = \begin{bmatrix} u_1 \\ u_2 \end{bmatrix}; [i] = \begin{bmatrix} i_1 \\ i_2 \end{bmatrix}; [L] = \begin{bmatrix} L & M_1 \\ M_1 & L \end{bmatrix};$$

$$[C] = \begin{bmatrix} C + C_p & -C_p \\ -C_p & C + C_p \end{bmatrix}.$$

In the previous relaionships $L_{11}$, $C_{11}$ represent the line parameters of line 1 in the presence of line 2 and $L_{12}(L_{21})$, $C_{12}(C_{21})$ the coupling parameters between two lines – the mutual line inductance and the line parasit capacitance. In case of lossless, symmetrical, with commun returning lines we have the following expressions :

$$L_{11}=L_{22}=L \quad L_{12}=L_{21}=M \quad L_{10}=M_1 \quad L_{20}=M_2 \quad M_1=M+M_1+M_2$$

$$C_{11}=C_{22}=C \quad C_{12}=C_{21}=C_p \quad C_{10}=C_{1p} \quad C_{20}=C_{2p} \quad C_p=C_p+C_{1p}+C_{2p}.$$

The equations (1) and (2) are showing the parasite phenomenon – the undesirable energy transfer between one circuit and the other. Thus, in (1) the voltage $u_1$ depends on the current $i_2$ from the other line. Similar $u_2$ depends on $i_1$, and so on. Line 1 couples in a parasite way line 2, but as well line 2 couples in a parasite way line 1. The equations (7), (8) are putting in evidence the coupling : the voltage $u_1$ depends as well on voltage $u_2$, and so on – it does not result differential equations of second order in the expresions of $u_1$ and $u_2$ like in the study of isolated lines.

To resolve the problem it is necessary resolving the systems (7) and (8) conditioned by the equations (1)÷(4).

## 4. FINITE-ELEMENT METHOD

The method used in this paper is the finite-element method (FEM). FEM is a more recent development than the finite-difference method. It was initially developed in the field of structural analysis, and as a result much of the literature on it involves mechanical and civil engineering. The essence of the method is the development of an approximatiom to the field vectors over the entire domain, rather than approximating the governing equations at a finite set of points as in the finite-difference method.This is done by subdividing the entire region into a set of elements (usually triangles or quadrilaterals for a two-dimensional region), and defining a set of basis

**functions** (or trial functions) to represent the variation of fields within each element. The field, $E_x$ for example, is then represented by

$$E_x(\mathbf{r}) \cong \sum_{i=1}^{N} \xi_i \psi_i(\mathbf{r}) \tag{9}$$

where $\psi_i$ is a set of $N$ basis functions, with unknown coefficients $\xi_i$.

A set of equations to determine the unknown coefficients is generated either by a variational approach or by the use of **weighting functions**, which effectively produce samples of the approximate solution, the governing equation and the boundary conditions. The resulting solution, which contains the set of coefficients $\xi_i$ is an approximation to the true fields over the entire domain.

The problems of interest in PCB have the following properties:

- the dielectric materials used for substrates can be assumed to be arranged in a layered structure, with each layer having constant, isotropic material properties.
- the arrangement of conductors can be extremely complex, but nearly all are in a plane parallel to the substrate interfaces.
- the applications are usually electrically small, or else all significant electromagnetic coupling occurs over electrically small distances.
- the applications are often unbounded.
- the results of the simulation have to be made available to circuit designers as circuit-theory parameters.

A typical configuration is represented in Fig. 2 and Fig.3.

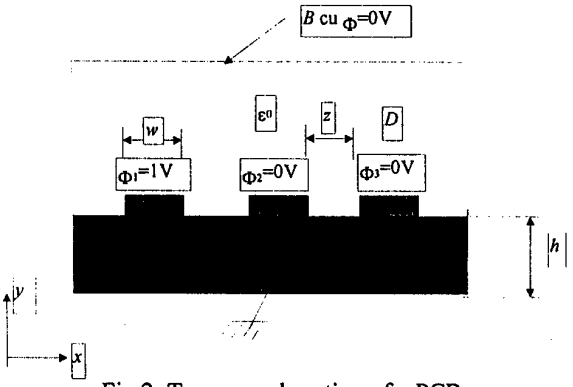



Fig.2. Transversal section of a PCB.

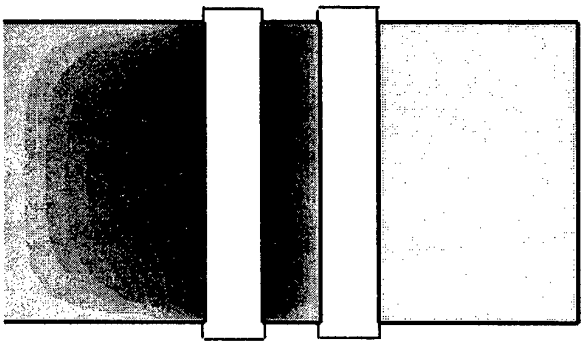


Fig.3.Upper view of a PCB with two tracks, with the potential applied to the left track.

## 5. CAPACITANCE AND INDUCTANCE MATRIX COMPUTATION

For a system of n+1 conductors such as that illustrated in Fig.2, let the potential on the n+1 reference conductor, the ground plane, be set to zero volts with respect to the potentials on the other conductors. If the first conductor is charged up to a nonzero potential $\phi_1 = u_1$, and the rest of the conductors grounded to the reference conductor ($u_2=u_3=\ldots=u_n=0$ volts), then the electrostatic field and charge on each conductor is uniquely determined by the value of $\phi_1$. In this manner [10], see Fig.3, the $j$th column of the per-unit length capacitance matrix is computed as

$$C_{ij} = \left.\frac{Q_i}{u_j}\right|_{(u_1,\ldots,u_{j-1},u_{j+1},\ldots,u_m)=0} \tag{10}$$

where for $i=j$, $C_{ii}$ is the self-capacitance between the $i$th conductor and ground; and for $i\neq j$, $C_{ij}$ is the mutual capacitance between the $i$th and the $j$th conductors.

Calculation of the per-unit length inductance matrix is obtained from the capacitance matrix calculated with the dielectric removed

$$[L] = \varepsilon_0 \mu_0 [C_0]^{-1}. \tag{11}$$

In the above expressions, $\varepsilon_0$ and $\mu_0$ are the permittivity and permeability of free space, respectively; and $[C_0]$ is the per-unit length capacitance matrix in the absence of the dielectric.

Applying a FEM-program Quickfield we may obtain Fig.4 and Fig.5. With the help of these pictures it is possible to determine the Quickfield values for the inductivity and capacity. Similar with the electrostatic analysis obtained in Fig.4 and Fig.5 it is possible to realize a magnetostatic analysis too as in Table 1. It is possible to propose a value for the density current obtaining the intensity of the magnetic field. Having these value it is possible to derive the magnetic flux. Knowing the values of the magnetic flux and current it is possible to obtain the values for the inductivities having a different permeability than $\mu_0$. The

inductivities values for $\mu_0$ have similar values with the theoretical ones obtained in Table 1.

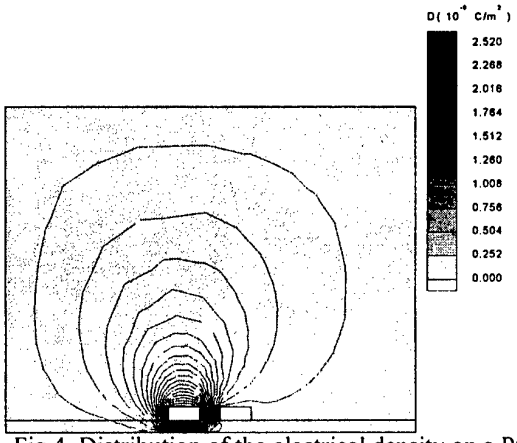



Fig.4. Distribution of the electrical density on a PCB with two tracks.

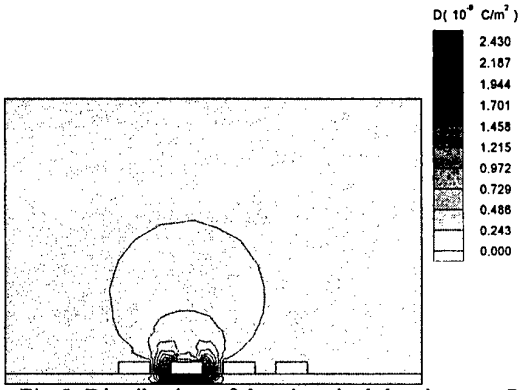



Fig.5. Distribution of the electrical density on a PCB with four tracks.

**Table 1. Theoretical and Quickfield values.**

| | | |
|---|---|---|
| T | $C_{11}$=9.23e-11 F/m | $L_{11}$=12.038e-8 H/m |
| Q | $C_{11}$=9.72e-11 F/m | $L_{11}$=11.431e-8 H/m |
| T | $C_{12}$=6.50e-12 F/m | $L_{12}$=17.094e-9 H/m |
| Q | $C_{12}$= 6.61e-12 F/m | $L_{12}$=16.809e-9 H/m |
| T | $C_{10}$=11.98e-11 F/m | $L_{10}$=9.91e-8 H/m |
| Q | $C_{10}$=12.579e-11 F/m | $L_{10}$=10.405e-8H/m |
| T | $C_{20}$=8.93e-12 F/m | $L_{20}$=15.84e-9 H/m |
| Q | $C_{20}$=9.3765e-12 F/m | $L_{20}$=14.832e-9 H/m |

In Table 1 are represented the self-capacitance, self-inductance and mutual capacitance and mutual inductance between the two tracks and the ground.

Analysing the obtained values we can see that the obtained values by the FEM method are similar with the theoretical ones.

## 6. CONCLUSIONS

The analysis presented in this paper would be useful to electromagnetic engineers and scientists, especially to those who are working in the area of PCB. The main task is to minimalize the perturbations between the tracks. The results of the inductivitues and capacities are validated by theoretical results obtained in literature. The proposed method is based on a circuital characterization of the structure with two and four tracks, via the FEM. The circuital characterization of PCB also allows one to study multiple perturbations problems.

## 7.REFERENCES

[1]. Radu, S. "Electromagnetic Compatibility" (Romanian), *Editura "Gheorghe Asachi"* Iasi, 1995.
[2]. Ignea, A. "Measuring and testing in electromagnetic compatibility" (Romanian) , *Editura Waldpress*, Timişoara 1996.
[3].Breaban, F. "Microwaves" (Romanian) , *U.T.T Timisoara*, 1991.
[4]. Angot, A. "Mathematical Complements" (French), *Editura Tehnica*, 1966.
[5]. S. Radu, "Introduction in electromagnetic compatibility" (Romanian). Iaşi: Editura "Gh.Asachi", 1995.
[6]. R. Laroussi and G.I. Costache, "Finite-Element Method Applied to EMC Problems", IEEE Electromagnetic Compatibility, vol.35, pp178-184, Mai 1993.
[7]. Gh. Mîndru and M.M. Rădulescu, "Numerical analysis of electromagnetic field"(Romanian), Editura Dacia, Cluj, 1986.
[8]. O.C. Zienkiewicz and R.L. Taylor, " La méthode des éléments finis. Formulation de base et problémes linaires", Afnor Technique, Paris,1991.
[9].*** QUICKFIELD-Finite Element Analysis System. Version 3.2. Tera Analysis 1995.
[10]. M. Lascu, "Contributions in the assurance of electromagnetic compatibility of electronic equipments", (Romanian) PhD, 1998.

## BIOGRAPHICAL NOTES

**Mihaela Ruxandra Lascu** was born in Timişoara, Romania, on May 7, 1962. She received the degree in electrical engineering from the "Politehnica" University of Timişoara in 1986 and the Ph.D. degree in electromagnetic compatibility in 1998. Since 1990 she was appointed Assistant at the University of Timişoara. Her main interest is in numerical techniques applied in electromagnetic compatibility, such as finite-element analysis and finite-difference time-domain methods, and their application to interference problems in steady-state and time-domain applications. Now she is lecturer at the University of Timişoara.

**Dan Florentin Lascu** was born in Timişoara, Romania, on June 30, 1961. He received the degree in electrical engineering from the "Politehnica" University of Timişoara in 1986 and the Ph.D. degree in power electronics in 1998.Since 1997 he was appointed Lecturer at the University of Timişoara. His main interest is in power processing topologies, modeling and control, power factor correctors and high power density switch mode power converters.

EMC 2000 INTERNATIONAL WROCŁAW SYMPOSIUM ON ELECTROMAGNETIC COMPATIBILITY

# Radio interference cases on broadcasting sites

Alain Azoulay
TDF / Centre Technique. 4 avenue Ampere . 78897 Saint Quentin en Yvelines . France
alain.azoulay@cetec.tdf.fr

## 1.Introduction

Radio broadcasting companies face sometimes strong interference cases where colocation of radio broadcast transmitters (FM and TV) and two-way private or cellular mobile radio could exist on the same site.

We present here some definitions and a typical case as well as the way to avoid interference between co-located services on transmitting sites. A prediction software has been developed to assess interference, particularly inter-modulation products and harmonics generation as well as blocking effect. Even if the prediction of intermodulation frequencies is quite achievable, the levels of these products are another matter as numerous cases of non-linearities can occur on a transmitting site. Radiated powers are quite high on a broadcasting site and rectification or non linear phenomena could occur at any place in the coupling link between one or multiple transmitters and a co-located victim receiver or sometimes distant receivers.

## 2. Typical organization of a broadcasting site.

Usually, in most cases, transmitters are located in dedicated rooms in broadcasting centers.
Electromagnetic compatibility for these centers are a mostly important issue. Not only, because of the various transmitters and receivers it is possible to find in such a center, but also for the electromagnetic protection against lightning or power lines surges. Broadcasting centers are often located on heights, over mountains or hills with masts which heights are well above 50 meters. So, lightning protection is also a concern from the EMC point of view.
In this paper, we will focus mainly on the radiofrequency compatibility aspect which is the other most important parameter that the broadcasters have to take in consideration to assess a good quality of reception and transmission on their site.
A number of documents prepared by various organizations (ITU-R, ETSI, EBU,..) reflect this topic. [1],[2],[3].



Figure 1. Broadcasting FM and TV transmitters in a dedicated room

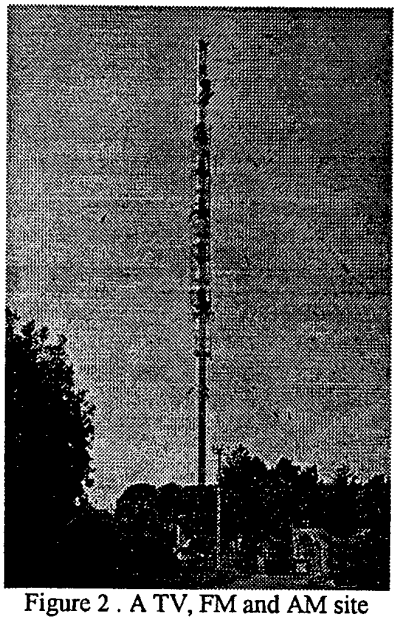


Figure 2 . A TV, FM and AM site

The figure 1 depicts a typical broadcasting center room and the figure 2 shows a broadcasting site in France.
Broadcasting centers are more and more subject to high demand not only for the broadcasting purposes, but also for communication purposes. On the same site, we can usually find , of course broadcasting transmitters in FM, analog TV Band III, IV, V, sometimes DAB, and in a starting phase DVB-T transmitters. In addition, it is more and more common to find Private Mobile

Radio (PMR) systems analog and digital, cellular GSM 900 and 1800, microwave relays in various microwave bands, satellite reception and other specific radio systems (GPS for example)
In short, there is a high density of transmitters, receivers and of course antennas covering various frequency bands.
Such a density of radio systems, mostly covering 30 MHz up to some 38 GHz implies to provide to the radio managers of the site and of the radio systems an appropriate level of electromagnetic compatibility between these systems which could comply with very different standards, which could be of very different generations and which compatibility is not always easy to verify.
One of the critical EMC issues is that on these sites, there are dedicated sensitive receivers with antennas which could be installed very close to powerful transmitters antennas.

### 2.2. Frequency bands found on typical broadcasting sites (transmit and receive frequencies)

If we exclude a limited number of specific sites dedicated to AM radio (long, medium, short waves), most of the broadcasting sites include radio systems which are located in various frequency bands. The table 1 indicates the frequency bands found in France on various sites.

| Radio Service / system | Transmit frequency band | Receive frequency band |
|---|---|---|
| Private mobile | 68 – 87 MHz | 68-87 MHz |
| FM | 87.5- 108 MHz | |
| Private mobile | 151-174 MHz | 151-174 MHz |
| TV Band III | 174-223 MHz | |
| PMR analog | 406-428 MHz | 406-428 MHz |
| PMR Digital | 410-430 MHz | 410-430 MHz |
| PMR analog | 440-470 MHz | 440-470 MHz |
| TV Band IV/V | 470-860 MHz | |
| GSM 900 receive band (BTS) | | 890-915 MHz |
| GSM 900 transmit band (BTS) | 935-960 MHz | |
| GPS (receivers) | 1575,42 MHz | |
| DAB | 1452-1492 MHz | |
| GSM 1800 receive band (BTS) | | 1710-1785 MHz |
| GSM 1800 transmit band (BTS) | 1805-1880 MHz | |
| Microwave relays | 4 GHz, 7 GHz, 23 GHz, 38 GHz | 4 GHz, 7 GHz, 23 GHz, 38 GHz |

Table 2. Frequency bands of some radio services or systems found usually in a broadcasting site

In addition, sometimes, specific broadcast receivers are also installed on the site in order to provide Ball-enfang reception.

### 2.3. Types of radio interference encountered on broadcasting sites

Generally speaking, only the radio receivers are affected by interference but sometimes, also transmitters could be affected by specific situations which will be described in this document.
The most common sources of interference to radio receivers in broadcasting sites come from two effects very different in their origin:

- the first effect comes from all unwanted emissions
- the second effect comes from the blocking of the receivers because of the presence of high power transmitters.

As defined by Radio Regulations (Article 1 (S1), No. 140 (S1.146) of the RR), unwanted emissions consist of spurious emissions and out-of-band emissions.

Out-of-band emissions (Article 1 (S1), No. 138 (S1.144) of the RR) are situated on a frequency or frequencies immediately outside the necessary bandwidth of the transmission which results from the modulation process, but excluding spurious emissions. These emissions affect sometimes other radio services closely located in frequency, but most of the time, it is the spurious emissions which affect most dramatically radio receivers installed on transmitting sites.

Spurious emissions consist of many radiated signals resulting of the presence of a single transmitter but could be worse whenever multiple transmitters are co-located on a same site.
Spurious emissions (Article 1 (S1), No. 139 (S1.145) of the RR) are emissions on a frequency, or frequencies, which are outside the necessary bandwidth and the level of which may be reduced without affecting the corresponding transmission of information. Spurious emissions include harmonic emissions, parasitic emissions, intermodulation products and frequency conversion products but exclude out-of-band emissions.

Spurious emission from FM stations can affect a number of radio services which are close in frequency to the FM band, namely PMR band below 87.5 MHz and airband above 108 MHz, additionally harmonics of the transmit frequencies and all types of broadband noise can also decrease the protection ratio of the receiver. On broadcasting sites, most of the spurious emission come from the intermodulation products related to the presence of multiple transmitters. It is not uncommon to have on the same site more than 6 FM transmitters and 3 to 6 TV transmitters.
Coupling combined to non-linear effects may produce intermodulation signals at various places.
If Fi are the transmitters frequencies, a non linear effect could provide signals at frequencies $F_{IMq}$ which are linear combination of the frequencies Fi.

$$F_{IMq} = |+/-m\ F1+/-\ n\ F2\ +/-\ p\ F3+ \ldots|$$

The order q of the intermodulation product is the sum of the coefficients of the linear combination

$$q = m+n+p+\ldots,$$

with m, n, p, q integers positive or equal to zero.
If we consider only two signals at F1 and F2, the generated intermodulation products will include :

- harmonics and intermodulation products of the second order F1+F2, F1-F2, 2F1,2F2
- harmonics and intermodulation products of the third order which can be very troublesome like 2F2-F1, 2F1-F2, 2F1+F2, 2F2+F1, 3F1, 3F2
- etc...

The levels of intermodulation products generally decrease when the order increase. From a practical point of view, the most disturbing orders are usually the third and the fifth. For the FM band, a number of cases have been identified with products of the third order.
The intermodulation phenomenon can occur in different locations on a broadcasting site. The transmitters and their infrastructures including the multiplexers, the antennas and the cables may be one source of non-linear effects. The final stage of a power amplifier can be a point of non-linearity by coupling of high field-strengths induced by another transmitter to the output of this amplifier, so there could be a mix of two signals at frequency F1 and F2 with an order three combination.
As defined in [3], the intermodulation conversion loss *Ai*, in dB, is the ratio of power levels of the interfering signal from an external source and the intermodulation product, both measured at the output of the transmitter.
Without any special precautions, typical values for semi-conductor transmitters are to be found in a range of 5 to 20 dB and for valve transmitters, in the range of 10 to 30 dB, in respect of the 3rd order product (2f1 - f2). The overall loss between a transmitter providing the unwanted emission giving rise to the intermodulation product and a receiver operating at the frequency of the product is:

$$A = Ac + Ai + Ap \qquad (2)$$

where Ac is the propagation loss between the interfering signal output and the transmitter output, A *p*, in dB, is the propagation loss of the intermodulation product between the relevant transmitter output and the receiver input and Ai is the intermodulation conversion loss.

The second possible point where intermodulation may occur, is the receiver input when two RF signals with high amplitude are present at the input.
For angle modulation systems, receiver inter-modulation performance is defined by the existing standard ETS 300 086 [5] as a ratio between an on-frequency wanted test signal of -107 dBm and two off-frequency unwanted signals at 70 dB above this level displaced to cause a third order intermodulation product on the wanted channel. Under these conditions an audio output approximately equivalent to a 7 dB RF carrier to interference ratio at the receiver input must be obtained. This definition therefore accepts that in the presence of the off-frequency signals, the receiver sensitivity required by standards may be degraded by 3 dB.

The third point, quite difficult to identify and handle is the site itself with its metallic infrastructure, masts and fence. Many reports state that the masts or the fence could be responsible for generating intermodulation products by non-linearities of the rust or various metallic oxides at contact points or bolts. There is here a type of semi-conductor acting as a non-linear device.

The second most important effect comes from the blocking effect or desensitization of the victim receiver which receives an important level of out of band incoming signal. Usually, the front end part of the receiver will have a gain reduction resulting in a degradation of sensitivity or sometimes some strange effects like rectification of the incoming high level signal.
This situation is generally qualified in the existing standards by the blocking performance. This blocking although not clearly defined by ITU-R, has been taken into account by ETSI in its various radio standards in order to provide protection of the receivers. These standards do not provide always efficient protection against blocking on difficult situations such as broadcasting sites with multiple powerful transmitters (often more than 1 kW) but they indicate that blocking can occur and give a typical protection against blocking.

## 3.Some typical situations of interference

One of the most typical situations of interference is caused by the presence of Private Mobile Radios (PMR) below 87 MHz and many FM transmitters on the same site. Intermodulation products are one of the major sources of trouble in assessing the radiofrequency compatibility of the site.
Intermodulation products come by combination of coupling and non-linearities at various places in the whole site.

Among the various cases, here is one interesting cases of FM / PMR compatibility.
One PMR equipment consists of transceivers connected on three whip antennas. These antennas are installed at various altitudes on the mast but the highest antenna is located between to sets of FM antenna. The PMR frequencies are the following: 83.150 MHz, 83.5125 MHz, 83.9375 MHz and 83.4125 MHz.
The FM transmitters are located in a specific room and consist of two racks:

| Public FM radios | Frequency (MHz) |
|---|---|
| FM1 | 97.2 |
| FM2 | 88.0 |
| FM3 | 95.4 |
| FM4 | 107.3 |

Rack1 : Public FM radios

| Private FM radios | Frequency (MHz) |
|---|---|
| FM5 | 106.7 |
| FM6 | 102.0 |
| FM7 | 95.9 |

Rack2 : Private FM radios

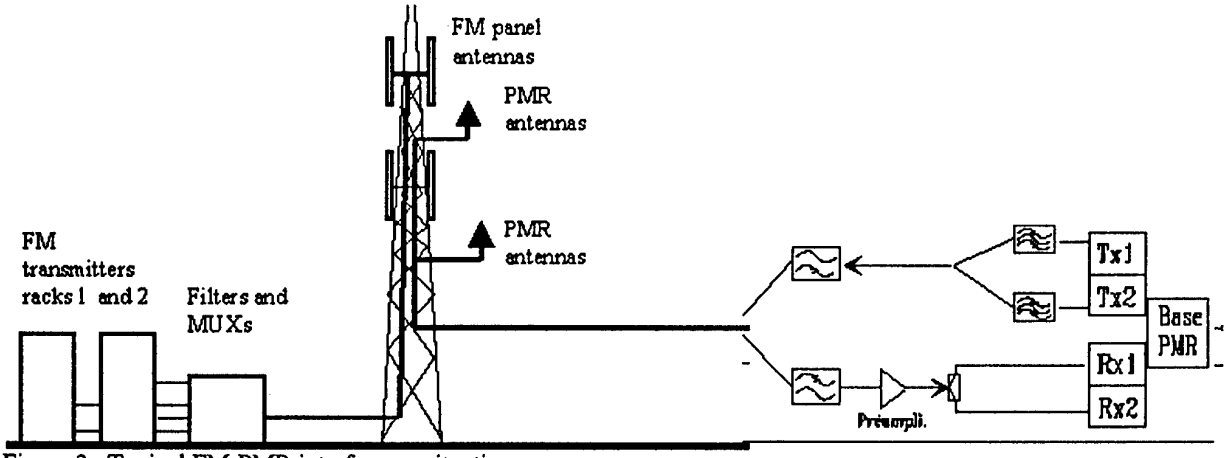



Figure 3 –Typical FM-PMR interference situation

## Interference identification

The first step to cope with interference is to identify the frequencies of the intermodulation products potentially provided by the FM transmitters. As in most of the cases, third order IM products are the most disturbing a full calculation of the frequencies have been conducted and the main IM frequencies coming close to the PMR frequencies are the following

| Third order IM product in the PMR band | Contribution of frequencies |
|---|---|
| 83.2 MHz | FM2 +FM7-FM4 |
| 83.3 MHz | FM2 + FM6 – FM5 |
| 83.5 MHz | 2.FM3 – FM4 |
| 84 MHz | FM3 + FM7 – FM4 |

Measurement have been performed all around the equipment and particularly at the output of the multiplexers of both FM radios groups; no intermodulation product appeared.
The FM levels measured at the output of the receiving PMR antennas are high , between 98 and 113 dB(µV).
The single intermodulation product measured is the 83.5 MHz frequency with various levels depending on the antenna, the highest PMR antenna receives 26 dB(µV), the other antenna at lower level receives 40 dB(µV)
To fix the problem these two antennas have been removed and replaced by a Ground Plane antenna placed well above the FM antenna panels and a global improvement of more than 10 dB has been achieved on the IM product as well as on the blocking parameters, and the PMR equipment could perform satisfactorily

## 4. Software to predict interference

In order to avoid to perform calculations and measurements on a case by case basis, TDF-C2R, the research center of TDF has developed a new software to provide a practical situation analysis of the radiofrequency compatibility of a broadcasting site. In a first phase, this tool is dedicated to the worst case encountered in broadcasting stations that is PMR – FM compatibility analysis

A new version is under way to cover most of the cases for radio EMC analysis purposes. This tool is a development and engineering tool and not a perfect model of all the phenomena which may occur in an interfering situation, but it is quite helpful and gives a quick overview of potential problems.

## 5. Some solutions to avoid interference on broadcasting sites.

First of all, to avoid interference a careful frequency planning should be started in order to eliminate any risk of intermodulation product as far as possible; additionally, coupling calculation must be conducted in order to avoid blocking effects as far as the blocking level of the potentially victim receiver is known or assumed based on standards or specifications.
From practical point of view, the broadcasting sites should be well maintained to avoid rust, to avoid equipment and antenna being left after their usage; good grounding and shielding of all equipment and cabling should be taken into account as well.
Additionally, high performance selective filters should be placed just between the antenna and the receiver amplifier to define the operational frequency band in order to limit any blocking problem.
Another important factor is the decoupling factor between the transmit antennas and the receive antenna. This decoupling factor should be maintained as high as possible to increase the loss between the interfering signals and the victim receiver.

## 6. Conclusion

Interference cases on broadcasting sites are a permanent subject to take care as compatibility between numerous high power transmitters and very sensitive receivers at close frequencies should be guaranteed. Many measurements have to be conducted to identify accurately all the physical mechanisms

(coupling, intermodulation and non-linear effects in general) and a software tool to improve EMC prediction seems more and more useful as the number of transmitters and receivers in various frequency bands increase every day and as the demand for new radio services is always stronger.

## 7. Acknowledgement

Special thanks are given for their collaboration and measurement efforts to Nicolas Daniau, Pascal Bary, Philippe Senegas and their group leader Henri Leclerc from the TDF Technical Centre and for the software models implementation and verification to Pierrick Seite, Francois Jacquin and Emmanuel Nicolas from the TDF-C2R, TDF Research and Development Centre.
This work has been and is still strongly encouraged and supported by the Methods and Production Division of TDF and particularly by Patrick Dupuis and Jacques Martin.

## 8. Bibliography

[1] - Recommendation ITU-R M.1072 - Interference due to intermodulation products in the land mobile service between 25 and 3000 MHz.

[2] – ITU-R Recommendation ITU-R SM.329-7- Spurious emissions . (1997)

[3] - ETSI - TR 100 053 V1.3.1 (1998-08)-Technical Report -Electromagnetic compatibility and Radio spectrum Matters (ERM)- Radio site engineering for radio equipment and systems in the mobile service

[4] – EBU - EMC at transmitter sites

[5]. ETS 300 384 . Radio broadcasting systems: Very High Frequency (VHF), frequency modulated, sound broadcasting transmitters

[6] – ETR 132 . Radio broadcasting systems: Code of practice for site engineering VHF, frequency modulated sound broadcasting transmitters. August 1994

[7] – MPT 1331 – Code of Practice for radio site engineering – April 1987 , reprinted in 1992

Biographical note

Alain Azoulay is the head of the Antenna, Radio and EMC measurement Branch of Telediffusion de France (TDF) technical center. After graduated from the Supelec engineering school in Paris in 1970, he worked at Thomson CSF in the microwave relays division up to 1974 and spent afterwards more than 20 years in the EMC and mobile radio division of CNET, France Telecom research and development center. He joined TDF in 1998.
He is currently delegate member of CISPR (International special committee for radio interference) and has been chairman of ITU-R TG1/3 on spurious emission of transmitters up to November 1997.

EMC 2000 INTERNATIONAL WROCŁAW SYMPOSIUM ON ELECTROMAGNETIC COMPATIBILITY

# OPTIMALLY PLACING BASE STATIONS IN A MICROCELLULAR URBAN ENVIRONMENT

Ranjan Bose
Dept. of Electrical Engineering, IIT Delhi, India 110016
Email: rbose@ee.iitd.ernet.in, Phone: 91-11-659-1048

*Abstract – With the increasing demand for cheaper and better wireless services from the customers, and the move towards smaller cell sizes, it is becoming very important to optimally design the cell geometries, and deploy the minimum number of base stations to provide maximum possible coverage. The gradual decrease in cell sizes with the objective of providing services to more number of users has lead to the design of microcells. These microcells have the base station antennas located well within the local environments and usually below the local building rooftops. In this paper we consider how to optimally determine the locations for the placement of base stations for a wireless system in an urban setting, given the data for building heights and their locations. The optimality of the base stations is with respect to the total coverage area using the minimum number of base stations. Coverage is being defined as the percentage of area from where it is possible to establish a communication link with at least one of the base stations. In an urban setting, where we expect a relatively high density of tall buildings, line of sight (LOS) links may not be always possible. Wherever LOS link is not possible, a non-LOS link might be considered, taking into account the attenuation of the radio waves through the building walls (and the roof, as the case may be).*

## 1. INTRODUCTION

Typically, in urban settings, the base station location is chosen to be on the top of the tallest building [1]. However, with the move towards smaller cell sizes in order to meet a larger user densities, micro-cellular environments are being deployed [7]. These microcells have the base station antennas located well within the local environments and usually below the local building rooftops. The location of the base station antenna below the level of the rooftop of the local buildings implies that the field strength dependence can no longer be adequately described in terms of a single radial distance variable. The streets and the rooftops will have a strong guiding effect. The microcellular systems designers require accurate estimation of carrier to co-channel interference in order to design interference limited high capacity mobile radio systems. The propagation modeling has to be 3-D so as to get reasonably accurate estimates.

Currently, in-building wireless service represents a significant and growing component of the cellular traffic [2]. This wireless service may not be limited to telephony alone. Traditionally, pedestrian mobility has been supported by high power systems that are more costly than necessary. But as the customer base is expanding, for increased network efficiency, the cell sizes have to be reduced [3]. The geometries of these small cells will be determined by the building locations building heights, street locations, location of the base stations, the transmitter power and the receiver sensitivity. A change in the location of the base station will alter the cell shape and hence the coverage provided by that base station. In order to provide *cheaper* but reliable wireless communication services with high coverage (both in-building and outdoors) to more and more users, it is essential to optimally plan the cell site locations and the base station location within the cells. This planning for cell sites and base station location has to be done taking into account the following:

(i) Locations and heights of the buildings within the area where the wireless communication service has to be provided.
(ii) Allowable base station locations (since all locations may not be accessible or permissible).
(iii) Attenuation of the radio waves by the walls and roofs of buildings (in order to determine the non LOS coverage).

This paper discuss the strategy to determine the optimal location of the base stations and the corresponding cell sites, given the environment variables (building locations in the area, building heights, attenuation through the walls and roof of buildings, the transmitter power and the receiver

sensitivity). The optimization is based on the principles of dynamic programming. A software package has been developed which implements this technique and assists in cell site and base station location. This paper briefly explains the algorithm and the working of this planning software. This software can be used for system level designing.

## 2. COVERAGE IN AN URBAN SETTING

Here coverage is being defined as the percentage of area from where it is possible to establish a communication link with at least one of the base stations. In other words, the strength of the radio signal is above a known threshold level (receiver sensitivity) in the area *covered* by the service provider. In any urban setting there are tall buildings, and the coverage is desired both indoors and outdoors. Besides, the streets and the building rooftops have strong guiding effects. It may be possible that line of sight (LOS) link is not feasible due to the presence of buildings and other obstructions (Fig. 1). In that case the attenuation of the radio signal through multiple walls (and roofs) will have to be taken into account. Depending upon the construction materials used in the building and the wall thickness, losses of 5 to 10 dB are typical [2].

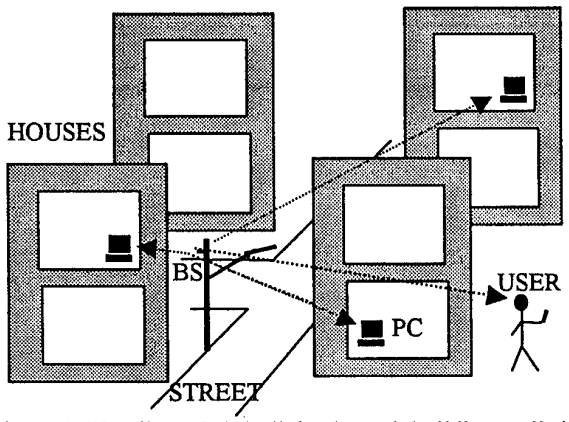



Figure 1. Non line-of-sight links through building walls in an urban setting. The wave propagation is determined by the building locations and heights.

Depending on the relative positions of the base station and the tall buildings in its neighbourhood, the cell geometry will get determined. Thus, the ideal location of the base station will be a function of the building heights and their relative locations in that area.

## 3. OPTIMAL BASE STATION LOCATION

The objective is to determine the optimal location of base stations given the building locations, building heights, attenuation through walls and the transmitter power. This is a resource allocation problem where our objective function (the function which is to be maximized/minimized in an optimization problem) is the coverage area. The decision variables are the base station locations, their corresponding heights and the total number of base stations required to provide the desired coverage. Here we approach the problem from the perspective of dynamic programming [4, 5].

Let us say that we have to set up the wireless communication network for an urban campus. We do not lay any restrictions on the size of the campus. First we divide the entire campus in rectangular grids. The grid size will depend upon the accuracy desired. Thus the entire campus can be represented by a set of grid points. Our objective, then, is to place minimum number of base stations in such a manner so as to cover maximum number of grid points. It may be possible that a single grid point is covered by more than one base station (overlapping cells). Intuitively, we must minimize the overlap areas of the different cells if we want to use the minimum number of base stations.

Let us say that $N$ base stations have to be deployed in order to achieve the desired total coverage. This value of $N$ is also to be determined. Let the set of all grid points in the campus be represented by $S$ and the size of this set be $m$. Thus there are $m$ grid points that span the campus. We assume that the possible locations of a base station can only be on any one of the grid points. Once we place a base station at a certain grid location, it will be able to cover (illuminate) a certain number of grid points around it. The algorithm is as follows:

We solve this resource allocation problem using concepts from dynamic programming. We begin by identifying the stages in the problem. The stage should be chosen so that when one stage remains, the problem is easy to solve. Then, given that the problem has been solved for the case where one stage remains, it should be easy to solve the problem where two stages remain, and so forth. It would be easy to solve if only one base station was to be placed optimally. Let us define stage to represent the case when the base station locations remaining to be determined are $t, t+1,\ldots, N$.

Next, define $f_t(d_t)$ to be the maximum total-coverage obtained by placing the $t, t+1,\ldots, N$ base stations at the grid locations contained in the set $d_t$. The size if $d_t$ will be $N - t + 1$. Further define $x_t$ to be the base station location at stage t in order to attain $f_t(d_t)$. We start working backwards by computing $f_N(g_i)$, $(i = 1,\ldots, m)$. That is, we place the $N^{th}$ base station at every grid point, one grid point at a time. Corrosponding to each location $g_i$ $(i = 1,\ldots, m)$, we determine the *set* of grid points $s_{i,N}$ to which the Nth base station would provide coverage. The set $s_{i,N}$ will be a function of the

buildings located near the base station location $g_i$. Thus, corresponding to a base station located at every grid point in the campus, we obtain a set of covered (illuminated) grid points.

We continue the process for the $N$-1$^{th}$ base station. To determine $f_{N-1}(d_{N-1})$ we look at all possible locations for the $N$-1$^{th}$ base station location. The location that maximizes $f_{N-1}(d_{N-1})$ is $x_{N-1}(d_{N-1})$. Let the $N$-1$^{th}$ base station located at $g_i$ provide coverage to the set of grid points $s_{i,N}$. It would be logical to avoid locating the Nth base station at a grid point already covered (illuminated) by the $N$-1$^{th}$ base station. Therefore, the possible locations for the $N^{th}$ base station, *given* a particular location of the $N$-1$^{th}$ base station, now belongs to the smaller set $S$ - $s_{i,N-1}$. The function to be maximized at stage $N$-1 can be expressed as:

$$f_{N-1}(d_{N-1}) = \max \{S_{i,N-1} \cup f_N(x_N \in S - s_{i,N-1})\} \qquad (1)$$

where S is the set of all grid points spanning the campus, $s_{i,N}$ is the set of grid points to which the $N$-1$^{th}$ base station (located at $g_i$) provides coverage, and $f_{N-1}(d_{N-1})$ represents the total coverage at stage $N$-1. Note that the algorithm works backward from the end of the problem towards the beginning, thus breaking up the large, unwieldy problem in to a series of smaller, more tractable problems. At each stage $t$, only the maximum value of $f_t(d_t)$ is retained (principle of optimality). We keep on working backwards until $f_t(d_t) = S$ (for the case of 100% coverage). This stopping criterion will also tell us how many base stations are required to achieve that coverage.

## 4. COMPUTATIONAL LOAD

As we have mentioned earlier, the actual number of base stations that will be needed to provide the desired coverage is not known, *a-priori*. Hence, the algorithm proceeds stage by stage, at each stage evaluating the maximum coverage achieved. As soon as the desired coverage (which is usually 100%) is obtained, the algorithm halts. Thus, the computational load of the algorithm is a function of the total number of base stations that are actually deployed.

The total number of base station that would be required to provide coverage depends upon three factors:

(i) The link budget: This accounts for the total path loss from the transmitter to the receiver. The link budget will actually determine the extent of the boundaries of the cell. The path loss depends upon the environment (dense-urban, urban or rural) where the wireless service is being provided as well as several other factors.

(ii) The capacity requirements: This depends on the user density and the user traffic (erlangs/user). Places with high user density coupled with high traffic would require a large number of base stations than dictated by the link budget [6].

(iii) Interference: The maximum allowable co-channel interference may limit the coverage and hence the total number of base stations required in interference limited, high capacity systems.

Let the total number of grid points spanning the area to be covered be $m$ (as mentioned earlier). Let the *average* number of grid points illuminated by a base station be $m_c$. The value of $m_c$ depends on the actual position of the tall buildings near the base station (besides other factors such as the terrain, foliage etc.), and is a statistical parameter. The average number of look-ups, comparisons, union operations and the memory requirements for placing $N$ base stations are given in Table 1.

Once a specified coverage area is fixed and the resolution of the grid points is decided, the parameter $m$ gets fixed. Also, the cell radius (which depends on the transmitter power, receiver sensitivity and the type and density of buildings, terrain and foliage) determines the value of $m_c$. It can be seen from Table 1 that the total number of look-ups reach a maximum value for $N \cong (m/m_c)$. Similarly, the number comparison peaks for $N \cong (m/m_c)$. It can be intuitively seen that if a base station covers $m_c$ grid points on an average, then, we would require $(m/m_c)$ base stations to cover all m grid locations. Thus, it can be inferred that the computational load (look-ups, comparisons and union operations) *grow* as $\alpha N - \beta N^2$ for fixed values of $m$ and $m_c$. Also, it can be observed that the increase in computational load while going from $N = 7$ to $N = 8$ is much larger than going from $N = 8$ to $N = 9$. Thus, there is *diminishing* increase in the computational load with increasing $N$.

**Table 1.** Computational load and memory requirements for placing $N$ base stations.

| Computational load/Memory requirement | No. of operations required |
|---|---|
| Look-ups | $mN - m_cN(N+1)/2$ |
| Comparisons | $m(m-1)N - mm_cN(N+1)/2$ |
| Unions | $m^2N - mm_cN(N+1)/2$ |
| Memory required | $m^2N + m(m-m_c)N(N+1)/2 - mm_cN(N+1)(2N+1)/6$ |

## 5. SIMULATION RESULTS

Some basic simulations were performed to test the computational load of the algorithm. The coverage provided by a base station has been modeled as a random variable. The extent of the coverage is determined by the transmit power. Assuming path loss

and receiver sensitivity remain fixed, we have varied the transmitter power (which would result in a smaller of $N$) and plotted the computational load in Figure 2. In order to put things in perspective, we have also varied the number of grid resolution) and observed its effect on the computational load.

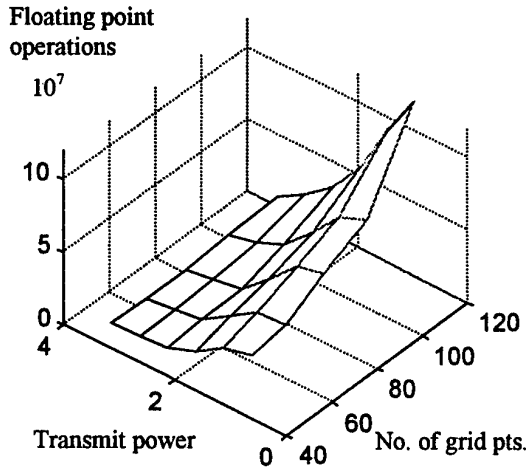



Figure 2. Computational complexity as a function of transmit power and the no. of grid points.

From another set of simulations it was observed that the total number of base stations required ($N$) increases almost linearly with m as expected (see Figure 3). Substituting $N = km$ ($k$ being the constant of proportionality), we observe from Table 1 that the computational load grows as $m^3$. This is corroborated by Figure 4.

## 6. DISCUSSION

For reducing costs, it is important to determine the optimal locations for placing base stations so as to obtain maximum coverage using minimum number of base stations. The determination of coverage by a certain base station depends upon various environmental variables, such as, the nearby building heights and locations (besides the transmitter power, the receiver sensitivity, multipath fading etc.). We have proposed an algorithm that determines where to optimally place the base stations. It also determines what is the minimum number of base stations required to provide the desired coverage. In the latter part of the paper we have discussed the computational load of the algorithm. The number of look-ups, comparisons and union operations have been considered, and their variation with respect to transmitted power and the total number of grid points have been analyzed.

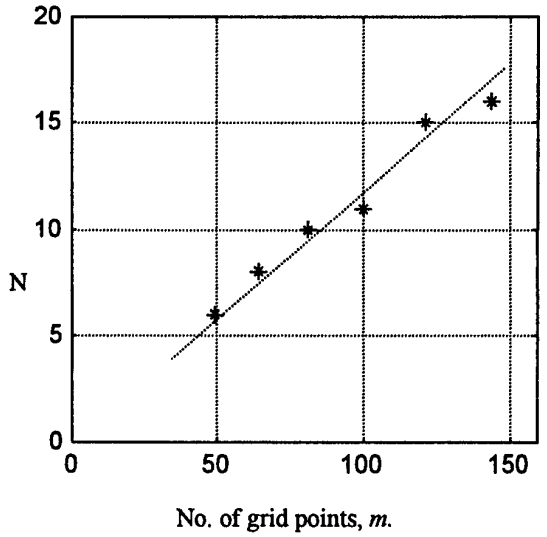



Figure 3. Linear relationship between the number of grid points, $m$, and the number of base stations, $N$.

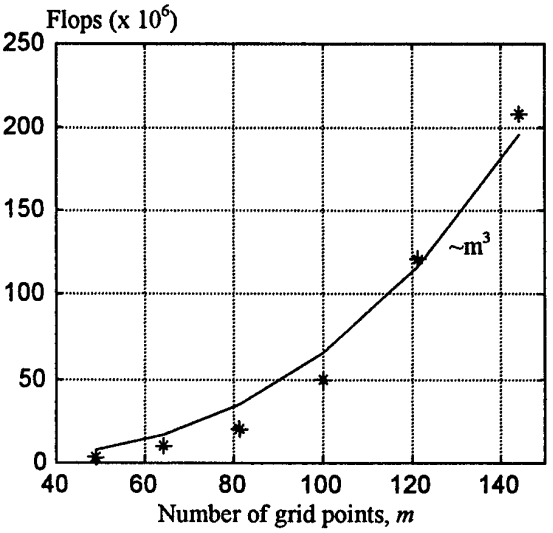



Figure 4. Variation of the number of floating point operations with the number of grid points, $m$.

## REFERENCES


[1] Clint Smith, *Practical Cellular and PCS design,* McGraw-Hill, 1998.

[2] J. Sarnecki, *et.al.*, "Microcell Design Principles", *IEEE Communications Magazine,* Apr. 1993.

[3] G.Calhoun, *Digital Cellular Radio,* Artech House, 1988.

[4] W.L. Wingston, *Introduction to Mathematical Programming,* Duxbury Press, 1995.

[5] R.Bellman, *Dynamic Programming,* Princeton University Press, 1957.

[6] Ravinder Kumar, "Implementation of a wireless communication system using cdma2000 in IIT (D) Campus", M.Tech. Thesis, Dept. of EE., IIT, Delhi, Dec. 1998.

[7] M. J. Mehler, "The microcell propagation challenge," *Inst. Elect. Eng. Colloq. Microcellar Prop. Modeling*, London, U.K., 1992, vol. 1992/234, pp. 1/1-1/4.

EMC 2000 INTERNATIONAL WROCŁAW SYMPOSIUM ON ELECTROMAGNETIC COMPATIBILITY

# RESISTANCE WELDING MACHINES – A CRITICAL POWER SUPPLY NETWORK LOAD CONCERNING POWER QUALITY AND ELECTROMAGNETIC EMISSIONS

Reinhard Doebbelin, Dirk Heyder, Hubert Mecke, Thoralf Winkler

Otto-von-Guericke-University of Magdeburg, Institute of Electric Power Systems
PSF 4120, 39016 Magdeburg (Germany), Phone: +49-391-6718592, Fax: +49-391-6712408

*Resulting from their power rating, circuit topology and discontinuous operation resistance welding machines show intensive mains current distortions and electromagnetic emissions. Considering the most important resistance welding machine types several aspects regarding these disturbances and relevant influencing factors are discussed.*

## 1. INTRODUCTION

Due to its versatility and effectiveness resistance welding has become one of the most important joining processes in engineering. It is widely used by means of welding robots incorporated into highly automated production processes and manually operated machines as well. The energy required by the welding process is provided and controlled by specific high-current power sources. Power rating covers the range of up to approximately 2.5 MVA at welding currents of up to about 350 kA. Most of resistance welding processes e.g. spot, projection and butt welding are carried out discontinuously. Thus, the operation of resistance welding machines results in remarkable surge loads of the power network which may cause voltage fluctuations and flicker. In addition voltage distortions occur depending on the specific mains current distortions of the applied power source type.

Furthermore, resistance welding machines proved to be a serious source of electromagnetic emissions (EME). The current aim to create an EMC product standard for these machines illustrates the importance of regulations in this field. As long as the existing draft for prEN 50240 [1] is not declared to be a valid standard, the regulations and limits of the generic standards concerning electromagnetic emission and immunity (mainly for industrial environment [2], [3]) have to be considered also in the field of resistance welding machines. After coming into force of the product standard for resistance welding equipment it will prevail over generic standards.

## 2. MAINS CURRENT DISTORTIONS

The types of power electronic converters mostly used in resistance welding machines are a.c. current regulators, three-phase d.c. current regulators and inverters. In case of a.c. current regulator resistance welding machines the frequency spectrum of mains current represents an uninterrupted series of odd harmonics. In contrast, following the laws of mains current harmonics [4] the mains current spectra of three-phase d.c. current regulator and inverter machines show distinct amplitudes of the harmonic numbers 5; 7; 11; 13; 17; 19; etc. In these power sources the included mains frequency operated rectifier modules determine the order of the harmonic components in the spectrum of mains current. Whereas the orders of the occurring harmonic currents thus can be predicted, the amounts of their amplitudes depend on output current adjustment, present process load, circuit details and further aspects. Therefore the amplitudes cannot easily be calculated by means of power electronic theory.

The implementation of different resistance weldments necessitates an adaptation of welding current to the technological requirements. Therefore, in terms of power quality the interrelation between output current adjustment and mains current distortion is of great importance. Here, the mentioned resistance welding machine types show a similar behavior. In case of all types an increase of output current results in a growing absolute value of most of the harmonics whereas their share of mains current rms value decreases because of the stronger increase of the share of the fundamental frequency. Therefore, the total harmonic distortion (THD) of the mains current decreases with an increasing output current (fig. 1).

Since the interrelation between output current adjustment and mains current distortion had been analyzed using a short circuit load of the machines the differences in mains current wave form and harmonics between short circuit load and welding process load had to be investigated. The comparison was made for the a.c. current regulator resis-

tance welding machine and the inverter machine using output current values chosen by typical welding applications.

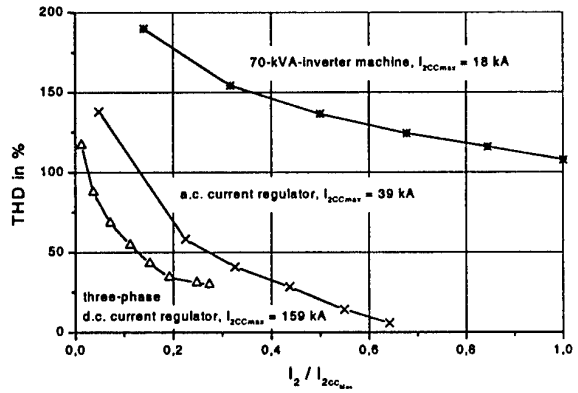



Fig. 1 Mains current THD of resistance welding machines versus output current referring to maximum short circuit output current of each machine

In case of the a.c. machine relatively low differences concerning mains current occur between short circuit and welding at the same output current value. This might be caused by the a.c. output circuit with its reactance reducing the influence of a load resistance alteration. The mains current wave form during welding process load

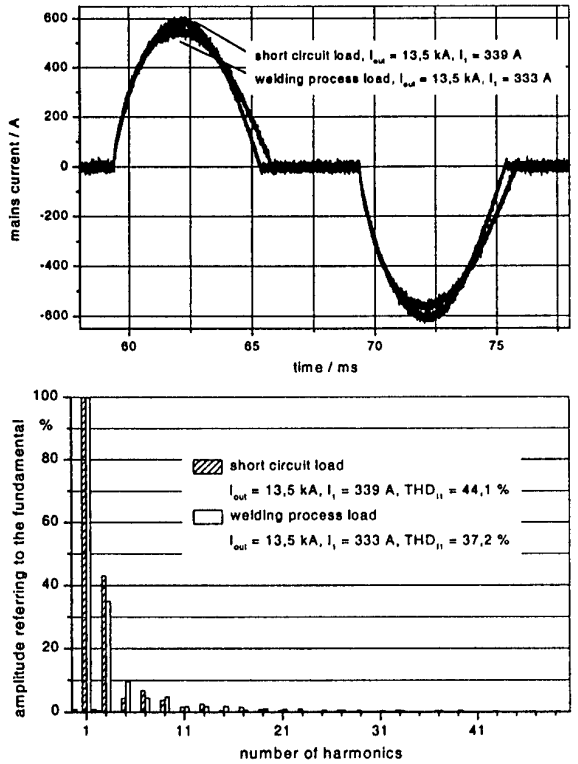



Fig. 2 Comparison between mains current of an a.c. current regulator machine during welding and under short circuit load

shows a little lower amplitude and a slightly longer duration of current flow resulting in a slightly lower distortion compared to short circuit load (fig. 2).

In case of the inverter machine the mains current rms value during welding is always higher than during short circuit load at the same output current value. Here the load resistance alteration has a greater influence on the mains current since, caused by the output rectification the influence of output circuit reactance is negligible. Determined by the three-phase diode-bridge mains rectifier with smoothing capacitor the power factor of the inverter power source is near 1. Resulting from the longer duration of current flow referring to the mains frequency period the mains current distortion during welding decreases compared to short circuit load (fig. 3).

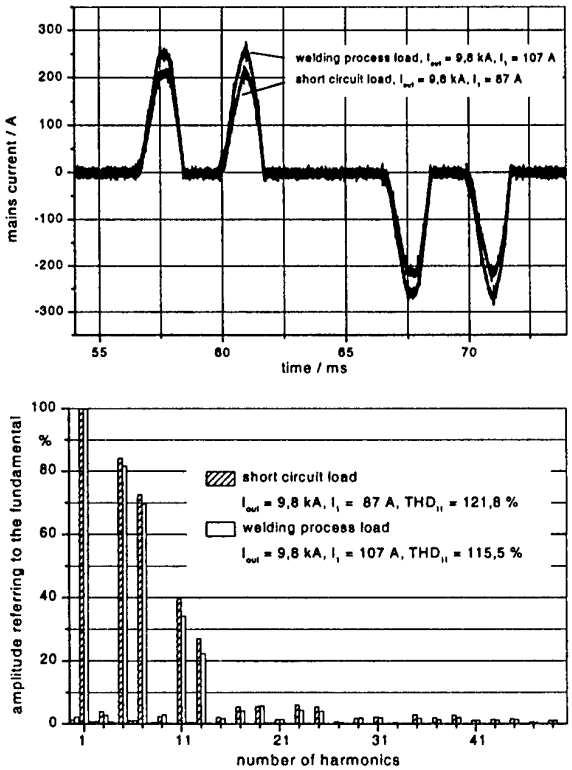



Fig. 3 Comparison between mains current of an inverter machine during welding and under short circuit load

In detail the actual mains current wave form of an inverter power source is influenced by the amount of the d.c.-link smoothing capacitance. This interrelation has been investigated by means of simulation (fig. 4).Considering idealized conditions (no power supply network impedance) the mains current distortion decreases generally with a reduction of the d.c.-link capacitance. Under realistic conditions, depending on the amounts of power supply network impedance and output current adjustment of the inverter the opposite interrelation exists in a certain range.

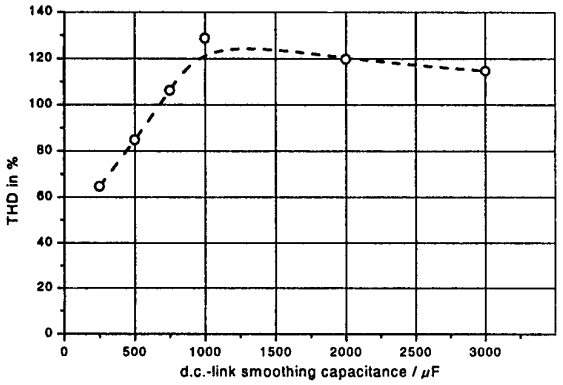



Fig. 4 Mains current THD of a resistance welding inverter versus amount of the d.c.-link smoothing capacitance, power supply network impedance: R = 1,5 mΩ, L = 50 μH, inverter output current $I_{out}$ = 10 kA

## 3. SPECIFIC ASPECTS OF EME MEASUREMENTS

To prove compliance with the EMC standards emission and susceptibility tests of the relevant devices have to be carried out. For manufacturers of resistance welding machines the question of test effort is of special importance because these machines represent exceptional DUTs. The susceptibility aspects are regarded as relatively uncritical. However, concerning electromagnetic emissions several specific aspects have to be considered [5].

So, for conducted emission measurements the noise voltages should be coupled out by means of a voltage probe instead of a LISN to maintain a sufficiently high short-circuit capacity of the supplying power system as it is required by resistance welding machines.

In contrast to most DUTs resistance welding machines work in an intermittent way. Thus, for emission measurements the measuring cycle of the EMI receiver has to be synchronized with the load cycle of the machine. In this way during one single welding time one frequency range of the disturbance spectrum is evaluated. Using this procedure the total measuring time for one operational parameter setting amounts up to approximately 2.5 h.

Concerning the evaluation of disturbances the peak evaluation should be preferred because using a quasi-peak or average evaluation the resulting spectra depend on the duration of the off-period within the duty cycle of the machines.

These measuring conditions have been considered concerning the investigations described in the following section.

Furthermore time domain measurements of conducted emissions using digital storage oscilloscopes can be taken into account [6]. In resistance welding machines the disturbance spectra are calculated by means of FFT based on the registration of one single on-period of the machine. In practice the validity of the resulting spectra is limited in the frequency range.

## 4. CHARACTERISTIC SPECTRA

As a supposition for limitation measures concerning the electromagnetic emissions of resistance welding machines the noise levels and existing dependencies have to be investigated. In [5] as an example spectra of conducted and radiated disturbances of one single resistance welding inverter had been shown. Based on an extended scope of machines some characteristics of each resistance welding machine type can be stated now. So, for instance resistance welding inverters show a relatively high noise level still in the upper frequency range of conducted emissions, because of the switching mode operation and the dynamic behavior of the applied power semiconductors.

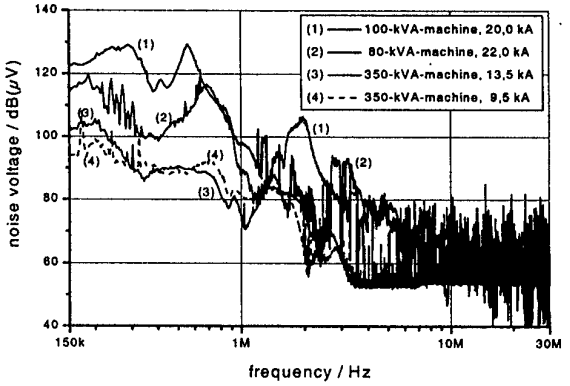



Fig. 5 Conducted emissions of a.c. current regulator resistance welding machines

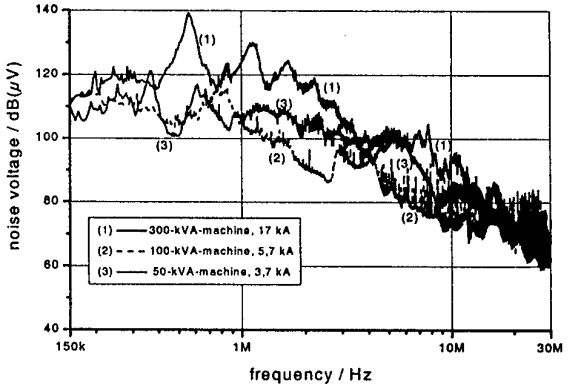



Fig. 6 Conducted emissions of inverter resistance welding machines

Whereas remarkably high noise voltage variations are typical for a.c. current regulator (fig. 5) and inverter (fig. 6) resistance welding machines, three-phase d.c. current regulator machines (fig. 7) show a relatively steady behavior.

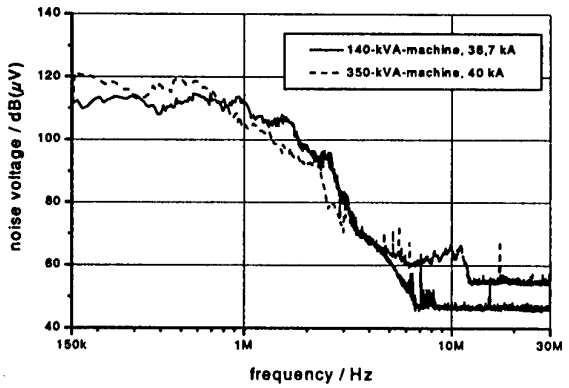



Fig. 7 Conducted emissions of three-phase d.c. current regulator resistance welding machines

Due to the phase-control of an a.c. current regulator resistance welding machine the conducted emissions of this machine type depend in a higher degree on the amount of mains voltage at the time of switching of the thyristor than on the level of output current.

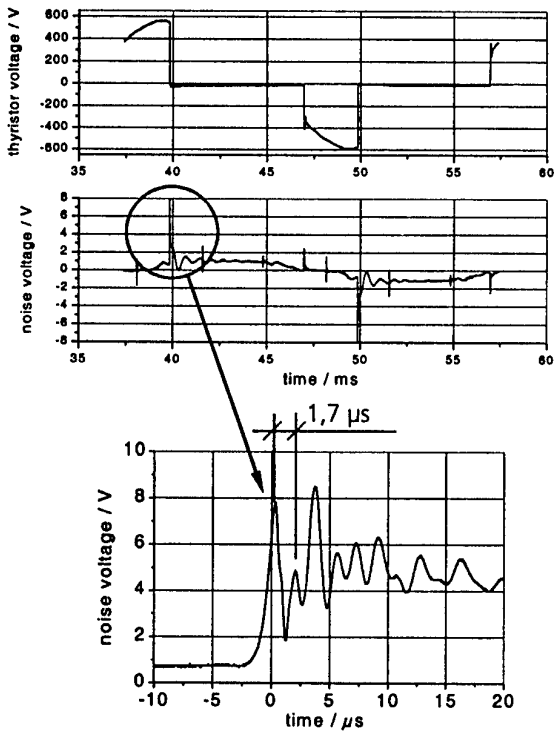



Fig. 8 Noise voltage time domain analysis

A time domain analysis of the noise voltage coupled out at the mains connection (fig. 8) demonstrates the interrelation to the switching operation of the applied power semiconductors (example 100 kVA a.c. current regulator resistance welding machine). The peak in the noise voltage spectrum of this machine (fig. 5) at about 580 kHz refers to the period of the oscillation in the interference voltage.

In fig. 9 typical spectra of radiated emissions of an inverter machine and a three-phase d.c. current regulator machine are presented. Evaluating the spectra it has to be considered that at frequencies in the region of 90 MHz and within the range from 930 up to 960 MHz a very high basic noise level appeared. Almost in the complete frequency range the inverter machine shows higher noise levels than the three-phase d.c. current regulator machine although the output current of the inverter machine is much lower. As well as in the field of conducted emissions this might be caused by the fast switching behavior of power semiconductors used in inverter topologies. In the main, typical noise levels of radiated emissions of a.c. current regulator resistance welding machines are between the noise levels of inverters and three-phase d.c. current regulators.

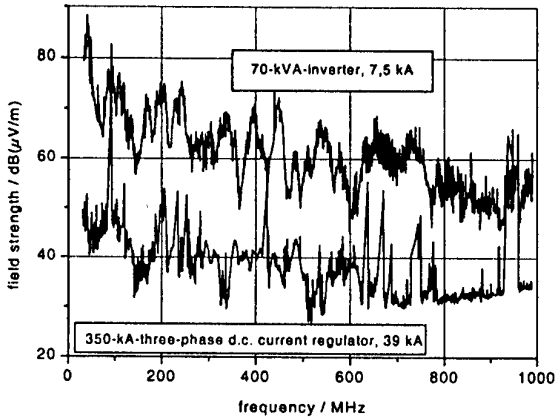



Fig. 9 Radiated emissions of resistance welding machines, measuring distance 3 m

## 5. CONCLUSIONS

All of the investigated resistance welding machine types show specific features concerning the considered disturbances. For the most part the resistance welding inverter generates the highest interference levels regarding conducted and radiated emissions and mains current distortions as well. Existing evident interrelations between voltage wave forms of internal parameters of the power source topologies, emitted noise voltage in time domain and the related spectrum can be used to localize internal sources of disturbances within the circuit topologies and to investigate appropriate remedial measures.

## ACKNOWLEDGEMENT

This work was sponsored by the German *Bundesministerium für Wirtschaft und Technologie / Arbeitsgemeinschaft industrieller Forschungsvereinigungen, AiF-Nr. 11379B* and supported by the *Forschungsvereinigung Schweissen und verwandte Verfahren des DVS* for which the authors wish to express their sincere gratitude.

## REFERENCES

[1] Draft for prEN 50240
Electromagnetic compatibility (EMC)
Product standard for resistance welding equipment

[2] EN 50081-2:1993
Electromagnetic compatibility (EMC)
Generic emission standard; Part 2: Industrial environment

[3] EN 61000-6-2-1999
Electromagnetic compatibility (EMC)
Part 6-2: Generic standards – Immunity for industrial environments

[4] D. A. Bradley
„Power Electronics" (English)
Van Nostrad Reinhold (UK) Co. Ltd, Wokingham, Berkshire, 1987, ch. 6, pp. 141-155

[5] D. Heyder, R. Doebbelin, H. Mecke, R. Neumann
„EMC- aspects of resistance welding machines" (English)
Proceedings of the Symposium on Electromagnetic Compatibility EMC Zurich, Switzerland, 1999, february 16 –18, pp. 331-334

[6] U. Reinhardt
„Comparative EMC investigations in time and frequency domain" (German)
Univ. of Stuttgart, doctoral thesis, 1996

## BIOGRAPHICAL NOTES

Reinhard Doebbelin received PhD degree (Dr.-Ing.) from the Otto-von-Guericke-University of Magdeburg in 1990. He works in the field of electronic power sources for arc and resistance welding processes and related EMC-problems.

Dirk Heyder has been a graduate electrical engineer since 1993. He works in the field of electronic power sources for technological processes and electric drives.

Hubert Mecke is professor (Prof. Dr.-Ing. habil.) of Power Electronic Equipment and Electrothermics and head of the Institute of Electric Power Systems of the Otto-von-Guericke-University of Magdeburg. Research activities concern power electronic equipment for electrothermic processes, in particular power electronic semiconducters, electronic process power sources and related EMC-problems, optimization of process control and analysis of electrothermic processes. Prof. Mecke received his doctor degrees from the Otto-von-Guericke-University of Magdeburg in 1970 and 1979.

Thoralf Winkler has been a graduate electrical engineer since 1991. He dealt with under water sparc discharges generating shock waves for pulse power technology. At present he works in the field of EMC-problems of electronic power sources.

EMC 2000 INTERNATIONAL WROCŁAW SYMPOSIUM ON ELECTROMAGNETIC COMPATIBILITY

# MONITORING OF ELECTROMAGNETIC INTERFERENCE IN HIGH VOLTAGE SUBSTATIONS

**Samir Shihab** **Gordana Felic**

*Department of Electrical Engineering*
*RMIT University*
*GPO Box 2476V, Melbourne 3001, Australia*
*Tel: +61 3 9660 2109, Fax: +61 3 9660 2007*
*sam.shihab@rmit.edu.au*

*ABSTRACT*

*This paper deals with characterisation of radiated and conducted interference in air-insulated high voltage substations. The sources of Electromagnetic Interference (EMI) studied are: the switching operation of circuit breaking equipment and the power frequency electromagnetic fields. The research interests of this study are the characterisation of these phenomena with their electrical properties and the theoretical interpretation of the conditions that cause their occurrence. Two different air insulated substations have been chosen for the investigation of the electromagnetic interference effects. A special transient recording system has been developed and installed in the substation for constant measurement and data collection. The research work includes a number of measurements and tests performed in the substations in the Melbourne metropolitan area and at the High Voltage Laboratory of RMIT University, Melbourne, Australia. The results of the complete research activity show that the radiated interference as transient electromagnetic wave propagates in broadband frequency spectrum (100 MHz). The amplitude of transient event compared to the power frequency electromagnetic field can be more than two times higher than the power frequency steady state electromagnetic field. Electromagnetic fields can couple energy in monitoring equipment and secondary low voltage wiring installed in a switchyard. Based on the results of the investigation and the associated data analyses practical solutions related to on-site measurement of EMI are proposed. Also, laboratory-testing procedures for substation control and protection equipment are addressed. Additionally, this work suggests the possible EMC measures for protecting substation control and protection equipment of potentially dangerous EMI.*

***Key words:*** *Electromagnetic Compatibility - Electric Transients – High Voltage Substations*

## 1. INTRODUCTION

The environment in a high voltage substation and the areas housing its low voltage protection and control equipment are 'polluted' by operations of high voltage components. Control and protection equipment utilizing electronic and digital circuits are potentially susceptible to this high level electromagnetic interference. Electromagnetic compatibility (EMC) of such equipment can only be guaranteed when two main factors are determined: EMI characterisation of the site of installation and the Interference Immunity of the equipment.

During its operation under normal steady state conditions, the substation as a complete system is a source of electric and magnetic field radiation. Opening and closing of switches or disconnects cause radiated and conducted interference in a form of transient electromagnetic fields and transient voltages and currents in a system. The research interests of this study are the characterisation of these phenomena with their electrical properties and the theoretical interpretation of the conditions that cause their occurrence. Once the substation interference phenomena are characterised and explained, the results of characterisation can be used to design the proper testing procedures for the substation's electronic equipment and to validate analytical models. Additionally, the characterisation can be used as the basis for electromagnetically compatible design of the same equipment that has to be installed in the substation's environment.

Two different air insulated substations have been chosen for the investigation of the electromagnetic interference effects. A special transient recording system has been developed and installed in the substation for constant measurement and data collection.

The research work includes measurements and tests performed in substations in the Melbourne metropolitan area as well as at the High voltage Laboratory of RMIT University.

All the collected data have been processed, analysed and compared with simulated models and the results obtained and published by other researchers.

## 2. MAGNETIC FIELD MEASUREMENTS

The experimental system for transient magnetic field measurements installed in the 66 kV switchyard of the 500/220/66 kV substation is shown in Figure 1. The system consists of the magnetic field sensor, fiber optic data transmission and the data acquisition, The 66 kV oil circuit breaker connects the 50 MVAR capacitor bank to and disconnects it from the 66 kV network. The oil circuit breaker (1600 A, 2500 MVA) is connected via the series reactor (1852 kVAr) to the capacitor bank. The switching operations of the breaker create current transients that generate transient magnetic fields in the vicinity of the breaker and the 66 kV bus-bar. The measurements of the magnetic fields were taken at the ground level and at the distance of 10 meters from the breaker. The loop-antenna designed according to [1] was placed in parallel position to the 66 kV bus.

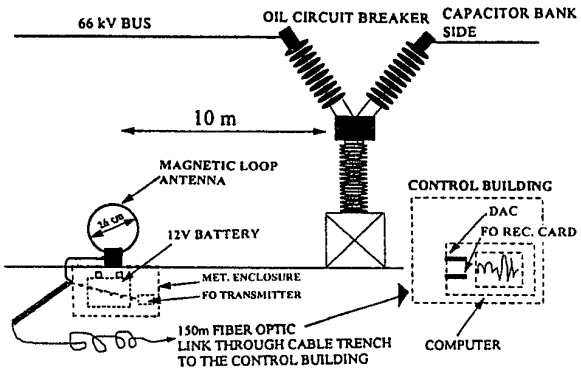



Fig. 1 Magnetic field transient measurement system installed in the switchyard (not to scale).

A typical waveform obtained by using this system is shown in Figure 2. It presents the horizontal component of the transient magnetic field that occurs during the energization of the capacitor bank by the oil circuit breaker. The captured waveform consists of pulse shaped transients occurred during the first 500 μs of the closing operation. The first single transient is produced by the occurrence of the first pre arcing (pre striking) between the breaker's contacts. 'fl-le amplitudes of the succeeding transients are lower as the distance between the contacts is decreasing. The frequency spectrum of the magnetic field waveform is in the range of 2 kHz up to 3 MHz. Due to the insensitivity of the sensor at low frequency components (50-1000 Hz) of the magnetic field the recorded transient contains only components of 5 kHz to 3MHz. They are caused mainly by the external capacitances of the, insulators at each side of the breaker. This measurement was taken at the distance of about 10 meters from the breaker. However, the components of much higher frequencies (up to 40 MHz) can be expected during the operation of the oil circuit breaker in the very close proximity to the breaker [4, 5]. All the waveforms measured in this work generally correspond to the expected transient current waveforms. However, it has to be taken into account that the magnetic field measured at a certain location over any interval of time may be a result of the superposition of three transients launched by the transient current of each phase.

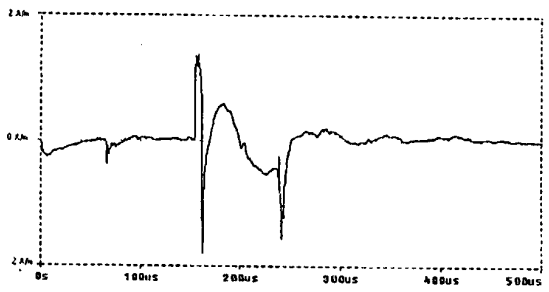



Fig. 2 Magnetic field due to the closing operation of the circuit breaker.

## 3. ELECTRIC FIELD MEASUREMENTS

The experimental system for transient electric field measurements in the 66kVswitchyard of the 500/220/66 kV substation is shown in Figure 3. The system consists of the electric field probes, fibre optic data transmission and the data acquisition. The short bus sections with the circuit breaker open at the end is to be connected to the network and the energized source side corresponding to Figure ' ). The 66 kV disconnect switch is hook-stick operated.

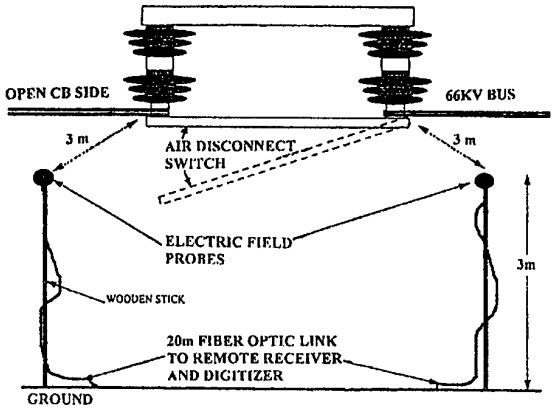



Fig. 3 Electric field transient measurement system installed in the switchyard (not to scale).

The electric field measurements were obtained by using Haefely E-field testing system during the operation of the disconnect switch (opening and closing). The electric field probes are spherical potential free field sensors designed according to [3]. They were placed high above the ground level according to Fig. 3.

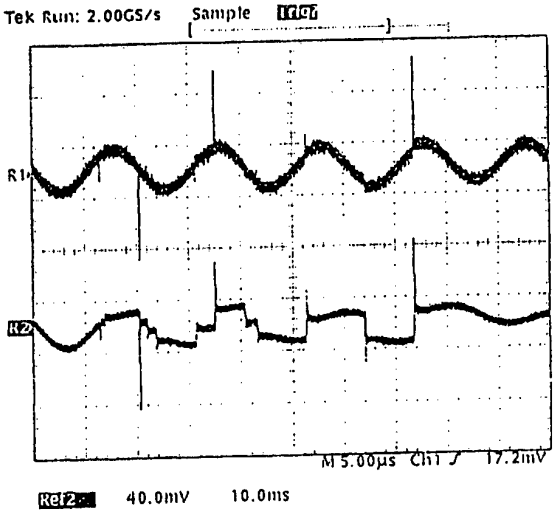



Fig.4: Electric field waveforms due to opening operation of disconnect switch. Vertical scale: upper trace (12.5 kV/m) / div, lower trace (25 kV/m) / div.

Fig.4 shows the electric field transient waveform measured close to the disconnect switch: supply side (upper trace), load side (lower trace) during the opening operation. The typical step shaped electric field waveform of the load side contact (open ended bus section) is corresponding to the expected transient voltage waveforms as it has been reported [2].

The amplitudes of the sparking transients increase and the time step between consecutive sparking events increases as the switch starts opening. The magnitude of the electric field strength close to the switch (about 3 m) was about 60 kV/m according to Figure 4 (lower trace). The obtained frequency of a single transient event was about I 0 MHz and the rise time of 20ns.

The electric field transient waforms correspond well with the measurements conducted in the laboratory as well as with the results of modelling using PSPICE simulation software. Electric field transients as high as 3 p.u. were recorded. The magnitude of the transient field strength close to the disconnect switch (about 2 m) were about 60 kV/m. It has t be taken into account that not all sparking transients could have been captured since with the sampling rate applied of 1 MHz/sample some transients could have been missed during acquisition. However, when higher sampling rate was applied it was possible to capture single striking events as well. Fig. 5 shows a record of a such single striking transient. The frequency recorded for this event is about 10 MHz and the rise time is approximately 20 ns. The maximum field intensity was about 80 kV/m.

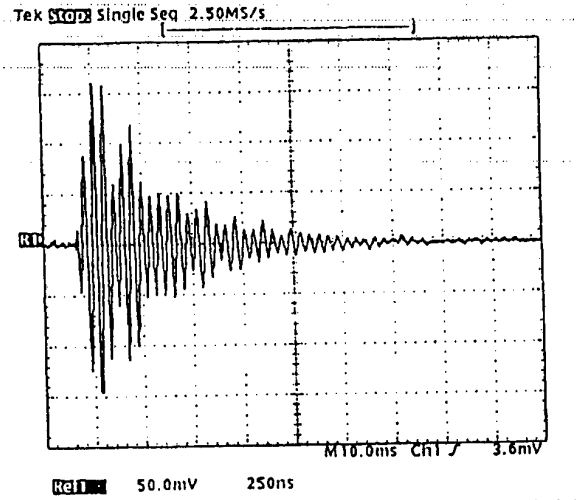



Fig. 5: Electric Field Transient recorded during opening of disconnect switch, Single Sparking event. Vertical scale: (31.25 kV/m)/div; horizontal scale: 250 ns/div.

## 4. CONCLUSIONS

The results of the complete research activity show that the radiated interference as transient electromagnetic wave propagates in broadband frequency spectrum (100 MHz). The amplitude of transient event compared to the power frequency electromagnetic field can be more than two times higher than the power frequency steady state electromagnetic field. Electromagnetic fields can couple energy in monitoring equipment and secondary low voltage wiring installed in a switchyard. The energy coupled in secondary wiring propagates through cables to control and protection equipment in a control building. If the amount of the coupled energy is above the immunity threshold of equipment, this finally results in malfunction or false operation of the protection and control circuits. It means the equipment for protection and control placed in a switchyard or inside a control building has to be tested prior to installation in a substation.

Disconnect switch transients can be a serious hazard for substations. Slow moving contacts during opening and closing operations can produce thousands of transients or arcing events that can last up to several seconds. Transient electric fields of order of several tens kV/m with frequency of several MI-TZ during the operation of a disconnect switch have to be expected.

The circuit breaker transients are characterized as far less hazardous than those produced by operation of disconnect switch. However in some applications, like in the one presented in this work (capacitor bank switching), they are switched quite frequently. Transient magnetic fields of the order of at least several

tens of A/m can be expected during the energization of the capacitor-bank.

In order to avoid malfunction, substation's electronic equipment has to be tested before installation in substations and protected against the coupling of these transients in substations. The results of EMI measurements of this work can be used for the design of more practical testing procedures.

The transient monitoring system developed in this research work proved to be reliable and, most importantly, much cheaper than the commercially available systems that are developed primarily for laboratory word and testing.

Further work is currently underway to improve the performance of the transient monitoring system. Also, further investigations are being undertaken for monitoring of conducted and coupled transients into the auxiliary systems of high voltage substations. This includes the influence and configuration of the earthing systems.

EMI measurements in high voltage substations can be expensive and to some extent cumbersome. The installation of the measuring equipment in the substation needs extra time for preparations and co-ordination with the relevant utility administering the substation. In this respect future work on analytical models that simulate solutions for more complex structures would reduce the cost of implementing practical transients monitoring systems in high voltage substations.

## 5. REFERCNCES


1. Baum C.E., Breen E.L., Giles J C, O'Neill J. and Sower G.D., "Sensors for Electromagnetic Pulse Measurements Both Inside and Away from Nuclear Source Regions", IEEE Transactions on Antennas and Propagation, Vol.AP-26, No. 1, January 1978, (p22-p35).

2. Boggs S. A., Chu F. Y., Fujimoto N., Krenicky A., Plessl A. and Schlicht D. "Disconnect Switch Induced Transients and Trapped Charge in Gas-Insulated Substations", IEEE Transactions on Power Apparatus and Systems, Vol. PAS-101, No, 10, October 1982, (pp3593-3602).

3. Feser K. and Pfaff W., "A Potential Free Spherical Sensor for the Measurement of Transient Electric Fields", IEEE Transactions on Power Apparatus and Systems, PAS-102, 1983, (pp2501-2508).

4. Wiggins C.M., Wright S.E., "Switching Transient Fields in Substations", IEEE Transactions on Power Delivery, Vol. 6, No. 2, April 1991, (pp591-600).

5. Wiggins C.M., Thomas D.E, Nickel E.S., Wright S.E., "Transient Electromagnetic Interference in Substations", IEEE Trans. on Power Delivery, Vol. 9, No. 4, October 1994, (ppl869-1884).


## BIOGRAPHICAL NOTES

**SAMIR SHIHAB** received his B.Eng.(Elec) from Cairo, Egypt and *Dipl.-Ing.* and *Dr.-Ing. (1972)* from the TU Braunschweig, Germany. Since 1975 he has been with RMIT University, Melbourne, Australia where he is now a professor. His areas of technical interests include: High Voltage Engineering, EMC, Energy Management and Engineering Education. He is a Fellow IE Aust., Member IEEE and Member of committees of CIGRE, IEC and Standards Australia.

**Gordana Felic** received her B.Eng.(Elec) from Zagreb University, Croatia and her M.E. degree from RMIT University, Australia. She did work in industry in Zagreb and from 1994-1998 she was a research assistant at RMIT University. Currently she is a Senior Tutor at the University of Melbourne. She is a Member of IEAust.

EMC 2000 INTERNATIONAL WROCŁAW SYMPOSIUM ON ELECTROMAGNETIC COMPATIBILITY

# EMC Aspects of High Speed Powerline Communications

Klaus Dostert
University of Karlsruhe
Institute of Industrial Information Systems
Hertzstr. 16, D-76187 Karlsruhe
Phone:+49 721-608-4597; Fax: +49 721-608-4500
Email: klaus.dostert@etec.uni-karlsruhe.de

## Abstract

*With the cessation of the German Telekom's monopoly significant changes are taking place in the field of fixed network telecommunications. In this context fast communication links over the so-called „last mile" are of major interest. The electrical power distribution grid could turn out to be an ideal alternative for existing standard communication links. Numerous experiments and theoretical investigations have demonstrated, that power lines generally exhibit the physical properties for rates up to several Mbits/s.*

*Based on these encouraging results, the vision of the INTERNET access via the standard wall-plug was born in industry and strongly supported by major utilities. Most of the frequency band of interest, however, is already in use for different kinds of wireless services, such as broadcasting, amateur radio or air traffic control. Although PLC is intended to be wire-bound, a certain impact on wireless services seems inevitable, because power distribution networks are electromagnetically open. This could invoke different EMC problems, which have to be carefully analyzed and avoided by appropriate measures. Currently the preparation of regulations is under way, defining portions of the spectrum between 1...30MHz, which could be opened for PLC. Furthermore allowable levels of the radiated fields have to be defined, including the corresponding measuring procedures.*

*This paper outlines the possibilities and limitations of high speed PLC, providing EMC with existing services. Towards this aim, broadband modulation schemes as well as measures of network conditioning are considered. The latter will reduce possible antenna effects of the power supply wiring system and suppress common mode signal propagation.*

## 1 INTRODUCTION

Most European power supply utilities (PSU) are owners of long-distance high-speed communication links in form of optical fibers along the high and medium tension lines. Until 1998, due to existing monopolies, this capacity could only be partially exploited. Although data transmission over energy distribution networks has been playing a role for quite a long time, systems operating beyond the frequency range of 150kHz, have not been taken into account in Europe in the past. Also the current use is still limited to data rates of several kilobits per second for low level applications such as tariff switching or remote meter reading. Research results, however, clearly indicate that the frequency range up to 30 MHz - and even beyond at building installations - offers various opportunities for high speed telecommunication [1]. Generally this field can be subdivided into telephony (i.e. speech transmission) and pure data transmission. The latter is of major interest for European power distribution systems, e.g. for fast INTERNET access. In developing countries standard telephone and digital services over power lines could be a very attractive alternative against a separate additional telecom wiring system.

The „data rate per user" requirements, the demand of real-time capability, and the allowable channel bit error rate considerably differ for the mentioned applications. Telephony, for example, needs a relatively low but constant data rate for each user, while the average duration of a telephone call is small compared with typical data transmission connections. For speech transmission, the source coded bit stream can be subdivided into more and less significant bits. Since transmission errors hitting significant bits of the data stream would cause severe disruptions, these portions have to be carefully channel coded. This way acceptable quality can be maintained e.g. at bit error rates as high as $10^{-3}$. On the other hand speech transmission demands real time capability. A repetition of lost data packets is not possible. Short disruptions, however, can easily be bridged almost unnoticeably for the user, e.g. by muting or by interpolation. Longer disruptions, however, in the range of seconds, are intolerable.

Pure data transmission has different requirements. E.g. for INTERNET access, the amount of data to be

transmitted during a session may be moderate most of the time. Sometimes, however, peaks may occur, e.g. for the download of software, sound or image files. Therefore a fixed, equally distributed assignment of the channel capacity cannot be recommended. A flexible assignment, distributing the capacity depending individually on the user's current demands appears sensible. A growing number of users will of course increase the probability of simultaneous demands for high data rates, but no general limitation for the number of users must be provided. Also for pure data transmission a low bit error rate is desirable. Lost or corrupted data packets, however, can be easily repeated as transmission is based on packet-oriented protocols (TCP/IP).

Although today the PSUs are able to use their networks for various telecommunication services without restrictions, the local loop fixed network access is still widely provided over standard copper wires owned by the former monopolists. Establishing true competition calls for a fast exploitation of the possibilities lying in the power distribution network. However, there are considerable differences in topology, structure and physical properties in comparison with conventional media, such as twisted pair and coaxial cables or fiber optic networks.

Due to the required data rates above 1 Mbit/s the frequency range up to 30 MHz must be considered. For the design of appropriate systems and for network planning, detailed models of the transfer characteristics as well as of the interference scenario are required. During the past most investigations of power line channel properties concentrated on the frequency range below 150 kHz [2]. Only recently papers were published, dealing with the MHz range [3]. Some of them are exclusively focused on indoor power line channels [4].

With powerline communications new broadband services will be operating in a network, which generally consists of unshielded and heterogeneous cable types. While transmitting signals at high frequencies over unshielded cables, such a wiring system may operate as an antenna and emit considerable radiation due to the lack of symmetry. Electromagnetic interference (EMI) with wireless services operating in the same frequency range may occur. Currently radiation out of the mains network is subject of new regulation initiatives [5]. In the following various EMC problems and solutions are discussed in detail, including the major efforts towards regulation and standardization.

## 2 EMC Problems and Solutions

PLC can be denoted as a new broadband service using the wide-spread mains network, which generally is an unshielded and heterogeneous wiring system. In the outdoor environment PLC will be established in the frequency range from 1MHz to about 10MHz and for indoor use in the frequency range between 10MHz and 30MHz seems to be appropriate. While transmitting signals at these frequencies over unshielded cables, radiation will occur due to the lack of symmetry. Electromagnetic interference (EMI) with wireless services operating in the same frequency range seems inevitable. Therefore frequency allocation and radiation from the mains network is currently subject of regulation.

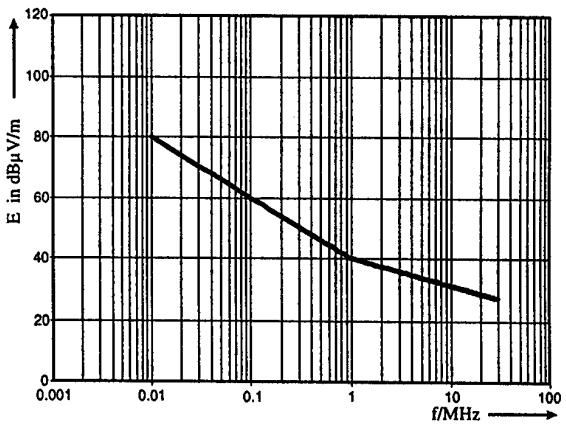



Fig. 1: Level limit proposals for the electrical field E

In Fig. 1 a proposal from the German regulatory authority (RegTP) is depicted which was published in a draft paper in January 1999. The curve Fig. 1 proposes the limits of the allowable electric field strength E at a distance of 3m from the network under test. By these limitations not only PLC is concerned, but every kind of wire-bound data transmission, including e.g. cable TV, telephone as well as computer local area networks.

The draft paper initiated a series of controversial debates, so that a time span until summer 2001 was set for amendments and corrections. Besides the rather hard level limitations, the most critical statement of the paper is, that frequency bands assigned to wireless security services must not be used on cables, independent of the level of possible radiation. Concerning the definition of those wireless security services, it should be noted, that no details about the exact allocation of the frequency bands to be protected have been published. The consequences of such kind of regulation would be dramatic economic impairments. The radiation from any data transmission cable would finally have to be brought down to the level of the atmospheric background noise, which can be as low as -40dBµV/m in certain frequency ranges. (Note that standard measuring equipment is hardly able to capture levels down to 0dBµV/m.)

For cable TV suppliers fulfilling the requirements would only be possible by shutting down the so-called special channels, which in Germany provide about 1/3 of the total TV programs. Economically this would mean a damage in the order of 15-20 billion Euros. The special channels have been used for decades without major EMC problems. Dangerous situations affecting e.g. health or causing damage to property were never reported.

Furthermore, fulfilling the above requirements would call for checking each data transmission network, including every computer local area network or the telephone wiring for possible radiation - even if the radia-

tion levels might be below the sensitivity limits of standard measuring equipment. Finally, in consequence the deactivation of numerous services would be necessary on the one hand, and on the other various new and innovative possibilities would be canceled in the stage of their introduction, including ASDL. So, hopefully amendments and corrections of the draft paper will soon lead to more sensible approaches.

Towards this aim cooperation of the regulatory authorities with industry, utilities and research institutions for compromises is paramount. The so-called „power line community" did an important first step by setting up a „regulation initiative". For manufacturers of PLC equipment it is important to be aware of usable frequency bands, as well as of the upper limits of radiation, while defining the voltage levels on the lines which are necessary for reliable communication. So first of all it is necessary to find unused portions of the spectrum, i.e. frequency bands which are currently not occupied by wireless services.

In cooperation with RegTP the overview given in Fig. 2 was obtained. In summary the gaps add up to about 7.5MHz, but the crucial point is, that the usable bandwidth is heavily segmented. No larger contiguous portions are available. This fact will of course impose significant restrictions on the choice of signaling and modulation schemes.

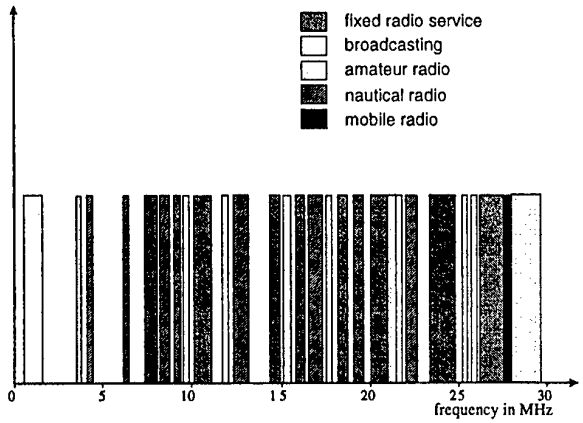



Fig. 2: Service allocation and possible gaps for PLC in the spectrum up to 30MHz

So it will e.g. be impossible to apply broadband single-carrier approaches. Multi-carrier modulation in form of OFDM, however, has turned out to be an ideal candidate for the exploitation of the spectral resources [6].

As already stated, for PLC equipment manufacturers it will be important to have clear and easy to measure limits of the voltage to fed into the power lines. Regulation, however, must not care for this voltage, but the possible radiation. In order to bridge this gap, a so-called „mains decoupling factor" similar to a definition in CISPR/A [7] is introduced. In contrast to CISPR/A, however, here the field strength is measured instead of the antenna terminal voltage - see Fig 3. This offers the possibility to express the radiated field independent of the injected voltage.

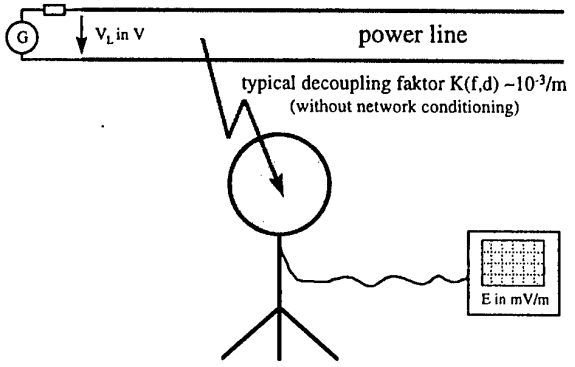



Fig. 3: Radiation measurement using an H-field probe

The newly defined decoupling factor K(f,d) must be determined for each configuration separately, e.g. for each a cable or substation. Once the decoupling factor of a certain geometry is known, it is possible to calculate the radiated fields for arbitrarily signals. Such results also offer the possibility to compare measurements for different signals. Thus, the decoupling factor will turn out to be an important figure for the future development of PLC. It can be regarded as a transfer function between the communication signals on the lines as input and the unintendedly radiated field as an output. The decoupling factor summarizes the impact of all parameters, which influence this transfer function. For determining K(f,d) a sinusoidal continuous wave signal is injected symmetrically into the power line wiring. The signal generator is swept over a certain frequency, interval and the radiated field is measured with an H-field loop antenna. According to EMC standards for the frequency range below 30MHz, this kind of loop antenna has to be used. During the sweep, the H-field amplitudes are determined. When measurements with a H-field loop antenna according to Fig. 3 are performed, exclusively magnetic fields are captured. The associated electrical field strength can be calculated by multiplying the magnetic field strength with the characteristic impedance $Z_H$=377Ω of the free space, i.e.

$$E = Z_H \cdot H \qquad (1)$$

Eq. (1) is correct only under far-field conditions, i.e. if the E- and H-field components are orthogonal and no components in the direction of propagation exist. If results form (1) are acquired under near-field conditions they can nevertheless be useful for comparative investigations, and finally even for the definition of limits for radiation. It must be noted, however, that an electrical field strength due to radiation from PLC determined this way cannot be compared with the field strength of a broadcasting station measured at the same place.

Under the assumption, that for reliable PLC a certain transmission level $V_L$ (in volts) is necessary on the power line, the question is, which electrical field strength E (in volts/meter) results from that at a certain

distance. The answer is everything but simple, because E substantially depends on the network structure, the way of signal coupling and various environmental conditions within a building, such as the presence of large metal parts.

Although Fig. 3 sketches the problem somewhat simplified, important basic statements can be made nevertheless. From various published results [8] and own measurements a rough estimation of the value of the decoupling factor K(f,d) is possible: For networks without conditioning, K(f,d) is in range of $10^{-3}$/m. I.e. for a transmission level $V_L$=1V on the line (unmodulated carrier) there is approximately an electrical field strength of E=1mV/m (≡ 60dBμV/m) at a distance of 3m. In order to estimate, which values of the electrical field strength are to be expected from real PLC signals, the following example considered:

The carrier amplitude is assumed to be 1V. For analysis a resistance of 1Ω is chosen, which allows simplified calculations, however, without affecting the general validity of the results. With this notation the total transmitted power is $P_{tot}=1/\sqrt{2}\,V^2$. For a data rate of 2Mbits/s and BPSK* modulation the transmitted power is approximately distributed over a frequency band of 4MHz. The distribution is in fact not even over this frequency range. For conciseness, however, the details are neglected here. Then we have the power spectral density of the transmitted signal:

$$S_s(f)=\frac{1V^2}{\sqrt{2}\cdot 4MHz}=17{,}67\cdot 10^{-8}\frac{V^2}{Hz}. \qquad (2)$$

Applying the measuring standard with a 9kHz band-pass filter, only the portion of power which falls into this bandwidth is received, i.e.

$$P_9=S_s(f)\cdot 9kHz=1{,}59\cdot 10^{-3}V^2 \qquad (3)$$

$P_9$ corresponds to a line voltage $V_L$=47mV. In case of a network without conditioning, the radiated field expected from such a voltage can now be estimated by the decoupling factor defined above: For $K(f,d)\approx 10^{-3}$, we have

$$E_E=K\cdot V_L=10^{-3}\cdot 47\cdot 10^{-3}V/m=33dB\mu V/m \qquad (4)$$

This result is obviously very close to the limits depicted in Fig. 1 and clearly indicates the feasibility of high speed PLC even under severe restrictions. In addition, however, the decoupling factor can be substantially lowered by network conditioning measures, which introduce a higher degree of symmetry. For reduced signal radiation the following actions seem to be suitable:

- symmetrical signal coupling
- insertion of HF barriers to prevent PLC signals from propagating into unwanted directions
- network conditioning for common mode rejection

* binary phase shift keying

When the PLC signals are symmetrically fed into the cable of interest, and at the same time also propagation is kept in differential mode along the cable, EMC problems will not occur, even for long distance transmission, i.e. over several hundred meters. In any case it makes sense to consider conditioning measures both for the transformer station and the house connection.

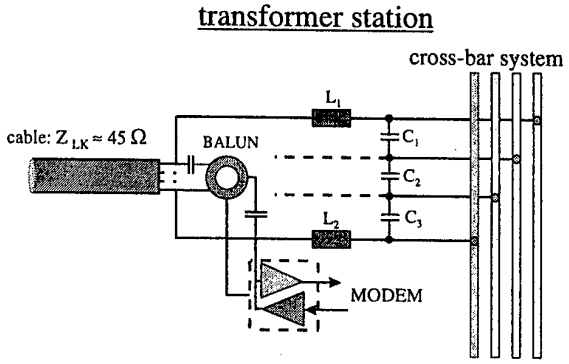



Fig. 4: Network conditioning at the transformer station

As Fig. 4 shows, an inductor for HF attenuation is inserted into the two conductors which have been selected to carry the PLC signals. The capacitors at the cross-bar system will shorten the remainder of the HF energy which eventually passes the inductors. Applying this kind of conditioning to each of the supply cables will put two barriers between the cables, yielding a high degree of decoupling. Also for the opposite direction this kind of conditioning will be advantageous, because received broadcast signals, for which mainly the cross-bar system has an antenna function, are kept away from the cable. The impedance of the output stage of a modem can now be matched to the characteristic impedance of the cable by means of a balun.

The construction of the inductors, however, turns out to be a severe challenge, although an inductance of less than 10μH is generally sufficient. Since they have to carry the full current load, which may exceed some hundred ampéres, the use of magnetic materials is problematic due to saturation. Solutions in form coreless coils will normally fail because of the necessary size. Appropriate core materials and constructions are currently tested by the author's research group in close cooperation with industry and PSUs. As soon as acceptable solutions for transformer stations are found, it will be easy to apply them in simplified form at the house connections, because here, due to the lower current loads the coils can be built substantially smaller. However, in order not to obstruct indoor PLC applications, additional inductors in each phase and the neutral conductor are necessary behind the capacitors. Also here the modem output impedance can be matched to the supply cable's characteristic impedance. Fig. 5 describes a perfect termination point which makes the behavior of the outdoor network stable and reliable, i.e. independent of the customer's indoor activities, which is an essential prerequisite for a service provider.

Unfortunately the above results cannot be transferred to the indoor network. High speed PLC within buildings will remain a severe EMC challenge, because there are no possibilities for conditioning. Both isolation and

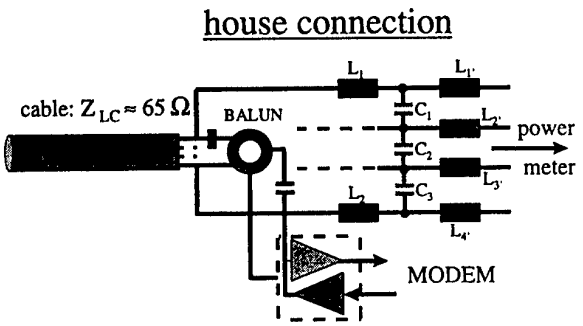



Fig. 5: Conditioning the house connection

symmetrical, differential mode signaling are unfeasible to a great extent. Strong coupling between the signal voltage $V_L$ on the line and the radiated field must generally be taken into account, i.e. the decoupling factor K(f,d) may take on values larger than $10^{-3}$/m. An advantage within buildings, however, are the relatively small distances which have to be bridged. So transmission levels can normally be chosen much lower than for outdoor applications. Capturing and evaluating interference effects, however, turns out to be very difficult. Indoor field measurements appear not very sensible, as usual procedures are hardly applicable. They prescribe a measuring distance of 3m from the mains wiring, which normally cannot be kept. Furthermore measurements at such a short distance will not capture true radiated fields, because inductive and capacitive coupling effects superimpose the results. For true field measurements a distance of at least one wavelength is required, i.e. 300m for 1MHz or 15m for 20MHz. For smaller distance a reasonable interpretation of the results is impossible. Especially a comparison with the field strength of an incoming broadcast station would be absolutely misleading. So true field measurements will make sense only outside of buildings.

## 3 CONCLUSIONS

From a realistic point of view no general electromagnetic disaster must feared through extended application of PLC. The necessary transmission levels for reliable PLC will not considerably enhance the probability of disturbance. A realistic estimation of today's electromagnetic pollution situation before the introduction of PLC clearly reveals that the reception of weak AM broadcast stations in the medium and HF frequency bands is practically impossible in most residential buildings, not to mention industrial environments. This is due to various interference caused by the operation of electrical and electronic devices, such as light dimmers, CD players, personal computers etc. Through PLC the situation should not become significantly worse, however. As guideline for acceptable AM quality in the medium-wave band, a field strength of 60dBμV/m can be assumed. If radiation from PLC always remains approximately 20dB below this value, no critical impairments will arise. The example given above has demonstrated that 27dB are achievable even with a rather simple modulation scheme.

Experimental and theoretical investigations clearly revealed, that the power distribution grid exhibits channel capacities beyond 100Mbits/s. So data rates exceeding several megabits per second are very realistic. PLC system concepts are currently centering around the multi-carrier signaling scheme OFDM. A first system generation successfully indicated the feasibility of this approach. The second system generation is under development and expected to be in operation by the end of the year 2000, while research institutions are already thinking about the next generation with enhanced performance concerning data rate and spectral efficiency, with modulation schemes such as QAM.

## 4 REFERENCES

[1] K. Dostert: RF-Models of the Electrical Power Distribution Grid. Proceedings of the 1998 International Symposium on Power Line Communications and its Applications, Tokyo (March 1998) 105-114.

[2] Hooijen, O: A Channel Model for the Residential Power Circuit Used as a Digital Communications Medium. IEEE Transactions on Eletromagn. Compat. Vol. 40 (1998), pp. 331-336

[3] Zimmermann, M., Dostert K.: A Multi-Path Signal Propagation Model for the Power Line Channel in the High Frequency Range. Proceedings of the Intern. Symp. on Power Line Communications and its Appl., Lancaster, United Kingdom 1999, pp.45-51

[4] Philipps, H. : Performance Measurements of Powerline Channels at High Frequencies. Proceedings of the Intern. Symp. on Power Line Communications and its Appl., Tokyo, Japan 1998, pp.229-237

[5] Rickard, James. A Pragmatic Approach to Setting Limits to Radiation from Powerline Communications Systems. Third International Symposium on Powerline Communications, Lancaster University, 30 March 1999.

[6] Lampe, L.H., Huber, J.B.: Bandwidth efficient power line communications based on OFDM. To be published in AEÜ Vol. 54/Heft 1, Feb. 2000.

[7] CISPR/A (Secretariat) 67, Report 60 (7/1985): Methods of measurement of mains decoupling factors.

[8] Smith report on project AY 3062 concerning a model to predict the radiation properties of certain line transmission systems. The Smith Group Limited, UK.

## BIOGRAPHICAL NOTE

Klaus Dostert received his Dipl.-Ing. degree from the RWTH Aachen in 1976 and the Dr.-Ing. degree from the University of Kaiserslautern in 1980. After some years as a post-doctoral fellow he finished his habilitation dissertation and received the „venia legendi" for RF communications. Since 1992 he has been a professor at the University of Karlsruhe. His current work centers around reliable high-speed data and voice communication over the electrical power distribution grid.

EMC 2000 INTERNATIONAL WROCŁAW SYMPOSIUM ON ELECTROMAGNETIC COMPATIBILITY

# EVALUATION OF POWER LINE COMMUNICATION SYSTEMS

G.Goldberg
Past Chairman IEC ACEC (Advisory Committee on Electromagnetic Compatibility)
Wannerstr. 43/61 8045 Switzerland Fax: +41 1 463 63 32 e-mail: gegegezurich@swissonline.ch

***Abstract***

*The utilisation of power lines for the transmission of signals superimposed on the mains voltage has been already proposed around 1895. In course of time, with the progress of the technology, systems have been developed with increasing sophistication and increasing performances. The last step of this evolution is the present development of systems in the radio frequency range 1 to 30 MHz with data rates of 1 or more Mbits per second and new applications. Aim of the paper is to summarise the characteristics of the previous and of the new systems in order to compare their performances and their fields of application. Attention will be given to the Electromagnetic Compatibility issues as a main concern with regard to the new systems is related to disturbances of the Radio Services by the radiation of the signals on the power lines.*

## 1. Short history of the mains signalling systems

First a terminological remark: All the systems using the power lines for the transmission of signals are embraced under the generic term "mains signalling". The systems operating in the Low Frequency (Hz) range (see 3.1) are called "Ripple Control Systems", the systems operating in the Medium Frequency (kHz) range (see 3.2) were called PLC systems whereby PLC means " Power line Carrier", the new systems using the High Frequency (MHz) range (see 3.3) are also called – in fact unfortunately – PLC systems but the acronym means here "Power line Communication". Confusion should be avoided.

The idea to use also the power network for the transmission of signals appeared for the first time by the end of the 19$^{th}$ century when two French engineers took 1899 a patent on this invention. A practical application of the idea started in the 20$^{th}$ with a French multifrequency Ripple Control System but a real expansion of this techniques took place after 1950 . Ripple Control enjoyed a good success and became and is still now a normal network equipment. There are several thousand emitters and probably ca 30 to 40 Mio receivers installed. Ripple control systems are one way systems. In the 70$^{th}$ several attempts were made with PLC(carrier) systems in the kHz range, up to ca 150 kHz for two ways systems but with a quite limited success. A new start began in the 90$^{th}$ with PLC (communication) systems in the MHz range for new applications and new technologies. It is still in course of development

## 2. Main features and requirements to "Mains signalling systems"

When developing or operating a mains signalling system it is necessary to have a clear idea of the requirements to its functions and its characteristics. The following list of topics may be considered in the evaluation of the systems;

Technical features:

- Frequency band and transmission frequency (transmission characteristics and disturbances)
- Signal characteristics: (type of signal : long or short pulses, spread spectrum, marking,...)
- Network structure and network characteristics (lines, loads, ....)
- Perturbation of the signals and reliability of the signal transmission
- Mutual influences of neighbouring systems,
- EMC issues: perturbation of other network items perturbation of the Radio services

Applications:
- Coding of the orders
- for Utilities: load control, remote meter reading, network control, ....newly data or voice transmission
- for the Users in Home/Building installations e.g. load control, switching operations, newly data or voice transmission

## 3. Characteristics of the various systems

In this chapter it will be tried to characterise the different types of systems in order to allow a systematic comparison

*3.1. Low frequency systems ( Ripple Control )*

Technical features:
- Single frequency systems
- Frequency in the band 110 to 725 Hz (earlier up to 3000 Hz) – Frequencies between the Harmonics
- Very good signal transmission , possible over three voltage levels - only problem: large capacitor banks
- Therefore signal injection possible on the High, Medium ; Low Voltage level (220 KV,....20 KV, O,4 KV).
- Therefore relatively high signal level: emission 2 to 5 % of Un, receivers 0,5% of Un
- Therefore quite high rating of the signal injection equipment
- But centralised installation of the whole system and centralised control makes system operation simple
- Impulse interval coding, quite slow but acceptable for the relevant applications
- EMC:
  effects of Ripple Control on other network items, nowadays no disturbances
  effects on the Ripple Control receivers: influence of the harmonics of the mains voltage – is avoided by a narrow filter curve and the relatively high response level

Applications:
- Only one way systems
- Applications: load control of domestic and industrial consumers (heating), tariff control of the electricity meters, network control (network switches, capacitor banks,...)
- Different types of receivers , from simple receivers to receivers with build in intelligence Centralised control of the whole network

*3.2. Medium Frequency systems ( Power Line Carriers)*

Ripple Control systems have two main disadvantages:
- the quite " heavy" emitters, partly due to the relatively high signal level
- that they are one way systems

Considering the developments of the field of electronic, in the techniques of signal coding and decoding, it has been tried in the $60^{th}$ and $70^{th}$ – particularly in the US - to develop for utilities new systems which avoid these disadvantages.
Different signal coding methods have been proposed :spread spectrum, frequency hopping, also shifting of the zero crossing of the power frequency voltage or current, marks on the mains voltages and others. The low emitter power allows also to have small systems for private installations

Some main features:
- Frequency in the band 9 kHz to 148,5 kHz (subdivided in several subbands : from 9 to 95 kHz for Utilities, from 95 to148,5kHz for private installations)
- Due to the higher frequency or the short pulses signal transmission quite difficult, only on two network levels MV and LV but in both directions.
- Low signal levels – in the range of 0,1..2 %. Un
- Accordingly low emitter rating
- For utilities "half" centralised system control – telecontrol of the substations from a central dispatching
- Generally quite rapid coding of the orders
- EMC:
  effects of the network disturbances on the tranceiver devices, immunity provided by an appropriate response level of the input circuit and the sophisticated signal coding
  effects of the system on other network items: no complains seem to have been stated
  effects on Radio services: although the radiated field exceed the radio frequency limits and there exist several important Radio Stations in this frequency range, also no complains seem to have been registered; the frequencies of these stations shall be avoided

Applications:
- like for Ripple Control: load control of domestic and industrial consumers, tariff control, network control,..
- additionally remote meter reading should be possible. In fact this application to our knowledge has been seldom implemented
- back signalling of network control operations

### *3.3 High Frequency systems (Power Line Communication)*

These fully new systems are now in course of development for fully new applications. Different technologies seem to be considered but no detail characteristics have been published. The main features can be summarised as follows:

Technical features.
- Frequency range 1 to 30 MHz
- Lower frequencies for Utilities (Outdoor); Higher frequencies for Buildings (Indoor)
- Intended transmission rate at least 1 Mbits per sec, possibly more
- accordingly broad band signals
- signal: spread spectrum coding or frequency chimneys (free frequencies according ITU)
- signal level: ???? (depends on the noise spectrum, less than 1 mV ?)
- reliable transmission range in the order of 300m (cables or overhead lines ? )
- therefore transmission only on one network level, primarily on the LV level to the consumers,
- necessity of a link from each emitter to a central control station, therefore quite complicated system architecture
- EMC: effects on other network items, no information available
- effects of conducted network disturbances on the system devices, no information available
- effects of radiated fields on the Radio services: presently a great concern, see chapter 4

Applications
- the promoters of these systems mention load control, tariff control, etc,...for Utilities or Building Automation like with Ripple Control or Power Line Carrier systems but this does not seem to be the main advantage of these systems.
- new intended applications would be the transmission of data like with Internet, possibly voice transmission,...as the for last mile for Radio Telecom.
- another application would be the transmission of data in a building without the necessity to install a special wiring.

PLC communication systems are in course of development. Several problems have to be solved:
- the technical solutions to assure the feasibility of the systems
- in particular the coexistence with the Radio services
- the operational aspects of the geographically spread system
- the reliability
- the economical aspects

## 4. EMC considerations

The EMC problems related to the Ripple Control Systems and the PLC carrier systems have been already solved and some short indications have been given above [1].

The situation is still subject of studies and standardisation for the PLC systems in the MHz range.
Three topics have to be examined:
- the effects of the linebound PLC signals on other network devices (no information is yet available)
- the effects of the network disturbances (noise) on the operation of the PLC devices determinant together with the signal coding method for the minimum response level of the PLC devices
- the effects of radiated fields on the Radio services presently the problem giving rise to the most concern determinant for the maximum emission level.[2,3,4,5]

Figure 1 shows a proposal for the limits of the radiated fields [6]

Several international technical bodies are studying the problem of the effects on the Radio Services: CEPT/ERC (PLT),CISPR,/G, ITU-R, CENELEC TC 205A and SC 210A, ETSI EP PLT, IEC TC 57. Final recommendations have not yet been established Also national bodies study the problem [6].

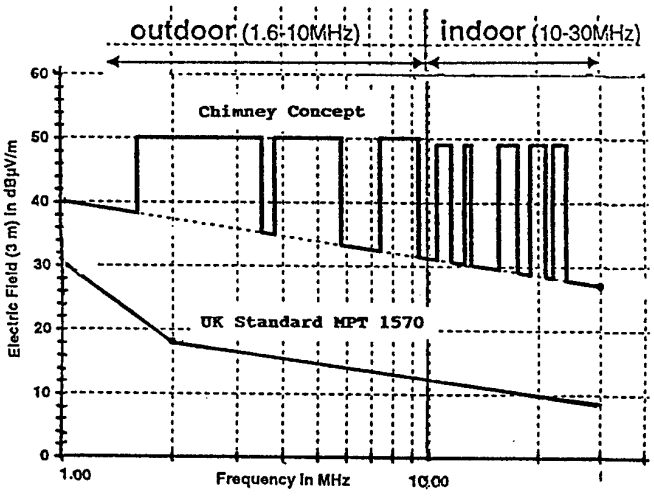



Figure 1. Proposals for the limitation of the radiated field of Powerline Communication Systems

## 5. Final remarks

There exist different kinds of "Mains signalling systems" and the question arises what could be the future.

Ripple Control in the low frequency range – below 1 kHz, one way -- is a successful system which belongs to the normal equipment of European and industrial overseas Utilities.

Power line carrier systems in the medium frequency range - 9 to 148,5 kHz, two ways – seem to have a limited success for Utilities. On the other hand they are appropriate for Buildings and House installations.

Power line Communication systems in the radio frequency range – 1 to 30 MHz, high transmission rate in the Mbits/s range – offer new utilisations of the power lines e.g. for data transmission. They are still in course of development and their success will depend on the feasibility, the operational aspects, their reliability and, last but non least, on the economical aspects. They can have two fields of application: Utilities and Buildings/House systems

## Bibliography

[1] G.Goldberg, "EMC of Signal Transmission on MV and LV Networks", Proceedings of the EMC Symposium Wroclaw 1998

[2] K.Dorset," EMC aspects of High Speed Powerline Communication Systems", Proceedings of the Symposium Wroclaw 2000

[3] R.Vick, "Radiated Emission of Domestic Mains Wiring Caused by Powerline Communication Systems,
Proceedings of the EMC Symposium Wroclaw 2000

[4] P.Wilhelmsen , " A Regulatory Authority's Evaluation of PLC and EMC", Proceedings of the EMC Symposium Wroclaw 2000

[5] D.Hansen, "Megabits per Second on 50 Hz Power lines ? Proceedings of the EMC Symposium Wroclaw 2000

[6] Radio communication Agency UK, "MPT 1570 Radiation Limits and Measurement Standard – Electromagnetic radiation from telecommunications systems operating over material substances in the frequency range 9 kHz to 300 GHz".

[7] CENELEC EN 50065-1 (1991/2/5): Signalling on low-voltage electrical installations in the frequency range 3 kHz to 148.5 kHz. Part 1: General requirements, frequency bands and electromagnetic disturbances

### *Biographical Note*

G.Goldberg graduated as Electrical Engineer at ETHZ - Federal School of Technology Zürich. He worked thereafter mainly in the field of Control Equipment for Power Systems and became there acquainted with the EMC problems. He was from 1985 to1994 Chairman of IEC TC 77- Electromagnetic Compatibility - and from1990 to 1996 of ACEC – Advisory Committee on Electromagnetic Compatibility. He is presently still active member of ACEC where he initiated the IEC work on Human Exposure to EMF

EMC 2000 INTERNATIONAL WROCŁAW SYMPOSIUM ON ELECTROMAGNETIC COMPATIBILITY

# MEGABITS PER SECOND ON 50 HZ POWER LINES ?

Diethard Hansen
EURO EMC SERVICE (EES) Dr.-Ing D. Hansen
Bahnhofstr. 39, CH-8965 Berikon 2, SWITZERLAND
Phone: +41 566337381, Email: euro.emc.service@t-online.de
http://www.euro-emc-service.de

*Digital Power Line Communications (PLC) is trying to increase the speed of data rates into the Megabits per seconds range. Therefore the short wave band of up to 30 MHz will be transmitted over the low voltage distribution network. The recent history of PLC in Germany together with the standardization and measurement procedures are given. Public opinion in Germany and technological alternatives to PLC like ADSL and wireless communications with low power are discussed. Reasons for the removal of the RegTP field trial license, based on numerous protests, are explained. The present approach of the remaining PLC consortia and their attempt to introduce the PLC technology nation wide is questionable.*

## 1. INTRODUCTION

Digital power line communications, e.g. mains signaling in the frequency range 3 to 148.5 kHz is a well recognized procedure. The EMC details are documented in EN50065-1 1991 as well as the amendments A1 1992, A2 1995 and A3 1996. The German equivalent is DIN EN50065-1 or VDE 0808 part 1 November 1996, respectively. This standard sets among others the limits for the injected signal level into the 230V/50Hz power grid for the various applications, e.g. for operating, controlling and measuring, in particular switching of the mains signaling receivers for low tariff heating systems.

The most prominent PLC activity in Europe was started about 3 years ago by the company NOR.WEB. The goal is to transmit data over a broad band medium above 148.5 kHz for telecommunications like ISDN and Internet. According to Shannon's information theory several Megabits per seconds data rate require corresponding transmission bandwidth of several Megahertz and therefore corresponding higher carrier frequencies. After lengthy considerations and pre-tests, regionally limited field trials were conducted in the U.K. The transmission path in this low voltage network started at the power transformer all the way down to the distribution into the individual homes, where the signal was decoupled. The preferred operation frequencies were 3 MHz and 5 MHz. The integral power transmission level was below 1 Watt. Using the standardized EMC receiver bandwidth of 10 kHz, according to CISPR 16 (150 kHz - 30 MHz), this results in approximately 0 dBm or -40 dBm/Hz respectively.

Under the observation of the radio communication agency in London the close monitoring of the trials was performed to explore PLC technology in general. In parallel this called for the development of a new measurement procedure MPT1570 with the title: Electromagnetic radiation from telecommunications systems operating over material substances in the frequency range 9 kHz to 300 MHz. Measurements are executed in peak mode using a magnetic loop and applying the limits of the electrical field strength:

$$E = 20\ dB(\mu V/m) - 7.7 \log_{10} (f / MHz) \qquad (1)$$

The test reality revealed excessive emissions above these limits. It is interesting to note, that in contrast to the U.K. emission limits, the German draft of the RegTP: Measurement procedure 322 MV 05 RegTP, is relaxed by approximately 20 dB. This MV 05 covers telecommunication lines and installations in the frequency range of 9 kHz - 3 GHz, using 3 Meter measurement distance.

Due to the enormous approval difficulties in the UK and the massive protests of civil and military frequency users in the short wave range, the PLC activity was shifted to the continent and Germany in particular.

## 2. PLC IN GERMANY

At the end of 1997 several consortia were formed in the German PLC arena. NOR.WEB tried to implement the British technology in Germany under Nortel DASA. In order to quickly conduct their own field trials with 1 Mbit/s in Herrenberg near Stuttgart, the south German utility company EnBW / Tesion installed the U.K. technology under license from NOR.WEB. BEWAG, the Berlin utility company, got together with HEW Hamburg and GEW Köln to develop a different

approach namely a certain spread spectrum technology, covering the total short wave range. This led to a patent claim 1997 and the granted German patent DE 197 14 386 C1 in 1998. Siemens Germany tried to develop their own solution for Internet over the mains, using multi-channel, multi-frequency technology with bit rates below 1 Mbit/s. The west German RWE teamed up with the Swiss Ascom company group to develop and establish a PLC system, which was tested near Düsseldorf with similar data rates as planned by Siemens. At the CEBIT 99 in Hannover this voice and video transmission system, using ISDN interfaces, was shown in a live presentation.

All the above mentioned consortia received a test license by the RegTP for locally and temporary restricted field trials. On the other hand the RegTP initiated a round table to deal with the compatibility in telecommunications (ATRT) under the working group 3 for PLC. For this working group the author was elected as chairman by industry, government and trade associations representatives in autumn 1998. Mr. Stecher from Rohde and Schwarz München accepted the secretariat. It was the main goal to evaluate the new PLC technology and use this input to drive national and international standardization.

## 3. STATUS AND DEVELOPMENT OF STANDARDS

PLC technology can not just simply be categorized by the historically grown EMC standards. One way to look at it, is to put a PLC modem into the frame work of the EMC act (EMVG). However, what is going to happen, if this equipment is used in a wide spread network. Moreover the power distribution grid has not been developed as a symmetrical telecom line. The proper definition, in telecom terms, of the media is almost impossible, because of mismatches, stubs, switches, lighting, outlets etc. Unshielded symmetrical, modern telecom cables have a minimum of 35 dB symmetry attenuation in the used frequency band. In the low voltage network inside buildings this value could be anything including 0 dB. Therefor common mode and not differential mode is mainly producing EMI. The equipment is hardly never going to be an impedance match. Additionally PVC installation cable by their insulation display much more path loss than telecom cables. 60 dB over 100 m at 20 MHz are not unusual. Even on one particular floor there is a lot of difference in attenuation, because outlets are installed in various locations, using different feeder systems of various phases and forming subs. The effective PLC signal transmission in the short wave range (3 MHz to 30 MHz) is perturbed by the legally necessary radio interference protection of the RFI bypass capacitors in the line filters of the associated equipment. These capacitors cause RF short circuits. For these obvious reasons low voltage networks have not been put into the group of telecom networks.

On the other hand radio transmitters have to go through national approval. This has not changed much with the introduction of TTE and R+TTE directive by the EU, because frequency spectrum use and frequency allocation have historically grown differently in the various countries. A change over night is impossible, harmonization will take time. It is also worth mentioning the duty of the national telecom authorities to ensure a certain transmission quality in the spectrum. Consequently this leads to the right of the German RegTP to control also the situation below 30 MHz along conductors, maintaining a peaceful coexistence of the various services. This may be, among others, public broadcasting, security services, the military, secret service and amateur radio. That is the coordination under the German frequency management plan, which is in it's final draft version presently. In former days there was basically no EMC conflict between cable systems and wireless applications. Unfortunately this has changed a lot with the introduction of cable TV systems and high speed digital signal transmission. In spite of using coaxial cables in the TV distribution systems there is a lot of shield leakage, based on technical imperfections and aging. Catastrophic emissions in the aeronautical security bands are jamming Germany. LANs and WANs are growing increasingly, adding to this critical situation.

The German telecommunication act (TKG §45 part 2) regulates the use of frequencies in and along conductors. Their is not much of a choice for PLC user. They either use low power spread spectrum systems with limits well below the EMC standards for ITE or apply for a national approval according to TKG, if they intend to use high power systems.

The fight over the last mile to the end customer in modern deregulated telecom and electricity markets requires solutions for wide spread networks on harmonized European level. This is presently happening under ETSI and CEPT/ERC, standardizing functional and EMC parameters more or less under one roof.

An important EMC compromise has been reached in CISPR 22 (EN55022 1998). This led to a relaxation for telecom ports under class B of about 10 dB conducted common mode emission between 6 and 30 MHz. This is, however, a temporary solution, which may have to be revised within the next 3 years, based on interference complains.

The German standardization subcommittee DKE UK 676.17 has founded a PLC working group in the forth quarter of 1999, closely cooperating with ATRT. The DKE represents the national committee of Germany, dealing with ETSI, CENELEC, CISPR and IEC. Of particular importance is presently CENELEC TC 205A, spanning the frequency range from 3 kHz to 30 MHz. Most PLC interested parties follow the high power approach with subdivisions in various unoccupied short wave windows and creating a product specific standard. This attempt, however, is problematic, due to international frequency allocations at the ITU in Geneva.

On the German side the RegTP under the ministry of economic affairs has issued a decree NB 30 - 1999. This contains the following 3 m limits:

1. 0.009 to 1 MHz
   40 dB(μV/m) - 20 $\log_{10}$(f / MHz)
2. greater 1 MHz to 30 MHz
   40 dB(μV/m) - 8.8 $\log_{10}$(f / MHz)
3. greater 30 MHz to 1 GHz
   27 dB(μV/m) equivalent to an effective radiated power 20 dBpW
4. greater 1 GHz to 3 GHz
   40 dB(μV/m) equivalent to effective radiated power 33 dBpW

The detailed measurements follows the procedure RegTP 322 MV 05.

## 4. PUBLIC'S RESPONSE AND PLC ALTERNATIVES

Shortly before CEBIT 99 the consortium RWE Ascom announced in a big PR campaign a fundamental breakthrough in PLC. The Ascom stocks rose sharply. However, PLC technical details were never published. It was interesting to watch the reaction of the other consortia in immediately launching their own success stories for projects, which were not even close to finish. Putting the pressure on the consortia in ATRT, clearly demonstrated, these experts were not in the position or willing to speak about technical details. Even the presentation of the inventor of the NOR.WEB PLC, Dr. Brown was only partly covering technical details. How can one standardize a proprietary black box PLC technology? It became finally clear by walking around at the CEBIT 99, that the whole PLC show was marketing driven. Only RWE Ascom demonstrated live. This, however, was not much more than ISDN quality. The show was accompanied by numerous protests of short wave users. The strongest opponents proved to be the RegTP licensed radio amateurs. Their club (DARC) with more than 60,000 members stated correctly PLC to be a lethal threat to the amateur radio service. This was demonstrated in various PLC field trials.

Security services like police, military and intelligence service (BND) contradict the assumption of the PLC activists, regarding the existence of many empty frequency windows. Naturally, these secret windows are not publicly listed, while at the same time radio and TV community was worried about potential increase of the noise floor throughout Germany. It was emphasized, that the introduction of digital broadcasting, leading to less radiation hazards, will only work, if the transmitter power is reduced maintaining the same background noise. The more sophisticated the modulation type, the higher the signal noise ratio has to be.

The prove for the premature push of PLC into the standardization becomes evident by analyzing the majority of the symposia, dealing with PLC at that time. Here it was mostly the business case highlighted, but the technical feasibility not to mention EMC was hardly discussed in detail. Services like video on demand superfast Internet access and Internet telephony kept the project manager's dreaming. This is partly supported by the observation of power network engineers, starting a new telecommunication career.

In the mean time German universities started Ph.D. PLC work, which naturally will take 3 to 5 years.

It is important, however, to recognize, there are many competing technologies of either conducted or wireless nature outside the field of PLC. There is tough competition in the race to the last mile. The broad band cable TV system can nowadays offering several 10 Mbit/s in about 100 MHz bandwidth at reasonable price. Bi-directional systems with the corresponding modems are commercial available for private homes with charges similar to cellular phones. The provider Netcologne is offering 52 Mbit/s without having to reserve a rented extra line.

The German Telekom is offering ADSL with approximately 1 Mbit/s expanding the old ISDN capabilities. This technology has less EMC problems, due to the symmetrical nature of the telecom lines. Fiber optic links are well known, but normally too costly to connect the end customer.

Wireless LANs today reach 1 to 10 Mbit/s at 20 dBm (100 mW) bridging several 100 m in 2.4 GHz and 5.8 GHz ISM bands. Long distance tests of up to 7.5 km at 2 Mbit/s and 100 mW have already successfully been conducted. Lately 155 Mbit/s have been achieved by wireless loops.

Looking at these advanced alternative technologies, the introduction of PLC within a relatively small window of 1 to 2 years is critical, knowing the PLC community is trying to catch up with the low side of the other high speed data rates.

## 5. WITHDRAWAL OF THE REGTP FIELD TRIAL LICENSES

After the presentation of the short wave propagation study by Ascom at the end of 1998 it was clear, -40 dBm/Hz PLC transmission level might increase the natural background noise in Germany by as much as 10 dB. The ionosphere would then mirror this effect into overseas regions. Short wave radio communications could therefore be seriously affected.

Amateur radio PLC simulations in the U.K. proved the effectiveness of Milliwatt powers for European wide radio traffic by using PLC typical end even symmetrical, buried cables. These tests were under the supervision of EMC professionals like competent bodies and EMC test labs.

Concern was also expressed by the German armed forces, the BND, the ministry of internal affairs and local federal government state agencies. Concern was also

expressed by telecom experts in the worldwide embassy radio link system. A similar situation was found in the broadcasting over long, medium and short waves. The often stated argument, this can all be covered by Internet is complete nonsense.

Many serious PLC studies and simulations in academia do not make the author believe, PLC could shortly be implemented on a nation wide base.

30 dB to 40 dB in excess of the RegTP NB 30 decree in well monitored field trials of the consortia, accompanied by accredited test labs and the RegTP, speaks for itself. These results, initially classified, are now publicly available in the minutes of the ATRT PLC meeting from 24. Sept. 1999.

Based on intensive discussions the RegTP has now withdrawn the granted licenses. Annother sensational news was, NOR.WEB is pulling out of the PLC business, mainly for economical reasons!

## 6. SUMMARY

The PLC results, in particular regarding EMC, did by far not meet the expectations. The time pressure in the market place by competing technologies is enormous. The consortia were unable to deliver adequate technical and normative drafts. ATRT, however, was able to input international normative requests for well coordinated PLC standardization. The first working groups are successfully acting. The author assumes, that in the near future there is only a chance to introduce PLC technology by using spread spectrum and keeping well below the EMC limits. This, however, will lead to more repeaters along the line. EES Germany has conducted positive pre-investigations. The EMC act with the higher limits, compared to the TKG limits, may have to be reconsidered in view of system and not only box requirements.

## BIOGRAPHICAL NOTE

Dr.-Ing. Diethard Hansen is president of the EES Switzerland and Germany, specializing in international consulting, training, innovative EMC test products, accredited testing and R&D. Further areas: LVD, radio, automotive and medical. He is holding a BS/MS in electrical engineering from Germany and a Ph.D. degree from TU Berlin. More than 20 years of industrial EMC/EMP experience, 35 patents (GTEM, EUROTEM, Poyntor sensor) and 140 professional publications as well as chairmanships are assigned to him. He was the manager of the EES Competent Body and acted as board member of European Competent Bodies ACB - Brussels. Memberships: IEEE/EMC, CENELEC, ETSI and IEC. He is the RegTP ATRT PLC chairman and a lead auditor for EMC labs and competent bodies in the DAR accreditation system. Since 1991 Dr. Hansen is a senior EMC engineer under USA NARTE accreditation.



EMC 2000 INTERNATIONAL WROCŁAW SYMPOSIUM ON ELECTROMAGNETIC COMPATIBILITY

# RADIATED EMISSION OF DOMESTIC MAIN WIRING CAUSED BY POWER-LINE COMMUNICATION SYSTEMS

Ralf Vick
EMV- Beratungs- und Planungsbüro Prof Gonschorek & Dr. Vick
Gostritzer Str. 106, 01217 Dresden, Germany
Phone: (+49) 351 3107161 Fax: (+49) 351 31071612
e-mail: info@emc-experts.com

***Abstract*** *- This paper shows the results of magnetic field strength measurement in the case of power-line carrier systems. The measurements were performed when RF signals in a frequency range of 150 kHz to 30 MHz were coupled into the 230 V main wiring of buildings. A relation between the unbalance of the power network and radiated fields is shown. However, applied models fail to predict the fields at frequencies below 4 MHz. The results show, that it is necessary to regulate power-line communication in order to protect the broadcast frequency band.*

## 1 INTRODUCTION

Transmission of data through a 230 V electric power line, called Power-line Communication (PLC), could find a intensified application within the next few years in households and industry. In a typical low-voltage system, several hundred households are connected star-like from a transformer station. Several new services could be operated without the installation of additional transmission mediums.

Data transmission through electric power-lines have already been installed in buildings to control functions, e.g. the brightness of lightning systems or the movement of shades etc.. Functioning systems based on the EIP protocol are still being commercialized. Transmission of data with a broader bandwidth is opening up new opportunities for communication technology. In US markets, systems are available which can transmit audio, television and Local Area Network signals at different carrier frequencies. This equipment right now is not allowed to be used in Europe, according to legal regulations, which also include existing restrictions of the carrier-frequency range.

In order to increase bandwidth, the transmission of signals in a frequency range above 150 kHz is necessary. With it comes a danger of radiated emission, since power lines act as an antenna at higher frequencies. This paper shows results of magnetic field measurements in case of PLC.

## 2 RADIATION BY UNBALANCED SYSTEMS

To transmit data through the power-lines, a modulated signal will be symmetrically coupled between the outer conductor and neutral or between two outer conductors of the three-phased system. The signal can be coupled to the power-line using a balun and coupling capacitors. More advanced systems adopt the output impedance of the transmitter to the power-system's impedance.

### 2.1 Unbalance of the system

It is known that the attenuation of symmetric signals along power-lines is much higher than the attenuation of asymmetric signals. On the other hand, asymmetric signals will be more efficiently radiated than symmetric signals, thus the real danger when doing PLC lies in generated asymmetrical signals along the lines.

Even if the signal is intentionally coupled symmetrically into the wiring, asymmetric voltages and currents will be generated along the line due to the system's unbalance, especially, at points with a high unbalance, i.e. electronic devices.

When a symmetrical voltage is feed into the power system one needs an appropriate method to estimate the generated asymmetrical voltage. The Longitudinal Conversion Loss (LCL) and the Transversal Conversion Loss (TCL) are defined in the ITU recommendations. They are ratios between the asymmetric and symmetric components at a specific test point, i.e. a power outlet.

The LCL of a specific test point is determined by coupling a asymmetrical voltage (longitudinal signal) into the system and measuring the resulting symmetrical voltage (transversal signal). The LCL is a logarithmic ratio between the asymmetrical ($E_L$) and the resulting symmetrical voltage ($V_T$).

$$LCL = 20 * \log_{10}(\frac{E_L}{V_T}) \quad dB \qquad (1)$$

The TCL is the ratio between the symmetrical and the asymmetrical voltage when a symmetrical voltage is feed into the system.

$$TCL = 20 * \log_{10}(\frac{E_T}{V_L}) \quad dB \qquad (2)$$

A probe can be used to measure the LCL or the TCL, [1].

Changing power-network conditions, especially the mismatch of the wave impedance between the measurement equipment and main wiring, lead to resonance in the TCL. This behavior requires the determination of the TCL at different test points within the building. Then an appropriate value, such as the minimum, should be used for interpretation of the TCL.

Once the TCL is known, one is able to calculate the asymmetrical voltage at a given amplitude of the symmetrical signal. This voltage can then be used to estimate the radiated emission with an appropriate model.

## 2.2 Measurement setup

Investigations were aimed to give an overview of the radiated fields during power-line communication. Furthermore, the relation between TCL and the radiated field should be shown. The setup was designed to measure the TCL and the radiated magnetic fields H ($0\ dB_{\mu A/m} = 51.5\ dB_{\mu V/m}$) without a change in the coupling conditions, Figure 1.

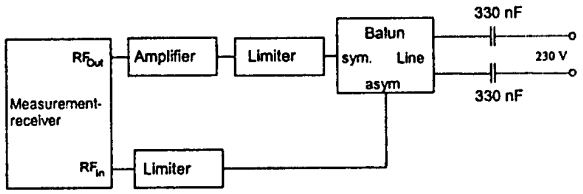



**Figure 1 TCL measurement setup**

An R&S ESHS30 measurement-receiver with an internal generator was used for the measurements. It allows the receiving frequency to be locked to the transmitting frequency. Using a balun, a symmetrical signal was coupled into the power-line system at specific power outlets. The resulting asymmetrical voltage was measured at the balun. Radiated magnetic fields within a range of approximately 30 m around the coupling point were measured by a magnetic loop antenna connected to the receiver.

# 3 MEASUREMENTS

Investigations were performed on five different buildings as well as an underground cable, but only the indoor measurements are mentioned in this paper. A symmetrical signal of 105 $dB_{\mu V}$ was coupled into different power outlets within the buildings and the radiated magnetic field was measured. The chosen buildings were an one family house, a rebuild villa, an office building, a two family house and a 12 story building from 1964.

## 3.1 Summarized magnetic field measurements

The magnetic field was measured at 192 field points within the buildings with at least two different coupling

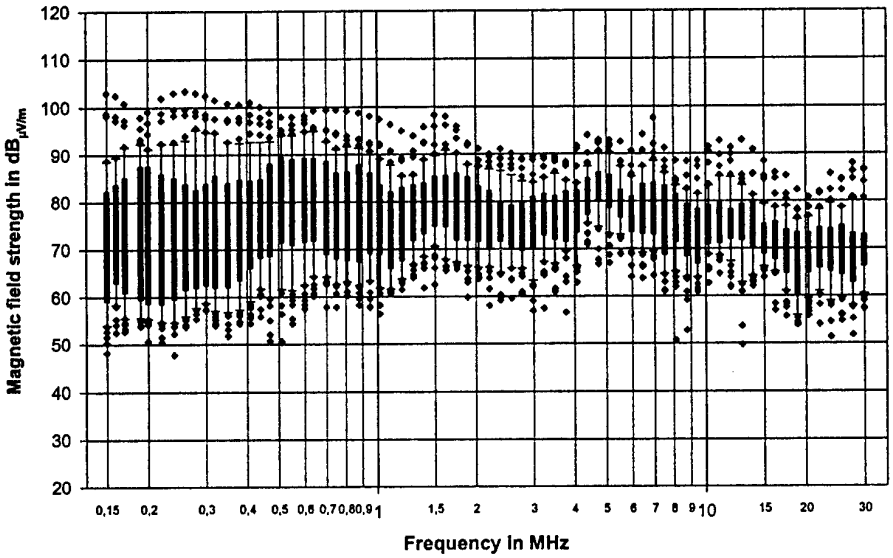



**Figure 2 Measured field strength H in a distance up to 3 m of the coupling point when a symmetrical signal of 105 $dB_{\mu V}$ was coupled into the power-line**

locations. The measurements were done at 70 pre-selected frequencies, which were chosen to have a low background noise. A high variability in the magnetic field was observed. In the case of resonance effects of the power-line system, the maximum measured magnetic field strength was 120 $dB_{\mu V/m}$. The results were grouped according to the distance, $d$, between the coupling and the measuring locations.

The following classes were chosen:

- measurements less than 3 m from the coupling point (48),
- measurements between 3 m and 5 m from the coupling point (57),
- measurements greater than 5 m from the coupling point (87).

The data are best displayed by Box-Plots. Box plots show the 25 % - 75 % interval of the values as a box, the median as a line within this box and the 10 % - 90 % values as a line interval. Additionally, all outliers are displayed as points. Thus, Box-plots give a good visual interpretation of the measured values, Figure 2 and Figure 3.

The variability in the magnetic field as well as the high resulting values are displayed in the figures.

One should use a specific value of the functions for interpretation. The demand, undisturbed reception for radio receivers should be possible in 90% of all cases, could be used to set this value.
Using this 90 % interval, it is possible to calculate a coupling factor for the magnetic field of approximately -15 $dB_{1/m}$ for frequencies lower 2 MHz, i.e. a symmetrical voltage of 105 $dB_{\mu V}$ would cause a magnetic field strength of lower than 90 $dB_{\mu V/m}$ in 90 % of the cases.

To show the dependence of the magnetic field on the frequency as well as on the distance between coupling and measurement points, the median for different distances is displayed in Figure 4.

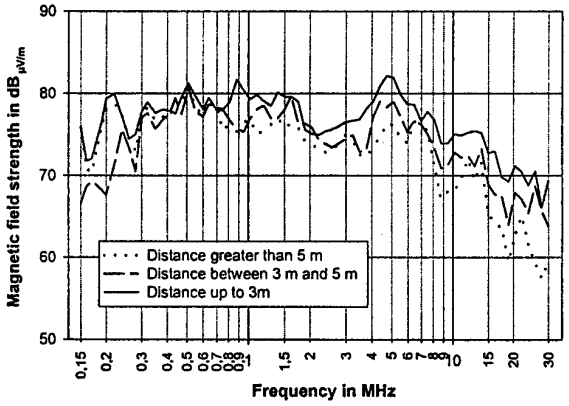



**Figure 4 Median of the measured field when a symmetrical signal of 105 $dB_{\mu V}$ is coupled into the power-line**

The curves may be interpreted as follows:

- $d < 3$ m:
  H remains around 79 $dB_{\mu V/m}$ up to 5 MHz, then falls by 15 dB per decade.
- $3\ m \leq d \leq 5$ m:
  H rises from 67 $dB_{\mu V/m}$ to 77 $dB_{\mu V/m}$ between 150 kHz to 500 kHz. Between 0.5 MHz to 5 MHz it remains around 77 $dB_{\mu V/m}$. Finally, it falls by 15 dB per decade for frequency greater than 5 MHz.
- $d > 5$ m:
  H stays around 76 $dB_{\mu V/m}$ up to 5 MHz, then falls by 20 dB per decade.

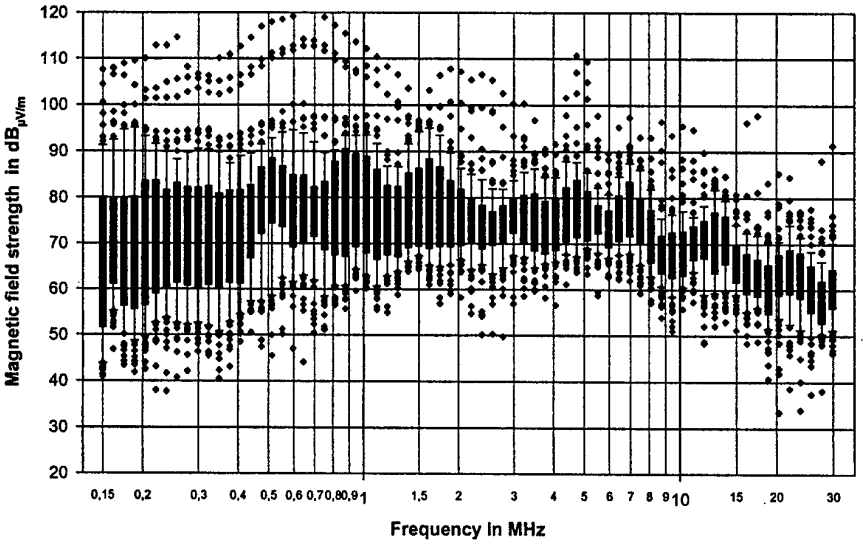



**Figure 3 Measured field strength in a distance greater 5 m of the coupling point when a symmetrical signal of 105 $dB_{\mu V}$ was coupled into the power-line**

A dependence on the distance of approximately 10 dB per decade is distinguishable at frequencies greater than 10 MHz.

### 3.2 Local distribution of the magnetic field

The local distribution of the magnetic field was measured in a single room of the one family house. The walls are situated at the coordinates (0,y), (x,0), (4m,y), (x,6m) and the power lines are installed along the walls and the ceiling (lamp outlet, z = 2.5 m).
For example, the local distribution of the magnetic field within the room at 30 MHz is shown in Figure 5.

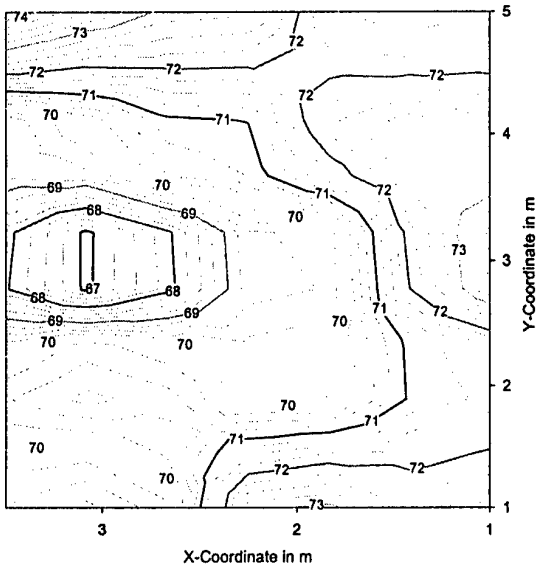



**Figure 5 Local distribution of the magnetic field when a symmetrical voltage of 105 $dB_{\mu V}$ is coupled into the power line at (0,0), z = 1 m**

It is obvious that the field varies only slightly within the room, which was already demonstrated in simulations. The maxima of the asymmetric current or voltage along the distributed lines leads to extended local maxima of the magnetic field within the room.
One will find the maxima of the field along the power line.

### 3.3 NB 30 related interpretation

The Regulation Authority of Post and Telecommunication in Germany set up limits for the magnetic field 3 m away from telecommunication equipment in the NB 30, Figure 6.
The symmetrical voltage that would cause a magnetic field according to these limits can be calculated,

$$U_{S,NB30} = U_{0,sym} \cdot \frac{H_{NB30}}{H_{ist}} \qquad (3)$$

where $U_{0,sym}$ is the symmetrical voltage used for the measurements, $H_{NB30}$ is the limit according to the NB 30 and $H_{ist}$ is the measured magnetic field.

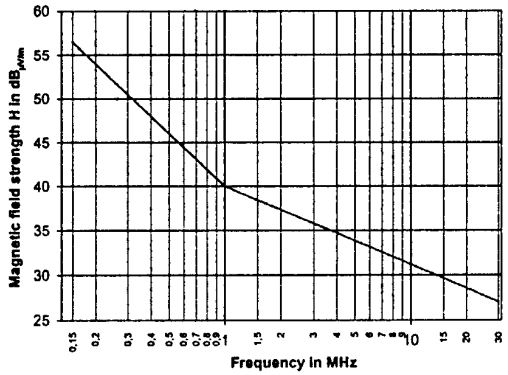



**Figure 6 Limits for the magnetic field of telecommunication systems according to the specification NB 30 of the German Regulation Authority of Post and Telecommunication**

This voltage, $U_{0,sym}$, is shown in Figure 7 for the 2 family house.

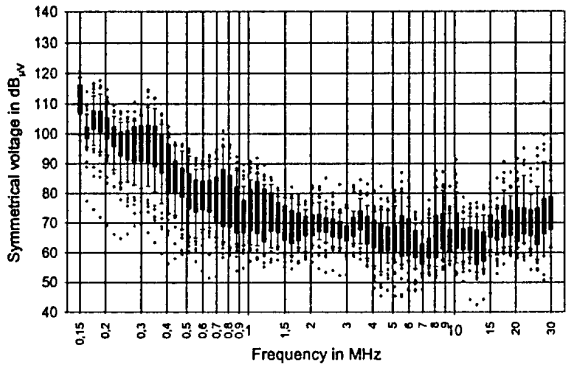



**Figure 7 Symmetrical Voltage that leads to magnetic fields according to the German regulation NB 30**

Using these voltages, one can limit the symmetrical or the unsymmetrical voltage. Therefore, it is a good assumption to assume the unsymmetrical voltage to be 6 dB less than the symmetrical voltage.

## 4 APPLYING SIMPLE MODEL

A have-wave dipole was applied to calculate the magnetic and electric field strength 10 m from the source. The amplitude of the source voltage was 105 $dB_{\mu V}$ and the dipole was in resonance for each selected frequency. The calculated field was reduced by the TCL of a specific test point in order to get an estimation for the magnetic or electric field. The median of the corresponding measurements was calculated. It is displayed along with the calculated approximation, Figure 8. The calculations were done for a number of test points and distances.
One can observe that there is a close correlation between TCL and the generated magnetic field. This simple Model underestimates the magnetic field. At 4 MHz the measured field is still around 20 dB higher

than the estimation. These discrepancy gets smaller at higher frequencies.

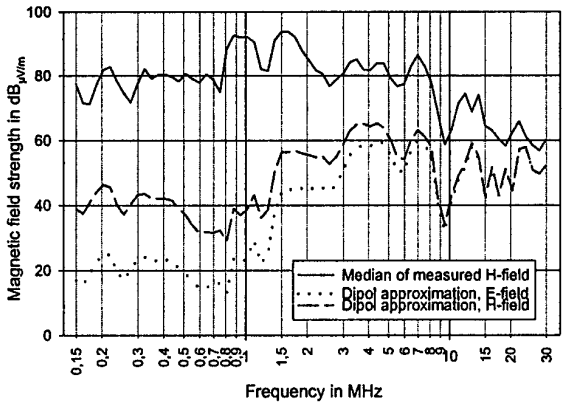



**Figure 8 Comparison between modeled and measured magnetic field strength at one coupling point**

At lower frequencies, estimation is not permitted. This is due to long wavelengths and the distributed power-lines. Even more advanced models of the wiring, which were used for numerical field calculations, are accurate in the frequency range below 1 MHz.

There are some effects that lead to these circumstances. One stems from the existence of single ended power lines. It was shown, [2], that the symmetrical signal can produce high electric fields even when the TCL, i.e. the balance of the system, is high. This is caused by unsymmetrical lines, e.g. single phased switched power-lines (lamp circuits). If the load is switched off, only one wire is connected to the load. That is why single ended line is driven as a antenna, with a source voltage equal to half of the symmetrical voltage (earth related). The result of this mode of operation is a high electric field.

There are additional undetected effects that lead to the mismatch between models and measurements in the lower frequency range. At this time, a statistical interpretation of the measurements should be used to overcome the inaccurate models. Therefore, limits of the symmetrical or the unsymmetrical voltages should be established. These limits should be related to the existing CISPR standards.

## 5 SUMMARY

The magnetic field radiated by power-lines was measured when a symmetrical signal was coupled into 230 V main wiring. The results show a potential danger related to unregulated power-line communications. The symmetrical voltage that may be coupled into the wiring is only in the order of 60 $dB_{\mu V}$ (1mV). This assumes that the generated field meets the German regulation NB 30 in 90 % of the invested cases. This is approximately valid for the entire frequency range of 150 kHz to 30 MHz. The generated fields within buildings are independent of the distance from the coupling point in the low frequency range, f < 10 MHz.

Simple models are not suitable to estimate the radiation due to PLC in the lower frequency range, especially below 4 MHz. There are some effects, related to the wiring of 230 V power networks that lead to high field strengths in the low frequency range, even when the balance of the system is still acceptable. One of the effects is a high electrical field, due to single ended wiring units, i.e. switched off lamps or loads. In this case the single ended conductor could be driven by half of the symmetrical voltage coupled into the power-line.

The results of the investigation showed the need for a regulation of the symmetrical or unsymmetrical voltage of power-line communication systems in order to protect broadcast services.

## 6 REFERENCES

[1] Macfarlane, I.P., "A Probe for the Measurement of Electrical Unbalance of Networks and Devices" (English). IEEE Transaction on Electromagnetic Compatibility, Vo. 41, No. 1, February 1999, pp. 3-14

[2] R. Vick; "PLC-Studie" (German), EMV- Beratungs- und Planungsbüro Prof. Gonschorek und Dr. Vick, Dresden, 2000 (published at www.regtp.de)

## BIOGRAPHICAL NOTES



**Ralf Vick** studied electrical engineering at Dresden University of Technology, Germany. After finishing his studies in 1991 he worked on the subject of immunity of microcontrollers to impulsive disturbances. He received his Ph.D. degree in 1995. Since 1995, he has been an EMC consultant in private practice. Projects he has involved with include the EMC of the German Frigate F124 and investigation of the radiation of power line carrier systems.

EMC 2000 INTERNATIONAL WROCŁAW SYMPOSIUM ON ELECTROMAGNETIC COMPATIBILITY

# A REGULATORY AUTHORITY'S EVALUATION OF PLC AND EMC

Per Wilhelmsen

Senior advisor, Norwegian Post and Telecommunications Authority
PO. Box 447, Sentrum, N-0104 Oslo, Norway
E.mail: per.wilhelmsen@npt.no, fax: +47 22824890

## 1. INTRODUCTION

Power Line Communications (PLC) have been discussed for some years. PLC offers a new channel "the last mile" to the customers' premises. It offers thereby an opportunity for increased competition on telecommunication services, which would be of benefit to the users. Trials have been made in several countries, and the first commercial systems are under introduction. Power lines are not constructed for telecommunication signals. This causes challenges for the development of equipment for the transmission of telecommunication signals. So far network owners and equipment producers seem to have under-estimated the challenges given by requirements on EMC and interference to radio communication systems.

The industry is busy developing equipment and solutions for PLC. The service providers and network owners want to use this equipment to offer services and increase revenue. They are testing pilot installations to be able to deploy equipment when available from the suppliers.

The authorities are discussing potential problems and possible regulations to ensure that PLC will not cause interference to radio communications. All parties meet at international organisations to develop standards and requirements for PLC. The work is not finished, but rapidly developing.

## 2. NPT AND EMC

Norwegian Post and Telecommunications Authority (NPT) is an EMC authority when radio communications are concerned. NPT is part of the telecommunication authority. NPT licence radio frequencies and controls the use of radio frequencies and noise and interference to radio communications systems.

The main EMC authority in Norway is The Norwegian Directorate for Product and Electrical Safety.

PLC is not the only new technology giving potential EMC problems. Increased frequency range for xDSL systems in telecommunication networks and two-way communications in CATV networks may also cause radiation and thereby interference to radio systems.

## 3. POWER LINES

Power line communications are as of particular interest between the distribution transformer and the end users. The distance may be up to a few hundred meters, and the number of connections about two hundred.

Power lines up to the end user connection could be
- ducted cables
- buried cables
- overhead cables
- overhead lines

From the distribution transformer a number of cables or lines go in different directions, customers are connected to taps terminated at input fuses at the customers' premises. Two main systems exists, the main system in Europe have 410 V between the three phase conductors and 230 V between any one phase and ground. Four conductors are used, in cable systems the ground conductor may act as shielding in a coaxial type cable.

In Norway a three conductor power distribution is used. Shielding may be provided in some cables, but the shielding is not used as a separate conductor. Norway and Albania are the two countries in Europe that use the three conductors distribution scheme.

We would expect buried and ducted cables to cause less radiation than overhead cables and lines. The earth layer above these cables may act as extra screening. The ground conductor will as a rule be provided as an outer conductor or sheath in cables. Cables with four conductors could therefore be used with a coaxial cable type function for high frequency signals.

Is radiation and interference from PLC unlicenced use of radio frequencies or is it an EMC problem? Seen from NPT it may be either one, regulations enforced by NPT cover both aspects.

## 4. NPT INTERESTS IN PLC

NPT started its work on PLC in 1998. The NPT interest in PLC and EMC was initiated by two examples of EMC and radio communications interference:

- Norwegian aerial cable networks in southern part of the country were some years ago disturbed by German VLF radio transmitters. Analogue carrier frequency systems (1+1 Systems) could no longer be used on certain cables. These cables had geographical orientation from the radio transmitter (north - south). Analysis and measurements are described in two articles in Telektronikk (a technical periodical from Telenor, Norway)[i] [ii]. The noise included contributions from electrical energy open wire lines that induced noise to parallel telecommunication cables.
- Information on an EMC problem, where a PLC-system internal in a building was disturbed by a PLC system at a passing medium to high voltage system with open wire lines.

Media could in 1998 report on the emerging interest for PLC for the provision of telecommunication services. The two cases mentioned above made us believe that PLC could mean interference and EMC problems if and when PLC systems were deployed in some scale. This made it necessary to initiate work to collect information on

- the possibilities for PLC systems
- the potential impact from PLC to radio communication systems
- other EMC aspects as seen from NPT as EMC authority in the field of radio communication systems.

To ensure that our work included all organisations and groups that could have a view on PLC, we formed an informal group with representatives from what was thought to be all interested parties:

- The Norwegian Directorate for Product and Electrical Safety (EMC authority in Norway)
- Norwegian Water Resources and Energy Directorate (Regulations, Norway has competition for the production part and a monopoly for the distribution part)
- NPT, with representatives from
  - Radio frequency planning and frequency licences
  - Radio frequency control
  - Technical regulation and control
- ElTele AS (a telecommunications company owned by companies for energy production and distribution)

The main task for the group was to build a common understanding of all aspects of PLC, and in particular the consequences regulations could have on PLC.

Information is collected from different sources:

1. Seminars in 1998 and 1999 on Power Line Communication systems (Arranged by IIR)
2. Standards and standardisation work in CENELEC and ETSI
3. CEPT Working Group SE (Spectrum Engineering)[iii]
4. Contact with companies developing PLC systems
   - NOR.WEB/Nortel Networks
   - Comuniq ASA (Norwegian, www.comuniq.com)
   - Alcatel Telecom AS
5. Companies studying PLC systems as their technical solutions on access, to offer telecommunication services through networks they own themselves:
   - ElTele AS
   - Viken Energinett AS (owns the distribution network in Oslo and some other municipalities)

## 5. PLC STRUCTURE

There are at least four different alternatives for PLC from the electrical energy distribution network. All alternatives include a PLC terminal at the distribution transformer, the main differences are connected to the terminations at the customers' ends:

1. PLC is terminated at the energy metering equipment and fuse box, where the telecommunication signals are transferred to an internal specialised network for telecommunications.
2. As above, but filters are introduced in the network, thus keeping the high frequency telecommunications signals in the relevant part of the cable network (only the part of the network leading to PLC customers will carry PLC signals)
3. Any of the above alternatives, but with the difference that PLC signals are lead directly into the internal power network at the customer's premises. The low voltage network will also act as at telecommunication network, any power outlet will also be a connection point for telecommunication services.
4. A two-stage PLC solution. The first stage consists of any of alternatives 1 and 2 above. The second stage is a PLC systems specialised for use on the internal power cable system at the customer's premises. Stage two may use other frequencies and signal levels than stage one.

The different solutions present different situations and effects as regards possible EMC and radiation aspects. The first two limit the high frequency signals to the cables between the distribution transformer and the customers. It will therefore be the connections between the PLC equipment and the cables themselves, including the cables, that must be investigated regarding EMC.

The use of filters to restrict the part of a distribution network where PLC signals are transmitted could reduce EMC and radio interference. Taps from cables to street light and other users of electrical energy could,

however, mean that such efforts have a moderate effect on the total emission of signals to the environment.

In alternative three there is no need to investigate the effects on PLC on the internal cabling at the customer's premises.

In alternative four the internal cabling and equipment using electrical energy will have to be evaluated regarding EMC and as source of radio interference. Equipment using electrical energy includes light bulbs, coffee machines, kitchen stoves and electrical heaters.

## 6. INTERNATIONAL STANDARDISATION

Work on PLC and associated EMC problems are going on in three different organisations. The different groups have its own field of work.

The CEPT WG SE co-ordinator on PLC has initiated a common meeting between the heads of the CEPT, ETSI and CENELEC groups. The results of such a meeting is by January 2000 not known. For those who have an interest to engage in a specific aspect, i.e. EMC, it may be difficult to see which group is the suitable one.

The different groups and areas of work are given below:

- CEPT (an organisation for post and telecommunications authorities)
  - WG SE. On possible problems on interference to radio communication systems and associated requirements on both PLC and radio systems. WG SE work in particular with problems on several users of the same radio frequencies and defining limits for signal strengths and sensitivity to interference from other signals.
  - WG FM. On possibilities to allocate frequencies dedicated to PLC. Such allocation would mean that some users of radio frequencies need to be transferred to new frequencies
  - ERM (EMC issues)
- CENELEC (an organisation open to authorities, users and industry):
  - TC 210, SC 205 (frequencies when using power lines for different types of use)
  - SC 210A (EMC, terminals)
- ETSI (European Telecommunications Standards Institute, open to authorities, users and industry):
  - Special project team on PLC standards, working in particular on protocols and architecture[iv]
  - ERM (EMC aspects)
- ITU (International Telecommunication Union):
  - ITU-R (Radio communicatons) WP 1A (relationship between PLC and radio communications, a global follow-up of work in ETSI and other regional organisations)
- CISPR
  - CISPR G (EMC for information technology equipment)
  - CISPR H (EMC limits for radio communication equipment)

One of the problems with five groups and organisations working on different aspects of PLC is the different schedules used. The CENELEC group working on standardisation on the use of frequencies up to 30 MHz is working very fast and should be finished by june 2000 (this is written 2000-02-06). The other groups have a two year schedule for their work. The CENELEC and ETSI groups are dominated by the industry developing and wanting to use PLC while the CEPT groups are working tools for the authorities in Europe and are looking at the EMC and interference that might be expected from PLC systems. The CEPT work could result in European regulations on limits for EMC and radiation from PLC and other cable media with high frequency signals.

## 7. IS RADIATION FROM PLC SYSTEMS AN EMC PROBLEM?

Power lines and telecommunications have for many years co-existed. Even if inductive coupling have resulted in noise in telecommunication cables, caused by harmonics and noise in high-voltage power lines, the measures of precaution have been covered by the power line owner if the noise source have been introduced after the telecommunications network was established. This solution could be used provided it is possible to find solutions to reduce noise and the power line owners are willing to pay.

If PLC introduces unacceptable noise to radio communication systems, it may not be possible to find measures to reduce the noise.

The CEPT group that met in December 1999 discussed PLC and with what type of regulatory framework the expected radiation and interference problem could be treated. The PLC group could not agree at that meeting. Some delegates expressed the view that the EMC directive and the following national regulations should be sufficient. Other delegates said that EMC regulations could not cover this type of situation. The latter opinion lead to the conclusion that special regulations are required to protect radio communication systems.

The EU Commission has advised the member states not to establish national regulations on limits for radiation from PLC or other cable media, but wait for the results from the studies in the different European groups working for a common view in this area.

NPT has found it necessary to ensure that we have the necessary regulatory framework in place before PLC or other new cable communication systems are deployed. This would create a predictable framework where the network owners could make their own calculations and

measurements and decide if the solutions used would create noise and interference below the defined limits.

The present regulations in Norway consist of The Telecommunications Act and secondary regulations authorised by this Act. The secondary regulations include national implementation of the EMC directive and the ITU and European radio regulations. We are of the opinion that this regulation could be sufficient. The lack of quantitative limits requires that users of radio communication systems make complaint on noise, and that the noise source is identified to a PLC system, before we could impose restrictions on the use of the source of interference. We would therefore prefer a regulatory framework where

- the PLC operator could make measurements themselves
- compare the results with limits defined in the regulations
- on this basis decide if a particular customer or part of the network may allow PLC without exceeding the given limits

## 8. THE MEASUREMENT PROBLEMS

The general measurement methods for EMC are given by CISPR:

- At frequencies below 30 MHz EMC is measured "conducted". PLC signals are below 30 MHz and should stay inside the cable. The EMC problem is connected to the signals that escape the cable.
- At frequencies above 30 MHz EMC is measured as radiated signals. At these frequencies PLC signals do not exist.
- There is no EMC requirement on cables and wires. Requirements are set for equipment and connected cables as a system. The cables exist and may be very costly to replace.

Seen from NPT this may be regarded as a small problem, as we below 30 MHz also measure radio noise sources. There seem, however, to be necessary to develop new standards for EMC measurement methods to take into account that EMC by radiation may also be a problem below 30 MHz.

Measurements of radiated field strength below 30 MHz are not very simple. Traditional dipole antennas would be too large. Active antennas of small size will simplify measurements.

The far field effect is another problem. If sky-waves are created, interfering noise signals could be a consequence very far away from the noise source. PLC and radio interference is in its nature therefore not necessarily national problems, but international.

## 9. MEASUREMENTS IN NORWAY

Measurements are planned during the summer 2000 in co-operation with Viken Energinett AS, the network operator in Oslo and some other municipalities in Norway. The trial will include different types of cables and lines. The PLC equipment will have a maximum bandwidth of 30 MHz. The network operator will deploy equipment for commercial service early 2001, if the pilot installation is working satisfactory.

There are at least two problems in measuring radiation or EMC from PLC systems.

- The power lines are not point sources, but distributed noise sources. Where should the measurements be made?
- The PLC system may be subdivided in two parts, on consisting of the network up to the customer, and the other of the network at the customers' premises.
- Buried or ducted cables (earth cables) may not always be below the surface, energy is needed for street lamps and possibly other purposes. These types of use require cables above the ground, and both cables and equipment using the energy may create radiating. How do we separate the different components of radiation?

## 10. INFORMATION ON MEASUREMENTS IN OTHER COUNTRIES

We have received information on measurements from the UK authority RA (Radiocommunications Agency) and Nor.Web/Nortel Networks. The information is on equipment and cables used for a test installation in Manchester, England. This test installation uses buried or ducted cables, centre frequencies of 3 and 5 MHz, and filters or termination equipment to avoid that PLC signals is transmitted to the internal power line network at the customers' premises.

The measurements showed radiation of very high field strength compared to usable signal levels for short wave radio communications. Radiation sources are mainly where the PLC equipment is connected to the power lines. In technical terms levels of 50 – 65 dBμV/m were measured at 10m distance from the power lines and equipment connected to them (bandwidth 9 kHz). The general background noise level is 0 dBμV/m (plus or minus 5 dB).

## 11. POSSIBLE SOLUTIONS TO PLC PROBLEMS

There are three main solutions to the expected EMC or radiation problem introduced by PLC:

- PLC solutions are allocated specific frequencies, and existing radio communication systems at these frequencies are transferred to other frequencies. This can only be a long term solution. The CEPT WG FM

is looking at the possibilities for this solution. A potential problem will occur if such frequencies are not found suitable for the capacity needed andcannot be used in networks available for PLC

- Limits for EMC or radiation of radio signals are defined for all PLC systems. The limits are set with co-existence of PLC and radio communications in mind. This solution will reduce the possibility to receive radio signals at present noise floors, as the noise floors will be higher. The CEPT WG SE is looking at this type of solution.
- Existing regulations are used. The authorities will look for the source of any problem on EMC or interference from radio signals received as complaints. Any PLC system identified as the noise source will be regarded as a system where the authorities can impose restrictions to end the noise. Such measures could mean the end of PLC used for telecommunications service for the customers in certain areas. Would it be necessary to ban the use of PLC in certain areas?

## 12. WHO WILL BE AFFECTED?

A large number of persons, companies, organisations and public services use radio communication. The use of radio frequencies up to 30 MHz include:

- Broadcasting (Long, medium and short wave)
- National defence units
- Aero mobile communications
- Maritime mobile communications
- Fixed services
- Navigation
- Frequency and timing references
- Radio astronomy
- Radio amateurs

We have heard from certain owners of power line networks interested in the use of PLC systems that the benefits of such systems are so great that a solution on possible EMC and radiation problems should be solved in a way that would allow PLC. Short wave radio communications are expected to be replaced by communications by satellite, they say. On some areas of use, their investigations show that no known users of radio communications are affected by the expected noise signals. Anyway, there are other and stronger noise sources in most environments, so the contributions from PLC systems are negligible.

Seen from the radio frequency authorities the problems are somewhat different. We have within Europe allocated all frequencies below 30 MHz to certain uses. To change the allocation of frequencies will take a lot of time and require that the present users of these frequencies are willing to change their solutions. And who should cover the costs of this solution?

NPT want to co-operate with the parties interested in PLC to find solutions that

- make the industry able to use PLC to offer services to their customers that today receive electrical energy over the power lines
- protect the radio communication users so they still may use their systems

We are at present (January 2000) in a dialogue with the industry. We follow the development in the international organisations developing standards for PLC and limits for EMC and radiation, and we are, if required, prepared to develop temporary national regulations to protect the present use of radio frequencies.

## 13. CONCLUSIONS

Information from authorities and manufacturers of PLC solutions show that PLC create increased noise levels. The increased noise levels may be a problem for ordinary reception of radio signals.

The PLC noise level measured at a distance of 10m is measured to 50 – 60 dB above the background noise level. On the other hand, the PLC noise level is significantly lower than the background noise level in an office environment.

At the moment it is therefore very difficult to draw any conclusions as to the level of EMC or radiation from PLC that might be acceptable to avoid too much degradation of radio communications.

---

[i] Knut Stokke: Travelling wave antennas. Telektronikk 4.94, p.63-66

[ii] Arne Thomassen: Telecom overhead cables as antennas for long wave radio signals. Telektronikk 4.94, p.41-43

[iii] CEPT/ERC/SE(99)PLT21rev1 Approved report of the ERC WG SE special meeting on PLT (20.12.99)

[iv] ETSI PLT#1 (99) 15, ETSI PLT 1st plenary meeting (13-14 October 1999)

EMC 2000 INTERNATIONAL WROCŁAW SYMPOSIUM ON ELECTROMAGNETIC COMPATIBILITY

Late paper to the session "EMC IN COMMUNICATION, POWER AND TRANSPORT SYSTEMS" (page 121)

# MODELLING AND SIMULATION OF INTERFERENCE AT THE RADIONAVIGATION SYSTEM OF THE MEXICO CITY

**Leopoldo Estrella and R. Linares y M**

**ESIME-SEPI-IPN,** National Polytechnic Institute **of México,** Unidad **Profesional Adolfo López** Mateos, Edif. 5, 3er. **Piso,** Col. Lindavista, **C.P.** 07738, México, **D. F. Tel+Fax:** (011525) **729-6000 ext.** 54622. E-mail: rlinares@maxwell.esimez.ipm.mx

**V. Ya. Kontorovitch**

**CINVESTAV,** México, Research and Advanced Studies Center of National **Polytechnic** Institute of México, Electrical Engineering Department, Telecommunication **Section, Av. IPN # 2508,** Esquina **con Av.** Ticomán, **Col.** San Pedro Zacatenco, **C.P.** 7000, México, D. F., **Tel+Fax:** (011525) 747-7088.E-mail: valeri@mvax 1 .red.cinvestav.mx

## ABSTRACT

Mexico City is not only big, it also has a high population density. The airport is in a metropolitan zone, surrounded by a residential area. The broadcasting services and radionavigation systems interfere with each other despite the fact that both systems obey the international standards. The problem is the location and sensitivity of the systems. In this paper a model and simulation of the radionavigation systems is presented for the Mexico City case. The model is obtained for the joint probability density function (PDF) of the phase and quadrature output signal of the complex cross-correlation when the input is a narrow-band partially correlated Gaussian signal. The results show that for signal uncorrelated is best to use a Gamma Function. Therefore a density function in accordance with the concept of the average distant using the Gamma Function is presented. These PDF are applied to the interference problem of the radionavigation system at the Mexico City airport. The results are presented as curves showing the value of input correlation coefficient, which is a practical form used to obtain the level of interference.

## 1. INTRODUCTION

The population in the world is growing. In some countries there is invasion some areas next to the airports. In Mexico city the airport is metropolitan zone and around there are residential zones, then communication services are interfered. For the airport case the mean problems is the radar that affect the population communication services such as broadcasting, radio cellular phone and etc. But the radar is affected too, due to high sensitivity. The interference power received from the emitter around of airport radar often exceeds the receiver noise by many dB, thereby limiting the system sensitivity.

Regulatory sanctions do not allow the increase of radar power. Therefore is important to analyze the interference problems around of the radar of Mexico city. Radio interference problems essentially involve three steps:

1. Finding a model to analyze the interfering signals;
2. Estimating the parameters of the interfering signals using measured data,
3. Using the estimated parameters to propose suppress methods of interference.

For modeling the interference problems is important to describe the environment as accurately as possible. In general, it is not possible due to interfering signals environment is random, then for analysis those problems is necessary to use probabilistic approach. In second section a probabilistic density function in accordance with correlation coefficient is presented. In section 3, distribution function for normalized distance in accordance with Gamma function is presented and finally apply of models.

## 2. JOINT PDF FOR THE OUTPUT VARIABLES

The radionavigation system of Mexico city is affected by different interference sources. In the system input the interference signals and useful signal can be considered as independent. However, in stage first these signal can be mixed and then in detector output the signals are correlated. The basic scheme of this process is shown in figure 1.

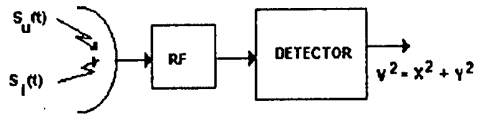



Figure 1 Radionavigation system interference scheme

Suppose we have one interfering signal $S_I(t)$ correlated with useful signal $Su(t)$. These signals are narrow band Gaussian with independent in phase and quadrature zero mean Gaussian modulation. It can be represented by conical form:

$$S_U(t) = v_1(t)\cos(2\pi f_c t) - v_2(t)\,\mathrm{sen}(2\pi f_c t) \quad (1)$$

$$S_I(t) = v_3(t)\cos(2\pi f_c t) - v_4(t)\,\mathrm{sen}(2\pi f_c t) \quad (2)$$

The correlation coefficients are:
In. phase

$$\rho\cos\phi = \frac{\sigma_{13}}{\sigma_1\sigma_2} = -\frac{\sigma_{24}}{\sigma_1\sigma_2} \quad (3)$$

quadrature

$$\rho sin\phi = \frac{\sigma_{14}}{\sigma_1\sigma_2} = -\frac{\sigma_{23}}{\sigma_1\sigma_2} \quad (4)$$

where $\sigma_1$=total power of useful signal, $\sigma_2$=total power of interference signal and $\sigma_{ij}$=covariance

The probabilistic density function (PDF) for the input signal is

$$w(v_1,v_2,v_3,v_4) = \frac{1}{(2\pi)^2\sigma_1^2\sigma_1^2\left(1-\rho^2\right)} * \exp\left[\frac{v_1^2+v_2^2}{\sigma_1^2} - 2\rho\cos\phi\,\frac{(v_1v_3+v_2v_4}{\sigma_1\sigma_2} + \frac{v_3^2+v_4^2}{\sigma_2^2} - 2\rho sin\phi\,\frac{(v_1v_4+v_2v_3}{\sigma_1\sigma_2}\right] \quad (5)$$

In detector the output signal is

$$V^2 = X^2 + Y^2 \quad (6)$$

where $X = V\cos\varphi$ y $Y = V\,\mathrm{sen}\,\varphi$

For $m$ samples with reference at the Nyquist interval (1/B), the characteristic function for output detector is:

$$\Phi_m(\omega) = E[\exp(j\omega V)]$$

As joint PDF is the inverse Fourier Transform, for V>0 we have

$$\Phi_m = \frac{4}{\sigma_1\sigma_2\left(1-\rho^2\right)(m-1)!} * \int_0^\infty \left[\frac{V}{\sigma_1\sigma_2}\right]^m * K_{m-1}\left[\frac{2V}{\sigma_1\sigma_2\left(1-\rho^2\right)}\right] * I_0 * \left[\frac{2\rho V}{\sigma_1\sigma_2\left(1-\rho^2\right)}\right]\exp(j\omega V)dV \quad (7)$$

$$W(V) = \frac{4}{\sigma_1\sigma_2\left(1-\rho^2\right)(m-1)!} * \left[\frac{V}{\sigma_1\sigma_2}\right]^m * K_{m-1}\left[\frac{2V}{\sigma_1\sigma_2\left(1-\rho^2\right)}\right] * I_0 * \left[\frac{2\rho V}{\sigma_1\sigma_2\left(1-\rho^2\right)}\right] \quad (8)$$

where $I_0(V) = \frac{1}{\pi}\int \exp(\pm V\cos\varphi)d\varphi$ is modified Bessel function

It can observe that PDF is independent of the phase of the process correlation coefficient. The behavior of the output detector in accordance with general feature of the PDF for different values of correlation coefficient and samples $m$>1, is shown in figure 2.

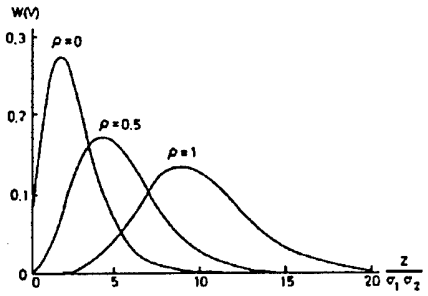



Figure 2. PDF for detector output

For uncorrelated signal the probability density function became to Gamma Function and then we can apply this function for interference analysis in radionavigation system

## 3. DISTRIBUTION FUNCTION FOR NORMALIZED DISTANCES

We assume a sequence of interference signals emitted from different source, where all of them are independent and identically distributed. This interference can be represented by mean of statistical ensembles as:

$$V_I = \sum_{i=1}^{N} v_i \quad ; \sigma_I^2 = \sum_{i=1}^{N} \sigma_i^2$$

Where N is the number of sources
In accordance with statistical model of path loss $V_I^2 = V_o^2 \langle R \rangle^{-n}$, where $V_o^2$ is voltage signal emitted by transmitter of the interference source; $\langle R \rangle$ is the average distance and $n$ is an empirical constant, which depend on environment; for free space n=2

Interference threshold is related with the receptor sensitivity, then $V_I$ can be measured in the receptor and in accordance with average distance is yield the power of the interference source.

The general assumption made here is that the space is limited by two radius: $R_k \le R \le R_m$, where $R_k$, $R_m$ are the normalized distances between the interference sources and the victim receptor as is shown in figure 3.

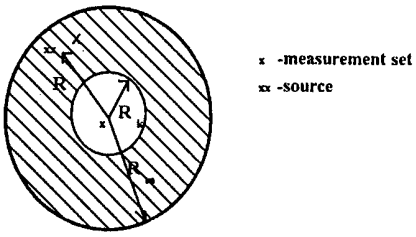



Figure 3. The measurement condition

For analysis of the interference, we use the average distance concept [1] that is:

$$\langle R \rangle = \frac{\gamma\left(R_m^{\gamma+1} - R_k^{\gamma+1}\right)}{(\gamma+1)\left(R_m^{\gamma} - R_k^{\gamma}\right)} \qquad (9)$$

where $\gamma = \begin{cases} 1 \text{ for axis location of the source} \\ 2 \text{ for plane location of the source} \\ 3 \text{ for sphere location of the source} \end{cases}$

The probability density of the signal that can interfere to victim receptor in the area limited by $R_k$, and $R_m$ can be calculate by

$$W(V_I) = \frac{[\gamma/n]\langle R \rangle^{\gamma}}{\left(R_m^{\gamma} - R_k^{\gamma}\right) V_I} \qquad (10)$$

For obtain information of envelope of the interfering signals in victim receptor can be used the Gamma distribution [1] which expression is:

$$W(x, V_I, \sigma_I^2) = \frac{1}{\beta\Gamma(\alpha+1)}\left(\frac{x}{\beta}\right)^{\alpha} \exp\left(-\frac{x}{\beta}\right) \qquad (11)$$

where $\alpha = \frac{V_I^2}{\sigma_I^2} - 1$; $\beta = \frac{\sigma_I^2}{V_o^2 \langle R \rangle^{-n}}$

## 4. EVALUATION OF INTERFERENCE

Around of the radar of Mexico city airport a lot of interfering sources, the first evaluation was to find the probability density in radii of operation of radar, where $R_m = 20\,km$ and $R_k = 0.5\,km$; the power measured interfering signals is -76 dBm. With $\gamma = 2$ and $n = 2$; $\langle R \rangle = 13341\,m$; $V_I^2 = 15.8\,\mu V^2$; $\sigma_I^2 = 5\,\mu V^2$; $\alpha = 2$ and $\beta = 3$.

Using (10) we can obtain the probability density of interfering signals, this is shown in figure 4.

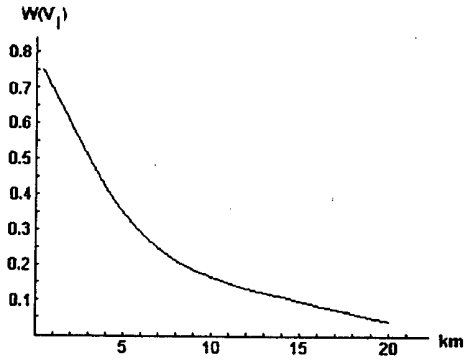



Figure 4. Probability density of interfering signals

With equation (11) is obtain the probability density function of envelope of the interfering signals, this is shown in figure 5

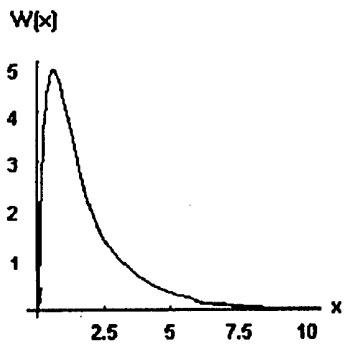



Figure 5. PDF of envelope of the interfering signals

## CONCLUSION

When the interfering signals are correlated in the process of the first stage of the receptor, the joint Gaussian density function can used with cross correator and equation (8) is performance. But if the useful signals and interfering signals are uncorrelated the better option are the equations (10) and (11), where only need the distance of coverage zone and the power of interfering signal in receptor.

## REFERENCES

[1] V. Ya. Kontorovich , R. Linares y M, H. Jardón A. B. Millan, "Theoretical approach to EMC measurements problems," International Journal of Modelling & Simulation, Vol. 19, No 4, 1999.

**EMC 2000** INTERNATIONAL WROCŁAW SYMPOSIUM ON ELECTROMAGNETIC COMPATIBILITY

Late paper to the session "EMC IN COMMUNICATION, POWER AND TRANSPORT SYSTEMS" (page 121)

# *Theoretical Experimental Investigation of EMC at Copper Subscriber Loop*

**Angel Romero R.**

Telefonos de México. Maintenance and Administration Section. Prolongación Diana 120 Col.Delicias, Cuernavaca, Morelos, C.P. 62290. México. Tel+Fax: (011527) 3225522+3162306. E-mail: arramire@telmex.net

**V. Ya Kontorovich**

CINVESTAV, México, Research and Advanced Studies Center of National Polytechnic Institute of Mexico, Electrical Engineering Department, Telecommunication Section, Av. IPN # 2508, Esquina con Av. Ticomán, Col. San Pedro Zacatenco, C.P. 7000, México, D. F., Tel+Fax: (011525) 747-7088. E-mail: valeri@mvax1.red.cinvestav.mx

**R. Linares y M.**

ESIME-SEPI-IPN; Becario COFAA, National Polytechnic Institute of Mexico, Unidad Profesional Adolfo López Mateos, Edif. 5, 3er. Piso, Col. Lindavista, C.P. 07738, México, D. F. Tel+Fax: (011525) 729-6000 ext. 54622, 54608, 54607.E-mail: rlinares@maya.esimez.ipn.mx

**Keywords: Psophometric noise, subscriber loop, higher-order statistics, alpha-stable distribution.**

## ABSTRACT

The subscriber loop connects the users to the network backbone, through the digital switching office. This loop exhibits EMC problem, because the speech and non-speech data signal are transmitted through time-continuous and amplitude-continuos waveform by means of copper wire. As a result, the signal is distorted and degraded due to several causes, such as: effects of 1/f noise, phase transition, power loss, noise, poor frequency response, and interference due to transient phenomena.

This paper shows a novel approach by means of alpha-stable distribution of the psophmetric noise at copper subscriber loops is developed for predicting disturbances at voice communication line. This approach it was used to determinate the effects that degrade the service quality at telephone-bandwidth in Mexico city. A higher-order statistical analysis was done for the psophometric noise, the noise data were given by the equipment in the central office to proportionate a methodology to quantify the noise and to solve the troubles of EMC at the subscriber loop and the results reached have been satisfactory, that's why the recommendation is to use the psophmetric noise beside the metallic noise, dBrn (dB above reference noise) to work out this kind of troubles.

## I. INTRODUCTION

Nowadays, there is not recommendation to measure in a satisfactory way the electromagnetic status of the copper rods from the analogical subscriber loop in a digital switching office to evaluate the noise immunity with accuracy, and for that reason is proposed the concept of the psophometric noise to apply it in EMC troubles at subscriber loop. The objectives for maximum levels of noise in the analogical networks from AT&T are 28 dBr (relative noise in dB's) for connections until 60 miles of length and 34 dBr for circuits of 1000 miles [1].

The current standards, in the telephone operation, for instance, it makes use of values for metallic noise less than 28 dBrnc [2], and this kind of evaluation is not good enough to detect and improve the EMC in the subscriber loop. The summary is shown by the following: The methodology starts with a brief explanation about the scenery of the telephone noise, beginning in the sixties when the mathematical models were devised by Mandelbrot

and Mertz, both of them had succesuful applications with hyperbolic distributions, such as, Mandelbrot's economic models adapted adequately in the German telephone network, completing the scenery with D. Middleton, who established the basis to generate a whole statistical communications theory as new subject of the signal processing in telecommunications. Lately, W. Willinger & V. Paxon they are working with mathematical models to represent the behavior of telephone traffic through internet.

Subsequently, to validate the psophometric concept, which is demonstred with the aid of experimental data obtained from a digital switching office ubiqueted in Mexico City, where the telephone numbers are sampled by random techniques for measure the psophometric noise in the subscriber loop by means of a software command in the computer to get the communication man machine in the telephone digital office, this exchange office was built with technology Alcatel and is known like as System 12, later on a statistical characterization of psophometric noise in a telephony digital networks with $\alpha$-stable distributions is made calculating higher-order moments, cumulants and the following four parameters; $\alpha$ (characteristic index), $\beta$ (skewness), $\gamma$ (dispersion) and a (location) to calculate the estimator for determinate the pdf of a characteristic function is the following equation:

$$f(x;\alpha,\beta)=\frac{1}{\pi}\int_0^{\infty}\exp(-t^{\alpha})\cos\left[xt+\beta t^{\alpha}\omega(t,\alpha)\right]dt. \quad (1)$$

To sum up, the function is graphed with the values estimated; histograms, quantiles or fractiles, box and whisker plot and goodness of fit to get an approach by means of alpha-stable distribution.

## II. SCENERY OF TELEPHONE NOISE

Berger and Mandelbrot have made an approach of cantor set to adjust a model with a recurrent process to describe the distribution of the ocurrence of errors in data transmission on telephone lines, i.e., processes governed by distributions of the Pareto type [3].

In 1965 Mandelbrot, uses a Levy set to build a fractal model that improves the Pareto model developed by himself in 1963.

Self-Similars stochastic processes are useful for multiscale analysis because the signals exhibiting long-range dependence and invariance in distribution under time scaling, when the model considered is fractional brown motion [4].

Based on a series of parameter estimation procedures, Stuck and Kleiner [5] modeled non-gaussian lines by a stable distribution with characteristic index = 1.95 (a gaussian has characteristic 2.0). The amplitudes of the noise bursts were adequately modeled by a log normal and power Rayleigh, or Gamma.

Nongaussian signal processing it was tried over the last twenty-five years for several authors, such as; D. Middleton in 1977 [6], who considered the impulsive interferences as the results of a large number of spatially and temporally distributed sources that produce random noise of short duration, hence probabilistic analytic models of physical nongaussian noise and interference processes are used in the development of the stable model for impulsive noise. The approach by mean of alpha-stable distribution is characterized by heavy tails on the pdf (probability distribution function) [7].

Recent mathematical discoveries concerning the temporal dynamics of internet traffic include its self-similar or monofractal scaling laws, multifractal scaling behavior over small time scales, and the emergence of wavelets as tools for analyzing network measurements, for example, internet traffic of data packets, which has been shown to be fractal with infinite variance, i.e., algebraic tails of the pdf for packet arrivals [8].

Non-Gaussian stochastic processes are encountered in many practical situations, in particular when the signal exhibits an impulsive behaviour, the wavelet analysis of fractal Poisson and self-similar processes with non-Gaussian distributions and the higher/lower-order moments of their wavelets coefficients. Stable processes have also turned out to be good models for many impulsive signals and noises, when the probability distributions of the highly variable data have heavy tails. These distributions have infinite variance and undefined higher-order moments [9].

## III. ELECTROMAGNETIC ENVIRONMENT

### A. Electromagnetic compatibility (EMC)

When the electrical and electronic devices are electromagneticly compatible, i.e., electronic noise is generated by each device involved in the whole system, and the noise doesn't interfere during the normal operation of the devices mentioned above in the introduction and it says that the system is electromagneticly compatible.

In this study it is researching the noise immunity in the subscriber loop, where the transmission lines and conmutation equipment are affected by interferences provoked by high voltages cables and atmospheric discharges; Therefore this topic is involved with the noise produced by the human being and the nature effects, both of them belong EMC and EMI (Electromagnetic interference) [10], which it refers to the undesireables voltages or currents that damage the operation of the subscriber loop.

### B. Measurements

There is a test in the digital exchanges to measure the psophometric noise with a frequency of 820 Hz, where it is got –5dBm and 0.435 Volts according to the weighting psophometric curve, this value is equivalent to 0.5 miliwatts. This test is known like; "verify" and consists in simulate two resistances;first a verification with 2000 ohms and the second a verification with 1500 ohms between the rods a & b in the subscriber loop all this is taken from the office exchange of technology "Sistema-12" from the supplier Alcatel [11], from a computer to get communication man machine the next command is sent:

**14:DN=K'XXXXXX,WTC=0,23=1&1&1,TSEGMENT=4,FULLREP,22=1,21=2;**

where XXXXXX, is the telephonic number within this test called "verify" where were found the next values of psophometric noise, which are shown in the next table:

**Table 1. Psophometric noise measurements**

| | | | |
|---|---|---|---|
| -78.34 dBp | -81.86 dBp | -81.86 dBp | -66.30 dBp |
| -68.80 dBp | -75.84 dBp | -78.34 dBp | -81.86 dBp |
| -81.86 dBp | -78.34 dBp | -72.32 dBp | -78.34 dBp |
| -81.86 dBp | -87.88 dBp | -60.28 dBp | -81.86 dBp |
| -81.86 dBp | -49.93 dBp | -73.90 dBp | -43.64 dBp |
| -78.34 dBp | -81.86 dBp | -78.34 dBp | -81.86 dBp |
| -78.34 dBp | -81.86 dBp | -81.86 dBp | -68.80 dBp |
| -69.82 dBp | -78.34 dBp | -81.86 dBp | -75.84 dBp |
| -81.86 dBp | -78.34 dBp | -75.84 dBp | -75.84 dBp |
| -81.86 dBp | -100 dBp | -81.86 dBp | -59.58 dBp |
| -100 dBp | -81.86 dBp | -75.84 dBp | -81.86 dBp |
| -78.34 dBp | -87.88 dBp | -81.86 dBp | -81.86 dBp |
| -78.34 dBp | -81.84 dBp | -55.84 dBp | -78.34 dBp |
| -78.34 dBp | -78.34 dBp | -41.77 dBp | -60.65 dBp |
| -87.88 dBp | -78.34 dBp | -78.34 dBp | -87.88 dBp |
| -72.32 dBp | -73.90 dBp | -78.34 dBp | -53.90 dBp |
| -64.36 dBp | -58.34 dBp | -62.78 dBp | -67.88 dBp |
| -67.88 dBp | -78.34 dBp | -81.86 dBp | -87.88 dBp |
| -63.80 dBp | -69.82 dBp | -75.84 dBp | -69.82 dBp |
| -44.07 dBp | -38.31 dBp | -78.34 dBp | -87.84 dBp |
| -73.90 dBp | -60.28 dBp | -68.80 dBp | -56.76 dBp |

## IV. STATISTICS

### A. Data collection

Classifing data after table 1 by frequency during the measures carried on from the exchange office of psophometric noise in the analogical subscriber loop to determinate the behavior of the the distribution in the telephonic noise.

To calculate the media, median, mode, standar deviation, variance, fractils, etc. We it got the next data:

**Table 2. Frequency of the data**

| Intervals (dB's) | Frequency (g) | Scale (x) | Product (xg) |
|---|---|---|---|
| 100-97 | 2 | -9 | -18 |
| 97-94 | 1 | -8 | -8 |
| 94-91 | 0 | -7 | 0 |
| 91-88 | 0 | -6 | 0 |
| 88-85 | 6 | -5 | -30 |
| 85-82 | 1 | -4 | -4 |
| 82-79 | 20 | -3 | -60 |
| 79-76 | 17 | -2 | -34 |
| 76-73 | 9 | -1 | -9 |
| 73-70 | 2 | 0 | -163 |
| 70-67 | 8 | 1 | 8 |
| 67-64 | 2 | 2 | 4 |
| 64-61 | 2 | 3 | 6 |
| 61-58 | 4 | 4 | 16 |
| 58-55 | 2 | 5 | 10 |
| 55-52 | 1 | 6 | 6 |
| 52-49 | 1 | 7 | 7 |
| 49-46 | 0 | 8 | 0 |
| 46-43 | 2 | 9 | 18 |
| | 80 | | 75 |

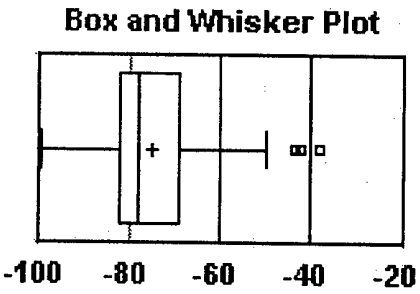



**Fig. 1 Box-and-Whisker Plot with the data from Table 1.**

From Fig.1 it has the following quantiles and it proceeds to normalize the data to get positives estimators taking the central value zero and interpoling:

05% = -86 dB → -1.8
25 % = -76 dB → -0.6

75 % = -68 dB → 0.4
95 % = -60 dB → 1.2,

**B. Probability function density.**

To calculate the probability density function, it uses the characteristic function from inverse Fourier transform:

$$f(x;\alpha,\beta)=\frac{1}{\pi}\int_0^{\infty}\exp(-t^{\alpha})\cos\left[xt+\beta t^{\alpha}\omega(t,\alpha)\right]dt. \quad (2)$$

Sustituting the normalized data from table 2:

$$f_{\alpha}(x)=\frac{1}{\pi\alpha}\sum_{k=0}^{\infty}\frac{(-1)^k}{2k!}\Gamma\left(\frac{2k+1}{\alpha}\right)x^{2k},1\le\alpha\le 2$$

$$f_{\alpha}=0.45 \quad (3)$$

An infinitely divisible characteristic function has no real zeros [12].

Now it employs Likehood-Ratio Test method:

$$\left(|f(t)|^2\right)^{1/2n}=|f(t)|^{1/n}=\exp\left\{\frac{1}{n}\log f(t)\right\},$$

$$f_{\alpha}(x)=\frac{\alpha}{|1-\alpha|}x^{1/(\alpha-1)}\int_0^{\pi/2}\upsilon(\theta)e^{-\alpha/(\alpha-1)\upsilon(\theta)}d\theta,$$

$$f_{\alpha}(0)=\frac{1}{\pi}\Gamma((\alpha+1)/\alpha)=0.28,$$

$$f_1(x)=\frac{1}{\pi(1+x^2)}=0.30,$$

$$f_2(x)=\frac{1}{2\sqrt{\pi}}e^{-x^2/4}=0.27.$$

**C. Estimators**

Now we can get the estimators using McCulloch's fractile method:

$$\upsilon_{\alpha}=\frac{\pounds_{0.95}-\pounds_{0.05}}{\pounds_{0.75}-\pounds_{0.25}}=\frac{1.2+1.8}{0.4+0.6}=3,$$

an estimate of $\alpha$ can be found from Table 5.1 after [12], using linear interpolation is obtained $\alpha = 1.563$ from $\upsilon = 3$.

Is calculated the Hurst parameter to quantify the strength of the fractal scaling, which it must be $0 < H < 1$ then $H = 0.64$, because $H = 1/\alpha$ [13].

The scale parameter c can be estimed from

$$\hat{C}=\frac{\pounds_{0.75}-\pounds_{0.25}}{\upsilon_c(\alpha)}=\frac{0.4+0.6}{1.939}=0.52$$

where the denominator is obtained from Table 5.2 after [12].

Once it has c, it calculates $\gamma$:

$$c=\gamma^{1/\alpha}$$

$$\gamma=c^{\alpha}$$

$$c=0.52$$

$$\gamma = 0.35.$$

With the generalized central limit theorem, their distribution function normalized converges in distribution to X where X is nondegenerate and the limit random variable X is stable [12]:

$$\lim_{n\to\infty} t^{\alpha}P(|X|>t)=\gamma C(\alpha)=0.18.$$

**D. Variance, Skewness and Kurtosis Measures**

To calculate the kurtosis and the average skewness:

$$\beta=\frac{median-\text{mode}}{\sigma}=-0.12,$$

there is a convergence in mode, median and mean in symmetric distributions, therefore is shown by the following equation:

Mode = media-3 (media-median)
-75.87=-72-3(-72+73)
-75.87=-75

Then we have an asimetrical and unimodal distribution with $\beta \le \sqrt{3}$ and we have $\beta = -0.12$.

To determinate the dispersion coefficient, its used the data from Table 2:

$$\delta_1=\int_{-\infty}^{\infty}\left|x-\mu_1'\right|dF$$

$$\delta_1 = 3.$$

The asimmetry and average skewness is the next:

$$\beta_1 = 0.82$$

$$\beta_2 = 7.1$$

$$\gamma_1 = 0.9$$

$$\gamma_2 = 4.1.$$

With the moments it can get other measures of the distribution

$$\gamma_1 = \sqrt{\beta_1} = \frac{\mu_3}{\mu_2^{3/2}} = \frac{k_3}{k_2^{3/2}}$$

$$\gamma_2 = \beta_2 - 3 = \frac{\mu_4}{\mu_2^2} - 3 = \frac{k_4}{k_2^2}.$$

### E. Moments and cumulants.

To find the higher-order moments and cumulants we use the next polynomials:

**Table. 3 Moments and cumulants.**

| Order | Moments | Cumulants |
|---|---|---|
| 1 | -1.85 | -1.85 |
| 2 | 13.7 | 10.27 |
| 3 | -33.6 | -65.27 |
| 4 | 698 | 532.38 |

Now we calculate the central moments with the cumulant with order 1 equal to zero from the tables of David & Kendall [14]:

**Table. 4 Central moments**

| Order | Moments |
|---|---|
| 2 | 10.28 |
| 3 | -122.29 |
| 4 | 758.84 |

### F. Goodness of fit.

With all the information obtained above, it proceeds to estimate a graphic with a non-Gaussian distribution that represents the behavior of the telephonic noise in the analogical subscriber loop:

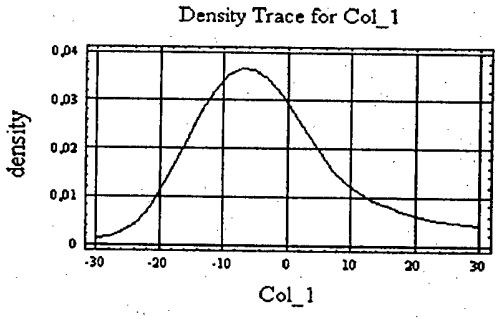



**Fig. 2 Stable symetric distribution with the data from the Table 2.**

### G. Function Spaces.

In order to generalize is considered the linear span of a stable process like a Banach space, where $\alpha$ =1.5. In terms of signal processing, the space L (L in honor of Lebesgue) is the space of functions with finite energy. The Lebesgue integration is called measure theory.

## V. Conclusion.

- The characteristic exponent with a value of 1.563, means that it has a stable distribution for telephone noise in the subscriber loop.
- To show the behavior of telephone noise in the subscriber loop with a stable symmetric distribution means use Banach's spaces instead Hilbert's spaces because it has Lebesgue spaces.
- The quality level it has actually is not the optimal, because it has an average of –72 dBp, when it should be about –90 dBp, beside this kind of measurement is not ruled in the telephone operation.
- The quality specifications are directed to the basic telephony and its necessary to actualize the norms for data transmission and the inernet use.

## VI. References.

[1]. Bellamy, *J.Digital Telephony* 2nd. Ed. USA, John Wiley & Sons, Inc.1991.

[2]. *Telmex, Manual de Planta Exterior: Parámetros eléctricos.* México, 1997.

[3]. Berger, J.M./Mandelbrot, B. "A New Model for Error Clustering in Telephone Circuits." IBM Journal July.1963.

[4]. Mandelbrot, B./ Van Ness, J.W, "Fractional Brownian Motions, Fractional Noises and Applications," SIAM Review Vol. 10. 1968.

[5]. Stuck, B.W./Kleiner, "B.A Statistical Analysis of Telephone Noise," B.S.T.J., Vol.53, No 7, September 1974.

[6]. Middleton, D. "Statistical-Physical Models of Electromagnetic Interference," IEEE transactions on EMC,Vol. EMC-19, No.3, August 1977.

[7]. Middleton, D., *Some Fundamental Problems, Results, and Tasks in Non-Gaussian Signal Processing.* New York. 1999.

[8]. Willinger, W/ Paxson, V. *Where Mathematics Meets Internet.*
*Notices of the American Mathematical* Society, 45(8), August 1998.

[9]. Pesquet-Popescu, B., "Statistical properties of the wavelets descomposition of certain non-Gaussian self-similar processes," Signal Processing Vol. 75 Elsevier. 1999.

[10]. Paul,C.R. *Introduction to Electromagnetic Compatibility.* U.S.A., John Wiley & Sons, Inc. 1992.

[11]. Alcatel *Información de soporte para comunicación hombre máquina. México,* SI014 (PAM 2.01). 1997.

[12]. Nikias,C.L./Shao, M., *Signal Processing with Alpha-Stable Distributions and Applications.* U.S.A., John Wiley & Sons, Inc. 1995.

[13]. Mandelbrot, B., *La Geometría Fractal de la Naturaleza.* España, Tusquets. 1997.

[14]. Stuart, A./Ord, K. *Kendall's Advanced Theory of Statistics, Vol 1. Distribution Theory.* 6th Ed. London Edward Arnold. 1994.

**EMC 2000** INTERNATIONAL WROCŁAW SYMPOSIUM ON ELECTROMAGNETIC COMPATIBILITY

Late paper to the session "EM HAZARDS AND TERRORISM" (page 466)

# A SOFT SYSTEMS METHODOLOGY – SYSTEM DYNAMICS (SSM-SD) BASED APPROACH TO RE-ENGINEERING EMI/EMC REGULATIONS AND STANDARDS TO COUNTER FUTURE TERRORIST THREATS

By (LCdr) RAJESH DEBNATH & (Cdr) VW KARVE

## ABSTRACT

***Most conventional approaches to the design of Electromagnetic Conflict (EC) systems are "hard" in nature, which presume EC to be a static, predictable encounter. This forms the basis of the standalone design philosophy for EC equipment adopted till date, from which flow various EMI / EMC and MIL standards. This reductionist approach is doomed to failure in the futuristic complex and dense electromagnetic environment, as Information Operations (IO) and Information Warfare (IW) become the chosen means to wage war against established authority and systems. The ultimate objective of EC is to affect the man, preferably the decision maker, and not the individual system(s) per se. In modern conflict, especially in Operations short of war and counter terrorist operations, any model of the prevalent EC environment also depends on non-quantifiable factors and the uncertainties of combat, which contribute to system entropy and emphasize the importance of the human decision maker. The terrorist – counter terrorist interaction (system) can therefore be classified as a Human Activity System (HAS). The authors propose a holistic system design philosophy for EC systems, based on the System Dynamics (SD) approach, incorporating the Soft Systems Methodology (SSM), to achieve a realistic representation of the terrorist – counter terrorist interaction in the futuristic electromagnetic environment. The SSM-SD paradigm is systematically developed, using the CATWOE model, system Root Definition (RD) and System Dynamics archetypes.***

## INTRODUCTION

*"The next Great War will be won by the side that best exploits the electromagnetic spectrum"*
*- Admiral Sergei Gorshkov*

This prophecy of the longest serving Admiral of the erstwhile Soviet Navy has come true in the numerous conflicts that have taken place around the world since the Second World War. Today, computers and allied networking and communication technologies, collectively known as **Information Technology (IT)**, have rapidly permeated into the hierarchy of the national law enforcement machinery, including the Armed Forces. The contemporary law enforcer or warrior cannot afford to remain insulated from the **Revolution in Military Affairs (RMA),** that has made information the most powerful weapon in the modern arsenal.

The sheer pace of technological transformation in IT is causing a paradigmatic shift in warfare itself, as well as in Operations Short of War (OSOW), changing it's very character and conduct from the Clausewitzian principle of mass concentration to demassification, force multiplication and information manipulation. [1] Today, counter terrorist operations form a major chunk of OSOW. Technology is a great leveller, which can change power equations entirely. Even the most "powerful" nation faces the danger of being "out-clicked" by sundry mafias and terrorist organizations. It is an increasingly difficult task to sustain the technological asymmetry against terrorism. Although technological advancement serves as a prerequisite for RMA, technology by itself cannot provide complete solutions. Only the synergistic effect of common preconditions of technological developments, doctrinal innovation and organizational adaptation alone can enable full realization of RMA.

## TERRORISM AND THE ELECTROMAGNETIC SPECTRUM

Terrorism is a manifestation of conflict in human society, which is easy to recognize but difficult to define. By it's very nature, any model of the terrorist threat to human society is fuzzy, incomplete and characterized by high entropy content, and is thus, a "soft" problem. A conceptual model of terrorism, based on David Easton's Systems Theory [2], is shown in Fig. 1.

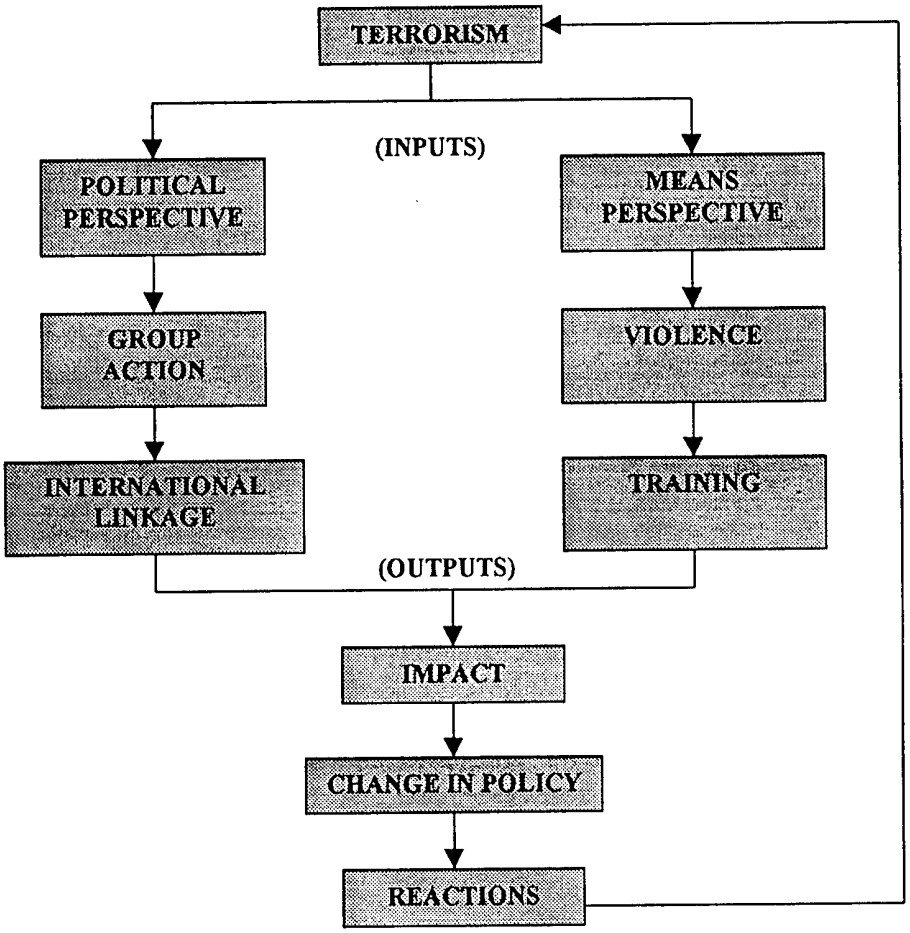



**FIG. 1 : CONCEPTUAL MODEL OF TERRORISM**

In this model, terrorism is defined as a political phenomenon, as well as a means to achieve political goals. For the purposes of this paper, the means perspective is of interest. Thus, terrorism is defined as a means in pursuit of realization of a political mission. Violence employed by terrorists is tactical in nature, to convey a message to the established authority. Contemporary tools of violence (conventional arms and explosives) demand professional training, and hence necessarily involve a long lead time and resources for training.

**Cyberterrorism** is the premeditated, politically motivated attack against information, computer systems, computer programs and data, invariably using RF links, which result in violence against noncombatant targets. In the contemporary polycentric global dispensation, the most likely and realistic threat is that of Information Warfare (IW) waged by subnational groups, clandestine agents or simply disgruntled individuals. Organized IW encompasses many traditional military disciplines, which require a new structure to orchestrate offensive and defensive operations at the **physical**, **informational** and

**perceptual** levels of conflict. IW requires restructuring of the coordination between the existing disciplines, as well as the mindset of the key protagonists. Today, new innovations and trends cause an order of magnitude increase in the **tempo** (rate of change of action) and **range lethality** (action at a distance) normally associated with warfare [3]. This necessitates;

- A **holistic** approach to understand the complex mosaic of IW, that has dramatically warfare in rather fundamental ways, and,
- A unified framework from which to design, manage and coordinate various information manipulation systems and functions, which requires a **process oriented architecture**, wherein the entire process from system conceptualization to deployment is undertaken by a multiskilled team of designers and users, as far as **EMI / EMC aspects** are concerned.

## CYBERTERRORISM AND ELECTRONIC WARFARE

**Electronic Warfare (EW)** is the most well known form of Electromagnetic Conflict, and it is enlightening to analyze cyberterrorism through the kaleidoscope of EW. At the macro level, EW is a subset of contemporary IW. Historically EW developed as a series of electronic countermeasures (ECM) to specific electronic systems. To understand how EW interacts with electronic systems to reduce their effectiveness or deny their use to the adversary, the **ECM-ECCM ladder model** has been used in the past.[4] In this model, an electronic system results in a counter system (ECM); the ECM in turn causes a counter-countermeasure (ECCM) to be implemented; and this process continues ad infinitum, as shown in Fig. 2.

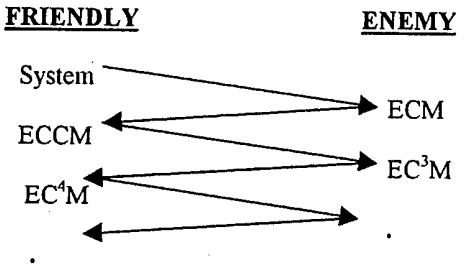



**FIG 2: THE ECM-ECCM LADDER**

The following conclusions can be drawn from the ladder model of EW:

- It tends to promote a binary evaluation of EW. Either it works, or it does not, depending on the ladder rung we are on.
- It tends to concentrate on the interaction of only two systems rather than consider the complexity and uncertainty of conflict, where many systems may be employed simultaneously.
- It excludes the human and organizational factors and the human decision maker (choice of technique, whether to deploy the system at all), hence represents the "**hard**" approach.

This conventional "hard" representation, which presumes EW to be a static, predictable, one on one encounter, forms the basis of the **standalone design philosophy** for electronic equipment adopted till recently. Most contemporary **EMI/EMC standards** (MILSTDs, EU EMC Directive 89/336/EEC, IEC/TC 77 etc.) flow from this philosophy. This **reductionist** approach for designing EW systems was suitable for the electromagnetic environment (EME) of the 1970s, when systems were few and non interacting, and terrorists relied on conventional weaponry to propagate violence.

## INADEQUACY OF EXISTING EMI/EMC PHILOSOPHY IN FUTURE ELECTROMAGNETIC CONFLICTS

The electromagnetic environment and the threats therein have increased tremendously in density and complexity since the 1970s. Today, signals emitted from the suspected threats must not only be detected and tracked by ESM systems, but they also need to be differentiated from the millions of pulses and CW emissions from allied and neutral sources. Severe weather and propagation conditions and hostile ECM (practiced by well financed and equipped cyberterrorists) further deteriorate the electromagnetic environment.

The **ultimate objective** of EW is to **affect the man**, preferably the decision maker, and not the individual systems, per se. In modern conflict, any model of the prevalent electromagnetic environment is fuzzy and incomplete, because the real effectiveness of an EC / EW system depends not only on quantitative factors such as the position on the ECM-ECCM ladder and adherence to EMI/EMC standards, but also upon non-quantifiable factors and the **uncertainties** of conflict. This emphasizes the importance of the human decision maker. Any terrorist – counter terrorist interaction (system) can therefore be classified as a **Human Activity System (HAS)**.

Though conventional wisdom suggests that every electronic system has to be either compatible or immune to EMI, in the futuristic electromagnetic scenario, systems need to be developed which will enable the law enforcer to exhibit **counterintuitive behaviour**,[5] which can be used as an **add-on deception technique** in the EC / EW arsenal. Without a holistic approach to adapting and incorporating EMI / EMC standards and practice to system design philosophy, we will invariably arrive at solutions that;

- Attack the problem piecemeal,
- Lead to suboptimization at the expense of complete system improvement, and,
- May never achieve the overall aim.

The anticipated dynamic terrorist – counter terrorist interaction in the futuristic EME is pictorially depicted in Fig. 3. [6] This representation is holistic, and is thus, a "**soft**" representation, which indicates the need for the **Soft Systems Methodology (SSM)** for the design philosophy of electronic systems. Therefore, the EC / EW system to deal with terrorist threats in the future can be described completely as a combination of;

- A "**hard**" part, in which individual systems are characterized by easy-to-define objectives, clearly defined decision making procedures and quantitative Measures of Performance (MOPs), and,
- A "**soft**" part, in which objectives are hard to define, decision making is uncertain, MOPs are at best qualitative, and human behaviour is unpredictable and irrational.

## DECEPTION

The tactical deception subset of EC / EW can be viewed as a viable defensive measure that can confuse a cyberterrorist skilled in Information Operations (IO). Daniel and Herbig [7] qualify deception as "*the deliberate misrepresentation of reality done to gain a competitive advantage*". There are three goals in any deception;

- The **immediate** aim is to condition the target's beliefs.
- The **intermediate** aim is to influence the target's actions.
- The **ultimate** aim is to benefit from the target's actions.

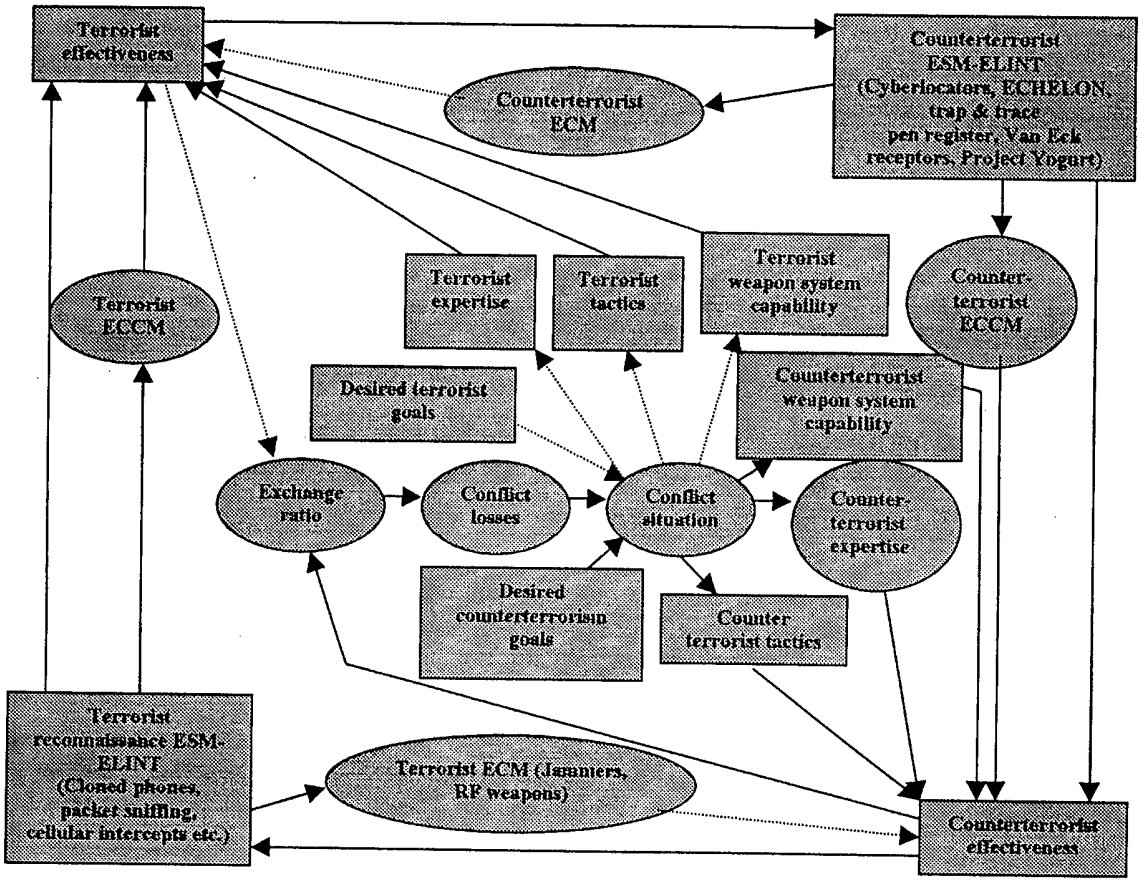



**FIG 3 : THE ANTICIPATED TERRORIST – COUNTERTERRORIST INTERACTION (SYSTEM) IN THE FUTURISTIC ELECTROMAGNETIC ENVIRONMENT**

Deception has two variants;

- **Ambiguity increasing (A-type)**, which confuses a target and seeks to compound the uncertainties confronting the target's attempt to determine the deceiver's intentions. A-type deceptions seek to ensure that the level of ambiguity always remains high enough to protect the secret of the actual operation or database.
- **Misleading (M-type)**, which reduce ambiguity by building up the attractiveness of one wrong alternative, which causes the target to concentrate his operational resources on a single (false) contingency, thereby maximizing the deceiver's chances for prevailing in all others.

Although the two variants are conceptually distinct and can be initiated with different intentions in the deceiver's mind, their effects often coexist. How one characterizes a particular deception partly depends on the perspective one takes. The outcome of the variants is a spectrum ranging from **convinced misdirection** at one end to **utter confusion**, in which all possibilities look equally likely, at the other end. It is illuminating to examine parallels between Information Operations (IO) and the classical Clausewitzian principles, one representation of which is the **Lanchester's Square Law**, or **Lanchester's Law of Modern Warfare**, named after FW Lanchester, given in Equation 1 [8];

$$B_0^2 - B^2 = E\,[\,R_0^2 - R^2\,] \qquad (1)$$

Where, $R_0$ and $B_0$ are the total number of Red and Blue combatants respectively at the start of the conflict, and R and B represent the numbers of surviving Red and Blue combatants at any given time t, after the battle has started. E is the consolidated exchange rate, defined as the ratio of the average number of Blue combatants lost to that of Red combatants lost. From the Lanchester combat theory, we can distil the following **Helmbold** type equations, which represent a more general combat model, containing many of the classic homogenous combat models as special cases:

$$\mathbf{dR / dt = - a(t). B. (R / B) \exp (1 - W_B)} \quad (2)$$

$$\mathbf{dB / dt = - b(t). R. (B / R) \exp (1 - W_R)} \quad (3)$$

where a, b are positive constants.

In equations (2) and (3),

- "***Perfect knowledge***" or complete information, corresponds to the *aimed fire* situation, where $W_R = W_B = 1$,
- "***Ignorance***" or utter confusion, corresponds to the *area fire* situation, where $W_R = W_B = 0.5$ (A-type deception), and,
- "***Misinformation***" corresponds to worse performance than even area fire, where $W_R = W_B$ is less than 0.5.
- "***Total misinformation***" is the theoretical limiting case, where $W_R = W_B = 0$, which implies that the combatant fires upon himself. In this case, the Helmbold type equations reduce to;

$$dR / dt = - aR \text{ and } dB / dt = - bB \quad (4)$$

In this case, the more units a combatant possesses, the larger are the combatant's losses, the combatant's attrition rate is proportional to the number of units he possesses.

## EC / EW MANAGEMENT BY THE SOFT SYSTEMS METHODOLOGY (SSM)

Deception involves those actions executed to deliberately mislead adversary decision makers as to friendly military capabilities, intent and operations, thereby causing the adversary to take specific actions that will contribute to the accomplishment of the friendly mission. [9] The quantum increase in EC / EW system capabilities, which are increasingly being driven be **commercial off-the -shelf (COTS)** products has led to **network centric warfare**. This is warfare unlike any other warfare in the past because it depends upon the quality and quantity of appropriate data to positively change the behaviour of the person receiving it. Any tactical deception scheme should provide a perception of the available data that will **change the behaviour of the adversary in a predictable way**, based upon the information s/he is allowed to intercept or intrude upon. Thus the aim of EC /EW is to **influence human behaviour**.

A Human Activity System (HAS), or, **soft system**, as it is called, is defined as **a system in which human beings interact with each other to achieve specific teleology**. The terrorist – counterterrorist interaction in the futuristic EME, depicted in Fig. 3, is a HAS as it's specific teleology is to affect human behaviour. Peter Checkland of the University of Lancaster, UK, proposed that whenever a system consists of "hard" and "soft" subsystems, the methods used for engineering the technology should not be applied to the human part of the system. **SSM** was developed to analyze and describe the relevant aspects of the HAS, and how it interacts with the technology system. [10] A HAS is a purposeful activity by people ( the actors) who can contribute meaning to what they **perceive** is being achieved by the system or organization. Checkland's observation is that there can never be a single objective of a HAS, only a set of possible views of it, according to the **Weltanschauungen** (world view) of the actors in and around the system. A human being perceives and cognizes a fact through a set of sensory mechanisms and stored knowledge base. While the world presents a fact, the human element of any system cognizes the fact from a particular perspective view, or Weltanschauung. The human cognition process is one in which an event is accepted

by sensory organs. This input is passed through a selective **attitude** filter, which only passes a **coloured** version of the original input. The colour is introduced due to a bias factor, which is an outcome of:

- Long term memory
- Knowledge base
- Conditioning

Consequently, the S-R (Stimulus-Response) paradigm, propounded by JP Seward, is modified into the **S-A-R (Stimulus-Attitude-Response)** paradigm. The SSM is depicted pictorially in Fig. 4.

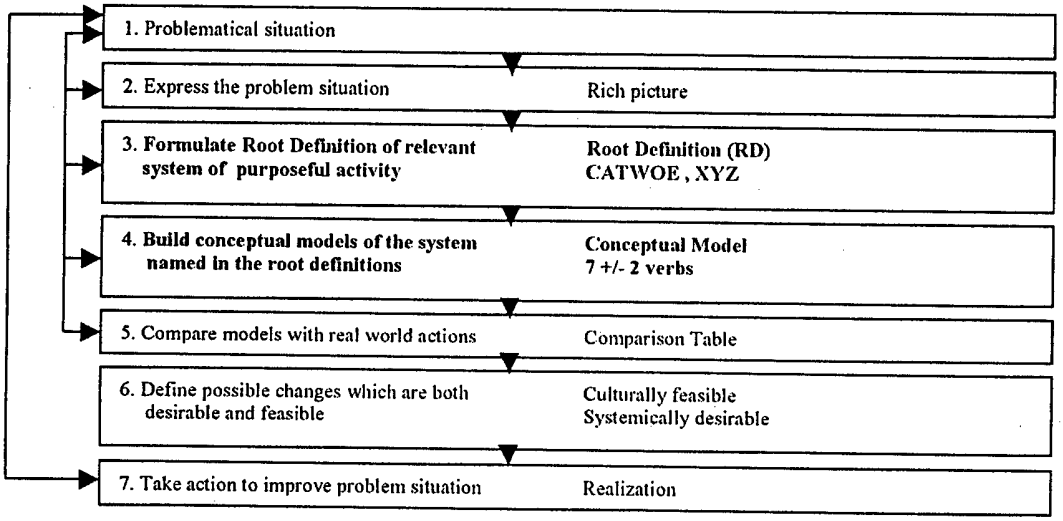



**FIG 4 : THE SEVEN STAGE MODEL OF THE SOFT SYSTEEMS METHODOLOGY (SSM)**

**Root Definition**

The core of SSM revolves around the formulation of a **Root Definition (RD)** for the subject system. The RD caters for the cognitive aspect through the **CATWOE** model, which is used to identify and categorize all the stakeholders as shown in Table 1. A **stakeholder** is any individual, group, organization or institution that can affect, as well as can be affected, by any changes in policy of the subject system.

A complete Root Definition (RD) is one which embodies the above areas in an explicit way, or failing that, any of these areas which is omitted, should be omitted consciously and with good reason. The Weltanschauung, however, may be implicit. A complete RD may be expressed as ;
**A system to do X, by Y, in order to achieve Z .**

## A HOLISTIC SYSTEM DESIGN PHILOSOPHY FOR THE FUTURISTIC ELECTROMAGNETIC SCENARIO

The current trend is towards the minimization of EMI and maximization of EMC. From the EW point of view, the above trend reduces the vulnerability of friendly systems to adversarial **Measurements and Signature Intelligence (MASINT)**. MASINT feeds on a target system's unintended emissive byproducts, or "**trails**", which form distinct signatures. These signatures, such as the EMI generated by an electronic system, can be exploited as reliable discriminators to characterize specific events or disclose hidden targets. [11] Conversely, the **EMI signature can be deliberately used** as part of an overall ECM deception strategy, to maximize the (mis)information available to the cyberterrorist, with the aim of altering

his / her behaviour ,as desired. Thus, a paradigmatic shift is required, from *risk avoidance* at all cost to *risk management*, on our own terms.

| Consideration | | Amplification |
|---|---|---|
| Customer | (C) | Client(s) (of the activity), beneficiary(s), or victim(s), the subsystem affected by the main activity(s). The indirect object of the main activity verb(s). |
| Actor(s) | (A) | The agents who carry out, or cause to be carried out, the transformation process(es) or activities of the system. |
| Transformation | (T) | The core of the RD, a transformation process carried out by the system. Assumed to include the direct object of the main activity verb(s). |
| Weltanschauung (World-view) | (W) | The outlook or taken-for-granted framework which makes this particular RD a meaningful one. |
| Ownership | (O) | Ownership of the system, control, concern or sponsorship; a wider system which may discourse about the system. A system that can change of stop the Transformation. |
| Environment (wider system constraints) | (E) | Environmental impositions; perhaps interactions with a wider system other than that included in Ownership above. |

**TABLE 1: THE CATWOE MODEL**

This indicates the need to incorporate a subsystem in the EC / EW suite, which gives the tactical flexibility to the law enforcer to select the type and quantity of EMI signature that s/he desires to use in a given scenario. For instance, in the context of information manipulation functions, the case of **deception** can be represented as;

$$\mathbf{dv/dt = a\,(1-u)\,(1-v)}\,, \qquad (5)$$

where, u, v represent ignorance of friendly and adversarial forces, and
(1-u), (1-v) represent the **situational awareness (SA)** of friendly and adversarial forces.

Equation (5) indicates that;

- Success is dependent on the individual situational awareness.
- The more we know about the adversary (through our MASINT), the more effective our deception techniques can be.
- The more the adversary can detect and know, the more knowledge s/he has to lose by effective friendly techniques.

However, when viewed in isolation, as in the standalone design philosophy, the various information manipulation functions, like suppression of EMI, could well be employed at cross purposes, and end up substantially negating one another. For instance, the system designer's strict adherence to EMI/EMC standards based on the standalone design philosophy will clash with the law enforcer's requirement of tactical deception in a unified EC / EW system. Such a situation can be pictorially depicted by the **accidental adversaries archetype** of **system dynamics** [12], shown in Fig. 5.

## CONCLUSION

The differing perceptions between the designer and the user in the context of the utility of EMI can be modelled using the **CATWOE model** described earlier, as shown in Table 2. As is evident, the most significant difference between the perceptions of the system designer and the user (law enforcers and , counterterrorism forces) is in the Weltanschauungen, and consequently, the Root Definitions of the system. This is the **core issue** that needs to be addressed from the EMI/EMC viewpoint, if EC / EW systems are to remain effective in the complex electromagnetic environment of the future.

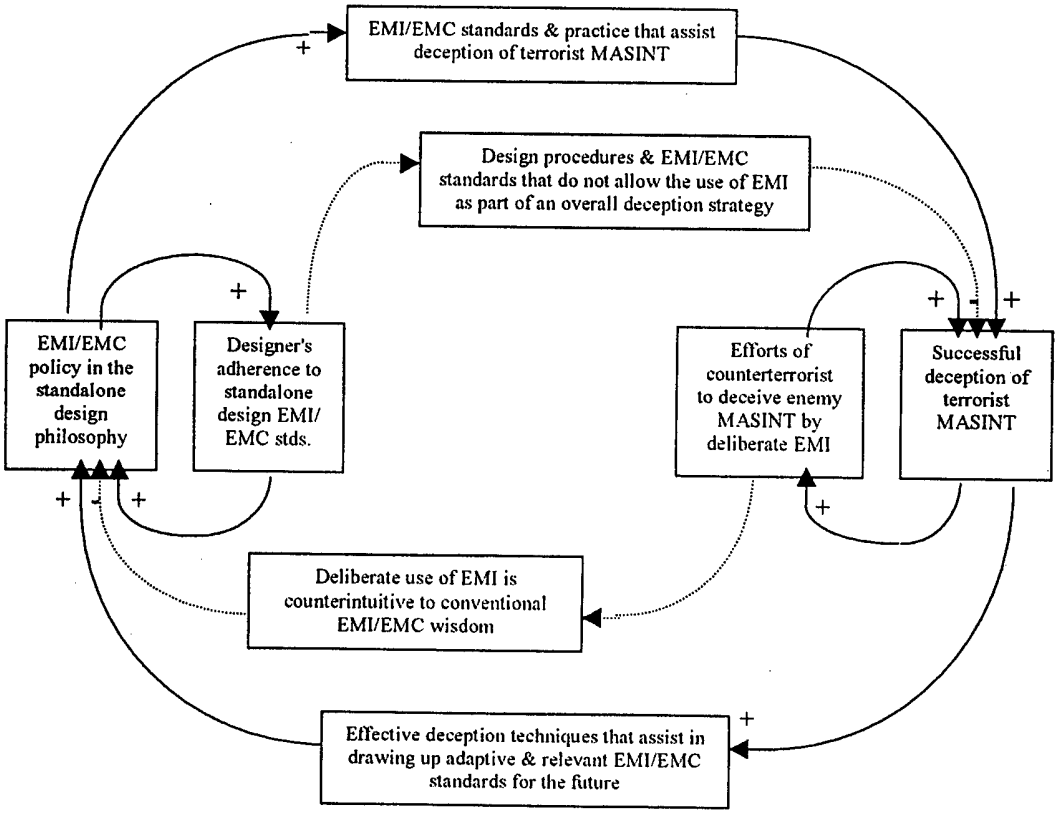



**FIG 5: THE SYSTEM DESIGNER AND TACTICAL USER AS ACCIDENTAL ADVERSARIES IN THE CONTEXT OF DESIRABLE EMI IN AN EC / EW SYSTEM**

| Consideration | The Designer's perspective | The user's perspective |
|---|---|---|
| Customer (C) | The law enforcers/counterterrorists | The law enforcers/counterterrorists |
| Actors (A) | The design team & users | The design team & users |
| Transformation (T) | Design & Development of effective EC/EW systems. | Use of the EC / EW systems with maximum effect in a given scenario. |
| **Weltanschauung (W)** | **Maximum inter/intra system compatibility, adherence to existing EMI/EMC standards. Aim is to minimize EMI & maximize EMC.** | **Seamless integration into a unified IO network. Option to use EMI signature to deceive enemy MASINT. Minimized EMI may not be desirable in a dense EW scenario.** |
| Owner (O) | The design organization | The user force |
| Environment (E) | EMI/EMC standards, MILSTDs, advances in electronics & computers. | EMI/EMC standards, MILSTDs, advances in electronics & computers. |
| **Root Definition (RD)** | **A design organization owned system comprising the design team for the development of EC / EW systems ensuring adherence to EMI/EMC standards, minimizing EMI & maximizing EMC.** | **A user force owned system for effective conduct of EW within a unified IO network, to defeat the (human) terrorist with deception ECM, for which a controllable threshold of EMI is desirable.** |

**TABLE 2: COMPARATIVE CATWOE MODELS OF THE SYSTEM AS PERCEIVED BY THE SYSTEM DESIGNER AND USER**

Information Technology and it's numerous offshoots are redefining conflict as we know it. It has created the fifth dimension, the **cyberspace**, where most conflicts will be take place in the future, after land, sea, air and space. In this dimension, we can expect to face nontraditional threats and adversaries, like terrorists, criminals and distant rogue states. Armed with the right technologies and modest budgets, these adversaries will be capable of inflicting great damage upon both military and civilian targets. Addressing the threat from an enemy nation is one circumstance, but the risks arising from terrorist activity will raise the ambiguity level, as it will be extremely difficult to find just who the adversary is and what s/he can do. An IW attack can be mounted from anywhere, at any time, and can be conducted from a distance via RF links or international communication networks. In such cases, the conventional tactic of retaliation *in kind* and *in proportion* will be difficult to implement, because the attacker's information dependence may be entirely different from that of the victim.

Confronted with such a scenario, we feel it is more prudent to concentrate on the **defensive aspect of IW**, with limited strike / offensive capability to attack a belligerent, when his / her identity is known and his / her information base is vulnerable. As human society becomes increasingly reliant on electronic gadgetry, computers and networked connectivity, we must expect IW attacks as a matter of course. Tactical and defensive deception is an effective answer to such threats. With the deliberate use of EMI, the adversary can be enticed to attack on our own terms, so that we can control what s/he accesses and lead him/her to believe s/he has succeeded. In doing so, the paramount goal of IW, that of influencing the enemy's perceptions to suit our aims and cause him/her to act in a more predictable manner, would have been achieved.

This calls for a twin track approach. One is to revamp the electronic system design philosophy to facilitate seamless integration of systems into a unified IO network. The second is to encourage **"out-of-the-box"** thinking to respond to the emerging threats. We propose the SSM-SD approach to achieve both the objectives.

## REFERENCE

[1] Kak, K, 'Revolution in Military Affairs – An appraisal', Strategic Analysis, vol. XXIV, no. 1, April 2000.
[2] Prabha K, 'Defining terrorism', Strategic Analysis, vol. XXIV, no. 1, April 2000.
[3] F.J. Ricci and D. Schutzer, 'US Military Communications', Computer Science Press, 1986
[4] Lt. Col. R.E. Fitts (ed.), The Strategy of Electromagnetic Conflict, Peninsula Publishing, Los Altos, California, 1980.
[5] J.W. Forrester, Collected Papers of J.W. Forrester, MIT Press, Cambridge, Massachusetts, 1975.
[6] Debnath R and Karve VW,' Design of futuristic Electromagnetic Conflict systems using Soft Systems Modelling – System Dynamics methodology', Proceedings of the 6th International Conference on Electromagnetic Interference and Compatibility, Society of EMC Engineers India, 1999.
[7] Daniel DC and Herbig KL (eds.), 'Strategic Military Deception', Pergamon Press, 1982.
[8] Morse PM and Kimball GE, 'Methods of Operations Research', John Wiley and Sons Inc., 1950
[9] Newland RK, 'Tactical Deception in Information Warfare: A New Paradigm for $C^4I$', Journal of Electronic Defense, December, 1998.
[10] Smyth DS and Checkland PB, 'Using a systems approach: The structure of Root Definitions', Journal of Applied Systems Analysis, Vol. 5, no. 1, pp. 75-78, 1976.
[11] Lum Z, 'The measure of MASINT', Journal of Electronic Defense, pp. 43-48, August, 1998.
[12] Senge PM, 'The Fifth Discipline', Currency Doubleday, 1994.

EMC 2000 INTERNATIONAL WROCŁAW SYMPOSIUM ON ELECTROMAGNETIC COMPATIBILITY

# RADIOCOMMUNICATION ASPECTS OF EMC ANALYSIS AND MEASUREMENTS ON A SHIP

Ryszard J. Katulski*, Andrzej Kosinski**, Wiktor Pawlowski*

*Technical University of Gdansk, PL-80-952 Gdansk, Poland

**Naval Academy, PL-81-919 Gdynia, Poland

*The subject of this paper is the EMC analysis of ship radiocommunication systems. Especially the EM coupling effects between the antenna systems, as well as the influence of the antennnas localization on the electric field strenght distribution at the ship deck are analysed. The results of the theoretical and measurement investigations are presented. First, the EMC problems on a ship are introduced. Next, the EM coupling analysis of ship antennas by use of the thin wire modelling method is presented. The obtained theoretical results are partially verified by measurements. In conclusion, taking into account the carried out research, the indications for a EMC project procedure radiocommunication systems are proposed.*

## 1.INTRODUCTION - EMC PROBLEMS ON A SHIP

The maritime radiocommunication service should assure two direction communication on sea-land paths and on ship to ship paths, in order to guarantee the safety of navigation and the security of human life and property on the sea. For this reason the ships of the mercantile marine as well as the fleet navy are equipped in a large number of different radiocommunication installations. All these equipments, especially the ship antenna system, radiate electromagnetic fields, wanted and unwanted. In such circumstances a carefully realized EMC analysis and suitable measurements are necessary to warrant that an undisturbed employment of all radio installations will take place.

The design of the ship radiocommunication systems requires that all antennas should be located within a limited area, i.e. at the same ship on a common or a different deck. In this situation the influence of the deck architecture on the antenna properties, as well as the mutual coupling between the ship antennas have been examined. A typical effect of this coupling is the worsening of the antenna directivity properties, as well as the change of the input impedance of the ship antennas. The mentioned last fact influences negative on the impedance adjustment between the antennas and the ship radiocommunication equipments.

Another coupling problem is the fact that on the input of a monitoring receiver unwanted signals are induced due to the power transmitted by the ship radio equipments.

Taking into account the safety conditions of peoples on a ship, the distribution of the electric field strenght and the distribution of the field power densitiy at several different ship decks should be known to determine the emergency zones, especially under the main deck in the marines cabins.

Another problem of great practical importance is connected with the mentioned above negative influence of the electric field on ship automatic systems. The unwanted field strength can disturbe the operation conditions of these systems.

## 2. SHIP ANTENNAS EM COUPLING ANALYSIS

The antennas of the ship radiocommunication systems have a linear structure, especially a monopole antenna - in practice called as wip antenna - is the main type of the ship antennas [1].

The ship antennas em coupling event can be presented in the schematic form, as it is shown in fig.1.

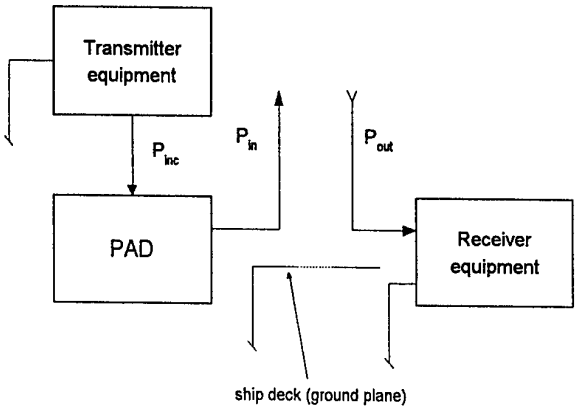



Fig. 1. Schematic form of the ship antennas coupling

Taking into account the ship antenna operation conditions - the installation of the ship antenna over a

ground plane in form of the ship deck - see fig. 2, the wire model of the analysed ship linear antennas and the masts installed on the ship deck have the form of a symetrically dipole antenna array, as it is shown in fig. 3. Therefore, the analysed ship antennas and masts can be represented as parallel thin wires with appropriate lenghts.

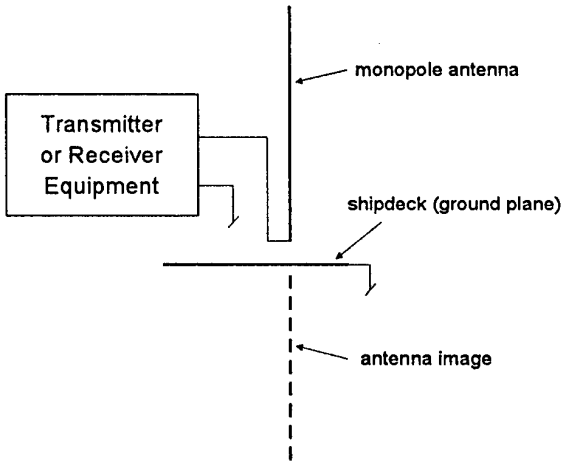



Fig. 2. The monopole antenna over ship deck

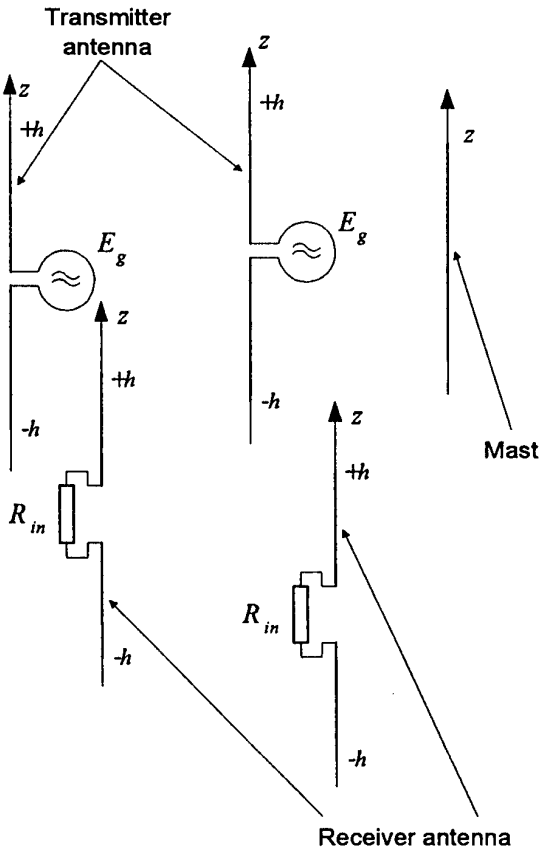



Fig. 3. The wire model of the ship linear antennas

The main parameter of the coupling phenomena between analysed ship antennas is the current distribution along the lenght of the antennas. The application of the wire model is intend to calculate the current distribution and next to determine the coupling ratio between selected ship antennas, taking into account the presence of other antennas and ship masts.

When the ratio of the radius to length of the ship antenna is small - the condition have place in practice - the only one significant component of the antenna current distribution is the axial component, which can be expressed in coordinate system as shown in fig. 3, by the following integro-diffrential equation:

$$\left(\frac{\partial^2}{\partial z^2}+k^2\right)\int_{-h}^{+h}\left[I(z')\cdot G(z,z')\right]dz=-j4\pi\cdot\omega\cdot\varepsilon\cdot E(z), \quad (1)$$

where: $I(z')$ - current density,
$E(z)$ - axial component of the electric field strenght,
$G(z,z')$ - free space Green function,
$k$ - wave number.

For $N$ ship linear antennas, the antenna array can be described by the set of equations, which is given bellow:

$$\left(\frac{\partial^2}{\partial z^2}+k^2\right)\sum_{i=1}^{N}\int_{-h_i}^{+h_i}\left[I_i(z')\cdot G(z,z')\right]dz'=-j4\pi\cdot\omega\cdot\varepsilon\cdot E_1(z),$$
$$\vdots \quad (2)$$
$$\left(\frac{\partial^2}{\partial z^2}+k^2\right)\sum_{i=1}^{N}\int_{-h_i}^{+h_i}\left[I_i(z')\cdot G(z,z')\right]dz'=-j4\pi\cdot\omega\cdot\varepsilon\cdot E_N(z).$$

The equation set (2) can be described in the integro-differential operator short form as:

$$\sum_{i=1}^{N}K_{1i}\left\{I_i(z')\right\}=E_1,$$
$$\vdots \quad (3)$$
$$\sum_{i=1}^{N}K_{1i}\left\{I_i(z')\right\}=E_N.$$

The set of operator equations (3) has been solved by use of the method of moments procedure [2]. Applying the above mentioned procedure, the operator equations set (3) can be described as a set of algebraic equations in the following matrix form:

$$[Z]\cdot[\alpha]=[V], \tag{4}$$

in which: $[Z]$ - impedance matrix with elements adequated for integro-differential form of equation (1),

$[V]$ - matrix of the known functions excited ship transmitter antennas,

$[\alpha]$ - matrix of the unknown coefficients of the unknown ship antenna current distribution due to the moments method approximation, described as:

$$I_i(z')\cong\sum_{m=1}^{M}\alpha_{im}\cdot b_{im}(z'), \tag{4.1}$$

where $b_{im}(z')$ denotes the $m-th$ basis function applied to approximation of current distribution in the $i-th$ ship antenna. Calculating the current density distributions along the analysed ship antennas one can determine the value of the coupling ratio $C_{ij}$ between the selected $i-th$ and $j-th$ ship antennas, which dependences on the power $P_i$ radiated by the $i-th$ antenna and the power $P_j$ induced in the $j-th$ antenna. The above mentioned coupling ratio can be described in the following form - as seen from fig. 1:

$$C_{ij}=\frac{P_j}{P_i}, \tag{5}$$

in which:

$$P_j=\left|I_j\right|^2\cdot\mathrm{Re}\{z_{Lj}\}, \tag{5.1}$$

and

$$P_i=\mathrm{Re}\{V_i\cdot I_i^*\}, \tag{5.2}$$

where $z_{Lj}$ denotes the impedance loaded the $j-th$ ship receiver antenna.

If the coupling ratio is known, then one can calculate the value of the voltage $V_j$ induced on the $j-th$ receiver due to the power $P_i$ of the $i-th$ transmitter:

$$V_j=\left\langle C_{ij}\cdot P_i\cdot\mathrm{Re}\{z_{Lj}\}\right\rangle^{1/2} \tag{6}$$

## 3. THE THEORETICAL AND MEASUREMENT INVESTIGATIONS

The presented coupling model first of all has been tested numerically and next has been verified by measurements. The wip radiocommunication antennas have been installed on main ship deck. The localizations of the antennas are shown in fig. 4.

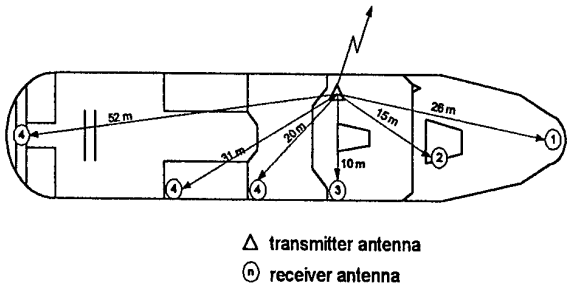



Fig. 4. The localization of wip ship antennas

The coupling analysis was made for different frequencies and different power of the ship transmitter equipments, with the aim to determining the values of the voltages induced on the inputs of the ship receivers due to the power radiated by the transmitter antenna. The lenght of the transmitter antenna was 10 m and the lenghts of the receiver antennas were 6 m. The differencies between theoretical and experimental results, for the localization of the ship antennas on the deck as it is shown in fig. 4, were not greater than 30%. These differencies arises from the fact that the conducting structure of the ship deck with their building form influence on the antennas operation conditions to a high degree. However, the accuracy of the obtained results is good for practical engineering applications [3].

Taking into account the safety conditions of the peoples on a ship, the electric field strenght distribution and the field power density distribution on different ship decks were measured to determining the emergency zones, especially under the main deck in the marines cabins. The field attenuation due to the deck structure has been investigated by means of measurements. The obtained results for different frequency bands are shown in fig. 5.

At the end, an unwanted radiation effect of the ship antennas switchboard has been observed, which negative influences on the ship automatic systems and disturbed the operation conditions of these systems.

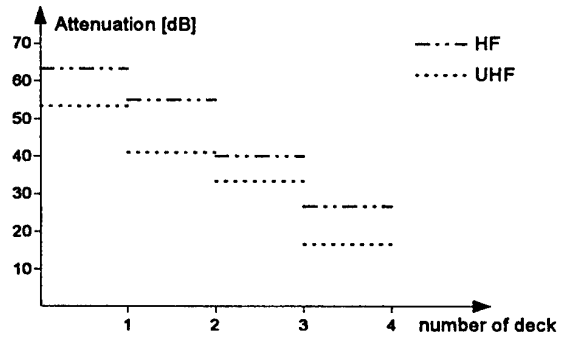



Fig. 5. The field attenuation due to the ship decks, 1 - main deck

## 4. CONCLUSION

The presented model for the coupling analysis between antennas on the ship deck has been tested numerically and was verified by the measurement way. The coupling of the wip radiocommunication antennas installed on the main ship deck was invetigated. This coupling analysis was made for different frequencies and different power of the ship transmitter equipment, with the aim to determining the values of the voltages induced on the inputs of the ship receivers due to the power radiated by the transmitter antenna. Coincidence between theoretical and measurement results satisfied practical requirements.

The electric field strenght and the field power density distribution on the ship different decks were measured to determining the emergency zones, especially under main deck in marines cabins. The field attenuation due to the deck structure has been investigated too.

Taking into account the all obtained results, one come to the conclusion that the two antenna groups, i.e. transmitter and receivers antennas, should be separated on ship deck with possible long distance. For example transmitter antennas should be at the ship stern and receiver antennas on the bow part of the ship deck.

## 5. REFERENCES

[1] Preston E. Law,
"Shipboard Antennas",
Artech House, London, 1986.

[2] J. Moor, R. Pizer,
"Moments Methods in Electromagnetics",
Researches Studies Press, London, 1984.

[3] R. J. Katulski,
"Numerical Design of Shipboard Communication Antenna,
Proc. of the Fifth Int. Conf. on HF Radio Systems and Techniques, Edinburgh 1991,
IEE Conf. Publ. No. 339, pp. 89-92.

## BIOGRAPHICAL NOTES

Ryszard J. Katulski graduated at the Technical University of Gdansk in 1975, and received Ph.D. degree from the Technical University of Wroclaw in 1984. Since 1968 he is with the Technical University of Gdansk, working on wireless communication with special interest in antenna theory and techniques with electromagnetic compatibility aspects.

Andrzej J. Kosiński graduated at the Military University of Technology of Warsaw in 1976, and received Ph.D. degree from the Military University of Technology of Warsaw in 1987. Since 1976 he is with the Naval Academy of Gdynia, working on radiocomunication with special interest in exploitation of military communication theory and techniques with elektromagnetic compatibility aspects.

Wiktor Pawlowski graduated at the Technical University of Gdansk in 1957 and received Dr. Ing. degree in Electronics from the Technical University of Warsaw in 1966. Since 1957 he is with the Technical University of Gdansk, working on radiocommunication systems with special interest in radiowave propagation in nonionised media.

EMC 2000 INTERNATIONAL WROCŁAW SYMPOSIUM ON ELECTROMAGNETIC COMPATIBILITY

# APPLICATION OF ELECTROMAGNETIC RADIATION OF HIGH-VOLTAGE EQUIPMENT FOR DIAGNOSTICS OF ITS TECHNICAL STATE

N.V. Kinsht, M.A.Katz, N.V. Silin, O.V. Preobragenskaya, Y.B. Petropavlovsky
Far-Eastern State Technical University, Pushkin st. 10,Vladivostok, 690600, Russia
Fax: +7(4232) 266988, E-mail: nicolay@mail.primorye.ru

*High-frequency electromagnetic noises created by electrical equipment of substation reflect in a great degree its serviceability state or proximity of failure. Principles for constructing of diagnostics model on the basis of measuring electromagnetic noises are discussed. Question of generating and distributing noises at a substation are analyzed. Equipment circuits for measuring noises and equations describing the solution of diagnostics problem are considered. Some experimental dates are presented.*

## 1. NOVEL USE OF EMC

The operation of the electric power equipment is always accompanied by its own intensive electromagnetic radiation with a wide frequency band. For instance, it was experimentally found, that the electromagnetic field, which is emitted by electrical equipment on outdoor substation by voltage >220 kV, is observed up to frequencies of hundreds and even thousand megahertz. The spectrums and the radiation levels of different parts of equipment essentially differ from each other. Sources of radiation are partial and corona discharges, breakthrough at switching, thunderstorm overvoltage, etc.

Thus, the overwhelming number of high-voltage and electric power equipment is a source of radio interference. Despite of small power compared with radio station these man-made interference substantially determine an electromagnetic environment in a radio-frequency range. The dependence of the interference from the frequency is investigated well enough. Devices, which emit the signals of continuous and discontinuous operation, create the interferences with a frequency spectrum usually up to several megahertz. The single signal with a steep front has wider spectrum, than continuous signals. The grouped together impulses (for example, from partial discharges) create the interferences in the widest frequency band.

The detection and elimination of electromagnetic noises from different industrial equipment is one of the main problems in support in a normal conditions of activity of radio electronics equipment [1]. The majority investigations in the field of electromagnetic compatibility is devoted to this problem.

On the other hand electromagnetic signals, emitted by the high-voltage and electric power equipment, can show a serviceability or faults of this equipment. This circumstance allows to generate a new direction in the field of an electromagnetic compatibility, namely, diagnostics of an electric power equipment on the basis of measurement and analysis of high-frequency electromagnetic noises. The main advantage of suggested method is the minimum meddling in the technological process. The data of regular or periodical measurements can be the base for early warning about the tendencies of the state of the technical equipment.

## 2. THE PROBLEMS OF CONSTRUCTION OF A DIAGNOSTICS MODEL

The analysis of availability index of product of the object presupposes the creation of a diagnostic model [2]. For its creation it is necessary to study the following problems: 1) physical nature of interfering sources; 2) influence of environmental conditions to intensity and levels of signals; 3) the paths of propagation of interferences from a source to a receiving antenna. It is necessary to distinguish the elements of the equipment and elements of the diagnostic model. So, the transformers and switches are the elements of the equipment of electrical substation. But their parts,

whose faults are coupled with appearance electromagnetic noises, select as elements of diagnostic model. For example, it can be the high-voltage leads-in.

The study of the processes of creation of signals in the elements of diagnostic model allows not only to determine diagnostic parameters of signals, but also to create the database for a construction of common diagnostic model by classificating of these parameters.

## 3. CONSTRUCTION OF A DIAGNOSTICS MODEL

The main source of electromagnetic radiation at substation is its capital equipment. Let us assume that the registered signal is a linear function of its source. The total equivalent circuit shown in figure 1 corresponds to the model where $e_1(t)$, $e_i(t)$ ... $e_n(t)$ are electromotive forces of *n* equivalent sources of electromagnetic radiation, $u_1(t)$, $u_i(t)$ ... $u_m(t)$ are voltages of *m* electromagnetic radiation measured in different parts of substation.

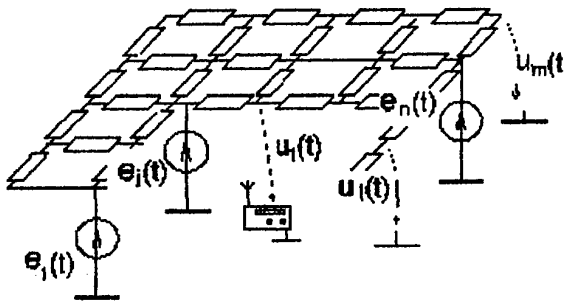



Fig. 1. The total equivalent circuit

The complex resistances in figure 1 correspond to the real electrophysical characteristics of air and to the presence of large number of units of connections. The analysis of the sources of radiation can be presented as a generalized equivalent circuit shown in figure 2.

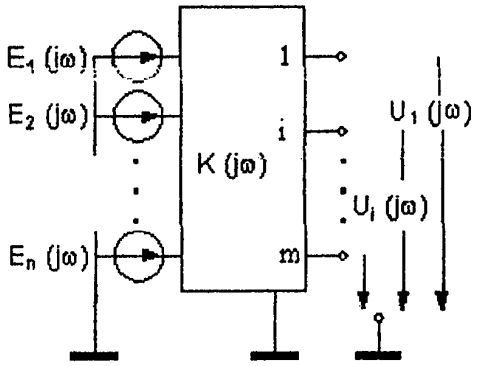



Fig. 2. Generalized equivalent circuit

The connection between sources of electromagnetic radiation and measured voltages must be written down in the matrix form:

$$\mathbf{U}(j\omega) = \mathbf{K}(j\omega)\,\mathbf{E}(j\omega),$$

where $\mathbf{U}(j\omega)$ and $\mathbf{E}(j\omega)$ are spectrum vectors of voltages and sources respectively, $\mathbf{K}(j\omega)$ is matrix of complex factor of a transfer.

If the matrix $\mathbf{K}(j\omega)$ is a square, the decision will look like:

$$\mathbf{E}(j\omega) = \mathbf{K}^{-1}(j\omega)\,\mathbf{U}(j\omega).$$

The spectrum voltages provide possibility to determine the spectrum of sources of a signal. The dynamics of change of voltages are connected with serviceability state of elements of the electrical equipment. For example, in figure 3 the spectrum voltages were measured:

a - near the autotransformer of 500 kV,

b - near the current transformer of 500 kV,

c - outside of power equipment.

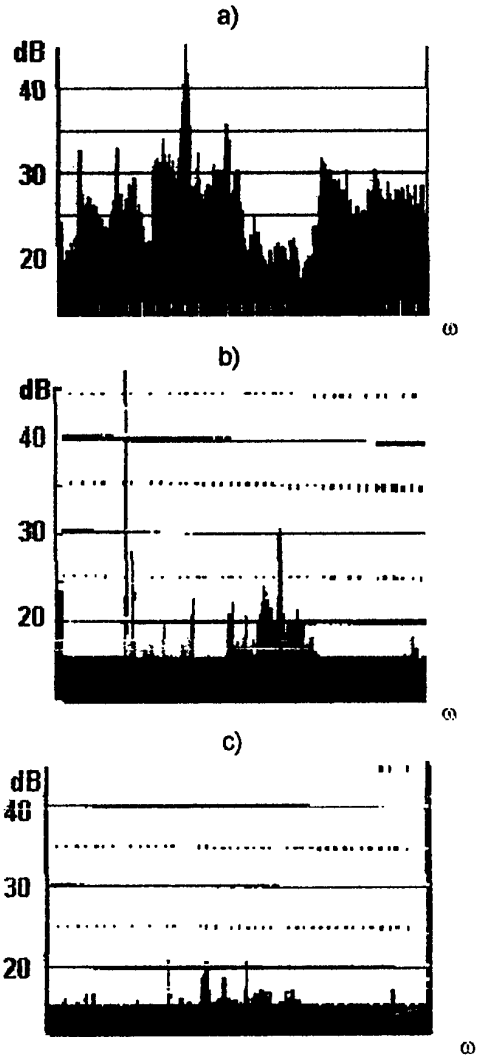



Fig. 3. Spectrum voltages

One of the main problems for the creation of a diagnostic model is determining of the elements of matrix $\mathbf{K}(j\omega)$ . Theoretically, this problem can be solved by methods of diagnostics of the multipolar circuits [3]. The number of sources of signals is usually more than number of measured voltages, that is $n > m$. Then the test methods of diagnostics are expedient for the decision of this task. According to these methods it is possible to make changes in the circuit of the power equipment at the substation, including modes of complete switching-off. Then in this case it is possible to find the test matrix $\mathbf{K}_T(j\omega)$ for $p \geq m/n$ experiments, based on the various circuits of electric equipment. Its elements are zero if the equipment is switched-off. The new test equation

$$\mathbf{U}_T(j\omega) = \mathbf{K}_T(j\omega)\, \mathbf{E}(j\omega)$$

can also be solved regarding a vector of sources of radiation. Naturally, the inexactitudes of measurements of high-frequency signals, variation of meteoconditions and other factors can interfere with the reception of reliable results. The regular supervision, accumulation of databank and use of statistical methods can essentially increase the reliability of methods of diagnostics of electric power equipment.

## 4. REFERENCES

1. V.P. Vdoviko, A.G. Ovsyannikov. "Utilization of partial discharges characteristics measurement for monitoring of 110-550 kV transformer insulation" (in Russian), Proceedings of the third Symposium on Elecrotechnics 2010, Ì /enigorod, Russia, May 23-26, 1995, pp. 117-122.
2. N.V. Kinsht, G.N. Gerasimova, M.A. Katz. "Diagnostic of network" (in Russian), Energoatomizdat, Moscow, 1983.
3. P.A. Butirin. "Diagnostic of the multipolar circuits" (in Russian), Power engineering and transport, No. 6, 1983, pp. 62-64.

## BIOGRAPHICAL NOTES

All authors of the paper work at the Far-Eastern State Technical University. N.Silin heads the Electrical Engineering Department from 1992. N.Kinsht and M.Katz are professors at the Department. N.Kinsht heads the research laboratory of Electrical Physics and Electrical Power at the Institute for Automation and Control Processes. O.Preobragenskaya is an associate professor, qualified in computer and information systems. Y.Petropavlovsky is a post-graduate student working on the high frequency signal measurements.

**EMC 2000** INTERNATIONAL WROCŁAW SYMPOSIUM ON ELECTROMAGNETIC COMPATIBILITY

# APPLICATION OF WAVELET TRANSFORM FOR ADJACENT CHANNEL TRANSIENT POWER MEASUREMENTS

Jerzy Kołakowski
Institute of Radioelectronics, Warsaw University of Technology
ul. Nowowiejska 15/19, 00-665 Warszawa
tel/fax +48 22 6607635 e-mail j.kolakowski@ire.pw.edu.pl

*Abstract*

*The paper deals with measurements of interference observed in adjacent channel during radiocommunication transmitter transient states. The method using digital filtering for signal envelope power evaluation is proposed. Application of wavelet transform for signal de-noising is presented and discussed. The paper contains results of simulations as well as measurements of an exemplary transmitter.*

## 1. INTRODUCTION

During transient states, which usually occur when transmitter is switched on or off, the transmitter can be a source of interference endangering communication in adjacent channels.

According to the most of EMC specifications concerning radiocommunication equipment the basic tests depend on determination of RF power and carrier frequency plots as a function of time. More complex measurements are carried out in case of transmitters intended for transmission of data (e.g. radio-modems, cellular phones etc.) They consist in evaluation of RF power delivered to adjacent channels. Generally, the point of the test is to catch a peak value of RF power detected in adjacent channels during transient state. The signal is measured at the output of the strictly defined band-pass filter tuned to the nominal frequency of the adjacent channel. Requirements, the filter should fulfil, depend on measured equipment. For transmitters intended for data transmission the filter attenuation outside the adjacent channel should be greater than 90 dB [5]. In case of cellular equipment filter specification is less stringent (eg. GSM phones should be tested with five-pole 30 kHz filter [4]).

An exemplary test arrangement is presented in fig. 1. The tests are performed for transmitters equipped with antenna connector as well as transmitters with integral antennas. In the latter case the use of specialised coupling device is necessary. Unfortunately the device introduces attenuation in the signal path. It can deteriorate the signal-to-noise ratio and thus can increase measurement uncertainty.

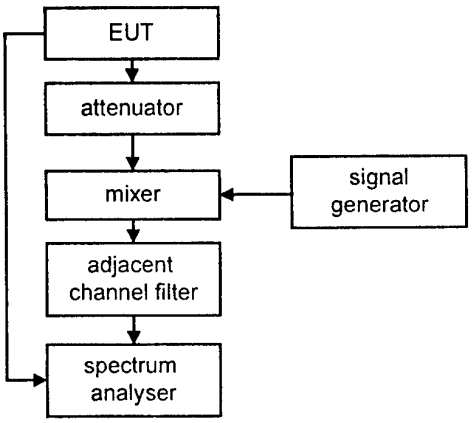



Fig. 1. Test arrangement for adjacent channel transient power measurements.

The paper contains proposal of the method that implements digital filtering and wavelet transform for measurement of transmitters during transient states.

## 2. WAVELET TRANSFORM

$$Wf(u,s) = \int f(t)\frac{1}{\sqrt{s}}\psi^*\left(\frac{t-u}{s}\right)dt \qquad (1)$$

The wavelet transform (1) converts time-domain signal *f(t)* to its time-scale representation *Wf(u,s)*. Function $\psi$ is so called mother wavelet, *s* and *u* correspond to scale and shift in time respectively. Scale value corresponds to frequency value so the transformation results in time-frequency representation of the signal. Time-frequency signal energy density can be expressed by scalogram - squared modulus of the wavelet transform. Scalogram maxima can be

used for evaluation of signal transient frequency.

Signal can be reconstructed from its wavelet transform according to formulae (2,3).

$$f(t)=\frac{1}{C_\psi}\int_0^\infty\int_{-\infty}^{\infty}Wf(u,s)\frac{1}{\sqrt{s}}\psi\left(\frac{t-u}{s}\right)du\frac{ds}{s^2} \quad (2)$$

where $C_\psi=\int_0^\infty\frac{|\hat{\psi}(\omega)|^2}{\omega}d\omega$ (3)

$\hat{\psi}$ - Fourier transform of $\psi$

Equations mentioned so far describe continuous version of the wavelet transform. Computer calculations require discretisation in time and scale domains. Usually scale and shift in time are discretised in the following way.

$$s=2^{\frac{m}{N}} \quad (4)$$

$$u=nu_0 2^{\frac{m}{N}} \quad (5)$$

where: m,n – integers, N – number of voices (intermediate scales per octave).

The choice of $u_0$ and N values should be done very carefully in order to provide precise signal reconstruction. These aspects are covered by wavelet frame theory [1][2].

Wavelet transform can be used for effective reduction of noise. The method known as time-variant filtering consists in reconstruction of the signal from its modified time-frequency representation. The most popular methods of modification use various ways of wavelet coefficient thresholding [2]. Hard thresholding method requires all coefficients lying below the threshold to be set to zero. In case of soft thresholding [3] coefficient modification depends on relation between the threshold and coefficient value. More sophisticated solutions assume elimination of wavelet transform coefficients lying outside the ridge regions.

The advantage of such de-noising methods originates from the fact that apart from traditional filtering they can diminish the noise in the signal bandwidth. The method can improve signal to noise ratio up to several decibels.

## 3. DESCRIPTION OF THE MEASUREMENT METHOD

The essence of the proposed method is the calculation of required parameters using set of transmitter output signal samples.

Simulations and measurements described in the paper have been done with the use of Gabor wavelet (6) (fig. 1).

$$\psi(t)=g(t)e^{-j\eta t} \quad (6)$$

where $g(t)$ is a Gaussian window:

$$g(t)=\frac{1}{(\sigma^2\pi)^{\frac{1}{4}}}e^{-\frac{t^2}{2\sigma^2}} \quad (7)$$

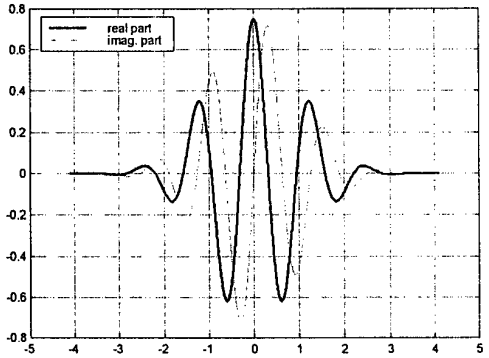



Fig. 2. Gabor wavelet in time and frequency domains ($\eta$=5, $\sigma$=1).

After calculation of the signal time-scale representation the wavelet transform coefficients have been modified using hard thresholding method. The threshold value was established by means of computer simulation. Calculations utilise approximate value of the recorded signal to noise ratio.

Before digital filtering reconstructed signal was zero-padded. This extension was necessary because of discrete convolution properties. Number of zeroes relates to the length of the adjacent channel filter impulse response. Zero-padding can be used for extension of the data record to the power of two value which provides reduction in time of calculations. Output signal is calculated as the inverse FFT from the product of signal spectrum and filter frequency response.

## 4. COMPUTER SIMULATIONS

Computer simulations covered two aspects of discussed method: noise level at the filter output and determination of threshold level to be used by de-noising procedure. Calculations have been made with the filter which frequency response is presented in figure 3. The digital filter corresponds to the RBW filter of the spectrum analyser. Results obtained from this instrument were used as a reference during measurements described below.

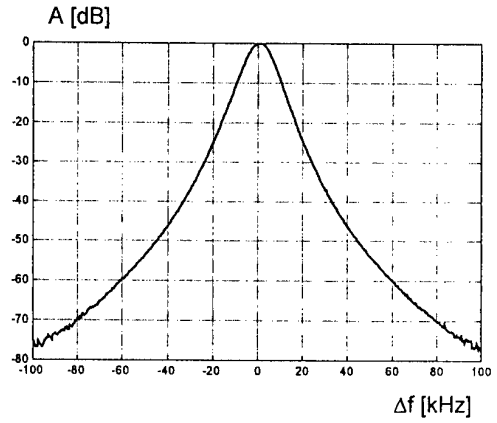



Fig 3. Spectrum analyser filter characteristics

Noise level at the output of adjacent channel filter can be calculated with analytical methods. In case of less regular filter frequency response it can be easily determined using appropriate simulations. Relation between signal-to-noise ratio (SNR) and output noise level is presented in fig. 4.

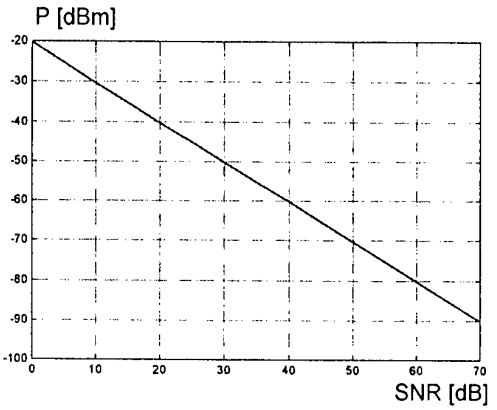



Fig. 4. Noise power at the output of adjacent channel filter versus SNR.

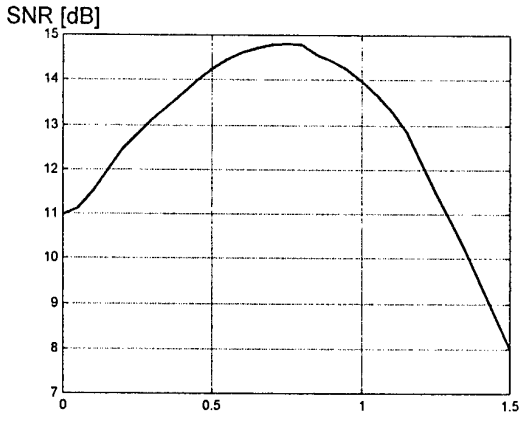



Fig. 5. Improvement in SNR ratio versus threshold value. (SNR before denoising – 10 dB).

Threshold level used by de-noising procedures was also determined by means of simulation. An amplitude step modulated signal with predefined SNR was processed with various threshold values. An exemplary plot of SNR improvement in case of noisy signal (SNR=10dB) is presented in fig. 5.

## 5. EXEMPLARY MEASUREMENTS AND RESULTS

The proposed procedure has been tested using test arrangement presented in fig. 6. Transmitter output signal was acquired with a vector signal analyser (HP 89441A). Envelope power was measured with a spectrum analyser E4402B.

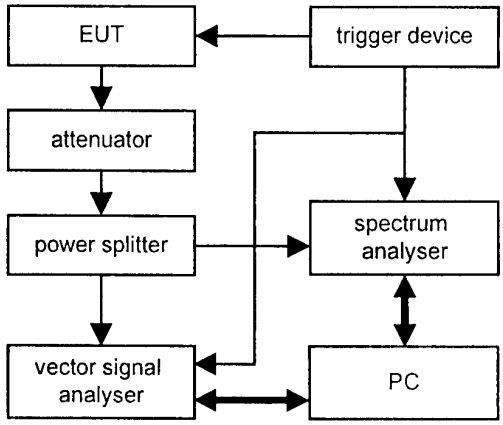



Fig. 6. Test arrangement.

Measurements described in the paper have been performed with the use of transceiver operating at 178 MHz. The envelope of the transmitter output signal is presented in figure 7.

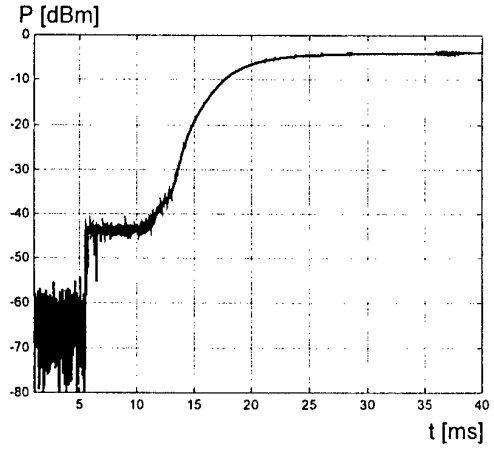



Fig. 7. Recorded transmitter output signal.

Emissions in adjacent channels have been measured using spectrum analyser internal RBW filter (10 kHz). Although the frequency response of

that filter (fig 3.) does not fulfil requirements of appropriate standards [5] the filter due to its short impulse response is convenient for experimental verification of the proposed method.

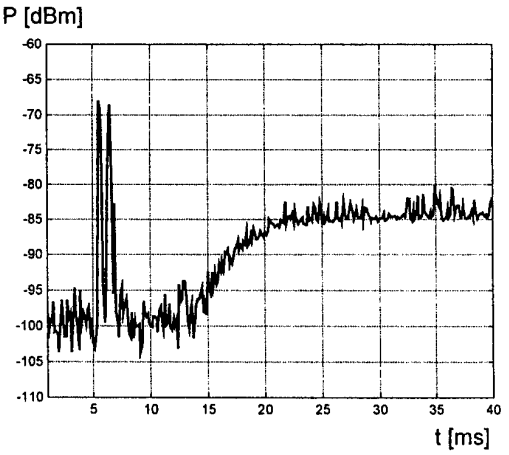



Fig. 8. Envelope power (measured with the spectrum analyser).

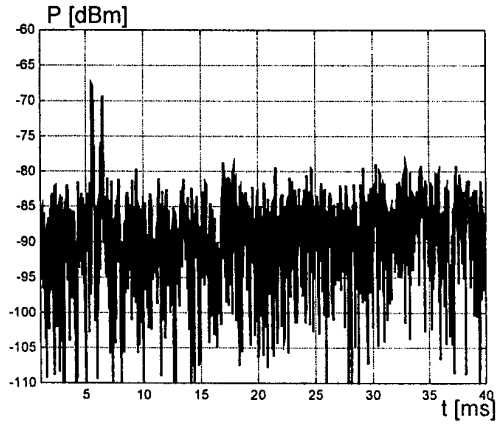



Fig. 9. Envelope power (calculated)

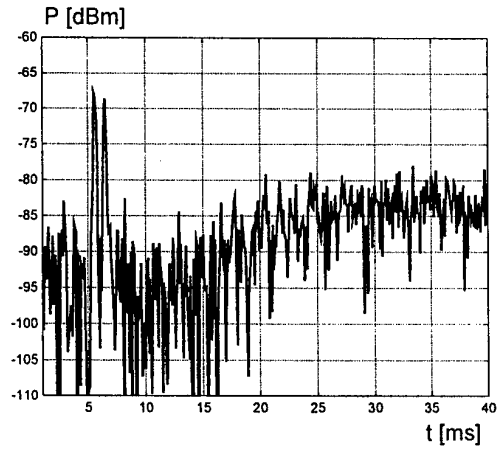



Fig. 10. Envelope power (calculated for de-noised signal).

Figures 8 and 9 presents envelope power measured and calculated. The offset of filter centre frequency was equal to 100 kHz. Peaks of the signal power have similar values, but in case of calculated signal the strong influence of noise is observed. Figure 10 presents signal after de-noising. De-noising procedure allows for observation of signal parts previously obscured by noise.

## 6. CONCLUSIONS

The method for adjacent channel transient power measurement described in the paper seems to be a valuable alternative to methods described in standards. It provides results comparable to those achieved with traditional methods. In case of low signal to noise ratio de-noising procedure based on wavelet transform enables more precise measurement of envelope power.

The hard thresholding procedure implemented in described measurements is a basic one. Further SNR improvement would be possible with more advanced processing of wavelet coefficients eg. by applying threshold value taking into account local (in time domain) signal properties.

## 7. REFERENCES

1 I. Daubechies, *Ten Lectures on Wavelets*, SIAM, 1992.

2 S. Mallat, *A Wavelet Tour of Signal Processing*, Academic Press, 1998.

3 D. L. Donoho, *Denoising by soft-thresholding.* IEEE Transactions on Information Theory, 41(3), 1995.

4 ETSI Technical Specification GSM 11.10 *Mobile Station Conformity Specification.*

5 ETS 300113; Technical characteristics and test conditions for radio equipment intended for the transmission of data (and speech) and having an antenna connector; ETSI, June 1996.

## BIOGRAPHICAL NOTE

Jerzy Kołakowski received his MSc degree in 1988 from Warsaw University of Technology. Since 1988 he is with Institute of Radioelectronics. His activity concerns methods and systems for measurements of radiocommunication equipment.

**EMC 2000** INTERNATIONAL WROCŁAW SYMPOSIUM ON ELECTROMAGNETIC COMPATIBILITY

# NUMERICAL MODELING OF NONLINEAR INTERFERENCE AND DISTORTIONS FOR WIRELESS COMMUNICATIONS

Sergey L. Loyka

Belorussian State University of Informatics & Radioelectronics, P. Brovki Str. 6,
Minsk 220027, Belarus, e-mail: sergey.loyka@ieee.org

*Nonlinear interference and distortions have a profound impact on wireless communication system operation, especially under conditions of severe electromagnetic environment (overcrowded spectrum, strong interfering signals, multipath and multi-signal environment etc.). In this paper, we propose a new behavioral-level simulation technique – the "instantaneous" quadrature technique, which can be employed for the EMC/EMI analysis of wireless systems in a computationally-efficient way taking into account nonlinear effects (over wide dynamic and frequency ranges) and, secondly, we discuss how to apply the instantaneous quadrature technique to simulating wireless receivers and transmitters for EMC/EMI problems.*

## 1. INTRODUCTION

Exponential increase in the number of wireless communication systems and in the complexity of their design greatly increases the risk of intra- and inter-system interference and distortions, which can degrade the system performance drastically, especially under conditions of over-crowded spectrum and limited space available (antenna towers, indoor communications, closely-located handheld phones etc.). Even carefully-made frequency planning does not guarantee the absence of interference in any scenario. Some possible kinds of nonlinear interference and distortions for wireless communication systems are the following [1, 2]:

1. Spurious radiation of transmitters: harmonics and sub-harmonics, intermodulation products (IMP), noise etc. Note that the intermodulation radiation can be caused by an external signal (from a nearby transmitter) as well as by several carriers (in CDMA systems, for example) in the transmitter's power amplifier.
2. Spurious responses of receivers: adjacent, image and intermediate frequency (IF) channels.
3. Nonlinear behavior of receivers may also cause the performance degradation (desensitization, IMPs, local oscillator noise and harmonics conversion etc.).

Analytical and semi-empirical methods were extensively used in the past for the analysis of these effects [1, 2]. Those methods were quite simple and allowed one to get some insight into the system operation. However, the accuracy of those methods is rather poor. Besides, the analysis of complex systems (present-day wireless systems) is rather difficult to do by the old methods.

Thus, nonlinear numerical methods should be used for these problems. System-level analysis (when one or even several systems are to be analyzed at the same time) requires for behavioral-level techniques [3] because circuit-level methods can not be applied due to very high demand for the computational resources.

## 2. QUADRATURE MODELING TECHNIQUE

The quadrature modeling technique is the most popular tool for behavioral-level nonlinear modeling and simulation of active stages of communication circuits and systems [3, 4]. This technique was introduced in early 1970s for nonlinear modeling and simulation of traveling wave tube amplifiers used in satellite communications [5]. The main idea of the quadrature modeling technique is the use of a complex envelope instead of real narrowband signals [3-5]:

$$x(t) = A(t)\cos(\omega_0 t + \varphi(t)) = Re\{A(t)\cdot exp[j\cdot(\omega_0 t + \varphi(t))]\} \quad (1)$$

where $A(t)$ and $\varphi(t)$ – are amplitude and phase that vary slowly with respect to carrier (amplitude and phase modulation), $\omega_0$ – is the carrier frequency. Its complex envelope is

$$\overline{A(t)} = A(t)\cdot exp[j\varphi(t))] \quad (2)$$

So, there is not any carrier information in the complex envelope, only modulation information (only the first harmonic zone is taken into account). It's very important from the viewpoint of computational efficiency, but it also limits the technique capabilities – only narrowband analysis is possible because the frequency response is assumed to be flat over the simulation bandwidth. The output signal of a bandpass nonlinear stage is

$$y(t) = K(A_{in}(t))\cdot A_{in}(t)\times \cos(\omega_0 t + \varphi_{in}(t) + \Phi(A_{in}(t))) \quad (3)$$

where $A_{in}$ and $\varphi_{in}$ are the input signal amplitude and phase. A nonlinear stage is characterized by its envelope amplitude and phase transfer factors:

$$K(A_{in}) = \frac{A_{out}}{A_{in}}, \quad \Phi(A_{in}) = \varphi_{out} - \varphi_{in} \qquad (4)$$

$K(A_{in})$ represents envelope amplitude-to-amplitude (AM-AM) nonlinearity, and $\Phi(A_{in})$ represents envelope amplitude-to-phase (AM-PM) nonlinearity. Note that both factors depend on the input signal amplitude, not on instantaneous value of the signal. It's due to the bandpass representation of signals and system stages (actually, lowpass equivalents of both are used). Thus, equation (4) constitutes the envelope nonlinearity.

In the quadrature modeling technique, in-phase and quadrature envelope transfer factors are used

$$\begin{aligned} K_I(A_{in}) &= K(A_{in})\cos\Phi(A_{in}) \\ K_Q(A_{in}) &= K(A_{in})\sin\Phi(A_{in}) \end{aligned}, \qquad (5)$$

and output lowpass signal is expressed as

$$Y(t) = K_I(A_{in})X_I(t) - K_Q(A_{in})X_Q(t) \qquad (6)$$

Two independent channels (in-phase (I) and quadrature (Q)) are used for the simulation. In this way this technique takes into account both the AM-AM and AM-PM nonlinearities. This nonlinear model is sometimes called a memoryless nonlinearity [3]. Strictly speaking, this nonlinearity is not a memoryless one because there is a phase shift (AM-PM), thus the output depends on the input at some past instants (however, there is indeed no any frequency dependence in this model). The input of the quadrature nonlinearity is also shifted by $-\pi/2$ and this operation is not a memoryless one (in fact, it is the Hilbert Transform that is an integral transformation [3]). Consequently, this channel and the entire quadrature structure are not memoryless ones. However, we can still use the term "memoryless" in the sense that the transfer factors $K_I$ and $K_Q$ depend on the input signal amplitude $A_{in}$ at the same instant only.

At the present time, this technique is mainly used for the simulation of solid-state power amplifiers. It has many advantages: it allows one to simulate the power amplifier with a digitally-modulated input signal using a PC in reasonable time and, consequently, to predict adjacent channel power ratio (ACPR), power spectral regrowth (PSR) and error vector magnitude (EVM). The technique can also predict IMPs and gain compression/expansion. The permissible number of input tones and the analysis dynamic range are quite large. However, the main drawback of the quadrature modeling technique is that it is a narrowband one, so it can not take into account frequency response, to predict harmonics of the carrier frequency and even-order nonlinear products, or to model the bias decoupling network effect [6]. This effect limits the analysis accuracy even for narrowband signals and systems [6]. The quadrature modeling technique also uses an explicit representation of the modulated signal, so multiple-carrier signals can not be simulated in a direct way. Thus, some improvements are desirable.

## 3. DISCRETE TECHNIQUE

The discrete technique was introduced in 1980s for the nonlinear simulation of a RF/microwave receiving path taking into account nonlinear interference and distortions [7-11]. It also accounts for the spurious receiver channels (adjacent, image, local oscillator noise etc.), IMPs and harmonics, gain compression/expansion etc. The main application of this technique was to EMC/EMI analysis in a group of RF/microwave systems. An important advantage of the discrete technique is that instantaneous values of the signals are used during the analysis, not the complex envelope.

The basis of the discrete technique is a representation of the system block diagram as linear filters (matching networks) and memoryless nonlinear elements (active elements) connected in series (or in parallel, or both) [7-11]. Input and output filters model input and output matching networks. This representation reflects characteristic peculiarities inherent to the construction of typical RF amplifying and converting stages. The utilization of the model with memoryless nonlinearity is not a significant limitation on the method. Non-zero memory effects can partially be factorized at the level of input or output filters, that is, this representation is equivalent with respect to the simulation of the "input-to-output" path. Signal passage through a linear filter is simulated in the frequency domain using the complex transfer factor of the filter,

$$S_{out}(f) = S_{in}(f) \cdot K(f), \qquad (7)$$

where $S_{out}(f)$- is the output signal spectrum, $S_{in}(f)$ – is the input signal spectrum, $K(f)$ - is the filter complex transfer factor, and $f$ - is frequency. An appropriate sampling technique is required in order to sample the spectrum. Signal passage through a nonlinear memoryless element is simulated in the time domain using the instantaneous transfer function of the element,

$$u_{out}(t) = F[u_{in}(t)], \qquad (8)$$

where $u_{out}(t)$ - is instantaneous value of the output signal at time instant $t$, $u_{in}(t)$ - is the same for input signal, $F$ - is an instantaneous transfer function of the nonlinear element. This function can be calculated using the measured or circuit-level simulated AM-AM characteristic [9-10].

Thus, the simulation is made over a wide frequency range. The technique allows one to predict harmonics and even-order nonlinear products, to take into account frequency response and to analyze multi-carrier systems. Both these techniques (the quadrature modeling technique and the discrete technique) are very computationally efficient as compared to circuit-level techniques (HB technique or SPICE), and still have a circuit-level accuracy in many cases. However, the discrete technique does not take into account AM-PM

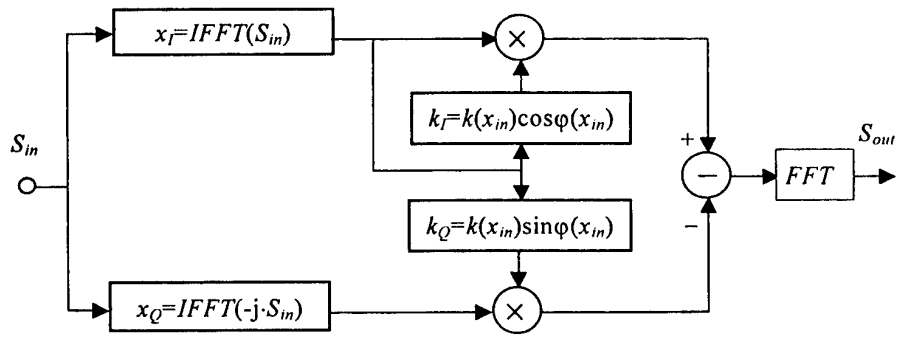



Figure 1. Modeling broadband nonlinear element by the 'instanteneous' quadrature technique.

nonlinearity that limits substantially the analysis accuracy.

## 4. "INSTANTANEOUS" QUADRATURE TECHNIQUE

Here we propose to combine the quadrature modeling technique and the discrete technique in order to build the combined "instantaneous" quadrature modeling technique which can model the circuit or system behavior over wide frequency and dynamic ranges taking into account both AM-AM and AM-PM conversions. In order to model signals and systems over a wide frequency range, the instantaneous values of the signals must be used, not the complex envelope. In order to model the AM-PM conversion, the quadrature modeling structure should be used for the nonlinear element modeling. Thus, the modeling process consists of the following items:

1. Linear filters are modeled in the frequency domain (the same as for the discrete technique).
2. Nonlinear elements are modeled in the time domain using the quadrature structure, but the instantaneous signal values are used, not the complex envelope.
3. The transform from the frequency (time) domain to the time (frequency) domain is made by IFFT (FFT) (very computationally efficient).
4. The Hilbert transform [3] is used to calculate in-phase and quadrature components,

$$x_Q(t)=\hat{x}(t)=\int_{-\infty}^{\infty}\frac{x(\tau)}{t-\tau}d\tau,\ x_I(t)=x(t), \qquad (9)$$

where $x_I(t)$ and $x_Q(t)$ – are instantaneous in-phase and quadrature components of the signal, $\hat{x}(t)$ is the Hilbert-conjugate signal of $x(t)$. In fact, we use the Hilbert Transform in the frequency domain to calculate the quadrature components because it does not require numerical integration and, thus, is much more computationally efficient:

$$x_Q(t)=IFFT(-j\cdot S(\omega)) \text{ for } \omega\geq 0,$$
$$S(\omega)=FFT(x(t)) \qquad (10)$$

where S(ω) – is the signal's spectrum. The signal itself is the in-phase component, and the Hilbert's conjugate signal is the quadrature component.

5. A system of two integral equations is used in order to convert the envelope transfer function into the instantaneous ones:

$$\frac{4}{\pi}\int_0^1 k_I(A_{in}t)\frac{t^2dt}{\sqrt{1-t^2}}=K(A_{in})\cos\Phi(A_{in})$$
$$\frac{4}{\pi}\int_0^1 k_Q(A_{in}t)\sqrt{1-t^2}\,dt=K(A_{in})\sin\Phi(A_{in}) \qquad (11)$$

where $k_I$ and $k_Q$ – are the instantaneous in-phase and quadrature transfer factors. Note also that using (11) only the even parts of the transfer factors can be calculated. In order to find the odd parts, some additional characteristics should be used (for instance, the second harmonic transfer factor). As a rule, the amplitude transfer characteristics can be measured or simulated using a circuit-level simulator, thus we need to solve equations (11) for $k_I$ and $k_Q$. This can be done using the method of moments. If we use piecewise constant basis functions and a point matching technique, the matrices of these equations appear to be upper triangular ones, so the systems of linear equations can be solved analytically (this semi-analytical approach speeds up computations substantially).

Fig. 1 gives an illustration of the nonlinear element modeling. It should be noted that the transfer function of the quadrature channel is not a usual transfer function in a conventional sense: it depends not only the input of the quadrature nonlinearity ($x_Q$) but also on the input of the entire structure ($x_{in}$) i.e., in fact, on the input of the in-phase nonlinearity ($x_I$). Consequently, we cannot use the usual methods of the transformation of the envelope transfer function into the instantaneous one [5]. At the same time, the transfer function of the in-phase channel is a usual transfer function and those methods can be applied in this case.

If one whishes to simulate even-order nonlinear products, then odd parts of the instantaneous transfer factors must be determined. It can be done using the second-order envelope characteristics (second harmonic zone AM-AM and AM-PM functions or second-order IMP at the output for the two-tone input):

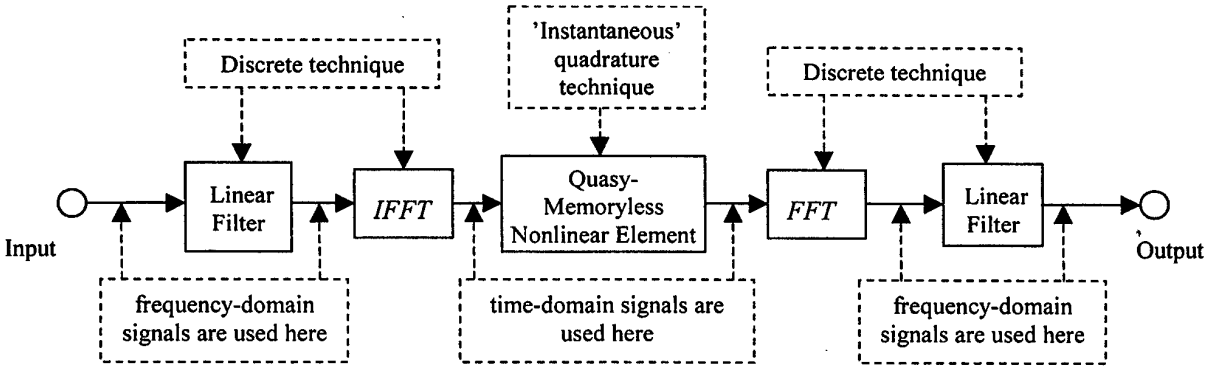



Figure 2. Simulating a single-stage radio amplifier by the 'instantaneous' quadrature technique.

$$\frac{4}{\pi}\int_0^1 k_I(A_{in}t)\frac{t(2t^2-1)}{\sqrt{1-t^2}}dx = K_2(A_{in})\cos(\Phi_2(A_{in}))$$
$$\frac{8}{\pi}\int_0^1 k_Q(A_{in}t)t\sqrt{1-t^2}\,dx = K_2(A_{in})\sin(\Phi_2(A_{in})) \quad (12)$$

where $K_2(A_{in})$ is the second-order envelope transfer factor and $\Phi_2(A_{in})$ is the second-order AM-PM characteristic. We can solve the integral equations (12) using the traditional method of moments approach. But, as practical experience shows, it requires even more sample points than for the even parts. Thus, it is much efficient to use the semi-analytical approach proposed above.

## 5. APPLYING INSTANTANEOUS QUADRATURE TECHNIQUE TO WIRELESS SYSTEMS

Let us now consider the simulation of typical wireless subsystems/systems using the instantaneous quadrature technique. Fig. 2 illustrates the simulation of a single stage RF amplifier (either power or low noise). The input and output filters model the matching networks, and the quasy-memoryless nonlinear elements model the amplifier nonlinearity (both AM-AM and AM-PM). Using this approach, we may simulate other RF and IF stages (like mixers and IF amplifiers) and even detectors [11] in a computationally-efficient way. Further, using the black-box approach, we may simulate the entire subsystem/system operation under real-world conditions and signals.

The simulation of a wireless transmitter using the instantaneous quadrature technique is quite straight-forward: we do it in the same way as for the quadrature modeling technique. The power amplifier is considered to be the main source of interference and distortions in this case (however, other stages can also be simulated). The simulation of a wireless receiver is not so simple because many its components can contribute to the overall interference and distortions. Thus, we consider (i.e. simulate) the receiver block diagram step by step: low-noise amplifier, local oscillator plus mixer, IF filter and IF amplifier, detector and baseband signal processing part. It should be noted that (i) frequency response is taken into account in every stage, and (ii) detector simulation is possible using the technique proposed that enables us to go further to the simulation of baseband signal processing.

Thus, the instantaneous quadrature technique can be used for the EMC/EMI simulation of an entire wireless communication system over wide frequency and dynamic ranges.

## 6. TECHNIQUE VALIDATION

In order to validate the technique proposed, extensive harmonic-balance simulations as well as measurements of microwave solid-state amplifiers have been carried out. Fig. 3 shows IMPs simulated by our technique (solid line) and measured (squares). One can note quite a good agreement between behavioral-level simulation and measurements. In general, the discrepancy is about few dBs except for some special areas, which should be further investigated. Fig. 4 shows harmonics simulated by our technique (solid line) and measured (squares). Behavioral-level simulation and measurements agree quite well in this case too. The discrepancy is rather large for several special areas, which should be further investigated. Note also that the analysis is made over wide dynamic range (130-180 dB) and wide frequency range (harmonics!). Thus, these results seems to be very satisfactory taking into account that the problem is a nonlinear one. Accuracy of even-order nonlinear products prediction is slightly worse but still satisfactory for practical purposes.

## 7. CONCLUSION

In this paper, we have presented the instantaneous quadrature technique as an efficient tool for behavioral-level simulation of wireless circuits and systems for EMC/EMI problems. This techniques combines the advantages of both the quadrature modeling technique and the discrete technique and, consequently, gives one possibility to simulate the circuit/system nonlinear performance over wide frequency and dynamic ranges. This technique should be used on the frequency planning phase in order to avoid possible system performance

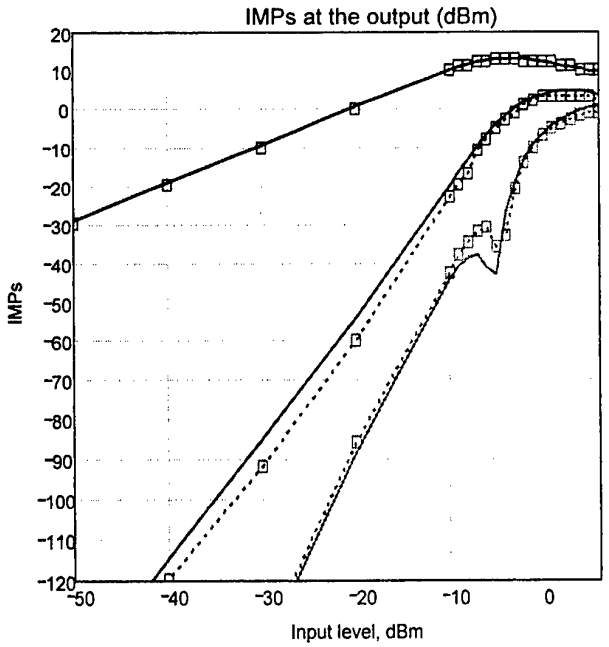



Figure 3. Fundamental, 3[rd] and 5[th] order IMPs (solid line – simulated, squares – measured) for 2 stage MMIC amplifier.

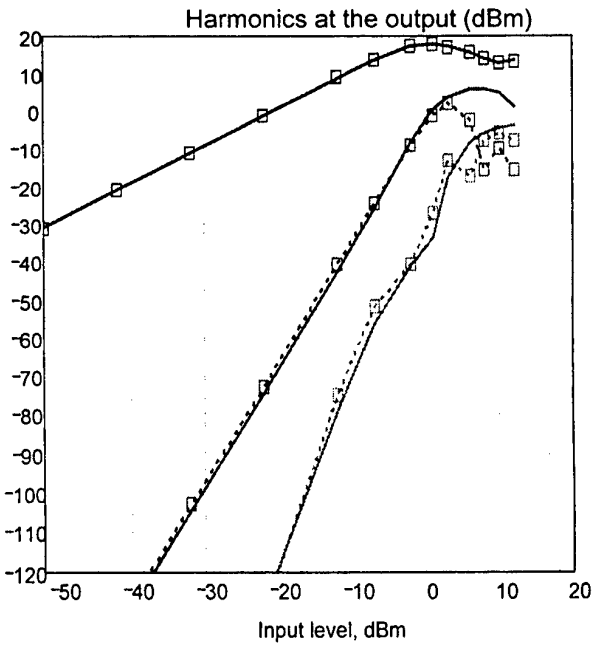



Figure 4. Fundamental, 3[rd] and 5[th] harmonics (solid line – simulated, squares – measured) for 2 stage MMIC amplifier.

degradation on the implementation phase and to ensure reliable and high-quality communication.

## 8. REFERENCES

[1] D.R.J. White, "*A Handbook Series on Electromagnetic Interference and Compatibility*", Don White Consultants Inc., Germantown, Maryland, 1971-1973.

[2] J. Gavan, "Principles of Radio System and Relevant EMI Environmental Effects, Analysis and Computation," in R. Perez (ed.), *Handbook on Electromagnetic Compatibility*, New York, Academic Press, 1995.

[3] M.C. Jeruchim, P. Balaban, K.S. Shanmugan, *Simulation of Communication Systems*, Plenum Press: New York, 1992.

[4] J. Staudinger, "Applying the Quadrature Modeling Technique to Wireless Power Amplifiers," *Microwave Journal*, vol. 40, No. 11, Nov. 1997, pp.66-86.

[5] A. R. Kaye, D. A. George and M. J. Eric, "Analysis and compensation of bandpass nonlinearities for communications", *IEEE Transactions on Communications*, vol. 20, No. 11, Nov. 1972, pp.965-972.

[6] J. Staudinger, Behavioral Analysis Method Applied to the Design & Simulation of Linear Power Amplifiers, *RAWCON'98 Workshop "Modeling and Simulation of Devices and Circuits for Wireless Communications"*, Colorado Springs, CO, Aug. 9-12, 1998.

[7] V.I. Mordachev "Express analysis of electromagnetic compatibility of radio electronic equipment with the use of the discrete models of interference and Fast Fourier Transform", *Proc. of IX Inter. Wroclaw Symp. on EMC*, Poland, Wroclaw, 1988, Part 2, pp.565-570.

[8] S. L. Loyka and V. I. Mordachev, "Identification of Nonlinear Interference Sources with the Use of the Discrete Technique," *IEEE EMC Symp.*, Denver, Colorado, Aug. 24-28, 1998, pp.882-887.

[9] S.L. Loyka, "Numerical Simulation of Nonlinear Interference in Radio Systems (Invited paper)," *The 26th URSI General Assembly*, Toronto, Canada, Aug. 13-21, 1999.

[10] S.L. Loyka, "The Influence of Electromagnetic Environment on Operation of Active Array Antennas: Analysis and Simulation Techniques," *IEEE AP Magazine*, 1999, accepted for publication.

[11] S.L. Loyka, Nonlinear EMI Simulation of an AM-Detector at the System Level, *IEEE Trans. on EMC*, 1999, accepted for publication.

## BIOGRAPHICAL NOTE

Dr. Sergey L. Loyka was born in Minsk, Republic of Belarus on August 6, 1969. Since 1995 he is a Senior Researcher of the EMC Laboratory, Belorussian State University of Informatics and Radioelectronics. Dr. Loyka is a member of the New York Academy of Sciences and of the IEEE. He has over 60 publications in the area of EMC, active antenna arrays, wireless communications, nonlinear circuit analysis and computer-aided modeling and simulation.

EMC 2000 INTERNATIONAL WROCŁAW SYMPOSIUM ON ELECTROMAGNETIC COMPATIBILITY

# NEW APPROACH TO SUPPRESS IMPULSIVE INTERFERENCE ON TRACK CIRCUIT OF ELECTRIFIED RAILWAYS

Yang Shiwu, Fei Xikang, Wu Yunxi
College of Electronic and Information Engineering, Northern Jiaotong University, Beijing 100044, China
Phone: 86-10-63240696, Email: ysw@center.njtu.edu.cn

*At first, we point out that the impulsive interference of unbalanced traction current is the principal reason causing degradation of 25Hz track circuit. After discussing the basic theory on anti-interference, we present a new apparatus called impedance-match transformer, which is composed of impedance bond (transformer) with air-gap and 50Hz series-resonant circuit. Some calculation results are given in this paper. Both simulation and application demonstrate that this solution can greatly alleviate impulsive interference and boost signal transmission.*
*Key words: impulsive interference, track circuit, impedance-match transformer.*

## 1. GENERAL DESCRIPTION

### 1.1. Problem

Generally, both AC traction current and track circuit use tracks as transmission channel in electrified railways. Impedance transformer (bond) acts as the joint part. If traction current of one rail doesn't equal that of the other, the unbalanced current will exert interference on track circuit.

As a common mode in electrified railway stations, 25Hz phase-sensitive track circuit chooses 25Hz as signal frequency for transmitting track circuit information to evade 50Hz alternating traction disturbance. Its principle can be expressed by (1):

$$V = k \times V_1 \times V_2 \times \sin\alpha \qquad (1)$$

Where V is the working voltage, k is coefficient, $V_1$ and $V_2$ are local and receiving (track circuit) voltage respectively, $\alpha$ is phase difference between $V_1$ and $V_2$. In fact, it has excellent performance against stable interference caused by 50Hz unbalanced traction current. At present, it has been applied in China and many other countries.

On the other hand, 25Hz track circuit has an undesired shortcoming in preventing the impulsive interference. Based on simulation data, its immunity to impulsive unbalanced current is approximately 20A, about 3.3% of 600A, i.e. capacity of impedance transformer. However, the actual unbalanced coefficient could reach 10% or more. Therefore, mistaken operations of 25Hz track circuit are often found in some particular sections with greater unbalance. The common phenomenon is that the track relay of receiving circuit falls down in a moment then picks up, then the signal consequently flashes "red" indicating danger, so trains have to operate emergency brake and sometimes wrongly enter the route. Clearly, transportation safety and efficiency are seriously threatened.

### 1.2. Reasons

Impulsive current happens when traction current changes suddenly and strongly on conditions such as intermittent bad contact between overhead conductor (power mains) and pantograph, starting and braking of locomotive. On account of equipment with non-linear voltage/current characteristic on electrified traction, impulsive current is actually a transient.

Impulsive interference is generated from unbalanced current. Unbalanced extent determines how strong the interference is. Because a great deal of rails are connected with screws but not by soldering in China, two rails easily become unbalanced.

We find that impulsive interference influences the track circuit mainly by two ways. Firstly, because impulsive current has approximate but asymmetric sine waveform, it contains plentiful composite of direct current. The ferromagnetic equipment such as impedance bond could be easily saturated, and 25Hz signal floating on 50Hz interference is vulnerable to clipping or attenuating, so the receiving circuit may get a voltage below normal value. Secondly, when interfered, the linear filter in receiving part of 25Hz track circuit will yield a 25Hz transient procedure or damped oscillation as its impulsive response, therefore it may definitely disturb the signal and cause false operation of receiving circuit.

Obviously, measures should be taken to solve saturation of impedance transformer and simultaneously assure signal transmission.

## 2. BASIC CONCEPTION

### 2.1. Essence of traction current

We ought to grasp the nature of traction current before considering any approach. The value of traction current *I* can be written as (2):

$$I = V_t / (Z_1+Z_2) \quad (2)$$

Where $V_t$ is traction voltage (25kV), $Z_1$ is impedance of locomotive load, $Z_2$ is the combined impedance of tracks and earth. Because of $Z_1 >> Z_2$, we can assume that traction current is mostly determined by traction power of the locomotive, in other word, it is independent of the track circuit, hence traction current, along with unbalanced current, can be regarded as an ideal current source.

### 2.2. Further analysis

There are two fundamental kinds of solution on filtering-circuit design, i.e. parallel and series resonant circuit. They should be applied in different situations.

Based on above result, the valid solution for track circuit to avoid interference of unbalanced current is to parallel series-resonant circuit with the interference current source (shown in Fig.1.).

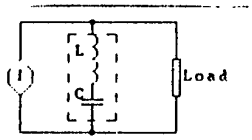



Fig.1. Series-resonant circuit

And interference voltage $V_L$ on the load $Z_L$ (e.g. track circuit) can be described as Equation (3):

$$V_L(f_0) = I_L(f_0) \times Z_L(f_0) \quad (3)$$

Where $f_0$ is the resonance frequency (50Hz) focusing on interference, $I_L(f_0)$ is the current passing load, $Z_C(f_0)$ is impedance of resonance circuit. Because of $Z_C(f_0) \to 0$, $V_L(f_0)$ approaches zero. Therefore it is clear that $V_L(f_0)$, as well as the power upon the load, is consequently minimized though interference current may be considerably large.

For ideal voltage source as interference, we should use the other kind of parallel-resonant circuit. If adopting this method against traction current, we might get little effect.

### 2.3. Saturation characteristic of impedance-bond

One of chief factors discussed is saturation of impedance-transformer without air-gap. According to its B-H curve, impedance-transformer is a non-linear device. Its inductance value $L_M$ is calculated by (4):

$$L_M = (N^2 \times \mu \times S) / l \quad (4)$$

Where N stands for turns of coil, $\mu$ for magnetic inductivity constant of iron-core, S for effective area of iron-core, l for average length of magnetic circuit.

As we know, opening air-gap of iron-core will decrease $L_M$ and boost linearity of impedance transformer. It means that saturation current now is greater than that without air-gap.

## 3. SOLUTIONS

Corresponding with the access of impulsive interference, we design a new type impedance transformer, called impedance-match transformer (IMT).

### 3.1. Requirements

IMT should ensure 25Hz track circuit against at least 60A (10% of 600A) unbalanced traction current.

Opening air-gap will improve saturation characteristic of impedance transformer but lower the impedance of 25Hz signal at the same time. IMT should meet its original demands.

Fail-safe must be considered in IMT design.

### 3.2. Structure of IMT

Structures of impedance transformer and IMT are given as Fig.2.

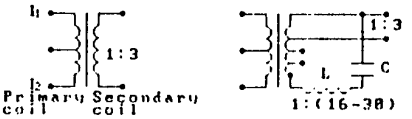



Fig.2. Structures of impedance transformer and IMT

Difference between traction current $I_1$ and $I_2$ is defined as unbalanced current. Three important measures are taken in IMT design.

As the first step, we increase the air-gap of iron-core of impedance transformer for purpose of increasing the value of its saturation current. This method makes track circuit receive 25Hz signal without loss in condition of larger unbalanced traction current.

As the second step, we additionally put a series-resonant circuit on the secondary coil (referred to signal-side) of impedance transformer, and its turns-ratio is 1:(16~30). This circuit, with resonant frequency 50Hz, consists of only two components, inductor L and capacitor C, and they meet (5):

$$2\pi \times 50 \times L = 1 / (2\pi \times 50 \times C) \quad (5)$$

Assume that resonant resistance is defined as *Z* and transformation ration as *n*, so the resistance is $Z n^2$ after reflecting to primary side. Compared with original structure, the value of this resistance is remarkably lessened, so that the interference current consumes its most energy in this circuit, and only a little part may enter track circuit.

What's more, this resonant circuit is equivalent to a capacitor at signal frequency 25Hz, its impedance Z is shown in Equation (6):

$$Z=3 / (4\times2\pi\times25\times C) \quad (6)$$

Because impedance transformer and rails have inductive resistance feature, we can design them close to parallel-resonance at 25Hz signal. Further, by adjusting its multi-taps, IMT could match with the impedance of the track circuit at 25Hz and $\alpha$ could reach 90°, it means we realize optimal transmission of 25Hz signal. So the unfavorable consequence of opening air-gap could be overcome.

3.3. Calculation data

Here is a group of calculation data about IMT based on analysis above (see Table 1.).

Table 1. Parameter and impedance at 50Hz

| C (μF) | L (H) | Q | $Z_0$ (Ω) | $Z_0'$(Ω) |
|---|---|---|---|---|
| 30 | 0.3377 | 20 | 5.6 | 0.0073 |

In Table 1., Q stands for quality factor, $Z_0$ for resonance resistance at 50Hz, $Z_0'=Z_0/27^2$ (typically n=27) for effective resistance from primary side.

And we can get its related data at 25Hz (see Table 2.)

Table 2. Impedance at 25Hz

| Z (Ω) | Z'(Ω) |
|---|---|
| 159.7∠−84.4° | 0.219∠−84.4° |

In Table 2., Z stands for impedance at 25Hz, Z' for effective impedance from primary side.

Effective capacitance $X'_C$ of Z' is 0.218 Ω, so we can simply open proper air-gap of impedance transformer and make its inductive resistance $X_{M25}$ equal to this value, or let $X_{M25}$=0.218 Ω.

3.4. Contrast

3.4.1. 50Hz exciting current

Impedance transformer's exciting current $I_M$ can be written as (7):

$$I_M = \left|\frac{\dot{I}_1 - \dot{I}_2}{2}\right| \quad (7)$$

Where ($I_1$ - $I_2$) stands for unbalanced traction current.

IMT's $I'_M$ can be written as (8):

$$I'_M = \left|\frac{(\dot{I}_1 - \dot{I}_2)}{2}\times\frac{\dot{z}_0}{\dot{z}_0 + j\dot{X}_{M50}}\right| \quad (8)$$

From data above, $Z_0'$ = 0.0073Ω, $X_{M50}$ = 2·$X_{M25}$ = 0.436Ω. Therefore we get $I_M / I'_M$ =59.5.

3.4.2 Transmission of 25Hz signal

Impedance transformer's rated input impedance $|Z_1|$ is 0.7 Ω.

IMT's input impedance $Z'_1$ can be calculated by parallel impedance of Z' and $X_{M25}$, as (9):

$$|Z'_1| = |Z' // X_{M25}| = 2.3\ \Omega \quad (9)$$

$|Z'_1|$ is about as 3.3 times as $|Z_1|$.

As discussed above, 50Hz exciting current is greatly decreased and transmission of 25Hz signal improved, so the signal-noise-ratio of 25Hz track circuit is remarkably boosted.

3.5. Combination with other track circuits

There is still another issue. To provide continuous information for cab signaling in railway station, 25Hz track circuit need to be combined with other styles including FSK (500~900Hz), France UM-71 (1700~2600Hz), and 25Hz alternating-counter. In this case, we need put another proper capacitance on series-resonance circuit so that IMT will appear required impedance.

## 4. APPLICATION AND CONCLUSION

Calculation and simulated experiment prove that this impedance-match transformer can successfully suppress the impulsive interference, 25Hz track circuit can be immunized against unbalanced traction current up to 180A. After it was applied on the electrified lines where degradation and malfunction used to occur at times such as Chenzhou-Shaoguan section of Beijing-Guangzhou Line in 1996, 25Hz track circuits have been working reliably and stably.

## 5. REFERENCES

5.1. Qin Zeng-huang, "Electrotechnics" (Chinese), Education press of China, Beijing, 1993, pp. 279-297.

5.2. Yang Shi-wu, "Study on computerized control systems of railways" (Chinese), Report of Northern Jiaotong University, Beijing, 1997.

5.3. Ministry of railway, "Signaling maintenance rules" (Chinese), Railway Press of China, Beijing, 1986.

## BIOGRAPHICAL NOTES

Yang Shi-wu, Lecturer, MSEE, graduated from Northern Jiaotong University, Beijing, in 1993. From then he has been a member of faculty in College of Electronics and Information Engineering and now takes charge of Signaling Division of EMC Research Center.

Fei Xi-kang, Professor, BSEE, graduated from Northern Jiaotong University in 1962.

Wu Yun-xi, Professor, BSEE, graduated from Leningrad Railway Institute, Russia, in 1961.

EMC 2000 INTERNATIONAL WROCŁAW SYMPOSIUM ON ELECTROMAGNETIC COMPATIBILITY

# *ELECTROMAGNETIC COMPATIBILITY ASSURANCE IN ELECTRIC POWER SYSTEM SUBSTATIONS*

Franc ŽLAHTIČ; Mateja ZORMAN, Tomaž ŽIVIC
Elektroinštitut Milan Vidmar, Ljubljana, Slovenia
Tel. no.: +386 61 1743001, Fax no.: +386 61 1253326, E-mail: franc.zlahtic@eimv.si

*ABSTRACT*

*The paper presents an approach followed during the preparation of the Slovenian technical legislation in the area of electromagnetic compatibility (EMC) in electric power system substations. The approach is based on the classification of substations and their parts in different categories of electromagnetic (EM) environment and takes into account probability, density and velocity of electromagnetic disturbances. Mitigation measures for a particular EM environment, requirements for the primary system, secondary systems and equipment are discussed as well. The approach, which comprises all type tests and their values for secondary systems and equipment adopted from IEC and EN EMC standards, is based on observations obtained through our on-site measurements.*

## *1. INTRODUCTION*

To a large extent, the reliability of the entire electrical power system depends on the reliability of secondary systems and equipment in its substations. To assure the rated operation of secondary systems[1] and equipment in a normal or faulty operating state at any predictable EM disturbance, an EMC assurance concept was set up for Slovenian Electricity Utilities.

Although relevant IEC Technical Committees have published several EMC product standards dealing with different application areas relevant for Electricity Utilities (TC 17 - switchgear and control gear, TC 57 - power system control and associated communications, SC 65A - industrial-process measurements and control – system aspects, TC 95 - measuring relays and protection equipment, etc.), their requirements cover only a part of the electromagnetic environment typical for power stations and substations. Moreover, even generic immunity standards for industrial environment, prepared by IEC and CENELEC, do not sufficiently cover the relevant electromagnetic phenomena of substations and do not give detailed acceptance criteria for testing of equipment.

To assist Slovenian Electricity Utilities, the Milan Vidmar Electroinstitute set up an EMC assurance concept for the Slovenian substations. The goal of our approach was to determine requirements that should be fulfilled not only as early as in the planning phase but also later during design, construction, operation and maintenance of substations. They include:

* Determination of EMC aspects for each step of substation planning;
* Determination of EMC requirements in the tender documentation, particularly for secondary systems and equipment, and partly for primary (i.e. high-voltage) equipment;
* Setting up EMC testing and checking procedures for secondary systems and equipment;
* Determination of EMC requirements for the construction documentation;
* Determination of procedures for installation of secondary systems and equipment and partly for primary equipment [3];
* Determination of requirements for equipment maintenance;
* Determination of requirements for periodic measurements.

Our aim was also a simultaneous preparation of foundations for a new Slovenian technical regulation in this field. In these efforts, we followed the steps foreseen in accordance with the state-of-the-art being

[1] Control, signal, measuring and protection devices, low voltage supply circuits, etc.

reflected in IEC [5] and EN standards [1, 2] and *Council Directive relating to EMC (89/336/EEC)*. So the concept of EMC assurance in substations, forming the foundations for technical legislation, consists of:

* Classification of substations and their areas (parts) with regard to anticipated EM disturbances into different categories of EM environment;
* Measurements for estimation of the extent of EM disturbances in substations;
* Requirements for secondary systems and equipment;
* Procedures to assure EMC in substations and their EM environment.

The analyses conducted by the Milan Vidmar Electroinstitute as well as experiences of Slovenian Electricity Utilities have lead to the following conclusions:

* The magnitude and intensity of EM disturbances and EM interferences differ from one location to the other within a substation.
* The greatest magnitudes are in the vicinity of the primary equipment and are independent of the primary network rated voltage.
* Disturbances are transmitted to secondary systems and equipment by conduction along secondary lines, induction and EM radiation.

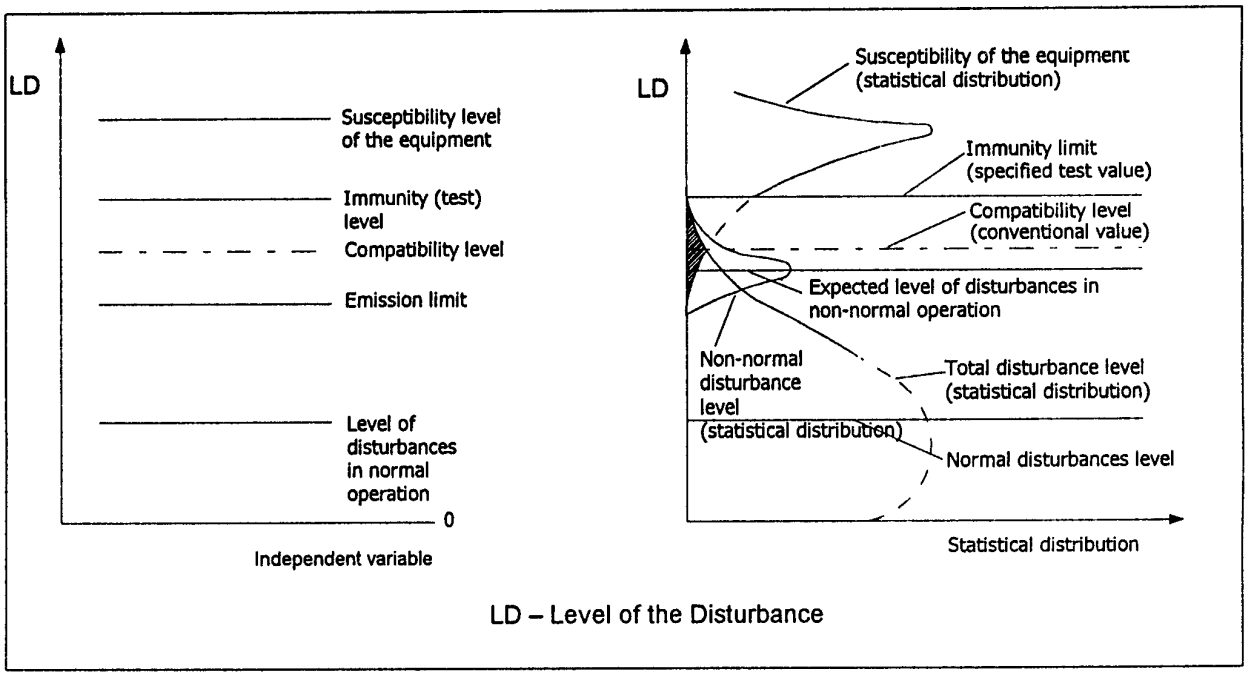



Fig. 1.

## *2. ELECTROMAGNETIC ENVIRONMENT IN SUBSTATIONS*

The EM disturbances occur due to activities and phenomena inside and outside of substations. Internal disturbances result from:

* switching operations and faults in substations;
* non-linear load characteristics in low-voltage supply systems (semiconductor devices, motor drives, etc....);
* voltage unbalances and other signals in low-voltage supply systems;
* operating and functioning of radio systems (including mobile telephones).

External disturbances result from:

* faults which occur outside of substations;
* atmospheric discharges and charges which due to their mutual inductance affect substations;
* The actual extent of a particular disturbance depends on implemented mitigation measures (i.e. on cables and cable shields, armour earthing, grounding grid design, shielding and armour in buildings, etc.).

The investigation of effects of EM disturbances [6] on secondary systems and equipment revealed that values of EM disturbances caused by atmospheric discharges and faults in high voltage (primary) networks are four to five times greater than values of disturbances due to normal switching operations. The probability density (distribution) of EM disturbances in the secondary systems and equipment in Slovenian power substations is in compliance with the distribution of EM disturbances as given in IEC 61000-1-1. The distribution of EM disturbances caused by faults and atmospheric discharges is in accordance with our observation and is shown in Fig. 1 as a non-normal disturbance level. It serves as a basis for the

determination of values for type tests and criteria for analyses of onsite measurements in substations.

Based on the anticipated magnitudes and frequency of EM disturbances, individual parts or areas of substations are classified in one of the three categories:

* **Environment I - protected environment**
* **Environment II – conventional environment**
* **Environment III - exposed environment**

The concept gives the following classification examples:

* **Environment I** comprises areas inside control centres where special mitigation measures were implemented to reduce the immunity requirements.
* **Environment II** comprises control areas in the vicinity of high voltage switchyards or generation facilities. During the construction of a substation and in particular during the circuit and equipment installation, special measures should be taken in order to reduce EM disturbances in control and signal circuits. Devices in these areas should be manufactured and installed in compliance with EMC requirements.
* **Environment III** comprises devices in kiosks in high-voltage switchyards or in generation facilities and their cable lines. In such environment, adequate measures should be taken during the construction and installation of substations.

### *3. TYPE TESTS FOR SECONDARY SYSTEMS AND EQUIPMENT*

Immunity type tests according to IEC and EN standards and *EMC Directive* are defined for all secondary systems and equipment installed in substations. Our concept includes a list of type tests and test procedures derived from IEC 61000-4-1, EN 50082-1 and EN 50082-2. Test values were adopted for each EM environment separately. The most rigorous test values were adopted for Environment III - Exposed environment.

### *4. CONTROL MEASUREMENTS*

Efficiency of implemented mitigation methods can be checked by on-site measurements. They should show

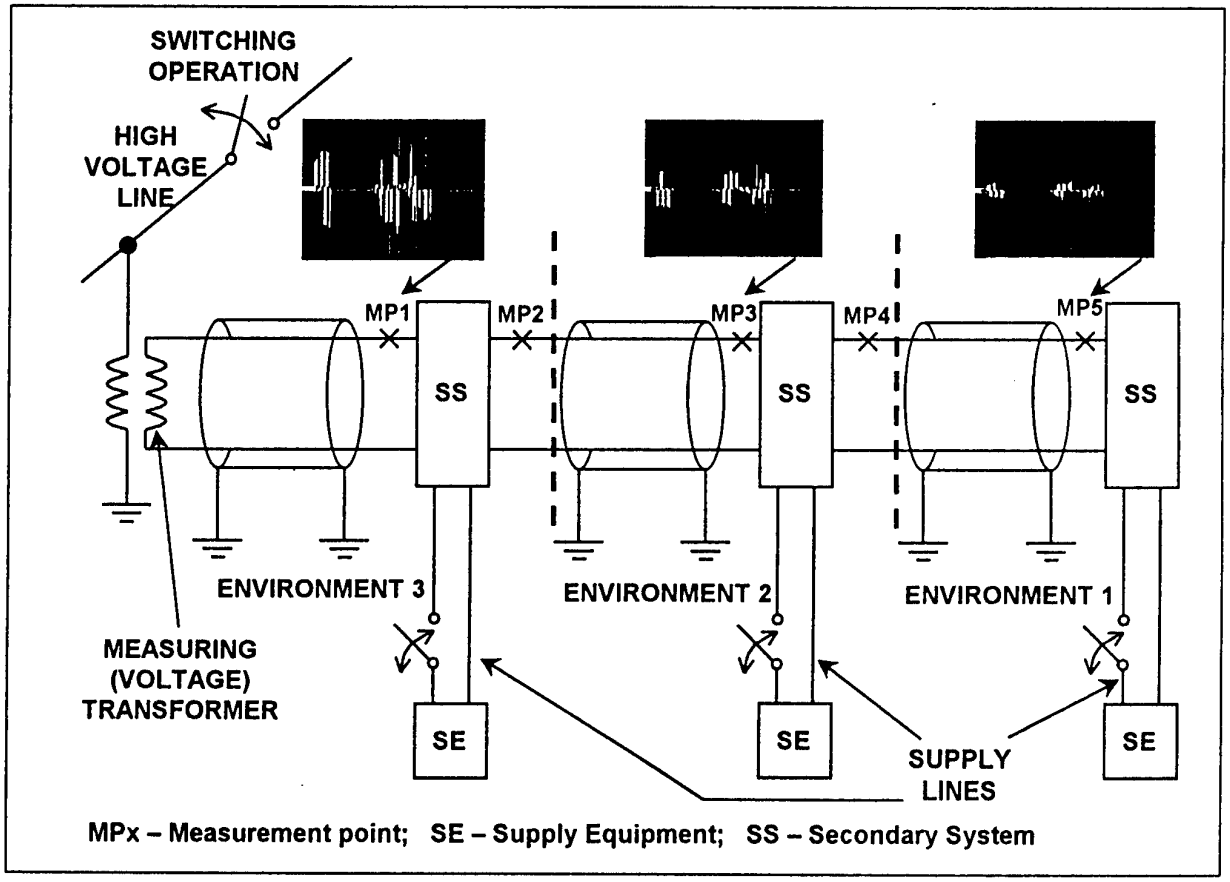



Fig. 2.

how EM disturbances diminish along the secondary circuit and what are their values at individual points (Fig. 2.). They are used to establish the general exposure of the secondary equipment and its general resistance to EM disturbances as well.

In order to perform measurements, disturbances are needed. The practice shows that the most convenient simulation of EM disturbances is achieved by opening or closing disconnectors or circuit breakers. For the analysis of EM phenomena on secondary system supply lines, it is convenient to perform switching operations on their supply devices too.

Our analyses proved that phenomena which take place during switching operations are identical to those which take place during non-normal states and type tests.

The advantage of these measurements is the fact that they enable repeatability of procedures and that they can be made during the normal operation of a substation. The adopted measuring procedure is fully compliant with the IEC 60816 standard. Each measurement is made at least on three locations of a laid secondary cable - line. Measurements are made on both ends of a secondary cable or on terminals of the secondary equipment. Measurements which have to be performed on the same circuit are made simultaneously. They are analysed according to criteria set up in our concept. Magnitudes of measured disturbances should not exceed values given in Table 1. We estimate that measured values are 4 to 5-times smaller than values of EM disturbances experienced during non-normal states.

Table 1

| | Longitudinal voltage - common mode | Transversal voltage – differential mode |
|---|---|---|
| Environment I | 0 V | 0 V |
| Environment II | 110 V | 220 V |
| Environment III | 210 V | 520 V |

## *5. CONCLUSION*

To assist Slovenian Electricity Utilities, the Milan Vidmar Electroinstitute has set up an EMC assurance concept for the Slovenian substations. The concept, based on application of EMC standards, represents a solid base for designers, investors and operators. It classifies substations and their parts in three categories of the EM environment and gives testing values for the secondary equipment for each environment. It defines on-site measurements with forced EM disturbances to check implemented mitigation methods. In this way weak spots are detected where EMC should be improved.

## *6. REFERENCES*


6.1. EN 50082-1 (1992) 1995: Electromagnetic compatibility - Generic immunity standard, Part 1: Residential, commercial and light industry

6.2. EN 50082-2, 1995: Electromagnetic compatibility - Generic immunity standard, Part 2: Industrial environment

6.3. EN 60694: Common specifications for high-voltage switchgear and controlgear standards, 1996

6.4. IEC 60816: Guide on methods of measurement of short duration transients on low-voltage power and signal lines, 1984

6.5. SIST EN 61000-4-1, 1994: Electromagnetic compatibility (EMC), Part 4: Testing and measurement techniques, Section 1: Overview of immunity tests, Basic EMC publication

6.6. Žlahtič F.: Electromagnetic Compatibility Assurance in Electric Power Substations, Ref. no. 1303, Milan Vidmar Electroinstitute, Ljubljana 1996

**EMC 2000** INTERNATIONAL WROCŁAW SYMPOSIUM ON ELECTROMAGNETIC COMPATIBILITY

# COMPARISON OF THE LUMPED- AND DISTRIBUTED-CIRCUIT MODEL OF THE LIGHTNING PROTECTION SYSTEM

Karol Aniserowicz
Bialystok University of Technology, Grunwaldzka 11/15, 15-893 Bialystok, Poland
tel. +48(85)7421651x.156, fax: +48(85)7421657, e-mail: aniser@cksr.ac.bialystok.pl

*ABSTRACT*

*Two methods of calculations of the current distribution into a lightning protection (LPS) system during a lightning stroke are discussed. The presented results were obtained using the lumped- and distributed-circuit model of the LPS.*

*A new idea of modelling of a lightning channel has been presented.*

*The validity range of the simple lumped-inductance model has been discussed. The received results may be useful while designing of LPS and predicting of the lightning current distribution.*

## 1. INTRODUCTION

The analysis of the lightning protection systems (LPS) under the conditions of the lightning action is one of the most important EMC problems. The prediction of the lightning current distribution in the protection conductors may show the most threatened parts of the building. Hazards due to conducted or induced overvoltages may be estimated when surge current distribution is known. Even very simplified calculations may be helpful while planning a room for electronic equipment.

There are many publications concerning the lightning current distribution in the conductors of the lightning protection systems (LPS), e.g. [1 - 5]. The contributions may be classified into two main groups according to the applied mathematical models of LPS. The authors use either the lumped-circuit models (including only the own inductance of wires or mutual inductance of wire loops) or the complicated field-theory models.

In the presented work some computations were made to compare the results obtained from these different models. Basing on the included examples the validity of application of the lumped circuit model may be considered. Particularly, it is important to know for what kind of structures and what kind of surges (first or subsequent lightning strokes) it is possible to predict the current distribution using the simple lumped-inductance model.

## 2. NUMERICAL EXAMPLES

Consider two examples of lightning protection systems shown in Fig. 1a and 1b. The LPS shown in Fig. 1a was analysed in [4] using different lumped-circuit approach and results were somewhat different from these presented below.

Assume that the ground is ideal (high conductive) and that all the conductors have the same diameter of 8 mm. The remaining dimensions are shown in Fig. 1.

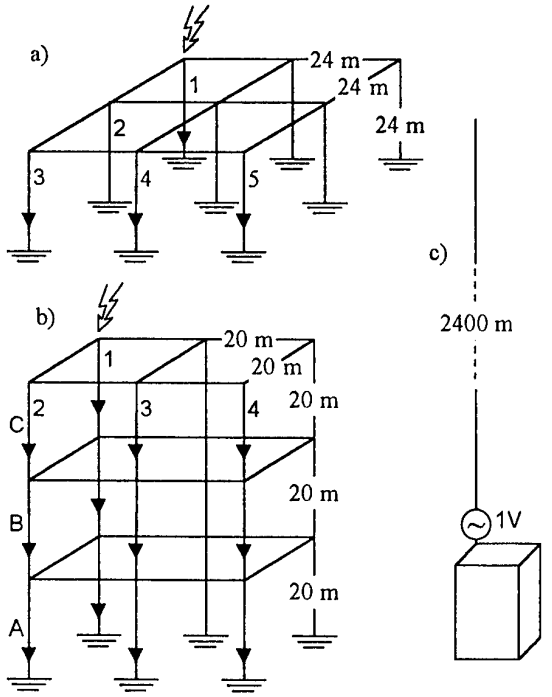



Fig. 1. Examples of the LPS to be analysed (a, b) and a model of lightning channel (c)

A point of the lightning stroke was chosen to be in the corner of the LPS.

Computations were executed for the chosen paths formed by the down-conductors. These paths were numbered respectively: 1, 2, 3, 4 and 5. For the LPS 1b the levels above ground were labeled: A, B and C.

## 3. METHODS OF COMPUTATIONS

### 3.1. A lumped-circuit model of the LPS

A most simplified mathematical model was applied and checked in this work. Lightning was modelled as a current source. Only the own inductances of the LPS conductors were taken into consideration:

$$L\,[\mu\mathrm{H}] = 0.2l\left(\ln\frac{4l}{d} - 0.75\right) \qquad (1)$$

where: $l$ – length, $d$ – diameter of the wire. Mutual inductances were neglected.

Assuming linear shape of rising slope of the current pulse and using the Laplace transform, such a model leads to a simple set of linear algebraic equations. Solving this system of equations it is possible to estimate the percentage distribution of the lightning current in the LPS.

Method of calculations basing on the own and mutual inductances of loops formed by the conductors has been described in [4].

### 3.2. A field-theory model of the LPS

A new idea of modelling of a lightning channel has been applied. It is near to the transmission-line model of a lightning [1-2]. The model under investigation was generated during the application of the commercial software AWAS [6] into the non-standard computations. The lightning channel has been modelled as a long vertical wire (Fig. 1c) with the ideal sine voltage source. Such a way of inserting of the generator makes it possible to model the upward movement of the return stroke current.

Only voltage sources may be modelled using the method implemented in [6]. The forced current was achieved by successive computations in the frequency domain basing on the mixed-potential equations combined with the method of moments for the polynomial approximation of the currents.

Mathematical model, combining the incident field $\mathbf{E}^i$ with the current distribution and with the scattered field $\mathbf{E}^s$, $\mathbf{H}^s$, comes from known equations formulated in the frequency domain:

$$\mathbf{E}^s = -j\omega\mathbf{A} - \nabla\Phi \qquad (2)$$

$$\mathbf{H}^s = \frac{1}{\mu_0}\nabla\times\mathbf{A} \qquad (3)$$

$$\mathbf{A} = \mu_0 \iint_S \mathbf{J}_S \frac{e^{-jkR}}{4\pi R} dS \qquad (4)$$

$$\Phi = \frac{1}{\varepsilon_0}\iint_S \rho_S \frac{e^{-jkR}}{4\pi R} dS \qquad (5)$$

$$\nabla\cdot\mathbf{J}_S = -j\omega\rho_S \qquad (6)$$

Forced voltage generator (Fig. 1c) has been introduced basing using the boundary condition on the conductor surface:

$$\mathbf{n}\times\mathbf{E}^s = -\mathbf{n}\times\mathbf{E}^i \qquad (7)$$

The influence of radiation of the wires and the mutual coupling between the LPS elements has been taken into account automatically during the formulation of integral equations.

The algorithm of computer simulation is as follows. First compute the current transmittance of the chosen point of the construction, defined as a quotient: the current spectrum in the analysed point divided by the current spectrum in the bottom of the model of lightning channel, for drive of frequency independent 1V generator. This transmittance is equal to the current in the given point for the driving by the 1A frequency independent current source. Then the current spectrum in the given point is achieved as a product of the computed transmittance and the spectrum of the lightning current pulse [5].

The Discrete Fourier Transform has been used to obtain the current waveforms in the time domain. 1024 spectrum samples with the interval of 5 kHz in the frequency domain were taken into account. Thus the analysed frequency band reaches 5.12 MHz, that allows to include several resonances of the explored structure during computations.

Application of the DFT makes it possible to compute arbitrary waveforms. A double-exponential equation has been introduced to describe the lightning waveform:

$$i(t) = k\,I_0\left(e^{-\alpha t} - e^{-\beta t}\right) \qquad (8)$$

Two groups of parameters have been applied, modelling two waveforms 2/25 μs and 0.2/25 μs, respectively:

$$k = 1.166,\ \alpha = 3.4\times10^4\ \mathrm{1/s},\ \beta = 1.0\times10^6\ \mathrm{1/s} \qquad (9)$$

$$k = 1.02,\ \alpha = 2.9\times10^4\ \mathrm{1/s},\ \beta = 1.1\times10^7\ \mathrm{1/s} \qquad (10)$$

The first waveform may be classified as a "slow" rising pulse and the second pulse – as a "fast" one. The maximum value $I_0$ was set to be 100 kA. Due to such data choice the numbers expressed in kiloamperes are equal to percentage distribution of the maximum value of lightning current in the conductors. Thus it is easy to analyse the results and compare them with the circuit-theory calculations. The comparison of selected results is presented below.

## 4. RESULTS OF COMPUTATIONS

Solution of the lumped-circuit linear set of equations makes it possible to estimate the percentage distribution of the maximum lightning current in the conductors. Of course, in point 3.1, the waveform of the currents in the LPS has to be assumed the same as the forced current.

The aim of the computations described in point 3.2 is to compare the results and to say when the simplified lumped-circuit theory may be applied. There are two main criterions of comparison:

- if the waveform of the currents may be assumed to be similar to the lightning waveform;
- if the maximum values of the currents computed by the two methods are of the same order.

The chosen results of field-theory computations have been presented in Fig. 2 – 9.

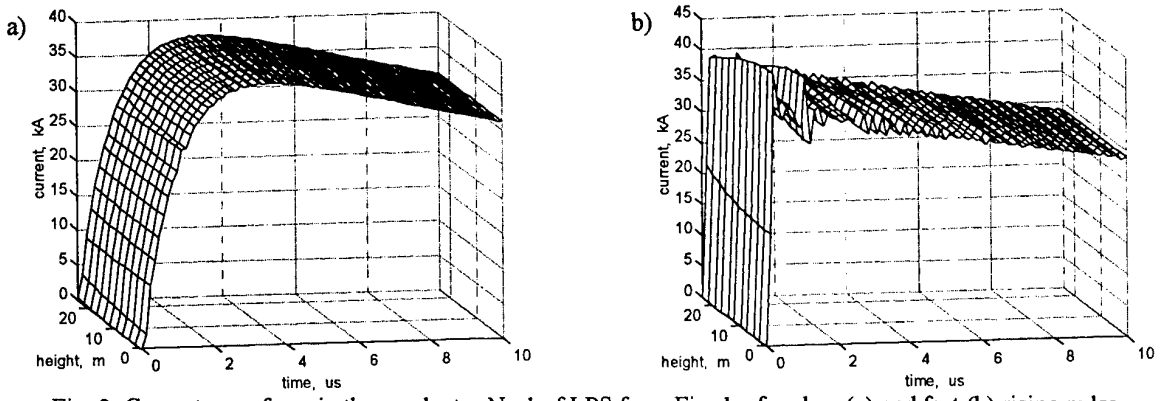



Fig. 2. Current waveform in the conductor No 1 of LPS from Fig. 1a for slow (a) and fast (b) rising pulse

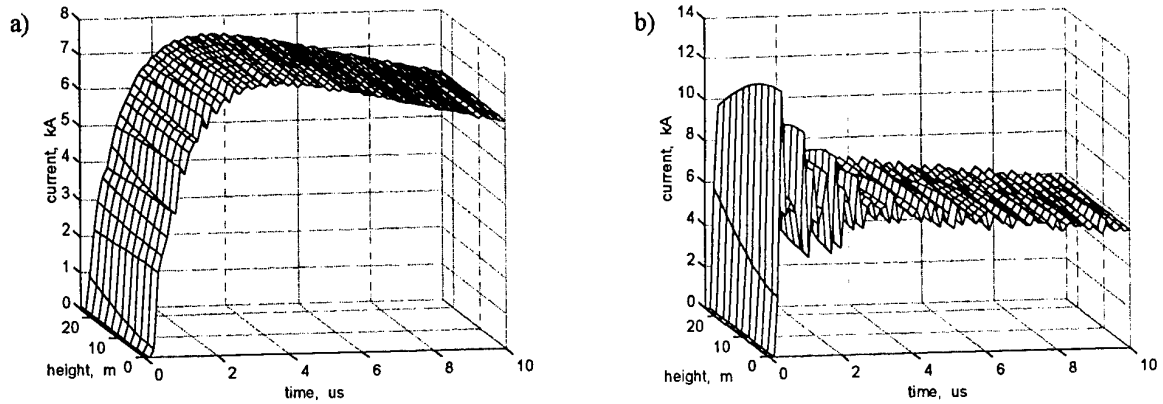



Fig. 3. Current waveform in the conductor No 3 of LPS from Fig. 1a for slow (a) and fast (b) rising pulse

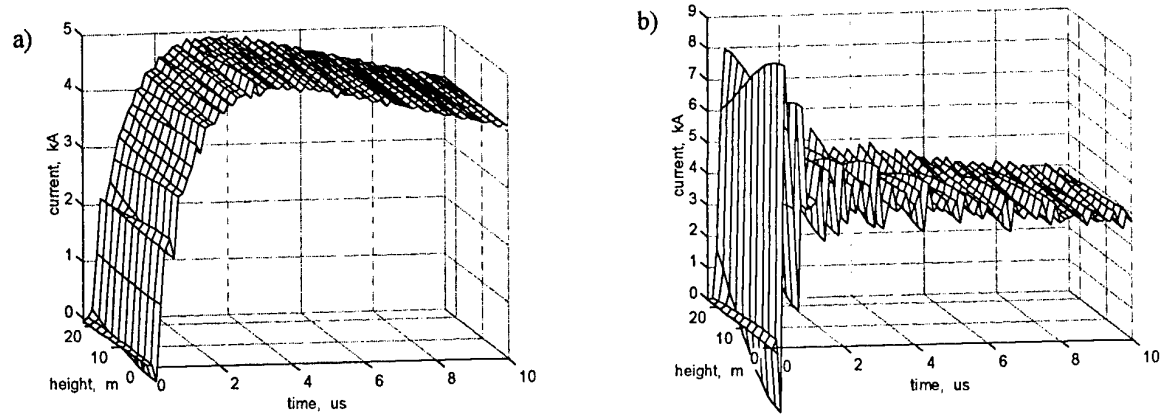



Fig. 4. Current waveform in the conductor No 4 of LPS from Fig. 1a for slow (a) and fast (b) rising pulse

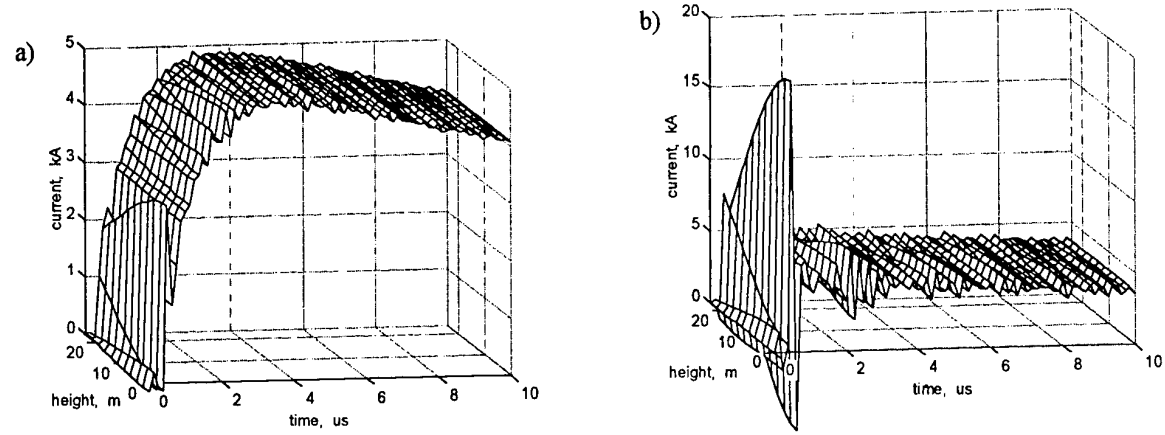



Fig. 5. Current waveform in the conductor No 5 of LPS from Fig. 1a for slow (a) and fast (b) rising pulse

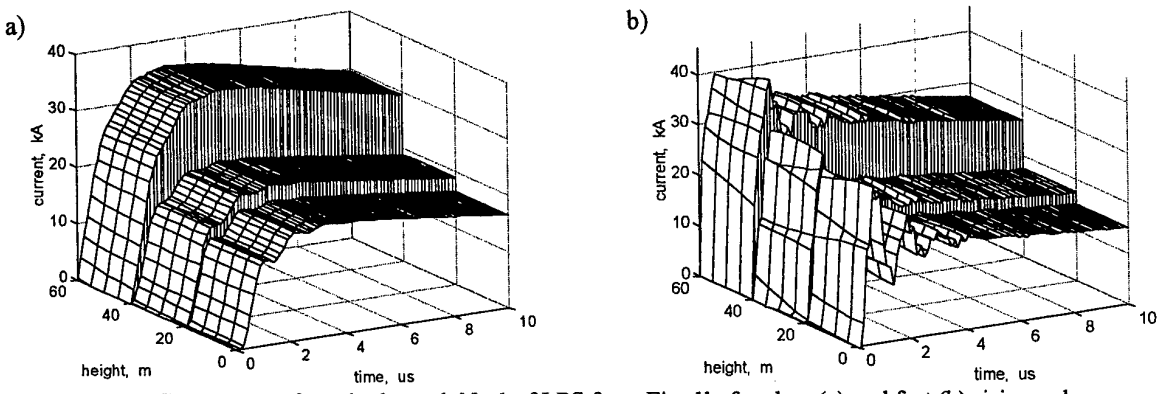



Fig. 6. Current waveform in the path No 1 of LPS from Fig. 1b for slow (a) and fast (b) rising pulse

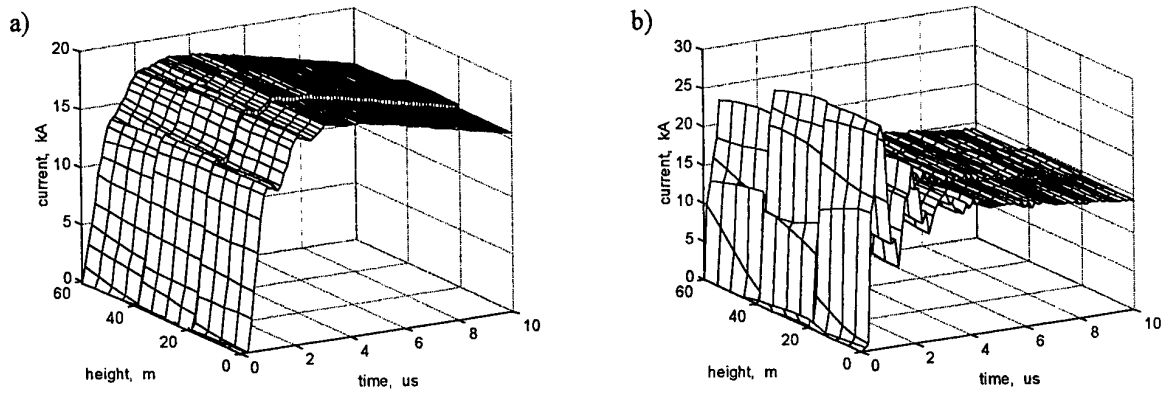



Fig. 7. Current waveform in the path No 2 of LPS from Fig. 1b for slow (a) and fast (b) rising pulse

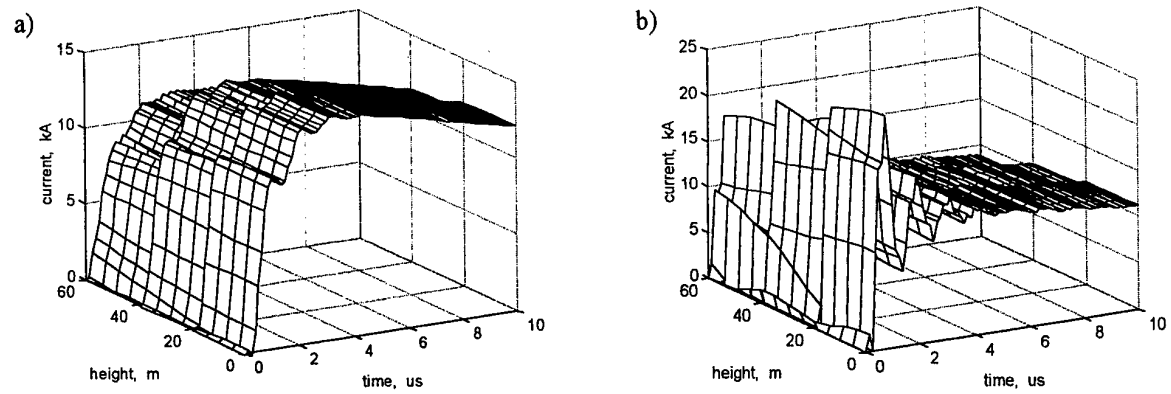



Fig. 8. Current waveform in the path No 3 of LPS from Fig. 1b for slow (a) and fast (b) rising pulse

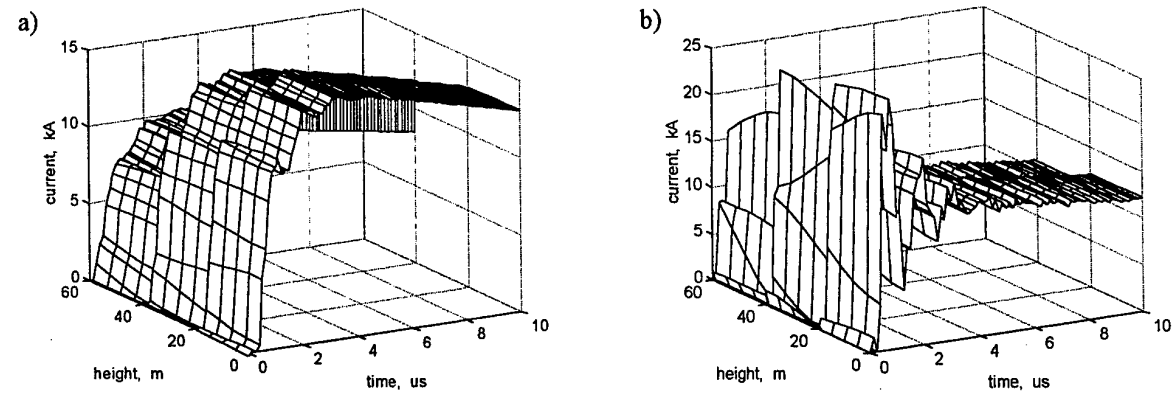



Fig. 9. Current waveform in the path No 4 of LPS from Fig. 1b for slow (a) and fast (b) rising pulse

As it is seen from Fig. 2 – 9, only response for the slow current pulse (front time of 2 μs) may be supposed to have a waveform similar to the forced current. This situation may be interpreted as a model of response to the first return stroke [7]. But the bigger distance from the lightning channel the greater oscillations occur (e.g. Fig. 5a, 9a). The bigger the structure the worse the conditions of quasi-stationarity are satisfied.

In the Tables 1 and 2 a comparison of current maximum values is presented. The results of the lumped-circuit and the field-theory model for the forced current parameters given by eq. (9) have been compared. The percentage difference $\varepsilon$ between the results has been defined as:

$$\varepsilon = \frac{I_{lump} - I_{field}}{I_{field}} \times 100\% \qquad (11)$$

where: $I_{lump}$, $I_{field}$ – results of the lumped-inductance and field-theory computations, respectively.

Table 1. Comparison of results for LPS from Fig. 1a

| conductor No. | $I_{lump}$, kA | $I_{field}$, kA | $\varepsilon$, % |
|---|---|---|---|
| 1 | 42.62 | 37.71 | +13 |
| 2 | 13.93 | 13.41 | +3.9 |
| 3 | 5.95 | 7.56 | –21.3 |
| 4 | 3.93 | 4.97 | –20.9 |
| 5 | 2.62 | 4.94 | –47 |

Table 2 Comparison of results for LPS from Fig. 1b

| conductor No. | $I_{lump}$, kA | $I_{field}$, kA | $\varepsilon$, % |
|---|---|---|---|
| 1A | 19.53 | 19.94 | –2.1 |
| 1B | 23.47 | 22.76 | +3.1 |
| 1C | 38.81 | 35.54 | +9.2 |
| 2A | 17.83 | 18.73 | –4.8 |
| 2B | 18.29 | 19.18 | –4.6 |
| 2C | 17.23 | 18.41 | –6.4 |
| 3A | 15.67 | 14.59 | +7.4 |
| 3B | 14.64 | 13.92 | +5.2 |
| 3C | 11.82 | 11.62 | +1.7 |
| 4A | 14.54 | 15.79 | –7.9 |
| 4B | 12.8 | 14.43 | –11.3 |
| 4C | 8.44 | 10.39 | –18.8 |

The oscillations that occur for the fast current pulse are the proof that not for each waveform the lumped-circuit theory may be applied. This case, typical for fast rising lightning subsequent return stroke [7], has to be analysed using only field-theory models.

## 5. CONCLUSIONS

The results presented above were obtained using the lumped- and distributed-circuit model of the LPS.

A new idea of modelling of a lightning channel has been presented.

For typical front-time pulses (of order of several microseconds) a simple lumped-inductance model leads to results that in most cases are in good agreement with complicated computations.

The bigger the electric dimensions of the structure the worse the conditions of quasi-stationarity are satisfied. The case of distinct disagreement between the lumped- and field-theory models has been presented for the forced current with parameters defined by eq. (10).

Typically, the lumped-circuit models of the LPS may be applied if the following conditions are satisfied:
- the LPS dimensions must be not greater than several tens of meters;
- only the first return stroke may be analysed.

The results received in this work may be used while designing of lightning protection systems and predicting of the lightning current distribution.

## 6. REFERENCES


1. A. Karwowski, A. Zeddam, "Transient currents on lightning protection systems due to the indirect lightning effect", IEE Proc.-Sci. Meas. Technol., Vol. 142, No.3, May 1995, pp.213-222.
2. D.J. Bem (ed.), "Electromagnetic Pulse Overstress" (in Polish), Wrocław Techn. University, Wrocław, 1994.
3. Z. Flisowski, "Evolution trends in lightning protection of buildings" (in Polish), PWN, Warsaw, 1986.
4. A. Sowa, "Analysis of lightning hazard for electronic equipment" (in Polish), Białystok Techn. University, Białystok, 1990.
5. G.G. Chavka, K. Aniserowicz, "Computer simulation of action of lightning current on the construction of antenna masts", 14th International Wrocław Symposium and Exhibition on EMC, June 23-25, 1998, pp.481-485.
6. A.R.Djordjević, M.B.Baždar, T.K.Sarkar, R.F.Harrington, "Analysis of Wire Antennas and Scatterers (AWAS)", Artech House, London, 1995.
7. IEC-1312-1:1993, International standard, "Protection against lightning electromagnetic impulse", Part 1: "General principles".


## ACKNOWLEDGEMENT

The author would like to acknowledge the support of this work by the State Committee for Science Research of Poland under the Rector's Project W/WE/1/98.

## BIOGRAPHICAL NOTE

**Karol Aniserowicz** was born in Białystok, Poland, in 1955. He received the M.Sc. degree in electronic engineering from the Warsaw University of Technology, in 1979 and the Ph.D. degree in electrical engineering from the Technical University of Szczecin, in 1987. Since 1979, he has been with the Faculty of Electrical Engineering, Białystok University of Technology. He was one of the founders of the Center of Protection from Overvoltages and Electromagnetic Interferences in Białystok, established in 1995. His research interests include electromagnetic compatibility, industry applications of microwaves, and numerical methods applied to the theory of electromagnetic fields.

EMC 2000 INTERNATIONAL WROCŁAW SYMPOSIUM ON ELECTROMAGNETIC COMPATIBILITY

# TIME DOMAIN MEASUREMENT OF VERY FAST TRANSITION DURATIONS DUE TO GAP DISCHARGE IN AIR AS A SIMULATION OF THE CDM ESD

Ken KAWAMATA*,
* Department of Electrical Engineering,
Hachinohe Institute of Technology,
88-1 Ohbiraki Myo Hachinohe-shi, 031-8501 JAPAN
E-mail: kawamata@hi-tech.ac.jp

Shigeki MINEGISHI** and Akira HAGA**
**Faculty of Engineering, Tohoku Gakuin University,
1-13-1 Chuo Tagajo-shi, 985-8537 JAPAN
E-mail: smine@tjcc.tohoku-gakuin.ac.jp
E-mail: ahaga@tjcc.tohoku-gakuin.ac.jp

*Abstract* : Very fast transition duration due to starting of gap discharge were investigated in time domain. Voltage rising time in positive polarity and falling time in negative polarity were observed with a very wide-band transient digitizer. The gap space was set very small for voltages below 1500 V as a simulation of the CDM ESD and the gap discharge of switch devices. The measurement system consists of a distributed constant line system with a tapered coaxial electrode, which has the matched impedance for the characteristic impedance of the distributed constant line system. The insertion loss of the tapered coaxial electrode was within -3dB in the frequency range below 4.5GHz. The atmosphere around the electrode is ordinary air. This experimental system enables to measure the high speed transients of about 100 ps due to gap discharge in time domain. As a consequence of the experiment, the relationship between the discharge voltage and the transition duration were confirmed.

## 1. INTRODUCTION

It is well known that the very fast transients of electromagnetic field are arisen from gap discharges of ESD (electrostatic discharge) and electrical contacts. The transient due to gap discharge is a very wide band (high frequency) electromagnetic noise source. Over the past few years a considerable number of studies have been made on electromagnetic noises of the ESD and contacts from the point of view of the electromagnetic compatibility. The electromagnetic noise characteristics of gap discharge are gradually becoming clearer [1]-[7].

However, there has been only a little amount of information about voltage waveforms of the transition duration (voltage rising time in positive polarity and voltage falling time in negative polarity) due to a starting of the discharge in very wide band time domain [8]-[11]. Very little is known about the duration of voltage rising time and voltage falling time due to gap discharge at voltages below 1500V. The main purpose of this paper is to clarify the transition duration due to gap discharge in voltages below 1500 V as the EMI source.

It is desirable to observe the transition duration due to gap discharge in distributed constant system, because the transients are very rapid. In the first place, a measurement system using the distributed constant system was established to observe the very fast transition duration. It was confirmed that the experimental system enables to measure the high speed voltage transients of about 100ps [12].

In this paper, relationship between source voltage and the transition duration were investigated using this experimental system.

## 2. DISTRIBUTED CONSTANT EXPERIMENTAL SYSTEM

The experimental system using distributed constant line system shown in Fig.1 was set up. The system consists of a power supply, a tapered coaxial electrode, a directional coupler (HP778D) as coupled transmission lines and semi-rigid coaxial cables (50 Ω) as distributed constant lines. The directional coupler was used to observe

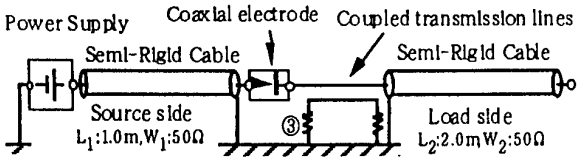



Fig. 1 Experimental system using the distributed constant line system

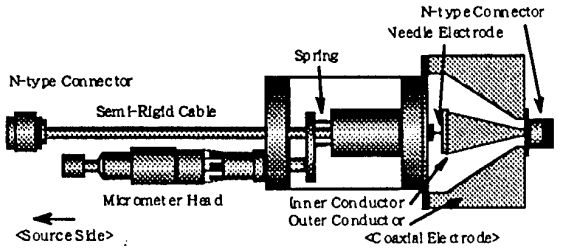
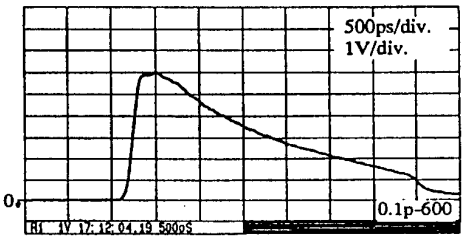
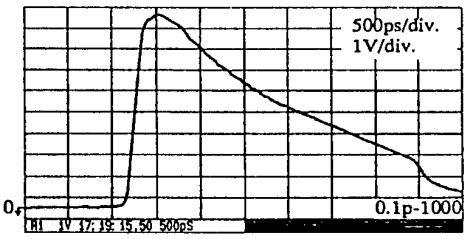



Fig. 2 Cross section view of the tapered coaxial electrode

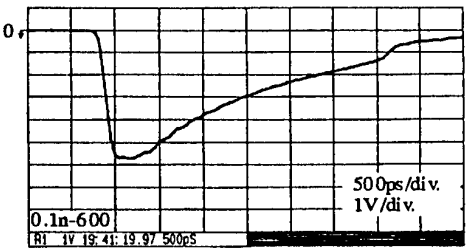



(a) source voltage is 600V

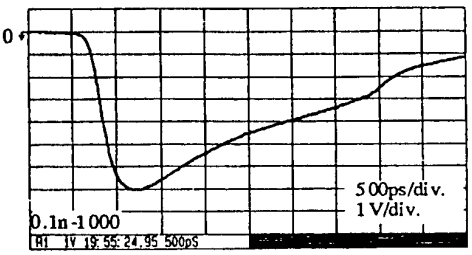



(b) source voltage is 1000V

Fig. 3 Waveforms of rising part in positive polarity




(a) source voltage is 600V




(b) source voltage is 1000V

Fig. 4 Waveforms of falling part in negative polarity

the transition duration. When the directional coupler was driven by 35 ps rise time pulse, it had a response of 68 ps rise time. The tapered coaxial electrode and a source side semi-rigid coaxial cable were constructed in a body. A wide band transient digitizer (TEKTRONIX SCD5000, 4.5GHz) connects an output of the coupled transmission lines at terminal ③ via coaxial attenuator of 10 dB.

Fig. 2 shows a cross section view of the tapered coaxial electrode. The electrode consists of an inner conductor as plane electrode, an outer conductor, a needle electrode and a micro meter head. Each conductor was made of copper. A diameter of the inner conductor is 20.0mm, an inside diameter of the outer conductor is 46.2 mm, and length of the taper is 50.0 mm. The taper is a linear physical taper. The characteristic impedance will be constant (Zc) at each point of the tapered coaxial electrode. So, impedance matching between the cable and the coaxial electrode was accomplished. The needle electrode was made from a sharpening the inner conductor of the source side semi-rigid coaxial cable. The two needle electrodes have curvature of radius r=0.1 mm, and r=0.5 mm, respectively. An insertion loss of the electrode measured by a network analyzer (HP8753D, 30kHz-6GHz). The connection between needle and plane electrodes was made by mechanical connection. These insertion losses are within -3dB in the frequency range below 4.5GHz.

In the experiment, the semi-rigid cable with the needle electrode is moved by the micro-meter head. The gap space is reduced gradually. A shingle-shot waveform of voltage transients at the instance of discharge was observed with the wide band transient digitizer. The duration time (10%-90%) of voltage rise curves and fall curves were observed, where the voltage of power source was increased from 400V to 1300V. Experimental parameters are the radius of curvature of needle electrode, the source voltage and the voltage polarity.

## 3. EXPERIMENTAL RESULTS AND DISCUSSION

### 3.1. Experimental results

The example voltage waveforms of transition duration are shown in Fig.3 and 4, when the radius of curvature of needle electrode is 0.1 mm. Fig.3 shows the rising part of transition duration in positive polarity and Fig.4 shows the falling part in negative polarity. In both figures, (a) is for the source voltage of 600 V, and (b) is for 1000 V,

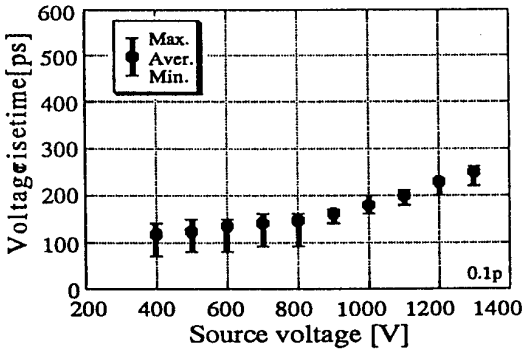
respectively. Converted voltage value of the vertical axis for an attenuation of 30 dB (20dB of the coupler and 10 dB of the attenuator) is about 33 V/div., and for the horizontal axis is 500 ps/div., respectively. The voltage on a distributed constant line at the load side should rise (fall) to a half amplitude of the source voltage. However, the peak value of the waveforms was lower because of the influence of the coupling characteristics of the coupled transmission lines. Especially, in Fig.4 (b), the peak value was low, because the high frequency components were decreased due to slowdown of transition duration. In this report, the study was limited only to the relative duration time of the voltage transients.

In Fig.3, the voltage rise time of (a), and (b) is about 130 ps, and 170 ps respectively. In Fig.4, the voltage fall time of (a), and (b) is about 150 ps, and 260 ps respectively. These waveforms show an acceptable reproducibility. Relationship between source voltage and the transition duration due to an increasing of the source voltage from 400 V to 1300 V in positive and negative polarity are shown in Fig.5. The source voltage polarity and radius of curvature of needle electrode are as follows; (a-p) needle of r=0.1 mm in positive, (b-p) needle of r=0.5 mm in positive, (a-n) needle of r=0.1 mm in negative, and (b-n) needle of r=0.5 mm in negative polarity. In these figures we show the minimum, maximum and average of sixty measurements. The voltage rise time of (a-p) and (b-p) is from 116 ps to 245 ps, and from 107 ps to 290 ps respectively. Furthermore, voltage fall time of (a-n) and (b-n) is from 142 ps to 450 ps, and from 110 ps to 285 ps respectively.

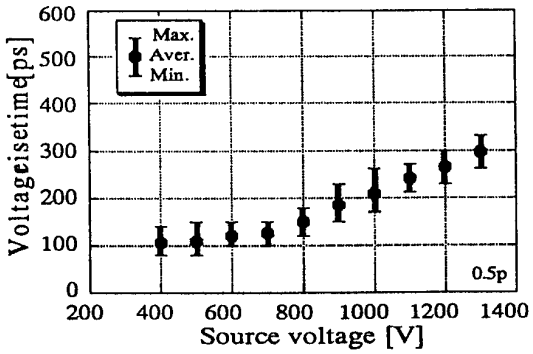
The relationship between the discharge voltage and the transition duration were confirmed from these results. The voltage rise time was slowed down proportionately to the source voltage in positive polarity, while the voltage fall time was slowed down remarkably in negative polarity for the r=0.1 mm needle. It can be considered that the cause of the difference in transition duration influenced the distribution of the electric field in the gap electrode.

### 3.2. Discussion for the distribution of electric field

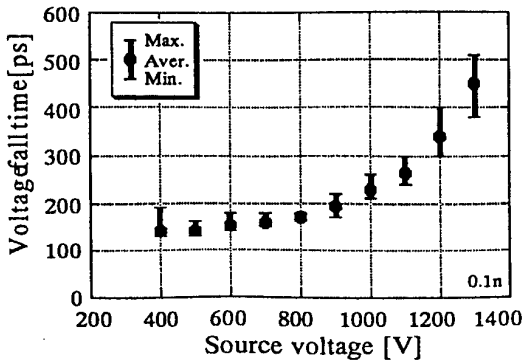
The fields distribution were decided by a gap length and a radius of curvature of needle electrode. The field becomes uniform when the gap length is very short in comparison with the radius of curvature of the needle electrode. In the reverse, it becomes a non-uniform field when the gap length is long. In the case of a sphere electrode and a grounded plan electrode, formative limits



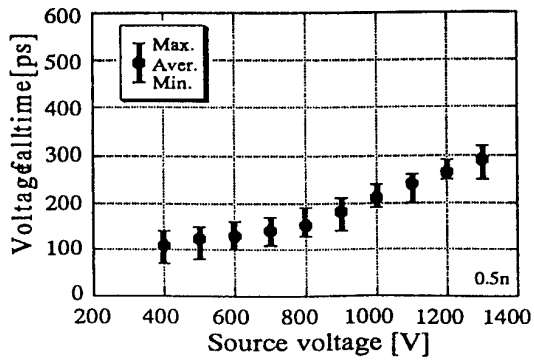

(a-p) r=0.1 mm needle in positive polarity




(b-p) r=0.5mm needle in positive polarity




(a-n) r=0.1 mm needle in negative polarity




(b-n) r=0.5 mm needle in negative polarity

Fig. 5 Relationship between source voltage and the transition duration due to an increasing of the source voltage.

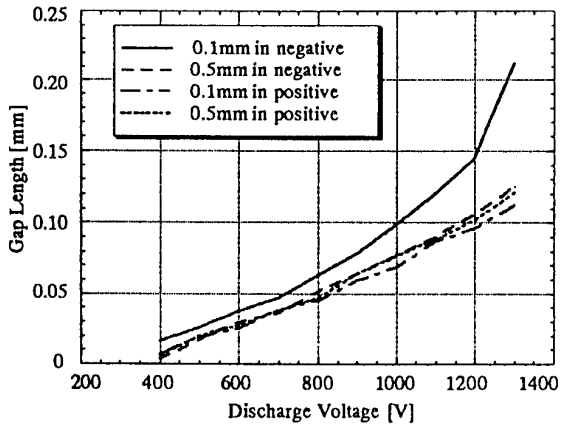



Fig. 6 Relation between discharge voltage and the gap length in this experimental system.

of the uniform field are given by (M.Topler's experimental equation in 1907)

$$d / (2 \cdot R) < 1.7 \qquad (2)$$

$$d / (2 \cdot R) < 0.9 \qquad (3)$$

where d is the gap length, R is the radius of sphere electrode, and equation (2) is in positive polarity and equation (3) is in negative polarity. When, this equation applied to our experimental system. The formative gap lengths of the uniform field are below 0.34 mm in positive polarity and below 0.18 mm in negative polarity at the needle of 0.1 mm radius of curvature. Furthermore, the formative gap length are below 1.7 mm in positive polarity and below 0.9 mm in negative polarity, where the radius of curvature is r=0.5 mm. Fig.6 shows a relation between discharging voltage and the gap length in this experimental system. When the radius of curvature of needle electrode was 0.1 mm in negative polarity, the field became non-uniform at more than 1200 V. This voltage agrees approximately with the results of Fig.5 (a-n) where the fall time of transition duration was slowed down remarkably.

It can be said that the discharge gives breakdown directly in the uniform field, while the breakdown in non-uniform field is reached via a complex process of corona discharge (partial discharge). This is one of the causes of the difference of transition duration.

### 3.3. Confirmatory experiment

Confirmatory experiment was proceeded to confirm the difference in the distribution of electric field. The tapered coaxial electrode was changed for the needle-needle type electrode to make the uniform electric field. Fig.7 shows

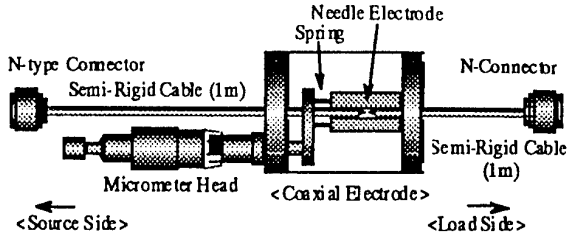



Fig. 7 Cross section view of the needle-needle type electrode

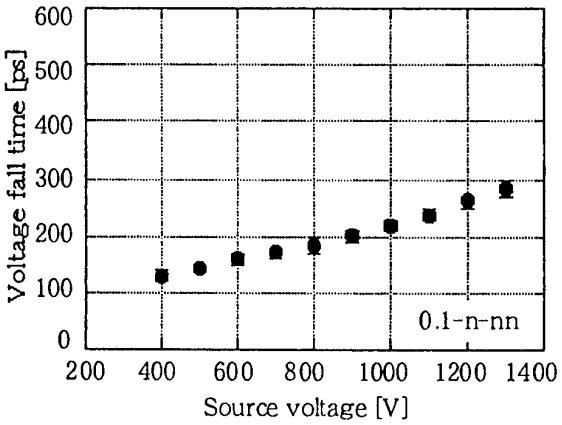



Fig. 8 Relationship between source voltage and the transition duration in the needle-needle electrode.

a cross section view of the needle-needle type electrode. The needle electrode was made from a sharpening the inner conductor of source side and load side semi-rigid coaxial cables. The radius of curvature of the needle electrodes is 0.1 mm, respectively.

The relationship between source voltage and the transition duration due to an increasing of the source voltage in negative polarity is shown in Fig.8. The voltage fall time was slowed down remarkably from about 130 ps to about 450 ps in the needle to plan type electrode. While in experiments of the needle to needle type electrode, the transition duration of voltage fall time was slowed down from about 130 ps to about 300 ps relatively with the source voltage.

## 4. CONCLUSION

The very fast transition duration due to the short gap discharge was investigated in time domain using the distributed constant line system.

As a consequence of the experiment using this

measurement system, the voltage rise time was slowed down from about 100 ps to about 300 ps for an increasing of the source voltage from 400 V to 1300 V in positive polarity. While, the voltage fall time was slowed down remarkably from about 130 ps to about 450 ps when experiment was performed in negative polarity for the 0.1 mm needle electrode. The relationship between the discharge voltage and the transition duration was confirmed from these results. That is, the rise time of the transition duration shows similar characteristics in positive polarity, while the fall time was slowed down remarkably in negative polarity when the radius of curvature of needle electrode was 0.1 mm. It was confirmed that the cause is the differential distribution of electric field in the gap of electrode.

## REFERENCES


[1] P.F.Wilson and M.T.Ma, "Field radiated by electrostatic discharges", IEEE Trans. on Electromagn. compat., EMC-33, no.1, pp.10-18, Feb. 1991.

[2] M.Honda, "Indirect ESD measurement using a short monopole antenna", 1990 IEEE Int'l. Symp. on Electromagn. Compat., pp.641-645, Aug.1990.

[3] L.M.MacLeod and K.G.Balmain,"Compact Traveling-Wave Physical Simulator for Human ESD", IEEE Trans. on Electromagn. Compat., vol. 39, no. 2, pp. 89-99, May 1997.

[4] D.Pommerenke:"ESD:transient fields, arc simulation and rise time limit", Journal of ELECTROSTATICS, vol.36, pp.31-54, 1995.

[5] R.Zaridze, D.Karkashadze, R.G.Djobava, D.Pommerenke, and M.Aidam, "Numerical Calculation and Measurement of Transient Fields from Electrostatic Discharge", IEEE Trans. on Components, Packaging, and Manufa. Tech., Part C, vol.19, no.3, July 1996.

[6] O.Fujiwara, "An Analytical Approach to Model Indirect Effect Caused by Electrostatic Discharge", IEICE Trans. on Commun., vol.E-79-B, no.4, April 1996.

[7] S.Ishigami, R.Gokita, Y.Nishiyama, I.Yokoshima and T.Iwasaki:"Measurements of fast transient fields in the vicinity of short gap discharges", IEICE Trans. on Commun., vol.E78-B, no.2, pp.199-206, Feb. 1995.

[8] K.Arai, W.Janischewskyj and N.Miguchi ,"Microgap Discharge Phenomena and Television Interference ", IEEE Trans.Power Appar.&Syst.,PAS-104,No.1, 1985.

[9] D.Pommerenke:"ESD:waveform calculation, field and current of human and simulator ESD", Journal of ELECTROSTATICS, vol.38, pp.31-54, 1996.

[10] B. Daout and H. Ryser,"The reproducibility of the rising slope in ESD testing", Proc. of 1986 IEEE Int'l Symp. on Electromagn. Compat., pp.467-474, Aug.1986.

[11] R.Wallace,"6GHz time Domain Measurement of Fast Transient Events", Proc. of 1992 IEEE Int'l Symp. on Electromagn. Compat., pp.460-463, Aug.1992.

[12] K.Kawamata, S.Minegishi,A.Haga and R.Sato, "Measurement of Very-Fast-Voltage Rise Curve Due to Gap Discharge Using Coupled Transmission Lines in Distributed Constant System",IEEE Trans. Instrum. Meas., vol.46, no.4, pp.918-921, Aug. 1997


## BIOGRAPHICAL NOTES

**Ken Kawamata** was born 1965, in Japan. He received the B.S., and M.S., degree in engineering from Tohoku Gakuin University in 1987, and 1989, respectively. He joined Tohoku Electric Power Co. in 1989. He became a Research Associate since April 1992 , and he has been an Assistant Professor since April 1998 at the Faculty of Engineering, Hachinohe Institute of Technology. He has Doctor of Engineering degree.

Dr. Kawamata is member of the Institute of Electronics, Information and Communication Engineers of Japan; the Institute of Electrical Engineers of Japan; and the IEEE..

**Shigeki Minegishi** was born 1951, in Japan. He received the B.S., M.S., and Doctor degree in engineering from Tohoku Gakuin University in 1976, 1978, and 1981 respectively. He became a Research Associate in April of same year; and after served as Assistant Professor, Associate Professor, and he has been Professor since April 1999 at the Faculty of Engineering, Tohoku Gakuin University.

Dr. Minegishi is member of the IEICE of Japan; the IEE of Japan; and the IEEE.

**Akira Haga** was born 1944, in Japan. He received the B.S., and M.S., degree in engineering from Tohoku Gakuin University, and Yamagata University in 1968, and 1970, respectively. He joined Technical Research Laboratory of Citizen Watch Co., Ltd. in April of same year. He became a Research Associate in April of 1972; and after served as Assistant Professor, Associate Professor, and he has been a Professor since April 1992 at the Faculty of Engineering, Tohoku Gakuin University. He has Doctor of Engineering degree.

Dr. Haga is member of Japan Applied Magnetism Society; IEICE of Japan; the IEE of Japan; and the IEEE.

EMC 2000 INTERNATIONAL WROCŁAW SYMPOSIUM ON ELECTROMAGNETIC COMPATIBILITY

# MODELING OF THE LIGHTNING ELECTRIC FIELD FOR DIFFERENT MODELS OF THE CHANNEL-BASE CURRENT WITH STANDARD PARAMETERS

Grzegorz Masłowski

Rzeszow University of Technology
35-959 Rzeszow, W. Pola 2
e-mail: masloprz@prz.rzeszow.pl

*This paper discusses a modeling procedure that permits calculation of lightning vertical and horizontal electric fields starting from the different functions of the channel-base current proposed in present publications. The MTL (Modified Transmission Line) model of the current wave propagation along the channel for all cases is the same. The peak value and other current parameters during modeling of the electric field are standard for the normalized subsequent return stroke.*

## 1. INTRODACTION

In the wide area of electromagnetic compatibility, all mathematical models of observable phenomena are based on Maxwell's equations [1]. For lightning return strokes the modeling process means the establishment of a relationship between a source of interference and the response of electrical system. Indirect lightning return strokes are more dangerous cause of damage power system and electronic equipment than direct strikes, because of their more frequent occurrence. Therefore it is very important to examine all aspects of models represent physical phenomenon describing lightning return strokes. Three specific models are necessary to evaluate lightning-induced voltages on transmission lines and cables [2]. On the beginning it should be consider a model for the current propagation in the discharge and channel-base current. The next problem is calculation of the lightning return-stroke electromagnetic field propagation over a real soil with finite conductivity. The final stage is coupling this field with different structures as transmission lines and cables [3-6]. The Agrawal model appears mechanism of the field-to-line coupling [7]. This model uses the vertical and horizontal electric field to calculate the induced voltages and current in the transmission lines. The horizontal electric component ought to account along the line. The hypothesis of perfect conducting ground, adopted in studies on the subject, correctly represent a nearby lightning return stroke. When the distance from lightning return stroke not exceed a few hundred maters it is necessary to investigate all components of the electric field (electrostatic, induction and radiation). Sommerfeld has treated general problem of a dipole above an imperfectly conducting ground [8]. His expression for the electric field depends on the slowly converting integrals. It is not convenient to apply these expressions in the numerical modeling. For the distance range that does not exceed a few kilometers from the lightning channel vertical electric field can be calculated with assuming the ground as a perfect conductor. The horizontal component of the electric field is more affected by the finite conductivity of the ground than the vertical one. For the few hundred meters horizontal component can be calculated with assumption the perfect ground conductivity [9].

## 2. SPATIAL-TEMPORAL DISTRIBUTION OF THE CURRENT ALONG THE LIGHTNING CHANNEL

A mathematical model that permits the calculation of vertical and horizontal electric field components of lightning, starting from MTL model for the current distribution in the discharge proposed in [9]. The lightning channel is assumed

to be the vertical antenna above a perfect ground plane. The assumption of the perfectly conducted ground can be adopted in the calculation nearby indirect lightning return stroke. The distribution of the lightning return stroke current can be expressed by

$$i(z',t) = i(0,t-\frac{z'}{v})\exp(-\frac{z'}{\lambda}) \qquad (1)$$

where:

$\lambda$ - Decay constant determined in the range of 1-2 km,
$v$ - Velocity of the return stroke current,
$z'$ - Spatial variable along the channel.

## 3. THE CHANNEL-BASE CURRENT

There are many different functions for the channel-base current. It will be examine three functions the most popular in present publications. For example in [10] the channel base-current is approximated by normalized function

$$i(0,t) = \frac{I_0}{\eta}\frac{(t/\tau_1)^n}{1+(t/\tau_1)^n}\exp(-\frac{t}{\tau_2}) \qquad (2)$$

where:

$I_0 = 25$ kA - Amplitude
$\eta = 0{,}993$ - Amplitude correction factor
$\tau_1 = 0{,}454\ \mu s$ - Front time constant
$\tau_2 = 143\ \mu s$ - Decay time constant
$n = 10$ - Exponent

These parameters reproduce the channel-base current of a typical subsequent lightning return-stroke with the peak value 25 kA, the front time $T_1 = 0{,}25\ \mu s$ and the half-delay time $T_1 = 100\ \mu s$. Several authors adopt for the channel-base current an analytical expression described by a sum of two functions similar to above presented

$$i(0,t) = \sum_{i=1}^{2}\frac{I_{0k}}{\eta_k}\frac{(t/\tau_{1k})^n}{1+(t/\tau_{1k})^n}\exp(-\frac{t}{\tau_{2k}}) \qquad (3)$$

The parameter $\eta_k$ is the amplitude correction factor, which can be expressed in the form

$$\eta_k = \exp[(-\frac{\tau_k}{\tau_{2k}})(\frac{n\tau_{2k}}{\tau_{1k}})^{1/n}] \qquad (4)$$

where:

$I_{0k}$ - Amplitude of the channel-base current
$\tau_{1k}$ - Front time constant
$\tau_{2k}$ - Decay time constant
$n$ - Exponent (2...10).

In particularly parameters of this function that are shown in Table 1 good reproduce the shape of current from Eq. (2).

Table 1. Parameters of two functions from (3)

| $I_{01}$ | $\tau_{11}$ | $\tau_{21}$ | $n_1$ | $I_{02}$ | $\tau_{12}$ | $\tau_{22}$ | $n_2$ |
|---|---|---|---|---|---|---|---|
| kA | μs | μs | - | kA | μs | μs | - |
| 24 | 0.20 | 75 | 2 | 6.1 | 50 | 200 | 2 |

Function from Eq. (3) is used instead the double exponential function of the following type

$$i(0,t) = \frac{I_{03}}{\eta_3}[\exp(-\alpha t) + \exp(-\beta t)] \qquad (5)$$

This function has non-continuous time derivative at $t = 0$. Parameters of this function are presented in Table 2. The channel-base currents describe by equations (2), (3) and (5) have the same peak value, front time and half-delay time but their time-derivatives are different (see Fig.1 and Fig.2).

Table 2. Parameters of the double exponential function (equation (5))

| $I_{03}$ | $\eta_3$ | $\alpha$ | β |
|---|---|---|---|
| kA | – | $\mu s^{-1}$ | $\mu s^{-1}$ |
| 24 | 0.985 | 0,007 | 4,5 |

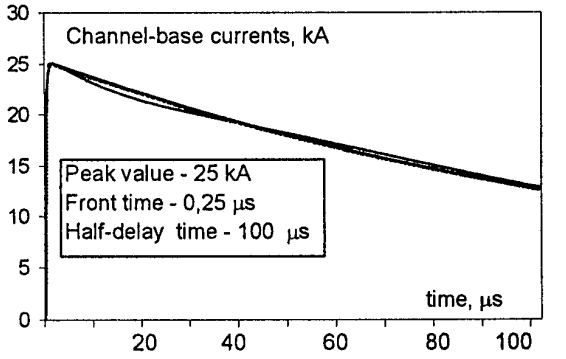



Fig.1. Channel-base currents for Eq. (2), (3) and (5)

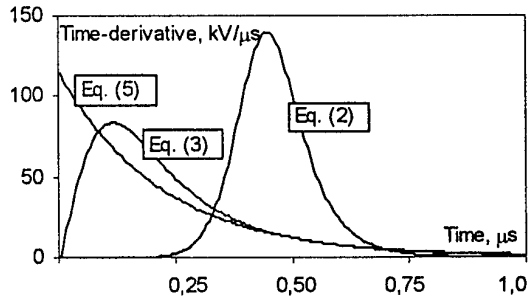



Fig.2. Time derivatives of the channel-base currents (for Eq. (2), (3) and (5))

## 3. LIGHTNING RETURN-STROKE ELECTROMAGNETIC FIELD

The lightning channel is assumed to be vertical antenna above a ground plain (see Fig. 3).

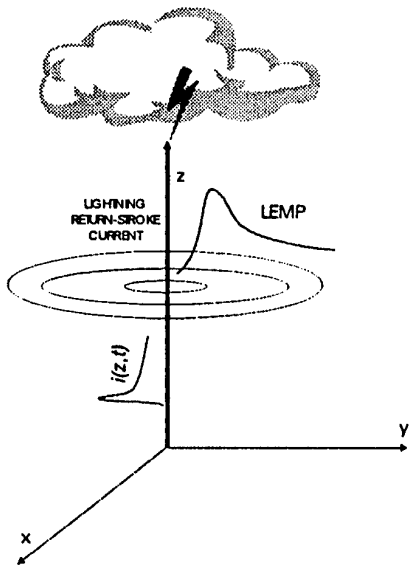



Fig.3. Geometry of the problem

By assuming the ground as a perfect conductor it is possible to derive the expressions for the horizontal and vertical electric field of the nearby lightning return stroke from Maxwell's equations [11]. These expressions, adopted to the MTL model, in the frequency domain become [12]

$$E_\rho(r,j\omega)=\frac{Z_0}{4\pi}\int_{-H}^{H}\left[\left(\frac{I(r,j\omega)}{j\omega}+\pi I(0)\delta(\omega)\right)\frac{3c\rho(z-z')}{r^5}+\right.$$
$$\left.+I(r,j\omega)\left(\frac{3\rho(z-z')}{r^4}+\frac{\rho jk(z-z')}{r^3}\right)\right] \qquad (6)$$

$$E_z(r,j\omega)=\frac{Z_0}{4\pi}\int_{-H}^{H}\left[\left(\frac{I(r,j\omega)}{j\omega}+\pi I(0)\delta(\omega)\right)\frac{2c\left[(z-z')^2-\sigma^2\right]}{r^5}+\right.$$
$$\left.+I(r,j\omega)\left(\frac{2(z-z')^2-\rho^2}{r^4}-\mathrm{j}kr\frac{\rho^2}{r^4}\right)\right] \qquad (7)$$

where

| | |
|---|---|
| $Z_0=120\pi$ | - Free space characteristic impedance |
| $H$ | - Height of the channel |
| $\rho=\sqrt{x^2+y^2}$ | - Distance from the lightning channel |
| $r=\sqrt{\rho^2+z^2}$ | - Distance from the $dz'$ element |
| $c$ | - Speed of the light in vacuum |
| $k=\omega/c$ | - Wave vector |

In the frequency domain, the traveling-wave current distribution is given by

$$I(r,j\omega)=I(\omega)\exp(-(1/\lambda+j\omega/v)|z'|)\exp(-jrk) \qquad (8)$$

where

| | |
|---|---|
| $I(\omega)$ | - Fourier transform of the channel-base current (Eq. (2), (3) or (5)) |
| $\alpha=1/\lambda+\mathrm{j}\omega/v$ | - The channel propagation constant |
| $\exp(-jrk)$ | - Phase related with the distance $r$ |

The total electric field is obtained by integrating along the vertical channel and its image. The electrostatic component is related to the integral of the channel current (the first component in equations (6) and (7)), the induction component is a consequence of the decomposition current along the lightning channel (the second component in equations (6) and (7)), and the radiation component is related to the time derivative of the channel current (the third component in equations (6) and (7)). Note that Fourier transform of the integral association with the electrostatic component includes the element $\pi I(j\omega)|_{\omega=0}\delta(\omega)$. Approximation of this relation is used in the numerical calculation because the electrostatic component for $\omega=0$ is not definite in the frequency domain.

## 4. NUMERICAL CALCULATIONS

In Fig 4 and 5 there are shown shapes of the horizontal and vertical electric fields and their components for three different channel-base currents. In all cases the parameters were the same in the MTL model of the current distributed along the channel ($\lambda=1{,}7$ km, $v=1{,}3\cdot10^8$ m/s). The high of channel, $H$, is also a parameter but it is not significant in determining the radiated waveforms [2]. The electric field was calculated for the one hundred meters away of the lightning return-stroke channel and ten meters above the perfectly conducting ground. The vertical electric field has negative sign and it is stronger than horizontal electric field about ten times (see Fig. 4 and Fig. 5). All plots show that different models of the channel-base current give very similar field. In fact only for current described by Eq. (2) can see less than 3-5% differences (that depends on a range time). Of course the greatest differences are for vertical and horizontal radiation components that depend on time derivatives of currents. Channel-base currents described by Eq. (3) and (5) have different time derivatives but the radiation components are very similar.

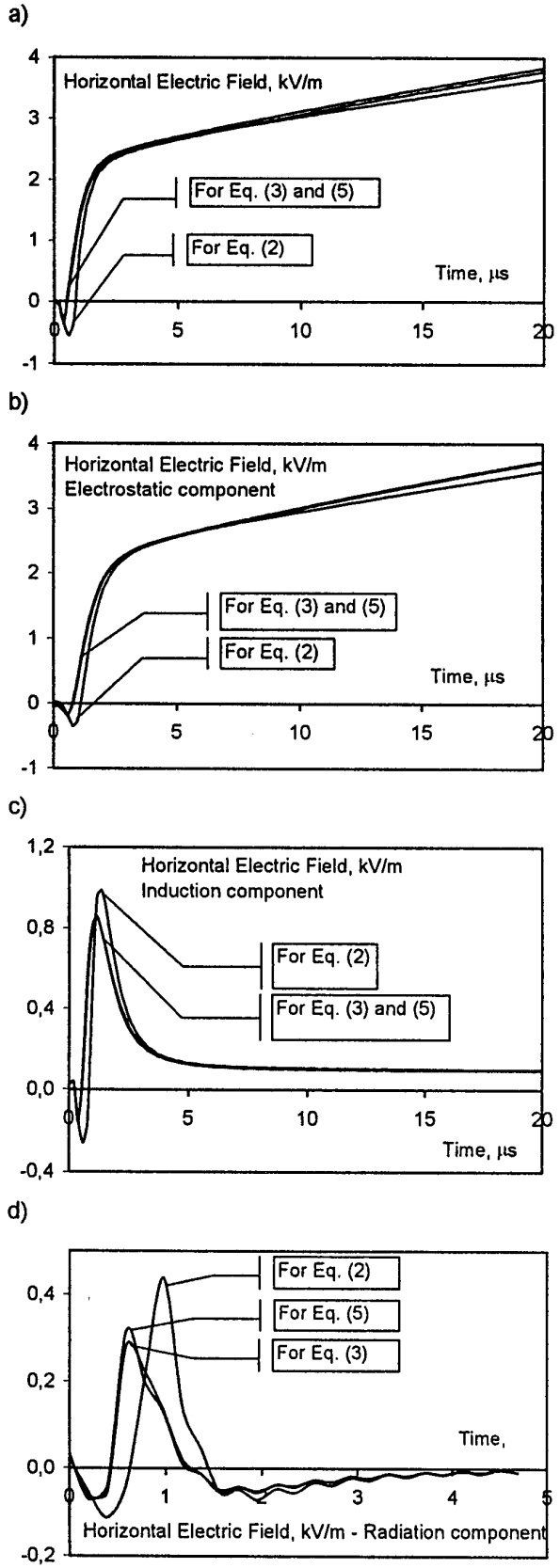



Fig. 4. Horizontal electric field (a) and its components (b), (c) (d), (ρ=100 m, h=10 m)

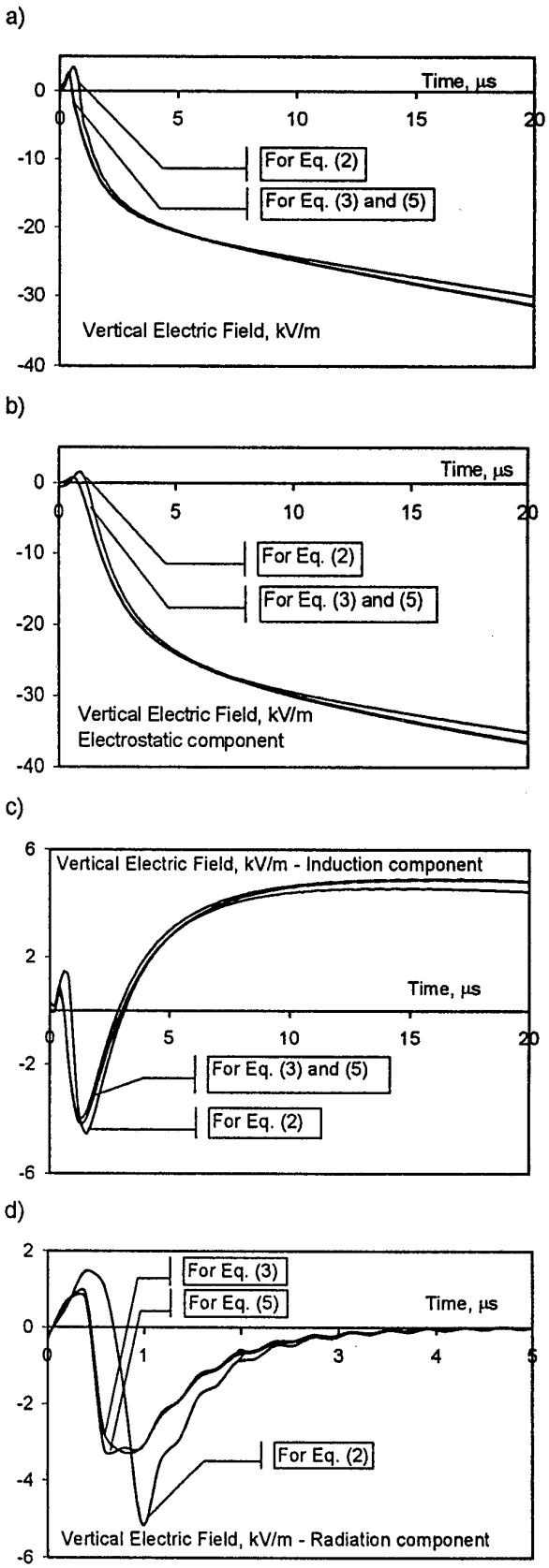



Fig. 5. Vertical electric field (a) and its components (b), (c) (d), (ρ=100 m, h=10 m)

## 5. CONCLUSIONS

Three different functions of the channel-base current were adopted in the MTL model for the mathematical modeling of the lightning electric field. The current describes by double exponential function gives the same horizontal and vertical fields as the channel-base current described by a sum of two normalized functions. Therefore electric fields can be calculated properly for MTL model with the double exponential function although the time derivative of such function is not consistent with measured return-stroke time derivative waveshape. An in the future study of lightning will be tested a simplified equations of the lightning electromagnetic field and coupling this field with transmission lines.

## 6. REFERENCES


[1] Paul C. R., "Introduction to Electromagnetic Compatibility", John Wiley & Sons, Inc., New York, 1992.

[2] Tesche F.M., Ianoz M.V., Karlsson T., "EMC Analysis Methods and Computational Models", John Wiley & Sons, Inc., New York, 1997.

[3] Bajorek J., Włodek R., "Mathematical modeling of the induced overvoltages in power lines", (Polish), Proceedings of the Symposium on Mathematical Metods in Power Engineering, Zakopane, Poland, 1993.

[4] Masłowski G., "Analysis of Influence of Lightning Return Stroke Electric Field on any Wiring Configuration. Proceedings of the Conference ELMECO, Liblin, Poland, 1994, pp. 239-244.

[5] Masłowski G., TLM method in modeling of the lightning overvoltages in transmission lines", (Polish), Proceedings of the Symposium on Overvoltages in Electric and Electronic Devices, Białystok, Poland, 1994, pp. 131-138.

[6] Bajorek J., Masłowski G., "Comparision of selected algorithms used to analyse of induced overvoltages in transmission lines", (Polish), Proceedings of the XVIII Symposium SPETO, Gliwice-Ustroń, Poland, 1995, pp. 291-296.

[7] Agrawal A.K., Price H.J., Gurbaxami S. H., "Transient response of multiconductor transmission lines excited by a nonuniform electromagnetic field". IEEE Trans. on EMC, No. 22, 1980, pp. 119-129.

[8] Sommerfeld A., "Uber die Ausbreitung der Wellen in der drahtlosen Telegraphie". Ann. Phys., Vol. 28, 1909, pp. 665.

[9] Nucci C.A., Rachidi F., Ianoz M. V., Mazzetti C., "Lightning-induced voltages on overhead lines". IEEE Trans. on EMC, No.1, 1993, pp. 75-94.

[10] VG 95 371, Teil 10, Elektromagnetische Verträglichkeit (EMV) einschließlich Schutzegen den Elektromagnetischen Impuls (EMP) und Blitz, August, 1993.

[11] Master M.J., Uman M.A., "Transient electric and magnetic fields associated with establishing a finite electrostatic dipole". Am. J. Phys., **51**, 1983, pp. 118-126.

[12] Bajorek J., Masłowski G., "Mathematical models of electromagnetic field of lightning", Proceedings of the XXII Symposium SPETO, Gliwice-Ustroń, Poland, 1999.


## BIOGRAPHICAL NOTES



Grzegorz Masłowski was born in Poland in 1965. He received the M.Sc. degree from the Rzeszow Technical University in 1991 and the Ph.D. degree in electrical engineering from the University of Mining and Metallurgy in Krakow, in 1999. Since 1992, he has been with the Department of Electrical Engineering, Technical University in Rzeszow. His research interests include physical and mathematical models of lightning, numerical modeling of the lightning electromagnetic impulse, and transmission lines excited by a nonuniform electromagnetic field.

**EMC 2000** INTERNATIONAL WROCŁAW SYMPOSIUM ON ELECTROMAGNETIC COMPATIBILITY

# LIGHTNING OVERVOLTAGES IN STRUCTURAL CABLING SYSTEMS

Andrzej W. Sowa Leszek K. Augustyniak
Technical University of Białystok
15-893 Białystok, ul Grunwaldzka 11/15, fax. 48 85 7421657

*Lightning discharge is one of the basic sources of electromagnetic impulses, which threats to devices working in complex computer nets. Especially dangerous are overvoltages during direct lightning stroke to building. Taking this fact into account, the investigation were made to estimate the levels and shapes of the induced overvoltages in structural cabling systems due to electromagnetic fields from surge currents in lightning protection systems (lps). Studies of lightning overvoltages are an important element in the reliability analysis of local area networks.*

## 1. INTRODUCTION

The wide usage of semi-conductor elements and integrated circuits in construction of electrical and electronic devices considerably decreases the dimensions and simultaneously increases possibilities of these devices. However newly built devices, without uses of protective elements or systems, characterize diminished resistance to electromagnetic disturbances. The most important natural source of electromagnetic interferences is lightning discharge, which interacts directly and indirectly with electrical and electronic systems.

One of the systems most affected by lightning interference is data transmission installation. When an external EM field, such as lightning electromagnetic pulse (LEMP), irradiates a data-network, the resulting induced voltage impulse across the electric load of the network (e.g. across a computer or telecommunication sub-assembly) is mainly due to two effects:

- the antenna characteristics of the data-network,
- the data-network response to the overvoltage and overcurrent surges coming from the external line which were induced in these lines by the same lightning event.

During a direct lightning stroke to building the surges in data-transmission networks are induced by the electromagnetic field which is caused by lightning current which propagated in lightning protection systems or conducting elements of building's construction. These surges may disturb or damage the electronic equipment. The level of interferences in a network strongly depends on the physical structure of the network itself. One of the biggest problems regarding the control of lightning induced overvoltages in a data-transmission installation is the evaluation of the response of a complex wiring system to a LEMP. The susceptibility of specific structural installation to transient waveforms of lightning origin is rather difficult and complex to calculate.

Nowadays the most popular kind of wiring applied to complex systems of connections between electronic devices is structural cabling. This is system of wiring, which makes possible realization of definite configuration of connections, but with possibility his future extensions and reconfiguration. Therefore wiring of building without earlier knowledge of devices, which will be making use of wiring is possible. However every type of wiring of building can create threat to devices joint to it as a result of induced overvoltages.

## 2. EXPERIMENTAL SET-UP

The most dangerous case is a direct lightning stroke to the building in which a computer system is installed. During such a stroke, additionally to the LEMP, the surge current of high amplitude and short rise time, which flows to the ground in a lightning protection system or a steel construction of the building, should be taken into account. In this paper selected results of the experimental studies on the structural cabling network of UTP category 5 cable are presented.

Already in line segments from several to tens metres long, interconnecting devices inside the building, induced overvoltages of relatively high values can occur.

The measurements were carried out on the real network of a brick building. During research the current generator was connected to the bottom end of the to the perpendicular aluminium pipe about 7.7 metre long placed inside building. The upper end of the pipe was connected to air terminal of lps on the roof of the object (node *x* on Fig. 1a). The second pole of generator was joint to earthing installation in building. In this arrangement the surge current flowed into aluminium pipe and subsequently in building's lps (Fig 1a.).

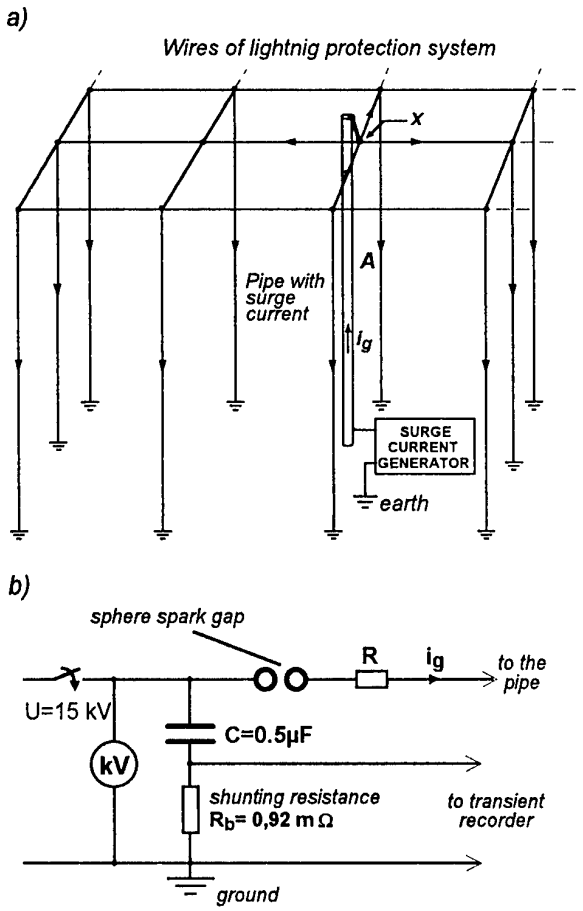



Fig. 1. Schematic diagram of experimental set-up
a) lightning protection systems with surge current,
b) surge current generator

The surge current was measured with a shunting resistance Rb = 0,92mΩ and transient recorder HP 54510A. The magnitudes and the shapes of surge currents were regulated by changing the values of resistance R (R = 10Ω, 22Ω, 50Ω and 100Ω) at $U_g$ = 15 kV.

In measurements the amplitudes of surge currents in the pipe reach the values from several hundreds A to several kA.

Some examples of surge current which flows in the pipe are presented in Fig.2.

Measurements were conducted in circuits of real structural installation arranged inside 2-storey building of brick.

This permitted to avoid some errors (which would be appear in model researches as a result of different simplifications) giving overvoltage image in typical installation.

The transverse and longitudinal induced voltages appearing in the structural installation were registered in selected sockets using HP 10441A and transient recorder HP 54522A.

The measurement system is shown in Fig. 3.

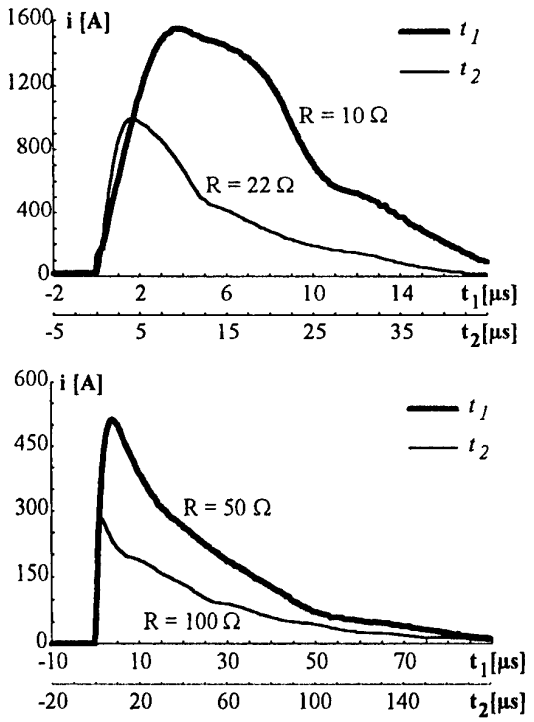



Fig. 2. Examples of surge currents, which flow in pipe and next in lightning protection system (R=10Ω, 22Ω, 50Ω and 100Ω)

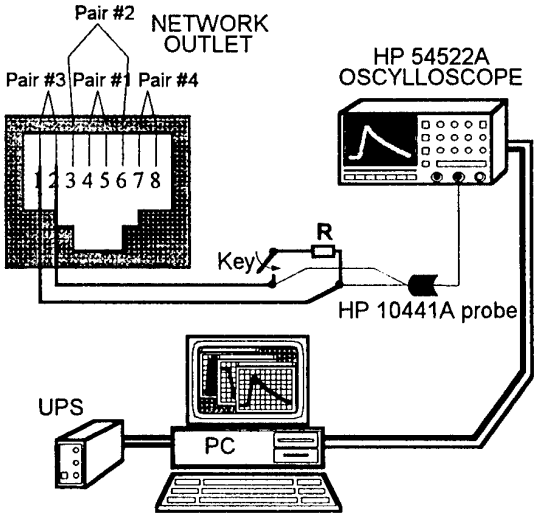



Fig. 3. Schematic diagram of the experimental set-up for induced voltages measurements

Figure 4 shows vertical projection of building's above-ground storey fragments, with marked point of test current introducing to the Ips and points of overvoltage measurements in structural cabling systems.

Structural cabling installation was performed with commonly applied unshielded twisted pair cable (4-pairs UTP category 5). All structural lines of building converged in cross-room (floor distributor in room no 022) on ground floor.

Lengths of lines were from several metres to several tens metres. The greatest line length, at which measurements were carried out was about 60 metres (room no 158).

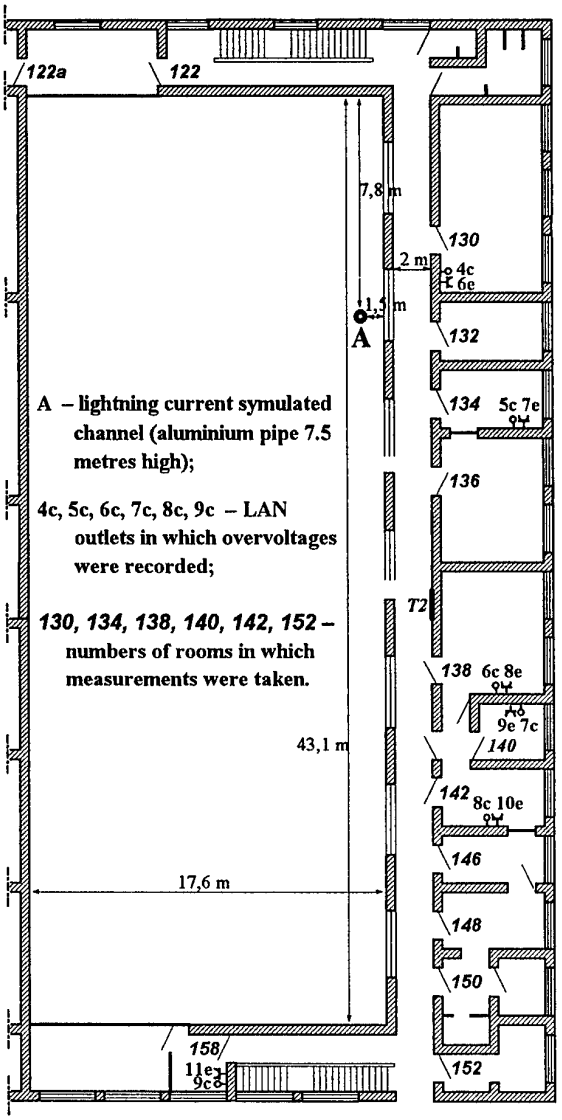



Fig. 4. Fragments of the first floor in object with structural cabling system in which the measurements of the induced overvoltages were made. In rooms the measuring points (sockets) of structural installation were marked.

## 3. EXPERIMENTAL RESULTS

Measurements of overvoltages induced by different shape currents *ig* were conducted among others in rooms no 024 and 140 (Fig. 4). In the experimental study the structural cabling systems was completely disconnected from computers.
Measurements were taken in two cases: without load and with load of a 100 Ω.
Figure 5 shows example oscillograms of voltages registered in two sockets of structural installation at test current peak value 1.55 kA and rise time 2.5 μs (fig. 2*a*).

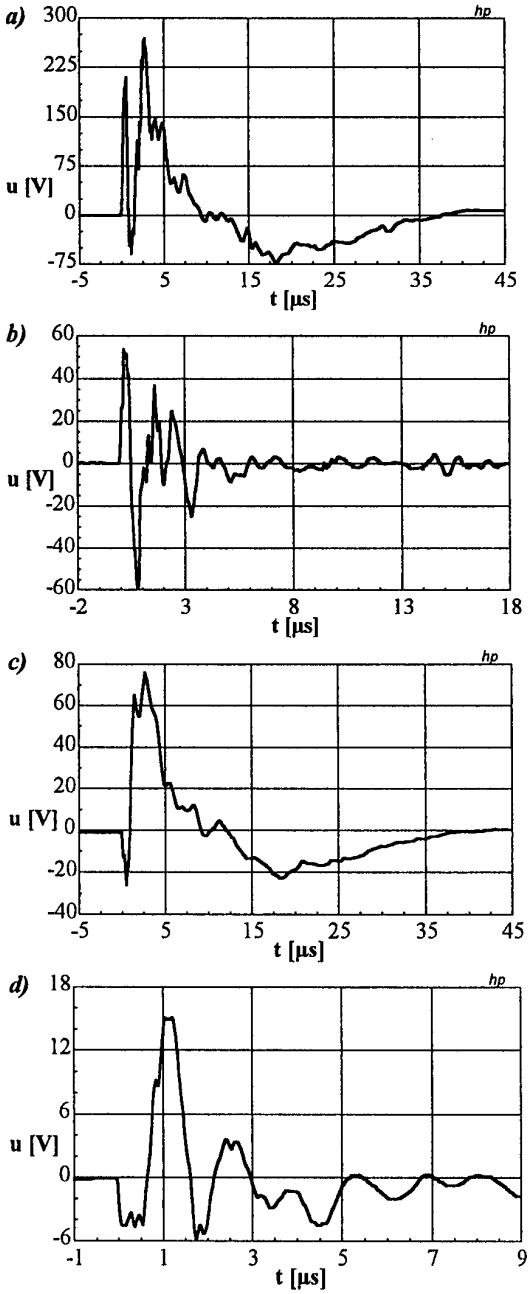



Fig. 5. Voltages induced in two sockets at 1st floor: a), b) in socket *1c* without load and with load 100Ω respectively, c), d) in socket *7c* without load and with load 100Ω respectively

Maximum values of overvoltages registered in selected sockets of structural installation for currents with:
- peak values 1550A and 274A,
- rise times respectively 2.5 μs and 1.2μs

which are put to the lightning protection systems are taken below in table 1.

Table 1: Overvoltage levels registered in selected sockets of structural installation

| Measurement point (socket) (fig. 5) | Surge current parameters | | Max value of overvoltage [V] positive / negative | |
|---|---|---|---|---|
| | peak value [A] | rise time [μs] | open circuit | load 100 Ω |
| 1c (room 024) | 1550 | 2,5 | 268,4 / -73,93 | 53,83 / -59,49 |
| | 274 | 1,2 | 17,64 / -13,88 | 4,12 / -5,07 |
| 3c (room 028) | 1550 | 2,5 | 15,00 / -36,15 | 5,66 / -5,33 |
| | 274 | 1,2 | 10,84 / -17,17 | 3,72 / -3,62 |
| 4c (room 130) | 1550 | 2,5 | 51,44 / -32,84 | 18,56 / -22,69 |
| | 274 | 1,2 | 23,01 / -22,64 | 12,62 / -11,93 |
| 7c (room 140) | 1550 | 2,5 | 76,99 / -24,69 | 15,19 / -5,71 |
| | 274 | 1,2 | 41,88 / -15,80 | 10,44 / -6,06 |

On the base of all registered in structural installation overvoltages some rules can be formulated:

- induced overvoltage values decreased with the length of line; the greatest values were registered in short sections of lines ending in rooms adjoining to the cross room; this may also result from the fact that the pipe with full current was located 5 metres away from this cross room;
- if line on certain piece ran vertically (in parallel to the pipe with surge current), overvoltage levels increased 2÷3 times;
- peak to peak values of overvoltage induced in structural wiring with load $R = 100\ \Omega$) were average about 1.5÷4 times smaller than in open circuit;
- overvoltage level in wiring grew about 2 times slower than value of test current.

Registered overvoltage values grew with increasing test current rise time. In spite of generating of current surges of different shapes and overvoltages registration in many points of installation did not succeed to fix of distinct relation between current rise time and overvoltage.
The same installation may be cause of these – its different parts ran different ways and in different horizontal directions and also in vertical direction in relation to the source of disturbances, therefore the resultant surge voltage being sum of voltages in different running sections of the line was accidental (similarly like in any other real installation).

## 4. CONCLUSIONS

Investigations showed high level of lightning overvoltages induced in structural wiring by simulated lightning current flowing in lps of the building. At current peak value only 1, 55 kA and rise time 2.5 μs voltages registered in different points of installation had peak to peak values of some tens ÷ some hundreds volts.

Attention should be paid, that in case of direct lightning strikes to objects the real lightning currents have multiple higher peak values and shorter or similar rise times. Then the levels of overvoltages induced in wiring arranged inside the building will exceed considerably the electric strength of the input elements of the computers or other devices in system and circuits and damaged them.
Some overvoltage measurements in real structural cabling during lightning current distribution in lps of the object confirm possibilities of damages.

Only well-chosen overvoltage protection devices in structural cabling systems assure the protection against this kind of danger.

## 5. REFERENCES

1. Augustyniak L. K.: "Analysis of lightning overvoltages in computer networks inside buildings". Doctor's thesis, Technical University of Białystok, Białystok 1999.

2. Harrison S., Wisdish M., Karmazyn H.: *Misapplication and poor instalation of transient overvoltage protection*; 23-rd ICLP, Firenze-Italy, September 23÷27 1996, vol. 2, pp. 628÷629.

3. Martzloff F. D., Tetreault M.: Characterization of disturbing transient waveforms on computer data communication lines. 6-th Conference on EMC, Zürich 1985, pp. 423÷428.

4. Sowa A., Jężak S.: Overvoltages Protection in Typical Energetic Buildings. Poznań 1999.

## 6. BIOGRAPHICAL NOTES

**Leszek K. Augustyniak** was born in Siemiatycze, Poland, in 1961. He received the M.Sc. degree in Electrical Engineering Technology from the Technical University of Białystok in 1987, and the Ph.D. degree in 1999. Since 1988 he has been with the Electrical Department at the Technical University of Białystok. He has been working in the area of overvoltage protection, high voltage technology and finally in the field of Electromagnetic Compatibility, particularly concentrating on fast pulse interferences like LEMP and NEMP. He is the author or co-author of over 40 papers, patents and conference presentation in the fields of lightning protection, over-voltage protection, lightning current distribution in buildings, electromagnetic compatibility.

**Andrzej W. Sowa** was born in Warsaw, Poland in 1951. He received M.Sc. and Ph.D. degrees from Warsaw University of Technology in 1974 and 1979 respectively. Since 1978, he has been with the Department of Electrical Engineering, Technical University of Białystok. He is the author and co-author of 5 books and above 200 papers, patents and conference presentation in the above fields.

EMC 2000 INTERNATIONAL WROCŁAW SYMPOSIUM ON ELECTROMAGNETIC COMPATIBILITY

# LEMP-LIKE EFFECTS ON RAILWAYS SYSTEMS

**G. Vercellotti, R. E. Zich**
Dipartimento di Elettrotecnica, Politecnico di Milano
P.za Leonardo da Vinci 32, 20133, Milano Italy
ph: +39-011-564-4118, +39-02-23993797
fax: +39-02-23993703, email: zich@polito.it

*In order to assess the impact of the possible EMC problems induced on an electric railway system by a fast transient electromagnetic field incoming on the considered structure the effects due to a LEMP has been here considered. Different models of LEMP itself and of the coupling LEMP-railway phenomena have been considered and compared. Further results and more analytical details will be directly presented at the symposium.*

## 1. INTRODUCTION

The electric railway system is characterized by the presence of an overhead line, two periodically grounded conducting lines and an impressed current system leading an electrically driven motor.

The catenary-pantograph-drive-railroad connection may be so considered as an impressed current loop possible victim of an incoming high power transient field.

In particular we focused our attention on the Italian traction system that is very untypical since, differently with respect to most other European systems, the traction system is driven by a DC impressed current, see Fig. 1.

Another important feature characterizing the considered problem is that every electric railway is an installation spread over a very large area and so it has an high probability of being exposed to natural lighting discharges or it can be easily exposed to similar artificial transient fields.

In fact the effects induced by direct, or even mostly by an indirect lighting discharge, are quite common and unfortunately they can cause damages both to the subsystems of feeding and to subsystems related to the safety.

In this context just indirect lightning discharge has been considered since first of all the endangered area where this phenomenon may occur, involving a practical railway system, is considerably much greater than for a direct discharge phenomenon.

Moreover a direct discharge is usually taken into account by severe safety standards and, for what concerns the EMC effects, by the European Standard EN-50123, while the electromagnetically coupled transient due to a nearby discharge is only considered by a particular part of the last EMC standards.

The last consideration just means that the introduction of specific systems for avoiding the direct stroke unwanted effects on the traction system are much more widely introduced, just for compliance, than those for reducing the indirect stroke coupling problems.

Furthermore due to the rising possibility of producing at low cost and high portability high power microwave transient generators, or other kinds of EMP-like generators, with a generated field with spectral characteristics close to the natural EMP (lightning), it is now of great importance to understand in detail the kind of the possible damages induced by these electromagnetic fields, *i.e.* the vulnerability of the railway systems to this kind of excitation.

In this paper just the overvoltages induced on the overhead lines have been now considered, while for what concerns the problems induced on the catenary-pantograph system [4] or on the pantograph-drive or on the electronic controls widely introduced on the rail-transit vehicles, these all will be object of the future work of the authors.

In fact in order to perform a fast transient vulnerability analysis of the whole railway system it is first necessary to focus the attention on the parts of the considered complex system that seems to have the highest probability of having problems due to the considered electromagnetic attack [5], and then to pass to consider all the others till the construction of a complete vulnerability model.

## 2. STROKE MODELS

In order to study in detail the overvoltages induced on the overhead line of a railway system due to a lightning indirect stroke, two different models of channel strokes have been here considered and compared.

In particular the stroke channel has been first considered straight, according to the model mostly present in literature [3].

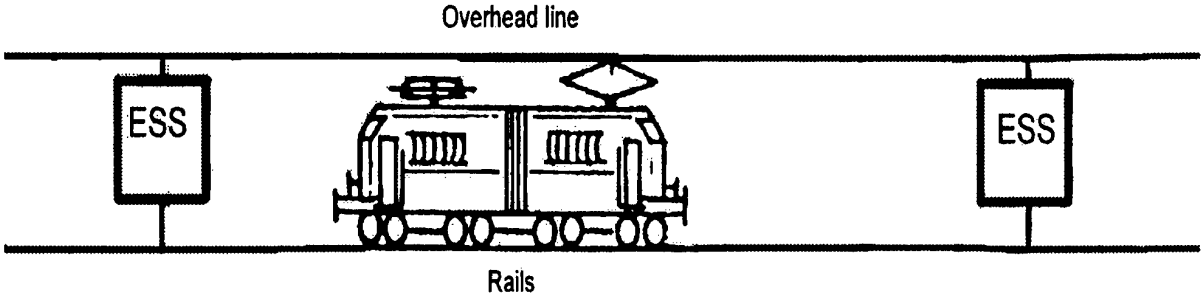



**Fig. 1:** Considered railway systems

Then the EMP natural source has been modeled through a piecewise-linear tortuous and branched model, see Fig.2, according to last model recently developed by the authors [1,2].

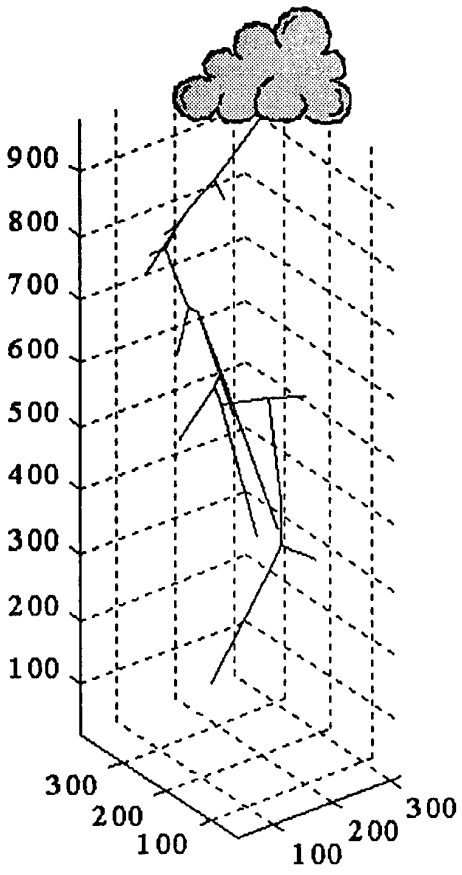



**Fig. 2:** Lightning geometry of the considered branched channel

For what concerns the first lightning channel model, the channel stroke has been considered, as usually, as a vertical linear antenna on which an impressed current with well-known frequency spectrum bandwidth is traveling.

Dealing with the physical characteristics of the considered current there several different models are available in literature.

Ad example the altitude distorted one [6,7], the heuristic Willet-Le Vine model [8] taking into account the height distortion, and a lot of others current models try to model, through the current properties itself, the physical characteristics of the measured parameters, such as light intensity and radiated field [9].

The model here considered and numerically implemented in the simulation tools among the previous ones, is the one described in detail in [3], that is a kind of first order but very effective approximation, for sake of numerical optimization with the coupling model, of the more detailed but even more complex one reported in [9].

On the contrary for what concerns the tortuous and branched channel model, the lightning channel has not been substituted by a vertical linear antenna for computing the radiated field since in previous works of the authors it has been demonstrated that this approximation do not let to take into account the higher portion of the radiated spectrum of the experimentally observed lightning strokes.

On the contrary the introduction of a tortuous, due to the kinks, and branched channel can easily manage even the higher portion of the radiated fields, higher portion that can be of particular interest for the coupling phenomena on the victim system.

Furthermore since it is useful to apply the results of the following considerations even for artificial transients, the most complex model has to be considered since the artificial EMP generators usually are designed for working in the microwave band

## 3. RADIATED FIELDS

The lighting discharge has been considered happening with a known distance from the line, with a known

length of the ground-to-cloud channel, with a known value of peak current.

All these parameters, distance, length and peak current value, have been assumed according to typical experimental data.

To obtain the electric field values induced by lighting discharge it were used two suitable numerical programs, one already available in literature [3] for the straight channel, and the other RADBR, (RADiation from BRanched channel), [1,2], that has been specifically designed in order to take into account that untriggered lighting discharge, i.e. natural lightning, does not necessarily occur trough a direct channel but usually trough a zigzag way.

For what concerns the first numerical program the considered geometry has been reported in Fig. 3.

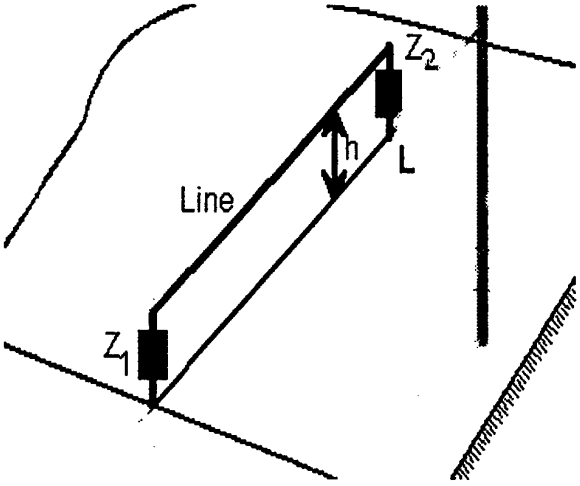



**Fig. 3:** Considered geometry of the lightning stroke and victim system in the straight approximation.

The discharge currents traveling in the two kinds of channel considered are again different, since these were developed for two different purposes.

Ad example in the straight channel the excited current has been reported in Fig. 4, where the decaying time constant was too high and the current do not fall down but assume a flat behavior for taking into account in a better way the low frequency part of the radiated spectrum as it is usually done in the papers working with that kind of model.

On the contrary the decaying time constant introduced in the branched channel model is much lower since that kind of model has been introduced not for approximating the low frequency portion of the radiated field but for a better consideration of the higher frequency components with respect to the standard straight channel model.

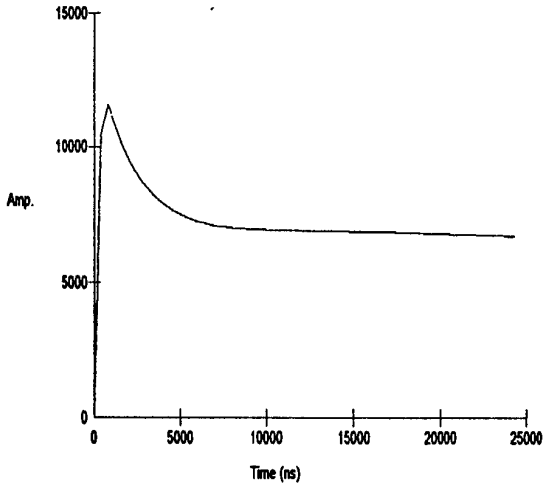



**Fig. 4:** Considered current for the straight channel model.

In fact assuming the branched channel model a typical example of the radiated electric fields that is possible to obtain is reported in Fig. 5.

In particular in this figure the considered observation point is very far from the stroke footpoint, $10^5$ m, the considered channel is a very tortuous one, with a lot of primary and secondary branches, and the ground and cloud reflections have been included.

In Fig. 5 it is also possible to compare the different time domain behavior of a branched channel with an equivalent straight channel with the same total length.

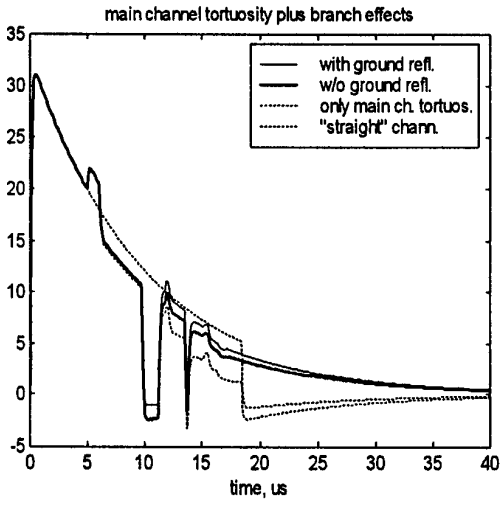



**Fig. 5:** Electric Field, measured in V/m, radiated by a tortuous channel with and without ground reflection and with and without branches.

From this comparison one can conclude that the high frequency contents of the radiated field is substantially affected by the geometrical properties of the discharge channel.

The discontinuity present in the equivalent straight channel radiated field it is due to the fact that in that

case the ground reflection was included through the model described in detail in [2].

The behavior of the radiated field as a function of time is also function of the distance between the observation point, it means the victim system, and the stroke footpoint.

In order to point out this kind of problem in Fig. 6 the behavior of the computed radiated electric field, vertical component as in the previous figure, as a function of that distance are reported.

The channel considered is a very simple branched channel with respect to the one considered for Fig.5 in order to try to focus now the attention just on the victim system position function.

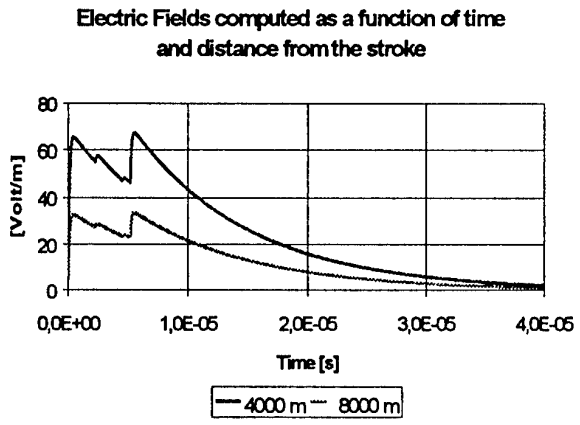



**Fig. 6:** Electric Field, measured in V/m, radiated by a tortuous channel.

## 4. INDUCED VOLTAGES

In order to try to understand how the electromagnetic field radiated by a lightning stroke can effectively couple with the considered victim target in this paper just the effects induced on the overhead line has been considered.

This kind of approach is of course just a first step of the complete vulnerability analysis of the railway system, but it is of particular importance since among the different possible ways of coupling of the killer signal with the target system the overhead lines seem to be one of the most effective for the following considerations.

- The overhead lines form a fixed installation spread over a very large area, and so there is high probability that an EMP generating phenomenon occurring somewhere can impact effectively on it. This point is absolutely not true concerning with the mobile electronics on board that if not present right there in the considered stroke area cannot be directly affected.
- The interferences due to a coupling with an incoming EMP on the overhead lines can propagate through them and impact on the mobile part of the system through a secondary coupling. On the contrary the other conducting lines present in the system are periodically grounded for safety reasons and overvoltages induced on them cannot damage any other part of the system.

For summarizing in a few words the previous points, it is possible and it may be very dangerous, and these are the reason why this it has been considered as the first point.

In particular the considered problem is the impact close to a line section 1km long, 5 m high, with the usual wire radius and considering an earth conductivity $\sigma$ =0.016 Siemens/m.

The obtained results have been reported in Fig. 7, 8 and 9 where first the coupling phenomena due to the straight channel has been considered as in [3] as a cylindrical wave radiated by the straight antenna (the considered channel).

The values of the total radiated electric field considering also cloud and ground reflections have been then considered and these results have been turned in a suitable format for the program NULINE, [3], modelling the coupling problem,. either in the frequency domain or in the time domain for the transient analysis of a single wire trasmission line located over a perfectly or lossy conducting ground plane.

Even if the program modelling the coupling phenomena considers an incident plane wave while the radiation program yields cylindrical waves we believe that their use gives better results than others programs which don't consider the branching of lighting discharge in order to perform a realistic forecast of natural or artificial unwanted effects.

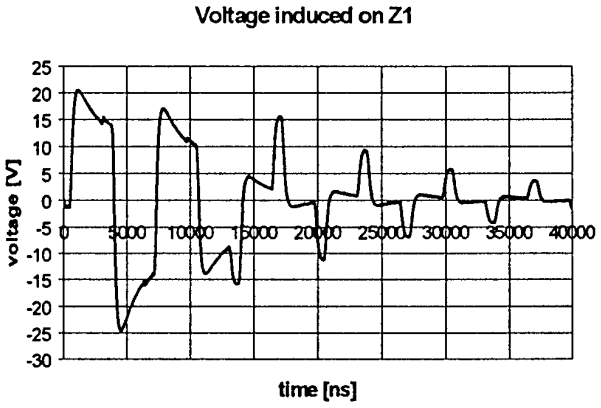



**Fig. 7:** Overvoltages induced by the LEMP on the railway overhead line. 8000 m far. Straight untortuous channel

For what concerns in detail the reported figures, Fig.7 considers the voltages induced on a victim system by a stroke modeled as a straight antenna 8 km far from the line on the normal to the line direction. Fig. 8 and Fig. 9 on the contrary consider the effects due to the tortuous and branched channel described in detail in the previous sections. The only difference in the two set of results is the different distance of the stroke footpoint, always on the normal to the line direction.

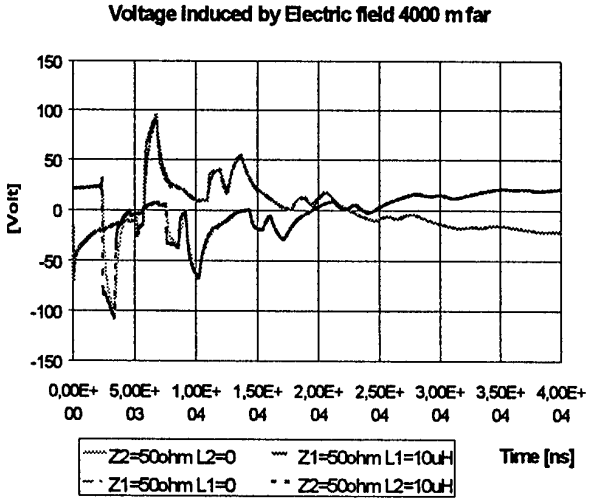



**Fig. 8:** Overvoltages induced by the LEMP on the railway overhead line.

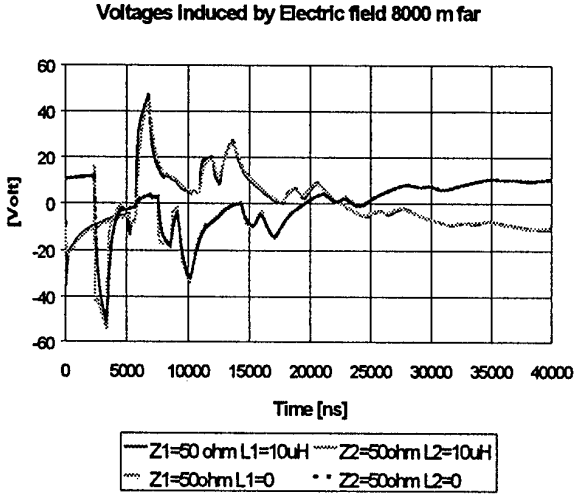



**Fig. 9:** Overvoltages induced by the LEMP on the railway overhead line.

## 5. CONCLUSIONS

The effects induced by an EMP on the overhead lines of a railway system has been considered. The results of the numerical simulations performed through different numerical tools show good agreement with the available set of measurement data and point out the necessity of developing a complete system vulnerability analysis of which this is only the first step.

## 6. REFERENCES

6.1. R.E. Zich, G.Vecchi, M. Sala, F.Canavero: "Return stroke radiation by a branched channel: a transmission-line discharge model", *Proceedings of the International Zurich Symposium on EMC,* 16-18 Feb. 1999, pp 593-596.

6.2. G. Vecchi, R.E. Zich, F. Canavero: "Disturbances Radiated by a Branched Lightning", *Proceedings of the 13th International Wroclaw Symposium on EMC,* 25-28 June 1996, pp. 504-507.

6.3. F. M. Tesche, M. V. Ianoz, T. Karlsson: "EMC Analysis Methods and Computational Models", *Wiley Interscience,* 1997.

6.4. S. Leva, A.P. Morando, R.E. Zich: "On the unwanted Radiated Fields due to the Sliding Contacts in aTraction System", IECIE Trans on Communication, Special Issue on Recent Progress in Electromagnetic Compatibility Technology, vol. E83-B, NO. 3, March 2000, pp. 1-6.

6.5. R.N. Ghose: "EMP Environment and System hardness design " Interference Control Technologies, 1984.

6.6 P. Idone, E. Orville: "Lightning return stroke velocities in the Thunderstorm Research International Program (TRIP)", Journal Geophys. Res., vol 87, no. C7, pp. 4903-4915, 1982.

6.7. D.M. Jordan, M.A. Uman, "Variation in light intensity with height and time from subsequent lightning strokes", Journal Geophys. Res., vol 88, pp. 6555-6562, 1983.

6.8. J.C. Willet, D.M. Le Vine, "On the current distribution in lightning subsequent return strokes", preprint volume of the 10th International Conference on Atmospheric Electricity in Osaka, pp. 492-495, 1996

6.9. C.A. Nucci, G. Diendorfer, M.A. Uman, F. Rachidi, M. Ianoz, C. Mazzetti, "Lightning return stroke current models with specified channel-base current: a review and comparison", Journal Geophys. Res., vol 95, no. D12, pp. 20395-20408, 1990.

## BIOGRAPHICAL NOTE

**Riccardo Enrico Zich**: Laurea summa cum laude (M.S.) and Ph.D. in Electronic Engineering Politecnico di Torino, Torino, Italy, in 1989 and 1993, respectively. Researcher in the same University from 1991. Since 1998 Associate Editor of the IEEE Trans. on EMC and joined the Politecnico di Milano, Dipartimento di Elettrotecnica as Associate Professor of Electrical Engineering.

EMC 2000 INTERNATIONAL WROCŁAW SYMPOSIUM ON ELECTROMAGNETIC COMPATIBILITY

# A HYBRID METHOD FOR THE ANALYSIS OF TRANSIENTS IN EMC PROBLEMS

R. De Leo, G. Cerri, S. Chiarandini, V. Mariani Primiani, P. Russo
Dipartimento di Elettronica ed Automatica
Università di Ancona
Via Brecce Bianche
60131 Ancona – Italy
fax. +39-071-2804334
e-mail: s.chiarandini@ee.unian.it

*This paper presents some applications of a hybrid method for the solution of EMC coupling problems, involving arbitrarily shaped wire structures, and complex scattering objects. The wire structures are solved with the Method of Moment and the objects with the FDTD. The method is briefly presented, together with the numerical aspects that the method involved. The applications pertain pulse penetration into shielded enclosures and coupling between helix and biological tissues.*

## 1. INTRODUCTION

The analysis of electromagnetic problems, and particularly of EMC problems, is often difficult because it is sometime impossible have a closed form solutions for Maxwell's equations in very complex environments, where sources and scattering objects are generally strong coupled. Also a high degree of analytical treatment in the problem formulation is allowed only if great simplifications are adopted, reducing the object geometry to canonical structures, with an obvious loss of accuracy.

Therefore most of cases has to be approached with numerical techniques. The most popular among them, suitable for EMC frequencies, are Method of Moment (MoM) , Finite Differences in Time Domain (FDTD), Transmission Line Matrix method (TLM), Finite Element Method (FEM).

However, also numerical techniques suffer some drawbacks. Integral equation approaches, like MoM, can be efficiently used to characterise a regular object, whose geometry is described by simple equations, but it becomes very cumbersome to model an irregular, inhomogeneous and penetrable objects.

On the other hand, differential equation approaches (FDTD, TLM) can treat medium inhomogeneities in a more straightforward manner, but they are not very suitable to describe thin or wire structures, especially when the wire orientation is not conformable to the axes of the structured grid. Moreover, the requirement of describing small details and of discretizing the whole domain can lead to an impracticable number of cells.

Therefore the basic idea is to combine various methods, using for each part of the overall complex structure the most efficient technique, in order to overcame the intrinsic limitations of using a single technique only.

This contribution presents typical EMC problems solved by a hybrid technique based on the combination of an integral equation method (MoM) and a differential equation method (FDTD).

The technique seems to be particularly suitable to treat scattering problems, where a source is strongly coupled to an object placed in its near field region. The use of the equivalence principle allows to analyse the overall problem separating the source region and the object region: this aspect makes the approach quite general because inside each sub-region any structure can be characterised and solved by the proper method.

## 2. FORMULATION OF THE PROBLEM

The problem of the electromagnetic coupling between radiating structures of arbitrary shape and inhomogeneous objects can be efficiently treated with hybrid numerical techniques.

The idea [1] is to reduce the complexity of the problem solving a number of simpler subproblems each of them dealing with one of the interacting structure. In this way for every structure we can choose the technique that best fits its features, achieving a great accuracy in the solution of the problem.

The equivalence principle is then used to take into account the electromagnetic coupling between the objects. Fig.1 shows a typical coupling problem between a wire structure of complex shape and a scattering object.

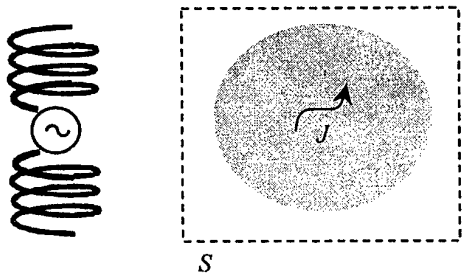



Fig.1 A helix antenna radiates a generic scattering object placed in its near field region: the region is divided by an equivalent surface S

The domain is divided in two subdomains by an equivalent surface *S*. A proper choice of the equivalent current distribution on *S* allows to set up a subproblem for the analysis of the source without the presence of the object (fig.2) and another subproblem for the analysis of the object without the presence of the source (fig. 3)

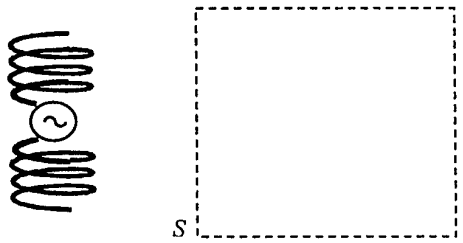



Fig. 2 First equivalent problem: the actual field is outside S

Fig. 2 shows the first equivalent sub-problem: outside S, in the source region. The actual total fields $\mathbf{e}_1(r,t)$, $\mathbf{h}_1(r,t)$ are the superposition of the fields $\mathbf{e}(j)$, $\mathbf{h}(j)$ radiated by the source and the fields $\mathbf{e}(j_s)$, $\mathbf{h}(j_s)$ radiated by the induced currents.

Inside *S*, any arbitrary field distribution can be chosen, in particular the fields $\mathbf{e}(j)$, $\mathbf{h}(j)$ radiated by $\mathbf{j}(r,t)$ in free space are considered. An equivalent current distribution is introduced to support the field discontinuity on *S* :

$$\mathbf{j}_1(r,t) = \mathbf{n} \times \mathbf{h}(j_s)|_{on\ S} \qquad (1)$$

$$\mathbf{m}_1(r,t) = \mathbf{e}(j_s)|_{on\ S} \times \mathbf{n}_1 \qquad (2)$$

Fig. 3 shows the second equivalent sub-problem, in the scattering object region. The actual total fields $\mathbf{e}_2(r,t)$, $\mathbf{h}_2(r,t)$ are the superposition of the incident fields $\mathbf{e}(j)$, $\mathbf{h}(j)$ and the scattered fields $\mathbf{e}(j_s)$, $\mathbf{h}(j_s)$. Inside *S*, the fields $\mathbf{e}(j_s)$, $\mathbf{h}(j_s)$ radiated by $\mathbf{j}_s(r,t)$ in free space are chosen, therefore the equivalent current distribution on *S* is

$$\mathbf{j}_2(r,t) = -\mathbf{n} \times \mathbf{h}(j)|_{on\ S} \qquad (3)$$

$$\mathbf{m}_2(r,t) = -\mathbf{e}(j)|_{on\ S} \times \mathbf{n} \qquad (4)$$

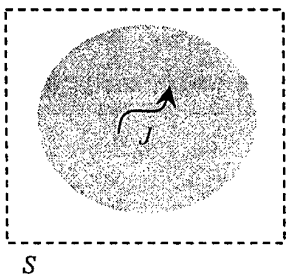



Fig. 3. Second equivalent problem: the actual field is inside the surface S

The Hybrid method presented here, solve the first subproblem by the Method of Moment in time domain, and the second one by the FDTD. This choice is made because the radiation of arbitrarily shaped wire antennas can be easily treated using an integro-differential equation where only the current flowing on the wire is unknown. On the other hand the scattering inhomogeneous object require the direct solution of Maxwell equations to be simulated accurately. Marching on in time procedure for the Method of Moment [2] is used in order to obtain an iterative solution of the problem similar to the FDTD one. In this way the two techniques can be easily interfaced.

## 3. NUMERICAL ASPECTS

The FDTD and the Method of Moment are time domain iterative techniques so they can be affected by problems of numerical instabilities.

Essentially the most critical parameter is the time discretisation step. For the FDTD technique the $\Delta t$ has a superior limit [3]:

$$\Delta t \leq \frac{1}{c\sqrt{\frac{1}{\Delta x^2}+\frac{1}{\Delta y^2}+\frac{1}{\Delta z^2}}} \qquad (5)$$

where $\Delta x$, $\Delta y$ and $\Delta z$ are the lattice spatial steps. More restrictive constraints limit the choice of the time step for the Method of Moment. An investigation of this problem has been made by the authors [4], leading to the conclusion that it strongly depends on the geometrical parameters of the antenna (curvature radius, wire radius and spatial discretisation step $\Delta s$). Some empirical criteria have been determined for the choice of the optimal $\Delta t$ for Moment Method technique, obtaining the following relation

$$\Delta t = \Delta s / nc \qquad (6)$$

In which $n$ is a parameter strictly related to the minimum curvature radius of the arbitrarily bent wire representing the geometry of the antenna. The Hybrid Method suffers from these limitations because the two techniques for being interfaced need a particular relation between the two time steps that have to be equal or at least one multiple of the other. Depending on the specific problem to be analysed, the choice of the $\Delta t$, for one of the two techniques can be very restrictive, compelling the other one to work in an oversampling condition. For example, if the problem is the analysis of the electromagnetic coupling between a cellular phone and a human head, when the radiating structure is a normal mode helical antenna, the Method of Moment need a very small $\Delta t$, compared to the upper limit of the FDTD. In this case the FDTD works in a temporal oversampling condition.

Another situation can be a straight dipole radiating a high dielectric constant scatterer. The upper limit of the FDTD could be less than the optimal $\Delta t$ for the MoM, so, because of the strict relation between the spatial and time step of MoM, it has to work in temporal and spatial oversampling conditions.

However these oversampling requirements do not affect the accuracy and efficiency of the Hybrid Method, that performs very well in the analysis of complex scattering electromagnetic problems.

## 4. RESULTS

The results presented here concern a transient EMC problem, and the coupling between antenna and biological tissue.

A typical EMC coupling problem can be a shielded enclosure with an aperture placed near a radiating source represented by a loop. This structure can be assumed as a simplified model of an electronic circuit or a discharge path of an ESD and generally whatever involved a differential mode current. This loop can behave as an antenna, so the signal can couple with the circuitry inside the enclosure.

The problem is modelled as in fig.4

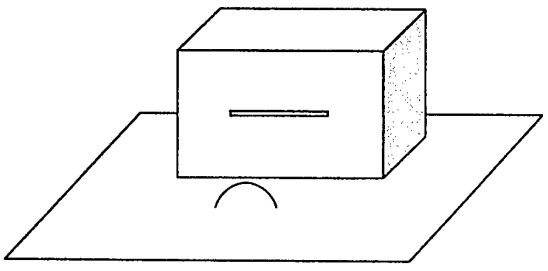


Fig. 4 Shielded box facing a loop.

A rectangular box with a horizontal slot is placed on a conductive plane. The electronic circuit is modelled with half loop facing the box, 7 cm apart from it. The loop is fed with a coaxial cable, and inside the box there is a monopole that senses the field that penetrates into the enclosure through the slot. The box and the slot dimensions are 27x7x16 cm and 12.5x0.25 cm respectively. The receiving monopole height is 6 cm with a wire diameter of 1.8 mm. The loop has a diameter of 4 cm and a wire radius of 0.5 mm.

The input signal is a very fast impulse that can represent as first approximation an ESD.

The parameters for the simulation are chosen considering that in this case the MoM is the technique with the more restrictive requirements. In fact for the simulation of the loop a spatial discretization step of 0.75 mm is the right compromise between an accurate description of the geometry and the stability condition. With this step the temporal $\Delta t$ is univocally determined (0.8 psec). The FDTD unit cell has a dimension of 5 x 5 x 2.5 mm, so from the Courant stability criterion the upper limit for the $\Delta t$ is 7 psec, so for the implementation of the hybrid method a $\Delta t$ of 3.2 psec is chosen for the FDTD.

The excitation used is a raised cosine pulse (fig.5)

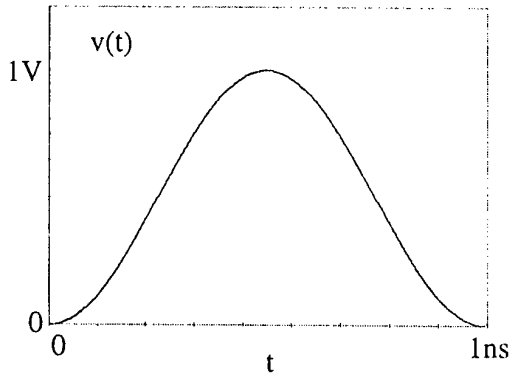



Fig.5. Voltage feeding the loop

$$v_o(t) = \begin{cases} \frac{1}{2}(1-\cos\frac{2\pi t}{T}) & 0 \le t \le T \\ 0 & elsewhere \end{cases} \quad (7)$$

with T = 465 ps.

In the simulation the monopole is loaded with 50 Ω to simulate the coaxial cable effect.

Fig.6 shows the voltage induced on the monopole inside the enclosure.

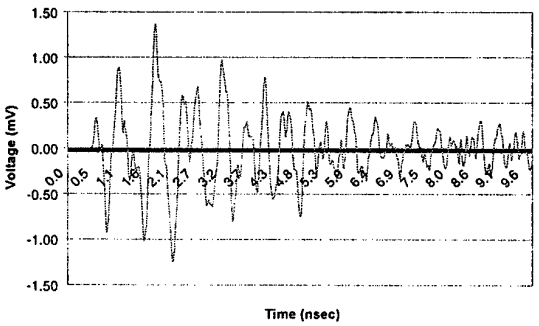



Fig.6 Calculated voltage received by the inner antenna

The induced voltage exhibits many oscillations due to internal reflections and a time duration much longer than the exciting pulse duration. The decay factor depends on the radiation efficiency of the slot. Moreover it can be observed that the induced voltage reaches significant values even if the box is placed along the direction of minimum radiation for the loop: this effect is essentially due to the resonant behaviour of the shielded enclosure.

Another class of problem that can be studied with the hybrid method is the coupling between cellular phone and the human head. Different canonical problems were studied in the past for the assessment of the worst case. The quantity that represents the electromagnetic exposure to RF sources is the Specific Absorption Rate (SAR), i.e. the time-rate of electromagnetic energy deposition per unit-mass: $SAR = \sigma |\mathbf{E}|^2 / \rho$, $\sigma$ being the equivalent conductivity of the medium, $\rho$ the density, and $|\mathbf{E}|$ the *rms* electric field magnitude.

Usually the canonical problems that were studied regard the straight dipole or monopole, so there are a lot of results on these structures. A more update problem needs the study of the more commonly used antenna in cellular phone, that is the helical antenna.

The canonical problem presented here is a helical antenna that radiates a three-layered sphere (fig. 7), representing three tissue of the human head (skin, skull and brain). The inner sphere (6.75 cm) is wrapped by two layers of thickness 2.5 mm each.

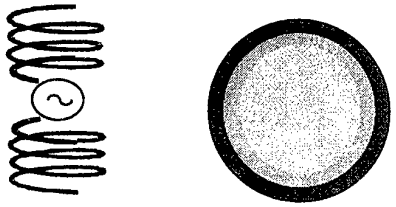


Fig. 7. Helical antenna radiates a three-layered sphere

The antenna is a 4+4 turns helix in the normal mode of radiation, with a 1 Volt feeding voltage characterised by the following geometrical parameters helical diameter D=5 mm, pitch angle $\alpha$=4.55°, helical step S=1.25mm, wire radius a=0.098 mm. The parameter for the MoM are $\Delta s$= 0.58 mm and consequently $\Delta t$= 0.65 psec. The FDTD unit cell is 2.5 x 2.5 x 2.5 mm, and the $\Delta t$ used is 1.3 psec.

Fig.8 shows the peak SAR inside the sphere for a 1.71 GHz excitation of the helix.

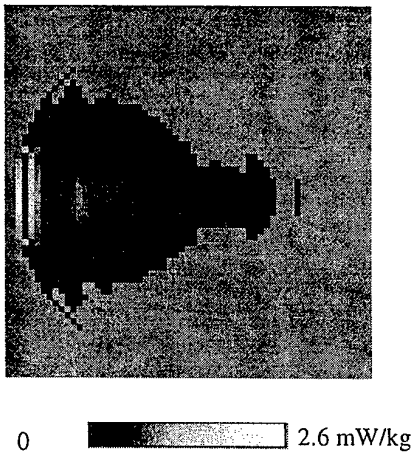



Fig. 8 Distribution of the peak SAR on the plane centered on the sphere.

This result highlights the capability of the hybrid technique to analyse very small and curved radiating structures, which could be not studied by a pure FDTD algorithm.
Concerning the SAR distribution, there is a hot spot concentrated in the region facing the antenna. As expected the maximum SAR occurs in the external layer, however a not negligible field penetration is observed inside the lossy sphere, because of the focusing effect of the curvature. In particular the field is characterised by oscillations due to the spatial resonances.

## 4. CONCLUSION

A hybrid technique in time domain is presented for the solution of EMC problem. The choice of the time domain allows the solution of transient problem involved very fast signal such as ESD. The use of the equivalence principle allows separating the problem in sub-domains where the more appropriate numerical technique can be applied. The results presented shows various cases that can be studied with this technique.
A further investigation of the method is being performed for allowing also the solution of problems that involve the coupling between scatterer and objects physically connected.

## 5. REFERENCES

5.1. G. Cerri, R. De Leo, V. Mariani Primiani, P. Russo, G. Tribellini, "Development of a Hybrid MOMTD/FDTD technique for EMC problems: analysis of the coupling between ESD transient fields and slotted enclosures" (English), International Journal of Numerical Modelling, Vol. 12, No. 4, July-August 1999, pp.245-256.

5.2. S.M. Rao, T.K. Sarkar, and S.A. Dianat, "A novel technique to the solution of transient electromagnetic scattering from thin wires", (English), *IEEE Trans. on Antennas and Prop., vol.34, no.5, May 1986*, pp.630-634.

5.3 A. Taflove, "Computational Electrodinamics. The Finite Difference Time Domain Method", Artech House, 1995.

5.4 G. Cerri, S. Chiarandini, P. Russo, "Numerical aspects in time domain modelling of arbitrarily curved thin wire antennas" (English), International Journal of Numerical Modelling, Vol. 12, No. 4, July-August 1999, pp.245-256.

## BIOGRAPHICAL NOTES

Graziano Cerri (MS '81) is associate professor of microwaves in the Department of Electronics at the University of Ancona. His research is mainly devoted to the EMC problems, to the analysis of the interaction between e.m. fields and biological bodies and to microstrip antennas.

Roberto De Leo (MS '65) is a Full Professor of EMC at the University of Ancona, Italy. From 1966 to 1980, he worked on microwaves at the University of Bari. In 1976 he was appointed Full professor of microwaves. In 1980, he joined the University of Ancona, where he currently works. His research interests are medical application of electromagnetics waves and EMC.

Valter Mariani Primiani (MS '90) is the responsible technician for the EMC laboratory at University of Ancona. His area of interest in electromagnetic compatibility concerns the prediction of differential and common mode radiation from digital PCBs, radiation from apertures in metallic enclosures, the effects of ESD indirect coupling and the analysis of emission and immunity test methods.

Paola Russo (MS '95) received the PhD degree in Electronic Engineering at the Polytechnic of Bari in April 1999. Presently, she is working with a research contract in the Department of Electronics at the University of Ancona. Her main research topics are on the application of numerical modelling to EMC problem.

Simona Chiarandini (MS '98) is currently working toward her PhD in Electronic Engineering in the Department of Electronics at the University of Ancona. Her main research interests are the numerical technique in EMC problems and the analysis of microwave antennas.

EMC 2000 INTERNATIONAL WROCŁAW SYMPOSIUM ON ELECTROMAGNETIC COMPATIBILITY

# ON THE MAXIMUM OVERVOLTAGES INDUCED IN LOW VOLTAGE POWER INSTALLATION NETWORKS DUE TO INDIRECT LIGHTNING FLASHES

Arturo Galván and Vernon Cooray
Institute of High Voltage Research, University of Uppsala, Sweden
Fax: +46 18 502619 e-mail: Arturo.Galvan@hvi.uu.se

*A comprehensive study about the maximum overvoltage induced in Low Voltage Power Installation (LVPIs) networks due to indirect lightning flashes is presented. The aim of this paper is to discuss and analyze the maximum overvoltage one might expect for different geometrical conditions and different loads connected to the installation. The analysis includes the effect of the angle of incidence of the lightning electromagnetic field and the role of the soil conductivity in the evaluation of the lightning induced voltages.*

*It is shown that the wave shape of the induced voltage strongly depends on the values of the loads connected to the LVPI. For infinite soil conductivities and high-value loads, a relation as simple as vertical electric field times the height of the electrical installation gives us the maximum induced voltage that one might expect. However, horizontally large structures located in low soil conductivity increases the total induced voltage. For low-value loads connected to the LVPI, the major contribution to the total induced voltage comes from the interaction of the horizontal electric field with those conductors located horizontally.*

## 1. INTRODUCTION

Several techniques have been proposed to estimate the lightning induced voltages of LVPI located inside buildings [2-5]. Although these techniques might be very effective in the prediction of induced voltages, they provide scant information about the effect of the geometrical and load conditions of the electrical circuit at the moment of the transient as well as the possible influence of the angle of incidence in the evaluation of the total induced voltage.

To be calculated by means of a rigorous theory and real LVPIs (including loads varying in time) the analysis needs important computation time, which, for the problem of interest, is still prohibitive. The complexity of analyzing real installations is overcome by using simple circuits and mathematical tools based on the superposition concept valid for linear systems. The transient response of LVPIs to lightning electromagnetic fields is evaluated by using the Agrawal et al. coupling model [1] to simulate the interaction between the lightning electric field components (vertical and horizontal) and the conductors of the LVPI.

The assumptions for the analytical simulations of the interaction between lightning electromagnetic fields and the electrical circuit are the following. a) Neglect propagation effects as the induced pulses travel along the conductors, b) LVPI is electrically small, c) LVPI contain purely resistive loads and d) Each branch of the LVPI is represented by a single conductor.

It is assumed that the electromagnetic fields that impinge the conductors have the same amplitude and wave shape at any point within the LVPI. This is valid as long as the distance between the LVPI and the lightning flash is larger than the size of the LVPI.

It is well known that the load values change in time and that they are better represented in terms of impedance rather than in terms of resistance. However, the absolute value of loads in frequency domain such as computers, washing machines, refrigerators, etc., ranges from only a few tens to several thousands of Ω, for the frequency spectrum of the lightning flash. For the sake of understanding, the loads were represented by purely resistive elements. These resistive elements were represented either by 50 Ω (small loads) or open circuit (large loads). They are referred to in this paper as S-loads and H-loads, respectively. In order to make the circuit even simpler, only one conductor was considered for the LVPI. With this assumption, aspects such as mutual effects between conductors (in case of using two or more

conductors very close each other) and the effect of the insulating sheath when a cable array is used are avoided. Also, the mutual effects generated in the intersections between vertical and horizontal conductors were neglected.

## 2. ANALYTICAL SET-UP

Figure 1 shows the electrical circuit used as LVPI network. The parameter *R#* corresponds to the resistive loads, *d* is the length of the circuit, *w* is the width, *h* is the height. The wave front of the electromagnetic field impinging the circuit is also depicted in Figure 1 and this single direction of incidence was used in all the cases for a fixed angle.

The incident vertical electric field pulse used in the analytical study was extracted from experimental data, corresponding to a cloud-to-ground flash 150 km far from the LVPI network measured in the meadow near the main building of the Institute of High Voltage Research. Thus, the vertical electric field is purely radiation and the horizontal electric field was calculated by using the wave tilt formulation [6-7]. Figure 2 shows the vertical and horizontal electric fields used as excitation. For the case of horizontal fields, soil conductivities of 0.01, 0.001 and 0.0001 S/m were assumed. In the analysis, two different circuits were used: one small referred to as c-small circuit (*d=3.0 m, w=1.0 m, h=3.0 m and a=1.5 m*) and one larger referred to as c-large circuit (*d=30.0 m, w=10.0 m, h=3.0 m and a=1.5 m*).

The Agrawal et al. coupling model [1] was used to simulate the interaction of the electric field parallel to ground with the horizontal conductors and the electric field perpendicular to ground with the vertical conductors of the network of conductors in the LVPI. The mathematical procedure is similar to that proposed by Galván et al. [8], in which the ATP-EMTP program is used to keep track the voltage and currents signals along the conductors.

## 3. RESULTS AND DISCUSSIONS

### 3.1 High loads and infinite soil conductivity

Figure 3(A) shows induced voltage in both c-small and c-large circuits with only one H-load connected at R1. Curve (a) represents the simple calculation Vertical Electric Field times the height of the installation *(Peak Voltage = 3.69 V/m x 3.0 m = 11.08 V)*. Curve (b) depicts the result for the c-large circuit (*10.94* $V_{peak}$ ). Curve (c) illustrates the result for the c-small circuit (*10.35* $V_{peak}$). Figure 3(B) shows how the induced voltage in the c-large circuit vary when the number of vertical conductors is changed from 1 to 11 (the cases 1, 2, 4, 6, 8 and 11 correspond to H-loads). In the calculation, the soil conductivity was assumed to be infinite. It can be observed that in both cases the induced voltage follows the signature of the vertical electric field and that the effect of increasing the number of vertical conductors is to decrease the amplitude of the induced voltage.

### 3.2 Small loads and infinite soil conductivity

Figures 4(A) and 4(B) show the induced voltage in the c-large circuit with one outlet and when the number of vertical conductors is increased. All the loads in the circuit were S-loads and the induced voltage was evaluated at R1. Observe that the induced voltage has a signature similar to that of the time derivative of the vertical electric field, especially for the case of only one outlet. For comparison purposes, the time derivative of the vertical electric field with the amplitude normalized to the amplitude of the induced voltage is also given in the figure.

### 3.3 Low soil conductivity

Figure 5(A) shows the induced voltage in the c-large circuit when 11 vertical conductors with H-loads were used. The induced voltage was evaluated using different soil conductivity values, as shown in the curves. Figure 5(B) shows the same case but for S-loads connected to the 11 vertical conductors. In both figures, curve (a) corresponds to the case when the soil conductivity was very high (reference voltage) and the induced voltage was measured at R1 having H-loads.

It is observed that the soil conductivity plays an important role in large circuits, especially when loads with low values are connected to the network. In the case shown in figure 5(A), observe that the wave shape of the induced voltage changes as the soil conductivity decreases. Moreover, the maximum induced voltage increases as the soil conductivity decreases. For the case shown in figure 5(B), the contribution of the vertical field to the induced voltage is negligible in comparison to the contribution of the horizontal field which increases with increasing horizontal extent of the conductors and decreasing ground conductivities.

### 3.4 Effect of the loads and angle of incidence

In reality, the magnitude of the loads connected to a LVPI varies in time and it is difficult to determine a representative value for calculations. Because of that many calculations were performed by changing the values of the load to estimate the response of the system. Due to lack of space it is difficult to show all the results. Consequently, only

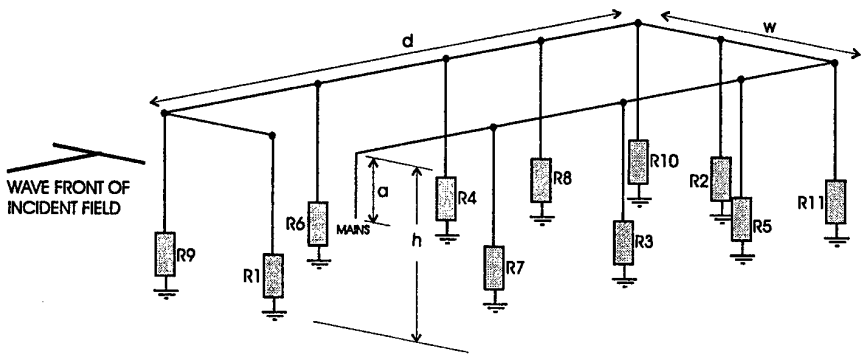



Figure 1. Electrical circuit used in the analytical simulations. The parameter *d* corresponds to the largest part of the circuit, *w* is the width, *h* is the height. The induced voltage was calculated across the loads R1 and R2. The load values were 50Ω (S-loads) and open-circuited condition (H-loads).

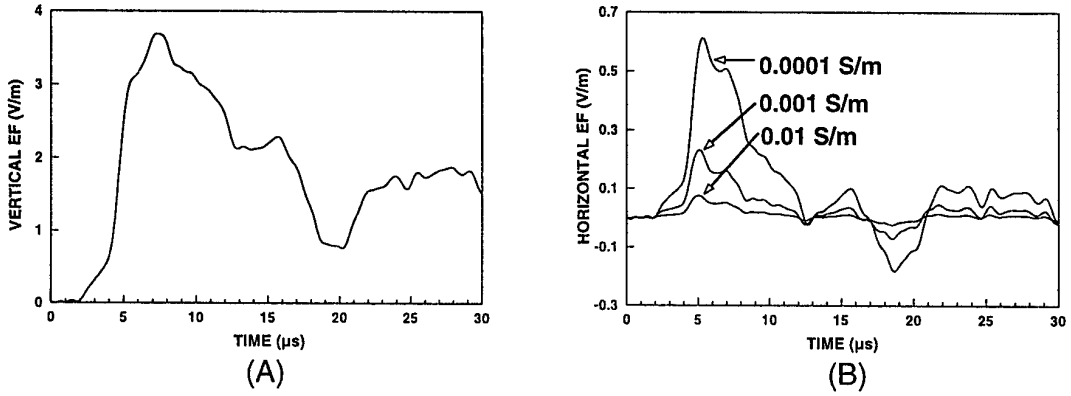



Figure 2. (A) Vertical electric field measured in the meadow near the Institute's building. (B) Horizontal electric field calculated using the wave tilt concept valid for radiation fields.

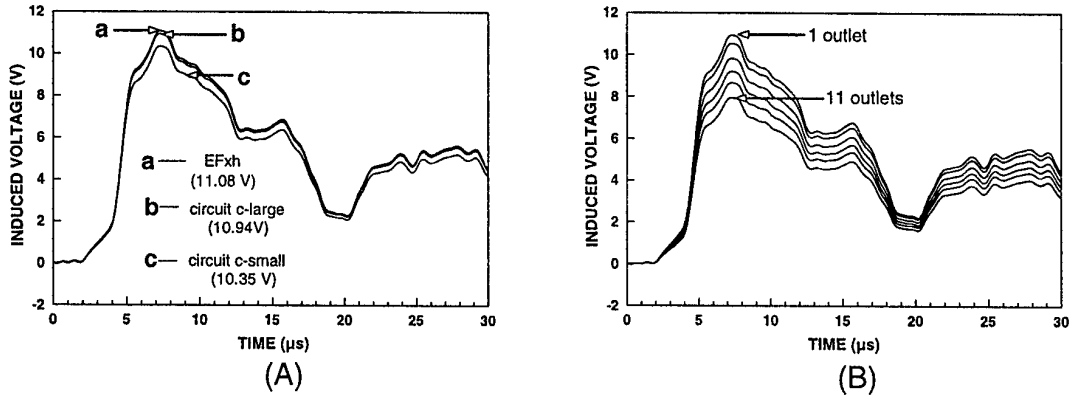



Figure 3. (A) Induced voltage for both c-small and c-large circuits. (B) Induced voltage for the c-large circuit, when the number of vertical conductors is increased (1, 2, 4, 6, 8 and 11) with H-loads. The induced voltage was evaluated at R1. The soil conductivity was assumed to be infinite.

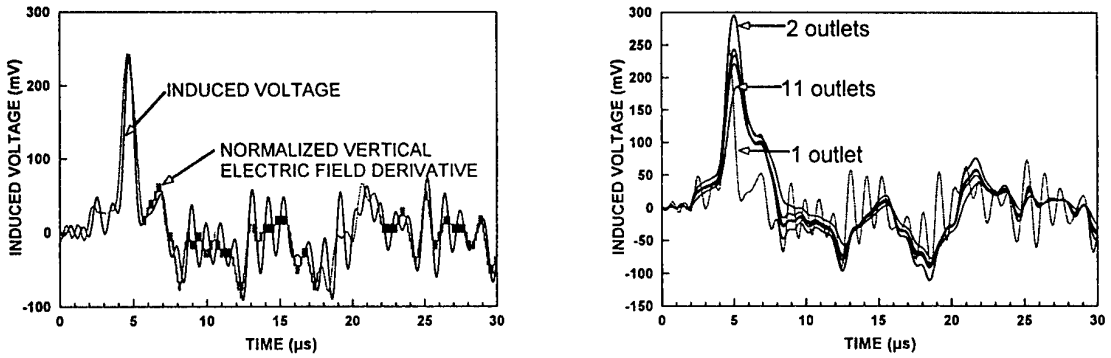



Figure 4. (A) Induced voltage calculated by using the c-large circuit with only one outlet and (B) Induced voltage calculated by using the c-large circuit with 1, 2, 4, 6, 8 and 11 outlets (vertical conductors). The induced voltage was evaluated at R1. Only S-loads were connected to the outlets. In (A) the vertical electric field derivative is normalized to the amplitude of the induced voltage. The soil conductivity was assumed infinite.

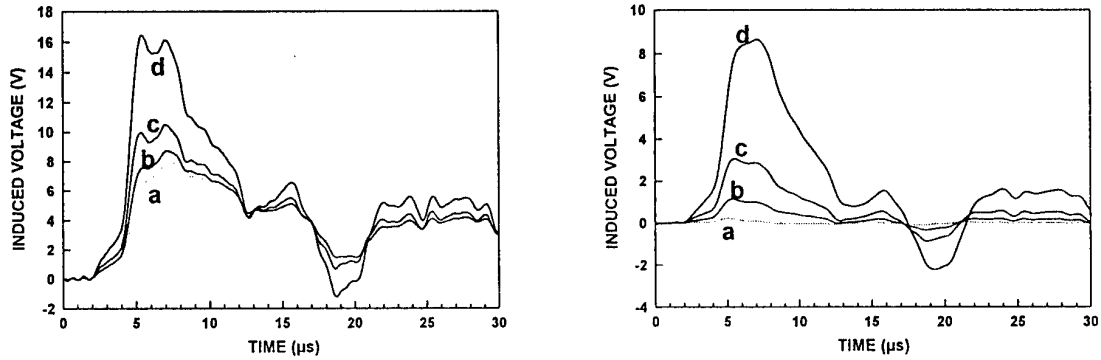



Figure 5. (A) Induced voltage for the c-large circuit with eleven H-loads. The induced voltage was evaluated at R1 with H-loads. A(a) Induced voltage for infinite soil conductivity (used as reference). A(b) Induced voltage for $\sigma$=0.01 S/m. A(c) Induced voltage for $\sigma$=0.001 S/m. A(d) Induced voltage for $\sigma$=0.0001 S/m. (B) Induced voltage for the large circuit with eleven loads. Curves (a) to (d) were evaluated for the same soil conductivity values as for the case (A). In this case, the induced voltage was evaluated at R1 with H-load and S-loads connected to the rest of the vertical conductors.

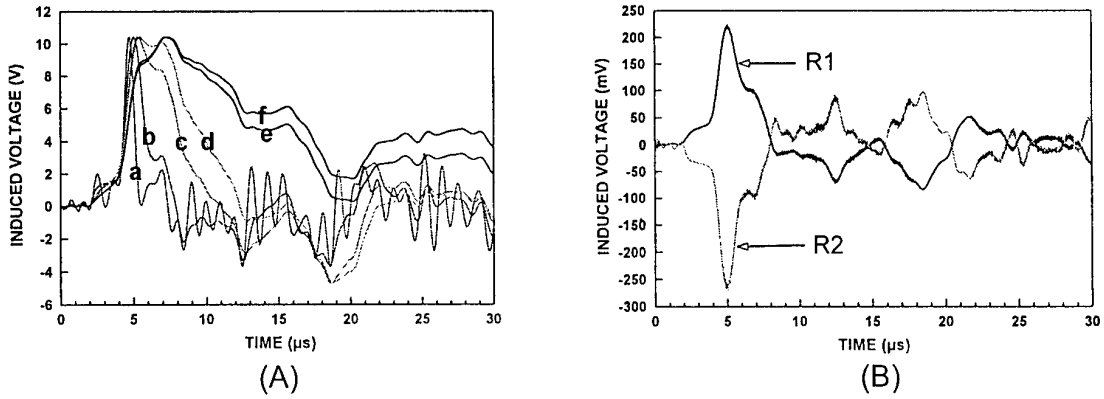



Figure 6. (A) Induced voltage evaluated at R1 for the c-large circuit with two outlets (R1 and R2=1M$\Omega$). A(a) R1=50$\Omega$. A(b) 1k$\Omega$. A(c) 5k$\Omega$. A(d) 10k$\Omega$. A(e) 100k$\Omega$ and A(f) 1M$\Omega$. The induced voltage is normalized to curve (f). (B) Induced voltage evaluated at R1 and R2 for the large circuit with eleven outlets. All the loads were S-loads except at the measuring point (H-load).

two cases will be shown here. One case shows the effects of changing the magnitude of the load and the other the effects of changing the angle of incidence.

Figure 6(A) shows the induced voltage for the c-large circuit when only two vertical conductors were used (R1 and R2). The load value at R2 was fixed at 1MΩ and the load value at R1 was varied from 50Ω to 1MΩ, as indicated in the figure. It can be observed that when R2 is large the wave shape of the induced voltage changes from that of the derivative of the vertical electric field to that of the vertical electric field as R1 increases. For the sake of comparison, all the pulses were normalised to the peak value of the pulse (f), which corresponds to the induced voltage across R1 for 1MΩ. Figure 6(B) shows the case for the c-large circuit with 11 vertical conductors and infinite soil conductivity. All the load values were S-loads, except at the measuring point. The curves illustrate the case when the induced voltage was evaluated at R1 and R2 with R1 = R2. Note that due to the symmetry of the LVPI, the voltage measured at R1 is identical to that observed at R2 when the angle incidence is changed by 180° keeping all other parameters the same. Note that the initial polarity of the induced voltage at R2 was opposite to that of the R1. Note however, that since the ground is perfectly conducting there is no contribution from the horizontal field to the induced voltage. This, we believe is an important result. This is the case since the change in polarity of the induced voltage at the termination of power lines when the angle of incidence is changed from 0° to 180° is caused by the interaction of the horizontal field with the conductors. The results presented here show that, depending on the loads and the angle of incidence, the polarity of the induced voltage may change from one point to another in the LVPI even in the case in which the vertical field is the only source that contributes to the induction.

## 4. CONCLUSIONS

By using computational simulations, it was shown that the amplitude and wave shape of lightning induced voltages in LVPI networks strongly depends on the values of the loads connected to the LVPI. A relationship as simple as vertical electric field times the height of the electrical installation gives us the maximum induced voltage when very high load values are connected and for infinite soil conductivity. However, the geometrical conditions of the installation and the soil conductivity impose severe restrictions in the use of that simple relationship. On the one hand, horizontally large structures located in soils with low conductivity values increases the total induced voltage due to the large contribution to the total induced voltage of the horizontal component of the electric field. On the other hand, the increase in the number of vertical conductors installed in the network reduces the maximum induced voltage impressed on the point of interest for the case of high loads. For very low values of the loads connected to the LVPI, the major contribution to the total induced voltage comes from the interaction of the horizontal electric field with those conductors located horizontally. Finally, it was shown that the change of polarity of the induced voltage is not only produced by the interaction of the horizontal electric field with horizontal conductors, but also by the interaction of the vertical electric field with vertical conductors when the loads and the angle of incidence are changed.

ACKNOWLEDGMENT. A. Galván thanks CONACYT and Instituto de Investigaciones Eléctricas, México, for their financial support. The work reported here is partly funded by a donation to the Institute of High Voltage Research by John and Svea Andersson.

## 5. REFERENCES

[1] A.K. Agrawal, H.J. Price and S.J. Gurbaxani, "Transient response of multiconductor transmission lines excited by a non-uniform electromagnetic field", IEEE Transac. on Electromagn. Compat., Vol. EMC-22, pp. 119-129, May 1980.

[2] H. Pérez, "Transient response of low voltage power installations to natural and simulated lightning electromagnetic fields", Ph.D. dissertation, Institute of High Voltage Research, Uppsala University, Sweden, 1994.

[3] H. K. Hoidalen, "Lightning-induced overvoltages in low voltage systems", Ph.D. dissertation, Norwegian University of Science and Technology, Norway, 1997.

[4] L. Liljestrand and V. Scuka, "Electromagnetic transients in public low voltage power installations", EMC-86, in Proc. *Int. Symp. EMC*, pp. K2:842-850, Wroclaw, Poland, 1986.

[5] Y. Ming, "Lightning electromagnetic environment and interaction to electrical systems", Ph.D. dissertation, Institute of High Voltage Research, Uppsala University, Sweden, 1994.

[6] Cooray V. "Horizontal fields generated by return strokes", Radio Science, Vol. 27, No. 4, pp 529-537, July-August, 1992.

[7] Wait, J.R, Electromagnetic waves in stratified media, Pergamon NY, 1962

[8] A. Galván, V. Cooray and V. Scuka, " Interaction of Electromagnetic Fields From Cloud and Ground Lightning Flashes with an Artificial Low Voltage Power Installation", IEEE-Transactions on Electromagnetic Compatibility, Vol. 41, No. 3, pp. 250-256, August 1999.

EMC 2000 INTERNATIONAL WROCŁAW SYMPOSIUM ON ELECTROMAGNETIC COMPATIBILITY

# MODELING OF THE BASE OF A LIGHTNING RETURN STROKE

Robert L. Gardner
Spectral Synthesis Labs
6152 Manchester Park Circle
Alexandria, VA 22310

*Lightning emits radio frequency energy across a wide spectrum. Most of the high frequencies emitted by the return stroke come from the lowest sections of the channel, where upward and downward channels join. In this paper we examine a theoretical model of the lowest part of the channel and compare the results to some recent optical measurements of the first 400m of the channel. The models are based on linear and nonlinear transmission line models where the elements of the transmission line evolve in response to the current flowing through the channel. Currents in the channel heat the channel and cause it to grow hotter and larger, decreasing its resistance per unit length. A resistive transmission line disperses the channel waveform as it travels causing the leading edge to flatten. A nonlinear resistance per unit length causes a flattening that is observably different from the flattening in the linear version. This same flattening is, at least, qualitatively similar to that observed in recent optical measurements. Evolution of the channel radius is predicted in this paper using a very simple model developed from fluid dynamics. The future role of more complex models is examined.*

## 1. INTRODUCTION

Lightning models can be used in two ways. The first is the first principles model, in which quantitative estimates for physical parameters are derived from assumptions and physical principles. The second method assumes a certain form for the behavior of a variable and derives parameters from fits to data. In the first method, usually pairs of variables are considered, such as current and brightness, or, more often, currents and fields. Transmission line models have been used for the current and an inverted, simplified Green's function used to derive the fields. In this paper, we will use such a model to consider the behavior of the channel near the junction. The lightning process transmits most of its high frequency content from this region so it is important to understand this region.

A lightning channel begins when leaders join, often near the ground, and the return stroke currents start to flow. As currents flow through the channels the air is heated so that the air glows and expands. The hot air acts as a resistor for additional current flow. While the current and brightness are not linear, they are monotonic so that regions of high brightness indicate regions of large current. Further, the resistance of the channel is dependent on the current that has flowed through it. That resistance then governs the current flowing through the channel and the whole process in nonlinear. Gardner [1] described such a system using a nonlinear, nonuniform transmission line model. That model used assumed inductance and capacitance to provide initial velocities similar to observed values and calculated the resistance of the channel from the plasma parameters. We expect the current waveform of such a model to show a softening as the waveform propagates along the resistive channel.

A full transmission line model can be used to treat the current flow in the channel. The losses in the channel will cause the peak current to decay and the channel to broaden as the waveform propagates up the channel. The actual conditions of the channel are not known, since the initial conditions of the arc are not known. This problem has caused these models not to be well accepted since the lack of information leads to final predictions that are not consistent with all observations. In this case, there are new observations that allow us to derive the losses in the channel from observed decay in the waveform.

Have recently published optical data on the behavior of the first 400 m of a lightning channel. The observed waveforms show, qualitatively, the described behavior. In this paper, we will compare and contrast the model and the published observations and use that data to derive a simple estimate of the conditions inside the channel.

## 2. BASE OF THE CHANNEL

A lightning return stroke begins when the upward going leader joins a downward moving leader about 10 m above the ground. A description of the process is in Gardner, et al. [2]. A current forms at the joining point and the two waves travel away from each other. The downward going wave travels only a short distance

before being reflected from the ground and then joins the upward going current. There is a schematic of the process in fig. 1. Since the channel has resistive losses, which manifest in the emission of electromagnetic waves, sound and light, the current wave distorts and flattens as it travels. The origin, then, of most high frequency waves is near the base of the channel.

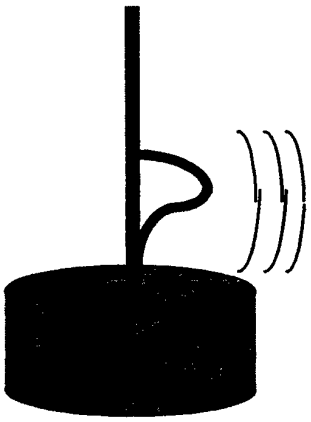


**Figure 1: Schematic of the Base of a Lightning**

In the remainder of the paper we will explore both experimental and theoretical evidence of this picture of the behavior of the base of the channel.

Transmission line models are often used in describing the behavior of a lightning return stroke current [3]. However, the models are only occasionally complete, in the sense that resistance and conductance losses are included. Even less often are nonlinear terms included. Equations 1-3 describe a low loss line.

$$V = Ae^{-\gamma z} + Be^{+\gamma z}, \gamma = \alpha + j\beta \quad (1)$$

$$\alpha \approx \frac{R}{2\sqrt{L/C}} + \frac{G\sqrt{L/C}}{2} \quad (2)$$

$$\beta \approx \omega\sqrt{LC}\left[1 - \frac{RG}{4\omega^2 LC} + \frac{G^2}{8\omega^2 C^2} + \frac{R^2}{8\omega^2 L^2}\right] \quad (3)$$

Equation (1) describes the movement of the channel in the frequency domain with $e^{i\omega t}$ time variation. $\alpha$ represents the decrease in magnitude as the wave travels up the channel and $\beta$ describes the dispersion of the wave as it travels. L, C, G and R are the inductance, capacitance, conductance and resistance per unit length of the channel.

The observable for the current traveling up the channel is the optical brightness of the channel. While the optical emission does qualitatively represent the current pulse as it travels up the channel, there are some important differences [4]. First, the brightness is not linearly proportional to the brightness. Second, the optical emission will lag the passage of the current since the channel requires time to heat the 1-2 eV threshold required for optical radiation. If we still approximate the current as being monotonic with the brightness, we can learn something of the behavior of the channel near the ground.

Derivation of a unique velocity of a wave traveling along a channel is somewhat difficult since the shape of the current waveform changes with height along the channel. Using the peak will give an under estimate of the velocity since the peak retreats away from the leading edge with propagation. Examination of equations 1-3 shows that the leading edge (high frequency limit) travels without reduction from the lossless transmission line velocity. As we move along the wave (admit lower frequencies) the peak recedes providing a lower and lower estimate of the velocity of the leading edge of the current. The proper way is to measure the velocity of the leading edge, but that measurement is often limited by signal to noise considerations.

It is sometimes difficult to effectively associate the capacitance of the channel with a transmission line model since the capacitance requires a second conductor. Part of the association is empirical, but part is represented in the storage of charge in the corona around the return stroke [5].

## 3. EXPERIMENTAL DATA

Uman [6] contains a general development of the theory and supporting experiments associated with the development of a lightning return stroke. Data supporting the transmission line like description includes both optical and electromagnetic measurements. The concept of the upward and downward leaders joining to initiate the return stroke is discussed in Uman [7] and Berger [8]. Recently, Wang, et al have presented some specific optical measurements that detail the optical emission of the lowest 400m of a return stroke.

Wang, et al [9] show a sequence of waveforms of the optical output of the channel. Their optical system provides approximately 30m spatial resolution and 100ns time resolution. In addition, some of the measurements were limited by saturation of the optical sensors.

There were two data sets for return strokes presented that were taken on 2 Aug 1997. The first and most interesting set for our purposes was the set taken at 21:17 UTC. The second set was taken 10 minutes later at 21:27 UTC. Both were measurements of rocket-triggered lightning. The triggering, of course, confuses our model of the way the channels joint near the ground, but the details of that argument are not critical to this paper.

The first brightness plot that was taken at 13m height in the first data set is not saturated, but shows a complete profile. The second one that is taken at 38m is saturated. If the joining model is correct there would be a doubling of the current in the channel as the ground reflection joins the direct wave, we would expect an increase in the brightness just above the joining point.

We estimated the current waveforms for those measurements that were saturated and concluded that the channel brightness decreased by a factor of about three with the propagation over the 400m observed length. The risetime also increased by about a factor of three over the observed length from a little less than a microsecond to a little less than three microseconds. These changes are estimates and could be improved if the complete data were available.

We also examined the leading edges of the waveforms in the published plots and estimated that velocity as 1.3 X $10^8$ m/s. Using the peaks of the plots would have yielded a lower value.

## 4. TRANSMISSION LINE MODEL

The methods of Tesche, Ianoz, and Karlsson [10] were used to construct a numerical transmission line model in the time domain. In the first model, only linear parameters were used, but otherwise all elements of the transmission line were present. The velocity of the leading edge of plots was used for one relationship for L and C. An estimate of the channel impedance of 200 Ω was used for the other relationship. A resistance of 1.6 Ω/m was found to fit the data best.

Figures 2 shows the results of the calculation at the base, middle and top of the channel. The magnitude of the pulse has decreased by a factor of three as it was forced to do by the choice of the resistance per unit length. The dispersion is not as large as it should be to match the data. The solid lines show the velocity of the leading edge, that is held constant at 1.3 X $10^8$ m/s.

The model's complexity was then increased to include a nonlinear resistance per unit length. This model based on what that was originally presented by Strawe [11] and is based on a channel model originally presented by Braginskii [12]. Data was not available at that time to support Strawe's parameter choices. The more complex model of Gardner [1] was not yet available for this presentation, but should be available for later additional calculations. It should be noted that the expansion of the channel in time and its energy balance is not a solved problem. The complex nature of the various reactions in air that result in the conducting channel require that we approximate the air's behavior. The model presented here is a compromise between a very detailed calculation of the air chemistry and properly treating the macroscopic behavior of the lightning channel.

Equation 4 shows the development of the conducting channel radius as a function of the integrated history of the current, i and conductivity σ. The initial radius is chosen as 1 cm and the radius then evolves in time. The resistance per unit length can be found from the radius by multiplying the assumed constant conductivity of 1.4 X $10^4$ S/m by the channel radius.

Detailed calculation of the air chemistry and properly treating the macroscopic behavior of the lightning channel.

Equation 4 shows the development of the conducting channel radius as a function of σ. The initial radius then evolves in time. The resistance per unit length can be found from the radius by multiplying the assumed constant conductivity, 2.22 X $10^4$ S/m, by the channel area.

$$a^2(t) = a_0^2 + \int_0^t \left[\frac{i^2(t)}{\sigma}\right]^{\frac{1}{3}} dt \qquad (4)$$

Fig. 3 shows the evolution of this model for the channel base, middle and top. The dispersion for this model is closer to that observed but not up to model fidelity that is likely to be possible. Increases in the model complexity and fidelity will, hopefully, improve agreement.

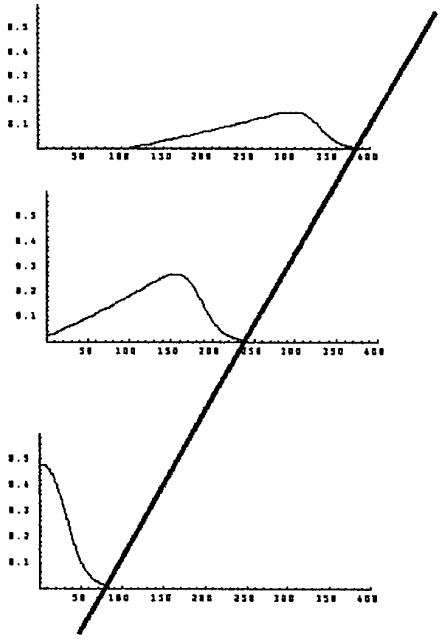


**Figure 3: Progression for Linear Transmission Line Model**

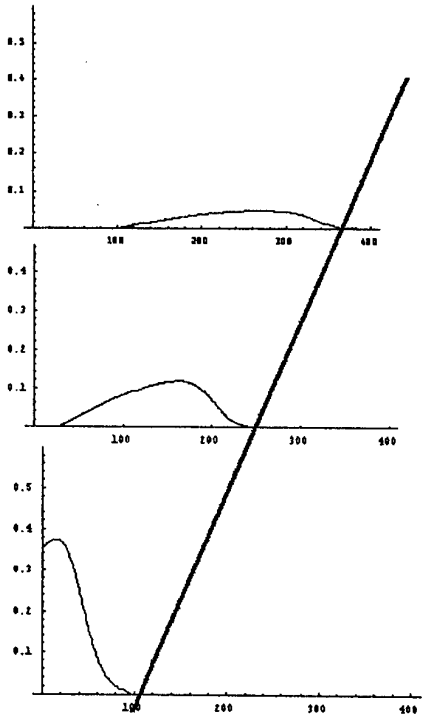


**Figure 2: Progression for Nonlinear Transmission Line Model**

## 5. CONCLUSIONS

Understanding the lowest part of the lightning return stroke is very important if one is to understand the high frequency radio frequency emission of the lightning channel. In this paper, linear and nonlinear transmission line models were applied to the evolution of the channel brightness in the lowest 400m of the channel. The models were effective at predicting certain changes in the optical waveform given that the brightness is monotonic with the current. The type of model development has not been often applied to lightning channels because of the difficulty in knowing the initial conditions required for effective use of such models. The author hopes that future lightning data will help improve this situation.

## 6. REFERENCES


6.1. R. L. Gardner, *A Model of the Lightning Return Stroke*, Thesis, University of Colorado, 1980

6.2. R. L. Gardner, et al., "Comparison of Published HEMP and Natural Lightning: in *Lightning Electromagnetics*, R. L. Gardner, ed., Hemisphere, New York,1990.

6.3. M. A. Uman, *The Lightning Discharge*, Academic Press, Orlando, 1987 p. 138.

6.4. A. H. Paxton, R. L. Gardner and L. Baker, "Lightning Return Stroke, A Numerical Calculation of the Optical Radiation, in *Lightning Electromagnetics*, R. L. Gardner, ed., Hemisphere, New York, 1990.

6.5. C. E. Baum and L. Baker, "Transmission Line Model", in *Lightning Electromagnetics*, R. L. Gardner, ed., Hemisphere, New York, 1990.

6.6. M. A. Uman, M, *The Lightning Discharge*, Academic Press, Orlando, 1987, App. A.

6.7. M. A. Uman, *Lightning*, McGraw-Hill, New York, 1969.

6.8. K. Berger, "The Earth Flash" in Lightning I, Physics of Lightning, R. H. Golde, ed., Academic Press, New York, 1977, p. 175.

6.9. Wang, Takagi and Watanabe, *J. Geophys. Res.*, **104**, No. D12, 14,369-14,376, June 27,1999

6.10. F. M. Tesche, M. V. Ianoz, and T. Karlsson, EMC Analysis Methods and Computational Models, Wiley, New York, 1997, p. 272.

6.11. D. F. Strawe, "Non-linear Modeling of Lightning Return Strokes" in *Proc. Fed Aviat. Administra./Florida Inst. Technol. Workshop Grounding Lightning Technol.*, Melbourne, FL, Mar. 1979, pp. 9-15, Rep. FAA-RD-79-6.

6.12. S. I. Braginskii, "Theory of the Development of a Spark Channel", *J. Exptl. Theoretical Phys.*, **34** (USSR), 1958, pp. 1548-1557.



Dr. Robert L. Gardner received his PhD from the University of Colorado in 1980. He has been active in High Power Electromagnetics since that time and has worked in the EMP, lightning, and high power microwave communities in a variety of positions with the US Navy and the US Air Force. He has published widely in these areas including being the editor and major contributor to *Lightning Electromagnetics*. Dr. Gardner is currently a consultant supporting the Joint Program Office for Special Technology Countermeasures located in Dahlgren, VA.

EMC 2000 INTERNATIONAL WROCŁAW SYMPOSIUM ON ELECTROMAGNETIC COMPATIBILITY

# Lightning Indirect Effects Modeling Applied to Protection Design and Evaluation

M. Ianoz[1], C. Mazzetti[2], C.A. Nucci [3], F. Rachidi [1]

[1] Swiss Federal Institute of Technology, Power Systems Laboratory, Lausanne, Switzerland
[2] University of Rome 'La Sapienza', Dip. Ingegneria Elettrica, Rome, Italy
[3] University of Bologna, Dip. Ingegneria Elettrica, Bologna, Italy

*Abstract* – Considerable progress has been achieved in the last 10-15 years on the modeling of the lightning phenomenon and on the electromagnetic field-to-transmission line coupling. The aim of this tutorial is to emphasize the last developments which took place in the last 2-3 years in particular concerning protection efficiency evaluation using these models and to remind some problems which are still under discussion.

## I. INTRODUCTION

Considerable progress has been achieved in the last 10-15 years on the modeling of the lightning phenomena and on the electromagnetic field-to- transmission line coupling methods (see e.g. [1-4])

The study of disturbances produced by external electromagnetic pulses on transmission and distribution lines, with particular reference to lightning-induced voltages, has been carefully reconsidered in the last years by several researchers. This was motivated by the widespread use of sensitive electronic devices in the power system equipment (circuit breakers, disconnectors, control and protection circuits) and, in parallel, by the increasing demand by customers for good quality in the power supply. Indeed, lightning-induced voltages are responsible of the majority of faults on distribution overhead lines, causing microinterruptions and, more in general, disturbances to sensitive electronic devices.

The so-called "engineering models" [2,3,5] describing the spatial-temporal distribution of lightning return stroke current permit a simple and straightforward approach useful for practical calculations. The use of these models together with the progress achieved in modeling the coupling of the electromagnetic field to multiconductor lines of various geometries as well as to shielded cables permits today to design or to check with a reasonable precision the degree of protection offered by suppressors and by buildings to sensitive equipment.

The aim of this tutorial to emphasize on the validation of these models, on the last developments which took place in the last 2-3 years and to remind some of the problems which are still under discussion.

## II. MODELS

### 2.1 Return Stroke Current Models

A return-stroke model to be employed in the calculation of lightning-induced voltages is a specification of the distribution of the return stroke current as a function of height and time along the lightning channel. This distribution is generally specified in terms of the current at the channel-base, which is a directly-measurable quantity and for which collected statistics are available. A certain number of return stroke models have been proposed in the literature (e.g. [2,3,6]) among which it has been shown that the TL and its more physically plausible modifications [7,8] are a good compromise between simplicity and accuracy in terms of predicted electric and magnetic fields.

### 2.2 Lightning electromagnetic field calculation

For distances not exceeding a few kilometers, the perfect ground conductivity assumption is shown to be a reasonable approximation for the vertical component of the electric field and for the horizontal component of the magnetic field [9,10]. The horizontal component of the electric field, on the other hand, is appreciably affected by the finite ground conductivity. Simplified expressions have been proposed [10-12] which are able to predict with a reasonable approximation electric field at various distance [10,11,13].

### 2.3 Field-to-transmission line Coupling Models

Three coupling models are commonly adopted in the power literature to describe the coupling between lightning return-stroke fields and overhead lines: the model by *Rusck* [14], the model by *Chowdhuri and Gross* [15], and the model by *Agrawal et al.* [16]. Only the *Agrawal* model and its equivalent formulations (*Taylor* et al. [17], *Rachidi* [18]) can be considered as rigorous

within the limits of the adopted hypothesis (transmission line approximations) [19,20].

## III. Experimental Validation of the Coupling Models

The coupling models have been tested by means of natural lightning [21-23] and triggered lightning [24,25]. The use of lightning is complicated by the intrinsic difficulty in performing a controlled experimenting, although triggered lightning is clearly more promising in this respect. The agreement regarding the wave shape can be considered satisfactory, but regarding the intensity, there are still unexplained discrepancies. Possible causes for the disagreement can be: calibration errors, an incorrect determination of the angle of incidence of the electromagnetic wave, uncertainties about the ground conductivity, the presence of trees and other objects in the vicinity of the line, etc..

More controlled conditions can be obtained using NEMP simulators [26-28] or reduced-scale models [29,30].

Indeed, for a relatively complex structure like the model of a three-phase power line with a grounding conductor (Fig. 1), a satisfactory agreement between calculations and measurements is obtained for instance for the current in the grounding wire (Fig. 2) [26].

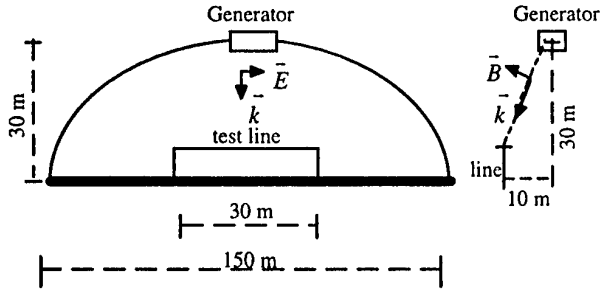



Fig. 1 - Relative position of the three-phase test line under the EMP simulator.

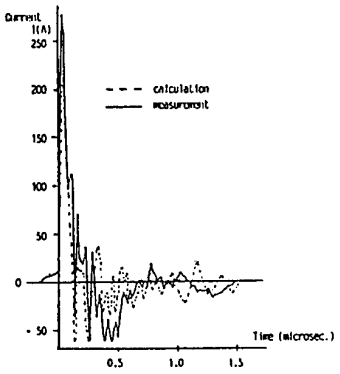



Fig. 2 - Example of comparison between calculation and measurement of current induced at one extremity of the grounding wire (adapted from [26]).

Another example of experimental test using a reduced-scale model developed at the University of Sao Paolo (Brazil) is shown in Fig. 3.

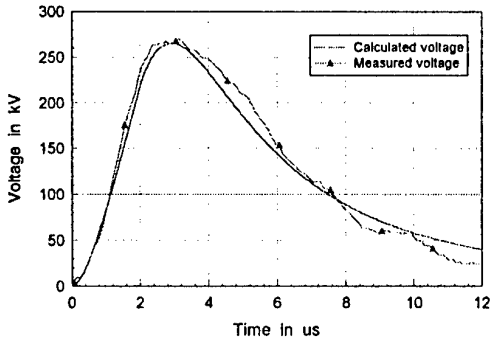



Fig. 3 - Comparison between measurements on a reduced-scale model at the University of Sao Paulo, and simulation results. (For details, see [30])

## IV. Coupling to Shielded Cables

Coupling to shielded cables must take into account a double coupling mechanism, an external one between the incident electromagnetic field and the cable sheath and an internal one between the current induced in the shield and the internal conductor. It is generally assumed that the external circuit is independent of the behavior of the internal circuit. The source terms in the internal circuit are related to the external line response through the transfer impedance and transfer admittance of the cable.

An experimental test of a coupling model to shielded cables [31] was performed using the EMP simulator SEMIRAMIS of the Swiss Federal Institute of Technology in Lausanne.

The considered shielded cable was a 3 m long RG58U connected to metallic boxes at its both ends. The whole arrangement was placed in the center of the working volume of the simulator.

The shield continuity between the cable and the boxes was achieved using good-quality connectors. The current induced in the inner conductor was measured inside the metallic box in order to avoid any interference from the excitation field.

Figure 4 shows a comparison between calculation and measurement for the current on the cable sheath. This comparison represents one more validation example for the field-to-transmission line coupling method discussed under Sect. III.

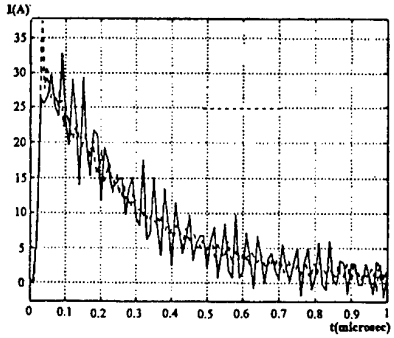



Fig. 4 - Comparison between experiment and calculation performed using the Agrawal model, for the current on the cable sheath. Solid line: measurement, dashed line: calculation (from [32]).

Figure 5 shows a comparison between calculation and measurement for the current on the inner conductor of the cable.

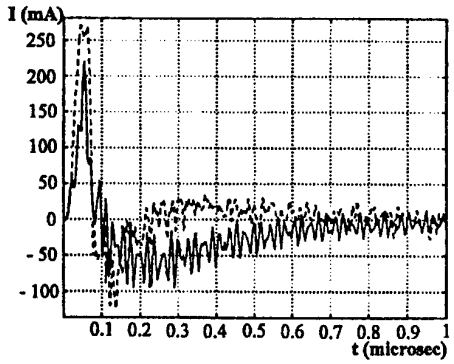



Fig. 5 - Comparison between experiment and calculation performed using the frequency-domain approach of the internal current for example 2. Solid line: measurement, dashed line: calculation (from [32].

## V. Analysis of Finite Ground Conductivity on Lightning-Induced Voltages

Some recent papers on lightning-induced voltages on overhead lines have considered the case of a finitely conducting ground [23,29,33-36]. This represents a major improvement compared to the previous works on the subject, which were assuming the ground as a perfect conductor. Indeed, as shown by the above papers, the ground resistivity can affect markedly the induced voltages, even for stroke locations close to the line. The effect of ground conductivity on lightning-induced voltages is rather complex. It affects both the lightning electromagnetic fields and the surge propagation along the line. Our studies have shown that depending on the position of the stroke location and of the observation point along the line, such a parameter can produce an increase, a decrease, and/or an inversion of polarity of the induced voltages [35-37]. Detailed explanation of the above results has also been given. In Fig. 6 an example is given of the profile of the induced-voltage amplitude along a 1 km long line for the case of a stroke location equidistant from the line terminations.

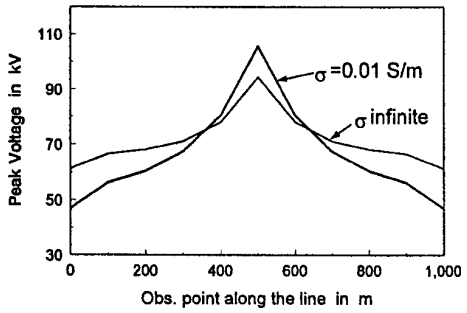



Fig. 6 – Illustration of the ground finite conductivity effect on the lightning-induced voltage peak along a 1-km long, 10-m high line. Lightning location: 50 m from the line center, symmetrical to the line ends (for details, see [37]).

## VI. Application to Realistic Line Configurations: Interface with EMTP

A computer program (LIOV) was developed by the authors which allow the evaluation of lightning-induced voltages on a multiconductor overhead line above a lossy ground (see [38,35] for the theoretical background). The line does not exhibit any discontinuity and is terminated at both extremities on impedances characterized by simple RLC-type circuits. In order to analyze realistic configurations such as a distribution network, the original LIOV code was interfaced with the Electromagnetic Transient Program (EMTP) [39]. Two interfacing methods were developed in collaboration with CESI [40] and EdF [41]. With the developed programs it is possible to compute the response of realistic distribution lines to nearby lightning, and therefore, they can be used for insulation coordination of specific distribution lines (e.g. the optimization of number and location of lightning surge arresters).

Figure 7 shows a low-voltage system configuration for which lightning-induced voltages were computed using the two above-described approaches (Figs. 8 and 9). The stroke location is indicated in the figure by letter F, and the conductors height is 10 m. The lightning return stroke electromagnetic field is calculated adopting the MTL model [7]; the return stroke velocity is assumed to be $1.9 \cdot 10^8$ m/s and the channel-base current peak is 30 kA.

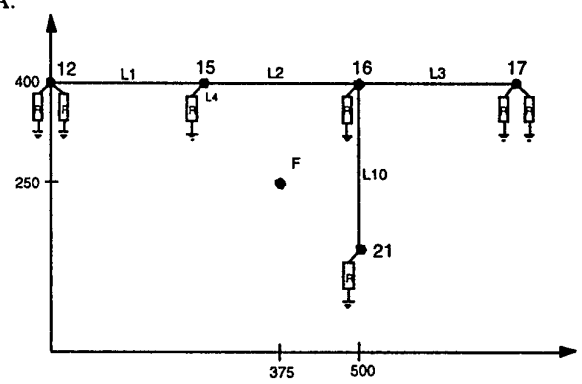



Fig. 7 - Case study system

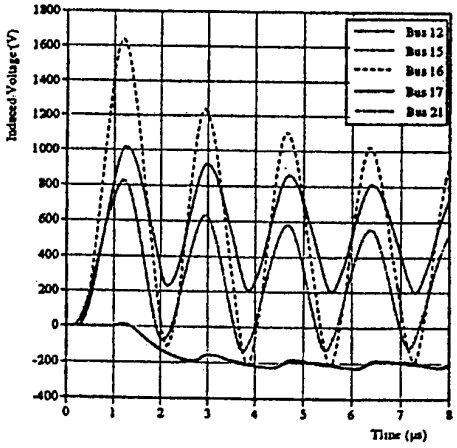



Fig. 8 - Induced voltages at the various buses of the system, with R=5 Ω (from [42]).

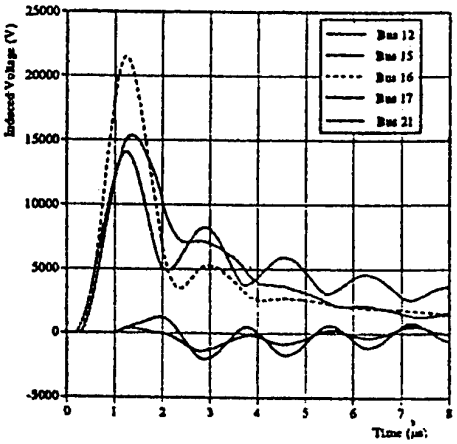
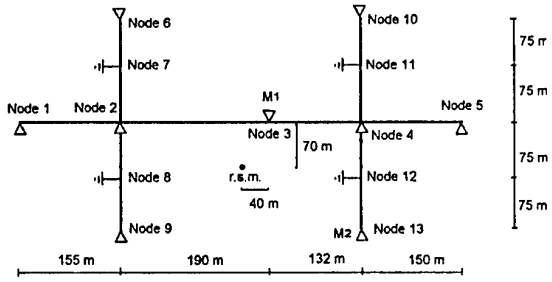



Fig. 9 - Induced voltages at the various buses of the system, with R=100 Ω (from [42]).

Another example of simulation using the LIOV-EMTP code developed in collaboration with CESI is presented in Fig. 10. The experimental results are obtained on a reduced scale model developed at the University of Sao Paulo [30].



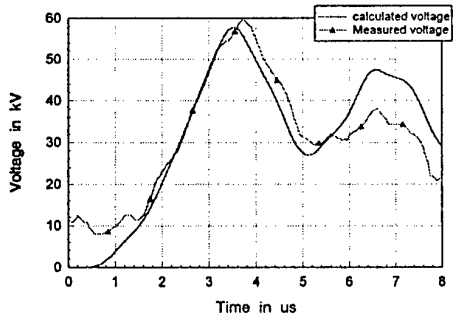




Fig. 10 – Computed and measured (at point M2) induced voltage on a reduced scale model for a complex configuration (see [30] for details).

## REFERENCES


[1] Nucci C.A., "Lightning-induced voltages on overhead power lines. Part II: Coupling models for the evaluation of the induced voltages", Electra, No. 162, pp. 121-145, Oct. 1995.

[2] Nucci, C.A., "Lightning-induced voltages on overhead power lines. Part I: return stroke current models with specified channel-base current for the evaluation of the return stroke electromagnetic fields", Electra, No. 161, pp. 74-102, August 1995.

[3] Rakov V., M.A. Uman, "Review and evaluation of lightning return stroke models including some aspects of their application", IEEE Trans. on EMC, Vol. 40, No. 4, pp. 403-426, Nov. 1998.

[4] R.L. Gardner, "Modeling of the base of a lightning return stroke", Proc. 13th Int. Wroclaw Symp. on EMC, Wroclaw, June 27-30, 2000.

[5] V.A. Rakov, "Lightning Electromagnetic Fields. Modeling and Measurements", Proc. 12th Int. Zurich Symp. on EMC, Feb. 18-20, 1997, paper 11C1.

[6] Thottappillil R, M.A. Uman, "Comparison of lightning return-stroke models", J. Geophys. Res., vol. 98, pp. 22,903-22,914, Dec. 1993.

[7] Nucci C.A., C. Mazzetti, F. Rachidi, M. Ianoz, "On lightning return stroke models for LEMP calculations", Proc. 19th Int. Conf. on Lightning protection, Graz, April, 1988.

[8] Rakov V., A.A. Dulzon, "A modified transmission line model for lightning return stroke field calculations", Proc. 9th Int. Symposium on EMC, Zurich, Switzerland, pp. 229-235, March 1991.

[9] Zeddam A., P. Degauque, "Current and voltage induced on telecommunications cable by a lightning return stroke", Lightning Electromagnetics, Edited by R. L. Gardner, Hemisph. publ. Corp., pp.377-400, 1990.

[10] Rubinstein M., "An approximate formula for the calculation of the horizontal electric field from lightning at close, intermediate, and long range", IEEE Trans. on EMC, Vol. 38, No. 3, Aug. 1996.

[11] Cooray V., "Lightning-induced overvoltages in power lines. Validity of various approximations made in overvoltage calculations", Proc. 22nd International Conference on Lightning Protection, Budapest, Hungary, 19-23 Sept. 1994.

[12] Wait J.R., "Concerning horizontal electric field of lightning", IEEE Trans. on EMC, Vol. 39, No. 2, May 1997.

[13] Rachidi F., C.A. Nucci, M. Ianoz, C. Mazzetti, "Influence of a lossy ground on lightning-induced voltages on overhead lines", IEEE Trans. on Electromagnetic Compatibility, Vol. 38, No. 3, pp. 250-264, Aug. 1996.

[14] Rusck S., "Induced lightning overvoltages on power transmission lines with special reference to the overvoltage protection of low voltage networks", Transactions of the Royal Institute of Technology, Stockholm, No. 120, 1958.

[15] Chowdhuri P., E.T.B. Gross, "Voltage surges induced on overhead lines by lightning strokes" Proc. IEE, Vol. 114, No. 12, pp. 1899-1907, Dec. 1967.

[16] Agrawal A.K., H.J. Price, S.H. Gurbaxani, "Transient response of a multiconductor transmission line excited by a nonuniform electromagnetic field", IEEE Trans. on EMC, Vol. EMC-22, No. 2, pp. 119-129, May 1980.

[17] Taylor C.D., R.S. Satterwhite, and C.W. Harrison, "The response of a terminated two-wire transmission line excited by a nonuniform electromagnetic field", IEEE Trans. on AP, Vol. AP-13, pp. 987-989, 1965.

[18] Rachidi F., "Formulation of the field-to-transmission line coupling equations in terms of magnetic excitation field", IEEE Trans. on EMC, vol. 35, no 3, August 1993.

[19] Nucci C.A., F. Rachidi, "On the contribution of the electromagnetic field components in field-to-transmission lines interaction", IEEE Trans. on Electromagnetic Compatibility, Vol. 37, No. 4, pp. 505-508, Nov. 1995.

[20] Nucci C.A., F. Rachidi, M. Ianoz, C. Mazzetti, "Comparison of two coupling models for lightning-induced overvoltage calculations", IEEE Trans. on Power Delivery, Vol.10, No1, pp 330-338, Jan. 1995.

[21] Yokoyama S., K. Miyake, H. Mitani, A. Takanishi, "Simultaneous measurement of lightning induced voltages with associated stroke currents", IEEE Trans. on PAS, Vol. PAS-102, pp. 2420-2429, Aug. 1983.

[22] Master M.J., M.A. Uman, W.H. Beasley, and M. Darveniza, "Lightning induced voltages on power lines: experiment", IEEE Trans. on PAS, Vol. PAS-103, No.9, pp. 2519-2529, Sept. 1984.

[23] De la Rosa F., R. Valdiviva, H. Pérez, J. Loza, "Discussion about the inducing effects of lightning in an experimental power distribution line in Mexico", IEEE Trans. on PWDR, Vol. 3, pp. 1080-1089, July 1988.

[24] Rubinstein M., A.Y. Tzeng, M.A. Uman, P.J. Medelius, E.W. Thomson, "An experimental test of a theory of lightning-induced

voltages on an overheda lines", IEEE Trans. on Electromagnetic Compatibility, Vol. EMC-31, pp. 376-383, Nov. 1989.

[25] Barker P.P., T.A. Short, A. Eybert-Berard, J.B. Berlandis, "Induced voltage measurements on an experimental distribution line during nearby rocket triggered lightning flashes", IEEE Trans. on PWDR, Vol. 11, pp. 980-995, 1996.

[26] Ianoz M., C. Mazzetti, C. A. Nucci, F. Rachidi, "Response of multiconductor power lines to close indirect lightning strokes", International CIGRÉ Symposium on Power System Electromagnetic Compatibility, Lausanne, Oct. 1993.

[27] Guerrieri S., F. Rachidi, M. Ianoz, P. Zweiacker, A. Borghetti, C.A. Nucci, "Effet d'une impulsion électromagnétique sur des reseaux électriques à plusieurs branches", Proc. 7ème Colloque International sur la CEM, pp. 475-480, Toulouse, 2-4 March 1994.

[28] Guerrieri S., M. Ianoz, F. Rachidi, P. Zweiacker, C.A. Nucci, "A time-domain approach to evaluate induced voltages on tree-shaped electrical networks by external electromagnetic fields", Proc. 11th Int. Symp. on EMC, Zurich, March 1995.

[29] Ishii M., K. Michishita, Y. Hongo, S. Ogume, "Lightning-induced voltage on an overhead wire dependent on ground conductivity", IEEE Trans. on PWDR, Vol. 9, No. 1, pp. 109-118, Jan. 1994.

[30] Nucci C.A., A. Borghetti, A. Piantini, J.M. Janiszewski, "Lightning-induced voltages on distribution overhead lines: comparison between experimental results from a reduced scale model and most recent approaches", Int. Conf. On Lightning Protection, Birmingham, Sept. 1998.

[31] Orzan D., F. Rachidi, M. Ianoz, P. Baraton, F. Audran, "Electromagnetic field coupling to shielded cables: methodology and experimnetal validation", International Symposium on Electromagnetic Compatibility, EMC'96 Roma, September 17-20, 1996.

[32] Orzan D., M. Ianoz, B. Nicoara, "Response of shielded cables to an external electromagnetic field excitation. Modeling and experimental validation", 13th International Zurich Symposium on EMC, Paper 36G3, pp. 185-190, Feb. 1999.

[33] Master M.J., M.A. Uman, "Lightning induced voltages on power lines: theory", IEEE Trans. on PAS, Vol. PAS-103, pp. 2502-2518, Sept. 1984.

[34] Hermosillo V.F., V. Cooray, "Calculation of fault rates of overhead power distribution lines due to lightning induced voltages including the effect of ground conductivity", IEEE Trans. on EMC, 1995.

[35] Rachidi F., C.A. Nucci, M. Ianoz, C. Mazzetti, "Calculation of lightning-induced voltages on an overhead line over a homogeneous lossy ground", IEEE Trans. on EMC, Vol. 38, No. 3, August 1996.

[36] Guerrieri S., M. Ianoz, C. Mazzetti, C.A. Nucci, F. Rachidi, "Lightning induced voltages on an overhead line above a lossy ground: a sensitivity analysis", Proc. 23rd ICLP, Firenze, 23-27 Sept., 1996.

[37] Guerrieri S., C.A. Nucci, F. Rachidi, "Influence of the ground resistivity on the polarity and intensity of lightning induced voltages", Proc. Int. Symp. on High Voltage, Canada, 1997.

[38] Nucci C.A., F. Rachidi, M. Ianoz, C. Mazzetti, "Lightning-induced voltages on overhead power lines", IEEE Trans. on Electromagnetic Compatibility, vol. 35, no 1, Feb. 1993.

[39] Electromagnetic Transient Program (EMTP) Rule Book, Bonneville Power Administration, Portland, Oregon, 1984.

[40] Nucci C.A., V. Bardazzi, R. Iorio, A. Mansoldo, A. Porrino, "A code for the calculation of lightning-induced overvoltages and its interface with the Electromagnetic Transient program", Proc. 22nd Int. Conf. on Lightning Protection, Budapest, 19-23 Sept., 1994.

[41] Orzan D., P. Baraton, M. Ianoz, F. Rachidi, "Comparaison entre deux approches pour traiter le couplage entre un champ EM et des réseaux de lignes", (in French), Proc. 8ème Colloque International sur la CEM, pp. 55-60, Lille, Sept. 1996.

[42] Borghetti A., S. Guerrieri, M. Ianoz, C.A. Nucci, D. Orzan, F. Rachidi, "Link of field-to-transmission line coupling codes to the Electromagnetic Transient Program", International Symposium on Electromagnetic Compatibility, St-Petersburg, Russia, June 1997.

Michel Ianoz (Senior Member IEEE 85, Fellow IEEE 96) was born in 1936. He is presently teaching EMC as a Professor of the Electrical Department of the Swiss Fedetral Institute of Technology of Lausanne and engaged in research activities concerning the calculation of electromagnetic fields, transient phenomena, lightning and EMP effects on power and telecommunication networks.

EMC 2000 INTERNATIONAL WROCŁAW SYMPOSIUM ON ELECTROMAGNETIC COMPATIBILITY

# ASSOCIATIVE MODELING OF INCOMING AND REFLECTED WAVES IN LIGHTNING CHANNEL AND IN STROKED OVERHEAD LINE

M.V. Kostenko
St.Petersburg State Technical University, Russia

*Abstract: The equivalent scheme with lumped parameters has been derived by integration of equations of the systems with distributed linear and non-linear characteristics. The scheme is based on the total current in the lightning channel and on the voltage on wires in the moment before the lightning stroke in a line. The wave processes in lines are also considered.*

**Keywords:** Lightning, Modeling, Waves, And Hyperbolic Equations

## 1. SETTING OF THE MODELING PROBLEM

The experience shows that lightning strokes in the lines even of the highest voltage class can often cause the insulation flashover, the emergency disconnection of lines and the equipment damage. Most of the lightning strokes in the overhead lines (more than 90% in flat country and more than 50% in mountains) have negative polarity. Within a part of millisecond they are developing from thunder center in a cloud towards the earth in a form of stepped leader [1]. The high volume charge surrounding the leader channel arises as a result of the intensive corona discharge. While the leader is approaching the earth from the high aboveground objects (in particular from wire of super high or ultra high voltage line that in this moment has operating voltage of opposite i.e. positive sign) the approaching leaders are developing. From the moment of breakdown of an interval between the converging leaders the wave of return stroke current is developing from earth to cloud. It causes the neutralization of the volume charge surrounding the lightning channel. In a process of switching from leader to return stroke the current in the lightning channel increases in thousands times during a few microseconds. The lightning channel is heating and enlarging. Voltage on the damaged line increases up to millions volts depending on the place of stroke (wire, tower or ground wire). If there are an operating voltage and the voltage induced by lightning on the damaged wire it leads to the increasing of return stroke wave amplitude. As far as heating and enlarging of lightning channel are in progress the velocity of spreading of next stages of return stroke is also increasing. It might be said that they leave behind its previous stages and 'crawl over' them. The spreading velocity of return stroke bright glow remains or even increasing at first in spite of intensive neutralization of surrounding volume charge [2], [3]. It results in a phenomenon that is similar to the ultra sound stroke in air [4]. All these increase the steepness of the front and instant current values are also increased under the first stroke. At the same time the repeat strokes develop along the previously heated lightning channel and their length of the front is decreased but its steepness is increased [5], [6]. The proposed model should reproduce these specific properties of the development of lightning return stroke wave current. The presently widely spread approach describing the return stroke of lightning as a source of 'forced' current with infinitely high internal resistance [5] looks doubtful due to the above mentioned reasons. Associative modeling of lightning stroke should be based on the integration the system of quasi-linear equations in partial derivatives and satisfaction of boundary and initial conditions for currents and voltages in the place of lightning stroke in a line. It is necessary to consider non-linear electrophysical parameters of lightning channel, the wave processes arising in a line, oncoming voltage on the damaged wire etc. However the direct field measurements and oscillogram are obtained only for the currents in the place of lightning stroke in the metallic tower with negligible small resistance of grounding ('calculated lightning currents' $I_{cal}$) [5], [7]. Therefore the model should be based on the logarithmically normal distribution of lightning current parameters [5] with the following density of distribution (Table 1):

$$f(x)=\frac{\exp(-x^2/2)}{\sqrt{2\pi}\cdot x\cdot\sigma_{\ln I}};\ x=\frac{\ln(x/M)}{\sigma_{\ln I}}, \qquad (1)$$

where $\sigma_{\ln I}$ is the logarithmic standard deviation and $M$ is the median parameter for the typical oscillogram $I_{cal}(t)$ (Fig. 1). It should also take into account the approaching voltage on the damaged wire $U_w$.

The rest of initial data can be chosen similar to electrophysical characteristics of breakdown of big air gaps or to the results of other investigations made in laboratory conditions. The oscillogram of currents in Ostankino TV tower [8] and the velocity of lightning channel bright glow [2] can be treated as an indirect check. This work is dealt with the systems of wave equations of hyperbolic type with non-linear parameters (depending on the instant current values) that are different for incoming wave of leader $(i_{Ls};u_{Ls})$ and for the lightning return stroke wave

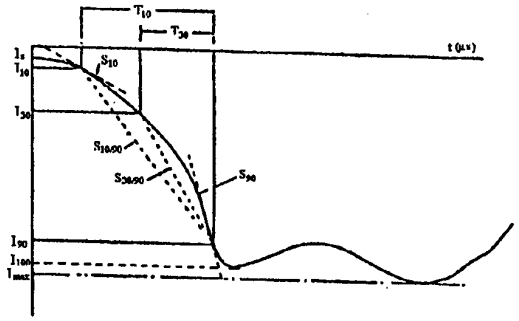


**Figure 1.** Typical oscillogram of the impulse of 'calculated' lightning current $I_{cal}(t)$ [5]

**Table 1.** Parameters of the logarithmic normal distribution for negative downward lightning (Fig. 1)

| Parameter | First impulse | | Subsequent impulse | |
|---|---|---|---|---|
| | M | σ | M | σ |
| Steepness (kA/μs) | | | | |
| $S_{10}$ at 10% | 2.6 | 0.521 | 18.9 | 1.404 |
| $S_{10/90}$ 10-90% | 5.0 | 0.645 | 15.4 | 0.944 |
| $S_{30/90}$ 30-90% | 7.2 | 0.622 | 20.1 | 0.967 |
| $S_{90}$ 90%(max) | 24.3 | 0.599 | 39.9 | 0.852 |
| Crest Current (kA) | | | | |
| $I_{cal}$ (Initial) | 27.7 | 0.461 | 11.8 | 0.530 |
| $I_{final}$(abs. max) | 31.1 | 0.484 | 12.3 | 0.530 |
| Duration (μs) | | | | |
| $t_{f10}=T_{10}/0.8$ | 5.63 | 0.576 | 0.75 | 0.921 |
| $t_{f30}=T_{30}/0.6$ | 3.83 | 0.553 | 0.67 | 1.013 |
| $t_{tail}$ (to 50%) | 77.5 | 0.577 | 30.2 | 0.933 |

outgoing from the place of stroke $(i_{sL};u_{sL})$. There are following expression for all wave: incoming in the node $S$ $(i_{js};u_{js})$ from the neighboring nodes $j$=1,2,$K$ and in the lightning $j$=$L$, reflected waves $i_{sj};u_{sj}$ and boundary conditions in this node $S$ (Fig. 2).

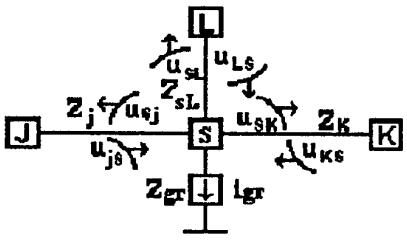



**Figure 2.** The principal scheme of the lightning stroke in the overhead line.

$$u_{js}=Z_{js}\cdot i_{js};u_{sj}=-Z_{sj}\cdot i_{sj};u_{js}+u_{sj}=u_s;$$
$$\sum_{s=1}^{L}(i_{js}+i_{sj})=i_{gr}=u_s/Z_{gr};(j=1,2,...,K,L) \quad (2)$$

The positive directions to node $S$ of the currents in every line $j$=1,2...K, L) including channel of the lightning are supposed to be positive. As a result of the transition from the leader stage to the return stroke the equivalent impedances of the lightning channel are different $(Z_{Ls}>>Z_{sL})$. The phase velocity of the return stroke has to increase with the current and with decreasing of its equivalent impedance [4]. The associative modeling should take these circumstances into consideration

## 2. EQUATIONS OF THE LIGHTNING STROKE IN OVERHEAD LINE

For the modeling of incoming and reflected waves in lightning channel it is necessary to integrate the following approximate system of differential equations in partial derivatives:

$$\partial i/\partial x+\partial q/\partial t+Gu\approx 0;\partial u/\partial x+\partial\Phi/\partial t+E_a\approx 0 \quad (3)$$

where $i,u,q,\Phi,E_a$ are the total current and voltage of the channel, total charge in the channel (taking into account surrounding volume charge), magnetic flux, and longitudinal electric field conductivity to the earth. In this paper an approximate solution of systems (2) is considered in the form of upward and downward current waves. To do this, the following assumptions are made.

### 2.1 Assumptions

1. The boundary effects of all lines ($j$=1,2...$K$, $L$) in node $S$ and the lightning channel conductivity to the earth $(G\cdot u\approx 0)$ will be disregarded.

2. The approximate volt-coulomb characteristics of the corona discharge will be taken similar to the results of the experimental investigations of $V$-$C$ characteristics in laboratory conditions [13,14]:

$$q^*=u^*+K\left(u^*-1\right)^{5/3};K^+=0.78;K^-=0.36 \quad (4):$$
$$q^*=A+B\cdot(u^*)^{4/3};A^-=0.15;B^+=1.02;B^-=0.85$$

where $q^*=q/q_{cr}=f_q(u^*);u^*=u/u_{cr}$, $u$ and $q$ are the total voltage and charge of the channel including surrounding space charge; $u_{cr}$ and $q_{cr}$ are critical corona voltage and charge respectively:

$$u_{cr}=E_{cr}\eta\ln(2h_s/\eta);q_{cr}=E_{cr}\eta/60c \quad (5)$$

where the critical corona field is equal [9]:

$$E_{cr}=3\cdot10^6\cdot\left(1+0.0301/\sqrt{r_L}\right) \quad (6)$$

But for lightning $u_{cr}$ and $q_{cr}$ depend also on the variable radius of the lightning channel $r_l$ unlike the constant radius $r$ of the overhead line conductors. In accordance with [10] it is supposed that the mean value of the current density in the range is $J\approx$22 kA/cm$^2$ for the high rate of the impulse current breakdown. So it leads to assumption that the radius of lightning depends on the current during the front of the current impulse. Thus it is necessary to substitute a new formula instead of formula (4):

$$C_d=\frac{\partial\ q}{\partial\ u}=f_C(i,u^*);\tau_d=\frac{\partial\ q}{\partial\ i}=f_T(i,u^*). \quad (7)$$

where $C$ is the dynamical capacitance of the lightning channel (taking into account the surrounding volume charges) and $T$ is the dynamical delay.

3. The inductance component of the voltage drop:

$$\frac{\partial\Phi}{\partial t}=L\cdot\frac{\partial i}{\partial t};L=\frac{d\Phi}{dt}=\frac{\partial\Phi}{\partial t}+\frac{\partial\Phi}{\partial r_l}\frac{dr_l}{di}\approx\frac{60}{c}\cdot\ln\frac{2h_s}{r_l}$$

Where $L$ is the dynamical inductance depending on lightning radius $r_L=f_r(i)$.

4. The active component of the voltage drop $E_a$ affects the results of calculations very strongly. But there is a little evidence about $E_a$ of the lightning channel. It is assumed that $E_a$ depends only on instantaneous value of the current at the same time and in the same node. In this paper the attempt is made to give an approximate solution of equations (2) in the form of the downwave of the leader and the upwave of the return stroke. A more precise calculation of $E_a$ is the task of further researches and a numerical integration [11] of systems (3).

We consider an approximate solution in the form of $E_a=\partial u_a/\partial x$ where $u_a\approx f_a(i)$ is an active voltage drop at the last streamer-leader zone. Thus $u_a$ depends only on $i$ according to falling volt-ampere static characteristics and dynamic impedance $Z_a$ becomes negative:

$$u_a\approx E_s h_s\left(I_s/i\right)^{\alpha};Z_a=du_a/di\approx-\alpha E_s h_s\left(I_s^{\alpha}/i^{1+\alpha}\right) \quad (9)$$

$$E_s\approx-5\cdot10^5;h_s\approx50;I_s\approx200;\alpha\approx0.15,.or.\alpha\approx0.5$$

where $E_s$, $h_s$ and $I_s$ are electric field, length, and current of the last streamer-leader zone and for $\alpha$ two values will be considered in order to estimate a possible error. So it is obtained:

$$E_a\approx\partial u_a/\partial x\approx(du_a/di)\cdot(\partial i/\partial x)=Z_a\cdot\partial i/\partial x \quad (10)$$

Thus it is supposed that the voltage drop in the arc $u_a$ and its dynamical impedance $Z_a$ depend only on the instant value of the current $i$: $Z_a=f(i)$.

By substitution of equations (4)-(10) into (3) the system of quasi-linear partial differential equations is obtained:

$$-\frac{\partial i}{\partial x}\approx C\frac{\partial u}{\partial t}+T\cdot\frac{\partial i}{\partial t};-\frac{\partial u}{\partial x}\approx L\cdot\frac{\partial i}{\partial t}+Z_a\cdot\frac{\partial i}{\partial x}, \quad (11)$$

where $C$ and $T$ depend on $i$ and also on $u=f_u(i)$ but $L$ and $Z_a$ depend only on $i$. In the first approximation all of them depend on $x$ and $t$ only indirectly through variations of $i$ and $u$. The lightning develops approximately perpendicularly to the Earth surface and $C$ and $T$ change comparatively slowly depending on the height, and these changes will be disregarded as $h_s>>r_l$.

### 2.2 The lightning equations and their solution

The solution: $i\approx i(t,x);u\approx u(t,x)$ of the system of quasi-linear differential equations (11) will be found according to the method of characteristics [12] within the region of change of the variables $t$, $x$, $i$, and $u$ that have the most practical significance where the hyper-surface $f(i,u,t,x)=0$ remains practically "smooth", i.e.:

$$df=\frac{\partial f}{\partial i}\cdot di+\frac{\partial f}{\partial u}\cdot du+\frac{\partial f}{\partial t}\cdot dt+\frac{\partial f}{\partial x}\cdot dx=\varepsilon_f\to0 \quad (12)$$

Under 'characteristics' $\phi(t,x)\approx0$ it is meant such 'geodesic' lines on the hyper-surface (12) on which and also not far from them the solutions for current $i(t,x)$ and voltage $u(t,x)$ remain practically constant and hence their differentials tend to zero

$$di=\frac{\partial i}{\partial x}dx+\frac{\partial i}{\partial t}dt\to0;du=\frac{\partial u}{\partial x}dx+\frac{\partial u}{\partial t}dt\to0 \quad (13)$$

We determine the partial derivatives of $t$ (or of $x$) $\partial i/\partial t=di/dt-(\partial i/\partial x)(dx/dt);\partial u/\partial t=du/dt-(\partial u/\partial x)(dx/dt)$. and substitute them into (11):

$$(\partial i/\partial x)(Z_a-L(dx/dt))+(\partial u/\partial x)=-L(di/dt);\ldots\ldots\ldots\ldots(14)$$

$$(\partial i/\partial x)(1-Tdx/dt)-C(\partial u/\partial x)(dx/dt)=-Tdi/dt-Cdu/dt$$

The solutions of the system (14) relatively to the partial derivatives give the formulae:

$$\partial i/\partial x=D_i/D;\partial u/\partial x=D_u/D, \quad (15)$$

where $D$, $D_i$ and $D_u$ are the determinants equal to:

$$D=\begin{vmatrix}Z_a-L(dx/dt & 1\\ 1-Tdx/dt & Cdx/dt\end{vmatrix},D_i=\begin{vmatrix}L(di/dt) & 1\\ -Tdi/dt+Cdu/dt & Cdx/dt\end{vmatrix};$$

$$D_u=\begin{vmatrix}Z_a-L(dx/dt) & -L(di/dt)\\ 1-T(dx/dt) & -T(di/dt)-C(du/dt)\end{vmatrix}\ldots\ldots\ldots\ldots\ldots\ldots(16)$$

If suppose that $D\neq0$ then it is possible to get the single values of derivatives for the lightning channel: $\partial u/\partial x;\partial u/\partial t;\partial i/\partial x;\partial i/\partial t$. It contradicts to the physical nature of lightning. In the case of $D=0,D_i\neq0;\ D_u\neq0$ derivatives tend to infinity that corresponds to the line of discontinuity and contradicts to the condition of smoothness (12). So $D$ is put to 0 and $D_i=0$ or $D_u=0$ that gives equations for the characteristics $dx/dt$ and for $du/di$:

$$dx/dt=\left(Z_a-T/C\pm\sqrt{(Z_a-T/C)^2+4L/C}\right)/2L;$$

$$du/di=\left(-Z_a-T/C\pm\sqrt{(Z_a-T/C)^2+4L/C}\right)/2 \quad (17)$$

Two real and different characteristics $dx/dt=f(i,u(i))$ are obtained. Thus the system (11) belongs to the hyperbolic type. As $Z_a<0$ the plus sign should be placed before the square root in the equation (17) for the characteristics of downward waves $u_{Ls};i_{Ls}$ of the leader. On the contrary if $dx/dt>0$ the minus sign in (17) for return-stroke upward waves $u_{sL};i_{sL}$ is placed. Thus the system of two differential equations in the form of Cauchy for $du_{sl}/di_{sl}$ and for $du_{ll}/diL_x$ are derived. The parameters $Z_a$, $C$, $T$, and $L$ are nonlinear dependencies on the instantaneous values of total current $i=I_{Ls}+I_{sL}$ and voltage $u=U_{sL}+U_{Ls}$ in the lightning channel.

By the numerical integration of equation (17) under wide variation of characteristics $Z_a=f_z(i)$, $C=f_c(u,i)$, $T=f_t(u,i)$ and $L=f_l(u,i)$ it is received the dependence:

$$Z_{eq}\approx Z_{sL}=u_{sL}/i_{sL}=f(i_L);i_L=i_{Ls}+i_{sL}\ldots\ldots\ldots(18)$$

According to equations (11) the equivalent scheme is obtained (fig.3) for calculating voltage $u_s=u_s(I_{cal})$ on the struck node of line.

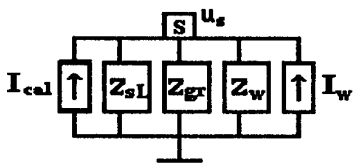



**Figure 3.** Equivalent scheme for calculating of the voltage at the place of lightning stroke in overhead line.

The equivalent impedances of the return stroke $Z_L$ are given in fig.4, according to (17) by increasing the total lightning current" $i_L$ from $i_L$=200 A to $i_L$= 250 kA.
The dependencies $Z_L(i_L)$ can be expressed for the practical calculations by the general approximate empiric formula for the equivalent impedance $Z_{eq} \approx Z_{sL}$ of the return stroke channel of the linear lightning (in Ohms):

$$Z_{eq} \approx 140 \cdot (1+240/i_l); i_L = I_{cal} - u_s / Z_{eq};$$
$$u_s = (I_{cal} + I_w) \cdot (Z_{sL}^{-1} + Z_{gr}^{-1} + Z_w^{-1}) \qquad (19)$$

where $i_L$ and $I_{cal}$ are the actual and 'calculated' (in the case of the stroke if the same lightning in the well-grounded object) [5], [7] lightning current (kA) in the place of stroke, $I_w$ and $Z_w$ are the total current of waves coming along the line wires and their wave impedance, $Z_{gr}$ is impedance of grounding ('watering') of an object damaged by lightning.

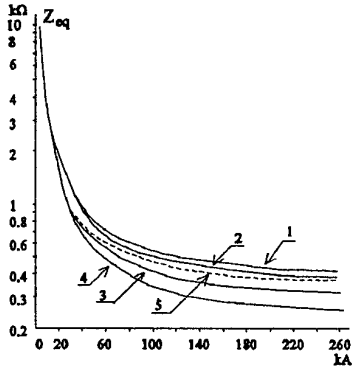



**Figure 4**. Equivalent lightning impedance Zeq calculated by formula (17) depending on the lightning current. Curves 1, 2, 3, 4 with $\alpha = 0.15$; and curve 5 with $\alpha = 0.5$. Volt-coulomb characteristics: [13]-curves 1, 2, 5; [14] curves 3, 4; polarity (-) curves1, 3, 5; and (+)-, curves 2, 4.

In the first moment $(t < 2l_{xj}/c; j = 1,2,...K)$ the voltages (i.e. the operating voltage and induced voltage from lightning in node $X$) are expressed by $2u_{js}=U_{x0}$. But from node $X$ to neighboring nodes $J$=1,2,...$K$ the waves $u_{sj} = -Z_{sj} \cdot i_{sj} = u_s - u_{js}$ are going and after the time $t_{sj} = 2l_{sj}/c$ in node S the waves $u_{js}$ will go. They will be determined by the reflection condition in neighboring nodes $J$. That is why the précised values of $u_s$ may be obtained after 1-2 iterations done according to equations (19). In some case when $u_s/Z_{sL} << I_{cal}$ it is possible to neglect $u_s/Z_{sL}$ and to suppose $I_L \approx I_{cal}$

## 3. BEADED AND GLOBE LIGHTNINGS

The processes connected with the globe and beaded lightnings are much less studied. It is possible to say that it is quite difficult to explain these amusing natural phenomena.
The time of glow of the globe lightning (seconds) and of the beaded lightning (parts of a second) is many orders higher than the time of the impulse of the linear lightning current. It seems that it can be explained by the luminescence of the metastable excited atoms or of the dissociated molecules of the air oxygen or nitrogen. It is especially true for the highly humid air. However at present time there is no convincing universally recognized explanation of the appearance of the luminous restricted in space convex "globe" or "beads".

### 3.1 Beaded lightning

The appearance of the beaded lightning can be explained by the "theta-pinch" instability of the linear lightning channel with quite large steepness of the return stroke current front. It was shown above that due to the current increase the next portions of the front spreads along the more heated channel with the less losses and the higher phase velocity than the previous ones and "leave them behind". It results that the lightning channel cannot enlarge and the "theta-pinch" of the thin lightning channel with the high current takes place (fig. 6).

### 3.2. Globe lightning

The appearing of the globe lightning may be caused by the high intensities of the electric field on the edges of the unfinished branches of the linear lightnings. It may be also caused by the high metal installations (the ship masts,

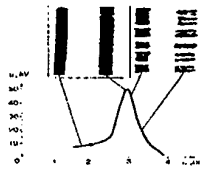


**Figure 6**. The scheme for the arising of MHD bursting instability of conductor as an analogue for appearance of the beaded lightning [15].

television towers, the bell towers etc). Or it may be caused by the "curved" electromagnetic instability of the linear lightning channel. They are especially possible at the places of the accidental curves or branches from the main channel of the linear lightning. Figure 7 displays the sequential stages of the toroid separating; arrows show the corresponding electrodynamics forces. Then due to the heat diffusion this toroid changes its form for the convex one that is the most stable. It becomes close to a sphere and continues to exist and shine due to the electrons returning from the metastable to the normal levels.

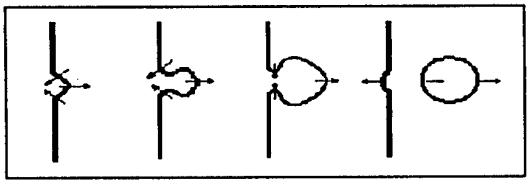


**Figure 7.** Scheme of the appearance of the globe lightning as an 'curved' instability.

## 4. CONCLUSIONS

The analysis of the obtained results allows us to make the following conclusions:

1. The equivalent lightning impedance changes in wide ranges depending on the lightning current but it has comparatively low dependence on the electro-thermal and physical characteristics obtained by the laboratory investigations. Impedance Zeq may be determined according to Figure 4 by the approximate empirical formula (19) with an error of about ±10%.

2.The equivalent impedance is equal to 3-4 kiloohms or more if the current is equal to or less than 10 kA. The main part of the energy is spent on warming up and expanding the lightning channel. An insignificant part of energy is spent on the neutralizing of the volume charges surrounding the channel and on recharging the leader channel. The input impedance of the line at the node of the lightning stroke is, as a rule, lower. So it is possible to regard lightning as a source of current with infinitely large impedance as it was previously recommend but only for the 'preliminary' current $i_L$ <10 kA.

3. The impedance Zeq decreases rapidly down to 800,...,700 ohms in the range of currents from 10 to 60 kA. Half of the energy is spent on the neutralizing of the volume charges and recharging the leader channel.

4. The impedance Zeq becomes stable fewer than 250,350 ohms if the lightning current is high (150,250 kA). It is found that the impedance of the electrical arc is only 10,20% of Zeq.

5. The dynamical characteristics $v = f_V(i,u)$ have the physical sense of the phase velocity and depend greatly on the electro-thermal and physical characteristics of the lightning channel; so it is necessary to make them more precise. It was obtained v << ç for $i_L$ < 10 kA. However the phase velocity increases rapidly while the current increases during the front of the impulse; it becomes stable for the currents 50-250 kA at the level of about 0.2 ç,...,0.4 c.

These results show that one must carry out further investigations concerning reflections from branching of lightning, neutralizing surrounding charges and the leader volt-ampere characteristics. The generalized rule of the equivalent wave (Figures 3) uses the field measurements of lightning current in the node with the stroke and takes into account all reflections from neighboring nodes according to equation (19) and Figure 3.

6.The above-mentioned hypothesis about phase velocity is supported by approximate calculations showing that wave velocity increases rapidly and the next portion of the wave overtakes the preceding one. As a result of this the shock current wave, shock UHF electromagnetic fields and shock wave in the gas (thunder) must arise.

7.The solutions obtained for the equivalent lightning impedance and phase velocity are based on assumptions and generalized characteristics of the impulse-corona discharge, the radius of the lightning channel, and the impedance of the arc. It makes possible to consider the process of transition from the leader-streamer zone to the return-stroke of lightning during initial stages. It also makes possible to solve the complicated system of partial differential equations of lightning in approximate but visual form for the current source, equivalent impedance, return stroke upwave, and leader downwave current. The further investigations are required and comparison of the measured and the calculated electromagnetic fields should be done. Authors believe that the obtained results do not contradict to the results of field measurements of average values of lightning impedance and phase velocity of the bright luminous domain in the return stroke.

## 5. REFERENCES


[1] M.A.Uman, *Lightning,* McGraw-Hill Book Company, New York, 1969

[2] D.M. Jordan and M.A. Uman, "Variations in light intensity with height and time from subsequent lightning return strokes" JGR, vol. 88, pp. 6555-6562, 1983

[3] M.V. Kostenko, *The paradigm of sustainable development: the bioelectromagnetic and informational ecology and higher education*, Textbook, Nestor, St.Petersburg, 1999

[4] M.V. Kostenko, "Electrodynamic characteristics of lightning and their influence on disturbances of high-voltage lines" *JGR*, vol. 100, no D2, pp. 2739-2747, February 1995

[5] "Guide to Procedures for Estimating the Lightning Performance of Transmission Lines", *Working Group 01 (Lightning) of Studies Committee 33 (Overvoltage and Insulation Co-ordination),* Paris, 1991. CIGRE

[6] "Manual on the 6-1150 kV electric nets protection from thunder and internal over-voltages", edited by N.N. Tikhodeev, 2-d edition, St.Petersburg, 1999 (in Russian:Руководство по защите электрических сетей 6-1150 кВ от грозовых и внутренних перенапряжений)

[7] R.B. Anderson and A.T. Eriksson, "Lightning parameters for engineering application" *Electra,* vol. 69, pp. 65-102, 1980

[8] B.N. Gorin and A.V. Skilev, "Measurement of lightning current in television tower in Ostankino" *Electrichestvo,* 8, pp. 64-65, 1984 (in Russian: Б.Н. Горин, А.В. Шкилев. Измерения токов молнии в Останкинской телебашне)

[9] F.W. Peek, *Dielectric Phenomena in High-Voltage Engineering,* 3-d edition, McGraw-Hill, New York, 1929

[10] V.S. Komelkov (Editor), *Techniques of Large Impulse Currents and Magnetic Fields*, Atomizdat,

Moscow, 1970 (in Russian: Техника больших импульсных токов и магнитных полей)

[11] B.N. Gorin, "The closing switch model of lightning return stroke", *Proceedings of 9-th International Conference on Atmospheric Electricity,* vol. I, pp. 206-211, St.Petersburg, 1992 (in Russian)

12] S.A. Christianovich, "About ultra-sound streams of gas *Trans.of TsAGI named after N.E. Zhukovsky, no* 543, pp. 1-43, 1941, (in Russian: С.А. Христианович. О сверхзвуковых течениях газа),

[13] I.M. Bogatenkov, N.I. Gumerova, M.V. Kostenko, A.V. Sozinov and N.N. Tsimerskaia, "Volt-Coulomb characteristics of corona at bundle conductors of impulse voltage. *Proc. Polytechn. Inst. Leningrad,* vol 340, pp. 8-13, 1974 (in Russian: И.М. Богатенков, Н.И. Гумерова и др. Вольт- кулоновые характеристики короны на расщепленных проводах при импульсном напряжении)

[14] B.B. Bochkovsky, "Impulse corona at single and bundle conductors", *Electrichesnvo,* pp. 22-28, 1996 (in Russian: Б.Б. Бочковский. Импульсная корона на одиночных и расщепленных проводах)

[15] A.M. Iskoldsky, N.B. Volkov, and O.V. Zubareva, "The dynamics of large-scale spatial structures in current-carrying fluids and the electric explosion of conductors", *Physica,* D 91, pp. 182-204, 1996 (in Russia)

## BIOGRAPHICAL NOTE

Mikhail Vladimirovich Kostenko was born in Nikolaev (Ukraine) in 1912, electrical engineer, DSc., Corr. Member of Russian Akademie of Science (1962), Foreign Member of Polish Akademie (1988), Professor of Electro-Physic and High Voltage Technique Department of Saint Petersburg State Technical University; Polytechnicheskaia 29, St. Petersburg, 195251, Russia. E-mail: Kostenko@stu.neva.ru

EMC 2000 INTERNATIONAL WROCŁAW SYMPOSIUM ON ELECTROMAGNETIC COMPATIBILITY

# ANALYSIS OF CONNECTOR BEHAVIOUR IN TERMS OF ELECTROMAGNETIC COMPATIBILITY

Edson MARTINOD*, Noël FEIX*, Michèle LALANDE-GUIONIE*, Bernard JECKO**

IRCOM CNRS UMR n° 6615
eMail : Martinod@brive.unilim.fr
WWW : http ://ircom.unilim.fr
* 7 rue Jules Vallès 19100 Brive la Gaillarde, France, phone (33) 05 55 86 73 18, fax (33) 05 55 86 14 26
** 123 rue Albert Thomas 87000 Limoges, France

*Abstract — Theoretical and experimental transient methods are proposed for connector behaviour analysis. From transient results S parameters and radiation losses are deduced, and an electrical far field magnitude is proposed.*

## 1. INTRODUCTION

In the EMC community, it is well known that many non-conformities are caused by electrical links. The identification of the undesired electromagnetic phenomena often comes too late to allow a simple, inexpensive corrective action. So, to reduce these additional costs, prediction tools must be developed. Time domain analysis can be used to evaluate electromagnetic parasitics like radiation losses [1]. Our contribution in this domain more particularly concerns the radiation of localized defect like connectors in a frequency range up to 1 GHz. Several test devices have been designed and analyzed in order to study discontinuity radiation. To illustrate the theoretical and experimental approaches, a slot on a coaxial cable shield is analyzed.

## 2. DISCONTINUITY ANALYSIS PRINCIPLE :

### 2.1. Electromagnetic study

The simulated structure is represented in figure 1 :

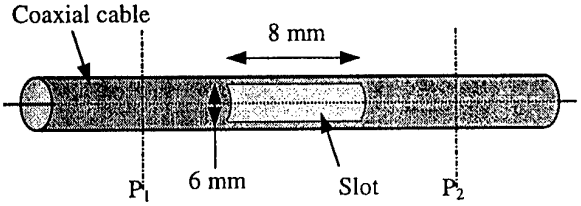



Fig. 1. Simulated structure

The characteristic of the studied structure are the following :

Coaxial cable diameter : 3,2 mm
Core diameter : 0,45 mm
Characteristic impedance of the coaxial cable : 50 Ω

This structure has been modeled and simulated using a 3D Finite Difference Time Domain (F.D.T.D.) algorithm which gives direct solutions of Maxwell's time dependent curl equations [2].
Two reference planes are chosen as shown in Fig. 1. The feeder is simulated by E field components in $P_1$. The components are gaussian shaped allowing a harmonic characterization in a frequency range up to 1GHz.
Transient current evolution on the structure is deduced from the H field circulation around the coaxial core (Fig. 2., Fig. 3.).

Scattering parameters are deduced from the Fourier transform of the incident (in $P_1$) and transmitted (in $P_2$) currents and from that reflected by the discontinuity (in $P_1$) as follows :

$$S_{11}(f)=\frac{F[I_{reflected}(t)]}{F[I_{incident}(t)]} \quad (1)$$

$$S_{21}(f)=\frac{F[I_{transmitted}(t)]}{F[I_{incident}(t)]} \quad (2)$$

The radiated power - incident power ratio is equal to the radiated losses and is deduced by $S_{11}(f)$ and $S_{21}(f)$ as follows :

$$\text{Radiated losses} = 1 - |S_{11}(f)|^2 - |S_{21}(f)|^2 \quad (3)$$

The dissipation power in both metal and dielectric substrate is ignored here.

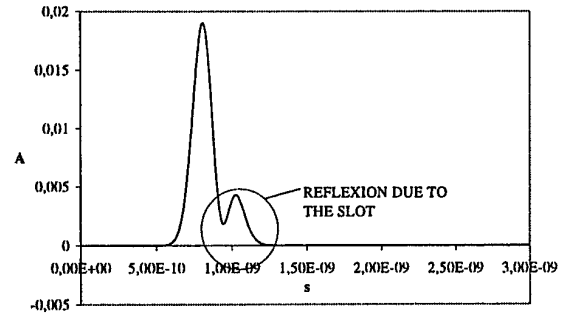



Fig. 2. Transient current before the slot in $P_1$

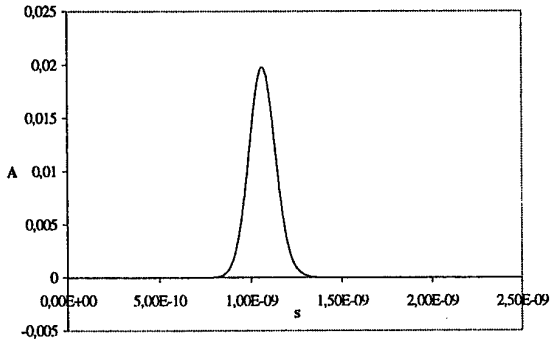



Fig. 3. transient current after the slot in $P_2$

2.2. Experimental configuration

A schematic view of the setup is shown in Fig.4.

All measurements are performed with a pulse generator (300ps rise-time, 2ns pulse width), a digitizing oscilloscope (6 GHz bandwidth) equipped with two voltage probes. All transmission lines used for the experimentation are semirigid coaxial cables.

First, reference voltage is measured while connecting a 50 Ω load directly to the first probe tip adapter (Fig. 5.). After that, the DUT is connected to the probe tip adapter and the voltage reflected by the slot is deduced from the voltage measure (Fig 6). The transmitted voltage is measured by using the second probe tip adapter connected after the DUT (Fig 7).We notice that the curve presented on Fig. 6. allows us to localize the defect and the second probe influences on the coaxial transmission line.

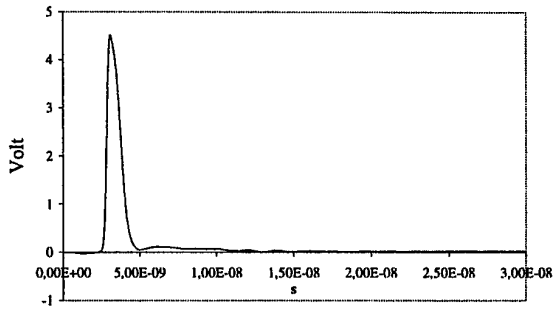



Fig 5 : reference voltage

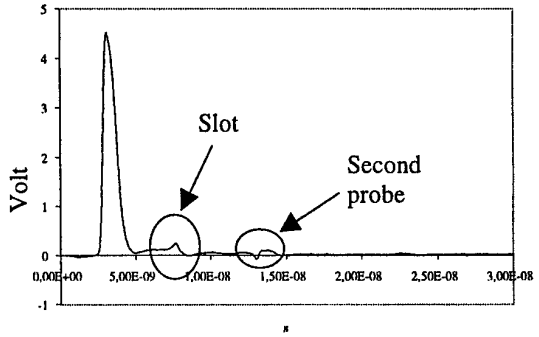



Fig. 6. voltage before the slot

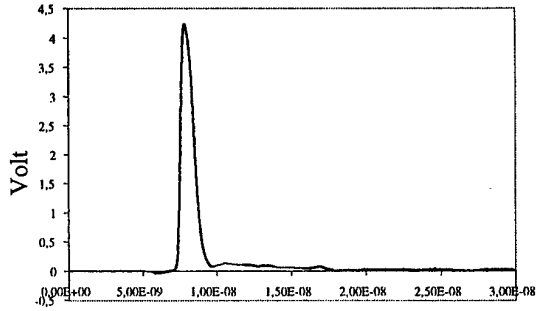



Fig. 7. voltage after the slot

## 3. FREQUENCY RESULTS

Scattering parameters are deduced from the Fourier transform of the incident, reflected and transmitted voltages.

In order to correct experimental systematic errors, a calibration procedure is necessary [3] [4]. This correction is done in frequency domain by using a Short Open Load Through procedure.

Here we present some significant results about the slot on coaxial cable shield (Fig.1.).

The scattering coefficient magnitudes for this discontinuity before and after calibration procedure are presented in the same Fig. 8.

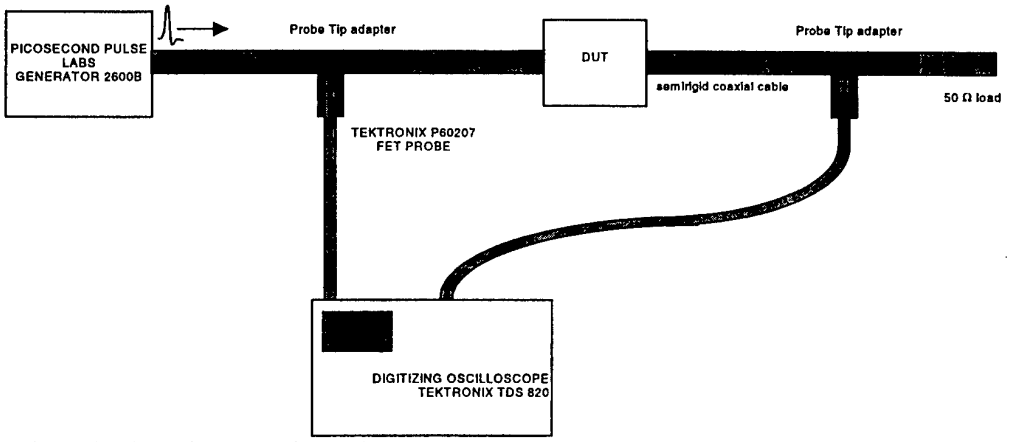
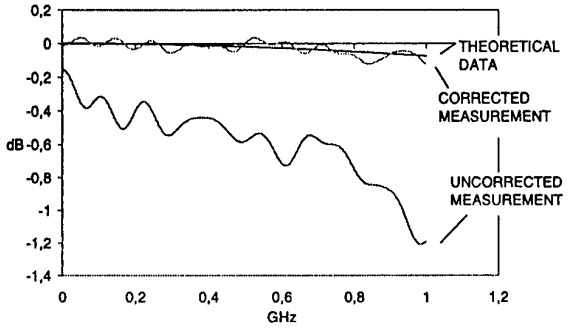
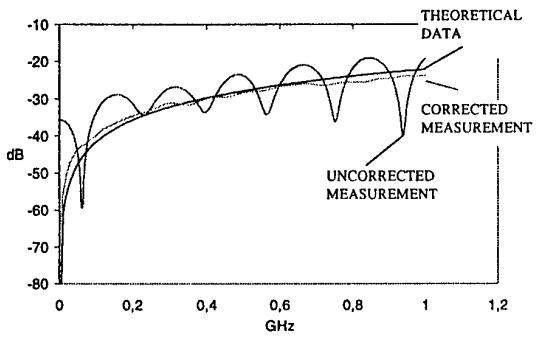



Fig. 4. : schematic view of the experimental test setup.




Transmission parameters $S_{21}$




Reflection parameters $S_{11}$

Fig. 8. experimental and simulation results

The curves representing the evolution of $|S_{21}(f)|$ and $|S_{11}(f)|$ as a function of frequency show a good agreement between corrected measurements and calculated data. We especially show the important influence of the calibration procedure .

From theoretical and experimental results, we deduce the radiated losses (Fig 9). The lost power evolution as a function of frequency shows a very good agreement between theoretical data and transient measurement. This curves show the efficiency of the transient experimental set up to characterize the defect influences on the radiated power by the line.

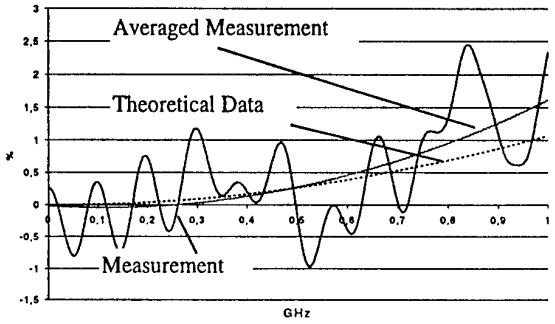



Fig. 9. lost power

## 4. ELECTRICAL FAR FIELD ESTIMATION

Knowing $P_{lost}$ we propose an estimation of the maximum electrical far field magnitude in the worst case.

In free space the relation associating the far field of an isotropic source to the lost power is the following :

$$r E_0(r) = \sqrt{60 P_r} \qquad (4)$$

Where r is the considered distance,
E(r) is the electrical far field,
$P_r$ is total radiated power by the isotropic source

When we consider this isotropic source placed at the beginning of a transmission line, this line behave as a travelling wave line which can present a radiation lobe (Fig. 10)

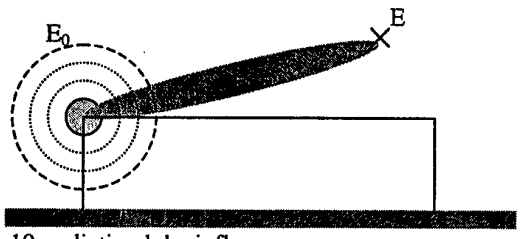


Fig.10. radiation lobe influence

Then, in the worst case, we consider the far field with the help of the following relation :

$$E_2 = 4.E_0 \quad (5)$$

For example, at 600 MHz, the lost power of the considered slot is about to 0.5 %. Then, knowing the injected power $P_{inj}$ and with help of (5), we deduce the maximum far field ten meters away in the worst case, $E_w$.

$$E_w = \left(0.1 \times \sqrt{60 \times 0.005}\right) \times 4 = 220 mV.m^{-1} \quad (6)$$

with 1Watt of injected power

## 5. CONCLUSION

Theoretical and experimental approaches are applied to localized discontinuity analysis and particularly to slot effects.

Simulation and experimental measurements give very similar S parameters results; this comparison shows the efficiency of the calibration procedure.

These results validate the experimental transient analysis for the prediction of discontinuity (like connectors) behavior and particularly radiation losses.

From the radiation losses we proposed an electrical far field estimation based on a worst case approximation. At this time we are working about the improvement of this approximation in order to take into account the relation between the line and the wave length.

Moreover, we are working about localized defects on other transmission links like bifilar and multifilar links which present a characteristic impedance different from 50Ω. For this study, another calibration procedure must be applied.

## 6. REFERENCES

[1] 'Time Domain Measurements in Electromagnetics' Ed. E.K. Miller, Van Nostrand Reinhold, USA, 1986.

[2] N. Feix, M. Lalande, B. Jecko, 'Harmonical characterization of a microstrip bend via the Finite Difference Time Domain Method' I.E.E.E. Transactions on Microwave Theory and Techniques, May 1992.

[3] P. Ferrari, G. Angenieux, B. Flechet, 'A complete calibration procedure for time domain network analyzers', I.E.E.E. MTT-S International Microwave Symposium Digest.

[4] L. A. Hayden, V.K. Tripathi, 'Calibration Methods for Time Domain Network Analysis' I.E.E.E. Transactions on Microwave Theory and Techniques, March 1993.

## BIOGRAPHICAL NOTES

**Edson Martinod** was born in Calais, France, in 1972. He received the Diplome d'Etude Approfondies in Electronic. He is presently studying for obtaining the Doctorat in Electronic from the University of Limoges, Limoges, France, in the laboratory of Electromagnetism of the Institut de Recherche en Communications Optiques et Microondes (IRCOM). He is now engaged on electromagnetic compatibility on connectors.

**Noël Feix** was born in Brive, France, in 1963. He received the Doctorat in Electronic from the University of Limoges, Limoges, France, in 1992.

Presently, he is Lecturer at University Institute of Technology of Limoges (Department Industrial Engineering) and he is member of the Electromagnetic Team of the Institut de Recherche en Communications Optiques et Microondes (IRCOM). He is now engaged on electromagnetic compatibility on connectors.

**Michèle Lalande-Guionie** was born in Noth, France, in 1962. She received the Doctorat in Electronic from the University of Limoges, Limoges, France, in 1986.

Presently, she is Lecturer at University Institute of Technology of Limoges (Department Electric Engineering and Industrial Computer Science, Brive, France) and she is member of the Electromagnetic Team of the Institut de Recherche en Communications Optiques et Microondes (IRCOM). She is now engaged on electromagnetic compatibility on connectors.

**Bernard Jecko** was born in Trelissac, France, in 1944. He received the Doctorat Third Cycle and the Doctorat es Sciences degrees from the University of Limoges, Limoges, France, in 1971 and 1972, respectively.

He is currently a Professor at the University of Limoges and leads the Electromagnetic Team of the Institut de Recherche en Communications Optiques et Microondes (IRCOM). His research interest is in the area of electromagnetic wave diffraction theory, particularly in the time domain.

**EMC 2000** INTERNATIONAL WROCŁAW SYMPOSIUM ON ELECTROMAGNETIC COMPATIBILITY

# Background, content and future of the EMC measurement standard prEN 50289-1-6, Open / shielded test methods,

Thomas Hähner
Alcatel Cable France
15, rue Lambin
60120 Paillart
France
Tel: +33 3 4480 6721
Fax: +33 3 4407 0149
thomas.haehner@paillart.alcatel.fr

Bernhard Mund
bedea Berkenhoff & Drebes GmbH
Herbornerstraße 100
35614 Aßlar
Germany
Tel.: +49 6441 801 133
Fax: +49 6441 98 32 30
bmund@bedea.com

*The following report gives an overview of common used and standardised measurement procedures of the screening effectiveness of communication cables. Furthermore a view to future EMC measurements of communication cables as well as of connectors is given.*

## 1 INTRODUCTION

### 1.1 General

Due to increasing use of all kind of electric or electronic equipment, electromagnetic pollution increases. To reduce this electromagnetic pollution, all components of a system, especially the connecting cables shall be screened.
To have a measure of the screening effectiveness and to compare different screen constructions with each other, international standardised measuring procedures are required.
The following report gives an overview of common used and standardised measurement procedures of the screening effectiveness of communication cables which are summarised in **prEN 50289-1-6.** Furthermore a view to future EMC measurements of communication cables as well as of connectors is given.

### 1.2 CLC TC46X/WG3

Following a decision of the CENELEC TC46X, Communication Cables, the Working Group CLC TC46X/WG3, Screening Effectiveness, was established in 1996. The task of this Working Group has been to develop standards to measure the screening behaviour of communication cables; especially for balanced data cables. The first meeting of this working group has been held on 10th of January 1997 in Hoersholm, Denmark.
At the moment a draft standard prEN 50289-1-6 is published, which includes 4 different measurement procedures to measure screening effectiveness of communication cables.

The CLC TC46X/WG3 is the mirror committee to the IEC TC 46/WG5, Screening Effectiveness. Since some Experts are members of both Working Groups a good co-operation between this both groups is given and double work is avoided.

## 2 PHYSICAL BASICS

### 2.1 General coupling equation

For the measurement of coupling it is expedient to use the concept of operational attenuation with the square root of power waves, like in the definition of scattering parameters [1,2]. The general coupling transfer function is then defined as:

$$T_{f}^{n} = \frac{\underline{U}_{f}^{2n} / \sqrt{Z_2}}{\underline{U}_{1} / \sqrt{Z_1}} = \frac{\sqrt{\underline{P}_{f}^{2n}}}{\sqrt{\underline{P}_{0}}} \qquad (1)$$

The electromagnetic influence between the cable and the surrounding is in principle the crosstalk between two lines and is caused by capacitive and magnetic coupling. At the near end the magnetic and capacitive coupling add where at the far end they subtract [2,3]. The coupling over the whole cable length is obtained by integrating the infinitesimal coupling distribution along the cable with the correct phase. The phase effect, when summing up the infinitesimal couplings along the line is expressed by the summing function S [2]. When the cable attenuation is neglected *S* could be expressed by the following equation.

$$S_{f}^{n}(lf) = \frac{\sin(\beta_2 \pm \beta_1) \cdot l/2}{(\beta_2 \pm \beta_1) \cdot l/2} \exp(-j(\beta_2 + \beta_1) \cdot l/2) \qquad (2)$$

**EMC 2000** INTERNATIONAL WROCŁAW SYMPOSIUM ON ELECTROMAGNETIC COMPATIBILITY

Late paper to the session "EMC PERFORMANCE OF SYMMETRICAL AND COAXIAL CABLINGS"
(page 198)

# CORRELATION BETWEEN RADIATED IMMUNITY AND COUPLING ATTENUATION

Michiel Pelt

Alcatel Cabling Systems, Competence Center
Alsembergsesteenweg 2 bus 3, B-1501 Buizingen, Belgium
Tel: (32) 2 363 39 10, Fax: (32) 2 363 09 60, E-mail: Michiel.Pelt@acs.alcatel.be

## ABSTRACT

A new test standard emerges to evaluate the EMC performance of cables and cable assemblies. With this test method called coupling attenuation balanced and unbalanced cables are investigated. The results are compared with radiated immunity tests inside a semi-anechoic chamber. Using simple antenna theory agreement between both test methods is illustrated. This enables to draw conclusions about the correctness of coupling attenuation.

## INTRODUCTION

A long time industry has been looking for a simple test methods to evaluate the EMC performance of symmetrical cables, connectors and cable assemblies. Over the years multiple parameters have been introduced into standards like balance, transfer impedance, screening attenuation, etc. However these parameters describe only partly the radiation and susceptibility properties. Balance describes the conversion between differential and common mode currents on a symmetrical pair. Transfer impedance describes the relation between the common mode voltage and the current on the outside of the screen. However a system engineer is only interested in the combined effect of balance and screening as this determines the noise induced on the cable and the Bit-Error Rate.

As cables and connectors are passive devices, the radiation from a cable and the susceptibility to external fields are reciprocal. Therefore the electromagnetic performance of a passive device can be presented by a single parameter which is the relation between the injected power on the cable and the radiated power. Such a parameter expresses the electromagnetic isolation between a signal pair and its electromagnetic environment.

Today a new test method called coupling attenuation is proposed within the European standardization organization CENELEC. Coupling attenuation measures the relation between the injected power and the maximum power of the radiating currents at either near or far end. The power of the radiating currents is measured using a current transformer around the device under test. For this reason coupling attenuation can be considered as a conducted emission test of the EMC performance. However shielding effectiveness in EMC depends on frequency and distance as an electric or magnetic field in the neighbourhood of a device does not necessary radiate in the far field. To that aim far field tests have been done to demonstrate agreement with coupling attenuation.

In order to make the correlation as precise as possible the experiments have been simplified. First agreement between both test methods is only done for a FTP, a UTP and a coaxial cable. Introducing connecting hardware or patch panels adds a supplementary uncertainty to the measurements. Secondly the far field tests are limited to radiated immunity inside a semi-anechoic room according to IEC 61000-4-3. In

this way uncertainties are avoided arising from rotating the device under test, changing antenna height, etc. Also the price for the test facility was much cheaper.

## COUPLING ATTENUATION

### Test procedure

The electromagnetic performance of an unbalanced cable is the effect of the screen. The electromagnetic performance of a symmetrical cable is the combined result of both balance and screening. The coupling attenuation of each cable is expressed in dB as:

$$a_c = 10.\mathrm{LOG}_{10}\left(\frac{P_1}{\max\left[P_{2,n};P_{2,f}\right]}\right)$$

where

$P_1$ input power of inner circuit
$P_{2,n}$ maximum near end peak power of outer circuit
$P_{2,f}$ maximum far end peak power of outer circuit

To measure this parameter the cable is fed with power $P_1$. Due to the electromagnetic coupling between the cable and its environment surface waves are exited and propagated in both directions along the screen surface. A surface current transformer is used for picking up the power of the surface waves with an absorber to suppress unwanted common mode currents. On the basis of the measured surface currents - $P_{2,n}$ or $P_{2,f}$ - it is possible to calculate the maximum peak power in the secondary system formed by the screen of the cable (or the cable itself) and the environment.

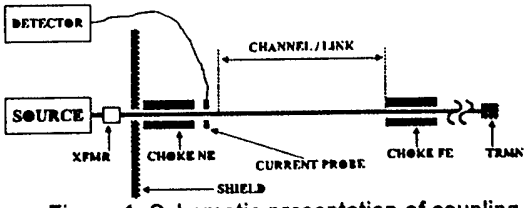



Figure 1: Schematic presentation of coupling attenuation

The cable under test is laid on a non-metallic table and connected to the generator via an impedance matching balun. The stationary absorbing clamp is placed as near as practically possible from the reflector plate for a near end measurement. For a far end measurement the absorbing clamp and the absorber are interchanged.
The power of the output of the absorbing clamp is measured for a linear frequency sweep from 30 MHz up to 1000 MHz in steps of 2.425 MHz. As the injected power injected is known the coupling attenuation can be calculated taking into account the attenuation of the set-up. For a symmetrical cable the test method is repeated for each individual pair.

### Experimental results

Three different cables were measured with coupling attenuation: A coaxial cable to observe the effect of the screen, a UTP to observe the effect of the balance and a FTP (dual foil) to observe the combined effect of balance and screen.

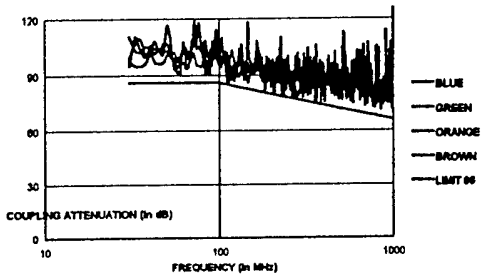



Figure 2: Coupling attenuation of a dual foil twisted pair cable

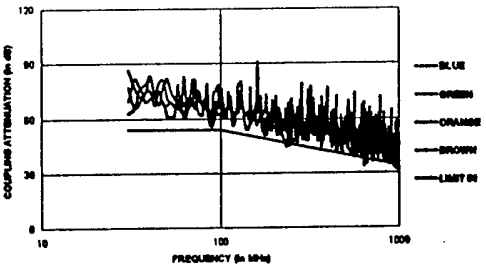



Figure 3: Coupling attenuation of an unshielded twisted pair cable

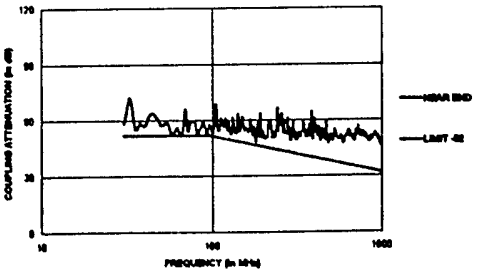



Figure 4: Coupling attenuation of a coaxial cable

The electromagnetic isolation provided by the dual foil cable is higher than for the other measured cables. The coupling attenuation of the FTP is 32 dB better than the UTP and 34 dB better than the coaxial cable.
For the symmetrical cables the recorded traces of the individual pairs remain close to a limit curve which is constant up 100 MHz but decreases with 20 dB/ decade from this frequency. This arises as electromagnetic isolation provided by the screen is independent on frequency whereas isolation provided by the balance decreases with 20 dB / decade. The level of the limit curve is a single parameter used to characterize the coupling attenuation over the entire frequency range. The same approach is proposed within the emerging draft standard for coupling attenuation.
For the unbalanced cable the isolation remains constant with frequency as the balance equals zero. The same limit curve is used to characterize the coupling attenuation over the entire frequency range although the recorded trace is nearly flat. Hence the electromagnetic isolation of the unbalanced cable increases by 20 dB/decade in comparison with the balanced cables.

## RADIATED IMMUNITY

A cabling set-up is radiated inside a semi-anechoic room as specified in the radiated immunity standard ISO/IEC 61000-4-3. The transmitting antenna is placed 3 m from the cabling set-up and generates an unmodulated field of about 3 V/m. The frequency range is covered by a biconical antenna from 30 to 200 MHz and with a log-periodic antenna with two amplifiers from 200 MHz to 500 MHz and from 500 to 1000 MHz.

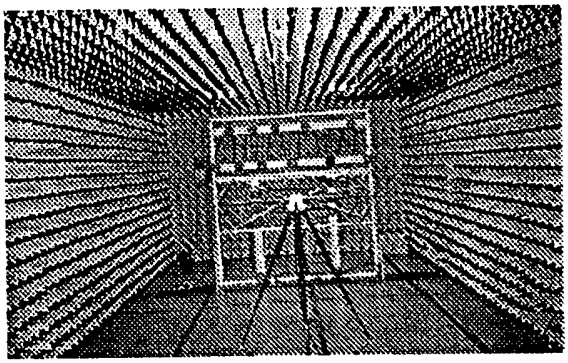


Figure 5: Picture of cabling set-up inside semi-anechoic chamber

### Cabling set-up

All radiated immunity testing must be performed in a configuration as close as possible to the installed case. However for cabling there is no standardized cabling set-up to get reproducible test results. Moreover in order that it is useful for EMC tests, the set-up should not suppress or enhance certain frequency ranges, and the direction to the test set-up and polarization of the receiving antenna should not be critical.
Therefore ISO/IEC JTC1 SC25 WG3 proposed to CISPR G a set-up during the London meeting in June 1996[4]. It consists of a 10 cm thick wooden frame on which 70 m cable is wound on the front side and on the back side. The cable is routed on both sides by circular non conducting cable supports with a bending radius of 5 cm.

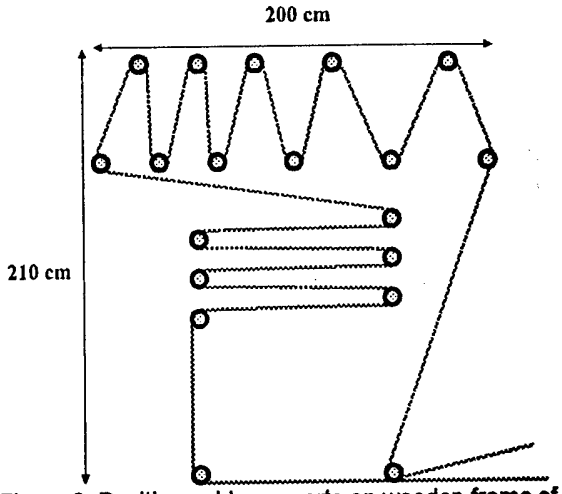



Figure 6: Position cable supports on wooden frame of cabling set-up

The properties of the cabling set-up as radiating element were investigated and compared to the emission of a dipole antenna[3,4]. It was concluded that the minimum attenuation is obtained when the cabling set-up is perpendicular to the direction of the antenna. Moreover the relative gain is quite constant over the frequency range and the set-up has no dominant polarization or directional characteristics. These results made us decide to construct an identical set-up.

### Incident field

For radiated immunity testing of equipment the incident field is 80% amplitude modulated. However for linear passive devices like cables this is useless and only gives arise to more

intricate calculations when correlating both test methods.
To achieve a constant field inside a semi-anechoic chamber the power fed to the antennas has to be adjusted continuously at each frequency. This makes a radiated immunity test extremely time consuming. Besides there is no reason to keep the incident field constant in order to characterize passive devices. The amount of power induced on the cable is directly related to the power density of the incident field. As cables are linear devices this ratio is totally independent of the field strength.
Therefore the power fed to the antenna was kept constant over the frequency range of each amplifier. As a consequence the incident field was not constant as function of frequency but altered due to the antenna factors and the characteristics of the semi-anechoic chamber.
Nevertheless particular care shall be taken to ensure the uniformity of the generated fields especially at lower frequencies. Because it is impossible to establish a uniform field close to an earth reference plane - i.e. the wall of the semi-anechoic chamber- the calibrated area is established at a height no closer than 0.8 m from the walls. Therefore the anechoic chamber must be sufficiently large for the cabling set-up. As the dimensions of the chamber equals 13.4 m x 4.7 m x 3.0 m this will not affect the measurements.

A „uniform area" is defined as a hypothetical vertical plane of the field in which variations are acceptably small. The size depends on the size of the device under test. For the cabling set-up the defined area is the part of the wooden framework 80 cm above the ground plane. Hence the two cable supports close to the ground plane are excluded from the measurements.

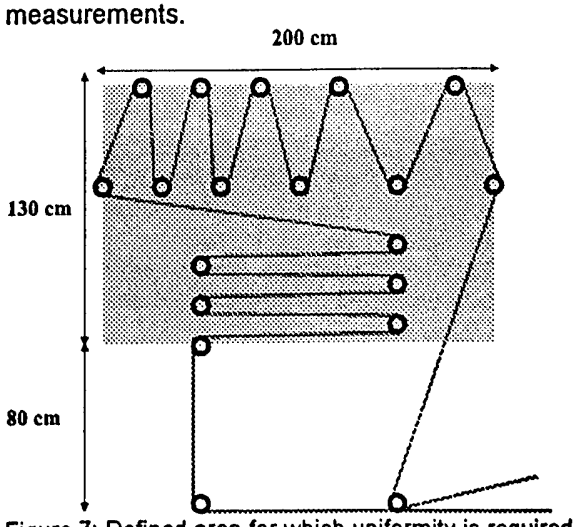



Figure 7: Defined area for which uniformity is required

The uniformity was verified over the defined area with an isotropic handhold field tester at five different locations along the area of interest, i.e. in the center and in corners of the defined area. At each location the field was measured in steps of 50 MHz up to 500 MHz and in steps of 100 MHz up to 1000 MHz for both the horizontal and vertical polarization state.

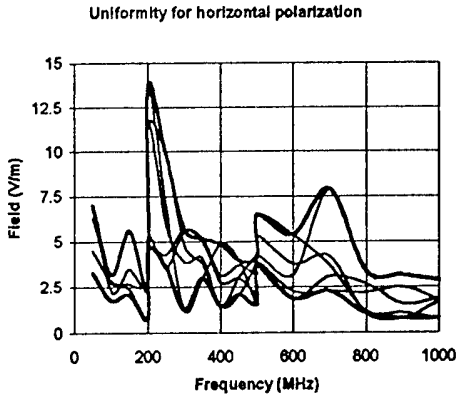



Figure 8: Uniformity of the horizontal field component - Dark traces indicates the maximum and minimum values at different locations; Light traces indicate field at each location versus frequency.

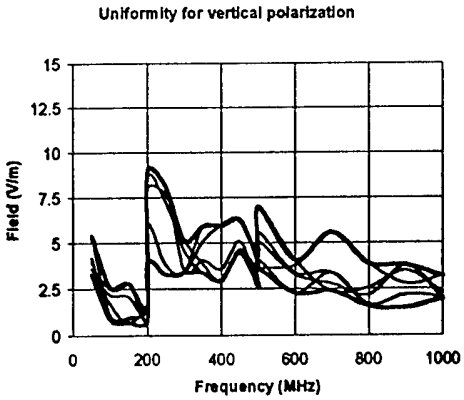



Figure 9: Uniformity of the vertical field component - Dark traces indicates the maximum and minimum values at different locations; Light traces indicate field at one location versus frequency.

According to the radiated immunity standard a field is considered uniform if its magnitude over the defined area is within - 0 dB to + 6 dB of a nominal value over 75 % of the surface. The tolerance of 6 dB is considered to be the minimum achievable in practical test facilities. By eliminating 17 % of the recorded values for the horizontal polarization and by eliminating 11 % of

the recorded values for the vertical polarization all the remaining values are within 0 dB to 6 dB limit over the defined area. Hence the field generated by an antenna placed 3 meters from the device under test is uniform.
For equipment testing the minimum field strength is of importance, i.e. the magnitude of field over the defined area which corresponds to the 0 dB value. This is logical because an incident field with a higher magnitude will certainly interfere with the equipment. However when characterizing passive devices it is the average incident field of all recorded values that is of interest.

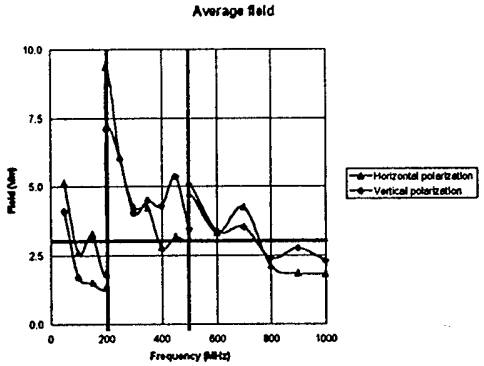



Figure 10: The average field strength over the defined area

The average field strength varies strongly from 1.8 V/m up to 9 V/m. When averaging over frequency the field strength varies slightly around 3 V/m.
Observe that the that the traces for horizontal and vertical polarization are very close to each other. This indicates the polarization insensitivity of the cabling set-up.
When an amplifier is changed, i.e. at 200 MHz and 500 MHz, the uniform field inside the semi-anechoic chamber changes drastically because the antenna is fed with different power levels.

## Monitoring noise power

The signal induced on the cable is measured outside the semi-anechoic chamber with a spectrum analyzer (bandwidth 100 kHz). To measure the balanced cables an impedance matching balun is inserted with a balance of 40 dB from 30 MHz to 1000 MHz. This is the same balun as used during the coupling attenuation tests and was put inside a small metallic box fixed to the wall inside the semi-anechoic chamber. The common mode rejection ratio was further improved with ferrite blocks just in front of the balun like for the coupling attenuation tests.

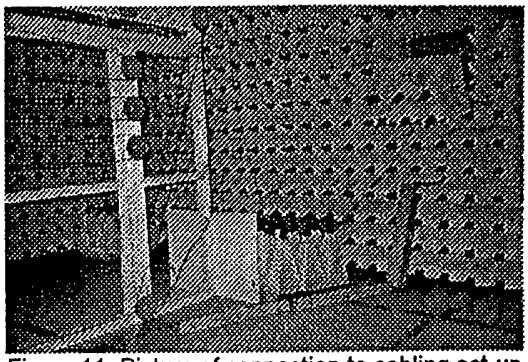


Figure 11: Picture of connection to cabling set-up inside the anechoic chamber

## Experimental results

In figures 12-13 the induced noise is shown for horizontal and vertical polarization of the antenna. For all cables the traces for the horizontal polarization are very close to the traces of the vertical polarization. This indicates again the polarization insensitivity of the cabling set-up.

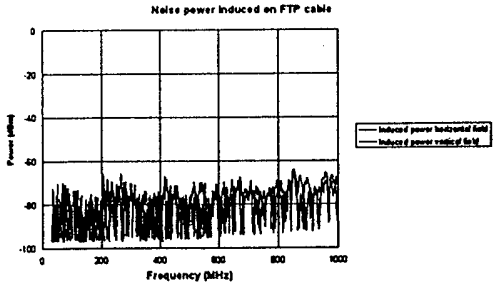



Figure 12: Noise power induced on a dual foil twisted pair cable

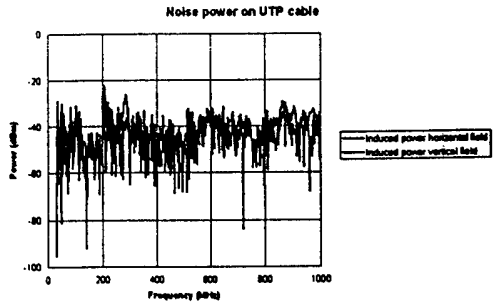



Figure 13: Noise power induced on an unshielded twisted pair cable

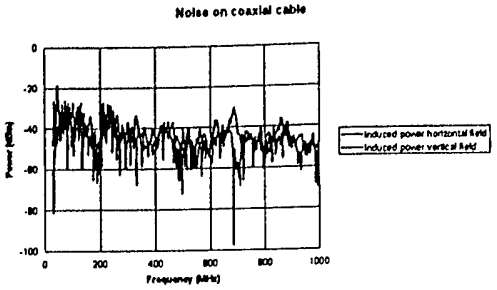



Figure 14: Noise power induced on a coaxial cable

Besides for the unbalanced cable the induced noise seems to be independent of frequency. This is not in contradiction with coupling attenuation as will be explained in next section. The traces for the dual foil cable are about 30 dB lower than the traces of the UTP cable. This difference was also observed with previous test method and applies also to the coaxial cable. However for the unbalanced cable the induced noise decreases with 20 dB/decade with respect to the symmetrical cables. This was also confirmed with previous test method.

## CORRELATION FAR FIELD - NEAR FIELD

### Theoretical calculations

The next step consists in calculating the noise induced on a cable with a certain level of coupling attenuation. However this requires knowing the amount of power captured in the outer circuit of the cabling set-up by the incident field.
The induced noise power in the outer circuit by a field of 3 V/m can be calculated using simple antenna theory. The amount of energy an antenna picks-up from the incident field depends on the antenna aperture. The latter is given by following equation:

$$G(\theta,\varphi) = \frac{4.\pi.A_f(\theta,\varphi)}{\lambda\lambda}$$

where

| | |
|---|---|
| $G(\theta,\varphi)$ | antenna gain |
| $A_f(\theta,\varphi)$ | antenna aperture |
| $\lambda$ | wavelength |

The gain of the cabling set-up has been investigated by comparing the radiation from the cabling set-up with a resonant dipole antenna[3,4]. It was concluded that the relative gain of the cabling set-up referred to a dipole was quite constant over the frequency range of interest and very close to that of a resonant dipole (gain = 1.64). Using this value the amount of power captured by the cabling set-up is found by multiplying the magnitude of the incident field with the effective aperture. For a constant field of 3 V/m (over the entire frequency range) the captured power in the outer circuit of the cabling set-up is shown in figure 15.

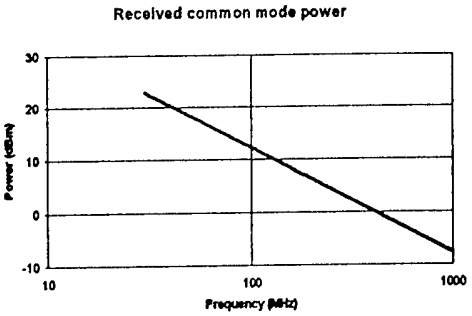



Figure 15: Power picked up from a 3 V/m field

Due to the wavelength dependence of the antenna aperture the power picked-up from the field decreases with 20 dB per decade. Part of the captured power is converted into signals that interfere with the data transfer due to non-infinite balance or non-zero transfer impedance. This electromagnetic isolation provided by the design of the cable is expressed by its coupling attenuation, unbalance attenuation or screening attenuation. The behaviour of coupling attenuation versus frequency is approximated by the limiting curve that fits very closely to the recorded values for the balanced cables. The limit curve is constant up to 100 MHz after which it decreases with 20 dB/decade. It gives the relation between the power inside the cable and the maximum power of the radiating currents outside the cable.

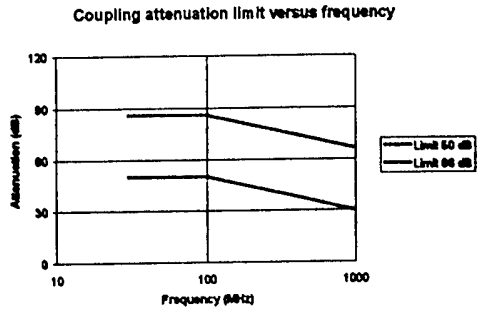



Figure 16: Approximation of coupling attenuation versus frequency

To find the power induced on the cable the coupling attenuation provided by the design of the cable has to be subtracted from the power captured by the cabling set-up.

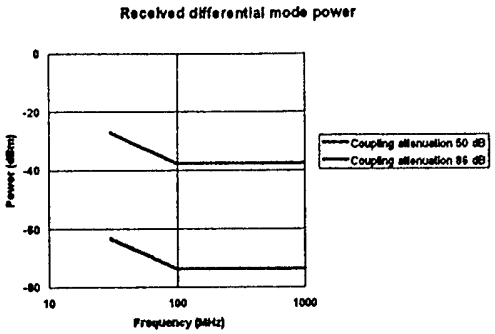



Figure 17: Noise induced on cables with different coupling attenuation by 3 V/m

The induced noise power is flat from 100 MHz like observed in the radiating immunity experiments for the balanced cables. This arises as both the received power in the outer circuit and the limit curve for coupling attenuation decrease by 20 dB/decade.
How well these calculated powers induced by a field of 3 V/m on the different cables fits the experimentally recorded values is presented in next clause.

## Correlation between both test methods

In the second clauses of this chapter it was shown that the incident field was uniform over the cabling set-up but not constant. However when averaging over frequency a value very close to 3 V/m was obtained. In the previous clause the induced power for an incident field of 3 V/m on the various cables were calculated for the outer circuit of the cabling set-up.

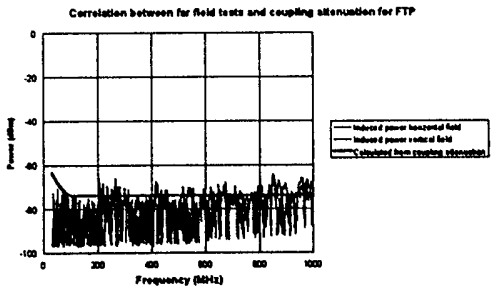



Figure 18: Correlation for dual foil twisted pair cable

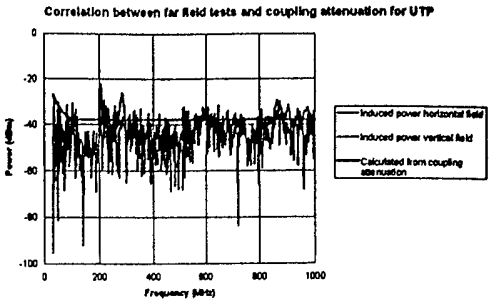



Figure 19: Correlation for unshielded twisted pair cable

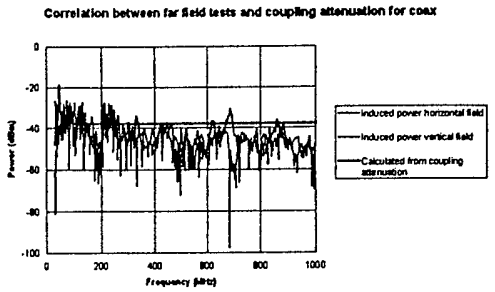



Figure 20: Correlation for coaxial cable

It can be observed that the values vary about 6 dB above and below the calculated noise power. This is acceptable as the accuracy of coupling attenuation and the incident field equals 6 dB. High peaks or dips occur especially at those frequencies where the average field is extremely high. For instance when changing the amplifier at 200 MHz the average field is 1.8 V/m at the end of the frequency range of the first amplifier whereas 9.0 V/m at the beginning of the frequency range of the second amplifier. This generates a dip just below 200 MHz and a peak just above 200 MHz on all graphs above.
Also the effect of approximating the coupling attenuation versus frequency by a limit curve can be observed at the low frequencies. When looking at the recorded data for coupling attenuation only the coaxial cable intersects the limit curve below 100 MHz. For the balanced cables this is not the case and therefore they are lower than the calculated noise power.
A more precise comparison between both test methods is beyond the scope of this paper. This would imply taking into account the field distribution over the cabling set-up, the coupling attenuation versus frequency (not approximating it by a limit curve), the change of the antenna gain versus frequency, a non-reflecting ground plane etc. Nevertheless satisfactory agreement between both test methods is found.

## CONCLUSIONS

Coupling attenuation can be considered as a conducted emission test of the EMC performance. However shielding effectiveness in EMC depends on frequency and distance as an electric or magnetic field in the neighbourhood of a device does not necessary radiate in the far field. To that aim correlation with a far field test like radiated immunity tests has been investigated for three cable constructions: A coaxial cable to observe the effect of screen attenuation, a UTP to observe the effect of unbalance attenuation and a FTP (dual foil) to observe the combined effect of screening attenuation and unbalance attenuation.

Using both test methods coupling attenuation and induced power for an incident field of 3 V/m was measured. The disparity between the coupling attenuation of the different cables was equal to the disparity between the induced power on the different cables. This applies to all cable constructions over the entire frequency range.

Experimentally it was observed that from 100 MHz the coupling attenuation of the balanced cables decreased by 20 dB/decade whereas the coupling attenuation of the coaxial cable was fairly independent of frequency. For the radiated immunity test the induced power on the balanced cables was independent of frequency whereas on the unbalanced cables decreased by 20 dB/decade. The discrepancy between both test methods was theoretically demonstrated using simple antenna theory. This enabled to calculate the noise power caused by a field - with an arbitrary field strength - and induced on a cable - with an arbitrary coupling attenuation if the characteristics of the outer circuit are known. So both relative and absolute agreement is found between both test methods.

## REFERENCES

[1] ISO/IEC 61000-4-3, *„Electromagnetic compatibility (EMC) - Part 4: Testing and measurement techniques - Section 3: Radiated, radio-frequency, electromagnetic field immunity test"*, International Standard, ISO, 1995.

[2] prEN 50289-6D, *„Generic specification for electrical test methods for cables used in analogue and digital communication and control systems - Part 6D: Coupling attenuation, absorbing clamp method"*, European draft standard, CENELEC, 1998.

[3] E. Bech, *„Evaluation of proposed generic cabling set-up to be included in EMC testing of information technology equipment based on electromagnetic field tests"*, Working document ISO/IEC JTC1 SC25 WG3 /BARCELONA/48, 1997.

[4] ISO/IEC JTC1 SC25 WG3 / N465, *„Liason letter to IEC CISPR G concerning a standard cabling set up for inclusion in CISPR 24"*, Liason report, ISO, 1997.

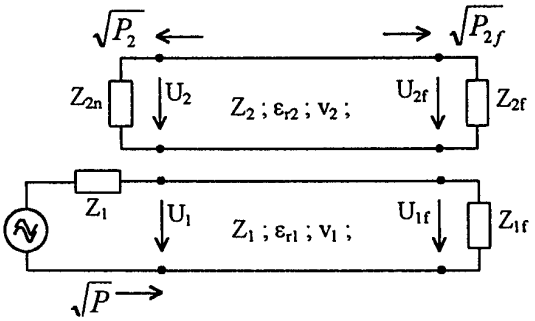



Fig. 1: Equivalent circuit

For high frequencies the asymptotic value becomes:

$$\left|S_{f}^{n}\right| \rightarrow \frac{2}{(\beta_1 \pm \beta_2)\cdot l} \qquad (3)$$

And for low frequencies the summing function becomes:

$$\left|S_{f}^{n}\right| \rightarrow 1 \qquad (4)$$

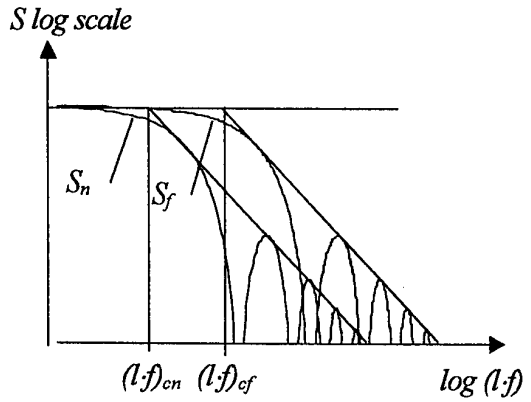



Fig. 2: Summing function S

The point of intersection between the asymptotic values for low and high frequencies is the so called cut-off frequency $f_c$. This frequency gives the condition for electrical long cables:

$$f_{c,f}^{n} \cdot l \geq \frac{c}{\pi \cdot \left|\sqrt{\varepsilon_{r1}} \pm \sqrt{\varepsilon_{r2}}\right|} \qquad (5)$$

where $\varepsilon_{r1,2}$ are the relative dielectric permittivity of the inner and the outer system and $l$ is the cable length.

## 2.2 Coupling transfer function

The primary screening quantities of a screen are the surface transfer impedance $Z_T$ and the capacitive coupling impedance $Z_F$ or the effective transfer impedance $Z_{TE}$ . For homogeneous screens they are constant along the cable length. The integration along the cable could then be easily solved. The coupling between the cable and the surrounding could then be expressed by the coupling transfer function. For matched lines it is [1,2]:

$$T_{f}^{s,n} = (Z_F \pm Z_T)\cdot \frac{1}{\sqrt{Z_1 \cdot Z_2}} \cdot \frac{l}{2} \cdot S_{f}^{n} \qquad (6)$$

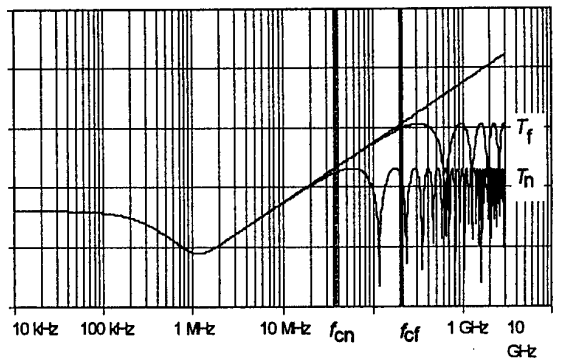



Fig. 3: Calculated coupling transfer function ($l$ = 1 m; $\varepsilon_{r1}$ = 2,3; $\varepsilon_{r2}$ = 1; $Z_F$=0)

For low frequencies, when S=1, the coupling transfer function corresponds to the frequency behaviour of the surface transfer impedance and capacitive coupling impedance. After a rise with 20 dB per decade the coupling transferfunction shows different cut off frequencies $f_{cn,f}$ for the near and far end. Above these cut off frequencies the samples are considered as electrical long.

Below the cut off frequencies the surface transferimpedance $Z_T$ is the measure of the screening effectiveness. The value of the transferimpedance $Z_T$ increases with the sample length.

Above the cut off frequencies in the range of wave propagation, resp. in the range where the samples are electrical long, the screening attenuation $a_S$ is the measure of the screening effectiveness. The screening attenuation is a length independent quantity.

Balanced cables which are driven in the differential mode will, due to irregularities in the cable symmetry, radiate a part of the input power.

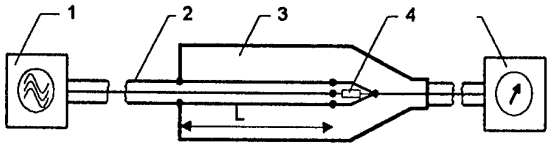
For unscreened balanced cables this radiation is depicted by the unbalance attenuation $a_U$. For screened balanced cables the disturbing power from the pair is additionally attenuated by the outer screen. The unbalance causes a current in the screen which is then coupled by the transfer impedance and capacitive coupling impedance into the outer circuit. Consequently the total effectiveness against electromagnetic disturbances of shielded balanced cable is the sum of the unbalance attenuation $a_U$ of the pair and the screening attenuation $a_S$ of the screen. Since both quantities usually are given in a logarithmic ratio, they may simply be added into the coupling attenuation $a_C$.

$$a_c = a_u + a_s \qquad (7)$$

## 3 MEASUREMENT PROCEDURES

### 3.1 Triaxial set-up to measure the surface transfer impedance

The triaxial procedure to measure the transfer-impedance is one of the classical methods to measure the transferimpedance. It is described in IEC 61196-1 and prEN 50289-1-6. The difference between the IEC and EN method is the interchange of generator and receiver. In the EN method the power is fed into the cable. The benefits of feeding the inner system, which is terminated by its characteristic impedance, are the matching of the generator and reflection free wave propagation over the cable length. The triaxial test set-up consists of a tube of brass or aluminium with an inner diameter of about 40 mm. The length is 0,5 m to 1 m.

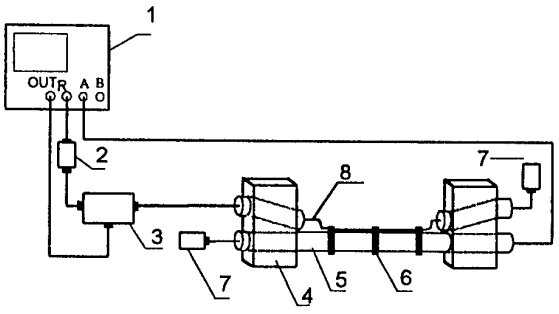



1 generator
2 cable under test
3 measuring tube
4 termination load
5 measuring receiver
L coupling length

Fig. 4: Principle of the triaxial set-up

### 3.2 Line injection set-up to measure the surface transfer impedance

A further method for the investigation of cable screens is the line injection of the Swiss PTT which is detailed described in IEC 96-1 Amendment 2/1993.




1 Networkanalyzer
2 attenuator 20 dB
3 power splitter
4 matching pads
5 cable under test
6 adhesive tape
7 termination load
8 injection wire

Fig. 5: Principle of line injection set-up, far end measurement

The injection wire, which is connected to the RF-generator injects RF-energy into the screen of the cable under test. The energy which is coupled into the cable under test is measured by the measuring receiver.

The transferimpedance $Z_T$ can then be calculated by the logarithmic ratio $A_T$ of the feeding voltage $U_1$ to the coupled voltage $U_2$ to:

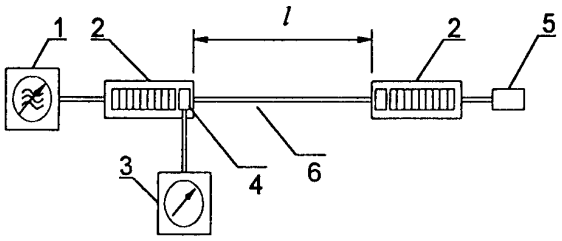
$$Z_T = \frac{2}{l} \cdot \sqrt{Z_1 \cdot Z_2} \cdot 10^{-\frac{A_T}{20}} \qquad (8)$$

where $A_T = U_2/U_1$

The upper frequency limit to which the transfer-impedance $Z_T$ can be measured depends on the length of the test section of the cable sample and of the differences in the velocities of propagation in the cable and the outer system. Theoretical the upper frequency limit is more than 3 GHz (see eq. 5). In practice this requires a well matched feeding system.

### 3.3 Absorbing clamp set-up to measure the screening attenuation

For the investigation of cable screens of coaxial cables in the higher frequency ranges, the screening attenuation $a_s$ was introduced (in the 70ths by Spatz and others). The screening attenuation is measured with absorbing clamps with the measuring set-up according to IEC 61196-1 clause 12.4. An absorbing clamp consists of a current transformer and a number of ferrite rings which are arranged in one housing.




1 Generator
2 Absorber
3 Receiver
4 Current transformer
5 Termination load
6 Cable under test

Fig. 6: Principle test set-up with absorbing clamps, near end measurement

The screening attenuation $a_s$ is the logarithmic ratio of the maximum radiated power $P_{2max}$ to the feeding power $P_1$ of the cable:

$$a_S = 10 \log (P_1/P_{2max}) \qquad (9)$$

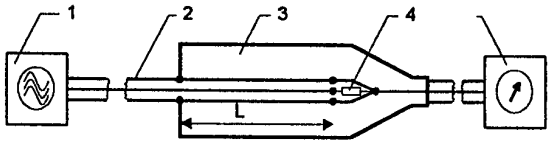
The generator feeds the cable with RF-Power. With the current transformer of one clamp the maximum power is measured while the other clamp matches the outer system and absorbs disturbances from outside the measuring length. The maximum power $P_{2max}$ in the outer system results from the near and far end measurement. With the now available absorbing clamps the screening attenuation can be measured up to 2,5 GHz.

### 3.4 Shielded screening attenuation set-up to measure the screening attenuation

A new development to measure the screening attenuation is the "Shielded screening attenuation"

test method. Although the principle were already described in the 60ths, it was Breitenbach who brought this idea back to the international standardisation in 1990 [4,5]. That measuring procedure is in principle an extension of the well known old IEC triaxial method. The new set-up allows the measuring of the transferimpedance $Z_T$ and, in the frequency range of electrical long cable samples, the measuring of the screening attenuation $a_S$ in one test set up. The procedure is standardised in IEC 61196-1, Amendment 1 and also in prEN 50289-1-6.

Contrary to the triaxial method of IEC 61196-1 the generator and the receiver are interchanged and the measuring tube is extended to a length of 2m to 3m. The advantage of the feeding into the matched cable under test (inner system) is, beside the screened test set-up, the matching of the generator and with that the propagation of the RF-energy in the CUT without reflection.




1 generator
2 cable under test
3 measuring tube
4 termination load
5 measuring receiver
L coupling length

Fig. 7: schematically arrangement for measuring the screening attenuation $a_S$ and the transferimpedance $Z_T$ with the Shielded Screening Measuring set-up

In the outer circuit, at the near end the screen under test is short circuited with the measuring tube. The electrical waves, which are coupled over the whole cable length from the inner system into the outer system, are travelling in both directions, to the near and the far end. At the short circuited end they are totally reflected, so that at the measuring receiver the superposition of near and far end coupling can be measured as the disturbance voltage ratio $U_2/U_1$. The screening attenuation as a power ratio is then related to a standardised characteristic impedance of the outer system $Z_s$=150Ω.

$$a_s = 20 \cdot \log\left(\left|\frac{U_2}{U_1}\right|_{max}\right) + 10 \cdot \log\left(\frac{2 \cdot Z_s}{Z_1}\right) \qquad (10)$$

where $Z_1$ is the characteristic impedance of the cable under test and $Z_s$ is 150 Ω.

### 3.5 Absorbing clamp set-up to measure the coupling attenuation of balanced cables

That set-up is in principle the same as the absorbing clamp set-up to measure the screening attenuation. It has been specially adapted in order to measure the coupling attenuation of symmetric cables, which is the combined result of unbalance attenuation and screening attenuation [6].

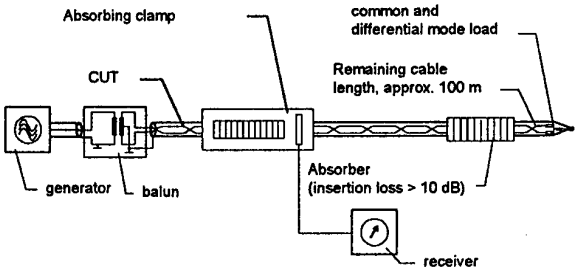



Fig. 8: Test set-up for the coupling attenuation absorbing clamp method

## 4 FUTURE

### 4.1 Coupling attenuation, injection clamp method

That injection clamp method is based on the same principle as the absorbing clamp method [7]. The difference is, that the power is fed to the surrounding of the cable (outer circuit), via the injection clamp. Also the outer circuit is matched to 150 Ω. The main benefits are, that the injection clamp make it possible to measure down to 100 KHz, instead of 30 MHz as in the absorbing clamp method. In addition the injection clamp has a about 15 dB less operational attenuation as the absorbing clamp. Thus a about 15 dB higher dynamic range is achieved.
This procedure is an approved new work item proposal in IEC, (IEC 46/86/NP).

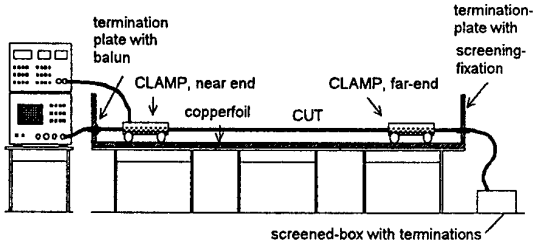



Fig. 9: injection clamp set-up

### 4.2 Coupling attenuation, Open tube method

As the clamp method could be used to measure the screening and coupling attenuation also the triaxial set-up to measure the screening attenuation can be extended to measure the coupling attenuation. Advantages are the wide frequency range, the high dynamic range and shielded surrounding of the sample under test [8,9,10].
The procedure is given to IEC TC 46 as a New work item proposal, NWP.
The set-up consist of:

- ∇ A metallic non ferromagnetic tube with a length sufficient to produce a superimposition of waves in narrow frequency bands which enable the envelope curve to be drawn.

- ∇ A signal generator with the same characteristic impedance as the cable under test.
- ∇ A balun for impedance matching of unbalanced generator output signal to the characteristic impedance of balanced cables.
- ∇ A receiver with a calibrated step attenuator or network analyser.
- ∇ Ferrite rings with an attenuation $a_{Ferrit}$ > 10 dB in the measured frequency range.
- ∇ Metallic boxes to shield the balun and the remaining cable length including the matching resistors

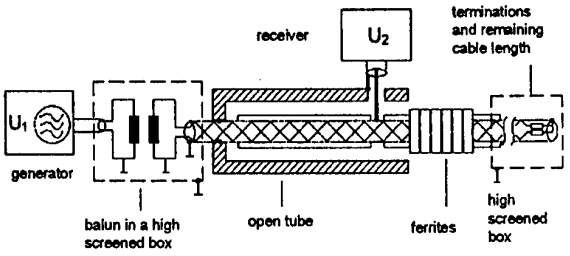



Fig. 10: Triaxial set-up to measure the coupling attenuation

### 4.3 Measurement of Connectors

An other procedure, which is under discussion is the screening effectiveness of coaxial, balanced and multipin connectors. The mechanical length of the connectors is usually short. Therefore in the frequency range of their application the summing function S=1. Thus only the transferimpedance may be measured. Since the capacitive coupling, specially for multipin connectors, can not be neglected, connectors can not be measured in a set-up with a short circuit at one end. Based on the open tube method, a possible test set-up is:

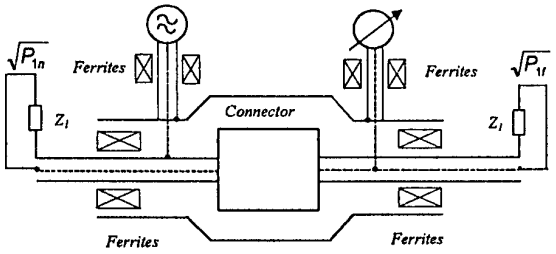



Fig. 11: Principle set-up to measure the transfer impedance of connectors

## 5 LITERATURE


[1] L. Halme, R. Kytönen, "Background and introduction to EM screening (shielding) behaviours and measurements of coaxial and symmetrical cables, cable assemblies and connectors", Colloquium on screening effectiveness measurements, Savoy Place London, 6 May 1998, Reference No:1998/452.

[2] Halme, L./Szentkuti, B, "The background for electromagnetic screening measurements of cylindrical screens", Tech. Rep. PTT(1988) Nr. 3

[3] W. Klein, "Die Theorie des Nebensprechens auf Leitungen", (German), Springer Verlag 1955 ,

[4] Breitenbach, O. , Hähner T, "Kabelschirmung im Übergang von MHz- zu GHz-Frequenzen", (German), ntz Bd. 46(1993) H.8, S. 602-608

[5] O. Breitenbach, T. Hähner, B. Mund, "Screening of cables in the MHz to GHz frequency range extended application of a simple measuring method", Colloquium on screening effectiveness measurements, Savoy Place London, 6 May 1998, Reference No:1998/452

[6] E. Bech, "Improvement of the absorbing clamp coupling and screening attenuation measurements and standards for symmetric and coaxial cables and connecting hardware", Colloquium on screening effectiveness measurements, Savoy Place London, 6 May 1998, Reference No:1998/452

[7] D. Wilhelm, "Measurements of coupled noise attenuation with special respect to frequencies below 30 MHz", Colloquium on screening effectiveness measurements, Savoy Place London, 6 May 1998, Reference No:1998/452

[8] T. Hähner, B. Mund, "EMC-performance of balanced (symmetrical) cables", Colloquium on screening effectiveness measurements, Savoy Place London, 6 May 1998, Reference No:1998/452

[9] Herrmann, R, "Weiterentwicklung von Meßverfahren zur Messung des EMV-Verhaltens koaxialer und symmetrischer Leitungen", (German), Diplomarbeit FH Gießen-Friedberg, Fa. Bedea Berkenhoff und Drebes GmbH, Asslar 1997

[10] T. Hähner, B. Mund, "test methods for screening and balance of communication cables", 13th international Zurich EMC Symposium, February 16-18 1999

EMC 2000 INTERNATIONAL WROCŁAW SYMPOSIUM ON ELECTROMAGNETIC COMPATIBILITY

# PRIMARY AND SECONDARY ELECTRO-MAGNETIC SCREENING (SHIELDING) PARAMETERS

Lauri Halme

HELSINKI UNIVERSITY OF TECHNOLOGY
Communications Lab./PO. Box 3000/FIN-02015 HUT
e-mail: lauri.halme@hut.fi Fax +358 9 4512345

*This paper serves as bases, background and introduction to better understanding of the work done in IEC [1--3] and CENELEC [4] in the field of the electromagnetic screening of cables, cable assembly and connecting hardware.*

## 1. GENERAL

With widening bandwidth, increasing use and demand of high security, the EMC capabilities of metallic communication access cablings (cables, cable assemblies and connecting hardware) have become of vital importance.

On cables and cable assemblies most of the test methods have been agreed upon. There is a big difference between screening and coupling limits of coaxial and symmetrical cables. For the time being there are no screening limits for mounted coaxial connectors and the limits for screened symmetrical connectors are very loose compared with the limits needed for coaxial connectors and their mounting to the cable.

To describe the EMC properties of screened (shielded) and unscreened (unshielded) constructions many parameters have been defined. They can be divided in primary and secondary parameters.

## 2. PRIMARY PARAMETERS

Outside electromagnetic fields induce currents into metallic screens which couple through screen resistivity, openings and anomalies, as cable screen currents flowing in a spiral, the electromagnetic fields to inside the screen. Measures of the screening quality of a screen are

- Surface Transfer Impedance ($Z_T$) and
- Capacitive Coupling Impedance ($Z_F$) or combined to
- Effective Transfer Impedance ($Z_{TE}$)

### 2.1 Surface Transfer Impedance $Z_T$

The surface transfer impedance $Z_T$ [Ω ] of an electrically short screen is defined as the quotient of the longitudinal voltage induced to the inner circuit by the current fed into the outer circuit or vice versa. $Z_T$ of an electrically short screen is expressed in ohms [Ω] or decibels in relation to 1Ω.

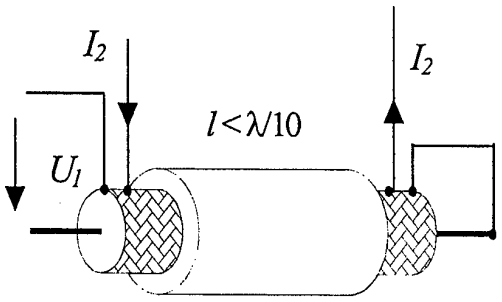



Fig. 1 Definition of $Z_T$

$$Z_T = \frac{U_1}{I_2} \qquad (1)$$

$$Z_T \text{ dB}(\Omega) = +20 \cdot \log_{10}\left(\frac{|Z_T|}{1\Omega}\right) \qquad (2)$$

### 2.2 Capacitive Coupling Impedance $Z_F$

The capacitive coupling impedance $Z_F$ [Ω] of an electrically short screen is defined as the quotient of the voltage induced to the near end impedance $Z_1$ of the inner system (open at the far end) by a current $I_2$ fed to

the far end termination $Z_2$ of the outer circuit (see fig. 2) to the current $I_2$.

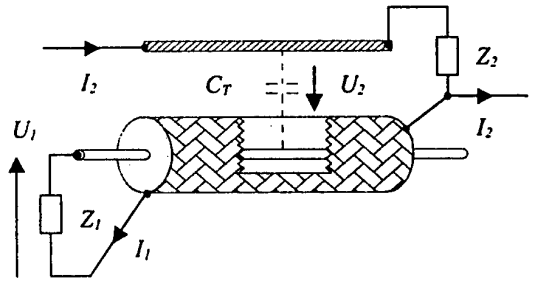



Fig. 2. Definition of $Z_F$

$$Z_F = \frac{U_1}{I_2} = \frac{I_1 \cdot Z_1}{\frac{U_2}{Z_2}} = \frac{I_1}{U_2} \cdot Z_1 \cdot Z_2 = Z_1 \cdot Z_2 \cdot Y_C \quad (3)$$

$$Y_C = \frac{I_1}{U_2} = j\omega C_T \quad (4)$$

$$Z_F\,[\mathrm{dB}(\Omega)] = +20 \cdot \log_{10}\left(\frac{|Z_F|}{1\Omega}\right) \quad (5)$$

$Y_C$ is the capacitive coupling admittance and

$C_T$ is the through capacitance

### 2.3 -Effective Surface -Transfer Impedance $Z_{TE}$

The Effective transfer impedance $Z_{TE}$ [Ω] is defined as maximum absolute value of the sum or difference of the $Z_F$ and $Z_T$ at every frequency.

$$Z_{TE} = \max|Z_F \pm Z_T| \quad (6)$$

$$Z_{TE}\,[\mathrm{dB}(\Omega)] = +20 \cdot \log_{10}\left(\frac{|Z_{TE}|}{1\Omega}\right) \quad (7)$$

The recommended limits for $Z_T$ and $Z_F$ are the same. They are behaving as the inductive and capacitive couplings in the crosstalk of symmetrical pairs, adding towards the near end and subtracting towards the far end.

### 2.4 Unbalance Coupling Impedance to Ground and Surroundings (1/e) [6]

$$\frac{1}{e(z)} = \left(\frac{1}{Z_c}\right) - \left(\frac{1}{Z_c} - \frac{1}{e(z)}\right) \quad (8)$$

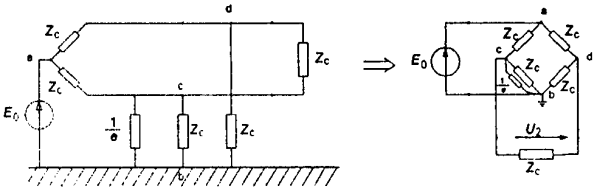



Fig. 3. Equivalent circuit to define the unbalance attenuation $a_{un}$ of a symmetrical pair.

$$\frac{E_0}{2U_2} = \left(\frac{4}{e(z)Z_c}\right) \text{ , when } \frac{1}{e(z)} >> Z_c \quad (9)$$

and the dimensions are electrically short.

$\frac{1}{e(z)}$ is the unbalance coupling impedance, which is a function of the length coordinate $z$.

The unbalance attenuation is for electrically short lengths

$$a_{un} = 20 \log_{10}\frac{\sqrt{P_0}}{\sqrt{P_2}} = 20 \log_{10}\frac{E_0\sqrt{Z_c}}{2U_2\sqrt{Z_c/2}} \quad (10)$$

$$= 20 \log_{10}\frac{4\sqrt{2}}{e(z)\,Z_c}$$

## 3. SECONDARY SCREENING PARAMETERS

### 3.1 General [5]

For measurement of couplings it is practical to define a general coupling transfer function, as the square root of power measured related to the unreflected square root of power sent into a system.

In cable techniques it is distinguished between near and far end coupling transfer functions $T_n$ and $T_f$.

$$T_{n,f} = \frac{\sqrt{P_{2n,f}}}{\sqrt{P_0}} \quad , \quad (11)$$

and expressed as complex coupling attenuation in dBs and radians

$$\Gamma_{n,f} = A_{n,f} + jB_{n,f} = \ln\frac{1}{T_{n,f}} \quad (12)$$

$$= -20 \log_{10}|T_{n,f}|\ [\mathrm{dB}] - j \cdot \arg(T_{n,f})\ [\mathrm{rad}]$$

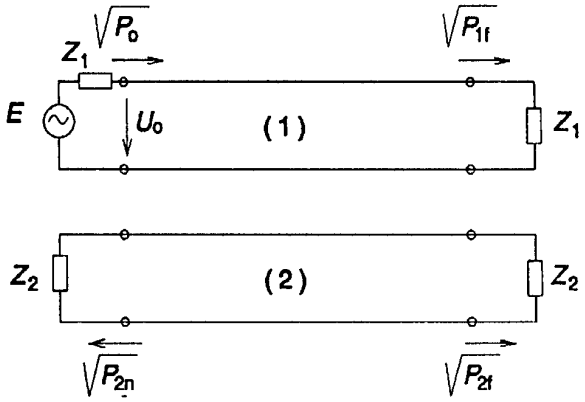



Fig. 4. Definition of coupling transfer function ($T_{n,f}$)

In cables the disturbance caused by couplings have to be integrated towards the far and near end respectively.

The summing functions achieved are of the form (sin x)/x and their envelopes are

$$\mathrm{Env}\left|S_{\substack{n\\f}}\{lf\}\right| = \frac{1}{\sqrt{1+\dfrac{(lf)^2}{(lf)^2_{\substack{cn\\f}}}}}, \qquad (13)$$

where the cut-off points are

$$(l\cdot f)_{C_{\substack{n\\f}}} = \frac{c}{\pi\left|\sqrt{\varepsilon_{r1}} \pm \sqrt{\varepsilon_{r2}}\right|} \qquad (14)$$

$c$ = velocity of light

$\varepsilon_{r1}$ and $\varepsilon_{r2}$ = relative permittivities of the inner and outer system

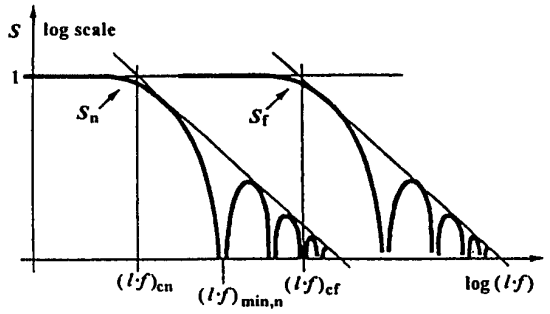



Figure 5. The summing function $S_{cn,f}$ for near (n) and far (f) end coupling. $(l\,f)_C$: cut-off point.
NOTE - $S_f > S_n$ above near end cut-off, yielding a directive effect

At lower frequencies $S$ is 1, but above a certain corner frequency $f_c$, S decreases 6dB/octave. The corner frequency is different for the near and far end.

Because at higher frequencies $Z_T$ and $Z_F$ are increasing 6dB/octave the result is a constant screening attenuation

### 3.2 Screening Attenuation [4]

Screening attenuation ($a_s$) is defined as quotient of the square root of power sent into coaxial system to the maximum square root of power travelling either to near or far end of the outer system,

$$a_s = 20\cdot\log_{10}\frac{\left|\sqrt{P_0}\right|}{\max\left|\sqrt{P_{2n}};\sqrt{P_{2f}}\right|} \qquad (15)$$

$$= 20\cdot\log_{10}\left(\frac{2\sqrt{Z_1 Z_2}}{Z_{TE}\,\ell\,S}\right)$$

#### 3.2.1 Screening attenuation of connector screens

It is practical to define connectors' screening effectiveness by measuring their effective transfer impedance $Z_{TE}$. Nevertheless, customers like screening attenuation in dBs. To be able to talk about screening attenuation of connectors the surroundings must be agreed upon. It is suggested to use the same standardised surroundings as for cables, i.e. a terminated outer 150 ohms' system (2).

Normally connectors can be regarded electrically short up to a few GHz. This means that the summing function is about 1.

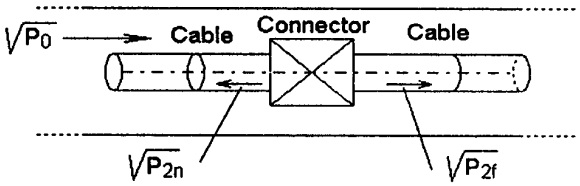



Fig. 6. Schematic drawing for definition of the screening attenuation of a connector

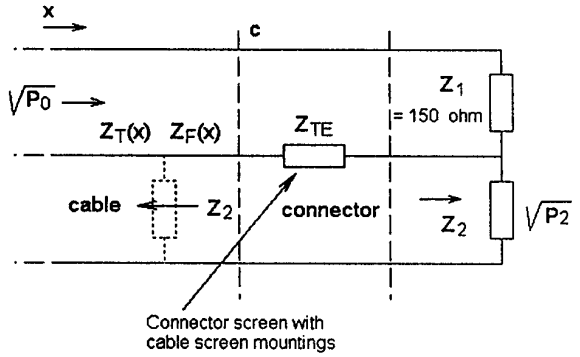



Fig. 7. Equivalent circuit to define the screening attenuation of a connector screen

In the above Fig.7 the square root of power is propagating in the outer system. Through connectors screens' effective transfer impedance two in opposite directions traveling waves are generated into the inner system (2). The screening attenuation of the connector is

$$a_{sc} = 20\log_{10}\frac{\left|\sqrt{P_0}\right|}{\left|\sqrt{P_2}\right|} = 20\log_{10}\left(\frac{2\sqrt{Z_1 Z_2}}{Z_{TE}}\right) \qquad (16)$$

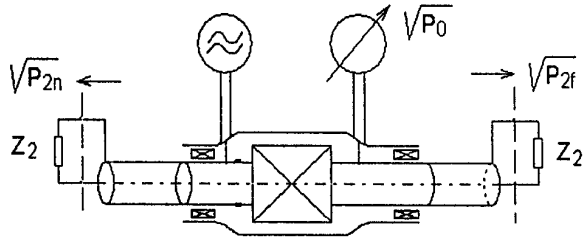



Fig. 8. Schematic practical arrangement for measurements of surface transfer impedances of connector screens

### 3.3 Screening attenuation test results' dependency on measuring set-up

As it can be seen from the Eqs above the screening attenuation is very much dependent on the velocity

difference of the outer and inner system. A velocity difference change from 40% to 10% decreases the screening attenuation with about 10 dB.

### 3.4 Coupling attenuation [4]

Coupling attenuation has been devoted to describe the screening effectiveness of symmetrical pair cables. It consists of two parts, unbalance attenuation and screening attenuation. A considerably good coupling attenuation is achieved by a careful balanced construction of a twisted pair cable, in the order of 50 dB up to 100 MHz and then decreasing maximum 6 dB/octave. If more screening is needed a metallic screen should be added around the individual pairs.

The coupling attenuation $a_c$ is equal to unbalance attenuation $a_{un}$ plus screening attenuation $a_s$.

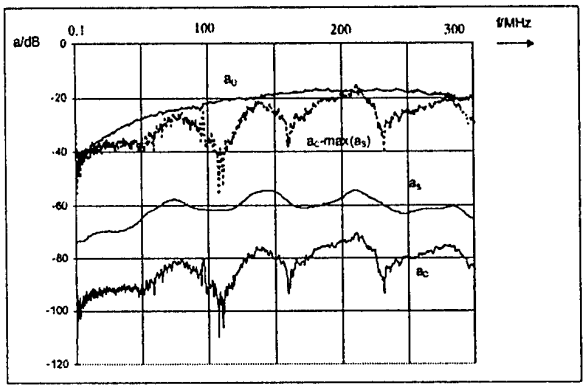



Fig. 9. Curves of unbalance screening attenuation, coupling attenuation and calculated unbalance of a screened twisted pair (Twinax 105). [8 /Fig13]

$a_U$ : measured unbalance attenuation (far end)
$a_S$ : measured screening attenuation (common mode)
$a_C$ : measured coupling attenuation (differential mode)
$a_C$ -max($a_S$ ): calculated unbalance attenuation

In the above Fig. 9 is with measurements demonstrated that the difference between $a_c$ and $a_s$ equals the unbalance attenuation. Care should be taken that a balanced cable has a sufficient amount of balance when fulfilling the coupling attenuation specification so that the whole coupling attenuation does not come from the screening attenuation.

## 4. LIMITS AND TEST RESULTS

In the Fig.10 are marked by points the screening limit values of a foil-braid screened CATV cable, foil screened data cable and screened CAT 7 connector. Characteristic is the big difference between the transfer impedances of screened balanced components and the coaxial cable. The difference is about two decades in the higher frequency range, corresponding to over 40 dB in screening or coupling attenuation. Fig. 11 the screening attenuation calculated from Fig.10 transfer impedance values are shown. Observe the behavior of the short connector screen and long cable screen. The connector summing function is 1 and the cable summing function is decreasing 6 dB/octave, which explain the behavior.

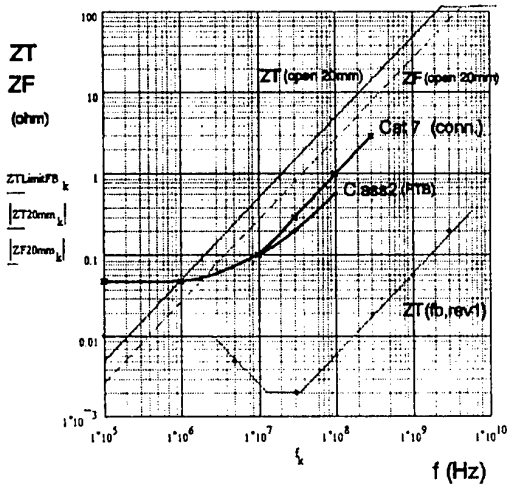



Fig. 10. Transfer impedance limits and $Z_T$ and $Z_F$ of a 20 mm open screen (screen consists of one wire)

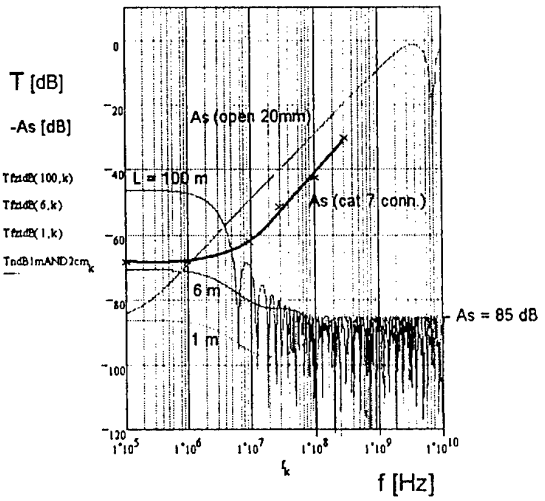



Fig. 11. Coupling and screening attenuation in dB

In the following Figs are shown typical measured and/or calculated screening, coupling and unbalance attenuation test results. [8]

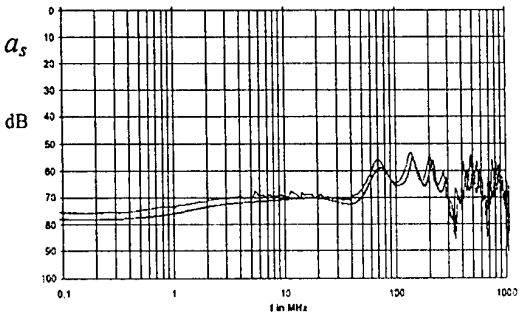



Fig. 12. Screening attenuation of RG 58 measured with the common and modified triaxial set-up; logarithmic frequency scale. [8 /Fig.11a]

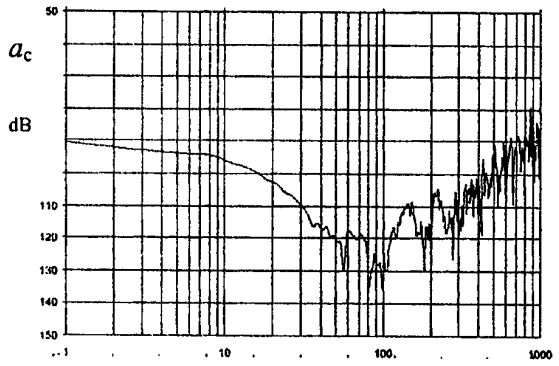



Fig. 13. Coupling attenuation of a common Cat 6 cable, coupling length 207 cm; logarithmic frequency scale. [8 / Fig.12a]

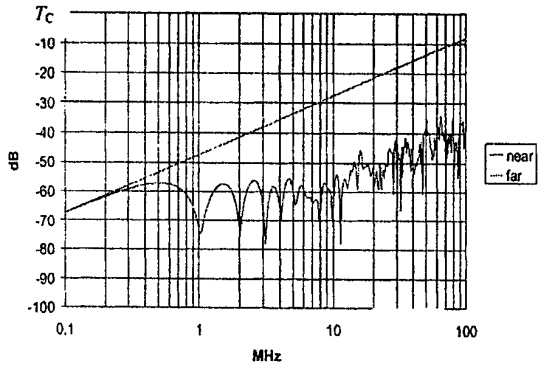



Fig. 14 Calculated coupling transfer function for a capacitive unbalance coupling of $e(z)$ = 0,4 pF/m + random(-0,4 up to + 0,4 pF/m), length =100 m, epsilon(1) = epsilon(2) = 2,3 . [9 /Fig. 9]

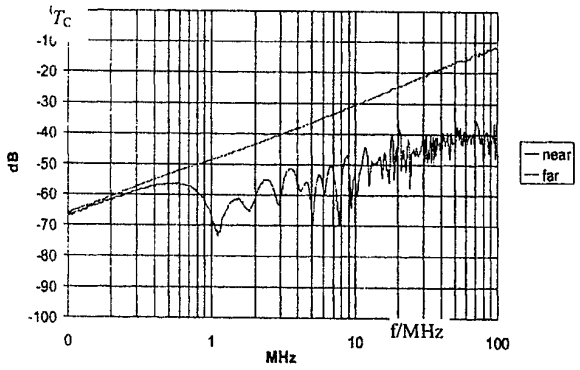



Fig. 15 Measured coupling transfer function of 100 m Twinax 105 ohm. [9 /Fig.2]

As it can be seen from Figs 14 and 15 of accuracy in manufacturing of balanced pair cables. The results can be interpreted that one has got about rid of the systematic unbalance coupling and the coupling left is a small random one.

## 5. REFERENCES

[1] IEC 61196-1, Amendment 1: Radio-frequency cables – Part 1: Generic specification – General, definitions, requirements and test methods

[2] IEC 61917, "Cables, cable assemblies and connectors - Introduction to electromagnetic (EMC) [EM] screening measurements "

[3] IEC TR 62064, Radio-frequency cables - Relationship between surface transfer Impedance and screening attenuation (A back-ground to the recommended limits contained in IEC 61196-1, clause 14), First edition 1999-07.

[4] prEN 502289-1-6 : Communication cables, Specification and test methods Part 1-6: Electrical test methods – Electromagnetic performance.

[5] Halme, l., Kytönen, R.,: Background and introduction to EM screening (shielding) behaviours and measurements of coaxial and symmetrical cables, cable assemblies and connectors. IEE Colloqium on Screening Effectiveness Measurements, IEE London, Proceedings No: 1998.

[6] Halme, L., K.,: Johtotransmissio ja sähkömagneettinen suojaus. (Transmission on lines and electromagnetic screening in Finnish), Parts A and B Otakustantamo 2nd Edition Helsinki 1989, 605 pages.

[7] Hähner, T., Mund, B.,:EMC –Performance of Balanced (Symmetrical) Cables, IEE Colloqium on Screening Effectiveness Measurements, IEE London, Proceedings No: 1998.

[8] Hähner, T., Mund, B.,: Test methods for screening and balance of communication cables. Zürich EMC Symposium Proceedings 1999, 100O4, pp. 533-538

[9] Hähner, T., : IEC draft CD 15.12.1999: Title: Amendment to IEC 61156-1, First Edition 1994-07: Addition of clause 2.1.7, 2.1.14 and 3.3.3: Unbalance attenuation [in the near end (LCL) and far end (LCTL)]

## BIOGRAPHICAL NOTE

Lauri Halme (D. Sc. E. E.). Since 1968 Specialist Lecturer at Helsinki University of Technology (HUT). 1962-1997 he worked in different leading positions in Telecom Finland: 1976-1988 as Director of Telecom Finland Research Laboratories and 1988-1997 at the CEO's staff as Director of Research, Development and Standardisation.

Halme is the chairman IEC TC 46 and CENELEC 46X dealing with standardisation and research of communications cables and accessories and Secretary of IEC SC100D dealing with CATV and Multimedia Network Systems.

EMC 2000 INTERNATIONAL WROCŁAW SYMPOSIUM ON ELECTROMAGNETIC COMPATIBILITY

# SHIELDED SCREENING ATTENUATION TEST METHOD DOWN TO 5 MHz

John Kincaid, Carl Dole
Belden Electronics Division
PO Box 1980, Richmond, IN 47375 USA
Fax: +1 765 983 5825
E-mail:jkbelden@globalsite.net, cdole@globalsite.net

*The electrical and physical characteristics of an elongated (30 meter length), resonant, cylindrical test fixture (triaxial) with a low-end test frequency limit which is less than 5 MHz are described. The fixture is in accordance with the principles of the shielded screening attenuation test method given in IEC 61196-1 amendment 1. Measured screening attenuation, and measured and extrapolated transfer impedance results for a selection of braid and multi-foil/braid shield designs are presented.*

## 1. INTRODUCTION

The shielded screening attenuation test method is being standardized in IEC 61196-1 [1], prEN 50289-6 and the SCTE test method IPS-TP-403B2 [2]. As originally conceived the test was applied to relatively short length copper coaxial cables and involved a resonant test fixture length of 1-3 meters [3]. The low end test frequency limit is primarily determined by fixture length, among other variables, and consequently is on the order of 50-100 MHz. The upper end test frequency limit is primarily determined by the TEM mode cut-off frequency and is on the order of 3-6 GHz depending on cable and fixture physical dimensions.

A complete test system is available commercially [4] and test fixture implementations involving standard commercially available components for a maximum fixture length of 6.7 meters have been reported [5,6].

However a 6.7 meter length is good for measurements down to about 20 MHz and a 30 meter length is required to arrive at about 5 MHz.

Development of such a long test fixture was undertaken to support applications such as CATV return path and data I/O and has been encouraged in IEC TC 46/WG5. Furthermore, a direct method for measuring screening attenuation at low frequencies is of interest for confirming extrapolation rules based on short fixture high frequency measurements of transfer impedance.

Another application for the fixture is evaluation of shield longitudinal structural uniformity or lack thereof. The chief drawback to such a fixture is it's very length. This issue has been resolved by mounting the fixture in overhead space along a seldom-used long corridor.

Another consideration was cost. However, standardized rigid transmission line hardware was found to provide an economical solution [7,8].

## 2. TEST FIXTURE DESIGN

The test fixture is outlined in figure 1. The main components are five sections of six meter length, 76.5 mm diameter rigid transmission line segments (without center conductor) which are cascaded together with gas tight coupling flanges.

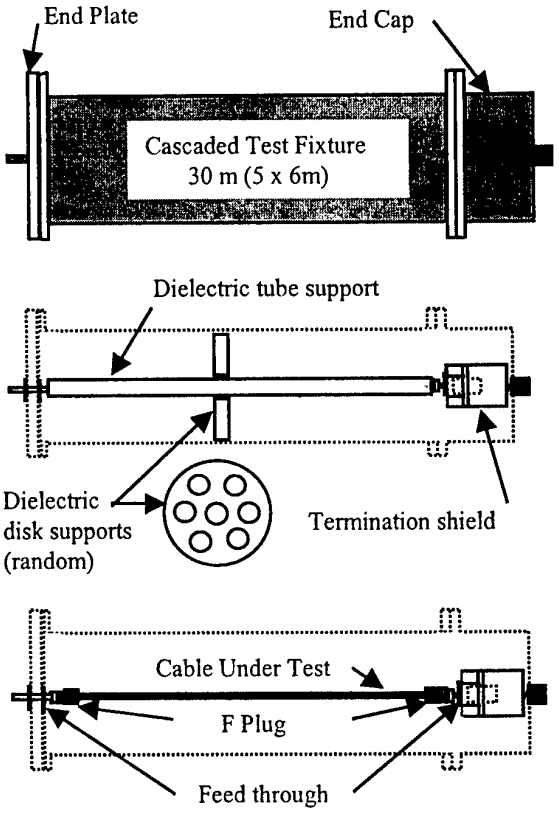



Figure 1. Triaxial Test Fixture Design

Low loss dielectric material is used to support the sample under test. Due to availability/time constraints the dielectric tube support was implemented in 1.8 meter lengths. This compromise created physical and electrical nonuniformities that are acceptable for the low frequency measurements but are less reliable for measurements above about 20 MHz.

An end plate closes the housing at one end and an end cap encloses the other. A feed-through connector is mounted in the center of the end plate. The end cap is fitted with a 50-ohm type N feed-through connector. The center pin of the N feed through connects into one end of an anchor connector. The sample termination shield consists of a split anchor connector that is mated to the end cap anchor connector. One side of the split anchor connector is fitted with a feed-through connector and the mated pair encloses and shields the cable sample termination. This arrangement provides for terminating the cable sample under test with a shielded resistive load and for connecting the shield to the center pin of the N feed through.

The cable sample under test is fitted with a plug type connector at each end and is connected between the feed-through connectors respectively located in the end plate and the split anchor connector.

## 3. ELECTRICAL CHARACTERISTICS

The shield of the cable under test defines the boundary between the two electrical regions within the fixture; the resonant region, which is located between the rigid transmission line cylindrical housing and the cable sample shield, and the cable sample. The diameter ratio of the housing and sample shield diameters is important for determining the impedance and percent velocity of the resonant region, which are approximately 150 Ω and 90 % respectively.

Figure 2 gives the return loss of the resonant chamber measured at the end cap. Shown are results for a 6.7 meter long fixture previously reported [6] and the prototype 30 meter long fixture. Nonuniformity due to the tube dielectric and flange mismatch are evident in the 30 meter results.

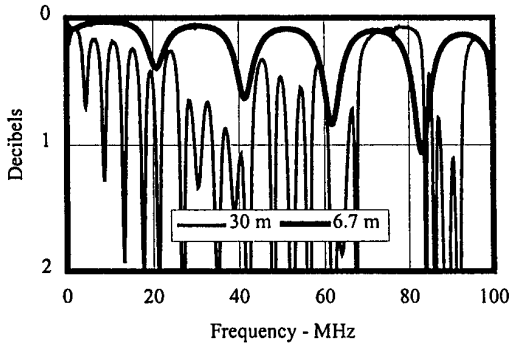



Figure 2. Return Loss of Test Fixture

## 4. DESCRIPTION OF SAMPLES TESTED

Several constructions of RG-6 type and RG-59 type coaxial cable were tested and are designated #'s 1-4. (#1 is RG-59 type and #'s 2-4 are RG-6 type cables). The details are given in tables 1 and 2.

TABLE 1.
Cable Shield Design Data

| # | Foil (inner) | Braid/ Angle (inner) | Foil (outer) | Braid Angle (outer) | Shield DCR mΩ/m |
|---|---|---|---|---|---|
| 1 | – | 95% b. c. /23° | – | – | 9 |
| 2 | a | 60% Al 27° | – | – | 31 |
| 3 | a | 80% Al /27° | b | – | 15 |
| 4 | a | 60% Al /27° | a | 40% Al /20° | 17 |

TABLE 2.
Shielding Tape Design Data

| | Layer Thickness (mm) | | | |
|---|---|---|---|---|
| Foil Type | Al Foil | Polyester | Al Foil | Width (mm) |
| a | .00889 | .02286 | .00889 | 19.05 |
| b | .0254 | .02286 | | 25.4 |

## 5. TEST PROCEDURE

### 5.1 Screening attenuation

The shielded screening attenuation test is closely related to the absorbing clamp test. With both of these methods the sample under test is energized and a signal which is proportional to the resulting leakage field is measured. However, with the shielded screening attenuation method, the leakage field is contained or shielded within a cylindrical metallic tube.

The equipment setup is given in figure 3 and the equipment is listed in table 3.

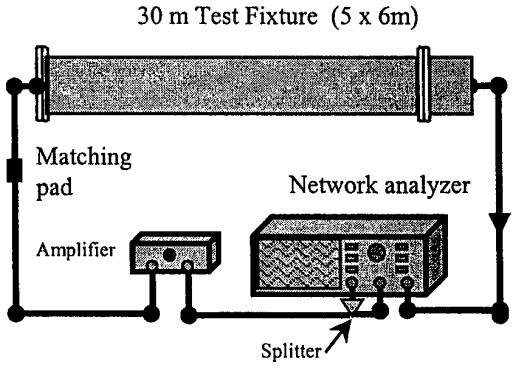



Figure 3. Test Equipment Setup

Screening attenuation is derived from the difference in power levels (insertion loss) between the end plate (energized sample) and the end cap (chamber).

TABLE 3.
Test Equipment

| |
|---|
| Network Analyzer:<br>HP8753ES, +10dBm, 10 Hz res. bandwidth |
| Power Splitter:<br>HP11850C, 9.5 dB loss nominal, DC-3 GHz |
| Matching Pad:<br>HP11852B, 5.7 dB loss nominal, DC-2 GHz |
| Power Amplifier:<br>HP8347A, 25 dB gain nominal, 100 kHz-3 GHz |
| Resistive Termination on sample under test:<br>75Ω type F for CATV applications |

The measured power ratio is normalized with the following formula. The screening attenuation curve is then obtained by drawing the envelope (not shown) formed by connecting the resonant peaks in the power ratio versus frequency plot.

$$a_n = \left| a_{meas} \right| + 10\log_{10}\left|\frac{2Z_S}{Z_1}\right| + 20\log_{10}\left( \sqrt{2}\,\frac{\left|1-\sqrt{\frac{\varepsilon_2}{\varepsilon_1}}\right|}{\left|1-\frac{\varepsilon_3}{\varepsilon_1}\right|} \right)$$

Where:

$a_n$ = normalized screening attenuation (decibels).
$a_{meas}$ = measured screening attenuation of sample in normalized and calibrated setup (decibels).
$Z_1$ = impedance of cable under test (ohms).
$Z_S$ = normalized impedance of screening attenuation fixture (150 ohms).
$\varepsilon_1$ = relative dielectric permittivity of cable under test.
$\varepsilon_2$ = relative dielectric permittivity of the environment of the cable.
$\varepsilon_3$ = relative dielectric permittivity of screening attenuation fixture outer circuit with respect to a 10% velocity difference.

## 5.2 Transfer impedance

The transfer impedance was measured on a short sample length using a triaxial fixture in accordance with IEC 61196-1. The measurement utilized a similar setup as for screening attenuation, however the fixture is driven at the end cap connector. Transfer impedance was determined with the following basic formula:

$$Z_t = \frac{100}{2l}\,10^{a_x/20}$$

Here $a_x$ is the measured power ratio and $l$ is the length.

# 6. TEST RESULTS

## 6.1 Screening attenuation

Screening attenuation results are plotted in figures 4,5 and 6. In figure 4 the lowest frequency peak is at about 4 MHz whereas in figure 5 the corresponding peak is at about 20 MHz.
Figure 6 shows the effect of test chamber nonuniformities around 30 MHz and 70 MHz.

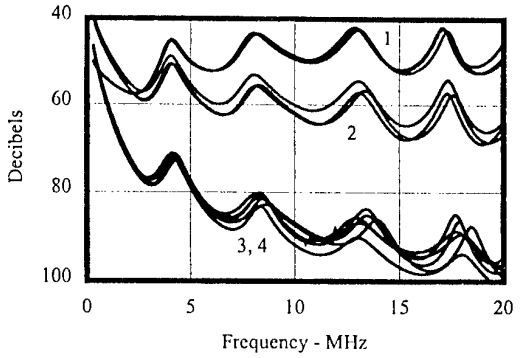



Figure 4. Screening Attenuation; 30 meter fixture
3 samples each cable type

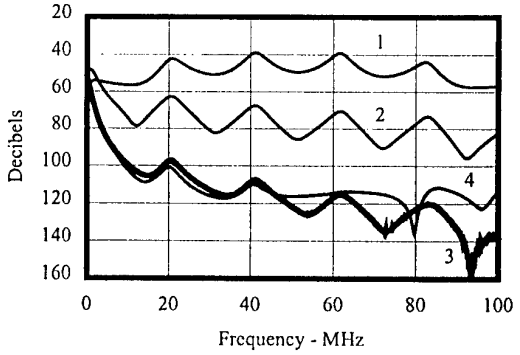



Figure 5. Screening Attenuation; 6.7 meter fixture

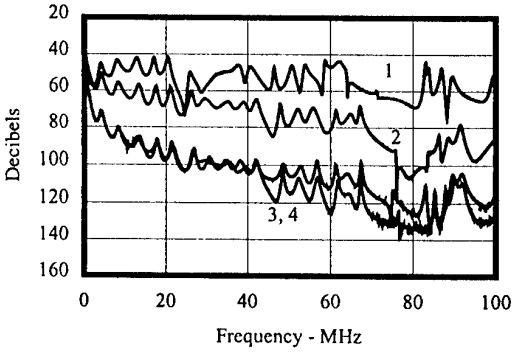



Figure 6. Screening Attenuation; 30 meter fixture

### 6.2 Transfer impedance

Transfer impedance results are shown on linear and logarithmic scales respectively in figures 7 and 8.

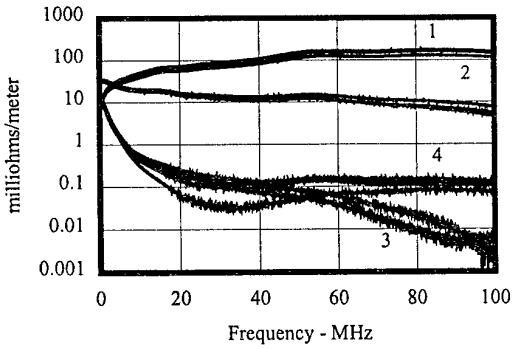



Figure 7. Transfer Impedance; linear frequency scale

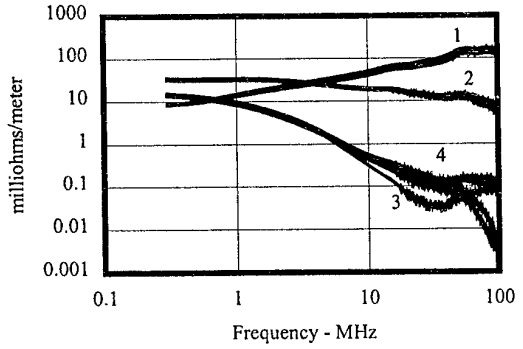



Figure 8. Transfer Impedance; log frequency scale

### 6.3 Transfer Impedance Correlation

Table 4 compares the measured transfer impedance and the extrapolated (from measured screening attenuation) transfer impedance for the four lowest peak frequencies.
Column A corresponds to the measured transfer impedance, and column B corresponds to the extrapolated transfer impedance.

Table 4.
Transfer Impedance Correlation

| Cable # | 1 | | 2 | | 3 | |
|---|---|---|---|---|---|---|
| Peak #. | A | B | A | B | A | B |
| 1 | 26.3 | 9.4 | 26.4 | 6.0 | 1.7 | 0.4 |
| 2 | 42.1 | 11.1 | 21.0 | 3.6 | 0.6 | 0.1 |
| 3 | 57.0 | 13.1 | 19.7 | 3.1 | 0.4 | 0.1 |
| 4 | 66.5 | 12.0 | 18.4 | 3.2 | 0.3 | 0.1 |

## 7. CONCLUSION

Screening attenuation measurements down to 5 MHz are feasible provided the facility exists for a very long triaxial test fixture (about 30 meters). The investment in hardware is relatively small.
Work with the prototype fixture has demonstrated the importance of maintaining uniform transmission line characteristics in the test chamber. Improvements to overcome these limitations are planned.
The measured data for the foil/braid shielded designs shows the frequency dependence of screening attenuation below about 100 MHz and this is particularly noted below 20 MHz.
Work is continuing to assess the correlation of measured transfer impedance on short samples (28 cm) with the measured screening attenuation of long samples (30 meters).

## 8. REFERENCES

8.1 61196-1 Amendment 1 Radio-Frequency Cables – Part 1: Generic Specification – General, definitions, requirements and test methods.

8.2 SCTE (Society of Cable Telecommunications Engineers, Inc.) IPS-TP-403B2 (preliminary-2/1/2000), Test Method for Shield Effectiveness: Screening Attenuation of Coaxial Cable.

8.3 Breitenbach, O; Hähner, T; Mund, B; "Screening of Cables in the MHz to GHz Frequency Range Extended Application of a Simple Measuring Method", IEE Colloquium on Screening Effectiveness Measurements, Savoy Place, London, May 6, 1998.

8.4 bedea/Rosenberger, CoMeT Coupling Measuring Tube. bedea BERKENHOFF & DREBES GMBH, Herborner Straβe 100 • 35614 Aβlar • Germany

8.5 Kincaid, J; Dole, C; "Test Fixture Design and Shielded Screening Attenuation Performance of CATV Coaxial Cable", IEE Colloquium on Screening Effectiveness Measurements, Savoy Place, London, May 6, 1998.

8.6 Kincaid, J; Dole, C; "Implementation of IEC 61196-1 Shielded Screening Attenuation Test Method", International Wire and Cable Symposium, Philadelphia, Pennsylvania, November 19, 1998.

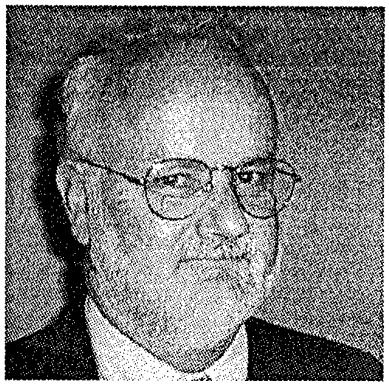
8.7 IEC 60339-1,2 General purpose rigid coaxial transmission lines and their associated flange ...

8.8 EIA-225 Rigid Coaxial Transmission Lines...

## ACKNOWLEDGEMENTS

The authors are grateful to the Belden Electronics Division for the support extended to develop screening attenuation measurement technology. Thanks to Benjamin Willett for assistance with the laboratory measurements.

BIOGRAPHICAL NOTES



John Kincaid

John is a Senior Product Engineer at the Belden Engineering Center. He holds BSEE and MSEE degrees from the University of Oklahoma and has over 25 years experience with Belden. His experience encompasses engineering management and product development positions in the USA as well as in Europe. He holds nine patents. John is a member of the IEEE and is active in IEC and TIA cable standardization activities. He is the US Technical Advisor to IEC SC 46A on coaxial cables, and is Convenor of IEC SC 46A/WG3 on data and CATV cable. He is also an expert on working groups 5 and 7 dealing with shielding and premises cabling issues.



Carl Dole

Carl is an Associate Product Engineer and has been at the Belden Engineering Center for ten years. He will be graduating highest distinction in December with a BS degree in Electrical Engineering Technology from Purdue University. Prior to joining Belden, Carl worked 10 years in television broadcast engineering and has a FCC General Class Radiotelephone License. Presently he is working on developing improved test methodologies for shielding and other tests at Belden. He is a member of IEEE, SMPTE, and SBE.

EMC 2000 INTERNATIONAL WROCŁAW SYMPOSIUM ON ELECTROMAGNETIC COMPATIBILITY

# FUTURE DEVELOPMENTS OF STANDARDISATION OF COUPLING ATTENUATION

Poul Villien

3P THIRD PARTY TESTING
Agern Allé 3, DK-2970 Hørsholm, Denmark
e-mail: Villien@3Ptest.dk Fax +4545765708

*This paper concerns the future developments of standardisation of coupling attenuation. After the assumed approval of the coupling attenuation test method for cables in July 2000 work will be continued to extend the method to cover patch cords, connecting hardware, and cable assemblies as both laboratory and in-field measurements. Principles, problems and time scale for completion of work are discussed.*

## 1. GENERAL

The coupling attenuation test method has got very high international attention as this parameter is a key to allow comparative identification of electromagnetic performance for both screened and unscreened components. As an example unscreened balanced cable standards from CENELEC for years could not be prepared until the introduction of coupling attenuation. Before then international agreement about the electromagnetic performance of unscreened cables for high speed applications could not be reached. Unscreened balanced cable standards in the CENELEC EN 50288-X-Y series will now soon be published and contain minimum coupling attenuation requirements for different types of cables. The requirements have been proposed, but the test method has not yet been agreed. This test document, CENELEC EN 50289-1-6, is now out for its final 3 months approval process and agreement is expected in July 2000.

The CENELEC standardisation committee TC 46X has stressed its great interest in coupling attenuation also as a test method for components other than cables. At their March meeting its Working Group 3 was urged to continue to prepare test standards for patch cords, connecting hardware and cable assemblies as fast as possible after the positive conclusion of the cable test voting process. This work is presently put on hold, but the basic principles of the test method for patch cords, connecting hardware and laboratory measurements of cable assemblies have already been discussed in Working Group 3. Only the in-field cable assembly test method has not yet been treated.

The future coupling attenuation test standards will be published in the CENELEC EN 50289-1-X series. It is expected that the CENELEC standards after agreement also will be issued as IEC standards.

## 2. PATCH CORDS

The coupling attenuation test method for patch cords is the first standard to be developed after the agreement of the cable test method.

Patch cords are cables terminated with connectors in one or both ends. The length of the cables may vary from below one metre to more than 10 metres. Compared with the cable specification the special issues to be addressed by the patch cord standard are therefore:

- Two adaptor cables, each with mating connector (test head), are needed to terminate the patch cord with the signal generator and the far end cable.
- The two ends of the patch cords may have different connectors and also very different coupling attenuation values.

To cover these two special points the test method is proposed to be based on the cable test method of EN 50288-1-6 with the following two modifications:

- The coupling attenuation of the test heads and adaptor cables must be verified in order to know the maximum coupling attenuation that can be measured for the patch cord in question. Selection of adaptor cables and test heads should of course be optimised in order to allow the highest possible patch cord measurement. Also the nature of the

adaptor cables must be the same as for the cable of the patch cord. For instance unscreened balanced cable and test heads must be used for unscreened balanced patch cords. Coupling attenuation of patch cords can never be measured better than the coupling attenuation of test heads and adaptor cables.

- The measurement is performed using a fixed position of the absorbing clamp. This means that measurement of the two ends of a patch cord is performed by reversing the patch cord in the test set-up and not by performing a near end and far end measurement (as done for the cable measurement). It will be necessary to use different lengths of adaptor cables in the two reversed measurements if the connectors in the two ends of the patch cables are not the same.

A likely procedure would be to place the absorbing clamp close to the test head in either the near or far end (to be specified by the standard) and with the absorbers six metres from the absorbing clamp. The absorbers are then placed on the patch cord itself or on the far end cable for patch cords shorter than six metres.

In every other respect the cable test procedure can be applied.

## 3. CONNECTING HARDWARE

The coupling attenuation test method for connecting hardware is the second standard to be developed.

Connecting hardware does not include the mating connector part. Compared with the cable specification the special issues to be addressed by the connecting hardware standard are therefore:

- Two adaptor cables without or with mating connector (patch cord) are needed to terminate the connecting hardware with the signal generator and the far end cable.
- The two ends of the connecting hardware may have different connectors or even just a direct cable termination.

To cover these two special points the test method is proposed to be based on the cable test method of EN 50288-1-6 and the patch cord test method discussed above with the following two modifications:

- The coupling attenuation of any patch cords and/or adaptor cables must be verified in order to know the maximum coupling attenuation that can be measured for the connecting hardware in question. Selection of adaptor cables and patch cords should of course be optimised in order to allow the highest possible connecting hardware measurement. Also the nature of the adaptor cables and patch cords must be the same as for the connecting hardware. Coupling attenuation of connecting hardware can never be measured better than the coupling attenuation of patch cords or adaptor cables.
- Like for the patch cords the measurement is performed using a fixed position of the absorbing clamp. It will be necessary to use different lengths of adaptor cables or patch cords for the two reversed measurements if the connectors in the two ends of the connecting hardware are not the same. This is a normal situation when measuring balanced connecting hardware.

A likely procedure would be to place the absorbing clamp close to the connecting hardware in either the near or far end (to be specified by the standard) and with the absorbers on the far end cable six metres from the absorbing clamp.

In every other respect the cable test procedure can be applied.

Presently a test method based on the above described principles has been included in the proposed IEC specification for connectors to be used in cabling according to the ISO/IEC IS 11801 and CENELEC EN 50173 specifications.

## 4. LABORATORY MEASUREMENTS OF CABLE ASSEMBLIES

The coupling attenuation laboratory test method for cable assemblies is the third standard to be developed.

Cable assemblies include combinations of connecting hardware, patch cords and/or cables. Common specific examples of cable assemblies are links and channels as defined in CENELEC EN 50173 and ISO/IEC IS 11801. Compared with the cable specification the special issues to be addressed by the cable assembly laboratory testing standard are therefore:

- A way to identify the "sum" of the coupling attenuation of all included components must be established.
- Two adaptor cables without or with mating connector (patch cord) may be needed to terminate the cable assembly with the signal generator and the far end cable.

To cover these two special points the test procedure is proposed to be based on the cable test method of EN 50288-1-6 and the patch cord and connecting hardware test methods discussed above with the following two modifications:

- The coupling attenuation of any adapting patch cords and/or cables must be concluded in order to know the maximum coupling attenuation that can be measured for the connecting hardware in question. Preferably selection of any adaptor cables and patch cords should be made from the same components as being part of the cable assembly

under test. Alternatively their coupling attenuation must be optimised in order to allow for the highest possible connecting hardware measurement.

- The measurement of a cable assembly is carried out as individual measurements of all its components, i.e. every type of **mated** connecting hardware and cable. The absorbing clamp is moved to the different key positions of the cable assembly which means to both sides of every connecting hardware type and on every cable type.
- The cable assembly should be terminated to the signal generator through adaptor cables or patch cords being of the same type as used in the cable assembly in question. If this is not possible other adaptor cables or patch cords may be used, but their coupling attenuation will define the maximum value that can be measured.

A likely procedure would be to connect the cable assembly to the signal generator and carry out the measurement of each component at a time. For a balanced cable assembly consisting of a patch cord (type 1), connecting hardware (type 1), horisontal cable, connecting hardware (type 2) and patch cord (type 1) (i.e. a typical channel) the measurements would be carried out in the following sequence:

A. Measurement with the absorbing clamp positioned at the extreme end of the first patch cord.
B. Measurement with the absorbing clamp positioned at the near end of the connecting hardware (type 1).
C. Measurement with the absorbing clamp positioned at the far end of the connecting hardware (type 1).
D. Measurement with the absorbing clamp positioned at the far end of the connecting hardware (type 1), but pointing at the horisontal cable part (horisontal cable measurement).
E. Turning cable assembly to connect opposite end to signal generator.
F. Measurement with the absorbing clamp positioned at the near end of the connecting hardware (type 2).
G. Measurement with the absorbing clamp positioned at the far end of the connecting hardware (type 2).

The coupling attenuation of the cable assembly is the worst case value of any performed measurement considering a 10 dB (to be agreed) relaxation of the connecting hardware measurements.

## 5. IN-FIELD MEASUREMENTS OF CABLE ASSEMBLIES

The in-field coupling attenuation test method for cable assemblies has not yet been discussed in Working Group 3. Consequently no safe indication can be given about the nature of the future specification. However, it seems important that a **quantitative method** is developed, and that this method is reproducible with an acceptable precision. A possible way could be to connect the installed cable to the signal generator by a known patch cord. The absorbing clamp should then be placed on the patch cord and the value of coupling attenuation for both ends of the cable assembly could be measured.

The worst case value of the two measurements, considering a 10 dB (to be agreed) relaxation, could be considered as the coupling attenuation of the installed cable assembly.

The correctness, reproducibility and uncertainty of any in-field test method must of course be demonstrated before it can be specified. Therefore the solution proposed above is only the authors ideas of a future possible test method.

## 6. TIMESCALES OF WORK

The coupling attenuation standard for cable testing needs to be agreed before work on other component types will be started. Based on discussions with experts from European countries it is expected that the outcome of the 3 months approval process will be an agreement in July 2000. After then, intensive work to complete the other documents will be started. It is expected that the patch cord, connecting hardware and laboratory method of cable assembly measurements will be completed as working group drafts for national inquiry by the end of 2000. The in-field test standard is scheduled for completion in the spring 2000, but might be delayed in case of necessary technical evaluations needed to conclude the test method.

The final standards are then in the best case scheduled for publication in the last part of 2001 and in 2002 for the in-field test method.

## BIOGRAPHICAL NOTE

Poul Villien is coordinating manager at 3P Third Party Testing. He is active in both IEC, ISO/IEC and CENELEC standardisation of cables, connecting hardware and cabling. Poul Villien is the chairman of CENELEC TC 46X Working Group 3, dealing with EMC related cable performance included development of the coupling attenuation standards for cables, patch cords, connecting hardware and cable assemblies.

EMC 2000 INTERNATIONAL WROCŁAW SYMPOSIUM ON ELECTROMAGNETIC COMPATIBILITY

# Introduction to the MOM and the GTD/UTD and their Combination

Prof. Dr.-Ing. Karl-Heinz Gonschorek

Carl Friedrich von Siemens-Foundation Chair on Electromagnetic Compatibility
Dresden University of Technology, Helmholtzstr. 9, 01069 Dresden, Germany

**Summary:** The Method of Moments (MOM) has proven to be a very useful tool for analysing electromagnetic fields in complex environments. The normal procedure within the MOM, the discretization of the metallic bodies into segments for thin wire structures or patches for larger surfaces, limits it's use. Not only the size of the so-called system matrix is a boundary, also the matrix becomes more and more ill-conditioned. To overcome these difficulties the Geometrical Theory of Diffraction (GTD) was introduced by Keller in 1962 [1], which was later on extended to the Uniform Geometrical Theory of Diffraction (UTD) [2]. In this theory the electromagnetic interaction between two points in space is described by a limited number of rays, the higher the frequency the better the results. Combining the MOM and the GTD/UTD allows to treat electromagnetic interactions within complex environments, containing both electrically small and electrically large bodies. In the contribution an introduction to both methods shall be given, concentrating more or less on GTD/UTD. Another main subject of the presentation describes the combination of both methods, which leads to a new class of problems to be solvable now. The paper will close with two examples investigated by the GTD/UTD or by a combined use of MOM and GTD/UTD.

## 1. Introduction

The Method of Moments (MOM) is a well established method for calculating electromagnetic interactions within complex environments containing metallic and dielectric bodies. Large and powerful computer packages, based on the Method of Moments, are available today, for instance CONCEPT, FEKO, NEC, which allow to investigate questions like near and far fields of linear antennas, coupling from antennas to interfaces and cables, coupling between cables and from electronics to antennas, always considering the whole electromagnetic environment. In this method a matrix of unknowns is build up, which becomes larger and larger with increasing frequency. A complete different method is given by the Geometrical Theory of Diffraction (GTD). In this theory the electromagnetic radiation within a complex environment between two points in space is described by a limited number of rays. In a first step no matrix is needed. The results become better and better with increasing frequency. Looking for arrangements of common interest which may have dimensions in the metre-region the Method of Moments can be used up to about 1 GHz, the Geometrical Theory of Diffraction can be applied starting with appr. 500 MHz. To repeat: In the MOM the structure parts have to be small compared to or in the range of the wavelength under consideration. In the GTD/UTD the scattering bodies have to be large in terms of the wavelength. There is really an overlapping range, where both methods can be applied, which makes it easy to check results or new developments. If an arrangement is given containing both electrically small and electrically large bodies a combined method has to be applied, which makes use of the advantages of both methods. After a short introduction to the Method of Moments (a status report will follow in the next contribution [3]) a more detailed explanation of the Geometrical Theory of Diffraction will follow. Having prepared both methods a way combining both will be explained.

## 2. Method of Moments

The Method of Moments, which belongs to the boundary element methods, describes the electromagnetic behaviour of an arrangement by surface currents, in case of very thin electrodes by currents flowing on their axes. Normally these currents are unknown and have to be predicted by variational procedures. It has turned out that subdividing the surfaces resp. the wires into subsections defining a current function on each subsection seems to be the most economic way for arbitrary arrangements. Furthermore most programs use triangle or roof-top

shapes for these current expansion functions. The equations combining the current with the electric field strength are given by

$$\vec{E} = -\,grad\,\phi - j\omega\,\vec{A}\ ,$$

with

$$\phi = \frac{1}{4\pi\varepsilon}\iiint_{V'}\rho\,(V')\cdot\frac{e^{-j\frac{2\pi}{\lambda}|\vec{r}-\vec{r}'|}}{|\vec{r}-\vec{r}'|}\cdot dV', \qquad (1)$$

$$\vec{A} = \frac{\mu}{4\pi}\iiint_{V'}\vec{J}(V')\cdot\frac{e^{-j\frac{2\pi}{\lambda}|\vec{r}-\vec{r}'|}}{|\vec{r}-\vec{r}'|}\cdot dV'\ ,$$

and $$\rho = \frac{j}{\omega}\,div\,\vec{J}\ .$$

Let's assume a λ/2-wire, driven by a voltage source of 1 V, which is subdivided into 6 segments leading to 5 overlapping triangles as show in Fig. 1. For 6 segments only 5 triangles are needed, because in reality a piecewise linear expansion is used. The amplitude of the triangles are unknown in the first step. To predict these unknowns boundary conditions have to be defined. For 5 unknowns 5 boundary conditions are needed. Boundary conditions are given by the fact that a tangential electric field strength is not allowed on the surface of a wire. And this is valid for the whole surface except the point of excitation. So 4 conditions can be derived from $E_{tan} = 0$ and one from the driving voltage. In table 1 the results for a wire radius of λ/1000, produced by CONCEPT, are stated.

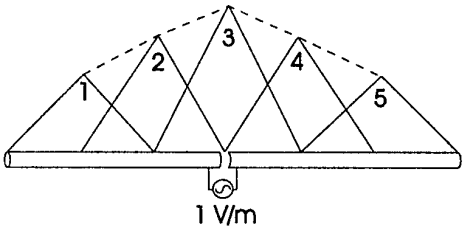



**Fig. 1:** λ/2-dipole with 5 triangle expansion functions

| | | |
|---|---|---|
| Driving voltage: | 1 | V/m |
| Input impedance: | 77.8 + j*33.6 | Ω |
| Current on segment 1 and on 5: | 5.7 - j*3.3 | mA |
| Current on segment 2 and 4: | 9.5 - j*5.0 | mA |
| Current on segment 3: | 10.8 - j *4.7 | mA |

**Table 1:** Results of a MOM-calculation (λ/2-dipole with wire radius of λ/1000)

To get the stated results a matrix of 5 x 5 elements is build up, considering all interactions between the 5 current functions. This very simple example should only demonstrate the procedure and give an impression that for rebuilding the real current distribution a certain number of segments is needed. The default value in CONCEPT is 8 triangles per wavelength.

In Fig. 2 an example is given, that shall show, what's also possible. An antenna installed on the roof of a car is fed at 88 MHz with a power of 100 W. The radiated electromagnetic field produces, as explained above, currents on the surface of the car. These currents are also shown in Fig. 2. The arrows represent these currents. Their length is a measure of their amplitude.

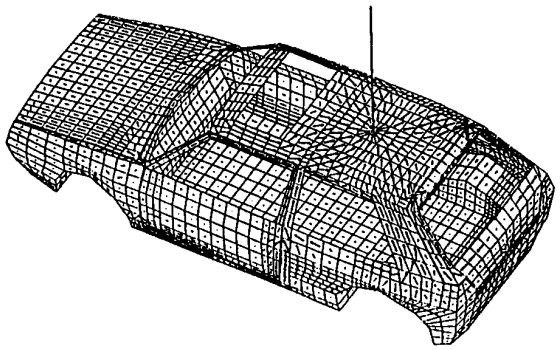


**Fig 2:** Antenna on the roof of a car, frequency f = 88 MHz

### 3. The Geometrical Theory of Diffraction

The best way to start explaining the Geometrical Theory of Diffraction seems to be making some general remarks:

1. Using the method of subsections within the Method of Moments restricts the size of objects which can be investigated. Usually a max. length of a subsection (in case of patches for a base line) of λ/10 is specified.
2. Depart from the fact that the system matrix becomes larger and larger with increasing frequency the matrix becomes more and more ill-conditioned.
3. In 1962 Keller introduced the Geometrical Theory of Diffraction. The idea is that at high frequencies the electromagnetic field can be described sufficiently by a limited number of rays.
4. The Geometrical Theory of Diffraction represents an extension of the classical theory of geometrical optics.
5. It permits the calculation of high-frequency fields in the vicinity of electrically large and complex bodies. By applying variational techniques asymptotic solutions of Maxwell's equations can be found.
6. Additionally to the direct ray and the well-known reflection process on the surface of a metallic body the Geometrical Theory of Diffraction uses three more processes
   * rays, diffracted at edges between surfaces,
   * creeping waves,
   * rays, diffracted at tips and wedges.

The two expressions GTD = Geometrical Theory of Diffraction and UTD = Uniform Geometrical Theory of Diffraction will be used interchangeably in this contribution. The UTD is an extension of the classical theory. It avoids some field inconsistencies at boundary lines, for instance between the light and the shadow region.

The GTD/UTD is based on rays. In Fig. 3 the wave front of a ray in it's general description is given. A general ray has two main curvatures $K_1$ and $K_2$ , which can easily be described by a direction and a curvature radius $\rho_i$. Such a ray propagates from a starting point up to a fieldpoint, in this case we have a direct ray, or up to a reflection or diffraction point

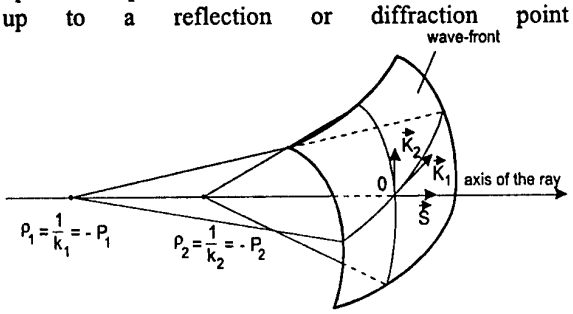



**Fig 3:** Description of a wave front

In Fig. 4 a reflection on a curved surface is shown. The incident ray $S_i$ touches the surface at the reflection point R, here the ray is modified, depending on the shape of the surface around the reflection point, and is leaving the surface as scattered ray $S_r$. At the reflection point locally the reflection law with respect to the angles has to be fulfilled.

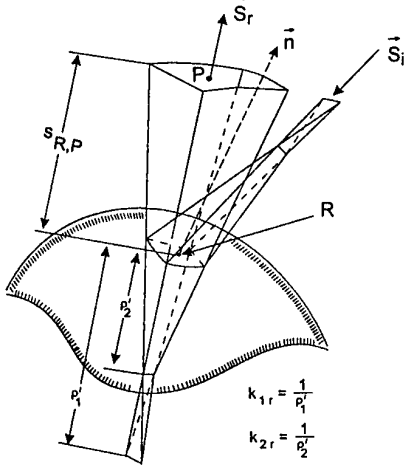



**Fig. 4:** Reflection on a curved surface

The edge, wedge and tip diffraction will not be explained here, they are a little bit more complicated, their contribution is normally small if direct and/or reflected rays are given. They cannot be denied because in shadow regions sometimes they deliver the only component. The reader may be point to the literature [2].

From physical observations it is known that also in the shadow region of smoothly curved bodies electromagnetic fields exist. To get these parts one more type of ray is needed, the so-called creeping wave. The creeping wave touches the surface tangentially (seen from the source or starting point) creeps within the surface for a certain distance and leaves the surface again tangentially in the direction toward the point of interest. In Fig. 5 such a creeping wave is depicted. The ray $S_i$ touches the surface at point $B_1$, creeps in a transmission tube up to the point $B_2$ and leaves the surface as modified ray $S_c$. On it's way from $B_1$ to $B_2$ it looses continuously energy because of it's permanent radiation.

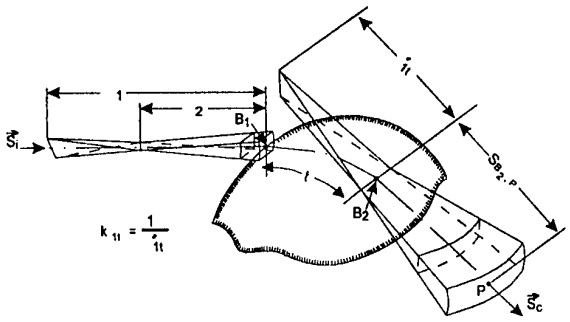



**Fig. 5:** Creeping wave

Rays must be predicted within the Geometrical Theory of Diffraction. Therefore a great part of work is more of geometrical than of electrical nature. A check can easily be carried out whether all or enough rays are considered by calculating not only the field in a certain field point but also in it's near vicinity. From physics it is known that the field cannot chance drastically for two field points having a spatial distance of less than $\lambda/2$.

$$\begin{aligned}\vec{E}(P) = {} & \vec{E}_i(Q)\ \frac{e^{-j\beta s_{Q,P}}}{\sqrt{\left(1+k_1 s_{Q,P}\right)\left(1+k_2 s_{Q,P}\right)}} \\ & + \left[R(R)\right]\ \vec{E}_i(R)\ \frac{e^{-j\beta s_{R,P}}}{\sqrt{\left(1+k_{1r} s_{R,P}\right)\left(1+k_{2r} s_{R,P}\right)}} \\ & + \left[D(K)\right]\ \vec{E}_i(K)\ \frac{e^{-j\beta s_{K,P}}}{\sqrt{s_{K,P}\left(1+k_{1d} s_{K,P}\right)}} \\ & + \left[T\left(B_{1,2}\right)\right]\ \vec{E}_i\left(B_1\right)\ \frac{e^{-j\beta s_{B_2,P}}}{\sqrt{s_{B_2,P}\left(1+k_{1t} s_{B_2,P}\right)}}\end{aligned} \qquad (2)$$

In equation 2 a complete description is given for the case of a propagation from a source point Q to a field point P if the direct ray, one reflected ray, one edge diffracted ray and a ray with a creeping part has to be considered.

One of the problems of the geometrical theory of diffraction is the knowledge of the diffraction dyades, R (R), D (K), T ($B_{1,2}$) with respect to eq. 2, which describe the modification of the rays at the surfaces. A diffraction dyade is a 2 x 2 matrix having only coefficients on it's main diagonal.

The following problems areas of GTD/UTD can be summarised:

1. Mathematical formulation of the diffraction dyades as mentioned,
2. Ray-tracing in order to predict all rays between source- and observation-point that fulfil Fermat's principle,
3. Suppression of rays which are not possible due to obstacles on their way from source- to observation-point,
4. Consideration of rays with multiple diffractions???,
5. Source description.

The mathematical formulation of the diffraction dyades is a special field of investigation, which shall not be treated here.

The points 2 to 4 are more or less geometrical questions.

The question marks closing point 4 have a double meaning:

a) formulation of a general procedure to find and describe the multiple diffractions taking into account all boundary conditions,
b) specifying a criteria which and how many multiple diffractions have to be considered.

## 4. Source description within GTD/UTD

The GTD/UTD in it's basic form is defined for or in rays. The MOM, as a boundary element method, relates the field to currents on the boundary between two media, in the case we are treating here, to currents on surfaces. To prepare the combination of GTD/UTD and MOM, but also for a better application of the geometrical methods, it is advisable to find a way to relate the rays to currents. There are several possibilities. The best seems to be the use of so-called Ekelman-sources, which are a rebuilding of sinusoidal current functions into a series of three point sources. In Fig 6 the transformations from piecewise constant (Hertzian Dipol) and from piecewise sinusoidal current distributions to far fields are shown.

## 5. Procedure for combining MOM with GTD/UTD

Having a MOM- and a GTD/UTD-program available the combination is easily realised. The complex environment under investigation is divided into two parts, the MOM-part, containing the electrically small bodies, and the GTD/UTD-part with the electrically large structures. A system matrix for the MOM-part is build up and modified by correction terms coming from diffraction processes at the large bodies. The procedure has been presented several times. By doing this some conditions have to be obeyed, for instance if the MOM-part consists of two spatial regions, which are partly or totally shadowed by the large objects.

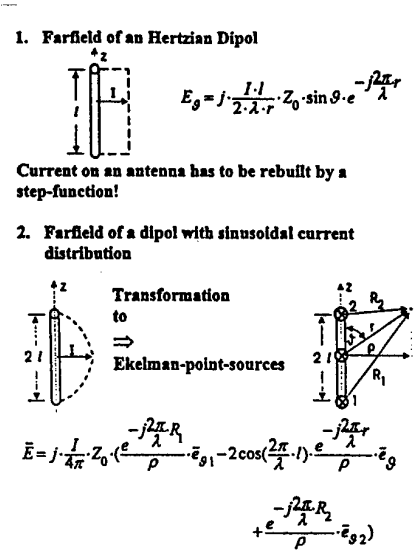



**Fig. 6:** Source description, coming from currents to fields

Also a special procedure is needed if the MOM-bodies are directly connected to the GTD/UTD-structure. Fig. 7 contains two wires near to a large scattering body. The electromagnetic interactions between the two wires can be decribed by the Method of Moments. The influence of the scattering body will be considered by diffraction coefficients. As a consequence we got two matrices for the wire coupling, one considering the direct coupling from segment to segment and one for the coupling via the scattering object from segment to segment. Adding both matrices and inverting the combined matrix yields the currents on the wires. Having these currents the whole field within the arrangement can be calculated now.

## 6. Examples for the application on GTD/UTD and the combination with MOM

Two examples shall demonstrate the features of the tools described above. In the first example a dipole-antenna is placed in front of a mast on a ship. The antenna has a length of $\lambda/2$ and a distance to the mast of 2.25 $\lambda$. The superstructure of the ship is rebuild by 14 building blocks. The investigation is carried out at 2 GHz. The influence of the superstructure to the current of the $\lambda/2$-antenna is not taken into account. In Fig 8 the arrangement and the far field pattern is presented.

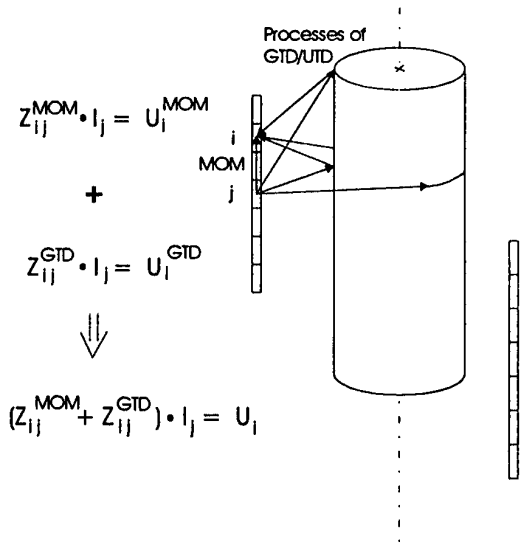



**Fig. 7:** Combining MOM with GTD/UTD

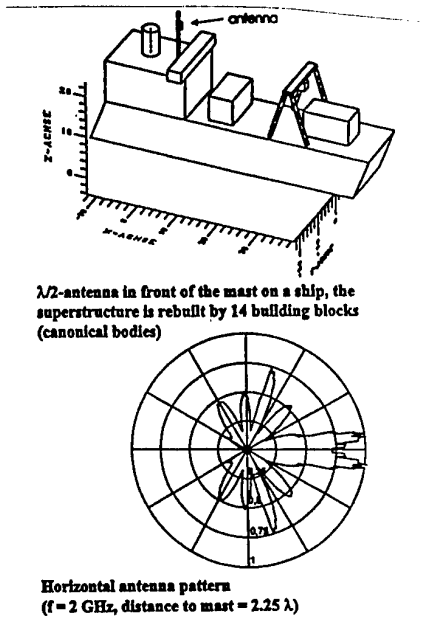



**Fig. 8:** λ/2-antenna on a ship in front of a mast

The second example was investigated by a hybrid-program, which combines both methods in the way stated above. A λ-dipole is located in the vicinity of two large scattering bodies. It is asked for the voltage coupled into a λ/2-sensor. The sensor is moved on a line behind the two large objects. In Fig. 9 the arrangement and the results are given. Additionally to the plot from the hybrid program (solid line) a first order result is shown which was produced by a procedure based only on optical considerations (dashed line). For the approximate solution the coupling between the λ-dipole and the λ/2-sensor was calculated by a MOM code, not considering the large scattering objects. The results were than modified by suppressing the sensor voltage for the cases where no optical sight is given between the dipole and the sensor. It is clearly to be seen that the fields between the two scattering objects cannot sufficiently be described by simple estimations.

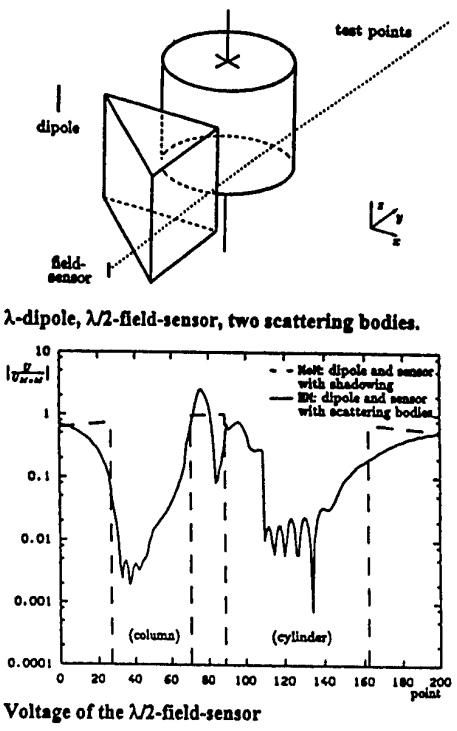



**Fig. 9:** Coupling between a dipole and a sensor

## 7. Conclusion

In the contribution an introduction to the Geometrical Theory of Diffraction (GTD/UTD) and it's combination with the Method of Moments (MOM) should be given. The main ideas have been presented. Two example demonstrate the features of a hybrid procedure.

## References

[1] Keller, J. B.: 'Geometrical theory of diffraction', J. Opt. Soc. Am. Vol 52, pp. 116-130

[2] Patak, P. H.: 'Uniform Geometrical Theory of Diffraction',AGARD Lecture Series No. 312 (1887), pp. 2.1-2.20.

[3] Jakobus, U.: 'Latest Developments in the Method of Moments for an Efficient Numerical Solution of Complicated and Large Scale EMC Problems', Sci. Contr. to Wroclaw Symposium on EMC 2000, Wroclaw, June 2000

**Karl-Heinz Gonschorek** studied high frequencies at the University of Hanover. From 1975 to 1980 he was an scientific co-worker at the University of the Armed Forces in Hamburg. Here he wrote his Ph.D. thesis about electromagnetic pulse-coupling in extended arrangements of thin wires. Today he is holder of the Carl Friedrich von Siemens-Foundation Chair on EMC at the Dresden University of Technology.

**EMC 2000** INTERNATIONAL WROCŁAW SYMPOSIUM ON ELECTROMAGNETIC COMPATIBILITY

# LATEST DEVELOPMENTS IN THE METHOD OF MOMENTS FOR AN EFFICIENT NUMERICAL SOLUTION OF COMPLICATED AND LARGE SCALE EMC PROBLEMS

Ulrich Jakobus

Institut für Hochfrequenztechnik, University of Stuttgart
Pfaffenwaldring 47, 70550 Stuttgart, Germany
Fax +49 (0)711/685-7412, Phone +49 (0)711/685-7420
E-Mail u.jakobus@ieee.org

*This paper discusses some recent extensions to the Method of Moments as implemented in the computer code FEKO, which enhance the capabilities with respect to modelling of large scale practical EMC problems. Amongst the presented extensions are frequency interpolation, iterative solution techniques for massively parallel supercomputers, and some improvements in a current based hybrid technique.*

## 1 INTRODUCTION

Amongst other numerical techniques, the Method of Moments (MoM) finds a very widespread application in the area of EMC e.g. for a variety of automotive applications. With increasing available computer power, there is the trend that EMC engineers try to solve more complex and larger problems, and this need seems to grow even faster than the available computer power. It is therefore essential to continuously improve the numerical techniques in order to increase the efficiency and to extend the range of application.

The present contribution aims at summarising some recent extensions of the MoM, which are already available, or will be made generally available soon, in the computer code FEKO [1].

## 2 INSULATED METALLIC WIRES

For some EMC applications it is essential to take a possible dielectric coating of metallic wires into account, or also the insulation of wires that are located in a lossy environment. Certainly a full MoM model could be constructed for dealing with such a configuration, by treating the coating as a dielectric tube around the wire and introducing equivalent electric and magnetic surface current densities within the framework of the MoM. But this approach is extremely expensive concerning memory and CPU-time requirements. Popovic has pointed out in his book [2] possibilities of transforming a wire coating into a distributed inductive load, which can be handled very efficiently by the MoM. His approach, however, fails in certain situations, e.g. if the loss tangents of the coating and the surrounding medium are different. A special technique has been developed, which makes use of the volume equivalence principle and directly relates the volume polarisation current to the line charge distribution along the wire, similar to the proposals in [3, 4].

An application example is depicted in Fig. 1. Two monopoles of heights $h = 11\,\mathrm{cm}$ and wire radii $r_w = 0.2\,\mathrm{mm}$ are placed at a distance of $d = 10\,\mathrm{cm}$ into a lossy liquid (water). Fig. 2 shows the resulting transmission coefficient $S_{21} = 2\,U_r/U_0$ versus frequency; the dashed line represents $S_{21}$ for uncoated wires (MoM solution with 132 unknowns). Taking the insulation with $\varepsilon_{r,2} = 2.5$ and $r_d = 1.7\,\mathrm{mm}$ into account by a rigorous full MoM formulation leads to the solid line in Fig. 2. One can clearly notice the effect of the insulation. However, by the full MoM so-

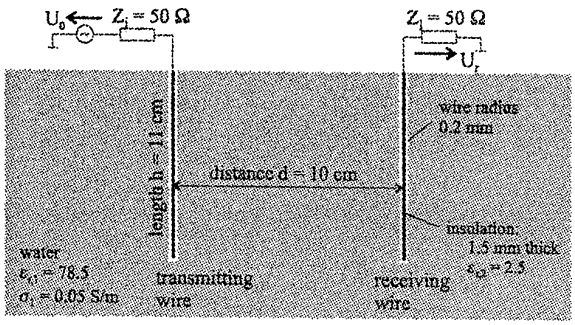



Fig. 1: Coupling between two insulated wires in a lossy environment.

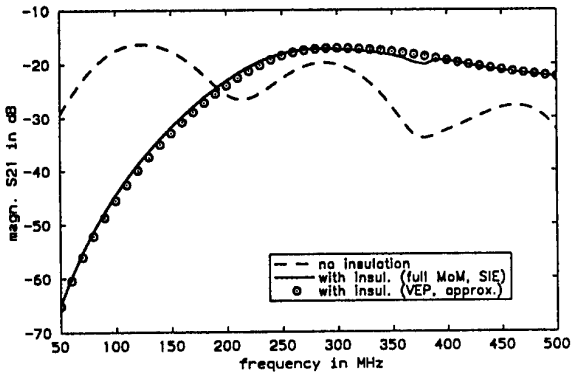



Fig. 2: $S_{21}$ coupling coefficient for the arrangement in Fig. 1 as a function of frequency.

lution, the number of basis functions increases from 132 (no insulation) to 4524 (with insulation). Applying the new approximate formulation based on the volume equivalence principle allows to account for the insulation with only 132 unknowns. The result is depicted in Fig. 2 by the circular symbols. There is an excellent agreement as compared to the full MoM reference solution.

## 3 MOM/UTD/PO HYBRID METHOD

For electrically large metallic or homogeneous dielectric bodies, FEKO offers the option to use a hybridisation of the MoM with high–frequency asymptotic techniques: MoM/PO (physical optics) or MoM/UTD (uniform theory of diffraction) [5]. Correction terms for the PO are available and lead to the IPO (improved PO) or to Fock currents.

One recent extension of this hybrid method is the application of Fock currents and PO edge and wedge correction terms to complicated structures where it may happen that part of the Fock region is shadowed by PO surfaces, or that part of the edge/wedge where the correction shall be taken into account, is shadowed as well.

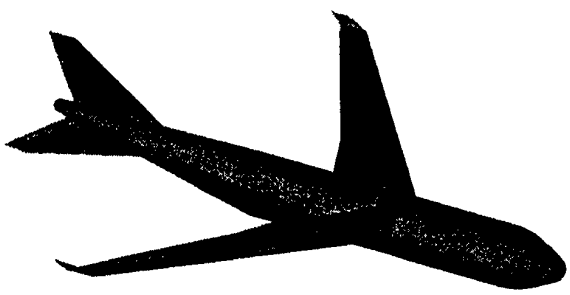


Fig. 3: Aircraft model with the surface current density as obtained by the improved PO and Fock currents.

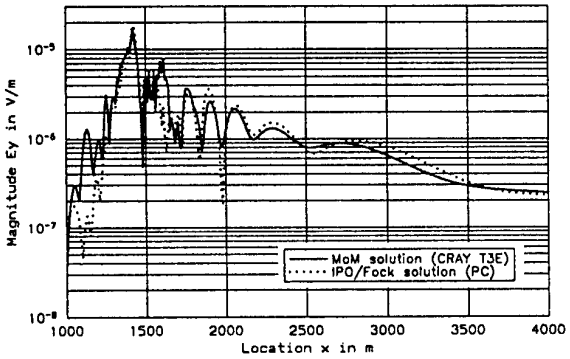



Fig. 4: Magnitude of the scattered electric field strength along the runway.

An application example from aviation shall be discussed. At a typical distance of 150 m parallel to the runway is the so–called taxiway, where aircrafts queue waiting for take–off. Such an aircraft is shown in Fig. 3 (the ground plane is taken into account in the computation, but not shown in the figure). The main problem to be investigated is, that this aircraft represents a metallic obstacle, and will disturb the signal of the localiser by superimposing scattered components. This situation is depicted in Fig. 4, where the scattered electric field strength is plotted along the runway in a height of 4 m above ground in a distance range from 1 to 4 km from the antenna.

Using the full, conventional MoM leads to the scattered field strength as indicated by the solid line in Fig. 4. Such an investigation, however, is quite expensive. For a segmentation with 27145 unknowns the solution time on a heterogeneous LINUX cluster with 6 nodes is about 1.6 days. Since not enough main memory is available, out–of–core techniques must be used.

Using the available hybrid methods in FEKO, the computational cost can be reduced significantly. For PO it is only about 25 min (sequential code), and by adding corrections terms leading to the improved PO (IPO) [6] and by using Fock currents [7] on the curved sections of the fuselage this increases to about 3 hours (also sequential FEKO version) with a rather small memory requirement of just 10 MByte. The surface current density for this asymptotic IPO/Fock solution is shown in Fig. 3, and even though this looks very smooth, the scattered electric field in Fig. 4 (dotted line) agrees very reasonably with the solid line based on the much more expensive MoM.

## 4 FREQUENCY INTERPOLATION

For a variety of EMC investigations, one is interested in the frequency response over a wide frequency range. For a frequency domain implementation of

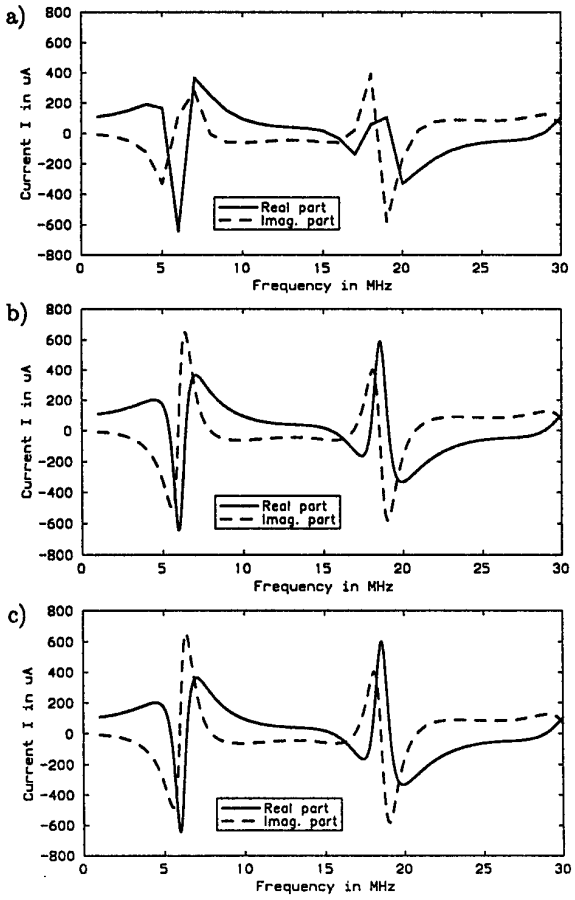



Fig. 5: Induced current versus frequency for an IEEE EMC benchmark problem using 30 sample points (a) or 581 samples (b). Application of MBPE on the data with 30 samples is shown in graph (c).

the MoM, this requires the solution at a large number of frequency sample points.

Techniques such as MBPE (model based parameter estimation) or AWE (asymptotic waveform expansion) [8–10] provide a means of accelerating MoM solutions. An application example is depicted in Fig. 5, where the induced current (real and imaginary part) is plotted as a function of frequency for a wire loop excited by a monopole antenna.

The MoM solution using only 30 frequency sample points is shown in Fig. 5 (a). As compared to using more samples (e.g. 581 in Fig. 5 (b)) one clearly realises the deficiencies, the resonance peaks are not predicted accurately.

Instead of now increasing the number of sample points from 30 to 581 (factor 19.4 longer run–time for the MoM solution), the MBPE is applied in Fig. 5 (c) to the raw data of only 30 sample points. One clearly realises again a very good agreement to the reference solution with 581 samples in Fig. 5 (b), while the computation time is identical to the 30 sample result in Fig. 5 (a).

## 5 ITERATIVE SOLUTION TECHNIQUES

In certain situations, e.g. when hybrid techniques cannot be applied or for validation purposes of the latter, one is forced to solve electrically large problems with the conventional MoM. For problems with typically 30000 to 50000 unknowns, the application of massively parallel supercomputers such as the CRAY T3E allows the solution in a reasonable time of 1 or 2 hours, whereas on a single PC or a parallel PC cluster the solution might even take a few days. The parallelisation of the MoM has been described in detail (e.g. [11]), and the most time–consuming phase of the solution process is the solution of the complex dense system of linear equations. For a sequential MoM implementation usually iterative solution techniques are problematic to apply for general composed metallic/dielectric scattering problems. Convergence depends very much on the structure of the problem, and only after having tried several combinations of different iterative solvers with different preconditioners, a method is found which outperforms the standard LU decomposition. This is, however, different for a massively parallel implementation of the MoM. Communication can be done very efficiently for iterative techniques that avoid a matrix–vector product involving the transpose of the matrix (e.g. CGS or TF–QMR), and examples show that these iterative techniques clearly outperform the default parallel LU–decomposition.

Two such examples have been included in the graph of Fig. 6, where the scattering at two different metallic objects is investigated using 9096 and 18468 basis functions, respectively.

The dashed lines indicate the scaling of the problem on the CRAY T3E using ScaLAPACK as standard solver based on a LU–decomposition. One clearly realises almost a stagnation using 64 or more nodes. On the other hand, CGS as an iterative solution tech-

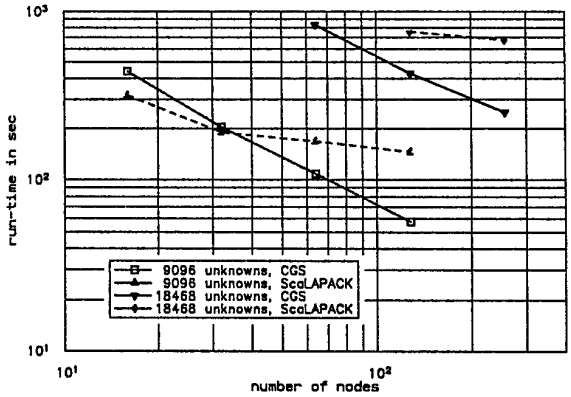



Fig. 6: Run–time for CGS and ScaLAPACK on the CRAY T3E as a function of the number of nodes for two metallic scattering problems.

nique, shows an almost ideal scaling behaviour, and except for the smaller problem solved on 16 nodes only, the run–time of CGS is also shorter than the ScaLAPACK run–time, albeit the fact that the convergence for CGS is not very overwhelming for these metallic problems.

## 6 CONCLUSIONS

Several recent extensions of the MoM have been discussed which make this method very suitable for an analyis of a large number of practical EMC problems.

## REFERENCES


[1] Electromagnetic Software & Systems (EMSS), Stellenbosch, South Africa, *FEKO User's Guide*, 1999. URL `http://www.feko.co.za`.

[2] B. D. Popović, *CAD of Wire Antennas and Related Radiating Structures*. New York: Research Studies Press, John Wiley & Sons, 1991.

[3] V. Hansen and T. Vaupel, "Berechnung der Eingangsimpedanz von Herzschrittmachern," *Newsletter — Edition Wissenschaft, Forschungsgemeinschaft Funk*, Apr. 1996.

[4] P. E. Atlamazoglou and N. K. Uzunoglu, "A Galerkin moment method for the analysis of an insulated antenna in a dissipative dielectric medium," *IEEE Transactions on Microwave Theory and Techniques*, vol. 46, pp. 988–996, July 1998.

[5] U. Jakobus and F. M. Landstorfer, "A combination of current– and ray–based techniques for the efficient analysis of electrically large scattering problems," in *Conference Proceedings of the 13th Annual Review of Progress in Applied Computational Electromagnetics*, (Monterey), pp. 748–755, Applied Computational Electromagnetics Society, Mar. 1997.

[6] U. Jakobus and F. M. Landstorfer, "Improved PO–MM hybrid formulation for scattering from three–dimensional perfectly conducting bodies of arbitrary shape," *IEEE Transactions on Antennas and Propagation*, vol. 43, pp. 162–169, Feb. 1995.

[7] U. Jakobus and F. M. Landstorfer, "Application of Fock–currents for curved convex surfaces within the framework of a current–based hybrid method," in *CEM'96, IEE 3rd International Conference on Computation in Electromagnetics, Bath, Conf. Publication Number 420*, pp. 415–420, Apr. 1996.

[8] E. K. Miller, "Model–based parameter estimation in electromagnetics: Part I. Background and theoretical development," *IEEE Antennas and Propagation Magazine*, vol. 40, pp. 42–52, Feb. 1998.

[9] E. K. Miller, "Model–based parameter estimation in electromagnetics: Part II. Applications to EM observables," *IEEE Antennas and Propagation Magazine*, vol. 40, pp. 51–65, Apr. 1998.

[10] E. K. Miller, "Model–based parameter estimation in electromagnetics: Part III. Applications to EM integral equations," *IEEE Antennas and Propagation Magazine*, vol. 40, pp. 49–66, June 1998.

[11] U. Jakobus, "Application of integral equation and hybrid techniques to the parallel computation of electromagnetic fields in a distributed memory environment," *Applied Computational Electromagnetics Society Journal*, vol. 13, pp. 87–98, July 1998. Special Issue on Computational Electromagnetics and High Performance Computing.


## BIOGRAPHICAL NOTE

Ulrich Jakobus received the Dipl.-Ing. and Dr.-Ing. degrees in electrical engineering from the University of Stuttgart, Germany, in 1991 and 1994, respectively. He completed his Habilitation in 1999 and became Privatdozent at the same university.

Since 1991 he is with the Institut für Hochfrequenztechnik, University of Stuttgart. There his main areas of research include numerical techniques in electromagnetics, antennas, electromagnetic compatibility, and bioelectromagnetics.

EMC 2000 INTERNATIONAL WROCŁAW SYMPOSIUM ON ELECTROMAGNETIC COMPATIBILITY

# ANALYSIS OF COMPLEX SYSTEMS WITH CABLES USING ELECTROMAGNETIC TOPOLOGY

Torsten Steinmetz* and Jürgen Nitsch
Otto-von-Guericke-University Magdeburg
Institute for Fundamental Electrical Engineering and EMC
Universitätsplatz 2, 39016 Magdeburg, Germany
Tel.: +49 391 67 11414
Fax: +49 391 67 11236
E-Mail: Torsten.Steinmetz@ET.Uni-Magdbeurg.DE

***Abstract:*** *Electromagnetic topology is a powerful tool to investigate disturbances in complex systems. It can be used to calculate voltages and currents that occur on the wiring of a system. However, in this approach so far only uniform transmission lines are included. In this paper, a method to treat nonuniform transmission lines (NMTL) in topological networks is presented and some frequently used nonuniform cables are analyzed. A wiring in a PC housing is investigated and a comparison with measurements, numerical simulation using a method of moments code, and with the results of the topological method is carried out.*

## 1. INTRODUCTION

Complex technical systems, like cars or aircraft, operate on a very low energetic level. In addition, more and more functions, also critical functions, are performed by electronic sensors and actors on these low energetic control-signal levels. On the other hand, the growing use of electronic equipment and its increasing package density inevitably lead to EMI problems.
Therefore a numerical analysis of the electromagnetic behavior of complex systems at the design level can help to ensure the EMC of the final system, and thereby avoid a very cost-effective post-hardening.
A full wave simulation of a complex system requires a large amount of computation time and memory. In addition to that the inclusion of cable harnesses makes a numerical solution almost impossible. For this reason **topological methods** are applied [1].

## 2. THE PRINCIPLE OF ELECTROMAGNETIC TOPOLOGY

In contrast to a full wave solution, the topological method is based on a decomposition of the whole system into different parts. These parts are collected into a topological diagram as a formal representation of the system. The interactions between the decomposed parts are then analyzed in the corresponding interaction graph to build a correct model of the system behavior in terms of coupled subsystems.
The topological diagram and interaction graph have to be transformed into a **network** representation with propagation tubes and scattering junctions [2]. Essentially, two networks have to be generated for an arbitrary system: one for the cable coupling and a second one for field coupling. Both are mutually linked together via source terms.
The mathematical description of these networks is based on the BLT-equation [3] and is formulated in frequency domain. The BLT-equation reads

$$([1]-[S][\Gamma])[W(0)]=[S][W^{(s)}(L)]. \qquad (1)$$

Here the supermatrix [S] describes the scattering behavior of the network junctions and the supermatrix [Γ] the propagation along the tubes. The supervector $[W^{(s)}(L)]$ characterizes all sources of the network.
The above equation has to be solved for [W(0)], the outgoing wave supervector. For this purpose one needs to know all entries of [Γ] and [S]. A whole variety of numerical methods is available to determine the scattering parameters of the sub-volumes, e.g., finite differences, finite elements, TLM, MoM, etc.. Also analytical solutions or measurements can be used to fill the entries of the scattering matrix. Even a combination of different methods can be applied.
For the calculation of [Γ] transmission line theory still provides a solution for a host of cases. Since the propagation matrix describes how energy propagates from the near end to the far end of a tube, one also may think to use other methods to estimate [Γ], in particular for very high frequencies when radiation starts to play a role.
Indeed, sometimes the propagation matrix is contained in an equivalent scattering matrix. Then, using equivalent sources at the ports, the previous BLT-equation can formally be simplified, giving

$$([1]-[\tilde{S}])[W(0)]=[\tilde{S}][W^{(s)}(L)]. \quad (2)$$

This equation describes a network of scattering subvolumes which are directly connected at their ports.

## 3. NONUNIFORM MULTICONDUCTOR TRANSMISSION LINES

We have included nonuniform multiconductor transmission lines (NMTL) in the topological network, discussed above. This is done in the following way. We start with a system of N transmission lines and a reference conductor, described with the telegrapher equation in frequency domain

$$\frac{\partial}{\partial z}\begin{bmatrix}\mathbf{u}(z,\omega)\\ \mathbf{i}(z,\omega)\end{bmatrix}=\begin{bmatrix}0 & -\mathbf{Z}'(z,\omega)\\ -\mathbf{Y}'(z,\omega) & 0\end{bmatrix}\begin{bmatrix}\mathbf{u}(z,\omega)\\ \mathbf{i}(z,\omega)\end{bmatrix}+\begin{bmatrix}\mathbf{u}'^{(s)}(z,\omega)\\ \mathbf{i}'^{(s)}(z,\omega)\end{bmatrix} \quad (3)$$

where z is the local coordinate along the NMTL. The voltage vector **u**, the current vector **i**, the per-unit-length series voltage source vector $\mathbf{v}'^{(s)}$, and the per-unit-length shunt current source vector $\mathbf{i}'^{(s)}$ have N components, whereas the per unit-length series impedance matrix **Z'** and the per-unit-length shunt admittance matrix **Y'** are N *x* N matrices, and in distinction to the uniform transmission line equation, dependent on the parameter z. Another useful representation of (3) is the one in terms of wave variables $\mathbf{w}_+$ and $\mathbf{w}_-$, where + indicates the direction of increasing z and - of decreasing z. This representation can be obtained from (3) using the transformation

$$\begin{bmatrix}\mathbf{w}_+(z)\\ \mathbf{w}_-(z)\end{bmatrix}=\begin{bmatrix}1 & \mathbf{Z}_c(z)\\ 1 & -\mathbf{Z}_c(z)\end{bmatrix}\begin{bmatrix}\mathbf{u}(z)\\ \mathbf{i}(z)\end{bmatrix}\equiv[\mathbf{T}(z)]\begin{bmatrix}\mathbf{u}(z)\\ \mathbf{i}(z)\end{bmatrix} \quad (4)$$

and

$$\begin{bmatrix}\mathbf{w}_+'^{(s)}(z)\\ \mathbf{w}_-'^{(s)}(z)\end{bmatrix}=\begin{bmatrix}1 & \mathbf{Z}_c(z)\\ 1 & -\mathbf{Z}_c(z)\end{bmatrix}\begin{bmatrix}\mathbf{u}'^{(s)}(z)\\ \mathbf{i}'^{(s)}(z)\end{bmatrix}=[\mathbf{T}(z)]\begin{bmatrix}\mathbf{u}'^{(s)}(z)\\ \mathbf{i}'^{(s)}(z)\end{bmatrix}. \quad (5)$$

The corresponding equation for the wave variables reads

$$\frac{\partial}{\partial z}\begin{bmatrix}\mathbf{w}_+(z)\\ \mathbf{w}_-(z)\end{bmatrix}=\begin{bmatrix}-\mathbf{P}(z)+\frac{1}{2}\mathbf{G}(z) & -\frac{1}{2}\mathbf{G}(z)\\ -\frac{1}{2}\mathbf{G}(z) & \mathbf{P}(z)+\frac{1}{2}\mathbf{G}(z)\end{bmatrix}\begin{bmatrix}\mathbf{w}_+(z)\\ \mathbf{w}_-(z)\end{bmatrix}+\begin{bmatrix}\mathbf{w}_+'^{(s)}(z)\\ \mathbf{w}_-'^{(s)}(z)\end{bmatrix} \quad (6)$$

with

$$\mathbf{P}(z)\equiv\mathbf{Z}_C(z)\mathbf{Y}'^{-1}(z)=-\mathbf{Z}'(z)\mathbf{Z}_C^{-1}(z)$$
$$\mathbf{G}(z)\equiv D_z\mathbf{Z}_C(z)=\frac{\partial\mathbf{Z}_C(z)}{\partial z}\mathbf{Z}_C^{-1}(z)=-\mathbf{Z}_C(z)\frac{\partial\mathbf{Z}_C^{-1}(z)}{\partial z}. \quad (7)$$

The characteristic impedance is obtained by

$$\mathbf{Z}_C(z)=\sqrt{\mathbf{Z}'(z)\mathbf{Y}'(z)^{-1}}. \quad (8)$$

The equations (3) and (6) are of the form

$$\frac{\partial}{\partial z}\mathbf{X}(z)=\mathbf{Q}(z)\mathbf{X}(z)+\mathbf{X}'^{(s)}(z) \quad (9)$$

where **X(z)** is the unknown supervector, **Q**(z) a nonconstant parameter matrix, and $\mathbf{X}'^{(s)}$(z) the source supervector. The standard solution of (9) with initial value $\mathbf{X}(z_0)$ is given by (see [4])

$$\mathbf{X}(z)=\mathbf{M}_{z_0}^{z}(\mathbf{Q}(z))\mathbf{X}(z_0)+\int_{z_0}^{z}\mathbf{K}(z,\xi)\mathbf{X}'^{(s)}(\xi)d\xi \quad (10)$$

where the matrizant $\mathbf{M}_{z_0}^{z}$ can be calculated via the expansion

$$\mathbf{M}_{z_0}^{z}(\mathbf{Q}(z))=1+\int_{z_0}^{z}\mathbf{Q}(\tau)d\tau+\int_{z_0}^{z}\mathbf{Q}(\tau)\int_{z_0}^{\tau}\mathbf{Q}(\delta)d\delta d\tau+\ldots \quad (11)$$

The Cauchy matrix **K**(z,ξ) is expressed by

$$\mathbf{K}(z,\xi)=\mathbf{M}_{z_0}^{z}(\mathbf{Q}(z))\left[\mathbf{M}_{z_0}^{\xi}(\mathbf{Q}(z))\right]^{-1}=\mathbf{M}_{\xi}^{z}(\mathbf{Q}(z)). \quad (12)$$

Thus, the general matrix vector equation is formally solved. The remaining problem is the nontrivial computation of the matrizant. Since equation (11) is not well suited for a numerical computation, we rather use the product integral representation of the matrizant [4,5]

$$\mathbf{M}_{z_0}^{z}(\mathbf{Q}(z))=\prod_{z_0}^{z}e^{\mathbf{Q}(z)dz}=\lim_{\Delta z\to 0}\prod_{k=1}^{n}e^{\mathbf{Q}(z_k)\Delta z_k}. \quad (13)$$

Assuming that the matrices **Q**(z), **Q**(z') commute for all z, z' along the line then we find the simple expression for the matrizant

$$\mathbf{M}_{z_0}^{z}(\mathbf{Q}(z))=e^{\int_{z_0}^{z}\mathbf{Q}(z)dz}. \quad (14)$$

In order to calculate equation (13) we have to segment the parameter interval along the line into discrete sections, the length of which depend on how strongly **Q**(z) changes its values in dependency of z. In special cases it is possible to estimate the matrizant analytically, e.g., for circulant lines [6].

Of course, NMTLs can be introduced in the representation of the BLT-equation, either as tubes via the propagation parameters or as junctions via equivalent scattering parameters. In the following the matrizant is transformed into a scattering matrix which is positioned between two tubes of zero length in the network. Therefore two steps have to be performed: Firstly the equivalent scattering matrix of the NMTL has to be calculated and secondly, sources along the line must be transformed into equivalent sources at the end of the line. Using the definition of the scattering parameters and the solution of (6) (with (13)), a transformation rule from the matrizant into scattering parameters can be derived:

$$[\mathbf{S}_{eq}]=\begin{bmatrix}-\mathbf{M}_{22}^{-1}\mathbf{M}_{21} & \mathbf{M}_{22}^{-1}\\ \mathbf{M}_{11}-\mathbf{M}_{12}\mathbf{M}_{22}^{-1}\mathbf{M}_{21} & \mathbf{M}_{12}\mathbf{M}_{22}^{-1}\end{bmatrix} \quad (15)$$

with

$$\begin{bmatrix}\mathbf{M}_{11(N\times N)} & \mathbf{M}_{12(N\times N)}\\ \mathbf{M}_{21(N\times N)} & \mathbf{M}_{22(N\times N)}\end{bmatrix}=\mathbf{T}(z_L)\mathbf{M}_{z_0}^{z_L}\begin{pmatrix}0 & -\mathbf{Z}'(z)\\ -\mathbf{Y}'(z) & 0\end{pmatrix}\mathbf{T}(z_0). \quad (16)$$

We use the transformation

$$\begin{bmatrix} \mathbf{u}_{eq}^{(s)} \\ \mathbf{i}_{eq}^{(s)} \end{bmatrix} = \int_{z_0}^{z_L} \mathbf{M}_{\xi}^{z_L} \begin{pmatrix} 0 & -\mathbf{Z}'(z) \\ -\mathbf{Y}'(z) & 0 \end{pmatrix} \begin{pmatrix} \mathbf{u}'^{(s)}(\xi) \\ \mathbf{i}'^{(s)}(\xi) \end{pmatrix} d\xi \approx \sum_{z_0}^{z_L} \mathbf{M}_{\xi}^{z_L} \begin{pmatrix} 0 & -\mathbf{Z}'(z) \\ -\mathbf{Y}'(z) & 0 \end{pmatrix} \begin{pmatrix} \mathbf{u}'^{(s)}(\xi) \\ \mathbf{i}'^{(s)}(\xi) \end{pmatrix} \Delta z_{\xi} \quad (17)$$

to evaluate the equivalent sources at the end of the line. Consequently, we get a model for the nonuniform tube which can be naturally included in the BLT equation. An example how to incorporate a NMTL into a BLT network is shown in Figure 1.

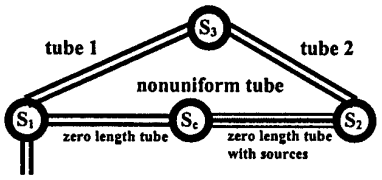



**Figure 1:** Example of a BLT network with a nonuniform tube modeled as an equivalent scattering junction

Now we are prepared to treat a network with uniform and nonuniform multiconductor transmission lines.

## 4. APPLICATION TO FREQUENTLY USED NONUNIFORM LINES AND UNKNOWN CABLE LAYINGS

To validate the previous described method, various frequently used types of nonuniform transmission lines are analyzed. Therefore we have to know the exact geometrical data of the cable harness. This means that at every cross section along the NMTL the location and thickness of every single conductor must be known.
Our first example is a wavy shaped line as shown in Figure 2.

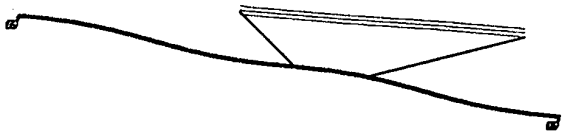


**Figure 2:** Example 1 - wavy shaped line

This tube consists of three single conductors above an ideal ground plane. Their mutual distance is constant, but the height of the wires above ground is changed sinusoidally in the range of ± 80% of the nominal height. The near end of the first wire is excited with a 1 Volt generator, and all other ends are loaded with 50 Ω resistors. The line is 1 m long, and the currents at the ends of the line are calculated from 1 MHz up to 1 GHz. Figure 3 shows the magnitude of the cross-coupled current at the far end of the second wire which was derived using the approach with the matrizant in comparison to a full wave calculation (with the method of moments code CONCEPT) and the solution for a uniform transmission line.

The full wave solution agrees very well with the matrizant solution. The differences to the results for a uniform transmission line are significant. The variation between the matrizant and the method of moments results in the higher frequency range are caused by radiation effects which are not included in the matrizant solution.

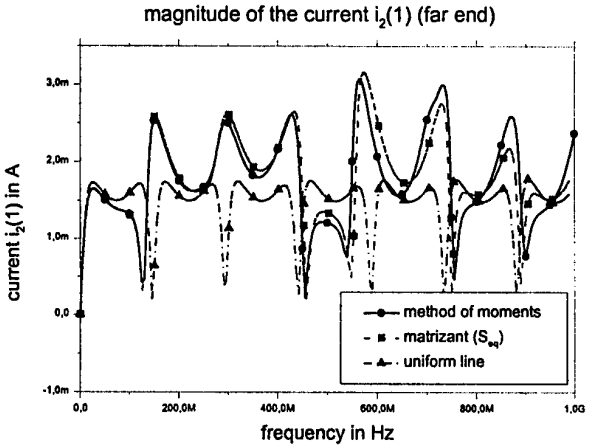



**Figure 3:** Example 1 - cross coupling at the far end

In the first example all geometrical data of the tube were well known. However, often the exact position of individual wires are only known at the near end and at the far end of the tube (e.g. at the connectors). This suggests the performance of a statistical analysis of such an unknown nonuniform tube. Thus, many calculations of randomly generated tube geometries have to be completed in order to estimate maximal and minimal bounds for the equivalent scattering parameters.
The second example treats such an unknown cable laying. We investigate a cable geometry of three wires above ground plane as in example 1, but the exact positions of individual wires are not known. We assume, that the wires are located in a tolerance area as sketched in Figure 4. Thus, both, height and distance, of the wires are changed over the length parameter z.

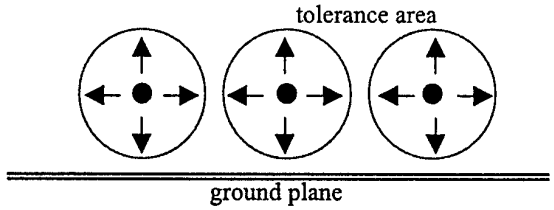



**Figure 4:** Example 2 – cross section of the "random tube", the wires are located within the tolerance area

For this "random cable tube" 100 possible geometries are calculated and analyzed using the matrizant approach. Figure 5 shows one example geometry for this tube.



**Figure 5:** Example 2 – one random geometry

First we want to illuminate, how the nonuniformity of the random line influences the cross coupling. The initial idea was, that there will be no difference to an uniform line, because the effect of stronger coupling, caused by a smaller distance, could be averaged out by the effect of weaker coupling, due to a larger distance of two wires. However, our results show a remarkable difference to uniform lines. In Figure 6 we display the near end cross-coupled current of the second wire which is very different from that of an uniform line.

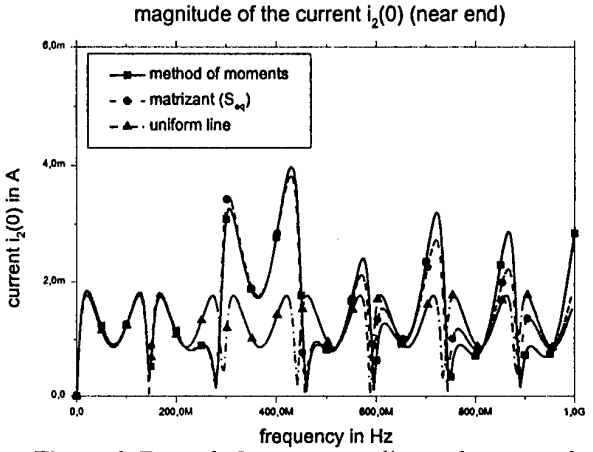



**Figure 6:** Example 2 – cross coupling at the near end

The analysis over 100 calculations leads to minimum, maximum and mean values of the differences between the equivalent scattering parameters and the uniform transmission line scattering parameters.

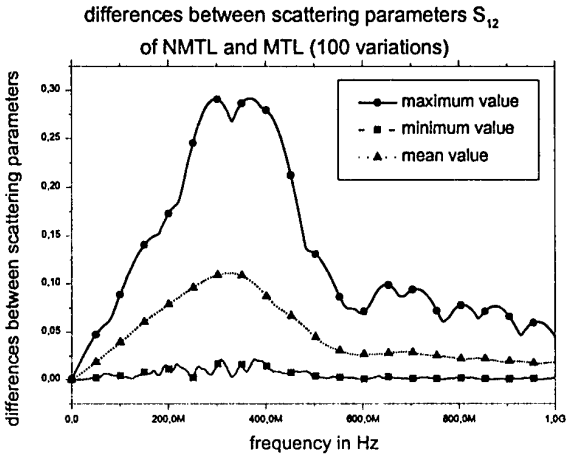



**Figure 7:** Example 2 – bounds in the statistical analysis of the deviation to a MTL

These bounding values are shown in Figure 7. With the aid of these bounds we are able to identify frequency regions of increased disturbances on the wires, where attention to a correct operation has to be paid (around 300 MHz in example 2).

## 5. A SIMPLE EXPERIMENT WITH A CABLE IN A PC HOUSING

We will elucidate the topological method with the aid of a general example and will present numerical results in comparison with measurements.

We chose a standard PC desktop housing, removed all interior components, installed two small boxes and connected them with transmission lines of different configurations. The slot of the floppy disk is left open to enable field coupling into the interior. This test set-up is shown in a geometrical method of moment model in Figure 8.

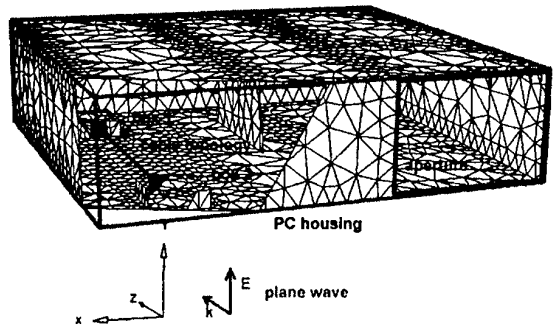



**Figure 8:** PC-housing with boxes and cables

The topological network of this problem is very simple because we only have to treat one tube (Figure 9).

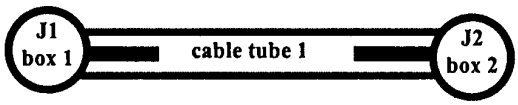



**Figure 9:** Topological network of the wiring of the PC

Since the topological network is located in a structure which is excited by a plane wave of 1V/m, we have to calculate the tangential E-field at all wire positions. For simple geometries this can be done analytically, but for our PC housing we used the method of moments. This allows the use of the Agrawal model [7] for the coupling of the fields to the transmission line structure. We calculated the E-field without the presence of the wiring. The mesh size of the structure depends on the maximum frequency and on other general meshing-rules.

The first transmission line configuration was a single wire above ground. The ends of the line were loaded with 50 Ω resistors. The measured interference voltage at the 50 Ω resistor is compared with a full wave solution (MoM) and with the solution of the topological approach (see Figure 10).

In general the results are in a good agreement. The method of moments and the topological approach deliver almost identical results. The measurements indicate the same resonance frequencies, and also the amplitudes are in the same range like the simulations.
One reason for the higher value at 600MHz is the non perfect model of the PC housing: The real housing exhibits a surrounding small slit which resonates at 600 MHz. This is not the case in the computational models. Another source of errors are the non perfect resistors. The simulation starts with ideal 50 Ω resistors for all frequencies but the parasitic effects of the used surface mounted devices are not to be neglected above 1 GHz.

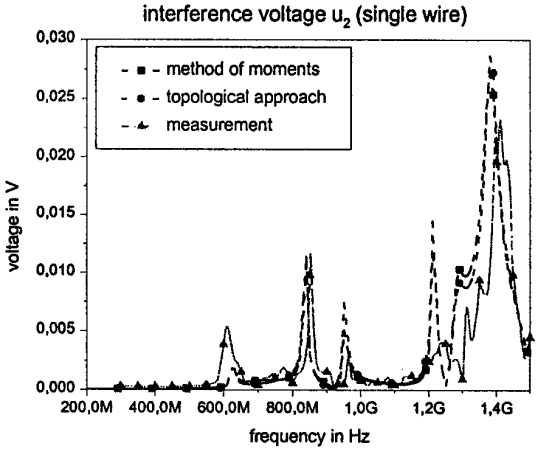



**Figure 10:** Interference voltage of a single wire configuration in the PC housing

In the above example we have treated a very simple configuration. Therefore the advantages of the topological method against a full wave method do not become very obvious. However, they will become significant in cases where the variation of load elements is required. Then a full wave method has to solve the full problem, whereas the topological method has only to solve the transmission line problem, since the external problem does not change (excitation and coupling to the interior), and the previous calculated E-field data can repeatedly be used. Also (for the full wave solution) the numerical effort increases rapidly for more complex cable bundles (real wiring with 10 or more wires and dielectric insulation) and exceeds the numerical effort for the external problem by far. In addition, the solution time of some full wave methods (e.g. method of moments) do not linearly scale with the number of unknowns.
Therefore, the advantage of the topological method depends on the problems under study. The benefit in time can be immense. We calculated problems where the topological method was 2000 times faster than the method of moments. Thus we can perform calculations within seconds instead of hours or days.

## 6. CONCLUSIONS

The electromagnetic topology can be considered as a helpful tool for the analysis of EMC in large complex systems. Many applications and validations have been performed in the past [2]. The above sections extend the application of the electromagnetic topology to non-uniform lines and thereby the discrepancies between theoretical or numerical models and the real world problems can be decreased.
The basis of our considerations was the telegrapher equation (3) with non-constant parameters. We hope that the solution of this equation is the solution of the electromagnetic problem we actually want to solve. However, one has to be aware that transmission line theory includes some approximations. In particular, these approximations are the assumptions of a TEM-mode and the absence of radiation effects. These assumptions may become invalid. The TEM mode is disturbed in a nonuniform line and also at the terminations of the line, and radiation becomes significant at higher frequencies.
On the other hand, we are meanwhile able to extend the multiconductor transmission line theory to include the above mentioned phenomena into the transmission line parameters, and the solution (with redefined, complex transmission line parameters) via the matrizant will be in agreement with Maxwell's theory [8,9].
The fast computation time allows a statistical analysis of unknown random cable layings. This leads to results on bounding values and probabilities of disturbances in complex systems, but can also include statistical variations of production series (e.g. tolerances of production).

## REFERENCES

[1] J.Nitsch, T.Steinmetz, R.Vetter, *Modelling and Simulation in Multiconductor Transmission Line Theory,* Proc. EMC Zurich 99, supplement, p. 57-65
[2] J.P.Parmantier, *Application of EM Topology on Complex Wiring Systems,* Proc. Int. Symp. on EMC 99, Magdeburg, p. 1-8, ISBN 3-929757-25-7
[3] C.E.Baum, T.K.Liu, F.M.Tesche, *On the Analysis of General Multiconductor Transmission Line Networks,* IN 350, November 1978
[4] F.R.Gantmacher, *The Theory of Matrices Vol. II,* Chelsa Pub., New York, 1989, ISBN 0-8284-0133-0
[5] J.D.Dollard, C.N.Friedman, *Product Integration with Application to Differential Equations,* Addison-Wesley Pub., London, 1979, ISBN 0-201-13509-4
[6] J.Nitsch, F.Gronwald, *Analytical Solutions in Nonuniform Multiconductor Transmission Line Theory,* IEEE Transaction on EMC, Vol. 41, No. 4, 1999, p. 469-479
[7] F.M.Tesche, *Principles and Application of EM Fields Coupling to Transmission Lines*, Proc. EMC Zurich 95, supplement, p.21-31
[8] J.Nitsch, H.Haase, *Field Coupling to Nonuniform Multiconductor Transmission Lines (in german),* Rep. E/F11B/X0268/X5174, EMV-Fachgebiet Gredingen, Sep. 1999
[9] H.Haase, J.Nitsch, *Parameter of Nonuniform Transmission Lines (in german),* EMV 2000, Tagungsbeitrag 7. Internationale Fachmesse und Kongreß für EMV, Düsseldorf, 2000

**EMC 2000** INTERNATIONAL WROCŁAW SYMPOSIUM ON ELECTROMAGNETIC COMPATIBILITY

# USING HYBRID PEEC-MTL MODELS FOR THE ANALYSIS OF INTERCONNECTION STRUCTURES

G. Wollenberg A. Görisch

Otto-von-Guericke-University Magdeburg, IGET
P.O. Box 4120, D-39016 Magdeburg, Germany
Tel.: +49-391-67 186 36, Fax: +49-391-67 112 36
e-mail: guenter.wollenberg@et.uni-magdeburg.de

*This paper describes a hybrid PEEC-MTL method for the simulation of interconnection structures in the time and frequency domain. The interconnection structure is analyzed and subdivided into PEEC parts modelling the nonuniform regions of the structure, and into transmission line parts for the homogeneous ones. To maintain the model accuracy the cross couplings between the PEEC and the TL parts and between different transmission lines are considered.*

## 1 INTRODUCTION

Short switching times and low signal levels raise the requirements on the EMC of circuits and systems. Fast switching leads to internal EMC problems (signal integrity, overvoltages...) and enlarges the radiation of electromagnetic fields while the decrease of signal levels increases the interference susceptibility.

Most of these problems are related to the wires and transmission lines between the components and units of a circuit. These interconnection structures may be effective transmitting and receiving antennas since they are often electrically long. Their parasitic capacitances and inductances influence the behaviour of the circuit and lead to switching impulse voltages, ringing, crosstalk etc. .

To keep the costs for EMC measures and redesigns low, accurate and efficient simulation models are needed, that allow the analysis of the electronic circuit including the effects of interconnections. This models have to be valid in the time and in the frequency domain, because electronic components are nonlinear and often a linearization is not allowed. A further requirement on the model is the possibility to integrate it into a circuit simulation.

A general method, that was developed to include interconnection effects into circuit simulations, is the **P**artial **E**lement **E**quivalent **C**ircuit (PEEC) method. This method was developed by Ruehli ([4] ) and gives a circuit interpretation of the **E**lectrical **F**ield **I**ntegral **E**quation (EFIE).

Another type of an interconnection model suitable for circuit simulations is the transmission line (TL) model. Compared to PEEC models TL models are fast to calculate. But they are limited in their applicability to long, straight conductors. Further, the conductor(s) in forward direction have to run near and parallel to their return conductor(s).

The idea is to analyze the interconnection structure and to use TL models for all possible parts of the structure. The remaining parts still have to be modelled using the PEEC method, and a coupling mechanism between the TL and the PEEC parts and between the transmission lines has to be included.

In the following the fundamentals of the PEEC method are described briefly. To show the relations between TL and PEEC models the telegraphers equations will be derived from a PEEC point of view. Basing on this the principle of the PEEC-TL coupling is explained in section 4.

## 2 THE PEEC METHOD

The derivation of the PEEC model starts from the equation of the electric field $\vec{E}(\vec{r})$ at an observation point $\vec{r}$ in space as the sum of an external, incident field $\vec{E}^{(i)}$ and the scattering field $\vec{E}^{(s)}$.

$$\begin{aligned}\vec{E}(\vec{r}) &= \vec{E}^{(i)}(\vec{r}) + E^{(s)}(\vec{r}) \\ &= \vec{E}^{(i)}(\vec{r}) - \frac{\partial \vec{A}(\vec{r})}{\partial t} - \operatorname{grad}\varphi(\vec{r})\end{aligned} \tag{1}$$

The scattering field is calculated with the help of the magnetic vector potential $\vec{A}$ and the scalar electric potential $\varphi$.

$$\vec{A}(\vec{r},t) = \mu \int_{V_q} G(\vec{r},\vec{r}_q)\, \vec{J}(\vec{r}_q, t-\tau) dV_q \qquad (2)$$

$$\varphi(\vec{r},t) = \frac{1}{\varepsilon} \int_{V_q} G(\vec{r},\vec{r}_q)\, \rho(\vec{r}_q, t-\tau)\, dV_q \qquad (3)$$

Including this equations into (1) and laying the observation point on the conducting structure the EFIE is derived.

$$0 = -\vec{E}^{(i)}(\vec{r},t) \qquad (4a)$$

$$+ \frac{1}{\kappa}\vec{J}_L(\vec{r},t) \qquad (4b)$$

$$+ \mu \int_{V_q} G(\vec{r},\vec{r}_q) \frac{\partial \vec{J}(\vec{r}_q, t-\tau)}{\partial t} dV_q \qquad (4c)$$

$$+ \frac{1}{\varepsilon} \operatorname{grad} \int_{V_q} G(\vec{r},\vec{r}_q)\, \rho(\vec{r}_q, t-\tau)\, dV_q \qquad (4d)$$

The term (4a) describes the external electric field $\vec{E}^{(i)}$. The second term is the electric field part caused by the the conduction current density $\vec{J}$ and the conductivity $\kappa$ at the observation point.

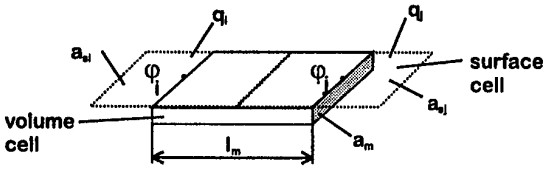



Figure 1: Volume cell with two surface cells

The term (4c) calculates the part of the electric field generated due to the time derivatives of the current densities in the source volume $V_q$. The contribution of the different current densities in the source volume to the electric field at the observation point is weighted with the Green's function $G(\vec{r},\vec{r}_q)$ for the free space.

$$G(\vec{r},\vec{r}_q) = \frac{1}{4\pi\,|\vec{r}-\vec{r}_q|}$$

The last term in the EFIE describes the contribution of the charges in the source volume to the electric field.

The PEEC method requires a particular discretization scheme. Like shown in figure 1, the structure has to be divided into two kinds of cells:

- surface cells that carry the charges
- volume cells that lead the currents.

Surface cells and volume cells are shifted against each other by half of the cell length $l_m$. This approximates the gradient at $\vec{r}$ in (4d) as the potential difference between the ends of the volume cell at $\vec{r}$.

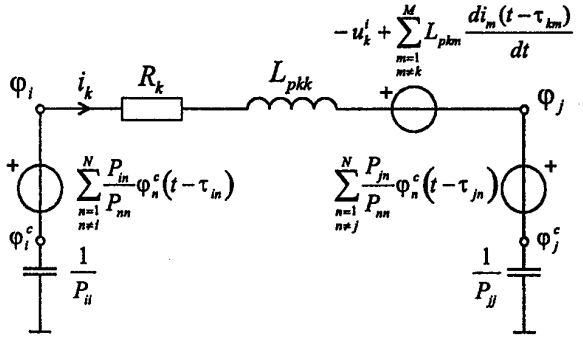



Figure 2: Equivalent circuit of a volume cell and two surface cells (see figure 1)

For the approximation of the charge and the current distribution constant spatial basisfunctions are used. To transform the discretized EFIE into an equivalent circuit, the electric field at the observation point is integrated along the cell length. Since the line integral of the electric field gives a voltage, the resulting equation can be interpreted with Kirchhoff's Voltage Law. In consequence, the equivalent circuit in figure 2 and the relations for the calculation of the circuit parameters are derived.

The calculation of the partial inductances $L_p$ and the coefficients of potential $P$ are of larger complexity. In general they are calculated as follows.

$$L_{pmn} = \frac{\mu}{a_m a_n} \int_{a_m}\int_{a_n}\int_{l_m}\int_{l_n} G(\vec{r},\vec{r}_q)\, d\vec{l}_n \cdot d\vec{l}_m da_n da_m \qquad (5)$$

$$P_{ij} = \frac{1}{\varepsilon\, a_{si} a_{sj}} \int_{a_{sj}}\int_{a_{si}} G(\vec{r},\vec{r}_q)\, da_{si} da_{sj} \qquad (6)$$

If the interconnections are divided into rectangular cells, closed form solutions for this integrals are available from [1].

# 3 PEEC AND TL MODELS FOR A HOMOGENEOUS TRANSMISSION LINE

Next the relations between TL and PEEC models will be considered in the frequency domain at the example of a lossless wire above perfectly conducting, infinite ground (see figure 3).

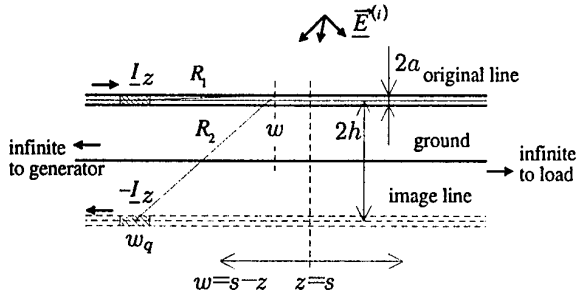



Figure 3: Round wire above perfectly conducting ground

Assuming the thin wire approximation

$$a << 2h \text{ and } 2h << \lambda \tag{7}$$

the volume integrals for the calculation of the potentials change to line integrals.

$$\underline{A_z}(w) = \frac{\mu}{4\pi} \int_{-\infty}^{\infty} \underline{g}(w, w_q)\, \underline{I_z}(w_q)\, dw_q \tag{8}$$

$$\underline{\varphi}(w) = \frac{1}{4\pi\varepsilon} \int_{-\infty}^{\infty} \underline{g}(w, w_q)\, \underline{q}(w_q)\, dw_q \tag{9}$$

The influence of the perfectly conducting ground is included using the image principle. Due to this the Green's function changes to

$$\underline{g}(w, w_q) = \frac{e^{-j\frac{2\pi f}{c}R_1}}{R_1} - \frac{e^{-j\frac{2\pi f}{c}R_2}}{R_2} \tag{10}$$

with

$$R_1 = \sqrt{(w - w_q)^2 + a^2} \tag{11}$$

$$R_2 = \sqrt{(w - w_q)^2 + 4h^2}. \tag{12}$$

Due to (7) the complex Green's function $\underline{g}(w, w_q)$ can be simplified to the static, real function

$$g_0(w, w_q) = \frac{1}{R_1} - \frac{1}{R_2}. \tag{13}$$

The reason for this is the strong selectivity of the Green's function. Only sources near the observation point have a significant influence on the values of the potentials $\vec{A}$ and $\varphi$. This has two consequences:

1. The retardation can be neglected for this sources, because $2h << \lambda$ has to be valid, too.
2. Since the unknowns $\underline{I_z}$ and $\underline{q}$ are inside the reaching distance of the Green's function approximately constant, they can be excluded from the integration.

$$\int g_0(w, w_q)\underline{X}(w_q)\, dw_q \rightarrow \underline{X}(w) \int g_0(w, w_q)\, dw_q$$

The calculation of the potentials changes then to:

$$\begin{aligned} \underline{A_z}(w) &= \underline{I_z}(w)\, \frac{\mu}{4\pi} \int_{-\infty}^{\infty} g_0(w, w_q)\, dw_q \\ &= \underline{I_z}(w) \underbrace{\frac{\mu}{2\pi} \ln \frac{2h}{a}}_{L'} \end{aligned} \tag{14}$$

$$\begin{aligned} \underline{\varphi}(w) &= \underline{q}(w)\, \frac{1}{4\pi\varepsilon} \int_{-\infty}^{\infty} g_0(w, w_q)\, dw_q \\ &= \underline{q}(w) \underbrace{\frac{1}{2\pi\varepsilon} \ln \frac{2h}{a}}_{1/C'} \end{aligned} \tag{15}$$

Applying eq. (1) in the frequency domain to our transmission line arrangement we obtain

$$\underline{E_z}(w) = \underline{E_z}^{(i)}(w) - j\omega \underline{A_z}(w) - \frac{\partial \underline{\varphi}(w)}{\partial w}. \tag{16}$$

Since the wire is ideal conducting, $\underline{E_z}(w)$ is zero. Inserting equation (14) into equation (16) leads to the first telegraphers equation:

$$j\omega L' \underline{I_z}(w) + \frac{\partial \underline{U}(w)}{\partial w} = \underline{\vec{E}_z}^{(i)}(w). \tag{17}$$

The voltage between the wire and the groundplane $\underline{U}(w)$ is equal the potential of the wire $\underline{\varphi}(w)$ if only the TEM mode exists. The second telegraphers equation

$$\frac{d\underline{I_z}(w)}{dw} + j\omega C' \underline{U}(w) = 0 \tag{18}$$

is derived from the continuity equation and eq. (15).

To show the relations between the per unit length parameters used in the telegraphers equations and the partial elements used in the PEEC models the thin wire approximation is applied to the equation for the partial inductances (5)

$$L_{pmn} = \int_{l_m} \left[ \frac{\mu}{4\pi} \int_{l_n} g_0(w, w_q)\, dw_q \right] dw. \tag{19}$$

The inner integral represents the contribution of the line element $l_n$ to the mutual per unit length inductance at the point $w$. The outer integration over $l_m$

sums up all these contributions to the mutual partial inductance $L_{pmn}$. To derive the per unit length inductance of a transmission line arrangement from the partial inductances all $N$ partial inductances of the wire to the cell $m$ at the observation point $w$ have to be summed up.

$$L'_m = \frac{1}{l_m} \sum_{n=1}^{N} L_{pmn} \qquad (20)$$

# 4 COUPLING PEEC AND TL MODELS

Our former work (e.g. [5]) was focused on TLs. We created a model for smooth coupling of PEEC and TL models in a homogeneous region of a TL. Thus we are able to model discontinuities and nonuniformities of TLs accurately by PEEC models and to couple them to TL models for the remaining homogeneous parts. In more general and comprehensive structures couplings may be along the whole transmission line and between different and even non parallel running transmission lines, too.

Unlike in [2] our basic idea is now *not to reduce* the size of the system matrix but to *make it more sparse* taking into account the knowledge about transmission lines. To do this, first the interconnection structure is analyzed to find wires, that run parallel to the groundplane. Further bends, junctions and changes in the cross-section are separated. Additional effort has to be spend, if wires run parallel in close vicinity. In this case multi-conductor transmission lines have to be generated.

In consequence a reordered PEEC-(M)TL model exists. The PEEC model is now separated in a PEEC part and a part of lumped LC transmission lines. The coupling between the PEEC cells and the LC segments is identical to the coupling between the PEEC cells. The values for the transmission line parameters are calculated like in equation (20).

# 5 EXAMPLE: MULTI WIRE CONFIGURATION ABOVE PERFECT GROUND PLANE

Our example is the problem 14 of the benchmark catalog [3]. A multi wire configuration above a perfect ground plane is excited by a homogeneous plane wave (see figure 4).

All wires have a radius of $a = 1,75mm$. In order to simplify the numerical analysis a resistance of $R' = 2\Omega/m$ shall applied to all wires. The configuration is excited by a homogeneous plane wave. The field strength rises to its end value of $E = 1V/m$ within $t_r = 3ns$. The wave vector $\vec{k} = \frac{k}{\sqrt{2}}(\vec{e}_x - \vec{e}_z)$ lies in the xz-plane, while the vector of the electric field $\vec{E}$ is directed in the negative y-direction. The task is, to calculate the current at the feeding points of the wires 3 and 4 in the time domain for $t = 0..100ns$.

The structure was subdivided into 5cm long cells. This allows a treatment up to about 500MHz. Because the height of the wires above the ground is 10cm, the transmission line models are valid up to about 150MHz.

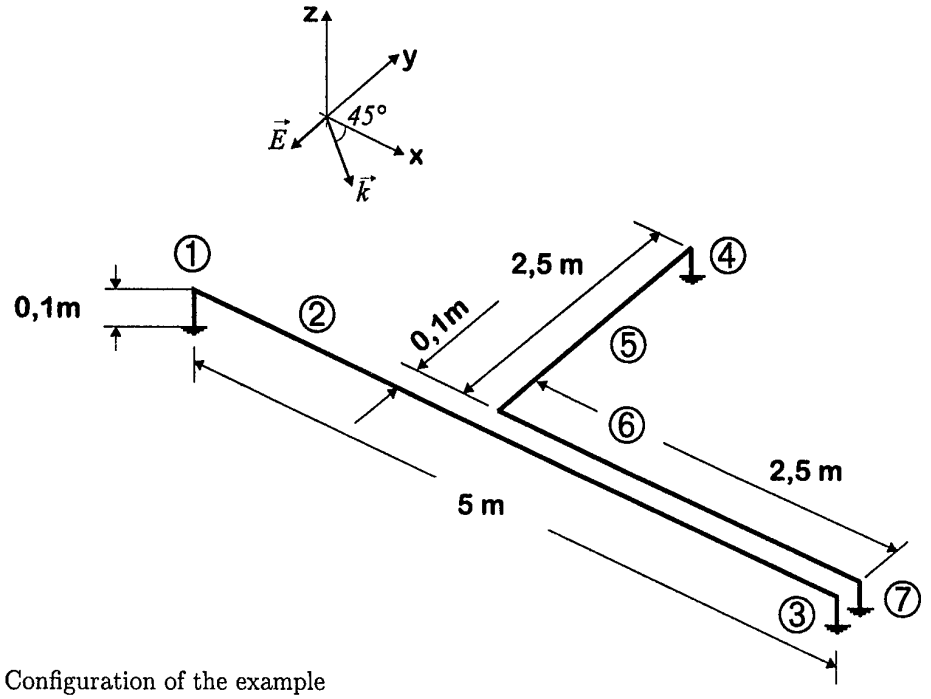



Figure 4: Configuration of the example

To verify the PEEC model, its results are compared with results from the Method of Moments code CONCEPT in figure 5. Since they show a good agreement, we use the PEEC model as the reference for the coupled PEEC-MTL model in the time domain. To the results in figure 5 it should be mentioned, that they were obtained using a constant electric field strength of $E = 1V/m$ for all frequencies.

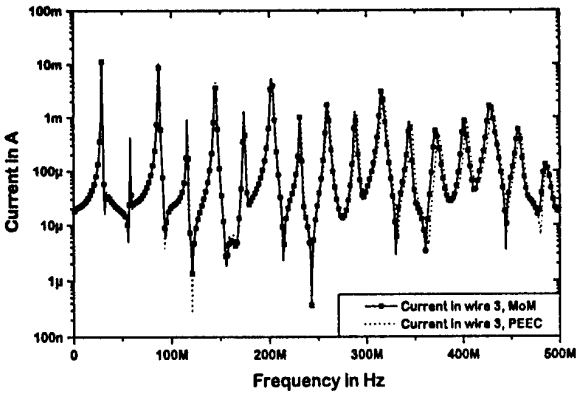



Figure 5: Verification of the PEEC model in the frequency domain

Next the results of the transient simulation of the PEEC and the PEEC-MTL model are compared in figure 6. Two kinds of PEEC-MTL models are treated. The model **PEEC-MTL 1** includes the couplings between the PEEC cells and the segments of the LC transmission lines and between the segments of different transmission lines. In the model **PEEC-MTL 2** both kinds of additional couplings are not included and it can be seen clearly, that this leads to larger errors in the calculated response.

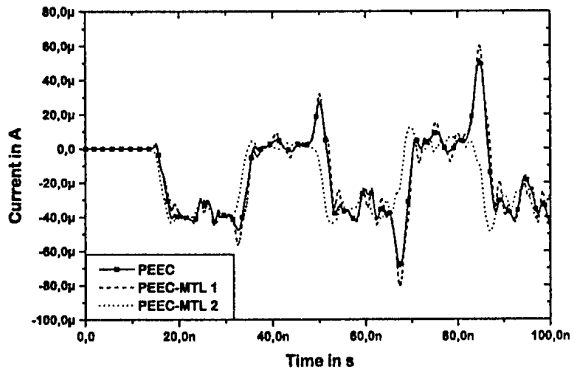



Figure 6: Current thru the feeding point of wire 3 in the time domain

The differences between the PEEC and the PEEC-MTL 1 model are caused mainly due to high frequency components in the excitation function. Since the transmission line part doesn't include retardation, radiation loss is not included and a larger overshot is obtained. The much larger differences between the PEEC and the PEEC-MTL 2 model result from missing couplings.

Finally the simulation times on a Pentium II / 400MHz processor are compared:

- 106s to simulate the PEEC model,
- 52s to simulate the PEEC-MTL 1 model and
- 14s to simulate the PEEC-MTL 2 model.

# 6 SUMMARY

Unlike other methods for the coupling of Full Wave models with TL models our basic approach speeds up the simulation by thinning out the system matrix. To maintain the accuracy of the model a cross-coupling between the PEEC cells and the TL models and between different transmission lines is necessary. To permit this cross-coupling no longer built-in distributed TL models can be used. Instead they are discretized models able to cross-coupling.

Since the approach outgoing from the PEEC system matrix is very general, it can be applied to all kinds of interconnection structures. The degree of thinning out the matrix nd speeding up the calculation depends on how many parts of the whole structure fulfil the presumptions formulated in section 4.

# References

[1] C. Hoer and C. Love. Exact inductance equations for rectanguler conductors with applications to more complicated geometries. *Journal of Research of the National Bureau of Standards–C*, 69C(2):127–137, April–June 1965.

[2] T. A. Jerse and C. R. Paul. A Hybrid Method for Efficiently Estimating Common-Mode Radiation from Transmission-Line Structures. In *IEEE EMC International Symposium (Atlanta, Georgia)*, pages 145–149, August 1995.

[3] G. Mrozynski, V. Schulz, and H. Garbe. A Benchmark Catalog for Numerical Field Calculations with Respect to EMC Problems. In *Proceedings of the 1999 IEEE International Symposium on EMC, Seattle, Washington*, volume 1, pages 497–502, 1999.

[4] A. E. Ruehli. Equivalent Circuit Models for Three-Dimensional Multiconductor Systems. *IEEE Transactions on Microwave Theory and Techniques*, 3:216–221, 1974.

[5] G. Wollenberg and A. Görisch. Coupling of PEEC Models with Transmission Line Models for Simulation of Wiring Structures. In *Proceedings of the IEEE International Symposium on EMC, Seattle WA*, pages 848–853, 1999.

EMC 2000 INTERNATIONAL WROCŁAW SYMPOSIUM ON ELECTROMAGNETIC COMPATIBILITY

# ANALYSIS OF THE SHIELDING PERFORMANCES OF LOADED PERFORATED SHIELDS

**Riccardo E. Zich[1], Hans A. Wolfsperger[2]**
[1]Dipartimento di Elettrotecnica, Politecnico di Milano
P.za Leonardo da Vinci 32, 20133, Milano Italy
ph: +39-011-564-4118, +39-02-23993797
fax: +39-02-23993703, email: zich@polito.it
[2]Universitaet Karlsruhe, IEH – Institut fuer Elektroenergiesysteme
und Hochspannungstechnik, Karlsruhe, Germany
ph:+49-721-608-3054, fax:+49-721-695244; email: **wolfi@ieh.etec.uni-karlsruhe.de**

*In a lot of cases the shielding effectiveness of a shielding structure is determined by apertures that have to be present for different practical reasons. In order to try to minimize the unwanted coupling between the external environment and the shielded volume due to the apertures, they are often loaded with different media. The analysis of the shielding performances of loaded perforated shields is here presented. The analysis is performed through a suitable formalism in the spectral domain, which leads to a circuit interpretation of the electromagnetic problem. The network analysis yields a sort of Wiener-Hopf equation that can be iteractively solved through the Method of Moments, until the required accuracy is reached. The considered analytical approach, suitable for any kind of aperture, is validated through an experimental analysis of a typical configuration of practical interest showing a good agreement of the measured and predicted data.*

## 1. INTRODUCTION

Electromagnetic shields are widely introduced in different systems in order to prevent unwanted coupling effects between the considered system supporting the shield and the electromagnetic environment in which it has to work.

In fact, on one hand, the proliferation of electronics in different applications and the increasingly higher working speed of it, and on the other side, the increasing number of possible sources of electromagnetic noise, natural (such as lightning) but now mostly artificially introduced (such as RF emissions, broadcasting systems, high power radars, high power microwave weapons [1] or even electromagnetic pulses produced by nuclear high altitude explosions [2], [3]), yields the importance of controlling effectively the penetration of unwanted electromagnetic fields into sensitive systems.

The typical solution to the previous problem is the introduction of a metallic enclosure in order to avoid electromagnetic coupling between the inner and the outer volume.

The shielding effectiveness that can be obtained by the introduction of a solid metallic shield, without any aperture, is extremely high, but unfortunately this is only a very ideal option; in fact, any real shielding enclosures presents, for different practical reasons, apertures, gaskets and other weak elements that affect dramatically the shielding effectiveness of the whole structure.

In order to minimize the coupling effects due to the presence of apertures, a possible solution is to try to load the apertures with different layered media [4].

Unfortunately, the computation of the shielding effectiveness of a structure containing a loaded perforated shield is not simple also from a numerical point of view, because of the complexity of the boundary conditions.

The analysis of the electromagnetic coupling between two different regions divided by a metallic shield presenting apertures has been widely studied in the spatial-natural domain by different authors, for example, in [5], [6], but these kinds of approaches, very effective considering a perforated shield in free space, do not stand if loaded apertures are considered.

Furthermore, in [4] the penetration of electromagnetic fields through loaded apertures is addressed, again in the spatial-natural domain, but just considering resistive loading media.

In order to develop a more general approach that let us consider any kind of linear stratified structure as loading medium, for example, isotropic or anisotropic dielectrics, with and without losses, chiral materials, biisotropic materials, pseudo-chiral omega media, bianisotropic media or any complex layered structure combining them, the double spatial Fourier transform is

introduced. This leads to a suitable formalism in the spectral domain rephrasing the electromagnetic problem in an equivalent circuit network model problem [7].

The circuit network approach in the spectral domain yields a sort of Wiener-Hopf equation that can be iteratively solved with requested accuracy through the Method of Moments in the spectral domain with the Galerkin testing scheme. This method does not have any restrictions on the kind of apertures or on the kind of linear loading materials chosen.

The results presented in literature [4], [5], [6] can be obtained again through the considered approach as particular cases (no loading media, resistive sheet as loading medium).

Furthermore, in order to validate the here presented method, an experimental analysis of a configuration of particular importance has been performed showing a good agreement between the measured and the predicted data, even considering just the first momentum in the mode expansion representation. In fact through the spectral approach it is also possible to obtain a better fitting of the experimental data taking into account more terms in the mode expansion representation.

## 2. THE CONSIDERED PROBLEM

Let us consider the structure of Fig.1 representing a perforated shield loaded by a sequence of general bianisotropic slabs.

The whole stratified structure will be modeled in terms of the characteristic impedance [7]. The characteristic impedance of the complete structure is obtained using a cascade matrix algorithm [8].

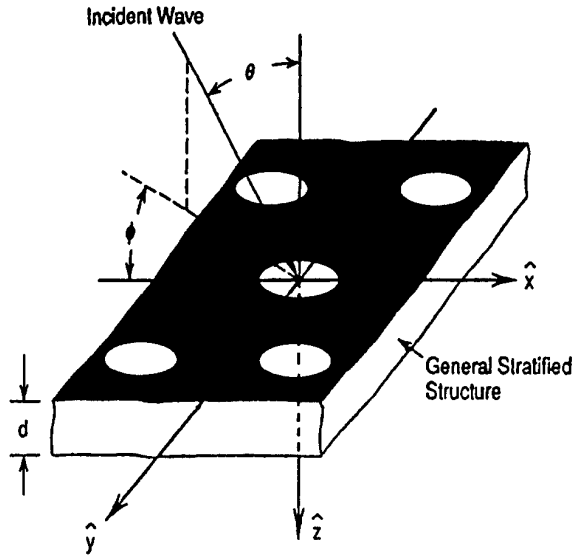



Fig. 1: The geometry of the problem.

The considered problem may be faced by the introduction of the equivalence theorem in both regions: region 1, free space with the electromagnetic source, and region 2, loading media and electromagnetic victim, splitting for a while the coupled problem in two subproblems.

In the first one, dealing with region 1, the perforated shield is replaced by a perfect electric conductor on which, in order to take into account the effects of the apertures, electric and magnetic surface current densities are induced:

$$\underline{\mathbf{J}}_{e\sigma} = \hat{\mathbf{n}} \times \underline{\mathbf{H}}_a$$
$$\underline{\mathbf{J}}_{m\sigma} = \underline{\mathbf{E}}_a \times \hat{\mathbf{n}}$$

where $\underline{\mathbf{E}}_a$ is the electric field and $\underline{\mathbf{H}}_a$ is the magnetic field induced by the source on the apertures. The electric current density does not radiate, while the magnetic one is the radiating term that acts as the source for the region 2, where again the shield is substituted a perfect electric conductor, with the same magnetic surface current density of region 1, laying on a multilayered structure.

Let us introduce the spectral representation of the magnetic current density and of the transverse components of the electric and magnetic fields in both regions

$$\underline{\mathbf{V}}(\underline{\sigma}) = \int_S \underline{\mathbf{E}}_t(\underline{\rho})\, e^{j\underline{\sigma}\cdot\underline{\rho}} d\underline{\rho}$$

$$\underline{\mathbf{I}}(\underline{\sigma}) = \int_S \underline{\mathbf{H}}_t(\underline{\rho}) \times \hat{\mathbf{z}}\, e^{j\underline{\sigma}\cdot\underline{\rho}} d\underline{\rho}$$

$$\tilde{\underline{\mathbf{V}}}(\underline{\sigma}) = \int_S \hat{\mathbf{z}} \times \underline{\mathbf{J}}_{m\sigma}(\underline{\rho})\, e^{j\underline{\sigma}\cdot\underline{\rho}} d\underline{\rho} = \int_S \underline{\mathbf{E}}_a(\underline{\rho})\, e^{j\underline{\sigma}\cdot\underline{\rho}} d\underline{\rho}$$

where $\underline{\sigma}$ is the spatial frequency vector, $\underline{\rho}$ the position vector.

It is now possible to rephrase the original electromagnetic problem in an equivalent circuit network problem in the spectral domain. In Fig.2, the equivalent circuit model for region 1 is depicted.

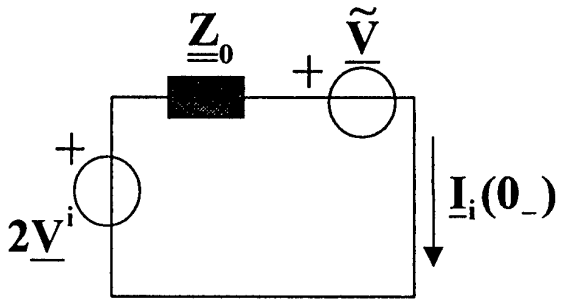



Fig. 2: Equivalent circuit model for region 1.

The circuit solution yields the following relation in the spectral domain

$$\underline{I}_i(0_-) = \underline{\underline{Z}}_0^{-1} 2\underline{V}^i - \underline{\underline{Z}}_0^{-1} \underline{\tilde{V}}$$

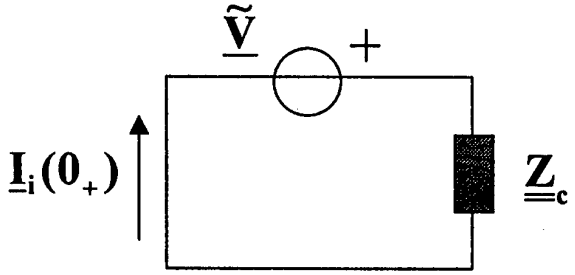



Fig. 3: Equivalent circuit model for region 2.

In a similar way, the equivalent circuit model for region 2 is reported in Fig.3, and the value of the equivalent current in the second circuit is

$$\underline{I}_i(0_+) = \underline{\underline{Z}}_c^{-1} \underline{\tilde{V}}$$

where $\underline{\underline{Z}}_c$ is the characteristic impedance of the whole loading structure seen by the shield [7].

The two currents are exactly the same on the aperture area while they are different on the shield; in fact their difference may be written as

$$\underline{I}_i(0_-) - \underline{I}_i(0_+) = \underline{A}_-(\underline{\sigma}) = \underline{\underline{Z}}_0^{-1} 2\underline{V}^i - (\underline{\underline{Z}}_0^{-1} + \underline{\underline{Z}}_c^{-1})\underline{\tilde{V}}$$

The previous one is a Wiener-Hopf equation since it involves in the same structure functions defined on complementary domains: $\underline{A}_-(\underline{\sigma})$ is a minus function defined only on the shield, while the equivalent voltage generator is just present on the apertures. (It is due to the magnetic equivalent current density at the apertures.)

It is possible to solve the previous equation in a very effective way by using of the Method of Moments in the spectral domain.

In order to compare the measured and the predicted data, let us consider now a very simple case as a test for our approach: the perforated shield considered from here on is a alluminium sheet, 1mm thick, with one circular hole, 20mm of diameter, loaded by an isotropic dielectric polyestere slab, 5mm thick, (relative dielectric constant reported in Fig.4), in the EMC typical band of interest for compliance testing, 30MHz-1GHz. Many other cases have been considered, both analitically and experimentally, but for sake of simplicity the easiest problem is here reported without loss of generality.

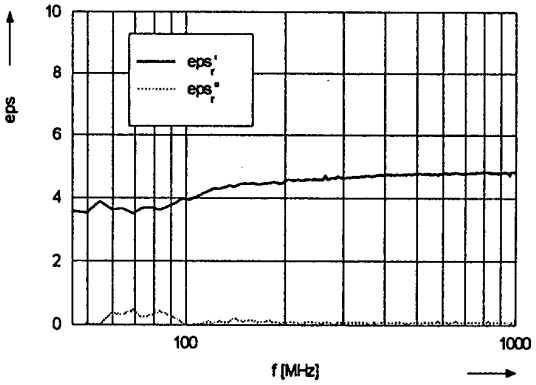



Fig.4: Complex dielectric constant of the inserted medium.

The main idea of an effective analytical application of the MOM (Method of Moments) is to choose a proper set of expansion function. The best choice in our test-case is to choose the eigenmodes of the circular waveguide as expansion function of the transverse electric field induced on the aperture:

$$\underline{E}_a(\underline{\rho}) = \sum_{mn} C_{mn} \underline{e}^{II}_{mn}(\underline{\rho}) + \sum_{mn} D_{mn} \underline{e}^{I}_{mn}(\underline{\rho})$$

Since the problem is considered in the low frequency range, only the first eigenmode can be taken into account:

$$\underline{E}_a(\underline{\rho}) \approx C_{11} \underline{e}^{II}_{11}(\underline{\rho})$$

where

$$e^{II}_{11}(\underline{\rho}) = \pm\sqrt{\frac{\varepsilon_1}{\pi}} \frac{J_1(\frac{\chi^I_1}{a} r)}{\sqrt{\chi^{I2}_1 - 1}} \frac{1}{J_1(\chi^I_1)} \sin\phi$$

is the scalar generating function for one polarization ($\cos\varphi$) for the first eigenmode ($TE_{11}$) of the circular waveguide from which it is easy to obtain [11] the vectorial eigenmode function $\underline{e}^{II}_{11}(\underline{\rho})$.

If a higher accuracy is needed it is sufficient to introduce more terms in the previous expansion.

In order to obtain the shielding effectiveness of the considered structure, the spatial Fourier transformation of the $\underline{e}^{II}_{11}(\underline{\rho})$ has to be computed:

$$\underline{\underline{e}}_{11}^{II}(\underline{\sigma}) = \int_S \underline{\underline{e}}_{11}^{II}(\underline{\rho})\, e^{j\underline{\sigma}\cdot\underline{\rho}} d\underline{\rho} =$$

$$= 2\pi \frac{\sigma a J_1(\chi_1^I) J_0(\sigma a) - \chi_1^I J_0(\chi_1^I) J_1(\sigma a)}{(\frac{\chi_1^I}{a})^2 - \sigma^2}$$

It is now possible to get the expansion in the spectral domain of the induced voltages

$$\underline{\hat{V}}\ (\underline{\sigma}) = C\, \underline{\underline{e}}_{11}^{II}(\underline{\sigma})$$

and the Wiener-Hopf equation becomes

$$\underline{A}_-(\underline{\sigma}) = \underline{\underline{Z}}_0^{-1} 2\underline{V}^I - (\underline{\underline{Z}}_0^{-1} + \underline{\underline{Z}}_c^{-1})\, C\, \underline{\underline{e}}_{11}^{II}(\underline{\sigma})$$

Introducing the primary current $\underline{I}^P(\underline{\sigma})$, just due to the source action, and the equivalent total admittance of the circuit $\underline{\underline{Y}}_t(\underline{\sigma})$

$$\underline{I}^P(\underline{\sigma}) = \underline{\underline{Z}}_0^{-1} 2\underline{V}^I$$

$$(\underline{\underline{Z}}_0^{-1} + \underline{\underline{Z}}_c^{-1}) = \underline{\underline{Y}}_t(\underline{\sigma})$$

the Wiener-Hopf equation becomes

$$\underline{A}_-(\underline{\sigma}) = \underline{I}^P - \underline{\underline{Y}}_t\, C\, \underline{\underline{e}}_{11}^{II}(\underline{\sigma})$$

By projection on the Galerkin testing scheme it is possible to obtain the unknown expansion coefficient C:

$$0 = \frac{1}{(2\pi)^2} \int_{\underline{\sigma}} \underline{I}^P(\underline{\sigma}) \underline{\underline{e}}_{11}^{II}(-\underline{\sigma}) d\underline{\sigma}$$

$$- C \frac{1}{(2\pi)^2} \int_{\underline{\sigma}} \underline{\underline{e}}_{11}^{II}(-\underline{\sigma})\ \underline{\underline{Y}}_t(\underline{\sigma}) \underline{\underline{e}}_{11}^{II}(\underline{\sigma}) d\underline{\sigma}$$

$$C = \frac{\int_{\underline{\sigma}} \underline{I}^P(\underline{\sigma}) \underline{\underline{e}}_{11}^{II}(-\underline{\sigma}) d\underline{\sigma}}{\int_{\underline{\sigma}} \underline{\underline{e}}_{11}^{II}(-\underline{\sigma})\ \underline{\underline{Y}}_t(\underline{\sigma}) \underline{\underline{e}}_{11}^{II}(\underline{\sigma}) d\underline{\sigma}}$$

In order to compare the predicted results with the measured results the shielding effectiveness just due to the introduction of the dielectric slab has been considered:

$$SE_{load} = 20 \log \frac{|\underline{E}_{w.diel}|}{|\underline{E}_{w/o diel}|}$$

where both the fields may be computed through the previous procedure, in fact

$$\underline{E}_{w.diel} = \frac{1}{2\pi} \int_{\underline{\sigma}} \underline{\underline{Z}}_c^{-1}\, C\, \underline{\underline{e}}_{II}^{II}\, e^{-j\underline{\sigma}\cdot\underline{\rho}}\, d\underline{\sigma}$$

and the other field may be computed in a similar way just replacing the free space impedance by the characteristic impedance and the correct value of the coefficient C.

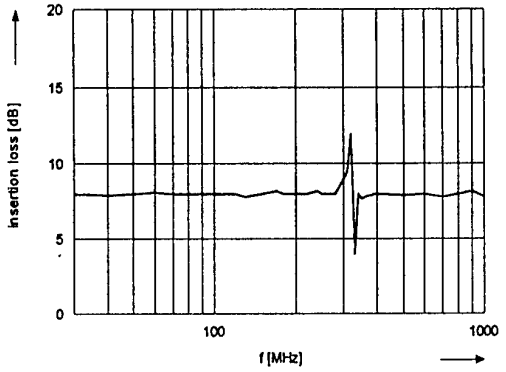



Figure 5: Total predicted shielding effectiveness just due to the introduction of a dielectric slab from 30 MHz-1GHz.

## 3. MEASUREMENTS

The measurements confirming the results of the calculations have been performed in a Dual-Coaxial-TEM-Cell, Fig.6, [10].

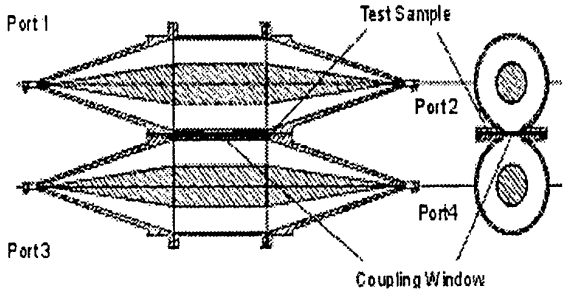



Fig.6: Longitudinal- and cross-section of the Dual-Coaxial-TEM Cell

It is possible to describe the magnetic and the electric coupling between the two single cells by a coupling capacitance and a coupling inductance between two transmission lines, shown in the circuit model, Fig. 7:

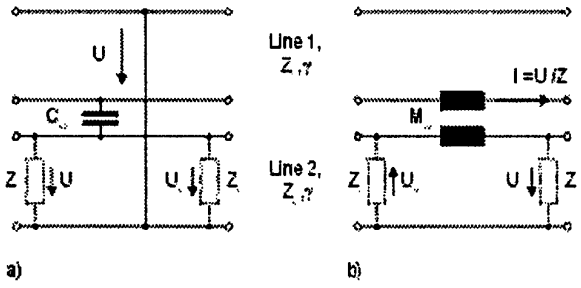



Fig. 7: Circuit model for a) electric coupling and b) magnetic coupling between two transmission lines.

Excitation of transmission line 1 influences in transmission line 2 the voltage

$$U_c = \frac{\frac{1}{2} j\omega C_{12} Z_L U_1}{\frac{1}{2} j\omega C_{12} Z_L U_1 + 1} \approx \frac{1}{2} j\omega C_{12} Z_L U_1 ,$$

$$\frac{1}{2}\omega C_{12} Z_L U_1 << 1$$

by autocapacitive coupling and induces the voltage

$$U_m = \frac{1}{2} j\omega M_{12} \frac{U_1}{Z_L}$$

by autoinductive coupling. Here $U_1$ is the voltage at the excited line 1, $Z_L$ the characteristic impedance of the lines and $C_{12}$, $M_{12}$ the coupling capacitance and inductance. Using the circuit model, for the voltages $U_n$ and $U_f$ measured at the near and the far end of transmission line 2 one obtains:

$$U_n = U_c + U_m$$

$$U_f = U_c - U_m .$$

With the previous equations and it is possible to obtain the electric and the coupling separately.

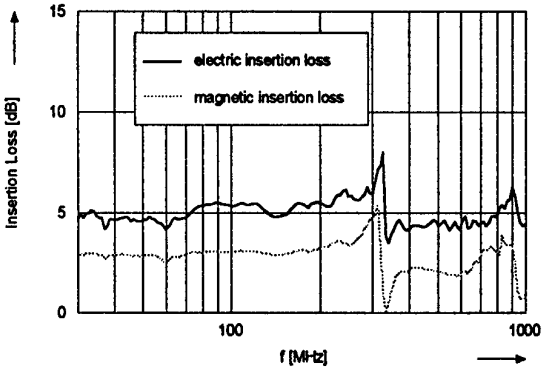



Fig.8: Insertion loss of a 20 mm circular aperture due to the insertion of a 5 mm polyester plate.

## 4. CONCLUSIONS

The effects of loading media on apertures have been here addressed. A general formalism has been presented and on the particular problem of a circular hole experimental and predicted data have been compared showing a good agreement. The same method applies also to other apertures loaded with general linear media without restrictions.

## 5. REFERENCES

5.1. C. D. Taylor, N. H. Younan, "Effects from high power microwave illumination", *Microwave J.*, p.80, June 1992.

5.2. C. E. Baum, D. F. Higgins, "EMP Principles and Techniques", *EMP Interaction: principles techniques and reference data*, Air Force Weapons Lab, 1980.

5.3. "EMP Engineering and Design Principles", Bell Telephone Laboratories, Whippany, New Jersey, 1975.

5.4 C. L. Gardner, G. I. Costache, "The penetration of EM waves through loaded apertures", *IEEE Transaction on EMC*, vol.. 37, No 3, Aug 1995.

5.5. F. De Meulenaere, J. Van Bladel, "Polarizability of some small apertures", *IEEE Trans.*, AP-25, 1977.

5.6 C.M. Butler, C. Baum, "EMP Penetration: Apertures", *EMP Interaction: principles techniques and reference data*, Air Force Weapons Lab, 1980

5.7. R.E. Zich: *Analysis of the shielding properties of Planar Wire-mesh Shields loaded by general stratified structures* IECIE Trans. Com, Feb 1995

5.8. R.D.Graglia, P.L.E.Uslenghi, R.E.Zich, "Reflection and transmission for planar structures of bianisotropic media", *Electromagnetics*, April 1991, pp. 193-208.

5.9. H.A.Wolfsperger, H. Strehlow, A.J. Schwab, "A New Dual-Coaxial-TEM Cell", Proc. 1999 EMC Tokio Symp.

5.10. N.Marcuvitz, "Waveguide Handbook", *IEE Books, Electromagnetic Waves Series* 1986.

EMC 2000 INTERNATIONAL WROCŁAW SYMPOSIUM ON ELECTROMAGNETIC COMPATIBILITY

# DOSIMETRIC ANALYSIS OF BASE STATION ANTENNAS VIA SIMULATION AND MEASUREMENTS

Zwi Altman[1], Andrzej Karwowski[2], Man-Fai Wong[1], Joe Wiart[1] and Laroussi Gattoufi[3]
[1] CNET, France Telecom, 38-40 rue du General Leclerc, 92794 Issy les Moulineaux, France
[2] Silesian University of Technology, Akademicka 16, 44-100 Gliwice, Poland
[3] Bouygues Telecom – R&D, 30, av de l'Europe, 78944 Vélizy, France

*Abstract – A simple and accurate model for base station panel antennas is proposed for dosimetric analysis. A unit cell of the antenna is modeled and is denoted as the generic model. The field of the entire antenna, denoted as the synthetic model, is obtained by superposing shifted field contributions of the generic model. Comparison of the synthetic model with the full antenna modeled and with measurements illustrates the accuracy of the synthetic model.*

## 1. INTRODUCTION

The densification of the mobile network in the last few years manifests the tremendous interest of the public in mobile communications. To assure the safety of the users, international recommendations such as ICNIRP Guidelines have been elaborated to define the authorized limits of exposure to electromagnetic fields [1].

The assessment of the radiated fields in the vicinity of Base Station (BS) antennas can be carried out using both measurements and simulations. Both approaches are complementary, and allow one to scan the entire volume surrounding the antenna. Simulation approach is of particular interest since it can be used to verify measurements on the one hand, and to extrapolate these results outside the accessible volume where measurements can be performed on the other hand.

Various types of antennas are used by mobile operators, although the most commonly used are panel antennas which comprise an array of radiating elements in front of a metallic reflector. These antennas can vary in size, in the reflector geometry and in the radiating elements, e.g., dipole or patch antenna, according to the need of geographical coverage. New antennas are regularly introduced in the network due to its fast evolution and the introduction of new technologies, such as cross polar dual band antennas etc. A full wave modeling of all the antennas in the network for dosimetric purposes is impractical. A more realistic approach is to introduce one or a few representative models for base station antennas that satisfies the manufacturer specifications.

The purpose of this work is to present a simple and accurate model for BS panel antennas which we denote as *synthetic model*. This model is generated in two parts. First, a one unit cell element of the entire antenna, denoted as a *generic model*, is derived. Then, the fields of the entire antenna are obtained by superposing shifted field contributions of the generic model. We consider a model of a BS antenna to be representative if it satisfies the specifications for the 3 dB aperture in the $E$ and $H$ (vertical and horizontal) planes and the maximum gain of the main lobe. A linear feeding law is assumed although the formulation remains identical for any type of feeding. The vertical aperture specification is obtained by choosing the appropriate number of elements in the array, whereas the horizontal aperture is obtained by adapting the unit cell geometry via an optimization procedure. The synthetic antenna model is validated by comparing its radiated near field to that of the full antenna modeled. The numerical simulations have been carried out using two Method of Moment (MoM) based codes: MOMIC [2], which is specialized to wires and wire-grid structures, and NEC-2 [3] which uses both wires and patches.

The radiated near fields have been measured in a volume surrounding the antenna using a detected probe located on the arm of a robot. The good agreement between measurements and simulations validates the synthetic model and put forwards the importance of numerical techniques to extrapolate measurement results.

## 1. THE SYNTHETIC ANTENNA MODEL

Consider an array of three dipoles with horizontal separators, behind a metallic reflector. The field at an observation point $P$ can be described as the sum of fields radiated by the three dipoles in the presence of the reflector (Fig. 1) as written in (1). The subscript '$i$' corresponds to the dipole number that generates the

field, and $z_i$ denotes the coordinate of the dipole center along the z-axis.

$$\mathbf{E}_{ant}(P) = \sum_{i=1}^{N_{dip}} \mathbf{E}_i\left(z_i\hat{\mathbf{z}} + \mathbf{r}_i\right) \qquad (1)$$

The separators are included to minimize the coupling between any given dipole and its neighboring dipole images.

Consider a unit cell comprising a dipole, a reflector and two separators as shown in Figure 2. The field at the point $P$ in front of the full antenna (Fig. 1) can be approximated by adding the contributions of the unit cell near field, $\mathbf{E}_{cell}$, at appropriate shifted points (Fig. 2). Assume for example that the unit cell coincides with the *j-th* unit cell of the full antenna. The total electric field is given by

$$\mathbf{E}_{ant}(P) \cong \sum_{i=1}^{N_{cell}} \mathbf{E}_{cell}\left(z_j\hat{\mathbf{z}} + \mathbf{r}_i\right) \qquad (2)$$

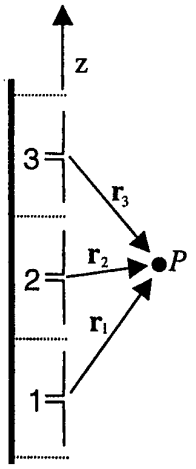



Figure 1. Three radiating dipoles in front of a metallic reflector.

The approximation (2) is particularly good due to the presence of the separators in the model, as will be illustrated in the numerical examples.

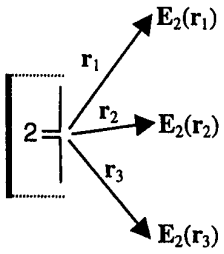



Figure 2. Generic model consisting of one unit cell of the antenna array.

The choice for the unit cell geometry is of particular importance since its dimensions can be varied to satisfy the antenna specifications:

(*i*) Maximum gain
(*ii*) 3 dB horizontal aperture
(*iii*) adaptation at nominal frequency bandwidth

For a linear array, the gain in dB of the antenna, $G_{ant}$, is given in terms of the gain of the unit cell, $G_{cell}$:

$$G_{ant} = G_{cell} + 20\log(AF) - 10\log(N_{cell}) \qquad (3)$$

where $AF$ is the array factor. The maximum gain satisfies

$$G_{ant}^{\max} = G_{cell}^{\max} + 10\log(N_{cell}) \qquad (4)$$

From (4) we get the value required for the maximum gain of the unit cell. The geometry of the unit cell that satisfies the conditions (*i-iii*) is obtained via a simple optimization procedure such as the Genetic Algorithm [4], and is denoted as the *generic model.*

In Figure 3 the geometry of the generic model, as prepared for NEC 2, with 3 dB horizontal aperture of $\theta_{ap}^{h}$ = 90°, and a gain of 8 dBi, is presented. We note that the reflector walls have been modeled as rectangular boxes as required by the magnetic field integral equation formulation used in NEC 2.

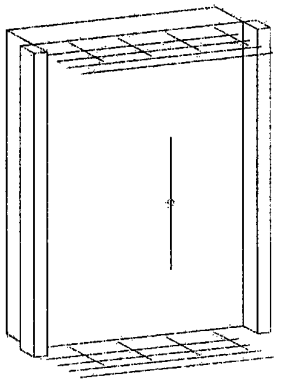


Figure 3. Generic model for $\theta_{ap}^{h}$ =90° and $G_{cell}$=8dBi.

Finally, we calculate the electric field radiated by the generic model at a volume surrounding it, big enough along the z-direction. The field of the synthetic model at each point is obtained by adding the shifted field contributions of the generic model using (2).

## 2. RESULTS

In this section we compare numerical and measurement results for a GSM Kathrein K730370 antenna. This BS antenna consists of an array of four dipoles, and will be analyzed at frequency of 900 MHz. First, we compare the numerical results for the of entire antenna models obtained by NEC-2 and a customized, extended version of MOMIC. As mentioned in the introduction, the main difference between the two codes is that MOMIC employs wire mesh (grid) to model conducting surfaces (the antenna reflector in the case at hand), whereas NEC-2 utilizes thick walls. The wire-grid model of K730370 prepared for the MOMIC code is shown in Figure 4. The model consists of 584 nodes and 1099 wires. Each wire used to model the antenna reflector was assumed to have a radius of 1 mm, and was split into two segments. Each of the four radiating dipoles was modeled by a cylindrical wire having a 3 mm radius; the wire was subdivided into 8 segments. The total number of unknowns (current modes) in the problem is 2737.

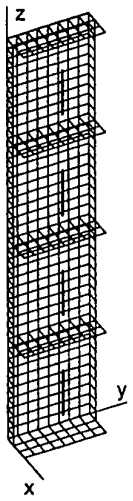



Figure 4. Wire-grid model of the Kathrein K730370 antenna for the MOMIC code.

In Figures 5 and 6, the iso-level lines for the electric field (RMS) using the two codes are plotted in the *E*- and *H*- plane respectively. An input power of 1 Watt has been used. The agreement between the two methods is very good, and the small differences is due to the different thicknesses used to describe the reflector walls.

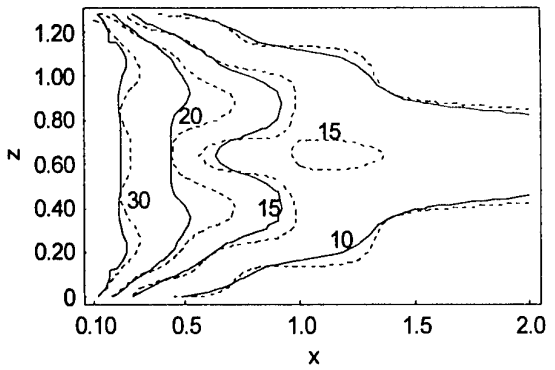



Figure 5. Iso-level lines of the electric field in the *E*-plane in front of the K730370 antenna, using the MOMIC (solid lines) and NEC 2 (dashed lines).

Next, we compare the synthetic model with the full antenna modeled. In Figures 7 and 8 the electric field iso-level lines calculated by NEC 2 are plotted in the *E*- and *H*- planes respectively. The input power of 1 Watt is used.

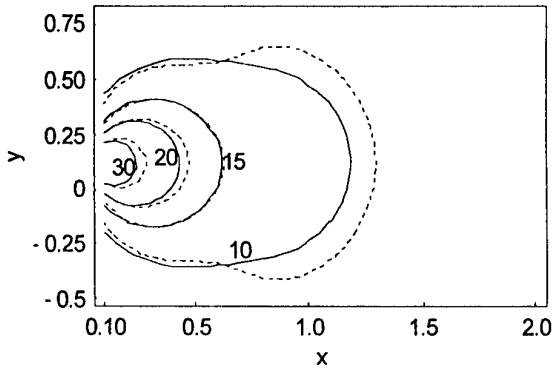



Figure 6. Iso-level lines for the electric field in the *H*-plane in front of the K730370 antenna at z=20cm, using the MOMIC (solid lines) and NEC 2 (dashed lines).

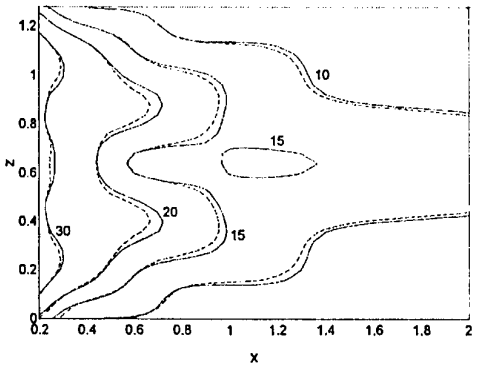



Figure 7. Electric field in the *E*- plane in front of the K730370 antenna using the synthetic model (dashed lines) and the full antenna modeled (solid line).

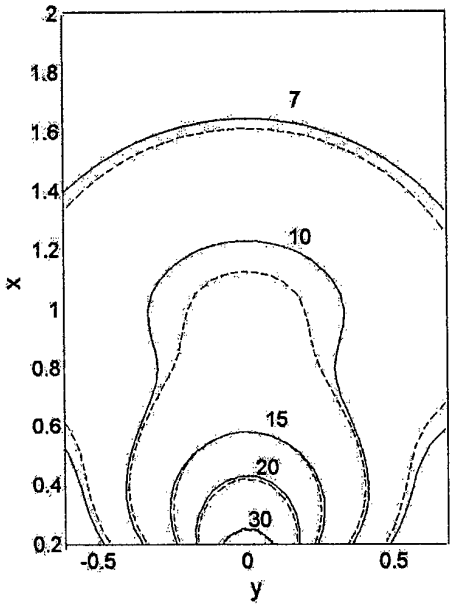



Figure 8. Electric field in the *H*- plane for the K730370 antenna at z=20 cm using the synthetic model (dashed lines) and the full antenna modeled (solid line).

The excellent agreement between the two approaches validates the synthetic model and put forwards this approach for dosimetric analysis of BS antennas. It is noted that due to the small number of unknowns required to model the unit-cell geometry, the computation time for the synthetic model is very short, of the order of several seconds. Moreover, the model remains accurate for bigger antennas, viz., arrays with larger number of radiating elements.

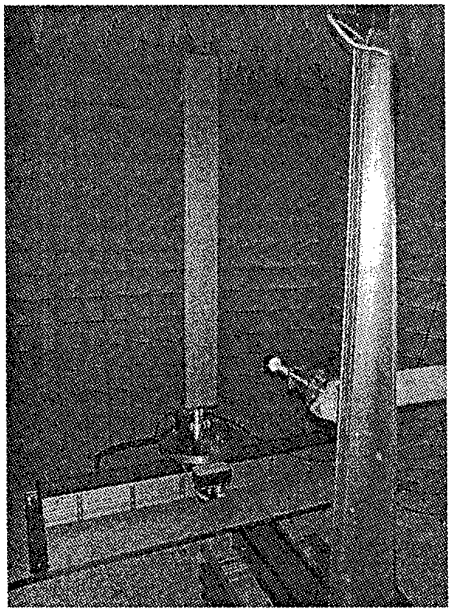


Figure 9. Measurement set-up for the electric field radiated by a base station antenna.

Measurements of the electric near field have been carried out in a semi-anechoic chamber of the CNET using an *E*-field probe that scans the entire volume surrounding the antenna. The measurement setup is shown in Figure 9. It is noted that for small distances from the antenna, below 2m, the reflections from the metallic ground can be neglected.

The comparison between measurements and simulations using the synthetic model are shown in Figure 10. A Kathrein K730370 antenna has been used with an input power of 10 Watt.

We can see that a similar field pattern is obtained using both approaches, and that the *E*-field simulated results tend to overestimate the measured results.

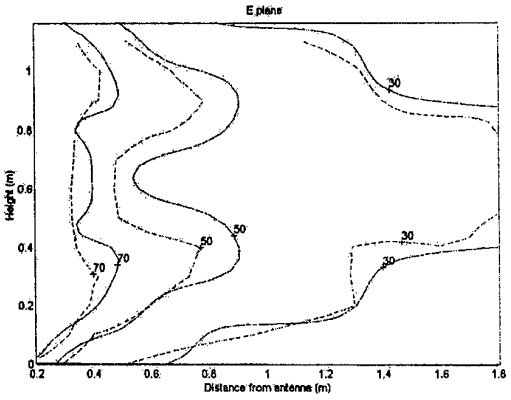



Figure 10. Comparison of the electric field in the *E*-plane using the synthetic model (solid line) and measurements (dashed line).

## 3. CONCLUSIONS

A synthetic model of BS panel antennas for dosimetric analysis has been presented. The model is based on the superposition of shifted fields radiated by a generic antenna which is a single unit cell of the antenna array. The comparison with the full antenna modeled as well as with measurement results illustrates the accuracy of the proposed model. The synthesis of a few generic antennas can be used, via the synthetic model, to represent all the panel antennas utilized by the operator.

One of the authors (AK) would like to acknowledge partial support of this work by the National Institute of Telecommunications, Wroclaw Branch, Wroclaw, Poland.

## 4. REFERENCES

[1] ICNIRP, "Guidelines for Limiting Exposure to Time-varying Electric, Magnetic and Electromagnetic Fields (10 kHz to 300 GHz)", Health Physics, vol. 74, no. 4, pp. 494-522, April 1998.

[2] A. Karwowski, "MOMIC - a computer program for analysis of wire antennas and scatterers" (in polish), *National Telecommunications Symposium KST'97*, Bydgoszcz, Poland, Sept. 10-12, 1997, Proceedings, vol. D, pp. 395-404 (see also http://emlib.jpl.nasa.gov/EMLIB/MOMIC/).

[3] Burke and Poggio, "Numerical electromagnetic code – Method of Moments". Lawrence Livermore National Laboratory, January 1981.

[4] D. E. Goldberg, Genetic Algorithms in Search, Optimization and Machine Learning, Reading, MA: Addison-Wesley, 1989.

## 4. BIOGRAPHICAL NOTES

**Zwi Altman** received the B.Sc. and M.Sc. degrees in electrical engineering from the Technion-Israel Institute of Technology, in 1986 and 1989 respectively, and the Ph.D. degree in electronics from the Institut National Polytechnique de Toulouse, France, in 1994. From 1994-1996 he was a Post-Doctoral Research Fellow in the Electromagnetic Communication Lab., at the University of Illinois at Urbana Champaign. In 1996 he joined the CNET- National Center of Telecommunication Studies of France Telecom.

**Andrzej Karwowski** received M.Sc. and Ph.D. degrees (equivalent of), both in electrical engineering, from the Wroclaw Technical University, Wroclaw, Poland, in 1969 and 1976, respectively. Since 1987 he has been affiliated with the Department of Automatic Control, Electronicsand Computer Science, Silesian University of Technology, Gliwice, Poland, where he currently holds the position of Professor. His research interests are primarily in computational electromagnetics. Dr. Karwowski is a member of the IEEE.

**Man-Faï WONG** received the Engineering degree in electronics from "Ecole Nationale d'Electronique, d'Electrotechnique, d'Informatique et d'Hydraulique de Toulouse", Toulouse, France in 1990 and Ph.D. degree in electronics from Paris 7 University in 1993. Since 1990, he has been with the Centre National d'Etudes des Télécommunications (CNET), France Telecom, in the fields of applied electromagnetics for telecommunications systems. He is currently working on the interactions of microwaves with human bodies and the electromagnetic compatibility of wireless systems. Dr. Wong is a senior member of IEEE.

**Joe Wiart** received the Engineer degree from the Ecole Nationale Supérieure des Telecommunication, Paris France, in 1992 and the PhD degree in physics from the ENST and P&M Curie University, Paris, France in 1995.He joined the CNET - the research center of France Telecom in 1992. He is currently the head of a group dealing with the interaction of radiowaves with the human body and on medical electronic devices in CNET.
Dr Wiart is Vice Chairman of the COST 244 bis, Chairman of the CENELEC Working Group in charge of mobile and base station standard, and vice chairman of the URSI French commission K. Since 1998 Dr Wiart is Senior member of the SEE.

**Laroussi Gattoufi** received the electrical engineering degree from Ecole Nationale d'Ingénieurs de Tunis, Tunisia, in 1992 and the Ph.D. degree from the University of Paris-XI (Supélec, Gif-Sur-Yvette), in 1998. He joined Bouygues Telecom (French Telecommunications Operator), in June 1998, as Head of Electromagnetic Phenomenas, Antennas and Propagation R&D Groupe. His research activity conducted in the Groupe since that time, has been devoted to general scattering, diffraction and telecommunication systems, both numerical and experimental aspects. Dr. GATTOUFI is a member of IEEE Antenna and Propagation Society.

**EMC 2000** INTERNATIONAL WROCŁAW SYMPOSIUM ON ELECTROMAGNETIC COMPATIBILITY

# DIRECTIONAL ANTENNAS FOR THE REDUCTION OF SAR INSIDE THE HUMAN HEAD

Paola Bertotto, Andrea Schiavoni, Gabriella Richiardi, Paolo Bielli
CSELT – Centro Studi e Laboratori Telecomunicazioni
Via G. Reiss Romoli 274, 10148 Torino
Tel: +39 11 228 7266, Fax: +39 11 228 5577, E-mail: andrea.schiavoni@cselt.it

*The purpose of the paper is the investigation of patch antennas for cellular phones in order to reduce the SAR (Specific Absorption Rate) inside the human head. The electromagnetic problem has been solved by using the FDTD (Finite Difference Time Domain) method. The phone-head position, as requested by standards, has been performed by using a developed in house pre-processor able to manage the 3D geometry and create the input data file for the electromagnetic solver. The anatomical model of the human head has been obtained by a MR Images segmented in order to distinguish different tissues. SAR reduction, radiation patterns and input reflection coefficient have been evaluated to satisfy design constraints.*

## 1. INTRODUCTION

Traditional cellular phones use wire or helix antennas whose radiation pattern in free space is omnidirectional. During the normal use of the phone the power in the angular region of the head is absorbed and doesn't contribute to the radiation. The use of directional antennas is of interest for the following reasons:

- reduction of the electromagnetic field, and as consequence the SAR, in the head's tissues with respect to traditional antennas;
- limited load effect of the head on the matching parameters of the antenna;
- greater life of the batteries with the same performances in terms of link's quality;
- more compact cellular phones.

The aim of this work is the evaluation of SAR inside the human head generated by models of cellular phones equipped with patch antennas, single band and dual band. SAR has been computed for different types of antennas and compared with SAR generated by $\lambda/4$ monopole phone in order to determine the reduction factor. The $S_{11}$ coefficient has been computed to evaluate the input matching and resonance frequency and the frequency bandwidth.

The patch antenna is enclosed inside the phone's case then hidden behind a plastic cover. The plastic cover could change the frequency characteristics of the antenna then has been taken into account. The effect of the source position on the frequency characteristics has been evaluated for one model of patch antenna and optimised in terms of matching.

The radiation patterns of the simulated antennas have been compared with the radiation pattern of the $\lambda/4$ monopole in presence and absence of the head.

## 2. ELECTROMAGNETIC MODELLISATION

The electromagnetic problem has been solved by using the FDTD technique; the grid has been truncated by using RTABC absorbing boundary conditions [1-3]. The standard technique has been extended with routines able to analyse:

- thin sheets [4] – model of dielectric or metallic sheets, parallel to the co-ordinated planes, whose transversal dimension is smaller than a space discretization step;
- coaxial cables [5] – analysis of coaxial cables inside the FDTD grid modelled as a transmission lines;
- thin wires [6] – analysis of metallic wires whose diameter is smaller than a space discretization step;
- near field to far field transformation.

The anatomical model of the head has been obtained by means of the following procedure:

- Magnetic Resonance acquisition (fig. 1a) of a volunteer head. The 3D model is the superimposition of a set of planar images;
- Recognition and labelling process based on neural network techniques. A label is associated to region having the same grey

level relevant to a tissue. The head model has been labelled with 36 tissues (fig. 1b).

- Validation by radiologists. Final check of the recognition process and correction of errors, if necessary.

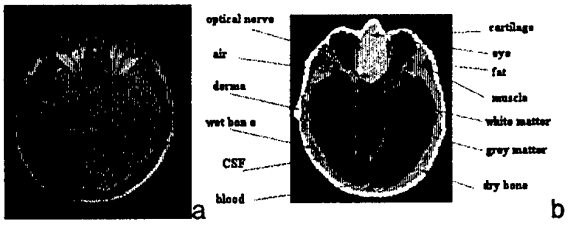



Fig. 1. Human head model: a) original image in grey scale; b) the same image labelled.

The geometry of the problem is managed by using a pre-processing system [7] in order to align the model of the phone to the head, as requested by CENELEC ES59005 standard [8] in the "Intended Use" position. The pre-processor performs the discretization of the space, creates the input data files for the electromagnetic solver and generates graphical file to check the correctness of the process; the discretization process is completely automated.

## 3. SIMULATIONS

The idea to integrate antennas for cellular phones inside the case offers many advantages with respect of the traditional antennas, like the wire and the helix antennas. Indeed, apart from a lower probability of breaks, this type of antenna reduces the power absorbed by the human head. In the same time there is a minimisation of the head effects on the antenna's radiation pattern and input impedance. For these reasons patch antennas are often indicated as "antennas with a low impact of SAR". On the other hand attention has to be paid the SAR inside the hand and its influence on the far field and matching behaviour of the antenna. The greater difficulty in the design of these antennas is to obtain a compromise on the dimensions, which have to be compatible to the reduced dimensions of the phone's case, and the operating characteristics such as the frequency bandwidth and reflection coefficient.

The body of the phone has been simulated as a metallic box covered by a plastic sheet, to represent the display and the keyboard. The dimensions of the box are 120x55x20 mm; the plastic layer is 5 mm thick; permittivity $\varepsilon = 2.4$ and conductivity $\sigma = 0.00325$ [S/m]. Figure 2 shows the position of the $\lambda/4$ wire antenna and patch antenna on the phone's case.

For all simulations the space has been discretized in cubic cells, 1 mm side, obtaining a very accurate definition both of the head and of the antenna, satisfying the FDTD constraints for all the considered frequencies.

An averaged power of 250 mW at 900 MHz and an averaged power of 125 mW at 1800 MHz has been considered.

The code runs efficiently on a parallel computer with low computation time.

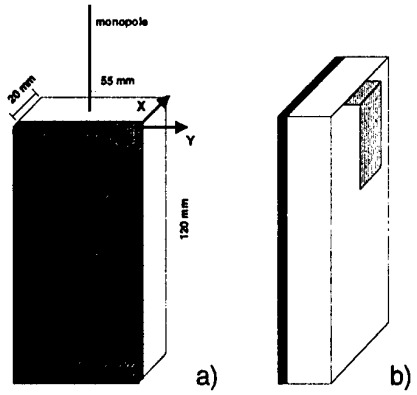



Fig. 2 a) Metallic box equipped with $\lambda/4$ wire antenna; b) Metallic box equipped with patch antenna

## 4. RESULTS

The output of the code consists of the field distribution in the analysed space. Results have been evaluated and compared in terms of:

- SAR values averaged as requested by standards [8-9] and reduction with respect to $\lambda/4$ wire antenna;
- Input reflection coefficient considering the phone radiating in free space;
- radiation patterns in absence and in presence of the head.

### 4.1 Dual band PIFA antenna

The dual band PIFA (Planar Inverted F Antenna) consists of two patches: the first has a rectangular shape and the second has an L shape working, respectively, in the band of 1800 MHz and 900 MHz. The antenna is connected to the ground plane by a short and it is feed by a coaxial cable (figure 3).

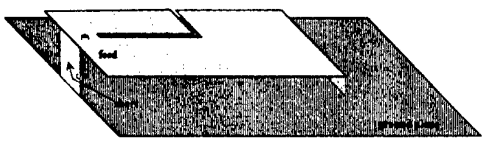


Fig. 3 The dual band PIFA antenna

A prototype has been manufactured; figure 4 shows the comparison on the $S_{11}$ parameter computed by the FDTD and measured in free space.

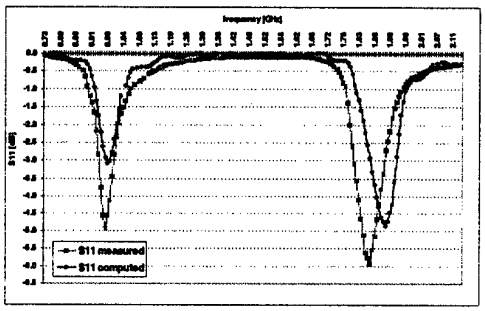
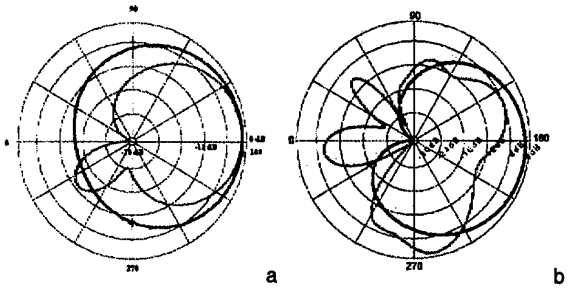



Fig. 4 Comparison between the reflection coefficient $S_{11}$ measured and computed for the dual band PIFA antenna

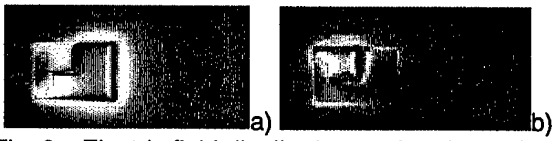
Figure 5a reports the radiation patterns for the dual band PIFA antenna in free space (black line) and in presence of the head (grey line) at 900 MHz; figure 5b shows the same comparison at 1800 MHz.



a b

Fig. 5 Radiation patterns for PIFA on the plane YX; black line in free space and grey line in presence of the head. a) at 900 MHz; b) at 1800 MHz.

The electric field distributions on the plane of the antenna are reported in the figure 6; it can noted the part of the antenna that is working at the relevant frequency.



a) b)

Fig. 6 Electric field distribution on the plane of the antenna: a) 900 MHz; b) 1800 MHz

4.2 WMSA antenna

The WMSA antenna (Window-reactance-loaded Micro Strip Antenna), figure 7, is constituted by a metallic plane on which there are two apertures to increase the electric path of the field's lines. The antenna works in the GSM1800 band.

The antenna is has been covered by a plastic sheet to consider the plastic cover of the phone's case. Figure 8 shows the $S_{11}$ as a function of the position of the feed point moved toward the aperture. This is another parameter that can be used, beside the dimensions of the antenna and apertures, to tune the antenna.

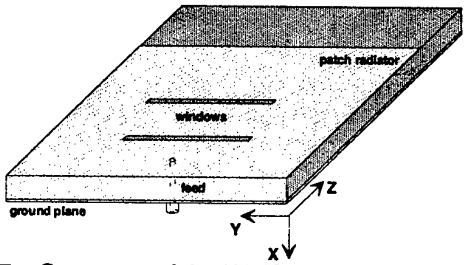



Fig. 7 Geometry of the WMSA antenna

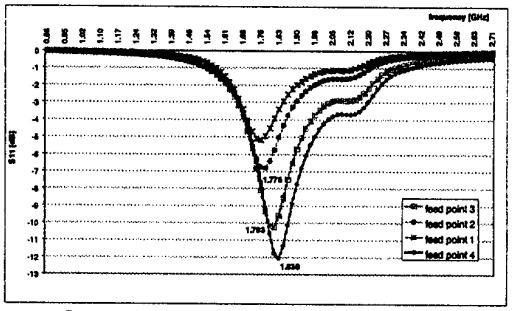
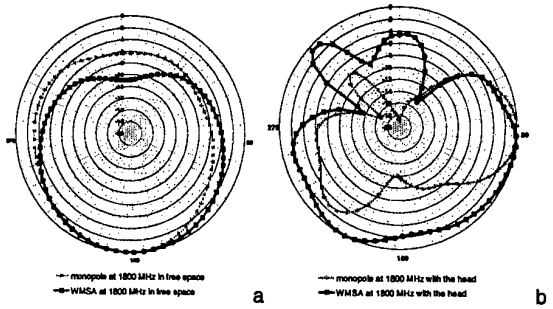



Fig. 8 $S_{11}$ parameter as a function of feed position. It can be noted the change in the centre frequency and bandwidth.

Figure 9 shows the radiation patterns in free space and in presence of the head, compared with the $\lambda/4$ wire antenna. Figure 10a shows the electric field distribution on the antenna's plane while figure 10b shows the plane cutting the antenna.



a b

Fig. 9 Radiation patterns on the plane YX at 1800 MHz. a) in free space; b) with the head.



a b

Fig. 10 Electric field distributions. a) on the antenna's plane; b) plane crossing the antenna.

4.3 WDBP antenna

The WDBP (Windowed Dual Band PIFA) antenna is modification of the dual band PIFA on which there are two apertures in the direction of the length, figure 11. The excitation is obtained by electromagnetic coupling through a plane below the plane of the antenna. Figure 12 shows the $S_{11}$ coefficient on both the GSM bands.

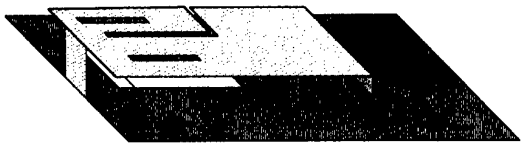


Fig. 11 WDPB antenna.

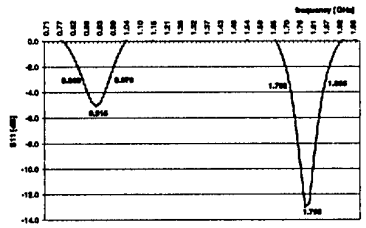
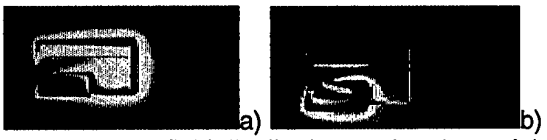


Fig. 12 Reflection coefficient for the WDPB antenna.

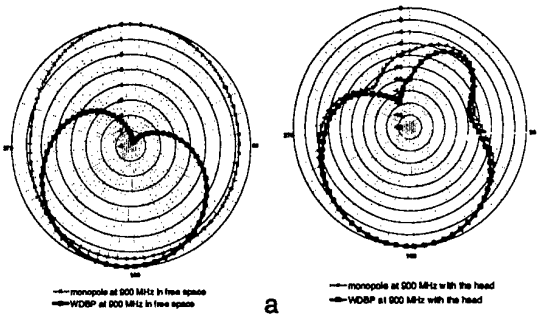
Figure 13 shows the electric field distributions for the antenna working respectively at 925 MHz and 1795 MHz.



a) b)

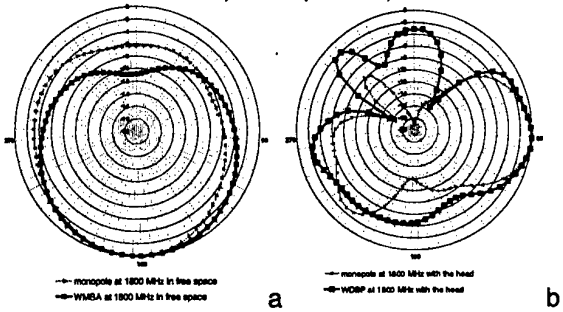
Fig.13 Electric field distribution on the plane of the antenna. a) at 925 MHz; b) at 1795 MHz.

Figure 14 reports the comparison on the radiation pattern, in free space and in presence of the head, with the λ/4 wire antenna at 925 MHz. Figure 15 shows the same comparison at 1795 MHz.



a b

Fig. 14 Radiation patterns on the plane YX at 900 MHz band. a) free space; b) with the head.



a b

Fig. 15 Radiation patterns on the plane YX at 1800 MHz band. a) free space; b) with the head.

Table 1 reports the SAR values for the different antennas at 900 MHz compared with SAR due to the λ/4 monopole antenna. SAR has been averaged on a cubic mass of 1.0 and 10.0 g as requested by standards [8-9]. Table 2 gives SAR values at 1800 MHz. SAR has been computed considering an averaged radiated power of 250 mW and 125 mW at 900 and 1800 MHz, respectively. The SAR difference, with respect to the λ/4 monopole, has been computed as:

$$\Delta = 100\frac{SAR_{\lambda/4} - SAR_{antenna}}{SAR_{\lambda/4}}$$

Table 1: SAR comparison at 900 MHz.

| | $SAR_{1.0g}$ | Δ | $SAR_{10.0g}$ | Δ |
|---|---|---|---|---|
| Antenna | [W/kg] | [%] | [W/kg] | [%] |
| λ/4 monopole | 0.62 | - | 0.49 | - |
| PIFA | 0.12 | 80.6 | 0.05 | 89.8 |
| WDBP | 0.33 | 46.7 | 0.27 | 44.9 |

Table 2: SAR comparison at 1800 MHz.

| | $SAR_{1.0g}$ | Δ | $SAR_{10.0g}$ | Δ |
|---|---|---|---|---|
| Antenna | [W/kg] | [%] | [W/kg] | [%] |
| λ/4 monopole | 0.31 | - | 0.16 | - |
| PIFA | 0.12 | 61.3 | 0.04 | 75.0 |
| WMSA | 0.11 | 64.5 | 0.05 | 68.8 |
| WDBP | 0.21 | 32.2 | 0.10 | 37.5 |

Figures 16 and 17 show the comparison on SAR distribution for the λ/4 monopole and WDBP antenna at 900 and 1800 MHz respectively. SAR has been normalised to the maximum SAR and reported in logarithmic scale since it decays exponentially inside the head. The pictures shows the plane where the maximum SAR was found.

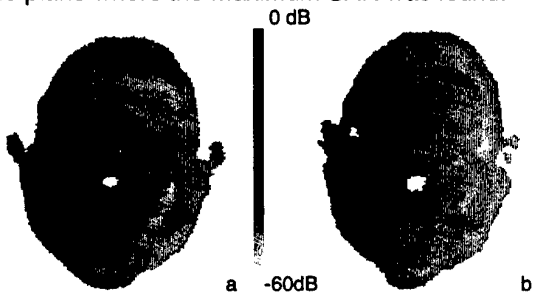



Fig. 16 SAR distribution at 900 MHz in the plane where maximum was found. a) λ/4 monopole; b) WDBP antenna.

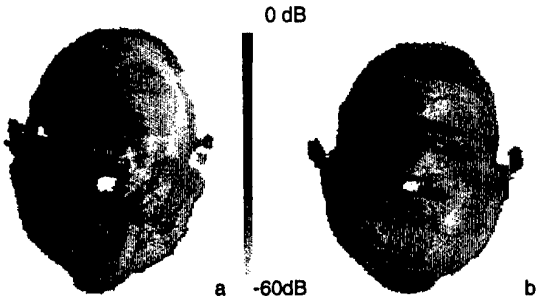



Fig. 16 SAR distribution at 1800 MHz in the plane where maximum was found. a) λ/4 monopole; b) WDBP antenna.

A SAR level placed at half grey scale means that it is reduced by a factor 1000 with respect to the maximum value. Even if the grey scale doesn't help in appreciate the SAR distribution it can be noted the different penetration at 900 and 1800 MHz and also the lower penetration of directional antenna with respect to the monopole.

By observing the radiation patterns it can be noted, for all the considered antennas, the lower influence of the head with respect to monopole antenna. In this sense the head affects lower the input parameters of the antenna maintaining matching with the RF amplifier.

The effect of the hand holding the phone has been not considered, anyway depending on the hand position it could affect the antenna behaviour. The effect of the hand on radiation patterns and SAR inside the hand should be investigated to increase performances of the antennas.

## 5. CONCLUSIONS

SAR has been evaluated inside an anatomical model of the human head radiated by different types of patch antennas working at GSM 900 and 1800 frequencies. SAR has been compared with SAR generated by a model of phone equipped with $\lambda/4$ monopole in order to evaluate the reduction factor due to the use of directional antennas.

For all the considered antennas both at 900 and 1800 MHz, there is a considerable SAR reduction inside the human head.

The dimensions of the antennas are compatible with the space at disposal on the phone's case. The effect of the cover and the effect of the position of the feeding point has been taken into account.

The FDTD technique has shown good performances in the analysis of antennas, especially if used on parallel computers permitting to obtain very low computation times.

## ACKNOWLEDGMENT

This work is fully supported by TIM – Telecom Italia Mobile. Authors wish to thank ing. Luca Caroli-TIM for the support.

## REFERENCES

[1] Taflove, "Computational Electrodynamics - The Finite Difference Time Domain Method", Artech House, 685 Canton Street, Norwood, 1995, MA 02062

[2] Taflove, "Advances in Computational Electrodynamics- the Finite-Difference Time-Domain Method", 1998 Artech House, 685 Canton Street, Norwood, MA 02062.

[3] Kunz, Luebbers, " The Finite Difference Time Domain Method for Electromagnetics", 1993 by CRC Press, Inc.

[4] Maloney, Smith, "The efficient modeling of the thin material sheets in the finite-difference time-domain (FDTD) Method", IEEE Trans. on AP, vol.40, No. 3, March 92.

[5] Maloney, Shlager, Smith, "A simple model for transient excitation of antennas by transmission lines", IEEE Trans. on AP. vol. 42, no. 2, Feb.94.

[6] Umashankar, Taflove, Beker, "Calculation and experimental validation of induced currents on coupled wires in a arbitrary shaped cavity", IEEE Trans. on AP. vol. 35, no. 11, Nov. 87.

[7] Richiardi, Vezzari, Schiavoni, Bertotto, Bielli, "Numerical representation of cellular phones: procedure and accuracy", EMC'98 Roma, September 14-18 1998.

[8] CENELEC ES 59005 "Consideration for evaluation of human exposure to electromagnetic fields (EMFs) from mobile telecommunication equipment (MTE) in the frequency range 30 MHz 6 GHz" Oct. 98.

[9] IEEE Std C95.1-1991 "IEEE standard for safety levels with respect to human exposure to radio frequency electromagnetic fields, 3 kHz to 300 GHz".

EMC 2000 INTERNATIONAL WROCŁAW SYMPOSIUM ON ELECTROMAGNETIC COMPATIBILITY

# ELECTROMAGNETIC FIELDS IN PROXIMITY OF GSM BASE STATIONS

Brunello Fabiano, Charrère Marco, Disco Daniele, Gambin Domenico, Gianola Paolo
CSELT (Centro Studi E Laboratori Telecomunicazioni), Via Reiss Romoli 274, 10146 Torino, Italy
Tel.: +39 (0)11 2287190, Fax +39 (0)11 2285577, E.mail: paolo.gianola@cselt.it

*In this paper we present evaluation techniques for the electromagnetic field levels radiated by antennas used in the Radio Base Station (RBS) for mobile services. Theoretical modelling and experimental results are explained for the electromagnetic field in the near zone of the antennas. Besides, a numerical technique for the calculation of the electromagnetic field levels in an urban area is presented.*

## 1. INTRODUCTION

The ever increasing presence in many countries of RBS for mobile communications caused, in recent years, a growing anxiety of people living close to RBS worried about the biological effects of electromagnetic pollution. Moreover, governments in many countries have established very stringent exposition limits for the levels of the EMF (electromagnetic fields) radiated in the radio-frequency range. The Italian law regarding the exposition limits for the electromagnetic fields [1] sanctions: (Art. 4): "*... in correspondence of buildings used for permanencies not less to four hours, it doesn't must to be exceed the fellow frequency independent values, averaged on a human body vertical section equivalent area, and over a time-slot of six minutes: 6 V/m for the electric field, 0.016 A/m for the magnetic field and for a range of frequency between 3 MHz and 300 GHz, 0,1 W/m$^2$ for the power density of the equivalent plane wave.*" As a consequence, operators must produce documentation more and more detailed on the compliance of their RBS to prescribed limits. In the paper we will present efficient methods for the evaluation of the EMF levels radiated by RBS-antennas and in proximity of the RBS in urban areas.

## 2. NEAR FIELD ANTENNA MODELS

As a rule the EMF radiated by a RBS-antenna is calculated under a far-field hypothesis, that is the gain function $G(\theta,\varphi)$ of the antenna is the product of the radiation patterns in the vertical and in the horizontal plane (fig. 1): so the radiated electric field results

$$E(R,\theta,\varphi) \cong \frac{\sqrt{30PG(\theta,\varphi)}}{R}$$

where R is the distance from the antenna and P is the input power.

However to estimate the EMF close to the above kind of antenna is necessary to have its near-field model, actually the far-field limit zone can be more than forty meters, but the distance between an antenna and an urban site is often less.

The well-know full-wave tool NEC (Numerical Electromagnetic Code) [2] gives an accurate model of the antenna in its near-field zone, but it requires a good knowledge of its structure, besides the computation time is expensive.

The methods explained in this paper, calculate the electromagnetic field radiated in the near and far zone of antennas by considering the radiation far-field patterns and the dimensions of the antenna only.

By thinking the RBS-antenna as a uniform array (this is true for a large variety of radio mobile services) as shows on fig. 1, a valid alternative to the full-wave tools was found. A first method, the so-called NFUA (Near Field Uniform Array) that is explained on [3], assumes that the near-field of the antenna is a sum of the far-field of each element.

The innovation of the method can be distinguished on two steps: in the first from the radiation patterns of the antenna an algorithm computes the number N of its elements and the distances to each others referred to the wavelength.

In the other step an FFT algorithm smoothes the discontinuous behaviour of the single element radiation pattern (for details see [3]).

The other method that we have developed is the so called NFUTD (Near Field UTD): it is based on the UTD (Uniform Theory of Diffraction) described in [4], and it takes [5] as one's starting point.

From the first step of the NFUA, the NFUTD can describe an antenna as shown in fig. 1: actually N and the various distances are known (the dimensions are got from the antenna data sheets).

The total electrical field for this antenna is the sum of the electric field radiated from the array elements with its components reflected and diffracted by the metallic plate used as a reflector:

$$\vec{E}_{TOT} = \sum_{i=1}^{N} \vec{E}_i^I + \vec{E}_i^R + \vec{E}_i^D .$$

Each array element is an electric dipole of finite length, which is supplied by a sinusoidal electric current: the method care is due to the kind of relation used for the EMF of the dipole. Actually the diffracted field is related to the incident one by the following expression:

$$\vec{E}^D = \vec{E}^I \cdot \underline{\underline{\mathbf{D}}} \cdot A(s) \cdot e^{-jks}$$

where $\underline{\underline{\mathbf{D}}}$ is the diffraction coefficient dyadic; if the incident field changes abruptly the diffracted field isn't able to reduce its discontinuity and that of the reflected one when they cross the shadow zone limits.

We have tested various forms of the EMF radiated by an electric dipole, but the expression achieved from the electric dipole far-field condition, has provided the best results: fig. 2 and fig. 3 shows the radiation patterns in the vertical and horizontal plane coming from measurements and NFUTD method: a good agreement was found over the 20dB level.

We have considered the $\vec{E}^D$ component diffracted by both edges and corners of the metallic plate (for details on NFUTD see [6]).

Both methods (NFUA and NFUTD) reduce the calculation time even for large number of points on which we evaluate the EMF, and they need a simple definition of the antenna structure.

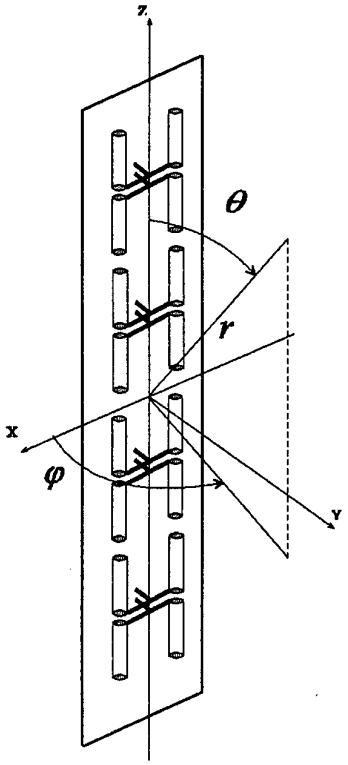



**Fig. 1** RBS-antenna as a planar array.

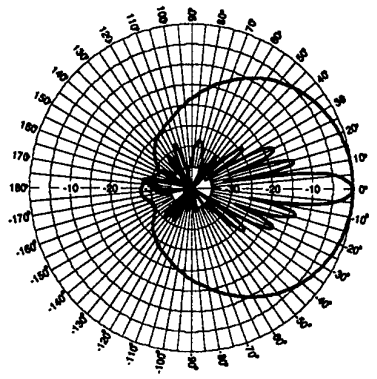


**Fig. 2** Radiation patterns got by far-field measurements.

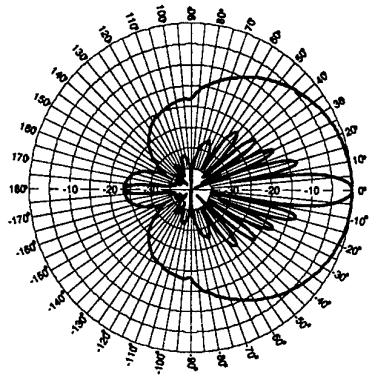


**Fig. 3** Radiation patterns got by NFUTD simulation.

## 3. NEAR FIELD MEASUREMENT SYSTEM

The antenna test stand is a system specifically designed for planar antenna measurements. It is outdoor equipment installed on the roof of CSELT building. The construction was mainly built of dielectric material and supports field strength measurements of antennas in the range of 2.5m (Z-axis) by 18m (X-axis) (fig. 4). The azimuth positioner supports the AUT at a centre height of 4.5 m, by means of a mounting pole. A complete rotation over 360 degrees can be accomplished through an R.F. rotary joint mounted in the positioner. Anechoic panels are installed on the roof in order to avoid reflections and the instrumentation and data recording system are located in an indoor laboratory. The antenna test system is controlled by professional stepping motor drives.

The measured results shown in fig. 5 and fig. 6 were obtained by using a frequency selective measurement set-up equipped as follows. The electric probe is a calibrated dipole (Anritsu MP663A). The magnetic probe is a calibrated loop Emco (mod. 902). These are connected through a cable to the receiver (HP 70000 spectrum analyser). A solid state power amplifier connected to the AUT amplifies the signal from the tracking generator of the spectrum analyser.

A monitor system, located at the azimuth positioner base, comprising the directional coupler, the power sensor (HP8481A) and the power meter (HP437), is

permanently connected to the feed line in order to continuously sample the RF power level.

Spectrum analyser measured data, power levels sampled by the monitor system and cable attenuation are used to compute electric field values.

A specific software manages the measurement system in order to control frequency, power level, azimuth speed, data collection as a function of the azimuth and X-Z positions, data storage and output.

By little modifying the instrumentation set-up, one could substitute the frequency selective test range (electric dipole and magnetic loop) with wide-band electric and magnetic sensors.

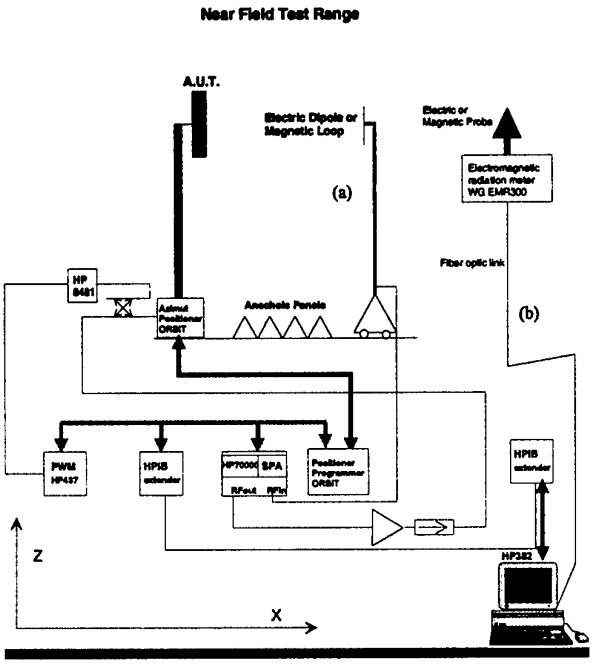



**Fig. 4** Frequency Selective (a) and Wide-Band (b) Near Field Test Range.

## 4. RESULTS

Now we give an overview on the results got from the numerical methods (i.e. NEC, NFUA, NFUTD) and measurements comparison: we have mapped a plane placed around the antenna to get an isoline ensemble at different values (for the electric field only): this is shows in the figures 7,8,9,10,11,12.

For the NEC model only we have done a measurements along the main antenna axle (they are showed on fig.5 and fig.6): the middle of each vertical stokes locates the measured value, while the length of the stoke is due to the measure uncertainty of the electric and magnetic field.

The uncertainties are due to different contributes: absolute uncertainty of the dipole calibration (±0.5 dB), linear uncertainty of the spectrum analyser (±0.5 dB), residual reflectivity of the measurement site (±0.2 dB).

The total uncertainty is obtained from the sum of the previous values as defined in the standard ISO TAG 4. As it appears from fig.5 and fig.6, the electric and magnetic field values provided by NEC lies in the uncertainty zone.

In the NFUTD besides the choice of the electromagnetic field relation, there is that the UTD is a valid theory when the distance between two elements that interacts each other (for example an electromagnetic source and an edge) is larger than a quarter of wavelength. In the GSM band this length is $L = \lambda/4 \cong 8$ cm : in our model an electric dipole may be far from a reflector edge less than 8 cm.

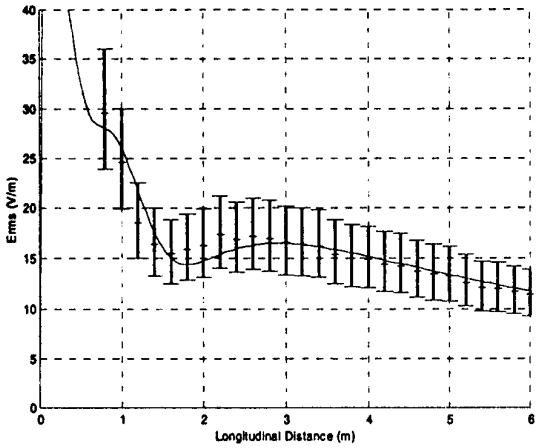



**Fig. 5** Electric field (V/m) computed and measured at 900 MHz.

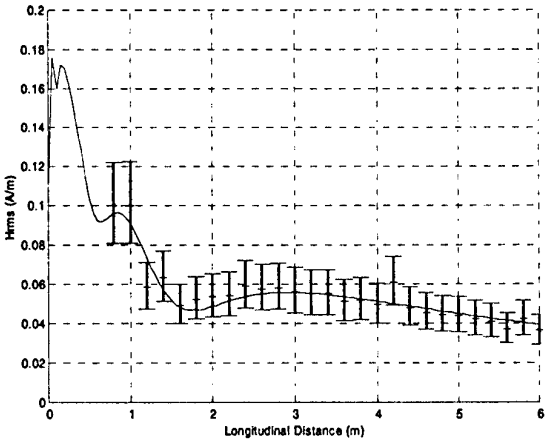



**Fig. 6** Magnetic field (A/m) computed and measured at 900 MHz.

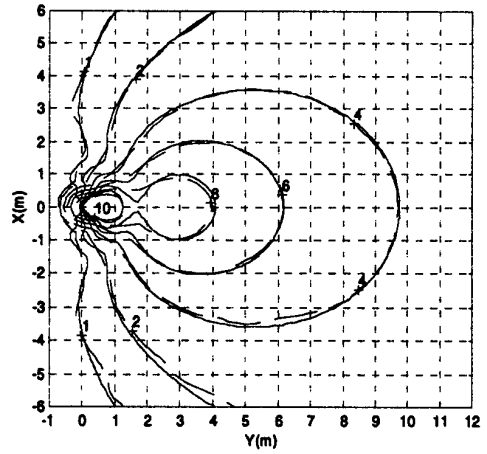



**Fig. 7** Electric field (V/m) measured (dashed line) and computed by NEC (solid line).

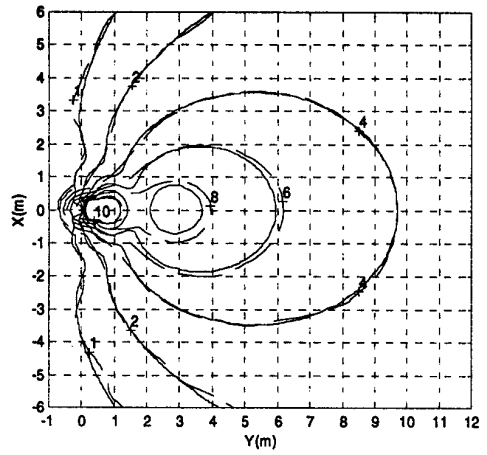



**Fig. 8** Electric field (V/m) measured (dashed line) and computed by NFUA (solid line).

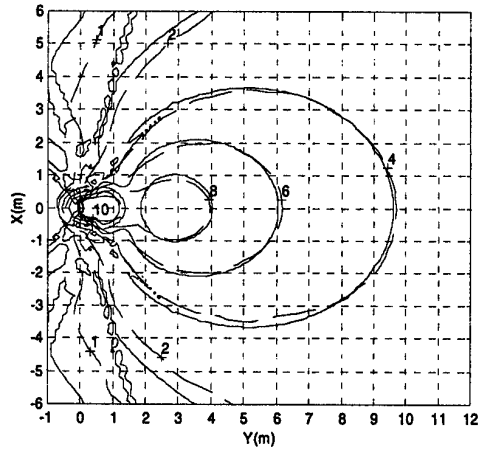



**Fig. 9** Electric field (V/m) measured (dashed line) and computed by NFUTD (solid line).

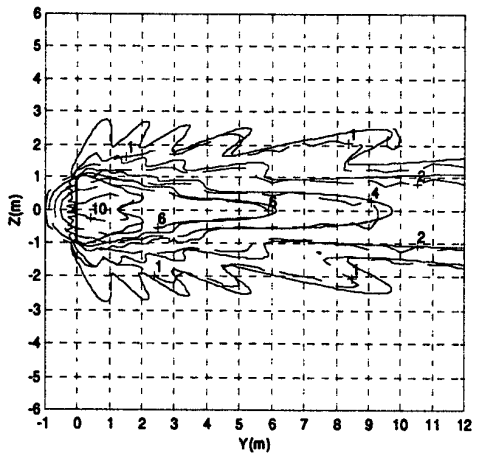



**Fig. 10** Electric field (V/m) measured (dashed line) and computed by NEC (solid line).

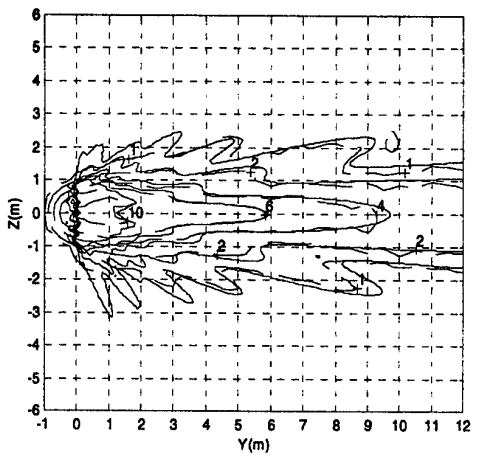



**Fig. 11** Electric field (V/m) measured (dashed line) and computed by NFUA (solid line).

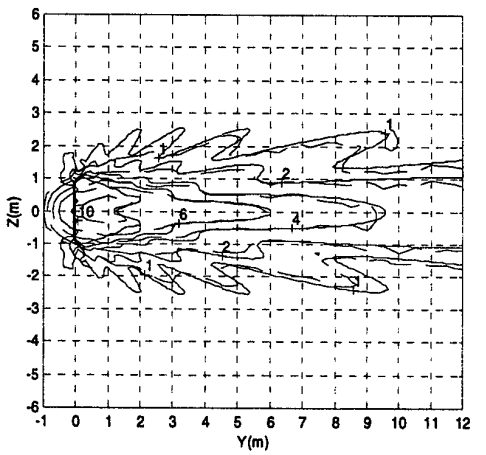



**Fig. 12** Electric field (V/m) measured (dashed line) and computed by NFUTD (solid line).

## 5. ELECTROMAGNETIC FIELDS IN URBAN AREAS

To calculate the EMF irradiated in an urban environment we have used the antenna models described above with a ray-tracer approach.

The high number of points that covers the urban areas, on which we estimated the EMF levels, forced us to developed an acceleration technique that reduce the number of surface (i.e. the building walls) considered.

Our acceleration technique is a combination of the painter's and z-buffer algorithms [7]: a 3-D image is reduced to a 2-D screen by a perspective view from a source point, so only the visible surface appeared on this new image. Applying this method to a ray-tracer, we have evaluated the direct and the reflected rays, therefore the EMF due to them. We compute the second order reflected field, in which the reflection coefficients depends on the electromagnetic feature and thickness of the buildings walls too.

In [8] there is an exhaustive description of the acceleration technique that we have developed.

In the calculation of the entire EMF, as a possible improvement, we will consider the diffracted field by the building edges: this will be done by the UTD.

Fig.13 shows a base station in an urban environment: the electric field (V/m) is computed on the buildings surfaces and on the ground; in the more darkness zones there is an high electric field value, while the existence of many white zone is due to the absence of the diffracted field.

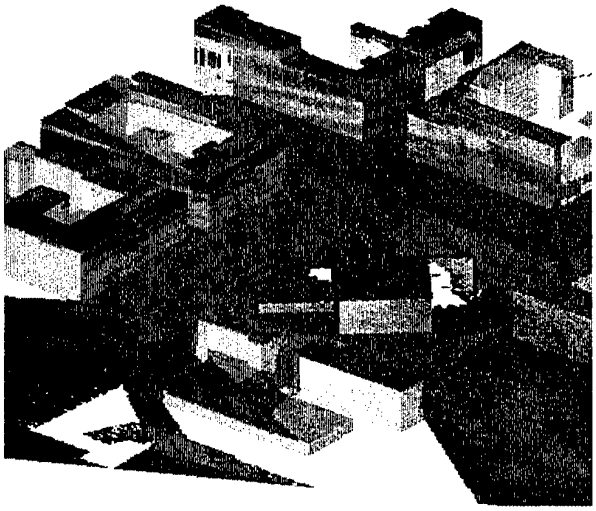


**Fig. 13** Three-sectorial site in an urban environment.

## 6. REFERENCES


6.1. Decreto del Ministero dell'Ambiente No. 381, Rome, Italy, 10 September 1998.

6.2. Burk G.J., Poggio A.J., "Numerical Electromagnetic Code-Method of Moment", Lawrence Livermore National Laboratory, January 1981.

6.3. Bizzi M., Gianola P., "Electromagnetic Fields Radiated by GSM antennas", IEE Electronic Letters, Vol.35, No.11, 1999, pp.855-857.

6.4. Kouyoumjian R.G., Pathak P.H., "Uniform Geometrical Theory of Diffraction for an Edge in a Perfectly Conducting Surface", in Proceedings of the IEEE, Vol.62, No.11, 1974, pp. 1448-1461.

6.5. Carli, Lombardi, Manià, Vescovo, Gianola P., "Antennas Models for Field-Level Evaluation in Proximity of GSM Base Stations", Proceedings of the Symposium EPMCC'99, Paris, France, 1999, pp. 296-300.

6.6. Brunello F., "Techniques for the analysis and the evaluation of electromagnetic fields in the GSM-band" (Italian), Thesis, Politecnico di Torino, October 1999.

6.7. Foley J.D., Van Dam A., Feiner S. K., Hughes J. F., "Computer Graphics: Principles and Practices", Addison-Wesley, New York, 1995.

6.8. Gambin D., Brunello F., Disco D., "An acceleration technique using a 3D representation for ray tracer in a urban environment", submitted to IEEE Antenna and Propagation Symposium 2000.

EMC 2000 INTERNATIONAL WROCŁAW SYMPOSIUM ON ELECTROMAGNETIC COMPATIBILITY

# THE ROLE OF HEAD TISSUE COMPLEXITY IN THE PEAK SAR ASSESSMENT FOR MOBILE PHONES

**Jianqing Wang and Osamu Fujiwara**

**Department of Electrical and Computer Engineering**
**Nagoya Institute of Technology**
**Gokiso-cho, Showa-ku, Nagoya 466-8555, Japan**

*The role of head tissue complexity in the peak SAR assessment for mobile phones was investigated by using the FDTD method in conjunction with an MRI-based human head model. The tissue complexity of the head model was changed from one type of tissue to 17 types of tissue. The results showed that, at 900 MHz and 2 GHz, the homogeneous modeling may result in an underestimate about 20% for the $\lambda/2$ monopole antenna mobile phones and an overestimate to the same extent for the helical antenna mobile phones. A head model with a simple skin-fat-muscle-bone-brain structure seems to be sufficient to obtain a fairly accurate one-gram or ten-gram averaged spatial peak SAR value from computer simulations for mobile phone compliance.*

## 1. INTRODUCTION

With the recent rapid increase in the use of mobile phones, safety guidelines for protecting human beings from the radio frequency exposure have been issued in various countries [1][2]. Especially, since 1996, the U.S. Federal Communication Commission (FCC) has required the routine specific absorption rate (SAR) evaluation prior to device authorization or use [3]. According to the FCC rule, any mobile phone has to be evaluated with respect to the SAR limit using either phantom measurement or computer simulation. For computer simulation, human head models being usually derived from magnetic resonance imaging (MRI) or computed tomography (CT) scans are used. However, the derived head models were reported with various tissue complexities, ranged from several to dozens of tissue types [4]-[7], while an actual head anatomically has over 800 tissue types. Hombach et al. and Meier et al. numerically analyzed the interaction between half-wave dipole antennas and human head models and they both concluded that homogeneous modeling of human head is suited for assessing the spatial peak SAR, although it is hard to avoid an overestimate which sometimes may exceed 40% [5][6]. To what extent the tissue structure complexity gives a reasonable SAR assessment remains unclear. Moreover, due to the difference in the interaction between different antenna types and the human head, the antenna type should affect the peak SAR, while its dependence on tissue complexity also remains unclear.

The objective of this paper is to investigate the role of head tissue complexity in the peak SAR assessment. An our newly developed MRI-based head model [8] was employed for this aim. The head model has a high tissue complexity, say including 17 tissue types. Based on the same MRI data, 16 other head models with tissue complexities from one tissue type to 16 tissue types were also developed. Then the finite-difference time-domain (FDTD) method was used to calculate the spatial peak SARs in the 17 head models for the two most popular antennas and two frequency bands. The two most popular antennas were a half-wave monopole and a helix both mounted on a plastic-covered metal box. The two frequency bands were 900 MHz and 2 GHz, which are being employed and will be employed in the near future in Japan, respectively.

## 2. MODEL AND ANALYSIS METHOD

### 2.1 MRI Based Head Model

The raw MRI data were taken from a Japanese adult head (male, 23 years old), which consists of 115 slices with 2 mm space in the axial plane. Each MRI slice was a 256 × 256 pixel and 9-bit grey scale image. The grey scale data of MRI images were interpreted into tissue types, which is known as a process of segmentation. The segmentation was performed under the guidance of a medical doctor. At first, the grey scale images were rescaled to produce cubic voxels of 2 mm. Then the images were segmented unambiguously as belonging to one of 17 different tissue types by assigning each 2 mm cube voxel to a RGB code, which identifies the discrete tissue type of that particular voxel. This process was performed manually with the aid of a commercial software Adobe Photoshop. The segmented tissue types are blood, bone, bone marrow, cartilage, cerebrospinal fluid (CSF), cornea, dura, eye humour, fat, grey matter, lens,

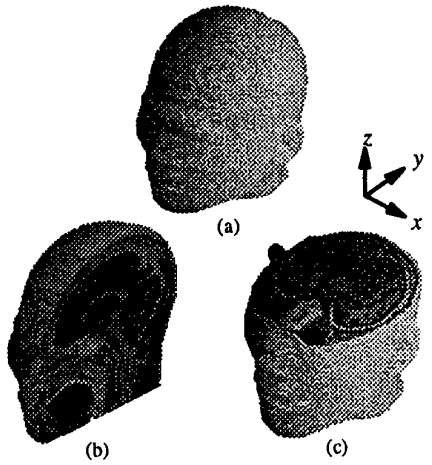



Figure 1: MRI-based head model. (a) appearance, (b) mid-sagittal vertical cross-section, (c) horizontal cross-section through the eyes.

mucous membrane, muscle, parotid gland, sclera, skin and white matter. Figure 1 shows the head model, a mid-sagittal vertical cross-section and a horizontal cross-section through the eyes of the head model. The 16 other head models with tissue complexities from one tissue type to 16 tissue types were developed based on the same MRI data. For example, the one-tissue model was composed of the brain tissue (whose dielectric properties were assumed to be the averages of the grey matter and white matter), the two-tissue model was composed of the skin and brain tissue, the three-tissue model was composed of the skin, bone and brain tissue, and so on. Table 1 shows the composition of each model as well as electrical properties for each tissue [9] where $\rho$ is the mass density, and $\varepsilon_r$ and $\sigma$ are the relative permittivity and conductivity, respectively.

### 2.2 Modeling of Mobile Phone with a Mono -pole Antenna

The handset of mobile phone was modeled as a dielectric covered rectangular metal box, with a length of 12.4 cm, a width of 4.4 cm and a thickness of 2.4 cm. The metal box was covered with a dielectric insulator of 2 mm thickness and $\varepsilon_r$=2.0. A $\lambda/2$ monopole antenna was mounted on the top of the handset, in the front of the 4.4 cm side and 2 cm far from the edge of the 2.4 cm side. This corresponded to a distance of 2 cm between the monopole and the the ear because the handset was barely touching the ear. The radius of the monopole was 0.5 mm, which was approached by the thin-wire approximation considering the effect of a wire with a radius smaller than the FDTD cell dimensions. $\delta$-gap feeding was employed to excite the monopole antenna.

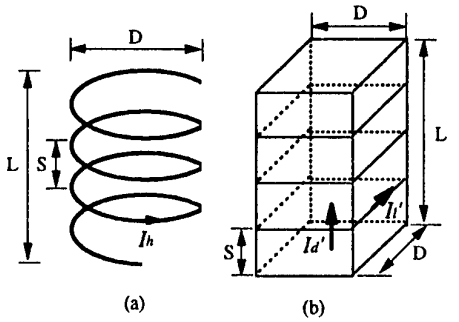



Figure 2: (a)Size of helical antenna, (b)stack used to model the helical antenna. The stack is composed of several layers. Each layer has a square area with one side equal to the diameter $D$ and a height equal to the pitch $S$ of the helical antenna.

### 2.3 Modeling of Mobile Phone with a Helical Antenna

The helical antenna, having a length $L$=1.6 cm, a pitch $S$=2 mm and a diameter $D$=4 mm, was mounted on the top of the same handset described above both at 900 MHz and 2 GHz. According to Lazzi and Gandhi's proposal for modeling a helical antenna in [7], a rectangular stack, as shown in Figure 2, was used to reproduce the fields generated by the helix. Referring to Figure 2(b), one layer of the stack has an equivalent dipole and an equivalent loop. Denoting the current in the equivalent dipole as $I'_d$, we can replace it with a displacement current, and have the equivalent electric field $E_z$ in lieu of $I'_d$, which is expressed as

$$E_z = \frac{I'_d \cdot 1/j\omega C}{s} = \frac{I'_d}{j\omega\varepsilon_0 D^2} \tag{1}$$

where $C$ is the capacitance between the layer, being given by $\varepsilon_0 D^2/s$.

On the other hand, denoting the current in the equivalent loop as $I'_l$, from Biot-Savart's law, we can obtain the equivalent magnetic field related to the current $I'_l$ in the center of the same layer, which is given as

$$H_z = \oint \frac{I'_l dl' \sin\phi}{4\pi R^2} = \frac{4}{\sqrt{2}\pi}\frac{I'_l}{D} \tag{2}$$

where $R$ is the distance from the current element $dl'$ to the center of the layer, $\phi$ is the angle between the direction of the current and the vector from the element to the center of the layer, and the integration is carried out along the boundary line of the layer. Thus, for one layer of the stack, we have

$$\frac{E_z}{H_z} = \frac{I'_d}{I'_l}\frac{\sqrt{2}\pi}{j4\omega\varepsilon_0 D}. \tag{3}$$

Table 1: Dielectric properties of tissue and composition of head models

| Tissue type | $\rho$ [kg/m$^3$] | 900MHz $\varepsilon_r$ | 900MHz $\sigma$ [S/m] | 2GHz $\varepsilon_r$ | 2GHz $\sigma$ [S/m] | n** |
|---|---|---|---|---|---|---|
| brain* | 1030.0 | 45.81 | 0.77 | 43.21 | 1.26 | 1 |
| skin | 1010.0 | 41.41 | 0.87 | 38.57 | 1.27 | 2 |
| bone | 1850.0 | 16.62 | 0.24 | 15.37 | 0.48 | 3 |
| fat | 920.0 | 11.33 | 0.11 | 10.96 | 0.21 | 4 |
| muscle | 1040.0 | 55.96 | 0.97 | 54.17 | 1.51 | 5 |
| dura | 1030.0 | 44.43 | 0.96 | 42.62 | 1.42 | 6 |
| CSF | 1010.0 | 68.64 | 2.41 | 66.91 | 3.07 | 7 |
| cartilage | 1100.0 | 42.65 | 0.78 | 39.76 | 1.42 | 8 |
| grey matter | 1030.0 | 52.72 | 0.94 | 49.69 | 1.51 | 9 |
| white matter | 1030.0 | 38.89 | 0.59 | 36.73 | 1.00 | 9 |
| parotid gland | 1050.0 | 60.55 | 1.21 | 58.27 | 1.83 | 10 |
| eye humour | 1010.0 | 55.27 | 1.17 | 68.47 | 2.16 | 11 |
| lens | 1100.0 | 41.21 | 0.64 | 39.78 | 1.06 | 12 |
| bone marrow | 1030.0 | 11.27 | 0.23 | 10.56 | 0.38 | 13 |
| blood | 1060.0 | 61.36 | 1.54 | 59.02 | 2.19 | 14 |
| mucous membrane | 1010.0 | 46.08 | 0.84 | 43.52 | 1.34 | 15 |
| sclera | 1170.0 | 55.27 | 1.27 | 53.27 | 1.72 | 16 |
| cornea | 1050.0 | 55.23 | 1.39 | 52.39 | 1.98 | 17 |

* Average of the grey matter and white matter.

** $n$ stands for the number of tissue constitutes a head model.

Since each layer of the stack had the same height as the pitch of helix, the currents $I_d'$ was equal to the actual helix current $I_h$. Moreover, since the actual loop of the helix has a circular shape, for inducing the same magnetic field in the center of the loop, the current $I_l'$ should be related to actual helix current $I_h$ by $I_l' = \frac{\sqrt{2}\pi}{4} I_h$. Thus Eq. (3) can be rewritten as

$$\frac{E_z}{H_z} = \frac{1}{j\omega\varepsilon_0 D}^1. \tag{4}$$

The excitation of the helical antenna was performed by using sinusoidal $E_z$ and $H_z$ according to the above relationship.

## 3. RESULTS AND DISCUSSION

Figures 3 - 6 show the dependence of the one-gram and ten-gram averaged spatial peak SAR on tissue complexity. The one-gram averaged and ten-gram averaged spatial peak SARs were obtained over a 1 cm$^3$ and 2.2 cm$^3$ cubics, respectively, which did not include air. All of the results were normalized to an antenna output of 1 W. As can be seen from the results, for the $\lambda/2$ monopole antenna mobile phones, the one-tissue model exhibited an underestimate feature at the two considered frequencies. With respect to the 17-tissue model, the one-tissue model gave underestimates of 18% at 900 MHz and 13% at 2 GHz for the one-gram averaged spatial peak SAR. The same feature can be observed for the ten-gram averaged spatial peak SAR, only the underestimated or overestimated level was smaller. However, for the helical antenna mobile phones, the one-tissue model gave an upper bound for the one-gram and ten-gram averaged spatial peak SAR. With respect to the 17-tissue model, at 900 MHz, the one-tissue model gave almost the same value, while at 2 GHz, the one-tissue model gave overestimates of 12% and 20% for the one-gram and ten-gram averaged spatial peak SARs, respectively.

From these results the dependence of the peak SAR on tissue complexity seems to be antenna - dependent. This may be explained from the different composition of tissue in the ear region and on the upper side of ear. Figure 7 shows the SAR distributions in the $zx$ plane for the $\lambda/2$ monopole antenna and helical antenna at 900 MHz. For the $\lambda/2$ monopole antenna the peak current appeared at the center of the monopole, which resulted in that the main EM absorption area was on the upper side of the ear. The volume of brain tissue is large in this region. However, due to the short length of helical antenna, the currents in this case concentrated at the bottom of the antenna and the upper part of the handset, which resulted in a concentrated EM absorption in the ear region having a more complex tissue composition.

[1] This is somewhat different from the relationship, say $E_z/H_z = 4/(j\omega\varepsilon_0\pi D)$, being derived by Lazzi and Gandhi in [7].

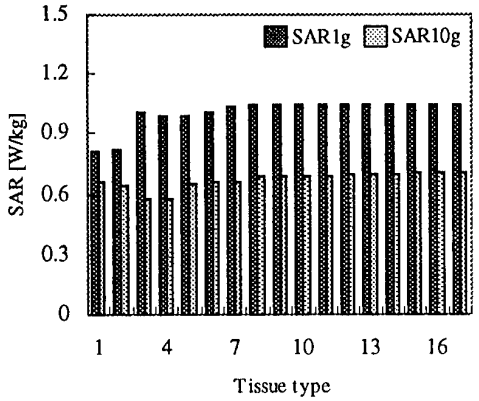



Figure 3: Dependence of the one-gram and ten-gram averaged spatial peak SAR on tissue complexity. Antenna: $\lambda/2$ monopole; Frequency: 900 MHz.

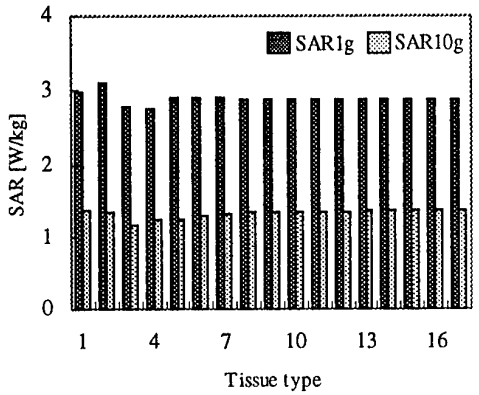



Figure 4: Dependence of the one-gram and ten-gram averaged spatial peak SAR on tissue complexity. Antenna: helical; Frequency: 900 MHz.

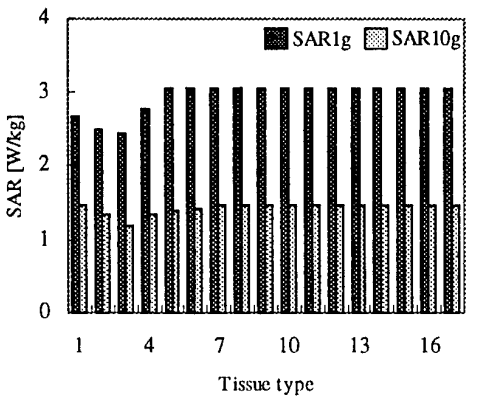



Figure 5: Dependence of the one-gram and ten-gram averaged spatial peak SAR on tissue complexity. Antenna: $\lambda/2$ monopole; Frequency: 2 GHz.

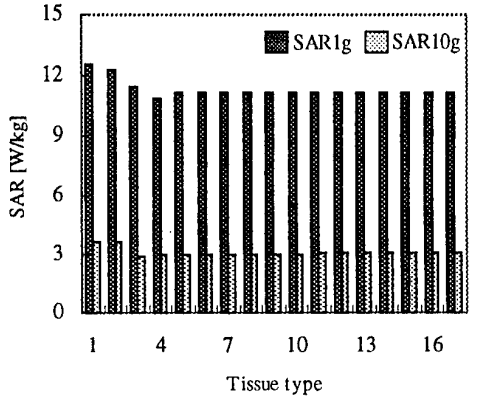



Figure 6: Dependence of the one-gram and ten-gram averaged spatial peak SAR on tissue complexity. Antenna: helical; Frequency: 2 GHz.

Furthermore, from Figures 3 - 6, when the tissue types were larger than 5, the peak SAR approximately converged to the value for the 17-tissue model. The 5-tissue model, i.e., the skin-fat-muscle-bone-brain model, was found to have a difference for the one-gram and ten-gram averaged spatial peak SAR within 5% with respect to the 17-tissue model. This relationship holds for both the $\lambda/2$ monopole and the helical antennas at both 900 MHz and 2 GHz. By comparing the SAR profiles for the head models with different tissue complexity, as shown in Figure 8, it is obvious that the SAR profiles close to the head surface, that determine the gram-averaged spatial peak SAR, have a similarity between the 5-tissue model and the 17-tissue model. This phenomenon attributes to the fact that the skin, fat, muscle, bone and brain are the main tissue types in the exposed region of head.

These findings leads to a conclusion that a head model with a simple skin-fat-muscle-bone-brain structure is sufficient to derive a fairly accurate peak SAR value from computer simulations for mobile phone compliance.

## 4. CONCLUSION

The role of head tissue complexity in the peak SAR assessment for mobile phones was investigated by using the FDTD method in conjunction with an MRI-based human head model. The tissue complexity of the head model was changed from one type of tissue to 17 types of tissue. The investigated frequencies were 900 MHz and 2 GHz, and the investigated antenna types were popular $\lambda/2$ monopole and helical antennas, both mounted on a dielectric covered metal box. The results showed that the homogeneous modeling may result in an underestimate about 20% for the $\lambda/2$ monopole antenna mobile phones and an overestimate to the same extent for the helical antenna mobile phones. A head model with a simple skin-fat-muscle-bone-brain structure gives almost the same peak SAR value as a highly complex 17-tissue model, which suggests that the 5-tissue head model is sufficient to obtain a fairly

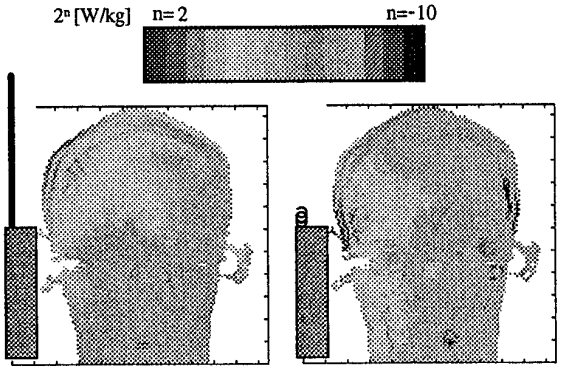



Figure 7: SAR distributions in the $zx$ plane. Left: $\lambda/2$ monopole antenna, right: helical antenna. Frequency: 900 MHz.

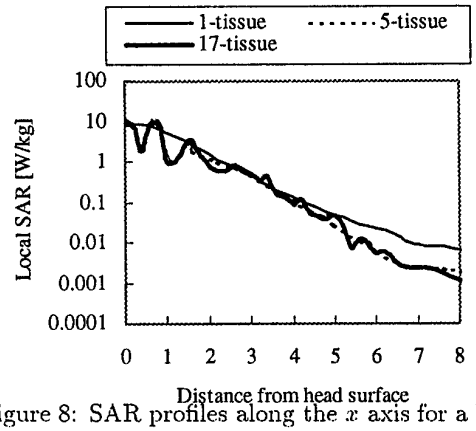



Figure 8: SAR profiles along the $x$ axis for a helical antenna mobile phone at 2 GHz.

accurate peak SAR from computer simulations for mobile phone compliance.

## REFERENCES

[1] American National Standards Institute, "Safety Levels with Respect to Exposure to Radio Frequency Electromagnetic Fields, 3 kHz to 300 GHz", ANSI/IEEE C95.1-1992.

[2] ICNIRP, "Health issues related to the use of hand-held radiotelephones and base transmitters", Health Physics, vol.70, pp.587-593, 1996.

[3] Federal Communications Commission, "Report and Order: Guidelines for Evaluating the Environmental Effects of Radiofrequency Radiation," FCC 96-326, Washington DC, 1996.

[4] M. Okoniewski and M. A. Stuchly, "A study of the handset antenna and human body interaction", IEEE Trans. Microwave Theory Tech., vol.44, no.10, pp.1855-1864, Oct. 1996.

[5] V. Hombach, K. Meier, M. Burkhardt, E. Kuhn and N. Kuster, "The dependence of EM energy absorption upon human head modeling at 900 MHz," IEEE Trans. Microwave Theory Tech., vol. 44, no. 10, pp. 1865-1873, Oct. 1996.

[6] K. Meier, V. Hombach, R. Kastle, R. Y. S. Tay and N. Kuster, "The dependence of EM energy absorption upon human head modeling at 1800 MHz," IEEE Trans. Microwave Theory Tech., vol. 45, no. 11, pp. 2058-2062, Nov. 1997.

[7] G. Lazzi and O. P. Gandhi, "On modeling and personal dosimetry of cellular telephone helical antennas with the FDTD code", IEEE Trans. Antennas Proprgat., vol. 46, no. 4, pp. 525-529, April 1998.

[8] J. Wang and O. Fujiwara, "FDTD analysis of dosimetry in human head model for a helical antenna portable telephone", IEICE Trans. Commun., vol.E83-B, no. 3, March 2000.

[9] http://www.fcc.gov/fcc-bin/dielec.sh

## BIOGRAPHICAL NOTE

**Jianqing Wang** received the B.E. degree in electronic engineering from Beijing Institute of Technology, Beijing, China, in 1984, and the M.E. and D.E. degrees in electrical and communication engineering from Tohoku University, Sendai, Japan, in 1988 and 1991, respectively. After he worked as a Research Associate at Tohoku University and a Research Engineer at Sophia Systems Co., Ltd., he moved to the Department of Electrical and Computer Engineering at Nagoya Institute of Technology, Nagoya, Japan, where he is currently an Assistant Professor. His research interests include electromagnetic compatibility, bioelectromagnetics and digital communications.

**Osamu Fujiwara** received the B.E. degree in electronic engineering from Nagoya Institute of Technology, Nagoya, Japan, in 1971, and the M.E. and the D.E. degrees in electrical engineering from Nagoya University, Nagoya, Japan, in 1973 and in 1980, respectively. From 1973 to 1976, he worked in the Central Research Laboratory, Hitachi, Ltd., Kokubunji, Japan, where he was engaged in research and development of system packaging designs for computers. From 1980 to 1984 he was with the Department of Electrical Engineering at Nagoya University. In 1984 he moved to the Department of Electrical and Computer Engineering at Nagoya Institute of Technology, where he is presently a professor. His research interests include measurement and control of electromagnetic interference due to discharge, bioelectromagnetics and other related areas of electromagnetic compatibility.

**EMC 2000** INTERNATIONAL WROCŁAW SYMPOSIUM ON ELECTROMAGNETIC COMPATIBILITY

# A PROBABILISTIC MODEL FOR TRANSMISSION LINE VOLTAGES INDUCED BY AN EXTERNAL FIELD

Diego Bellan and Sergio Pignari
Dipartimento di Elettrotecnica, Politecnico di Milano, Italy
Tel.: +39-02-2399-3726 – Fax: +39-02-2399-3703
e-mail: diego.bellan@polimi.it, sergio.pignari@polimi.it

*In this work, a probabilistic approach for the characterization of wiring harness susceptibility to external interference is presented. The problem of field-coupling onto a uniform, two-conductor transmission line is considered by modeling the external field as a plane wave with random parameters. The probability density function of the voltage induced in one of the line loads is derived analytically, under a low-frequency assumption. The proposed model allows computation of statistical parameters of interest, such as expected values, variances, and confidence intervals of voltages and currents in the line loads.*

## 1. INTRODUCTION

Field coupling to transmission lines is an issue of paramount importance in the area of electromagnetic compatibility (EMC). After the pioneering work of Taylor *et al.* [1], several papers have been written on this subject [2], with the aim to explain interference effects that an external electromagnetic source plays on complex wiring structures.

However, in the majority of the works available in the literature such a problem is examined from a deterministic standpoint. Only in recent years contributions to this subject have been cast in terms of new prediction techniques, based on statistical or probabilistic approaches. In particular, techniques belonging to this category have been employed for the description of crosstalk in random wire bundles [3-5], for modeling the electromagnetic field and cable response in over-moded enclosures [6], for electromagnetic field representation in reverberation chambers [7], and for modeling EMP conducted environments [8].

The need for applying probabilistic modeling to the problem of radiation onto transmission lines can be viewed as a way to overcome the lack of information that the designer/analyst usually encounters when he tries to characterize the interfering field.

This work addresses the problem of field coupling onto a lossless two-conductor transmission line by means of a probabilistic approach. The line is supposed to be uniform, and composed by a signal conductor running above an infinite ground plane. Line terminations are modeled by equal resistances, connected between each wire-end and ground. The offending field is modeled as a random plane wave: amplitude, polarization, and direction of incidence of the wave are treated as random variables with suitable probability density functions (PDFs).

Under a low-frequency assumption (i.e. for wavelengths greater than the line length), the proposed model enables one to derive analytical expressions of the PDFs of the voltages (currents) induced in the line terminations. Consequently, statistical parameters of interest, such as expected values, variances, and confidence intervals can be evaluated and used for an effective description of the line susceptibility.

Statistical simulation has confirmed the consistence of the obtained analytical results, and the potential of the probabilistic characterization of wiring harnesses.

## 2. PROBABILISTIC MODEL DESCRIPTION

This section is devoted to the description of the probabilistic model. The structure under analysis is sketched in Fig. 1. It shows a two-conductor transmission line exposed to an external plane wave field. In the Figure, $E_0$ is the amplitude of the electric field, angles $\vartheta, \psi$ identify the direction of incidence, angle $\eta$ specifies the wave polarization. The line length is $\mathcal{L}$, and its height above ground is $h$. The signal conductor is loaded at both ends by equal resistances $R$.

Voltages and currents induced by an external wave in the line loads are readily evaluated by resorting to lumped equivalent voltage sources, placed at the line terminations [9]. In particular, if the right end of the line is considered, and a low frequency expansion of the induced voltage is derived, we get

$$V_R \approx j\omega \frac{E_0 h \mathcal{L}}{c_0}\left[\cos\psi\cos\eta + \sin\psi\sin\eta\cos\theta - \frac{R}{Z_C}\cos\eta\sin\theta\right], \qquad (1)$$

where $\omega$ is the angular frequency, $c_0$ is the speed of light in free space, and $Z_C$ is the line characteristic impedance. Expression (1) holds for low-frequencies, i.e. for wavelengths much greater than the line length ($\ell/\lambda << 1$). A similar expression can be derived for the voltage induced in the left load.

If all the quantities involved in equation (1) are regarded as known parameters, such an expression has to be viewed as the result of a deterministic model. Alternatively, if the deterministic model assumption is released, and some of the parameters involved in the description of the field-to-wire coupling phenomenon are treated as random quantities, the model becomes probabilistic, and results should be cast in terms of suitable estimators.

In the present analysis, all the quantities related to the description of the transmission line (i.e. $\ell$, $h$, $Z_C$, $R$) are considered as deterministic data, while the wave parameters (i.e. $E_0$, $\vartheta$, $\psi$, $\eta$) are treated as random quantities. This means assuming a sufficient knowledge of the geometrical and electrical characteristics of the line, but recognizing uncertainties in the description of the interfering field. Such a point of view is representative of many practical circumstances, in which circuitry is operated in harsh environments, but only partial information is available regarding interference.

From the mathematical point of view, this is equivalent to describe some or all the wave parameters as random variables, with by specific PDFs. Consequently, also voltages (currents) induced in the line loads are random variables, related to the wave variables by specific functional relationships.

As far as the voltage $V_R$ induced in the right end of the structure of Fig. 1 is concerned, such a functional relationship is specified in equation (1). The statistical properties of such a variable may be investigated by applying to (1) the theorem on the transformation of random variables [10].

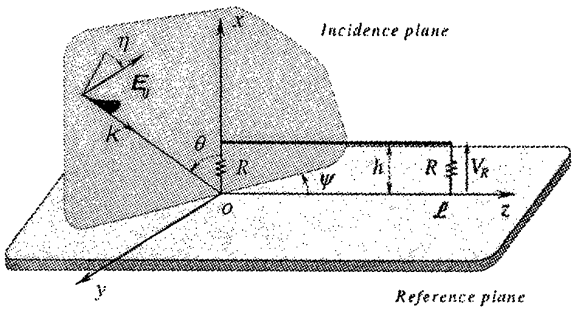



Fig. 1. Two-conductor uniform transmission line exposed to an external plane-wave field. The incidence direction of the wave is identified by angles $\vartheta$, $\psi$, the wave polarization is described by angle $\eta$. The symbol $\ell$ denotes line length, and $R$ is the terminal resistance used to connect both wire-ends to ground.

Equation (1) is therefore the basis of the considerations developed in this paper.

The degree of uncertainty introduced in the model may be controlled via the selection of the wave parameters that will be described as random variables, and by the statistical properties adopted for their description. This is a point of paramount importance, since in practice the degree of uncertainty related to the interfering field may strongly depend on the specific application.

The procedure adopted for the probabilistic characterization of the field-to-line coupling is described in the following. The magnitude of the voltage induced in the right termination of the line is rewritten from (1) as

$$|V_R| \approx \omega P E_0 \left|\cos\psi\cos\eta + \sin\psi\sin\eta\cos\theta - a\cos\eta\sin\theta\right| \tag{2}$$

where $a$ and $P$ are constant factors, defined by

$$a = \frac{R}{Z_C}, \qquad P = \frac{h\ell}{c_0}. \tag{3}$$

Subsequently, two auxiliary random variables $\zeta, \xi$ are introduced, defined as

$$\zeta = \left|\cos\psi\cos\eta + \sin\psi\sin\eta\cos\vartheta - a\cos\eta\sin\vartheta\right| \tag{4a}$$

$$\xi = E_0\,\zeta\,. \tag{4b}$$

Random variable $\zeta$ accounts for the effect of random variables $\vartheta, \psi, \eta$ (incidence and polarization angles). Random variable $\xi$ is defined as the product of random variable $E_0$ (wave amplitude) times the auxiliary random variable $\zeta$. By virtue of (4a) and (4b), equation (2) is rewritten in compact form as

$$|V_R| \approx \omega P \xi\,. \tag{5}$$

Equation (5) expresses the magnitude of the induced voltage as the product of a deterministic factor $\omega P$ times the auxiliary random variable $\xi$.

After having specified which of the wave angles behaves as a random variable, the PDF $f_\zeta(z)$ of $\zeta$ will be obtained by applying to (4a) the theorem of transformation of random variables [10]. Subsequently, the PDF $f_\xi(x)$ of $\xi$ will be obtained from equation (4b) in terms of the PDFs of the amplitude of the external wave $f_{E_0}(w)$, and $f_\zeta(z)$, as

$$f_\xi(x) = \int_{\alpha(x)}^{\beta(x)} \frac{1}{w} f_{E_0}(w)\, f_\zeta\left(\frac{x}{w}\right) dw\,, \tag{6}$$

where the endpoints of the interval of integration $[\alpha(x), \beta(x)]$ are functions of $x$ that depend on the domain of $f_{E_0}(w)$.

Finally, the PDF of $|V_R|$ will be derived from equation (5), as

$$f_{|V_R|}(y) = \frac{1}{\omega P} f_\xi\left(\frac{y}{\omega P}\right). \tag{7}$$

In (7) $y$ is used to denote the independent variable of PDF $f_{|V_R|}(\cdot)$.

## 3. PDF OF VOLTAGE INDUCED IN THE LINE LOAD

In this Section explicit expressions of the PDF of the magnitude of the induced voltage $|V_R|$ are derived, for specific characterizations of the impinging wave.
In particular, we concentrate on the case of uncertainty on the wave amplitude and direction of incidence. Wave polarization is supposed to be known. A similar situation occurs whenever the relative position of the wiring with respect to the source of interference is not completely known and, at the same time, precise indications are given on the way in which the disturbing field is generated. For example, this could be the case of interference emitted by the antenna of a RF transmitting station, placed on the roof-top of a building, onto a device that may be installed at different floors in a neighboring building.
As a specific case, we consider a vertically polarized wave, travelling parallel to the transmission line, with a random elevation angle. In terms of the wave parameters defined in Fig. 1, this means setting $\eta = 0$, $\psi = 0$, and considering the elevation angle $\vartheta$ as well as the wave amplitude $E_0$ as random variables.
In this case, the magnitude of the voltage induced in the right load is derived from (2) as

$$|V_R| = \omega P E_0 |1 - a \sin\vartheta|. \tag{8}$$

In order to get explicit expressions for $f_{|V_R|}(y)$, we need to specify the PDFs associated with the incidence angle $\vartheta$ and the wave amplitude $E_0$.
Since no information is available on the elevation angle $\vartheta$ under which the line sees the arriving wave, we assume $\vartheta$ uniformly distributed in the interval $[0, \pi/2]$, i.e.:

$$f_\vartheta(t) = \begin{cases} 2/\pi & 0 \le t \le \pi/2 \\ 0 & elsewhere \end{cases}. \tag{9}$$

For what concerns the wave amplitude $E_0$, indications can be found in the literature for the PDF of electric fields generated in specific environments. For example, in [9] it is shown that in mode-stirred chambers the magnitude of any of the electric field components is $\chi$ distributed with two degrees of freedom (Rayleigh distribution), and the total electric field magnitude is $\chi$ distributed with six degrees of freedom. We have to refer to the specific information available on the source of interference, for a proper selection of the PDF of $E_0$. In the following, we will derive the PDF of $|V_R|$ for different choices of the PDF of $E_0$.
The first step is to resolve the random variable transformation of equation (4a). Such a transformation reveals that the role played by the elevation angle $\vartheta$ on the induced voltage essentially depends on the value of parameter $a$, defined in (2). From the mathematical point of view, this means that subsequent steps of the analysis need to be distinguished on the basis of the value of $a$.

### 3.1. $a = 1$

This is the case of a line with matched loads. The PDF $f_\zeta(z)$ is obtained from (4a) as

$$f_\zeta(z) = \frac{2}{\pi\sqrt{z(2-z)}}, \qquad 0 < z \le 1, \tag{10}$$

and, by substitution of (10) into (6), the implicit expression of PDF $f_\xi(x)$ becomes:

$$f_\xi(x) = \frac{2}{\pi}\int_x^\infty \frac{f_{E_0}(w)}{\sqrt{x(2w-x)}}\,dw. \tag{11}$$

Explicit expressions of $f_\xi(x)$ can be derived from (11) by specifying the PDF $f_{E_0}(w)$ of the amplitude of the external wave. A summary of the results obtained for uniform, exponential, and beta distributions is presented in Table I.

### 3.2. $a << 1$

In this case equation (8) shows that the induced voltage is insensitive to the effect of a random elevation angle $\vartheta$. The PDF of $\xi$ is directly obtained from (4b), as

$$f_\xi(x) \equiv f_{E_0}(x). \tag{12}$$

### 3.3. $a >> 1$

In this case the sinusoidal term in equation (8) prevails over 1. The relationship between the auxiliary variable $\zeta$ and the angular variable $\vartheta$ simplifies to $\zeta = a\sin\vartheta$, and the PDF $f_\zeta(z)$ becomes:

$$f_\zeta(z) = \frac{2}{\pi}\frac{1}{\sqrt{a^2 - z^2}}, \qquad 0 \le z < a. \tag{13}$$

By substitution of (13) into (6), the PDF of $\xi$ is then expressed in terms of the PDF of $E_0$, as

$$f_\xi(x) = \frac{2}{\pi} \int_{x/a}^{\infty} \frac{f_{E_0}(w)}{\sqrt{(aw)^2 - x^2}} dw \,. \qquad (14)$$

In this case, explicit results for $f_\xi(x)$ have been obtained for uniform, Rayleigh, and beta distribution of $E_0$.

### 3.4. $\frac{1}{10} < a < 1$ or $1 < a < 10$

There are cases in which $a$ is less (greater) than one, but not so little (large) to allow considering only one of the two terms that appear in the argument of the absolute value of equation (8).
From the mathematical point of view, the description of such cases is more complicated. For sake of brevity, it is not reported in this work.

## 4. NUMERICAL SIMULATIONS

In this Section, numerical simulation is used to validate the probabilistic model, and to investigate its validity limits. We consider a transmission line with length $\mathcal{L} = 1$ m, height $h = 0.1$ m, and wire radius $r_w = 0.5 \times 10^{-3}$ m. The line is supposed to be matched at both ends ($a = 1$).
In the simulation we analyze the case of impinging waves with random amplitude $E_0$ and random elevation angle $\vartheta$. The incidence angle $\psi$ as well as the polarization angle $\eta$ are considered as fixed parameters, and are set to zero. We suppose the wave amplitude $E_0$ is beta distributed with PDF parameters $\nu_1, \nu_2$ set to 2 and 3, respectively. The elevation angle $\vartheta$ is unknown, and therefore treated as a random variable with uniform distribution in $[0, \pi/2]$.
Ten thousands waves with the above-described statistical properties have been randomly generated, and the voltage induced by each wave in the right load, at the frequency of 100 MHz, has been computed. An estimate of the PDF of the magnitude of the induced voltage has been obtained by proper normalization of the histogram. This result has been compared with the analytical expression of the PDF derived in Subsection 3.1, and reported in the last row of Table I. Fig. 2 shows the comparison.
The good agreement of the two curves is a check of correctness of the proposed probabilistic model. Moreover it is worth noting that, despite the proposed model is based on a low-frequency assumption, the above-described result has been obtained for a line-length-to-wavelength ratio of $\frac{1}{3}$.
However, it is recognized that the frequency range in which the model is valid is influenced by the value of the line loads, the widest range being obtained in the case of matched loads. Matched terminations represent a particular, but also practically significant case. In fact, design strategies are usually intended to avoid reflections at the line ends.

## 5. CONCLUSIONS

The problem of field-coupling onto a two-conductor transmission line is analyzed from the probabilistic standpoint. The probability density function of the voltage induced in the line load is derived analytically, for different statistical descriptions of the impinging wave. The choice of a two-conductor line simplifies the analysis; however some of the results presented in this paper can be extended to multiconductor transmission lines [11].
The proposed model allows one to characterize line susceptibility in terms of statistical parameters of interest, and may be useful at the design stage, whenever information on the source of interference is partially or completely unknown.

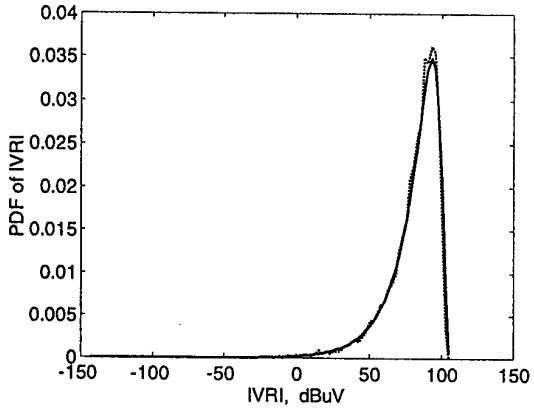



Fig. 2. PDF of the magnitude of the voltage induced in right load of the line. Solid curve is the analytical expression of the PDF, derived in Subsection 3.1. Dotted curve is the normalized histogram, obtained by repeated simulations ($10^4$ random waves have been employed). The operation frequency is 100 MHz, angles $\psi$ and $\eta$ are set to zero, wave amplitude $E_0$ and elevation angle $\vartheta$ are treated as random variables.

## 6. REFERENCES

6.1. C. D. Taylor, R. S. Satterwhite, C. W. Harrison Jr., "The response of a terminated two-wire transmission line excited by a non-uniform electromagnetic field," *IEEE Trans. Antennas Propagat.*, vol. AP-13, pp. 987-989, Nov. 1965.

6.2. C. R. Paul, "Frequency response of multiconductor transmission lines illuminated by an electromagnetic field," *IEEE Trans. Electromag. Compat.*, vol. EMC-18, pp. 183-190, Nov. 1976.

Table I. PDF of the auxiliary random variable $\xi$, for different choices of the PDF of the wave amplitude $E_0$, in the case of a matched line $(a=1)$.

| $f_{E_0}(w)$ | $f_\xi(x)$ |
|---|---|
| Uniform distribution:<br>$\frac{1}{E_{0\max}}, \quad 0 \le w \le E_{0\max}$ | $\frac{2}{\pi E_{0\max}}\left(\sqrt{\frac{2E_{0\max}}{x}-1}-1\right), \quad 0 < x \le E_{0\max}$ |
| Exponential distribution:<br>$\lambda e^{-\lambda w}, \quad w \ge 0$ | $e^{-\frac{\lambda x}{2}}\sqrt{\frac{2\lambda}{\pi x}}\left(1-erf\sqrt{\frac{\lambda x}{2}}\right), \quad x > 0$ |
| Beta distribution ($\nu_1 = 2$, $\nu_2 = 3$):<br>$\frac{1}{E_{0\max}^4 \beta(\nu_1,\nu_2)} w^{\nu_1-1}(E_{0\max}-w)^{\nu_2-1}$,<br>$0 \le w \le E_{0\max}$ | $\frac{16}{35}\frac{1}{\pi b^4}\left[\sqrt{\frac{2b}{x}-1}\left(3x^3-11bx^2+8b^2x+4b^3\right)-18x^3+49bx^2-35b^2x\right]$,<br>$b = E_{0\max}, \quad 0 < x \le E_{0\max}$ |


6.3. G. T. Capraro and C. R. Paul, "A Probabilistic approach to wire coupling interference prediction," Proceedings of the 4th International Zurich Symposium on Electromagnetic Compatibility, ETH, Zurich, 1981, pp. 267-272.

6.4. S. Shiran, B. Reiser, and H. Cory, "A probabilistic model for the evaluation of coupling between transmission lines," *IEEE Trans. Electromagn. Compat.*, vol. EMC-35, no. 3, pp. 387-393, Aug. 1993.

6.5. S. Pignari, L.Konè, F. Canavero, A. Ciccolella, B. Demoulin, "Statistical Approach to crosstalk in random cable bundles," (invited paper), International Symposium on Electromagnetic Theory, Thessaloniki, Greece, May 25-28, 1998, pp. 662-664.

6.6. R. Holland and R. H. St. John, "Statistical response of EM-driven cables inside an overmoded enclosure," *IEEE Trans. Electromagn. Compat.*, vol. EMC-40, no. 4, pp. 311-324, Nov. 1998.

6.7. D. A. Hill, "Plane wave integral representation for fields in reverberation chambers," *IEEE Trans. Electromagn. Compat.*, vol. EMC-40, no. 3, pp. 209-217, Aug. 1998.

6.8. M. Ianoz, B. I. C. Nicoara, and W. A. Radasky, "Modeling of an EMP conducted environment," *IEEE Trans. Electromagn. Compat.*, vol. EMC-38, no. 3, pp. 400-413, Aug. 1996.

6.9. S. Pignari, F. Canavero, "Theoretical assessment of bulk current injection versus radiation," *IEEE Trans. Electromagn. Compat.*, vol. EMC-38, no. 3, pp. 469-477, Aug. 1996.

6.10. A. Papoulis, *Probability, Random Variables and Stochastic Processes*, Mc-Graw-Hill, 1991.

6.11. D. Bellan, S. Pignari, "Statistical characterization of multiconductor transmission lines illuminated by a random plane-wave field," accepted for presentation in the *IEEE Int. Symp. on Electromagn. Compat.*, Washington, D.C., USA, Aug. 21-25, 2000.


## BIOGRAPHICAL NOTES

**Diego Bellan** received the Laurea degree and the Ph.D. degree in Electrical Engineering from the Politecnico di Milano, Italy. Currently he is with the Department of Electrical Engineering of the Politecnico di Milano, Italy. His research interests are in the field of EMC, and include distributed-parameter circuits, shielding, and numerical methods.

**Sergio Pignari** received the Laurea degree and the Ph.D. degree in Electronic Engineering from the Politecnico di Torino, Italy. Currently he is an Associate Professor of Circuit Theory with the Department of Electrical Engineering of the Politecnico di Milano, Italy.
His research interests are in the field of EMC, where he works on the modeling of distributed circuits, characterization of interference effects, and statistical methods.

EMC 2000 INTERNATIONAL WROCŁAW SYMPOSIUM ON ELECTROMAGNETIC COMPATIBILITY

# A PREDICTION MODEL FOR CROSSTALK IN LARGE AND DENSELY-PACKED RANDOM WIRE-BUNDLES

Diego Bellan and Sergio Pignari
Dipartimento di Elettrotecnica, Politecnico di Milano, Italy
Tel.: +39-02-2399-3726 – Fax: +39-02-2399-3703
e-mail: diego.bellan@polimi.it, sergio.pignari@polimi.it

*This paper addresses the problem of statistical prediction of crosstalk in densely packed wire-bundles, with a large number of conductors. The wire-bundle is modeled as the cascade of equal-length, uniform multiconductor transmission lines, characterized by the same cross-section. Bundle non-uniformity is described via random permutation matrices that are used to describe wire-interchange at section-to-section junctions. The model allows high numerical efficiency, and permits consistent statistical estimation of parameters of interest, such as upper and lower bounds, mean value and variance. Model validity has been checked by means of experimental tests.*

## 1. INTRODUCTION

The prediction of crosstalk between wires in cable bundles is an important step in the quantitative evaluation of the overall system electromagnetic compatibility. In recent years several contributions to this subject have been brought out, by addressing the problem from the statistical point of view. In particular, in [1] strong variations of crosstalk in cable bundles due to variations in relative wire position have been evidenced via experimental measurements. In [2] a probabilistic model for the evaluation of crosstalk in a uniform three-conductor line has been presented. In [3] a technique based on the numerical solution of the multiconductor transmission line (MTL) equations, combined with a Monte Carlo method has been proposed for the statistical characterization of crosstalk. In [4, 5] models based on the chain connection of different uniform MTLs have been adopted to describe bundle non-uniformity.

The above-mentioned numerical techniques allow a rather precise statistical characterization of crosstalk. However, their weakness relies in the need of repeated evaluations of the per-unit-length matrix parameters of the bundle. Such a requirement reduces the overall numerical efficiency, especially in the case of bundles with a large number of conductors. Unhappily, most of the bundles encountered in practical applications are composed by a very large number of densely packed conductors.

This paper concentrates on the problem of statistical prediction of crosstalk in densely packed wire-bundles, with a large number of conductors. In the proposed technique the random wire-bundle is modeled as the cascade of equal-length uniform MTLs, characterized by the same cross-section. Bundle non-uniformity is described via generation of proper random permutation matrices, which are used to describe wire-interchange at section-to-section junctions. This approach can be viewed as the generalization of the method proposed in [6] for the analysis of twisted-wire pairs.

The novelty as well as the crucial point of the proposed method are to resort to a unique cross-section for the description of the bundle. This simplifying approximation allows to overcome the problem (shown by previous techniques) of extensive evaluations of per-unit-length matrix parameters.

For what concerns wire routing, the random permutation matrices inserted at section-to-section junctions are chosen so to determine minimum-distance wire-movements.

The result is a simple, effective, and numerically efficient model, which allows the precise characterization of crosstalk in the frequency domain, via suitable statistical estimators. In particular, the proposed method permits to identify upper- and lower-bounds, mean value, variance, and probability density function of crosstalk.

Experimental tests have also been performed, with the aim to check robustness of the approximations introduced in the model. The voltage transfer ratio between victim and generator wire-pairs (crosstalk) has been measured in 100 different realizations of a 16-wire bundle. Successful comparison of predicted results *versus* measured quantities shows the powerful of the proposed technique, and proves the adequacy of the adopted simplifying approximations.

## 2. CROSSTALK PREDICTION MODEL

This Section is devoted to the description of the proposed prediction model.

Randomness implies that relative wire positions are unknown and non-constant along the bundle. This means

dealing with random variations of the shape of the bundle cross-section. Hence, modeling variations of the bundle cross-section is a crucial point of the method.
We restrict the analysis to a special family bundles. In particular, we consider densely packed wire-bundles, characterized by the following two properties: (a) bundles contain a large number of conductors, (b) the dielectric jacket of each wire is in contact, or nearly in contact, with some of the neighboring wires. Model validity is not related to the total number of conductors in the bundle; however, such a number should be large enough for the above-mentioned assumptions to hold. The bundle is supposed to be placed over an infinite ground-plane, acting as the reference conductor.
The crosstalk analysis is based on the following prediction model. The bundle is broken down into the cascade of equal-length sub-sections, treated as uniform MTLs and characterized by the same cross-section. Bundle non-uniformity is modeled by randomly deciding wire-interconnections at section-to-section junctions.
The overall chain parameter matrix of the bundle is then evaluated as the ordered product of the chain parameter matrix describing each bundle sub-section by the chain parameter matrices of the section-to-section junctions.
Detailed considerations on the bundle cross-section generation scheme, as well as on the algorithm adopted for wire routing at section-to-section junctions are given in the following.

### 2.1. Bundle cross-section

Densely packed wire-bundles containing a large number of conductors typically satisfy properties (a) and (b) mentioned above. In such circumstances, bundle cross-section is forced to be pseudo-circular. Based on these considerations, we introduce a standard cross-section geometry, composed by adjacent wires placed on a regular grid.

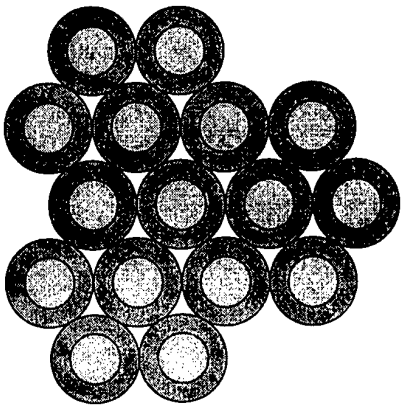


Fig. 1. Standard cross-section in the specific case of a bundle with 16 signal conductors. The same cross-section is used for modeling all the bundle sub-sections.

As an example, Fig. 1 shows the standard cross-section in the specific case of a bundle with 16 signal conductors. Since the larger is the number of conductors in the bundle, the more exact is the pseudo-circular cross-section shape assumption, the same cross-section is used for modeling all the elementary sub-sections in which the bundle is broken down. Hence, from the geometrical point of view, all the bundle sub-sections are identical uniform MTLs.
In line with this strategy, per-unit-length matrix parameters need to be numerically evaluated just once. In other words, a unique pair of per-unit-length inductance and capacitance matrices is used to describe every sub-section of a bundle, as well as every realization of the entire set of bundles under analysis.
From the numerical point of view this fact represents a great advantage, entailing high numerical efficiency of the overall procedure for crosstalk prediction.

### 2.2. Section-to-section junctions

Since the bundle model employs a cascade of equal and uniform MTLs, the description of bundle non-uniformity is done via random wire routing at section-to-section junctions.
As a matter of fact, wire interchanges at section-to-section junctions are modeled by resorting to random permutation matrices. In particular, each section-to-section junction is treated as a wire-interconnecting device of infinitesimal length, and it is characterized in terms of the chain parameter matrix. Due to the infinitesimal-length assumption, the entries of such matrix can take only the value of 0 or 1. This approach can be viewed as the generalization of the method proposed in [6] for the analysis of twisted-wire pairs.
Wire routing is based on the minimum-distance criterion. This means that, among all the possible random permutation matrices, only those corresponding to minimum-distance wire-movements are selected.

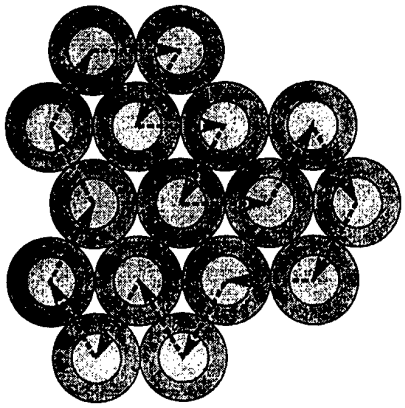


Fig. 2. Schematic representation of a possible sequence of wire-movements at the junction between two adjacent bundle sub-sections. The sequence of movements represents a hamiltonian cycle of the graph associated with the cross-section.

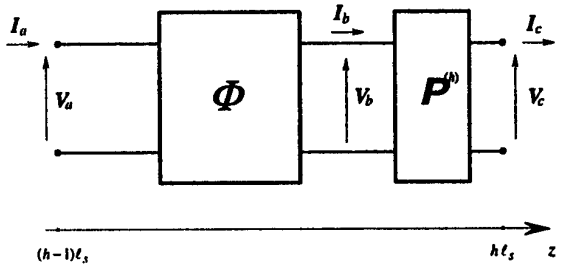



Fig. 3. Circuit model of a bundle sub-section. Matrices $\Phi$ and $P^{(h)}$ are the chain parameter matrices of the uniform sub-section and the wire-interchange section, respectively.

As an example, Fig. 2 schematically shows a possible sequence of wire-movements at the junction between two adjacent line-sections. An arrowed segment between wire $w_i$ and wire $w_j$ indicates that wire $w_i$ of the line-section at the left of the junction is connected with wire $w_j$ of the line-section at the right of the junction.

From the algorithmic point of view, the problem of identifying and randomly selecting minimum-distance permutation matrices has been solved by resorting to graph theory. The bundle cross-section is treated as a graph, in which the wires constitute graph nodes and the possible wire-movements represent graph branches. According to this point of view, the minimum-distance permutation matrices used to describe wire routing are recognized to be the *hamiltonian cycles* of the graph [7].

According to this model, the $h-$th sub-section of the bundle is considered as the cascade of a uniform line section of length $\ell_s$ and a wire interchange section. Fig. 3 shows the block diagram of the $h-$th sub-section. Matrix $\Phi$ is the chain parameter matrix of the uniform MTL, matrix $P^{(h)}$ is the chain parameter matrix of the random wire-interchange which precedes $(h+1)-$th sub-section. These matrices are defined by the following relationships:

$$\begin{bmatrix} V_B \\ I_B \end{bmatrix} = \Phi \cdot \begin{bmatrix} V_A \\ I_A \end{bmatrix}, \tag{1}$$

$$\begin{bmatrix} V_C \\ I_C \end{bmatrix} = P^{(h)} \cdot \begin{bmatrix} V_B \\ I_B \end{bmatrix}. \tag{2}$$

Matrix $P^{(h)}$ takes the form [6]

$$P^{(h)} = \begin{bmatrix} \hat{P}^{(h)} & 0 \\ 0 & \hat{P}^{(h)} \end{bmatrix}, \tag{3}$$

and sub-matrix $\hat{P}^{(h)}$ is the random permutation matrix for wire voltages and currents, at the interface with the $(h+1)-$th sub-section.

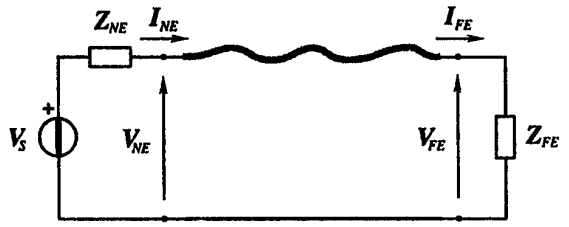



Fig. 4. Schematic representation of a random wire-bundle running above a ground plane. Vector $V_S$ and matrices $Z_{NE}$, $Z_{FE}$ characterize bundle terminal networks, that are modeled in terms of Thévenin equivalent circuits. Quantities $V_{NE}$, $V_{FE}$, $I_{NE}$, $I_{FE}$ are the vectors of wire voltages and currents at the bundle ends.

The global description of the $h-$th elementary segment of the bundle is obtained by combining equations (1) and (2). This gives:

$$\begin{bmatrix} V_C \\ I_C \end{bmatrix} = P^{(h)} \cdot \Phi \cdot \begin{bmatrix} V_A \\ I_A \end{bmatrix}. \tag{4}$$

The overall chain parameter matrix of the bundle $\Phi_B$ is derived as the ordered product of the chain parameter matrices of the elementary line sections, i.e.:

$$\Phi_B = \prod_{h=1}^{N_S} P^{(N_S+1-h)} \cdot \Phi. \tag{5}$$

## 2.3. Crosstalk estimators

Bundle equations together with terminal load equations describe the whole system, i.e. a specific bundle realization, in the frequency domain.

Bundle terminal networks have been specified in terms of Thévenin equivalent circuits. Fig. 4 schematizes the global circuit model of the bundle. Vector $V_S$ and matrices $Z_{NE}$, $Z_{FE}$ characterize bundle terminal networks, quantities $V_{NE}$, $I_{NE}$, $V_{FE}$, $I_{FE}$ identify the vectors of wire voltages and currents at near- and far-end, respectively.

Expressions for crosstalk can be derived by combining bundle equations with terminal loads equations, i.e.:

$$\begin{bmatrix} V_{FE} \\ I_{FE} \end{bmatrix} = \begin{bmatrix} \Phi_{11} & \Phi_{12} \\ \Phi_{21} & \Phi_{22} \end{bmatrix} \cdot \begin{bmatrix} V_{NE} \\ I_{NE} \end{bmatrix} \tag{6a}$$

$$V_{NE} = -Z_{NE} \cdot I_{NE} + V_S \tag{6b}$$

$$V_{FE} = Z_{FE} \cdot I_{FE}, \tag{6c}$$

where quantities $\Phi_{11}$, $\Phi_{12}$, $\Phi_{21}$, and $\Phi_{22}$ represent the four sub-matrices of the bundle chain parameter matrix $\Phi_B$.

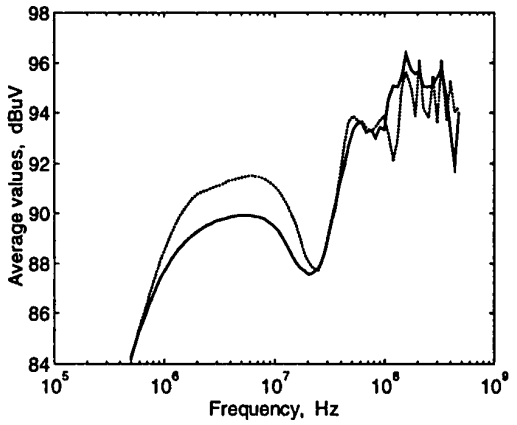



Fig. 5. Comparison between numerical predictions (solid line) and experimental measurements (dotted line). Average values of experimental data (output of the spectrum analyzer) are compared with the same quantities obtained from prediction. See text for more details.

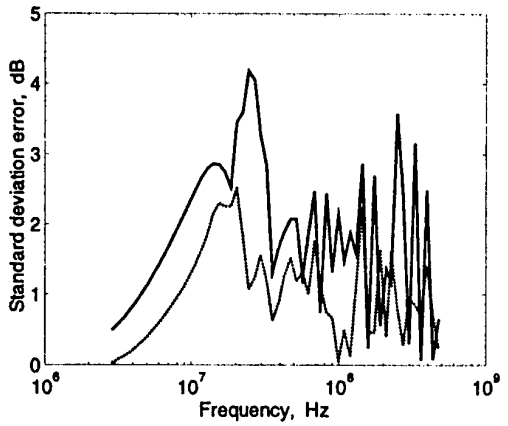



Fig. 6. Standard deviation error of crosstalk data. Difference between the standard deviation of predicted crosstalk values, and the standard deviation of measurement data. Curves differ only for the number of sub-sections adopted for bundle modeling. Solid and dotted curves refer to 4 and 20 sub-section models, respectively. It is worth noting that the choice

Solution of equations (6a), (6b), and (6c) yields to the following expression for near-end currents:

$$\boldsymbol{I}_{NE} = -\left[\boldsymbol{\Phi}_{12} - \boldsymbol{Z}_{FE}\cdot\boldsymbol{\Phi}_{22} - (\boldsymbol{\Phi}_{11} - \boldsymbol{Z}_{FE}\cdot\boldsymbol{\Phi}_{21})\cdot\boldsymbol{Z}_{NE}\right]^{-1} \cdot(\boldsymbol{\Phi}_{11} - \boldsymbol{Z}_{FE}\cdot\boldsymbol{\Phi}_{21})\cdot\boldsymbol{V}_{S}, \quad (7)$$

and back substitution of expression (7) into equation (6b) also gives near-end voltages. Finally, far-end voltages are derived from equation (6a):

$$\boldsymbol{V}_{FE} = \boldsymbol{\Phi}_{11}\cdot\boldsymbol{V}_{NE} + \boldsymbol{\Phi}_{12}\cdot\boldsymbol{I}_{NE}\,. \quad (8)$$

Repeated solutions of the above-described equations for different bundle realizations allows one to generate a data set describing the range of possible crosstalk levels, at the operation frequency.
Statistical manipulation of such data permits a detailed characterization of crosstalk in terms of suitable estimators. Typical computable quantities are upper- and lower-bounds, mean value, variance, and probability density function of crosstalk levels.

## 3. NUMERICAL SIMULATION AND EXPERIMENTAL MEASUREMENTS

In this section results of numerical simulations based on the method presented in the previous sections are described, and compared with data obtained by experimental measurements.
The wiring harness under analysis is a bundle composed by 16-wires. The bundle is placed at the height of 2 cm over a metallic ground plane, and terminated with 50 Ω resistances. The bundle length is 1.9 m, the metallic-core radius of bundle's wires is 0.25 mm, the dielectric-jacket radius (external radius) is 0.4 mm.

For what concerns prediction, the bundle cross-section has been modeled as in Fig. 1. Per-unit-length matrix parameters have been evaluated by means of the technique developed in [8], and based on the Fourier expansion of the electric charge distribution on the wire surface. Twenty equal-length sub-sections have been used for bundle modeling. One hundred bundle realizations have been generated at random, and the voltage transfer ratios between victim wire and generator wire at the near end of each bundle have been computed. In this process, also the generator-victim wire pairs have been randomly selected.
For what concerns experimental characterization, the same wiring structure previously described has been assembled, and 100 realizations of the same bundle have been obtained by repeated re-wrapping of the same set of 16 wires. The crosstalk between victim wire and generator wire at near end has been measured by means of a spectrum analyzer, in the frequency range from 500 kHz to 300 MHz.
In Fig. 5, average values of data obtained by measurement (dotted line) are plotted *versus* frequency, and compared with the same quantities obtained by prediction (solid line). Of course, such quantities do not have the physical meaning of mean value of crosstalk, since they have been obtained as the average values of data expressed in dBμV (output of the spectrum analyzer); however here they are used only for comparison purposes.
The good agreement of the two curves (maximum error is approximately 3 dB) confirms the validity of the one-cross-section approximation adopted in the model.
The decision of breaking down the bundle into 20 sub-sections is worth for some comments. In fact, the number of uniform sub-sections used for bundle modeling is a crucial parameter. Both underestimation and

overestimation of the number of sections leads to low-quality predictions. The choice of such a parameter must be driven by careful observation of the bundles under analysis. Of course, the faster are wire movements in the bundle cross-section, the greater must be number of sub-sections.

In order to describe quantitatively the impact of the choice of the number of sub-sections, Fig. 6 shows the difference between the standard deviation of predicted crosstalk values, and the standard deviation of measurement data. Curves refer to simulations that differ only for the number of sub-sections adopted for bundle modeling, and are plotted *versus* frequency.

Solid and dotted curves refer to 4 and 20 sub-section models, respectively. It is worth noting that the choice of 20 sub-sections implies a global reduction of the standard deviation error of crosstalk, even in the frequency range associated with bundle resonances. Further simulations employing 30 to 40 sub-sections have been performed. Related results, not reported in Fig. 6, have shown a larger standard deviation error.

This means that, in the present case, the choice of 20 sub-sections is the closest to the real evolution of wire coordinates in the bundle.

Also load configurations that yield to essentially capacitive (inductive) crosstalk, have been investigated, and predictions compared with data obtained by experimental measurements.

Predictions have confirmed the consistence the proposed technique, and have put in evidence its powerful in characterizing crosstalk in large and densely-packed wire-bundles.

## 4. CONCLUSIONS

In this work, a statistical approach for the description of crosstalk in densely packed wire-bundles has been presented. The bundle is decomposed into a cascade of equal-length MTL segments, with the same cross-section. Bundle randomness is modeled via random wire-interchange at section-to-section junctions. Advantages of the proposed technique are to be found both in the high numerical efficiency (only one evaluation of per-unit-length parameters is required), and in the statistical characterization of crosstalk.

## 5. REFERENCES


5.1. C. R. Paul, "Sensitivity of Crosstalk to Variations in Cable Bundles," Proceedings of the International Symposium on EMC, Zurich, 1987, pp. 617-622.

5.2. S. Shiran, B. Reiser, and H. Cory, "A probabilistic model for the evaluation of coupling between transmission lines," *IEEE Trans. Electromagn. Compat.*, vol. EMC-35, no. 3, pp. 387-393, Aug. 1993.

5.3. A. Ciccolella, F. Canavero: "Statistical simulation of crosstalk in bundles," Proceedings of the 11th International Zurich Symposium on Electromagnetic Compatibility, ETH, Zurich, March 1995, pp. 83-88.

5.4. S. Pignari, L.Konè, F. Canavero, A. Ciccolella, B. Demoulin, "Statistical Approach to crosstalk in random cable bundles," (invited paper), International Symposium on Electromagnetic Theory, Thessaloniki, Greece, May 25-28, 1998, pp. 662-664.

5.5. S. Salio, F. Canavero, J. Lefèbvre, W. Tabbara, "Statistical description of signal propagation on random bundles of wires," Proceedings of the 13th International Zurich Symposium on Electromagnetic Compatibility, ETH, Zurich, Feb. 1999, pp. 499-504.

5.6. C. R. Paul, and J. W. McKnight, "Prediction of crosstalk involving twisted pairs of wires–Part I: A transmission-line model for twisted-wire pairs," *IEEE Trans. Electromagn. Compat.*, vol. EMC-21, no. 2, pp. 92-105, May 1979.

5.7. B. Bollobas *Graph Theory*, Springer-Verlag, New York, 1979.

5.8. J. C. Clements, C. R. Paul, and A. T. Adams, "Computation of the capacitance matrix for systems of dielectric-coated cylindrical conductors," *IEEE Trans. Electromagn. Compat.*, no. 4, pp. 238-248, Nov. 1975.


## BIOGRAPHICAL NOTES

**Diego Bellan** received the Laurea degree and the Ph.D. degree in Electrical Engineering from the Politecnico di Milano, Italy. Currently he is with the Department of Electrical Engineering of the Politecnico di Milano, Italy. His research interests are in the field of EMC, and include distributed-parameter circuits, shielding, and numerical methods.

**Sergio Pignari** received the Laurea degree and the Ph.D. degree in Electronic Engineering from the Politecnico di Torino, Italy. Currently he is an Associate Professor of Circuit Theory with the Department of Electrical Engineering of the Politecnico di Milano, Italy.

His research interests are in the field of EMC, where he works on the modeling of distributed circuits, characterization of interference effects, and statistical methods.

EMC 2000 INTERNATIONAL WROCŁAW SYMPOSIUM ON ELECTROMAGNETIC COMPATIBILITY

# ANALYSIS OF THE SHIELDING EFFECTIVENESS OF A TRUNCATED CHIRAL CYLINDER

**M.G. Floreani, R.E. Zich**
Dipartimento di Elettrotecnica, Politecnico di Milano
P.zza Leonardo da Vinci 32. 20133 Milano, Italia.
Ph: +39-011-564-4118, +39-02-2399-3797;
fax: +39-02-23993703, email:zich@polito.it

*The analysis of the shielding effectiveness of a truncated chiral cylinder is here presented. An E-polarized cylindrical wave, coming from the region outside the cylinder, impinges onto the chiral shield. The chirality of the medium induces a coupling between TM and TE waves. The truncation of the practical shield has been taken into account in two different ways here compared. The analytical expression of the shielding effectiveness has been derived in a closed form.*

## 1. INTRODUCTION

The attempt of describing real shielding through ideal models has to take into account the necessity of representing different ways of access from outside, such as apertures, joints, slits or cables.

In fact, all these elements necessarily present for practical reasons usually are able to reduce drastically the shielding effectiveness of the whole shielding system.

The last consideration implies that it is practically useful to have sections in which it is easy to access to the shielded area or to the shielded volume and in order to consider the decayment of the shielding properties of the system in an analytical way it is necessary to develop a complete electromagnetic model even dealing with unideal structures.

Although it's impossible to give such a faithful and rigorous representation in these cases, the theory of electromagnetic shielding has so far suggested descriptions in terms of circuital models in case of transversal illimited planar cross sections of shieldings formed of homogeneous layers, if isotropic, or anisotropic and bianisotropic.

A better attempt to improve the model was to describe coupling via apertures into enclosed regions containing additional dielectric or metallic bodies and scattering from reflector structures having canonical geometry, such as spherical or cylindrical shells.

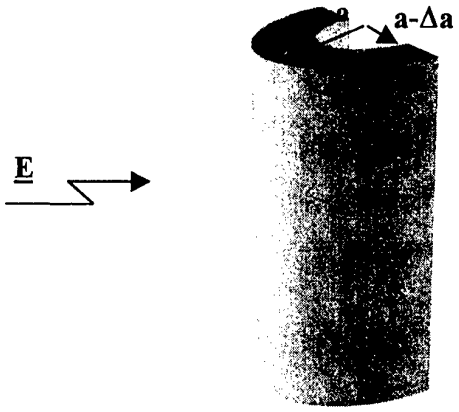



**Fig.1:** Geometry of the considered structure

The model here presented is concerned with a fundamental generalization of the previous representations and it considers the attempt to give a local description of a real shielding in terms of a homogeneous truncated chiral cylinder.

Starting from writing the components of electric and magnetic field vectors on the cylindrical surface and using the constitutive relationships of the material, the boundary conditions allow to obtain the coefficients of the expansion in terms of Bessel and Hankel functions.

The cylinder is characterized by $\varepsilon_{eff}$, $\eta_{eff}$, $\mu_{eff}$ which can be evaluated numerically.

Another possible approach has been then applied to a dielectric truncated cylinder. In this second case the considered volume including the incoming field and the truncated cylinder has been divided into four subvolumes and writing the boundary conditions it is

possible to obtain a coupled set of equations.

The solution of these equations permits to obtain the shielding effectiveness in a closed form even in this way.

Both the proposed approaches present positive features and practical problems but it must be enhanced since now that through the first one a very useful and powerful interpretation of the problem in terms of equivalent circuit network theory may be deduced.

## 2. CHIRAL MATERIALS

Chirality is a pure geometrical concept, related to the bilateral symmetry properties of the considered object. An object is defined chiral if it cannot be brought into congruence with its mirror image by rotation or translation, i.e. if it lacks bilateral symmetry.

The absence of bilateral simmetry implies the possibility of introducing an intrinsic laterality of the object, pointing out, between the same class, right- and left-handed elements.

From an electromagnetic point of view chirality has been studied since 1920-1922 by Lindman, that considered microwave sources lightening suitable materials where some chiral wire-helics were embedded.

A chiral medium can be modeled by a collection of chiral objects of same handedness; if the objects are randomly oriented the material is chiral isotropic.

A homogeneous, isotropic chiral medium can be electromagnetically described by the following constitutive relations:

$$\underline{D} = \varepsilon \underline{E} - \eta \underline{H}$$
$$\underline{B} = \eta \underline{E} + \mu \underline{H}$$

where $\eta$ is the chiral admittance of the medium.

## 3. ANALYTICAL APPROACH

Chiral media have been studied over many years for many applications and for example they have been examined as possible coating for reducing radar cross sections, for antennas and arrays, and in waveguides.

The chiral material is a reciprocal medium characterized by different phase velocities for right-hand and left-hand circularly polarized waves, as it is possible to deduce from the previous set of constitutive equations. In a lossless chiral medium any linearly polarized wave undergoes a rotation of its polarization as it propagates.

For a chiral cylinder the chirality itself induces an interesting coupling between $TM^z$ e $TE^z$ scattering waves.

The problem is concerned with a E-polarized plane wave incident on a chiral truncated cylinder (fig. 1).

The material is characterised by using $\varepsilon_{eff}$, $\eta_{eff}$, $\mu_{eff}$ instead of the real parameters $\varepsilon$,$\eta$, and $\mu$, in order to take into account the effects of the truncation as it is usually done for example dealing with microstrip structures. The effective parameters may be numerically obtained with a suitably developed code.

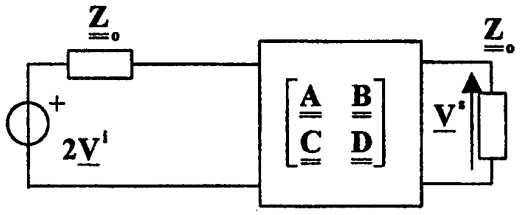



**Fig 2:** The equivalent circuit model

In order to rephrase the electromagnetic problem in terms of circuit network models a convenient way is the introduction of the Double Spatial Fourier Transform of the transverse electric and magnetic fields in the cylindrical coordinates, where $\underline{\sigma}$ is the spatial frequency vector.

The equivalent circuit network model of the considered problem is reported in Fig.2.

The voltage generator on the left models the incoming field, the two matrices $\underline{\underline{Z}}_0$, on the left and on the right, model the free space regions, the two-port models the equivalent untroncated chiral cylinder characterized in terms of effective physical parameters deduced in terms of the physical ones and of the kind of truncation introduced.

In order to obtain a two-port representation in terms of the transmission matrices, it is necessary to start previously from the transversal form of Maxwell equation in cylindrical coordinates.

Starting from the classical Maxwell curl equations and imposing the chiral constitutive relations for the chiral media:

$$curl\underline{E} = -j\omega\mu_{eff}\,\underline{H} - j\omega\eta_{eff}\,\underline{E}$$
$$curl\underline{H} = j\omega\varepsilon_{eff}\,\underline{E} - j\omega\eta_{eff}\,\underline{H}$$

It is possible to express the radial component of **E** and **H** in order to express the above equations only in function of the transversal components of the electric and magnetic fields; the results are given by the following set of coupled equations that, in the spectral domain lead to the equivalent circuit model.

$$\frac{\partial\left(R\underline{E}_t\right)}{\partial R}=\frac{1}{R^2}\frac{\eta_{eff}}{j\omega\left(\varepsilon_{eff}\mu_{eff}+\eta_{eff}^2\right)}grad_{\varphi z}div_{\varphi z}\left(\underline{R}\times\underline{E}_t\right)+$$

$$-\frac{1}{R^2}\frac{\mu_{eff}}{j\omega\left(\varepsilon_{eff}\mu_{eff}+\eta_{eff}^2\right)}grad_{\varphi z}div_{\varphi z}\left(\underline{R}\times\underline{H}_t\right)+$$

$$+j\omega\mu_{eff}\left(\underline{R}\times\underline{H}_t\right)+j\omega\eta_{eff}\left(\underline{R}\times\underline{E}_t\right);$$

$$\frac{\partial\left(R\underline{H}_t\right)}{\partial R}=\frac{1}{R^2}\frac{\varepsilon_{eff}}{j\omega\left(\varepsilon_{eff}\mu_{eff}+\eta_{eff}^2\right)}grad_{\varphi z}div_{\varphi z}\left(\underline{R}\times\underline{E}_t\right)+$$

$$+\frac{1}{R^2}\frac{\eta_{eff}}{j\omega\left(\varepsilon_{eff}\mu_{eff}+\eta_{eff}^2\right)}grad_{\varphi z}div_{\varphi z}\left(\underline{R}\times\underline{H}_t\right)+$$

$$+j\omega\varepsilon_{eff}\left(\underline{R}\times\underline{E}_t\right)-j\omega\eta_{eff}\left(\underline{R}\times\underline{H}_t\right).$$

On the contrary for what concerns the direct representation of the field in the three regions, outside the equivalent effective shield, in the equivalent shield and inside it, the components of **E** and **H** have to satisfy the following boundary conditions:

$$E_{z1}^{tot}(r=a)=E_{z2}^{tot}(r=a);H_{z1}^{tot}(r=a)=H_{z2}^{tot}(r=a)$$

$$E_{\phi1}^{tot}(r=a)=E_{\phi2}^{tot}(r=a);H_{\phi1}^{tot}(r=a)=H_{\phi2}^{tot}(r=a)$$

$$E_{z2}^{tot}(r=a-\Delta a)=E_{z3}^{tot}(r=a-\Delta a)$$

$$E_{\phi2}^{tot}(r=a-\Delta a)=E_{\phi3}^{tot}(r=a-\Delta a)$$

$$H_{z2}^{tot}(r=a-\Delta a)=H_{z3}^{tot}(r=a-\Delta a)$$

$$H_{\phi2}^{tot}(r=a-\Delta a)=H_{\phi3}^{tot}(r=a-\Delta a)$$

where cylindrical coordinates have been used.

The solution of the equations obatined by introducing the suitable expression of the electric and magnetic fields propagating in the considered cylindrical coordinates, gives the following expression of the scattered electrical field in the region r < a - Δa :

$$E_{z3}=E_0\sum_{m=-\infty}^{+\infty}G_m j^{|m|}J_{|m|}(kr)e^{jm(\phi-\phi^\circ)}$$

$$E_{r3}=\frac{jE_0}{kr}\sum_{m=-\infty}^{+\infty}mH_m j^{|m|}J_{|m|}(kr)e^{jm(\phi-\phi^\circ)}$$

$$E_{\phi3}=-E_0\sum_{m=-\infty}^{+\infty}H_m j^{|m|}J'_{|m|}(kr)e^{jm(\phi-\phi^\circ)}$$

where J and H are the Bessel and Hankel functions and the coefficients of the series are given by:

$$G_m=\frac{J_{|m|}(ka)H_{|m|}\left[k_{eff}(a-\Delta a)\right]}{J_{|m|}\left[k.(a-\Delta a)\right]H_{|m|}(k_{eff}a)}e^{-jm(\phi_{inc}-\phi^\circ)}\Psi$$

$$\mathrm{H}_m=\frac{\eta_0 J'_{|m|}(ka)e^{-jm(\phi_{inc}-\phi^\circ)}}{\beta_1}H_{|m|}\left[k_{eff}(a-\Delta a)\right]\varepsilon_6\varepsilon_7$$

with:

$$\Psi=1-\Omega+\frac{\varepsilon_5 H_{|m|}\left[k_{eff}(a-\Delta a)\right]}{\varepsilon_1}\left\{\frac{J'_{|m|}(ka)H_{|m|}(k_{eff}a)\eta_{eff}}{\eta_0 J_{|m|}(ka)}+\right.$$

$$\left.-H'_{|m|}(k_{eff}a)+-\frac{\Omega\varepsilon_4}{\eta_0 H_{|m|}(ka)}\right\}$$

where Ω, and the other parameters are the following expressions of Bessel and Hankel functions:

$$\Omega=\frac{\left[\alpha_1-\alpha_2+\alpha_3\frac{J'_{|m|}(ka)}{J_{|m|}(ka)}-\alpha_4-\alpha_5\frac{J'_{|m|}(ka)}{J_{|m|}(ka)}+\alpha_6\right]}{\left[\alpha_1-\alpha_2+\alpha_3\frac{H'_{|m|}(ka)}{H_{|m|}(ka)}-\alpha_4-\alpha_5\frac{H'_{|m|}(ka)}{H_{|m|}(ka)}+\alpha_6\right]}$$

$$\alpha_1=\frac{H_{|m|}\left[k_{eff}(a-\Delta a)\right]J'_{|m|}\left[k(a-\Delta a)\right]\varepsilon_1}{J_{|m|}\left[k(a-\Delta a)\right]\tau};$$

$$\alpha_2=\frac{\eta_0 H'_{|m|}\left[k_{eff}(a-\Delta a)\right]\varepsilon_1}{\eta_{eff}\tau}$$

$$\alpha_3=\frac{\eta_{eff}J'_{|m|}\left[k(a-\Delta a)\right]H_{|m|}(k_{eff}a)}{\eta_0 J_{|m|}\left[k(a-\Delta a)\right]};$$

$$\alpha_4=\frac{J'_{|m|}\left[k(a-\Delta a)\right]H'_{|m|}(k_{eff}a)}{J_{|m|}\left[k(a-\Delta a)\right]}$$

$$\alpha_5=H_{|m|}(k_{eff}a);\alpha_6=\frac{\eta_0 H_{|m|}(k_{eff}a)}{\eta_{eff}}$$

$$\varepsilon_1=H_{|m|}(k_{eff}a)H'^{(2)}{}_{|m|}(k_{eff}a)+$$

$$-H'_{|m|}(k_{eff}a)H^{(2)}{}_{|m|}(k_{eff}a)$$

$$\tau=H_{|m|}(k_{eff}a)H^{(2)}{}_{|m|}\left[k_{eff}(a-\Delta a)\right]+$$

$$-H_{|m|}\left[k_{eff}(a-\Delta a)\right]H^{(2)}{}_{|m|}(k_{eff}a)$$

$$\varepsilon_4 = \eta_{eff} H'_{|m|}(ka) H_{|m|}(k_{eff} a) + -\eta_0 H'_{|m|}(ka) H'_{|m|}(k_{eff} a)$$

$$\varepsilon_5 = H_{|m|}(k_{eff} a) H^{(2)}{}_{|m|}\left[k_{eff}(a-\Delta a)\right] + -H^{(2)}{}_{|m|}(k_{eff} a) H_{|m|}\left[k_{eff}(a-\Delta a)\right]$$

$$\beta_1 = H'_{|m|}(k_{eff} a)\varphi\left\{\eta_{eff} J'_{|m|}\left[k(a-\Delta a)\right] H'_{|m|}\left[k_{eff}(a-\Delta a)\right] + -\eta_0 H_{|m|}\left[k_{eff}(a-\Delta a)\right] J'_{|m|}\left[k(a-\Delta a)\right]\right\}$$

$$\varphi = H^{(2)}{}_{|m|}(k_{eff} a) - H_{|m|}(k_{eff} a) H'^{(2)}{}_{|m|}(k_{eff} a)$$

$$\varepsilon_6 = H'^{(2)}{}_{|m|}\left[k_{eff}(a-\Delta a)\right] + -H^{(2)}{}_{|m|}\left[k_{eff}(a-\Delta a)\right] H'_{|m|}\left[k_{eff}(a-\Delta a)\right]$$

$$\varepsilon_7 = H_{|m|}(k_{eff} a) - \Theta\left(H_{|m|}(ka) H'_{|m|}(k_{eff} a) - H_{|m|}(k_{eff} a) H'_{|m|}(k\,a)\right)$$

$$\Theta = \frac{\beta_1 + H_{|m|}(k_{eff} a)\left(\eta_0 J'_{|m|}\left[k(a-\Delta a)\right]\varepsilon_2 - \eta_{eff} J_{|m|}\left[k(a-\Delta a)\right]\varepsilon_3\right)}{H_{|m|}(k_{eff} a)\left(\eta_0 \varepsilon_2 \beta_2 - \eta_{eff}\varepsilon_3\beta_3\right) - \eta_{eff} H'_{|m|}(ka)\beta_1}$$

$$\varepsilon_2 = H'_{|m|}(k_{eff} a) H^{(2)}{}_{|m|}\left[k_{eff}(a-\Delta a)\right] - H'^{(2)}{}_{|m|}(k_{eff} a) H_{|m|}\left[k_{eff}(a-\Delta a)\right]$$

$$\varepsilon_3 = H'_{|m|}(k_{eff} a) H'^{(2)}{}_{|m|}\left[k_{eff}(a-\Delta a)\right] - H'^{(2)}{}_{|m|}(k_{eff} a) H_{|m|}\left[k_{eff}(a-\Delta a)\right]$$

$$\beta_2 = \eta_{eff} J'_{|m|}\left[k(a-\Delta a)\right] - \eta_0 H'_{|m|}(ka) J_{|m|}\left[k(a-\Delta a)\right]$$

$$\beta_3 = J_{|m|}\left[k(a-\Delta a)\right]\left(\eta_{eff} - \eta_0 H'_{|m|}(ka)\right)$$

Consequently the shielding effectiveness may be obtained in the following closed form:

$$E = 20\log_{10}\left|\frac{\hat{E}_i}{\hat{E}_t}\right| = 20\log_{10}\frac{1}{\sqrt{G_m^2 + \frac{1}{k}H_m^2 + H_m^2}}$$

A second alternative approach has been also here considered.

A dielectric truncated cylinder is divided into four parts: the outside region, the inside region, the shield, and the portion of the cylinder that has been truncated.

Its impedance is $\eta$. The truncated cylinder angular range is:

$$\left[-\phi_0, +\phi_0\right]$$

$$\phi_1 = \mathrm{Im}\left\{\vec{k}_1 \cdot \Delta\vec{a}\right\}; \phi_2 = \mathrm{Im}\left\{\vec{k} \cdot \Delta\vec{a}\right\}.$$

In the four regions the electric and magnetic field components have to satisfy the following conditions:

$$E_{z_1}^{tot}(r=a) = E_{z_2}^{tot}(r=a);$$

$$H_{\phi_1}^{tot}(r=a) = H_{\phi_2}^{tot}(r=a)$$

$$E_{z_2}^{tot}(r=a-\Delta a) = E_{z_3}^{tot}(r=a-\Delta a);$$

$$H_{\phi_2}^{tot}(r=a-\Delta a) = H_{\phi_3}^{tot}(r=a-\Delta a)$$

$$E_{z_3}^{tot}(r=a-\Delta a) = E_{z_4}^{tot}(r=a-\Delta a);$$

$$E_{z_1}^{tot}(r=a) = E_{z_4}^{tot}(r=a)$$

From the solution of these equations we can obtain:

$$D_m = -\frac{\varepsilon\pi k_1 a e^{jm\phi_1}}{2j\eta_0 \alpha J_{|m|}\left[k(a-\Delta a)\right]}\left\{\frac{\gamma\cdot\rho_1}{\rho_2} + \delta\right\}$$

*where*

$$\rho_1 = \left[2j\eta_0 \alpha J_{|m|}(ka) + \pi k_1 a \delta\Omega\right]$$

$$\rho_2 = \left[2j\eta_0 \alpha H_{|m|}(ka) - \pi k_1 a \gamma\Omega\right]$$

i.e. the coefficient of the following component:

$$E_{z_3} = E_0 \sum_{m=-\infty}^{+\infty} D_m j^{|m|} J_{|m|}(kr) e^{jm(\phi-\phi_1)}.$$

The value of the coefficients defining $D_m$ are the following ones:

$$\alpha = \left\{\eta_0 J'_{|m|}\left[k_1(a-\Delta a)\right] J_{|m|}\left[k(a-\Delta a)\right] + -\eta J'_{|m|}\left[k(a-\Delta a)\right] J_{|m|}\left[k_1(a-\Delta a)\right]\right\}$$

$$\Omega = \alpha H_{|m|}(k_1 a) - \beta J_{|m|}(k_1 a);$$

$$\varepsilon = \alpha H_{|m|}\left[k_1(a-\Delta a)\right] - \beta J_{|m|}\left[k_1(a-\Delta a)\right]$$

$$\beta = \left\{\eta_0 H'_{|m|}\left[k_1(a-\Delta a)\right] J_{|m|}\left[k(a-\Delta a)\right] + -\eta J'_{|m|}\left[k(a-\Delta a)\right] H_{|m|}\left[k_1(a-\Delta a)\right]\right\}$$

$$\gamma = \eta H'_{|m|}(ka) J_{|m|}(k_1 a) - \eta_0 H_{|m|}(ka) J'_{|m|}(k_1 a)$$

$$\delta = \eta_0 H_{|m|}(ka) J'_{|m|}(k_1 a) - \eta\ J_{|m|}(k_1 a) J'_{|m|}(ka)$$

Finally the shielding effectiveness for the dielectric case in the considered approach so follows:

$$SE = 20\log_{10}\left|\frac{\hat{E}_i}{\hat{E}_t}\right| = 20\log_{10}\frac{1}{D_m}.$$

## 4. REFERENCES


4.1 R.E. Zich "Analysis of the shielding properties of chiral slabs" *IECIE Trans. On Communication, Special Issue on EMC*, vol. E78, Feb.95, pp 230-237.

4.2 D.L. Jaggard, N. Engheta "Novel use of layered chiral materials for control of absorption, reflection and transmission" *IEEE International Symposium on Electromagnetic Compatibility*, Zurich, Switzwerland, 1991.

4.3 R.E. Zich "Analysis of the shielding properties of Planar wire-mesh shields loaded by stratified structures" *IECIE Trans. On Communication, Special Issue on EMC*, vol. E78, Feb.95, pp 238-246.

4.4 R.E. Zich "Analysis of shielding structures for emc" (invited paper) *International U.R.S.I. Symposium on Electromagnetic Theory*, 25-28 Maggio 1998, Salonicco, Greece.

4.5 S.Bassiri, N. Engheta, "One- and Two-Dimensional Dyadic Green Function in Chiral Media", *IEEE Transaction on Antennas and Propagation*, vol.37, Apr. 1989, pp. 512-515.

4.6. R.D. Graglia, P.L.E. Uslenghi and R.E. Zich, "Dispersion relation for Bianisotropic Materials and its symmetry properties", *IEEE Transaction on Antennas and Propagation*, vol.39, Jan.1991, pp. 83-91.

4.7. H. Cory, "Chiral Devices – an overview of canonical problems", *Journal of Electromagnetic Waves Applications*, vol. 9, 1997, pp. 805-829.

4.8. P.Pirinoli, R.E.Zich, "Analysis of the radiated emissions of printed structures on chiral substrate", *the 1994 International Symposium on Electromagnetic Compatibility*, Sao Paulo, Brazil, 1994.

4.9 J.A. Stratton, *Electromagnetic Theory*. New York: McGraw-Hill, 1941.

4.10. Abramovitz, Stegun, *Handbook of Mathematical Functions*, Dover Book, 1956

4.11. N. Marcuvitz, "Waveguide Handbook", *IEE Books, Electromagnetic Waves Series* 1986


## BIOGRAPHICAL NOTE

**Riccardo Enrico Zich**: Laurea summa cum laude (M.S.) and Ph.D. in Electronic Engineering Politecnico di Torino, Torino, Italy, in 1989 and 1993, respectively. Researcher in the same University from 1991. Since 1998 Associate Editor of the IEEE Trans. on EMC and joined the Politecnico di Milano, Dipartimento di Elettrotecnica as Associate Professor of Electrical Engineering.

EMC 2000 INTERNATIONAL WROCŁAW SYMPOSIUM ON ELECTROMAGNETIC COMPATIBILITY

# THEORY AND EXPERIMENT ON RADIATION FROM A BENT TRANSMISSION LINE

N. Ishibashi, S. K. Lee and M. Hayakawa

Department of Electronic Engineering, The University of Electro-Communications, 1-5-1 Chofugaoka, Chofu Tokyo 182-8585, Japan fax: +81 (0)424 43 5783 e-mail: hayakawa@whistler.ee.uec.ac.jp

*This paper deals with the radiation from a transmission line with a bend from both theoretical and experimental points of view. First of all, the radiation loss has been estimated by means of the method of moments, and it is fond to become significant from the line height of h/λ~0.1(λ:wavelength). Also, the radiation loss is found to increase significantly for larger bend angle(α) especially for higher h/λ values. Then, radiation patterns from a bent transmission line have been numerically computed, which may indicate that the radiation is originated mainly at the bend, but other part is also found to contribute to the overall patterns with many additional lobes. These numerical estimations are compared with the corresponding experiments by means of a network analysis, and they are in excellent agreement with the theoretical expectations.*

## 1. INTRODUCTION

An important aspect of electromagnetic interference is the coupling of external (either intentional or unintentional) electromagnetic waves to the transmission lines and electronic systems, and there have been published a lot of papers on this subject [see our recent paper by Omid et al. (1997) [1] and references therein].

The problem opposite to this electromagnetic coupling, is the radiation of undesired electromagnetic waves from various electric devices, which may lead to their interference to other electronic systems. However, there have been carried out very few investigations on this radiation phenomenon, even though it is essentially fundamental for EMC studies. Some works [2] have been performed, in which radiation from a transmission line (without a bend) is treated as being reciprocal to the electromagnetic coupling. However, the PCB configuration and some transmission lines have generally a bend, and we could expect some radiation from such a bend. Reineix and Jecko [3] have dealt with an approximate solution of radiation losses from a transmission line with an elbow (bend), on the assumption that radiation is generated at the discontinuity. Then, Nakamura et al. [4] have adopted the full-wave analysis for a bent transmission line, but the same approximation was made. So, this paper will deal with the quantitative (exact) estimation of such a radiation from a bent transmission line by means of the full-wave electromagnetic theory, which is confirmed by the corresponding experiments.

## 2. NUMERICAL ESTIMATION AND EXPERIMENTS

The configuration of the problem is illustrated in Fig.1, together with the coordinate system used in the paper. The transmission line (with a radius (0.006λ) much smaller than a wavelength λ) is suspended at a height h above an infinite perfectly conducting ground, and the line without a bend goes further in the x-direction. But, when the line is bent at the position of x=0 from the x axis toward the y axis by an angle α, we have the situation in the upper panel of Fig. 1. In the conventional situation as a transmission line, the height h is taken to be sufficiently small with respect to the wavelength λ, so that the principal propagation mode is quasi-TEM mode. The input voltage is assumed to be 1 Volt. In order to use the numerical electromagnetic

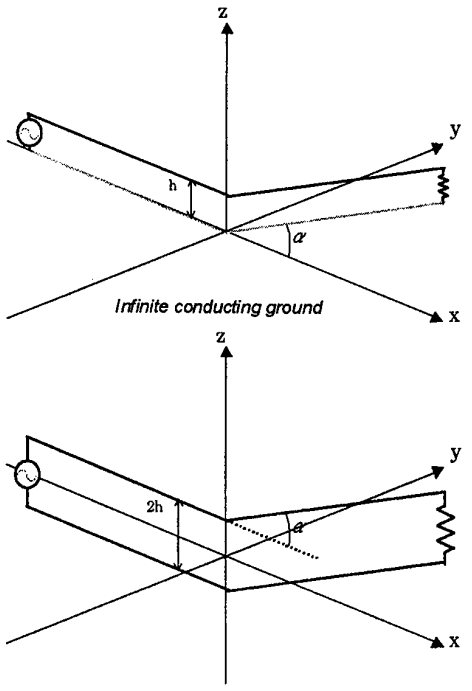



Fig.1 Configuration of the problem and coordinate system used.

code (NEC) [5] based on the conventional method of moments, we have to consider the two-wire line as shown in the lower panel of Fig. 1, which is equivalent to the bend situation in Fig. 1 by considering the image.

NEC 2 [5] is a program, which solves, by means of the method of moments, the integro-differential equations derived from Maxwell's equations with boundary conditions, in which we have to divide the line into many segments. The length of such a small segment is taken as follows; 0.05λ in the vicinity of the bend (within ±1λ from the bend), and 0.1λ for other parts. These values for segmentation are finally determined, based on the different runs with changing the segment length, such that we have confirmed the accuracy of less than 1% for these segmentations when computing the current distributions.

Next, the experimental setup is shown in Fig. 2, in which we intend to measure the radiation loss by means of the use of a network analyzer. A bent transmission line is placed as in Fig. 2 over an aluminum ground plane with an area of 1.8m x 1.8m. The whole length of the bent line ($2\ell$) is fixed as 90cm (corresponding to 3λ at 1GHz), and the analyzed frequency band is from 50MHz to 2GHz. The height of the line is fixed at three different values of h=6mm, 18mm and 30mm (corresponding to λ/50, λ/17, λ/10 at 1GHz). The radiation loss (expressed as a percentage of the input power) is estimated as $1-(|S_{11}|^2+|S_{21}|^2)$, where $S_{11}$ and $S_{21}$ indicate the coefficient of reflection and transmission, which can be measured by the network analyzer. Fig. 3 illustrates another experimental setup for the measurement of radiation patterns from a bent

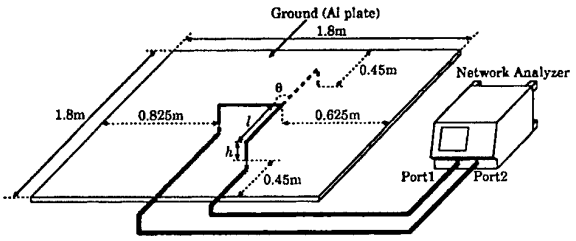



Fig.2 Experimental setup for the measurement of radiation loss from a bent line.

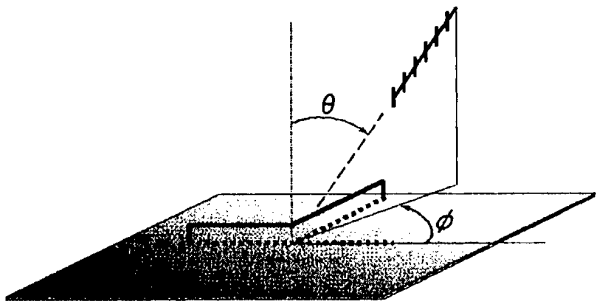



Fig.3 Experimental setup for the measurement of radiation patterns of a bent transmission line.

transmission line, in which the angles, θ and ϕ are defined. In order to measure the electric field, we have used a Yagi antenna.

## 3. RESULTS OF COMPUTATIONS AND EXPERIMENTS

### 3.1 Radiation loss

First of all, we estimate the current distribution by means of the method of moments, then estimate the electromagnetic fields at far distances and we can obtain the total radiation power. Fig. 4 illustrates the numerical estimation at a particular frequency (1GHz) for the radiation loss as a function of line height. Bend angle (α) is treated as a parameter. As is easily understood from the figure, when the line height is extremely small (h/λ~1/30) for which the propagation mode is purely TEM, the radiation loss is found to be of the order of a few percents. Also, the bending does not significantly increase the radiation loss. While, when the value of h/λ increases up to 0.1 (we still consider that the propagation is quasi-TEM mode), the radiation is significantly enhanced up to the order of over 10% in the case of α=0° (without any bend). With the increase in α, about 15% of the input power is seen to be radiated for α=90° and its radiation loss becomes even larger for α>90°.

Fig. 5 illustrates the result of comparison with the experiment, in which the line height is fixed as h=18mm and α=90°. Then, the frequency dependence of radiation loss is plotted in the figure. The oscillation of the overall pattern is only resulted from the wave interference over the whole length. First of all, the general patterns obtained by the theory and experiment are found to exhibit very similar behaviors, which means that the theoretical estimation as in Fig. 4 is excellently confirmed by the experiment. As is shown in this figure, the radiation loss is increasing with increasing frequency, which is consistent with the previous figure (Fig. 4).

### 3.2 Radiation patterns

The radiation pattern is calculated by using the estimated current distribution on the bent line. Fig. 6 illustrates the radiation pattern from the whole part of a bent transmission line (h=6mm, and α=90°), in which $E_\theta$ and $E_\phi$ are plotted (see the coordinates in Fig. 3). The right panel indicates the theoretical estimation, while the left, the corresponding experimental result. It is found that both radiation patterns are in good agreement with each other. Nakamura et al.[4] have estimated the radiation by using the full-wave analysis just like ours, but they have had an assumption that the radiation is only from the bend. In order to have a comparison with theirs, we extract a piece of current for the bend region (in the vicinity of the bend within ±1λ) and we compute the radiation patterns. Those computed ones are found to be in good agreement with Nakamura et al.'s result. However, the radiation patterns in Fig. 6 are considerably different from Nakamura et al.'s, and this difference may indicate that

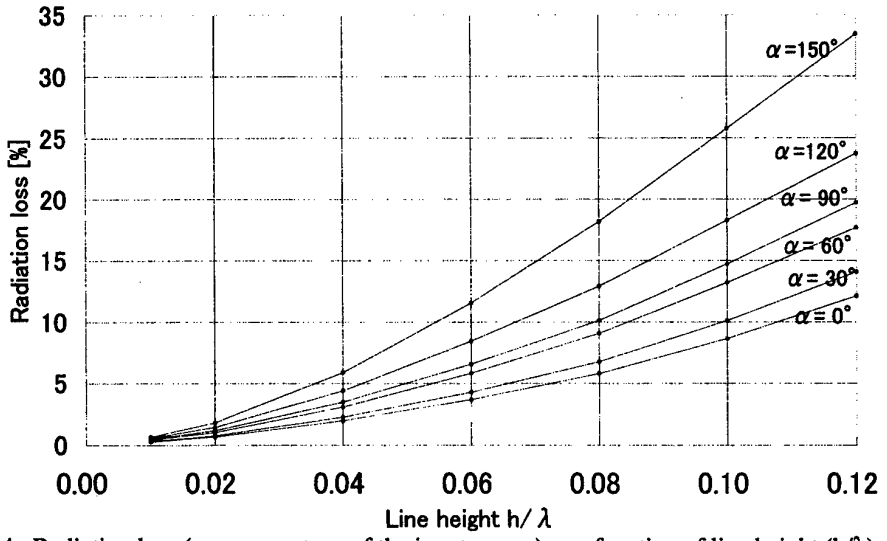



Fig.4 Radiation loss (as a percentage of the input power) as a function of line height (h/λ).

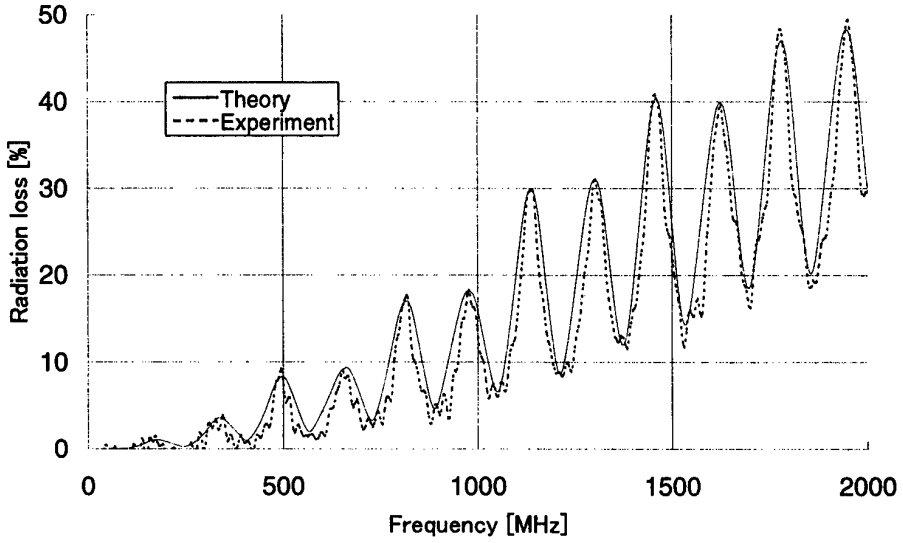



Fig.5 Radiation loss versus frequency. h=18mm and α=90°.
A full line refers to the experiment, while a broken line, the theoretical estimation.

even if the radiation is mainly from the bend region, the whole line is also contribution to the overall patterns. This is because the number of side lobes increases considerably as compared in the case of the radiation only from the bend. This point is clearly demonstrated in Fig. 7 by changing the total length of the transmission line. As is seen in the figure, the general tendency (or behavior) in the radiation patterns is strictly reserved, but the number of side lobes increases significantly.

By looking at Fig. 6 in the case of α=90°, we think of the physical mechanism of radiation from a bent transmission line. There are two travelling wave antennas; one is the current up to the bend, and the other is that after the bend. As we can notice from the current distribution in Fig. 3, the standing wave pattern in the current distribution enables us to calculate the reflection coefficient at the bend to be of the order of 0.1. Of course, the antenna before the bend is the type of a standing wave due to the reflection at the bend, but the reflection is so small that it seems to be considered more like a traveling wave antenna. So, we can simply consider that there are two travelling wave antennas, one in the x-direction (up to the bend), and another in the y-direction (after the bend). Correspondingly, we can anticipate, for $E_\phi$ pattern, one main lobe in the x-direction due to the travelling wave before the bend and another main lobe in the y-direction due to that after the bend. As for $E_\theta$ radiation pattern, we have the

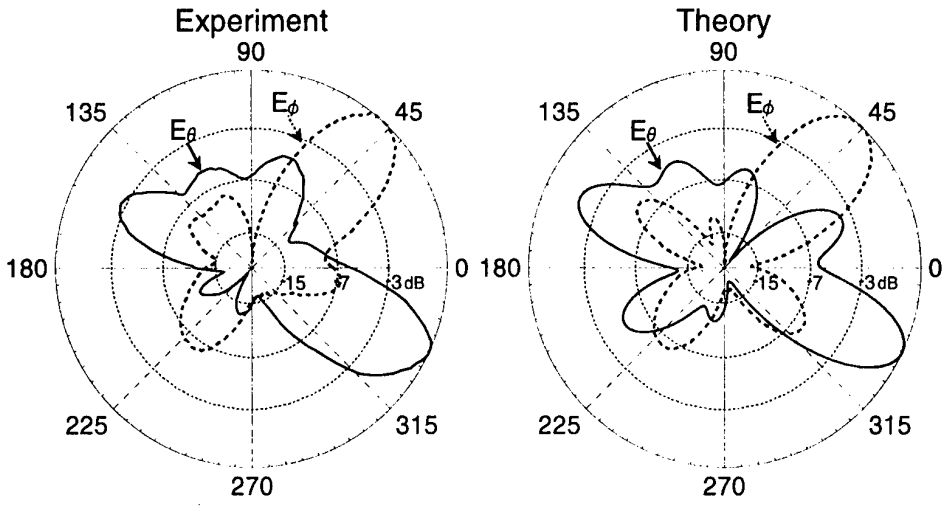



Fig.6 The radiation patterns for the $E_\theta$ (in full line) and $E_\theta$ (in broken line) components with taking into account the whole contribution. The same θ is assumed to be 45°.

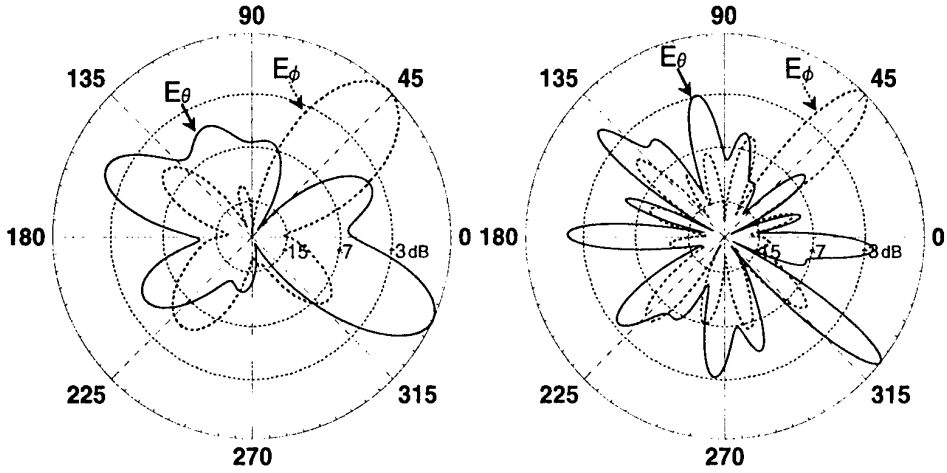



Fig.7 Change in radiation patterns due to the change in the total length ($2\ell$=2.2λ, left and $2\ell$=6.2λ, right). h=6mm and α=90°.

combined effects of those two antennas in the intermediate direction between the two antenna directions.

## 4. CONCLUSION

The radiation from a bent transmission line has been investigated theoretically and experimentally, which is of fundamental importance in EMC studies. The radiation loss is principally determined by the line height. When h/λ is less than 1/30, a few percent of radiation is expected, but it increases up to 10% for h/λ=0.1. Also, the bend angle (α) is found to play an important role in the radiation. Furthermore, the radiation is found to be not only just around the bend, but also over a whole length.

## 5. REFERENCES

5.1. M. Omid, Y. Kami, and M. Hayakawa, "Field coupling to non-uniform and uniform transmission lines", IEEE Trans. Electromag. Compat., vol. EMC-39, pp.201-212, 1997.

5.2. Y. Kami, "Mechanism of electromagnetic radiation from a transmission line", Trans. Commun., Inst. Electr. Inform. Comm. Engrs. Japan, vol. E75-B, 115-123, 1992.

5.3. A. Reineix and B. Jecko, "Radiation losses in the time domain transmission line method", Proc. Int'l Symp. on Electromagnetic Compatibility (EMC) '94 Roma, Rome, Italy, September 13-16, 1994, pp.402-407.

5.4. T. Nakamura, N. Hayashi, H. Fukuda, and S. Yokokawa, "Radiation from the transmission line with an acute bend," IEEE Trans. Electromagn. Compat., vol. EMC-37, no. 3, pp. 317-325, 1995.

5.5. G. J. Burke and A. J. Poggio, "Numerical

electromagnetic code (NEC)-method of moments", NOSC Tech. Doc. 116, Naval Ocean Systems Center, San Diego, CA, 1980.

## BIOGRAPHICAL NOTE

Naomitsu Ishibashi is now in the 2nd grade of Master Course of Department of Electronic Engineering, The University of Electro-Communications, Tokyo Japan. He graduated from the same university in 1998. He is studying the radiation phenomenon from a bent transmission line, coupling of external signals to transmission lines etc.

Sungkyu Lee is a Ph. D student in the University of Electro-Communications, Tokyo Japan. His interest is general EMC study by means of numerical analysis, including the radiation from a bent line, cross-talk etc.

Masashi Hayakawa is now a professor of Department of Electronic Engineering, The University of Electro-Communications, Tokyo Japan. He graduated from Department of Electrical Engineering, Nagoya University, and obtained B. Eng., Master of engineering and Doctor of engineering, all from Nagoya University. He worked at Research Institute of Atmospherics, Nagoya University and studied space physics and atmospheric electricity. After moving to the present university, he extended his work very much, including EMC general problems, inverse problems, seismo-electromagnetics in addition to the previous works (space physics, atmospheric electricity).

EMC 2000 INTERNATIONAL WROCŁAW SYMPOSIUM ON ELECTROMAGNETIC COMPATIBILITY

# AN EFFICIENT METHOD FOR CALCULATION OF THE RADIATION FROM COPPER INSTALLATIONS WITH WIDEBAND TRANSMISSION SYSTEMS

Piotr Zawadzki
Silesian Technical University, Akademicka 16, 44-100 Gliwice

Rabah Tarafi, Olivier Daguillon, Ahmed Zeddam
France Telecom / BD-CNET, DTD/SFE, Technopole Anticipa, 22307 Lannion Cedex

*The recent innovations in connecting hardware and smart encoding schemes make it possible the old copper installations are capable to support T1/E1 bit rates. It is obvious that old networks destined for POTS, will intensively dissipate energy transmitted by new wideband services and they should be regarded as a potential source of electromagnetic hazards. This note reports results of the study towards developing a computer-aided method for numerical modeling of an electromagnetic environment in a close vicinity of cables carrying signals of wideband transmission systems. The proposed method is formulated in the frequency domain and uses multiconductor transmission line theory for determination of field sources. Subsequently, fullwave approach is applied to find near electromagnetic field in the vicinity of the cable.*

## 1 INTRODUCTION

Bandwidth "hungry" computing applications, the increasing need for information sharing and the explosive growth in higher data transmission rates demand the greater speed and larger bandwidth from LANs (Local Area Networks) or local premises telephone installations. One method of improving the information infrastructure is to install an all-fibre network. However, the all-fibre premises distribution network has its price: implementing it requires the replacement of copper cables with fibre and the installation of more expensive active components, such as fibre optic interface devices. With recent innovations in the design of connecting hardware and smart encoding schemes UTP (Unshielded Twisted Pair) or FTP (Foiled Twisted Pair) cables are now capable of supporting high bit rates.

DSL (Digital Subscriber Line) refers to several types of advanced modems that enable fast access at speeds 300 times faster than most analog modems. Since DSL works on regular telephone lines they are considered a key means of opening the bottleneck in the "last mile" of the existing telephone infrastructure. It is obvious that old premise networks, destined for the POTS, will intensively dissipate energy for the new modulation schemes and they might become a source of not negligible electromagnetic radiation. The above observation leads to the conclusion that new services installed on existing networks should be treated not only as victims of the external noise, but also as potential sources of electromagnetic emissions. This, in turn, calls for the elaboration of the fast, reliable, computer aided method for prognosis of electromagnetic hazards arising in this new environment.

## 2 NUMERICAL MODEL

Numerical models for the radiation of the cable with the given parameters can be derived on a basis of computational intensive methods based on a direct solution of Maxwell equations. However, everyday EMC engineering practice requires maybe less accurate but more efficient methods.

We use multiconductor transmission line theory to determine current distribution along the cable [1] and full-wave approach [2] to determine field of a specified current distribution.

### 2.1 Calculation of the current distribution

For a system of $N$ conductors (plus reference conductor) telegraphers equation can be written in the matrix form

$$\frac{d\mathbf{V}(s)}{ds} + \mathbf{Z}'\mathbf{I}(s) = \mathbf{0} \qquad (1a)$$

$$\frac{d\mathbf{I}(s)}{ds} + \mathbf{Y}'\mathbf{V}(s) = \mathbf{0} \qquad (1b)$$

where $\mathbf{V}(s)$ and $\mathbf{I}(s)$ are the voltage and current vectors and $\mathbf{Z}'$ and $\mathbf{Y}'$ are the square $N \times N$ matrices describing per unit length line parameters. These

two first order differential equations can be transformed into second order equation for the current distribution

$$\frac{d^2\mathbf{I}(s)}{ds^2} - \mathbf{R}'\mathbf{I}(s) = \mathbf{0} \tag{2}$$

where $\mathbf{R}' = \mathbf{Y}'\mathbf{Z}'$. The solution of this equation has the form

$$\mathbf{I}(s) = \mathbf{Z_c}^{-1}\mathbf{S}^{-1}\left[\mathbf{E}^{+}(s)\,\mathbf{a} - \mathbf{E}^{-}(s)\,\mathbf{b}\right] \tag{3}$$

where

$$\mathbf{Z_c} = \mathbf{S}^{-1}\left[\frac{1}{\gamma_i}\right]\mathbf{S}\mathbf{Z}' \tag{4}$$

$$\left[\frac{1}{\gamma_i}\right] = \begin{bmatrix} \frac{1}{\gamma_1} & 0 & \dots & 0 \\ 0 & \frac{1}{\gamma_2} & \dots & 0 \\ \dots & \dots & \dots & \dots \\ 0 & 0 & \dots & \frac{1}{\gamma_n} \end{bmatrix} \tag{5}$$

$$\mathbf{E}^{\pm}(s) = \begin{bmatrix} e^{\mp\gamma_1 s} & 0 & \dots & 0 \\ 0 & e^{\mp\gamma_2 s} & \dots & 0 \\ \dots & \dots & \dots & \dots \\ 0 & 0 & \dots & e^{\mp\gamma_n s} \end{bmatrix} \tag{6}$$

and matrix $\mathbf{S}$ is a diagonalisation matrix of $\mathbf{R}'$, $\gamma_i$ is a propagation constant of the $i$-th mode and vectors $\mathbf{a}$ and $\mathbf{b}$ have to be calculated from the boundary conditions.

### 2.2 Decomposition on elementary dipoles

Due to linearity of Maxwell equations linear extended source (i.e. cable) can be decomposed into collection of short sections and each section can be treated as elementary dipole. If the cable section length $l$ holds the condition [2] $l < \lambda/10$ ($\lambda$ is the wavelength) then one can neglect the current spatial dependency on a dipole. We have in this case the staircase approximation of the current distribution along the cable, and in the net effect the entire structure is replaced by a set of elementary dipoles. The resulting field can be determined as a sum of respectively retarded contributions.

The rigorous approach to field calculation in the presence of a lossy ground requires computation of the so called Sommerfeld integrals [3]. The computation cost of those integrals is prohibitively large and unacceptable in most practical implementations. Fortunately, the finite ground conductivity has in many cases only a small impact on field values and it is acceptable to use approximated method based on perfect soil assumption and method of electrical images.

### 2.3 Field of an elementary dipole

The elementary dipole is characterized by its directional vector $\mathbf{1}_l$, length $l$ that is small compared to all distances of interest, and current $I_0$ constant over dipole. The solution of Maxwell equations in free space for this source configuration has the form [4]

$$\mathbf{E} = -j\frac{\eta I_0 l}{4\pi k}\left\{\left[(kR)^2 - (1+jkR)\right]\mathbf{1}_l - \left[(kR)^2 - 3(1+jkR)\right](\mathbf{1}_l\cdot\mathbf{1}_R)\,\mathbf{1}_R\right\}\frac{e^{-jkR}}{R^3} \tag{7a}$$

$$\mathbf{H} = \frac{I_0 l}{4\pi}(\mathbf{1}_l \times \mathbf{1}_R)(1+jkR)\frac{e^{-jkR}}{R^2} \tag{7b}$$

where $\eta$ is the wave impedance, $R$ distance from the source to observation point, $\mathbf{1}_R$ respective directional vector and $k = 2\pi/\lambda$.

## 3 METHOD VALIDATION

Method validation can be performed by comparing its results with predictions of other methods that implement commonly accepted and verified models or by the comparison with independently conducted computations based on the same mathematical model of the reality. In the following sections we present method validation as a two stage process:

1. comparison with independent multiconductor transmission line analysis code developed by Excem [5]
2. comparison with MOMIC code implementing rigorous full-wave approach to scattering and radiation problems [6]

The mentioned above programs were used for verification of current and field distributions for some canonical examples. All field calculations are performed with perfect ground assumption. Keys for presented plots have the following meaning: *line code* denotes results obtained with the validated program, *Excem code* – results from [5], *MOM code* – results obtained by a rigorous approach to electromagnetic waves radiation based on solution of an integral equation for current distribution with method of moments [6].

### 3.1 Comparison with Excem code

The distribution of sources uniquely determines the electromagnetic field. The effective, nonbalanced current flowing along the multiconductor cable is the field source in our case. The report [5] was chosen as a source of reliable data to validate current distribution along the cable. We considered four pair UTP cable with each pair loaded with $R_0 = 120\ \Omega$ and one pair forced with voltage $V_0 = 2$ V. The cable has length $L = 10$ m and was positioned on height $h = 10$ cm. The current distribution along cable for frequency 2.818 MHz is presented on Fig. 1

### 3.2 Comparison with method of moments

Lets consider transmission line composed by a horizontal conductor over perfectly conducting ground

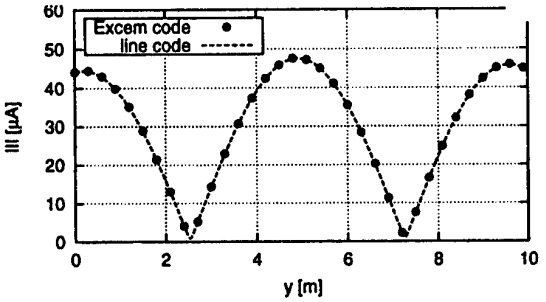



Figure 1: Effective current distribution along multiconductor line.

(see Fig. 2) and grounded at both ends by loading impedances. This structure (together with its elec-

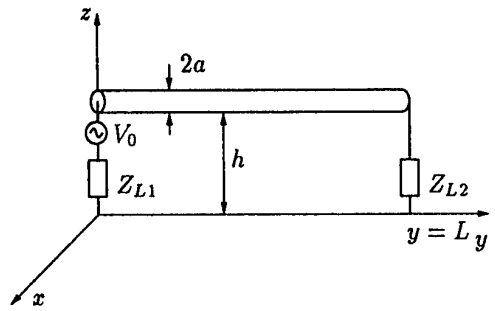



Figure 2: Transmission line geometry, $L = 2$ m, $h = 1$ cm, $a = 1$ mm, $Z_{L1} = Z_{L2} = 50\ \Omega$.

trical image) was analysed by a rigorous approach and with proposed method. The observed quantity was an electric field produced at point $P\,(L, L/2, 2h)$.

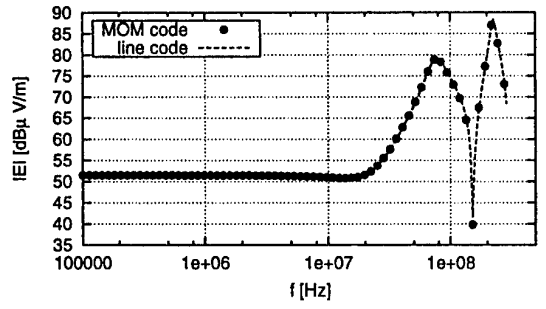



Figure 3: Field at point $P\,(L, L/2, 2h)$.

It is clearly seen from Fig. 3 that antenna mode gives no contribution to the current on the line, and in consequence, radiated fields predicted by the transmission line theory and rigorous approach are the same.

## 4 PARAMETRIC STUDY

A motivation in developing a model is to have the capability to perform parametric studies, in which independent model parameters can be varied in order to gain a global understanding of the phenomenon. We used presented method to investigate the field dependence in the vicinity of the multiconductor transmission line on the following parameters:

- cable type,
- geometrical configuration of the line,
- line forcing.

### 4.1 Calculation setup

The considered line is composed from sections of different length of UTP four pair cables S278 and S298. Each pair is terminated with the resistance 120 Ω. Two cases of line forcing were considered: first pair forced by a sinusoidal voltage of amplitude 2 V, or all pairs forced with the voltage same as previously. This forcing conditions are identified on graphs by keys V1 and V4, respectively. Geometrical configurations further referenced as I-like and U-like are presented on Fig. 4 and Fig. 5. Configura-

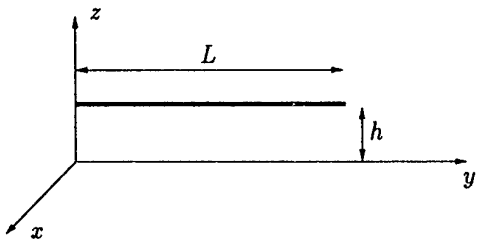



Figure 4: "I-like" geometry.

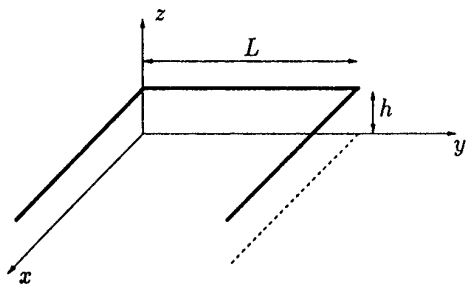



Figure 5: "U-like" geometry.

tions are parametrized by the cable section length $L$ and the height $h$ above ground, which is assumed to be ideal. Observation point was positioned at point P(1m,$L$/2,1m). The calculations were performed for two heights and three lengths.

Table 1: Parameters of calculations

| cable | height | geometry | length | forcing |
|---|---|---|---|---|
| S278 | $h = 15$ cm | I-like | $L = 5$ m | V1 |
| S298 | $h = 1$ m | U-like | $L = 10$ m | V4 |
| | | | $L = 15$ m | |

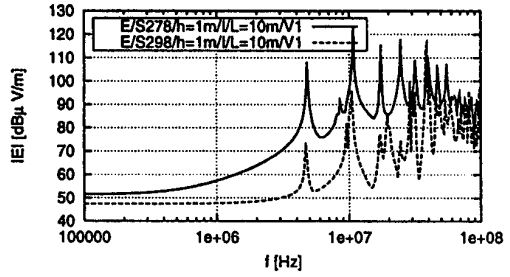



Figure 6: Amplitudes at resonant frequencies.

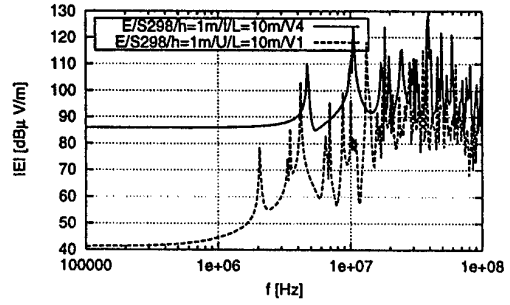



Figure 7: Dependency of resonant frequencies on geometrical configuration.

### 4.2 Discussion

The strength of the field at the resonant frequency strongly depends on cable type but resonant frequency itself does not (see Fig. 6).

The resonant frequencies are determined by geometrical configuration (see Fig. 7) of the system, and it is not possible to design modulation schemes to program them out i.e. make PSD (Power Spectral Density) function small at resonant frequencies. However, it is still possible to design new modulation schemes to avoid resonant frequencies of potential victims, for instance radio amateur receivers.

## 5 CONCLUSION

The proposed method is general and flexible. Virtually, it is capable to analyse any service supported over any cable, unless reliable cable model and PSD function of the transmitted signal are known. The method is also fast as the computation time grows with square of the number of pairs in a cable and linearly with the cable length. Moreover, method is able to analyse not only straight section of the cable, but also handles networks with cable bends.

## REFERENCES

[1] C. R. Paul, *Analysis of Multiconductor Transmission Lines.* New York: John Wiley & Sons, 1994.

[2] W. L. Stutzman and G. A. Thiele, "Antenna Theory and Design" John Wiley & Sons, New York, 1981.

[3] A. Somerfeld, "Uber die ausbreitung der wellen in der drahtlosen telegraphie," Annalen der Physics, Vol. 28, 1909, p. 665.

[4] P. Zawadzki, "Elaboration of software for prediction of signals induced by a lightning discharge on telecommunication cables placed inside buildings," Tech. Rep. NT/LAB/QFE/143, CNET, Lannion, December 1996.

[5] "Comaparaison de l'emission des cablages de telecommunication." Excem doc. no. 98042102A.

[6] R. F. Harrington, "Field Computation by Moment Methods" MacMillan, New York, 1968.

## BIOGRAPHICAL NOTES

PIOTR ZAWADZKI was born on February 26, 1964. He received Ph.D. degree in electronics from the Silesian Technical University in 1998. He is employed therein since 1989. He is involved in research of electromagnetic field numerical modelling.

RABAH TARAFI was born on October 20,1968. He is engineer of the Ecole Nationale d'Ingenieurs de Brest (ENIB). In 1998, he received the title of Docteur of the University of Brest. He joined the National Research Center of France Telecom in 1998 where he is in charge of studies relating to EMC of France Telecom telecommunication network.

OLIVIER DAGUILLON was born on November 23, 1967. In 1995, he received the title of Docteur of the University of Clermont-Ferrand. He joined the National Research Center of France Telecom in 1995 where he is in charge of studies relating to electric and electromagnetic stresses on telecommunication network.

AHMED ZEDDAM was born on April 9, 1952 . He received Ph. D. degree in electromagnetics from the University of Lille. From 1979 to 1982, he was an assistant professor of electronics at Lille University. Since 1982, he has been employed at the National Research Center of France Telecom in Lannion where he is engaged research in the area of electromagnetic compatibility. Dr Zeddam is the author and coauthor of about 60 scientific papers, published in reviewed journals and international conferences.

EMC 2000 INTERNATIONAL WROCŁAW SYMPOSIUM ON ELECTROMAGNETIC COMPATIBILITY

# EMC ANALYSIS FOR FREQUENCIES ABOVE 1GHZ IN NAVAL SHIPBUILDING

Harm-Friedrich Harms, Thyssen Nordseewerke Emden,
Elchstr. 77, D-26603 Aurich, Germany, fax: + 89 2443 47194, e-mail: HarmsHF@nwn.de

*It is very important for operating naval ships to know the distribution of electromagnetic fields on the upper deck. This knowledge is needed for a proper work of the communication system as well as for electromagnetic sensors, radar systems, weapon systems etc. Furthermore it is to guarantee the personal safety and the safety of ammunition against electromagnetic fields. The Method of Moments (MoM) is a useful way for field analysis on naval ships within frequencies up to HF region. Starting at UHF region the Uniform Geometrical Theory of Diffraction (UTD) is an appropriate method. How to operate UTD is presented in this paper.*

## 1 INTRODUCTION

The analysis of electromagnetic fields is mainly divided into two frequency ranges, the classic communication frequencies up to 30 MHz and a region starting about 1 GHz in majority radar systems. The lower frequency analysis can be done by Method of Moments (MoM) [4, 1, 6]. For the higher region starting with frequencies about 1 GHz the Uniform Geometrical Theory of Diffraction (UTD) [5, 7] is a very efficient tool. One important precondition of UTD is that the structures of the investigated arrangements have to be greater than a wave length ($\lambda$). Also they must have a good conductivity. These conditions are fundamentally fulfilled for a ship. Apart from a direct incident field UTD considers field components which are reflected and diffracted. Additionally parts caused by creepy waves and multiple scattered field components are included [7].

Some extra problems occur by using UTD for field analysis on a naval ship. Most of the antenna systems in the frequency region above 1 GHz have a large gain. The main lobe has multiple directions for different modes. So how to describe the sources of the electromagnetic fields? What kind of model can be used for the superstructure of the ship? A useful representation of the field sink, the equipment which might be disturbed by the fields, has to be found.

## 2 EMC ANALYSIS

EMC work for systems like naval ships and submarines starts with the collection of the data of the equipment and subsystems. Then the sources and the sinks of electromagnetic influences (EMI) are ordered into a column and a line which build up a coupling matrix. The elements of the matrix represent combinations of sources of disturbance and sinks of disturbance.

| sink of dist. / source of dist. | ... | sink 2 | ... | sink 4 | ... |
|---|---|---|---|---|---|
| ... | | | | | |
| source 2 | | − | | × | |
| ... | | | | | |
| source 4 | | × | | ⊗ | |

Table 1: Part of the coupling matrix of a system with the sinks and sources of disturbance (dist.).

Each combination has to be regarded. Using the experience of other projects one is able to considerably reduce the combinations which have to be analysed. These combinations are marked with a minus (−) (Tab. 1 sink2, source 2). Combinations which have to be observed furthermore are marked with a × (Tab.1 sink 2, source 4). If the result of the analysis delivers that there is still an Electromagnetic Interference (EMI) the sign remains a × (Tab.1 sink 4, source 2). Otherwise a ⊗ indicates that the result of the analysis delivers no EMI (Tab.1 sink 4, source 4).

### 2.1 Field Source Modelling

In practical operation there is less data of an antenna system available for the EMC specialist of the ship yard to do a field analysis. Perhaps the system is still under development, maybe the (more detailed) data is secret. Usually there is a specification describing only the Isotropic Radiated Power (EIRP) and the attenuation of the side lobe.

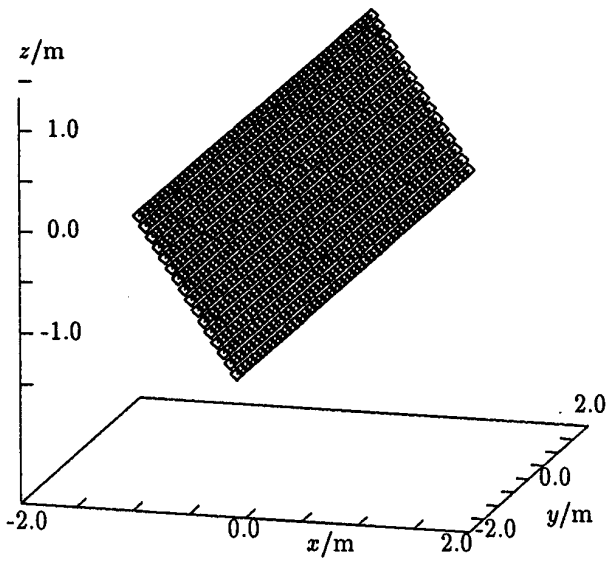



Fig. 1: The aft phase array radar antenna of the ship. The arrangement of the point sources of the antenna, its orientation and dimensions are shown.

Additionally it is not possible for the EMC analysis to observe all realizable directions of the main lobe. So in a first step the source is modelled by an isotropic radiator with the EIRP of the antenna system. It is a true "worst case" estimation of the fields on the ship deck caused by the field source. This model represents the main lobe of the antenna illuminating the complete upper deck structures.

If the calculated field strength is lower than the susceptibility limit of the field sink, work is already done. Providing this is not the case the question has

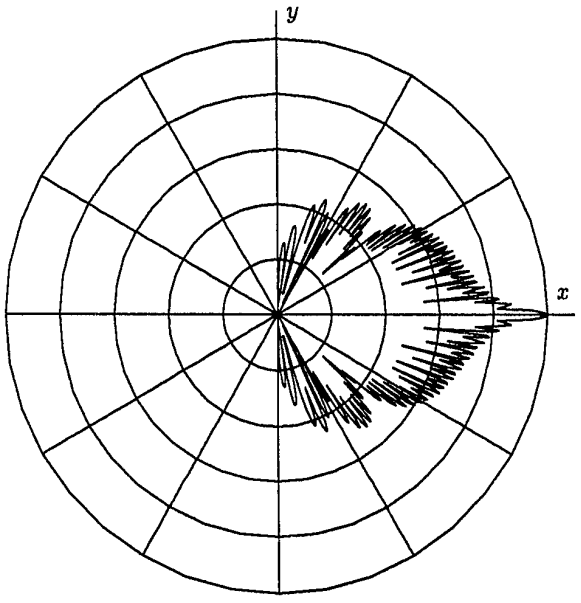



Fig. 2: Horizontal antenna diagram of the array antenna for horizon main lobe with a range of 100 dB.

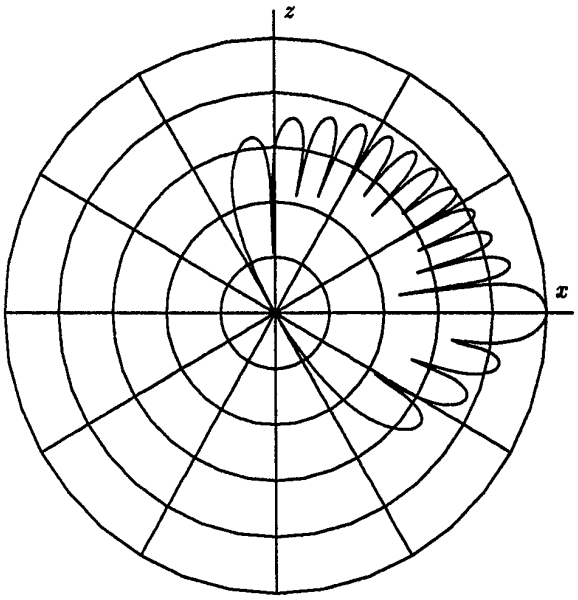



Fig. 3: Vertical antenna diagram of the array antenna for horizon main lobe with a range of 100 dB.

to be answered if one can assume that the main lobe will never hit the upper deck. Usually for functional reasons there is no need to illuminate these structures by the main lobe. Then the field value delivered by the analysis can be reduced by the side lobe attenuation.

Fig. 1 shows the aft radar antenna face of the ship. The horizon diagram is shown in Fig. 2, Fig. 3 represents the vertical diagram of this antenna for main lobe with horizon direction. The range of the diagrams is 100 dB. It can be seen that according to Fig. 3 a side lobe attenuation of about 12 dB can be assumed.

Perhaps the field strength for the field sink is still too high. So more detailed information about the behaviour of the transmitting antenna can help to find a better description for its radiation to do an optimized new analysis [3]. If there is no more additional information measures have to be taken to eliminate this EMI.

## 2.2 Modelling of Ship Structure

The ship which has to be investigated is shown in Fig. 4. Using MoM for the HF band the structure of the ship has to be described by patches. These patches must be small in terms of the wave length. To use UTD for field analysis the structures of the model have to be large compared with the wave length. The surface of the ship can be described by a polyhedron (Fig. 5). All parts of the ship above water-line are modelled. The surface of the water is also included and represented by an infinite plane.

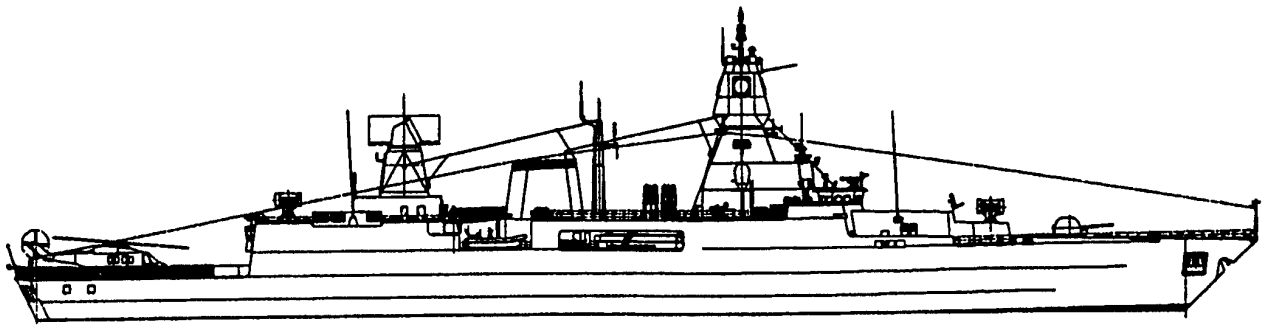


Fig. 4: Side view of the ship with the antenna systems for communication and radar. The radiation of antennas up to **HF** region is analysed with the Method of Moments. For frequencies starting at **UHF** region Uniform Geometric Theory of Diffraction is used.

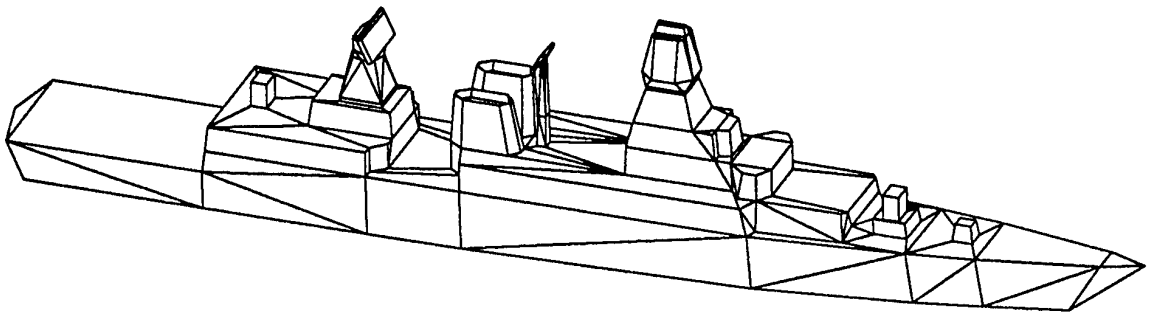


Fig. 5: Model of the ship for **EMC** analysis in frequency region above 1 GHz with **UTD**. The model consists in approximately 400 flat surface elements, triangles and quadrangles.

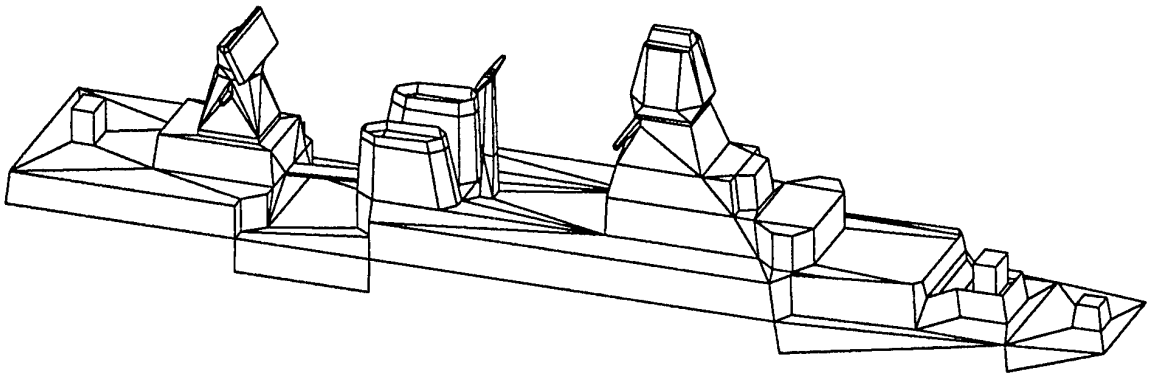


Fig. 6: Optimized model of the ship with additional components of the superstructure for **EMC** analysis in frequency region above 1 GHz. The structure is described in more details. Therfore again about 400 elements have to be used.

The polyhedron model consists in triangles and quadrangles. Also patches limited by $n$ straight lines can be used [2]. But attention has to be paid that theses patches are plain. Their dimensions have to be large in terms of the wave length. To consider all the **UTD** scattering processes with important field contribution it is useful to regard reflections, diffractions and parts caused by creepy waves. Multiple diffracted fields deliver less field strength but need much more time for the calculation. So it is useful to consider only double scattering processes containing at least one reflection.

The model of the ship according to Fig. 5 can be optimized to save time. The surface of the sea has no influence on the field distribution at the superstructure of the ship. The helicopter deck and other parts do not influence the field distribution at the investigated points. So they are removed (Fig. 6).

## 2.3 Describing of Field Sinks

The valid field strength for the EMC susceptibility of an equipment is measured in the test range in absence of the equipment. Therefore the field calculations on the ship are also done without modelling the equipment. So a plain model of the ship is used (Fig. 6) for the EMC analysis. The electric field has to be calculated at the most susceptible part of the subsystem, mainly the antenna. To consider the dimensions of the equipment field calculations should not be done for a single point. Therefore fields are calculated in a field region. Another aspect should

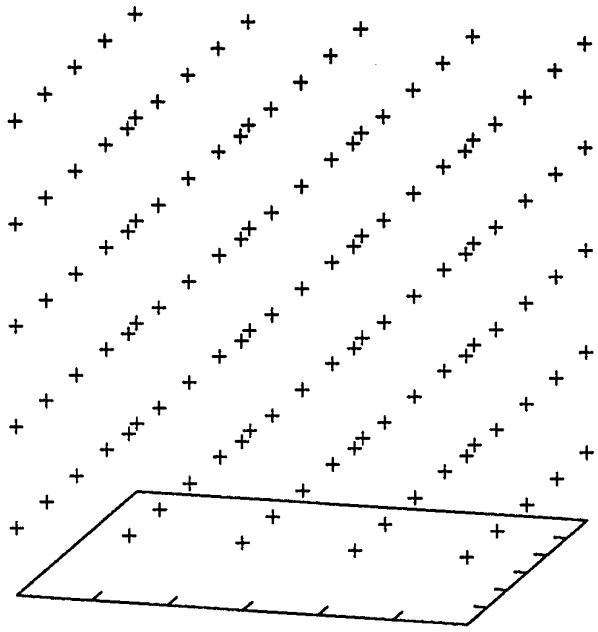


Fig. 7: Field region with $5 \times 5 \times 5$ test points (+) in a cube with the dimensions of $\lambda/2 \times \lambda/2 \times \lambda/2$.

be observed. It is possible that the field distribution is caused by resonant effects. If a single field point is chosen it might happen that the field value is much too low. A cubic field region with the dimension of a half wave length is chosen to regard all of these items (Fig. 7). The maximum field strength in the cube is the relevant value to compare with the susceptibility of the equipment.

# 3 Examples

In the following two examples are presented. They show the advantages of modern field analysis tools for EMC analysis in naval shipbuilding in the frequency region above 1 GHz.

## 3.1 Field Sink on a Mast

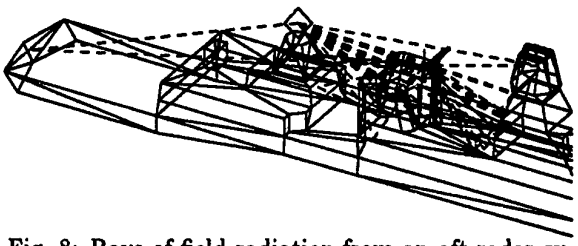


Fig. 8: Rays of field radiation from an aft radar system into an antenna on the middle mast.

Fig. 8 shows the rays between an aft radar antenna of the ship and a field sink on a mast in the middle of the ship. Direct field propagation, reflections and diffractions are regarded. Additionally the following double scattered fields are included into the analysis: reflection – reflection, reflection – diffraction, diffraction – reflection. Only one test point is selected to represent the field sink. For this simple example already 25 rays deliver contributions to the field at the position of the field sink.

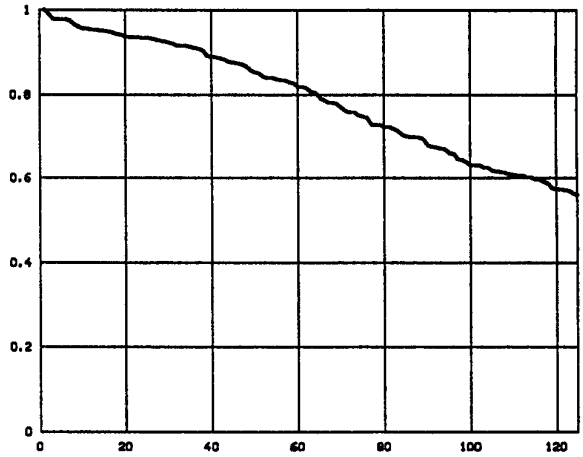



Fig. 9: Field diagram of the field radiation from an aft radar system into an antenna on the middle mast. The results for the test points are scaled and sorted according to the height of the values.

Fig. 9 shows the diagram generated by the analysis tool. It is already stated, that a field region with test points is chosen to represent the field sink. The field strength in the test points is arranged by falling amplitudes. The maximum value is relevant for the susceptibility level of the field sink. The minimum value is about 56% of this field and significantly lower than the maximum.

## 3.2 Field Sink on the Bridge Roof

The rays between the aft radar antenna and a field sink at the roof of the bridge is shown in Fig. 10. Direct field, single scattered fields and double scattered fields are considered. Looking at the two dimensional drawings of the ship, nobody would expect that there

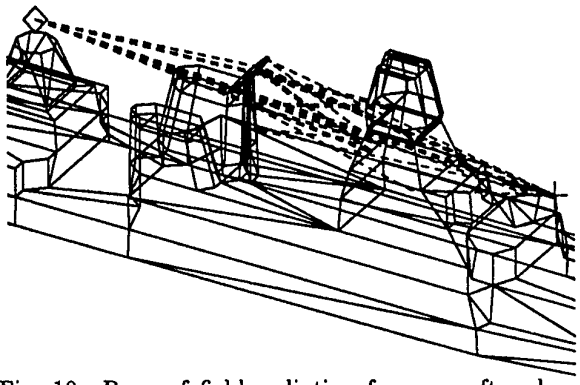


Fig. 10: Rays of field radiation from an aft radar system into an antenna on the roof of the bridge.

might be a a direct ray between the radar antenna and the field sink. But the numeric calculation shows that there are 17 different paths from the source to the sink: One direct ray, 5 rays representing single scattered fields and 11 rays caused by double scattered processes (Fig. 10).

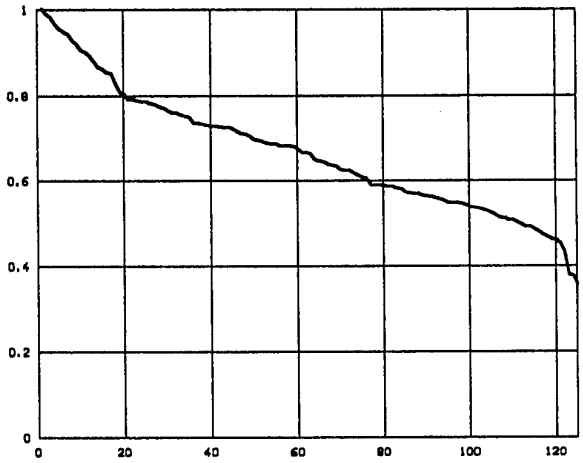



Fig. 11: Field diagram of the field radiation from an aft radar system into an antenna on the roof of the bridge. The results for the test points are scaled and sorted according to the height of the values.

The corresponding field diagram is shown in Fig. 11. The minimum value is 36% of the maximum value. So a field calculation in only one point could cause a field strength which might be only about one third of the maximum value at the position of the real field sink.

## 4 Conclusion

The UTD is an adequate method for field calculations in the frequency region starting about 1 GHz. So UTD is a useful tool for a EMC analysis of a ship's superstructure. Therefore suitable descriptions for the radiation of the antennas are presented. The structure of the ship has to be build up by a polyhedron. For the source of disturbance a field region has to be defined. Using the results of this calculation one is able to evaluate the EMC of an equipment on the superstructure of a ship.

## References

[1] H.-D. Brüns. *Pulserregte elektromagnetische Vorgänge in dreidimensionalen Stabstrukturen.* PhD thesis, Universität der Bundeswehr, Hamburg, Germany, 1985.

[2] Harm-Friedrich Harms. *Hybridmethode - Erweiterung der Momentenmethode um das Verfahren der Einheitlichen Geometrischen Beugungstheorie.* PhD thesis, Technische Universität Hamburg-Harburg, 1996. Shaker Verlag GmbH, Aachen, Germany.

[3] Harm-Friedrich Harms. Phased Array Radar Antenna – Modelling for EMC Analysis . In *Symposium Record of 1999 International Symposium on EMC in Magdeburg*, pages 343–348, 1999.

[4] R. F. Harrington. *Field Computation by Moment Methods.* The Macmillan Company, New York, 1968.

[5] J. B. Keller. Geometrical Theory of Diffraction. *Journal of the Optical Society of America*, 52:116–130, 1962.

[6] T. Mader and H. Singer. Numerical Solution of the EFIE Using Arbitrarily-Shaped Quadrangular and Triangular Elements. In *7th Annual Review of Progress in Applied Computational Electromagnetics, Monterey, CA*, pages 292–303, March 1991.

[7] P. H. Pathak, Burnside, W. D., and R. J. Marhefka. A Uniform GTD Analysis of the Diffraction of Electromagnetic Waves by a Smooth Convex Surface. *IEEE Transactions on Antennas and Propagation*, 28(5):631–642, September 1980.

## Biographical Note

Harm-Friedrich Harms was born in Aurich, Germany on January 11, 1960. In 1979 he finished his vocational education (Funkelektroniker, radio engineer). He received the Dipl.-Ing. (MSEE) degree from the University of Hanover in 1990 and the Dr.-Ing. (PhD EE) degree from the Technical University Hamburg-Harburg in 1996. He wrote his doctor thesis about the Hybrid Method - The Combination of MoM and UTD. Since 1996 he has been working for the Thyssen Nordseewerke Emden (shipyard) in the naval department. His field of work is the Electromagnetic Compatibility on ships and submarines.

**EMC 2000** INTERNATIONAL WROCŁAW SYMPOSIUM ON ELECTROMAGNETIC COMPATIBILITY

# Calculation of Electromagnetically and Thermally Coupled Fields in Real Soil Decontamination

M. Heidemann, H. Garbe
University of Hanover
Institut für Grundlagen der Elektrotechnik
und Messtechnik
Appelstraße 9A, D-30167 Hannover, Germany
e-mail: *heideman@geml.uni-hannover.de*
fax: +49-(0)511-762-3917

R. Kebel
DaimlerChrysler Aerospace AG
Military Aircraft
Hünefeldstraße 1-5, D-28199 Bremen, Germany
e-mail: *Robert.Kebel@m.dasa.de*

***Abstract:*** *One application of electromagnetic fields is to purify contaminated soil by vaporizing liquid pollutions via dielectric heating. Depending on the relevant material, the interaction between thermal and electromagnetic fields is of considerable influence on the temperature. A new procedure for the coupled calculation of electromagnetic and thermal fields in 3-dimensional objects is presented, using the FEM (Finite Element Method). The procedure is based on the considerable difference between the time constants of the field propagation. By alternately calculating the electromagnetic and the thermal field the interaction of the fields is taken into account. Therefore the temperature dependency of the electromagnetic material properties must be known. For this reason a new test setup and a time-domain measurement method have been developed for measuring permittivity and conductivity. Simulation results visualize the difference between electromagnetically and thermally coupled and uncoupled field calculation.*

## 1 Introduction

For determination of a required energy feed via electromagnetic fields or for the estimation of a possible thermal hazard, the calculation of electromagnetically and thermally coupled fields is of rapidly growing importance. The soil decontamination is one of several applications for this principle. Well-known are also dielectric heating in the microwave range, diathermy as medical therapy or absorbtion of electromagnetic fields.

It can be said that, in the majority of cases, temperature dependencies of electromagnetic material properties are rarely taken into account or the resulting reaction on applied electromagnetic fields is being neglected.

This paper shows a solution for the determination of interacting thermal and electromagnetic fields (Fig. 1). The origins of power loss in real dielectric material are the polarization effects, caused by the electric field and described by $\varepsilon_r''$, and additional the dielectric conductivity $\sigma_d$. For harmonic excitation both, dielectric loss and conduction loss, can be considered together in an effective conductivity $\sigma_{eff}$. The power loss is described by the dissipation factor $\tan\delta$:

$$\underline{\varepsilon} = \varepsilon_0(\varepsilon_r' - j\varepsilon_r''), \quad \sigma_{eff} = \sigma_d + \omega\varepsilon_0\varepsilon_r'', \quad \tan\delta = \frac{\sigma_{eff}}{\omega\varepsilon_0\varepsilon_r'}$$

where $\varepsilon_r'$ and $\varepsilon_r''$ represent the real and imaginary part of the complex relative permittivity $\underline{\varepsilon}_r$. $\varepsilon_0$ is the dielectric constant for free space and $\omega$ the angular frequency. Inside an infinitesimal small volume the field strength is constant. The power loss density or heat generation rate $p$ is given by:

$$p(\vec{x},t,T) = \frac{1}{2}\cdot\sigma_{eff}(T)\cdot\left|\vec{E}(\vec{x},t)\right|^2 \qquad (1)$$

where $\vec{E}$ represents the electric field strength, $T$ the temperature, $t$ the time and $\vec{x}$ the location. Calculation examples for dominant heat conduction are given in section 4. Convection and radiation on the objects surface are boundary conditions for Fourier's law

$$\vec{q}(\vec{x},t,T) = -\lambda_{th}(\vec{x},T)\cdot\nabla T(\vec{x},t) \qquad (2)$$

where $\vec{q}$ and $\lambda_{th}$ represents the total heat flux vector and the thermal heat conductivity respectively. Thus, the law of heat conduction for a resting, isotropic, incompressible medium in a closed system is

$$\rho(T)\cdot c_p(T)\cdot\frac{\partial T}{\partial t} = \nabla\left[\lambda_{th}(T)\cdot\nabla T\right] + p(\vec{x},t,T) \qquad (3)$$

($\rho$: density, $c_p$: specific heat). So, the differential equations of the electromagnetic and the thermal field are coupled by the power loss density $p$ and the temperature dependency of electromagnetic material parameters like $\sigma_{eff}$ and $\varepsilon_r'$.

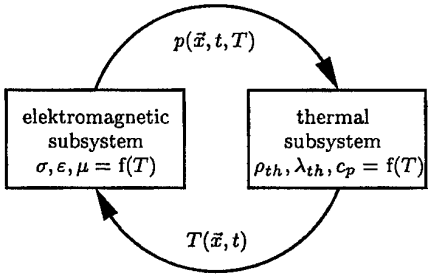



Figure 1: electromagnetic-thermal interaction

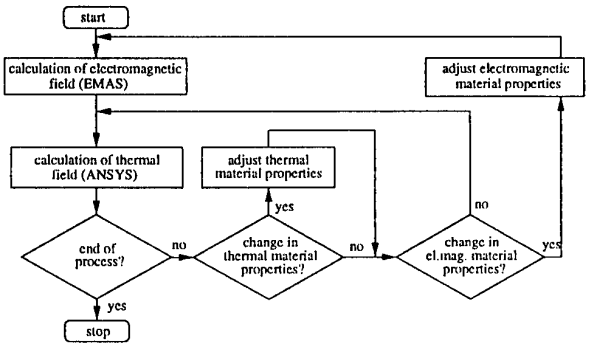



Figure 2: Flow chart showing algorithm

## 2 Coupled Field Calculation

This paper presents a procedure where the interaction of the fields is taken into account by alternating calculation of electromagnetic and thermal field (Fig. 2)[1]. The method is based on the considerable difference between the time constants of electromagnetic and thermal field propagation.
Because of local heat generation and temperature dependent material properties, the program must be able to change these properties locally. Therefore the Finite Element Method (FEM) is applied to a 3-dimensional model. The electromagnetic field is calculated with the help of the program EMAS and the temperature field by means of ANSYS (Fig. 2). The calculated electromagnetic field is assumed to be constant for a small time intervall $\Delta t$. The power loss density of the finite elements in EMAS is interpreted as heat generation rate and introduced into the temperature field calculation. The temperature distribution for $t + \Delta t$ is calculated, the material properties of the elements are adapted in accordance with element temperature and the procedure repeats until the end of the heating process is reached. The calculation procedure can be applied to models with any temperature- and frequency-dependency of the electromagnetic and thermal parameters.

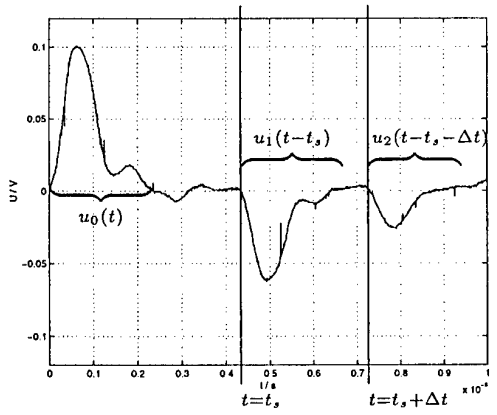



Figure 3: Measuring pulse $u_0(t)$, first and second reflection ($u_1(t)$, $u_2(t)$) for $l = 50\,\text{mm}$ water level (20°C)

## 3 Measurement of Permittivity

The temperature dependencies of the electromagnetic material properties must be known, but they are generally not given in literature. For this reason, a test setup has been developed for measuring $\epsilon'_r$ and $\sigma_{eff}$. Well known measurement procedures for permittivity use the frequency-domain and require a network analyzer. The complex functions used to analyze the measurement yield to ambiguous results.

This new measurement is based on time domain signals and therefore uses an oscilloscope. The measurement setup consists of an expanded, short-circuited, coaxial transmission line – similar to a TEM cell – (Fig. 4), which is filled with a material probe and used like a TDR (time domain reflectometer)[2]. A fast rising pulse passes through the feeding section to the conical wave expansion section. The temperature dependency of permittivity and conductivity is determined by temperature measurement in the electric field, using a fiber optical thermometer. The measurement apparatus is warmed in a climate cabinet up to the constant measurement temperature.
Fig. 3a shows a typical measurement signal, in this case for pure water at a load length of $l_1 = 50\,\text{mm}$ (cp. Fig. 4). The pulse $u_0(t)$ is partially reflected at the planar material surface ($u_1(t)$). The transmitted wave propagates through the dielectric to the planar short circuit termination at the end of the line and is reflected there. The measurement is performed for the load lengths $l_1$ and $l_2 < l_1$. The permittivity is determined with the Fourier transformations of the reflections $u_{2,l_1}(t)$ and $u_{2,l_2}(t)$ [2]:

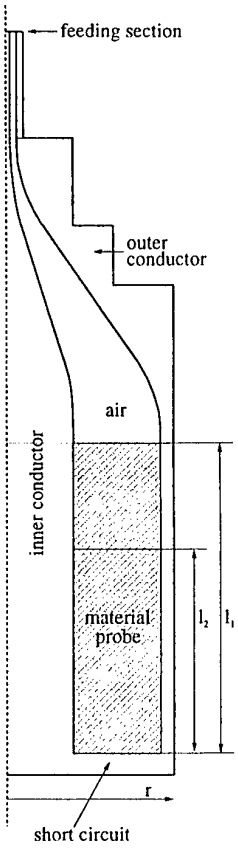
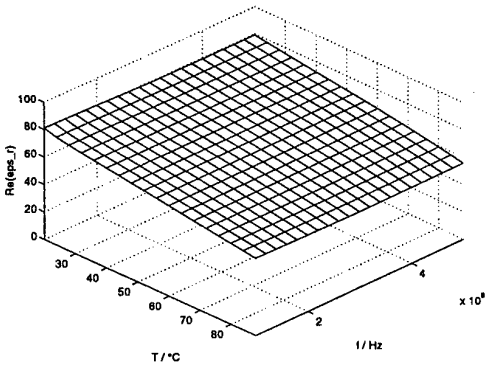



Figure 4: short-circuited coaxial transmission line

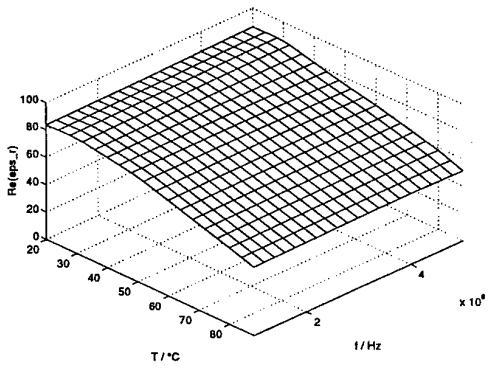
$$u_{2,l_1}(t) \quad \circ\!\!-\!\!\bullet \quad U_{2,l_1}(\omega)$$
$$u_{2,l_2}(t) \quad \circ\!\!-\!\!\bullet \quad U_{2,l_1}(\omega)$$

Both measurement signals have the same excitation pulse and the same reflection at the material surface, so:

$$\frac{U_{2,l_1}(\omega)}{U_{2,l_2}(\omega)} = e^{-\jmath k_0 (l_1 - l_2)\left(\sqrt{\epsilon'_r - \jmath \frac{\sigma_{eff}}{\epsilon_0}} - 1\right)} \qquad (4)$$

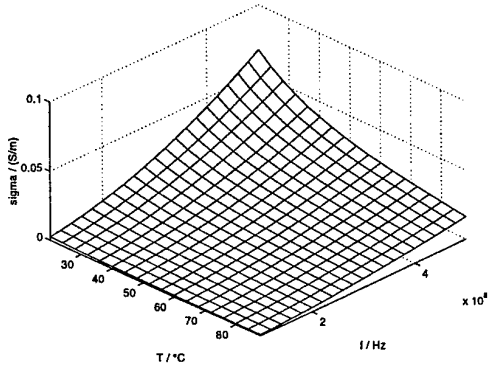



a) Data from [3]

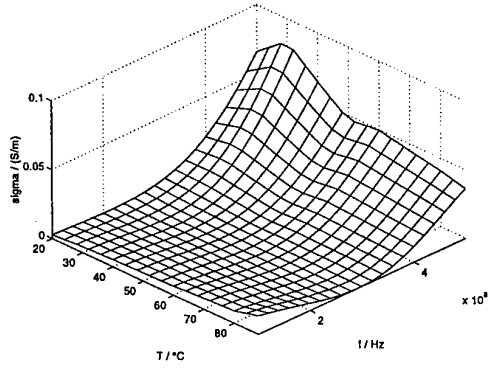



b) Measurement data

Figure 5: water: real part $\varepsilon'_r$ of relative permittivity $\underline{\varepsilon}_r$, depending on temperature and frequency




c) Data from [3]




d) Measurement data

Figure 6: water: effective conductivity $\sigma_{eff}$, depending on temperature and frequency

$k_0 = \omega/c_0$, where $c_0$ represents the speed of light. Eq. 4 yields after a rearrangement to

$$\varepsilon'_r - \jmath \frac{\sigma_{eff}}{\varepsilon_0} = \left[ \frac{\jmath \ln\left(\frac{U_{2,l1}(\omega)}{U_{2,l2}(\omega)}\right)}{k_0 (l_1 - l_2)} + 1 \right]^2 \qquad (5)$$

The periodicity of the natural logarithm must be taken into account. Therefore the wave velocity

$$|c| = \left| \frac{1}{\sqrt{\mu_0 \varepsilon_0 \left(\varepsilon'_r - \jmath \frac{\sigma_{eff}}{\varepsilon_0}\right)}} \right| \quad , \quad \mu_r = 1 \qquad (6)$$

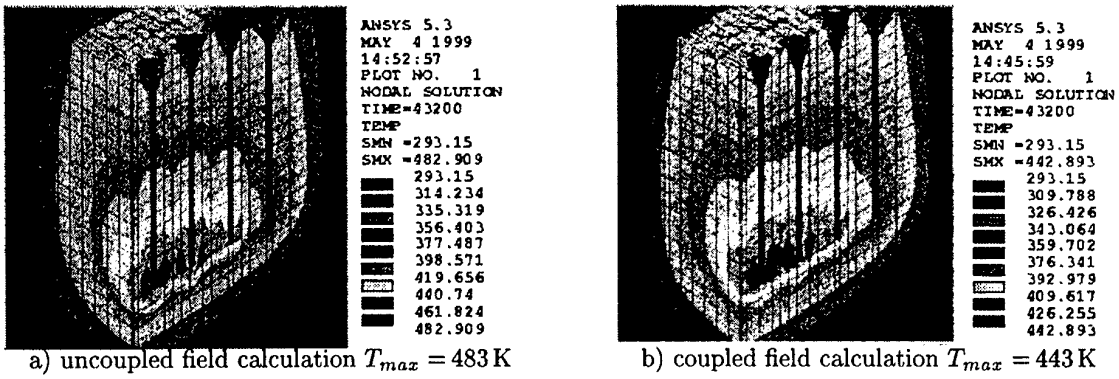
must be in the range of $2l/\Delta t$ (cp. $\Delta t$ in Fig. 3).

This method includes several advantages. The influence of the measurement setup, e.g. losses in the aluminium, is the same in both measurements. So they cancel out in Eq. 4. In addition, Fresnel losses or the excitation of higher order modes need not be considered [2]. Ambiguities are excluded in opposition to frequency-domain pocedures. Also heterogen materials can be tested. Good correspondence of measurement data and tabulated data is found for $\varepsilon'_r$ [3] and also for $\sigma_{eff}$ (Fig. 5,6).

## 4 Electromagnetic Soil Decontamination

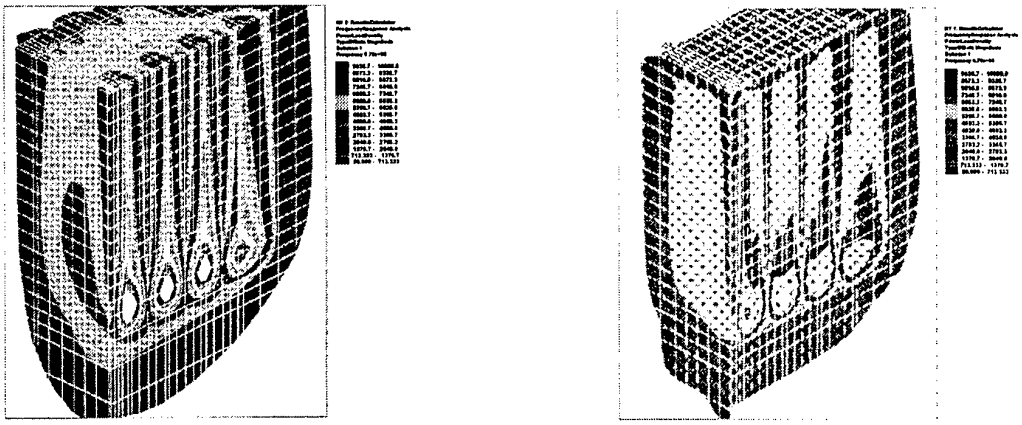
For electromagnetic soil decontamination, the soil is dielectrically heated via electrodes (Fig. 4). For reasons of symmetry the magnetic field is normal to the cut surfaces A and B in Fig. 4. So, the calculation model is reduced to a quarter of the whole geometry. The soil data used is the same as sand with 6 %vol water, where the water is the electrically relevant material. The simulation uses current-excitation at a frequency of $f = 6.78\,\mathrm{MHz}$. Due to $\sigma_{eff}$ (Fig.6) the power loss density decreases during the heating process from 20.1 kW at $t = 0\,\mathrm{s}$ within 6 hours to 18.5 kW ($\widehat{=}\,92\,\%$) and after 12 hours to 16.3 kW ($\widehat{=}\,81\,\%$). Apart from that, the power loss at a chosen point depends on the local loss angle. The ratio of apparent power $Q$ to active loss $P$ changes from 1 ($t = 0\,\mathrm{h}$) to 3.73 ($t = 12\,\mathrm{h}$) in the maximum. The comparison of coupled to uncoupled simulation results leads to a temperature difference of 40 K ($\widehat{=}\,26.7\,\%$) after 12 h of heating (Fig. 7).

The uncoupled electromagnetic field calculation for this setup has been verified with the help of the simulation tool CONCEPT, based on the moments method (MoM). There is a good agreement between the MoM simulation results and the results of the uncoupled electromagnetic FEM simulation (Fig. 9).




a) uncoupled field calculation $T_{max} = 483\,\mathrm{K}$ b) coupled field calculation $T_{max} = 443\,\mathrm{K}$

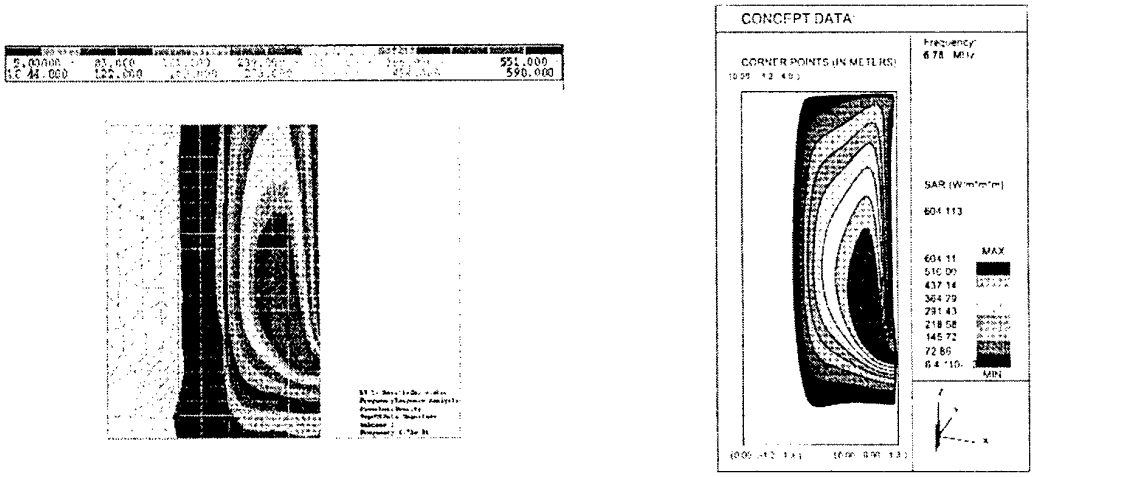
Figure 7: Electrode setup for soil decontamination: temperature distributions after 12 h at $P_{t=0} = 20\,\mathrm{kW}$, $T_{t=0} = 293\,\mathrm{K}$. Difference of temperature changes: 26.7 %



a) uncoupled field calculation, $p(t = 0\,\mathrm{h}) = p_0 = const$, $p_{max} \approx 11\,\mathrm{kW/m^3}$

b) coupled field calculation, $p(t = 12\,\mathrm{h})$, $p_{max}(t = 12\,\mathrm{h}) \approx 9\,\mathrm{kW/m^3}$

Figure 8: Electrode setup for soil decontamination: local power loss density for $P_{t=0} = 20\,\mathrm{kW}$, $T_{t=0} = 293\,\mathrm{K}$. Difference of max. power loss density after 12 h: 22 %




a) Finite Element Method (EMAS) b) Method of Moments (CONCEPT)

Figure 9: Power loss density for uncoupled field calculation. Front view of electrode setup.

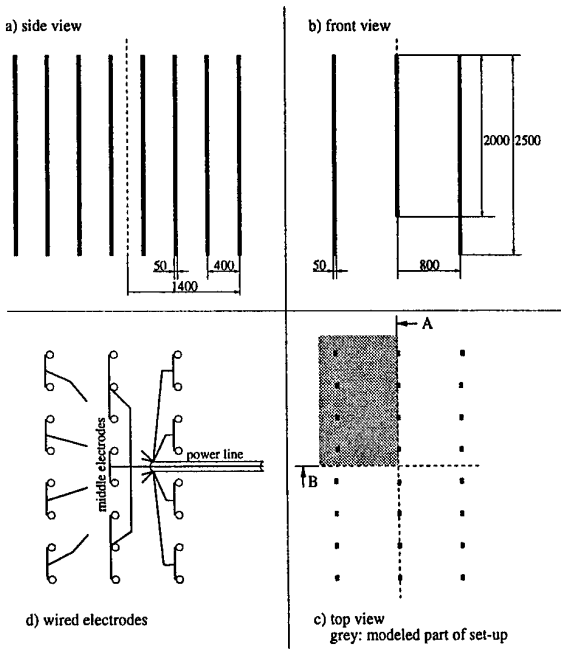



Figure 10: Electrode setup for soil decontamination (measures in mm)

## 5 Conclusion

The interaction between electromagnetic and thermal field can have considerable influence on results of a process. Depending on the material properties the interaction must not be neglected in many cases of dielectric heating. The relevant material properties permittivity and conductivity can easily be determined with the help of the described measurement setup and procedure. A simulation tool was presented which takes interactions of the fields into account. As a result dielectric heating for the purpose of decontaminating soils needs much more energy than calculated with the uncoupled method.

## Acknowledgement

The authors would like to thank the Wehrwissenschaftliche Institut für Schutztechnologien (WIS), Munster, Germany, for supporting this work.

## References

[1] Dibben, D.C.; Metaxas, A.C.: *Finite Element Analysis of Multi-Mode Cavities with coupled Thermal and Electromagnetic Fields*, International Microwave Power Institute Symposium, Chicago, July 1994

[2] Farr, E.G.; Frost, C.A.: *Time Domain Measurement of the Dielectric properties of Water in a Coaxial Test Fixture*, Measurement Notes, Note 49, 1996

[3] v. Hippel, A.R.: *Dielectric Materials and Applications*, Wiley, New York, 1954

[4] Kebel, R.: *Elektromagnetisch-Thermisch gekoppelte Feldberechnung für Erdböden* (Electromagnetic-Thermal coupled Field Calculation for Soil), Universität Hannover, Fachbereich Elektrotechnik, Dissertation (Ph.D. Thesis), 1999

## Biographical Notes



**Markus Heidemann** was born in Bielefeld, Germany, in September 1971. He received the Dipl.-Ing. degree in electrical engineering from the University of Hanover, Germany, in March 1999.
On April 1999 he joined the Institut für Grundlagen der Elektrotechnik und Messtechnik at the University of Hanover as research assistant. He works on the field of TEM-waveguides including the measurement and calculation of electromagnetic fields. Markus Heidemann is a member of VDI and IEEE.



**Heyno Garbe** was born in Germany in 1955. He received his Dipl.-Ing. and Dr.-Ing. from the University of the Federal Armed Forces, Hamburg, Germany, in 1978 and 1986 respectively. From 1974 to 1986 he served as an officer in the German Army. From 1986 to 1991 he was with the Asea Brown Boveri Research Center in Baden, Switzerland. There he was involved in research activities on TEM-waveguides, the numerical calculation of electromagnetic fields, and other EMC related topics. From 1991 to 1992 he was the Research Manager for EMC Baden Ltd. Since 1992 he has been with the University of Hannover where he holds a professorship in the department of electrical engineering and information technology. In addition to lecturing on basic electrical engineering, measurement technology, and EMC, he has developed an active research program related to electromagetic field effect modelling, testing, and measurement as applied to EMC. Prof. Garbe is also very active in several EMC related national and international standardisation committees. He is a Senior Member of IEEE and member of URSI Comm. E. Prof. Garbe is an associate editor of the IEEE EMC Transactions.



**Robert Kebel** was born in Hanover on December 6, 1967. He received his Dipl.-Ing. and Dr.-Ing. degree in electrical engineering from the University of Hanover in 1995 and 1999 respectively. From 1995 to 1998 Dr. Kebel worked as research associate at the Institute of Basic Research in Electrical Engineering and Measurement Techniques at the University of Hanover, where he was in charge of the "Absorption of Electrical Energy" project. During this time, he prepared an EMC test laboratory for its accreditation. 1999 he joined DaimlerChrysler Aerospace AG as systems engineer where he works in the field of signature technology in Bremen. Robert Kebel is a member of IEEE and VDE.

EMC 2000 INTERNATIONAL WROCŁAW SYMPOSIUM ON ELECTROMAGNETIC COMPATIBILITY

# A STATISTICAL APPROACH FOR COMPUTATIONAL ELECTROMAGNETICS.

C.J. Macdonald-Bradley, P.A. Jennings, R.J. Ball, P.H. Lever & S.D. Baker
Warwick Manufacturing Group,
University of Warwick,
COVENTRY, UK. CV4 7AL.

Contact: chris.mb@warwick.ac.uk (tel: +44 24 7652 8445, fax: +44 24 7652 4783)

*Causes of uncertainties associated with computational electromagnetic modelling are identified and discussed. The paper aims to show how to quantify these uncertainties and uses a case study that examines the variations on induced wire current, as a result of small wire-position changes, to demonstrate the methods introduced. Using statistical methods it is shown that, in this example, current variations of 100% can be expected as a result of these small changes.*

## 1. INTRODUCTION

This paper discusses methods to identify the uncertainties associated with simulated results for computational electromagnetics (CEM). For CEM, uncertainty between the results of computational simulation and physical data comes from both the numerical methods being used in the simulation *and* from critical variations between the computer model of the physical set-up and the physical experiment itself.

These two sources of uncertainty are inter-twined, and this makes it difficult to accurately determine the suitability of a CEM model, for particular applications, when comparing it with experimental data. The methods in this paper describe a process whereby any two sets of results can be compared. These sets of results may be derived from changes to the model *or* changes to the modelling process. By further investigating each of these aspects using such methods, it is suggested that any CEM results can be more fully stated by including limits of uncertainty and levels of confidence. The case example given analyses results from changes to a model, but the same process can be applied equally to results from changes to the modelling process.

This work has been done as part of a study into the effects of interfering radiation on the wiring of passenger cars [1].

[For the purposes of this paper, the Finite Difference Time Domain (FDTD) method has been used to generate numerical results, but the analysis methods are not specific to this CEM.]

### 1.1. Changes to the Model

Using a simplified model that retains a particular characteristic can provide a result that indicates more clearly the effect of that characteristic on the results. By repeating modelling for many individual characteristics, varied by many small increments, each aspect of a much more complex model can be 'compiled' statistically to give a final solution. Rather than looking at every combination of factors that have an effect on the results, an understanding of the mechanisms of the effect each factor has can provide a more thorough understanding of the results. This work aims to satisfy a number of issues raised by the industrial mass production of any distributed electrical system, such as passenger cars:

- Spotting errors in results due to the model definition being wrong, by comparisons between similar models. (That is, if a result lies outside an expected distribution of results from similar models, then it is possible that the result is wrong, and the cause can be investigated.)
- Giving greater confidence levels from observing many models giving similar results.
- Providing statistical information that can be interpreted to show probability of EMC failure due to production variations.
- Making it easier for development engineers to understand how modelling 'many' units relates to their design needs, rather than using one single model.
- Reducing demand on computing power and memory, making the method available to less well resourced companies and projects.

The case model in section 2 is an example of these principles.

### 1.2. Changes to the Modelling Process

There are hundreds of papers on the FDTD method published each year; testing, developing, improving and hybridizing with other methods [2]. Perhaps one of the reasons there is a proliferation of FDTD work, and CEM work in general, is the continual improvement of computing power. With every new release of faster processors, new ideas that were not possible with older technology suddenly become an attractive target to test. The problem with this is that older, simpler methods are not tested thoroughly enough to determine if their output, that may have appeared inaccurate or wrong, has simply been misinterpreted. The temptation to produce a more complex CEM model that can take a greater account of all the electromagnetic mechanisms at work becomes too great, and inevitably the validation work for the simpler variants is wasted as attention is drawn to the new model.

But focusing on whether the simulation method correctly imitates every physical effect can still only provide a limited accuracy, because there are other sources of error throughout the modelling process. Not exhaustively, these include;

- whether all the mechanisms in the simulation are represented or understood,
- approximations to the differential equations that provide the simulation algorithms,
- meshing types, density and associated algorithms, (for 3-D finite element methods),

- geometric definitions sympathetic to the simulation approach (e.g. designing the model so structures lie along grid-lines, or can take advantage of special algorithms)
- algorithm step intervals and lengths of simulations (typically time-steps or frequency steps),
- material properties and material interaction algorithms,
- definition of output sources (i.e. how/where the simulation is interrogated for the results),
- post-processing and errors resulting from transformations.

Developing new algorithms that can take advantage of greater computing power is certainly often beneficial to simulation accuracy, but exactly *how* beneficial it is needs to be qualified and quantified otherwise it is impossible to determine the success of a new approach.

Attention should also be paid to how such simulation results are compared, and what they are compared to. Production engineers will say that the accuracy of a simulation is how well the results match those they get out of their test facilities; after all, the purpose of a simulation is to simulate the real world. However, mathematicians will point to theoretically solvable canonical models, and compare those results. Both approaches are wrong when the level of accuracy associated with the simulations has not been calculated.

[As a simplistic example to show the importance of finding confidence limits correctly, if two estimates of the length of an object 1m long are 0.95m±0.02m and 1.10m±0.20m, then it is clear that neither value, without the uncertainty, is correct as it is a physical measurement and can never be stated exactly. Together, these estimates indicate that the object is 0.93-0.97m long, because the uncertainty put on the first is too optimistic. But if the estimate was, instead, 0.95±0.10m, then the indicated estimate would be 0.90-1.05m, which is correct because the estimates are now both reasonable.]

### 1.3. Combining Results

Building up a statistical sample of measures, each with a correct uncertainty boundary, can therefore lead to a much better statement of a result than can any single result. To do so for CEM methods, and indeed any other simulation method, therefore relies on being able to determine an uncertainty associated with any single result. Failure to do so means that the 'correct' value can never be found. Failure to do so correctly results in the wrong answer.

Many times functions that represent the EM response of a system (simulated or measured) are compared with other such functions. These differing functions might actually be giving the same answer, but without confidence limits attached, it is impossible to say.

The case study aims to pursue methods that will provide some initial methodologies for calculating confidence limits on simulation results. The objective is to test and display the results in a statistical manner that provide information about small changes to a model.

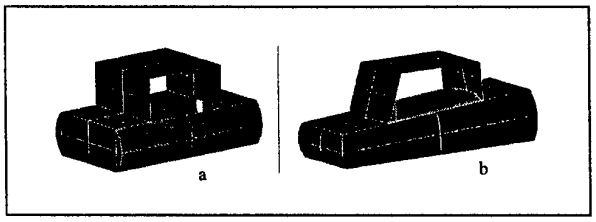



Figure 1. The two metallic structures used in the case study. The dimensions of the structures are approximately 3.6m x 1.8m x 1.8m.

## 2. A CASE STUDY

## VARIATION IN FDTD RESULTS FOR WIRE CURRENTS IN CAR-LIKE STRUCTURES.

### 2.1. Aims and Objectives

As an example of what is achievable using comparative principles, this case looks at analysing likely differences from modelling currents on a wire in an automotive-type metal cavity. The objectives here are to derive, qualitatively, the differences between a particular 'exact' model, as may be used in a typical simulation, and other models in which the wire is not precisely located. The aim of such a study is, therefore, not only to find out what *is* a critical factor (in the way wire position is shown to be critical here), but also to put some measure on that, so that results from different approaches or different methods may be directly compared.

### 2.2. Method

A metallic structure is generated for the FDTD simulation, and current is modelled for a wire in a given position, excited with an external plane wave source. That position is then altered in a series of stages, in this case by up to 10cm in any direction for either end of the wire, and the simulation repeated for each wire position. (This process aims to reproduce the situation where a simulation has been performed that represents an experimental set-up, but the wire in the experiment is actually in a slightly different position.) The result is a function for transferred current from the interfering EM field for each of the wire positions. From this set of functions, an assessment of differences between them can be established. The statistical implication, from a large set of results, is that all such small variations in the wire would result in a measured value that lies in the distribution obtained.

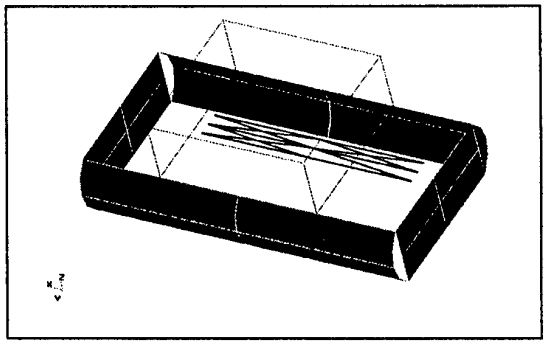


Figure 2. The range of positions of the wires.

Figure 1 shows basic structures that have already been used in previous work for the determination of the effects of cell size in FDTD modelling [3]. Figure 2 indicates the location of the wires that were modelled. The 'control' wire is indicated by the centre-most line, and would be typical of how a wire might be modelled in a FDTD simulation. The model is repeated for the situation of the wire being altered around the centre-line by a number of variations, which are indicated as an overlapping network of wires in the figure.

Figure 3 shows the results from the analysis for a sample of such wires. It can be seen from these graphs that the variation between differing wire positions often reaches a magnitude range over 10dB (without frequency corrections). To quantify these differences, bearing in mind that there are likely to be magnitude *and* frequency differences, it is necessary to characterise these transfer functions in a way that will allow them to be compared directly. The main impetus of this work is

to look at EMC susceptibility, so an obvious characteristic is the set of maximum turning points on the function. This stage requires matching the functions - which is easy for the human eye to do, but presents difficulties to an automated computer process. In this particular case, there is a reasonable correlation for frequency (all peaks appear to compare within 10% by frequency) and a simple match of closest turning points is sufficient.

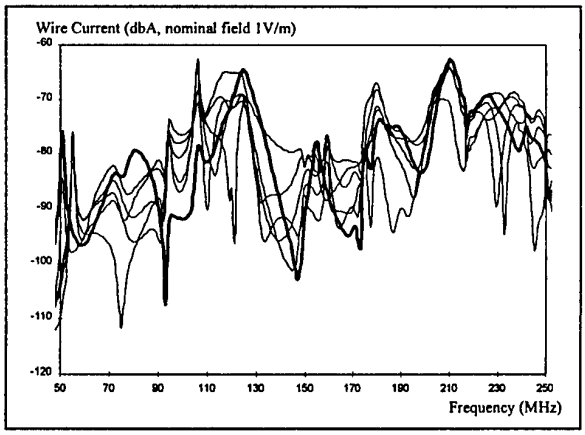



Figure 3. A sample of transfer functions for different wires positions inside structure 'a', as shown in figure 1. The 'control' (centre) wire's function is shown bold.

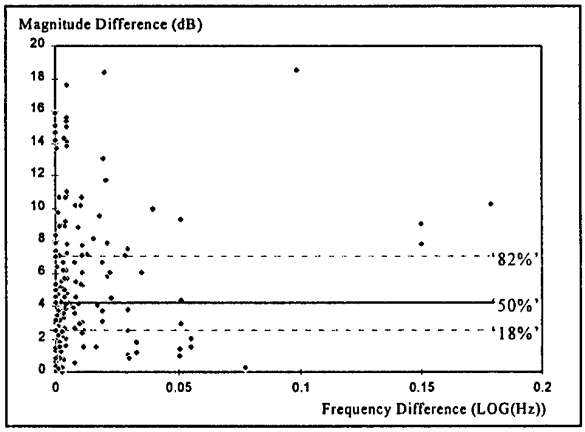



Figure 4. Magnitude and frequency differences between the turning points of transfer functions of different wires, compared to the control wire.

Figure 4 shows all the magnitude and frequency differences as points. Each point represents the difference between a peak on the control transfer function and the corresponding peak on the function of another wire. (For those points showing a large frequency difference, it is likely that the function-matching routine has failed and has matched two peaks that do not correspond, and these points can be rejected upon inspection of the functions.) This distribution of points represents all the differences between the modelled corresponding peaks on the transfer functions of closely placed wires. The statistical inference is that this distribution is representative of any such set of differences for similarly placed wires. As this aims to be a general method it would be unnecessary to look for a match to a known distribution. Instead, non-parametric measures of the data set are taken in place of arithmetic ones. The 50 (median), 18 and 82 percentile points are taken to describe the distribution (indicated on the graph). [The 18 and 82 points are taken to indicated an equivalent range of ±1 standard deviation, as it would be if the distribution was normal.)

These are quantitative measures of the variations associated with changes in wire positions within the structure. They can be taken on their own, to indicate what the likely uncertainties might be, when the wire is not located in the 'control' position. However, they can also then be used for direct comparisons with similar experiments where the modelling has been changed. Here, the changes are the structure and the angle of the incident radiation. By performing this comparison, a conclusion can be drawn about the likely variations in wire currents for these changes. The difference points for the wire currents, as shown in figure 3, are for an incident field of a specific direction and polarisation. Figure 5 shows the same three statistical measures for different incident angles for the two different structures (as shown in figure 1). It shows a composition of results from 432 transfer functions (24 propagation/polarisation angles, 2 structures, 9 wires) ordered in ascending median values. Each pair of lines represent the 18, 50 and 82 percentile statistics for the same experimental conditions applied to each of the two structures. For example, the centre pair show that, for all the incident field angles tested, there is a 50% expectation that the variation between different wires will be of the order of 3 to 4dB. The trend line (which is included for illustration purposes) indicates that this holds true for both of the structures examined.

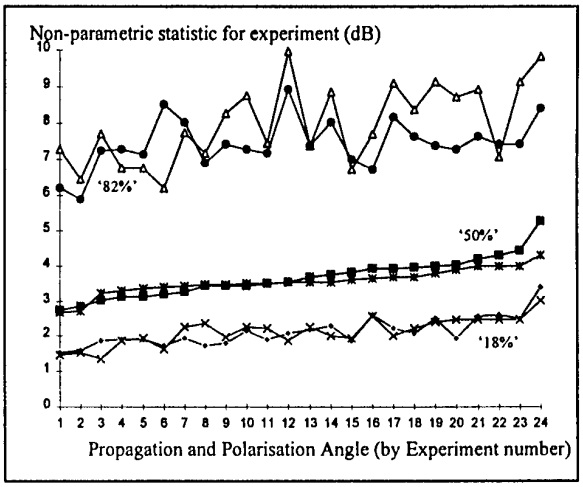



Figure 5. Composition of results for changes to the model.

It can be seen that the statistical measures are generally similar for all the experiments. Inspection of this data also shows that for those propagation angles where the distribution of wire current differences is largest for one structure, it also tends to be large for the other. Transfer functions can also be compared with this data to establish if they come from the same experiment. For example, the function for the current on the control wire where the incident field was from the side and vertically polarised was compared with the data from the wires in the same experiment but with horizontal polarisation. The results for this are 2.9dB(18%), 6.0dB(50%) and 13.4dB(82%). This suggests they are not in the same data sets of figure 5, showing that the function from this control wire does not come from this experiment.

## 2.3. Conclusions to the Case Model

Two sample automotive-style structures have been examined, and the variations of current on a wire, whose geometry has been altered by up to 10cm (1-2 cell displacement), have been processed statistically. The results show these variations in wire currents are consistent between two different structures, with the implication that this variation would be similar for other structures of similar size and shape. The models have been analysed across a range of propagation and polarisation angles, and show the same trends in wire currents. These trends

show a likely variation of up to 2.6dB to 5.0dB for 50% of the data obtained.

[The total percentage of data points between 3dB and 6dB variation for all these experiments was 35%, which means in about 1 in 3 cases the variation in current can be expected to be between 40% and 100%, for displacements of upto 10cm in the wire position. About 25% of the data exceed a variation of 6dB, so 1 in 4 times it is likely to exceed 100% variation. This is comparable with aerospace and automotive results, where wire currents in nominally identical production models have been found to typically vary by 100% [4].]

## 3. COMPARING TRANSFER FUNCTIONS

The case study looking at changes in the transfer functions for wire currents is an easier example than is often found to be the case in EM simulation. The functions of current are reasonably similar, and it has been satisfactory here to simply compare the peak turning points to provide the necessary statistical data. This is often not the case, and it is therefore necessary to discuss these additional methods to those used above to provide the means to apply this approach in a general case.

### 3.1. Frequency Errors

One particular problem to EM measurement and simulation is the number of degrees of freedom in any result. Most simulations for engineering applications involve a vector quantity at a 3 dimensional point. This can then be conveniently turned into a single magnitude value along a given directional component, such that a peak flow rate or stress, for example, might be compared with a maximum allowable value.

In CEM, at best the result can be turned into a frequency and magnitude value pair at a given point and directional component. As a consequence, in both measurement and simulation, the result will have an associated magnitude *and* frequency error pair. The problem this represents is best explained in practical terms. If an EMC test is conducted to look for a peak value that a CEM method predicts at a given frequency, is the prediction wrong because no peak is found at that frequency? It may be that the frequency value is wrong, and looking at a higher frequency reveals that peak.

This seems a trivial example at a single frequency, but how can a continuous frequency error be predicted and displayed across a simulated spectrum? The method developed in this work has been a frequency-band matching technique, as shown in figure 6. Two transfer functions are compared by taking a small section of one function, starting at a given point on the x-axis and shifting it left or right against the x-axis. A match is found when the area difference between that section and the other function is minimised. This is repeated for every point along the x-axis within the required range of testing. Failure of the algorithm can be seen when the frequency displacement necessary to find that minimised area becomes discontinuous between points, implying that it is unclear what the frequency shift should be.

### 3.2. Using Global (model) variables to determine frequency correction

There have been a number of studies into the magnitude accuracy of the FDTD method for different circumstances. They generally look at the errors prevalent in the finite difference solutions that generate the FDTD method's algorithms [5]. However, in actual FDTD simulations, errors accumulate from one timestep to another that also have the effect of shifting the results with respect to frequency. If two such functions are compared but the frequencies do not match, quoting a magnitude error without a frequency error becomes meaningless because there would be no indication of which two points are being compared.

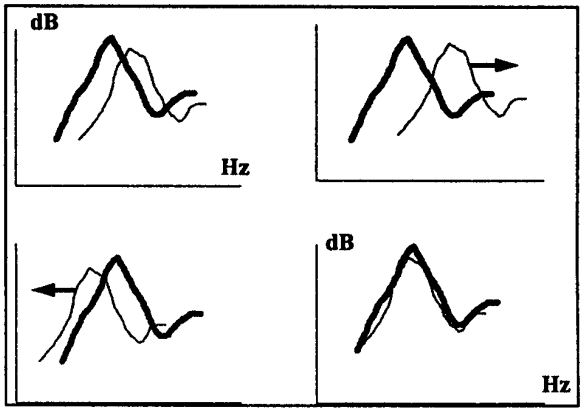



Figure 6. A frequency-band matching technique for functions.

The frequency-band matching described above aims to solve this, but an alternative approach which will form future work from the content of this paper is to use Global, or model-wide, variables. Global variables are any measures which can represent some aspect of the whole model's state as a single variable (or simplified set of variables).

Figure 7 is an example of using this idea in determining frequency errors. In this example, a composite aircraft fuselage was being modelled. To determine the likely accuracy as a function of the finite element cell size being used, two experiments were run with different cell sizes in which data from several thousand cells was taken. This data was then reduced to a single percentage value of those cells, at each frequency, whose field magnitude exceeded that frequency component of the interfering radiation (i.e. those points that are showing resonant behaviour). This results in a percentage versus frequency function which indicates those frequencies where there is the most and least resonance occurring. This removes absolute measures of magnitude, and although the percentages are different between the cases, as a result of the set of probes representing different space within the structure, it is clear in this example what the frequency shifts are between the cases.

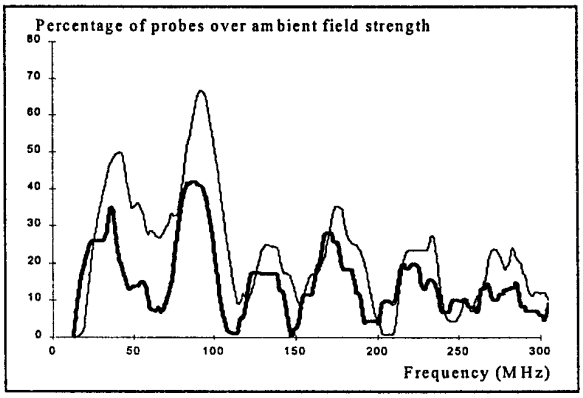



Figure 7. The EM response of a modelled composite fuselage, using two models with different cell-sizes (larger cell results shown in bold).

These approaches allow frequency uncertainties to be adjusted, and magnitudes of correctly corresponding points to be compared. Any conclusions regarding the magnitude accuracy of CEMs are therefore only complete with correction for

frequency variations, but the frequency corrections for different models tend to be different. It is therefore necessary to establish the possible frequency variations, and the frequency-band matching and the global-variable methods provide means to achieve that. Figure 8 shows an example of using the frequency-band matching technique, applied to structure 'a' of figure 1.

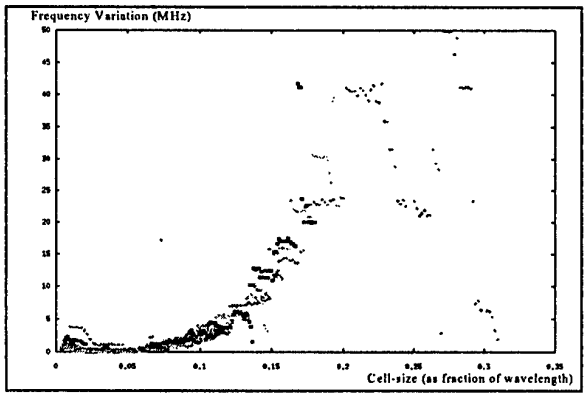



Figure 8. Frequency variations characteristic of structure 'a' in the case study. The points show matches between transfer functions obtained by using different cell-sizes in the modelling. (Cell-size is shown as a fraction of wavelength, e.g. a 5MHz variation for frequencies whose wavelengths are 10 x cell-size.)

### 3.3 Application of Frequency Corrections

Establishing a frequency variation characteristic for a model, as shown in figure 8, allows for a more detailed study of magnitude differences. Once such a characteristic is established, it becomes an easier process to perform any comparison between two functions for that model. Calculating a frequency variation function, along with determining which aspects of a model have the greatest effect on frequency variation, should be seen as an essential part of a complete solution.

## 4. CONCLUSIONS

This paper has presented some methods that pursue the aim of evaluating CEM uncertainty. By examining the differences that exist between different sets of results, an assessment of the effect of changes to models can be made. These changes may be in the form of actual changes to the structure of the model, as has been shown for wire positions in a case study. The method for comparison used is, however, equally applicable if sets of results are from different modelling approaches - such as changes to EM fields, material properties, geometric definitions (including finite element meshing) and changes to the simulation algorithms themselves.

Further, the whole process can be compared with physically derived results, as the source data that leads to the derivation of statistical measures comes only from the transfer functions themselves. Even if there is only one set of physical data, by generating sets of results numerically from differing models and using the physical data as the control data, the same statistical comparisons can be made as described in the case study.

## 5. ACKNOWLEDGMENTS

This work has been done under the WHEELS project (Wiring Harnesses: Electromagnetic Effects of Lightweight Structures) [1], which is part of EPSRC's Innovative Manufacturing Initiative [6].

Our thanks to the continued support from our sponsors on this project; Lucas Rists Wiring Systems, Rover Group, FEGS Ltd. and Electro Magnetic Applications Inc..

## 6. APPENDIX

### 6.1. Technical Details

The FDTD implementation used was the EMA3D code, supplied by Electro Magnetic Applications, Inc. [7]. A graphical user interface was provided by FEGS Ltd..

All experiments in the case study used a 10,000 time step analysis, over 1.5μs, with an incident Gaussian pulse (<25dB variation for 0-600MHz, >100dB attenuation over 1.2GHz) in various polarisations. The cell size used was 9cm.. A 5000 point DFT was used to calculate the Z-transform.

### 6.2. Frequency-band matching

The comparative analysis is performed by frequency-band matching two frequency transfer functions, g(x) and h(x). The magnitude error is the value for which

$$\int_f^{f+D} |\log(h(x)) - \log(g(x+\sigma))| . dx$$

is a minimum, the frequency shift being σ in that case (taken as a point frequency at f+D/2), and D is the analysis bandwidth (typically 50 MHz).

## 7. REFERENCES

7.1. P.A. Jennings, R.J. Ball, P.H. Lever, C Macdonald-Bradley & S. Baker, "W.H.E.E.L.S.: A Statistical Approach to EMC Model Validation", *Proceedings of IEEE 1998 Int'l Symposium on Electromagnetic Compatibility,* Denver USA, August 1998.

7.2. K.L. Shlager & J.B. Schneider, "A Selective Survey of the Finite-Difference Time-Domain Literature.", *IEEE Antennas and Propagation Magazine,* Vol.37, No. 4, pp 39-56, August 1995.

7.3. C.J. Macdonald-Bradley, P.A. Jennings, R.J. Ball, P.H. Lever & S.D. Baker, "The Effects of Cell Size on FDTD Calculations for Cubic Structures.", *Proceedings of 13th International Zurich Symposium on Electromagnetic Compatibility,* Zurich, Switzerland, February 1999.

7.4. P.A. Jennings, "Achieving correlation between system-level and whole vehicle radiation susceptibility tests", *MPhil Thesis,* University of Warwick, Coventry, UK, May 1992.

7.5. A. Taflove, "Review of the formulation and application of the finite-difference time-domain method for numerical modelling...", *Wave Motion,* Vol.10, No.6, pp. 547-582, 1988.

7.6. "The Foresight Vehicle", *Technology Foresight No.5: Transport,* pp 74-83, Office of Science and Technology, HMSO 1995.

7.7. R.A. Perala, T.H. Rudolph, P.M. McKenna, "Application of the Time Domain Three Dimensional Finite Difference Method to a Wide Variety of EMC Problems", *Proceedings of 1992 Regional Symposium on Electromagnetic Compatibility,* Tel Aviv, Israel, November 1992.



Chris Macdonald-Bradley received the HND qualification in Software Engineering, and began research work in multi-phase fluid flow. After receiving the BEd degree in Mathematics, he was engaged in teaching and engineering training before taking a post at the University of Warwick in 1997, where he is currently a Research Fellow working on EMC design tools for the automotive industry.

EMC 2000 INTERNATIONAL WROCŁAW SYMPOSIUM ON ELECTROMAGNETIC COMPATIBILITY

# MODELS FOR SIMULATION OF FIELDBUS TRANSMISSION LINE EMC TESTING

Tadeusz Missala

Industrial Research Institute for Automation and Measurements, Al. Jerozolimskie 202,

02-486 WARSZAWA, fax +(48)(22)874 02 20, e-mail: tmissala@sg.piap.waw.pl

*The IEC 61158-2 standard contain the EMC requirements for the equipment, which is connecting to the transmission line, but don't contain any requirement for the complete equipped line [3]. To obtain the answer, is sufficient such a testing, author propose the simulation by use of the models of signals and equipment. Such models are proposed in the paper.*

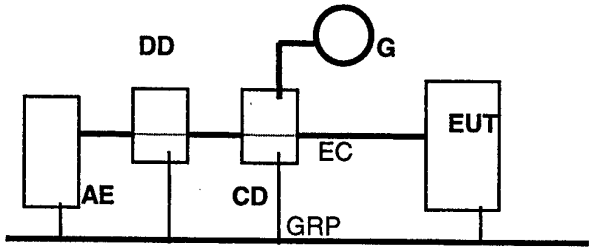
## 1. INTRODUCTION

The typical EMC immunity requirements for industrial-process measurements and control equipment are formulated in IEC 61326-1 standard [4]. All these requirements shall be met by the complete installations, not only by the instruments only, because the interaction between the instruments, the supply and signal lines and the whole industrial environment is to taken into account. The space configuration of the installation can have an important influence on the EMC immunity and this implicate, the tests „in situ" to execute.

The Fieldbus standard [3] don't require such a tests. The author have made an extensive literature revue, that has presented, the problem isn't investigate and probably is a new research topic. The relevant IEC standards series 61000-4-xx deal with the immunity testing of apparatus and comprehensive systems only; the problem of the testing of the installation as a whole is neglected [5 to 8]. The relevant basic publication, e.g. Gonschorek and Singer or Kohling contain the advises only, for the theoretical analysis of the installation conditions to reach probably the required immunity of the industrial system [1,2]. The tests of the manufactured installation, as well as the methods for the simulation investigations aren't presented.

This is the reason, the author have decided a proposal for the first step for such a testing to make. This step there are the mathematical models of the test signals and components of the test path, that are the object of the paper.

The block diagram of the typical test circuit is presented on the fig. 1.




Symbols: G - test generator; CD. - coupling device; DD - decoupling device; AE - auxiliary equipment; EUT - equipment under test ( transmission line loaded by the measuring and control equipment); EC - external circuit/port of EUT; GRP - ground reference plain.

Fig.1. The typical test circuit for immunity testing (block diagram)

The models of the components of the test circuit will be presented sequentially . EUT is composed of the transmission line and equipment, connected to it.

## 2. MODELS OF THE TEST SIGNALS

Two most important output signals of the test generators will be discussed. There are:

- EFT/B signal, described in IEC 61000-4-4 [6]
- surge signal, described in IEC 61000 - 5 [7].

### 2.1. EFT/B signal

The pulse of this signal is presented on the fig. 2.

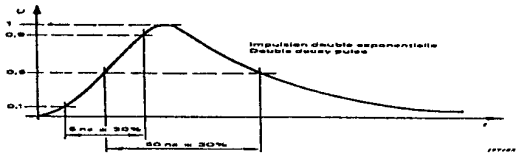


Fig. 2. Pulse 5 ns / 50 ns

The considered signal can be approximated on two ways:

- the more precise mathematical model is an exponential one;
- the more simple model can be linear one.

2.1.1. Exponential model

The rise slope of the pulse can be approximated by the decay curve second order, as below:

$$u(t) = U[1 - \frac{T_1}{T_1 - T_2} e^{-\frac{t}{T_1}} + \frac{T_2}{T_1 - T_2} e^{-\frac{t}{T_2}}] \quad (1)$$

where: $T_1$ and $T_2$ - the time constants, U - the pulse amplitude.

The detailed calculations led to the following values for the time constants:

$$T_1 = 1{,}95 \text{ ns}; T_2 = 0{,}55 \text{ ns}; \quad (2)$$

that give the following approximating formula:

$$u(t) = U[1 - \frac{1{,}95}{1{,}4} e^{-\frac{t}{1{,}95}} + \frac{0{,}55}{1{,}4} e^{-\frac{t}{0{,}55}}] \quad (3)$$

The verification in the check points 0,1U and 0,9U gives the values:

t = 0,55 ns, u = 0,094U;t = 5,55 ns, u = 0,919U;(4)

This accuracy is recognised as sufficient.

The fall slope of the pulse can be approximated by the decay curve first order, as below:

$$u(t) = Ue^{-\frac{t-t_p}{T_3}} \quad (5)$$

where: $T_3$ - the time constant; $t_p$ - the value of time shifting, equal the time for the pulse maximum value.

The detailed calculations led to the following values for the time constant and the time shifting:

$$T_3 = 65{,}64 \text{ ns}; t_p = 7{,}7 \text{ ns}; \quad (6)$$

that give the following approximating formula:

$$u(t) = Ue^{-\frac{t-7{,}7}{65{,}64}} \quad (7)$$

The verification in the check points U and 0,5U gives the values:

$$t = 7{,}7 \text{ ns}, u = U; t = 45{,}3, u = 0{,}501U \quad (8)$$

[note: 45,3 = 53(value red from the fig.2) - $t_p$]

This accuracy is recognised as sufficient.

This way :

for $\mathbf{0 \le t \le 7{,}7}$ ns is valid the formula (3);

for $\mathbf{7{,}7ns \le t \le \infty}$ is valid the formula (7); (9)

2.1.2. Linear model

Sometimes the more simple mathematical model can be useful; the linear model is a such one. This model is presented on the fig. 3.

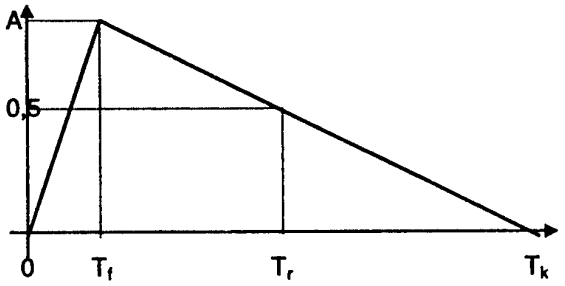



Fig. 3. The linear model of the pulse

The mathematical description is:

$$\mathbf{0 \le t \le T_f}, y(t) = \frac{A}{T_f} t;$$

$$\mathbf{T_f \le t \le T_k}, y(t) = -0{,}5A \frac{t - 2T_r + T_f}{T_r - T_f}; \quad (10)$$

where: $T_f$, $T_r$ - times, as presented on the fig. 3; A - the amplitude of the pulse

For the EFT/B pulse are valid the values as follows:

$$T_f = 5 \text{ ns}; T_r = 50 \text{ ns}; \quad (11)$$

This leads to the particular formulas:

$$\mathbf{0 \le t \le 5\ ns}, y(t) = \frac{U}{5} t;$$

$$\mathbf{5\ ns \le t \le 95\ ns}, y(t) = U \frac{95 - t}{90}; \quad (12)$$

where: U - the amplitude of the pulse, volts; t - time in nanoseconds.

2.2. Surge signal

The pulses of this signal are presented on the fig. 4a, 4b, 4c.

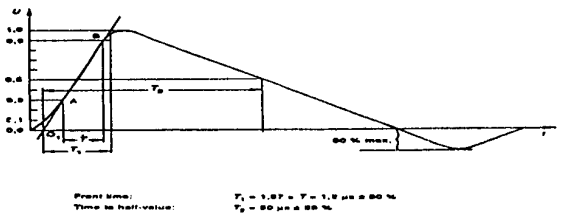
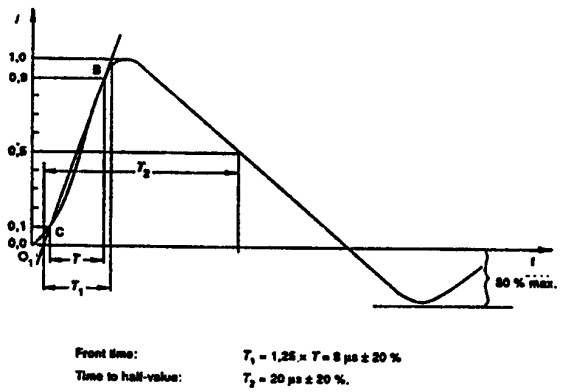
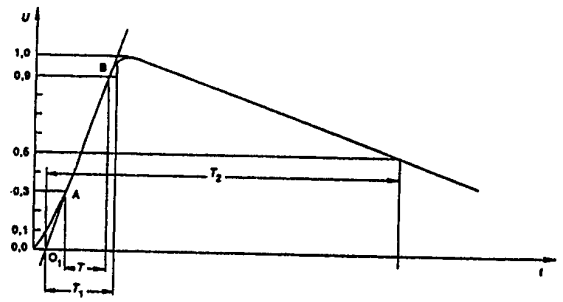


Fig. 4a. Surge pulse 1,2 µs / 50µs




Front time: $T_1 = 1{,}25 \times T = 8\ \mu s \pm 20\ \%$
Time to half-value: $T_2 = 20\ \mu s \pm 20\ \%$.

Fig. 4b. Surge pulse 8 μs / 20 μs




Front time: $T_1 = 1{,}67 \times T = 10\ \mu s \pm 30\ \%$
Time to half-value: $T_2 = 700\ \mu s \pm 20\ \%$.

Fig. 4c. Surge pulse 10μs / 700 μs

All these pulses are very near to the linear model as presented on the fig. 3. The assumption is adopted, the mathematical model is done by the formulas (10). On that basis for the particular pulses one obtains the formulas, as follows:

- voltage pulse 1,2 μs/50 μs :

$$\mathbf{0 \le t \le 1{,}2\ \mu s}\ ,\ y(t) = \frac{U}{1{,}2}t\ ;$$

$$\mathbf{1{,}2\ \mu s \le t \le 98{,}8\ \mu s},\ y(t) = U\frac{98{,}8 - t}{97{,}6}\ ; \qquad (13)$$

where: U - the amplitude of the signal, volts; t - time in microseconds.

- current pulse 8 μs/20 μs :

$$\mathbf{0 \le t \le 8\ \mu s}\ ,\ y(t) = \frac{I}{8}t\ ;$$

$$\mathbf{8\ \mu s \le t \le 32\ \mu s},\ y(t) = I\frac{32 - t}{24}\ ; \qquad (14)$$

where: I - the amplitude of the signal, amperes; t - time in microseconds.

- voltage pulse 10 μs /700 μs :

$$\mathbf{0 \le t \le 10\ \mu s}\ ,\ y(t) = \frac{U}{10}t\ ;$$

$$\mathbf{10\ \mu s \le t \le 98{,}8\ \mu s},\ y(t) = U\frac{1390 - t}{1380}\ ; \qquad (13)$$

where: U - the amplitude of the signal, volts; t - time in microseconds.

## 3. TRANSMISSION LINE

### 3.1. General

The Fieldbus transmission line shall be treated as an electrical long line; this is a result of the signal transmission rate. The transmission rate of the slowest signal is: $f_r$ = 31,25 kHz (PROFIBUS PA, Fieldbus Foundation), and of the most fast one is 12 MHz (PROFIBUS DP). The corresponding wave lengths are:

$\lambda_{max}$ = 9524 m ; $\lambda_{min}$ = 25 m ;

As the length of the line can be from 200 m (fast Fieldbus) to 1200 m (slow Fieldbus), it is of the range or greater than λ/4).

This way to consider is the phenomenon of interaction between the pulse interfering signals, as described above, and the work transmission signal. To complete the signal data, the interfering pulse lengths are listed below:

- for the pulse 5 ns/50 ns - is: $\lambda_i$ = 28,5 m;
- for the pulse 1,2 μs/50 μs - is: $\lambda_i$ = 29640 m;
- for the pulse 8 μs/20 μs - is: $\lambda_i$ = 9600 m;
- for the pulse 10 μs./700 μs - is: $\lambda_i$ = 417000 m.

In case of the nanosecond pulse have place the interference of the short wave interfering signal and the work signal, that wave length is the same range or many times greater. In others cases, the wave length of the interfering signal is many times greater than the wave length of the work signal. One can expect, the results of the interference are various.

### 3.2. Parameters and four pole model

In the Fieldbus Standard are given the required parameters of the transmission line, as follows [3]:

- characteristic impedance at $f_r$ = 31,25 kHz: $Z_o$ = 100 Ω ± 20 %;
- maximum attenuation at 39 kHz = 3,0 dB/km;
- maximum capacitive unbalance to shield = 2 nF/km;
- maximum d.c. resistance (per conductor) = 24 Ω/km;
- maximum propagation delay change 0,25 $f_r$ to 1,25 $f_r$ = 1,7 μs/km;

The four pole model of the electric long line is:

$$\begin{bmatrix} U_x \\ I_x \end{bmatrix} = \begin{bmatrix} ch\gamma x; & -S_o sh\gamma x \\ -\frac{sh\gamma x}{S_o}; & ch\gamma x \end{bmatrix} \times \begin{bmatrix} U_1 \\ I_1 \end{bmatrix} \qquad (15)$$

where:

$U_x$ , $I_x$ - voltage and current at the point x;

$U_1$ . $I_1$ - voltage and current at the input point;

x - variable - the distance from the input point;

γ - wave propagation constant:

$$\gamma = \beta + j\alpha = \sqrt{ZY}$$

$S_o$ - characteristic (wave) line impedance;

$$S_o = \sqrt{\frac{Z}{Y}}$$

$$Z = R + j\omega L; \quad Y = G + j\omega C$$

R, L, G, C - respectively line :resistance, inductance, conductance, capacity;

ω - angular frequency of the signal.

Values of the all above mentioned variables can be derived from the parameters done in this item.

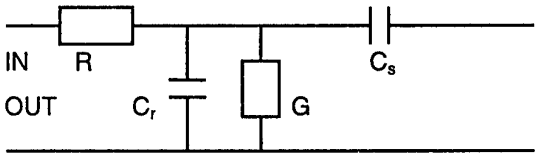
## 4. COUPLING DEVICES

### 4.1. Capacitive coupling clamp [6]

The total coupling capacitance between cable and clamp, required in the standard, is:
50 pF to 200 pF;

The other parameters, such as frequency response and resistance as well as the particular value of the capacitance is the function of recommended mechanical arrangement and shall be measured, before simulation.

The four-terminal schema of the clamp (with the connecting cable) is a very simple one, as shown on the fig. 5. It is assumed, the inductance of the clamp and the connecting cable is negligible, grace to they construction.




R - resistance of the connecting cable;
$C_s$ - capacity of the clamp;
$C_r$ , G - respectively capacity and conductivity of the cross coupling to earth.

Fig. 5. Schema of the capacitive clamp

The corresponding four-pole equation is:

$$\begin{bmatrix} 1 + RG + j\omega RC_r; & R + \dfrac{1 + RG + j\omega C_r}{j\omega C_s} \\ G + j\omega C_r; & 1 + \dfrac{G + j\omega C_r}{j\omega C_s} \end{bmatrix} = [A]$$

$$\begin{bmatrix} U_2 \\ I_2 \end{bmatrix} = [A] \times \begin{bmatrix} U_1 \\ I_1 \end{bmatrix} \qquad (16)$$

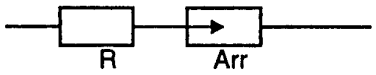
### 4.2. Capacitive coupling for interconnection lines [7]

The coupling network is composed of the resistor R = 40 Ω and the capacitor C = 0,5 μF, connected in series. The corresponding four-pole equation is:

$$\begin{bmatrix} U_2 \\ I_2 \end{bmatrix} = \begin{bmatrix} 1 & R + \frac{1}{j\omega C} \\ 0 & 1 \end{bmatrix} \times \begin{bmatrix} U_1 \\ I_1 \end{bmatrix} \qquad (17)$$

### 4.3. Coupling via arrestors [6.7]

The schema of the coupling path via arrestors is shown on the fig. 6




R = 40 Ω ; Arr - gas arrestor

Fig. 6. Coupling path via arrestors for transmission signals frequency above 5 kHz.

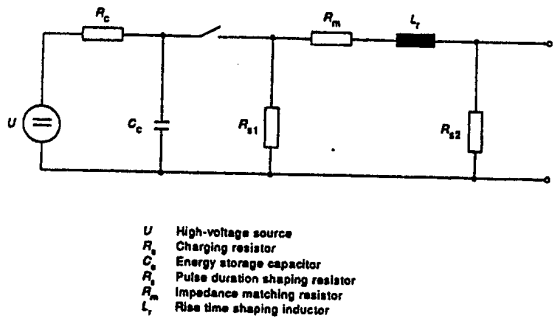
For the test modelling, the object of interest is the conductivity state of the arrestor i.e. the state when the test signal voltage is higher than the activation voltage of arrestor. In this state, the resistance of arrestor is negligible. This way the four-pole equation of the coupling path is:

$$\begin{bmatrix} U_2 \\ I_2 \end{bmatrix} = \begin{bmatrix} 1 & R \\ 0 & 1 \end{bmatrix} \times \begin{bmatrix} U_1 \\ I_1 \end{bmatrix} \qquad (18)$$

## 5. TEST GENERATORS

As an example will be considered the test generator, which generate the combined voltage/current wave, such as presented on the figures 4a and 4b.

The schema of it is shown on the fig. 7.




$U$ High-voltage source
$R_c$ Charging resistor
$C_c$ Energy storage capacitor
$R_s$ Pulse duration shaping resistor
$R_m$ Impedance matching resistor
$L_r$ Rise time shaping inductor

Fig. 7. Schema of the combined surge test generator.

The corresponding four-pole equation is:

$$\begin{bmatrix} U_2 \\ I_2 \end{bmatrix} = \begin{bmatrix} A_g & B_g \\ C_g & D_g \end{bmatrix} \times \begin{bmatrix} U_1 \\ I_1 \end{bmatrix} \tag{19}$$

where:

$$A_g = 1 + j\omega R_c C_c + \frac{R_c}{R_{s1}} +$$

$$+ \frac{1}{R_{s2}} \left\{ (1 + j\omega R_c C_c + \frac{R_c}{R_{s1}})(R_m + j\omega L_r) + R_c \right\};$$

$$B_g = (1 + j\omega R_c C_c + \frac{R_C}{R_{s1}})(R_m + j\omega L_r) + R_c;$$

$$C_g = j\omega C_c + \frac{1}{R_{s1}} +$$

$$+ \frac{1}{R_{s2}} \left\{ \left( 1 + j\omega C_c + \frac{1}{R_{s1}} \right) \left( R_m + j\omega L_r \right) + 1 \right\}$$

$$D_g = \left( 1 + j\omega C_c + \frac{1}{R_{s1}} \right) \left( R_m + j\omega L_r \right) + 1$$

The mathematical models of the others generators can be obtain on the similar way.

## 6. CONCLUSIONS

In the paper there are presented:

- the set of the problem;
- the indication of the phenomena to investigate;
- the first steps to reach the solution: the mathematical models of the interference signals, transmission line, coupling devices and of one of the signal generators.

The work will be continued.

## 7. REFERENCES

7.1. K. H. Gonshorek, H. Singer, „Electromagnetic Compatibility. Fundamentals, Analyses, Measures". (Elektro-Magnetische Verträgligkeit.Grundlagen,Analysen,Maßnahmen), B.G. Teubner, Stuttgart, 1992.

7.2. A. Kohling, „EMC system planning for industrial installations and non-military objects" (EMV-Systemplannung für Industrieanlagen und civil genutzte Objekte), Mesago, Stuttgart, 1997.

7.3. IEC 61158-2: 1993, Fieldbus standard for use in industrial control systems - Part 2: Physical layer specification and service definition.

7.4. IEC 61326-1: 1997, EMC requirements for electrical equipment for measurement, control and laboratory use:- Part 1: General requirements + A1:1998 - Particular requirements for equipment used in industrial locations; Particular requirements for equipment used in laboratories or test and measurement areas with a controlled electromagnetic environment, particular requirements for equipment that is powered by battery or from the circuit being measured

7.5. IEC 1000-4-3:1995 (EN 61000-4-3:1995), Electromagnetic Compatibility (EMC) - Part 4: Testing and Measurement Techniques - Section 3: Radiated, radio-frequency, electromagnetic field immunity test. Basic EMC Standard.

7.6. IEC 1000-4-4:1995 (EN 61000-4-4:1995), Electromagnetic Compatibility (EMC) - Part 4: Testing and Measurement Techniques.- Section 4: Electrical fast transient/burst immunity test. Basic EMC publication.

7.7. IEC 1000-4-5:1995 (EN 61000-4-5:1995) Electromagnetic Compatibility (EMC -. Part 4: Testing and Measurement Techniques. - Section 5: Surge immunity test. Basic EMC publication.

7.8. IEC 1000-4-6:1996 (EN 61000-4-6:1996) Electromagnetic Compatibility (EMC) - Part 4: Testing and Measurement Techniques.- Section 6: Immunity to conducted disturbances, induced by radio-frequency fields. Basic EMC publication.

## BIOGRAPHICAL NOTE

Tadeusz MISSALA, received the MSc degree in electric engineering from Technical University of Łódź at 1949, then worked as chief designer in the aircraft industry, The degree PhD in electrical engineering received from Technical University of Warszawa at 1963. From 1967 works in Industrial Research Institute for Automation and Measurement in Warszawa, from 1978 as Professor. From 1982 is also a Professor in Technical University of Worszawa. His research interests include industrial automation, automation components and EMC.

**EMC 2000** INTERNATIONAL WROCŁAW SYMPOSIUM ON ELECTROMAGNETIC COMPATIBILITY

# COST-EFFECTIVE EMC-CONFORMING DESIGN OF SWITCHED-MODE POWER SUPPLIES

Philip Fosu Okyere, Ernst Habiger

Dresden University of Technology
Institute for Automation
Mommsen street. 13
D-01062 Dresden/Germany
Tel: +49-351-4633180; Fax. +49-351-463 7726
pokyere@ieee.org
ernst.habiger @mailbox.tu-dresden.de

***Abstract:*** *This paper focuses on a computer-aided method for cost-effective EMC-conforming design of switched-mode power supplies (SMPSs). PSPICE-compatible models for the components of switched-mode power supplies such as conductor tracks and high frequency transformers as well as EMI-Filter elements such as common-mode chokes are provided. Formulas to calculate the model parameters from the geometrical properties of the components are given. Experimental results validate the accuracy of the models.*

## 1 INTRODUCTION

The design of electrical and electronic devices, equipment and systems to conform with today's national and international EMC-norms has gained increasing awareness and necessity from designers and manufacturers of electronic and electrical devices worldwide, especially from those within the member states of the European Union (EU). This is due to the fact that, since January 1, 1996, designers and manufacturers of electrical equipment, which can generate and emit electromagnetic disturbance or whose functional behavior can be interfered with or detrimented by electromagnetic disturbances are obliged by law to comply with the directive 89/336/EEC on Electromagnetic Compatibility (EMC).

Typical examples of such devices are Switched-Mode Power Supplies (SMPS). Modern switched-mode power supplies are operated at high switching frequency (from kHz in the MHz range) and at high rate of change of current and voltages and generate high conducted electromagnetic disturbances (conducted noise) as a result of this switching action.

Figure 1 summaries the different EMC-aspects of switched-mode power supplies which need to be considered in the design process; namely, the prevention and reduction of noise emission, increasing the immunity of the SMPS against interference due noise from other electromagnetic noise sources and prevention of high frequency noise coupling from the source into the sensitive load and vice versa.

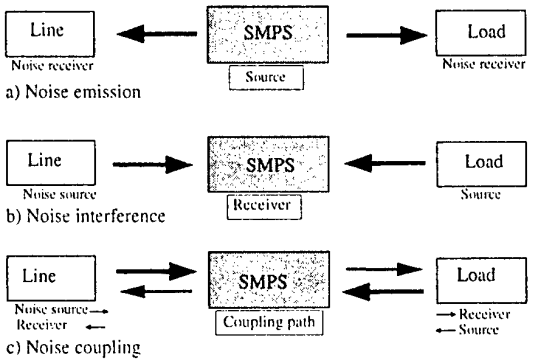



Fig. 1. EMC-Aspects of SMPS

Traditionally, the conducted noise are suppressed to levels which are acceptable to and in compliance with EMC regulations on conducted electromagnetic Interference (e.g. EN 55022) by adding low pass filters (EMI-filters), which usually consist of inductors and capacitors. Prototypes of the switched-mode power supplies are usually developed first before the EMI-filters are designed, whereby the components of the EMI-filters are selected by "try and error" in an EMC-Laboratory. In some cases, the physical configuration of the switched-mode power supplies might require modification before the limits on the conducted EMI can be met. This procedure of designing SMPSs for conformity with EMC-regulatory limits is time consuming and results in the increase of the total cost of the switched-mode power supplies. The method presented here enables the fulfillment of EMC regulations effectively and with minimum cost.

## 2 COST-EFFECTIVE DESIGN PROCEDURE

The flow chart summary of Fig. 2 explains the computer-aided method for the cost-effective design of switched-mode power supplies with regards to elec-

tromagnetic compatibility. Unlike the traditional EMC-Conforming Design procedure, with this method the required EMI-Filter and other suppression technique (e.g. Shielding) are determined and incorporated in the design process. The cost for the developing of the SMPS's are also estimated before the construction of the first prototype.

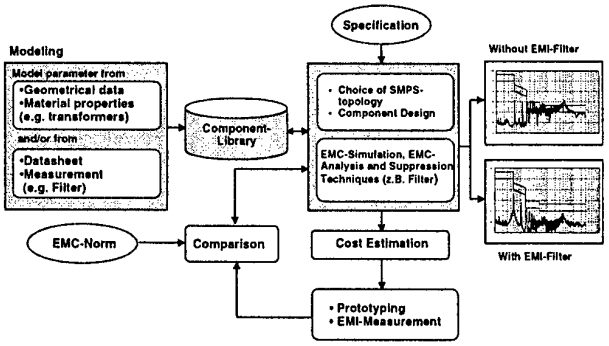



Fig. 2. Cost-effective procedure for the EMC-conforming design of SMPSs.

## 3 COMPONENT MODELING

This novel method is based on simulation. Its effectiveness depends therefore on the accuracy of the models of components such transformers, common-mode chokes, X- and Y-capacitors, conductor tracks, semiconductor devices which are implemented in the simulation. The parasitic properties of these components are to be considered in order to achieve realistic simulation results.

Figure 3 shows, as example, the circuit diagram of a commonly used switched-mode power supply with EMI-Filter, namely the forward converter. Its main components are the transformer Tr, the semiconductor switch M, the rectifier diode D1, the free wheeling diode D2, the demagnetization diode D3 and the output filter elements L and C.

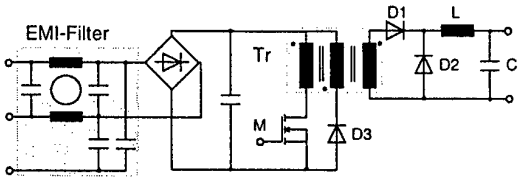



Fig. 3. Example of SMPS with EMI-Filter

Table 1 gives an overview of simply PSpice-compatible models for conductor tracks, inductors and capacitors.

| Component | Model |
|---|---|
| Conductor | $L_t$ $R_t$ |
| Inductor L | Rd, Rw, L, Cp |

| Capacitor | C Rp Lp |
|---|---|

Table 1. Model of selected components

### 3.1 Conductor track

The behavior of a conductor track at frequencies (in the kHz range) is approximately modeled as a series connection of the resistance $R_t$ and the inductance $L_t$. Their values are determine by:

$$R_t \approx \frac{l_b}{\kappa \cdot w \cdot d} \text{ and } L_t \cong 2 \cdot l_b \cdot \ln\left(\frac{8d}{w} + \frac{w}{4d}\right) \quad (1)$$

where $l_b$ represents the length, $w$ the width, $d$ the thickness and $k$ the conductivity of the conductor.

In SMPSs where we have high rate of change of voltages the parasitic capacitance $C_k$ between a conductor track and the ground plane, as illustrated in Fig. 4, plays a very vital role in the generation of high frequency conducted noise (common-mode noise) $i_{st}$:

$$i_{st} = C_k \frac{d u_{st}}{dt} \quad (2)$$

A simple formula to predetermine the value of this parasitic capacitance is given by [4]:

$$C_k \cong \varepsilon_r \varepsilon_o K_{c1}\left(\frac{w}{h}\right) l_b \quad (3)$$

where $K_{C1}$ is the fringing factor. Its value depends on the relative geometry $w$ and $h$ as well as on the relative permittivity $\varepsilon_r$ of the material between the conductor and the ground plane. Reference [4] gives a detailed analysis for the fringing factor and its corresponding values in dependency of the relative geometry.

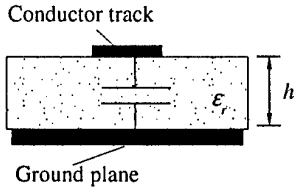



Fig. 4. Parasitic capacitance of a conductor track.

### 3.2 Capacitors

Capacitors are vital components of switched-mode power supplies and are useful for the suppression of conducted EMI. There are many different types of capacitors available but in general they all can be represented by the simplified circuit model shown in Figure 5.

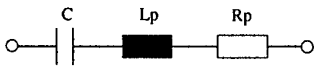



Fig. 5. Equivalent circuit of a capacitor.

This equivalent circuit includes the parasitic elements of a capacitor which are detrimental to their suppres-

sion effect. Figure 6 depicts a comparison of the insertion loss of a real capacitor with that of an ideal one (i.e. without parasitic elements). The insertion loss of the ideal capacitor rises continuously at 20dB/decade whilst that of the real capacitors falls after the resonant frequency as a result of the parasitic inductance.

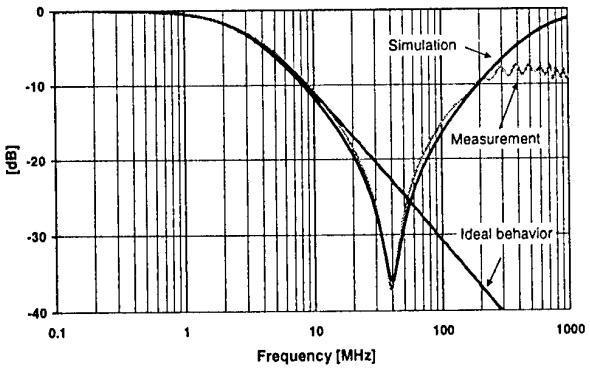



Fig. 6. Frequency behavior of a capacitor.

The model parameters $R_p$ and $L_p$ are determined from an existing insertion loss graph of a capacitor as follows:

$$R_p = \frac{R}{2\cdot(k-1)} \text{ and } L_p = \frac{1}{(2\cdot\pi\cdot f_R)^2\cdot C} \quad (4)$$

with R=50Ω and $k = 10^{\left|\frac{a_{emax}}{20}\right|}$, where $a_{emax}$ is the maximum insertion loss of the capacitor at the resonance frequency $f_r$.

### 3.3 Magnetic Components

Fig.7 shows the a novel PSPICE compatible model for high-frequency transformers of any number of winding layers which has been presented in the references [1] and [2] for the first time. The individual winding layers can either be connected in series or in parallel.

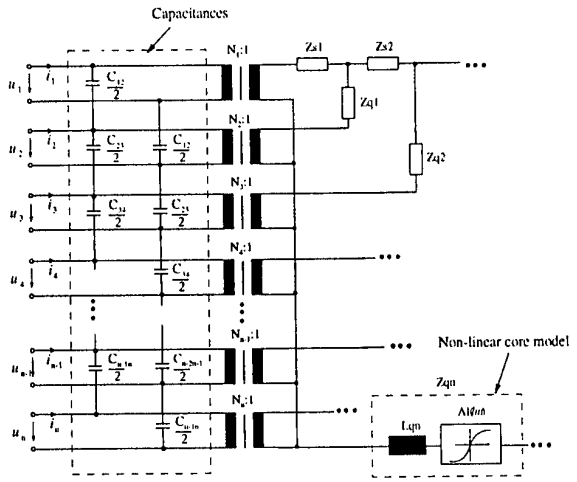



Fig. 7. Transformer model including, parasitic capacitances and a core Model.

This transformer model consists basically of three main parts, namely:

1. The parasitic capacitances between adjacent winding layer
2. Ideal transformers whose turn ratios represents the number winding turns of a winding layer and
3. The Impedance elements $Z_{s1}$ to $Z_{qn}$ which contain the geometrical and material properties of the windings, of the insulation between winding layers and of the magnetic core.

The impedance elements are given in the frequency domain and in dependency of the geometrical parameter of the transformer by the following complex expressions:

$$z_{s1}(p) = \frac{l_{tL1}\alpha_1}{\kappa_1 b_0}\coth(\alpha_1 h_{L1}) + \frac{l_{tL2}\alpha_2}{\kappa_2 b_0}\tanh\left(\frac{\alpha_2 h_{L2}}{2}\right) + \frac{\mu l_{tI1} h_{I1}}{b_0} p$$

$$z_{si}(p) = \frac{l_{tLi}\alpha_i}{\kappa_i b_0}\tanh\left(\frac{\alpha_i h_{Li}}{2}\right) + \frac{\mu l_{tIi} h_{Ii}}{b_0} p + \frac{l_{tLi+1}\alpha_{i+1}}{\kappa_{i+1} b_0}\tanh\left(\frac{\alpha_{i+1} h_{Li+1}}{2}\right)$$

$$z_{qi}(p) = \frac{l_{tLi}\alpha_{i1}}{\kappa_i b_0}\left(\coth(\alpha_i h_{Li}) - \tanh\left(\frac{\alpha_i h_{Li}}{2}\right)\right)$$

$$z_{qn}(p) = \frac{l_{tLn}\alpha_n}{\kappa_n b_0}\tanh\left(\frac{\alpha_n h_{Ln}}{2}\right) + pA_L$$

with

$\kappa_i, \mu$ conductivity, permeability

$l_{tLi}$, $l_{tIi}$ mean turn length of the ith conductor layer (index L), and ith insulation region (index I)

$h_{Li}$, $h_{Ii}$ height of the $i^{th}$ conductor layer (index L), and of the $i^{th}$ insulation region (index I)

$b_0$ winding width

$A_L$ inductance factor

$\alpha_i = \sqrt{\kappa_i \mu p}$: Skin constant

These complex functions would lead to a model of an infinite number of reactive elements in the time domain. Their approximation by means of continuous fractions will yield linear networks consisting of linear inductors and resistors, the accuracy of which, is dependent on the order of the approximation [2].

Figure 8 shows, for example, the corresponding linear network in their order of approximation for the impedance element Zs1(p). The first approximation models the behavior of a transformer at low frequency or by dc excitation .

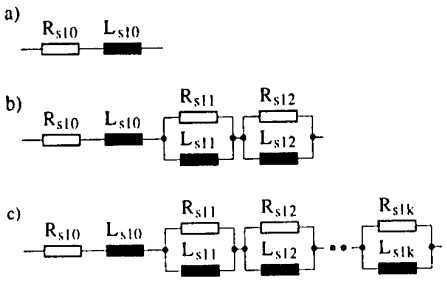



Fig. 8. Approximation of $z_{S1}(p)$, a) quasi-static b) quasi-stationary c) generalized.

It is termed quasi-static approximation. The second network represents the behavior of the transformer at higher frequency and includes the skin-effect in the transformer windings. It is termed quasi-stationary approximation. The third network represents the approximation of higher order.

The values of the network elements for the quasi-static approximation are determined by

$$R_{s10} = \frac{l_{tL1}}{\kappa_1 b_0 h_1}; \quad L_{s10} = \frac{l_{tL1}\mu h_1}{3b_0} + \frac{l_{tL2}\mu h_2}{2b_0} + \frac{l_{tI1}\mu h_{I1}}{b_0}$$

In the case of the quasi-stationary (first order) approximation, the values are obtained from

$$R_{s10} = \frac{l_{tL1}}{\kappa_1 b_0 h_1} \qquad L_{s10} = \frac{l_{tL1}\mu h_1}{10b_0} + \frac{l_{tL2}\mu h_2}{12b_0} + \frac{l_{tI1}\mu h_{I1}}{b_0}$$

$$R_{s11} = \frac{49 l_{tL1}}{20\kappa_1 b_0 h_1} \qquad L_{s11} = \frac{7 l_{tL1}\mu h_1}{30b_0}$$

$$R_{s12} = \frac{25 l_{tL2}}{6\kappa_2 b_0 h_2} \qquad L_{s12} = \frac{5 l_{tL2}\mu h_2}{12b_0}$$

Similarly, the other complex functions can be represented by their corresponding equivalent network. This is however beyond the scope of this report. The reader should therefore refer to [5] for a complete list of all the linear network parameter of this transformer model.

The parasitic capacitance between adjacent conductor layer is given by

$$C_{i,i+1} = \varepsilon_I \frac{b_o}{h_i}\left(\frac{l_{tL,i} + l_{tL,i+1}}{2}\right), \qquad (1)$$

where $l_{Lt,i}$ and $l_{Lt,i+1}$ are the mean turn length of the conductor layers, $h_i$ the thickness of the insulation layer between them and $b_o$ their width.

Fig. 9 shows the PSPICE-model for an ideal transformer. The number of turns of the individual windings is given by the transformation ratio $N_i$:1.

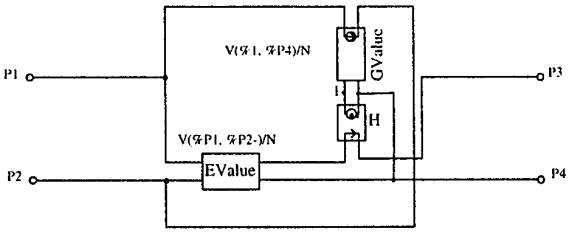



Fig. 9. PSPICE-model of an ideal transformer.

## 3.4 Example

A three winding transformer (see fig 3) was used as an example to verify the accuracy of the transformer model. The transformer consists of six individual layers, as shown in Fig. 10. The first layer consists of 44 turns, the second of 40 turns and the third of 36 turns. These layers are connected in series to form the secondary side of the transformer. Two solid wires with a diameter of about 0.23 mm each, were wound side by side for all these first three layers. The fourth, the fifth and the sixth individual layer consist each of 13 turns. The fourth winding layer serves as the primary side of the transformer. A solid wire with a diameter of d4 = 0.35 mm was used for this layer and three of these wires were wound side by side (3 in parallel). The fifth and the sixth layers were constructed with four solid wires wound side by side (parallel) with a diameter of about 0.23 mm each. The fifth layer forms the demagnetization winding. The sixth layers serves as a monitor winding. An insulation layer of thickness $h_I$=0.15 mm was used to isolate the first, the second and the third individual layer. The thickness of the insulation layer between the third and fourth is about 0.4 mm. Between the fourth and the fifth the insulation layer was also 0.15 mm thick.

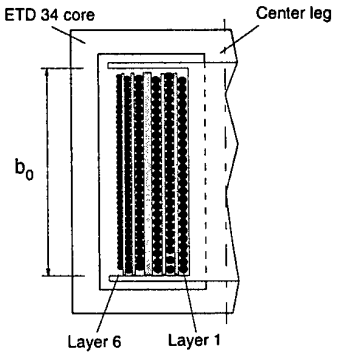



Fig. 10. Original transformer geometry.

Figure 11 shows the corresponding PSPICE-compatible model of the transformer. The impedance elements are realized as PSPICE-subcircuits [5]. $C_{12}$ and $C_{23}$ are the capacitances between the conductor layers of the secondary side of the transformer. $C_{34}$ is the capacitance between the primary and secondary side. This capacitance is responsible for noise coupling between the input and output of the converter. $C_{45}$ represents the capacitance between the primary and the demagnetization windings whilst $C_{56}$ forms the capacitance between the demagnetization and the monitor windings.

Simulations in the frequency domain (AC-analyse) were performed to determine the short circuit impedance of the transformer with both the quasi-static and quasi-stationary model.

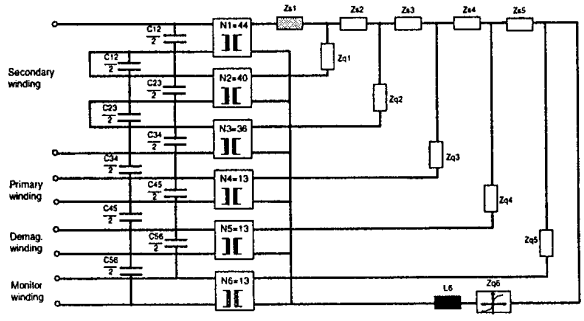



Fig. 11. Model of the transformer.

The first three layers were connected in series to form the secondary side of the transformer. The fourth and

the fifth layer were shorted whilst the sixth remain opened.

Figure 12 shows the short circuit resistance and fig. 13 the short circuit inductance (=leakage inductance) of the transformer. Experimental results are also included for comparison.

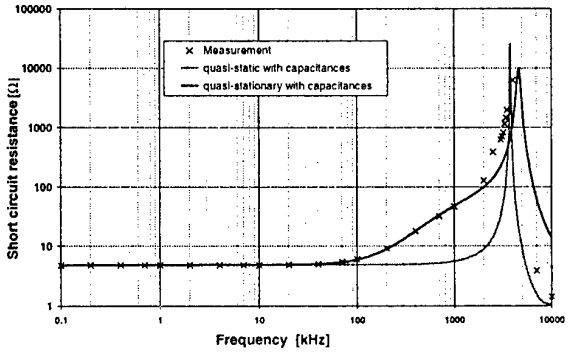



Fig. 12. Short circuit resistance of the transformer in dependence of the frequency.

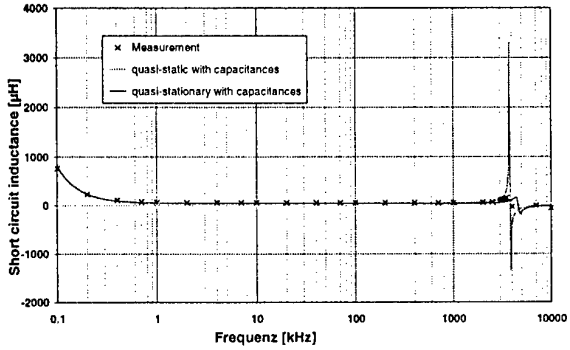



Fig. 13. Short circuit (leakage) inductance of the transformer.

It is obvious from the comparison that:
In the low frequency range, all the calculated results are in good agreement with measurement. The same applies to the short circuit inductance (fig. 13). The short circuit resistance is constant and corresponds with the value of the DC- resistance of the transformer. The short circuit resistance with the quasi-stationary model increases at higher frequencies (>100kHz). This is due to the skin-effect inside of the transformer windings.

## 4 SIMULATION OF CONDUCTED EMI

Figure 14 shows the simulation template for conducted EMI analysis and prediction. It consists basically of a model of the switched-mode power supply itself, that of a load, the model of the EMI-filter and one for an ideal Line Impedance Stabilizing Network (LISN). The line impedance stabilizing network is usually inserted between the input source and the power supply to isolate the line impedance from affecting the results of measurement.

The conducted EMI noise voltage is first measured in the time-domain across the resistance $R_{m1}$ and $R_{m2}$ and then transformed by means of the Fourier analysis in the frequency domain. The common-mode conducted noise is the arithmetic mean

$$U_{CM} = \frac{1}{2} \cdot (U_{s1} + U_{s2}) \tag{5}$$

and the differential-mode conducted EMI noise the difference

$$U_{DM} = U_{s1} - U_{s2} \tag{6}$$

of these noise voltages.

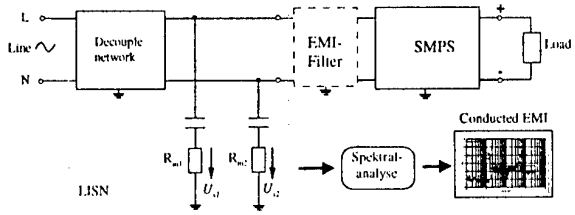



Fig. 14. Simulation template for Conducted EMI prediction.

## 5 CONCLUSION

A procedure for cost-effective design of switched-mode power supplies with regards to electromagnetic compatibility has been presented. The method is based on modeling and simulation. As such Pspice compatible models of the conductor tracks, capacitors and magnetic components has been given. The accuracy of the models were verified by experiment. Due to the limited space allowed for this paper, conduct EMI results predicted with the help of these models have been left out. The reader may refer to [3] for such.

## 6 REFERENCES

[1] P. F. Okyere; L. Heinemann, "An advanced PSPICE-Modell for high frequency Multiwinding Transformers", IEEE Power Electronics Specialists Conference 1999, U.S.A. pp. 592-597

[2] L. Heinemann; A novel SPICE-compatible high frequency multiwinding transformer model; IEEE Industrial Application Society Annual Meeting 1998

[3] P. F. Okyere, L. Heinemann, "Computer-Aided Analysis and Reduction of Conducted EMI in Switched-Mode Power Supplies" IEEE Applied Power Electronics Conference 1998, Anaheim, California. pp 924-928.

[4] *C.S. Walker:*: Capacitance, inductance and cross-talk analysis. U.S.A. Artech house, inc 1990.

[5] P. F. Okyere, "E. Effektivierung und Qualifizierung des EMV-gerechten Entwurfs von Schaltnetzteilen". Phd thesis of the Dresden University of technology. 1999

[6] P. F. Okyere, E. Habiger, "A novel physically based PSPICE-compatible model for common-mode chokes". 1999 International symposium on Electromagnetic Compatibility; Tokyo 1999.

EMC 2000 INTERNATIONAL WROCŁAW SYMPOSIUM ON ELECTROMAGNETIC COMPATIBILITY

# A SOFTWARE FOR THE EVALUATION OF FIELD PENETRATION INSIDE SHIELDING BOX WITH APERTURES

R. Azaro[1], S. Caorsi[2], M. Donelli[1], G.L. Gragnani[1] and M. Raffetto[1]

[1]Department of Biophysical and Electronic Engineering
University of Genoa, Via Opera Pia 11/A, 16145 Genova - ITALY
Tel. +39 010 3532244, Fax +39 010 3532245, e-mail:azaro@dibe.unige.it, gragnani@dibe.unige.it, raffetto@dibe.unige.it

[2]Department of Electronics
University of Pavia, Via Ferrata 1, 27100 Pavia - ITALY
Tel. +39 0382 505661, Fax +39 0382 422583, e-mail: caorsi@ele.unipv.it

*This paper describes the mathematical approach used to develop an electromagnetic simulator for the predictive analysis of the radiated immunity on printed circuit boards in metallic enclosures. The results calculated by using the developed simulator are compared with the ones obtained with a MST based measurement technique, a numerical method (FEM) and an analytical model. The most important features of the software implementation of the simulator are also provided.*

## 1. INTRODUCTION

Electromagnetic shields are usually adopted to solve both susceptibility and emission problems of an electrical or electronic device. An ideal electromagnetic shield is constituted by a closed surface made of perfect conductor that guarantees a perfect degree of isolation between the enclosed region and the external one [1], [2]. However, practical applications of shielding devices to electrical and electronic products imply the presence on the shield surface of a certain number of apertures and discontinuities (I/C ports, displays, cooling apertures, etc.). All these reductions in shield integrity result in a dramatic degradation of the attenuation capability of the enclosure. Due to the great number of applications of shielding devices in electronic industry, is quite important to develop CAD tools able to efficiently simulate the effects of apertures on shield performances by calculating the coupling of external electromagnetic field with the shielded region.

The numerical evaluation of the penetration of an electromagnetic field inside a metallic enclosure with apertures may be faced with a high degree of accuracy by means of different numerical methods: MoM, FEM, FDTD and TLM, for istance, allow the accurate modeling of electromagnetic compatibility problems, but they generally need a great amount of computational resources.

In this paper we describe a code that implements a semi-analytical model based on a modal expansion of the electromagnetic field inside the shielding box [3] and on the evaluation of the coupling, due to the presence of apertures, of the external field with the terms of the field expansion.

The validation process of the software is presented comparing the data obtained for a rectangular metallic box having a rectangular aperture on one face with the corresponding data obtained by means of a FEM code. The comparison is also done with another very efficient approximating analytical formulation based on a transmission line modelling of electromagnetic phenomena, proposed by Robinson et al. [4].

Furthermore the validation process has also involved an experimental activity; to this end the data obtained by means of the presented code, for the considered metallic box, are compared with the corresponding measured data obtained by means of an electromagnetic field measurement system based on the Modulated Scattering Technique [5], [6], [7].

Finally the comparisons are also extended to the case of a circuit enclosed in the shielding box.

## 2. ELECTROMAGNETIC PROBLEM

The problem is to determine the electromagnetic field inside a metallic box with a rectangular aperture in one of its faces, when an electromagnetic plane wave impinges on it. It is assumed that a metallic sheet (representing a PCB) is contained in the box and that the incident plane wave can have an arbitrarily (user-) defined incident direction, a frequency in the range

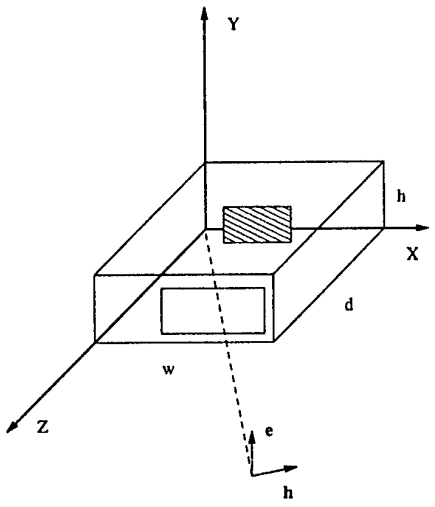



Fig.1 Problem geometry.

30 MHz - 1 GHz, and an arbitrary polarization. See Figure 1.

## 3. MATHEMATICAL PROBLEM

The problem described above is formulated as a scattering problem whose solution requires the use of numerical or semi analytical techniques. Since the geometries of the metallic box, aperture, and metallic sheet are fixed (even though their dimensions and relative positions are not), it was possible to solve the problem in an approximate way by using a semi analytical method based on a series expansion of the fields inside the box. Once the semi analytical approach was chosen, we firstly assumed the electromagnetic field on the rectangular aperture to be equal to the unperturbed electromagnetic field of the incident wave. In this way the original scattering problem was turned into an electromagnetic boundary-value problem. Moreover, it is well-known [3], [8] that, once the electromagnetic field on the aperture and the conduction currents present inside the box are known, the field inside the box is uniquely determined, being the tangential components of the electric field on the metallic walls equal to zero. As a matter of fact, the electromagnetic field inside the box can be calculated by using formulas (10.27) and (10.28) on page 299 of [3], which we report here for reader convenience.

$$\mathbf{E} = -\frac{1}{j\omega\varepsilon_0}\sum_n \frac{\int_v \mathbf{J}\cdot\mathbf{f}_n dV}{\int_v |\mathbf{f}_n|^2 dV}\mathbf{f}_n +$$

$$\sum_n \left[ -\frac{\int_s (\mathbf{u}_n \times \mathbf{E})\cdot \mathrm{curl}\,\mathbf{e}_n dS}{(k_n^2 - k_0^2)\int_v |\mathbf{e}_n|^2 dV} - \right.$$

$$\frac{k_n \int_v \mathbf{J}_m \cdot \mathbf{h}_n dV}{(k_n^2 - k_0^2)\int_v |\mathbf{h}_n|^2 dV} -$$

$$\left. \frac{j\omega\mu\int_v \mathbf{J}\cdot\mathbf{e}_n dV}{(k_n^2 - k_0^2)\int_v |\mathbf{e}_n|^2 dV} \right] \mathbf{e}_n \qquad (1)$$

$$\mathbf{H} = \frac{1}{j\omega\varepsilon_0}\sum_n \left[ -\frac{\int_s (\mathbf{u}_n \times \mathbf{E})\cdot \mathbf{g}_n dS}{\int_v |\mathbf{g}_n|^2 dV} - \right.$$

$$\left. \frac{\int_v \mathbf{J}_m \cdot \mathbf{g}_n dV}{\int_v |\mathbf{g}_n|^2 dV} \right] \mathbf{g}_n +$$

$$\sum_n \left[ -\frac{k_n \int_v \mathbf{J}\cdot\mathbf{e}_n dV}{(k_n^2 - k_0^2)\int_v |\mathbf{h}_n|^2 dV} - \right.$$

$$\frac{j\omega\varepsilon_0 \int_v \mathbf{J}_m \cdot \mathbf{h}_n dV}{(k_n^2 - k_0^2)\int_v |\mathbf{h}_n|^2 dV} -$$

$$\left. \frac{j\omega\varepsilon_0 \int_s (\mathbf{u}_n \times \mathbf{E})\cdot \mathbf{h}_n dS}{(k_n^2 - k_0^2)\int_v |\mathbf{h}_n|^2 dV} \right] \mathbf{h}_n \qquad (2)$$

$k_0$ is the free space wave number, $\varepsilon_0$ is the free space dielectric permittivity, $\mu_0$ is the free space magnetic permeability, $\omega$ is the angular frequency, $k_n$ is the wave number corresponding to the n-th mode, $\mathbf{J}$ is the electric current density vector field, $\mathbf{J}_m$ is the hypothetical magnetic current density vector field, and $\mathbf{e}_n$, $\mathbf{f}_n$, $\mathbf{g}_n$, and $\mathbf{h}_n$ are the "modes" of the cavity [9]. By the way, note that these series expansions can be applied to metallic boxes of any shape (different shapes, of course, affect the actual expressions of the modes of the cavity involved in the above series expansions).

However, while the boundary conditions are known, the current flowing on the metallic sheet which is present inside the box are not. This would prevent the use of the above formulas.

To overcome this problem, we firstly considered the problem of determining the electromagnetic field inside the empty box with the aperture. This determination

could be done by using the series expansions indicated above, as no unknown conduction currents are present in this case. In particular, the electromagnetic field could be calculated at the point of interest and at the center of the metallic sheet if it were present inside the box. Secondly, we used the value of the electric field at the center of the metallic sheet inside the box to enforce the tangential components of the electric field on the metallic sheet to zero. In particular, we considered a uniform surface current flowing on an equivalent circular metallic sheet. The only unknown was its amplitude. The electric field generated by this current, at the center of the circular metallic sheet itself, is given by

$$\mathbf{E} = \frac{1}{2}\sqrt{\frac{\mu_0}{\varepsilon_0}}\left(e^{-jk_0R} - 1\right)\mathbf{J} \qquad (3)$$

where R is the radius of the circular sheet and **J** is the vector representing the uniform tangential electric current density flowing on the sheet. This field is determined up to the arbitrary amplitude of **J** which could then be chosen so to enforce, at the center of the sheet, a zero tangential electric field.

Once its amplitude is determined, by using again the parts of the above formulas involving an electric current density (3), we can calculate the field at the point of interest due to this contribution only. By superposition, the sum of the two values of the electric field at the point of interest so far calculated gives the solution to the problem.

## 4. SOFTWARE IMPLEMENTATION

It is firstly necessary to define the problem. During this phase the following data must be provided to the procedure. Three numbers defining the depth, d, width, w, and height, h, are required to define the box dimensions. Afterwards aperture position and dimensions, are required. It is assumed that the rectangular aperture is always on the plane $z = d$. The position is then specified by providing the procedure with two numbers representing the x and y coordinates of the aperture center. The dimensions are given by its width (in the x direction) and height (in the y direction).

For the metallic sheet position and dimensions it is assumed that the metallic sheet is rectangular and that the plane containing it, is parallel to one of the coordinate planes, i.e. on this metallic sheet all points have the same coordinate x, or y, or z. The coordinates of the two vertices (six numbers) placed along the same diagonal of the rectangle must be provided. In order to describe the angle of incidence and polarization of the plane wave the following three angles are used. It is assumed that the propagation vector of the wave is incident on the origin of the coordinate system, that forms an angle $\theta$ with the x axis and that its projection onto the y-z plane forms an angle $\phi$ with the y axis. These two angles uniquely determine a line passing through the origin. Let us consider one plane orthogonal to this line. It is well known that the electric field vector is on this plane. For this reason the polarization of the electric field vector is described in terms of the angle $\varphi$ from the unit vectors $\mathbf{e}_\phi$ of the spherical coordinate system. The amplitude, and the frequency of the incident plane wave and the point of measurement of the electromagnetic field inside the metallic box (the three coordinates of the point) are required to complete the definition of the problem. Once these data are available the problem can be solved by using the mathematical approach described in the previous section. The calculated electric field at the point indicated by the user is then shown to the user by providing the following numbers: the three coordinates of the observation point, real part, imaginary part and amplitude of the three components of the electric field at that point.

## 5. NUMERICAL TESTS

In order to assess the capabilities of the software, some preliminary numerical tests were carried out.
The first test consider an empty metallic box with dimensions w=300mm, d=300mm and h=120mm. The box has an aperture of 100x5 mm, and the center of the aperture was positioned at the center of the box face. The structure is the same considered by [4] where an efficient model to study the shielding effectiveness was proposed. The electromagnetic wave considered was a uniform plane wave with a polarization along y axis and an intensity of 1 V/m; the frequency of the plane wave was varied from 400 MHz to 1 GHz. Figure 2 shows the electrical shield effectiveness against the frequency. The results are compared with the ones given in [4], in order to give a consistence check. From Figure 2 one can observe that the lower shielding effect is localized near 707 MHz, which is the resonance frequency of the structure thought as a rectangular resonator. The second example, is more interesting because considers the same box of the first example but with an aperture of 200x30 mm. As expected the shielding effectiveness is reduced with respect to the first example because the aperture is larger. The results of the simulation were compared with the results given in [4] and with the measured data obtained by using an MST based measurement technique [5], [6], [7]. The modulated scattering technique (MST) is a perturbative measurement tool based on the scattering properties of antennas and of electrically small loaded objects, used as field probes [10], [11]. These comparison are reported in Figure 3. Since the MST techniques works without any RF connection between the probe and the measurement system, the perturbations introduced in the field under measurement, inside the shielding box can be very limited if compared with traditional measurement technique. The data obtained by the modal simulator are

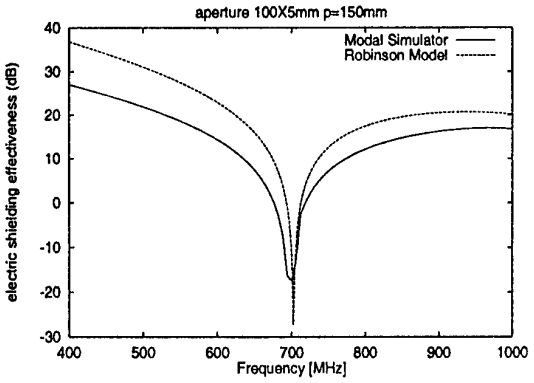



Fig. 2 Comparison between the model proposed by [4] and simulated value for an aperture of 100x5mm.

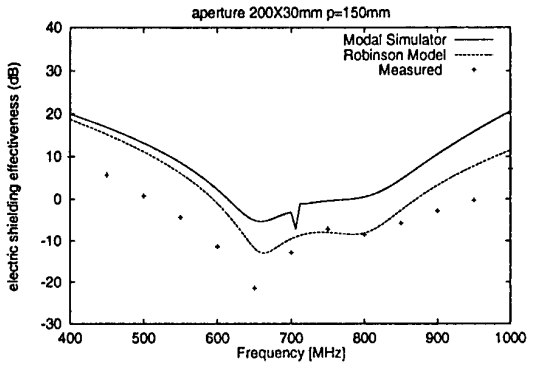



Fig.3 Comparison between measured data obtained by a MST measurement based system, Robinson et al. [4] model and the modal simulator.

in good agreement with the measured data and the model proposed in [4].

The third example considers a box of 200x100x300mm with a very large aperture of 100x80mm.

The field was computed along the z axis passing across the center of the box. Thirty uniformly spaced samples were considered. The amplitude of the incident wave was equal to 1V/m and polarized along the y direction.

Into the box a PCB of 100x90mm was placed; the PCB laid on the yz plane. Figure 4 shows the component Ey of the electric fields along the z axis in the two cases considered. The results were compared with the ones obtained by using a FEM code and the agreement was good.

## 6. CONCLUSIONS

An efficient software able to evaluate the shielding effectiveness of a metallic box has been presented. The validation process has been performed comparing the results obtained for a rectangular box with the data obtained by using an MST measurement system and the

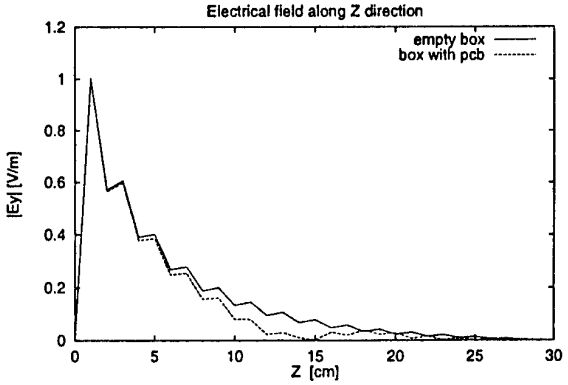



Fig.4 Simulation of the effects caused by insertion of a PCB into the box (f=30 MHz).

model proposed by Robinson et al. [4]. Due to the semi-analytical formulation of the problem the presented software results to be sufficiently accurate. This is also confirmed by the comparisons with other techniques.

## 7. REFERENCES

7.1 G. Cerri, R. De Leo and V. M. Primiani, "Theoretical and experimental evaluation of the electromagnetic radiation from apertures in shielded enclosures, "IEEE Trans. on Electromagnetic Compatibility, vol. 34, n. 4, November 1992, pp. 423-432.

7.2 H. A. Mendez, "Shielding theory of enclosures with apertures," IEEE Trans. on Electromagnetic Compatibility, vol. 20, n. 2, May 1978, pp. 296-305.

7.3 J. Van Bladen, "Electromagnetic Fields," McGraw Hill, New York, 1964.

7.4 P. Robinson, T. M. Benson, C. Christopoulos, J. F. Dawson, M. D. Ganley, A. C. Marvin, S. J. Porter and D. W. P. Thomas, "Analytical formulation for the shielding effectiveness of enclosures with aperture," IEEE Trans. On Electromagnetic Compatibility, vol.40, n. 3, August 1998, pp. 240-248.

7.5 J. H. Richmond, "A modulated scattering technique for measurement of field distributions," I.RE Trans. Microwave Theory Tech., vol. MTT-3, pp. 13-15, July 1955.

7.6 J. C. Bolomey, B. Cown, G. Fine, L. Jofre, M. Mostafavi, D. Pichard, J. Estrada, P. Fried Erich, and F. Cain, "Rapid near-field antenna testing via arrays of modulated scattering probes,"IEEE Trans. on Antennas and Propagat., AP-36, 1988, pp. 804-814.

7.7 R. Azaro, S.Caorsi, M.Pastorino, "On the relationship for the bistatic modulated scattering technique in scattering applications using scattering properties of antennas", IEEE Trans. on Antennas and

Propagation, vol. 46 n.9, September 1998, pp.1399-1400.

7.8 G. Franceschetti, "Elettromagnetic Fields," (italian) Boringhieri, Turin, 1983.

7.9 G. Conciauro, "Introduction to electromagnetic waves," (italian) McGraw-Hill, Milan, 1993.

7.10 R. Azaro and S. Caorsi, "Field uniformity test using modulated scattering probes," Proceedings 14 th International Wroclaw Symposium and Exhibition on Electromagnetic Compatibility, Wroclaw, Poland, 23-25 June 1998, pp. 183-187.

7.11 R. Azaro and S. Caorsi, "Field uniformity measurement in a TEM cell using the modulated scattering technique," Proceedings International Symposium on Electromagnetic Compatibility, EMC'98 ROMA, Rome, Italy, 14-18 September,1998, pp. 796-801.

## BIOGRAPHICAL NOTES

Renzo Azaro received the "laurea" degree in Electronic Engineering from the University of Genoa, Italy, in 1992. At present he is a Ph. D. student in "Computer science, applied electromagnetics and telecommunication engineering" at the same University. His main research interests are in electromagnetic compatibility and measurements.

Salvatore Caorsi is a full professor of Electromagnetic Compatibility at the Department of Electronics of the University of Pavia, Italy; he is also teaching the course of Antennas at the University of Genoa. He is the Past-President and founding member of the Inter-university Research Center for Interactions Between Electromagnetic Fields and Biological Systems (ICEMB). His primary activities are focused on applications of electromagnetic fields to telecommunications, artificial vision and remote sensing, biology, medicine and electromagnetic compatibility. Prof. Caorsi is a member of the AEI, EBEA and ESHO.

Massimo Donelli received the "laurea" degree in Electronic Engineering from the University of Genoa, Italy, in 1998. His main research interests are in electromagnetic compatibility.

Gian Luigi Gragnani received the "laurea" degree in electronic engineering from the University of Genoa, Genoa, Italy, in 1985. Since 1989 he has been responsible for the DIBE Applied Electromagnetics Laboratory at the University of Genoa. His primary research interests are in the field of electromagnetic scattering (both direct and inverse). In particular, he is engaged in doing research work on numerical methods for addressing electromagnetic problems, on microwave imaging, on biomedical applications of electromagnetic fields (especially microwave hyperthermia and radiometry), and on electromagnetic compatibility.

Mirco Raffetto received the "laurea" degree in Electronic Engineering ("summa cum laude") from the University of Genoa, Italy, in 1990, and the Ph. D. degree in "Models, Methods and Tools for Electronic and Electromagnetic Systems" from the same University, in 1997. Presently he is a postdoc research assistant. His main research interests are in electromagnetic direct scattering, microwave boundary value problems, and numerical methods in electromagnetism.

EMC 2000 INTERNATIONAL WROCŁAW SYMPOSIUM ON ELECTROMAGNETIC COMPATIBILITY

# PREDICTING EMI REJECTION REQUIREMENTS USING EXPERT SYSTEM BASED MODELING & SIMULATION TECHNIQUES

Andrew L. Drozd
ANDRO Consulting Services
Beeches Technical Campus
Bldg. 2, Ste. 1, Rte. 26N, Turin Road
Rome, NY 13440 USA
Fax: 315-334-1397
andro1@aol.com

Timothy W. Blocher
AFRL/IFSB
525 Brooks Road
Rome, NY 13441-4505 USA
Fax: (315) 330-7083
blochert@rl.af.mil

Anthony J. Pesta
AFRL/IFSE
525 Brooks Road
Rome, NY 13441-4505 USA
Fax: (315) 330-7083
pestaa@rl.af.mil

Donald D. Weiner, Pramod K. Varshney & Ilteris Demirkiran
Syracuse University
Department of Electrical and Computer Science, Link Hall
Syracuse, NY 13244 USA
Fax: (315) 443-4441/443-2583
ddweiner@ecs.syr.edu, varshney@cat.syr.edu & ilteris_d@yahoo.com

## ABSTRACT

*This paper describes a knowledge-based modeling and simulation capability called E³EXPERT that is being developed to predict interference cancellation requirements for co-located RF systems. An expert system is used to generate a valid computational model including all transceivers of interest. A coarse, conservative EMI analysis cull is then performed in the frequency domain. Coupling interactions are computed based on high-frequency GTD theory for high probability EMI cases. Results are ranked to determine the severity of EMI and to specify initial corrective measures with the aid of the expert system. A time-domain analysis is performed to confirm frequency-based predictions for persistent EMI cases. The knowledge base is being developed to monitor the signal environment in both domains and select the interference rejection schemes most appropriate for mitigating the effects of interferers.*

## 1. INTRODUCTION

The Electromagnetic Environment Effects Expert Processor with Embedded Reasoning Tasker (E³EXPERT) is a new capability that is being developed to model and analyze the operational compatibility of large, complex systems and their electronic subsystems. E³EXPERT is built upon an enhanced version of the Intrasystem Electromagnetic Compatibility Analysis Program (IEMCAP). Improvements and additional capabilities include: (a) a nonlinear prediction model to study receiver third-order intermodulation effects, (b) spread spectrum modulation signal models (direct sequence and slow, coherent frequency hoppers), (c) a limited non-average power receptor modeling capability, and (d) the availability of a time-domain simulation tool. The US Air Force Research Laboratory under Contract F30602-98-C-0034 sponsors the research and development to establish this capability [1, 2].

This paper provides definitive descriptions of several of these new capabilities and addresses the relative successes achieved thus far as part of a typical modeling and simulation scheme. Example problems are postulated which explain how the models are used and what results were obtained. These focus on complex aerospace systems with AM radios and spread spectrum wireless telecommunications transceivers. The approach is also relevant to analyzing the EMC of virtually any class of system consisting of multiple, co-located RF components (e.g., auto vehicles, marine vessels, radar stations, etc.). The knowledge-based aspects of the automated EMC analysis methodology captured in E³EXPERT are also explained. The knowledge base is a constantly evolving component that enhances the quality of the simulation as additional rules and knowledge about EMC problem solving methods are incorporated into its structure. Its application is illustrated for pre- and post-processing steps in the modeling, simulation and analysis scenario.

## 2. GENERATING COMPUTATIONAL MODELS

### 2.1. Creating and Validating Models

Computational electromagnetic (CEM) models can be generated in one of two basic ways. The first is by importing certain types of computer-aided design (CAD) or existing model data for selected CEM codes, and then transforming these into smooth surface models. The present capability can read in models consistent with the General Electromagnetic Model for the Analysis of Complex Systems (GEMACS), the Numerical Electromagnetic Code - Method of Moments (NEC-MOM) and the Basic Scattering Code (NEC-BSC) as well as several other CEM codes. The second way of generating a computational model is by manually creating it within a graphical editor/model building environment. Here perfectly electrically conducting (PEC) canonical objects (elliptical cylinders, cones, frusta, plates, toroids, boxes, patches and wires) are individually defined, sized, and assembled

to represent an actual system. Frequency selective surface properties (dielectrics and other non-PEC electrical characteristics) as well as loads on wires and dielectric patch elements can also be specified.

In either case the expert system pre-processor surveys the model, performs validity checks on all objects in the model, and identifies potential modeling anomalies, Feedback is provided to the analyst to correct any errors that are detected prior to committing the model to the analysis stage. An example of this is given in Figure 1 for the case of a plate (wing) that is not properly attached to a cylinder (fuselage). The final model that is generated can be displayed in the graphical editor/renderer environment, and can be further edited (i.e., trimmed or augmented). The present capability can produce valid computational models that are in accordance with the input requirements of IEMCAP, GEMACS, and several other CEM codes.

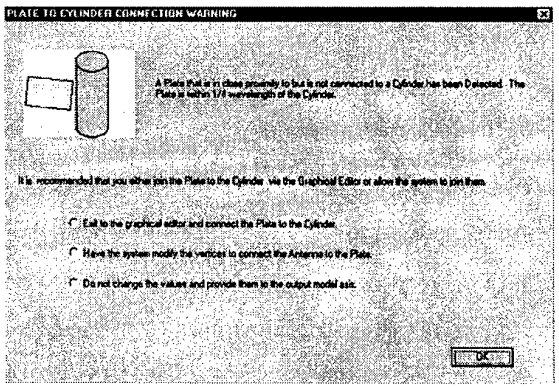



**Figure 1. Plate-to-Cylinder Error Screen**

### 2.2. Defining the Analysis Problem

In this paper, we focus on E$^3$EXPERT models for IEMCAP and GEMACS GTD coupling analyses. Figure 2 shows a graphical editor view of a detailed GTD model to be analyzed. For the IEMCAP analysis, a coarse version of this model is created. These models are identical except for the structural details (i.e., the coarse model excludes the aft stabilizers). The simplified model is "abstracted" from the detailed model to accommodate the use of IEMCAP for a coarse analysis cull.

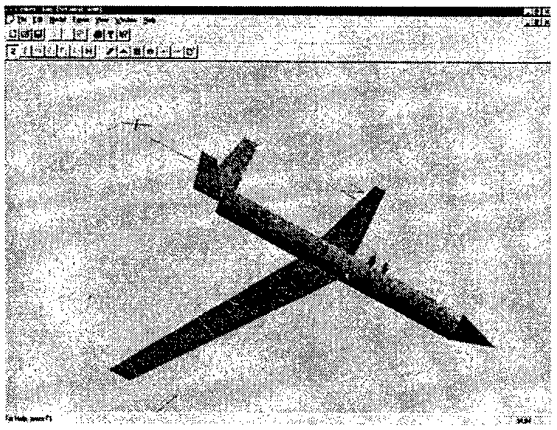


**Figure 2. Detailed Computational Model**

Both models contain several RF communications transmitting and receiving antennas that are effectively co-located on top of the cylindrical fuselage. These antennas are spaced within one meter of each other in a triangular configuration. For illustrative purposes, we only consider the problem of two transmitters coupling to a single receiver, where one transmitter produces a desired signal and the other is a potential interferer. The two transmitters and the receiver will first be treated as conventional amplitude modulated (AM) antenna ports. We will then consider the same example using direct sequence spread spectrum (DSSS) modulation for these ports. Medium frequencies (<<10 MHz regime) are considered in our example in order to keep sampling rates for FFT computations low and to reduce corresponding computation times. However, the problem can readily be extended to HF and higher frequencies. This simple scenario can also be expanded to analyze more complex models consisting of many types of RF and baseband ports, and mixed modulation signals.

After the basic CEM structure model and the location of all radiating ports have been defined, the analyst enters information about other electromagnetic, physical, and electrical properties relevant to the problem. These include transmitter power levels, receptor sensitivities, filtering characteristics, tuned and sample frequencies, modulation signals, harmonics, amplifier gains (for nonlinear interference simulations), time waveform parameters, and so on. Once all parameters have been entered, one is in the position to perform an initial coarse cull. It seems as though this step may not be necessary for our simple problem because of the small number of ports involved. However, this step becomes very important when there is a potentially large number of electromagnetic ports in the system problem. E$^3$EXPERT offers three types of solution approaches: (1) coarse, conservative baseline survey cull, (2) detailed analysis mode using a refined structure model and selected ports, and (3) a time-domain solution. In this case, the coarse model will be analyzed using the enhanced IEMCAP computational engine. The detailed model can (optionally) be run through a refined GTD computational module to more accurately compute structure and path propagation losses for selected pairs of RF antenna ports. One can also step into the time-domain mode. In particular, we will illustrate the application of modes (1) and (3), and briefly highlight the usage of mode (2) in our postulated problem.

The role of the expert system module at this point is to guide the analyst through each step of the automated modeling and simulation process. This capability is presently being implemented, tested, and refined. In effect, E$^3$EXPERT functions as an advisor to make sure that "mixed mode" models and analyses are avoided. For example, if the analyst attempts to run a detailed model through the coarse analysis stage, the built-in "expert" alerts the user about this inconsistency and walks the analyst through the proper sequence of steps to complete the modeling and analysis. This method is being further developed and implemented in the form of a "Modeling Assistant" or "Advisor".

## 3. NEW SPECTRUM MODELS

### 3.1. Power Spectral Density Representations

In view of E$^3$EXPERT incorporating a modified version of IEMCAP, we now discuss several enhancements to the code in the form of new spectrum models. The original version of IEMCAP included spectrum models for a

number of signaling waveforms (e.g., AM, FM, PDM, BFSK, Radar Pulses, etc.). These spectrum models were determined by bounding the actual spectrum of the signal. This procedure followed the worst-case design philosophy employed in the code.

More recently, spread spectrum communication systems have become quite popular. Spread spectrum techniques are currently being used quite extensively in mobile wireless communications and personal communication services (PCS) due to their interference rejection ability for handling multi-path fading and due to their ability for providing a multiple access mechanism known as code-division multiple access (CDMA). As opposed to the conventional IEMCAP signaling waveforms, spread spectrum signals are wideband in nature. There are two main spread spectrum techniques, namely direct sequence spread spectrum (DSSS) and coherent frequency hopping spread spectrum (FHSS). These two techniques differ in the manner in which they achieve spectral spreading. Although spectrum models for DSSS and slow coherent FHSS systems have been developed and incorporated in the enhanced IEMCAP code, the focus in this paper is on the DSSS model.

In DSSS systems, digitally modulated data using binary phase shift keying (BPSK), for example, is further modulated by a spreading or signature code resulting in a wideband signal. The spreading code is a pseudo noise (PN) or some other pseudo random sequence. A symbol in the PN sequence is called a chip and its duration is called a chip duration. It is usually much smaller than the message bit duration. The ratio of the message bit duration to the chip duration is known as the processing gain. This quantity determines the interference rejection capability of the system. A spectrum model for DSSS systems has been developed and incorporated in the enhanced IEMCAP. It follows the worst-case analysis philosophy of IEMCAP and is based on the bounding envelope of the actual DSSS spectrum. The two-sided power spectral density (psd) equation for the DSSS RF signal modulation model is of the form

$$S(f) = 1/2PT_{ch}\{\text{sinc}^2(f-f_c)T_{ch} + \text{sinc}^2(f + f_c)T_{ch}\} \quad (1)$$

where

$P = E_b/T_b$ is the data modulated carrier average power

$T_{ch}$ = Spreading code chip duration

$f_c$ = Carrier frequency

$E_b$ = Energy per message bit

$T_b$ = Message bit duration.

The addition of these two new spread spectrum models to IEMCAP as part of $E^3$EXPERT has significantly enhanced its utility as it can now be used for the compatibility analysis of modern communication systems and for co-site interference analysis.

## 4. FREQUENCY DOMAIN CULLS

### 4.1 Coarse Culling Procedure

An interaction matrix is developed which lists all possible interactions that could occur among the various receptors and emitters in a system. A major objective of this strategy is to isolate those elements of a matrix that can result in EMI. The initial size of the matrix can be reduced using first-order engineering culls which involve eliminating those interactions that have a high probability of not being troublesome. Only those cases that require further or more precise investigation using refined EMC tools and complementary analysis procedures remain. Therefore, the first step in the intrasystem assessment task is to model and analyze the remaining cases using a coarse culling approach.

The initial cull using $E^3$EXPERT for the simple structure model described earlier is a two-step procedure involving discrete models and numerical techniques. First, a linear cull is performed where coupling is computed on an individual port-pair (one-to-one) basis and then for multiple emitters to a singe victim receptor (many on one). To analyze receiver intermodulation effects due to nonlinearities in the receiver (i.e., RF and IF amplifiers, mixers, etc.) and because of multiple transmitter frequencies present at the receiver, a nonlinear cull is also performed. A nonlinear prediction capability has been developed and incorporated into $E^3$EXPERT for this purpose. The new model predicts 3rd-order intermodulation products, but can be extended to compute second- and higher-order terms.

### 4.2 Short Term Fourier Transform (STFT)

$E^3$EXPERT and the modified IEMCAP engine use the conventional Fourier transform to generate a time-invariant frequency-domain characterization of a signal, which reveals how the power in that signal is distributed with respect to frequency. This representation has been a powerful tool in assessments of EMC. However, there are applications where a time-frequency representation of signals would be more effective. For example, consider a complex environment consisting of several frequency-hopping emitters and receptors. Each emitter hops from one frequency to another as do the tuned frequencies of the corresponding receptors. Even though all of the equipments are active simultaneously over the same frequency band, there will be no interference provided the frequency-hopping patterns are designed such that the hopping frequencies are widely separated relative to the receptor bandwidths and, during each hopping interval, the emitter-receptor pairs utilize different frequencies. In this way, multiple operators can simultaneously use the same frequency band. The conventional Fourier transform of an emitter signal would reveal the hopping frequencies utilized by that signal, but would imply that all these frequencies were radiated together. To enable $E^3$EXPERT and its modified IEMCAP engine to determine which frequencies are actually radiated at a given instant, the short-time Fourier transform (STFT) has been added. With this new capability, a frequency-hopping signal is sliced into time segments consisting of consecutive frequency hops. The STFT is then taken of each time segment to determine its frequency content during that time interval. The IEMCAP computational engine is then employed in the usual way to determine whether or not interference situations exist for each of the time segments.

Since our simple example does not employ frequency-agile transceivers, this additional culling step is omitted. The automated methodology provided by the $E^3$EXPERT Modeling Advisor would alert the analyst of the possible need for employing the STFT technique had frequency hoppers been encountered in the analytical model.

## 5. DETAILED FREQUENCY DOMAIN ANALYSIS

### 5.1. Computing Detailed Coupling Coefficients

If the initial culls predict interferences, the next step in the analysis scheme using $E^3$EXPERT would be to then select offending emitter-receptor pairs one at a time and

analyze them using the refined analysis mode for the detailed structure model (assuming one has been generated). This involves the use of a robust GTD computational method to more accurately calculate coupling between individual pairs of emitters and receptors at critical or worst-case frequencies. Here we employ the GEMACS GTD module to illustrate how this is accomplished. To perform this step, we generate an equivalent GEMACS model for the given problem and specify the location, excitation, and loading properties of the selected emitter and receptor RF antenna ports. This is done automatically from within E$^3$EXPERT while in the "Detailed Frequency Analysis" mode. With the user involved, a GEMACS input model is created and run through the code. We obtain from this step in the analysis the coupling transfer loss based on the formula

$$\text{Power Ratio} = P_r/P_i. \qquad (2)$$

where

$P_i$ = Power input into the selected source

$P_r$ = Power received into the selected receptor load.

The power ratio is indicative of the coupling between the antenna pairs in the presence of the system structure. Alternatively, a simple equivalent circuit model method can be used to compute coupling between pairs of radiators. The authors are currently refining the design and implementation of this analysis mode.

## 6. TIME-DOMAIN ANALYSIS

### 6.1 SystemView Simulation Approach

If interferences still persists after frequency domain analyses, a time domain simulation can be performed to further verify their extent or severity. To accomplish this, an RF simulation tool called SystemView by Elanix has been incorporated within E$^3$EXPERT. SystemView applies a communications and signal processing approach to study the coupling of intended and unintentional sources to receptors in the time domain. The parameters for the time-domain analysis are input at the beginning of the E$^3$EXPERT model definition stage. The authors are presently investigating methods for automatically generating the SystemView model in accordance with the tool's input modeling requirements based on the predefined parameters.

## 7. ILLUSTRATIVE EXAMPLES

### 7.1. Linear and Nonlinear AM Example

This example is based on the simple problem postulated earlier. It primarily illustrates the nonlinear capability added to E$^3$EXPERT. For the given desired signal and interferer there is no interference when the AM receiver behaves linearly. However, a severe interference situation results when a nonlinearity is included in the RF amplifier of the receiver. E$^3$EXPERT correctly predicts both situations. SystemView by Elanix is used to visualize the demodulated waveform for each case.

The signal at the AM receiver input is given by

$$r(t) = s_d(t) + s_i(t) \qquad (3)$$

where the desired signal is the AM signal

$$s_d(t) = A_d\,(1 + \cos 2\pi f_{md} t)\cos(2\pi f_{cd} t) \qquad (4)$$

and the interferer is the AM signal

$$s_i(t) = A_i\,(1 + \cos 2\pi f_{mi} t)\cos(2\pi f_{ci} t) \qquad (5)$$

with

$f_{md}$ = 8.192 kHz, $f_{cd}$ = 1 MHz

$f_{mi}$ = 10.240 kHz, $f_{ci}$ = 1.065536 MHz.

Taking into account the emitter power levels and the coupling paths involved, E$^3$EXPERT predicted the values given in Table 1 for the various input frequencies assuming a 50-ohm receiver input impedance.

**TABLE 1. E$^3$EXPERT/IEMCAP Predicted Levels**

| Frequency (MHz) | Power (dBm) | Amplitude (V) |
|---|---|---|
| $f_{cd}$ = 1.0 | -56.2 | $A_d = 490.6\times10^{-6}$ |
| $f_{cd} + f_{md}$ = 1.008192 | -62.2 | $A_d/2 = 245.3\times10^{-6}$ |
| $f_{cd} - f_{md}$ = 0.991808 | -62.2 | $A_d/2 = 245.3\times10^{-6}$ |
| $f_{ci}$ = 1.065536 | -18.3 | $A_i = 38.6\times10^{-3}$ |
| $f_{ci} + f_{mi}$ = 1.075776 | -24.3 | $A_i/2 = 19.3\times10^{-3}$ |
| $f_{ci} - f_{mi}$ = 1.055296 | -24.3 | $A_i/2 = 19.3\times10^{-3}$ |

The linear receiver case is considered first. The AM receiver employed the following filters. The RF amplifier passband was centered at 1 MHz with a 200 kHz bandwidth while the IF amplifier passband was centered at 500 kHz with a 75 kHz bandwidth. Consequently, the frequency components of both $s_d(t)$ and $s_i(t)$ fall within the passband of the RF amplifier. However, after down conversion by a mixer with a local oscillator at 500 kHz, the frequency components of $s_i(t)$ fall outside the IF amplifier passband while those of $s_d(t)$ fall within. Hence, the interferer is removed and the 8.192 kHz message tone appears undistorted at the AM demodulator output. This scenario was simulated using System View as illustrated in Figure 3.

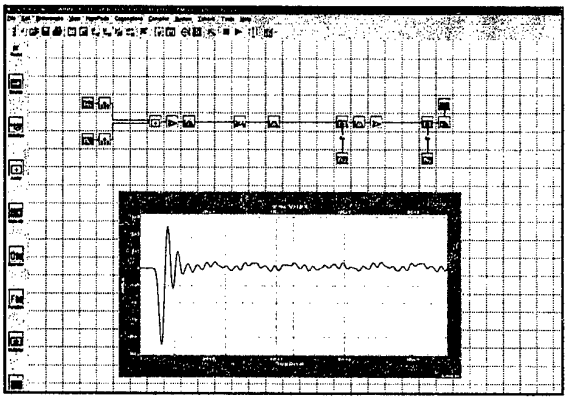


**Figure 3. SystemView AM Model**

The nonlinear receiver case is considered next. Everything remained the same except for a zero-memory nonlinearity, which was inserted into the RF amplifier. The nonlinearity was characterized by

$$y = a_1 x + a_3 x^3 \qquad (6)$$

where

$$a_1 = 3.162 \text{ and } a_3 = -168.89.$$

Because of the presence of the cubic nonlinearity, many different intermodulation components are generated at the RF amplifier output. Analysis reveals that the intermodulation component produced at ($f_{ci}$ - $3f_{mi}$) = 1.034816 MHz is the dominant interfering component which falls within the demodulator filter bandwidth of 35 kHz. This mix is of the form ($2f_1 - f_2$) where

$$f_1 = f_{ci} - f_{mi} \text{ and } f_2 = f_{ci} + f_{mi}. \qquad (7)$$

Corresponding to $a_1$ = 3.162, the linear power gain of the RF amplifier is

$$G = 10 \text{ dB}.$$

Corresponding to $a_3$ = -168.89, the 3rd-order intermodulation coefficient for the component at ($f_{ci} - 3f_{mi}$) is

$$K_3 = 82.9 \text{ dB}.$$

Utilizing G and $K_3$, the power levels at the RF amplifier output for the desired frequency component at ($f_{cd} + f_{md}$) and the interfering frequency component at ($f_{ci} - 3f_{mi}$) are predicted to be –52.2 dBm and –50 dBm, respectively. This is clearly an interference situation that was successfully predicted by E$^3$EXPERT/IEMCAP. The distorted demodulated output, as predicted by SystemView, is shown in Figure 3. Note that this interference could be eliminated by slightly narrowing the IF amplifier and or baseband filter bandwidths. This type of mitigation technique is being included in the E$^3$EXPERT knowledge/rule base.

### 7.2. Direct Sequence Spread Spectrum Example

As is well known, E$^3$EXPERT by virtue of the modified IEMCAP computational engine predicts interference based upon a worst-case approach. Accordingly, given an interference situation, IEMCAP is likely to predict the interference. However, because of this worst-case approach, IEMCAP may predict interference in a situation where, in fact, there is no interference. This example illustrates how the detailed analysis mode and SystemView can be used to check whether or not interference actually exists in such cases.

The received signal at the input to a DSSS receiver consists of a single interfering DSSS signal in addition to the desired DSSS signal. The power of the interfering signal is 50 times that of the desired signal resulting in a signal-to-interference ratio of –17 dB. The desired DSSS signal employed a chip rate of 2,000 chips/sec and a bit rate of 25 bits/sec. Consequently, the processing gain of the DSSS system for the desired signal is 19 dB. The processing gain is a measure of the antijam capability assuming a narrowband jammer. For this example, the jammer is not narrowband and there is some question as to whether the processing gain has a meaningful interpretation. Nevertheless, because the interferer is 17 dB larger than the desired signal, E$^3$EXPERT correctly flagged an interference situation using the new DSSS signal models recently incorporated into IEMCAP.

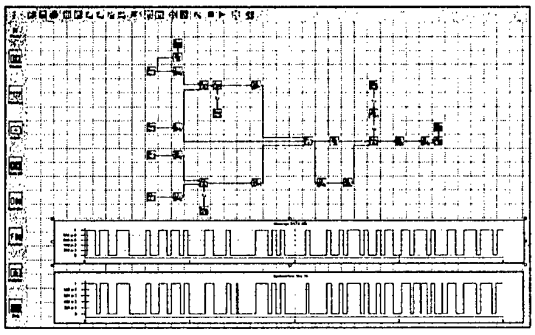


**Figure 4. SystemView DSSS Model**

SystemView was used to simulate the system in order to assess the severity of the problem. The desired signal carrier frequency was equal to the tuned frequency of the RF amplifier. The interfering DSSS signal employed a chip rate of 3,000 chips/sec and a bit rate of 25 bits/sec. The interfering signal carrier frequency was offset from the tuned frequency of the RF amplifier by 1 kHz. The bandwidth of the RF amplifier was 20 kHz. This scenario was simulated using SystemView as shown in Figure 4. The demodulated data bits are also shown in this figure along with the original message data bits. The system seems to experience a small number of errors even though the interference-to-signal power ratio is less than the processing gain of the system.

## 8. AUTOMATED EMC METHODOLOGY RULES

### 8.1 Post-Processing Interference Rejection

The knowledge base is being developed to contain rules about EMC problem-solving methods and procedures which mimics the way an experienced EMC engineer-analyst performs such tasks. This ensures that a proper analysis "flow" is maintained and a range of alternative interference mitigation techniques can be selected. Rules are employed to: (a) assist in generating valid computational models; (b) orchestrate the EMC analysis procedures to compute frequency-domain transfer functions and interference margins; (c) rank results in terms of severity and automatically specify an initial set of corrective measures to eliminate EMI in the frequency domain; and (d) deduce detailed EMI cancellation requirements. The expert system provides corresponding information to the analyst in order to work out a solution and to select one or more suitable interference rejection schemes from a library of predefined techniques depending on the type of problem, the severity of predictions, and the practicality of the mitigation solution. Mitigation techniques currently considered are: swapping equipment positions, adjusting frequencies and/or power levels to maintain RF links, specifying shielding requirements, modifying transmitter modulation parameters, time blanking, and use of filters.

## 9. SUMMARY

E$^3$EXPERT is a modeling and simulation tool which applies a knowledge-based approach to electromagnetic interference rejection analysis. Computer simulation results are shown which clearly demonstrate its effectiveness for several linear and nonlinear interference scenarios involving a collection of external RF transceivers mounted on a complex airborne structure. Research and development continues on behalf of testing and refining the tool's capabilities for EMC problem solving.

## 10. REFERENCES

[1] A. Drozd, A. Pesta, et. al. 1998. "*Application and Demonstration of a Knowledge-Based Approach to Interference Rejection for EMC*", Conference Proceedings of the 1998 IEEE International Symposium on Electromagnetic Compatibility, Denver, CO, 23-28 August 1998, pp. 537-542.

[2] A. Drozd, C. Carroll, J. Miller, et. al., "*E$^3$EXPERT - A Knowledge-Based, Object-Oriented Modeling and Simulation Capability for Predicting Detailed Interference Rejection Requirements*", Conference Proceedings of the 31st Annual Society for Computer Simulation Summer Computer Simulation Conference, Chicago, IL, 11-15 July 1999, pp. 499-504.

## BIOGRAPHICAL NOTES

Andrew L. Drozd is Owner and Chief Scientist for ANDRO. He received a B.S. degree in Physics/Mathematics in 1977 and an M.S. in Electrical Engineering in 1982, both from Syracuse University. He currently researches and applies innovative EMC modeling and simulation techniques to complex system problems. His co-authors are involved in research related to EMC, signal processing, wireless communications, radar technology, information technology, and nonlinear phenomena.

EMC 2000 INTERNATIONAL WROCŁAW SYMPOSIUM ON ELECTROMAGNETIC COMPATIBILITY

# MODELING THE MEASUREMENT OF THE TRANSIENT WAVE FROM THE OBJECT LOCATED OVER EARTH SURFACE

N. N. Kolchigin, N. P. Egorova, and S. N. Pivnenko
Radiophysics Department, Kharkov National University, 4, Svobody sq., 61077, Kharkov, Ukraine
E-mail: Nicolay.N.Kolchigin@univer.kharkov.ua

*The problem of modeling the transient electromagnetic wave beam scattering on a limited object located nearby the interface between two media is described. The solution to the problem is obtained by means of the Green's function for corresponding boundary problem and Fourier transform technique. The object surface is modelled with a set of confined plane sections of dielectric halfspace. The analysis of the considered direct scattering problem gives an opportunity to solve the problem of detection and identification of the objects located over the interface or buried into the dielectric halfspace.*

## 1. INTRODUCTION

The problem of object detection with radar exists both in the case of object location over the earth or sea surface and in the case when we wish to find and recognize the object buried under the surface. The improvement of radar measurement accuracy as well as identification problems include such actual questions as the need to account for limited nature of existing electromagnetic fields in space and time resulting in local interaction of the object and incident field. It is important to take into account the influence of nearby interface between two media when obtaining some information about the object.

In this report, the problem of modeling the transient electromagnetic wave beam scattering on a localized object located near the interface between two media is described. We restrict our problem with consideration of only dielectric objects and with case of two-dimensional transient wave beam.

## 2. STATEMENT OF THE PROBLEM

The geometry of the problem for two cases of object location regarding to the interface is shown in Figure 1.

The coordinate system Y, Z is situated in such way that the interface between two media is coincided with plane z = 0. The upper medium is implied to be the free space with permittivity $\varepsilon_0$, while the lower medium is the dielectric halfspace of permittivity $\varepsilon_1$. A dielectric object of permittivity $\varepsilon_2$ is situated near the interface and can be both over (Fig. 1a) and under it (Fig.1b).

When solving the problem, we model the object surface with a set of plane sections in such way that the object shape is well approximated.

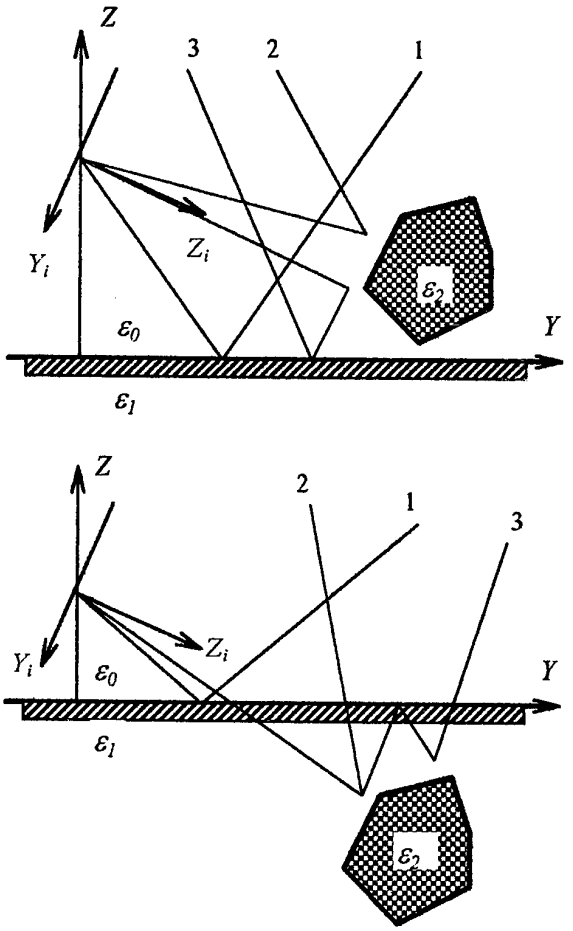



Figure 1. Arrangement of the object corresponding to two cases: (a) - the object is over interface, (b) - the object is under interface.

An antenna is modeled by the set of point sources placed at the plane $z_i = 0$ of coordinate system $Y_i$, $Z_i$. The field of the point sources represents an incident transient wave beam. This incident field can be expressed as a continuos set of plane time-harmonic

waves. Some part of spatial components of the field experienced the scattering both from the object and from the surface. After multireflections, the polarization of primary field may be changed. Such particular feature obliges determination of the reflected field of both polarization on every surface of the reflector. Thus to solve the problem it is necessary to consider both polarization of the field calculating their mutual transformation at the reflector surface.

## 3. THE METHOD OF SOLUTION

In consideration of the scattering process, we will take into account three paths of wave propagation. The ray 1 is connected with field reflected from the interface of two media. The ray 2 characterises field directly scattered on the object. And, at last, the ray 3 we connect with field scattered both on the interface and on the object. The total scattered field is the superposition of the mentioned fields scattered on all plane sections approximating the object. In that way, we reduce the solution of the stated problem to the solution of the scattering problem of transient wave beam on a confined section of dielectric halfspace that forms an arbitrary angle with nearby interface of two media followed by summation of the obtained field according to the geometry of particular problem. In order to account for transient feature of the incident field, we used the Fourier transform technique to obtain spectral representation of the field at the plane $z_i = 0$.

The method of solution of the described scattering problem is based on the use the Green's function. It consists of four stages.

At first the scattering problem of wave beam with known amplitude and phase distributions on the dielectric half-space with permittivity $\varepsilon_2$ placed at $y = L$ (surface 1) is considered (Fig. 1). The incident field is produced by electric dipoles placed at the plane $z_i = 0$ and directed normally to this surface:

$$u_{1zi} = \int_{-\infty}^{\infty}\int f(y_i',t)\, G^B(y_i, z_i, t; y_i')\, dy_i'\, dt$$

where $f(y_i', t)$ is a distribution function of the dipoles density given at the plane $z_i = 0$; $G^B(y_i, z_i, t; y_i')$ is the Green's function which in considered case is determined as [1]

$$G^B(y_i, z_i, t; y_i') = \frac{1}{2\pi}\int_{-\infty}^{\infty} \frac{\exp(ikR_1 + i\pi/4)}{2^{3/2}(\pi k R_1)^{1/2}}\, g(\omega)$$

$$\times\left(V(\gamma_{01}) - \frac{2(2\pi\exp(i\pi/2)^{1/2})}{kR_1^{1/2}} N(\varepsilon_2^{1/2}, \gamma_{01})\right) d\omega$$

where

$N(\varepsilon_2^{1/2}, \gamma_{01}) = \left((1-\gamma_{01}^2)V''(\gamma_{01}) - \gamma_{01}V'(\gamma_{01})\right)/2$;

$\gamma_{01} = \cos\Theta_{01}$; $g(\omega)$ is the spectral representation of the field at the plane $z_i = 0$. In this formulas the prime means derivative with respect to $\gamma$, and $\Theta_{0i}$ is an incidence angle in the integral representation of the field of the point source in the boundary problem solution

$$\Theta_{01} = \arccos\frac{2L - z_i}{R_i};$$

$$R_1 = \left((-y_i + y_i')^2 + (2L - z_i)^2\right)^{1/2}.$$

At second stage the scattering problem of part of incident wave beam by the interface at $z = 0$ (Fig. 1) is solved. The source's dipole moments are oriented parallel the plane $z = 0$. Along with $u_{2zi}$ component, $u_{2yi}$ component is also present in the scattered field due to four boundary conditions for $E_{yi}$, $E_{zi}$, $H_{yi}$ and $H_{zi}$. The Green's functions of the boundary problem for considered orientation of electric dipoles were determined in [1]. The perturbation introduced by the edge is neglected.

The field scattered by the interface is defined from the Green's theorem by substituting the corresponding Green's functions for Hertz components $u_{2zi}$ and $u_{2yi}$.

$$\begin{Bmatrix} u_{2yi}(y_r, z_r, t) \\ u_{2zi}(y_r, z_r, t) \end{Bmatrix} = \int_{-\infty}^{\infty} f(y_i', t) \begin{Bmatrix} G_{yi}^g(y_r, z_r, t; y_i') \\ G_{zi}^g(y_r, z_r, t; y_i') \end{Bmatrix} dy_i'$$

At the third stage the solution of scattering problem for the field defined in stage two and then scattered by the surface 1 is obtained.

And at last at the fourth stage the scattering problem of summary field found in stages one and three by the interface is solved. In that way we obtained the total reflected field at the plane $y = 0$.

Determination of space distribution of the field scattered by the dielectric surfaces is performed by the integration over considered cross-section of product of the Green's function of boundary problem and distribution density of the point sources for each polarization.

## 4. DISCUSSION

The analysis of the total scattered field allows to separate in it individual parts corresponding to various reflected rays which was described earlier. It is possible due to the time-limited nature of the incident field as well as due to the space locality of the scattering object. When time of interaction of the incident field and the object is smaller than time for the wave scattered on the object to travel to the interface and back, it is possible also to separate the part of signal corresponding to the interaction of the incident field with a single object. At that, we obtain the scattering characteristic of the object without the nearby interface.

In the case when the object is situated over the interface, the signal reflected from the object will come to the point of observation first of all. If the conditions

described above are satisfied then we obtain the scattering characteristic of the single object making use of the time separation of the observed signals. After the signal corresponding to the field scattered from the object, the signals corresponding to the field multireflected between the object and the interface in that or another sequence are follow.

When the object is situated under the interface, the signal reflected from the interface is the first one. In the absence of the object, the field in the point of observation is the only field reflected from the interface. The signal following after that is the wave reflected from the object which could be separated using the "time window". Further on, as in the previous case, the signals corresponding to the field multireflected between the object and the interface will come to the point of observation.

Thus, the analysis of the direct scattering problem gives an opportunity to solve the problem of detection and identification of the objects located nearby the interface of two media (that is the inverse problem).

The process of measurement of scattering characteristics of objects based on the described solution of scattering problem was modeled for several objects of simple shape. An experiment was carried out for the case when three re-reflected signals are taken into account which show good agreement of theoretical and experimental data.

## 5. CONCLUSION

The problem of transient electromagnetic wave beam scattering on a limited object located nearby the interface between two media is described. The proposed method of solution allows to describe many geometries of the scattering object. It also gives an opportunity to take into account various scattered waves depending on the strictness of the problem statement.

## 6. REFERENCES

6.1. L. M. Brekhovskikh. Waves in stratified media. Moscow, Nauka, 1973. (in Russian)

## BIOGRAPHICAL NOTES

**Nikolay N. Kolchigin** received combined B.Sc. and M.Sc degree in radiophysics and electronics, the Cand. Phys.-Math. Sci. (Ph.D. equivalent) degree in radiophysics, and Doctor of Phys.-Math. Sci. degree from Kharkov State University, Kharkov, Ukraine, in 1964, 1973 and 1996, respectively.

He is Deputy Head of the Chair of Theoretical Radiophysics at Kharkov National University. His current research interests include transient wave interaction with complex objects, radar cross-section measurements, design and modeling antennas for transient signals.

**Nataliya P. Egorova** received combined B.Sc. and M.Sc degree in radiophysics from Kharkov Technical University of Radioelectronics and the Cand. Phys.-Math. Sci. (Ph.D. equivalent) degree in radiophysics from Kharkov State University, Kharkov, Ukraine, in 1970 and 1999, respectively.

She is a Research Fellow at the Chair of Theoretical Radiophysics at Kharkov National University. Her research interests include wave beam interaction with dispersive and lossy dielectric media, analytical and numerical modeling of wave beam scattering on complex objects.

**Sergey N. Pivnenko** received combined B.Sc. and M.Sc degree in radiophysics and the Cand. Phys.-Math. Sci. (Ph.D. equivalent) degree in radiophysics from Kharkov State University, Kharkov, Ukraine, in 1995 and 1999, respectively.

He is a Research Fellow at the Chair of Theoretical Radiophysics at Kharkov National University. His current research interests include transient wave radiation/reception and scattering from stratified media and inclusions in that media; computer-aided design, experimental and theoretical analysis of passive microwave-circuit components, antennas and antenna arrays.

EMC 2000 INTERNATIONAL WROCŁAW SYMPOSIUM ON ELECTROMAGNETIC COMPATIBILITY

# SQUARING AND SMOOTHING IN EMC MODELS: A STATISTICAL SOLUTION

Eduard G. Kourennyi*, Viktor A. Petrosov**, Natalia N. Pogrebnyak*
*Chair of EPG, The Donetsk State Technical University, Artema St., 58, Donetsk 830000 Ukraine,
led@dgtu.donetsk.ua
**Chair of EPP, The Priasovsk State Technical University, Republic alley., 7, Mariupol 87500 Ukraine

*The task of EMC estimation subject to capacity of a casual noise disturbance and sluggishness of object - by squaring and smoothing is considered. It is shown that distribution low of the casual process after squaring and smoothing is beta-distribution. The solution of the problem is illustrated by an example of an estimation of permissible voltage unbalance.*

## 1.PROBLEM DEFINITION

A dynamic EMC-model of an object usually includes a linear filter, a squaring and smoothing (SS) unit and a statistical analysis unit: for example the flickermeter (IEC, Publication 868, 1986). The filter simulates reaction $y(t)$ of object to noise disturbance, and the SS unit takes into account the fact that the consequences of EMC infringement depend on capacity of reaction and sluggishness of object. We will conditionally refer to the ordinates of process $\Psi_T(t)$ after SS as doses (by analogy to a dose of flicker). The relation between the processes before and after SS is described by the differential equation

$$T\Psi_T' + \Psi_T = y^2 \qquad (1)$$

where $T$ is the time constant of the sluggishness of the object.

The heart of the problem is definition of density of distribution $f(\Psi_T)$ or distribution function $F(\Psi_T)$, based on which the peak value $\Psi_{T\max}$ of the dose is calculated (excess of $\Psi_{T\max}$ is possible with the given probability $E_x$). The right part of the equation is generally nonlinear, therefore the exact solution only exists for the special case of a telegraph signal. The approximate solution in expanded form of Edgeworth series is known, but the necessary initial information is inaccessible in practice.

The statistical solution of the SS problem by methods of simulation (synthetic sampling) is given in this report. For brevity the elementary EMC-model without the filter, when $y = x$ is considered. Such a model is applied to estimate an additional overheating of objects from non-sinusoidal and unbalanced voltage. In these cases the acceptable continuous value $[y]$ of the noise disturbance is standardised, and purpose of the study is determination of "an inertial maximum" $y_{T\max} = \sqrt{\Psi_{T\max}}$. The requirement of EMC is that $y_{T\max} \le [y]$.

Estimated value of the dose is calculated on the acceptable probability $E_x$ of its excess by the solving of the equation

$$F(\Psi_{T\max}) = 1 - E_x. \qquad (2)$$

In the standard of the quality of the electric power in the countries of Commonwealth of Independent States, a value $E_x = 0{,}05$ is accepted. Since objects with different time constant of sluggishness can be connected to electric power supply network, a dependence of inertial maximum on $T$ should be generally obtained.

## 2. SIMULATION OF THE DOSE

There are various methods for simulation of casual processes. In systems of power supply, which carry group of noise disturbance sources, it is expedient to use summation of individual noise disturbances with casual shifts. When realisations follow the law of normal distribution, each realisation $y(t)$ is formed by sum of a large number of $n$ "elementary" processes ($n = 100 \div 1000$) of the simple form. The elementary process has a mean value equal to zero and correlation function (KF) $n$ times smaller than the desired KF $k_y(\tau)$ of the simulated process. The mean value $\bar{y}$ of a process $y(t)$ is added to $y(t)$ after summation of elementary processes and before the operation of squaring.

To determine the statistical solutions, it is necessary to simulate an ensemble of a large number $N$ of realisations of process $y(t)$. Fig. 1 shows a sample of 5 of $N = 500$ realisations of normal process of negative sequence voltage changes with mean value

$\bar{y} = 1{,}6\%$, standard deviation $\sigma_y = 0{,}5\%$ and exponential correlation function having time of correlation $\tau_к = 5\,\text{c}$.

Each realisation $y(t)$ -is squared, and the corresponding realisations of doses are calculated using Duamel integral:

$$\Psi(t) = \frac{1}{T}\int_0^t e^{-\xi/T} y^2(t-\xi)d\xi = \int_0^t (1 - e^{-\xi/T})\left[y^2(t-\xi)\right] d\xi \qquad (3)$$

where $\xi$ is integration variable.

In practice, a transient comes to the end during the time $t_p = (5-6)T$. When, due to nature of the task, it is enough to compute only a distribution function, simulation stops at $t = t_p$. If, in addition, it is necessary to calculate KF of doses over the range of argument from 0 to $\tau_{max}$, then the time of simulation is equal to $t_p + \tau_{max}$. In Fig. 1b, five realisations of doses are shown at $T = 10\,\text{S}$. Realisations of doses correspond to realisations in Fig. 1a.

As simulation methods provide new knowledge, the requirements for the quality of simulation must be greater than for processing experimental data. It is also necessary to take into account, that the operation of squaring increases an error Therefore, in addition to checking the fidelity of reproduction of distribution function and KF of process $y(t)$, it is necessary to check reproduction of distribution function of process $y^2(t)$, which can be determined analytically from $f(y)$ or $F(y)$. The additional check at $T = 0$ ensures quality of simulation of doses at $T > 0$, as the smoothing reduces the error.

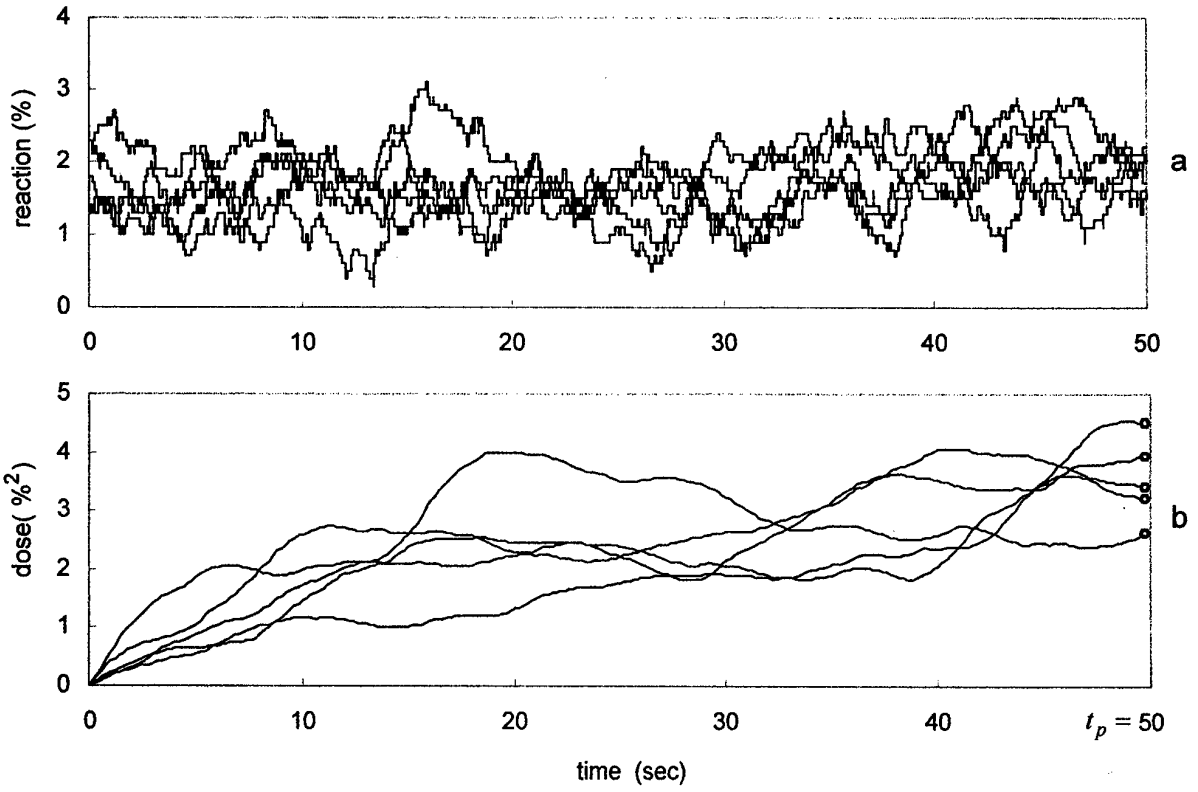



Figure 1.

## 3. STATISTICAL DECISION

The desired laws of statistical distribution are found from the corresponding cross-section of the ensemble of realisations Under stationary conditions, it is sufficient to consider only one cross-section (circles in Fig. 1b).

Only the mean value of a dose is known a priori:

$$\overline{\Psi}(t) = \left(\bar{y}^2 + \sigma_y^2\right)\left(1 - e^{-t/T}\right). \qquad (4)$$

Based on ensemble of realisations, it is possible to calculate the distribution moment coefficients of any

order as well as to select approximation by multi-parametrical Jonson's or Pirson's formulas. However the accuracy of definition of the moment coefficients for orders higher than two is poor. Therefore it is necessary to limit the calculation of the standard deviations of doses $\sigma_T$ and to select two-parametrical approximation law. Generally, the range $(\Psi_{Tm}, \Psi_{TM})$ of possible values of doses is finite. The numerous simulations showed that it is possible to accept for approximation beta-distribution with parameters expressed through quantities $\overline{\Psi}$ and $\sigma_T$ by the formulas:

$$\gamma = c(\overline{\Psi} - \Psi_{Tm})/\chi, \quad \eta = c(\Psi_{TM} - \overline{\Psi})/\chi \qquad (5)$$

where $\chi = \Psi_{TM} - \Psi_{Tm}$,

$$c = (\overline{\Psi} - \Psi_{Tm})(\Psi_{TM} - \overline{\Psi})/\sigma_T^2 - 1.$$

Distribution density of doses is:

$$f(\Psi_T) = \frac{\Gamma(\gamma+\eta)}{\chi^{c-1}\Gamma(\gamma)\Gamma(\eta)}(\Psi_T - \Psi_{Tm})^{\gamma-1} \times \times (\Psi_{TM} - \Psi_T)^{\eta-1} \qquad (6)$$

where $\Gamma(x)$ - gamma- function .

For a telegraphic signal with impulse value of $\pm B$ and the same central tendencies of duration ($t_1 = t_2$), equation (6) coincides with the known solution, provided that $\Psi_{Tm} = -B$, $\Psi_{TM} = B$, $\chi = 2B$. However there is no analytical solution at $t_1 \neq t_2$. Fig. 2 shows statistical density of distribution (curve 1) and curve 2, calculated on the formula (6) for $t_1/t_2 = 0{,}7$ and $\alpha T = 4{,}8$.

In this specific case of the normal distribution of the reaction, the doses are confined only by lower limit $\Psi_{Tm} = 0$. In addition to the average mean value, the standard deviation of doses is also known in this case. For example, for exponential KF

$$\sigma_T^2 = \frac{2\sigma_y^4}{1+2\alpha T} + \frac{4\bar{y}^2\sigma_y^2}{1+\alpha T}.$$

Here it is possible to use gamma-distribution with parameters $s = \overline{\Psi}^2/\sigma_T^2$, $\lambda = \overline{\Psi}/\sigma_T^2$ and distribution density

$$f(\Psi_T) = \frac{\lambda^s}{\Gamma(s)}\Psi_T^{s-1}e^{-\lambda\Psi_T}. \qquad (7)$$

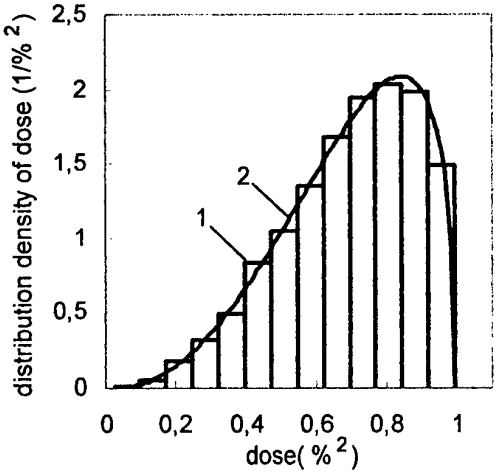



Figure 2.

Statistical and theoretical distribution functions (curves 1 and 2) are shown in Fig. 3 for an example of the negative sequence voltage. In Fig. 4, the satisfaction of the EMC requirement on permissible value $[y] = 2\%$ is checked: the same noise disturbance is inadmissible for objects with small inertia (crosshatched region), while it is admissible for the objects with large inertia. Neglecting sluggishness results in overestimating the requirements to EMC.

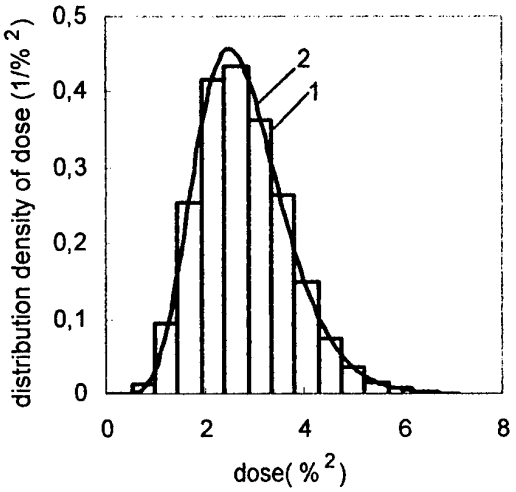



Figure 3.

In the practical applications, the number of terms in Edgeworth series is limited to 3-4. Indeed, due to lack of information about the distribution moment coefficients with the orders higher than three, an uncontrollable error and, in some cases, senseless results (negative value for the doses or ordinates of distribution density) occur. Thus we do not recommend using

Edgeworth series for the approached solution of an SS-problem.

It is known that the linear inertial systems normalise processes. The methods of simulation enable determination of the minimal value of time constant $T$, at which a hypothesis about normal distribution of doses can be accepted. In many cases it is only acceptable at very large values of $T$, at which the maximum and the mean value of a dose are become indistinguishable.

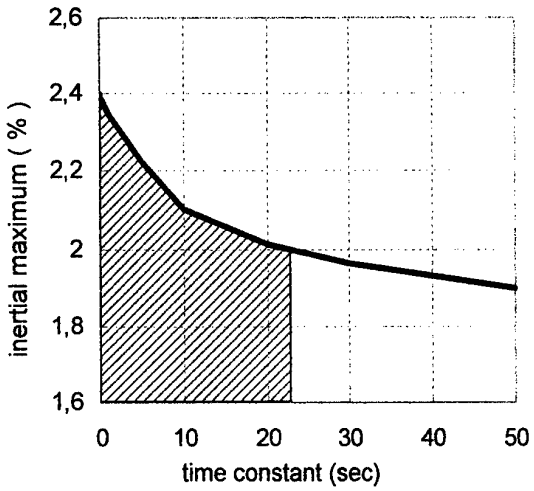



Figure 4.

## 4. CONCLUSIONS

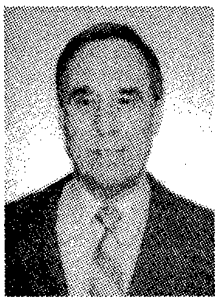
For the solution of the SS-problem, it is necessary to use methods of simulation of casual processes as an ensemble of realisations.

Generally, it is expedient to apply beta-distribution as an approximation of the statistical distribution laws for doses.

For the normally distributed reactions, acceptance of the hypothesis about gamma-distribution of doses gives the analytical solution.

The application of of Edgeworth series and hypothesis about normal distribution of doses is not recommended.

## BIOGRAPHICAL NOTES



Eduard G. Kourennyi. M. Eng. (The Novocherkask Polytechnical Institute), Doctor of Sciences, Professor of the Department of Electrical Supply of Industry and Sities (ESIS) of the Donetsk State Technical University (DSTU), Expert of the Ukraine Superior Certifying Commission, S. A. Lebedev Award of Ukrainian Academy of Sciences, Consulting of the joint-stock company «Stirol» (Ukraine), Member of IAEE. Scientific interests: ESIS, EMC, electrical saving, statistic dynamics of energy systems.



Victor A. Petrosov. M. Eng. (The Priazovsk State Technical University), Ph. D, deputy mayor of Mariupol (Ukraine). Scientific interests: EMC, electrical saving.



Natalia N. Pogrebnyak. M. Eng. (DSTU), Ph. D., junior lecture of the Department of ESIS of the DSTU. Scientific interests: EMC, electrical saving.

EMC 2000 INTERNATIONAL WROCŁAW SYMPOSIUM ON ELECTROMAGNETIC COMPATIBILITY

# MAGNETIC ANALYSIS OF INHOMOGENEOUS DOUBLE-LAYER SHIELDS AT LOW FREQUENCIES

Eugeniusz Kurgan
University of Mining and Metallurgy, Dept. of Electrical Engineering
al. Mickiewicza 30, 30-059 Krakow, Poland

*This paper describes an analysis of double layer shields at low frequencies by mixed finite and boundary element method in the case where material parameters depends spatially from co-ordinates.*

## 1. INTRODUCTION

Double-layer shields in the last years have received attention in magnetic shielding of devices at low frequencies. Both theoretical and experimental papers were published in this topic. It was proved that such shields could be optimal when thickness of these two layers has some prescribed thickness ratio[1]. This means that for optimal shielding the reduced field has a lowest value compared with any other material thickness combination.

Most of the previous works was done with the assumption that all layers were made of materials, which are linear, isotropic and homogeneous [6]. This is a frequent case. However, there are cases when we need to analyse shields produced from inhomogeneous materials, that is materials which conductivities depend spatially from co-ordinates. Such case is considered in this paper.

In such problems, generally it is impossible to analyse shielding defectiveness using analytical methods. The reason is that associated partial differential equations describing electromagnetic fields in these cases are inhomogeneous and generally for any prescribed vales of $\sigma$ and $\mu$ are very difficult to solve analytically [2]. The only approach is throughout numerical simulation.

In such situation, generally two methods are used: finite element method and boundary element method. The first of these methods has ability to easy treat inhomogeneous materials but has also some disadvantages. The main disadvantage is that one needs to divide on finite elements the domain where we do not want to calculate the field. This unnecessarily increases a number of unknowns in resulting system of equations [5].

The boundary element method (BEM) on the other hand is recognised in electromagnetic field computations as a powerful alternative to the finite element method. Design engineers have noticed that with the continuing increasing in computer power, the major part of the overall cost of performing a numerical analysis is the preparation of the data describing the problem. In contrary to FEM, when using boundary elements the only part of the problem geometry that requires discretisation are boundary surfaces. Thus, boundary element discretisation is always one dimension less then the dimension of the analysed problem. Unfortunately, BEM has serious problems with treating inhomogeneous materials. So the logical conclusion is to use both of them simultaneously: finite element method to discretize the inhomogeneous material domains and boundary element method to calculate the field outside material, that is in the air, which is always homogeneous [3,5].

This paper extents the previous results on the double-layer shielding to the cases where material constants depend spatially from co-ordinates and uses numerical approach based on combined finite element and boundary element approach.

## 2. THEORETICAL BACKGROUND

At low frequency shielding is one of effective approach against electromagnetic field interference. Recently, magnetic shielding is being considered as an promising alternative approach in a device design at power frequencies. Successful application of magnetic shielding can be found in some scientific papers [1,6]. In resent years double year shields are one that drown attention of many device designers. Usually it is assumed linear, isotropic and homogenous material properties. This is indeed a frequent case. But in many cases the material the shielding layers are made are inhomogeneous. This can be caused by manufacturing factors or even introduced intentionally. One can suspected

that spatial non-linear dependence of conductivities in cylindrical shields can makes shielding even more effective. Therefore numerical methods of calculation of electromagnetic shielding effects are of great importance. One of the most promising method is combined finite element and boundary element (FEM-BEM) method. In this paper this method will be applied to calculation of shielding effectiveness of cylindrical double layer magnetic shield.

Figure 1 shows the multiply connected eddy current problem investigated in this paper. It is assumed that eddy currents are present only in region $\Omega_e$, where conductivity and permeability are assumed to be dependent from spatial coordinates. Region $\Omega_0$ is a free space region (air region) with given current density **J**, which is considered as given. In finite element region $\Omega_e$ both permeability $\mu_e$ and conductivity $\sigma_e$ can depend from spatial coordinates. The boundary element region can contain only linear, isotropic and homogeneous materials. In the case when for some part of the boundary $\Gamma_e$ the filed doesn't extends beyond this boundary, this part doesn't need to contact with boundary element region. In the other cases, the BE-region should surround the FE-region. It is assumed, that current excitation is placed in air BE-region. The electromagnetic phenomena can be described in terms of electric field **E** and magnetic field **H** which are intimately related to the electric and magnetic flux densities **D** and **B**. The other choice it to use magnetic vector potential **A** end electric scalar potential $\varphi$.

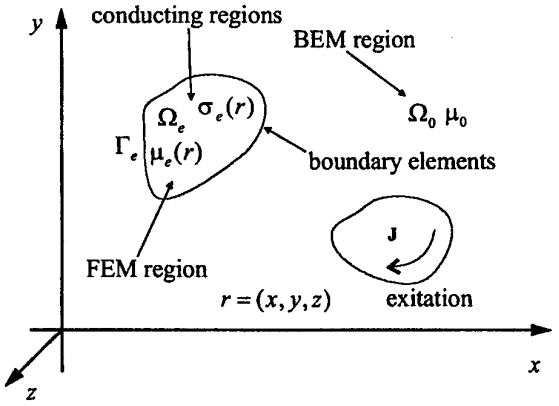



Fig1. FEM and BEM regions for hybrid FE-BE solution of open boundary electromagnetic quasi static problem.

From Maxwell's equations, neglecting the displacement current, the fundamental equation for eddy current problem may be describe as follows [3]:

$$\nabla\times\left(\frac{1}{\mu_e}\nabla\times\mathbf{A}\right)+\sigma_e\frac{\partial\mathbf{A}}{\partial t}+\sigma_e\nabla\varphi=0 \tag{1}$$

$$\nabla(\nabla\varphi)+\nabla\left(\frac{\partial\mathbf{A}}{\partial t}\right)=0 \tag{2}$$

Both of these equation have to fulfil adequate boundary conditions, if it is necessary. In derivation of these equation it was assumed that

$$\mathbf{B}=\nabla\times\mathbf{A} \tag{3}$$

$$\mathbf{E}=-\nabla\varphi-\frac{\partial\mathbf{A}}{\partial t} \tag{4}$$

In sinusoidal steady state we can define following complex amplitudes [2]:

$$\mathbf{A}=\mathrm{Re}[Ae^{j\omega t}] \quad \varphi=\mathrm{Re}[\varphi e^{j\omega t}] \tag{5}$$

where $A$ and $\varphi$ are complex amplitudes

$$A=A_r+jA_i=Ae^{j\Psi_A} \quad \varphi=\varphi_s e^{j\Psi_\varphi} \tag{6}$$

In this case equations (1) and (2) will have following form:

$$\nabla\times\left(\frac{1}{\mu_e}\nabla\times A\right)+j\omega\sigma_e A+\sigma_e\nabla\varphi=0 \tag{7}$$

$$\nabla\cdot\left(j\omega A+\nabla\varphi\right)=0 \tag{8}$$

## 3. FINITE ELEMENT FORMULATION

In FEM-BEM model where boundary elements are superimposed on $\Gamma_e$, the scalar potential $\varphi$ is essential to maintain the continuity between regions of different conductivity. In order to avoid ambiguity in definition of the magnetic vector potential $A$, the Coulomb gauge $\nabla\cdot A=0$ should be imposed and the term $-\nabla\left(\frac{1}{\mu_e}\nabla\cdot A\right)$ should be inserted into equation (7):

$$\nabla\times\left(\frac{1}{\mu_e}\nabla\times A\right)+j\omega\sigma_e A-\nabla\left(\frac{1}{\mu_e}\nabla\cdot A\right)+\sigma_e\nabla\varphi=0 \tag{9}$$

Unfortunately, when we discretize (9) and (8), the overall system matrix, which corresponds to FE part of the problem, is non-symmetric. Authors in [3] have proposed a variable transformation from $\varphi$ to $\varphi'$, which makes resulting matrix symmetric:

$$\varphi=\frac{\partial\varphi'}{\partial t} \tag{10}$$

Thus the final set of symmetric equation is:

$$\nabla\times\left(\frac{1}{\mu_e}\nabla\times A\right)+j\omega\sigma_e A-\\ -\nabla\left(\frac{1}{\mu_e}\nabla\cdot A\right)+j\omega\sigma_e\nabla\varphi'=0 \tag{11}$$

$$\nabla\cdot\left(j\omega A + j\omega\nabla\varphi'\right) = 0 \tag{12}$$

The usual Galerkin weighted residual method is applied to the above equations [5], which gives:

$$\sum_{i}^{N_{fe}}\int_{\Omega_{ei}}\left[-\left(\nabla N_i\times\frac{1}{\mu_{ei}}\times A\right)+j\omega\sigma N_i A+\right.$$
$$\left.+\frac{1}{\mu_{ei}}\nabla N_i\nabla\cdot A+j\omega\sigma N_i\nabla\varphi'\right]d\Omega- \tag{13}$$
$$-\sum_{i}^{N_{be}}\int_{\Gamma_{ei}}N_i\left(\frac{1}{\mu_{ei}}\nabla\times A\times\mathbf{n}\right)d\Gamma = 0$$

$$\sum_{i}^{N_{fe}}\int_{\Omega_{ei}}\sigma\nabla N_i\cdot\left(j\omega A+\nabla\varphi'\right)d\Omega-$$
$$-\sum_{i}^{N_{be}}\int_{\Gamma_{ei}}\sigma N_i\left(j\omega A+\nabla\varphi'\right)d\Gamma = 0 \tag{14}$$

where $N_i$ are shape functions for given problem, $\Omega_{ei}$ are finite elements, $N_{fe}$ is a number of finite elements, $\Gamma_{ei}$ are boundary elements, $N_{be}$ is a number of boundary elements and $\mathbf{n}$ is unit normal vector to the boundary $\Gamma$ at given point.

## 4. BOUNDARY ELEMENT FORMULATION

The boundary element method is applied to current carrying region with $\sigma = 0$ and $\mu = \mu_0$. It can be shown, that in this region the electromagnetic field is given by relation

$$\nabla\times\nabla\times A = \mu_0\mathbf{J} \tag{15}$$

and can be described only by vector potential $A$ alone. The vector $\mathbf{J}$ is an exiting current density. Utilising also in this case the weighted residual approach, we get the integral equation, which is the starting point in derivation of boundary integral equation for the air region:

$$\int_{\Omega}\left(\nabla\times\nabla\times A\right)\cdot\mathbf{G}d\Omega = \int_{\Omega}\mu_0\mathbf{J}\cdot\mathbf{G}d\Omega \tag{16}$$

where $\mathbf{G}$ is weighting function which in this case can be assumed as equal

$$\mathbf{G} = G\mathbf{a} \tag{17}$$

where $\mathbf{a}$ is any unit constant vector and $G$ is a Green's function defined by the following partial differential equation:

$$\nabla^2 G(\mathbf{r},\mathbf{r}') = -\delta(\mathbf{r}-\mathbf{r}') \tag{18}$$

Thus, $G(\mathbf{r},\mathbf{r}')$ *is* the free space Green's function of the Laplace equation (18) and for two dimensional problems has for 2D the value

$$G(\mathbf{r},\mathbf{r}') = -\frac{1}{2\pi}\ln|\mathbf{r}-\mathbf{r}'| \tag{19}$$

and for 3D problems

$$G(\mathbf{r},\mathbf{r}') = \frac{1}{4\pi|\mathbf{r}-\mathbf{r}'|} \tag{20}$$

where $\mathbf{r}$ and $\mathbf{r}'$ are observation point and source point, respectively. In order to transform (16) to into boundary integral equation we have to use vector form of the second Green's identity [2]. Thus we have:

$$\int_{\Omega}A\cdot\left(\nabla\times\nabla\times\mathbf{G}\right)d\Omega+$$
$$+\int_{\Gamma}\left(A\times\nabla\times\mathbf{G}-\mathbf{G}\times\nabla\times A\right)d\Gamma = \int_{\Omega}\mu_0\mathbf{J}\cdot\mathbf{G}d\Omega \tag{21}$$

The first integral in the above equation can be further transformed to the form using Gauss theorem:

$$\int_{\Omega}A\cdot\nabla\times\nabla\times G\mathbf{a}\,d\Omega = \mathbf{a}\int_{\Gamma}\nabla G\left(A\cdot\mathbf{n}\right)d\Gamma \tag{22}$$

and both surface integrals in (21) can be written as

$$\int_{\Gamma}\left(A\times\nabla\times\mathbf{G}-\mathbf{G}\times\nabla\times A\right)d\Gamma =$$
$$=\mathbf{a}\cdot\int_{\Gamma}\left[\left(\mathbf{n}\times A\right)\times\nabla G+\left(\mathbf{n}\times\nabla\times A\right)G\right]d\Gamma \tag{23}$$

After substitution the above both relations to (21) and using definition of Green's function in free space

$$\nabla^2 G(\mathbf{r},\mathbf{r}') = -\delta(\mathbf{r}-\mathbf{r}') \tag{24}$$

we finally get the boundary integral equation in free space as:

$$c_i A_i - \int_{\Gamma}G\left[\left(\nabla\times A\right)\times\mathbf{n}\right]d\Gamma - \int_{\Gamma}\nabla G\times\left(\mathbf{n}\times A\right)d\Gamma$$
$$-\int_{\Gamma}\nabla G\left(A\cdot\mathbf{n}\right)d\Gamma = \int_{\Omega}\mu_0\mathbf{J}G d\Omega \tag{25}$$

$c_i = c_i(\mathbf{r}_i)$ is a constant determined from the Cauchy's principal value integration of the Geern's function singularity [8] and $\mathbf{r}_i$ is a collocation point and depends only on problem geometry.

Equations (13), (14) and (25) can now be coupled together, because the term $(\nabla\times A)\times\mathbf{n}$ is present in both equations and thus making possible the linking process between the FEM and BEM easy. The discretization of (13), (14) and (25) can be done in standard way and will be not described here [7].

After discretization, integrating and linking a system matrix equation is solved for variables $A$ and $\varphi'$. Induction vector $\mathbf{B}$ can be calculated as $\mathbf{B} = \nabla\times A$ as follows:

$$\mathbf{B} = -\int_{\Gamma}\left[\mathbf{n}\times(\nabla\times A)\times\nabla G\right]d\Gamma - \\ -\int_{\Gamma}\left[\mathbf{n}\cdot(\nabla\times A)\right]\cdot\nabla G d\Gamma + \int_{\Omega}\mu_0\mathbf{J}\times\nabla G d\Omega \qquad (26)$$

This is an extension of Biot-Savart's law to an air region bounded by a surface $\Gamma$.

## 5. AN ILLUSTRATIVE EXAMPLE

To demonstrate the capability of the method an example of a cylindrical shielding structure is considered. Two metallic cylindrical shields with a source conductor located inside together with dimensions are shown in Fig. 2. The inner layer is made from aluminium and external layer from iron. The current carrying inner strand is assumed to be laminated and not exhibits eddy current induction properties.

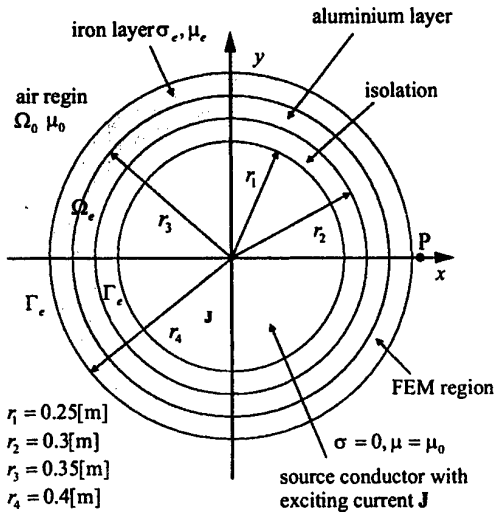



Fig.2. Problem geometry of double layer shield.

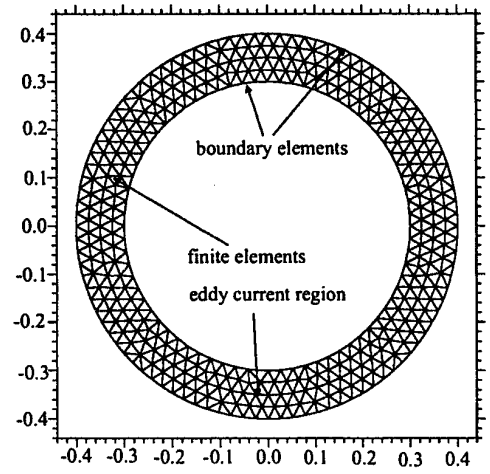



Fig3. Conducting eddy current domain is divided into finite elements and its boundary into boundary elements.

The inhomogeneous material conductivities and permeabilitis in conducting regions are given by:

– in aluminium layer:

$$\sigma_e = 3.4\cdot 10^6 \frac{1}{r_3^2}\left(x^2+y^2\right)\left[\frac{\mathrm{S}}{\mathrm{m}}\right]$$

$$\mu_e = 100\mu_0$$

– in iron layer:

$$\sigma_e = 1.6\cdot 10^6 \frac{1}{r_2^2}\left(x^2+y^2\right)\left[\frac{\mathrm{S}}{\mathrm{m}}\right]$$

$$\mu_e = \mu_0$$

The current density in source cylinder has a value:

$$\mathbf{J} = 10000\left[\frac{\mathrm{A}}{\mathrm{m}^2}\right]$$

The frequency in numerical experiments was changed from 10 [Hz] to 10000[Hz]. First the conducting eddy current region was divided into 669 finite elements with together 2592 nodes and boundary of this region into 168 quadratic elements.

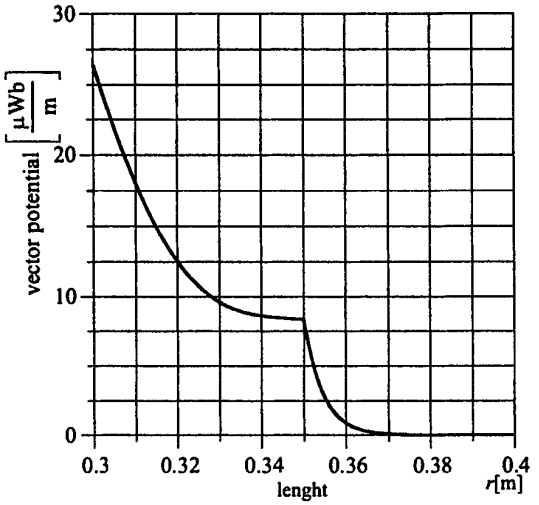



Fig4. Plot of the modulus of the magnetic vector potential along cable radius in conducting region at 50[Hz].

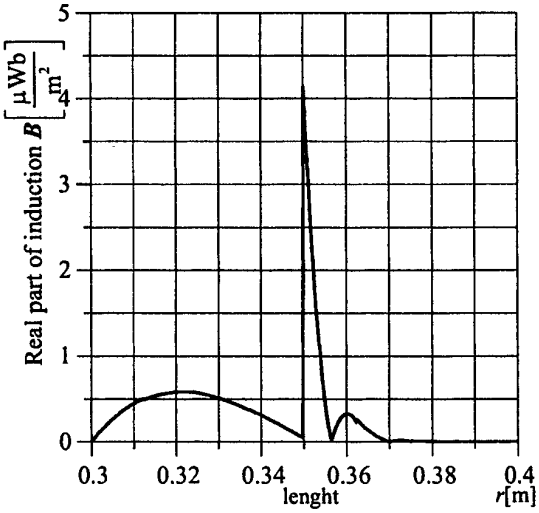



Fig5. Plot of the real part of the induction vector along cable radius in conducting region at $f$ = 50[Hz].

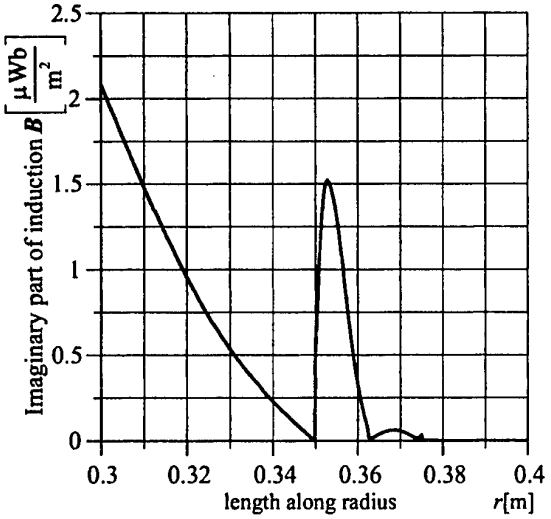



Fig6. . Plot of the imaginary part of the induction vector along cable radius in conducting region 50[Hz].

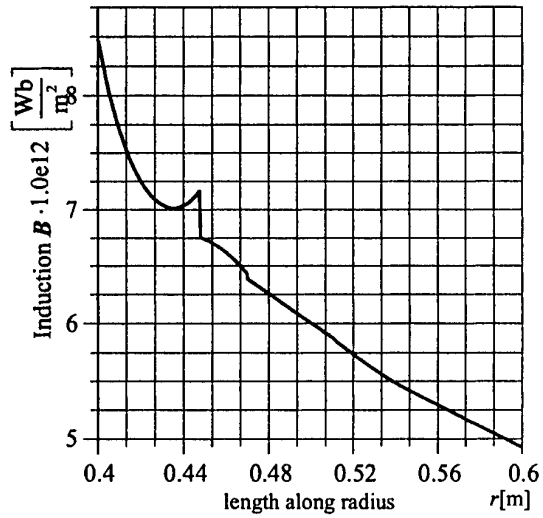



Fig7. . Plot of the modulus of the induction vector in region outside of double layer shield for frequency 50[Hz].

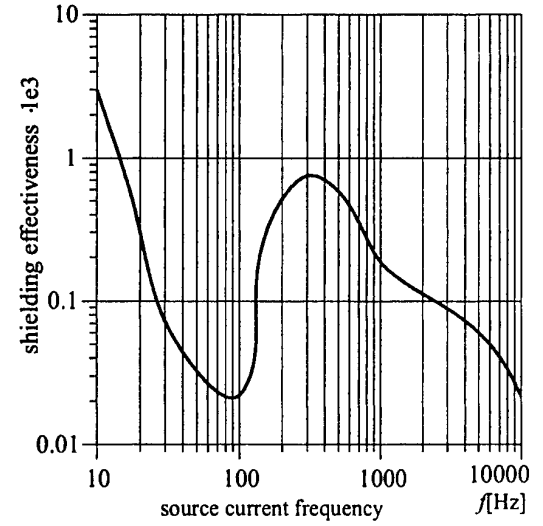



Fig8. Plot of the shielding effectiveness at point P (see Fig.2) in terms of frequency.

## 6. CONCLUSIONS

A inhomogeneous double layer shield was studied in this paper. It was shown that combined FEM-BEM method is very effective in calculation of electromagnetic field distribution in devices with inhomogeneous distribution of material properties. This method gives the lower number of degrees of freedom because it needs to discretize only conductive eddy current region.

In an example it was examined the dependency of shielding effectiveness in relation to exciting frequency. The shielding effectiveness is here defined as a ratio of modulus of induction of the vector $|\boldsymbol{B}|$ with double layer being present, to modulus of induction vector without any shield, in vicinity of the cable. In Fig.2 it is a point P placed at distance $\Delta l = 0.0001$[m] outside from it.

Looking at Fig.8 one can see that in frequency range from 50[HZ] to 100[Hz] we have first minimum. This means that for these frequencies the shielding effectiveness takes the lower values. This can be, probably, explained throughout existence of resonant frequency between the inner strand and outer shielding layers.

## ACKNOWLEDGEMENTS

This work was supported by the University of Mining and Metallurgy, under grant 10.120.247.

## REFERENCES

[1] Y. Du, J. Burnett, "Optimal magnetic shielding of double-layer shields at power frequencies", Proc. of IEEE 1997 Int. Symposium on EMC", Austin, Texas, USA, pp. 191-196.

[2] A.J. Stratton, *Electromagnetic Theory*, McGrow-Hill, New York, 1941.

[3] O. Biro, K. Preis, "On the use of magnetic vector dy currents", *IEEE Trans. on Magn.*, vol. 25, 1989, pp. 3145-3159.

[4] W.M. Rucker, K.R. Richter, "A BEM code for 3-D eddy current calculation", *IEEE Trans. on Magn.*, vol. 26, no 2, pp. 462-465, 1990.

[5] A. Kost, "*Numerische Methoden in der Berechnung elektromagnetischer Felder*", Springer Verlag, Berlin, 1994.

[6] K. Kawasaki, M. Inami, T. Ishikashielda, "Theoretical considerations on eddy current losses in non-magnetic and magnetic pipes for power transition system", IEEE Trans. On PAS, vol. PAS-100, no 2, 1981, pp. 474-479.

[7] Kurgan E.: *Non-linear magnetostatic field analysis by dual reciprocity boundary element method.* in V. Kose, J. Sivert (eds), Non-linear electromagnetic systems, IOS Press, Amsterdam, 1998, 93-396

[8] E. Kurgan, "Regularisation of nearly singular integrals in the current density field problems", *Journal of Technical Physics*,. 1997, vol. 38, pp. 563-574.

**EMC 2000** INTERNATIONAL WROCŁAW SYMPOSIUM ON ELECTROMAGNETIC COMPATIBILITY

# RADIOSIGNALS DYNAMIC RANGE IN SPACE-SCATTERED MOBILE RADIOCOMMUNICATION NETWORKS

V.I. Mordachev, 6 P.Brovka str., Minsk 220027, Belarus,
E-mail: nilemc@gw.bsuir.unibel.by, Fax: (375-17)-2398994

*The aim of the present paper is to outline and illustrate possible ways to practically implement the technique for tentative prediction of signals ensemble dynamic range at the receiver input in cellular networks. To illustrate the practicability of this technique the results of its utilization for prediction of reception conditions in FDMA, TDMA and CDMA networks are presented as well as the results of its comparison to the technique based on theoretical probabilistic evaluation of sample range of signal levels at the reception point.*

## INTRODUCTION

Intensive development of radiocommunication systems made modern urban radio environment substantially more complex. Rational frequency planning of this systems as well as shrinking of cell sizes along with the base station transmitter power decrease to several watts/channel or less makes it possible to substantially lower the probability of mutual interference on the main, adjacent and spurious receive channels. Under these conditions, however, we have to reckon with the probability that there are comparatively strong signals from the nearest mobile stations present at the mobile or base station:

- signals whose frequencies does not coincide with the receiving frequency but can cause communication quality deterioration due to nonlinear effects in the receiver: intermodulation, blocking, cross modulation and local oscillator voltage noise conversion;
- signals whose frequencies coincide with the receiving frequency of the weak signal from a distant mobile station (for example, if CDMA or TDMA radio interface standards are employed), which may cause the radio signal amplification/conversion path to be overloaded and thus introduce the requirement for provision of a wide power adjustment range (where this procedure exists at the system level) when communication with the nearest mobile stations is taking place.

This paper is aimed at development of a viable technique for probability evaluation of strong input signals under conditions of reception in space-scattered radiocommunication networks, particularly high-capacity cellular or trunking networks.

## INITIAL MODELS AND DEFINITIONS

1. As the radio environment parameter which characterizes the strong signals at the receiver input we use the value of the dynamic range $D$ of the ensemble $N$ of input signals:

$$D_P = \frac{P_{max}}{P_0} = \frac{\Pi_{max}}{\Pi_{min}} = \left(\frac{E_{max}}{E_{min}}\right)^2 = D_E^2, \qquad (1)$$

$$D = 10\,lg\,D_P = 20\,lg\,D_E.$$

This expression contains the following terms:

- power characteristics of the predominant input signal - the power flux density $\Pi_{max}$ and the field strength $E_{max}$ of the predominant field at the point of receiving antenna location; the power $P_{max}$ of this signal at the receiving antenna output;
- the values $\Pi_{min}$, $E_{min}$ of the receiver sensitivity limit "over the field" and the receiver antenna input sensitivity value $P_0$ of the in power measurement units.

2. As the radiowave propagation model we use the well-known hyperbolical approximation of the electromagnetic field power flux density $\Pi$ on the distance $R$ to its emitter:

$$\Pi = C_\nu P_{etr} / R^\nu, \; P_{etr} = G_a P_{tr}, \; C_\nu = const, \qquad (2)$$

where $P_{etr}$ - the equivalent isotropic radiated power (EIRP), $P_{tr}$ - the power fed to the emitter antenna; $G_a$ - the antenna gain, $C_\nu$ - the constant ($\nu$=2 for free space propagation, $\nu$=4 may be used in some cases (for radiowave propagation with interference of direct and reflected rays in the far zone for the VHF range and the lower part of the UHF as well as in cases when propagation path shadowing by urban buildings, structures and foliage is initially taken into account [1,2], $\nu$=2÷12 when the "regressive" in-building propagation model [3,4] for the UHF range is used).

3. As the receiver parameter which characterizes the receiver susceptibility to influence of strong signals outside the receiver (operating) bandwidth we use the value of the interference effects free input dynamic range of receiver [5]:

$$D_{in} = P_{max}/P_0 \in \{D_{im}, D_{ds}, D_{cm}, D_{onm}, D_{inm}, D_b\}, \qquad (3)$$

where $P_0$ is the lower signal power limit of a receiver antenna input sensitivity; $P_{max}$ may be defined using, particularly, the intermodulation criterium for determining the intermodulation free dynamic range $D_{im}$ of the receiver, the desensitization criterium for determining the desensitization free dynamic range $D_{ds}$ of the receiver, the cross modulation criterium for determining the cross modulation free dynamic range $D_{cm}$ of the receiver, and the respective criteria for determining the local oscillator noise mixering free dynamic range $D_{onm}$, the intermediate frequency paths interference free dynamic range $D_{inm}$, or the border frequency paths interference free dynamic range $D_b$ of the receiver.

4. The area of the radius $R_{max}=(C_v P_{etr}/\Pi_{min})^{1/v}$ around the location point of the victim receiver with the sensitivity limit $\Pi_{min}$ shall be considered as the spatial area of potential interfering interaction of radiotransmitters. Spatial arrangement of emitters within this area shall be characterized by the average spatial emitter density function of coordinates: the function $\rho(\alpha,\theta,R)$ in spherical coordinates for three-dimensional emitters arrangement or $\rho(\alpha,R)$ in polar coordinates for two-dimensional emitters arrangement; here $\alpha,\theta$ are the azimuth and elevation angles of the signal arrival direction; $R$ is the distance from the center of the area. We shall consider the functions $\rho(\alpha,R)$ and $\rho(\alpha,\theta,R)$ as slowly varying functions; thus the spatial density of emitters in the vicinity of the receiver location point which corresponds to the zero of coordinate system may be assumed as constant. In the general case, we shall assume $\rho=const$ for the $m$-dimensional vicinity of the receiver.

5. As the model of probabilistic character of spatial distribution of emitters in the vicinity of he radio receiver we shall use the known Poisson model of random distribution of points in space:

$$p_k(N_{\Delta V}) = \frac{N_{\Delta V}^k}{k!} exp(-N_{\Delta V}), \qquad (4)$$

where $p_k(N_{\Delta V})$ is the probability that exactly $k$ point emitters will fall into a certain element of space $\Delta V$ if the average number of emitters within this element is equal to $N_{\Delta V}$.

6. At the initial stage of analysis we shall assume that all emitters are isotropic and have equal EIRP $(C_v P_{etr}=const.)$ and that the receiver antenna is omnidirectional and its equivalent area is $S_e$ $(P_0=S_e\Pi_{min}=const)$.

7. We shall neglect the dependence of characteristics of the emitter antennas, receiver antenna and propagation model (2) characteristics on frequency assuming that the transmitting frequency range of emitters is limited.

For these conditions, the predominant signal with the power $P_{max}=S_e\Pi_{max}$ at the receiver input belongs to the nearest emitter whose potential influence on the victim receiver has not been compensated by regulatory or technical measures. Since distances from the victim receiver to interferers are random, the magnitude $P_{max}$ and the dynamic range $D_P$ of oscillations in the ensemble of input signals are functionally related random values and can be characterized by the corresponding probability distributions. The type of these distributions is determined by models (2),(4).

## PROBABILITY DISTRIBUTION OF SIGNALS DYNAMIC RANGE AT THE RECEIVER INPUT

For $m$-dimensional spatial distribution of emitters, the distance $R_{min}$ to the nearest emitter may be defined as the maximum radius of the spherical receiver vicinity $\Delta U$ free from emitters. Taking account of possible regulatory and technical ways to

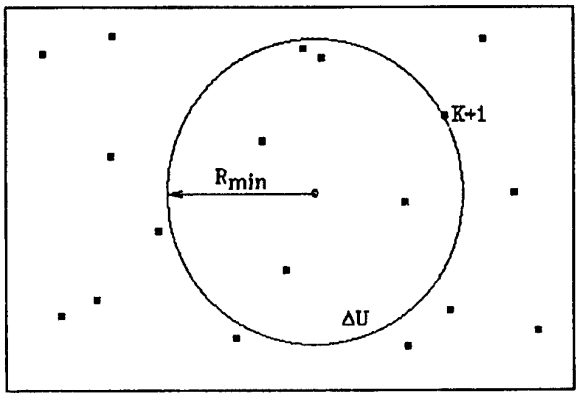



Fig. 1

provide electromagnetic compatibility of neighboring radio stations (compensation, blanking, spatial EMI shielding, coordination of transmit times), which allow one to rule out the influence of signals from a certain number $K$ of the nearest emitters (see Fig.1), the radius of this vicinity will be equal to the distance from the receiver to the $K+1$-th distant emitter. This emitter may be considered as the nearest interferer. Therefore the probability distribution density for the distance $R_{min}$ to the nearest interferer is [6]:

$$w(R_{min}) = \frac{G^H m}{\Gamma(H)} R_{min}^{Hm-1} exp(-GR_{min}^m); \qquad (5)$$

$$G = \rho a_m > 0, \quad H = K+1 > 0, \quad m > 0, \quad R_{min} \geq 0;$$

$\Gamma(*)$ -gamma function. $GR_{min}^m = N_a(R_{min})$ represents the average number of emitters within the $m$-dimensional spherical vicinity $\Delta U$ with the radius $R_{min}$ around the receiver location point. Using the apparent functional relationship between the dynamic range $D_P$ and the minimum distance $R_{min}$

$$D_P = \frac{c_v P_{etr}}{\Pi_{min} R_{min}^m},$$

we obtain from (5) the law for probability distribution of the signals dynamic range at the receiver input; the distribution is determined by the level of the signal from the $H$-th distant emitter and this law

has the form of the exponential-hyperbolic distribution [6]:

$$w(D_P) = \frac{N_a^H m}{\nu\Gamma(H)} D_P^{-(Hm+\nu)/\nu} exp(-N_a D_P^{-m/\nu}); \quad (6)$$

$$D_P \geq 0, N_a \geq 0, \nu > 0; m > 0.$$

In this distribution, $N_a$ represents the average number of emitters within the spherical area of potential interfering field interaction with the radius $R_{max}=(C_v P_{etr}/\Pi_{min})^{1/\nu}$ limited by the receiver sensitivity on the main receive channel in case the average spatial density of emitters within this whole area is constant and equal to the average density $\rho$ of the random spatial distribution of emitters in the vicinity of the receiver:

$$N_a = GR_{max}^m = \rho\pi^{m/2} R_{max}^m / \Gamma(1+m/2) \geq 0. \quad (7)$$

The expression for the distribution (6) moments is:

$$m_n(D_P) = N_a^{n\nu/m} \frac{\Gamma(H - n\nu/m)}{\Gamma(H)}, \; H - n\nu/m > 0. \quad (8)$$

The expressions (6),(8) thoroughly characterize probabilistic properties of the dynamic range of emissions (signals) at the receiver location point in the simplest case when EIRPs of emitters that are randomly located within the potential interfering interaction area are constant in time and equal in the direction to the radio receiver. In these expressions, $D_P \geq 0$, although the domain $D_P > 1$. The condition $D_P < 1$ means that if the Poisson model of spatial emitters location (4) is used then the probability that these emitters are absent within the area around the receiver with the radius $R_{max}$ is not equal to zero for any finite $\rho$, $R_{max}$ although this probability is generally extremely low.

It is necessary to point out that $n\nu/m \geq H$ and the distribution (6) have no initial moments in the most practically important cases. Nevertheless the obtained expressions make it possible to predict the dynamic range of signals during radio reception in space-scattered radio equipment groups on the basis of the evaluation of the upper boundary of the confidence interval $[0, D_{P0}]$ which includes the evaluated value of $D_P$ with the probability $p$:

$$D_{P0} = arg\{P(D_{P0}) = p\}, \quad (9)$$

$$P(D_{P0}) = \Gamma(H, N_a D_{P0}^{-m/\nu}) / \Gamma(H);$$

$\Gamma(H, N_a D_P^{-m/\nu})$ is the incomplete gamma function of the second kind.

For example, if in the considered situation the receiver antenna input dynamic range $D_{in}$ is known then the probability $p(D_P > D_{in})$ that it will be exceeded by the dynamic range of input signals is determined by the simple relationship:

$$p(D_P > D_{in}) = 1 - \Gamma(H, N_a D_{in}^{-m/\nu}) / \Gamma(H). \quad (10)$$

The distribution (6) is obtained using model (2) and the dynamic range of signals is determined using the power flux density (or power of individual signals at the receiver antenna input). If we use the propagation model of the type (2) based on the field intensity, in which the exponent is two times less than $\nu$, then the form of expressions (6),(8) and the meaning of their parameters will not change, but the condition for existence of moments in this distribution will be improved.

The arguments given below allow one to substantially improve limitations on applicability of models and relationships derived above; these limitations were assumed for derivation of the distribution (6).

*Signals dynamic range estimation for FDMA mobile stations*

Let us consider only the two-dimensional spatial mobile distribution ($m=2$). It is necessary to take $\nu=4$ in the model (2) for propagation conditions. In the case under consideration radio stations generally have equal power and omnidirectional antennas and employ broadband frequency filters at the receive input; these filters are transparent to signals on all the channels utilized by systems of the corresponding standard. Besides, these stations are emitters, are owned by independent users and are randomly and scatteredly distributed over the territory, which allows one to use the Poisson model of their distribution in the receiver vicinity.

Mobile usage patterns in these systems do not assume that any limitations are placed on signals of neighboring stations. Therefore it is interesting to discuss two possible scenarios of the situation [6]:

Scenario 1: The dynamic range $D_P$ of emissions (signals) at an arbitrarily selected surface point ($H=1$).

Scenario 2: The dynamic range $D_P$ of emissions at the mobile location point or the signals dynamic range at the mobile receiver input (in receive mode, the mobile's own signal is absent (simplex operation mode) or is suppressed by the duplexer frequency filter ($H=2$)).

In the first scenario, the distribution (6) has no initial moments. Therefore it is possible to carry out systems analysis of the dynamic range of emissions at the selected point using (9); this analysis implies that we need

- to substantiate the required value of the prediction reliability coefficient $p$ which is the probability that the emissions dynamic range will not exceed the desired value of $D_{P0}$;
- to solve the equation (9) over $D_{P0}$ analytically, using numerical methods or using the set of curves for the distribution (6).

In the discussed case, an analytical solution is possible: using the properties of the known representation of the incomplete gamma function of the second kind as

$$\Gamma(1+n,x) = n!\,e^{-x}\sum_{i=0}^{n}\frac{x^i}{i!}, \qquad n = 0,1,2,\ldots, \qquad (11)$$

we have:

$$p = \Gamma\left(1, N_a D_{P0}^{-2/4}\right) = exp\left(-N_a/\sqrt{D_{P0}}\right), \quad \text{hence}$$

$$D_{P0} = \left(N_a/ln\,p\right)^2; \qquad (12)$$

for $p \geq 0.9$ $D_{P0} \approx \left(N_a/(1-p)\right)^2$.

For equal values of $N_a$ the difference in values of $D_0$ for $p=0.9$ and for $p=0.99$ is approximately 20 dB.

In the second scenario, the distribution (6) for $D_P$ also has no (initial) moments. Therefore, using (11), we reduce the equation (9) to:

$$D_{P0} = arg\left\{\left(1+N_a/\sqrt{D_{P0}}\right)exp\left(-N_a/\sqrt{D_{P0}}\right) = p\right\}, \qquad (13)$$

Numerical solution of this equation for $p=0.9$ and $p=0.99$ allows us, for instance, to a obtain the following estimations:

$$D_{P0}(0.9) \approx 3.54N_a^2, \; D_{P0}(0.99) \approx 45{,}3N_a^2; \qquad (14)$$

the difference between these estimations for equal values of $N_a$ is approximately 11 dB.

The parameter $N_a$ in the given relationships represents the average number of mobile stations in transmit mode within the potential interfering interaction area with the radius $R_{max}$ if the spatial mobile density within this whole area is the same and corresponds to the mobile density in the vicinity of the considered point. For conventional mobile stations (2-5W transmit power, 1.5 - 2.0 m antenna height above the surface) and assumed propagation conditions $(\nu=4)$ this area can be as large as 10-30 square kilometers (taking into account the interference of the direct and reflected rays, the shielding introduced by buildings and Earth surface, the effect of foliage etc). For mobile density $\rho \in [1000,10000]$ stations/square kilometer and relative mobile transmit time of 2-5% we obtain $N_a \in [200,10000]$, which generally corresponds to the most severe operation environment. For actual operation conditions, the spatial emitter density range may be assumed as $\rho \in [100,1000]$ stations/square kilometer, which approximately corresponds to $N_a \in [20,1000]$. For these conditions, the table below contains the expected space ranges for values of $D_0 = 10lgD_{P0}$ for $p=0.9$ and $p=0.99$ in accordance with (12) and (14).

| Table 1 | Scenario 1 (H=1) | | Scenario 2 (H=2) | |
|---|---|---|---|---|
| $\rho$, stations /km$^2$ | $10^2 \div 10^3$ | $10^3 \div 10^4$ | $10^2 \div 10^3$ | $10^3 \div 10^4$ |
| $D_0(0.9)$, dB | 46÷ 80 | 66÷100 | 32÷66 | 52÷86 |
| $D_0(0.99)$, dB | 66÷100 | 86÷120 | 43÷77 | 63÷97 |

If in the second discussed scenario we define the dynamic range using the electromagnetic field strength and the analysis is based on the propagation model of the type (2) using the field strength and $\nu=2$, then the conditions are fulfilled for existence of the 1st (initial) moment in (8) for the distribution (6). For this scenario, $m_1(D_E)=N_a$. As a result of this, for the operation conditions discussed above we obtain the space range $20lg(m_1(D_E))=46 \div 80$dB for the interval $N_a \in [200, 10000]$ and the space range $20lg(m_1(D_E))= 26 \div 60$dB for the interval $N_a \in [20,1000]$.

The tentative estimations presented above do match the practical outlook on modern urban radio environment characteristics.

*Signals dynamic range estimation for TDMA frequency channel*

In TDMA systems signals of numerous space scattered radio stations sequentially fall into the main receive channel bandwidth of the receiver. The Figure 2 illustrates the time variation pattern of the signal level $P(t)$ in the receiver main receive channel for the TDMA network; the labels 1,2,...,N on the pattern denote signals of each of $N$ mobile

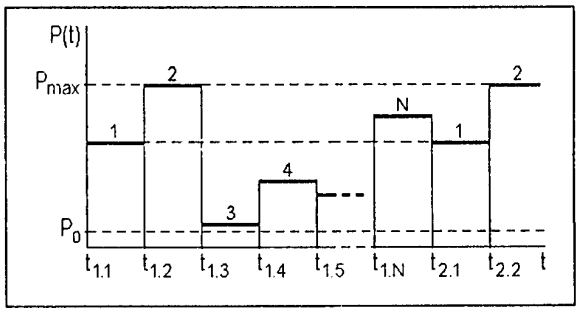



Fig. 2

stations. For $H=1$ the estimation of the probability that the dynamic range of signals from individual subscribers in the TDMA frequency channel will not exceed the value of the main receive channel dynamic range $D_{mp}$ may be carried out on the basis of the following relationship which is a consequence of the model (6)-(8):

$$p\left(D < D_{mp}\right) \approx \left[exp\left(-ND_{mp}^{-m/\nu}\right)\right]. \qquad (15)$$

Hence, for the receiver which carries out radio reception using the TDMA network frequency channel, the value of the main receive channel dynamic range $D$ whose expected probability is equal to $p$ is determined by the relationship

$$D \approx \left(-\frac{N}{ln\,p}\right)^{\nu/m}. \qquad (16)$$

Table 2 contains estimated values of $D$ for channels with $N=4$ (TETRA), $N=8$ (GSM) and $N=12$ (DECT) for different propagation conditions and two-dimensional emitter distribution $(m=2)$.

| Table 2 | p=0.9 | | p=0.99 | |
|---|---|---|---|---|
| | ν=2 | ν=4 | ν=2 | ν=4 |
| **D** for **N=4**, dB: | 16 | 32 | 26 | 52 |
| **D** for **N=8**, dB: | 19 | 36 | 29 | 58 |
| **D** for **N=12**, dB: | 21 | 42 | 31 | 62 |

*Estimation of possible CDMA network cell shrinkage due to predominant signal presence*

One of CDMA features is that cells can grow and shrink subject to existing load (traffic) [7]. The model (5) make it possible to relate CDMA network cell size variations to operating mobile stations spatial density variations.

If the maximum recommended (design) network load corresponds to $Z$ subscribers simultaneously served by a cell ($Z \approx 13 \div 14$), then for nominal spatial subscriber density $\rho_N$ the probability distribution, the mathematical expectation $m_1(R_S)$ and the variance $M_2(R_S)$ of the cell radius $R_S$ can be determined according to (5) as:

$$w(R_S|\rho_N) = \frac{G^Z m}{\Gamma(Z)} R_S^{Zm-1} exp(-GR_S^m);$$

$$m_1(R_S|\rho_N) = \frac{\Gamma(Z+1/m)}{\Gamma(Z)G^{1/m}};$$

$$M_2(R_S|\rho_N) = \frac{\Gamma(Z+2/m)}{\Gamma(Z)G^{2/m}} - \left[\frac{\Gamma(Z+1/m)}{\Gamma(Z)G^{1/m}}\right]^2;$$

$$G = \rho_N a_m > 0, \quad Z \geq 1, \; m > 0, \quad R_S \geq 0.$$

Hence, for spatial subscriber density $\rho_P$ that exceeds $\rho_N$ and corresponds to the peak network traffic, the expected average cell size shrinkage $\Im$ may be determined as the ratio of mathematical cell size expectations for peak and nominal spatial subscriber densities:

$$\Im = \frac{m_1(R_S|\rho_P)}{m_1(R_S|\rho_N)} = \left(\frac{\rho_N}{\rho_P}\right)^{1/m}. \qquad (17)$$

For instance, if the spatial emitter density is increased by 2 times as compared to $\rho_N$ then the average cell size radius will expectedly decrease by 1.41 times for two-dimensional subscriber distribution ***(m=2)*** and by 1.26 times for three-dimensional subscriber distribution ***(m=3)***, for example, in a multistoried building.

*Prediction of maximum allowable radio environment complexity*

The relationships (9),(10) make it possible to determine the maximum radio environment complexity which is allowable with regard to the probability that the receiver antenna input dynamic range will be exceeded by the input signals dynamic range. Taking into account the known incomplete gamma function representation (11), the equation (9) can be represented as:

$$p = \frac{\Gamma(H,Z)}{\Gamma(H)} = exp(-Z)\sum_{i=0}^{H-1}\frac{Z^i}{i!}, \quad Z = N_a D_{p0}^{-m/\nu}. \quad (18)$$

Solution of this equation about $D_{p0}$ for different values of $N_a$ and for fixed values of $p$, $H$ and $\nu/m$ makes it possible to estimate the highest average number of input signals $N_a$ which may be allowed for the receiver whose antenna input dynamic range is equal to $D_{in}$.

## CONCLUSION

The approaches presented above make it possible to predict in various scenarios the dynamic range of signals that create the radio environment at the observation point. The author tends to think that the material presented above has a potential for further development with regard to specific systems and provides opportunities for investigation of EMC problems in mobile communication systems.

## REFERENCES:


1. K.Siwiak, "Radiowave Propagation and Antennas for Personal Communications" (English), Artech House, Boston, 1995.

2. "Prediction Methods for the Terrestrial Land Mobile Service in the VHF and UHF Bands", Rec. ITU-R P.529-2, 1995.

3. W.Honcharenko, H.L.Bertoni, J.L.Dailing, J.Quan and H.D.Yee, "Mechanisms Governing UHF Propagation on Single Floors in Modern Office Buildings" (English), IEEE Transactions on Vehicular Technology, vol.41, pp.496-504, Nov. 1992.

4. M.J.Feuerstein, K.L.Blackard, T.S.Rappaport, S.Y.Seidel, H.H.Xia. "Path Loss, Delay Spread, and Outage Models as Functions of Antenna Height for Microcellular System Design" (English), IEEE Transactions on Vehicular Technology, vol.43, pp.487-498, Aug. 1994.

5. D.D.Weiner, "Nonlinear Interference Effects in EMC" (English), Proceedings of the Tutorial Lectures at the 10-th Zurich Symp. On EMC, March 1993, pp.114-127.

6. V.I.Mordachev, "Statistical Characteristics of Dynamic Range of Inadvertent Disturbances with Space-Scattered Groupings of Their Sources" (Russian), Proceedings of the 9-th Wroclaw Symp. On EMC, June 1988, pp.571-576.

7. V.V.Veeravalli and A,Sendonaris, "The Coverage-Capacity Tradeoff in Cellular CDMA Systems" (English), IEEE Transactions on Vehicular Technology, vol.48,pp.1443-1450, Sept. 1999.


## BIOGRAPHICAL NOTES


Vladimir Mordachev (Ph.D) is Head of the EMC Laboratory of Belarusian State University of Informatics and Radioelectronics, Minsk, Belarus. He works in the areas of EMC system and nonlinear circuit analysis, computer-aided modeling and design, EMC statistical theory and EMC measurement technique. He is a member of IEEE.

**EMC 2000** INTERNATIONAL WROCŁAW SYMPOSIUM ON ELECTROMAGNETIC COMPATIBILITY

# REBUILDING THE SCREEN OF A CABLE BY A DOUBLE LAYER OF PARALLEL WIRES

Roland Tiedemann Karl-Heinz Gonschorek

Technische Universität Dresden
ETI/EMV
01062 Dresden, Germany
tiedeman@eti.et.tu-dresden.de

***Abstract*** *In this contribution the coupling into a spezial coaxial screen is described. The screen consists of parallel wires which are arranged in a two layer system. A derivation is presented to determine the interference coupling through this screen. The screen is called* **P***arallel* **D***ouble* **L***ayer* **S***creen (PDLS). The analytical result of the interfence coupling is verified by a Method of Moment simulation.*

## 1. INTRODUCTION

To analyze the physical phenomena of interference coupling into shielded cables, simples models of the cable screen have to be developed. Hoping that every model improves a little bit the understanding of the complicated coupling mechanism. Here the **P**arallel **D**ouble **L**ayer **S**creen (PDLS) is presented.

The cross section of such a PDLS system is shown in Fig 1. The screen is rebuild by two layers. Each layer consists of $n$ parallel wires arranged equidistantly on a circle. The distance between two wires on one layer is substantially greater than the wire radius $r_0$, also the distance between the two layers is much greater. Furthermore the relations $r_0 \ll r_1 < r_2$ are given. The proximity effect is neglected. To determine the interference coupling into a coaxial cable the knowledge of the transfer impedance is necessary.

The cable transfer impedance is a purely cable specific quantity which describes the relation between the current $I_a$ on the cable screen and the induced voltage $U_T$ between the inner conductor and the screen. The transfer impedance is defined by the arrangement of Fig. 2 [4]. The cable screen and the inner conductor are short circuited at the left end. The induced voltage $U_T$ is measured across the open end on the right side. The transfer impedance can

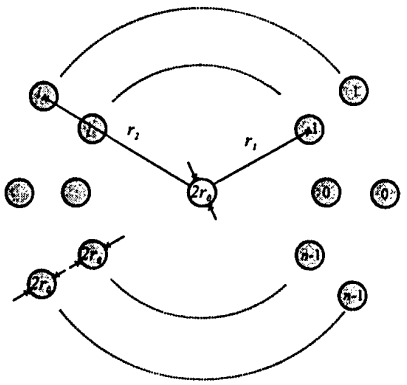



Figure 1: Model of a PDLS system

be written by:

$$Z'_T = \frac{U_T}{I_a\, l} \tag{1}$$

for cable lengths of $l \ll \lambda$.

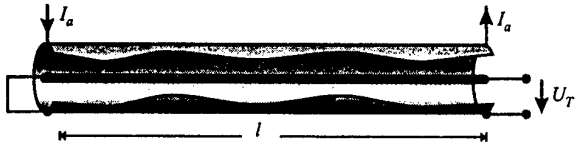



Figure 2: Definition of the Transfer Impedance

## 2. DERIVATION

To start the determination of the transfer impedance of a PDLS system the magnetic field of one wire has to be described. Fig. 3 shows the field of one wire.

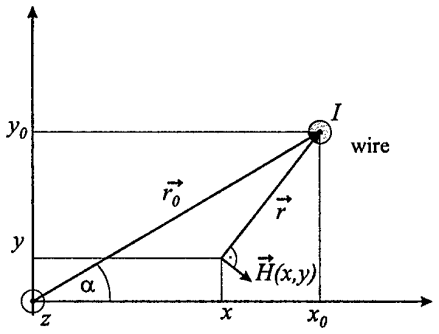



Figure 3: Magnetic field of one wire

The components of $\vec{H}$ are given by

$$H_x = \frac{I}{2\pi[(x_0-x)^2+(y_0-y)^2]}(y_0-y) \qquad (2)$$

and

$$H_y = -\frac{I}{2\pi[(x_0-x)^2+(y_0-y)^2]}(x_0-x) \ . \qquad (3)$$

The whole field of several wires is gained by a vectorial addition of the single parts. In Fig. 4 a section of the PDLS structure is shown. The current on one wire $i$ of the inner layer produces the field $\vec{H}_1 i$, the current on a wire i of the outer layer the field $\vec{H}_2 i$ respectively. From reasons of symmetrie it seems to be allowed to treat only one loop created by two opposite wires of the different layers for the current displacement process. In our case we choose the two wires on the positive $x$-axis. On the $x$-axis the $y$-component of $\vec{H}_1 i$ is given by

$$H_{1iy} = -\frac{I_1}{2\pi n[(x_{10}-x)^2+y_{10}^2]}(x_{10}-x) \ , \qquad (4)$$

analogous

$$H_{2iy} = -\frac{I_2}{2\pi n[(x_{20}-x)^2+y_{20}^2]}(x_{20}-x). \qquad (5)$$

In Fig. 5 a rebuilding of the loop created by the mentioned opposite wires 10 and 20 from both layers is shown. This loop is located in the $xz$-plane. The layers and therefore also the loop are short circuited at the ends. Kirchhoffs voltage law leads to:

$$-j\omega\phi'_{12} - \frac{I_1}{n}Z'_D + \frac{I_2}{n}Z'_D = 0. \qquad (6)$$

In this equation,

$$Z'_D = \frac{1}{(1+j)\pi\kappa r_0 d}\cdot\frac{J_0(\frac{1-j}{d}\cdot r_0)}{J_1(\frac{1-j}{d}\cdot r_0)}, \qquad (7)$$

[5] represent the internal impedance of one wire, $I_2$ the current on the outer layer and $I_1$ the current of

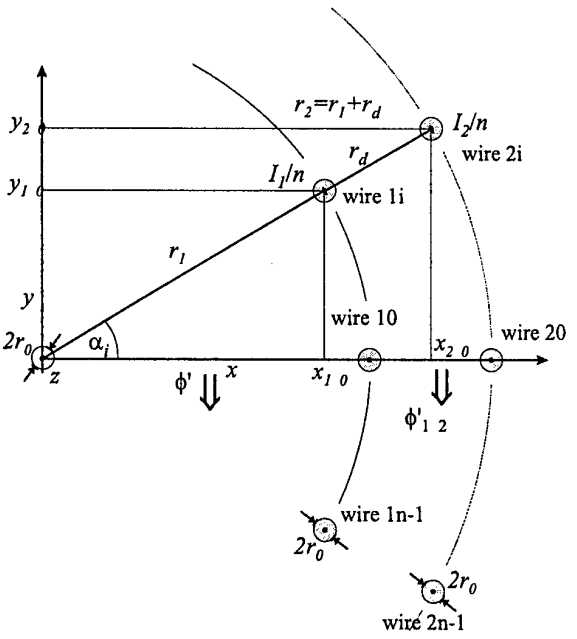



Figure 4: Part of the cross-section of a PDLS structure

the inner layer. The magnetic flux $\phi'_{12i}$ between the wire 10 and the wire 20 (Fig. 4) can be written as

$$\begin{aligned}\phi'_{12i} &= \mu_0 \int_{r_1+r_0}^{r_2-r_0} [H_{1iy}+H_{2iy}]dx. \qquad (8)\\ &= \mu_0 \int_{r_1+r_0}^{r_2-r_0} \Big[ -\frac{I_1}{2\pi n[(x_{10}-x)^2+y_{10}^2]}(x_{10}-x)\\ &\quad -\frac{I_2}{2\pi n[(x_{20}-x)^2+y_{20}^2]}(x_{20}-x)\Big]\, dx \ .\end{aligned}$$

The solution of the integral [1] is given by

$$\begin{aligned}\phi'_{12i} = \frac{\mu_0}{4\pi n}\Big[ & I_1 \ln|(x_{10}-x)^2+y_{10}^2| \qquad (9)\\ & + I_2 \ln|(x_{20}-x)^2+y_{20}^2|\Big]_{r_1+r0}^{r_2-r_0} \ .\end{aligned}$$

Because the logarithmic terms are always positive it is allowed to omit the amount lines. Furthermore $x_{10}, y_{10}, x_{20}$ and $y_{20}$ can be substituted by trigonometric terms. So, Eq. 9 can be rewritten by:

$$\begin{aligned}\phi'_{12i} = \frac{\mu_0}{4\pi n}\Big[ & I_1 \ln[(r_1\cos\alpha_i - x)^2 \qquad (10)\\ & +(r_1\sin\alpha_i)^2]\\ & + I_2 \ln[(r_2\cos\alpha_i - x)^2\\ & +(r_2\sin\alpha_i)^2]\Big]_{r_1+r0}^{r_2-r_0} \ .\end{aligned}$$

Considering the integration limits we obtain

$$\begin{aligned}\phi'_{12i} &= \frac{\mu_0}{4\pi n}\Big[ \qquad (11)\\ & I_1 \ \ln[r_1^2 - 2r_1\cos\alpha_i\cdot(r_2-r_0)+(r_2-r_0)^2]\\ -\ & I_1 \ \ln[r_1^2 - 2r_1\cos\alpha_i\cdot(r_1+r_0)+(r_1+r_0)^2]\\ +\ & I_2 \ \ln[r_2^2 - 2r_2\cos\alpha_i\cdot(r_2-r_0)+(r_2-r_0)^2]\\ -\ & I_2 \ \ln[r_2^2 - 2r_2\cos\alpha_i\cdot(r_1+r_0)+(r_1+r_0)^2]\Big].\end{aligned}$$

In the next step the influence of all wires has to be considered. The whole flux $\phi'_{12}$ is given by a sum of all $\phi'_{12i}$. The angle $\alpha_i = 2\pi i/n$ depends only on the variable $i$. So, the following equation for the whole flux can be derived:

$$\begin{aligned}\phi'_{12} &= \frac{\mu_0}{4\pi n}\sum_{i=0}^{n-1}\Big[ \qquad (12)\\ & I_1 \ln[r_1^2 - 2r_1\cos(\frac{2\pi i}{n})\\ & \quad\cdot(r_2-r_0)+(r_2-r_0)^2]\\ & -I_1 \ln[r_1^2 - 2r_1\cos(\frac{2\pi i}{n})\\ & \quad\cdot(r_1+r_0)+(r_1+r_0)^2]\\ & +I_2 \ln[r_2^2 - 2r_2\cos(\frac{2\pi i}{n})\\ & \quad\cdot(r_2-r_0)+(r_2-r_0)^2]\\ & -I_2 \ln[r_2^2 - 2r_2\cos(\frac{2\pi i}{n})\\ & \quad\cdot(r_1+r_0)+(r_1+r_0)^2]\Big].\end{aligned}$$

Using Eq. 12 within Eq. 6 leads to Eq. 13 which depends only on the currents $I_1$ and $I_2$, from the electrical point of view:

$$\begin{aligned}0 &= \qquad (13)\\ & -\frac{j\omega\mu_0 I_1}{4\pi n}\\ & \cdot\sum_{i=0}^{n-1}\ln\frac{r_1^2 - 2r_1\cos(\frac{2\pi i}{n})(r_2-r_0)+(r_2-r_0)^2}{r_1^2 - 2r_1\cos(\frac{2\pi i}{n})(r_1+r_0)+(r_1+r_0)^2}\\ & -\frac{j\omega\mu_0 I_2}{4\pi n}\\ & \cdot\sum_{i=0}^{n-1}\ln\frac{r_2^2 - 2r_2\cos(\frac{2\pi i}{n})(r_2-r_0)+(r_2-r_0)^2}{r_2^2 - 2r_2\cos(\frac{2\pi i}{n})(r_1+r_0)+(r_1+r_0)^2}\\ & -\frac{I_1}{n}Z'_D+\frac{I_2}{n}Z'_D.\end{aligned}$$

Rewriting Eq. 13 yields an explicit expression for the ratio $I_1/I_2$:

$$\frac{I_1}{I_2} = \xi = \frac{\frac{j\omega\mu_0}{4\pi n}\sum_{i=0}^{n-1}\ln k_1 - \frac{1}{n}Z'_D}{-\frac{j\omega\mu_0}{4\pi n}\sum_{i=0}^{n-1}\ln k_2 - \frac{1}{n}Z'_D} \qquad (14)$$

with

$$\begin{aligned}k_1 &= \frac{r_2^2 - 2r_2\cos(\frac{2\pi i}{n})\cdot(r_2-r_0)+(r_2-r_0)^2}{r_2^2 - 2r_2\cos(\frac{2\pi i}{n})\cdot(r_1+r_0)+(r_1+r_0)^2}\\ k_2 &= \frac{r_1^2 - 2r_1\cos(\frac{2\pi i}{n})\cdot(r_2-r_0)+(r_2-r_0)^2}{r_1^2 - 2r_1\cos(\frac{2\pi i}{n})\cdot(r_1+r_0)+(r_1+r_0)^2}.\end{aligned}$$

Considering Kirchhoffs law ($I = 1_1 + I_2$) leads to

$$I_1 = \frac{I}{1+\frac{1}{\zeta}} \qquad (15)$$

and

$$I_2 = \frac{I}{1+\zeta}\,. \qquad (16)$$

To calculate the voltage between the inner conductor and the screen we need the flux $\phi'$ (compare Fig. 5). The flux which is caused by the wire $i$ of the inner and the wire $i$ of the outer layer is given by:

$$\begin{aligned}\phi'_i &= \mu_0\int_{r_0}^{r_1-r_0}[H_{1iy}+H_{2iy}]\,dx. \qquad (17)\\ &= \mu_0\int_{r_0}^{r_1-r_0}\Big[-\frac{I_1}{2\pi n[(x_{10}-x)^2+y_{10}^2]}(x_{10}-x)\\ &\quad -\frac{I_2}{2\pi n[(x_{20}-x)^2+y_{20}^2]}(x_{20}-x)\Big]\,dx\,.\end{aligned}$$

Solving this integral in the same manner as Eq. 8 with the assumption that the radius of the inner conductor can be neglected, we get:

$$\begin{aligned}\phi'_i = \frac{\mu_0}{4\pi n}\Big[ & I_1\ln[1-\frac{2\cos\alpha_i}{r_1}\cdot(r_1-r_0)\\ & +\frac{(r_1-r_0)^2}{r_1^2}] \qquad (18)\\ + & I_2\ln[1-\frac{2\cos\alpha_i}{r_2}\cdot(r_1-r_0)\\ & +\frac{(r_1-r_0)^2}{r_2^2}]\Big]\,.\end{aligned}$$

Substituting the angle $\alpha_i$ by $2\pi i/n$ the whole flux can be written by

$$\begin{aligned}\phi' = \sum_{i=0}^{n-1}\frac{\mu_0}{4\pi n}\Big[ & I_1\ln[1-\frac{2\cos\frac{2\pi i}{n}}{r_1}\cdot(r_1-r_0)\\ & +\frac{(r_1-r_0)^2}{r_1^2}] \qquad (19)\\ + & I_2\ln[1-\frac{2\cos\frac{2\pi i}{n}}{r_2}\cdot(r_1-r_0)\\ & +\frac{(r_1-r_0)^2}{r_2^2}]\Big]\,.\end{aligned}$$

Substituting $I_1$ (Eq. 15) and $I_2$ (Eq. 16) within Eq. 19 yields to:

$$\phi' = \sum_{i=0}^{n-1}\frac{\mu_0}{4\pi n}\Big[\frac{I}{1+\frac{1}{\zeta}}\cdot\ln g_1 + \frac{I}{1+\zeta}\cdot\ln g_2\Big] \qquad (20)$$

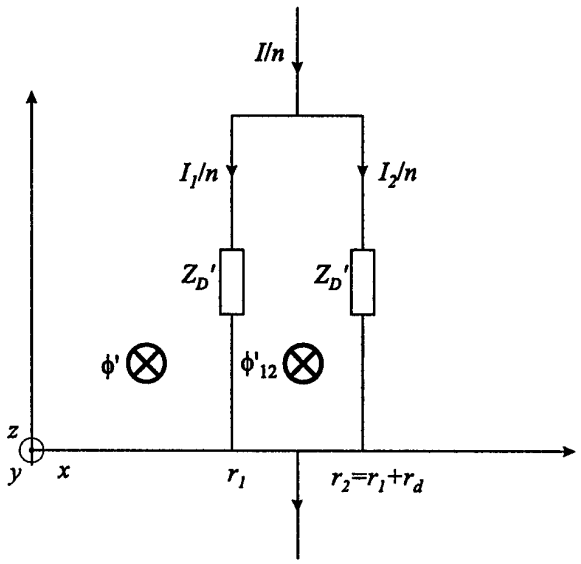



Figure 5: Loop formed by two opposite wires of both layers.

with

$$g_1 = 1 - \frac{2\cos\frac{2\pi i}{n}}{r_1} \cdot (r_1 - r_0) + \frac{(r_1 - r_0)^2}{r_1^2} \quad (21)$$

$$g_2 = 1 - \frac{2\cos\frac{2\pi i}{n}}{r_2} \cdot (r_1 - r_0) + \frac{(r_1 - r_0)^2}{r_2^2} .$$

A division of Eq. 20 by the current $I$ leads to an expression which can be considered as the mutual inductance between the PDLS and the inner conductor:

$$M'_{DR} = -\sum_{i=0}^{n-1} \frac{\mu_0}{4\pi n} \left[ \frac{1}{1+\frac{1}{\zeta}} \cdot \ln g_1 + \frac{1}{1+\zeta} \cdot \ln g_2 \right] . \quad (22)$$

The internal impedance of all parallel wires from the inner can be derived to:

$$Z'_{Du} = \frac{Z'_D}{n} \cdot \frac{1}{1+\frac{1}{\zeta}}. \quad (23)$$

And therefore the transfer impedance of a PDLS system can be written by

$$Z'_{TDR} = Z'_{Du} + j\omega M'_{DR}. \quad (24)$$

## 3. VERIFYING THE MODEL BY MOM

In this chapter the analytical derivation of the PDLS-model will be verified. The program CONCEPT [3] a useful tool to compute currents on wires which bases on the Methods of Moments (MoM) [2], is used. A piece of a coaxial PDLS is rebuilt for the verification [6]. This piece is shown in Fig.6. One

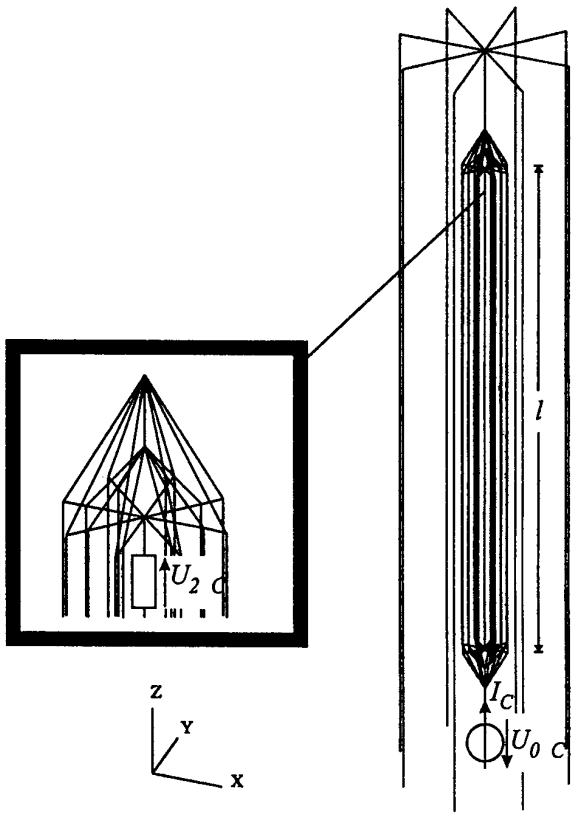



Figure 6: MoM model of a PDLS

end is connected by a wire with a ground plane. The generator $U_{0C}$ (Fig. 6) on this wire drives the system. An additional outer layer leads the current back to ground plane. The PDLS has a length of $l = 12.0$ cm, an inner radius of $r_1 = 3.9$ mm and an outer radius of $r_2 = 5.4$ mm. Up to appr. 100 MHz the current $I_C$ can be assumed to be constant. In the middle of the PDLS a wire represents the inner conductor. To determine the coupling voltage $U_{2C}$ a resistance with $R = 100\ \Omega$ is positioned at the inner conductor. 100 $\Omega$ are high enough for the simulation to get the needed open circuit voltage. The transfer impedance for this modeled braid can easily be predicted by

$$Z'_T = \frac{U_{2C}}{I_C l}. \quad (25)$$

For several numbers of wires the transfer impedance was computed by MoM and by the analytical solution (which is shown in chapter 2). In these calculations the screen was modeled by eight, sixteen, thirtytwo, and forty wires in each layer. The MoM and analytical results of the transfer impedance are given in Fig. 7. The parameter $n$ is the number of wires used for one layer. Up to 10 MHz the results of the MoM-calculation and the analytical description are the same. The MoM simulation considers the electric and magnetic coupling, the analytical so-

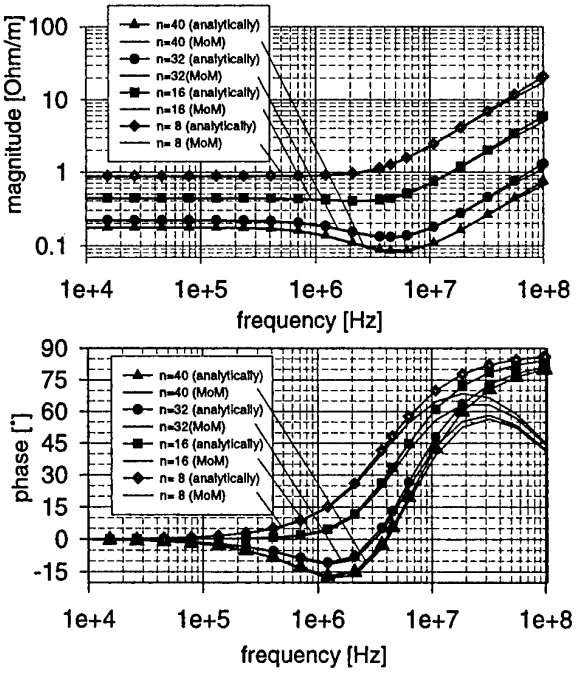



Figure 7: Transfer Impedance of a PDLS

lution only the magnetic coupling. For that reason it becomes clear that both curve cannot completely match in the higher range.

The results of the analytical solution shows that in the low frequency range the transfer impedance is equal to the DC resistance of the screen. In the higher range the magnitude increases. The phase reaches appr.+90°. At a frequency of appr. 1 MHz a minimum of the magnitude can be seen in the models with $n = 32$ and $n = 40$. This minimum is caused by the current displacement from the inner to the outer layer. The current displacement is considered by the factor $\xi$. In the higher range the inductive coupling dominates, so the transfer impedance increase.

## 4. CONCLUSIONS

The PDLS-system is a simple model of a coaxial cable. In this contribution a derivation is presented which allows to predict the transfer impedance of the PDLS. This derivation considers the inner impedance of the wires, the current distribution of the layers and the inductive coupling. A MoM simulation of the PDLS verifies the derivation. It clarifies the current displacement from the inner to the outer layer.

## REFERENCES

[1] BRONSTEIN, I.N.: *Taschenbuch der Mathematik.* 24. Auflage. Frankfurt/Main : Harri Deutsch, 1989

[2] BRÜNS, H.-D.: *Pulserregte Elektromagnetische Vorgänge in dreidimensionalen Stabstrukturen.* Hamburg, Hochschule der Bundeswehr, Disseratation, 1985

[3] BRÜNS, H.-D. ; SINGER, H.: *CONCEPT Homepage.* http://www.tu-harburg.de/~tebr/concept.html, Dec. 1998

[4] KADEN, H.: *Wirbelströme und Schirmung in der Nachrichtentechnik.* Berlin : Springer, 1959

[5] SIMONYI, K.: *Theoretische Elektrodynamik.* Johann Ambrosius Barth, 1993

[6] TIEDEMANN, R. ; GONSCHOREK, K.-H.: Minimizing the Interference Coupling into Standard Coaxial Cables with Braided Shield. In: *International Symposium on Electromagnetic Compatibility* Bd. 1. Denver, Colorado : EMC Society, August 1998

### About the Authors

**Roland Tiedemann** was born in Hamburg, Germany, in May 1970. From 1989 to 1992 he studied electrical engineering at the Universität Hannover and from 1989 to 1992 at the Technische Universität Hamburg-Harburg. In 1996 he joined the Siemens-Stiftungsprofessur at the Technische Universität Dresden. Today, his mayor research interests are: cable coupling, numerical simulation of electromagnetic fields and measurement techniques.

**Karl-Heinz Gonschorek** studied high frequencies at the University of Hanover. From 1975 to 1980 he was an scientific co-worker at the University of the Armed Forces in Hamburg. Here he wrote his Ph.D. thesis about electromagnetic pulse-coupling in extended arrangements of thin wires. Today he is holder of the of the Carl Friedrich von Siemens-Foundation Chair on EMC at the Dresden University of Technology

EMC 2000 INTERNATIONAL WROCŁAW SYMPOSIUM ON ELECTROMAGNETIC COMPATIBILITY

# DETERMINATION OF THE FIELD REDUCTION PROPERTIES OF SHIELDING DEVICES BY MODULATED SCATTERING MEASUREMENTS

R. Azaro[1], S. Caorsi[2]

[1] Department of Biophysical and Electronic Engineering
University of Genoa, Via Opera Pia 11/A, 16145 Genova - ITALY
Tel. +39 010 3532245, Fax +39 010 3532245, e-mail: azaro@dibe.unige.it

[2] Department of Electronics
University of Pavia, Via Ferrata 1, 27100 Pavia - ITALY
Tel. +39 0382 505661, Fax +39 0382 422583, e-mail: caorsi@ele.unipv.it

*The use of the Modulated Scattering Technique (MST) for the determination of the field reduction properties of shielding devices is proposed. The main advantages derive from the very limited perturbations introduced by a MST based field probe in the electromagnetic field under measurement. In the paper the theoretical basis of the MST are briefly discussed and a MST based measurement system is described. Finally some measurement data are presented and compared with data obtained by means of an analytical formulation.*

## 1. INTRODUCTION

Every electrical or electronic device usually has an enclosure which provides some different mechanical and electrical functions. Among them, especially in the case of devices sensitive to external electromagnetic field, plays an important role the one that provides the apparatus with an adequate degree of immunity to electromagnetic phenomena. Such a property is usually named as the *shielding effectiveness* $S_E$ of an enclosure and is one of the most important parameter that can determine the electromagnetic compatibility properties of the enclosed apparatus (both for emission and immunity). Traditionally shielding devices are based on the well known properties of metals, whose high conductivity in an ideal shielding configuration guarantees very high values of attenuation of electromagnetic fields. However nowadays, due to great demand of consumer electronics, there is the need of low-cost shielding enclosures based on the field attenuation properties of materials more light and cheap than metals. Consequently in industry there is the interest in fast and efficient methods for the determination of the shielding properties of real enclosures, in order to compare different shape and materials.

Shielding effectiveness measurements usually involve the evaluation of the coupling between a source and a receiver first with the enclosure under test removed (measurement of the *reference level*), and then with the enclosure under test inserted as shielding for the receiver (measurement of the *loaded level*). The ratio of the received power by the measurement system in the two configurations (*loaded level/reference level*), or *insertion loss*, gives the $S_E$ measure, usually expressed in decibels. In order to evaluate the *loaded level*, conventional measurement techniques involve a direct connection between a receiver and the receiving antenna, the last placed inside the shielding device. Perturbations introduced by the cable connecting the probe antenna and the receiver may be relevant, especially during the measurement of the loaded level. Furthermore, when the shielding device has limited size, it may be difficult to place a conventional field probe inside it.

Such problems con be overcome using the Modulated Scattering Technique (MST) [1] [2] [3] [4] for the measurement of electromagnetic field values. The main advantage deriving from the use of the MST derives from the possibility to perform the measurements without any connections with the MST probe antenna placed inside the enclosure, so the perturbations introduced during the measurement process can be very limited. In addition a MST probe, due to its limited size and its simple structure, introduce little perturbations to the field distribution under measurement, and can be efficiently used to evaluate small sized enclosures.

Finally, employing the *monostatic* set-up of the MST technique, the measurements can be performed directly at the RF port of the radiating system that generates the electromagnetic field to which the enclosure under test is exposed.

In this paper, to demonstrate the applicability of the technique to shielding properties evaluation of real enclosures, an experimental measurement system based on the MST is described and the data obtained for a brass rectangular box are reported and compared with the corresponding data obtained by means of an analytical formulation.

The study of the electromagnetic phenomena related to the presence of apertures in shielding enclosures has been faced by various authors [5] [6] [7] [8], at different level of approximation, presenting numerical simulations and analytical formulations. Due to its effectiveness and to its fast implementation, to obtain the data to compare with the measured data has been chosen the formulation of Robinson et al. [8] [9] [10]; in this formulation the enclosure is considered as a waveguide with only a mode of propagation ($TE_{10}$) and all the phenomena are modeled by suitable transmission lines.

## 2. THE MODULATED SCATTERING TECHNIQUE

The Modulated Scattering Technique (MST) is a perturbative measurement tool introduced in the fifties [1] [2] [3] for the investigation of electromagnetic field distributions generated by antennas, especially at centimeter wavelength. Subsequently many experimenters have proposed measurement systems, based on the MST, devoted to rapid and accurate near-field measurements for the characterisation and diagnostic of antennas [11] [12] [13]. The technique has also been used for mapping the field distribution in the close surrounding of printed circuits and components [14], for investigating the fields radiated by industrial applicators [15], and as a fast measurement technique for biomedical imaging systems [16] [17]. Recently the Modulated Scattering Technique has also been proposed as a tool to carry out the field uniformity verification in radiated field immunity sites [18] and as a tool to investigate on field uniformity inside TEM cells [19].

The Modulated Scattering Technique is based on the scattering properties of small probe antennas [20] and the signals related to the electromagnetic field under measurement are not delivered by the measuring probe, but re-radiated by the probe itself and received by the antenna generating the field in the *monostatic set-up*, or by an auxiliary antenna in the *bistatic set-up*..

As can be shown [3] [21] [22], in the *bistatic* set-up the received voltage is proportional to the field present where the probe antenna is placed, while in the *monostatic* set-up the received voltage turns out to be proportional to the square of the field.

In particular the relationship existing in the monostatic set -up can be derived starting form the

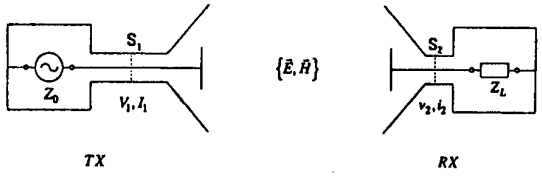



Fig. 1: The basic monostatic Modulated Scattering Technique set-up.

application of the Lorentz reciprocity theorem [23] [24] in a general configuration as sketched in figure 1. In such a configuration we consider a transmitting antenna *TX* which generates the electromagnetic field under measurement $\left\{\vec{E},\vec{H}\right\}$, and a receiving antenna *RX*, here employed as field probe. In figure 1 are also defined voltages and currents, $V_1, I_1$ and $v_2, i_2$, existing in the transversal sections $S_1$ and $S_2$.

If we assume that the hypothesis of applicability of the Lorentz reciprocity theorem are satisfied, starting from the expression of the theorem:

$$\int_S \hat{n}\cdot\left(\vec{E}_a\times\vec{H}_b-\vec{E}_b\times\vec{H}_a\right)dS=0 \qquad (1)$$

where $\left\{\vec{E}_a,\vec{H}_b\right\}$ and $\left\{\vec{E}_b,\vec{H}_b\right\}$ are two different field distributions that can be generated by means of two different functional state of the system and $\hat{n}$ is the unity vector normal to surface $S$ enclosing the system, we obtain the reciprocity relationship:

$$V_{1a}\,I_{1b}-V_{1b}\,I_{1a}+v_{2a}\,i_{2b}-v_{2b}\,i_{2a}=0 \qquad (2)$$

Here we consider as probe antenna (RX) a *minimum scattering antenna* [25] and we assume to connect to it an open circuit and a matched load in order to generate the two different fields distributions $\left\{\vec{E}_a,\vec{H}_b\right\}$, $\left\{\vec{E}_b,\vec{H}_b\right\}$.

After writing voltages and currents in the transversal sections $S_1$ and $S_2$ as sum of incident and reflected quantities, starting from (2) one can obtain the relationship:

$$V_{1b}^{\,refl}=\frac{Z_0}{Z_L}\frac{1}{V_{1b}^{\,inc}}\left(\vec{E}\cdot\vec{h}\right)^2 \qquad (3)$$

where $V_{1b}^{inc}$ and $V_{1b}^{refl}$ are the incident and reflected voltages in section $S_1$, $\vec{h}$ is the equivalent height of the receiving antenna, $Z_0$ the characteristic impedance of

TX system and $Z_L$ the matched load of the RX antenna.

The equation (3) constitute the fundamental relationship for the monostatic Modulated Scattering Technique set-up; for a given $V_{lb}^{inc}$ voltage incident in transmitting antenna, it allows one to evaluate the electric field $\vec{E}$ in the probe position measuring the reflected voltage $V_{lb}^{refl}$ in the transmitting system.

Since the field scattered by the probe produces very weak signal in the measurement system, usually a low frequency modulation of the scattered field is impressed. The modulation allows one to improve the sensibility of the measurement system by using some tuned amplifiers in the receiving system and, at the same time, to distinguish the field scattered by the probe from all other scattering contributions. Since the intensity of the scattered field depends on the value of the load connected to the probe [26], the modulation can be achieved impressing an impedance modulation. In practice the modulation is obtained switching periodically the electrical state of a non-linear device, connected as load for the probe, between two different electrical states.

## 3. THE EXPERIMENTAL SETUP

In order to investigate on the applicability of the technique to shielding evaluation of real enclosures and on the performances of the experimental system developed, measurements have been carried out, in the frequency range 400 - 1000 MHz, on a brass rectangular box (30 cm x 30 cm x 12 cm, wall thickness 1 mm) having a rectangular aperture (20 cm x 3 cm) on one face. This enclosure has been placed on a dielectric support and it has been exposed to the electromagnetic field generated in a semianechoic chamber (with additional anechoic material placed on the floor) by a logperiodic antenna. As sketched in figure 2, the experimental system was composed by a signal generator, a power amplifier, a dual directional coupler and a monostatic MST measurement system.

All the devices forming the experimental set-up system was arranged outside the semianecoic chamber, in order to improve the overall measurement accuracy.

As depicted in figure 2, the enclosure has been exposed to the incident electromagnetic field with the aperture directed towards the source antenna and, for every considered frequency, the received MST voltage has been detected and registered first without the box and then with the box present, as represented in figure 3*a* and 3*b*. As already mentioned there is no physical connection between the measurement system and the field probe, so the perturbations introduced in the electromagnetic field under measurement are very limited.

Since the measurement system is based on the monostatic set-up of the MST, the low frequency voltage obtained is propotional to the square of the

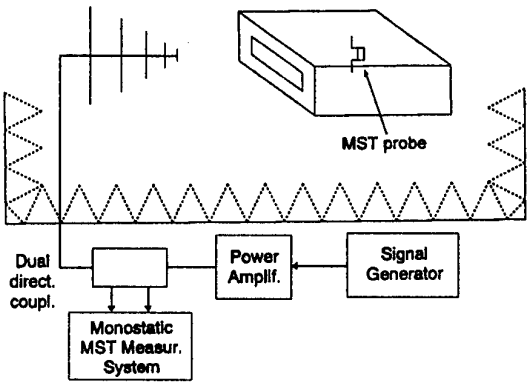



Fig. 2: Experimental set-up for shielding effectiveness evaluation of a rectangular box via a monostatic MST.

electromagnetic field present where the probe is placed.

Then if $\vec{E}_0$ is the electric field present when the box is removed, $\vec{E}$ the electric field when the box is present, $V_0^{MST}$ and $V^{MST}$ the corresponding low frequency voltages available from the measurement system, then the shielding effectiveness can be calculated as:

$$S_{E\,[dB]} = 20\,Log_{10}\frac{|\vec{E}_0|}{|\vec{E}|} = \\ = 20\,Log_{10}\sqrt{\frac{V_0^{MST}}{V^{MST}}} = 10\,Log_{10}\frac{V_0^{MST}}{V^{MST}} \qquad (4)$$

The measurement results obtained for the center of the rectangular box in the frequency range 400–1000 MHz are reported in figure 4 and are compared with the corresponding data obtained by means of an analytical formulation, based on a transmission line modeling of the electromagnetic phenomena, recently proposed by Robinson et al. [8].

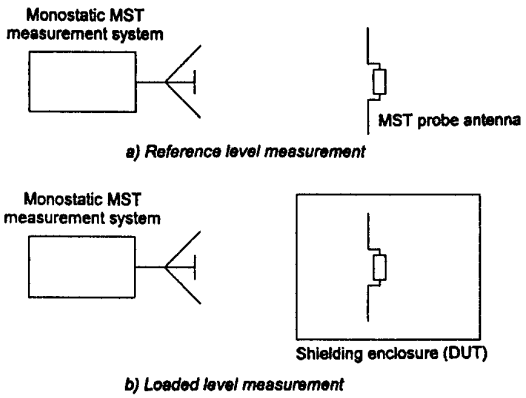



Figure 3: Field reduction properties of an enclosure via MST: 3*a* reference level measurement, 3*b* loaded level measurement.

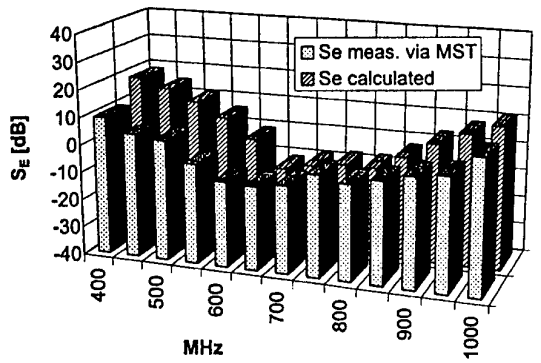



Figure 4: Shielding effectiveness evaluation via MST of a rectangular box (30x30x12 cm) having a rectangular aperture (20x3 cm).

As can be observed in figure 4 there is an acceptable accordance between the two data set, especially in the frequency range where resonance phenomena inside the rectangular box occur. Due to the limited power level available and to the weak signals detected from the MST experimental measurement set-up, it was very difficult to acquire the *loaded level* in the frequency ranges where the box presents shielding effectiveness values greater then 10 dB. As a consequence, further developments of this application will be devoted to obtain a more sensitive measurement system.

## 4. CONCLUSIONS

The use of the Modulated Scattering Technique (MST) for the determination of field reduction properties of real enclosures has been proposed. Some experimental results obtained via laboratory prototype system for a rectangular box, having an aperture, have been presented in the frequency range 400-1000 MHz. The results have also been compared with the corresponding data obtained by means of an analytical formulation, showing the applicability of the technique.

## 5. REFERENCES

5.1. J. H. Richmond, " A modulated scattering technique for measurement of field distributions," Inst. Radio Eng. Trans. Microwave Theory Tech. MTT-3, 1955, pp. 13-15.

5.2. R. Justice, V. H. Ramsey, "Measurement of electric field distributions," Inst. Radio Eng. Trans. on Antennas and Propagat. AP-3, 1955, pp. 177-180.

5.3. A. L. Cullen, J. C. Parr, "A new perturbation method for measuring microwave fields in free space," IEE Proceedings part B 102, 1955, pp. 836-844.

5.4. J. C. Bolomey, B. Cown, G. Fine, L. Jofre, M. Mostafavi, D. Pichard, J. Estrada, P. Friederich, and F. Cain, "Rapid near-field antenna testing via arrays of modulated scattering probes," IEEE Trans. on Antennas and Propagat., AP-36, 1988, pp. 804-814.

5.5. R. Azaro, S. Caorsi, M. Donelli, G.L. Gragnani, M. Raffetto, "A software for the evaluation of field penetration inside shielding box with apertures," Proceedings 14th International Wroclaw Symposium and Exhibition on Electromagnetic Compatibility, Wroclaw, 27-30 June, 2000.

5.6. H. A. Mendez, "Shielding theory of enclosures with apertures," IEEE Trans. on Electromagnetic Compatibility, vol. 20, n. 2, May 1978, pp. 296-305.

5.7. G. Cerri, R. De Leo and V. M. Primiani, "Theoretical and experimental evaluation of the electromagnetic radiation from apertures in shielded enclosures, " IEEE Trans. on Electromagnetic Compatibility, vol. 34, n. 4, November 1992, pp. 423-432.

5.8. M. P. Robinson, T. M. Benson, C. Christopoulos, J. F. Dawson, M. D. Ganley, A. C. Marvin, S. J. Porter and D. W. P. Thomas, "Analytical formulation for the shielding effectiveness of enclosures with aperture," IEEE Trans. on Electromagnetic Compatibility, vol. 40, n. 3, August 1998, pp. 240-248.

5.9. M. P. Robinson, J. D. Turner, D. W. P. Thomas, J. F. Dawson, M. D. Ganley, A. C. Marvin, S. J. Porter, T. M. Benson and C. Christopoulos, "Shielding effectiveness of a rectangular enclosure with a rectangular aperture," Electronic Letters, vol. 32, n. 17, August 1996, pp. 1559-1560.

5.10. Turner, T. M. Benson, C. Christopoulos, D. W. P. Thomas, M. P. Robinson, J. F. Dawson, M. D. Ganley, A. C. Marvin, S. J. Porter, "Characterisation of the shielding effectiveness of equipment cabinets containing apertures, " Proceedings International Symposium on Electromagnetic Compatibility EMC'96 ROMA, Rome, 17-20 September, 1996, pp. 574-578.

5.11. Liang, G. Hygate, J. F. Nye, D. G. Gentle, R. J. Cook, "A probe for making near-field measurements with minimal disturbance: the optically modulated scatterer," IEEE Trans. on Antennas and Propagat., AP-45, 1997, pp. 772-780.

5.12. M. Mostafavi, J. C. Bolomey, D. Picard, "Far-field accuracy investigation using modulated scattering technique for fast near-field measurements," IEEE Trans. on Antennas and Propagat., AP-33, 1985, pp. 279-285.

5.13. J. C. Bolomey, B. Cown, G. Fine, L. Jofre, M. Mostafavi, D. Pichard, J. Estrada, P. Friederich, and F. Cain, "Rapid near-field antenna testing via arrays of

modulated scattering probes," IEEE Trans. on Antennas and Propagat., AP-36, 1988, pp. 804-814.

5.14. T. P. Budka, S. D. Waclawik, G. M. Rebeiz, "A coaxial 0.5-18 GHz near electric field measurement system for planar microwave circuits using integrated probes," IEEE Trans. on Microwave Theory and Techniques, Vol. 44-12, 1996, pp. 2174-2184.

5.15. Roussy, Agbossou, Dichtel, Thiebaut, "High electromagnetic field measurements in industrial applicator by using an optically modulated sensor," Journal of microwave power and electromagnetic energy, vol. 27, n.3, 1992, pp. 164-170.

5.16. J. C. Bolomey, C. Pichot, "Microwave tomography: from theory to practical imaging systems," International Journal of Imaging System and Technology, vol. 2, 1990, pp. 144-156.

5.17. R. Azaro, S. Caorsi, M. Pastorino, "A 3 GHz microwave imaging system based on a modulated scattering technique and on a modified Born approximation," International Journal of Imaging System and Technology, vol. 9, n. 5, August 1998, pp. 395-403.

5.18. R. Azaro, S. Caorsi, "Electromagnetic field uniformity test using modulated scattering probes," Proceedings 14th International Wroclaw Symposium and Exhibition on Electromagnetic Compatibility, Wroclaw, 23-25 June, 1998, pp. 183-187.

5.19. R. Azaro, S. Caorsi, "Field uniformity measurements in a TEM cell using the modulated scattering technique," Proceedings International Symposium on Electromagnetic Compatibility EMC'98 ROMA, Rome, 14-18 September, 1998, pp. 796-801.

5.20. F. Harrington, "Small resonant scatterers and their use for field measurements," Inst. Radio Eng. Trans. Microwave Theory Tech. MTT-10, 1962, pp. 165-174.

5.21. J. C. Bolomey, D. Picard, M. Mostafavi, "Evaluation des cadences de mesure de champs proches au moyen de sondes modulées," Annales des Télécomunication, vol. 40, n. 1-2, Jan./Fév. 1985, pp. 26-36.

5.22. R Azaro, S. Caorsi, M. Pastorino, "On the relationship for the bistatic modulated-scattering technique in scattering applications using scattering properties of antennas", IEEE Trans. on Antennas and Propagation, vol. 46, n. 9, September 1998, pp. 1399-1400.

5.23. G. C. Someda, Electromagnetic Wave (in italian), Turin, UTET, 1986.

5.24. G. D. Monteath, Applications of the electromagnetic reciprocity principle, New York, Pergamon Press, 1973.

5.25. W. K. Kahn, H. Kurss, "Minimum scattering antennas," IEEE Trans. on Antennas and Propagation, pp. 671-675, September 1965.

5.26. R. E. Collin, "The receiving antenna" in R. E. Collin, F. J. Zucker, "Antenna Theory - Part 1" McGraw-Hill, New York, 1969, pp. 123-133.

## BIOGRAPHICAL NOTES

Renzo Azaro received the "laurea" degree in Electronic Engineering from the University of Genoa, Italy, in 1992. At present he is a Ph. D. student in "Computer science, applied electromagnetics and telecommunication engineering" at the same University. His main research interests are in electromagnetic compatibility and measurements.

Salvatore Caorsi is a full professor of Electromagnetic Compatibility at the Department of Electronics of the University of Pavia, Italy and he is also teaching the course of Antennas at the University of Genoa. He is the Past-President and founding member of the Inter-university Research Center for Interactions Between Electromagnetic Fields and Biological Systems (ICEMB). His primary activities are focused on applications of electromagnetic fields to telecommunications, artificial vision and remote sensing, biology, medicine and electromagnetic compatibility. Prof. Caorsi is a member of the AEI, EBEA and ESHO.

EMC 2000 INTERNATIONAL WROCŁAW SYMPOSIUM ON ELECTROMAGNETIC COMPATIBILITY

# AN INVESTIGATION ON MEASUREMENT METHOD OF DISTURBANCES AT TELECOMMUNICATION PORTS BY USING BOTH VOLTAGE AND CURRENT PROBE

Nobuo Kuwabara, Yoshiharu Hiroshima, and Fujio Amemiya
NTT Lifestyle and Environmental Technology Laboratories
3-9-11 Midori-cho, Musashino-shi, Tokyo 180-8585, Japan
Fax. +81-422-59-3314 e-mail:kuwabara@ntttqn.tnl.ntt.co.jp

*Method of measuring disturbances at telecommunication ports have been published by IEC/CISPR 22. A method using both the disturbance voltage and current is useful because it does not require any impedance stabilization networks (ISNs). In this paper, the values measured using this method are theoretically and experimentally compared with the values measured using ISN. The results shows that the method can be used to measure the disturbances by taking into account the margin, and the margin can be reduced to improve the phase angle characteristics of the common mode impedance with ISNs.*

## 1. INTRODUCTION

In 1998, CISPR published CISPR Publication 22 Third edition (CISPR 22) [1], which contained the limits and measurement method for disturbances at telecommunication ports of information technology equipment (ITE).

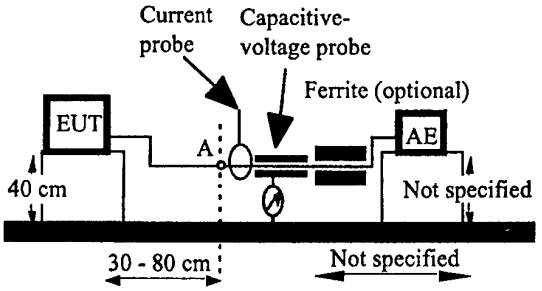
Disturbances at the telecommunication ports of ITE are generally measured using an impedance stabilization network (ISN) as specified in CISPR 22 [1]. There are many kinds of telecommunication ports; for example, a private branch exchange (PBX) has several thousand wire terminals and the latest high-speed LAN [2] use an 8-wire telecommunication port, but CISPR 22 only specifies ISNs for 2- and 4-wire ports.

The method measured both the voltage and the current of the disturbance is describes in annex C of CISPR 22 [1] as one of the alternative methods that should be applied when a suitable ISN is not available. The method can be used to measure disturbances at any kind of ports as well as high-speed LAN ports because it does not use any ISN. According to the report [3], the disturbances measured by this method are always larger than those measured by ISN. However, this has not yet been confirmed.

In this paper, we investigate the deviations of the measured disturbances using the method described in annex C 1.3 and using ISN. An equivalent circuit is studied for the measurement set-up of the disturbances. The disturbance levels measured using both methods are calculated based on the equivalent circuit. An equation to calculate the margin, which means the value added to the disturbances level measured by the method of annex C 1.3 is always guaranteed to be large compared with the level measured by ISNs, is derived from the simulation results. Experiment an actual equipment is described to confirm the theoretical result.

## 2. MEASUREMENT METHOD IN ANNEX C 1.3

The test set-up described in annex C 1.3 of CISPR 22 is illustrated in Fig. 1. It is used to measure both the voltage and current of the disturbance, and the most severe value compared with the relevant disturbance limits is used for the test results [6]. Ferrite clamps or similar devices can be inserted between the measurement point and the associated equipment (AE) to reduce the deviation of the common-mode impedance when an ISN is used.

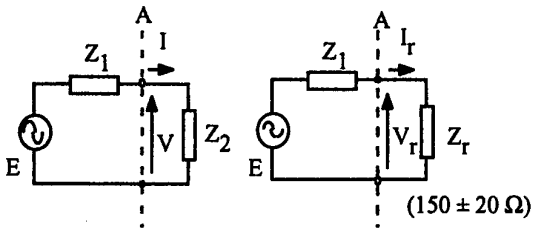



EUT: equipment under test AE: associate equipment

Fig. 1 Test set-up described in annex C.1.3.

The equivalent circuit for the test set-up in Fig. 1 is shown in Fig. 2. In Fig. 2, V and I are the voltage and the current of disturbance, respectively, and $V_r$ and $I_r$ are the voltage and the current using ISN. The common-mode impedance $Z_r$ is specified by CISPR 22. E is a disturbance source, $Z_1$ is the internal impedance of the disturbance source, and $Z_2$ is the common mode impedance when we show the AE from A point in Fig. 1. The effect of the current probe and the capacitive voltage probe are not considered in this circuit because the impedance between the current probe and the cable is less than 25 pF, as described in CISPR 16-1 [4]. The

capacitive voltage probe used in this experiment also satisfies this specification.




(a) Using annex C. 1.3. (b) Using ISN.

Fig. 2 Equivalent circuit for measuring disturbances at telecommunication ports.

From the equivalent circuit, the deviations between the measured results using the method in annex C 1.3 [1] and using ISN is given by,

$$F_v = V/V_r = \{Z_2(Z_1+Z_r)\}/\{Z_r(Z_1+Z_2)\}, \quad (1)$$
$$F_I = I/I_r = (Z_1+Z_r)/(Z_1+Z_2), \quad (2)$$

where V and I are the measurement results using the method in annex C 1.3 and $V_r$ and $I_r$ are the measurement results using ISN. Here, we present

$$Z_1 = |Z_1|\cos\theta_1 + j|Z_1|\sin\theta_1, \quad (3)$$
$$Z_2 = |Z_2|\cos\theta_2 + j|Z_2|\sin\theta_2, \quad (4)$$
$$Z_r = |Z_r|\cos\theta_r + j|Z_r|\sin\theta_r, \quad (5)$$

Substituting Eqs. (3), (4), (5) into Eq. (2), we get

$$|F_I| = \sqrt{\frac{|Z_1|^2+|Z_r|^2+2|Z_r||Z_1|\cos(\theta_1-\theta_r)}{|Z_1|^2+|Z_2|^2+2|Z_2||Z_1|\cos(\theta_1-\theta_2)}}. \quad (6)$$

From Eq. (1),

$$|F_v| = \{|Z_2|/|Z_r|\}|F_r|. \quad (7)$$

The larger the deviations from $V_r$ and $I_r$, the more severe the measured value is to the specified value. Thus, the test results are given by

$$F_t = \begin{cases} |F_v| & (|F_v| > |F_I|) \\ |F_I| & (|F_I| > |F_v|). \end{cases} \quad (8)$$

The amplitude of $Z_1$ and $Z_2$ can change from 0 to an infinite value and these phase angels can change from $\pi/2$ to $-\pi/2$. The amplitude of $Z_r$ can change from 130 Ω to 170 Ω [1] and its phase angle can change from $(-2/9)\pi$ to $(2/9)\pi$ according to the specifications [1]. These are changes independently. In such conditions, we should confirm whether $F_t$ is always more than 1 or not.

This paper investigate it theoretically and experimentally.

## 3. CALCULATION OF $F_t$

The $F_t$ value is calculated to investigate whether $F_t$ is larger than 1 or not in all cases. The range of the parameters and these steps are shown in Table 1. The amplitude of $Z_1$ and $Z_2$ changes from 1 to 10,000 for the typical range. The angle of $Z_1$, $Z_2$, and $Z_r$ and the amplitude of $Z_r$ changes in the allowable range. The step sizes in Table 1 are selected to get a sufficient accuracy.

Table 1 Calculation parameters

| Parameters | Range | Step |
|---|---|---|
| $\|Z_1\|$ | 1 - 10,000 | $_{10}\log(10000)/50$ |
| $\arg(Z_1)$ | $-\pi/2$ - $\pi/2$ | $\pi/18$ |
| $\|Z_2\|$ | 1 - 10,000 | $_{10}\log(10000)/50$ |
| $\arg\|Z_2\|$ | $-\pi/2$ - $\pi/2$ | $\pi/18$ |
| $\|Z_r\|$ | 130 - 150 | 10 |
| $\arg(Z_r)$ | $-\pi/9$ - $\pi/9$ | $\pi/18$ |

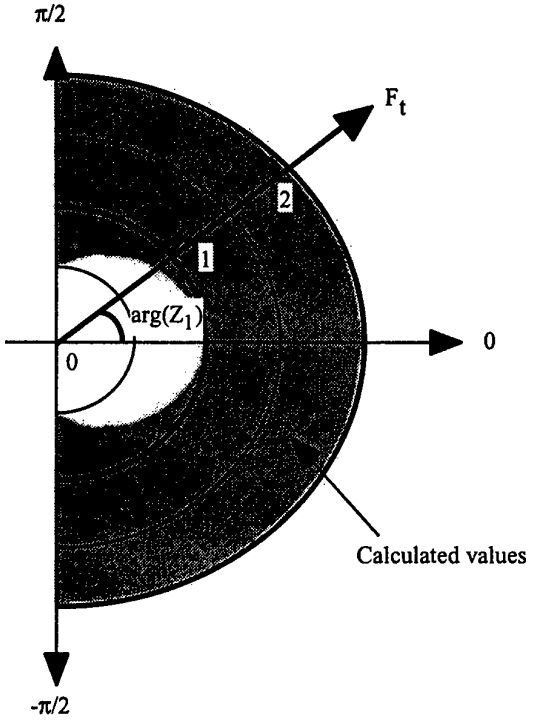



Fig. 3 Calculation results of $F_t$ values

The calculation results of the $F_t$ value are shown in Fig. 3 when the $Z_1$, $Z_2$, and $Z_r$ change. The gray part in Fig. 3 represents the calculated $F_t$ values. When $F_t$ is more than 2, we set $F_t$ to be 2. The results show that the minimum value of $F_t$ is less than 1. There is a possibility that the values measured using the method described in Annex C 1.3 is lower than those using ISNs, which is the formal method of CISPR 22. So, the minimum value of $F_t$ is calculated when this is lower than 1. It is difficult to calculate the $F_t$ value analytically

because the calculation results changes by the values of $|F_v|$ and $|F_l|$ as shown in Eq. (8). First, we investigate the conditions when $F_t$ is the minimum value.

There are six parameters as shown in Table 1. Here, we set

$$a = |Z_l|/|Z_r| \quad (10^{-4} \le a \le 10^4), \tag{9}$$
$$b = |Z_2|/|Z_r| \quad (10^{-4} \le b \le 10^4), \tag{10}$$
$$c = \theta_l - \theta_2 \quad (-\pi \le c \le \pi), \tag{11}$$
$$d = \theta_l - \theta_r \quad (-(11/9)\pi \le d \le (11/9)\pi). \tag{12}$$

The range of a, b, c, and d are determined by the range of the parameters listed in Table 1.

Substituting Eqs. (9)-(12) into Eqs. (6) and (7), we get

$$|F_l| = \sqrt{\{a^2+1+2a\cos(d)\}/\{a^2+b^2+2ab\cos(c)\}}, \tag{13}$$

$$|F_v| = b|F_l|. \tag{14}$$

These parameters change independently of each other. When we calculate the dependence of one parameter, the other parameter is considered as a constant.

Comparing Eqs.(13) and (14) with Eq. (6) and (7), the number of parameters is reduced from 6 to 4. The conditions, where $F_t$ is the minimum, are investigated using Eqs. (8), (13), and (14).

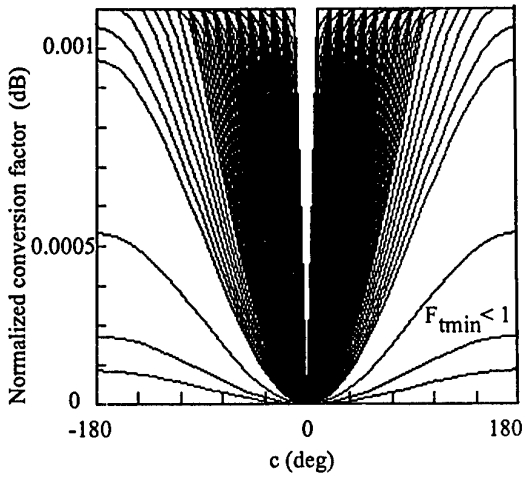



Fig.4 Calculation results of normalized conversion factor when a, b, and d are parameters.

Figure 5 shows the $F_t(a,b,0,d)$ values when the b value changes from 0.01 to 100. The parameters of a and d Figure 4 shows the $F_t(a,b,c,d)$ values when c value changes from $-\pi$ to $\pi$. The parameters of a, b, and d change as shown in Eqs. (9), (10), and (12). The step size of a and b is $10^{8/50}$ and that of c and d is $\pi/18$. The vertical axis presents $F_t(a,b,c,d)$ normalized by $F_{tmin}(a,b,c,d)$, which is the minimum value of $F_t(a,b,c,d)$. When $F_{tmin}(a,b,c,d)$ is more than 1, the calculated results are not shown in this figure because we do not need to consider these conditions. When c is zero, the $F_{tmin}(a,b,c,d)$ is the minimum for all a, b, and d ranges. We therefore get

$$F_{tmin}(a,b,c,d) = F_{tmin}(a,b,0,d). \tag{15}$$

Figure 5 shows the $F_t(a,b,0,d)$ values when the b value changes from 0.01 to 100. The parameters of a and d change as shown in Eqs. (9) and (12). When the $F_{tmin}(a,b,0,d)$ is more than 1, the calculated results are not shown in this figure. The vertical axis is the $F_t(a,b,0,d)$ value normalized by $F_{tmin}(a,b,0,d)$. This figure shows that the $F_{tmin}(a,b,0,d)$ is the minimum for all cases when b is 1. Therefore, we get

$$\begin{aligned} F_{tmin}(a,b,c,d) &= F_{tmin}(a,1,0,d) \\ &= F_{vmin}(a,1,0,d) \\ &= F_{lmin}(a,1,0,d) \\ &= \sqrt{\{a^2+1+2a\cos(d)\}/\{a^2+1+2a\}} \\ &= \sqrt{1 - 2\{1 - \cos(d)\}/F_a(a)}, \end{aligned} \tag{16}$$

where

$$F_a(a) = a+(1/a)+2. \tag{17}$$

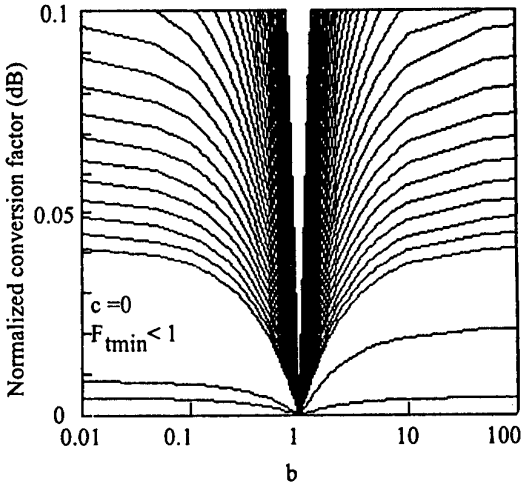



Fig.5 Calculation results of normalized conversion factor when a,and d are parameters.

In Eq. (16),

$$\{1 - \cos(d)\} \ge 0. \tag{18}$$

Then, when $F_a(a)$ is the minimum, $F_{tmin}(a,1,0,d)$ is the minimum. The value of a, when $F_a(a)$ is the minimum, is obtained in the following;

$$dF_a(a)/da = (1-1/a^2) = 0. \tag{19}$$

Using $a > 0$, a of 1 is obtained. Then,

$$\begin{aligned} F_{tmin}(a,b,c,d) &= F_{lmin}(1,1,0,d) \\ &= \sqrt{0.5 + \cos(d)/2} \end{aligned} \tag{20}$$

From Eq. (20), d value of $-(11/9)\pi$ or $(11/9)\pi$ is obtained when $F_{tmin}(a,b,c,d)$ is the minimum. From

Table 1 and Eq. (12), d of -(11/9) $\pi$ means $\theta_r$ is -(2/9) $\pi$ and $\theta_l$ is -$\pi$/2 while d of (11/9) $\pi$ means $\theta_r$ is (2/9)$\pi$ and $\theta_l$ is $\pi$/2. This means that $F_{tmin}(a,b,c,d)$ is the minimum when $\theta_l$ is $\pi$/2 or -$\pi$/2.

Figure 6 shows $F_{tmin}(1,1,0,\pi/2-\theta_r)$, $\theta_r<0$ and $F_{tmin}(1,1,0,-\pi/2-\theta_r)$, $\theta_r>0$. The vertical axis in Fig. 6 is the $F_{tmin}$ which means the minimum value of the conversion factor in dB, and the horizontal axis is $\theta_r$ which means the allowable deviation of ISN phase angle. The value of 0 dB means that the values measured using the method in annex C 1.3 agrees with the values measured using ISNs. This figure shows that $F_{tmin}$ is the maximum when $\theta_r$ is 0 and decreases in proportion as increase of absolute value of $\theta_r$.

The -$F_{tmin}$ in Fig. 6 can be considered as a type of the margin because the value adding -$F_{tmin}$ and the value measured using the method in annex C 1.3 is always larger than that of ISNs. So, Eq. (20) shows that the margin decreases in proportion with the deviation of the ISN's phase angle. When $\theta_r$ is $\pi$/9, which is the specification of CISPR 22 [9], $F_{tmin}$ of -4.8 dB is obtained.

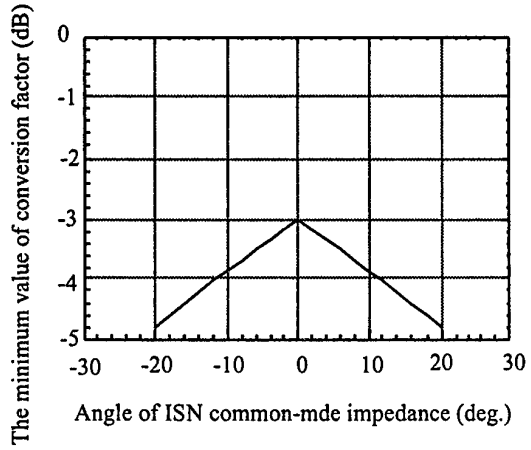



Fig. 6 The minimum value of conversion factor when the angle of an ISN common-mode impedance changes

## 4. EXPERIMENT

The set-up used to measure disturbances is illustrated in Fig. 7. Telecommunications equipment was used as the equipment under test (EUT). A 4-wire telecommunications line was used to connect the EUT to the AE. An ISN, an absorbing clamp, and a capacitive clamp were used to stabilize the common-mode impedance between the wires and ground. A current probe satisfying the requirement in CISPR 16-1 [4] was used to measure the common mode current. The capacitive-voltage probe with an electrostatic shield [5] was used to measure the common mode voltage, and it was placed 30 cm away from the EUT. The conversion factor of the capacitive-voltage probe was measured by a network analyzer where the same cable used in the experiment is inserted in the probe and is terminated by 50 $\Omega$. The disturbance value $V_r$ was also measured using an ISN for reference. The values subtracting 44 dB from $V_r$ are used as the reference $I_r$ for the measurement using a current probe. The absorbing clamp, the capacitive clamp, and an ISN, which are used to stabilize the common-mode impedance, are inserted between the voltage probe and AE to investigate the effect of the common-mode impedance stabilization.

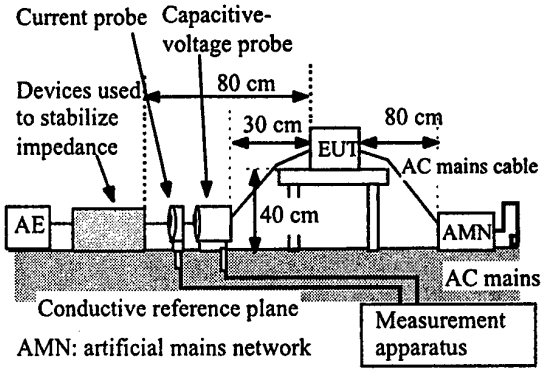



Fig. 7 Experimental set-up used to measure disturbances at telecommunication ports using both current probe and capacitive-voltage probe.

The measurement results are shown in Fig. 8. In this figure, the vertical axis is the deviations, which are the larger values of $V/V_r$ or $I/I_r$ for each frequency.

The measured values, when the ISN was used for impedance stabilization, are almost the same as the reference values. This means that the measured results using the method described in annex C 1.3 [1] agree with the results of ISNs when the common-mode impedance is the same value of ISN.

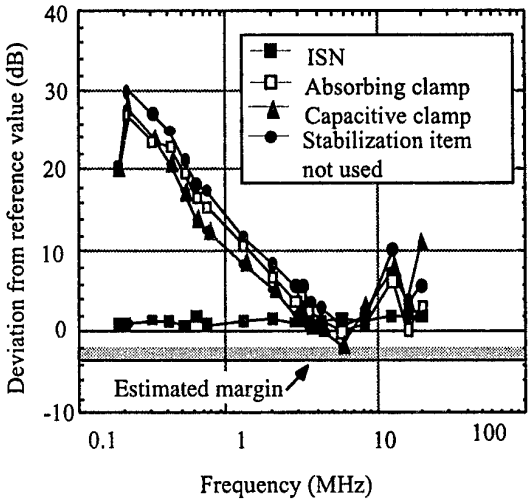



Fig. 8 Measured deviation from reference value.

The measured values not using ISN are different from the values using ISN in most of the measured frequency points, and the maximum deviation was more than 20 dB at 0.2 MHz. The values not using ISN are less than those using ISN at around 6 MHz. Therefor, some

margin is needed to guarantee that the measured values using this method are always larger than those of ISNs.

The estimated margin in Fig. 8 indicate 0 dB line when the margin calculated using Eq. (20) is considered. Seven degrees, which is the measured value of ISN in the experiment, is used as the deviation of the angle with the common-mode impedance. All measured values are above this line. The results show that the disturbances were measured by the method described in annex C 1.3 taking into consideration with the margins calculated using Eq. (20).

The measured disturbances, when the absorbing clamp and the capacitive clamp were used, were almost the same as the value when stabilization devices were not used. This means that other methods should be studied so as to reduce the deviation between the value measured using this method the value measured using an ISN.

## 5. CONCLUSION

The disturbances at telecommunication ports were measured by using the method described in CISPR 22 annex C 1.3. This method is useful to measure the disturbances at telecommunications ports because it can apply to any kind of telecommunication port. This paper investigated whether the method can always measure larger values than the values using ISNs.

The theoretical analysis and experiment indicate that the values using this method were lower than those using ISNs and this is not so rare because of the disturbances measured for a wide frequency range. The theoretical analysis shows that the margin can be calculated by using a simple equation, and the margin can be reduced to improve the phase angle deviation of ISNs. The experiment also indicates that the method can be used to measure the disturbances by taking into account the margin.

Future work will the study methods of stabilizing the common-mode impedance.

## 6. REFERENCES

[1] CISPR Publication 22 Third edition, "Information technology equipment -Radio disturbance characteristics - Limits and method of measurement", Nov. 1998.

[2] IEEE Draft P802.3ab/D2.0, "Physical layer specification for 1000 Mb/s operation on four pairs of Category 5 or better balanced twisted pair cable (1000BASE-T)", 1998-03.

[3] Ryser, H., "Additional comments to the proposed informative Annex D", CISPR/G/WG2 (Ryser) 96-2, Sep. 1996.

[4] CISPR Publication 16-1 First edition, "Specification for radio disturbance and immunity measuring apparatus and method, Part 1 Radio disturbances and immunity measuring apparatus", August 1993.

[5] Kobayashi, R., Kuwabara, N., and Hattori, M., "A method for determining the transmission direction of common-mode electromagnetic noise by measuring its energy flow", 12th International Zurich Symp. 38G5, Feb. 1997.

## BIOGRAPHICAL NOTES

**Nobuo Kuwabara** received B.E and M.E. degrees in electronic engineering from Shizuoka University in 1975 and 1977, respectively. He also holds a Dr. Eng. degree from Shizuoka University, granted in 1992. Since joining the Electrical Communication Laboratories of NTT in 1977, he has studied EMC problems related to telecommunications systems. He is currently a manager of Electromagnetic Environment Research Groupe at NTT Lifestyle and Environmental Technology Laboratories.

**Yoshiharu Hiroshima** received the B.E.and M.E. degrees in electrical and communication engineering from Tohoku University. He is currently a Research Engineer in the Electromagnetic Environment Research Group of Lifestyle and Environmental Technology Laboratories at NTT. Since joining NTT, he has been engaged in research and development of EMC measurement for telecommunication systems.

**Fujio Amemiya** received B.E and M.E. degrees in electronic engineering from Tohoku University in 1971 and 1973, respectively. He joined the Electrical Communication Laboratories of NTT in 1973, he went work on telephone systems. From 1973 to 1988, he engaged in development research on electronic and digital telephone sets. From 1988, he has been engaged in research and development of EMC in telecommunications systems. From 1992 to 1995, he was a manager of EMC Projects at Technical Assistance & Support Center. He is currently Senior Research Engineer, Supervisor in NTT Lifestyle and Environmental Technology Laboratories.

**EMC 2000** INTERNATIONAL WROCŁAW SYMPOSIUM ON ELECTROMAGNETIC COMPATIBILITY

# WEIGHTING OF INTERFERENCE FOR ITS EFFECT ON DIGITAL RADIOCOMMUNICATION SERVICES

Manfred Stecher
Rohde & Schwarz GmbH & Co. KG
Postfach 801469 D-81614 München, Germany
Phone: +49-89-4129-2152 Fax: +49-89-4129-3055
Email: Manfred.Stecher@rsd.rsd.de

*Abstract*

*Weighting of interference for its effect on modern digital radiocommunication systems is a prerogative for the future definition of emission limits. The effect on radiocommunication services depends on the type of interference (e.g. broadband or narrowband, pulse rate etc.). The paper explains the classical concept of pulse weighting to analog radio systems defined in CISPR standards, introduces a concept for the definition of weighting of interference to digital radiocommunication systems and gives new experimental results of weighting curves. Finally the results are analysed with respect to their common response and shape.*

## 1. INTRODUCTION

### 1.1 Origin and function of the quasi-peak detector

When broadcasting services started to enter homes in the twenties, it became obvious that radio interference had to be limited in order to enable an acceptable reception of the new service. As a consequence the International Special Committee on Radio Interference (CISPR) was founded in 1934 [1] for the development of measuring equipment and procedures. It took several publications until in 1975 all necessary CISPR publications had been developed establishing quasi-peak detection for all frequency ranges up to 1000 MHz.

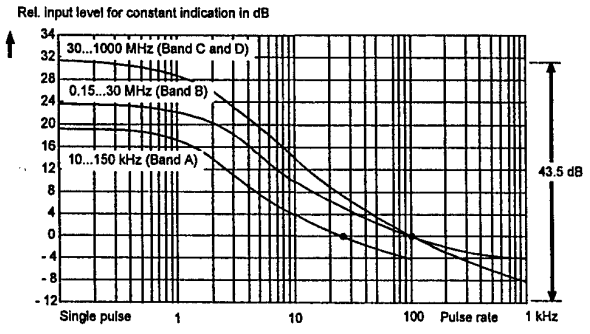



Fig. 1: Weighting curves of quasi-peak measuring receivers for the different frequency ranges as defined in CISPR 16-1 [2].

It is necessary to add that the effect of narrowband interference was found to be typically 10 dB higher than that of impulsive interference, which had to be taken into account in different limits for narrowband and broadband disturbances (now limits for the average and the QP detector).

### 1.2 Other detection functions

#### 1.2.1 Peak detector

The peak detector follows the signal at the output of the IF envelope detector and holds the peak value until discharge is forced. The indication is independant of the pulse repetition frequency.

#### 1.2.2 Average detector

The average detector determines the linear average of the signal at the output of the IF envelope detector. Since 1985 the CISPR specifies emission limits using the average detector in addition to QP limits for conducted emissions.

#### 1.2.3 RMS detector

The RMS detector determines the rms value of the signal at the output of the IF envelope detector. It is described in CISPR 16-1, but it has no practical use in EMI measurements up to now.

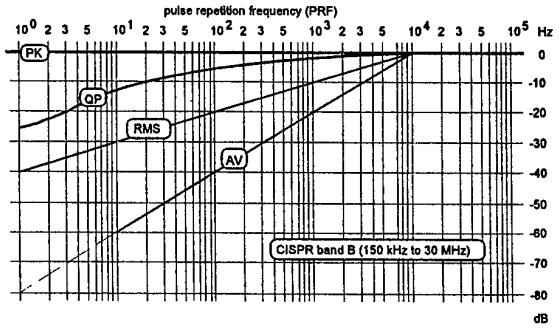



Fig. 2: Weighting curves of peak, QP, rms and average detectors in CISPR Band B

#### 1.2.4 Amplitude probability distribution (APD)

For the assessment of the interference effect on a radio channel, the APD is a suitable basis [3]. This however

cannot be called a weighting detector because it does not give one measurement result per frequency but the probability of occurrence of certain amplitudes as a function of the amplitude. The APD has been proposed for standardization in CISPR recently.

## 2. DIGITAL RADIOCOMMUNICATION SERVICES

### 2.1 General

All modern radio services use digital modulation schemes. This is not only true for mobile radio but also for audio and TV. Procedures for data compression and processing of analog signals (voice and picture) are used together with data redundancy for error correction. Usually, up to a certain critical bit-error rate (BER), the system can correct errors so that perfect reception occurs.

### 2.2 System characteristics

Whereas analog radio systems require signal-to-noise ratios of as much as 50 dB for satisfactory operation, in general, digital radio communication systems allow error-free operation down to signal-to-noise ratios of e.g. 10 dB. However the transition region from error-free operation to malfunction is small. Therefore planning guidelines for digital radio are based on almost 100% coverage. When the digital radio receiver operates at low input levels, the sensitivity to radio disturbance is important. In mobile reception, the sensitivity to radio disturbance is combined with the problem of multi-path propagation.

### 2.3 A CISPR Project and an ITU-R-Study question

Both CISPR [4] and ITU-R [5] adopted Study Questions dealing with the effect of different kinds of interference on radio signals. ITU-R Study Question 202/1 is titled: "Characterization and measurement of various interference sources to digital communication services (according to their interference effect)".

## 3. WEIGHTING OF INTERFERENCE TO DIGITAL RADIOCOMMUNICATION SYSTEMS

Up to now there has been little progress in both CISPR and ITU-R. The work to do is to determine the interference effect, find a compromise solution for a weighting detector including measurement bandwidth, define limits etc.

### 3.1 Principle of Weighting Function Measurement

The significance of the weighting curve for Band B in Fig. 1 is the following: the degradation of reception quality by a 100-Hz pulse observed by a radio listener is equal to the degradation by a 10-Hz pulse, if the pulse level is increased by an amount of 10 dB. In analogy to the above, an interference source with certain characteristics will produce a certain bit error rate (BER), e.g. $10^{-3}$ in a digital radiocommunication system, when the interfering signal is received in addition to the radio signal. The BER will depend e.g. on the pulse repetition frequency (PRF) and the level of the interfering signal. In order to keep the BER constant, the level of the interfering signal will have to be readjusted while the PRF is varied. This level variation vs. PRF determines the weighting function.

Measurement systems with BER indication are needed to determine the required level of the interfering signal for a constant BER.

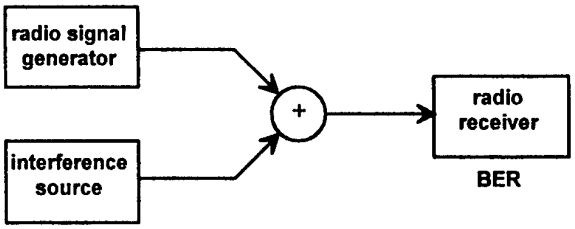



Fig. 3: Test setup for the determination of the interference signal level for a certain BER.

In a system as shown in Fig. 3 the radio receiver will have to decode the transmitted information and compare it with the undisturbed correct information in order to determine the BER. Such systems are available and have been used in [6]. In other systems the decoded information is looped back to the radio signal source and compared there to get the BER. The latter is true for Mobile Radio Testers.

Different digital radiocommunication systems will of course not respond in the same way to interference. Therefore a compromise solution will have to be found to cover as many digital radiocommunication systems as possible.

### 3.2 Generation of Interference signals

A signal generator with pulse-modulation capability can be used to generate the interference signal. For correct measurements, the pulse modulator requires a high ON/OFF ratio of more than 60 dB. Using the appropriate pulse width, the interference spectrum can be broadband or narrowband, where the definition of broadband and narrowband is relative to the communication channel. Fig. 4 gives an example of an interference spectrum used for the determination of weighting functions.

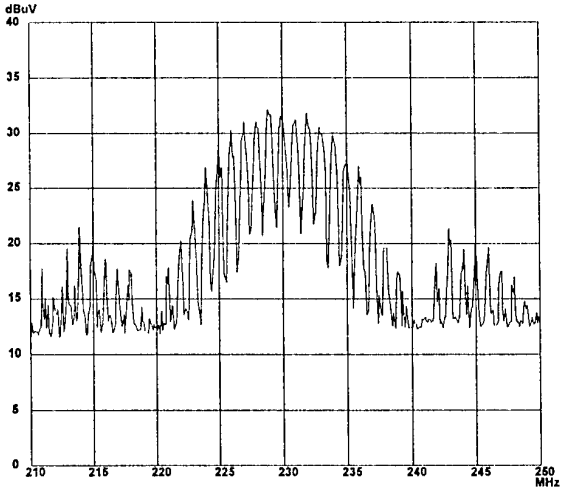



Fig. 4: Interference signal consisting of a pulse width of 0,1 µs with a pulse repetition frequency of 1 MHz. The signal generator level is 47 dB(µV). The spectrum above was measured with a impulse bandwidth of 1 MHz and the peak detector.

The advantage of using a band-limited pulse spectrum instead of a broadband pulse generator is to avoid overloading of the receiver under test. Otherwise the weighting function would be deteriorated by non-linearity effects. In addition to pulse-modulated carriers, unmodulated carriers were used to determine the sensitivity of different systems to different types of EMI.

### 3.3 Other principles of measurement

The receiver under test should receive a signal which is just sufficient to give quasi error-free reception (e.g. a BER = $10^{-7}$ or a factor of $10^{-3}$ lower than the critical BER). Thus the receiver operates like a receiver at the rim of a coverage area, where a disturbance above the emission limit can easily cause interference.

For radio telephone systems, where downlink (to the mobile) and uplink (to the base station) frequencies are in different bands, the use of a pulse modulated carrier helps to concentrate the interference on the mobile receiver and thus avoids to interfere with the loop-back connection.

## 4. MEASUREMENT RESULTS

Coding for error correction is characteristic of all digital radiocommunication systems. In most cases this is accomplished by adding e.g. tail bits within data frames and convolutional coding and by interleaving to avoid error bursts. GSM, DECT and TETRA are based on Time Division Multiple Access (TDMA), whereas IS-95 and J-STD 008 are based on Code Division Multiple Access (CDMA). DAB and DVB-T use Orthogonal Frequency Division Multiplex (OFDM). For the tests below, BER values have been chosen individually for each system.

### 4.1 GSM system

The European digital cellular telecommunication system operates in the 900 MHz (GSM 900) and 1800 MHz (GSM 1800) frequency bands. The offset between uplink (mobile to base station) and downlink is 45 MHz (GSM 900) resp. 95 MHz (GSM 1800). The occupied bandwidth is 300 kHz and channel spacing is 200 kHz. Modulation for constant spectrum envelope is achieved with Gaussian Minimum Shift Keying (GMSK). The error correction mechanisms applied are different for traffic channels (1b bits) and other bits (Class 2 bits). Therefore different bit error rates apply: BER, RBER 1b and 2 (residual BER) and FER (Frame error rates).

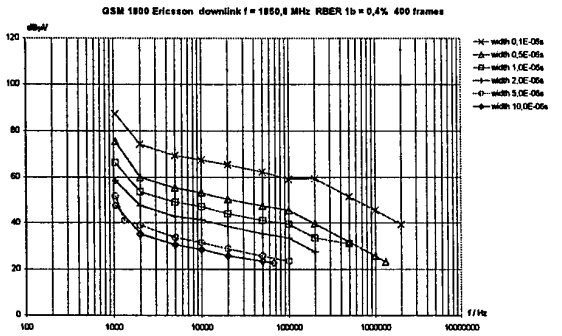



Fig. 5: Weighting functions for RBER 1b of GSM. The curves are characteristically rising below 2 kHz PRF.

The results shown in Fig. 5 are very similar to the BER and RBER 1b curves of Fig. 6. Fig. 6 presents results obtained by Dr. U. Neibig of Bosch, Germany, using the simulation software COSSAP. Unfortunately measurements below a PRF of 1 kHz were not possible due to instability of the test system.

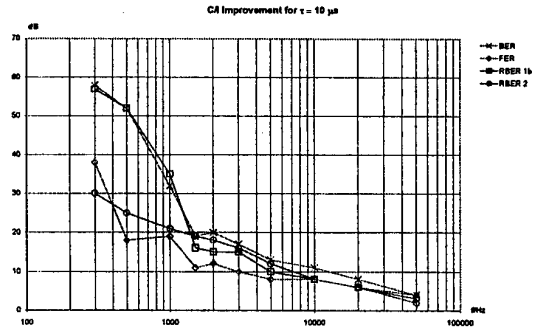



Fig. 6: Carrier-to-interference improvements in dB computed for GSM using COSSAP

### 4.2 DECT system

DECT stands for Digitally Enhanced Cordless Telephone and is used in homes and offices for distances up to 300 m (in picocells). It provides 10 channels spaced 1,728 MHz apart in the frequency range 1,88 to 1,90 GHz. The occupied bandwidth is ≈ 1,5 MHz. For speech data reduction Adaptive Differential Pulse Code Modulation (ADPCM) is used. Modulation is done with GMSK. The data stream for testing is Pseudo Random Binary Sequence (PRBS).

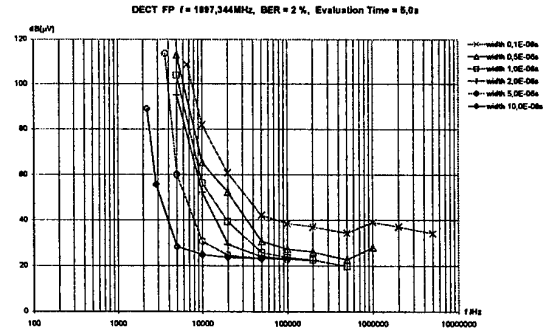



Fig. 7: Weighting functions for DECT show a flat response in the upper PRF areas and a sharp rise below about 10 kHz PRF.

### 4.3 TETRA system

TETRA stands for Terrestrial Trunked Radio and is used by workshops, the building and construction industry, airports, haulage business and safety services. It operates in the frequency range 380 to 520 MHz (in some areas also in 870 to 990 MHz) with a data rate of 36 kbit/s per carrier, an occupied bandwidth of ≈ 25 kHz and channel separations of 12,5, 20 or 25 kHz. Speech data reduction is done using Algebraic Code Excited Linear Prediction (ACELP) to 4,8 kbit/s per traffic channel. Up to four traffic channels are normally transmitted on one carrier. The error protection may be high or low, depending on the code rate. The modulation procedure is $\pi/4$-DQPSK. Fig. 8 shows the measured weighting curves for a high code rate = 1 (low error protection).

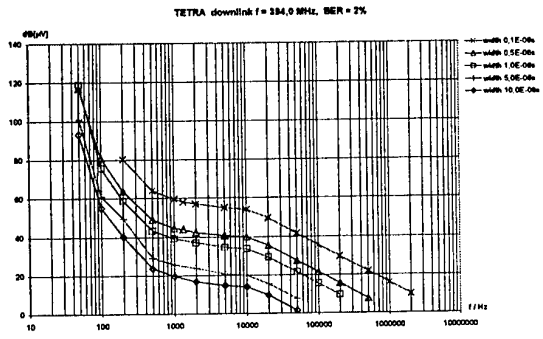


Fig. 8: Weighting functions for TETRA. Since the pulse spectrum is much wider than the channel bandwidth, all weighting curves are separated by the PRF ratio in dB.

4.4 CDMA systems IS-95 and J-STD 008

IS-95/J-STD 008 have been specified by TIA (US Telecommunications Industry Association) and are used in the frequency ranges 825 to 900 MHz (IS-95) and 1,8 to 2,0 GHz. The occupied bandwidth is ≈ 1,4 MHz (3 dB: 1.23 MHz). The modulation is done with Quadrature Phase Shift Keying (QPSK). For the uplink (mobile to base station) the optimum setting of the receive power at the base station is controlled via power control bits.

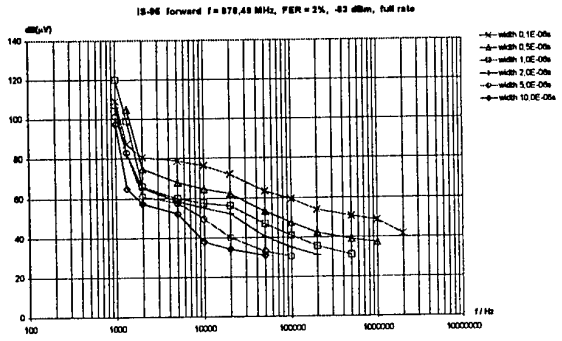


Fig. 9: Weighting curves for IS-95. The immunity to interference is rather high compared with other systems.

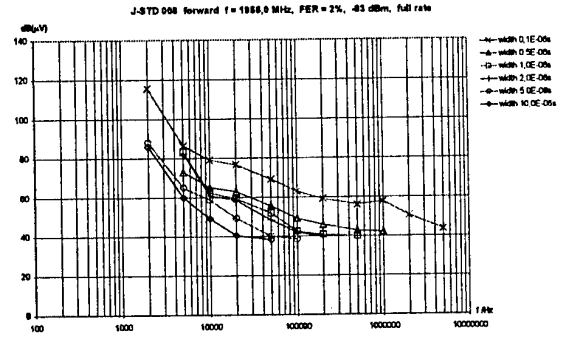


Fig. 10: Weighting curves for J-STD 008

4.5 Digital Audio Broadcasting DAB

DAB is operating in the VHF (174 to 230 MHz) and the L (1452 to 1492 MHz) bands with a bandwidth of 1,5 MHz per channel using Coded Orthogonal Frequency Division Multiplex (COFDM) to minimise multipath fading. The audio signal data rate is reduced by MUSICAM (Masking pattern adapted Universal Coding and Multiplexing), which is a part of the MPEG-2 (Moving Picture Expert Group) standard. The total transmitted bit rate is 2,4 Mbit/s. The 1500 subcarriers are modulated using Differential QPSK (DQPSK).

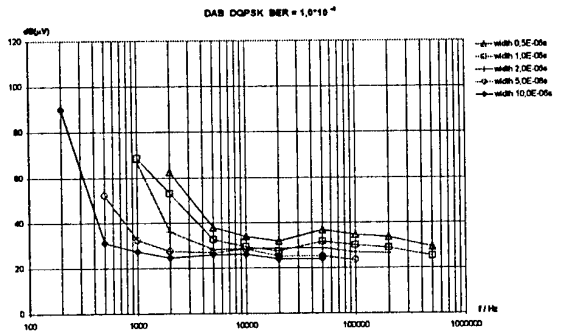


Fig 11: Weighting curves for DAB. The flat response down to approx. 1 kHz is characteristic of this system.

4.6 Digital Video Broadcasting Terrestrial DVB-T

DVB-T is intended to replace the existing analog TV systems. Data reduction is applied using MPEG-2. Each OFDM spectrum may contain 1705 carriers (2k modus) or 6817 carriers (8k modus). The individual carriers are modulated using QPSK or 16 QAM or 64 QAM (Quadrature Amplitude Modulation). The code rate CR is important for the amount of error protection (CR = ½ is a high amount of error protection):

$$CR = \frac{No.\,of\ information\ bits}{No.\,of\ information\ bits + No.\,of\ protection\ bits}$$

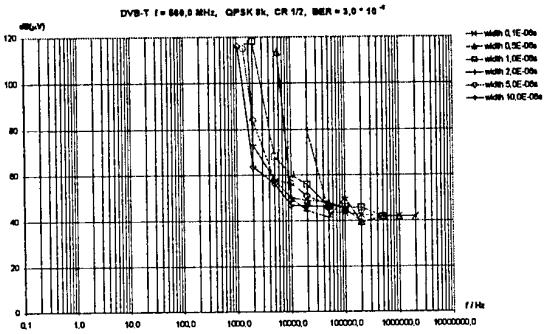


Fig. 12: Weighting function for DVB-T with QPSK and CR=1/2, i.e. the highest amount of error protection.

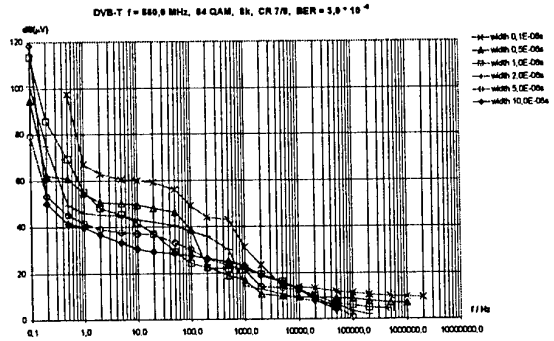


Fig. 13: Weighting function of DVB-T with 64 QAM and CR = 7/8, i.e. an extremely low of error protection.

Figs. 12 and 13 show two extremes of weighting functions for the DVB-T system. For other system parameters the weighting functions lie between these two.

4.7 Immunity to unmodulated sinewave signals

Each system has its individual sensitivity to unmodulated sinewaves - a special type of narrowband interference. This has been measured for the same amount of BER as for impulsive interference (see Fig. 14).

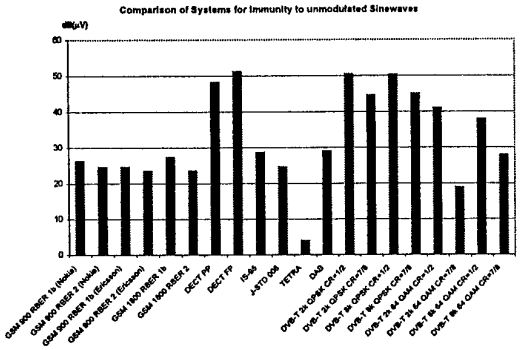



Fig. 14: The individual systems show different response to unmodulated sinewaves: especially the high immunity of DECT and the low immunity of TETRA are unexpected.

## 5. PROCESSING OF MEASUREMENT RESULTS

It is not easy to derive a unified weighting curve for future EMI measurements from the above presented results. Before we try to find a compromise solution, we should analyse the results as far as possible. Various facts have to be taken into consideration: e.g. the measurement bandwidths should be an average of the system bandwidths, e.g. 10 kHz for 150 kHz to 30 MHz, 100 kHz for 30 to 1000 MHz and 1 MHz for the frequency range above 1 GHz. Also further systems (e.g. DRM as the replacement of AM broadcasting or W-CDMA for future mobile telecommunications systems) will have to be measured as soon as equipment becomes available.

5.1 Values referred to a reference PRF

For comparison, the curves should be referred to a reference PRF as is done for the CISPR Quasi-Peak. A simple average of the measured curves will however not be adequate for universal weighting curves. Each individual curve will need to be weighted with a factor $c_i$ corresponding to the importance of the service.

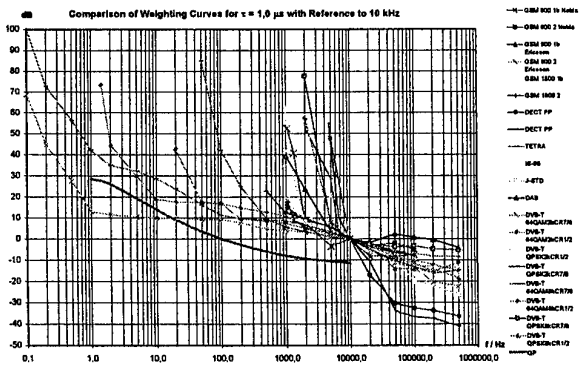



Fig. 15: Comparison of weighting curves for impulse widths of 1 µs, all referred to the value of 10 kHz (QP has been added for comparison)

5.2 Values referred to the system bandwidth

When looking at the curves of Figs. 5 through 13, it is obvious that all curves start with a flat response near the PRF corresponding to the system bandwidth and rising then faster some decades below.

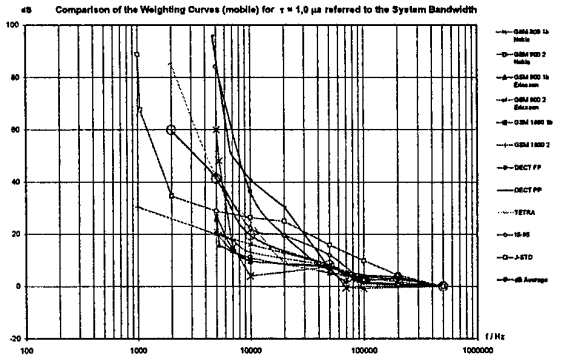



Fig. 16: Weighting curves for the mobile telecommunication systems referred to the individual system bandwidths and then compared and averaged.

Before final weighting curves can be defined, further investigations are needed and an expert group will have to weight the importance of the individual systems.

## 6. CONCLUSION

The concept and a first step towards weighting detectors of interference to digital radiocommunication services has been presented in [6]. The present paper gives further experimental results for mobile radio systems and DVB-T and one numerical example for GSM. All curves are starting with a flat response near the system bandwidth and are then rising increasingly fast. Pulse repetition frequencies below about 100 Hz will not have to be measured since they do not cause an interference effect. Some further results and weighted combined curves are to be agreed among the experts.

## REFERENCES

[1] Jackson, G.A.: "The early history of radio interference", Journal of the IRE, Vol. 57(1987), No. 6, pp. 244 - 250.

[2] IEC CISPR 16-1/1999-10: Specification of radio disturbance and immunity measuring apparatus and methods. Part 1: Radio disturbance and immunity measuring apparatus.

[3] Uchino, M.; Hayashi, Y.; Shinozuka, T.; Sato, R.: "Development of low-cost high-resolution APD measuring equipment", Proc. 1997 Int'l. Symp. EMC, Beijing, China, pp. 253 -256.

[4] CISPR Study Question 94: Determination of measurement and calculation of limits for the protection of radio services from man made radio noise.

[5] Question ITU-R 202/1: contained in ITU-Doc. 1/1-E, 30th Nov. 1995.

[6] Stecher, M.: "Weighting of interference according to its effect on digital communication services", Proc. IEEE EMC Symp., Denver, USA, 1998.

EMC 2000 INTERNATIONAL WROCŁAW SYMPOSIUM ON ELECTROMAGNETIC COMPATIBILITY

# SCREENING EFFECTIVENESS OF CATV NETWORKS - FIELD MEASUREMENTS

Antero Väänänen
Vaasa Polytechnic University, Wolffintie 30, FIN-65200 Vaasa, Finland; now at
Sodankylä Geophysical Observatory, Tähteläntie 112, FIN-99600 Sodankylä, Finland
Fax: +358 16 615529, Tel: +358 16 619829, E-mail: av@sgo.fi

*The shielding effectiveness of cable TV distribution networks and access networks in residential and other buildings has been investigated bidirectionally: by measuring the leakage emissions caused by the network, and by generating a known interference field with a transmitter and an antenna, and measuring the level of the interference leaked into the network. The shielding effectiveness of TV receiver connection cables was measured. The field strength of interference-causing on-the-air DAB transmissions was also measured, at several sites at the actual TV receiver locations inside buildings. Most measurements were done using both horizontal and vertical polarizations.*

## 1. INTRODUCTION

Terrestrial digital audio broadcast (DAB) transmissions have been started in Europe using frequencies around 200 MHz. This created a new EM interference problem affecting a large number of TV viewers. These frequencies are actually TV channels, and were "free" in the sense that they were not used for the existing terrestrial on-the-air TV transmissions at any DAB transmitter location. For the same reason they have been used for the cable distribution of TV signals. Now the on-the-air DAB transmissions were started right on the same channels which were already occupied in cable. In this new situation, the shielding effectiveness of the whole cable TV distribution chain, including the receiver, proved in many cases to be insufficient. TV reception was disturbed by the DAB signal on the same frequency.

The shielding effectiveness of CATV distribution networks of cable TV operators and of the CATV access networks in residential and other buildings has been investigated, to give the CATV operators a survey of the quality of these networks. The CATV operators use this information when they make decisions about necessary preparations for the coming DAB transmissions in other cities. The shielding effectiveness was investigated both by measuring the leakage emissions caused by the network, and by generating a known interference field with a transmitter and an antenna and measuring the level of the interference leaked into the network. The field strength of the on-the-air DAB transmissions was also measured, at several sites at the actual TV receiver locations inside buildings, to get to know the real signal levels at the point where the possible interference situations arise. The sites were selected by the cable operator on the basis of real interference complaints.

## 2. EMISSIONS FROM THE CATV NETWORKS

Emissions, which are possibly radiated by a CATV access or distribution network due to a leakage of the distributed signals, were measured at several locations representing different network types and different generations of equipment. The sites were chosen by the local cable operator. Measurements were done with EMC receiver or spectrum analyzer and wideband measurement antenna. It was very difficult to find buildings with really poor quality networks radiating so strongly that the emissions could be easily measured at a sufficiently large distance. The more recent the installation was, the less were the leakage emissions. No measurable emissions could be found at all from the most recent installations. No clear or systematic difference could either be found between horizontally and vertically polarized emissions.

The difference between the distributed signal level in the network and the leakage field strength measured at a suitable distance (5 m) can be used as a figure describing the relative shielding effectiveness of a distribution network of a building. For those older networks, where strong enough leakage was measured, this difference was about 55-60 dB. The signal level in the better quality networks was 60-80 dB higher than the noise floor of the emission measurement.

If it is necessary to try to transform an emitted interference field strength measurement result at certain distance to another distance, the nature of the source must be known. At those distances that are meaningful here, a radiating building network is not a point or line source, and simple basic formulas cannot be applied. We wished to be able to describe the nature of this type of source, and made sets of measurements at several different distances at many of the measured sites, but did not (yet) succeed in finding a general behaviour due to two reasons:

1) Too small field strengths; could not get reliable results at several (larger) distances, at least not with nondirectional antenna.
2) The directional pattern (beamwidth) of the measurement antenna introduces difficulties: emission level can even seem to increase with increasing distance, when the antenna sees a larger part of the radiating network when taken farther away from it.

We feel that it is not probable that a general formula could be found easily.

A survey of some results:

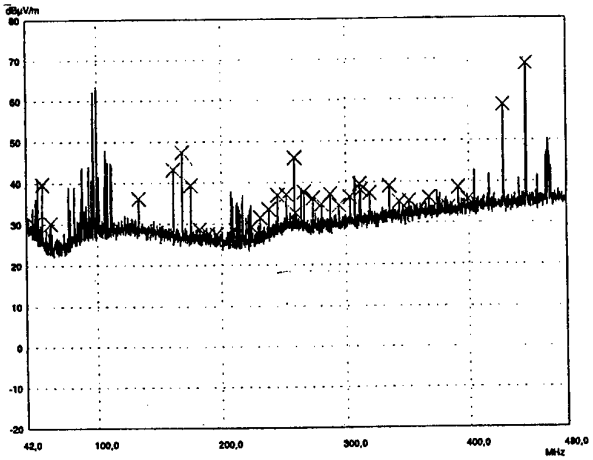



Fig. 1. Leakage emission measurement at location A.

Location A: 5-floor stone/brick town houses from the 1920's along two sides of a city block as well as in the neighbouring block, measurement being done close to one of the house walls. One of the houses had a TV signal distribution network from the 1960-1970's with 60 ohm cables. The original single-TV-cannel amplifiers had been replaced with a wideband CATV amplifier about 15 years ago, when a CATV network was constructed for the city and the building was connected to it. The access network of the other building was totally renovated to a star configuration very lately. Leakage emissions from the network could be recorded on all distributed channels, E2-S34. The levels were mostly around +35 dBµV, with highest peaks at about +39 dBµV/m, at a distance of 5 meters from the wall of the building.

Location B: A new student apartment building. No leakage at all, only the on-the-air FM and TV signals, mobile phone signals etc. could be seen.

Location C: Suburban area of single-family houses, constructed mainly of wood. The CATV network is about 13 years old; cabling is in the air, hung from poles together with the electricity distribution cabling. Measurement was done at 5 m distance from the crosspoint of a trunk cable and an access cable for two houses. All channels E2-S33 were leaking clearly, peaking mostly at +36...43 dBµV/m with the highest peaks at +44 dBµV/m. The emissions are clearly too strong, when compared with the limits set in the relevant standards, but this part of the network will be soon totally renovated using underground cabling.

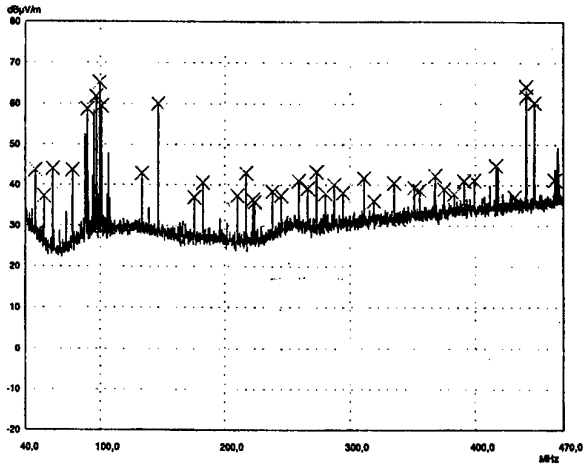



Fig. 2. Leakage emission measurement at location C.

Location D: Like location C, but a totally new housing area, where everything is new and cabling is underground. No measurable leakage was found, only the on-the-air signals like those at location B.

## 3. IMMUNITY OF THE CATV NETWORKS

The shielding effectiveness of the CATV distribution and access networks against radiation from outside sources was tested at some of the locations which were used for the emission tests and also at some new locations. Sites represent again different network types and different equipment generations, and were proposed by the CATV operator.

A known interference source was set up near the network or building to be tested. The interference signal leaked into the network was measured with a spectrum analyzer. The field strengths of existing on-the-air TV or other transmissions were not high enough to produce any measurable leakage signals into the networks. The source was 145 MHz or 435 MHz 30-50 W amateur radio transmitter and a directional antenna (calibrated hybrid quad or log-periodic) at 3 m height, generating 120...140 dBµV/m field strength.

The most recent installations were very good also when tested this way: no interference at all leaked into the networks. Different results were obtained with horizontal and vertical interference polarizations, but no clear general relationship was applicable to all cases. Horizontally polarized interference gave max 20 dB stronger leakage than vertical when it was stronger, vertical max 12 dB stronger than horizontal when it was stronger. Horizontal polarization generated slightly stronger leaked signals than vertical in most cases. 435 MHz interference gave about 6 dB stronger leakage than 145 MHz leakage in most cases, and about no difference in the rest.

Difference between calculated interference field strength at building center and measured leaked interference

signal level in the distribution network was in most cases 60-75 dB. For the oldest measured network it was only 43 db and for the newest at least 110 dB (interference buried in noise). For the oldest measured trunk/branch network (with air cabling, scheduled for complete renovation with underground cables this summer) the corresponding difference was about 60 dB, for other trunk/branch networks at least 100 dB.
For those sites, where also the leakage field strength measurement gave results clearly above noise floor, the relative shielding effectiveness figures obtained with both methods did not differ from each other by more than 1 dB.

A survey of some immunity measurements:

Location A1: The incoming cable from the CATV trunk network at location A. The highest peaks of the displayed noise are at a level of around +25 dBµV and the median level is about 6 dB lower. The interference source was located at 25 m from the center of the building, giving a field strength of +123...127 dBµV/m for the site. As no interference signal can be found from this cable, the trunk network at this point has a relative shielding effectiveness figure of merit of about 100 dB, corresponding to the difference between these two levels.

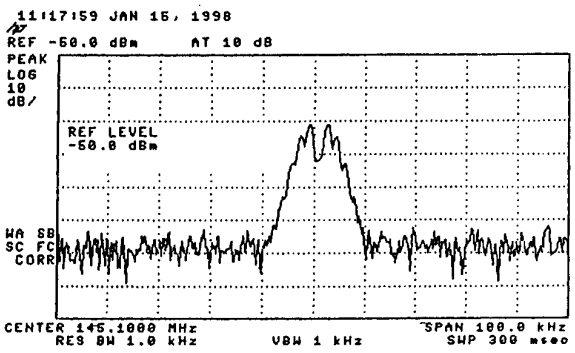



Fig. 3. Leakage signal in network at location A2.

Location A2: The measurement tap at the output side of the amplifier for this building. The interfering signal can now be seen at about +68 dBµV (taking all attenuations into account ). This figure is about 55 dB lower than the interference signal field strength value (source about 35 m from this point), the difference again representing the relative shielding effectiveness figure of merit. The distributed signal levels in the network at this point were around +95 dBµV and the leakage emissions were measured to be at +39 dBµV/m. The difference of these two figures is 56 dB which corresponds well with the 55 dB obtained from the preceeding calculation for the opposite direction leakage. The value would probably be better for a recently constructed or renovated star network.

Location A3: This is the other building of the city block at location A. The measurement is again from the output-side measurement tap of the amplifier. Interference signal at +77 dBµV while interfering field strength is at +120 dBµV/m (source about 45 m from this point) gives a difference of 43 dB as the shielding effectiveness. This was the old access network with 60 ohm cables and chain-connected outlets.

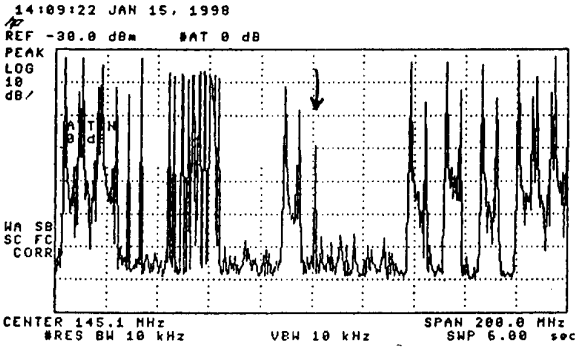



Fig. 4. Leakage signal in network at location C.

Location C: The same location C as earlier. The interference source was now positioned 5 meters from the air cabling. The signal was measured from the output side of the amplifier about 100 meters away and was at a level corresponding to +79 dBµV. With the interference level at +140 dBµV/m, the difference figure of merit is 61 dB. The sync peak signal levels were at +106 dBµV and the highest peaks of the leakage emissions were at +44 dBµV/m. These values have a difference of 62 dB, again closely corresponding to the other difference figure.

Location E: A branching point of branch network and trunk network air cables, but now of newer construction than at C, about 8 years old. The interference source was again 5 meters from this point and the signal leaked into the network was measured from an ordinary TV outlet in a wooden single-family house nearby. The level was around +27 dBµV, over 110 dB lower than the interference field strength figure. The good-quality cables clearly tolerate high interfering field strength values very well.

Table 2. Comparison of some emission and immunity measurement results.

| Location | A/ A2 | C | A1 | A3 | E |
|---|---|---|---|---|---|
| Signal level in cable | 95 | 106 | | | |
| Leakage field strength out | 39 | 44 | | | |
| Difference | 56 | 62 | | | |
| Interference field strength out | 123 | 140 | 125 | 120 | 140 |
| Leaked interf. level in cable | 68 | 79 | <25 | 77 | 27 |
| Difference | 55 | 61 | >100 | 43 | 113 |

## 4. MEASUREMENTS OF TV RECEIVER CONNECTION CABLES

Connection cables between the TV set and antenna outlet were found to be the real cause of interference leakage in all DAB interference complaint cases. Several hundreds of customer cables were changed by both the CATV operator and the broadcasting company.

Table 3. Leakage into connecting cables, referenced in decibels to a half-wave dipole.

| Cable | Meas 1 | | Meas 2 | | Note |
|---|---|---|---|---|---|
| | Open | Term | Open | Term | |
| 1 | -46 | -54 | -46 | -53 | |
| 2 | -48 | -54 | -53 | -54 | |
| 3 | -56 | -64 | -52 | -65 | |
| 4 | -42 | 0...-30 | -37 | -5... -40 | 1 |
| 5 | -55 | -70 | -53 | -66 | |
| 6 | -15 | -18 | -23 | -27 | |
| 7 | -50 | -67 | -49 | -69 | 2 |
| 8 | -32 | -26 | | | 3 |
| 9 | -24 | -26 | -21... -24 | -20... -54 | 4 |
| 10 | -40 | -10... -46 | -48 | -53 | 1 |
| 11 | -40 | -44 | -46 | -56 | |
| 12 | -32 | -26 | -27 | -34 | 4 |
| 13 | -56 | -58 | -50 | -56 | |
| 14 | -42 | -48 | -44 | -48 | |
| 15 | -55 | -70 | -52 | -72 | |
| 16 | -20 | -28 | -15 | -32 | |
| 17 | -54 | -64 | -53 | -69 | |
| 18 | | | -33 | -39 | |
| 19 | | | -34 | -46 | |
| 20 | | | -27 | -33 | |
| 21 | -85 | -85 | -75 | -78 | 5 |

Notes:
1) Loose contact of the connector shield part
2) Same as nr 15, but 1.5 m instead of 2 m
3) Same as nr 12
4) Slightly loose contact of connector shield part
5) Measurement setup only

Measurements were done on some cables in the lab as a by-product of the antenna and interference field-strength checking and calibration. The voltage induced to the tested cable from the interference generation setup 10 m away was measured, and the measured cable was moved a little around so that a maximum reading was found. This measured level was compared to a level received at the same position with a calibrated measurement antenna comparable to a half-wave dipole (G = 0,64 dBd). Two slightly different places and setups were used. Repeatability of this type of measurement cannot be very good, but the measurement setup was chosen to imitate the actual use of the cables. The measurement was conducted on 145 MHz. Cable lengths were from 1.5 to 15 m. A short summary of the results is given in Table 3.

With a shielded matched termination, the leakage levels were –18 ... -72 dB compared to half-wave dipole. Without the termination (end open) the leakage levels were -15 ... -53 dB. An ordinary TV receiver probably does not represent a laboratory grade termination. Most cables had about 5-20 dB better shielding attenuation with the matched load, but there were also some exceptions, which were worse with the load than without. A part of these cases is explained by the looseness of the connector outer part: the load transforms to an antenna, if the outer shield of the load resistor is not properly connected to the cable shield. This explanation was, however, not applicable to all cases. The length of the cable in wavelengths at the measurement frequency has significance, but it was not possible at this time to do a wide sweeped frequency test for all these cables. The frequency dependence was tested with some of the cables. In all, quality differences between the samples were significant. The samples were collected from several shops selling TV receivers.

Good quality double shielded measurement connection cables were tested as reference. No leakage was found with the available transmitter power, corresponding to a leakage level lower than –75 ... -85 dB compared to the half-wave dipole reference.

## 5. DAB SIGNAL LEVEL MEASUREMENTS

Measurements were done at actual TV receiver locations. The sites were selected mainly by the CATV operator on the basis of bad interference problems. Measurements were performed using EMC measurement receiver and spectrum analyzer, and with an antenna specially constructed and calibrated for this purpose (a folded dipole with a 1.5 m fibreglass tube handle). Field strength values were measured also outside the buildings. Building attenuation proved to be about 4-5 dB when the location was in direct free field, and about 8-15 dB, when the measurement was from a place without a clear free visibility to the transmitter. Horizontally (nominal) and vertically polarized measurements were done at every site; level difference detween these was greater in weak (indirect) fields. No direct measurable leakage to CATV distribution networks was found at any site. According

to information obtained from the Finnish Broadcasting Co, the DAB transmitters operating in Helsinki had a rf output power of 800 W and ERP of 2 kW in the main lobe of the antenna. We could not get directive diagrams of the antennas or field strength maps.

A description of some field strength measurements:

Location 1: An office on the ground floor of a 4-floor stone/concrete/brick building, distance from the transmitter about 4,5 km, in the main lobe. Signal level indoors in this office was +75...78 dBμV/m. Taking the measuring antenna deeper inside the house did not essentially decrease the signal level. In a closet about 6 m from the outer walls, behind a second thick brick wall, the DAB signal level was decreased by 6-8 dB. Outdoors, near the wall and about 1,5 m above ground level, the level was +80...82 dBμV/m. If a correction factor of 12 dB [1] is added to compare this value with the free field signal strength at 10 m, we arrive at the same level as in Table 1 for this distance. The windows of the office were not exceptionally large, but one of them had a rather free view towards the transmitter. This probably explains the smaller difference between the indoor and outdoor signal levels here compared to the next location. The difference, 4-5 dB in this case, represents the attenuation caused by the building.

Location 2: An apartment on the second floor of an 9-floor apartment house in an area having several tall buildings of this type. Signal level indoors, near the site of the TV receiver, was +55 dBμV/m and outdoors, on the balcony next to this room, was +63 dBμV/m. Distance from the transmitter is 5,5 km and the place is probably in the main lobe of the transmitter antenna. The position of the house is such that this side of the house is not directly towards the tx, but rather at right angles to it. The attenuation due to the building is now 8 dB.

Location 3: A large office in the first floor of a 4-floor office building; large windows, but not directly towards the transmitter. Distance 6 km, in the main lobe. Signal level indoors +72...74 dBμV/m; it was not possible to do the measurement outdoors.

Location 4: Top floor of a 10-floor apartment house with other buildings of the same type around. Distance from the transmitter is 4,2 km and at approximately right angles to the main lobe direction. YLE (the F.B.C.) had estimated that the signal could not be received at all at this location. Signal level was +60...62 dBμV/m indoors.

Location 5: A lobby in the first floor of a hospital building, 5,5 km from the transmitter and about 60 degrees off the main lobe. Signal level indoors, 4 m from the outer wall, still +70...72 dBμV/m. It was not possible to measure the signal level outdoors.

Location 6: An apartment on the top floor of a 6-floor building in the city center. The outer wall of this flat is facing the court of a city block consisting of buildings which are as tall as this house or still taller. The distance from the nearest one of the two DAB transmitters is 7 km and 16 km from the other. Signal level inside the apartment, at the TV receiver location (2m from outer wall and not next to a window) was +45...50 dBμV/m, and outdoors, on the balcony, +60 dBμV/m. The attenuation due to the building is here 10-15 dB.

Not a trace of the DAB signal could be detected at the antenna outlets connected to the CATV network at any of these measurement sites. The displayed noise level was about +8 dBμV on the analyzer with 1 kHz RBW. As the strongest estimated field strength in free field corresponding to the measured f.s. found at any of these measurement locations was about +95 dBμV/m, the difference between these two figures, 87 dB, can be used as a relative figure of merit representing the shielding effectiveness of the CATV network at that location. A corresponding figure can be easily calculated for the other locations, too. Because no interference could be seen in the network, the real shielding effectiveness is better than these values at every location.

## 6. CONCLUSIONS

With the measured DAB signal levels at TV receiver locations and the shielding attenuations of the measured ordinary connecting cables, the leaked interference level due to the connection cable leakage can be only 25 dB below signal level. This is not enough to protect the TV signal against interference from the DAB signal. The DAB signal field strength must be below 45...50 dBμV/m, if the leaked interference is to be buried in the noise when using the bad cables.

It seems to be possible to arrive to the same figure describing the shielding effectiveness of a CATV access network, by calculating either the difference between the signal level value in the network (in dBμV) and the leakage field strength value at 5 m distance (in dBμV/m), or the difference between the interference field strength (in dBμV/m) and the level of the interfence signal leaked into the network (in dBμV). This figure, given in dB, could be called the relative shielding effectiveness of the network.

When the quality of the network is not poor in shielding sense, it is clearly easier to measure a value for the relative shielding effectiveness with the method based on the use of the known interference transmitter. However, this alternative is available only if there is a legal way to use a transmitter for this purpose.

The attenuation of signal field strength inside a building due to the building (its walls) was 4...5 dB when there was a reasonably free path from the transmitter to the measurement point. When the measurement point was not in a direct field, the attenuation was 8...15 dB.

## BIOGRAPHICAL NOTE

Antero Väänänen, researcher at University of Oulu / Sodankylä Geophysical Observatory. On leave of absence from Vaasa Polytechnic University, where head of EMC lab and senior lecturer (oberlehrer), electronics & telecommunication technology. Earlier at ASA Radio Co, Teleste Co. and Tampere University of Technology, from where M.Sc. (Electr. Eng.).

EMC 2000 INTERNATIONAL WROCŁAW SYMPOSIUM ON ELECTROMAGNETIC COMPATIBILITY

# ANTENNA FACTORS OF THE NEW EUROTEM CELL FOR FULLY COMPLIANT EMISSION AND IMMUNITY TESTING

Diethard Hansen and Detlef Ristau
EURO EMC SERVICE (EES) Dr.-Ing. D. Hansen
Bahnhofstr. 39, CH-8965 Berikon, Switzerland
Tel: +41 566337381, Fax: +41 566337381
E-Mail: euro.emc.service@t-online.de
Homepage: http://www.euro-emc-service.de

*The EUROTEM® is a patented compact symmetrical TEM device with 4 striplines which are surrounded by a fully absorber-lined ferrite enclosure. Due to the broad band nature of the device, it is well suited for radiated emissions and immunity testing, compliant with the standards. In order to perform compliance measurements, the corresponding antenna factors have to be determined. Correlation to OATS measurements must be established. The EUROTEM devices are scaleable and can be built in different sizes. The range of test objects starts at printed circuit boards all the way up to two metre high racks. For large test objects, the arrangement can be fitted into an existing fully absorber-lined room. This arrangement is called EUROTEM-Antenna. By this retrofit, the conventional antenna mast and the typical EMC antennas are substituted with the EUROTEM antenna leading to savings in driving power and consequently in considerable cost savings for the amplifier. In contrast to the 10 year old GTEM technology, the EUROTEM is equipped with polarisation switching. The test object will be put on a turntable in the same manner as in any open area test site or absorber chamber. There is no rotation through the three spatial axes which is required using a GTEM cell and the corresponding manipulator. The EUROTEM is superior to the conventional technology by showing better field quality, better suppression of the non-TEM field components and in particular, the better cost efficiency factor.*

## 1. INTRODUCTION

The number of EMC standards is permanently growing. This is particularly driven by the European EMC Directive, which mostly harmonises IEC and CISPR standards under CENELEC EN norms. Due to this legal and economical pressure, there is a great interest in alternative test sites for field emissions and immunity. It does not seem to be justifiable to erect a large 10 m semi anechoic chamber to test a small EUT like a TV set or telephone. The typical emission standards are EN55022 and EN55011, with their antenna factors according to CISPR16 and ANSI C63.4. Using this OATS procedure with the ground plane requires changes of the set-up for emissions to immunity according to EN61000-4-3 with the 16 point calibration. This triggers the question, of how much field quality (substitution method in an empty facility) is actually needed, to be able to compare test results from different laboratories and facilities.

The implementation of the EMC Act, 1996 has induced a world-wide increase in demand for measurement cells and test facilities of various kinds [1-14]. The corresponding manufacturers claim these facilities to be fully compliant or at least suitable for measurements during the development phase of the product. It is a questionable argument to claim repeatability and relative measurement results to be sufficient for development testing. The danger is to operate with too high tolerances with respect to the final compliance test of the various devices under test.

IEC and CISPR standardisation committees increasingly realise the existence of historically-grown deficiencies and contradictions regarding the measurement procedures. This is in particular true for the sector of Information Technology.

The main interest for radiated emission testing today is the frequency range from 26 MHz to about 2 GHz. That was one of the main development goals of the EUROTEM. Additionally the aim was to simplify the operation, to improve the field quality and to reduce the investment cost, not only of the EUROTEM, but rather including the additionally required test equipment. In contrast to the OATS, there is less measurement time required because there is no change in the antennas and no antenna height scan. Naturally one has to measure the antenna factors for emission and immunity and establish the emission correlation to a 10m OATS, once.

## 2. THE EUROTEM FAMILY

Presently the EUROTEM® 2 (figure 1) is the smallest member of the family [15] with a typical test volume of 0.35 cm x 0.35 cm. In addition to the basic set-up with AC mains and DC filters, as well as fibre-optic feed-throughs and several connectors such as BNC, N and RS232, an electromagnetically transparent turntable with a typical load of 20 kg can be retro-fitted. The shielding effectiveness of the device reaches 100 dB above 150 kHz. Switching of the polarisation of the electromagnetic field is performed by rotating the balun enclosure against the 4 inner striplines.

The biggest member of the EUROTEM family is the EUROTEM antenna. This arrangement is shown in figure 2, demonstrating the way to fit it into an existing fully absorber-lined ferrite chamber with the dimensions 7 x 4 x 3 metres. Figure 2 shows our antenna device in an early design stage. Experience taught us to fit some foam absorber lining in front of the termination of the device. This greatly improved

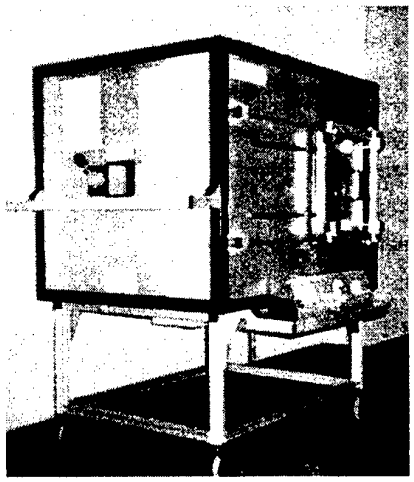


Fig. 1: EUROTEM 2

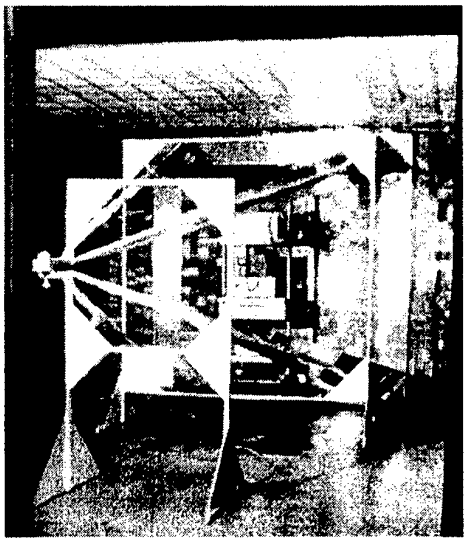


Fig. 2: EUROTEM-Antenna with 2 m Test Object on the Turntable

the field quality. To ease the access to the test object, the EUROTEM antenna can be fitted into the absorber room with it's rear end facing the door. In this area in particular, the quality of the absorbers has to be high because there is a stronger interaction with the back wall in comparison to the side walls.

The electromagnetic fields are mainly concentrated in the space defined by the four outer striplines. The field strength decreases rapidly moving aside from these lines. This relatively small stray field could be used to further reduce the absorber lining of the side walls and consequently saving absorber cost.

## 3. THE EUROTEM PRINCIPLE

Figure 3 shows the cross-section of the stripline arrangement as well as the principle of polarisation switching. Figures 4, 5 demonstrate the longitudinal cross-section of various EUROTEM arrangements.

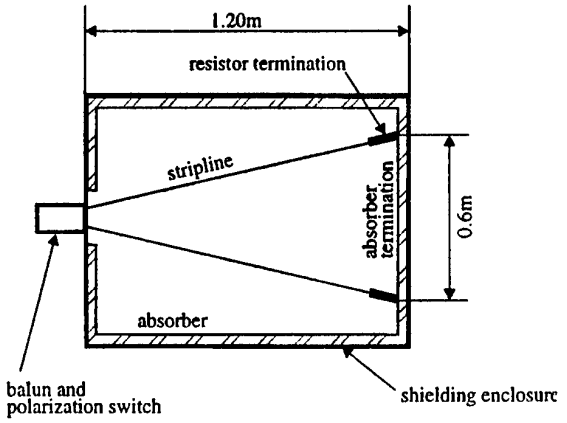



Fig. 4: Longitudinal Cross-section of EUROTEM 2

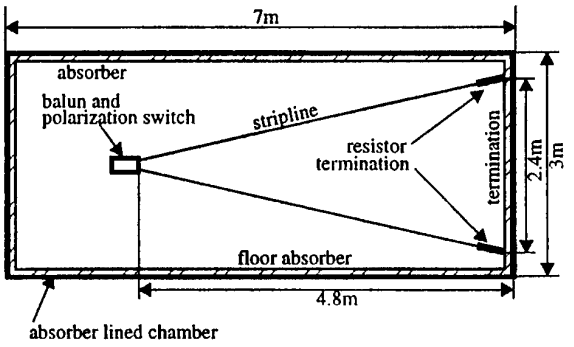



Fig. 5: Longitudinal Cross-section of EUROTEM -Antenna

In front of the back wall, which connects the four resistor termination modules of the EUROTEM antenna, there are additional foam absorbers fitted.

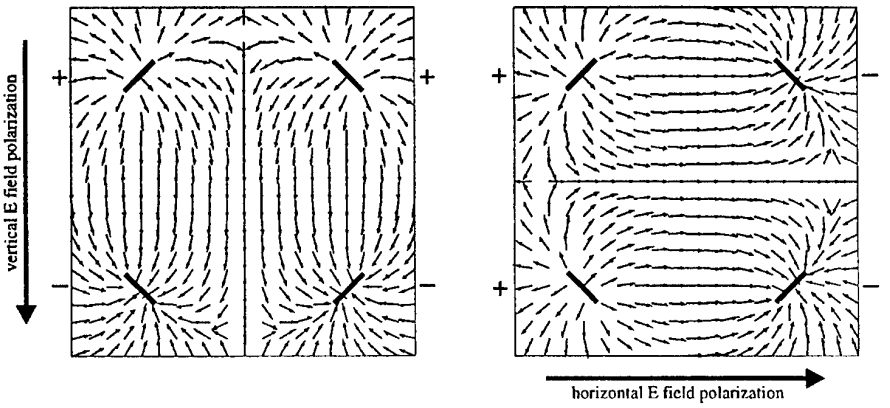



Fig. 3: Cross-section of the EUROTEM with Polarisation Switching

One of the main advantages of the four stripline arrangement is the freedom to route the supply cables of the EUT. In contrast to the GTEM cell for example, there is no need to penetrate metallic walls, which are not ferrite lined. Normally, the lines are fed through the centre opening of the turntable. By definition, the maximum coupling length of the connecting cables which are subjected to field illumination are naturally dependant on the size of the TEM device. Looking at the EUROTEM antenna, this is not a problem because the cables are exactly configured in the same way as on any OATS by using an 80 cm high electromagnetically transparent Styrofoam support on the turntable. Another nice feature, due to the perfect symmetry of the device, is the ability to route cables along the longitudinal symmetry axis through the centre of the back wall. Ideally this should not lead to any cable coupling, in reality however, there is a small curvature of the E & H field due to a spherical wave propagation within the TEM device. If this poses a problem, for example in very precise calibration measurements, compensation by a dielectric lens could be introduced. The ± 1 dB area of the EUROTEM-Antenna is 72 x 72 cm.

## 4. ANTENNA FACTORS FOR FIELD GENERATION

For immunity testing between 27MHz and 1GHz (lately 80MHz - 2GHz), the standard usually requires a three metre test distance between the tip of the antenna and the face of the test object. To generate 10V/m modulated with 1kHz 80% modulation, amplifiers of up to 500 Watts are needed for the low frequency range, for example, 60 MHz. This very high power is required because of the relatively bad matching between the 50 Ohm output impedance and the transmitting antenna which is physically too small compared to the wavelengths. An already optimised version of such a broad band antenna is the X-Wing BiLog manufactured by Chase, model number CBL 6140. Figure 6 compares the drive power of this antenna to our EUROTEM antenna. It is worth mentioning the distance from the feed point of our antenna to the placement of the EUT is about 3 metres. The high efficiency of the EUROTEM antenna however, is directly related to the mode of well-controlled field propagation within the stripline.

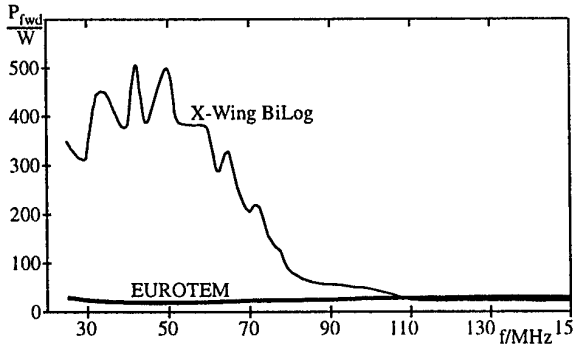



Fig. 6: Driving Power to Generate 10 V/m Modulated in 3m Distance

The BiLog antenna does not have this propagation mode but rather, uses the conventional type of radiation by an antenna. In order to improve such a conventional antenna system, the size of the antenna should electrically reach half a wavelength. This makes it rather impractical at 30MHz because five metres space is simply not available in small anechoic chambers. This requirement will hold true for vertical as well as horizontal polarisation of the antenna.

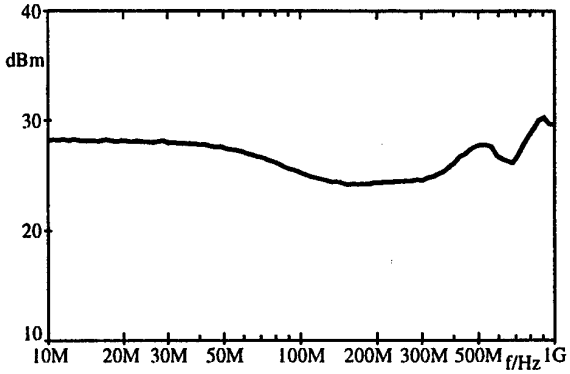



Fig. 7: Drive Power of the EUROTEM 2 to Generate 10V/m Unmodulated in the Test Volume

The difference in power consumption according to EN 61000-4-3 modulated and unmodulated signal is the factor 3.24 which equals 5.1 dB. For calibration, the unmodulated signal is being used. For the EUROTEM 2, this results in a drive power for the unmodulated signal of about 1 Watt to generate 10 V/m in the test volume (figure 7). 1 Watt equals +30 dBm in a 50 Ohm system. To determine the according drive power for the EUROTEM-Antenna, it is important to consider the larger test volume. Tripling the stripline distance results in 10 dB higher power requirements for the same field strength of 10 V/m.

The immunity antenna factors for the EUROTEM 2 have been deduced from the 16 point calibration, according to EN 61000-4-3, and are given in fig. 8. The maximum tolerable field deviation in the points (-0dB, +6dB) was fulfilled for all points without data reduction using 10V/m. For the antenna factors we used only the centre point results. The antenna factors were determined, measuring the input power in dBV at 50 Ohm and subtracting this from the generated field strength in dBV/m. A calibrated Holaday field strength sensor FM 2000 and a R&S power meter (NRVD) were used to establish the reference to national standards.

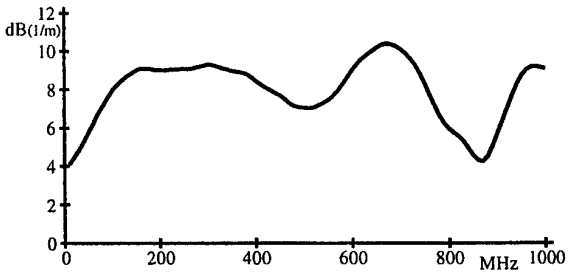



Fig. 8: Antenna Factors for Field Generation in the EUROTEM 2

## 5. ANTENNA FACTORS FOR EMISSION MEASUREMENTS

It is well-known since the early time of research and from the Crawford cells, that due to the law of reciprocity, TEM cells may be used both ways for radiated emissions and immunity. Reciprocity, in this context, means the attenuation between the transmitted and the receiving signal is the same when transmitter and receiver are interchanged at the antenna. To compare different emission facilities, a comparison noise source (VSQ) is used. One way to realise such a radiation source is to use a 10 MHz comb generator. Another way of doing this is

using a frequency synthesiser with an appropriate frequency multiplier or simply a source generating white noise. Our VSQ generates a needle spectrum which rolls off pretty strongly towards higher frequencies. This spectrum is additionally shaped by the use of the small 200 MHz resonant broad band dipole. Figure 9 shows the measurements using such a test radiator being placed in the centre of the test volume of the EUROTEM 2. By spatially rotating this dipole through the three room co-ordinates, the suppression of the non-TEM components can be demonstrated. Experience teaches however to cover the metallic surface of the self-contained, battery-driven comb generator by ferrite lining. This results in an improved symmetrical behaviour of the device and the suppression of unwanted unsymmetrical surface currents which would normally appear by forming a corner dipole of 90° angle to the rotational symmetry axis of the broad band dipole arrangement. This asymmetry could reach values as high as 20 dB.

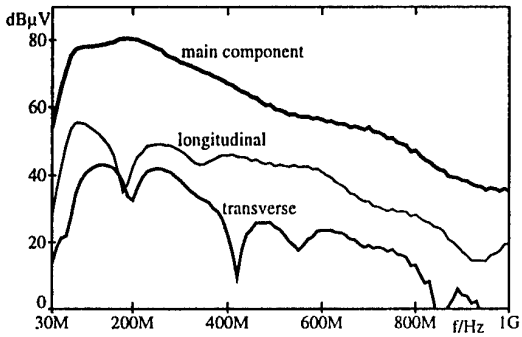



Fig. 9: Direct VSQ Emission Data from the EUROTEM 2 (example of non-TEM-component suppression)

This decoupling data must be considered as being excellent regarding the fact that the 40 cm long broad band dipole antenna almost short-circuits the available space between the striplines of 50 cm. For the EUROTEM-Antenna the data is similar however 10 dB lower (1,5 m to 0,5 m gap). In the lab the non-TEM wave suppression sometimes exceeded 40 dB

To determine the emission antenna factors (fig. 10) we used the VSQ as a transfer standard for comparison. This transfer standard was tested in three different accredited EMC labs on 10m OATS. The results in dBµV/m were tabled for horizontal and vertical polarisation between 30MHz and 1000MHz. These values were averaged, consequently there was one average table for horizontal polarisation and one for vertical. These average values were converted to free space

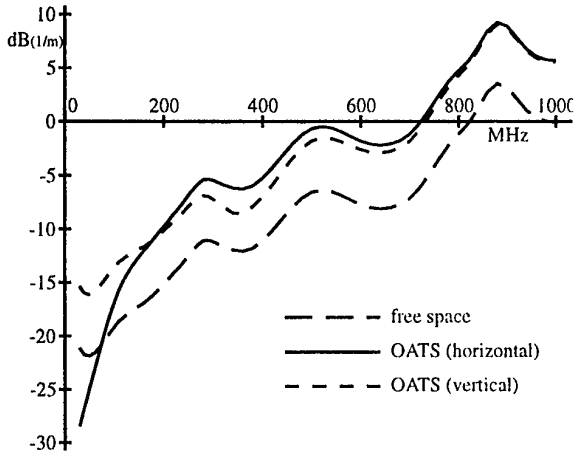



Fig. 10: 10m Emission Antenna Factors for the EUROTEM 2

mean values [16] and averaged again. Finally the transfer standard was tested in the EUROTEM 2 with the VSQ antenna in the centre position and a list of dBµV voltage measurements taken. The cable attenuation was considered. The difference to the averaged free space signals results in antenna factors for free space. From here the antenna factors for vertical and horizontal antenna polarisation on the OATS result from the free space factors, if the averaged field strength value is backwards calculated [16].

Using these antenna factors, resulted in a very good agreement of the used accredited OATS facilities with respect to our EUROTEM measurements. An additional, fourth OATS and an anechoic chamber were used for this comparison (figure 11).

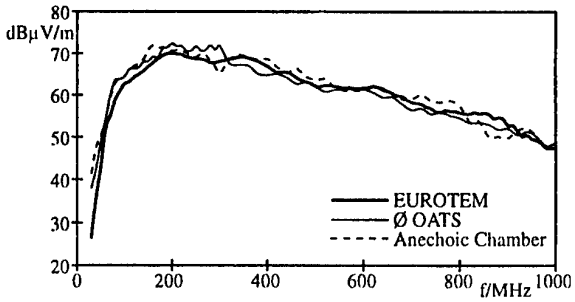



Fig. 11: Emission Measurements by VSQ and Various Test Facilities (curve shape determined by antenna of test radiator)

## 6. SPECIFICATIONS OF THE EUROTEM IN COMPARISON TO OTHER FACILITIES

Table 1 shows the comparison of the necessary drive power, the investment cost as well as the maximum dimensions of the test object for various facilities. The EUROTEM 2 cannot necessarily be directly compared to the other facilities because of its limited test volume. One major advantage of all EUROTEM devices is the simple way of changing the polarity of the electromagnetic field, in contrast to the GTEM cell.

Table 1: Comparison of Test Facilities

| | EUROTEM 2 | EUROTEM Antenna, short FALC | GTEM 1750 | FALC (3m site) |
|---|---|---|---|---|
| Maximum EUT size (metres) | 0.3x 0.3x 0.3 | 1.8x 1.5x 1.0 | 1.0x 0.5x 1.0 | 1.0x 1.5x 1.0 |
| Polarisation switch h/v | Yes | Yes | No | Yes |
| Facility size in metres | 1.0x 1.0x 1.3 | 3.0x 3.0x 6.0 | 4.0x 2.4x 8.0 | 4.0x 3.0x 7.0 |
| Input power for 10 V/m, 80% AM at 80 MHz | 1.6 W | 16 W | 17 W | 65 W |
| Input power for 10 V/m, 80% AM at 30 MHz | 2.5 W | 25 W | 26 W | 250 W |
| Input power for 100 V/m, automotive at 80 MHz | ca. 25 W | 252 W | 525 W | 2 kW |
| Input power for 100 V/m, automotive at 30 MHz | ca. 77 W | 630 W | 800 W | (7.5 kW) |
| Facility investment without equipment | ca. 27 % | ca. 70 % | ca. 60 % | 100 % |
| | | | | FALC = fully anechoic chamber |

The EUROTEM-Antenna has been mainly developed for integration or retrofit of an existing fully absorber-lined chamber. The lower corner frequency is only limited by the characteristics of the balun. The upper frequency limit is given mainly by the absorber performance of the EUROTEM termination and the existing absorber chamber. A comparison to the conventional radiated immunity equipment using a 3m test distance versus the EUROTEM antenna is shown in table 2.

Additionally there is the need for measurement software, a controlling computer and a generator to be considered. For precise calibrations, one would need an additional field strength sensor system.

Table 2: Differences between Conventional 3m Solution and Using a EUROTEM-Antenna

| | Conventional solution for a 3m site, using broad band antennas | Solution, using EUROTEM-Antenna, stand alone |
|---|---|---|
| **Antenna** | 6.5 %<br>(X-Wing BiLog) | 25 % |
| **Antenna mast**<br>(including control unit) | 15.5% | Not applicable |
| **Power amplifier** | 27.5 %<br>(0.01 - 100 MHz, 500 W)<br>50.5 %<br>(80 - 100 MHz, 200 W) | 31 %<br>(1 - 1000 MHz, 100 W) |
| **Total** | 100 % | 56 % |

## 7. CONCLUSION

In particular the EUROTEM 2 is suited for fully compliant radiated emission and immunity testing of smaller test objects. The non-TEM wave component is well suppressed. By using a calibrated and traceable power meter to read the input power of the cell and simultaneously measuring the generated E field strength through the test volume by a DKD traceable field probe the immunity antenna factors have been determined. With a calibrated test radiator the emission correlation to OATS could be established too.

## 8. REFERENCES


[1] S. Berger: „A User's perspective on GTEM testing." In: EMC Test & Design, USA, December 1993, pp. 38-43.

[2] J. Nedtwig: „Vermeidung störender Vielfachreflexionen in TEM-Wellenleitern: GTEM ---> TRIGATEM." In: EMV 92, 3, International Fachmesse und Kongreß für EMV in Karlsruhe, February 1992, pp. 243-251.

[3] F. Leferink: „A Triple-TEM cell: three polarisations in one setup." In: EMC 1993, 10th International Zurich Symposium and Technical Exhibition on EMC, Zurich, March 1993, pp. 573-578.

[4] L. Jendernalik, D. Peier: „Expanding the bandwidth of a TEM-cell with a planar terminator." In: EMC 1993, 10th International Zurich Symposium and Technical Exhibition on EMC, Zurich, March 1993, pp. 579-582.

[5] W. Bittinger: „Properties of open striplines for EMC measurements." In: IEEE 1993 International Symposium on EMC, Dallas, USA, August 1993, pp. 120-125.

[6] P. Wilson: „Higher Order mode field distribution in asymmetric TEM cells." In: URSI International Symposium on EM Theory, Stockholm, August 1989, 3 sides.

[7] L. Carbonini: „A transmission line device for EMI susceptibility measurements with enhanced field uniformity." WTEM, In: EMC 92, International Wroclaw Symposium on EMC, pp. 219-223.

[8] L. Carbonini: „ Comparison of analysis of a WTEM cell with standard TEM cells for generating EM fields." In: IEEE transactions on EMC, Vol. 35, No. 2, May 1993, pp. 255-263.

[9] D. Hansen, D. Ristau et al.: „Analysis of the measured field structure in a GTEM 1750." In: 1994 IEEE International Symposium on EMC, Chicago, August 1994, pp. 144-149.

[10] R. Lorch, G. Mönich: „Mode suppression in TEM cells." In: IEEE 1996 International Symposium on EMC, Santa Clara, August 1996, pp. 40-42.

[11] L. Jendernalik, D. Peier, R. Schaller: „TEMpact: Resonanzfreie TEM-Zellen in Kompaktbauweise." In EMV 96, 5. Int. Fachmesse und Kongreß für EMV in Karlsruhe, February 1996, pp. 317-324.

[12] A. Podgorski, G. Gibson: „Broadband Electromagnetic Field Simulator." Canadian Patent No. 2047999, 1991.

[13] A. Podgorski, J. Baran: „New concept of emission and susceptibility testing." In: IEEE 1997 International Symposium on EMC, Austin, August 1997, pp. 497-499.

[14] L. Carbonini: „A new TEM cell: Test results up to 3 GHz and a comparison to alternative solutions." In: ITEM UPDATE 1997, ROBAR Industries Inc., R & B Enterprises Division, West Conshohocken, PA, USA, pp. 31-40.

[15] D. Hansen, D. Ristau: „Characteristics of the EUROTEM Family", In Proceedings of the 1999 International Symposium on EMC, Tokyo, Japan, 1999, pp. 86-89

[16] D. Ristau, D. Hansen: „Correlating fully anechoic to OATS measurements." In: Proceedings of the 13th Wroclaw EMC Symposium, 1996, pp. 402-405.


## BIOGRAPHICAL NOTES

Dr.-Ing. Diethard Hansen is president of the EES Switzerland and Germany, specialising in international consulting, training, innovative EMC test products, accredited testing and R&D. Further areas: LVD, radio, automotive and medical. He is holding a BS/MS in electrical engineering from Germany and a Ph.D. degree from TU Berlin. More than 20 years of industrial EMC/EMP experience, 35 patents (GTEM, EUROTEM, Poyntor sensor) and 140 professional publications as well as chairmanships are assigned to him. He was the manager of the EES Competent Body and acted as board member of European Competent Bodies ACB - Brussels. Memberships: IEEE/EMC, CENELEC, ETSI and IEC. He is the RegTP ATRT PLC chairman and a lead auditor for EMC labs and competent bodies in the DAR accreditation system. Since 1991 Dr. Hansen is a senior EMC engineer under USA NARTE accreditation.



Dr.-Ing. habil. Detlef Ristau is vice president of EES Teltow near Berlin. He is leading the EES R&D division. Dr. Ristau is holding all engineering, Ph.D. and lecturer degrees from the university of transport Dresden, Germany. He has published numerous scientific contributions in major professional journals and symposia and he is one of the inventors of the EUROTEM, Poyntor. His particular interest includes sophisticated electromagnetic field problems. He is a member of the IEEE EMC society of the United States.



EMC 2000 INTERNATIONAL WROCŁAW SYMPOSIUM ON ELECTROMAGNETIC COMPATIBILITY

# SEMI-ANECHOIC CHAMBER BGF FACILITY FOR MEASUREMENTS OF EMISSION AND IMMUNITY - LATEST ADVANCEMENTS

A. Podgorski [1] E. Podgorski [1] M. Michalak [2]

[1] ASR Technologies, 332 Crestview Rd. Ottawa, Canada K1H 5G6
tel: (613) 737-2026, fax: (613) 737-3098, a.podgorski@ieee.org

[2] Nat. Inst. of Telecommunications, Swojczycka 38, 51-501 Wroclaw, Poland
tel: (48-71) 372-8812, fax: (48-71) 372-8878, m.michalak@il.wroc.pl

*New EMC Facility that allows fully automated radiated immunity and emission testing in both polarizations simultaneously was introduced in a form of a Dual Polarization Broadband Gigahertz Field (BGF) Simulator, first time four years ago. This publication details currently achieved BGF parameters such as: frequency range, obtainable field strength, etc. As well it indicates how these parameters are expanded, since the BGF was presented for the first time. The paper also addresses additional use of the BGF Facility as a magnetic field (H-field) Simulator.*

## 1. INTRODUCTION

Broadband Gigahertz Field (BGF) Facility (US Patents 5440316 and 5982331, European and Japanese Patents pending), can be used for automated emission and immunity testing in CW or Pulse mode, in both polarizations, in the frequency range from DC to 40 GHz or any upper frequency required.

The BGF Facility allows combining tests that are normally done in H-field coil, TEM-Cell and Anechoic Chamber. The Facility can either be built as a new construction, or it can be introduced as a modification to existing Anechoic or Semi-Anechoic Chambers and Open Area Test Sites [1]. Easily scaled by design, the Facility can be customized, so that objects of any dimensions (as large as an aircraft or ship, or as small as individual electronic components) can be tested at the required field strength, using the most modest power sources. In the BGF, the need for test antenna changing and rotating (changing the polarization), that exists with all current testing methods, is eliminated. Consequently, the full automation of measuring system and testing is possible. This results in substantial reduction of testing time and therefore a drastic reduction of testing cost.
The BGF Facility is based on a hybrid concept as it consists of a TEM-mode parallel line and a broadband horn antenna joined together. Initially, the Facility was developed to operate in either vertical or horizontal polarization. Later on, the vertical and horizontal polarizations Facilities were integrated into Dual Polarization Facility [2]. In Dual Polarization Facility, due to the independence of vertical and horizontal antenna systems, that allows testing to be conducted in both polarizations simultaneously, further significant cost and time saving is achievable.

Semi-Anechoic Chamber, CW Dual Polarization BGF - built for the AST Computer, was approved by the FCC for testing of emission and by the European Certified Body of Norway for testing of immunity [3,4].

This publication describes currently achieved Semi-Anechoic Chamber BGF Facility parameters and as well it indicates how the parameters were expanded ever since the BGF was conceived. Additional use of Semi-Anechoic Chamber BGF as an H-field Simulator is also addressed. Furthermore, the emphasis is being placed on possible BGF development.

## 2. BGF FACILITY EVOLUTION

Over the years numerous testing facilities and methods for the measurements of radiated immunity and emission, such as: Open Area Test Sites, Anechoic and Semi-Anechoic Rooms, Reverberation Chambers,TEM Cells, GTEM Cells and recently BGF Facilities, were developed.

Initially, the BGF was conceived as a single, either horizontal or vertical, polarization Facility where a large horn antenna and TEM Cell septum were incorporated into Semi- or Anechoic Room. Such single polarization BGF was operating in the frequency range from DC to 5 GHz and provided testing volume of 3m x 3m - substantially exceeding the testing volume of the largest in the world GTEM Cell.

In an attempt to shorten the required testing time Dual Polarization BGF, initially operating up to 5 GHz, was developed - see Fig. 1 and 2. The Facility was fully automated, so that not only the instantaneous change from susceptibility to emission, but also an automatic change from horizontal to vertical polarization was possible. Currently, Dual Polarization BGF Facility operates with the upper frequency limit of 40 GHz - further expansion of the upper frequency limit without limiting the testing volume or field level of testing is possible. The ability to expand the upper frequency limit of the BGF already proved to be very important factor in view of the fact that the maximum frequency of testing specified by some requirements is being increased. Just recently issued Bellcore's Generic Requirements Criteria GR-1089-CORE, for telecommunications equipment, indicates the need for testing up to 10 GHz.

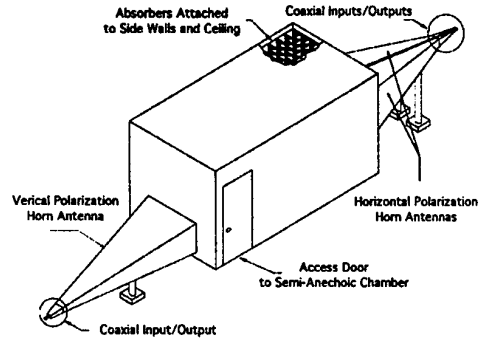



Figure 1. Dual Polarization Broadband Gigahertz Field (BGF) Facility - External view

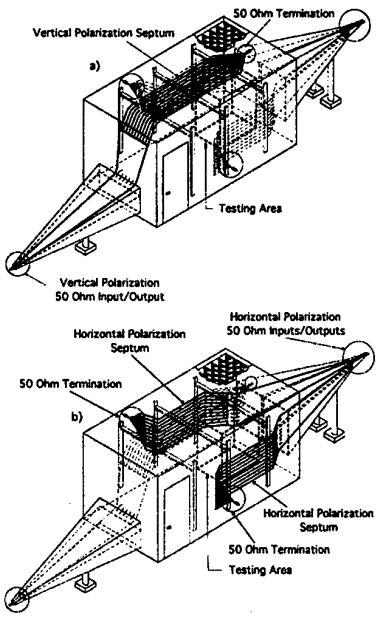



Figure 2. Dual Polarization Broadband Gigahertz Field (BGF) Facility - Internal view:
a) vertical polarization,
b) horizontal polarization.

Initially the CW BGF Facilities were built to accommodate EM field levels of 100 V/m up to 40 GHz. However, recent research resulted in development of CW BGF Facilities operating at field levels of 20 kV/m - using a single antenna. Further increase of the field level to 200 kV/m is possible with the use of a multiple antenna array system consisting of 100 antennas. Ability to generate such strong EM fields makes the BGF Facility one of the most advanced tool in the world for CW immunity and emission testing in a broadband frequency range.

An Open Area, Pulse BGF Facility for susceptibility testing was built - see Figure 3. The system [5] consisting of 150 kV Integrated Pulse Generator and Pulse BGF Antenna, if used without TEM-mode antenna (Figure 3a), allows simulation of electromagnetic field environment characterized by 100 kV/m peak field level, rise time as fast as 100 ps and pulse duration of 3 ns. If TEM-mode antenna is added (Figure 3b), the BGF system allows simulation of electromagnetic field environment characterized by 100 kV/m peak field level, rise time of 200 ps and pulse duration of 30 ns.

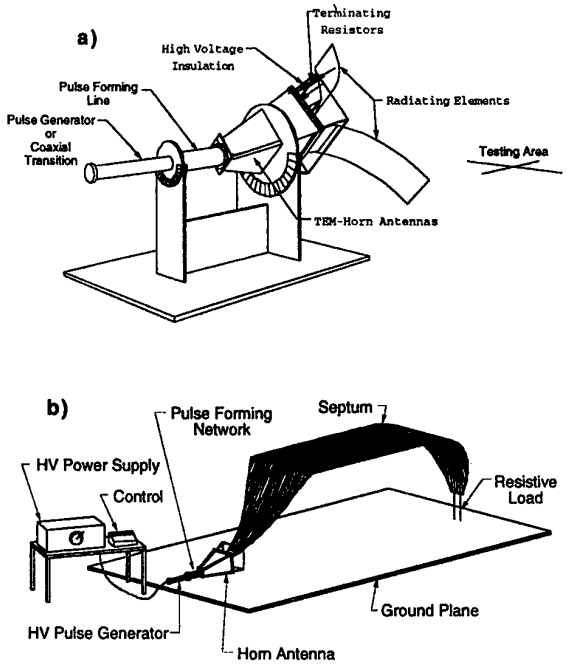



Figure 3. Pulse BGF Facility
a) without TEM-mode antenna
b) with TEM-mode antenna

With the rise time of 100 ps, the Open Area, Pulse BGF Facility, is one of the most advanced tools presently available for susceptibility testing in the Pulse mode. Figure 4 shows the comparison of the E-field bandwidth factors of the Pulse BGF Facility width currently available NEMP Threat Simulators. The BGF E-field band-

width factor is an order of magnitude higher than the E-field bandwidth factor of the fastest NEMP Simulators.

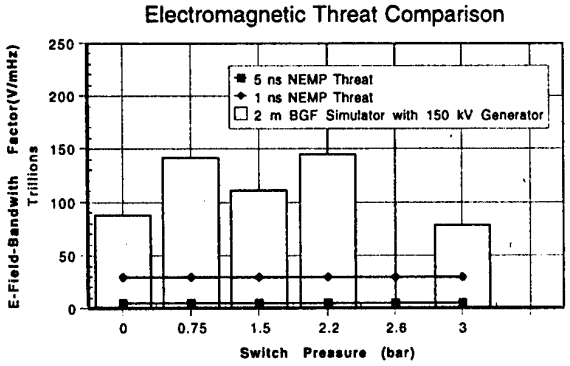



Figure 4. Comparison of the E-field bandwidth factor of the Pulse BGF Facility with currently available NEMP Threat Simulators

## 3. APPLICATION OF BGF FACILITY FOR MAGNETIC FIELD MEASUREMENTS

In a Semi-Anechoic BGF Facility, the TEM-line (terminated with 50 ohm resistor) is operating in the frequency range from DC to 50 MHz, while the broadband horn antenna starts operating at 80 MHz. In the region from 50 to 80 MHz, the operation of the TEM-line and the horn antenna are overlapping to ensure a uniform frequency coverage extending from DC to gigahertz frequencies. In spite of the BGF Facility capability to operate from DC, initially the Facility was used only from 27 MHz to conduct E-Field (electric field) radiated immunity and emission testing in accordance with IEC 61000-4-3 and ANCI C63.4 and FCC Part 15 criteria.

However, as per recently issued Bellcore's Generic Requirements Criteria GR 1089-CORE for telecommunications equipment, there is a need for: E-field radiated immunity and emission testing from 10 kHz to 10 GHz, and, H-field (magnetic field) radiated emission testing from 60 Hz to 30 MHz. Considering the BGF Facility operational capability from DC to 40 GHz, no modification to the Facility will be needed to perform E-field radiated immunity and emission testing from 10 kHz to 10 GHz. As well, if 50 ohm termination at the end of the TEM-line in the BGF is replaced with a "short", the Facility becomes suitable for the measurements of H-field radiated emission testing from 60 Hz to 30 MHz.

Theoretical analysis of H-field radiated emission measurements indicates that, using the BGF Facility, the Bellcore Generic Requirements Criteria GR-1089 CORE can be met in the whole frequency range of 60 Hz to 30 MHz. In accordance with GR-1089, the H-field radiated emission from the EUT shall not exceed the field strength given by Figure 5 and the emission measurements, in the frequency range 60 Hz to 30 MHz, should be conducted using a loop antenna. The antenna should be positioned with its plane vertical at a specified distance from the EUT. The antenna shall then be rotated, about its vertical axis, for maximum response at each azimuth about the EUT. The center of the loop shall be 1 meter above the ground floor.

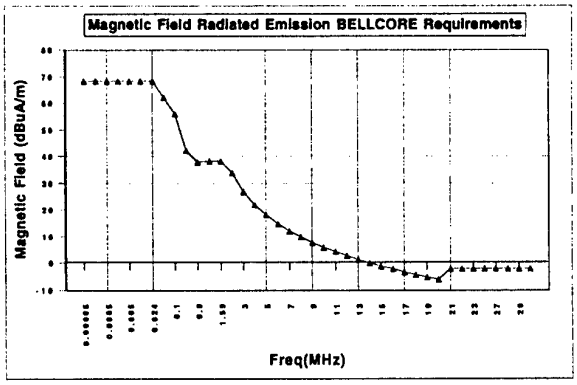



Figure 5. Telecommunications equipment H-field radiated emission limits, in the frequency range 60 Hz to 30 MHz - Bellcore Generic Requirements Criteria GR-1089-CORE

Following the GR-1089 recommendations, we calculated the radiated emission signal and measurements noise level in the Semi-Anechoic BGF Facility. The voltage induced in the BGF vertical polarization septum, by a magnetic field equal in amplitude to the H-field radiated emission limits specified by GR-1089, is always 40 dB higher than the measurements noise level - see Figure 6.

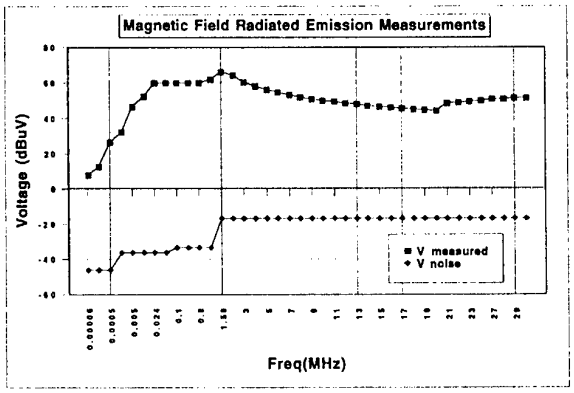



Figure 6. The H-field radiated emission signal and measurements noise level in the Semi-Anechoic BGF Facility

The calculation was done assuming that the required by GR-1089 magnetic field was generated by current flowing in a single 1 meter square loop located just above the floor of the BGF Facility. Preliminary laboratory measurements of the H field radiated emission signal correspond very well with our calculations.

## 4. SUMMARY

In comparison to presently used facilities for measurements of radiated immunity and emission, the BGF Facility is currently the only facility capable of operating from DC to 40 GHz. No need for changing or rotating test antennas exists, therefore full automation of the testing system is possible, resulting in substantial testing cost and time saving. The Facility can be used for electric and magnetic field emission and immunity testing in CW and Pulse mode.

For the E-field radiated immunity testing in accordance with IEC 61000-4-3 and MIL-STD-461, the required electric field strength can be achieved in the BGF using the most modest power sources. As well, the maximum height of the anechoic or semi-anechoic chamber needs to be only two times the height of the tested objects - this will further result in substantial cost saving.

For the E-field radiated emission testing in accordance with the ANCI C63.4 and FCC Part 15 criteria, in the BGF Facility (since there is no need for changing the height of the receiving antenna), the maximum height of the Chamber needed is equal to half of the height of the Standard Chamber. As such the cost of BGF Facility is lower than the standard facility required per ANCI C63.4 and FCC Part 15 criteria.

The BGF Facility can be used for the H-field radiated emission testing in accordance with GR-1089, without a need for having to use an additional loop antenna.

The BGF can be incorporated as a modification to existing facilities such as Open Area Test Site, Semi- or Anechoic-Chamber, Reverberation Chamber or it can be built as a self-sustained facility.

## 5. REFERENCES

[1] A.S. Podgorski and G. Gibson, "New Broadband Gigahertz Field Simulator", Proc. of the 1992 IEEE International Symposium on EMC, Anaheim, California, USA, August 17-21, 1992.

[2] A.S. Podgorski, "Dual Polarization Broadband Gigahertz Field (BGF) Simulator for Emission and Susceptibility Testing - Principles and Applications", Proc. of the 1996 International Symposium on EMC, Wroclaw, Poland, June 25-28, 1996.

[3] A.S. Podgorski and J. Baran, "New Concept of Emission and Susceptibility Testing", Proc. of the 1997 IEEE International Symposium on EMC, Austin, Texas, USA, August 18-22, 1997.

[4] A.S. Podgorski and J. Baran, "Radiated Emission Measurements Conducted in the AST Semi-Anechoic Chamber Dual Polarization Broadband Gigahertz Field Simulator and their Verification with the Measurements done on the Open Area Test Site", Proc. of the 1998 IEEE International Symposium on EMC, Denver, Colorado, USA, August 24-28, 1998.

[5] A.S. Podgorski and A. Kaelin, "Neuartige elektromagnetische Systeme fur Emissions- und Suszeptibilitatsprufungen mittels braitbandigen CW- und Impulsmessungen", EMV'98 - Int. Fachmesse und Kongress fur Electromagnetische Vertraglichkeit, Dusseldorf, Germany, February 10-12, 1998.

## BIOGRAPHICAL NOTES

A. Podgorski is holding MASc and PhD degrees from the Department of Electrical Engineering, University of Waterloo, Waterloo, Canada. He has published over hundred scientific papers and he is holding 10 patents. Since 1992 he has been on the Board of Directors for the EMC Society of IEEE. He is the EMC Society Life Member and has served as the EMC Society "Distinguished Lecturer". His name is listed in the Canadian "Who's Who".

E. Podgoorski is holding MASc degree from the Department of Electrical Engineering, McMaster University , Hamilton, Canada. Over the years she has been involved in numerous programs of national significance in the area of electromagnetics for Canadian Government and Industry.

M. Michalak is holding MASc degree from the Department of Electrical Engineering, University of Wroclaw, Poland. He is currently working towards his PhD. His interests concentrate on EMC measurements and study of EMC test facilities.

EMC 2000 INTERNATIONAL WROCŁAW SYMPOSIUM ON ELECTROMAGNETIC COMPATIBILITY

# TEST CHAMBER CHARACTERISTICS – IMPORTANT FACTOR DETERMINING REQUIRED RF POWER OF AMPLIFIER IN RADIATED IMMUNITY TESTS

A.E.Sowa, P.Kowalczyk

Wroclaw University of Technology
Institute of Telecommunication and Acoustics
Wybrzeże Wyspiańskiego 27
50-370 Wroclaw, Poland

phone: (+4871) 3203276, fax: (+4871) 3203189, e-mail: asowa@zr.ita.pwr.wroc.pl

*Field uniformity on a hypothetical vertical plane (uniform field area) is the only criterion regarding the field distribution in a test site which must be fulfilled according to applicable immunity standards. In the paper it has been shown that the required field uniformity can be obtained even in case of the sites which characteristics restrict the practical usefulness of them in a very serious way. This is due to very high power demands for the RF amplifiers providing antenna drive to the necessary field strength level. Computing the required value of the RF amplifier output power disregarding the influence of test chamber characteristics on it can cause serious underestimate of this power with all technical and (first of all) economical consequences of the purchase of improperly sized amplifier.*

## 1. INTRODUCTION

An immunity test site due to high strength levels which can be employed in the tests must be located in a shielded room.

The size of the room determines the resonant frequencies of the cavity created by the room. In case of bare metallic walls of the room the resonances can be very deep. The difference in the field strength can reach 25 dB when the position of a transmitting antenna or a field probe is changed by only 10cm [1]. It causes that all trials of practical use of an unlined screened enclosure meet very serious troubles. To limit the phenomenon the resonances should be effectively suppressed. According to [1] the resonances could be suppressed quite well using the technique of a partial lining of the chamber walls with ferrite absorber. The hot spots are exactly pointed out computationally.

Most commonly an immunity test site is located in an anechoic chamber – fully anechoic or semi-anechoic, where the resonance of the chamber is suppressed by lining all interior metallic surfaces of it (with a floor or without – respectively) with RF absorber. The exact demands regarding the chamber are not published by the standards [2,3]. According to them, the immunity tests should be performed in an anechoic chamber and in case of a semi-anechoic one, the chamber floor can be partially covered by additional absorber to reduce floor reflections. A minimal size of the room is indirectly determined by the distance between the tip of a transmitting antenna and an EUT and by the dimensions of the uniform field area [2,3]. In case of a compact chamber equipped with ferrite absorber its length is about 6 to 7m and the width and height about 3m. Of course any particular room can have different size.

Wroclaw Anechoic Chamber [4,5] is an example of a small anechoic chamber that fulfils the standards requirements [2,3] regarding test field uniformity. When the calibration procedure was carried out in WAC it appeared that a high difference between the value of the field strength vs. frequency obtained from measurements and predicted through computing in some particular frequency range existed. The existence of high maximum and minimum was observed. The phenomenon was observed for both antenna polarities – vertical and horizontal. Due to the fact that these effects took place in a low frequency range (26 to 130 MHz) where the effectiveness of pyramidal absorber used in WAC is low, it is clear that anechoic chamber characteristics play a key part for occurrence of these particular effects in the mentioned frequency range.

While conducting immunity tests according to IEC-1000-4-3 requirements, high strength of test field is demanded. It results in high power of broadband RF power amplifiers which provide antenna drive to the necessary field level. These amplifiers are very expensive and their proper choice is of great importance.

The influence and significance of the anechoic chamber characteristics on immunity testing will be developed in subsequent points of this paper.

## 2. CALIBRATION PROCEDURE . FIELD STRENGTH MEASUREMENT: OBTAINED RESULTS

Field immunity tests are to be carried out in accordance to the standards [2,3]. Based on these standards calibration procedure of a "uniform field area" is required. A "uniform field area" is a 1.5m square area situated on a vertical measurement plane 3m from the tip of a transmitting antenna. Calibration measurements are conducted in 16 points located every 0.5m (shown in fig.1) on a discussed square area for every measurement frequency in the basic range of 80MHz to 1000MHz [2].

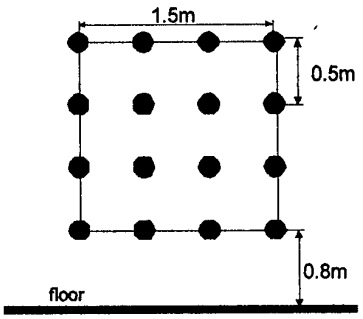



**Fig.1 Uniform field area and points where measurements of field strength are taken**

The method of immunity measurement conducted in WAC is described in [5]. For the purpose of this paper an automated calibration procedure was carried out in WAC. A compact combination antenna BTA-L (Frankonia) was used for the measurement. In the calibration measurement the input signal of the amplifier was kept constant for the whole frequency range. Field strength was measured in every point on the "uniform field area" in the frequency range of 26 to 1000MHz. To visualise the outcome, for every measuring frequency, the mean value of the field strength was computed (for 16 points). Calibration measurements were carried out for horizontal and vertical polarity of the transmitting antenna. The mean value was computed for both polarities and for every measurement frequency. Obtained results are shown in fig. 2 (horizontal polarity of the antenna) and 3 (vertical polarity of the antenna) .

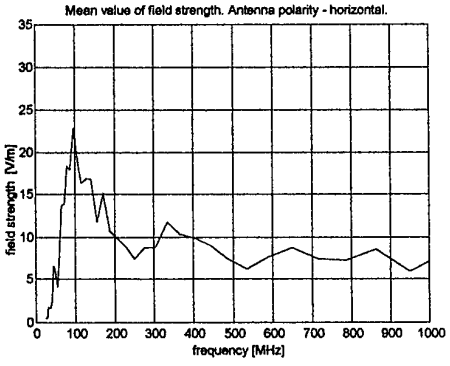



**Fig. 2 Mean value of field strength in the frequency range 26 to 1000MHz. Results for horizontal polarity obtained in WAC**

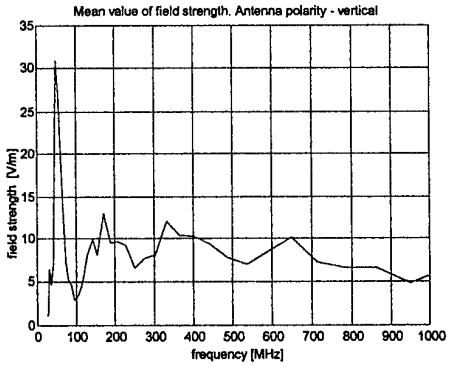



**Fig. 3 Mean value of field strength in the frequency range 26 to 1000MHz. Results for vertical polarity obtained in WAC.**

## 3. ELECTRIC FIELD STRENGTH VALUE AT THE DISTANCE R FROM THE TRANSMITTING ANTENNA. COMPUTING.

An electric field strength value at the distance R from the transmitting antenna is given by a Friss equation :

$$E_{[\frac{V}{m}]} = \frac{\sqrt{30 * P_t * G_t}}{R} \qquad (1)$$

where:

$P_t$ – transmitting power from the antenna [W]
E - electric field strength value [V/m]
$G_t$ – gain of transmitting antenna [ numerically]
R – distance from the antenna [m]

The real value of transmitting power from the amplifier (for an input signal equal to :–16dBm; this value of an input signal was used in the calibration test ) was substituted for $P_t$. Antenna factor was given by a producer thus $G_t$ can be computed. The distance R was equal to 3m. Substituting this data to equation (1) for the frequency range 26 to 1000MHz the value of the field strength vs. frequency for free space could be achieved. Moreover, correction factors were taken into account concerning VSWR of the transmitting antenna, attenuation of cables, an error in defining the antenna factor in the middle point of a transmitting antenna while the distance R is measured from the tip of it [6,7]. A computed plot of the field strength for the data mentioned above (a computed plot is the same for both

antenna polarities) is shown in fig 4 and fig.5 and compared with the plots from fig 2 and 3.

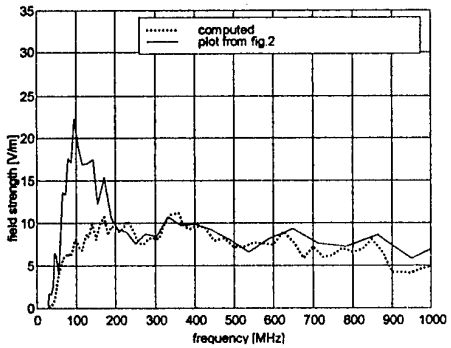



**Fig. 4 Comparison between measured value of field strength in the frequency range 26 to 1000MHz and field strength value obtained through computing (with the correction factors). Horizontal polarity of the transmitting antenna.**

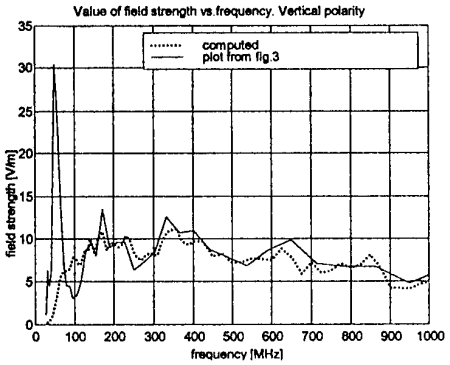



**Fig. 5 Comparison between measured value of field strength in the frequency range 26 to 1000MHz and field strength value obtained through computing (with the correction factors). Vertical polarity of the transmitting antenna.**

The results of the calibration measurements conducted in WAC appeared to be in accordance with the results obtained through computing except frequency ranges below 120MHz for the vertical polarity of the antenna and about 200MHz for the horizontal polarity. For the horizontal polarity there is a high maximum in the field strength for about 100MHz (this value exceeds 2.8 times the value of the field strength predicted through computing) and a minimum for 50 MHz (which can be of no concern – the basic frequency range of concern according to the standards is 80 to 1000MHz). For the vertical polarity there is a high maximum for 50 MHz (behind the basic range) and a minimum for 100MHz. The value of this minimum equals to 3.1V/m (fig.3) and the value of the field strength for this frequency obtained through computing equals to about 8V/m (fig.5). Thus, the predicted value of the field strength is 2.6 times higher than that measured in WAC (for this particular frequency range – around 100MHz, for vertical polarity). The point is that in this case to achieve the value of the field strength equal to the predicted through computing, a transmitting power of the amplifier must be about seven times higher than the power applied in the calibration measurements (value of power changes proportionally to the square value of field strength).

Resonant phenomena existing in WAC, esp. in a frequency range 50 to 100 MHz for both antenna polarities, are responsible for described effects of high maximum and low minimum in the value of field strength. To visualise the influence of WAC characteristics on field strength value, characteristics which show the ratio of field strength in WAC to field strength in the free space were computed, provided that the same equipment and driving power were used. Obtained results are shown in fig. 6 and 7.

## 4. CHAMBER CHARACTERISTICS INFLUENCE ON REQUIRED RF AMPLIFIER POWER

Figures 6 and 7 show the above mentioned influence of WAC characteristics on the field strength . A ratio of the measured field value to the computed value of field for free space is expressed in dB. When the plot is above the x axis it means that electric field value is higher in WAC than that in a free space provided the same equipment and driving power are used. When the plot lies below the x axis it means that the field value is lower in WAC than that in a free space under the same condition as previously.

As it can be noticed from figures 6 and 7 there is a very high influence of anechoic chamber characteristics on an electric field value for low frequencies – in the case presented in this paper for 26 to 120MHz (200MHz). When estimating amplifier power required to achieve a certain level of electric field strength (in accordance to IEC 1000-4-3) for immunity measurements, characteristics of a chamber must be taken into account.

For WAC the critical range lies below 130MHz. The ratio of the amplifier RF output power for both polarities is about 50 times for about 97MHz.

For the vertical polarity in this region the power driving the transmitting antenna necessary to produce a given field level will be significantly bigger than that computed or measured outside the chamber. As it was shown for 97MHz the necessary power will be about 7 times bigger!

In case of WAC for 97MHz the value of amplifier RF output power necessary to produce a field level of 10V/m will be about 210W. The power for a free space is equal to 31.2W. This power is the power of a linear amplifier for continuous wave (CW).

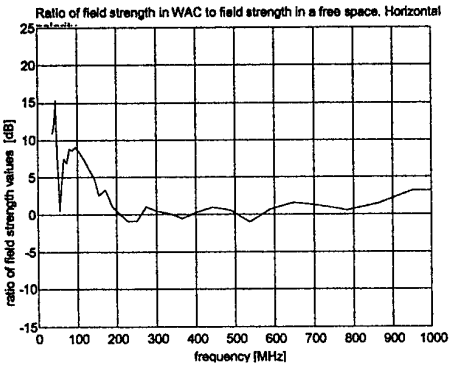



**Fig. 6 Ratio of field strength measured in WAC to field strength computed for free space, provided the same equipment and power drive. Horizontal polarity**

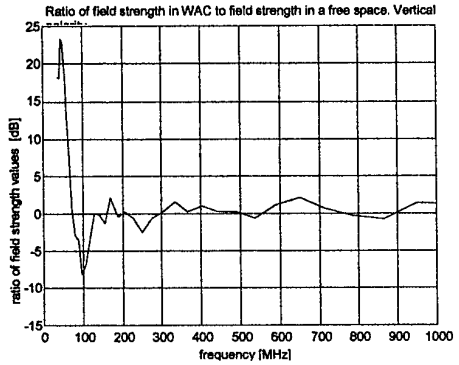



**Fig. 7 Ratio of field strength measured in WAC to field strength computed for free space, provided the same equipment and power drive. Vertical polarity**

IEC-1000-4-3 demands 80% amplitude modulation. It means that the linear output range of the amplifier must be 1.8 times larger than that for CW. The output power of the amplifier must be 3.24 times larger (5.1dB). It gives in the described case the value of 675W. Computed power for a free space is equal to 101W.

The price of a 100W broadband amplifier up to 1GHz is about 30k$. The amplifier price rises with the output power and can reach in particular cases the unrealistic numbers comparable with the price of a whole anechoic chamber.

## 5.CONCLUSION

Anechoic chamber characteristics may highly influence the value of field strength in a chamber. In some frequency ranges (where effectiveness of used absorber is low) in the chamber may occur the resonant phenomena strongly affecting field distribution.

Field uniformity on the hypothetical vertical plane (uniform field area) should not be the only criterion regarding the field distribution in a test site that is taken into account. The uniform field plane is only a plane of a certain specific crossection of the field inside the chamber. Our experiments have shown that it is possible to obtain a uniform field in accordance to the applicable standards demands in spite of the deep resonances in the spatial field distribution in the chamber.

A field distribution along the line connecting the tip of a transmitting antenna and the uniform field area should be carefully considered as well. At least the dependence of the field strength at a middle point on the uniform field plane vs. antenna driving power or the dependence of the mean value of this field strength (for 12 or 16 points) vs. antenna driving power should be known prior to the purchase of the power amplifier. If a test site already exists the above mentioned functions can be measured or in case of well known parameters of the chamber and adequate computational capabilities can be computed as well. The knowledge of these functions allows to correct the value of the required RF amplifier output power, computed for a free space (or OATS ), predict the value which is really needed and avoid all the consequences of the purchase of the improperly sized amplifier. If following cost analysis is performed, it can point out an optimum solution for any particular case – the purchase of an amplifier sized in accordance to the predicted power value or prior enhancement of the chamber reflectivity characteristics, which can decrease the necessary amplifier power. The latter calls for a change or improvement of chamber absorber. Optimisation of the transmitting antenna choice should also be considered.

## 5. REFERENCES

[1] Dawson L., Dawson J.F., Marvin A.C.,"The use of TLM modelling to predict the performance of ferrite tiles in damping resonances within a screened enclosure",Proc. of the 1999 IEEE Intl. Symp. on EMC, Seattle, WA, August 2-6, 1999, pp. 867-872

[2] IEC1000-4-3, Electromagnetic compatibility (EMC). Part 4: Testing and measurements techniques-Section 3: Radiated, radio-frequency, electromagnetic field immunity test., Feb.1995

[3]EN 61000-4-3 Electromagnetic compatibility (EMC). Part 4: Testing and measurements techniques-Section 3: Radiated, radio-frequency, electromagnetic field immunity test.,.1996

[4] Bem D.J., Kucharski A.A, Sowa A. E., Więcek M., "Wroclaw Anechoic Chamber", Proc. of Intl. Wroclaw Symp. on EMC, Wroclaw, 1994

[5] D.J. Bem, A.E. Sowa, M.Więcek, J.S.Witkowski, "Automated field calibration and immunity testing in Wroclaw Anechoic Chamber", Proc. of Intl. Wroclaw Symp. on EMC, Wroclaw, 1998

[6] Williams T.,"EMC amplifiers for immunity testing", ITEM 1997, pp. 183,186,188,284,286

[7] Osburn J.D.M, "Computing required antenna RF input power for a given E-field level at a given distance", ITEM 1998, pp. 18,20,24

**EMC 2000** INTERNATIONAL WROCŁAW SYMPOSIUM ON ELECTROMAGNETIC COMPATIBILITY

# ON THE PROPER USE OF THE INJECTION CLAMPS IN IEC/EN 61000-4-6 TEST

Jan Sroka
SCHAFFNER EMC AG
Nordstr. 11
CH-4542 Luterbach
tel. +41/326816743 fax. +41/326816715
e-mail: jsroka@schaffner.com

*ABSTRACT*

*The basic standards IEC and EN 61000-4-6 define different appliances for injection of RF disturbances. Coupling Decoupling Networks are preferred although injection clamps such as Electromagnetic (EM) Clamp or Current Injection (CI) clamp are also acceptable but only if application of CDNs is not possible.*
*The big advantage of injection clamps versus CDNs is the noninvading character of the coupling, however CDNs, unlike injection clamps, are insensible to impedance variations at the AE-Port.*
*A decoupling clamp at the AE-Port of the injection clamp makes the EUT impedance in high frequency range (above 26MHz) practically independent of the load impedance at the AE-Port.*
*But how to ensure stable impedance conditions in low frequency range by using an injection clamp?*
*The author proposes a method concerning the supply line. It is based on application of the Artificial Mains Network (AMN) which is anyway indispensable for conducted emission tests.*
*Impedance of the EM Clamp with the AE-Port loaded with AMN is stable up to about 26MHz. The AMN in low frequency range and additional decoupling clamp in high frequency range are complementary measures to ensure stable impedance conditions by using the injection clamp.*

## 1. INTRODUCTION

The preferred appliances for injection of RF disturbances according to the basic standard IEC 61000-4-6 (EN61000-4-6) [5.1] are Coupling Decoupling Networks (CDNs) built of lumped RLC components. Injection clamps such as Electromagnetic (EM) clamps or Current Injection (CI) clamps are also accepted but only if application of CDNs is not possible. The big advantage of the injection clamps versus CDNs is the noninvading character of the coupling. It should be not underestimated by *in situ* measurements of large systems or installations, particularly by injecting disturbance into the supply lines. The reason, however for the CDNs to be preferred in the standard is obvious. CDNs unlike injection clamps ensure stable impedance conditions versus load at the AE port.
In the paper comparison of frequency characteristic of all the above mentioned injection appliances is presented. Furthermore the application of the EM clamp for injection of disturbance into the supply line is discussed in details below. In a high frequency range an additional decoupling clamp stabilises the impedance. For a low frequency range a very simple solution is proposed. It consists in application of the Artificial Mains Network (AMN). The AMN must anyway be mounted in the supply line because of the conducted emission test. The method can be directly applied if a CI clamp is used.

## 2. IMPEDANCE CHARACTERISTIC OF DIFFERENT INJECTION APPLIANCES

All type of injection appliances can be regarded as a 3-ports with the:

1. Equipment Under Test (EUT) Port,
2. Auxiliary Equipment (AE) Port,
3. Radio Frequency (RF) Port.

The standard defines the common mode impedance of the injection appliances visible from the EUT-Port[1] with matched resistance (50Ω) at the RF-Port.

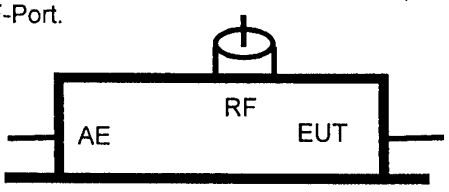



Fig.1. The injection appliance as a 3-port.

[1] This is called EUT impedance.

It should be 150Ω ±20Ω in the frequency range from 150kHz to 26MHz and $150\Omega^{+60\Omega}_{-45\Omega}$ in the frequency range from 26MHz to 80MHz, independently of the load impedance at the AE-Port. The EUT impedance is measured with an open circuited and a short circuited AE-Port. It is easy to fulfil this requirement with the CDNs. An example of the EUT impedance characteristic of the CDN 801-6 M3 is shown in Fig.2 and Fig.3.

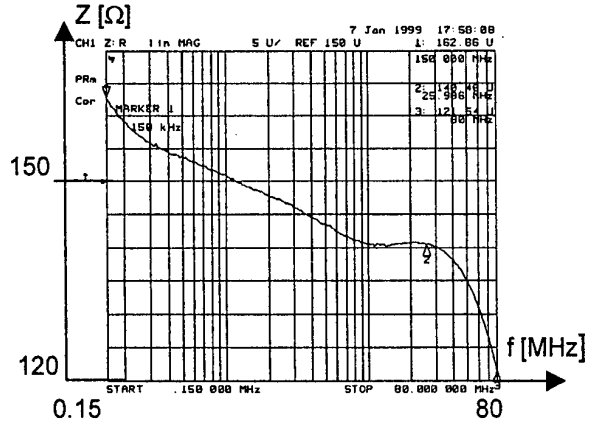



Fig.2. The EUT impedance of a CDN with the AE-Port opened.

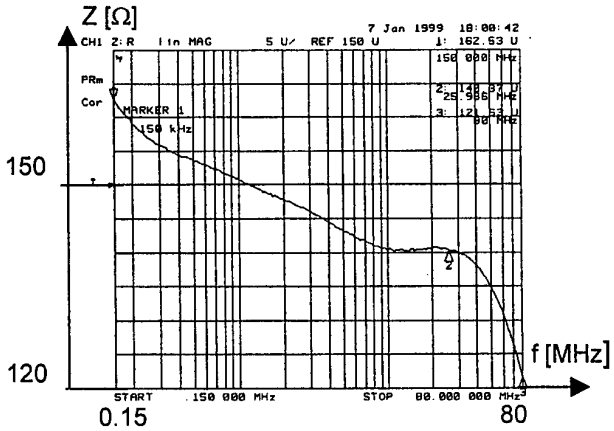



Fig.3. The EUT impedance of a CDN with the AE-Port short circuited.

The injection method defined in the standard IEC 61000-4-6 (EN 61000-4-6) consists in substitution i.e. the stress level to be injected during the test at the RF-Port is set prior to the test, with defined impedances at the EUT-Port (100Ω to 50Ω adapter) and AE-Port (150Ω) [5.1].
Because the EUT impedance of CDNs is practically insensible to a variation of a load impedance at the AE-Port, the stress injected to the EUT during the test corresponds to the level set before, regardless of the impedance of the Auxiliary Equipment connected to the AE-Port[2].

[2] Impedance of the Equipment Under Test connected to the EUT-Port can strongly vary from 150Ω but it does not meter. It can be increased with ferrite beads or decreased with leakage capacitors but it is the way to suppress the stress reaching the EUT.

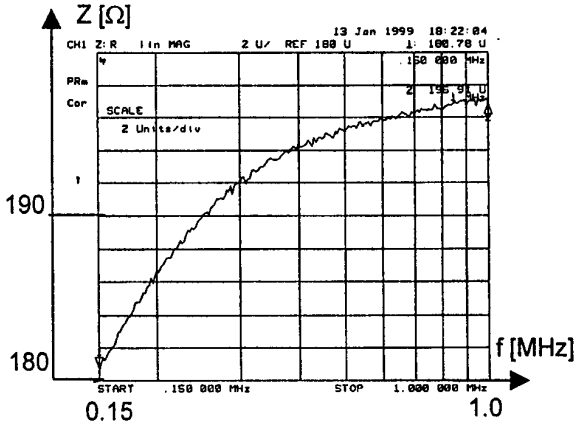



Fig.4. The EUT impedance of an EM Clamp in low frequency range with 150Ω resistance at AE-Port.

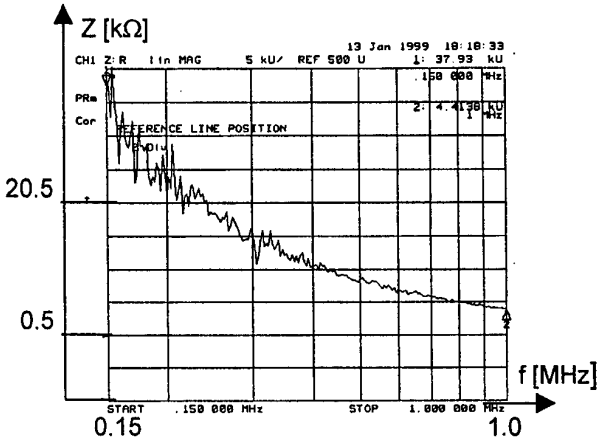



Fig.5. The EUT impedance of an EM Clamp in low frequency range with the AE-Port opened.

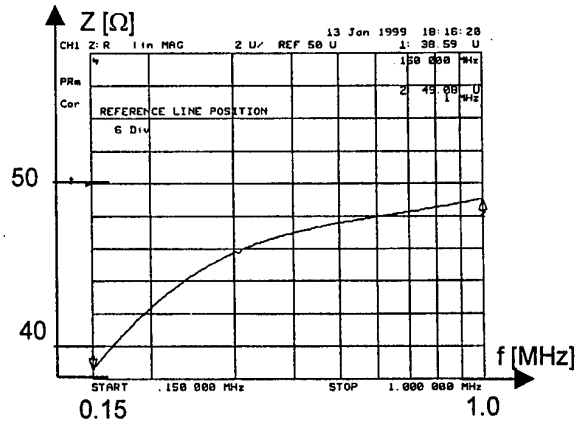



Fig.6. The EUT impedance of an EM Clamp in low frequency range with the AE-Port short circuited.

As it is visible from Fig.4, 5, and 6 the EUT impedance of an EM clamp, in a low frequency range (from 150kHz to 1MHz) varies unacceptably strongly with the impedance connected to the AE-

Port. For quantification of this variation the following coefficient is defined

$$d = \frac{Z\left\{\begin{matrix} short \\ open \end{matrix}\right\}(f) - Z_{150}(f)}{Z_{150}(f)}$$

where $Z_{open}$, $Z_{short}$ and $Z_{150}$ means the EUT impedance with the AE-Port opened, short circuited and with 150Ω load respectively. The biggest $d$ for the AE-Port open circuited is $d_{MAX}$ = +210, at 150kHz and for the AE-Port short circuited $d_{MAX}$ = –0.79, also at 150kHz.

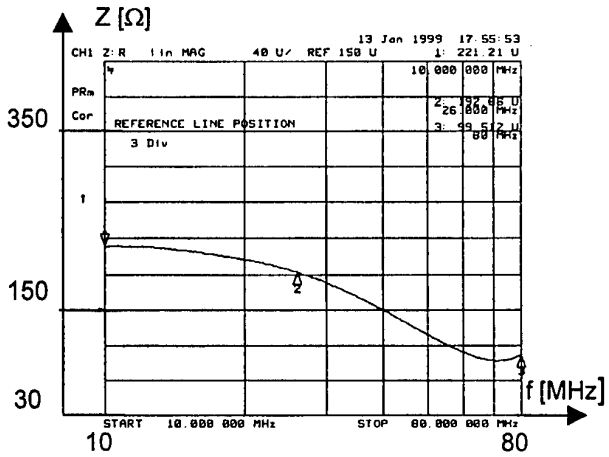



Fig.7. The EUT impedance of an EM Clamp in high frequency range with 150Ω load resistance at the AE-Port.

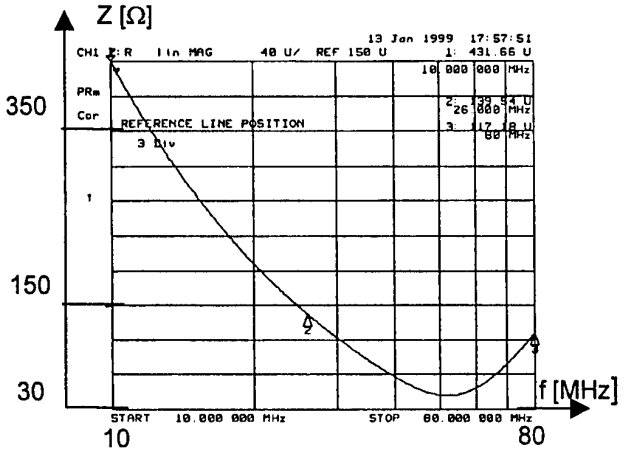



Fig.8. The EUT impedance of an EM Clamp in high frequency range with the AE-Port opened.

The EUT impedance is to some extent stabilised in a high frequency range, from 10MHz to 80MHz (see Fig. 7, 8 and 9) but deviation is still great, $d_{MAX}$ = +0.95 for the AE-Port opened by 10MHz and $d_{MAX}$ = +1.83 for the AE-Port short circuited at 39.7MHz.

The application of an additional decoupling clamp at the AE-Port of the EM clamp gives the improvement (see Fig.10, 11 and 12). In frequency range from about 26MHz to 80MHz the EUT impedance is practically independent of the load impedance at the AE-Port, $d_{MAX}$ = +0.22 for the AE-Port opened by 26MHz and $d_{MAX}$ = +0.03 for the AE-Port short circuited by 26MHz.

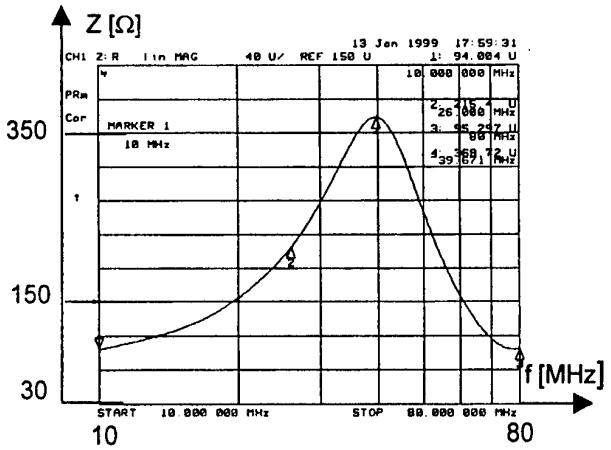



Fig.9. The EUT impedance of an EM Clamp in high frequency range with the AE-Port short circuited.

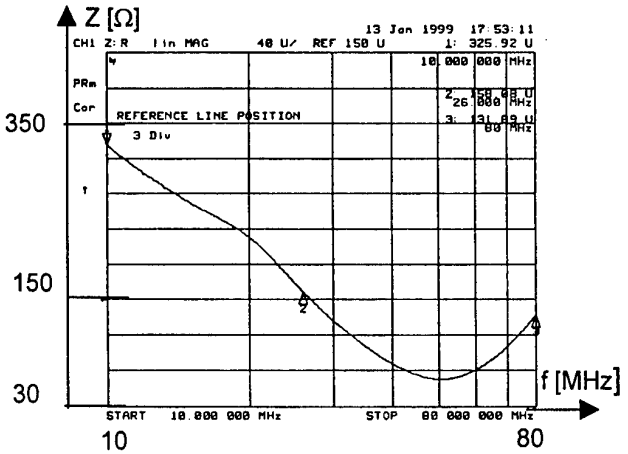



Fig.10. The EUT impedance of an EM Clamp extended with decoupling clamp, in high frequency range with 150Ω load resistance at the AE-Port.

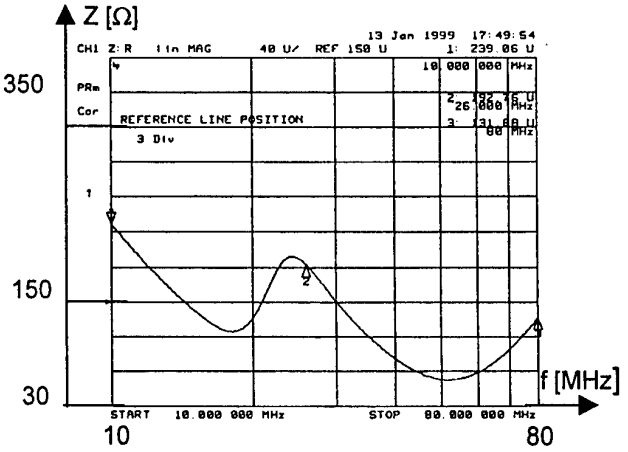



Fig.11. The EUT impedance of an EM Clamp extended with decoupling clamp, in high frequency range with the AE-Port opened.

The generic standards and many product family standards demand, however the start frequency strictly 150kHz.

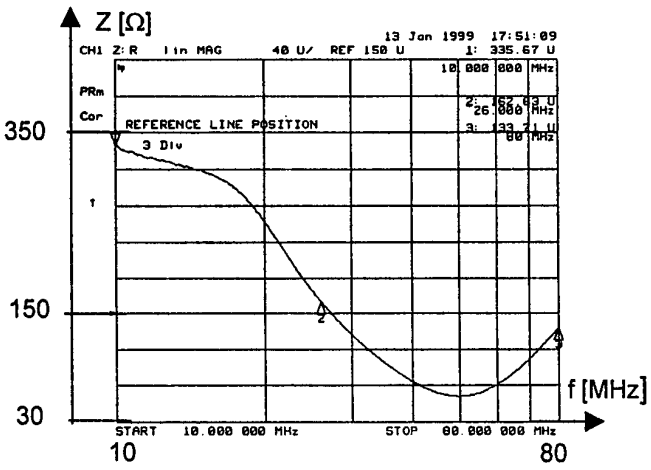



Fig.12. The EUT impedance of an EM Clamp extended with decoupling clamp, in high frequency range with the AE-Port short circuited.

## 3. HOW TO ENSURE THE DEMANDED STRESS LEVEL IN LOW FREQUENCY RANGE USING INJECTION CLAMP?

EMC practicians advice as follows:

1. connect a casing of the auxiliary equipment with 150Ω to the HF-Reference or
2. set the level prior the test with auxiliary equipment connected to the AE-Port of the clamp, instead of 150Ω.

Both these measures have disadvantages. The common mode impedance of the AE line is unknown. Moreover setting the level with the auxiliary equipment is realistic only with the AE[3] switched off. The common mode impedance can be different if the AE operates.

The method proposed by the author consists in using Artificial Mains Network (AMN) for the supply line. The AMN must anyway be mounted for conducted emission tests.

By setting the disturbance level and by performing the test, the AMN must be isolated from the HF Reference plate. Resistance must be connected between the AMN casing and the reference plate. Its value depends on the number of used lines. It must be such that the resulting common mode resistance of all lines to the HF Reference is equal to 150Ω. It is 133Ω in the case of one phase, three lines supply i.e.: phase, neutral and protective earth. Impedance in the Protective Earth (PE) line in the 50Ω/50μH V-AMN is different from the impedance in the rest over lines [5.2]. Therefore additional measures must be taken in order to avoid transformation of the injected common mode disturbance into the differential mode. They consist in connecting 50Ω/50μH and 250μH components in the PE line at the EUT side and mains side of the AMN respectively (see Fig. 15).

It must be noted that the Radio Frequency Generator [5.1] must be supplied with separation transformer (see Fig. 15) as otherwise the resistance between the AMN case and the HF-Reference plate will be short circuited.

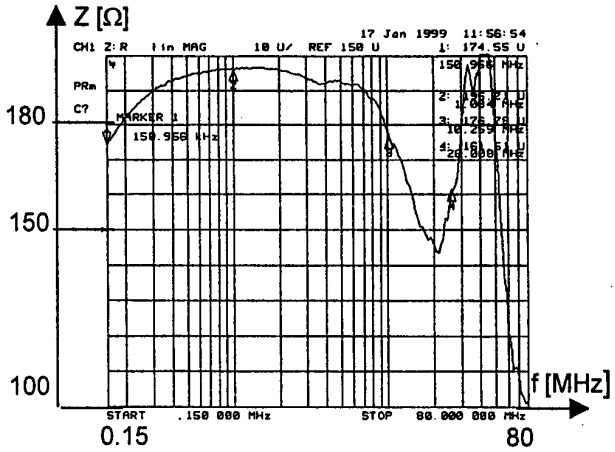



Fig. 13. The EUT impedance of an EM Clamp with the AMN at the AE Port. The lines at the network side of the AMN .- opened.

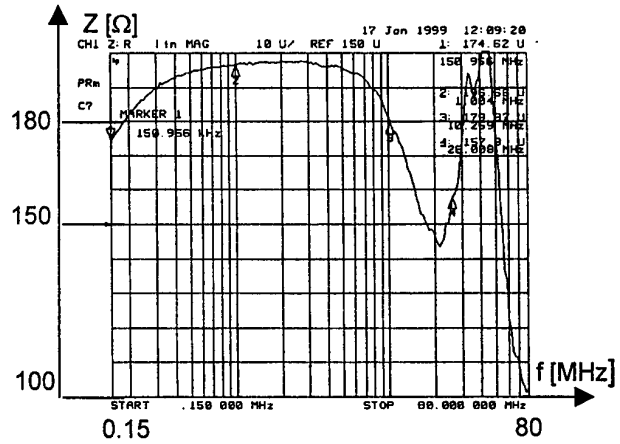



Fig. 14. The EUT impedance of an EM Clamp with the AMN at the AE Port. The lines at the network side of the AMN .- short circuited.

As it is visible in Fig. 13 and 14 the EUT impedance with the AE-Port loaded with the AMN and corresponding additional components is insensitive to the impedance at the network side of the AMN in the whole frequency range, up to 80MHz. Because of high impedance variation above 30MHz, it is recommended to set 30MHz as upper frequency limit of application of the proposed solution.

[3] In this context also AC Supply Network is understood as AE.

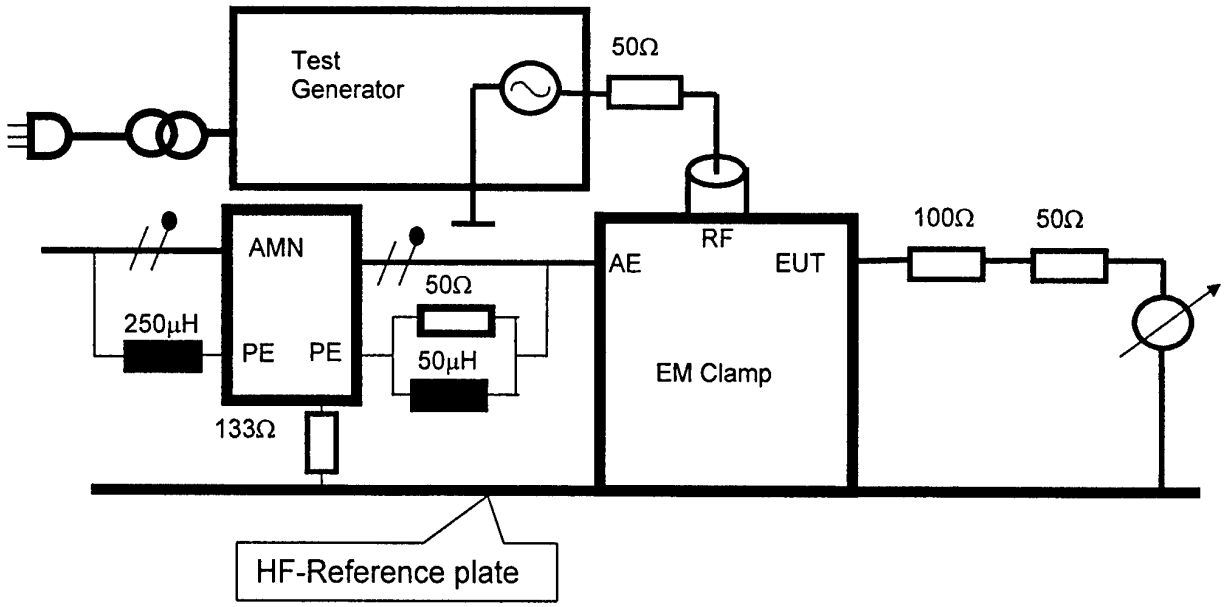



Fig. 15. The set-up for setting the stress level with AMN.

## 4. CONCLUSIONS

The EM Clamp itself does not ensure a stable EUT impedance, so it is negligent not to take any measures if the load impedance at the AE-Port is unknown. Extension of the EM clamp with a decoupling clamp makes the EUT impedance insensitive only from about 26MHz. In the frequency range from 150kHz to about 30MHz the commonly used 50Ω/50μH AMN stabilises EUT impedance very well. For this application the AMN must be connected to the HF Reference plate with a resistance. The resistance between the AMN casing and the HF Reference depends on the number of supply lines.

PE line in the AMN has a different HF impedance than the rest over lines. Additional RL components therefore have to be connected to the PE connector in the AMN in order to avoid transformation of the common mode disturbance into the differential mode. In order not to short circuit the resistance between the AMN casing and the HF Reference, the RF Generator must be supplied with the isolation transformer.

The modified AMN in low frequency range (up to 26MHz) and additional decoupling clamp in high frequency range are complementary measures to ensure stable impedance conditions.

The proposed method cannot be applied if the tested system or installation is equipped with additional installation lines which are independently, galvanically connected to the earth system, such as: metal water or metal gas pipes. Such connections makes short circuit of the resistance connected between the AMN and the HF Reference.

The same procedure can be applied for CI clamps.

## 5. REFERENCES

5.1 EN 61000-4-6 *Immunity to conducted disturbances, induced by radio-frequency fields* 1996-08.

5.2 CISPR 16-1 *Specification for radio disturbances and immunity measuring apparatus and methods, Part 1: Radio disturbances and immunity measuring apparatus*, 1993-08.

## BIOGRAPHICAL NOTE



**Jan Sroka** was born in Szczercόw in Poland on January 02 1952. He received MSc, Ph.D. and D.Sc. degrees in electrical engineering from Warsaw University of Technology in 1974, 1982 and 1991 respectively. From 1974 to 1991 he was with the Department of Electrical Engineering at the Warsaw University of Technology. From 1991 to 1994 he was at the post doctorate scholarship by the Group of Electromagnetic Fields at the Swiss Federal Institute of Technology in Zürich. Since 1994 he has been in the EMC accredited laboratory by SCHAFFNER EMC AG in Switzerland.

**EMC 2000** INTERNATIONAL WROCŁAW SYMPOSIUM ON ELECTROMAGNETIC COMPATIBILITY

# INSTRUMENTS FOR THE NATURAL MAGNETIC FIELDS REGISTRATION IN THE CITY CONDITIONS: THE MAGNETIC STORM INDICATORS

**Vladimir V. Lyubimov**

*The Institute of Terrestrial Magnetism, Ionosphere and Radio Wave Propagation of Russian Academy of Sci., Troitsk, Russia, 142190.* **Phone/Fax: +7 (095) 3340908; E-mail: lyubimov@izmiran.rssi.ru**

*In the paper application of the new instruments – the magnetic storm indicators (MSI) for the natural magnetic field registration in the city conditions has been described.*

*The construction of devices using fluxgate sensors allow to use MSI in various conditions and premises with the larger level of electromagnetic noises.*

*The description of main characteristics of MSI are shortly presented.*

## 1. INTRODUCTION

Necessity to make defences measure from the influence of magnetic storm (***MS***) in the first place dictate need for the means of its revelation in the real time scale in the industrial big city conditions with strong artificially created electromagnetic radiations and by noises, amplitude which can achieve 1... 10 μT and more [2, 8, 11, 16, 19]. Till recent time was believed, what to fix **MS** you may only in places with comparatively quiet magnetic field, without strong industrial noises [5]. Knownly, what level of noise with the net frequency in ordinary laboratory conditions or in the urban hospitals condition and clinic can exceed the variations of natural geomagnetic field (***GMF***) in thousand and more time [5, 8]. Noise from electrify transport have impulse character and compose as to amplitude dozens of nT at a distance in the hundreds of metres [2, 8, 11]. The spectral structure of urban noises practically superimpose the spectra of all known signals from biological objects. The maximum of the spectrum of **GMF** variations generally it is necessary on the domain of approximately twenty-four hours periods, depending on the geomagnetic latitude of the observation place, with the sharp decrease in the domain of short periods. During strong **MS** the spectrum of geomagnetic variations shift in the domain of short periods [10, 11].

## 2. PRELIMINARY INVESTIGATIONS AND PROBLEME SOLVING

From the point of view of medicine and magnetobiology that fact now does not cause any more of doubts, that electromagnetic fields (**EMF**) of a natural origin should be considered as one of the major ecological factors [1, 2, 8, 9, 11, 18, 20]. The presence of natural **EMF** in an environment is completely necessary for existence of normal ability to live, and their absence or the deficiency - results to serious negative, at times even to irreversible consequences for alive organism [1, 11, 17, 18, 20].

Our investigations [1, 3-8, 11, 14-16, 18, 20] showed the principle possibility of diagnistic magnetometers (***DM***) application, realized on the basis of fluxgate sensors, in the sity conditions with the larger level of electromagnetic noises. Therefore in 1990 in ***IZMIRAN*** begin to creation of simple and inexpensive instruments for the equipment of medical establishments, capable visualized the process of the GMF change in real time [10-14]. As a result was created a new class of ***DM*** - the magnetic storm indicators (***MSI***).

Are carried out of investigations, purpose which was creation reliable and inexpensive instruments for **MS** revelation in the conditions with the high level of technogenic hindrances and noises, for the realization of local electromagnetic control in hospitals, clinics, in the rest zones, in residential and manufacturing premises. In the process of experimental works were created special computer programs allowing to conduct correlation analysis receivable medical and geophysical information.

Manufactured in period from 1992 to 1999 models of ***MSI*** were received small, simple in exploitation and maintenance [10, 13]. The experimental samples of a number of instruments passed clinical and laboratory tests in research centers and organisations. Accumulated the experience of various types ***DM*** and ***MSI*** application in clinic showed the principal possibility of application created magnetometrical equipment in the conditions with the larger level of technogenic electromagnetic noises [3, 5, 13]. It was shown experimentally the possibility and the necessity of **MS** registration in the clinic conditions [4, 8, 15, 16]. Main characteristics of created analog and digital ***MSI*** are presented below.

## 3. MAGNETIC STORM INDICATORS

The MSI ***MF-01*** [10, 13] is high sensitivity analog magnetometer includes in itself two units: the magnetic measuring converter – ***MMC*** (250x80x40 mm) and the

indication unit – *IU* (110x90x55 mm), connected between each other cable by length 10..15 m. Information about the MS intensity change, its instantaneous significance on the 6-level luminous indicator are represented. Weight of instrument is not above 1,2 kg.

The MSI *MF-04 MAGIC* [13] was create as a laboratory device consisting two units: *MMC* and *IU*, connected between each other cable by length 6...10 m. Information about the change of MS intensity, its instantaneous and middle significance for the 60-minute interval of time, visualized on luminous indicator of *IU*. For the current time indication are used built-in timer and digital display. Is provided the possibility of the MS value indication at the help of switch on the acoustic signalling and possibility of around-the-clock receivable information fixing in the real time scale at the help of analog recorder. Number of fixed by the indicator of the MS gradation is 6. The weight of instrument is not above 3 kg.

Small-size diagnostic magnetometer - MSI *MF-05* [12-14] was create as a home appliances wall-instrument. Information about the change of MS intensity, its instantanous significance, visualized on luminous indicator. Are provided the possibility of the MS value indication at the help of sound signalling and the possibility of fixing and visualize its maximal significance at the help of luminous indicator. Instrument lets around-the-clockly to fix receivable information in the real time scale at help of analog recorder. Number of MS gradations fixed by the indicator is 6. The remote magnetometer cable length is 6...10 m. Units dimensions are 160 mm (length) and 70 mm (external diameter). Weight of MSI *MF-05* is not above 0.5 kg. Instrument is handy to work and MS registration in inhabited room conditions [20].

Created MSI: *MF-01, MF-04 MAGIC* and *MF-05* successfully were used for realization electromagnetic monitoring in conditions of clinics Moscow, Yalta and Kislovodsk sityes [4-8, 13-16]. For example, *MF-01*, established in branch of reanimation Central Railway Hospital (*CRH*) No.3 of Moscow, has studied in a continuous mode more than six years. Use MSI in clinic has allowed us to produce the necessary recommendations for revealing and to treatment of the magnetodepending cardiological patients [4, 18].

By the beginning of active realization of research work on study of biotropical influence of natural and artificial EMF creation has per capita served experimental model of the Geophysical Data Logger - MSI *IDL-04* [13, 21]. MSI *IDL-04* is appointed for registration, storage, processing, analysis and representation of slowly changeable in real time information from eight analog sensors, as an one of which is used *MMC* (140x80x40 mm). *IDL-04* carries out visualization of "*signal-time*" schedule on display, transmitting the measuring data in PC, the output of data in analog recorder, the production of the "*hard copy*" of display on printer, calculation and demonstration of the magnetic activity index. Instrument will realize the original algorithm of work which lets using receivable in the tempo of experiment data, to signallized about the MS, to calculate and visualize *K-index* of magnetic activity on base of the search, detections and the definitions of days with quiet geomagnetic situation. At the calculation of magnetic disturbance and the index of magnetic activity the registration data undergo by digital filtration. The volume of nonvolative memory lets to data accumulation during 14...113 days. The instruments weight is not above 3 kg.

At present time MSI *IDL-04* already four years is used for monitoring realization and MS registration in clinic conditions (in Moscow *CRH* No.3), where is organized continuous service of tracking for an environmental electromagnetic conditions in real time scale, that allows to have constantly data about current magnetic field disturbance and in due time to carry out therapy of magnetosensitivity ill at the MS beginning [3, 4].

Magnetic Activity Recorder - MSI *IDL–04M* [10] appear a modern model of *IDL-04*. It is appointed for measurement in real time of **D-*component*** of GMF variations, for registration, accumulation, processing, analysis and the data representation of this measurements, for the arranging of monitoring works as to the investigation of surrounding environment, for arranging medical and magnetobiological researches. *IDL-04M* has two measuring channel for *MMC* connecting by cables (8...10 m). Instrument has built-in graphic indicator. Fixed magnetic field data undergo digital filtration. The volume of nonvolative memory lets to accumulate information during 65 days. The instruments weight is not above 2 kg.

Now MSI *IDL-04M* during one year in Research Laboratory of Moscow Physics-Technical Institute is used successfully.

Universal Data Logger –MSI *IDL-07* [13, 21] can decide a lot of scientific, research and applied problems in geophysics, to find broad application for monitoring works realization on multiparametrical research of an environment, to help of preventive measures realizations in medicine, to be applied in magnetobiological researches. On the basis of *IDL-07* it is possible construction of autonomous observatories and stations for a measurement of various physical fields.

The MSI *IDL-07* is functionally independent compact device of a continuous operation intended for registration, accumulation, processing, analysis, visualization and transfer to PC informations from analog sensors on 8 measuring channels. It includes *IU* (200x140x230 mm) and two of analog magnetometer converters *MMC*, which are connected accordingly to first and second measuring channels. Remaining the measuring channels can be used for connection of electrical field, pressure, humidity, temperature and other sensors, have an electrical output.

Both *MMC* represent highly sensitive and high-precision one-component fluxgate magnetometers, ***first***

of which (140x80x40 mm) allows to conduct measurements of GMF *D-component* variations in any region of Globe without additional tuning, and *second MMC* (60x20x20 mm) is intended for an amplitudes measurement of artificially created constant or variable magnetic fields for want of realizations of researches in coil systems, in magnetic shielded rooms and cameras, in locations and observatories.

The MMC *IDL-07* realizes the following operations: visualization on the indicator of the schedule "*signal - time*", transfer accumulated datas through the serial port, accumulation of datas in internal memory, account and demonstrating of a magnetic activity index. The possibility of digital indication of outcomes is stipulated measurements of a magnetic field on each from magnetometric channels for want of realizations of their preliminary adjustment, calibration and for want of realizations of discrete measurements.

In a mode of long continuous work *IDL-07* automatically watchs current magnetic disturbations. For the notification about the fixed disturbation the MSI is supplied with the sound signalisation. For want of account of amplitude of magnetic disturbation and index of magnetic activity the datas of *IDL-07* are subjected of digital filtration. The main parameters and operational modes of *IDL-07* are selected with the help of functional buttons located on forward board of *IU*, agrees the menu or can be make by the program depending on the users problems. The *IU* is supplied with the liquid-crystal graphics display with sizes of 320 x 240 points. For want of realizations long continuous measurements with *IDL-07* the power-down mode is stipulated. It is appointed for the carrying out of monitoring works as to the investigation of surrounding environment, for execution of medical and magnetobiological researches. On the basis of instrument is possible of autonomous stations and observatory construction.

Magnetic Activity Recorder - MSI *IDL-09* [10] is appointed for detection and the indications of the MS amplitude *in any regions of Globe* in the real time scale, for measurement, regisration, logging, analysis and data representation about the magnetic field change. The volume of nonvolative memory lets to accumulate the information during 3...5 days. Instrument has analog output and equipped by built-in digital (*graphic*) display.

The power supply of all devices is carried out as from storage battery by voltage 9...12V DC or from network AC by standard network adapter. The more detailed characteristics of the created devices are given in [10, 13, 21].

## 4. CONCLUSIONS

In *IZMIRAN* during last 10 years experimental samples of *DM* on base of the one component fluxgate sensor are created, which main advantages are: economy, small sizes and weight, and also rather low cost. Our researches have shown, that these devices can be used for measurement of natural GMF variations and magnetic fields created by artificial sources in any premises in conditions of industrial city. For use in the field of medicine and magnetobiology the new class of devices - magnetic storm indicators is created. *MSI* allow to determine and visualized of MS amplitude in any area of Globe in real time scale and by that to help practical medicine in rendering the duly help to the people subject to heightened sensibility to changes of a magnetic field.

New generation of digital MSI *IDL-04, IDL-07* and *IDL-09* allow to fix physical fields and processes, to connect the analog sensors, placed in city, as basic meteorological parameters (temperature and humidity of air, atmospheric pressure, speed of a wind etc.), and geophysical parameters (electrical and magnetic components of a natural field). At the same time with magnetometrical information such devices allow the information to spend of multiparametrical monitoring work on research of an environment, it is more effective visualized occuring processes at realization of magnetobiological researches.

## 5. REFERENCES


5.1. "Cosmic Ecology and Noosphere" (in russian), Proceedings of the International Crimean Seminar, Partenit, Crimea, Ukraine, October 4-9, 1999. –146 p

5.2. "Electromagnetic Fields and Human Health", Proceedings of the Second International Conference 'Problem of Electromagnetic Safety of the Human Being, Fundamental and Applied Research. Development of EMF Standards: Philosophy, Criteria and Harmonization'. Moscow, Russia, September 20-24, 1999. –406 p.

5.3. GURFINKEL Yu.I., KIRIAKOV V.Kh., LYUBIMOV V.V. "The IDL-04 Magnetic Activity Recorder Application in Clinic Conditions", Proceedings of the International Scool-Seminar on Automation and Computing in Science, Engineering and Industry ACS'98, Moscow, Russia, June 27 – July 05, 1998. PP.160-162.

5.4. GURFINKEL Yu.I., LYUBIMOV V.V. "Use of Diagnostic Magnetometers and Magnetic Storms Indicators in Clinic as Information Instrument to Revealing of the Magnetodepending People", Proceedings of the International Scool-Seminar on Automation and Computing in Science, Engineering and Industry ACS'98, Moscow, Russia, June 27 – July 05, 1998. PP.162-163.

5.5. GURFINKEL' Yu.I., LYUBIMOV V.V., ORAEVSKY V.N. "Experience in the Use of a Diagnostic Magnetometer in the Emergency Clinic", Biophysics, V.40, No.5, 1995. P.1047-1054.

5.6. GURFINKEL Yu., LYUBIMOV V. and ORAEVSKY V. "Geomagnetic Monitoring: Experience and Prospects in Medicine and Biology", Proceedings of the Third International Congress of the European Bioelectromagnetic Assotiation,. Nancy, France, 1996. PP.24-26.

5.7. GURFINKEL Yu., LYUBIMOV V., ORAEVSKY V., PARFENOVA L. "Geomagnetic Monitoring: Experiments and Prospects in Biology and Medicine", Biophotonics, Proceedings of the International Conference "Non-equilibrium and Coherent Systems in Biology, Biophysics and Biotechnology", Dedicated to the 120-th birthday of Alexander Gavrilovitch Gurwitch (1874-1954), Moscow, Russia, September 28 – Oktober 02, 1995. PP.473-476.
5.8. GUSEVA T.A., KANONIDI Kh.D., LYUBIMOV V.V., GURFINKEL Yu.I. "Electromagnetic Monitoring of an Environment in Industrial City, Health Resort Zones and Clinics Conditions", Proceedings of the 8-th Scientific Assembly of IAGA with ICMA and STP Symposia, Uppsala, Sweden,.August 4-15, 1997. P.380.
5.9. KHOLODOV Yu.A. "The Man in Magnetic Web (Magnetic Field and Life)" (in russian), Znanie, Moscow, 1972. -144 p.
5.10. LYUBIMOV V.V. "Artificial and Natural Electromagnetic Fields in Environment, Environmental the Man, and Devices for their Detection and Fixing" (in russian), Preprint No.11 (1127), IZMIRAN, Troitsk (Moscow Region), Russia, 1999. -28 p.
5.11. LYUBIMOV V.V. "Biotropicity of Natural and Created Artificial Electromagnetic Fields. The Analytical Review" (in russian), Preprint No.7 (1103), IZMIRAN, Moscow, Russia, 1997. -85 p.
5.12. LYUBIMOV V.V. "Compact, Efficiency and Inexpensive Component Variometers for Science and Medicine Needs", Proceedings of the International Workshop & Exibition on Geophysics, Hanoi, Vietnam, March 14-17, 1996. P.163.
5.13. LYUBIMOV V.V. "Diagnostic Magnetometers for Electromagnetic Monitoring Realization in City Conditions both Modern Methods and Means Individual - Mass Visualization of his Results. The Review" (in russian), Preprint No.6 (1116), IZMIRAN, Moscow, Russia, 1998. -20 p.
5.14. LYUBIMOV V.V. "Fluxgate Magnetometers for Diagnostic and Research Work Realisation", Proceedings of the 8-th Scientific Assembly of IAGA with ICMA and STP Symposia, Uppsala, Sweden, August 4-15, 1997. P.455.
5.15. LYUBIMOV V.V. 'Modern Equipment for Monitoring Works Realisations. Diagnostic Magnetometers for Geophysics and Medicine", Proceedings of the International Scool-Seminar on Automation and Computing in Science, Engineering and Industry ACS'98, Moscow, Russia, June 27 – July 05, 1998. PP.156-157.
5.16. LYUBIMOV V.V., GURFINKEL Yu.I., KANONIDI Kh.D. "On the Possibility of Electromagnetic Weather Monitoring and Electromagnetic Control in Conditions of Moscow Clinics", Proceedings of the Fours International Pushchino Symposium on "Relations of Biological and Physico-Chemical Processes With Space and Helio-Geophysical Factors", Pushchino, Moscow Region, Russia, 1996. P.29.
5.17. MAKAROVA I.I. "Influence of Natural and Artifical Created Magnetic Fields on Organism" (in russian), Preprint No.7 (1123), IZMIRAN, Moscow, Russia, 1998. –42 p.
5.18. "Relations of Biological and Physico-Chemical Processes with Space and Helio-Geophysical Factors", Proceedings of the Fours International Pushchino Symposium, Pushchino (Moscow Region), Russia, September 23-28, 1996. –144 p.
5.19. SERDYUK A.M. "Social - Hygienic Aspects of Influence of Electromagnetic Fields on Organism of the Man" (in russian), J. "Social Hygiene, Organization of Public Health Services and History of Medicine", Vol.7, 1974. PP.95-98.
5.20. "Solar Activity Influence upon Medical, Biological and Physico-Chemical Processes", Proceedings of the International Crimean Seminar, Frunsenskoye, Crimea, Ukraine, October 11-14, 1995. –80 p.
5.21. ZVEREV A.S., KIRIAKOV V.Kh., LYUBIMOV V.V. "New Equipment for Geophysics and Medicine" (in russian), Preprint No.2 (1098), IZMIRAN, Moscow, Russia, 1997. -21 p.
5.22. ZVEREV A.S., KIRIAKOV V.Kh. and LYUBIMOV V.V. "Universal Data Logger IDL-07", Proceedings of the International Scool-Seminar on Automation and Computing in Science, Engineering and Industry ACS'98, Moscow, Russia, June 27 – July 05, 1998. PP.108-110.

## BIOGRAPHICAL NOTE



Vladimir V. Lyubimov was born in Moscow, Russia, in 1947. In 1971 he received the master degree (Dipl.-Ing.) of radio engineering at the Moscow Electrotechnical Institute of Communication (MEIC). Since 1971 repeatedly participated in various experimental and field geophysical work, spent on research ships on the various seas of the World ocean.

He works now as Senior Scientist for the Institute of Terrestrial Magnetism, Ionosphere and Radio Wave Propagation of Russian Academy of Sci. (IZMIRAN). His scientific interests are connected to development and creation magnetometrical equipment, intended for realization geophysical field-work, magnetobiological and medical researches.

EMC 2000 INTERNATIONAL WROCŁAW SYMPOSIUM ON ELECTROMAGNETIC COMPATIBILITY

# ANALYSIS OF NOISE PARAMETERS OF HIGHLY SENSITIVE INDUCTION SENSORS FOR MEASUREMENT OF VERY WEAK ELECTROMAGNETIC FIELDS

Vitalij Nichoga, Petro Dub
Karpenko Physico-Mechanical Institute of National Academy of Sciences of Ukraine, Ukraine, 79601, Lviv,
5 Naukova St., tel.: +380 (322) 65-42-92, fax: +380 (322) 64-94-27, e-mail: nich@ah.ipm.lviv.ua

*Highly sensitive sensors for measurement of electromagnetic radiation are necessary when carrying out experimental investigations of electromagnetic compatibility problems. Some peculiarities of choice of highly sensitive induction sensors (IS) parameters from the point of view of achievement of minimal discrimination threshold are considered in the paper. Especially great attention is devoted to the problem of inadmissibility of using noise factor, in general, for determination of optimal parameters of IS and to the problem of necessity of taking into account correlation among noise sources of IS pre-amplifier.*

## 1. INTRODUCTION

When solving many applied problems of electromagnetic compatibility, measurement of shielding factor, monitoring of electromagnetic environment contamination, applied geophysics and others it is necessary to use highly sensitive sensors, with the help of which the discrimination threshold $1 \cdot 10^{-5} \div 1 \cdot 10^{-7}$ nT/Hz$^{0,5}$ can be achieved within the frequency range 1 Hz ÷ 1 MHz [1].

In principle such discrimination threshold can be realised with the help of IS. But the problems of realisation of such discrimination threshold is complicated because of limited mass and dimensions of IS. Even usage of precious operational amplifiers [2] do not guarantee achievement of needed discrimination threshold.

Investigations show that even application of modern materials for sensors and electronic components often can not lead to the expected results if the conditions of matching of that structural parameters of sensors, which determine signal-to-noise ratio, with noise parameters of preliminary amplifier are not executed [3].

## 2. BASIC NOISE PARAMETERS OF SENSORS AND PRE-AMPLIFIERS

For analysis of problem of achievement of minimal IS discrimination threshold we use the following equivalent signal-noise scheme (Fig. 1). Noise parameters of an amplifier (transistor, integrated circuit) can be described with the help of linear noisy four-pole, in which the equivalent noise current and voltage sources reduced, more often, to the input of an amplifier, are used. In such case the real noisy four-pole is substituted by two sequentially connected four-poles: first includes only equivalent noise sources, which have, in general case, cross-correlation, second is noiseless and characterise only amplification properties (Fig. 1).

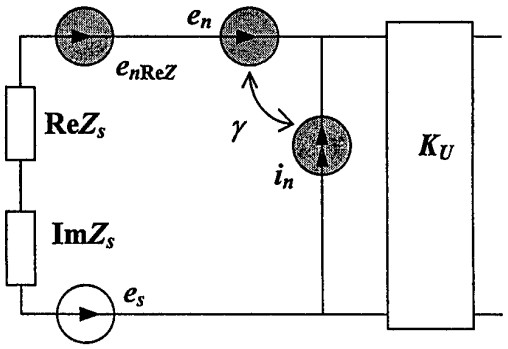



Fig. 1. Equivalent signal-noise scheme of sensor with pre-amplifier

The dispersions of noise e.m.f $\overline{e_n^2}$ and current $\overline{i_n^2}$, shown on the Fig. 1 equivalent noise scheme, can be determined experimentally by measuring output noise voltage in a narrow frequency band in the modes of short-circuit and open circuit on its input accordingly.

Complex correlation coefficient can be defined in the following way:

$$\gamma = \alpha + j\beta = \overline{e_n^* i_n} \Big/ \sqrt{\overline{e_n^2} \cdot \overline{i_n^2}} = |\gamma| \cdot e^{j\varphi}, \qquad (1)$$

where $\alpha$ and $\beta$ are real and imaginary parts of a complex correlation coefficient $\gamma$, $e_n$* - conjugate value of a noise e.m.f; $|\gamma|$ and $\varphi$ - module and phase of a complex correlation coefficient.

Signal source parameters are defined in Fig. 1 in the following way: $Z_s$ - complex source impedance, $ReZ_s$ and $ImZ_s$ - real and imaginary components of signal source impedance, which are, in general,, functions of structural parameters of signal source, $e_s$ - signal e.m.f, $e_{nReZ}$ - e.m.f of thermal noise of signal source resistance,

which value is determined by expression $4kT\mathrm{Re}Z_s$, where $k$=1,38·10$^{-23}$ J/K - Boltzmann's constant, $T$ - temperature, K. Here and below we consider that spectral densities are determined in the band $\Delta f_n$=1 Hz.

Correlation coefficient of amplifier noise sources can be found by using specific values of signal source impedance. Real component of correlation coefficient $\alpha$ can be determined when using pure real resistance at the amplifier input, and imaginary component $\beta$ - when using pure imaginary impedance. These problems are considered enough in literature [4-6].

## 3. LIMITATION OF USING NOISE FACTOR FOR OPTIMISATION OF PARAMETERS OF INDUCTION SENSORS

Noise factor $F$ is often used for comparison of pre-amplifiers qualities [4,7,8]. It shows how many times a signal-to-noise ratio decrease when passing through an amplifier:

$$F = \left(e_s^2 / e_{n\mathrm{Re}Z}^2\right) / \left(U_{si}^2 / U_{ni}^2\right), \qquad (2)$$

where $\left(U_{si}^2 / U_{ni}^2\right)$ - relation of signal and noise powers at an amplifier output.

As $U_s^2 / e_s^2 = K_U^2$, where $K_U$ - amplification coefficient, so

$$F = \frac{\overline{U_{ni}^2}}{e_{n\mathrm{Re}Z}^2}. \qquad (3)$$

For scheme in Fig. 1:

$$F = 1 + \frac{\overline{e_n^2} + \overline{i_n^2}\left|Z_S\right|^2 + 2P_{ni}(\alpha \mathrm{Re}Z_S + \beta \mathrm{Im}Z_S)}{P_t \mathrm{Re}Z_S}. \qquad (4)$$

The value $e_n i_n = P_n$ is often named noise power of an amplifier [3].

Eq. 4 characterise sufficiently noise properties of different amplifiers when using the same signal source. But Eq. 4 is often used mistakenly for determining optimal values of signal source impedance [4, 7, 8]. From conditions $\partial F / \partial \mathrm{Re}Z_s = 0$ and $\partial F / \partial \mathrm{Im}Z_s = 0$ one can find

$$\mathrm{Re}Z_{s.opt} = \sqrt{1-\beta^2}\,\frac{e_n}{i_n}, \qquad (5)$$

$$\mathrm{Im}Z_{s.opt} = -\beta \frac{e_n}{i_n}. \qquad (6)$$

But such approach, named determining of noise matching mode [4,8], does not guarantee achievement of maximal signal-to-noise ratio. From Eq. 2 we can receive

$$\left(U_{si}^2 / U_{ni}^2\right) = \frac{e_s^2 / e_{n\mathrm{Re}Z}^2}{F}. \qquad (7)$$

It is clear that maximum of $U_s/U_n$ is achieved when $F$ is minimal only in the case when signal-to-noise ratio in IS is itself invariable. But in almost all cases changing signal source impedance lead to change of this ratio. This condition is fulfilled when using matching transformer but it itself is a source of additional noise [9].

Thus in spite of achievement of noise factor minimum, which equals

$$F_{\min.mat} = 1 + \frac{e_n i_n}{2kT}\left(\alpha + \sqrt{1-\beta^2}\right), \qquad (8)$$

when conditions (5) and (6) are executed, maximum of signal-to-noise ratio can be far from optimal. Little value of noise factor can mean only that sensor parameters are chosen in such a way that it becomes worse a little when pre-amplifier is connected to IS. That is why application of noise factor for impedance optimisation of signal source (IS also) is inadmissible.

## 4. CORRECT OPTIMISATION OF INDUCTION SENSOR PARAMETERS

We consider, for example, optimisation of IS impedance with some limitations of mass and dimensions of a sensor. Such limitations are obligatory because IS, that are used for investigations of electromagnetic compatibility, must be carried easily and be small enough in order to have a possibility to consider the magnetic field in IS volume as homogeneous. Analysis can be realised with the help of scheme in Fig.2. Here additional capacitance $C_a$, which is connected parallel with IS, is used. It does not practically change signal-to-noise ratio in sensor. IS turn number is another parameter that is used together with $C_a$ to regulate module and phase of source. The point is (as it is shown in [10]) that such parameters as $e_s$, $r$, $L$ can be written, when mass and dimensions are limited, as functions of the only structural parameter of IS - turn number:

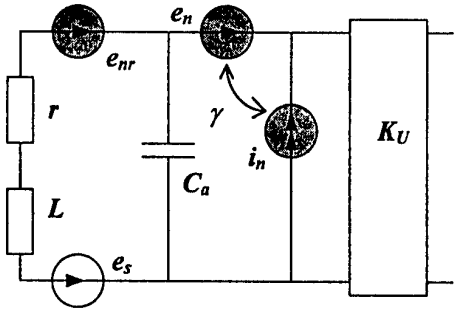



Fig. 2. Equivalent scheme of induction sensor with pre-amplifier and additional capacitance

$$e_s = k_e w \omega H, \quad (9)$$

$$r = k_r w^2, \quad (10)$$

$$L = k_L w^2. \quad (11)$$

Thus for scheme in Fig. 2 can be obtained

$$\frac{U_s}{U_n} = k_e \omega w H \Big/ \Big(4kTk_r w^2 + e_n^2\Big(\big(1-\omega^2 k_L w^2 C_a\big)^2 + \\ + \omega^2 C_a^2 k_r^2 w^4\Big) + i_n^2 w^4 \big(k_r^2 + \omega^2 k_L^2\big) + 2e_n i_n w^2 \big(\alpha k_r + \beta\omega\big(k_L - \\ - k_r^2 \omega^2 C_a^2 - k_L^2 w^2 \omega^2 C_a\big)\big)\Big)^{1/2}, \quad (12)$$

or expression for discrimination threshold:

$$H_{th} = \Big(4kTk_r w^2 + e_n^2\Big(\big(1-\omega^2 k_L w^2 C_a\big)^2 + \\ + \omega^2 C_a^2 k_r^2 w^4\Big) + i_n^2 w^4 \big(k_r^2 + \omega^2 k_L^2\big) + 2e_n i_n w^2 \big(\alpha k_r + \beta\omega\big(k_L - \\ - k_r^2 \omega^2 C_a^2 - k_L^2 w^2 \omega^2 C_a\big)\big)\Big)^{1/2} \Big/ k_e \omega w. \quad (13)$$

Optimal values of $w$ and $C_a$ when Eq. 12 reaches maximum and Eq. 13 - minimum, are equal to

$$w_{opt} = \sqrt{\frac{e_n k_r}{i_n \sqrt{1-\beta^2}\big(k_r^2 + \omega^2 k_L^2\big)}}, \quad (14)$$

$$C_{a_{opt}} = \frac{i_n\big(\omega k_L \sqrt{1-\beta^2} + \beta k_r\big)}{\omega e_n k_r}. \quad (15)$$

In this case signal-to noise ratio equals

$$\left(\frac{U_s}{U_n}\right)_{\max} = k_e \omega H \Big/ \sqrt{2k_r\Big(2kT + e_n i_n\big(\alpha + \sqrt{1-\beta^2}\big)\Big)}. \quad (16)$$

As it is visible from Eq. 16, $\left(\frac{U_s}{U_n}\right)_{\max}$ is proportional to expression $k_e/\sqrt{k_r}$, which is determined only by peculiarities of IS structure and its mass and dimensions. Thus designing of highly sensitive IS should be started from choice of structural parameters in such way that $k_e/\sqrt{k_r}$ becomes maximal and then optimal values of $w$ and $C_a$ must be found.

The considered example is simplified and is suitable, certainly, only for elaboration of IS, that work in a very narrow frequency band. In particular in this case it is supposed the resonance frequency of IS coil is sufficiently higher than operating frequency. We have consider first of all this case with the aim to illustrate the principle of highly sensitive IS optimisation itself.

In this case module of IS impedance together with additional capacitance is equal to

$$|Z_\Sigma| = e_n / i_n = R_{n_{in}}, \quad (17)$$

that is a value, which is named equivalent input noise impedance of pre-amplifier [3]. This result coincides result obtained by using Eqs. 5 and 6 but now matching is realised correctly because it takes into account changes of IS signal value. Real and imaginary components of impedance, calculated by Eqs. 14 and 15 also coincide Eqs. 5 and 6.

## 5. INFLUENCE OF CORRELATION COEFFICIENT ON OPTIMISATION OF INDUCTION SENSOR

Neglect of correlation coefficient of pre-amplifier noise sources must be discussed thoroughly. Firms that elaborate integrated circuits and other amplifiers do not give information about $\gamma$ [11]. In such cases we are forced to consider that $\gamma$=0 and then Eqs. 12÷15 transform to the following expressions:

$$\frac{U_s}{U_n} = k_e \omega w H \Big/ \Big(4kTk_r w^2 + e_n^2\Big(\big(1-\omega^2 k_L w^2 C_a\big)^2 + \\ + \omega^2 C_a^2 k_r^2 w^4\Big) + i_n^2 w^4 \big(k_r^2 + \omega^2 k_L^2\big)\Big), \quad (18)$$

$$H_{th} = \Big(4kTk_r w^2 + e_n^2\Big(\big(1-\omega^2 k_L w^2 C_a\big)^2 + \\ + \omega^2 C_a^2 k_r^2 w^4\Big) + i_n^2 w^4 \big(k_r^2 + \omega^2 k_L^2\big) + 2e_n i_n w^2 \big(\alpha k_r + \beta\omega\big(k_L - \\ - k_r^2 \omega^2 C_a^2 - k_L^2 w^2 \omega^2 C_a\big)\big)\Big)^{1/2} \Big/ k_e \omega w, \quad (19)$$

$$w_{opt} = \sqrt{\frac{e_n k_r}{i_n\big(k_r^2 + \omega^2 k_L^2\big)}}, \quad (20)$$

$$C_{a_{opt}} = \frac{i_n k_L}{e_n k_r}. \quad (21)$$

Thus it seems that $U_s/U_n$ is equal after substitution of Eqs. 20 and 21 in Eq. 18 to the following expression:

$$\left(\frac{U_s}{U_n}\right)_{\max} = k_e \omega H \Big/ \sqrt{2k_r\big(2kT + e_n i_n\big)}. \quad (22)$$

But $U_s/U_n$ is equal really to lesser value because substitution of Eqs. 20 and 21 must be done in Eq.12. Thus

$$\left(\frac{U_s}{U_n}\right)_{\max} = k_e \omega H \Big/ \sqrt{2k_r\big(2kT + e_n i_n(\alpha+1)\big)}. \quad (23)$$

This expression is less than Eq. 16. Thus neglect of correlation coefficient can lead to impossibility of

achievement of needed threshold when designing highly sensitive IS.

So it is necessary to pay more attention to the problem of measuring correlation coefficient because, as literature analysis [4-6] shows, possible errors and choice of optimal modes and input impedance are not studied thoroughly during such measurements. In particular, some times *Z*-parameters of transistors are not considered correctly [6].

## 6. CONCLUSIONS

1. Application of noise factor for optimisation of highly sensitive inductive sensors is, in general, inadmissible.

2. Maximum of signal-to-noise ratio or minimum of discrimination threshold of induction sensors must be used as a optimisation criterion.

3. When choosing optimal parameters of IS the total impedance of IS (together with additional elements) must be determined by Eqs. 5 and 6, but with condition that in expression for signal-to-noise ratio the dependencies of the signal on these parameters are used.

4. When designing highly sensitive inductive sensors the correlation coefficient of pre-amplifier noise sources must be taken into account necessarily.

## 7. REFERENCES

7.1. V. Nichoga, "Measurement of very weak low-frequency magnetic fields in geophysical and space investigations" (Russian), Selection and Processing of Information, Vol. 9, 1993, pp. 70-77.

7.2. V. Nichoga, P. Dub, "Measuring Sensors for Investigation of Magnetic Field on the Board of Space Apparatuses", Proceedings of the Fourteenth International Wroclaw Symposium and Exhibition on Electromagnetic Compatibility, Wroclaw, Poland, June 23-25, 1998, pp. 220-223.

7.3. P. Dub, L. Miziuk, V. Nichoga, "On a New Approach to an Evaluation of Noise Parameters of Amplifiers for Signals Preliminary Processing", Proceedings of the EURASIP Conference on DSP for Multimedia Communications and Services (ECMCS'99) Krakow, Poland, 24-26 June 1999, CD-ROM, paper 14, 4 pages.

7.4. V. Zalud, V.N. Kuleshov, "Noise in semiconductor devices" (Russian), Sovietskoie Radio, Moscow, 1977, 421 p.

7.5. J. Dostal "Operational amplifiers" (Russian), Mir, Moscow, 1982, 512 p.

7.6. V.Gromov, A. Moshinskiy, "Mesuring of primary noise parameters of amplifiers of different types" (Russian), Selection and Transmission of Information, Vol. 71, 1985, pp. 93-99.

7.7. A. van der Ziel, "Noise in Measurements" (Russian), Mir, Moscow, 1979, 296 p.

7.8. M. J. Buckingham, "Noise in electronic devices and systems" (Russian) , Mir, Moscow, 1986, 400 p.

7.9. P. Dub, V. Nichoga, "On a noise matching of an induction sensor with a pre-amplifier by using transformer scheme of input circuit" (Russian), Selection and Transmission of Information, Vol. 61, 1980, pp. 79-86.

7.10. P. Dub, L. Miziuk, V. Nichoga, "Optimisation of constructive parameters of induction sensors for achievement of the lowest discrimination threshold" (Russian), Selection and Processing of Information, Vol. 3(79), 1989, pp. 70-77.

7.11. "Analog Devices linear products databook": April 1998; Analog Devices, Inc., 1998.

## BIOGRAPHICAL NOTES

Vitalij Nichoga is a leading scientific researcher and the manager of laboratory of primary measuring transducers of Karpenko Physico-Mechanical Institute of National Academy of Sciences of Ukraine. He graduated Radio Engineering Faculty of State University "Lvivska Politechnika" in 1960, obtained his Dr. eng. degree in 1966 and Dr. hab. degree in 1996.

Petro Dub is a leading engineer of the same Institute. He graduated Automatics Faculty of State University "Lvivska Politechnika" in 1977. Investigation of electromagnetic fields and manufacturing of instrumentation for their measuring are both V. Nichoga and P. Dub main scientific interests.

EMC 2000 INTERNATIONAL WROCŁAW SYMPOSIUM ON ELECTROMAGNETIC COMPATIBILITY

# SLOTLINE SENSOR FOR PULSE MEASUREMENTS

S. N. Pivnenko
Radiophysics Department, Kharkov National University, 4, Svobody sq., 61077, Kharkov, Ukraine
E-mail: Sergey.N.Pivnenko@univer.kharkov.ua

*A new type of sensor made of a stub of slotline of special form for reception of transient electric field is developed. The experimental results on investigation of the slotline sensor are given. The time shape of the received signal in E- and H-planes and cross-polarization level were measured. The reflection coefficient in time domain of the slotline sensors was measured as well. The proposed slotline sensor has grater directivity as compared to a thin-wire dipole while keeping the same time shape of the received signal and the same cross-polarization level.*

## 1. INTRODUCTION

The problem of measurement of transient field characteristics is very important and, at the same time, is very complicated for realization due to specific features and nature of these signals. Several types of antennas and sensors such as linear antennas loaded nonuniformly and continuously with resistance, or with both resistance and capacitance, conical antenna, bow-tie antenna, TEM-horn was proposed for radiation, reception and measurement of characteristics of radiated transient fields [1-3].

In this paper, a new slotline sensor with improved characteristics for reception of transient impulsive signals is described. The experimental results on investigation of the sensor are given.

## 2. SLOTLINE SENSOR DESIGN

Three basic types of the slotline sensor of various shapes and sizes were investigated. An a-type sensor is a piece of metallized dielectric substrate of rectangular form with cutted slotline [4]. The sensor has length $L$ and width $W$ (Fig. 1a). Dimensions of the investigated a-type sensors are given in Table 1.

TABLE 1
DIMENSIONS OF THE SLOTLINE SENSORS OF A-TYPE.

| Type | Length, mm | Width, mm | Relative dimensions |
|---|---|---|---|
| a1 | 10 | 40 | $\tau/10 \times \tau/3$ |
| a2 | 20 | 40 | $\tau/6 \times \tau/10$ |
| a3 | 40 | 40 | $\tau/3 \times \tau/3$ |

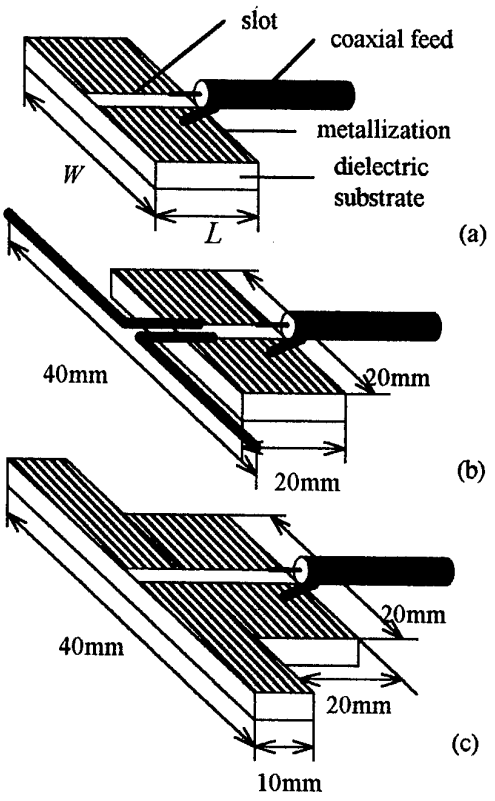



Fig. 1. Slotline sensors.

The slotline used for design of the sensors is made on 1.5 mm thick dielectric substrate with $\varepsilon = 4.2$. The width of the slot (0.2 mm) is choosen in order that the wave impedance of the slotline consists of about 75Ω at the frequency of 2 GHz.

A b-type sensor consists of a square stub of the slotline with soldered dipole at the front end. The dipole is made of 2mm diameter copper wire and have whole length of 40 mm (Fig. 1b). A c-type sensor is a piece of the slotline having form of capital T (Fig. 1c). This type of the sensor is some modification of b-type sensor. All dimensions of the c-type sensor are given in Fig. 1c.

All the sensors are fed directly by a 50Ω coaxial cable of 4 mm outer diameter with a few ferrite rings putted on the cable near the transition from the cable to

the slotline. As it follows from our early investigations, such type of the transition from the coaxial line to the slotline show small return losses in a wide band (DC to > 2.5 GHz) and good transient performance.

For comparison, the characteristics of usual thin-wire dipole were measured as well. The dipole was made of copper wires of 2 mm diameter and had whole length of 40 mm. It was fed by the same 50Ω coaxial cable with several ferrite rings placed near the feeding point to form matching transformer.

## 3. TIME DOMAIN MEASUREMENTS

The measurements were carried out in time domain making use of the set of following devices: short pulse generator (SPG), transmitting tapered slot antenna, stroboscopic oscilloscope C7-13 (10 GHz), analog-digital converter, and personal computer AT 386. The SPG produces a series of videopulses of triangle shape of 30 V amplitude and of duration $\tau$ = 0.4 ns. The transient field of linear polarization which is incident on the sensor under test was formed with the tapered slot antenna on dielectric substrate excited by the videopulse form SPG [5]. The signal received by the sensor is scaled in the stroboscopic oscilloscope and then digitized with the analog-digital converter. The developed software allows to perform an acquisition and processing of experimental data. The accuracy of the set is of about 2-3% when measuring both magnitude and time intervals.

The magnitude and the time shape of the signal received by the slotline sensors in E- and H-planes as well as the cross-polarization level were measured. The time shape of the signal received by the slotline sensors of a1-, a2-, and a3 types is the same of that received by the thin-wire dipole. As an example, the time shapes of the signal received by the a2-type sensor in both planes are depicted in Fig. 2. In the figure, the angle $\theta$ is an angle between the direction on the observation point and the line coinciding with the slot on the sensor. It is seen from the figure that the received signal has an approximate form of the third derivative of the excitation pulse. The time duration of the received signal is of about 1 ns.

The reception patterns on peak magnitude of the investigated sensors as well as of the thin-wire dipole are shown in Fig. 3. All patterns are normalized on value of signal received by the thin-wire dipole from the direction $\theta$ = 0°. In the direction of main maximum ($\theta$ = 0°), the signal received with the a1- or a2-type sensors is of about 2 dB grater then the signal received with the thin-wire dipole. An increase of the magnitude can be explained by the fact that the slotline sensor has enlarged area as compared to the thin-wire dipole and, hence, it has enlarged effective length.

In H-plane the reception patterns of this sensors are isotropic (Fig. 3b, 3c).

The a3-type sensor has almost omnidirectional reception patterns in both planes (Fig 3d). Slight nonsymmetry of the patterns with regard to the direction $\theta$ = 0° should be assigned to insufficient matching of the sensor with feeding cable. The cross-polarization level for the aforementioned slotline sensors and dipole is the same (of about −20 ÷ −25 dB).

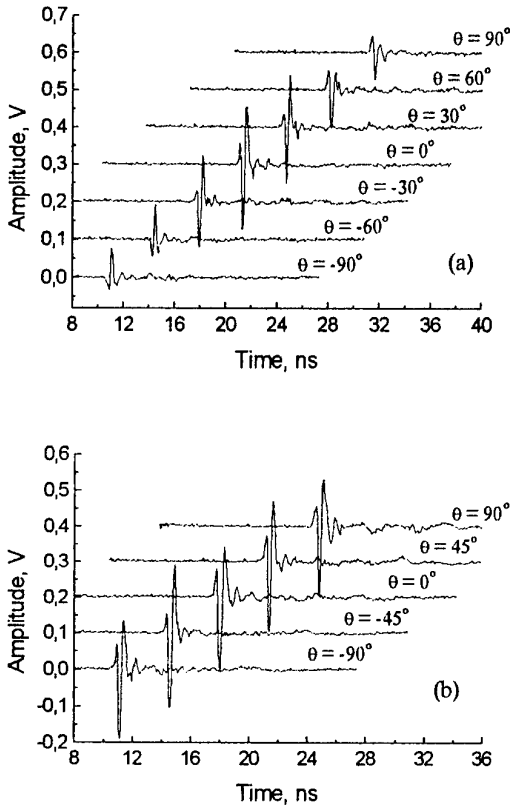



Figure 2. Time shapes of the signal received with the a2-type slotline sensor: a - E-plane, b - H-plane.

The slotline sensors of complex form bring some distortions into the received signal. At the same time, the magnitude of the received signal is smaller by 20 - 30% in comparison with the signal received with the thin-wire dipole (Fig. 3e, 3f). Apparently, this is due to the fact that in this case an interaction between signals received by soldered dipole and matching section of the slotline (b-type sensor) or by front and back edges of the sensor(c-type sensor) is take place. Therefore, the resulting signal has distorted form and reduced magnitude.

## 4. FREQUENCY DOMAIN RESULTS

The reflection coefficient of the slotline sensors as well as of the thin-wire dipole was measured in time domain using the same set of the devices. The frequency dependencies of the reflection coefficient in the range from 0.2 - 3 GHz were calculated from the

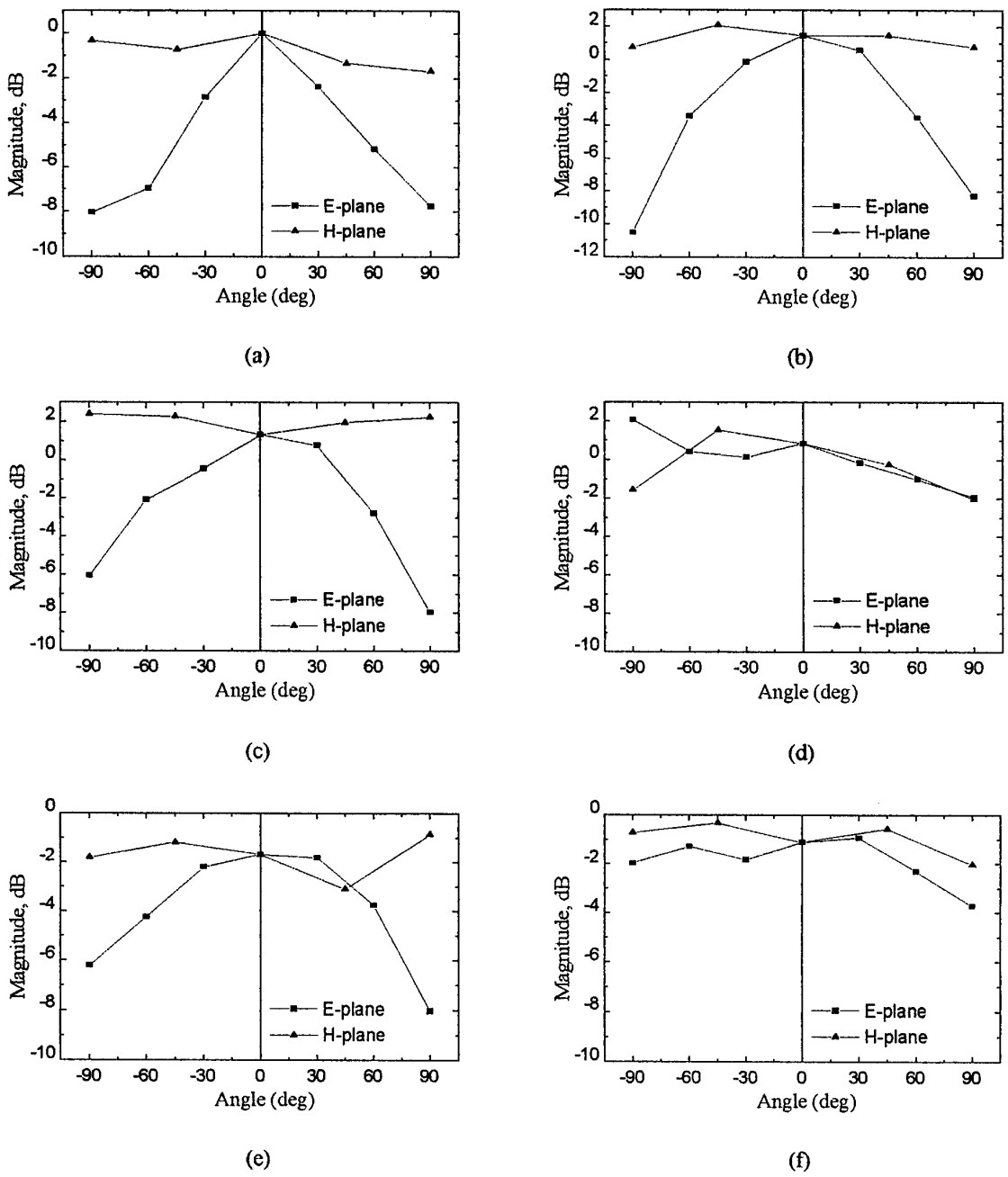



Figure 3. The reception patterns on peak magnitude of the thin-wire dipole (a), the a1-type sensor (b), a2-type sensor (c), a3-type sensor (d), b-type sensor (e), and c-type sensor (f).

measured time domain data making use of the Fast Fourier Transtorm and "time windowing" technique. The obtained results are shown in figure 4. One can see that the return losses for all sensors are very large values through whole band. It could be anticipated, because at this frequencies all investigated sensors are small in comparison with space duration of the radiated pulse (see Table 1).

## 5. CONCLUSIONS

A new type of sensor for transient electromagnetic fields based on a piece of the slotline was developed and experimentally investigated.

The proposed sensor has grater directivity as compared to a thin-wire dipole while keeping the same time shape of the received signal and the same cross-polarization level. It is easy for fabrication and can

find application in checking and measurements of both sinusoidal and transiend fields.

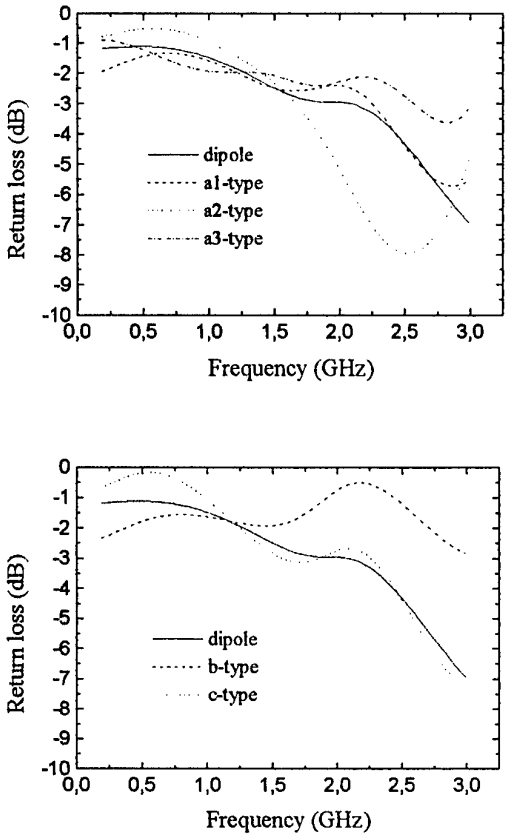



Figure 4. Frequency dependence of the return losses of the slotline sensors.

## 6. REFERENCES

6.1. M. Kanda, "Time domain sensors for radiated impulsive measurements," IEEE Trans. Antennas Propagat., Vol. 31, No. 5, 1983, pp. 438-444.

6.2. E. A. Theodorou, M. R. Gorman, P. R. Rigg, and F. N. Kong, "Broadband pulse-optimised antenna," IEE Proceedings, Vol. 128, Part H, No. 3, 1981, pp. 124-130.

6.3. K. L. Shlager, G. S. Smith, and J. G. Maloney, "Optimization of bow-tie antennas for pulse radiation," IEEE Trans. Antennas Propagat., Vol. 42, No. 7, 1994, pp. 975-982.

6.4. S. B. Cohn, "Slot line on a dielectric substrate," IEEE Trans. Microwave Theory Tech., Vol. 17, No. 10 1969, pp. 768-778.

6.5. S. N. Pivnenko, and N. N. Kolchigin. "Transient excitation of tapered slot antennas on a sharpen substrate", Proceedings of the XXVI General Assebly URSI, Toronto, Canada, 1999, p. 109.

## BIOGRAPHICAL NOTE

**Sergey N. Pivnenko** received combined B.Sc. and M.Sc degree in radiophysics and the Cand. Phys.-Math. Sci. (Ph.D. equivalent) degree in radiophysics from Kharkov State University, Kharkov, Ukraine, in 1995 and 1999, respectively.

He is a Research Fellow at the Chair of Theoretical Radiophysics at Kharkov National University. His current research interests include transient wave radiation/reception and scattering from stratified media and inclusions in that media; computer-aided design, experimental and theoretical analysis of passive microwave-circuit components, antennas and antenna arrays.

EMC 2000 INTERNATIONAL WROCŁAW SYMPOSIUM ON ELECTROMAGNETIC COMPATIBILITY

# LOOP ANTENNA IN THE EMISSION MEASUREMENTS

**Tadeusz W. Więckowski**

Wrocław University of Technology
Institute of Telecommunication and Acoustics
Wybrzeże Wyspiańskiego 27, 50-370 Wrocław, POLAND
Phone: +48 71 3214998, Fax. +48 71 3223473

*The paper herein presents various issues related to the use of loop antennas for alternative emission measurements. The theoretical possibilities to use a half of the loop antenna supplied relative to a conductive surface have been presented for an emission measurement stand. The calibration procedures and sample measurement results have also been presented.*

## 1. INTRODUCTION

Loop antennas have wide application in device EMC tests. They are widely used as electromagnetic field component (electrical and magnetic) measurement probes allowing for measurements in the frequencies and time domain. They are also used as simulators to test the test objects resistance to impulse electromagnetic stress. Within the last few years they also have found their way into test stands, used for alternative measurements of device electromagnetic emissions.

The issues related to establishing the level of emissions radiated by the devices, systems and installations (objects) is important not only for electromagnetic compatibility reasons, but also because of the frequent need to maintain a certain secrecy of the transmitted or processed information. There are devices available today that allow for such information to be retrieved based on spurious electromagnetic fields. This is the main reason why highly developed countries pay so much attention to emission research. The emission requirements of telecommunications systems are nowadays considered as basic parameters, similar to the mechanical and environmental requirements.

The possibilities to use double loaded loop antennas for alternative measurement of emissions have been presented for the first time, by the author of the paper herein, in 1990. The Alternative emission measurement methods consist of determining the parameters of the electromagnetic interference source instead of the radiated electromagnetic field. Based on the works of Hansen and Wilson it is clearly evident, that the source of the interference (the tested object) can be replaced by equivalent dipoles: and electrical one with the moment ($\overline{p}$), a magnetic one with the moment ($\overline{m}$) and a quadrupole with the moment ($\overline{q}$).

If the size of the tested object is less then the minimum wavelength of the radiated electromagnetic field, then in order to properly determine the value of the vector magnetic potential characterizing the radiating object, it is necessary to consider just the moments of the equivalent dipoles: the electrical and magnetic ones [1,2]. Knowing the moments of the equivalent electrical and magnetic dipoles of the interference source (tested device), the level of the radiated interference can be determined using analytical methods.

The double loaded loop antennas allow for an independent and simultaneous measurement of the electrical moments of both the electrical and magnetic equivalent dipoles.

Our works concentrated mostly on a measurement stand consisting of three orthogonal double loaded loop antennas. The works of Kanda are especially interesting in this field. However, the analytical relations presented by him are true only for the lower frequencies. Further on in the paper we present a measurement stand using a half of a double loaded antenna supplied relative to a conductive surface. We also present additional analytical relations allowing for the determination of the level of radiated interference even for the high frequencies.

## 2. MEASUREMENT STAND

The analysis herein covers a measurement stand consisting of a half of a double loaded loop antenna placed perpendicular to a perfectly conductive surface. The tested object has been placed in the middle of the antenna. The voltages measured at the antenna load points are caused by the currents induced by the electromagnetic field radiated by the tested object.

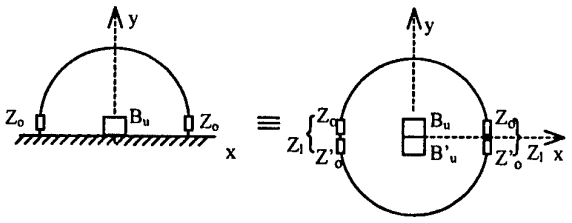



Fig.1. Block schematic of the test stand and its substitute diagram

For the purpose of analysis, it is convenient to replace the half of the antenna placed above a perfectly conductive surface along with the tested object, with an antenna and its mirror reflection along with an object and its mirror reflection placed in the middle of the loop antenna (Fig.1.).

Based on the works of Hansen and Wilson it is clearly evident, that the tested object and its mirror reflection can be replaced with the equivalent dipoles: an electrical one with the moment ($\overline{p}$ '), a magnetic one with the moment ($\overline{m}$ ') and a quadrupole with the moment ($\overline{q}$ '). If the size of the tested object is less then the minimum wavelength of the radiated electromagnetic field then in order to properly determine the value of the vector magnetic potential characterizing the radiating object, it is necessary to consider just the moments of the equivalent dipoles: the electrical and magnetic ones [2,3,9,10]. Thus:

$$\overline{A}(\overline{r}) \approx \frac{\mu_0}{4\pi} \cdot \frac{e^{-jk_0 r}}{r} \left[\overline{p}' - jk_0 r \times \overline{m}'\right] = \frac{\mu_0}{4\pi} \left[\overline{A}_p(\overline{r}) - jk_0 \overline{A}_m(\overline{r})\right] . \quad (1)$$

The total magnetic potential vector at the point of observation, which is caused by the radiation from the tested object, consists of the superposition of the vector magnetic potentials from the equivalent electrical dipole

$$\overline{A}_p(\overline{r}) = \frac{e^{-jk_0 r}}{r} \overline{p}' , \quad (2)$$

and the equivalent magnetic dipole

$$\overline{A}_m(\overline{r}) = \frac{e^{-jk_0 r}}{r} \overline{1}_r \times \overline{m}' . \quad (3)$$

The electrical field component tangent to a loop antenna with the radius b and loaded with the same impedance $Z_l$ at both opposite points ($\varphi = 0$) and ($\varphi = \pi$) is described by the following relation:

$$E'(b,\varphi) = A_0 + A_1 \cos\varphi + B_1 \sin\varphi , \quad (4)$$

in which:

$$A_0 = m'_z g_m , \quad A_1 = p'_y g_e , \quad B_1 = -p'_x g_e , \quad (5)$$

$$g_m = \frac{\varsigma_0}{4\pi} \left[\frac{k^2}{b} - \frac{jk}{b^2}\right] e^{-jkb} , \quad (6)$$

$$g_e = \frac{-\varsigma_0}{4\pi} \left[\frac{jk}{b} + \frac{1}{b^2} + \frac{1}{jkb^3}\right] e^{-jkb} . \quad (7)$$

Using the boundary conditions for the electrical field components tangent to the surface of the antenna wire:

$$E'(b,\varphi) + E(b,\varphi) = 0 \quad (8)$$

in which $E'(b,\varphi)$ is the electrical field component caused by the equivalent electrical and magnetic dipoles, and $E(b,\varphi)$ is the electrical component caused by the current flowing in the antenna, we obtain the following equation:

$$\frac{j\varsigma}{2} \sum_{n=-\infty}^{\infty} \left[a(n) I(n) - b E'_b(n)\right] e^{-jn\varphi} = -Z_l I(0) \delta(\varphi) - Z_l I(\pi) \delta(\varphi - \pi) \quad (9)$$

in which:

$$a(n) = \frac{kb}{2} \left[\mu(n+1) + \mu(n-1)\right] - \frac{n^2}{kb} \mu(n) , \quad (10)$$

$$\mu(0) = \frac{1}{\pi} \ln\left(\frac{8b}{a}\right) - \frac{1}{2} \int_0^{2kb} \left[\Omega_0(x) + jJ_0(x)\right] dx , \quad (11)$$

$$\mu(n)=\mu(-n)=\frac{1}{\pi}\left[K_0\left(\frac{na}{b}\right)I_0\left(\frac{na}{b}\right)+c_n\right]-\frac{1}{2}\int_0^{2kb}\left[\Omega_{2n}(x)+jJ_{2n}(x)\right]dx \quad , \tag{12}$$

$$c_n=\ln(4n)+\gamma-2\sum_{m=1}^{n}\frac{1}{2m+1}, \quad \gamma=0{,}577216 \tag{13}$$

where: I(n) is the Fourier distribution coefficient for the currents flowing in the antenna; $E_b^i(n)$ are the Fourier distribution coefficients for the electrical fields tangent to the antenna wire caused by the equivalent electrical and magnetic dipoles; $\Omega_n(x)$ are the Lommel-Weber functions; $J_n(x)$ are the Bessel functions of the first kind an n-th order; $I_0(na/b)$ are the modified Bessel function of the first kind and 0 order; $K_0(na/b)$ is the modified Bessel function of the second kind and 0 level and where $\delta(\varphi)$ is the delta function.

Solving the equation (9) for I(n) and substituting the resulting expression in the equation:

$$I(\varphi)=\sum_{n=-\infty}^{\infty}I(n)e^{jn\varphi} \tag{14}$$

we obtain a relation describing the current flowing in the antenna.

$$I(\varphi)=\sum_{n=-\infty}^{\infty}\frac{1}{a(n)}\left[2\pi bE_b^i(n)e^{-jn\varphi}-I(0)Z_l e^{-jn\varphi}-I(\pi)Z_l e^{-jn(\varphi-\pi)}\right] \tag{15}$$

If in place of the ( φ ) argument we substitute the angle values characteristic to the antenna loads we obtain a system of equations, which if solved for I(0) and I(π) give us the relations describing the currents flowing through the antenna loads.

$$I(0)=\frac{2b}{j\varsigma}\left[\frac{m_z' g_m}{(1+2Y_0Z_l)a(0)}+\frac{2p_y' g_e}{(1+2Y_1Z_l)a(1)}\right] \tag{16}$$

$$I(\pi)=\frac{2b}{j\varsigma}\left[\frac{m_z' g_m}{(1+2Y_0Z_l)a(0)}-\frac{2p_y' g_e}{(1+2Y_1Z_l)a(1)}\right] \tag{17}$$

where:

$$Y_0=\frac{1}{j\pi\varsigma}\left[\frac{1}{a(0)}+\sum_{n=1}^{\infty}\frac{1}{a(2n)}\right], \tag{18}$$

$$Y_1=\frac{2}{j\pi\varsigma}\left[\sum_{n=1}^{\infty}\frac{1}{a(2n-1)}\right]. \tag{19}$$

The admittance values $Y_0$ and $Y_1$ in the relation (16) and (17) are the relevant admittance values of the magnetic and electrical fields. Adding up the currents flowing through the antenna loaded with the two opposite identical impedance values, we obtain a resultant signal dependant only on the component moment of the magnetic dipole normal to antenna surface moment.
Summing up the currents flowing at the antenna load, we obtain a resultant signal depend only on the component moment of the electric dipole tangential to the antenna surface. Once we know the sum and difference of the currents flowing through the antenna loads, we can determine the components of the electrical moments for the equivalent electrical and magnetic dipoles.

$$m_z'=\frac{j\varsigma I_S\left[1+2Y_0Z_l\right]a(0)}{4bg_m}, \tag{20}$$

$$p_y'=\frac{j\varsigma I_d\left[1+2Y_1Z_l\right]a(1)}{8bg_e}. \tag{21}$$

In an actual measurement setup the sums and differences of the currents flowing through the loads are determined by measuring the voltage differences and sum between $U_d$ and $U_s$ present at the loads $Z_o=0.5Z_l$. Taking the above into account and the fact that the moments of the electrical and magnetic dipoles meet the following condition:

$$\overline{m'}=2\overline{m} \quad \overline{p'}=2\overline{p} \tag{22}$$

the relations (20) and (21) can be written as:

$$m_z=F_m I_S, \tag{23}$$

$$p_y=F_e I_d, \tag{24}$$

where:

$$F_m=\frac{j\varsigma_S\left[1+4Y_0Z_o\right]a(0)}{8bg_m}, \tag{25}$$

$$F_e = \frac{j\varsigma[1+4Y_1Z_o]a(1)}{16bg_e} \quad . \qquad (26)$$

The remaining components $(m'_x, m'_y, p'_x, p'_z)$ of the moments for the electrical and magnetic dipoles can be determined by measuring the sums and differences of currents flowing through the remaining two orthogonal placements of the object within the test space area (center of the antenna).

## 3. CALIBRATION OF THE TEST STAND

The issues presented above pertained to a loop antenna placed above a conductive surface with an infinite surface area. An actual test stand consists of a half of the loop antenna above a conductive surface with finite dimensions. Additional considerations need to be also taken into account for the external influences affecting the transfer function relating the electrical moments of the equivalent electrical and magnetic dipoles to the sum and difference of the currents at the antenna loads. Considering the above, the key consideration for an accurate determination of the interference radiated by the tested device into the external environment, is the knowledge of the transfer function. This function can be determined experimentally. It is recommended to determine the transfer function at the actual location of the test stand, right before performing the interference measurements. The calibration process starts with the placement of an electrical dipole with a known electrical moment into the center of the loop antenna (measurement space) and measuring the voltage difference present at the loop antenna loads.

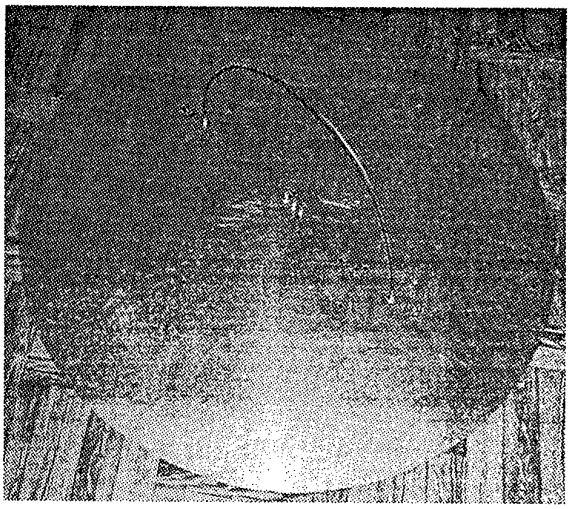


Fig. 2. Electrical and magnetic dipole in the center of the loop antenna (the measurement space)

The comparison of the measured values to the values calculated based on the relation (26) for the transfer function for the electrical dipole has been presented in Fig. 3. The occurring differences arise from the fact that the measurement antenna is placed above a shield having finite dimensions (diameter of the shield 1 m, diameter of the loop antenna 0,4 m) as well as by external influences.

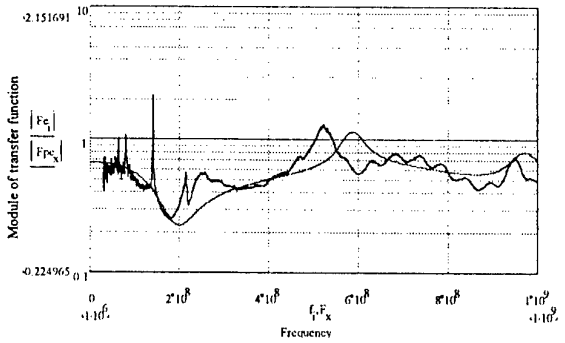



Fig. 3. Module of the transfer function relating the equivalent electrical dipole moment to the voltage difference at the antenna loads ($F_{ei}$ – calculated value, $F_{pex}$ – measured value)

The process for calibrating the transfer function relating the equivalent magnetic dipole moment to the voltage sum at the antenna loads is also similar - in place of the elementary electrical dipole in the previous setup, an elementary magnetic dipole is place and the sum of the voltages at the antenna loads is measured. The comparison of the measured values to the ones calculated based on transfer function (25) for the magnetic dipole is presented in Fig.. 4.

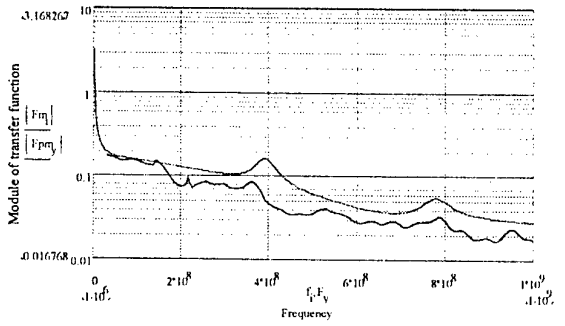



Fig. 4. Module of the transfer function relating the magnetic dipole moment to the voltage sum present at the antenna loads ($F_{mi}$ – calculated value, $F_{pmy}$ – measured value)

The measured transfer functions serve as the basis for calculating the electrical moments for the equivalent electrical and magnetic dipoles of the tested devices.

## 4. CLOSING NOTES

A practical example of a test stand using a half of a loop antenna supplied relative to a conductive surface has been presented in Fig. 5.

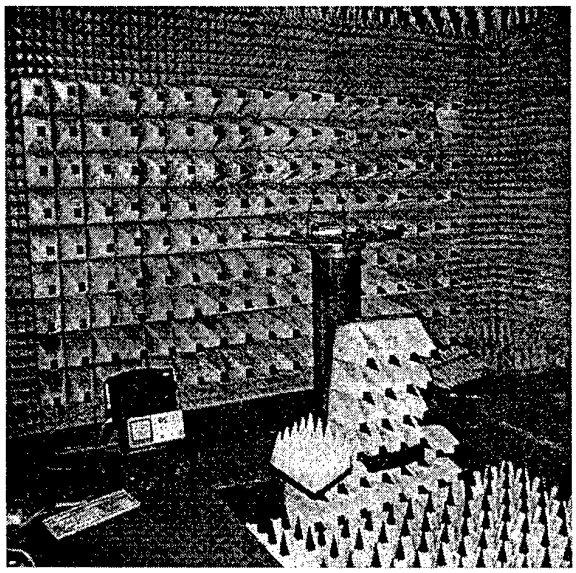


Fig. 5. Example test setup located in a an echoic room

In order to determine the electrical moments of the equivalent electrical and magnetic dipoles, the tested device shall be placed in the measurement space of the stand (the center of the loop antenna) and measurements are to be taken for the sum and difference of the voltages at the antenna loads for all three orthogonal placements of the tested object (Fig. 6).

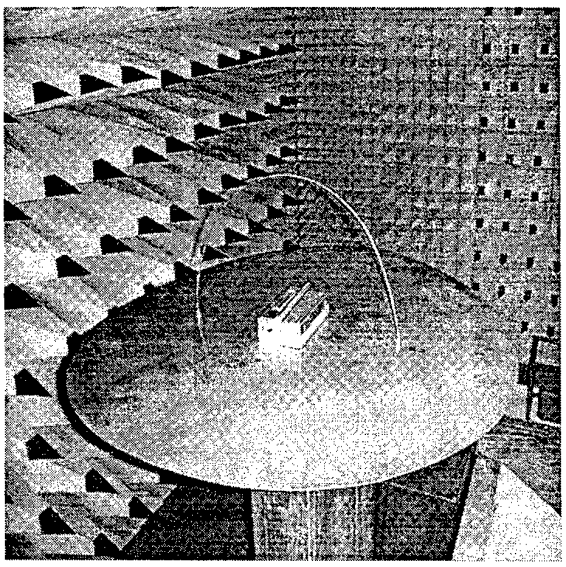


Fig. 6. The tested object within the measurement space

Having measured the transfer functions for the electrical and magnetic dipoles and also knowing the sums and differences of the voltages at the antenna loads for all three orthogonal placements it is possible to determine the electrical components of the moments of the equivalent electrical $(p_x, p_y, p_z)$ and magnetic $(m_x, m_y, m_z)$ dipoles. Knowing the electrical moments of the equivalent electrical and magnetic dipoles it is possible to determine the field radiated by the tested object in an open space. For a test object placed over a conductive surface (open area test site or an echoic room conditions), the radiated field is not only a superposition of the fields of the equivalent electrical and magnetic dipoles, but also of their mirror reflections [2,3,9].

$$\bar{E}(\bar{r}) = -j\frac{k_0 \zeta_0}{4\pi}\left[\begin{array}{l}\left[\dfrac{e^{-jk_0 r_1}}{r_1}\bar{F}_p(\bar{r}_1,\bar{p}) + \dfrac{e^{-jk_0 r_2}}{r_2}\bar{F}_p(\bar{r}_2,\bar{p})\right] + \\ jk_0\left[\dfrac{e^{-jk_0 r_1}}{r_1}\bar{F}_m(\bar{r}_1,\bar{m}) + \dfrac{e^{-jk_0 r_2}}{r_2}\bar{F}_m(\bar{r}_2,\bar{m})\right]\end{array}\right] \tag{27}$$

where:

$$\bar{F}_p(\bar{r},\bar{p}) = \left[\begin{array}{l}\bar{1}_x\left[p_x\left(\dfrac{x^2z^2}{\rho^2 r^2} + \dfrac{y^2}{\rho^2}\right) - p_y\dfrac{xy}{r^2} - p_z\dfrac{xz}{r^2}\right] + \\ +\bar{1}_y\left[-p_x\dfrac{xy}{r^2} + p_y\left(\dfrac{y^2z^2}{\rho^2 r^2} + \dfrac{x^2}{\rho^2}\right) - p_z\dfrac{yz}{r^2}\right] + \\ +\bar{1}_z\left[-p_x\dfrac{xz}{r^2} - p_y\dfrac{yz}{\rho^2} + p_z\dfrac{\rho^2}{r^2}\right]\end{array}\right], \tag{28}$$

$$\bar{F}_m(\bar{r},\bar{m}) = \left[\begin{array}{l}\bar{1}_x\left[m_y\dfrac{z}{r} - m_z\dfrac{y}{r}\right] + \\ +\bar{1}_y\left[-m_x\dfrac{z}{r} + m_z\dfrac{x}{r}\right] + \\ +\bar{1}_z\left[m_x\dfrac{y}{r} - m_y\dfrac{x}{r}\right]\end{array}\right]. \tag{29}$$

in which ($r_1$) is the distance of the observation point to the tested object,

$$r_1 = \sqrt{r^2 + (z-h)^2}\ , \tag{30}$$

and ($r_2$) is the distance of the observation point to the mirror reflection of the tested object.

$$r_2 = \sqrt{r^2 + (z-h)^2}\ . \tag{31}$$

We would like to remind that the mirror reflection of the equivalent electric dipole with the moment ( $\bar{p}$ ) having the components ( $p_x, p_y, p_z$ ) is a dipole with a moment ( $\bar{p}'$ ) having the components ( $-p_x, -p_y, p_z$ ). On the other hand the mirror reflection of the equivalent magnetic dipole with the moment ( $\bar{m}$ ) with the components ( $m_x, m_y, m_z$ ) is a dipole with a moment ( $\bar{m}'$ ) with the components ( $m_x, m_y, -m_z$ ).

Based on the moment method calculations it is clearly evident, that the maximum size of the tested objects cannot exceed one third of the antenna diameter and that the size of the conductive surface should be at least twice the diameter of the loop antenna. The upper measurement frequency depends only on the size of the tested object. The proposed method can be used for a frequency range, within which it can be substituted with equivalent electrical and magnetic dipoles.

## 5. REFERENCES


[1] H. Koepke, M. T. Ma, *„A New Method for Determining the Emission Characteristics of Unknown Interference Source"*, Proc. of the 5th Symposium and Exhibition on EMC, Zurich, March 1983, pp.35-40.

[2] P. Wilson, D. Hansen, D. Hoitink, *"Emission Measurements in a GTEM Cell: Simulating Free Space and Ground Screen Radiation of a Test Device"*, Research Report, Baden, June 1988.

[3] P. Wilson, D. Hansen, D. Koenigstein, *"Simulating Open Area Test Site Emission Measurements Based on Data Obtained in a Novel Broadband TEM Cell"*, International IEEE Symposium on EMC, Denver, 1989, pp. 171-177.

[4] S. Berger, "A Variable Position, Gravity Down G-TEM Configuration", Proc. of the International Symposium on EMC, Zurich, March 1995.

[5] L. Carbonini, "A New Procedure for Evaluating Radiated Emissions from Wideband TEM Cell Measurements", Proc. of the International Conference on Electromagnetic in Advanced Application, Turin, Italy, Sept. 1995, pp. 133-136.

[6] A. Nothofer, A.C. Marvin, T. Konefal, *"Radiated Emission measurements in GTEM Cells Compared with Those of an OATS"*, Proc. of the 12th International Symposium on EMC, Zurich, 1997, pp. 317-320.

[7] T. W. Wieckowski, *"Loop antennas in electromagnetic field metrology"*, Scientific Papers of the Institute of Telecommunication and Acoustics of the Technical University of Wrocław, No. 34, Wrocław 1992.

[8] M. Kanda, D. A. Hill, "New Emission Measurement Method for an Electrically Small Source: a Three Loop Method and TEM Cell Method", Proc. of the 11th Symposium on EMC, Wrocław, June 1992, pp. 310-312.

[9] M. Kanda, D. A. Hill, *"A Three Loop Method for Determining of an Electrically Small Source"*, IEEE Transactions on EMC, Vol. 34, No. 1, August 1994, pp. 1-3.

[10] T.W. Wieckowski, Z.M. Jóskiewicz, *"Loop antennas in the EMC metrology"*, Proc. of the 14th Symposium on EMC, Wrocław, June 1998, pp. 242-246.

[11] M. Kanda: *An Optically Linked Three-Loop Antenna System for Determining the Near Field Characteristics from an Electrically Small Source*, Supplement of Proc. of the 13th International Symposium on EMC, Zurich, 1999, pp. 155-160.


## Biographical note

**Tadeusz W. Wieckowski** is with the Institute of Telecommunication and Acoustics of the Wrocław University of Technology (Poland), where he works as a Professor in the field of communications systems and electromagnetic compatibility. He received his MSc and Ph.D. degrees in telecommunication in 1976 and 1980, respectively. He is a member of the Association of Polish Electrical Engineers and the Organizing Committee of the Wrocław Symposia. Mr. Wieckowski is an author of some 120 papers presented on international and national conferences.

EMC 2000 INTERNATIONAL WROCŁAW SYMPOSIUM ON ELECTROMAGNETIC COMPATIBILITY

# CALIBRATION OF THE MICROWAVE OVEN FOR STUDIES OF MICROWAVE ELECTROMAGNETIC RADIATION EFFECTS ON CELL CULTURES

S.Kharkovsky[1,2], A.Allahverdiyev[1], M.Can[1]

[1]Department of Electrical and Electronics Engineering Cukurova University, 01330 Balcali, Adana, TURKEY
Tel. 90 322 338 68 68. Fax 90 322 338 63 26.
E-mail: kharkovsky@mail.cu.edu.tr
[2]Institute for Radiophysics & Electronics National Academy of Sciences of Ukraine, 310085 Kharkov, UKRAINE

*The results of investigation and calibration of the microwave oven for study microwave electromagnetic radiation effects on the cell cultures are reported. A new method for the measurement of heating distribution in standard microwave oven (MWO) is developed. It is shown that it allows to measure and record field patterns in unloaded and loaded MWO and the heating distribution in it with load movement. The calibration protocol for microwave irradiated cell culture in the MWO is reported.*

## 1. INTRODUCTION

Microwave energy can result in pathophysiological manifestations and also can affect neural and immunological functions in humans and animals. Some reactions may lead to effects which constitute potential or actual health hazards [1]. The microwave electromagnetic field influence on biological systems have been explored in vitro and in vivo. However, the information available at the present time is not sufficient to explain microwave-induced biological effects because the investigations of a microwave influence on the cells, the microorganisms are still carried out [2]. Besides, the methods of microwave treatment have been used for fast fixation [3], denaturation, hybridization [4], sterilization [5] etc. Most of these methods use microwave oven (MWO) which is designed for household use because of its availability, low cost, safety conditions etc.

The use of microwave oven for biological studies of microwave effects without its calibration often causes irreproducible results because it has some disadvantages. These disadvantages are non-uniformity of field distribution ("hot" and "cold" spots), multi-mode spectra, effect of load etc. Besides, features of the sample (cell suspensions) are: small size, presence of water and different medium etc. The composition of sample container and the volume of solution around the sample are among the most important determinants of uniform microwave irradiation.

It should be noted that in a recent paper by G. R. Login and A. M. Dvorak [3], an excellent review of the use of microwave oven for fixation in morphologic studies and a calibration method to improve fixation results are given.

In this paper the results of the investigation and the calibration of the microwave oven for study microwave electromagnetic radiation effects on the cell cultures are reported.

First, we investigate the microwave oven without and with loads and give results of the measurement of field distribution in large oven cavity by using a new method. Then, on the basis of these results, we present the calibration protocol for microwave irradiated cell suspensions in the cavity of the microwave oven. Finally, results of the investigation of microwave influence on the cancer cell line of human (HEp – 2) contained in medium EMEM are reported.

## 2. INVESTIGATION AND CALIBRATION OF THE MICROWAVE OVEN

In principle, the standard MWO is a closed metal box with some means of coupling in power from generator and the dimensions of the box are several wavelengths in three dimensions. Such a box supports a large number of resonant modes in a given frequency range. However, when such an oven is partly filled with a workload, the resonance curves of the modes will overlap in frequency to give a continuous coupling into the load. The field distribution in a closed box is given by the sum of all the modes excited at the given operating frequency, each mode giving a basic sinusoidal power variation in space along the principal coordinate axes, and satisfying the well-known field equations. There is, therefore, fundamentally a spatial non-uniform complex distribution of field within a multi-mode oven [6].

In practice, the field distribution in the oven is more complicated than indicated above, because the characteristic impedance of the workload is substantially different from free space, giving secondary reflections from the surface of the workload. That is why it is important to study the mode pattern with the given workload in the MWO.

2.1. Field and heating distributions

A temperature and a power intensity map in empty MWO were determined by using a fiberoptic sensor [7], a probe method [6,8],. These techniques minimally perturb the microwave field, but they are very complex because the box is closed. Several methods were used for identifying hot spots (i.e., areas of microwave energy maximums). For example, the field distribution can be demonstrated by using a neon bulb array [3], a water-filled tube array [9], a radar absorbent material that changes color following the microwave absorbance [3] etc. But these methods only demonstrate the field distributions in MWO.

We have developed a new method for the investigation of field distribution in MWO using wet thermal paper. The lists of this paper are kept in special light forms and located in different planes within MWO. Developed method of the field distribution measurement provides a quick and easy method to identify and record the mode patterns in the oven cavity with and without a load.

We have investigated microwave field distribution on a little above the floor of MWO according to the demands of our future experiments with several samples of cell culture ( about 1-2 ml) in glass tubes. In fact, a list of the wet thermal paper is located on a MWO rotary plate with a diameter of 300 mm which can rotate or not.

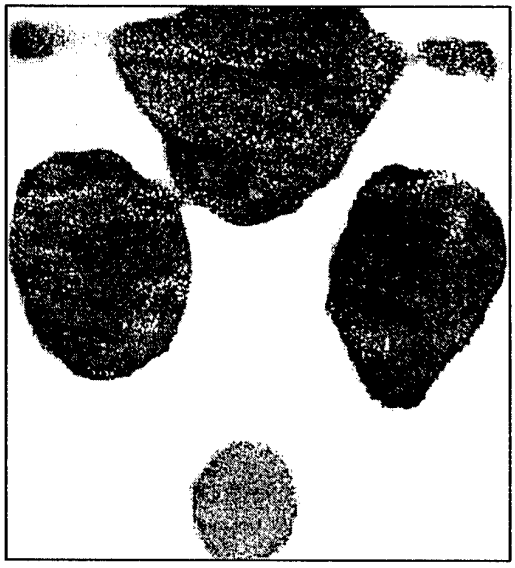


**Fig.1**. The field pattern on the thermal paper after irradiation in the unloaded microwave oven (360 watts, 30 sec) without the rotation of the plate.

Fig.1 and Fig.2 show the views of thermal papers after irradiation in MWO without rotation of the plate for unloaded (Fig.1) and loaded (Fig.2) MWO. A coupling element (output of magnetron) is located on the top of these figures. The load is water (100 ml) in a glass. Dark spots correspond to the maximum of the microwave field.

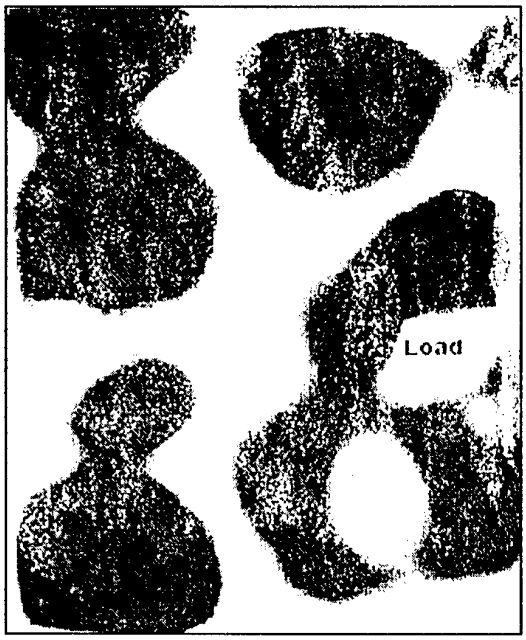



**Fig.2**. The field pattern on the thermal paper after irradiation in the loaded microwave oven (max power, 30 sec, 100 ml water load) without the rotation of the plate.

It can be seen from Fig.1 that the field distribution on the unloaded MWO plate is non-uniform, but there is at least one symmetry plane here. The location of the load in the MWO changes this field distribution (Fig.2). It becomes more non-uniform. The load in MWO not only changes the field distribution but also reduces the field intensity in maximum of the field. It should be noted that, in this shown case, the load is located in the area of the plate where the microwave field is absent in unloaded MWO (Fig.1) but it can be above this area of the plate because there are field variations in vertical planes.

Fig.3 and Fig.4 show the views of thermal papers after irradiation in MWO with the rotation of plate for unloaded (Fig.3) and loaded (Fig.4) MWO. The location of wet thermal paper and the load are the same as described in Fig.1 and Fig.2. But dark area shows the heating distribution as a result of the field influence on different places of the paper because both the thermal paper and the load move through maximum and minimum (nodes) of the microwave field.

We can see that the heating distribution in unloaded MWO (Fig.3) is uniform with the circle symmetry and the field is absent at the MWO center. The load do not markedly changes the heating distribution but rather reduces the field intensity.

As a result, the movement of the load in MWO can extend the area of the field influence uniformity. It is important for the irradiation of several samples of the same type instantaneously.

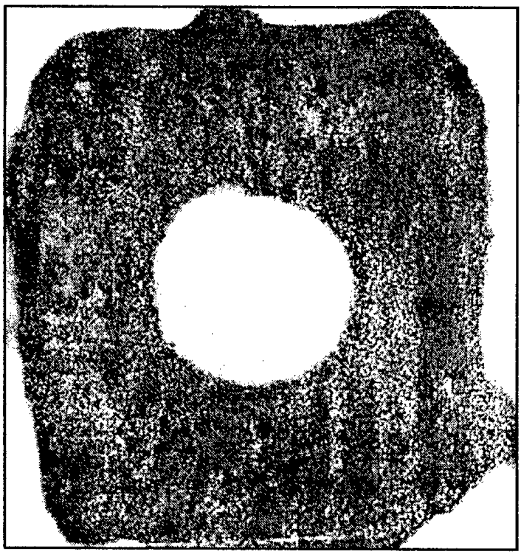


**Fig.3.**The view of the thermal paper after the irradiation in the unloaded microwave oven (360 watts, 30 sec) with the rotation of the plate.

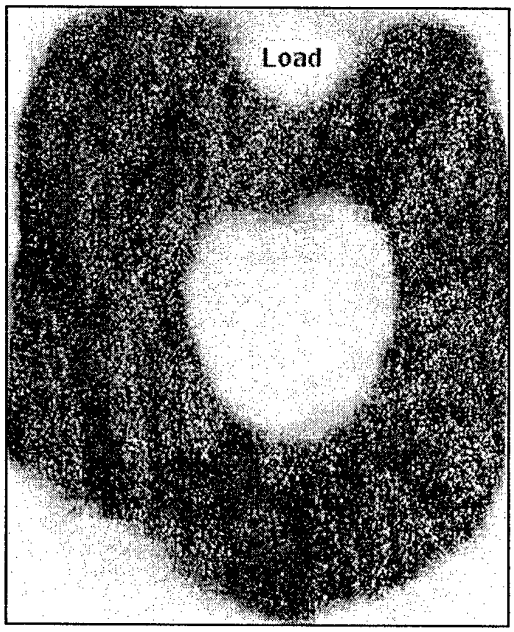



**Fig.4.**The view of the thermal paper after the irradiation in loaded microwave oven (360 watts, 45 sec, 100 ml water load) with the rotation of the plate.

2.2. Calibration protocol

We modeled the microwave field absorption in biological samples to predict their heating by using a medium EMEM irradiation and a final temperature measurement after microwave exposure. Each sample had volume which was approximately equal to 2 ml. The containers were metal-free glass tubes. Several tubes with this medium were irradiated at the same time.

As a result of these investigations, we can give the calibration procedure protocol as following:

1) The MWO power is set on minimum (90 or 180 W).
2) The load (200-300 ml water in glass) is located on the rotary plate of the MWO which is then pre-warmed for 1-2 min.
3) The microwave field distribution in the empty MWO is determined by using the wet thermal paper which is located on its rotary plate.
4) The load (200 ml room temperature water in a glass) and the needed number of tubes each of those containing about 2 ml of the same type of medium that will be used for cell culture are located uniformly on the areas of the ring where maximum microwave power distribution was recorded in step 3 on the new wet thermal paper.
5) The microwave field distribution in MWO with the load and the samples is determined by using the thermal paper. This paper can also be used to evaluate the time delay between the turning on of MWO (i.e., the paper is clean) and the beginning of the microwave influence (i.e., dark spots arise on the paper).
6) The dependence of the medium temperature on the irradiation time is determined by using temperature measurements of the medium after exposure.
7) The locations where the cell culture samples should be put are identified by determining the regions of the MWO plate that give the most uniform and the same type of fields in area of each sample and the need to raise the medium temperature from 20 to 50°C according to step 5 and 6.
8) The temperature of one of the tubes filled with medium (without cell) is measured after the microwave irradiation for checking.

By using this protocol, the microwave influence on the cancer cell line of human (Hep-2) containing in medium EMEM have been investigated. It's cell suspension which a final temperature must be less than 50°C.

## 3.CONCLUSIONS

The results of the investigation and the calibration of the microwave oven for study microwave electromagnetic radiation effects on the cell cultures are reported. Developed method of measurement of heating distribution in standard microwave oven by using wet thermal paper allow quickly and easily to measure and record the field patterns in unloaded and loaded MWO and heating distribution in it with load movement. The calibration protocol for microwave irradiated cell

culture in the MWO is reported. The main parts of it are 1) the measurement of the heating distributions in empty and loaded microwave oven with the rotary plate by using wet thermal paper, 2) the determination of the temperature of the same type of medium that will be used for cell culture after irradiation in the area where the maximum microwave power distribution was recorded in step 1. 3) the locations of the samples and the setting of the irradiation time according to the needed final temperature of themselves.

## 4. REFERENCES


4.1. S. M. Michaelson, "Microwave biological effects: an overview", Proc.IEEE, vol.68, N1, 1980, pp.40-49.

4.2. E. Marani, "Microwave applications in neuro-morphology and neurochemistry: safety precautions and techniques", Methods, vol. 15(2), June, 1998, pp.87-99.

4.3. G.R. Login, A.M. Dvorak, "Methods of microwave fixation for microscopy. A review of research and clinical applications: 1970-1992", Prog. Histochem. Cytochem., vol.27(4), 1994, pp.1-127.

4.4. M. Durm, F.M. Haar, M. Hausmann, H. Ludwig, C. Cremer, "Optimized Fast-FISH with alpha-satellite probes: acceleration by microwave activation", Braz. J Med. Biol. Res., vol. 30(1), Jan., 1997, pp.15-23.

4.5. S. K. Young, D. C. Graves, M. D. Rohrer, R. A. Bulard, "Microwave sterilization of nitrous oxide nasal hoods contaminated with virus", Oral Surg. Med. Oral Pathol., vol.60(6), Dec., 1985, pp.581-585.

4.6. A. C. Metaxas, R. J. Meredith, "Industrial microwave heating", Peter Peregrinus Ltd, London, 1988, ch.6, pp.130-150.

4.7. M. K. Sun, K. A. Wickersheim, A. Kamal, W. R. Kolbeck, "Fiberoptic sensor for minimally-perturbing measurement of electric fields in high power microwave environments", In : Microwave Processing of Materials 11 (Synder W. B., Sutton W. H. , Iskander M. F., Johnson D. L., eds.), 189, 141-145. –Materials Research Society, Pittsburgh, 1991.

4.8. T. G. Minran, " Microwave oven mode tuning by slab dielectric loads", IEEE Trans. Microwave Theory Techn., vol.26, N6, 1978, pp.381

4.9. L.L. Germash, E. D. Shlifer, "Device for an evaluation of the electromagnetic field distribution in microwave ovens", (in Russian) Electronic Techniques, Microwave Electronics, N3, 1982, pp.44-46.


## BIOGRAPHICAL NOTES

**Sergey N. Kharkovsky** was born in 1952. He graduated from Kharkov Institute of Radioelectronics (MC), Ukraine, in 1975, and received Ph.D. and D.Sc. degrees in radio physics from the Kharkov State University, Ukraine, in 1985, and from the Institute for Radiophysics & Electronics (IRE), Ukrainian Academy of Sciences, Kharkov, Ukraine, in 1994, respectively. Since 1975, he has been a Member of the Research Staff at the IRE. He has been a Visiting Professor at Electrical & Electronics Engineering Department of Cukurova University, Adana, Turkey, since 1998. His research interests include experimental investigations of open and shielded structures (dielectric wave guides and resonators, quasi-optical elements, diffraction gratings), devices (solid-state oscillators with quasi-optic metal-dielectric resonators, microwave oven) at microwaves and millimeter waves and their applications for a study of materials.

**Adil M. Allahverdiyev** was born 1951. He graduated from Medical School, Baku, Azerbaijan R. in 1974. He received Ph.D.,(1981) ,Dr. Med. Sc.(1990) degree at the Marcinovsky Institute of Medical Parasitology and Tropical Medicine, Moscow former USSR. He has been The Head of Labor Cultivation and Cryoprezervation of Cells Eukaryotos at the National Medical Research Institute of Prophylactic Medicine, Baku Azerbaijan Rep. He has been a invited as visiting scientist (Professor) at Dept. Microbiology, Medical Faculty of Cukurova University, Adana, Turkey, since 1993. His research interests include the mechanism of hemolysis induced by anti-malarial drugs; research on parasites, viruses -In vivo, in vitro biochemistry and biology of parasites, viruses , parasit host interactions, cultivation, cryoprezervation, pathophysiology, chemotherapy (combination by microwave) ,vaccine development.

**Memduh Can** was born in 1975. He received the B.S. degree from Cukurova University, Electrical-Electronics Engineering Department in 1998. He is currently enrolled to the M.S. program of the same department and working as a Research Assistant. His research interests include Telecommunications Systems, antenna design, microwave measurement techniques and microwave devices.

EMC 2000 INTERNATIONAL WROCŁAW SYMPOSIUM ON ELECTROMAGNETIC COMPATIBILITY

# THE NEAR-FIELD OF GSM 900/1800 HANDSET TERMINALS WITH BUIL-IN ANTENNAS

*Wojciech J. Krzysztofik*

**Wrocław University of Technology,** Institute of Telecommunication & Acoustics
The Radio Department
Wybrzeże Wyspiańskiego 27, 50-370 Wrocław, POLAND
e-mail: ***wojka@zr.ita.pwr.wroc.pl***

*This paper deals with the influence a handset phone, with new build-in compact planar antennas, on a human and surrounding medium. Simulations using the method of moments (MoM) for a wire-grid model of the planar inverted-F antenna (PIFA) treated together with a portable radio case have been carried out to evaluate radiation characteristics. The radiation pattern in both polarisation planes, and a near-E-field magnitude have been calculated. The modelling approach is compared with experimental results and previous work and good agreement is obtained.*

## 1. INTRODUCTION

Today we are poised to enter a world in which the conventional telephone-type instrument is no longer the medium we use to communicate but employ the wireless personal communication system (PCS) instead for sending messages and data to anyone, anytime and anywhere in the world. PCS systems are widely diverse and include fixed, low as well as high mobility systems, all of which rely upon the public network to some extent. Applications of these systems include direct broadcasting satellite (DBS), pagers, wireless phones, wireless local loops and data terminals. The latter can utilize radio ports to deliver fixed applications to homes or businesses, whereas a base station is needed for highly mobile applications that connects to the public network via switching office. In the near future several mobile satellite communication systems will provide global coverage to complement the existing terrestrial systems. A key component in providing high performance from such systems is the antenna of the handheld terminal. Accordingly, considerable attentions have been focused on antenna concept design and stringent requirements placed upon antenna performances have come to be extensively studied, specifically taking very nearby environmental radiating context into account.
Presently, whips or helices are typically used for cell-phones, wire or loops for pagers, and a variety of whips, small arrays or microstrip antennas are employed for wireless local area networks (WLANs) [1]. However, we include in this paper other antenna configurations (Fig. 1) that may have some desirable advantages over conventional design.

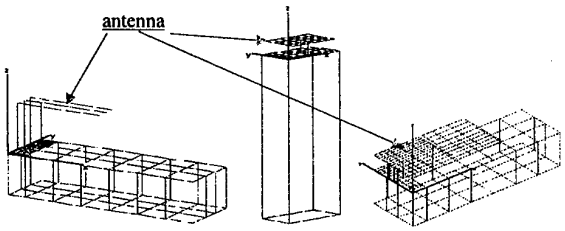



Fig. 1. Wire-grid models of various build-in antennas onto the handset: a) wire inverted-F antenna with two parasitic elements (IFA-PE), b) compact planar aerial (CPA), c) a planar inverted-F antenna (PIFA).

Cellular telephone handsets are now being designed to have dual- or multi-mode capabilities. In particular, there is requirement for internal antennas for GSM 900/ 1800 system and for terrestrial/satellite (e.g. GSM/IRYDIUM) personal global mobile communications systems.
Different system types require different antenna characteristics: terrestrial terminals require omnidirectional radiation patterns in the horizontal plane while satellite handhelds require a hemispherical radiation pattern.
So, it is suggested that there is a need for multi-frequency handset antennas. At present, some dual-band handset antennas have been developed based on the extension of wire antennas [2]. These antennas were made to resonate at two frequencies by simply adding another wire to the original antenna. However, there is now much interest in internal antennas, which have the desirable features of robustness and compactness. Some

internal handset antennas have now been developed to give small antenna size, improved bandwidth, and gain. Work on the effect of human interaction is receiving interest.

The aim of this paper is to present the performances of a new kind of miniature planar antenna designed for small-sized hand-held transceiver in presence of the human body. The analysis of dual-frequency PIFA's mounted on a radio case was done using the wire-grid model and method of moments (MoM).

## 2. SIDE-MOUNTED PIFA

The growing desire to replace the monopole or helix with more conformal, less obstructive elements has focused considerable attention on antennas such as the planar inverted-F antenna (PIFA) (Fig. 1c). Among existing built-in antenna schemes, the PIFA is one of the most promising case dates considering its compactness. In addition to portability, the PIFA exhibits sensitivity to both vertically and horizontally polarized radio waves and therefore is suitable for use with portable radio equipment in which antenna orientation is not fixed.

The linear inverted-F antenna , IFA, which is the original version of the PIFA, has been described by R.W.P. King et al. (1960) as a "shunt-driven inverted-L antenna-transmission line with open-end". The PIFA is constructed by replacing the linear radiator element of linear inverted-F antennas with a planar radiator element. These side-mounted elements consist simply of probe-fed conducting plate suspended above the conducting chassis. A short circuiting wire or strip is attached to one end of the suspended plate – a configuration that allows considerable reduction in the element resonant size.

Antennas are usually installed on a body with good conductivity, such as portable radio or automobile, and sometimes other antennas or conducting bodies are nearby, as on a tower. Thus, it is important to know the effects of nearby conducting bodies on the antenna performance.

The characteristics of a PIFA mounted on portable radio cases are different from those of PIFA on the infinite ground plane, and depends on both the antenna position on the case and dimensions of the radio case, because of the existence of surface currents on the radio case. To design the optimum antenna configuration for portable radio units, it is necessary to analyze the radiation and bandwidth characteristics inclusive of the radio case effects.

Modeling of the antenna problem in the presence of the head also shows that the pattern of the antenna, which is omni-directional in the azimuth plane when is isolated, becomes considerably asymmetrical due to the absorption by the head.

Nowadays, antenna performance prediction by computers gives satisfactory results quickly. When conducting body is less than about 5λ, the MoM method can successfully be used to calculate the characteristics of an antenna on the conducting body.

### 2.1. An antenna on a portable radio

The dual-band antenna consists of two separate radiating elements [3], [4], [5], as shown in Fig. 2, with the rectangular radiating element for 1.8 GHz-band and the L-shaped radiating element for 900 MHz-band, and has almost the same size as single-band planar inverted-F antenna operating at 900 MHz.

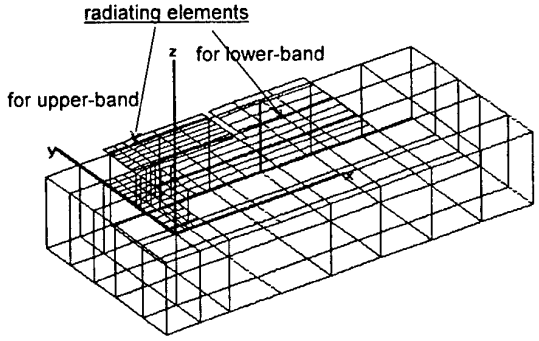



Fig. 2. Wire grid model of a PIFA antenna on a rectangular conducting body

The two radiating elements are grounded to the case at its corner and fed near the shorting pins using coaxial cable. An antenna element and a conducting bodies are treated in one unified system, that is, the conducting body is not taken as a ground plane but as a part of the antenna system itself.

### 2.2. MoM analysis

In this paper, the method of moments has been implemented to allow modeling and simulation of the build-in dual-band handset antenna.

An antenna and any other conducting objects in its vicinity that affect its performance may be modeled with strings of segments following the paths of wires (*wire-grid* model) and with patches covering closed surfaces. The basic devices for modeling structures (wires and flat patches) are short straight segments. Proper choice of the segments for a model is the most critical step to obtaining accurate results. The number of segments should be the minimum required for accuracy.

A conducting body is modeled by wire grids (wire radius: 0.0015λ): the six parallel wires perpendicularly intersecting nine parallel loops replace the conducting surfaces of the rectangular radio case (all 236 wires crosspoints are connected). Furthermore, the PIFA planar radiators are replaced by 121, and by 82 wires, for 0.9 and 1.8 GHz respectively. The feed in Fig. 2 is connected offset point from the corner of the radiator, where the wire-grid is highly dense.

The electric field integral equation (EFIE) for thin-wire-L-long structures of small or vanishing conductor volume has following form:

$$\vec{E}(\vec{r}_o) = \frac{j60\pi}{\lambda}\frac{\exp(-jkr_o)}{r_o}\int_L[(\hat{k}\cdot\vec{I}(l)\hat{k}-\vec{I}(l)]\exp(j\vec{k}\vec{r})\,dl \quad (1)$$

where $\vec{r}_o$ is the position of the observation point, $\hat{k} = \vec{r}_o / |\vec{r}_o|$, $k = 2\pi/\lambda$, and $\vec{k} = k\hat{k}$. The time convention exp(jωt) is omitted.

The EFIE is preferred to model surfaces for thin structures where there is little separation between a front and back surface.

The analysis is accomplished by numerical solution of integral equations for induced currents I(l) along wires into a grid model covering the surface. The integral equation is solved numerically by a form of the method of moments which applies to a general linear-operator equation,

$$\mathbf{L}\, l = e, \qquad (2)$$

where I is unknown response (current distribution), e is known excitation, and **L** is a linear operator (an integral in the present case).

The excitation may be an incident plane wave or voltage source on a wire, while the output may include current distribution, electric or magnetic field in the vicinity of the structure (near-field), and radiated fields (far-field).

In the NEC computer code [6] the unknown function I is expanded in a sum of basis functions, $I_j$, as

$$I = \sum_{j=1}^{N} \alpha_j I_j = \sum_j A_j + B_j \sin k(l - l_j) + C_j \cos k(l - l_j) \qquad (3)$$

where $|l - l_j| < \Delta_j / 2$, $l_j$ is the value of a l at the center of segment j and $\Delta_j$ is the length of segment j.

It means that wires are modeled by short straight segments with the current on each segment represented by three terms – a constant, a sine, and a cosine.

The set of equations for the coefficients $A_j$, $B_j$, $C_j$ are then obtained by taking the inner product of equation (2) with a set of weighting functions $\{w_i\} = \{\delta(\vec{r} - \vec{r}_i)\}$ ($\{\vec{r}_i\}$ is a set of points on the conducting surface). The result is a point sampling of the integral equations known as the collocation method of solution. Wires are divided into short straight segments with a sample point at the center of each segment. The solution, in matrix form, is then

$$[A, B, C] = [\langle w_i, \mathbf{L}\, I_j \rangle]^{-1} [\langle w_i, e \rangle] \qquad (4)$$

On the base of evaluated current distribution all circuit (e.g. input impedance) and field (e.g. near-, far-filed, power gain) parameters of the radiating structure can be determined.

## 3. EXPOSURE TO RF ENERGY AND SAFETY OF THE USER

Mobile and portable two-way wireless communication radios emit RF energy, which is as low as a fraction of a watt in the case of some portable phones and as high as 130 W for certain mobile stations. In normal use, handheld radios have the potential for causing higher exposure than mobiles because, although portable equipment rarely emits more than 7 W of RF power, a person's vital organs (e.g. the head) are in the immediate vicinity of the RF source. The interaction of the terrestrial mobile handheld terminal with human head has been widely investigated by many researchers [7], [8], [9].

There are two separate electromagnetic problems with regard to the effects of the human body. The first, of primary concern there, is the influence that the human body has on the field strength pattern of a body-mounted transceiver. This is the question of radio system performance and, rather coarse models give accurate representations of fields external to the body. The second electromagnetic problem concerns wave coupling into the body tissues. This problem is extensively covered elsewhere with respect to biological issues and dosimetry, and accurate representations of near fields, and its specific subject of standards. We will explore this issue only in the context of radio performance, and in terms of compliance to exposure standards and guidelines.

The perturbation of the antenna's free-space radiation pattern and the level of the energy absorbed by the human body are both significant, but are affected in detail by parameters such as operating frequency, antenna type and configuration of the human head and handset casing.

Let us now define what is relevant in a RF exposure. Until 1982, the exposure to RF electromagnetic fields (EMF) in the band of 100 kHz to 100 GHz was quantified in terms of the incident power density measured in $W/m^2$. This method of measurement proved to be grossly unsatisfactory at some RF frequencies due to fact that EM fields are coherently absorbed and has complicated structure in the vicinity of sources. Coherent absorption is a typical resonance phenomenon. The near-field exposure makes the use of the term power density practically meaningless. Clearly, the relevant exposure from low-power (7 W or less) portable devices happens within a few centimeters' distance from the antenna, where some high EM energy density values may be found.

Clearly using the specific absorption rate $SAR = \sigma E^2/\rho$ ($\sigma$–conductivity and $\rho$ density of medium) methodology in assessing the exposure of a human to incident EM energy totally bypasses the issue of near to far fields from sources. It is still desirable to relate the SAR distribution of an exposure to the structure of the incident EM fields, but it is not strictly necessary.

Note that SAR and it limits are generally frequency independent. The coupling mechanism that results in the internal body fields, as E, however, involves resonances, hence is frequency dependent.

We shall concern ourselves the external fields with the resulting field and the power density exposure criteria. The basic promise of modern standards is that the severity of an effect is directly related to the rate of radio-frequency energy absorbed, hence the introduction of the concept of SAR. Fields external to the medium are not easily related to fields in the medium, so the determination of SAR is complex and often relies on precise measurements, difficult or even impossible to process inside the human.

It can be model numerically or measure using phantom. So, we will try to determine the near-field of a handset in a free-space.

The CENELEC (Comite Europeen de Normalisation Electrotechnique) safety regulations, standard 50166-2; 1995 [10], states that the uncontrolled exposure of humans in the frequency band f = 0.4 to 2-GHz must be limited to an averaged E-field express as

$$E=1.37\ f^{1/2}. \quad (5)$$

In our case, the peaks of electric field are E= 41.1 and 58.1 V/m i.e. 32.3 and 35.3 dB, for f= 0.9 and 1.8 GHz, respectively.

## 4. EXPERIMENTAL AND CALCULATED RESULTS

### 4.1. Radiation patterns

The calculated vertical and horizontal radiation patterns are shown in Fig. 3 with the measured results.

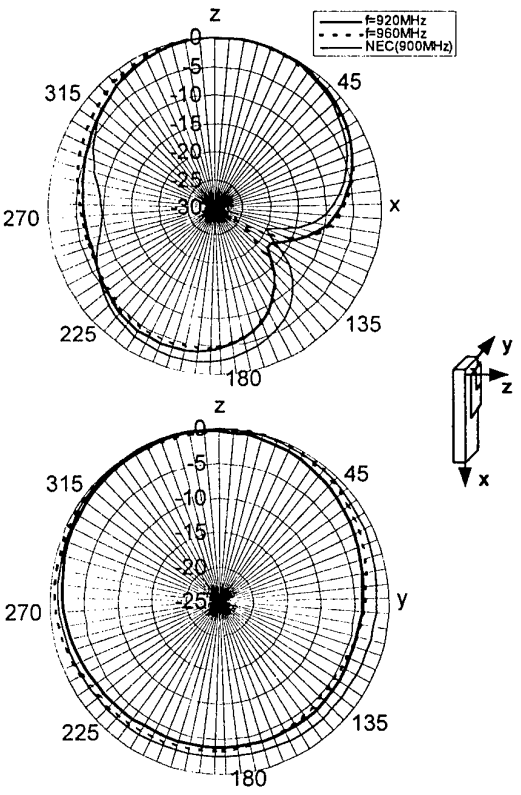



Fig. 3. Calculated and measured radiation patterns of a PIFA antenna on rectangular conducting body, operating at lover frequency [4], [5].

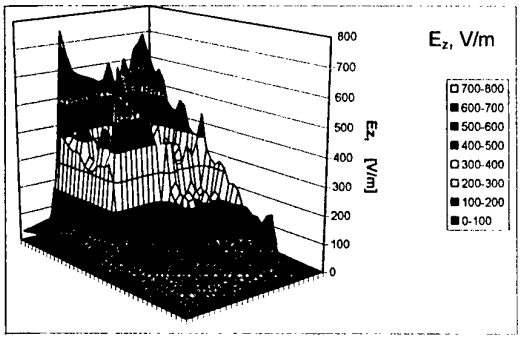
The $E_\theta$ component in the z-y plane shows an approximately omnidirectional pattern caused by surface currents on the radio case. Such desirable features for handset antennas are obtained at both frequencies. The effects of a conducting body can most clearly be seen in x-z plane pattern, where there are nulls around θ= 135 and 270 deg, which could not appear without the conducting body. $E_\phi$ component in the x-y plane is mainly the radiation from the feed line because the amplitude of the current on the feed line is much higher than that on other wires.

The calculated values have good agreement with the measured one, although null depth is not well predicted, so that the wire-grid model is confirmed to be useful in analyzing the radiation characteristics.

### 4.2. Near-E-field underneath radiators

The electric field distributions underneath the antenna radiators give insight into antenna operation. In Fig. 4, the magnitude of the electric field at both resonant frequencies are presented.

a)




b)

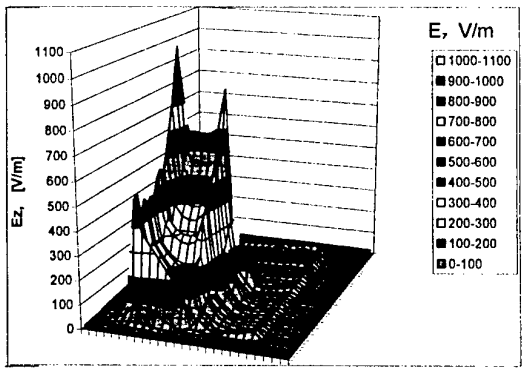



Fig. 4. Computed $E_z$-field component underneath the plane radiators (z=8 mm) of dual-band PIFA antenna, at the first – 0.9 GHz (a) and the second - 1.8GHz (b) resonant frequencies [5].

*Note: In both cases antenna is supplied with $U_{feed}$=1V, and a distance between radiators and metal case is H=9 mm.*

The results clearly show that $E_z$ is equal to zero in the position of the short pins and considerably larger at the opposite edge. The magnitude of the electric field of the nonresonant element is much lower than that of the resonant one as expected. This confirms good decoupling between the two separated radiating elements at both frequencies.

### 4.3. Exposure of portable radio operators

Because of the relatively low power of portable transmitters (usually less than 7W), the exposure of

concern is only in the very close proximity to the antenna, where the head of the user is located during the normal operation of the device.
The effects due the presence of the human body were examined from the point of view of fields external to the body.

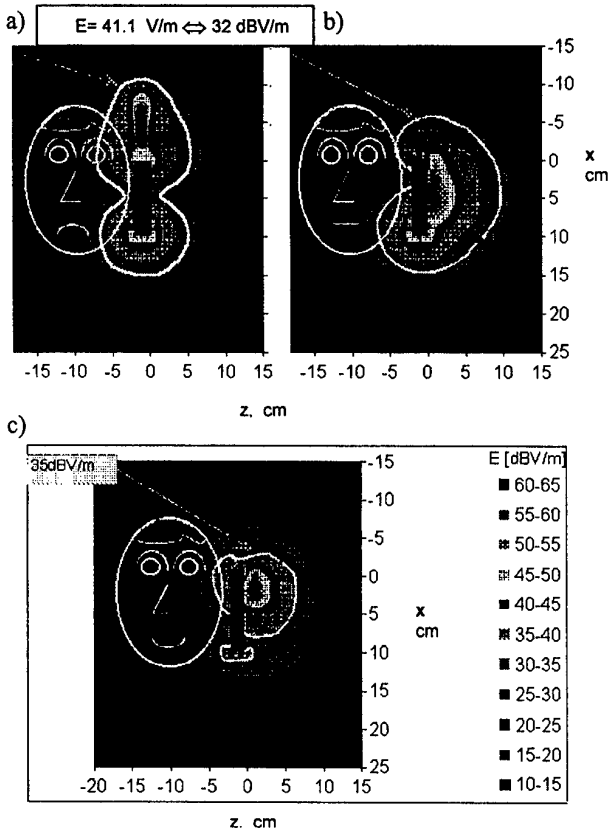



Fig. 5. Near-field distribution around handset with λ/4-whip antenna (a), and with build-in PIFA (b), at f= 900 MHz, and for PIFA at 1800 MHz (c), $P_{feed}$= 0.1 W [5].
*Note: The CENELEC protection area is bordered by white-line.*

Comparison the near-field of the traditional quarter-wave-whip and planar build-in handset antenna shows the advantage of the last one. The EM field less exposes the head, and for upper frequency also - hand.
The fields scattered by the body and external to it are the ones of most interest to the communications problem. The analytical results of Chuang [8] suggest that the radiation efficiency of a resonant 840-MHz dipole antenna proximate to the body may be reduced to as little as 29% near the head and to 15% at belt level compared to the efficiency in free space conditions. Furthermore, because the body is asymmetric with respect to the antenna, there is coupling of energy from the nominal to the cross-polarization.

## 5. CONCLUSIONS

The two chief design characteristics of any portable radio telephone antennas are that it must be mounted on the housing of portable telephone and that during operation the set will be held by a human, who may randomly point the set in any direction. Because antenna is forced into close proximity with the housing, the antenna current is induced not only into antenna element, but also into the conductive housing. This current dispersion changes the shape of the original radiation pattern. Radiation efficiency is further degraded by the antenna's forced proximity to the human body, since the antenna is necessarily used near an operator. The polarization of radiation pattern is also changed by the changes in antenna direction caused by operator movements and habits. These difficult design constraints are complicated by the need to develop very small antenna elements to meet the demand for compact, portable equipment; it is common knowledge that radiation efficiency and bandwidth degrade as antenna element size is decreased.
In this paper the wire-grid models for PIFA's mounted on portable radio case have been described, and it was confirmed that the calculated radiation patterns have good agreement with measured one. The near-E-field emitted toward operator is meaningful reduced.

## ACKNOWLEDGMENTS

Author wish to thank his former MSc student Tomasz Rotko, now employed in NOKIA Poland, for the valuable contribution to this work.

## 6. REFERENCES

[1] K. Fujimoto, J.R. James (ed.), **Mobile Antenna Systems Handbook**, Artech House Inc., Boston-London, 1994
[2] K. Siwiak, **Radiowave Propagation & Antennas for Personal Communications**, Artech House, Boston-London, 2nd ed., 1998
[3] Z.D. Liu, P.S. Hall, **Dual-frequency planar inverted-F antenna**, IEEE Trans. on Antennas & Prop. vol. 45, no. 10, Oct. 1997, pp. 1451-8
[4] W.J. Krzysztofik, T. Rotko, **New terminal antennas of mobile communication systems**, (in Polish), National Conference on Radiobroadcasting & Radiocommunication, May 18-20 1999, Poznan, Poland, pp. 359-62
[5] T. Rotko, **Antennas for portable radio units of mobile communication systems**, (in Polish) MSc Thesis, Wroclaw University of Technology, Wroclaw, Poland, July, 1999
[6] G.J. Burke, A.J. Poggio, **Numerical Electromagnetic Code – Method of Moments**, Lawrence Livermore Laboratory, Livermore, California
[7] P. Suvannapattana, S.R. Saunders, **Satellite and terrestrial mobile handheld antenna interactions with the human head**, IEE Proc. Microw. Antennas. Propag., Vol. 146, No. 5, Oct. 1999, pp. 305-10
[8] H.R. Chuang, **Human operator coupling effects on radiation characteristics of a portable communication dipole antenna**, IEEE Trans. on Ant. & Prop., Vol.42, No.4, April 1994, pp. 556-60
[9] A. Karwowski, **Radiation hazard of a cellular-telephony devices**, (in Polish), Review of Telecommunication, LXX, No. 12/1997, pp.758-65
[10] CENELEC, **European Prestandard ENV 50166-2, Human Exposure to Electromagnetic Fields High- Frequency, 10 kHz-300GHz**, January 1995

EMC 2000 INTERNATIONAL WROCŁAW SYMPOSIUM ON ELECTROMAGNETIC COMPATIBILITY

# Electromagnetic Environment in Railway Systems

Eisuke MASADA
Science University of Tokyo
2641 Yamazaki, Noda- city Chiba- pref., 278- 8510
masada@ee.noda.sut.ac.jp

Takeshi MIZUMA
Traffic Safety and Nuisance Research Institute
6- 38- 1 Shinkawa, Mitaka- city Tokyo,181- 0004
mizuma@tsnri.go.jp

Recently, electromagnetic fields by some electric facilities are discussed mainly with the point of view of human effects. Until now, it was generally said that there were little problems in the electromagnetic field by electric railways because of not such high voltage. But, international commision of ICNIRP has shown the guidelines of electromagnetic field to human body in 1998, and of course electric railways must keep these guidelines.Therefore, we must measure such electromagnetic field by railway systems accurately and evaluate them with justice .

In this paper, we will show the measurement examples of magnetic field by railways and show that these fields are fully under the present guidelines.

## 1. Introduction

Recently, according to the development of magnetically levitated vehicle ( Maglev ) systems , it has been said that electromagnetic field by linear motors were noteworthy. Fortunately, magnetic field by JR- Maglev are fulfilled the environment requirement of local government. After this, as these problems will be spread to general electric railway systems we must measure several data of electromagnetic field by these systems and evaluate accurately these data under the international guidelines for example ICNIRP.

In this paper, we will show the measurement examples of magnetic field by railways and show that these fields are fully under the present guidelines.

## 2.Characteristics of magnetic field on railway

2.1 Magnetic fields in the vehicle

The sources of magnetic fields in the vehicle are classified into figure 1.

It is generally considered that magnetic fields by electric equipments are leaked from connected cables and coils rather than boxes themselves. And, these magnetic fields have several modes by running pattern ( powering, braking, coasting) and continuous changing frequencies by time.

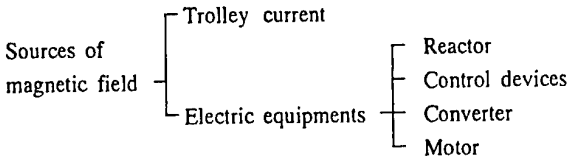



Fig.1 The sources of magnetic fields in the vehicle

Moreover, these magnetic fields are radiated with complexity on time and space in the vehicle.

2.2 Magnetic fields outside the vehicle

It must be considered for evaluating magnetic fields outside the vehicle to divide measuring modes into two patterns that is vehicle running mode and absence mode. And , it is noted that in the case of vehicle running changing magnetic field by currents flow and electric devices on the vehicle have several frequency and amplitude features according to running modes for examples powering, braking or coasting.

## 3. Measurement method of magnetic field on railways

Generally speaking, the distributions of magnetic fields on railways are largely different by conditions ( in or outside the vehicle, and even more on the ractor or inverter in the vehicle , running, standstill or absence , and even more powering , coasting or braking on running ). But, as to choose optimum measuring method every measurement condition is not so effective because of huge time requiring, it is reasonable to take the unified measurement method for fair comparison of magnetic fields on the railway systems.

It is required for measure magnetic field on the railway that large direct magnetic fileds of several mT order superposing small AC ( alternating current ) magnetic fields from some $\mu$ T to 10 $\mu$ T order that change frequencies from 0 to several 100 Hz order every time can be measured accurately by the order of 0.1 $\mu$ T order. Therefore, we developed measurement device for magnetic field on railway to

measure the range of maximum 2 mT DC and 0.5 mT AC up to 500 Hz magnetic field on real time.

Table 1 shows the main specification of this measurement device.

Table 1 Main specification of magnetic measurement instrument for railway systems

| | | | |
|---|---|---|---|
| Detecting method | Flux gate form | | |
| Frequency range | 0 ~ 500 Hz | | |
| Measurement range | DC | 0.1 μ T ~ 2 mT | |
| | AC | 0.1 μ T ~ 0.5 mT | |
| Sensor length | 5 cm | | |
| Dimensions | Width | Height | Depth |
| | 395mm | 383mm | 191mm |
| Weight | 13 kg | | |

## 4. Measurement examples of magnetic fields on railways

In this chapter some examples of magnetic fields on railway systems that were measured by proposed method are shown.

4.1 Conventional railway of DC feeder system

In Japan , major business transportation systems in the urban areas are adopted DC 1500 V feeding. Therefore, we measured magnetic fields of vehicles feeded by DC 1500V. Figure 1 , 2 and 3 shows the example of magnetic fields on the reactor, on the inverter and on the SIV ( Static Inverter ) in the vehicle respectively.

It is confirmed that magnetic fields on the reactor have DC and AC components. It is estimated that DC component is caused by DC currents from trolley and AC components are formed by harmonics currents of inverters on the vehicle.

On the contrary, magnetic fields on the inverter have almost AC components of inverter frequencies. So, the frequencies of magnetic fields on the inverter are synchronized to them of inverter frequencies.

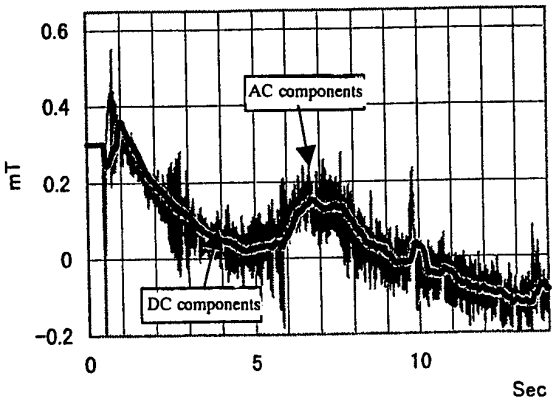



Fig.1 Example of magnetic field on the reactor in the vehicle

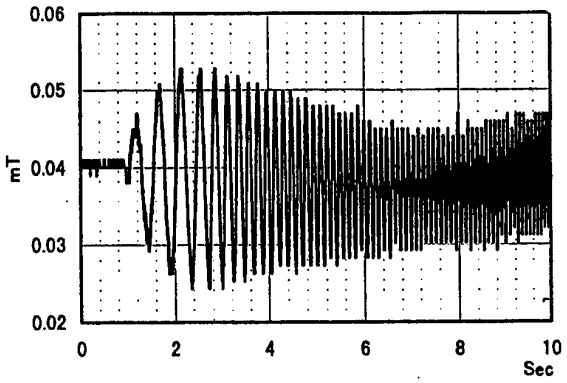



Fig.2 Example of magnetic field on the inverter in the vehicle

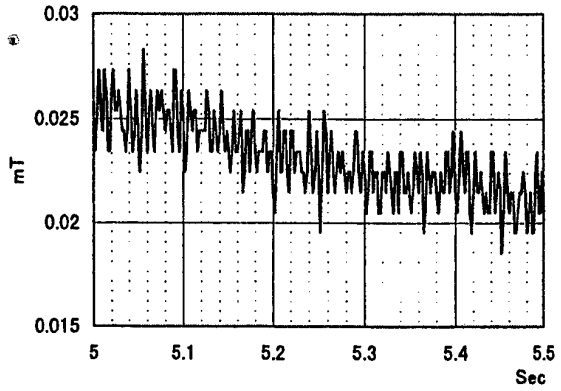



Fig.3 Example of magnetic field on the SIV in the vehicle

On the other hand, It is shown that magnetic fields on the SIV have AC component of carrier frequency of SIV that is 140 Hz.

Thus, It is clarified that magnetic fields in the vehicle have distributed widely on each electric equipment and are changed as time goes by according to running modes.

Table 1 shows the maximum values of magnetic fields of DC and AC components on each device in the vehicle and figure 4 shows the magnetic field on the reactor every running mode.

Table 1 Measurement results of magnetic field in the vehicle

(mT)

| | | Reactor | Inverter | SIV |
|---|---|---|---|---|
| DC | Powering | 0.59 | 0.04 | 0.06 |
| | Coasting | 0.13 | 0.04 | 0.05 |
| | Braking | 0.51 | 0.05 | 0.05 |
| AC | Powering | 0.06 | 0.02 | 0.002 |
| | | 20Hz | 3Hz | 140Hz |
| | Coasting | 0 | 0 | 0.002 |
| | | | | 140Hz |
| | Braking | 0.04 | 0.01 | 0.002 |
| | | 15Hz | 13Hz | 140Hz |

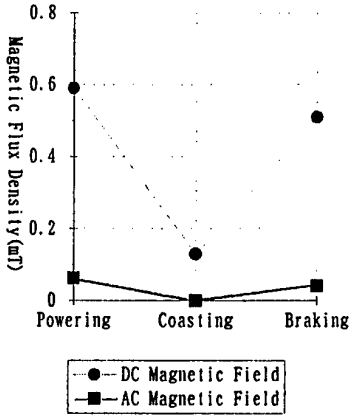



Fig.4 Magnetic field on the reactor every running mode

Moreover , Some examples of magnetic field outside vehicle are shown in figure 5.

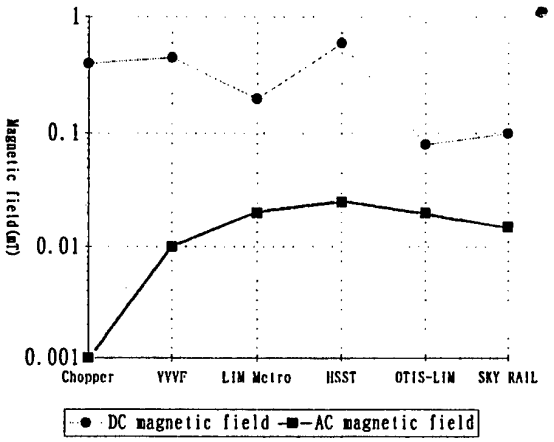



Fig.5 Magnetic field outside vehicle

In this figure, it is cleared that magnetic fields outside vehicle are mainly consisted of DC component and AC components that are about one tenth of DC for DC feeding systems.

4.2 Magnetic field on linear motor driven systems

In Japan, several linear motor driven systems are developing and practical uses in part. For these systems, the subjects of human effects by magnetic fields on linear motors are arrested now.

In this section, some results of measurements and evaluations about magnetic fields on linear motor driven systems with primary side on vehicle systems ( linear metro ) and on ground systems ( sky- rail ) are described. However, these systems are all used linear induction motors.

Figure 6 shows the example of magnetic fields on the linear motors with primary side on vehicle . Figure 7 shows the example of magnetic field of linear motors outside vehicle.

Though magnetic fields in the linear motor driven vehicle are similar to its of conventional railway on the inverter, they are quite different outside vehicle.

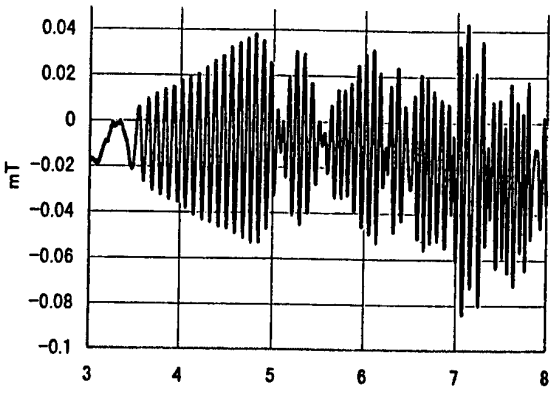



Fig.6 Magnetic field on the linear motor in the vehicle

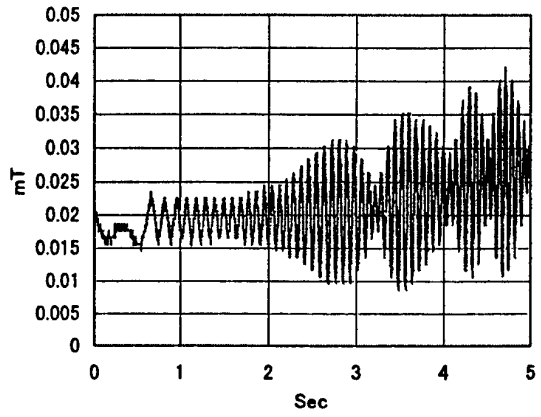



Fig.7 Magnetic field of liner motor outside vehicle

Judging from these figures , magnetic fields of linear motors are radiated in and outside vehicle.

Figure 8 shows the example of AC magnetic fields on the linear motor in the vehicle.

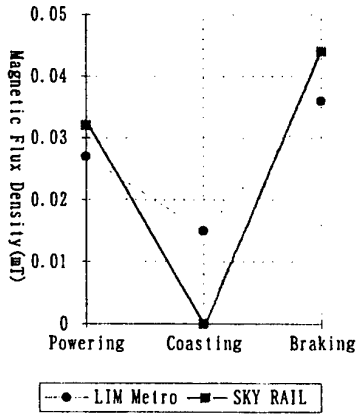



Fig.8 AC magnetic fields on the linear motor in the vehicle

It is confirmed that AC magnetic fields by linear motors are more remarkable on powering and braking than coasting and are larger than conventional railway about one figure up.

However , it must attend to evaluate that these main frequencies of AC magnetic fields are low range under 100Hz order and its amplitudes are less than 0.1 mT.
Table 2 shows the measurement results of maximum magnetic fields of linear motors outside the vehicle.

Table 2 Measurement results of magnetic fields outside vehicle of linear motor drives

| | | Primary side on | |
|---|---|---|---|
| | | Vehicle | Ground |
| Vehicle passing | DC mT | 0.07 | 0.06 |
| | AC mT | 0.02 | 0.01 |
| | | 17 Hz | 6 Hz |
| Vehicle absence | DC mT | 0.07 | 0.06 |
| | AC mT | 0.002 | 0 |
| | | 100Hz | —— |

It is cleared that AC magnetic fields by linear motors outside vehicles are amaller than its in the vehicles about one figure down and have low frequency components like as in the vehicle.

## 5. Relationship between measurement results and guideline

5.1 Measurement results and ICNIRP guideline

ICNIRP has published the guideline for limiting exposure to time-varying electric magnetic , and electromagnetic fields in 1998.

Figure 9 shows the guideline of reference magnetic flux density level and the status range by measuring outside vehicle on railways.

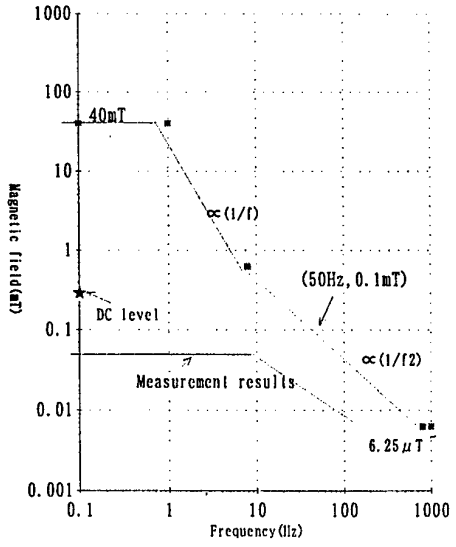



Fig. 9 Reference level of ICNIRP and measuring results

As shown in this figure, in the present time magnetic fields by railways outside vehicle have enough margins against reference level of ICNIRP. However, considering that large capacity IGBT inverter will be used in the near future this margin will be limited especially in the middle frequency ranges of some kHz order. Moreover , in the vehicle , because of nearness from electric equipments , this margin will be more shorter and close to the reference levels.
In this case , we must consider the basic restriction.

5.2 Simple modeling of magnetic fields distributions on railways

If magnetic flux density is exceeded the reference level, we must calculate induced currents in the human body. But, magnetic fields on railways have two characteristic features. One is to attenuate remarkably with length from the sources and the other is to have low frequency componetns on maximum values. Therefore, under several assumptions show below , we establish simple calculation methods of induced currents in the human body on railways.

( Assumptions )

① Magnetic fields on railways attenuate with one-order function by length of sources.
② Human body is composed of several cylinders of supposed radius , length and equivalent conductivity.
③ Maximum magnetic flux density and it's frequency are taken as the representative value for calculations.

( Calculation example )

Calculated value of induced current is about under 0.1 $mA/m^2$ for adult person at 50 Hz in regard to 2 $mA/m^2$ of basic restrictions.

For railways as attenuations of magnetic fields by length on railways are large, many margins can secure for the basic restrictions.

## 6. Conclusion

The characteristics of magnetic feilds on railways were arranged above, and real measurements were executed by proposal measurement method. Moreover, measurement results were compared with present guideline for human body on ICNIRP . As the result, magnetic fields on railway systems have enough margins against present guideline of ICNIRP under the present technology stage, but in the near future, this margin will be supposed to be short because of high power and high frequency. However, as this margin is restricted on reference level, it will be calculated under the basic restrictions by modeling of magnetic field distributions on railways. In this paper, we propose simple modeling and calculation sequences and show that enough margins will be secured even if magnetic fields on railways are exceeded reference level in the future.

But, hereafter we must measure more magnetic field on several railway systems and grasp its characteristics more accurately, and need to propose accurate measurement methods and evaluation method for international guidelines.

EMC 2000 INTERNATIONAL WROCŁAW SYMPOSIUM ON ELECTROMAGNETIC COMPATIBILITY

# REGULATION FOR THE PROTECTION OF THE GENERAL POPULATION IN SWITZERLAND

Jürg Baumann[1], Georges Goldberg[2]
[1]Swiss Agency for the Environment, Forests and Landscape, CH-3003 Bern, Switzerland
Fax +41-31-324 01 37; juerg.baumann@buwal.admin.ch
[2]Wannerstrasse 43/61, CH-8045 Zürich, Switzerland
Fax +41-1-463 63 32: gegegezurich@swissonline.ch

*The Swiss government has put into force a new ordinance on the protection of the general population from non-ionizing radiation. The ordinance regulates non-ionizing radiation originating from stationary installations. It enforces the reference levels for the general population which were recommended by ICNIRP. In addition emphasis is given to the precautionary reduction of long term exposure.*

## 1. INTRODUCTION

On 1 February 2000 the Swiss government has put into force a new ordinance on the protection of the general population from non-ionizing radiation (NIR) in the frequency range from 0 Hz to 300 GHz. It applies to stationary sources, e.g. high voltage overhead transmission lines and underground cables, substations, transformer stations, electric in-house wiring, railways, transmitters and radar stations. No restrictions are imposed on mobile equipment like cellular phones or electric appliances because emission reducing strategies for such consumer products must be standardized at the international level. This is already the case for e.g. microwave ovens or video display units. Also excluded are intentional medical applications of NIR as well as exposure of workers at the work place from sources within the enterprise.

## 2. LEGAL FRAMEWORK

The legal framework is laid down in the Swiss federal law relating to the protection of the environment. According to this law NIR in the environment must be limited to a level which is neither harmful nor a nuisance to humans.

This level has to be defined in terms of exposure limit values. The basis for deriving these exposure limit values is – according to the law – the state of scientific knowledge or the general experience.

In addition exposures which *might* be harmful or a nuisance shall be limited in the sense of precaution as much as technology and operating conditions will allow provided this is economically acceptable. This precautionary principle applies irrespective of the actual level of exposure. A risk needs not to be proven for precautionary measures to be implemented. The precautionary approach is designed to reduce potential risks, specifically potential long term risks which, due to limited knowledge, can not yet be assessed in a satisfactory way.

## 3. THE ORDINANCE ON PROTECTION FROM NON-IONIZING RADIATION

### 3.1 Exposure limit values

The ordinance enforces the reference levels for the general population as recommended by the International Commission on Non-Ionizing Radiation Protection (ICNIRP) [1]. These exposure limit values must be respected at all places accessible to the general public irrespective of the emitting installations being old or new. They are shown in figure 1 for the case that an exposure is made up of one single frequency. If fields at several frequencies are simultaneously present all contributions have to be appropriately summed up according to the summation rules of ICNIRP. These exposure limit values therefore limit the overall exposure which is present at a given location.

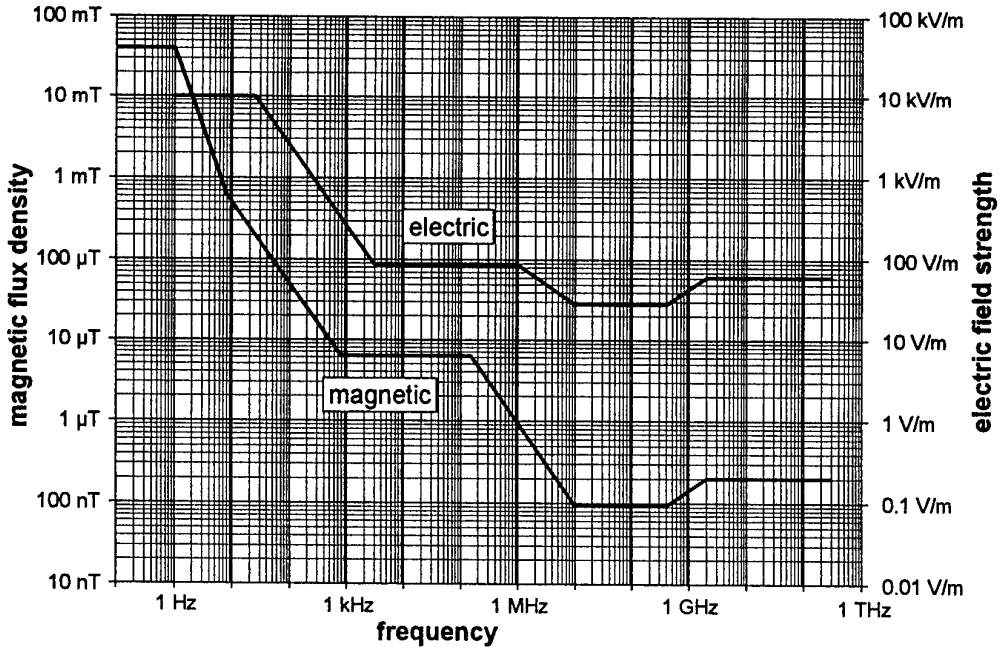



**Figure 1**: Reference levels for the general population recommended by ICNIRP [1]

The ICNIRP reference levels protect humans from scientifically proven harmful effects. However, the data base which underlies ICNIRP's reference levels is rather limited. Only short term biological effects at rather high intensity were considered by ICNIRP to be sufficiently validated. Other scientific findings of biological effects at much lower levels – so called non-thermal effects – and some epidemiologic evidence that low level NIR could be a risk factor in cancer development were not considered. Consequently there are some doubts as to whether the ICNIRP guidelines provide the degree of protection requested by the Swiss law on environmental protection. Specifically, open questions remain concerning health effects under long term exposure. Despite these deficiencies the ICNIRP reference levels were adopted as exposure limit values because no convincing alternative was available.

### 3.2 Precaution

Given the incomplete knowledge about long term health effects it is important to avoid any unnecessary exposure. This is exactly what is intended by the principle of precaution.

The principle of precaution is focused to those situations where people are exposed for a prolonged duration. Exposure is considered long term if a source emits for at least 800 hours per year and if the radiation of this source impinges on a place where humans can stay for a prolonged time. The latter places are called "places of sensitive use".

In order to be applicable in practice the principle of precaution has been put into numbers by means of so called installation limit values (ILV). In contrast to the exposure limit values the ILV do not refer to the overall exposure but only to that radiation which is produced by one single installation. The ILV are expressed in terms of magnetic flux density for power lines, transformers, sub-stations and railways or in terms of electric field strength for telecommunication, broadcast and radar transmitters.

The ILV are compiled in table 1. They are substantially lower than the exposure limit values. Contrary to the exposure limit values they are not based on health effects but on the technical and economic practicability. The experience shows that long term exposure from a single source at places of sensitive use can in the great majority of cases be kept far below the exposure limit values without unduly impeding the construction and operation of installations. The ILV are therefore not new, lower safety limit values. They simply reflect today's state of technology to reduce long term exposure.

**Table 1**: Installation limit values (ILV) for various installations

| Installation | ILV (RMS value) | Reference operational state |
|---|---|---|
| Electric power lines; transformer stations; sub-stations | 1 μT | Maximum rated current |
| Electric railways | 1 μT | 24 hour average, at operation according to schedule |
| Cellular phone base stations<br>900 MHz<br>≥1800 MHz<br>mixed frequency | <br>4 V/m<br>6 V/m<br>5 V/m | Maximum rated emitted power |
| Long- and mediumwave broadcasting | 8.5 V/m | Maximum rated emitted power |
| Radar | 5.5 V/m | Average over a complete survey scan, at maximum rated power |
| All other radio transmitters | 3 V/m | Maximum rated emitted power |

The ILV must be respected only at places of sensitive use. The measures to be taken in order to comply with the ILV are not defined in the ordinance but rather left to the skills and responsibility of the owner of an installation. Measures are either of technical nature or they influence the siting of installations (keeping away from places of sensitive use). Technical measures for high power lines are e.g. the optimum arrangement of conductors and phases as well as the height of conductors above ground. For cellular base stations the technical options refer to the choice of the antenna (radiation pattern), to the height of the antenna above ground and to minimizing the transmitted power.

The ILV have been set at a level which generally can be respected by newly constructed installations. This is not necessarily true for existing installations. The ordinance therefore allows exceptions either for certain installation categories in general or for individual installations on a case by case basis. Existing power lines and railways e.g. are generally exempt from respecting the ILV because reconstruction and new siting would in many cases be necessary which is considered too expensive. On the other hand cellular phone base stations must respect the ILV without exception and irrespective of their being old or new.

The ordinance concerns first of all the owner of an installation. Installations must be constructed and operated in such a way that they comply with the requirements of the ordinance. Secondly, also land use planning is affected. The ordinance demands that new zones of construction must only be assigned where the ILV of an existing or planned installation is not exceeded.

## 4. CONCLUSIONS

The precautionary approach is laid down in general terms in the Swiss law on Environmental protection and further supported by preliminary indications of health effects at long term, low intensity exposure. The new Swiss ordinance puts the precautionary principle into numbers. The extent of precaution has been established by the government following an evaluation of the technical possibilities to reduce exposure and the economic consequences. With the chosen approach the long term exposure of the population in Switzerland to NIR will remain as low as is today considered technically possible and economically feasible.

## 5. REFERENCES

[1] Guidelines for limiting exposure to time-varying electric, magnetic and electromagnetic fields (up to 300 GHz)
International Commission on Non-Ionizing Radiation Protection.
Health Phys. 1998, 54, 115-123

**EMC 2000** INTERNATIONAL WROCŁAW SYMPOSIUM ON ELECTROMAGNETIC COMPATIBILITY

# BIOLOGICAL EFFECTS OF ELECTROMAGNETIC FIELDS WITH EMPHASIS ON HEALTH AND SAFETY

Kenneth R. Foster* and Michael H. Repacholi**
*Department of Bioengineering, University of Pennsylvania, Philadelphia PA 19104 USA
**Radiation Protection and Global Hazards Assessment
Office of Global and Integrated Environmental Health
World Health Organization, CH-1211 Geneva 27, Switzerland
Tel: +41 22 791 3427, Fax:+41 22 791 4123, E-mail: repacholim@who.ch

This paper reviews biological effects of electromagnetic fields, and their relation to risk assessment and *standards* development. A great many biological effects have been reported from electromagnetic fields, but only few such reports have influenced the development of major exposure standards in effect at present. Major exposure standards have been based on hazards such as shock and burn, resulting from acute, high level exposures. We review briefly current controversies about possible chronic effects of electromagnetic fields, and the WHO EMF Project, which is co-ordinating a health risk assessment of electromagnetic fields.

## 1. INTRODUCTION

The subject of biological effects of electromagnetic fields is vast. One database includes approximately 28,000 abstracts of papers on biological or health effects, or biomedical applications of electromagnetic fields [1]. This is subject is far too large to review here.

This talk will review some major issues related to the interaction of electromagnetic fields with biological systems and standards development. Finally, we describe the WHO EMF Project, which addresses important issues in health risk assessment related to electromagnetic fields.

## 2. DOSIMETRIC CONSIDERATIONS

As with any potentially toxic substance, the potential hazards of electromagnetic fields depends on the exposure as well as other characteristics such as frequency. For a comprehensive review see [2].

Appropriate measures of exposure include:

- External field strength. At low frequencies or in the near-fields of antennas, the appropriate dosimetric quantity is the electric or magnetic field strength; commonly investigators cite the magnetic flux density instead.
- Incident power density (intensity), in $W/m^2$, typically used for far-field exposures at radiofrequencies and above.
- Contact current, in amperes.

These exposure parameters pertain to fields outside the body. The magnitude of the biological response typically depends on the fields induced within the body, i.e. the dose. Appropriate measures of dose include the internal field strength, current density, or specific absorption rate (SAR). The SAR is defined as the rate of heat generation in watts per kilogram of tissue.

The coupling between an external electric or magnetic field and the body is a complex issue that depends on field and body geometry and frequency, among other factors. (For a comprehensive review see [3]). An important consideration is the wavelength in relation to the body size. The coupling properties can be discussed in three very loosely defined frequency ranges:

- The quasi-static range (frequencies from about 100 kHz to less than about 20 MHz). At these frequencies, the body dimensions are far smaller than the wavelength of an electromagnetic wave, and the coupling can be considered separately for external electric and magnetic fields, both of which induce electric fields within the body. In general, the coupling is extremely weak at low frequencies, but increases roughly linearly with frequency. The induced current is distributed throughout the body in a complex way depending on body geometry and electrical properties. For example, for a person standing on a ground plane in a vertically polarized electric field, the induced current density in the neck and legs can be considerably higher than in the torso because of the smaller cross sectional areas of these body parts.
- The resonance region (frequencies from about 20 MHz to 10 GHz), at which the wavelength of the

incident field is comparable to the size of the body or body parts. In this frequency range, wave propagation effects are very important. The body and body parts exhibit multiple electrical resonances due to antenna effects. Relatively high absorption can occur in the whole body near its resonant frequency of about 70 MHz (for an adult standing erect in a vertically polarized field). At higher frequencies, localized regions of comparatively high SAR can occur in parts of the body (e.g., head) due to electrical resonance.

The quasi-optic range (frequencies above about 10 GHz), at which most of the energy absorption occurs within a few mm or less from the body surface.

The above considerations pertain to whole-body or nearly whole-body exposure. For near-field exposures, or when there is contact with external conductors (both common scenarios in acutely hazardous exposure situations involving high-powered sources) the coupling properties depend in complex ways on the field and body geometries.

These considerations are essentially related to dosimetry, i.e. determining the fields that are induced within the body from exposure to an external electromagnetic field. Apart from dosimetric considerations, the frequency is also important in determining the biological response. Biological processes have intrinsic response times, which imparts a low-pass characteristic to most biological responses to fields.

## 2. BIOPHYSICAL MECHANISMS

A great many mechanisms are established by which electric or magnetic fields can interact with biological systems, either thermal or nonthermal. (For a recent review focusing on modulation-dependent mechanisms see [4]. Most nonthermal mechanisms involve the electric field. Electric fields exert forces on charges and torques on molecules; in addition, higher-order interactions occur between field gradients and induced dipole moments or charges. These forces are opposed by random thermal agitation. Biophysical considerations suggest that thresholds for producing significant responses via these nonthermal mechanisms in biological systems are very high.

Excitation of cell membranes (a physiological process responsible for electrical shock) is a nonthermal effect that is both well documented and potentially hazardous. For typical cells, stimulating excitatory phenomena generally requires changing the membrane potential by tens of mV, which in turn requires electric field strengths in the surrounding tissue in the range of V/m or more. However, the thresholds vary widely depending on cell type. Because of the response time of membrane gates, membrane excitation is a low-frequency phenomenon. For a detailed discussion see Reilly [5].

Thermal mechanisms, by contrast, are related to temperature increase, or rate of temperature increase, in the exposed tissues. Thermal effects can be elicited by fields of any frequency, but because of the frequency-dependent coupling properties of the body, they are most apparent with high frequency fields.

## 3. BIOLOGICAL EFFECTS OF ELECTROMAGNETIC FIELDS IN HUMANS

A number of biological effects have been well established to occur in humans, some of which are potentially hazardous. We first consider effects observed under acute (short term) exposure conditions, and then comment about possible effects of chronic exposure to electromagnetic fields in humans.

### 3.1 Static fields

The strongest DC magnetic field that a human is li' ly to encounter is in the low-Tesla range, e.g. during imaging by MRI. No biophysical mechanism has been established that might lead to pronounced effects in humans at such levels, and limited testing with animals has disclosed only subtle effects. Humans exposed to 4 T fields in an MRI system have reported mild sensory phenomena [6]. The threshold for human perception of DC electric fields is 40-45 kV/m [7].

### 3.2 Low (power) frequency fields

The threshold for human perception of 50/60 Hz electric fields is 2-10 kV/m, and the perception arises from movement of hairs on the subject's skin. Other sensory effects are produced by contact current when a subject touches a conductive object while located in a field.

Alternating or pulsed magnetic fields will induce electric fields in the body, which at sufficient can be life threatening (e.g. by inducing cardiac fibrillation). However, the estimated flux densities needed to produce such effects are very high, e.g. magnetic flux densities above 100 mT at 60 Hz.. Some clinical devices use pulsed magnetic fields to stimulate nerve and muscle tissues. These typically employ pulsed magnetic fields, usually of millisecond duration and with magnetic slew rates (dB/dt) of tens of T/s and peak magnetic fields ranging from several hundred mT to several T.

Stimulation of fracture repair is a poorly understood but seemingly well established effect of pulsed magnetic fields; magnetic bone stimulators have been approved for sale in the U.S. since the late 1970's. These devices employ a variety of pulsed fields, and induce electric fields in the body with peak levels of the order of 0.1 V/m. The corresponding peak current densities are of the orders of tens of $mA/m^2$ in soft tissue, which are

above the level of naturally occurring (endogenous) fields but are well below anticipated thresholds for eliciting action potentials in excitable tissue.

A well established effect, first observed by d'Arsonval in 1896, is the production of visual sensations, called magnetophosphenes, when the head is exposed to alternating magnetic fields (10-20 mT, 50 Hz). These effects are caused by small currents (20-200 $mA/cm^2$) that are induced in the retina of the eye.

A final effect we consider, which has some bearing on electrical injuries under special conditions, is electrical breakdown of cell membranes. This effect, termed electroporation, occurs when the induced potential across a cell membrane exceeds about 1 V. Such effects require high current densities in the surrounding medium, at frequencies below ca. 1 MHz, i.e. current levels that would also be thermally hazardous if sustained. However, electroporation is a very fast process, and can be produced in the absence of damaging heating if the current pulse is very short. Electroporation has been implicated in some forms of electrical injury [8].

2.3 High frequency (radiofrequency) fields

At frequencies above 1-3 kHz, cell membranes become progressively less sensitive to electrical stimulation, and thermal phenomena predominate. A variety of effects, some hazardous, have been reported from high-frequency electromagnetic fields (mostly at radiofrequencies and above).

Humans can perceive microwave energy through a number of thermal mechanisms. The most straightforward is perception of skin temperature increase produced by microwave irradiation. The threshold for warmth perception corresponds to skin temperature increases of about 0.07 C [9]. The threshold for thermal pain corresponds to temperature increases 50-100 times higher. Pulsed microwaves can elicit auditory sensations if absorbed in the head, due to perception of thermally generated acoustic transients [10].

One unequivocal potential hazard from electromagnetic fields is thermal injury, i.e. burns. The thresholds for producing thermal damage in tissue depend on the temperature rise and duration of the heating. Thermal damage to tissue can be modelled as a first-order rate process with a threshold of about 43 C, i.e. temperatures below this level can be tolerated indefinitely, while higher temperatures will lead to thermal damage, in progressively shorter times at higher temperatures. Thus the microwave exposure needed to produce thermal damage depends on several factors, including the time over which irradiation persists, the size of the heated region, and the rate at which heat is transported from the heated region.

Other thermal effects can be produced by interacting with the thermoregulatory system, even in the absence of hazardous temperature increases. Characteristic thermoregulatory changes include alterations in blood flow, respiration, sweating, and many more subtle physiological and behavioral responses. These responses can be interpreted as normal physiological responses to heat, and are not necessarily adverse to the individual.

The basal metabolic rate in man is about 1 W/kg of body mass, and whole-body exposures somewhat below this level can be expected to produce thermoregulatory responses. Animals of different species differ widely in their thermoregulatory capabilities and responses.

This creates the need for care in evaluating data on biological effects of radiofrequency energy, including the need to distinguish carefully between whole body and partial body exposures. Handsets of mobile telephones, for example, may produce a partial body exposure of several W/kg in small regions of the head, although the total absorbed power might be thermally insignificant. Effects reported in animals at similar (whole-body) exposures are not necessarily indicative of those that might be produced by partial body exposure in humans at such levels.

A wide variety of other thermal effects have been demonstrated from radiofrequency fields in animals, which can be anticipated to occur in humans as well. Some of the more significant include thermally induced cataract and adverse reproductive effects (birth defects and other adverse effects). These effects require quite high exposure levels (tens of W/kg) and the effects are clearly related to excessive heating.

Behavioral disruption has been observed in several species of animals exposed to microwaves at whole body exposures of 4-6 W/kg, at several frequencies above 100 MHz. In such studies, the animals are trained to carry out a task (for example, pressing a lever to obtain food pellets) and exposed to microwave energy. At some exposure level, the animals stop performing the assigned task and begin a different behavior, typically one associated with thermoregulation (for example, spreading saliva on the tail in rats).

The two classes of mechanisms described above (membrane excitation and thermal effects) are thus the underlying cause of many different effects, some of which are clearly hazardous. Membrane excitation is a low frequency response, limited by the response time of ion channels in nerve membranes (which is typically of the order of tens of milliseconds). By contrast, heating is nearly equal to the tissue conductivity times the root-mean-square current density, which is a rather slowly varying function of frequency. This implies that the thresholds for membrane excitation will increase with

frequency, eventually becoming higher than that for thermal effects.

3.4. Relation to standards

The general picture that emerges from the above discussion is that the dominant effects at low frequencies are related to nerve excitation or electrical burn (depending on the exact exposure situation).

Because of the weak coupling between external fields and the body at low frequencies, electrical injuries from low-frequency fields require extremely high field strengths (in the absence of direct contact with conductors). By far the most common injury scenario involves contact of the victim with a conductor from which current is passed directly into the body.

By contrast, the obvious mechanism for injuries at higher frequencies involves excessive heating of body tissues. The reported injuries from radiofrequency fields involve burns from exposure to strong fields in close proximity to high power transmitters, or burns from excessive contact currents.

Thus, to simplify a complicated picture, major exposure standards are designed to avoid membrane excitation phenomena (principally, shocks) and burns at low frequencies, and excessive body heating at high frequencies. These effects result from acute (short-term) exposure and do not imply the existence of hazards from chronic (long term) exposures at low levels. Major exposure guidelines are explicitly not designed for protection against chronic hazards from long-term exposures, but focus on acute hazards.

3.5 Unresolved issues

Studies of biological effects of electromagnetic fields has been remarkably contentious for several reasons.

First, the scientific literature on biological effects of electromagnetic fields includes many (hundreds) of reports of biological effects of electric or magnetic fields in the frequency range of DC through microwaves, some at levels below present exposure guidelines. These have not driven exposure standards, either because of lack of apparent health significance, lack of independent confirmation, or lack of publication in sufficient detail to permit scientific committees to evaluate the studies (among other reasons). They do, however, give an impression that fields have biological activity even at rather low exposure levels.

Second, the epidemiology literature contains reports of associations between adverse health outcomes and presumed exposure to electromagnetic fields. The most-studied issue is the possible association between residential exposure to power-frequency fields and childhood cancer. But other statistical associations have been reported between various cancers and job titles that suggest exposure to electromagnetic fields. Some reported associations involve very specific forms of electrotechnology. For example, scientists have reported clusters of cases of testicular cancer among police officers using radar guns and have speculated in medical journals about testicular cancer from use of a laptop computer. There have been, in addition, many reported associations between electromagnetic fields and health problems other than cancer.

The interpretation of these studies is limited in part by inadequate (or no) exposure assessment or other methodological problems, and results of animal studies have been mixed but generally unsupportive of the existence of hazard. Expert committees that have examined this literature have uniformly concluded that no convincing evidence for hazard has emerged from these studies. These reports have, however, created a significant public issue and there is considerable scientific uncertainty in how to interpret them.

Addressing these scientific issues is substantially different from typical standards setting activities undertaken by the engineering community, and involves difficult problems of toxicology and environmental risk assessment.

4. WHO INTERNATIONAL EMF PROJECT

WHO established the International EMF Project to provide a mechanism for resolving the many and complex issues related to possible health effects of EMF exposure. The Project assesses health and environmental effects of exposure to static and time varying electric and magnetic fields in the frequency range 0 - 300 GHz, with a view to the development of international guidelines on exposure limits. It commenced at WHO in 1996 and will end in 2005.

The EMF Project has been designed in a logical progression of activities and outputs to allow improved health risk assessments to be made, and to identify any environmental impacts of EMF exposure. The Project objectives are to:

(1) Provide a co-ordinated international response to the concerns about possible health effects of exposure to EMF,

(2) Assess the scientific literature and make a status report on health effects,

(3) Identify gaps in knowledge needing further research to make better health risk assessments,

(4) Encourage a focused research programme in conjunction with research funding agencies,

(5) Incorporate the research results into WHO's Environmental Health Criteria monographs that provide formal health risk assessments for exposure to EMF,

(6) Facilitate the development of an international consensus on limits for EMF exposure,

(7) Provide information on the management of EMF protection programmes for national and other authorities, including monographs on EMF risk perception, communication and management, and

(8) Provide advice to national authorities, other institutions, the general public and workers, about any hazards resulting from EMF exposure and any needed mitigation measures.

WHO, through its International EMF Project, has recently conducted in-depth international reviews of the scientific literature on the biological and health effects of exposure to radiofrequency (RF), and static and extremely low frequency (ELF) fields. These reviews were conducted with the purpose of identifying;

1. health effects that can be substantiated from the literature, and

2. biological effects that are suggestive of possible health effects, but require further research to determine if exposure to electromagnetic fields (EMF) at the low levels of exposure normally encountered in the living and working environment has any impact on health.

The results of these reviews have been or are being published in the journal Bioelectromagnetics. Research still needed to fill these gaps in knowledge form the WHO EMF Research Agenda that is available on the EMF Project home page (http://www.who.int/peh-emf/) or from WHO.

Having completed the initial international scientific reviews, WHO is now urging EMF funding agencies world wide to give priority to this research, if it is their intention to obtain results that will assist both WHO and the International Agency for Research on Cancer (IARC) to make better health risk assessments.

Both WHO and IARC have already established a timetable for assessing health effects of EMF fields. In 2001 IARC will conduct a meeting to formally identify and evaluate the evidence for carcinogenesis from exposure to static and extremely low frequency (ELF) fields. IARC will publish the results of this meeting in the IARC Monograph Series. The International EMF Project will accept the IARC conclusions on carcinogenesis and incorporate them into the results of a WHO evaluation of non-cancer health risk assessment of exposure to static and ELF fields in 2002. The results and conclusions will be published in the Environmental Health Criteria series. It is anticipated that sufficient results will be available for IARC to conduct a similar evaluation of evidence for carcinogenicity of RF fields in 2003. WHO would then complete an overall health risk assessment of exposure to RF fields in 2004.

BIOGRAPHICAL NOTES

Kenneth R. Foster (F) is Professor of Bioengineering at the University of Pennsylvania, Philadelphia PA. Since 1971 his research has been related to the interaction of electromagnetic field with biological systems, including medical applications, mechanisms of interaction, and biological effects of electromagnetic fields, in which subjects he has published numerous scientific papers. He is former President of IEEE Society on Social Implications of Technology, and former chair of the IEEE EMBS Committee on Man and Radiation. Michael H. Repacholi is Coordinator, Occupational and Environmental Health, Department of Protection of the Human Environment, WHO, and Director of the EMF Project. He has been a member of numerous expert committees involving possible health effects of EMF and is the author or coauthor of 150 scientific publications.

4. REFERENCES

1. Information Ventures, Inc. EMF Database (CD-ROM). Information Ventures, Inc. 1500 Locust St. Philadelphia PA 19102-4321, 1994
2. C. H. Durney, H. Massoudi, M. F. Iskander, "Radiofrequency Radiation Dosimetry Handbook", Fourth Ed. San Antonio TX: Brooks Air Force Base. Report USAFSAM-TR-85-73 (available on World Wide Web at http://www.brooks.af.mil/AL/OE/OER/handbook/cover.htm).
3. C. Polk and E. Postow, eds., Handbook of Biological Effects of Electromagnetic Fields, Boca Raton: CRC Press, 1996, pp. 581-595.
4. K. R. Foster, "Thermal and nonthermal mechanisms of interaction of radiofrequency energy with biological systems," IEEE Trans. Plasma Science, Vol. 28, No. 1, 2000.
5. J. P. Reilly, "Applied Bioelectricity: From Electrical Stimulation to Electropathology", New York: Springer-Verlag, 1998.
6. J. F. Schenck, "Health and physiological effects of human exposure to whole-body four-Tesla magnetic fields during MRI", Ann. NY Acad. Sci., Vol. 649, 1992, pp. 285-301.
7. J. P. Blondin, D.-C. Nguyen, J. Sbeghen, D. Goulet, C. Cardinal, P. S. Maruvada, M. Plante, W. H. Bailey, "Human perception of electric fields and ion currents associated with high-voltage DC transmission lines", Bioelectromagnetics, Vol. 17, 1996. pp 230-241.
8. R. C. Lee, D. C. Gaylor, D. Bhatt, D. A. Israel, Role of cell membrane rupture in the pathogenesis of electrical trauma, J Surg Res 44:709-719, 1988.
9. D. W. Blick, E. R. Adair, W. D. Hurt, C. J. Sherry, T. J. Walters, J. H. Merritt, "Thresholds of microwave-evoked warmth sensations in human skin", Bioelectromagnetics, Vol. 18, 1997, pp. 403-409.
10. J. C. Lin, "The microwave auditory phenomenon", Proc. IEEE, Vol. 68. No. 1, 1980, pp. 67-73.

**EMC 2000** INTERNATIONAL WROCŁAW SYMPOSIUM ON ELECTROMAGNETIC COMPATIBILITY

# THE DIFFERENT KINDS OF EMF STANDARDS

G.Goldberg
Past Chairman IEC ACEC (Advisory Committee on Electromagnetic Compatibility)
Wannerstr. 43/61 8045 Switzerland Fax: +41 1 463 63 32 e-mail: gegegezurich@swissonline.ch

## *Abstract*

*The tremendous development of the use of electricity in all kinds of applications leads to the need for regulations to prevent or avoid negative effects on human health due to Electromagnetic Fields. These regulations concern the various aspects of the problem and are issued, by different bodies in different forms: standards, recommendations, guidelines. Aim of this paper is to explain the general structure of this standardisation work..*

## Background

Caused by the tremendous expansion of the use of electricity in all aspects of life: power applications, telecommunications, medical applications,.... the problems raised by the influence of Electromagnetic Fields (EM Fields) on human beings become more and more important. This field of interest and of concern encompasses a large number of activities:

- *biological/medical research and studies* in relevant institutes and laboratories (on humans, on animals, on cells .... for all kinds of EM fields)
-the specification of *exposure limits*(depending on the kinds of EM field and their effects )
-epidemiological investigations (for a practical and statistical assessment of the health effects)
- the development of *measurement equipment* and *procedures*
-*mitigation* methods (e.g. for the reduction of the field strength)
-*legal regulations* (e.g. by governmental bodies)

The non negligible possibility of adverse health effects on humans leads to a need for regulations for the prevention of these effects. These regulations cover two aspects: the *biological/medical aspect* with regard to the "victims", a *technical aspect* a with regard to the "sources" of EM Fields and their measurement.

Which are the relevant parameters?

First there is to consider different *frequency ranges,* depending on their health effects :
- *low frequency fields* in the frequency range 0...16'2/3 ....50/60 ....Hz produced for example by power lines, railways, industrial equipment, domestic devices, etc,
- *intermediate frequency fields* in the range of ca 10 kHz to 100kHz (1 MHz) emitted by domestic devices or industrial equipment
- *high frequency fields* above (0,1) 1MHz and up to 6 GHz or more, emitted by all kinds of radio transmitters, in particular by cellphone base stations, the handheld phones, also by industrial equipment, etc,

One can note that as for the formal boundary between the low frequency range and the high frequency range, the " classical" limit of 9 kHz used with regard to EMC has been slightly shifted and that another frequency range may be defined around 100 kHz.

Depending on the frequency range there is further to make a difference between the different *kinds of fields* which are to be analysed:
- in the low and intermediate frequency ranges the electric and magnetic fields separately
- in the high frequency range electromagnetic fields, the combination of both.

Depending also on the frequency range different *biological effects* are observed, whereby in the context of standardisation only, or mainly, in-vivo effects may be the subject of regulations (it seems inappropriate to develop standards for in vitro investigations in laboratories) .

It can be observed [3]:
- in the low and intermediate frequency ranges *non-thermal effects* like the stimulation of nerves and muscles, effects on the hormone production (e.g. melatonine), possibly carcinogenic effects,... (whereby there is to say that adverse effects have not been established with certitude and have still to be studied)
- in the high frequency range mostly *thermal effects* (clear limitations for the temperature rise in the tissues have been established)

## The different kinds of EMF regulations.

The standardisation organisations define in principle three kinds of regulations:
- *"standards"* which are - or should be - precise documents and should be strictly applied
- *"Recommendations"*, the application of which allows some flexibility
-*"Guides", "Guidelines* " which are rather informative documents and the application of which is also less compulsory

It should be noted that in scientific meetings the term "standard" is used indistinctly for these different kinds of documents (somebody said even "loosly") and it may be useful, from the viewpoint of the standardisation organisations, to take care of a clear distinction and apply above structure.

Apart of the documents developed by standardisation organisations there is to consider all the legal documents: *laws, ordinances, etc,...* issued by governmental or similar bodies. They may be documents developed specially for this purpose; they may be also documents taken over from scientific organisations or standardisation bodies

The term *"Regulation"* can be understood as a generic term encompassing all above documents.

Considering the whole range of topics covering the field of Human Exposure to EMF, it seems that the following topics could be considered [1]:

-**Technical Descriptions and Specifications of the Electromagnetic Environment** (in fact these documents should be common with the EMC Standards)

-Physiological Regulations or Legal Documents specifying **Exposure Limits**

-Technical Product Standards related to the sources of EM Fields and mitigation measures for the **Limitation of the emissions**

-Technical Standards related to the **Measurement Instrumentation, Measurement Procedures and Calculations** of the EM Fields

-(Possibly) Rules for **Epidemiological inquiries**

- **Regulatory Documents** (Laws, etc,..)

However it seems difficult to issue standards for scientific activities although this could useful in order to guarantee comparable results. If this seems difficult for particular scientific studies, it may be appropriate to establish some common rules for epidemiological enquiries in order to get comparable results..

Bibliography

[1] G.Goldberg," Regulations for the limitation of Human Exposure to EM Fields – An Overview", Proceedings of the Wroclaw Symposium on EMC 2000, Wroclaw, Poland, June 2000

[2] International EMF Project, Minutes of the meeting 3-4 June 1999, WHO,Geneva

[3] ICNIRP ." Guidelines for Limiting Exposure to Time-varying Electric, Magnetic, and Electromagnetic Fields (up to 300 GHz)", 1998 Health Physics 74, p.494-522

***Biographical Note***

G.Goldberg graduated as Electrical Engineer at ETHZ - Federal School of Technology Zürich. He worked thereafter mainly in the field of Control Equipment for Power Systems and became there acquainted with the EMC problems. He was from 1985 to1994 Chairman of IEC TC 77- Electromagnetic Compatibility - and from1990 to 1996 of ACEC – Advisory Committee on Electromagnetic Compatibility. He is presently still active member of ACEC where he initiated the IEC work on Human Exposure to EMF

NOTE: THIS PAPER IS THE INTRODUCTION TO THE SESSION ON EMF REGULATIONS OF THE EMC SYMPOSIUM WROCLAW 2000

EMC 2000 INTERNATIONAL WROCŁAW SYMPOSIUM ON ELECTROMAGNETIC COMPATIBILITY

# EUROPEAN EMF LEGISLATION

**turning the threat of trade barriers into an opportunity by means of standardisation**

Herman A.W. Leenders
Philips Corporate Standardization Department, P.O. Box 218, 5600 MD Eindhoven, the Netherlands
Fax: +31. 40. 27 33 929, email: herman.leenders@philips.com

*Abstract*

*There is an increasing worldwide concern about the effects of electromagnetic fields (EMF) on the health of human beings.*
*On 12 July 1999 the Council of European Health Ministers has approved a European EMF Recommendation, including limits for exposure of the general public.*

*The Recommendation leaves it open to EU member states to define national legislation. In some countries legislation with diverging (notably more stringent) limits has come into operation, and in other countries such legislation is under preparation. This tendency has the threat to become a serious barrier to trade.*

*On the other hand the Recommendation has accelerated the development of harmonised standards, to be connected to the European LVD and RTTE Directives. These harmonised standards, once operational, offer a powerful opportunity to convergence, thus diminishing the trade barriers.*

## 1 BACKGROUNDS

In 1998 new guidelines [1] have been issued by **ICNIRP**, the International Committee on Non-Ionizing Radiation Protection, linked to the World Health Organisation.

These guidelines are based on an extensive survey of research results, mainly of a biomedicine nature. The guidelines apply to exposure levels. They define levels to which the following categories of individuals can be exposed:

- the general public
- occupational workers.

This publication focuses on the general public, the area where the majority of the current efforts in legislation is carried out.

ICNIRP distinguishes 2 categories of upper values:

- Basic Restrictions. Although they include a safety factor, ICNIRP considers the basic restrictions as upper limits for exposure. The Basic Restrictions are expressed in the quantities B, J, SAR, and S [1]) as they occur in the human body.
- Reference Levels. These are developed because some of the Basic Restrictions are difficult to measure in the human body. The Reference Levels are derived from the Basic Restrictions under worst-case conditions, such as maximum coupling of the exposed fields into the human body. The Reference Levels are expressed in E, H, B, S, $I_L$, with additional quantities $I_C$ and, for pulsed fields, SA [2]).

In assessment of exposure levels in a given situation, it may sometimes be practical to start with assessment against the Reference Levels because that is often easier[3]). Exceeding the Reference Levels is not a violence of the ICNIRP guidelines, it only means that an assessment against the Basic Restrictions still has to be done.

---

1 B = magnetic flux density (T)
J = current density ($A/m^2$)
SAR = specific absorption rate (W/kg)
S = power density ($W/m^2$)

2 E = electric field strength (V/m)
H = magnetic field strength (A/m)
SA = specific energy absorption (J/kg)
$I_L$ = limb current (A)
$I_C$ = contact current (A)

3 Assessment against the Reference Levels is not a necessary step: direct assessment against Basic Restrictions is also a good practice.

The Basic Restrictions can be compared to a red traffic light: you are not allowed to pass it.



Basic Restrictions

The Reference Levels are to be compared with a sign for approaching a traffic light: it means that you must take special care not to pass a red light, but you may pass when the light is green.



Reference Levels

Based on the ICNIRP guidelines The Council of Health Ministers of the European Union have issued the **Council Recommendation**[4]) "on the limitation of exposure of the general public to electromagnetic fields (0 Hz to 300 GHz)" of 12 July 1999 [2].

This Recommendation advises the member states to adopt it into national legislation. Within 5 years the European Commission will report about the adoption. In addition, it recommends member-states and the European Commission to encourage research.

The Recommendation leaves the door open for member states to develop legislation, which is more stringent. If such legislation is applicable to equipment, this will contribute to trade barriers, as will be discussed in the following chapter.

Another important statement in the Recommendation is, that the Council invites the European Commission to "Work towards the establishment of European standards ....., including methods of calculation and measure". This has become the basis of the Mandate that the European Commission has given to CENELEC and ETSI for the development of such standards. This mandate will be discussed in chapter 3.

A very positive effect of the Recommendation is the harmonising tendency: it advises the adoption of ICNIRP limits & levels in member states, and to take these into account in European standards.

[4] A Recommendation is an instrument of the European Council of Ministers to *recommend* member states to incorporate European policy into national measures.

On the other hand, because a recommendation is a non-mandatory instrument, it leaves an opening for divergence: member states may establish their own limits.
Chapter 4 will deal with a strategy on how to let the harmonising tendency prevail over the divergence.

## 2 BARRIERS TO TRADE

Various countries in the European Union have legislation and/or standardisation in place which deviates from the Council Recommendation and the ICNIRP guidelines. In some cases the differences are very substantial. Other speakers will highlight a number of examples. Also outside the EU various regulations are not consistent with ICNIRP. Sometimes the differences are rather arbitrary, just like we have small differences in speed limits in Europe. In other cases the differences are more fundamental, often coloured by the "flavour of the day" in the local politics. Some countries apply no limits at all.

This has lead to the current situation of a variety of limits applied, inside and outside Europe. The ICNIRP guidelines and the Council Recommendation have triggered a revision of laws and standards right at this moment in a number of countries, which adds up a dynamic uncertainty apart from the divergence.

An further unclarity is, how exposure legislation can be applied to equipment emission:

- Exposure applies to the field values in which individuals are situated.
- Emission values describe the field that is emitted by equipment.

Health authorities for example are concerned with exposure. Equipment manufacturers keep their products under emission limits, but can not assume responsibility for exposure of individuals to fields emitted by multiple sources.

An important part of the legislation applies to exposure rather than emission, and in most of these situations there is no litigation yet to clear up if exposure legislation can be applied to equipment.

This whole situation is far from optimal, not for consumers and not for manufactures. For consumers there is a lack of transparency: it is hard to understand why a certain product is good for British people and not acceptable in Italy. For manufacturers it leads to trade barriers and higher costs.

## 3 HARMONISED STANDARDS

Fortunately there is not only the tendency of divergence. The same Council Recommendation also urges the European Commission to work towards European standards. It is only logical that these will be based on the Council Recommendation.

Even though the application of the Recommendation means a rather stringent regime, most industries embrace it because they prefer a rather stringent situation above a scattered and uncertain one.

The encouragement to standardisation takes place on the basis of a European Commission mandate to CENELEC and ETSI, which was in a state of finalisation when writing this paper. The mandate urges the standardisation bodies to develop standards, which are directly linked to the Recommendation. There will probably three types of standards, which typology is derived from the EMC world:

- Basic standards, defining the assessment methods.
- Generic standards, defining the general performance criteria and compliance limits.
- Product standards and product family standards, containing more detailed performance criteria and specific assessment elements for certain products or product families (e.g. GSM phones, domestic equipment etc.).

The Basic Standards are for reference only. The other two types are called "harmonised standards", to be connected with European legislation (as will be elucidated in chapter 4).

The central platform for EMF standardisation in Europe is CENELEC TC 211, "Electromagnetic fields in the human environment".
This committee has just been restructured and has now product-oriented working groups and a few horizontal working groups.

This structure facilitates the development of the basic and generic standards in the horizontal WG's, while the product (family) standards are made in co-operation between the product-oriented working groups in TC 211 and product-oriented Technical Committee's (such as TC 61 for domestic appliances, TC 92 for consumer electronics, but also ETSI for telecom equipment). CENELEC TC 211 has established a liaison with ICNIRP in order to safeguard the link between its guidelines, the standards and the Council Recommendation.

The mandate as well as the public interest in EMF triggers acceleration in the standard development. A draft product standard for cellular phones is already produced, and other working groups will soon reach this stage.

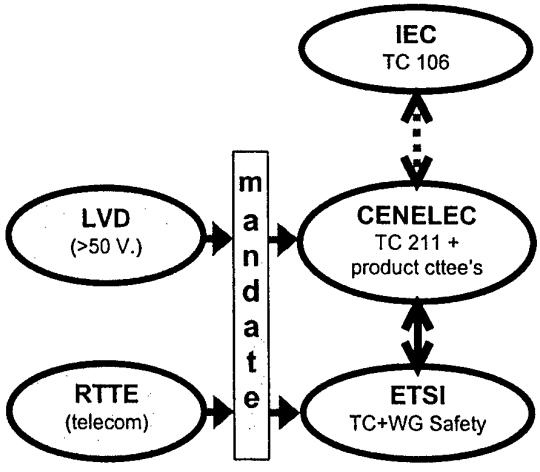
Even more meaningful than European convergence is the development towards global standardisation. IEC TC 106 has just been established at the end of 1999 with the provisional title "Testing Instrumentation and Methods for Measuring Electric and Magnetic Fields Associated with Human Exposure". It is logical that an exchange mechanism between the relevant Technical Committee's in IEC and CENELEC will soon be realised.

## 4 HOW STANDARDS AFFECT LEGISLATION

In Europe the harmonised standards will be connected to legislation, in casu two European Directives[5]):

- The Low Voltage Directive (LVD) which covers the safety of products with an operating voltage between 50 and 1000 Volts.
- The Radio Equipment & Telecommunications Terminal Equipment (R&TTE) directive.

The harmonised standards will be listed in the Official Journal of the European Communities. From that moment on, products that comply with these standards will automatically comply with the radiation requirements of these directives. In this way the apparatus emission levels will in the future be linked to the Council Recommendation.




the link between European legislation and standardisation

[5] A Directive is an instrument of the European Council of Ministers to impose European policy into legislation of the member states. As such it has a stronger regulatory power then a Recommendation.

It may be expected that this link to the LVD and the R&TTE directive will overrule the differences in national legislation, if these block the free trading of goods. Trade barriers will diminish as a consequence of article 95 (previously article 100A) of the European Treaty.

## 5 CONCLUSIONS

The current threat of diverging national legislation on EMF can be converted into an opportunity for achieving harmonised standards. These will discourage national authorities to come with deviating legislation. In this way harmonised standards reduce the danger of trade barriers.

CENELEC TC 211 in its collaboration with ETSI is an appropriate platform for developing the standards. A global convergence can be achieved when a liaison with the new IEC TC 106 is established.

## 6 REFERENCES

1. International Commission on Non-Ionizing Radiation Protection (ICNIRP): "Guidelines for limiting exposure to time-varying electric, magnetic, and electromagnetic fields (up to 300 GHz)", Health Physics Vol. 74, No. 4, April 1998.

2. European Council of Health Ministers: "Recommendation of 12 July 1999 on the limitation of exposure of the general public to electromagnetic fields (0 Hz to 300 GHz)" Official Journal of the European Communities L.199/59-61, 30-07-1999.

## THE AUTHOR

Herman A.W. Leenders works as senior standardisation officer in Philips Electronics in the Netherlands. He is involved in national and international standardisation committee's in the area of electromagnetic fields in the human environment.

He graduated in electrical engineering at Eindhoven University of Technology in 1981, after which he worked in government and small companies before joining Philips in 1996.



**EMC 2000** INTERNATIONAL WROCŁAW SYMPOSIUM ON ELECTROMAGNETIC COMPATIBILITY

# STANDARDISATION AND REGULATION IN GERMANY

Holger Schwarz
Narda Safety Test Solutions, Mühleweg 5, D-72800 Eningen u. A., Germany,
Tel.: +49 7121 86 1277, Fax: +49 7121 86 1480, e-mail: holger.schwarz@safety-test-solutions.de

*Every country has it own limits and procedures for safety in electromagnetic fields. This article shall visualise some of the differences between the ICNRP standard and the German regulations.*

Since January 1, 1997, in the Federal Republic of Germany exists a law for the protection of the public against electric and magnetic field, the *26. Verordnung zur Durchführung des Bundesimmissionsschutzgesetz (Verordnung über elektromagnetische Felder* - 26. BImSchV) (= 26. ordinance ("Electromagnetic Fields) to the German Emissions Control Act) – in brief: 26. BImSchV [1]. This refers exclusively to persons of the private sector and not to industry and handicraft. The law was proclaimed by the German Federal Ministry of Environment.
The limit values of the 26. BImSchV refer to the IRPA/INIRP standard of 1988 [2]. At the moment, the 26. BImSchV is revised and the limit values of ICNIRP 1998 [3] were considered. The requirements on the measurement technique and the valuation of the signals and measurement results refer to DIN VDE 0848, part 1 [4]. This is also in revision at the moment and will be published July 2000. The VDE will have consequences on the European standard and their workgroup TC 211.

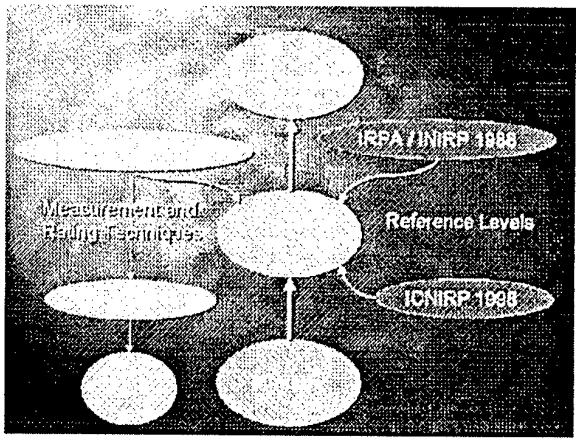



Figure 1) Legislation in Germany, General Public

To protect people in the industry and handicraft, the Professional Association Regulatory Standard for Occupational Safety and Health - BGV B11 - is in preparation. It should become legal force this year. Therefore the German Federal Ministry of Work will advise the Professional Association (Social Insurance), to establish the BGV B11 in the companies. The limit values in the high frequency are on the same level like them of ICNIRP 1998, but in the low frequency, there are relevant differences. Concerning the requirements on the measurement technique and the valuation of the signals and measurement results, the BGV B11 refers partly to DIN VDE 0848, part 1. The BGV B11 has no influence on branches, like for example the military.

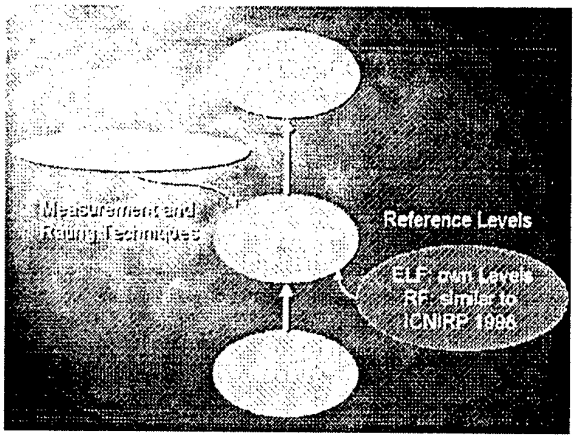



Figure 2) Legislation in Germany, Occupational

The Professional Associations take the insurance cover for work accidents and are an obligatory insurance for all companies. If the employer can prove that he fulfilled all duties that the Professional Association imposed on him, the Professional Association assumes all payments for injuries. If not, the Professional Association can make the company liable for compensation.

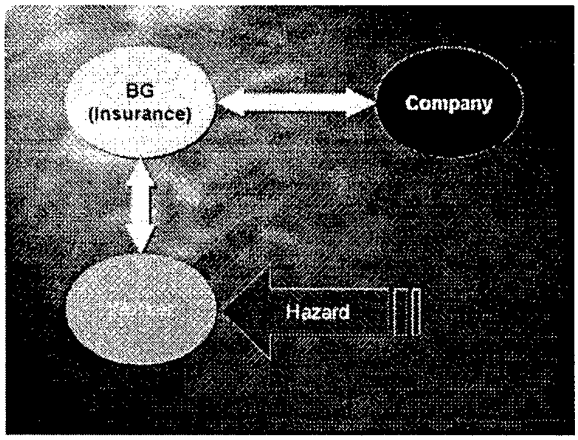



Figure 3) Role of "Berufsgenossenschaft"

Figure 4 shows the difference for the RF between the BGV B11 and ICNIRP. Over 30 MHz, both standards have the same limit values. The two standards differ only at frequencies below 30 MHz where ICNIRP shows partly significantly lower limit values.
BGV B11 Area 1 concerns to safety at workplace. The BGV B11 Area 2 concerns persons at workplaces, e.g. secretaries, who are not directly engaged in production lines. The Area 2 limit values agree with the 26. BImSchV, the limit values for the general public.

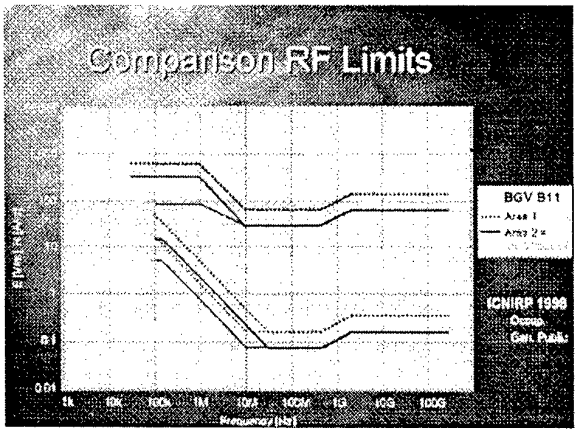



Figure 4) Comparison RF Limits

In the low frequency, this trend of drastically lower limit values for the ICNIRP standard continues. The 26. BImSchV has specified only two frequencies in the low frequency: 16 2/3 Hz, the frequency of the German railways and 50 Hz. The values are taken from the limit values of ICNIRP "General public".

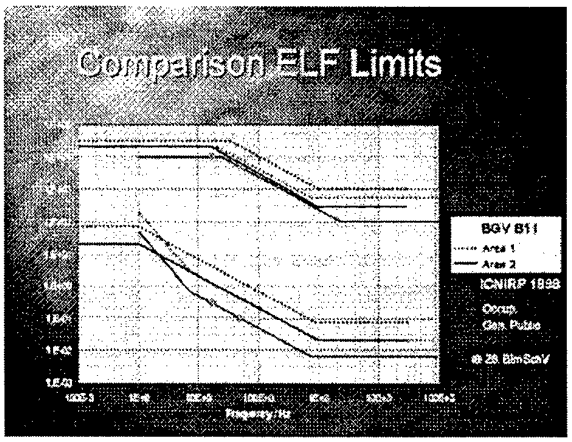



Figure 5) Comparison ELF Limits

Another – and very important – difference between ICNIRP and BGV B11 is the definition of the 30 % law. The 30 % law says that all frequencies that are less than 30 % of the highest carrier, have not to be considered. The BGV B11 makes one step more and uses the 30 % law for the limit value only after standardisation. That means the other spectral lines are normalised on the standard, what can signify a distinctly raise. After this, it is checked if they are still under 30 %. So it may be that the signals correspond to ICNIRP, but are over the limit values of the BGV B11.

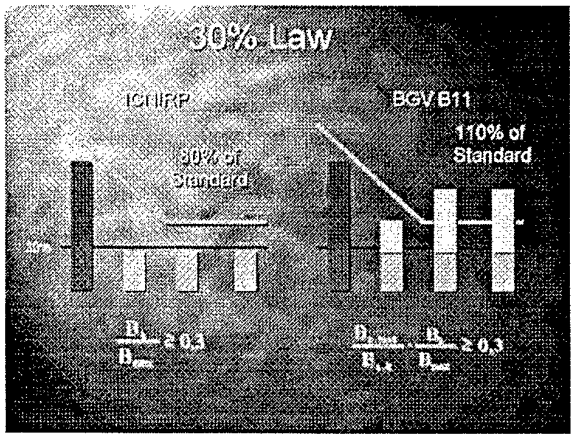



Figure 6) The 30% Law

References

[1] Hauptverband der gewerblichen Berufsgenossenschaften. BG-Vorschrift Elektromagnetische Felder BGV B11. Berufsgenossenschaftliche Vorschrift für Sicherheit und Gesundheit bei der Arbeit (26. ordinance ("Electromagnetic Fields) to the German Emissions Control Act). Redaktionell überarbeiteter Entwurf vom 31. Mai 1999

[2] International Non-Ionizing Radiation Committee of the international Radiation Protection Association. Guidelines on the limits of exposure to radiofrequency electromagnetic fields in the frequency range from 100 kHz to 300 GHz. Health Physics 54: 115-123;1988

[3] International Commission on Non-Ionizing Radiation Protection ICNIRP. Guidelines for limiting exposure to time-varying electric, magnetic, and electromagnetic fields (up to 300 GHz). Health Physics October 1998, Volume 75, Number 4

[4] Deutsche Elektrotechnische Kommission im DIN und VDE (DKE). Sicherheit in elektrischen, magnetischen und elektromagnetischen Feldern Teil 1: Definitionen, Meß- und Berechnungsverfahren ( Safety in electric, magnetic and electromagnetic fields – Part 1: Definitions, methods for measurement and calculation). DIN VDE 0848-1. Juli 1998.

Biographical Note

Holger Schwarz studied electrical engineering, field communications engineering, at the advanced technical college in Kiel, Germany. In 1986 he began to work at Wandel & Goltermann in the marketing department for spectrum analysis. Since five years he works in the department for measurement technique for electromagnetic fields which changed to Narda in January 2000.



EMC 2000 INTERNATIONAL WROCŁAW SYMPOSIUM ON ELECTROMAGNETIC COMPATIBILITY

# REGULATIONS FOR THE LIMITATION OF HUMAN EXPOSURE TO EM FIELDS- AN OVERVIEW

G.Goldberg
Past Chairman IEC ACEC (Advisory Committee on Electromagnetic Compatibility)
Wannerstr. 43/61 8045 Switzerland Fax: +41 1 463 63 32 e-mail: gegegezurich@swissonline.ch

***Abstract***

*A great activity takes place presently world-wide regarding Human Exposure to Electromagnetic Fields and one of the current tasks is to specify regulations for the protection oh humans against possible adverse health effects caused by these fields. The term "regulation" is to be understood in a general manner and encompasses standards, recommendations or guidance documents. They are issued by official bodies or relevant scientific organisations. Aim of the paper is to give an overview on this activity: who, what, how, ...? It will also give a summary of the some relevant international or national regulations .It should be noted that this activity has common aspects with EMC and it may be useful for EMC experts to be informed of the work on EMF and vice-versa.*

## 1. Who ? Which Organisations develop EMF Regulations

The term "Regulations" is, in the context of this paper, a generic term for documents dealing with the limitation of Human Exposure to EMF and the protection against adverse health effects. It encompasses standards, recommendations, guidelines, the application of which may be either mandatory or voluntary (see definitions in Annex 2)

1.1. The "world-wide "organisation of the standardisation work on EMF is quite complicated (and diversified) From a general view point there is to make a difference between scientifically oriented organisations – which develop biological/medical standards- and technically oriented organisations which develop measurement and similar standards. The most important organisations may be the following:

- *World-wide Scientific Organisations like*
  - WHO ( World Health Organisation) ICNIRP (International Commission for Non–Ionising Radiation Protection)
  - These two organisations have a clear separation of responsibilities which are complementary:
    WHO is responsible for scientific studies (e.g. The International EMF Project)
    ICNIRP is responsible for the specification of the exposure limits (e.g. the ICNIRP Guideline)

- *World-wide Technical Standardisation Organisations like*
  - IEC ( International Electrotechnical Commission),
  - ITU (International Telecommunication Union)
  - IEEE ( for the USA but also for other countries) which develop mostly technical standards but also recommendations or guidelines

- *Political Organisations e.g.*
  - the Commission of the EUROPEAN UNION which issues general Directives for the Member Countries of the EU

- *Regional Technical Organisations e.g.*
  - CENELEC (Comité Européen de Normalisation Electrotechnique)
  - ETSI (European Telecommunication Standardisation Institute) in charge of the implementation of the EU directives.

- *Governmental, in some countries Regional or even Municipal, Authorities*

- *Electrotechnical Organisations like*
- VDE, SEV, BS, ANSI, etc, which issue National Regulations

- *Industrial Organisations e.g.*
- ARIB in Japan,) Association of Radio Industries and Business) for their specific apparatus and systems

All these bodies develop documents which may be standards, recommendations or guides ( however their titles do not always correspond to the formal definitions).

1.2. IEC, the world-wide Electrotechnical Standardisation organisation, has decided only recently to deal with the problems of Human Exposure to EMF. Because of the subject of Electromagnetic Fields has some common points with EMC, the work started in a "Task Force EMF" of ACEC, which suggested the creation of a new Technical Committee and prepared a proposal for the programme of work of this committee (see Annex 1).
It is the general opinion that IEC shall not deal with biological/medical issues which should remain in the responsibility of relevant bodies : research institutes or organisations like WHO or ICNIRP. IEC shall deal only with technical matters like measurement techniques or the evaluation of EM fields sources.
In September 1999, the Committee of Action of IEC decided to set up a TC 106 with the provisional title " Testing Instrumentation and Methods for measuring Electric and Magnetic Fields Associated with Human Exposure". This title and accordingly the scope of the TC is somewhat restrictive compared to the ACEC proposal and may be revised. Liaison with TC 77 - "Electromagnetic Compatibility" - and CISPR -" Protection of the Radio services"- would be appropriate (see Annex 1)

1.3 For European experts and those who have a close relationship with the European Union it is useful to be informed of the particular organisation in this body:
- the EU issues Directives or Recommendations which specify general requirements.The Council of the EC has recently circulated a "Recommendation of 12 July 1999 on the limitation of exposure of the General Public to Electromagnetic Fields (0 Hz to 300 GHz)" [3] [5]
- the task to develop the necessary regulations is allocated to the standardisation bodies of the EU, in our case CENELEC or ETSI
- however it happens that the Directorates of the Commission set up special Working Parties to deal with specific problems, e.g. Cost 244 for the study of the biological effects (Directorate V) or CEPHOS for the problems related to cellular phones (Directorate XIII)

CENELEC has set up a TC 211 which original task was to specify exposure limits and measurement methods. However the responsibility for specifying exposure limits has passed from CENELEC to the Commission itself and the task of TC211 has been changed in that sense that the committee should deal now only with technical issues. In fact the scope of TC 211 is quite similar to the scope of IEC TC106 and a close co-ordination between the two committees would be very appropriate.

## 2. What? The topics of the EMF Regulations

It is assumed that the relevant factors are well known: E-fields, H-fields, SAR, contact current,...

From a general view point three kinds of regulations should be considered in the context of EMF protection:
- general biological/medical standards,
- general technical standards
- national protection regulations

2.1. General Biological/ medical standards

A tremendous number of studies are carried out about the EMF effects which should lead to protection regulations. However the present state of knowledge is such that if a wide amount of partial results on specific subjects is available but that there is still an incomplete overall view on general problems. For example, adverse effects on humans seem well recognised for short term exposure and immediate health consequences but long term effects have not yet been scientifically clearly established. In order to respond to this need WHO has started an "International EMF Project " which aim is" to assess the scientific literature and reports on health effects ....and provide a co-ordinated international response to concerns about possible health effects of exposure to EMF" It should be noted that the resulting document will be a scientific report, not a standard.[15]

Two general documents are important for the specification of exposure limits
- the ICNIRP Guidelines, which becomes nowadays a world-wide reference [1] [2] .. see Fig. 1
- the EU Recommendation, which is relevant for the EU countries [3] (note that this document is a Recommendation, not a Directive so that its application is in principle not mandatory)

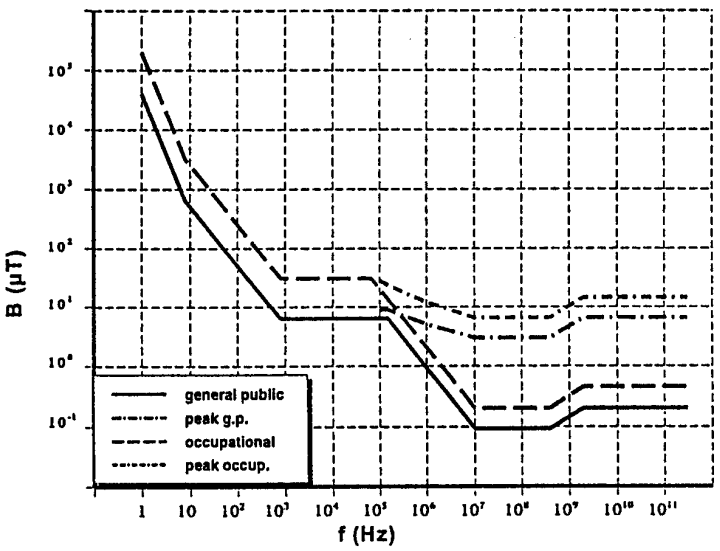



Figure 1: Reference levels for exposure to magnetic fields according ICNIRP Guidelines

A future standard could be useful establishing common rules for epidemiological enquiries in order to allow a systematic comparison of the results.

The specification of Exposure Limits is a specific biological/medical problem and therefore not in the province of IEC or now of CENELEC

2.2. General Technical standards

Only very few international technical standards exist for the time being and the work is starting in IEC (or CENELEC). The main standardisation subjects could be the following:

- description and specification of the EM environment (which fields, magnitude, frequency of occurrence,...)
- measurement instrumentation and procedures (LF, HF, SAR,.....)
- field distribution around the field sources (LF fields from Power Lines, Industrial equipment, domestic devices, etc, or HF fields originating from all kinds of Radio Transmitters, Mobile Telephones, industrial equipment,...( practically "product" related documents)
- emission limits for individual sources (and summation rules)
- mitigation measures when necessary (and possible)
- calculation methods (for theoretical assessments and for the cases where measurement are not possible)

It should be remembered that the field to which a person is exposed may be emitted by a single source or resulting from the superposition of several sources. In order that the resulting field does not exceed the exposure limit it is necessary to specify emission limits for the individual sources.

A programme of work proposed for IEC is given in Annex 2. CENELEC has practically the same programme

2.3. National Regulations

National Regulations are issued by the national Regulatory Authorities for the practical implementation of the protection of their citizens. Possibly for lack of international recognised standards, they are quite different from one country to the other . Table 1 summarises the main features of several relevant ones and leads to some general comments:[6] [7] [8] [9]

a) practically there are three aspects to consider:
. exposure limits
. emission limits for individual emitters
. measurement or calculation methods

b)exposure limits refer often to the ICNIRP Guidelines but also to other values

c) the regulations do not always specify emission limits

d) an important principle is the "Principle of Precaution" to take into consideration the not yet established conclusive effects: unknown effects, long term effects,...Regulatory authorities wants to be very cautious! This is particularly the case in Switzerland and Italy

| Country | Main features |
|---|---|
| Germany | Exposure limits refer to ICNIRP<br>Emission limits:<br>30 % rule: fields less than 30% of the limit are not considered<br>In the power frequency range only two frequencies are considered: 50 and 16 2/3Hz |
| Japan | No intention to apply the ICNIRP limits<br>No limitation regulation for power frequency fields<br>Limitations in the range 10 kHz to 300 GHz in term of V/m and A/m and SAR |
| Poland | Limits in terms of kV/m ,A/m and Power density W/m2<br>Zone concept: safe, intermediate, hasardous, dangerous zones |
| Switzerland | Principle of precaution<br>Places of sensitive use<br>Exposure limits: ICNIRP field limits (SAR limits not yet)<br>Emission limits: severe safety factor in order to take into consideration long term effects and the superposition of several fields |

Table 1: Some particular features of national EMF regulations

**Annex 1 A programme of work for IEC and CENELEC**

The EMF Task Force of IEC/ACEC has identified a number of tasks which could serve to establish the programme of work for the next future.. This proposal makes a difference between "Horizontal standards" for general use and "Vertical standards" related to specific sources and fields.

A.- Horizontal standards

1. Measurement of LF magnetic and electric fields with regard Human Exposure
2. Measurement of HF electromagnetic fields with regard Human Exposure
3. Calculation methods for low frequency induced currents
4. Calculation methods for high frequency fields

B. Vertical standards or Technical Specifications

*B.1 Low and intermediate frequency range*

1. Domestic Equipment
2. Power lines - Public Exposure
3. Power lines – workers
4. Industrial power equipment(heating)
5. Small and medium sized industrial equipment
6. Railways

*B.2. High Frequency range*

7. Hand-held and body mounted wireless communication devices
8. Base stations for cellular phone
9. Antitheft devices
10. Smart cards readers
11. Broadcast emitters
12. Radars

B.3. Low and high frequency range

13. Active medical implants

CENELEC TC 211 has established a programme of work which is very similar to above proposal and of course a close co-ordination between the two bodies would be very appropriate.
Some of the problems are also subjects of work in other organisations but to our knowledge such a consistent programme does not exist , the items are considered case by case.

**Annex 2 The different types of ( EMF) Regulations**

It appears that there is some confusion about the meaning of the words " standard", "recommendation",
"guide/guidelines", particularly among people not working in standardisation bodies. It seems useful to remind how they are understood and applied in such bodies like IEC, ISO, CENELEC, etc ,...It should be noted that they have generally a different legal status.

"Standards": This term is used in the standardisation work for documents which specify as exactly as possible their field of application, their rules of application, etc,... and in this sense they have a mandatory character. In above organisations they are generally written in a strict and short style without detailed justifications or explanations.

"Recommendations": This term is used for documents with the same technical character as standards but their application may be not so strict and allow some flexibility.

"Guides/Guidelines": These are rather general technical or scientific documents, with a more tutorial and informative character .

The term "Regulations" is used in this paper as a generic term which encompasses these three kinds of documents. In IEC Recommendations and Guidelines are called "Technical Specifications" (in CENELEC European Specifications)

It would be appropriate if the same terminology would be used outside the standardisation organisations in order to avoid confusions.

It should be noted that American standards are generally written in a much broader style than the European ones ,with detailed comments and justifications

**Bibliography:**

[1] ICNIRP ." Guidelines for Limiting Exposure to Time-varying Electric, Magnetic, and Electromagnetic Fields (up to 300 GHz)", 1998 Health Physics 74, p.494-522
[2] ICNIRP." Response to questions and comments on ICNIRP Guidelines" , 1998 Health Physics 75, p. 438-439
[3] European Union. "Council Recommendation of 12 July 1999 on the limitation of exposure of the general public to electromagnetic fields (0 Hz to 300 GHz)", Official Journal of the European Communities 30.7.1999, p.59 - 70
[4] Dr. K.R.Foster and Dr. M.H. Repacholi. "Biological Effects of Electromagnetic Fields with Emphasis onHealth and Safety"
Proceedings of the 15th International EMC Symposium Wroclaw 2000.
[5] H.A.W. Leenders "European EMF Legislation".
Proceedings of the 15th International EMC Symposium Wroclaw 2000.
[6] Dr. J. Baumann. ".Regulations for the protection of the general population in Switzerland".
Proceedings of the 15th International EMC Symposium Wroclaw 2000.
[7] H. Schwarz. ".EMF Standardisation and Regulations in Germany".
Proceedings of the 15th International EMC Symposium Wroclaw 2000.
[8] Prof. E. Masada. "Regulations for the Limitation of Human Exposure to EM Fields in Japan".
Proceedings of the 15th International EMC Symposium Wroclaw 2000.
[9] S.Rozycki,."Regulations for the Limitation o of Human Exposure to EM Fields in Poland ".
Proceedings of the 15th International EMC Symposium Wroclaw 2000.
[10] IEC 61786 " Measurement of low-frequency magnetic and electric fields with regard to exposure of human beings – Special requirements and guidance for measurements"
[11] IEC 61983 "Measurement and assessment of Human Exposure to High Frequency Electromagnetic Fields (9 kHz to 300 GHz)" –Presently Committee draft 85/ ../ CD
[12] IEC 61566 " Measurement of exposure to radio-frequency electromagnetic fields - Fields strength in the frequency range 100 kHz to 1 GHz".
[13] IEC 61000-2-7 "Electromagnetic compatibility – Environment – Low frequency magnetic fields in various environments"
[14] IEC Document CA/1545/DV 1999-07. "Proposal of ACEC for a new field of technical activity" (Human Exposure to EMF)"
[15] International EMF Project, Minutes of the meeting 3-4 June 1999, WHO,Geneva

***Biographical Note***

*G.Goldberg graduated as Electrical Engineer at ETHZ - Federal School of Technology Zürich. He worked thereafter mainly in the field of Control Equipment for Power Systems and became there acquainted with the EMC problems. He was from 1985 to1994 Chairman of IEC TC 77- Electromagnetic Compatibility and from1990 to 1996 of ACEC – Advisory Committee on Electromagnetic Compatibility. He is presently still active member of ACEC where he initiated the IEC work on Human Exposure to EMF*

EMC 2000 INTERNATIONAL WROCŁAW SYMPOSIUM ON ELECTROMAGNETIC COMPATIBILITY

# REGULATIONS FOR THE LIMITATION OF HUMAN EXPOSURE TO EM FIELDS IN JAPAN

Eisuke Masada
Science University of Tokyo, Dept. of Electrical Engineering
2641 Yamazaki, NODA 278-8510, Japan
FAX: +81-471 24 1810 E-mail: masada@ee.noda.sut.ac.jp

*The safety regulations in Japan are separated into ordinances of various ministries. The limitation of human exposure to EM fields has been mainly studied by MITI and MPT in relation with regulation. At present MPT sets a guideline for human protection against radio wave applications. The association of Radio Industries and Businesses (ARIB) has introduced a standard to follow this guideline voluntarily.*

## 1. INTRODUCTION

The health effects of exposure to the electro-magnetic fields (EMF) has been much concerned by publics in relation with the construction of UHV transmission lines, spread of utilization of mobile phones and the development of the magnetically levitated transportation system in our country. Though the Environment Agency represents our country for WHO/EMF project and the Ministry of Welfare administers public health, the problem of the exposure to EMF has been discussed mainly in relation with safety of products and installations, and studied for regulation by the Ministry of Post and Telecommunication (MPT) in high frequency area, as well as the Ministry of International Trade and Industry (MITI) in low frequency area.

In academic institutes the problem has been also investigated with many specialists and the field measurements have been carried out [1],[2]. The industries of electronics manufacturers, telecommunication systems and power utilities, have had much concern on the matter and performed experimental researches in their own facilities. Those results have been taken into account in the discussion related to the regulation of exposure to EMF in ministries.

## 2. REGULATION IN HIGH FREQUENCY EMF

The emission level of the high frequency EMF is regulated both for products safety and for safety related to telecommunication systems. In the former case, the leakage EMF from micro- wave ovens only is controlled in the Electrical Appliance and Material Control Law of MITI. In the latter case, MPT sets a protective guideline. Industries for telecommunication equipments has introduced a standard to comply with it and made their products follow it voluntarily. The manufacturer association of personal computers and related materials, Japan Electronic Industry Development Association (JEIDA) has introduced a voluntary control for the computer display to suppress EMF emission to the level required by MPR-II regulation of Sweden.

### 2.1. Regulation for appliances

The safety of appliances and materials like wires used in our home is regulated with the Electrical Appliance and Material Control Law of MITI. In relation with health effect of exposure to EMF from appliances, the leakage EMF from the microwave oven is only limited for safety in the law. The details on the limiting value are given in a ministerial ordinance as:

- leakage EMF power less than 1mW/cm$^2$ at 5cm from the surface of the equipment under operation with the door closed.
- leakage EMF power less than 5mW/cm$^2$

at 5cm from the surface of the equipment just before the moment when its door is opened and it is automatically switched off.

- The above-stated conditions are satisfied after 100,000 times of operation.

2.2 Protective guideline of TTC/MPT

The telecommunication technology council of the ministry of post and telecommunication (TTC/MPT) submitted a guideline, " protective guideline for human exposure in the application of the electromagnetic wave", (protective guideline of radio wave) to MPT in 1990. It was based on the ANSI standard of 1982 and covered the frequency range of 10kHz – 300GHz. The Research and Development Center for Radio Systems (the present Association of Radio Industries and Businesses ARIB) established a standard, "Standard for Protection against Radio wave" (RCR STD-38) following the guideline. Manufacturers and operators of the tele-communication system have fulfilled this standard voluntarily.

With the spread of mobile phones and community broadcasts with FM, public concern has been increased on installations related to them. MPT requested to the council to consider the situation and reexamine the guideline. TTC/MPT reported a recommendation on human protection in applications of radio wave in 1997 as:

(1) The allowable limits of the electromagnetic field strength in the 1990 guideline are still appropriate.

(2) The regulation of the EMF should be introduced first into the area, where the measurement and assessment methods have been established enough. The subjects of the safety regulation related to public health should be limited to radio wave applications utilized in the neighborhood of human bodies such as mobile phones for the time being.

On this basis the guideline was revised partly.

The guideline classifies the environment into two categories as:

(1) controlled environment as working places where the radio wave is utilized with consideration on the guideline.

(2) General environments other than (1) as our home.

The allowable limit of EMF is shown in Table 1. The guideline for the local absorption of the radio wave from equipment used in the proximity of the human body as mobile phones, is given on the limit of the specific absorption ratio (SAR) and the contact current as Table 2. However, the equipment with the rated output less than 7W is assumed to comply with this guideline with the distance of 7cm to the human body and exempted from the application of the guideline. ARIB has established a standard to assess SAR for cellular phone, "Specific Absorption Rate (SAR) Estimation for Cellular Phone" (ARIB STD-T56). The manufacturers and operators of portable cellular phones and terminals are expected to use this standard voluntarily, in order to comply with the SAR guideline.

2.3 Radio wave law of MPT

The progress of the telecommunication technology and the spread of its applications have aroused more concern on the public health problem. With the advise of the Radio wave Control Council, MPT decided to implement the protective guideline of radio wave into its regulation, in order to promote the utilization of radio wave smoothly for the establishment of info-telecom society in future and revised enforcement regulations of the radio wave law in 1998. The operator of a radio station is obligated to take measures to prevent general publics to enter the area, where the strength of the radio wave generated from the installation is over the limit specified with the guideline. Such stations as :

- the station with the average antenna output power less than 20mW
- mobile stations
- temporary stations for emergency use

## 3.REGULATION IN LOW FREQUENCY EMF

The human exposure to the low frequency EMF has been concerned mainly in relation with the high voltage transmission lines and installations of the electric power utilities. The electric utility industry law of MITI regulates installations and equipment utilized in electric power utilities for the safety problems of publics. If EMF generated by them gives serious influence on human health, it should be controlled in this law. The low frequency EMF is also produced with home appliances and electric wiring in house. The Electrical appliance and Material Control Law of MITI covers the problems of human safety on them.

3.1 Regulation of electric field

The high voltage transmission line generates electric field on the ground surface. If a person stands under the line, this field induces a potential

difference between its head and feet. To avoid the phenomenon to be perceived by the person, the electric field is limited to be less than 3kV/m at the height of 1m from the ground surface under the line in the electric utility industry law. The installation should be built to comply with this limit. However, this limit is not applied to the installation built at the location where general public is not influenced.

3.2 Exposure to magnetic field

The health effect of the low frequency magnetic field has been investigated in MITI in relation with its regulation. MITI set up a study committee on the health effect of EMF with specialists of basic medical science, physiology, pathology, bio-electronics and electrical engineering in 1993. On the basis of analysis over scientific publications related to biological effects of the low frequency magnetic field and epidemiological studies, as well as the investigation of the level of low frequency magnetic field in the residential environment, it concluded that it could not find clear evidence of injurious influences on human health due to the line frequency magnetic field in the residential environment at the moment, and the magnetic field strength in the residential environment was low enough in comparison with the protective level shown in WHO environmental health criteria and so on.

Simultaneously, it recommended to carry out long term research with the support of the ministry on the subject like:

- Detailed investigation on the sources of magnetic field and the state of human exposure to them.
- Collection and analysis of scientific results of researches inside and outside of the country related to the subject.
- Experimental studies of biological effects of the magnetic field.

A research program covering these objectives has been running with the support of the agency for energy and resource of MITI.

Under these situations, no regulation on the low frequency magnetic field exists.

## 4. HARMONIZATION WITH INTERNATIONAL STANDARDS

Under globalization of industrial activities, our government has introduced deregulation for the commercial activities and products. It has also followed to WTO/TBT agreement and been trying to harmonize the laws and national standards with international ones.

Then safety regulations as the Product Safety Law are modified into the functional ones. The requirements for products and installations to comply with the specified value for their functions, are transferred into standards or enforcement regulations, which are referred in the law.

Most of the Japan Industry Standard (JIS) have been harmonized with international standards. Other technical standards referred in the enforcement regulations are also being harmonized. The introduction of the mutual recognition agreement for the compliance tests of products accelerates it in future.

Therefore, if the international standard would be established for the allowable limits of EMF in the industrial and residential environment, it would be taken into the regulations of our society. For the time being, there exists no positive activity in our government to introduce ICNIRP guideline into the safety regulation of products and installations.

## 5. CONCLUSION

The technical standardization has not been developed enough for the area of EMC and EMF. Only a limited number of phenomena are taken into regulations. They are mainly controlled with guidelines of ministries. The manufacturers and operators follow them voluntary and the safety requirements are satisfied practically.

At present the regulation of EMF in relation with the health problem, including those voluntary approaches, is limited to the high frequency field and a few applications in our country. Fast development of such regulation is not foreseen in other field. In general, it is considered to discuss deliberately with established scientific facts.

Another problem related to the regulation for EMF is the divided responsibility for administration between a number of ministries. Though no positive studies on the health effects of EMF from the points of regulation ministries other than MITI and MPT, it should look very complicated from outside of the country. From January 1$^{st}$ of 2001, the ministries will be reorganized and combined into smaller number than at present. It will make the safety regulation in Japan including the exposure limit to EMF more transparent and easier to be understood. However, this situation makes the decision related to the subjects to be discussed pending.

Table.1 Guideline for Electromagnetic Field Strength
(Protective Guideline of Radio Wave of MPT)

| | General Environment (Ex. Residential) | | | Controlled Environment (Ex. Office) | | |
|---|---|---|---|---|---|---|
| Frequency | Electric Field Strength (V/m) | Magnetic Field Strength (A/m) | Power Density ($mW/cm^2$) | Electric Field Strength (V/m) | Magnetic Field Strength (A/m) | Power Density ($mW/cm^2$) |
| 10 – 30kHz | 275 | 72.8 | – | 614 | 163 | – |
| 30kHz – 3 MHz | 275 | 72.8-0.728 | – | 614 | 163-1.63 | – |
| 3 – 30MHz | 275-27.5 | 0.728-0.0728 | – | 614-61.4 | 1.63-0.163 | – |
| 30 – 300MHz | 27.5 | 0.0728 | 0.2 | 61.4 | 0.163 | 1 |
| 300MHz-1.5GHz | 27.5-61.4 | 0.0728-0.163 | 0.2-1 | 61.4-137 | 0.163-0.365 | 1-5 |
| 1.5 – 300GHz | 61.4 | 0.163 | 1 | 137 | 0.365 | 5 |

The numerical value means the average value over 6 minutes.

Table. 2 Guideline for Local Absorption Ratio of Radio Wave
(Protective Guideline of Radio Wave of MPT)

| | General Environment | Controlled Environment |
|---|---|---|
| Specific Absorption Ratio Average over the Whole Body | 0.08W/kg | 0.4W/kg |
| Specific Absorption Ratio Local Level | 2W/kg<br>4W/kg (the limbs)<br>per 10g of arbitral tissue | 10W/kg<br>20W/kg (the limbs)<br>per 10g of arbitral tissue |
| Contact Current | 45mA<br>(No measure is equipped against hazard of direct contact of the body. Frequency range between 100kHz-100Mhz) | 100mA<br>(No measure is equipped against hazard of direct contact of the body. Frequency range between 100kHz-100MHz) |

This guideline is applied to small radio communication devices, which are used in the proximity of a body and operate in the frequency range of 100kHz – 3GHz. The numerical value means the average value over 6 minutes.

**EMC 2000** INTERNATIONAL WROCŁAW SYMPOSIUM ON ELECTROMAGNETIC COMPATIBILITY

# REGULATIONS FOR THE LIMITATION OF HUMAN EXPOSURE TO EM FIELDS IN POLAND

Stefan Różycki, Research Institute of Energetics, Warsaw, Poland
Marek Kałuski, National Telecommunications Institute, Wrocław Branch, Poland
Marta Macher, National Telecommunications Institute, Wrocław Branch, Poland
tel: 071/3728812, fax: 071/3728878
e-mail: StefanR@post.pl, M.Kaluski@il.wroc.pl, M.Macher@il.wroc.pl

***Abstract*** *- This article presents a short review of legal regulations concerning the protection of the human health, and the environment against electromagnetic field (EMF) in Poland. The characteristics and specifics of the Polish regulations are presented, with regard to separate standards and ordinances for the labour environment, managed by the Minister of Health, and separate standards and ordinances for the general population, created by Parliamentary Acts, and the ordinances issued by the Minister of Environmental Protection.*

## 1. REVIEW OF THE POLISH REGULATIONS

Polish regulations on protection against EMF (non-ionising radiation) have a long tradition. The oldest of the regulations still in force, goes back to 1972. It is the ordinance of the Government, from May 1972, on health and safety at work with equipment generating microwave EMF [1]*). These are the administrative regulations. Generally, EMF regulations fall into two categories:

- concerning the safety at work,
- concerning the protection of general population.

In the first category, there are three regulations:

a) the above mentioned ordinance [1] for EMF with frequencies above 300 MHz,
b) the joint Ordinance of the Minister of Labour and the Minister of Health from February 1977, on health and safety at work with equipment generating EMF in the frequency range 0.1 MHz to 300 MHz [2],
c) the Ordinance of the Minister of Labour from December 1989, on the greatest permissible strength and concentration of agents harmful to health in the labour environment [3].

The newest regulations now in force is the Ordinance of the Minister of Environmental Protection from August, 1998 on

a) the detailed rules of protection against radiation harmful to people and the environment,
b) the permissible levels of radiation in the environment,
c) the requirements for inspection measurements of radiation.

All the regulations [1], [2], [3] on labour protection, are based on the principle that limits are set to the time of exposure to EMF. The time limits and rules of exposure to EMF have been estimated in dependence of EMF frequency, and such parameters, as strength of the magnetic component, strength of the electric component, the power density, and on the field's type, i.e.: whether it is stationary or non-stationary. According to the ordinance [1] on protection against EMF of frequencies from 300 MHz to 300 GHz, for areas in the vicinity of the equipment emitting EMF, three types of protection zones have been established:

- intermediate,
- hazardous,
- dangerous.

*) Full official headings of the ordinances, exact dates of issuing, place of publication, and full names of the relevant Ministries are given in the References.

The rules and time limits for worker's exposure in these zones are diversified.

In stationary fields, the limit values for particular zones, are as follows:

- in areas outside the zones (defined in [1] as „safe") the maximum value of energy flux density must not exceed 0.1 W/m$^2$;
- for intermediate zone, the limit values of energy flux density are: minimum 0.1 W/m$^2$, and maximum 2 W/m$^2$
- for hazardous zone, the limit values of energy flux density are: minimum 2 W/m$^2$, and maximum 100 W/m$^2$;
- in dangerous zone the value of energy flux density exceeds 100 W/m$^2$.

In non-stationary fields, the limit values for particular zones are as follows:

- in areas outside the zones (defined in [1] as „safe") the maximum value of energy flux density must not exceed 0.1 W/m$^2$;
- for intermediate zone, the limit values of energy flux density are: minimum 1 W/m$^2$, and maximum 10 W/m$^2$
- for hazardous zone, the limit values of energy flux density are: minimum 10 W/m$^2$, and maximum 100 W/m$^2$;
- in dangerous zone the value of energy flux density exceeds 100 W/m$^2$.

The definition of non-stationary fields has been given in ordinance of the Minister of Health [5]. Non-stationary fields are the ones generated by the equipment with mobile antennas or antenna beams, where their irradiation frequentness is greater than 0,02 Hz, and the coefficient C is less than 0,1

$$C = \frac{t_0}{T} \qquad (1)$$

where:

$t_0$ - time of occurrence for EMF with power density $P_0$ equal to or greater than 0,5 $P_{max}$ during one cycle of the antenna beam movement,

T - duration of one cycle of the antenna beam movement.

Only workers who, as a result of medical examination, have no contraindications against EMF exposure are allowed to stay in the protection zones, i.e. in the areas where EMF may occur of frequency over 300 MHz, and of energy flux density over 0,1 W/m$^2$. It is worth mentioning that regulation [1] does not specify what should be considered as a contraindication against EMF exposure.

In the zones defined as "intermediate", workers operating the equipment are allowed to stay for the whole working day, 8 hours on the average. In the "hazardous zones", workers operating the equipment are allowed to stay for shortened period of time. The shortening of the exposure time depends on the average energy flux density. Rules for calculating the permissible exposure time in the hazardous zone have been specified in the ordinance of the Minister of Health from 1972 [5]. The permissible time is to be calculated due to the following formulas:

- for a stationary field

$$t = \frac{32}{p^2} \qquad (2)$$

where

t - working time in hours

p - average density of energy flux in W/m$^2$

- for a non-stationary field

$$t = \frac{800}{p^2} \qquad (3)$$

where

t - working time in hours

p - average density of energy flux in W/m$^2$

In hazardous zone, i.e. in the zone in which the density value of energy flux density for the fields with frequencies over 300 MHz is greater than 100 W/m$^2$, exposure of workers not equipped with means of personal protection is forbidden. The delimitation of protection zones is determined by measurements.

Ordinance [2] deals with the labour protection in the fields with frequencies between 0,1 MHz and 300 MHz. For this frequency range, likewise in ordinance [1], intermediary, hazardous and dangerous zones exist. The frequency range extending from 0,1 MHz to 300 MHz has been divided into two sub-ranges: from 0,1 MHz to 10 MHz, and from 10 MHz to 300 MHz.

For the sub-range 0,1 MHz to 10 MHz, the following limit values have been set:

- in the areas beyond the zones, (defined as „safe") the maximum strength value of electric field must not exceed 20 V/m, and that of magnetic field 2 A/m;
- for intermediary zone, limit values of electric field strength are over 20 V/m up to 70 V/m, and of magnetic field over 2 A/m up to 10 A/m.
- for hazardous zone, limit values of electric field strength are over 70 V/m up to 1000 V/m, and of magnetic field over 10 A/m up to 250 A/m.
- in dangerous zone, electric field strength is greater than 1000 V/m, and magnetic field strength is greater than 250 A/m.

For the sub-range 10 MHz to 300 MHz, the following limit values have been set

- in areas beyond the zones (defined as „safe") the maximum value of electric field strength must not exceed 7 V/m;
- for intermediate zone, limit values of electric field strength are over 7 V/m up to 20 V/m.
- for hazardous zone, limit values of electric field strength are over 20 V/m up to 300 V/m.
- in dangerous zone, strength of electric field is greater than 300 V/m.

In order to calculate the permissible time for workers' exposure in a hazardous zone, likewise in the above description, for the frequency range 0,1 MHz to 300 MHz, the following formulas are used:

- for fields in the frequency sub-range 0,1 MHz to 10 MHz:

$$T_d = \frac{80}{H} \qquad (4)$$

for magnetic field,

$T_d = 560/E$

for electric field;

- for fields in the frequency sub-range 10 MHz to 300 MHz

$$T_d = \frac{560}{E} \qquad (5)$$

where
$T_d$ - permissible time in hours,
H - average strength of magnetic field in A/m
E - average strength of electric field in V/m.

$$T_d = \frac{3200}{E^2} \qquad (6)$$

The conditions of protection of work in the static fields, in the fields with frequency 50 Hz, and in the frequency range from 1 kHz to 100 kHz, have been determined in Ordinance of the Minister of Work issued in 1989 [3]. For EMF with frequencies greater than 0,1 MHz, hazardous and dangerous zones have been specified. Unlike the ordinances [1] and [2], the ordinance [3] does not introduce the intermediary zone.

In the vicinity of sources of static magnetic fields, and of the industrial frequency 50 Hz, three zones of field influence are differentiated

- Dangerous zone in which presence of workers is forbidden
- Hazardous zone in which permissible time for workers' exposure depends on the field strength
- Safe zone in which presence of workers is permitted without time limits

Dangerous zone is defined as an area in which the strength of a static magnetic field exceeds 80 kA/m (which corresponds to magnetic induction of about 100 mT), and the strength of a magnetic field with the industrial frequency 50 Hz exceeds 4 kA/m (approx. 5 mT). Should exposure concern only limbs (from feet up to knees, and from palms up to elbows) the limits of dangerous zone, as quoted in paragraph 2, are to be enlarged 5 times.

Hazardous zone is defined as an area, in which the field strength H (induction B) is within limits:
8 kA/m (approx. 10 mT) < H(B) < 80 kA/m (approx. 100 mT) for static magnetic fields,
and
0.4 kA/m (approx. 0.5 mT) < H(B) < 4 kA/m (approx. 5 mT) for magnetic fields with the industrial frequency 50 Hz.

Permissible exposure to magnetic fields in this zone is determined by the value calculated from the following expression

$$D = H^2 t_{(b)} \qquad (7)$$

where H -the strength of the magnetic filed to which a worker is exposed over a period t of time, while $t_{(b)} < 8h$.

In a hazardous zone the value of the expression must not exceed:

- 512 $(kA/m)^2h$ for static magnetic fields,
- 1.28 $(kA/m)^2h$ for magnetic fields with the mains frequency 50 Hz.

Should exposure in a hazardous zone concern only limbs (from feet up to knees, and from palms to elbows) the respective values in the expression are to be enlarged 25 times.

Safety zone is an area where the strength of a static magnetic field is less than

8 kA/m (approx. 10 mT),

and the strength of a magnetic field with the industrial frequency 50Hz, does not exceed

0,4 kA/m (approx. 0,5 mT).

For EMF in the frequency range between 1 kHz and 100 kHz, the 24 hours exposure of the workers is limited, where one differentiates between the occurrence of the fields with large, medium or small impedance, in the workplace.

For EMF of large impedance, the electric field strength should not exceed $E_d$ = 1000 V/m in a workplace. In the fields of smaller strength the total dose ($D_{rE}$) of the workers' exposure to electric field should not exceed the permissible dose of $D_{dE} = 80000\ (V/m)^2$, according to which a worker is

allowed to stay in the electric field of the strength of 100 V/m for eight hours.

For EMF of small impedance, the magnetic field strength in a workplace should not exceed H = 100 A/m. In weaker fields, the total dose ($D_{rH}$) should not exceed permissible value of $D_{dH} = 800\ (A/m)^2h$, according to which a worker is allowed to stay in magnetic field of the strength of 10 A/m for eight hours.

For the EMF of medium impedance, the strength of electric field (E) and magnetic field (H) in a workplace, should not exceed values, for which

$$E/E_d + H/H_d \leq 1 \qquad (8)$$

In weaker fields, exposure ratio/$k_{EH}$ should not exceed one. The following relation should be fulfilled:

$$k_{EH} = D_{rE} / D_{dE} + D_{rH}/D_{dH} \leq 1 \qquad 9)$$

In the vicinity of field sources, the range of dangerous zone (E> 1000 V/m, H> 100 A/m), and hazardous zone (E ≥100 V/m and H ≥ 10 A/m) should be delimited and marked.

Beside the described above legal regulations, many technical standards have been elaborated and published in Poland. They concern definitions, methods of EMF measurements, and the methods of designating the protection zones. The standards, however, do not specify the permissible levels of EMF, and therefore they have been omitted here.

The fundamental regulation relevant to the protection of the population, i.e. people exposed to EMF outside their working place, is the ordinance of the Minister of the Environmental Protection from August 1998 [4] on

- the detailed rules on protection against radiation, harmful to people, and to the environment,
- the levels of radiation, permissible in the environment,
- the requirements for inspection measurements of radiation [4].

The ordinance [4] gives definitions of the following dimensions:

- the permissible levels of non-ionising EMF radiation that might occur in the environment,
- the detailed rules for protection of people and the environment against electromagnetic non-ionising radiation in the form of
  - static electric and magnetic fields,
  - electric and magnetic fields of industrial frequency 50 Hz, emitted by stations and power lines,
  - EMF in the frequency range from 1 kHz to 300000 MHz, emitted in particular by radiocommunication, radionavigation, and radar equipment.

This ordinance also specifies the requirements for the inspection measurements of non-ionising electromagnetic radiation.

In Poland, in residential areas, and in the areas where there are located, in particular, hospitals, crèches, kindergartens, and boarding schools, the electric component of electromagnetic non-ionising radiation of 50 Hz, must not exceed 1 kV/m. The permissible levels of non-ionising radiation, specified in the ordinance, do not apply to the places not accessible to the public.

| Physical quantity → / Frequency range ↓ | | Electric component | Magnetic component | Power density | Ionic current density |
|---|---|---|---|---|---|
| | 1 | 2 | 3 | 4 | 5 |
| 1 | Static fields | 16 kV/m | 8 kA/m | - | 100 $nA/m^2$ |
| 2 | 50 Hz fields | 10 kV/m | 80 A/m | - | - |
| 3 | 0,001 - 0,1 MHz | 100 V/m | 10 A/m | - | - |
| 4 | 0,1 -10 MHz | 20 V/m | 2 A/m | - | - |
| 5 | 10 - 300 MHz | 7 V/m | - | - | - |
| 6 | 300 - 300000 MHz | - | - | 0,1 $W/m^2$ | - |

Table 1. Permissible levels of non-ionising electromagnetic radiation characterised by limit values of physical quantities

*Notes:*

Limit values of physical quantities characterising permissible levels of radiation refer to:

a) RMS value of electric and magnetic field strength of 50 Hz, and in the range from 0.001 MHz to 300 MHz,
b) Average power density values of electromagnetic field strength in the range from 300 MHz to 300000 MHz.

The quoted above permissible levels of EMF that may occur in the environment, defined in the Appendix to the ordinance [4] refer to 24-hours exposure of people.

## 2. CONCLUSIONS

Limits (standards) for influence of fields, now in force in Poland have been settled in a way diverging from the ones accepted in recommendations of the international organisations dealing with protection against radiation, for example, in the recommendations of ICNIRP - International Commission on Non-Ionising Radiation Protection, in the CENELEC prestandards of 50166 series, or

finally in the last year recommendations of the EC (European Council).

In Poland, like in other countries, location of objects emitting EMF is often controversial. The controversy is based on almost universal common belief that the influence of exposure to non-ionising radiation in the environment is harmful.. One of the obvious reasons for such an atmosphere is the substantial difficulty in communicating to the public the specialised, professional information in a simple and comprehensible way. The technical criteria for location of objects, in particular the radiocommunication ones, are entirely above understanding of a person who is not provided with adequate knowledge.

The lack of sufficient knowledge amongst population, about the principles of operation of objects emitting EMF, the rules of field pattern determination in the vicinity of such objects, and rules for setting the permissible, ensuring the harmlessness to people field strength levels as well as administrative procedures – are just few among other reasons of conflicts lively reflected in the media. The lack of the common acceptance of location, of the EMF emitting objects, is broadly believed to be the proof of their harmful impact.

The scenario of conflicts on EMF emitting objects in Poland, does not much differ from the course of similar conflicts in other countries.

The golden rule of any action undertaken in relation to this problem should be: spreading and popularising information on the nature of non-ionising radiation, on EMF, and on the results of competent scientific research in this area.

The works currently carried on in Poland, aimed at amendments of the Polish regulations are concentrated on:

- unification of definitions used,
- decrease the number of legal acts in force.

Taking into account the mentioned above social conditions, as well as the fact that the on-going world wide discussion on the effects of EMF exposure is far from its end, the set of permissible levels of field strength, accepted many years ago, should not be soon expected to change.

## 3. REFERENCES


[1] Ordinance of the Government dated May 25th, 1972 on health and safety at work with equipment generating EMF in the microwave range (Journal of Laws, No 21, item 153).

[2] Ordinance of the Ministers of Work, Pay and Social Affairs and the Minister of Health and Social Welfare dated February 19th, 1977 on health and safety at work with equipment generating EMF in the frequency range from 0.1 MHz to 300 MHz (Journal of Laws, No 8, item 33)

[3] Ordinance of the Minister of Work and Social Policy dated December 1st, 1989 on the greatest permissible strength and concentration of agents harmful to health in work environment (unified/body text, Journal of Laws, No 69, dated 1995, item 351, with later changes)

[4] Ordinance of the Minister of the Environmental Protection Natural Resources and Forestry dated August 11th, 1998, on the detailed rules on protection against radiation harmful to people, and the environment, permissible levels of radiation which may occur in the environment as well as the requirements for the inspection measurements of radiation (Journal of Laws No 107, item 676).

[5] Order of the Minister of Health and Social Welfare dated August 9th, 1972, on defining the electromagnetic fields in the microwave range and permissible exposure time in a hazardous zone (Journal of the Department of the Ministry of Health and Social Welfare No 17,


## BIOGRAPHICAL NOTES


**Marek Kałuski** received the M.Sc. degree in electronics engineering from Technical University, Wroclaw in 1970. He is a Researcher of EMC Group of National Telecommunication Institute, Wroclaw Branch. His experience includes a wide range of government and commercial client consultations in Poland, in the region of antenna measurements. His main research interests comprise the EMC problems and numerical modeling of the near EM field distribution for antennas and radiation devices.

**Marta Macher** received the M.Sc. degree in physics from Institute of Mathematics, Physics and Chemistry, Wroclaw University, in 1973. She is employed in the Working Group on human environment protection against EM fields in the National Telecommunication Institute, Wroclaw Branch. Her interests comprise the numerical modeling of the near EM field distribution for antennas and radiation devices.

**Stefan Różycki** received the M.Sc. degree in electric engineering from the Warsaw Technical University in 1980. He is resercher in Environmental Impact Laboratory in Institute of Power Engineering in Warsaw. At the part time he is a consultant in the Ministry of Environment in the matters of electromagnetic radiation protection. Also he has experience with experimental tests in area of the electric pulse influence to the living cell membrane.

EMC 2000 INTERNATIONAL WROCŁAW SYMPOSIUM ON ELECTROMAGNETIC COMPATIBILITY

# Presentation of CISPR/H activities

Alain Azoulay[1] and Bernard Despres[2]
[1] TDF/ Technical Center. Saint Quentin en Yvelines . France
[2] France Telecom Research and Development – DMR/URF – Issy les Moulineaux . France

## 1.Introduction

In 1998, the international special Committee on radio interference (CISPR) decided during its Frankfurt, Germany meeting to establish a new sub committee designated as CISPR/H. This subcommittee was created because of the considerable evolution of the radio services particularly in the bands above 860 MHz.
The ITU-R, in its new organization and according to the international pressure to allocate new frequency bands for a number of new services (cellular radio, digital audio, fast internet radio access, wireless local loop, new satellite services etc.), has induced the need for CISPR to study the impact of radio disturbances on these new services.
This paper, presented on behalf of the CISPR/H Chairman, describes the terms of references and the latest activities of the newly formed CISPR/H subcommittee.
CISPR/H has various activities, among them a coordination activity between all the partners (industry, regulators, operators...) in order to establish limits and guidelines on radio services protection.
This paper gives the methodology used by CISPR/H to achieve all its tasks in the future and what it has already proposed to do.

## 2. Scope of CISPR/H

The CISPR General Assembly, when establishing CISPR/H, defined its terms of reference. They have been slightly amended at the subsequent CISPR/H meetings, to now read :

a) To develop and maintain generic emission standards.

b) To develop a rationale for the setting of emission limits for the protection of radio communications while taking the interest of CISPR product committees into consideration.

c) To make a survey of EMC product standards on emission.

d) To develop and maintain a database on the characteristics of radio systems to be protected.

e) To maintain an archive of reasons provided by CISPR product committees in justification of product limits that exceed generic limits.

f) To establish limits of radio disturbances above 1 GHz for the generic emission standards.

CISPR/H task covers assistance to all other CISPR sub committees to guide them on the evolution of radio services not only because of the reassignation of new frequency bands but to take into account new modulation and access schemes to assess the interfering potential to these new services. Digital radio has drastically changed the world of radiocommunications and the definition of radio interference, as with digital technique, the degradation of quality is more sudden and more complete than with analog communications for which the interference is mainly progressive when the interfering level increases for a given usable received level.

Additionally, liaison with ITU-R is very important and will be included in the tasks of CISPR H, especially in order to get access to the relevant information on the characteristics of the new radio systems to protect (for example, IMT 2000)

## 3. Organization of the CISPR H work

The tasks related to CISPR/H have been listed and it has been identified which tasks will be covered by CISPR/H alone, which tasks should be dealt with by CISPR/H in co-operation with other sub-committees, and which tasks should be covered solely by the other CISPR sub-committees.

Table 1 shows the general ideas which have been agreed in principle for the CISPR/H responsibilities with regard to the other CISPR subcommittees

| Exclusive CISPR/H responsibilities | CISPR/H and others | CISPR/A responsibilities | Product subcommittees responsibilities |
|---|---|---|---|
| Radio services database | Other factors | Measurement methods under lab. conditions | Limits for specific products. CISPR/H is the horizontal committee for generic emission standards. |
| Objective numbers and calculations. "Worst case" limits when reception is reduced to a minimum acceptable service in accordance with specifications for particular radio services | Factors e.g. economics – probability – characteristics of interference sources | Measurement bandwidth - antennas - test sites - detectors etc. | Specific measurement set-up and adaptation of limits to specific products |

Table 1 – CISPR H responsibilities versus other CISPR sub-committees

For practical reasons, CISPR/H will establish only one working group (WG 1) and will assign all tasks to this WG. The working group will in its turn establish some lifetime-limited Project teams (PTs) which will deal with the accepted New Work Item Proposals (NWIP, see below). The Working group would collect the results of PTs and build final documents according to the CISPR/H requests.

To summarise, WG1 shall be responsible for:
- the management of project teams
- the maintenance of the two IEC generic emission standards

According to the new IEC rules, subsequent amendments to existing standards that do not extend their scope are part of the normal maintenance activity of the Sub-Committee and do not require the approbation of New Work Item Proposals (NWIP) before the work can start. In the case of CISPR/H, the work to amend the two existing IEC generic emission standard will take place under this maintenance regime.

For new areas of activities or new standards, a NWIP needs first to be submitted to the IEC National Committees (NCs) for Voting and it's only if the majority of the NCs agree to it and at least five countries intend to participate actively in the work that the corresponding deliverables can be prepared.

In the case of CISPR/H, four NWIPs have been submitted in October 1999.

NP 1: To develop a database on the characteristics of radio services to be protected, with an initial priority on the frequency range above 1 GHz.
NP 2: To develop a rationale for the setting of emission limits for the protection of radio services, with an initial priority on the frequency range above 1 GHz.
NP 3: make a survey of EMC product standards on emission
NP 4: maintain an archive of reasons provided by CISPR product committees in justification of product limits that exceed generic limits.

The voting results distributed in February 2000 showed a positive result for all these four new proposals, so the work will effectively start at the next CISPR/H meeting on June 7 and 8, 2000 in St Petersburg.

## 4. Generic emission standards

A new concept among the CISPR, generic emission standards, appeared after the CENELEC and ETSI development of such standards at the European level.
The need of such standards has appeared for the equipment that are not fully covered by the present CISPR emission standards which are listed in appendix (table 2).
A generic standard is the « default » standard when no product specific standard exists. IEC/CISPR has developed two generic emission standards and the relevant one to be used depends on the environment in which the equipment is intended to be used (residential, commercial and light-industrial or industrial). Generic emissions standards also constitute guidance documents for the preparation of EMC product standards as they provide the appropriate emission limits for a product not to produce undue disturbances in a given environment.

In 1996,before CISPR/H was established, a first work has been carried out by IEC/CISPR and two IEC standards have been published. The first one is the IEC/CISPR 61000-6-3: 1996 with the following title, Generic Emission Standard for residential, commercial and light-industrial environment The present content of IEC 61000-6-3 includes for the enclosure, application of the CISPR 22 Class B radiated limits and for the AC mains port the application of the IEC 61000-3-2 & -3 for low frequencies and the application of CISPR 22 Class B conducted limits and the CISPR 14 click noise limits.

The second standard is the IEC/CISPR 61000-6-4: 1996 which title is Generic Emission Standard for Industrial environment.
The present content of IEC 61000-6-4 includes for the enclosure the application of CISPR 22 Class A radiated limits, for the AC mains port the application of CISPR 22 Class A. These standards are supposed to be fully revised by CISPR/H in the future.

In particular, one of the major development for the future will be to extend the present radiated limits to frequencies above 1 GHz to cover all the new radio services operating in this range.
Another possible development is to add radiated limits below 30 MHz. Presently, there is no radiated

measurement or limit below 30 MHz with one possible exception (ISM Class1 Group B)
Is there some needs in this area ? Is the present situation satisfactory or not ?

## 5. Conclusion

This paper is an introduction of the CISPR H tasks and organization. CISPR H establishment is fully justified if we take into account the fast evolution of the RF technology and radio services to protect.
It is now necessary that CISPR introduces a new vision of the protection of radio services. Digital radio services, multimedia application and integration of services in general make very difficult to maintain the organization of subcommittees and the emission standards only by product categories.
The CISPR/H will be the link between the radio services spectrum management and protection (through the ITU-R) and the other CISPR subcommittees; it will be a hard task to identify the protection ratio of all these new radioservices, particularly versus the type of interference generated by non radio devices and define objective acceptable limits to avoid as far as possible interference. The new techniques in digital radio like TDMA or frequency hopping make quite difficult the identification of an interference or a channel blank.
So, definition of the criteria for deriving limits, and harmonization of limits in the future will be a hard task that CISPR H will surely have to face. We definitely hope that CISPR H will succeed in all the missions which have been allocated to this new subcommittee.

## 6. Appendix: List of emission product-standards established by CISPR

| CISPR Standard Number | Title |
|---|---|
| CISPR 11 | Limits and methods of measurement of electromagnetic disturbance characteristics of industrial, scientific and medical devices (ISM) radio-frequency equipment |
| CISPR 12 | Vehicles, motorboats and spark ignited engine-driven devices – Radio disturbances characteristics –Limits and methods of measurement |
| CISPR 13 | Limits and methods of measurement of radio interference characteristics of sound and TV broadcast receivers and associated equipment |
| CISPR 14 | Limits and methods of measurement of radio interference characteristics of electric-motor operated and thermal appliances for household and similar purposes, electric tools and similar electric apparatus. |
| CISPR 15 | Limits and methods of measurement of radio interference characteristics of electrical lighting and similar equipment |
| CISPR 22 | Information technology equipment –Radio disturbance characteristics – Limits and methods of measurement |
| CISPR 25 | Limits and methods of measurement of radio interference characteristics for the protection of radio receivers used on board vehicles |

Table 2 . List of emission product standards established by CISPR

Biographical notes

Alain Azoulay is the head of the Antenna, Radio and EMC measurement Branch of Telediffusion de France (TDF) technical center. After graduated from the Supelec engineering school in Paris in 1970, he worked at Thomson CSF in the microwave relays division up to 1974 and spent afterwards more than 20 years in the EMC and mobile radio division of CNET, France Telecom research and development center. He joined TDF in 1998.
He is currently delegate member of CISPR (International special committee for radio interference) and has been chairman of ITU-R TG1/3 on spurious emission of transmitters up to November 1997.

Bernard Després is head of the EMC and spectrum engineering group in France Telecom R&D where he works since 1992 after graduating from the ISEP engineering school in 1990.

He is member of several standardisation committees on EMC (CISPR Sub-Committees A, B and G and CENELEC SC 210A) and on spectrum engineering (CEPT WG SE). He is since 1998 the Chairman of IEC/CISPR/H, and since February 2000 the Chairman of a new CEPT SE Projet Team SE35 on "Power Line Telecommunication and cable transmission in general".

EMC 2000 INTERNATIONAL WROCŁAW SYMPOSIUM ON ELECTROMAGNETIC COMPATIBILITY

# DETERMINATION OF RATED EMC PARAMETERS BASED ON THE PROBABILISTIC APPROACH AND CONSIDERATION OF ACTUAL CONDITIONS

K.A. Bochkov, and N.V. Ryazantseva
Belorussian State University of Transport
246653, Belarus, Gomel, Kirov Str., 34
Tel. (0232)553361, e-mail: bochkov1999@mail.ru

*This presentation deals with the development of a new method of determinations of rated EMC parameters of microelectronic systems maintaining safety using the probabilistic approach recommended in reference guide IEC 61000-401. The rated EMC parameters are determined using probabilistic criteria of EMC levels in which a numerical value of error probability of the systems is assumed. A software package "EMCpar" has been elaborated for Windows allowing to determine the rated parameters of noise and noise immunity levels for specified EMC levels. The new method is better adequate than the existing "deterministic" method since it allows to determine the EMC parameters for specified conditions of reliable and safe performance of microelectronic systems.*

## 1. INTRODUCTION

Microelectronic systems controlling safety (SCS) of transport and industries perform extremely responsible functions, hence the problem of their electromagnetic compatibility with the electromagnetic environment requires more precise solution. Traditionally the rated EMC parameters are determined at the final stage of EMC problem solution. The problem itself of rating the norms ignored the need to take into consideration of numerous factors, hence it is a challenging scientific task and requires further studies of the theory of EMC problems. The existing approach to selecting the rated EMC parameters reflected in various international and national standards is deterministic. The essence of this approach is to select the rated parameters using the principle of the "method of most adverse conditions", the strictness of tests is determined by a set of several qualitative parameters. In this case the parameters of actual EME are ignored and are replaced with some maximum noise level (the strictness of tests is determined subjectively using several qualitative characteristics. This approach has two disadvantages implying that the strictness of tests may be unjustifiably exaggerated resulting in a significant cost of achieving EMC in standard microelectronic systems controlling safety, or oppositely the tests may be too lax upsetting the conditions of ensuring safety. Hence it is essential to analyze new methods of determining the EMC rated parameters using a probabilistic approach.

## 2. DETERMINATION OF RATED EMC PARAMETERS USING THE PROBABILISTIC APPROACH

It is an intricate task to rate the EMC parameters for SCS since it should be solved with the consideration of some specified safety level and a number of technological, economic and other aspects. The new method of rating EMC parameters is based on the application of probabilistic statistical EMC models [1,2] which take into account both the qualitative parameters of the existing electromagnetic environment (EME) and the parameters of noise immunity of such systems. It has been demonstrated [1,2] that it is exactly the value $P_{err}$ can qualitative reflect the compatibility of devices with a specific existing EME. In this case the existing EME is determined by processing statistic characteristics of noise of a definite type and it is determined by the distribution of noise levels. Following this model an error occurs when noise level exceeds the noise immunity level of a system (a device) and can be quantitatively determined by the magnitude of error probability $P_{err}$. This magnitude characterizes also the performance and safe performance of devices in a specific EME.

Analytic expressions of determination of $P_{err}$ of microelectronic SCS for most frequent practically combinations of distributions of noise and noise immunity levels in order to develop new methods of determination of rated values using the probabilistic approach what is treated in detail in [1-3]. For example, the error probability (the quantitative EMC level) for a combination of normal laws of distribution of noise and noise immunity levels is determined from the expression

$$P_{err} = \frac{1}{2} - \Phi\left(\frac{\mu_R - \mu_N}{\sqrt{(\sigma_R^2 + \sigma_N^2)}}\right) \qquad (1)$$

and for the exponential law of distribution of noise levels and normal distribution of noise immunity levels from the expression

$$P_{err} = 0{,}5 * \exp\left\{-\frac{1}{2}\left(2\mu_R\lambda - \lambda^2\sigma_R{}^2\right)\right\} + \Phi\left[\frac{\mu_R - \lambda\sigma_R^2}{\sigma_R}\right] \quad (2)$$

By using these dependencies and by specifying individual parameters the following problems of determination of the rated EMC parameters can be solved:

— by using a specified $P_{err}$ and known EME characteristics (in this case it the known law and the parameters of distribution of noise levels) to determine the rated noise immunity level for specified criteria using the standard deviation (the first problem of rating);

— by using a specified $P_{err}$ and the known law and parameters of distribution of noise immunity level to determined the rated value of noise levels for specified criteria and the standard deviation (the second problem of rating).

The first variant deals with the case when an answer is to be found for a specific EME which should the characteristics of noise immunity levels of the equipment to ensure that it functions with a specified error probability. The second problems appears in the case when, for example, the characteristics of some new newly designed equipment are known, i.e. the noise immunity level and its scatter. Then it can be answered what specified error probability will the equipment have and in which noise environment. It will allow to reduce cost or achieving exaggerated norms specified at present by the existing standards based on the deterministic approach. This will make the equipment cheaper for end-users. With this approach the problem of rating has many solutions, its intricacy lies not in purely mathematical problems of deriving analytical expressions for determination of the rated parameters, it is rather the necessity to specify correctly the remaining parameters. In fact, a rated value is a function of many variables. For example, in case of a combination of the normal laws of distribution of noise and nose immunity levels the parameter to be determined is a function of many variables

$X_{rat} = f(P_{err}, \mu_R, \sigma_R, \sigma_N)$.

When solving the problem of determination of the rated values the existing noise and noise immunity levels should taken into consideration, for example, the noise level is determined by the features of noise sources and it always has limits; the scatter of the noise immunity of equipment is determined by the technological levels, etc.

The noise immunity levels of devices are governed by a great variety of factors, such as the scatter of the parameters of the production process, compactness of parts, etc., each contributes into the type of the law of distribution. Then, according to the postulates of the central extreme theorem, it can be concluded about the normal law of distribution of noise immunity levels of SCS. According to [1] distribution of the EME parameters, the amplitude and duration in particular, well correlates in many cases with normal, logarithmic normal, exponential, Gamma distribution and laws of Raleigh and Waybull.

## 3.DETERMINATION OF THE RATED EMC PARAMETERS

Consider in detail how to obtain the rated EMC parameters using an example of combination of the normal laws of distribution of noise and noise immunity levels (see Fig. 1).

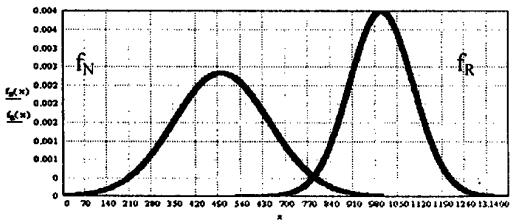



Fig. 1. Probabilistic EMC model for combination of normal distributions of probability density of noise and noise immunity levels

For this model the error probability of microelectronic devices is determined by the expression [1]

$$P_{err} = \frac{1}{2} - \Phi\left(\frac{\mu_R - \mu_N}{\sqrt{(\sigma_R^2 + \sigma_N^2)}}\right) \quad (3)$$

where

$$\Phi(z) = \frac{1}{\sqrt{2\pi}}\int_0^z e^{-\frac{z^2}{2}}\,dz$$

is the rated Laplace function.

The rated noise immunity level (the first problem of rating) can be determined from expression (3) for a specified error probability $P_{err}$ according to the standards of reliable and safe performance and fixed standard deviations of the noise immunity level $\sigma_R$ and noise level $\sigma_N$ . Designate with Z the rated Laplace function argument in expression (3)

$$Z = \frac{\mu_R - \mu_N}{\sqrt{\sigma_R^2 + \sigma_N^2}} \quad (4)$$

then

$$P_{err} = 0{,}5 - \Phi(Z);\ \Phi(Z) = 0{,}5 - P_{err}$$

Using the results of the Laplace function and determine Z in order to satisfy equality (3), then use the determined Z to determine the rated noise immunity level $\mu_R$.

From (4) directly determine

$$\mu_R = Z\sqrt{\sigma_R^2 + \sigma_N^2} + \mu_N \quad (5)$$

Consider a numerical example. Assume that according to the requirements of reliable and safe performance the error probability is specified as $P_{err} <= 10^{-6}$, then $\Phi(z) = 0.5 - P_{err} = 0.499999$ and $z = 4.76$, respectively. Also, the type and the statistical parameter of EME distribution are known: $\mu_N = 1000$ V (the second degree of strictness of tests for standard IEC 61000-404), $\sigma_N = 100$ V. Also the characteristic of the parameter of scatter of noise immunity level is known to be $\sigma_R = 10$ V. Smaller $\sigma_R$ values would correspond to a more advanced

technological level of fabrication of microelectronic equipment. Proceeding from these conditions (5) yields

$$\mu_R \geq 1478{,}37 \text{ V}.$$

Hence, the rated noise immunity level to achieve $P_{err} = 10^{-6}$ at $\mu_N = 1000$ V, $\sigma_N = 100$ V and $\sigma_R = 10$ V is equal to 1478.37 V in this example. The deterministic approach in this case would specify the strictness of test for noise immunity equal to 2 kV.

This example apparently demonstrates the advantage of the probabilistic approach to ratting and smaller cost needed to achieve the EMC of microelectronic SCS and making them cheaper.

The deterministic approach to rating the EMC parameters of microelectronic systems controlling safety may lead to another situation. Assume another case using the conditions of the previous example, but now the second strictness degree is specified 1 kV. According to (3) the error probability of microelectronic SCS equal to $P_{err} = 10^{-6}$ may fail to satisfy customer's parameters of reliable and safe performance of these systems.

Hence, the analyzed example evidences that determination of the rated EMC parameters with the help of the probabilistic approach allow to optimize (reduce) the cost of achieving the EMC of microelectronic SCS while satisfying the specification of their reliable and safe performance. The rated noise levels at specified $P_{err}$ values and known parameters of distribution of noise immunity levels of microelectronic SCS was based on (3). Analysis of expression (3) evidences that determination of the rated noise levels in any way requires to know also the scatter $\sigma_N$ of noise level parameters. The value $\sigma_N$ in this case can be determined only by analyzing the statistical data about the nose levels for various types of EME.

In its turn the equipment is needed to obtain the statistical data about the types and parameters of distribution capable to measure noise and register the noise parameters.

After the parameter $\sigma_N$ is determined and similarly to the previous example it is possible to determine the rated noise levels and below them to determine numerically the EMC levels as $P_{err}$.

Consider the methods of solving the problem of rating EMC parameters using the case of combination of distributions of noise levels based on the Raleigh law

$$f(x) = \frac{x}{\sigma_N^2} \exp\left\{-\frac{x^2}{2\sigma_N^2}\right\} \qquad (6)$$

and noise immunity based on the normal law.

Knowing the EMC level,, the $P_{err}$ for this combination of the laws of distribution can be derived from expression [1]

$$P_{err} = \frac{\sigma_N}{\sqrt{(\sigma_N^2+\sigma_R^2)}}\left(\frac{1}{2}+\Phi\left(\frac{\mu_R\sigma_N}{\sigma_R\sqrt{\sigma_N^2+\sigma_R^2}}\right)\right)\exp\left\{-\frac{\mu_R^2}{2(\sigma_N^2+\sigma_R^2)}\right\} \qquad (7)$$

In this case the solution of the first problem of rating is accomplished by determining the noise immunity level $\mu_R$ using the known $\sigma_N$ and the specified $\sigma_R$, solution of the second problem of rating is accomplished by determining $\sigma_N$ (sine the Raleigh distribution is a single-parameter law, hence it is enough determine just $\sigma_N$ to determine the noise level) based on the known $\mu_R$ and $\sigma_R$ . Yet, equation (7) is transcendental it can be solved only with numerical methods.

For the combination of the exponential law of distribution of noise levels and the normal law of distribution of noise immunity level the $P_{err}$ of EMC can be determined from [1]

$$P_{err} = \exp\left\{-\frac{1}{2}\left(2\mu_R\lambda - \lambda^2\sigma_R^2\right)\right\}\left[\frac{1}{2}+\Phi\left(\frac{\mu_K-\lambda\sigma_R^2}{\sigma_R}\right)\right] \qquad (8)$$

It is also transcendental. For other combinations of the laws of distribution, for example, when the noise levels are determined based on the Waybull law

$$f_N(x) = \frac{\alpha}{x_0}x^{\alpha-1}\exp(-x^\alpha / x_0)$$

and noise immunity levels follow the normal law, the error probability is described by the expression containing an integral which can be calculated if $\alpha$ is specified and only for some values of $\alpha$:

$$P_{err} = \frac{1}{\sigma_R\sqrt{2\pi}}\int_0^\infty \exp\left\{-\frac{(x-\mu_R^2)^2}{2\sigma_R^2}-\frac{x^\alpha}{x_0}\right\}dx$$

Analysis indicates that the parameters rated analytically can be obtained only for a limited number of combinations of the laws of distribution.

In the general case there are ceilings and floors of the parameters of each type of noise. Hence they can be represented by the truncated laws of distribution. It is a specifically essential consideration for determination of the EMC rated parameters for highly reliable systems. Moreover, the noise immunity levels for a number of instruments are more adequately described by the truncated laws of distribution (by the truncated Gaussian law in most cases).

Consider the solution of the problem of rating using the truncated laws of distribution, specifically the truncated normal laws.

In this case the function of the density of distribution of noise levels and the degree of noise immunity will be [1]

$$f_N(x) = \frac{1}{\sigma_N\sqrt{2\pi}} * \exp\left\{-\frac{(x-\mu_N)^2}{2\sigma_N^2}\right\} * \left(\Phi\left(\frac{d-\mu_N}{\sigma_N}\right)-\Phi\left(\frac{c-\mu_N}{\sigma_N}\right)\right)^{-1} \qquad (9)$$

$$f_R(x) = \frac{1}{\sigma_R\sqrt{2\pi}} * \exp\left\{-\frac{(x-\mu_R)^2}{2\sigma_R^2}\right\} * \left(\Phi\left(\frac{d-\mu_R}{\sigma_R}\right)-\Phi\left(\frac{c-\mu_R}{\sigma_R}\right)\right)^{-1} \qquad (10)$$

where a, b, c, d are the limits of variations of random noise and noise immunity levels of devices.

The error probability of devices in this case is described by the expression [1]

$$P_{err} = 1 - \frac{\Phi\left(\frac{b-c-\mu_u}{\sigma_u}\right)-\Phi\left(\frac{-\mu_u}{\sigma_u}\right)}{\Phi\left(\frac{b-c-\mu_u}{\sigma_u}\right)-\Phi\left(\frac{a-d-\mu_u}{\sigma_u}\right)} \qquad (11)$$

where $\mu_U = \mu_R - \mu_N$ , $\sigma_U = (\sigma^2_N + \sigma^2_R)^{0.5}$ .

Before solving the problem of rating the effect of truncation upon the error probability should be evalu-

ated. Analysis of such truncation upon the $P_{err}$ indicates that a combination of the truncated laws of distribution yields more accurate results when calculating the EMC level. When the values of $\mu_U$ are small, the $P_{err}$ calculated using (3) and (11) differ insignificantly, yet in this case $P_{err}$ is quite high. For SCS determination of the rated parameters ignoring truncation is costlier when effort is made to achieve the specified $P_{err}$. Meanwhile using more adequate truncated laws yields the same result cheaper.

Hence, it can be concluded that expression (11) is suitable for determination of the rated EMC parameters. The routine of determination of the rated EMC parameters is like in the previous case assuming that $P_{err}$, a, b, c, d are known, $\sigma_R$ is specified, then $\mu_N$ can be determined as a function of $\mu_R$, $\sigma_R$ , a, b, c, d, $\sigma_N$ and correspondingly $\mu_R$ =f ($\mu_N$ , $\sigma_R$ , a, b, c, d, $\sigma_N$). Analysis of the effect of "truncation" of the laws of distribution of noise levels upon the accuracy of determination of $P_{err}$ indicates hat the truncated laws should be used when using the Waybull, Raleigh and exponential laws of distribution, otherwise the error of determining $P_{err}$ becomes comparable with the probability $P_{err}$ itself.

The software package "EMCpar" for Windows is specifically intended to solve the problems of rating when no analytical solution is possible (see Fig.2).

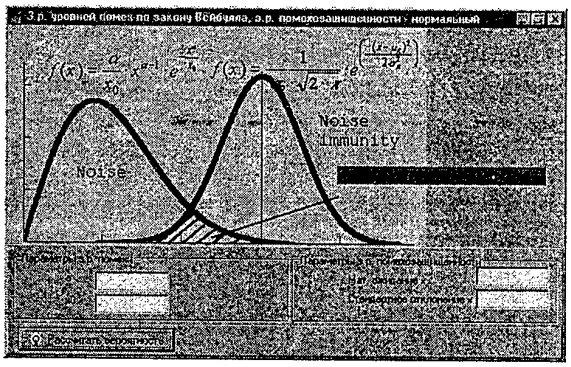



Fig. 2. Displayed information

The package allows to solve the problem of rating using any specified error probability (a specified degree of compatibility) and known noise levels, to determine what noise immunity level is required in each specific case for an individual or a group of instruments. The package allows to determine $P_{err}$ for all possible combinations of the laws of distribution of noise and noise immunity levels and error probability. The user interface is easy to use, requires no special training and runs in the interactive mode.

## 4. CONCLUSION

The new method of determination of the EMC rated parameters respects the guides of standard IEC 61000-4-1. Algorithms have been created to determine (to calculate) the rated EMC parameters. The advanced method of rating allows to optimize the cost of achieving the EMC and the required standards of reliable and safe performance of microprocessor circuits.

It is noteworthy that implementation of this approach requires the necessary instruments to register and analyze the EME (to determine the parameters and the type of the laws of noise distribution). Quantitative determination of the parameters of noise levels allows also to set more accurately the strictness of tests using the existing approach.

Also, in order to determine the parameters and the type of the law of distribution of levels and noise immunity, the noise simulators should be able to vary the characteristic of simulated noise smoothly. There are such test generators, like Haefely, EM-test, Schaffner, and others. The advanced approach to rating is easily implementable using the "EMCpar" package and suitable equipment. The novel advanced method of rating is more optimal since it respects the probabilistic nature of both noise levels and noise immunity levels and allows to determine the rated EMC parameters numerically for specified criteria of reliability and safety.

## 5. REFERENCES

5.1. K.Bochkov, D.Sc. Dissertation ( in Russian), Moscow, MIIT, 1993.

5.2. K.Bochkov, "Principles of Achieving EMC of Microelectronic Systems Controlling Major Sequences of Operations" ( in English), Proceedings of Int. Symp. on Electromagnetic Compatibility EMC'94, Sendai, Japan, 1994, pp. 601-613.

5.3. K. Bochkov, I. Zakharov, and N. Ryazantseva, "Determination of EMC Degrees Based on Probability Models of Microelectronic Systems Ensuring Railway Traffic Safety" Proceedings of Int. Symp. on Electromagnetic Compatibility EMC'98, Rome, Italy, 1998, pp. 707-709.

## BIOGRAFICAL NOTES

Konstantin A. Bochkov, Professor, Doctor of Engineering Sciences, born 1950, chief of the chair "Automatics and Telemechanics" and head of research laboratory "Safety and EMC of hardware" of the Belorussian State University of Transport. Specialist in EMC of microelectronic safety systems, over 100 publications. Graduate of the Belorussian State University of Transport (Dipl. Eng.), Post-graduate, Saint-Petersburg University of Transport, Ph.D. Dissertation, Saint-Petersburg University of Transport, D.Sc., Moscow State University of Transport Communications, IEEE member.

Natalia V. Ryazantseva , Associated Professor of the electrical Engineering Faculty of the Belorussian State University of Transport. EMC problems during the last decade. Graduate Moscow State M.V. Lomonosov University, Ph.D. Dissertation, Saint-Petersburg Electrical Engineering University.

EMC 2000 INTERNATIONAL WROCŁAW SYMPOSIUM ON ELECTROMAGNETIC COMPATIBILITY

# TECHNICAL EMC SPECIFICATIONS FOR TELECOMMUNICATION PRODUCTS

**Marin Radulescu** - INSCC National Communications Research Institute, Calea Victoriei 37B - 70101 Bucharest. ROMANIA
**Dan Cristian Rucinschi** - University "Politehnica" of Bucharest - Power Engineering Department, Splaiul Independentei 313 - 77206 Bucharest, ROMANIA
**Ioannis Charalampakis** - INTRACOM Hellenic Telecommunications & Electronics Industry - R&D Department Markopoulo Ave. 190 02 Peania, Athens, GREECE

*The paper intends to contribute to the implementation of the EMC Directive, proposing a model for technical EMC specifications dedicated to telecommunication products. The considered products are the telephone set with analogue interface and the multiplexer PCM-PG system, both belonging to the access network. Their choice is based mainly on their wide use, small size and influence they have on the quality of the transmitted signals.*

*The structure of the EMC specification contains aside scope, normative references, definitions etc., some specific topics like EMC requirements (emission and immunity), performance criteria, test methods, test plan.*

*In close relation with the above problems, the authors describe their achievements related to the automation of tests and testing results.*

## 1. INTRODUCTION

The development of digital communications leads to the growth of the EMC problems, especially as a consequence of the application of the "essential requirements" stated by EMC Directive 89/336/EEC and other related Directives.

On the other hand, the multiplication of standardization documents, issued at different dates and by different standardization bodies (international or regional) like IEC, ITU-T, CISPR, ETSI, CENELEC, CEN, CEPT implies the use of a great number of publications, sometimes having non-correlated provisions. This can give rise to different meanings on the applicable tests, testing procedures and performance criteria, with undesirable consequences related to the comparison of test reports, issued by different laboratories and to the reliability of the product certification with respect to EMC requirements (mainly when a declaration of conformity is allowed).

This is the reason why the authors propose a model for EMC technical specification, product oriented, which should be elaborated in a similar way with the standards. The work must be done in the frame of national authorities (certification body, regulation authority) or professional associations and will be hopeful to reach at least a regional consensus. Such document will include all the relevant tests for the product, testing conditions and performance criteria, eliminating in this way the possible disagreement between different publications dealing with similar products.

The paper describes EMC technical specifications for telecommunication products, widely used, as are the telephone set with analogue interface and the PCM-PG system. These are relative simple products marketed by many producers. The diversity of manufacturers on the one hand and the possibility of their testing in small laboratories, on the other hand was the main reasons for the choice of these products in order to apply them our model for EMC technical specification. Moreover they present all type of coupling ports, they have both analogue and digital interfaces, each with their specific disturbances and the presence of these products in the access network influences the quality of the transmitted signals and data.

## 2. THE STRUCTURE OF THE EMC TECHNICAL SPECIFICATION FOR TELECOMMUNICATION PRODUCTS

All the above mentioned considerations, also related to the drafting of EMC specifications [1,2], led us to the following specification's structure:

1. Scope and object
2. Normative references
3. Definitions (if necessary)
4. Product description
   - 4.1. Generalities
   - 4.2. Main functions and functional states
   - 4.3. Priority of service (see [2])
   - 4.4. Installation electromagnetic environment
   - 4.5. Definitions of ports
5. EMC essential requirements
   - 5.1. Emission limits
   - 5.2. Immunity levels
   - 5.3. Resistibility
   - 5.4. Performance criteria
     - 5.4.1. Normal operation
     - 5.4.2. Performance criterion A
     - 5.4.3. Performance criterion B
     - 5.4.4. Performance criterion C
     - 5.4.5. Performance criterion R
6. Measuring / testing procedures
   - 6.1. General conditions during tests
   - 6.2. Test plan
   - 6.3. ⎫ Description of each emission
   - 6.4. ⎪ measurement/immunity test required in
     - ⎧ Clause 5: test set-up, test equipment,
     - ⎩ test methods (with specific particularities
   - 6.X. ⎭ for the <product> involved.

7. Final provisions like the implications of safety requirements on the test results and the required content of the test report [3,4].

## 3. COMMENTS ON THE PROPOSED STRUCTURE

The proposed structure for EMC technical specifications dedicated to telecommunication products is the result of a common work of a team composed by EMC specialists and telecommunication specialists. During this work the main aspect which needed to be solved was the selection of EUT's relevant functions together with the adequate performances to be fulfilled during tests, in order to give to the EMC specialists all the necessary information for the determination of the applicable tests. This is necessary because not all "essential requirements" must be tested in all functional states.

### 3.1. Product description (4)

The approach of product description must be oriented to lighten the evaluation of EMC aspects and therefore is correlated with the others clauses as follows:

- main functions (4.2) are implied in the structure of the test plan (6.2);
- priority of service (4.3) is tied with EMC requirements (5.1 - 5.3). For instance, in the case of "normal priority" the EMC requirements for the telephone set must comply with EN 55022 and EN 55024[5,6] and for PCM-PG system with EN 300386-2 [7], while in the case of "high priority" the severity of immunity test must be higher and reference shall be made to ETS 300386-1[2];
- installation electromagnetic environment (4.4) is to be considered with regard to emission limits (5.1) and immunity levels (5.2);
- the definition of ports by a block diagram (4.5) is necessary both for the specification of EMC requirements (5.1 - 5.3) and for test set-ups, test equipment etc. (6.3 - 6.X)

### 3.2. Performance criteria (5.4)

Here the authors propose a new concept called **normal operation**, to be included in all products dedicated EMC technical specifications. The proposed definition may be: "**normal operation** - one or more states and/or functions which are relevant for the <product> and for a specific test. The <product> must be in **normal operation** condition during the whole process of verifying the conformity with the essential requirements".

Regarding the **normal operation** conditions (5.4.1), they may differ from a test to another, taking into account the relation between EMC sensitivity of EUT in different operating states and the involved disturbances, respectively tests. It must be specified for each case: the functional states, the monitored parameters and their values or limits.

The performance criteria are defined in several standardization documents, both for immunity tests and for resistibility tests [2,6,7,8,9]. As their definitions and their designation also, are rather different it is necessary an effort from the part of standardization bodies to unify their viewpoints regarding the definitions. For the purpose of proposed EMC technical specifications, the authors used the following equivalence of criteria.

**Table 1 Equivalence of performance criteria**

| Type of test | Type of disturbance | Performance criteria |
|---|---|---|
| EMC Immunity | Continuos | A[6,7,8] or NP[2] |
| | Transient | B[6,7,8] or RP[2] |
| | | C[6,7,8] or (LFS + LFC)[2] |
| Resistibility | Continuos / Short duration | R[7] or $A_{ITU-T}$[9,10] or LFO[2] |

When one describes a performance criterion in a product EMC technical specification (5.4.X) it is important to emphasize the allowed deviations from the **normal operation** already defined (5.4.1) (degradation of performances or permissible loss of performances).

Any <product> is deemed to be compliant with a requirement only after the checking of the normal operation, after the cessation of the applied disturbance.

### 3.3. General conditions during tests (6.1)

This clause shall specify environmental conditions (climatic and electromagnetic) in order to assure the repeatability and traceability of tests (e.g. for ESD test the humidity range is more limited than for the other tests). Also here shall be specified operational conditions for EUT (like power supply quality) and requirements for the test site. In some cases may be necessary to specify a minimum test configuration in order to allow EUT to operate as intended. A complex system like PCM-PG must be tested successively on the subscriber unit and the exchange unit as EUT, in each case the other unit acting as auxiliary equipment (AE).

### 3.4. Test plan (6.2)

The test plan may be conceived in tabular form, in order to offer a comprehensive presentation of several aspects:

- the sequence of functional states;
- the applicable tests;
- the performance criteria, correlated with the function(s) and the applied test(s).

The Annex 1 gives an example of test plans for the telephone set.

### 3.5. Some considerations about relations between EMC and safety tests (7)

Although the safety tests are very distinct of EMC tests, they must be considered when a <product> is to be EMC certified, because it may become dangerous or unsafe as a result of EMC tests [8]. Moreover, in Clause 8, Table 1 of IEC Guide 107 this subject is included between the typical subjects of EMC publications.

It is well known that during EMC tests a <product> may be the subject of a stress (especially with voltage surges or impulses) which would not be envisaged in the frame of safety tests. As regard the telephone set and PCM-PG system, one must keep in mind some aspects:

- the user is in direct contact with some parts (metallic or non-metallic) when dialing or during the conversation;
- it is not sure that an apparatus which complies with ITU-T P360:1998 requirements regarding the effectiveness of limiting devices for prevention of excessive acoustic pressure, will continue to be safe in this respect during impulse immunity tests.
- as a result of a loss of function of the limiting devices of remote supply current, the service crew working on lines

equipped with PCM-PG systems could be endangered.

For this reason, the proposed EMC technical specifications for telecommunication products must require for EUT the following combined sequence of tests:

A. **Safety tests** according to the applicable standard (EN 60950 or EN 41003);
B. **EMC tests** according to Clause 5 of the actual EMC technical specification;
C. **Safety tests** - at least the electrical tests whose effect is not cumulative, like the measurement of insulation resistance or the measurement of touch current.

Normally after the application of EMC tests the <product> must not be damaged and must function as intended by its manufacturer. That is why it may be assumed that the application of safety tests after EMC tests on the same <product> will not increase the severity of the safety tests.

## 4. AUTOMATIZATION OF THE EMC TESTS

The large number of measurements and tests to be done and of the functions to be checked, in order to evaluate the compliance with the EMC essential requirements, leads to the solution of automated testing.

This is sometimes recommended from the relevant standards because of the complexity of the test calibration and test execution procedure.

Emphasis is given to immunity testing to continuous phenomena because it is:

- a very time consuming procedure,
- the standards require normal performance of the product under test.

The test engineers have thus to adjust the test equipment, to observe the test item and to measure several parameters that are critical for a proper functioning of the product.

The use of a software for implementing the test is essential not only for automatically adjusting the test equipment but also for measuring parameters like telecommunication signals on lines, acoustic levels on handsets, BER on digital lines etc.

An automated measurement system was developed based on the industrial IEEE interface.

Test parameters can be adjusted and displayed together with measured data in a user-friendly Windows environment, but also recorded for later investigation.

For the development, the Labview environment was used because of its easiness to function with modular programs that can be readily combined to produce a larger program. The Labview environment is specially developed and addressed to instrumentation people.

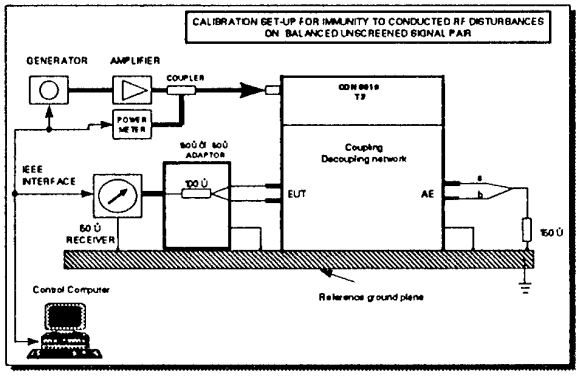
The test environment is thus free to include easily new test equipment and also to measure additional functional parameters of the products under test, making testing in the development phase easy, quick and accurate.

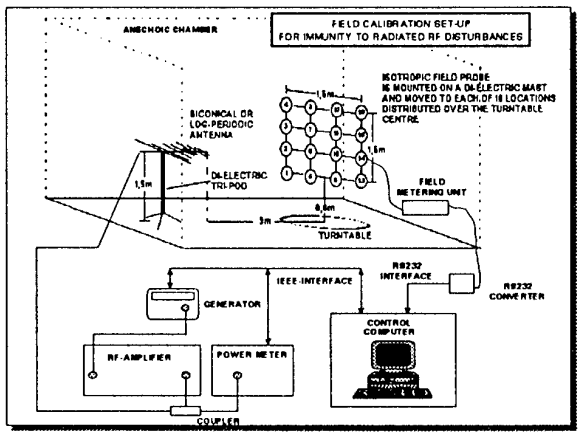
The test software is divided in two main parts, the conducted immunity and the radiated immunity test. Each part is further divided into two main routines one: for the calibration procedure and one for the actual test procedure.

The calibration of the conducted immunity has the purpose to apply a defined common mode voltage on the equipment under test terminals.

The calibration of the radiated immunity has the purpose to apply a uniform electromagnetic field around the equipment under test.

The calibration routines are running using a set up and a procedure as described in the relevant standards with the results automatically stored for later use during the test procedure.

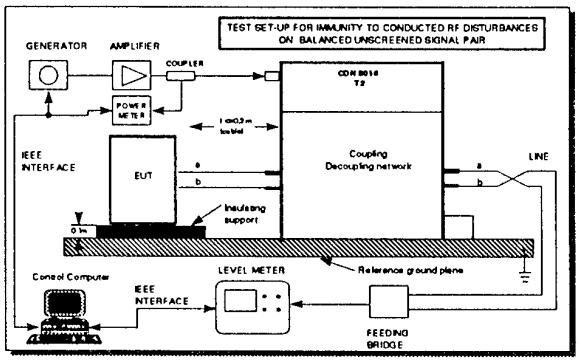


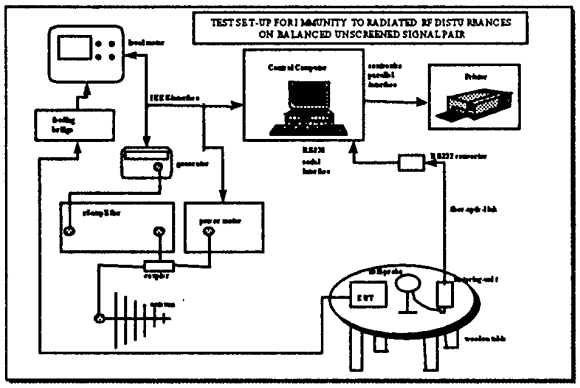




The automatically running calibration routines give the advantage to use them as often as it is required, having so always verified test conditions.

Extensive tests have been conducted using the software and with measurements of the following signals:

- 1 kHz demodulated signal selectively on a telecom line
- wide band noise on a telecom line
- psophometric noise on a telecom line
- acoustic noise on telephone handsets






For investigation purposes the software has the ability to make a quick test run and if the results are sufficient to proceed with the normal test steps which are time consuming.

The automatization offered many advantages during the development phase of the products:

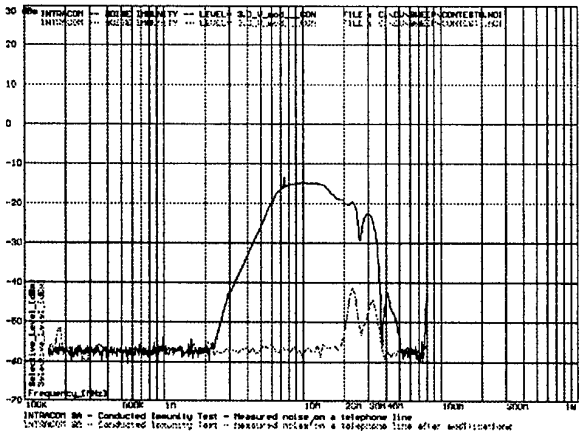
- The test results can be saved for later use
- Different test results can be compared
- The fast execution procedure minimizes the investigation time
- The human error has been eliminated during a very tiresome test procedure.

From the extensive testing a lot of experience has been gained on the behavior of telephone equipment to continuous RF disturbances. Generally, it can be said:

- Equipment with no acoustic interface needs a careful design following the rules that are well know from other tests made until now.
- Equipment with acoustic interface needs a lot of work to fulfill requirements of modulated RF disturbances.

## 5. CONCLUSIONS

The paper tries to emphasize some important aspects to have in mind when drafting EMC technical specifications, with application to the above mentioned telecommunication products:



- **the necessity of a close co-operation between EMC specialists and telecommunication specialists, in order to well define the normal operation and the test plan;**
- **the harmonization of performance criteria** (if needed) and a <product> oriented definition, taking into account that IEC (EN) and/or ETSI basic, generic or product family standards give only general definitions;
- the general approach is that product standards concerns mainly the manufacturers, which must have their own standards or specifications related to a particular <product>. The reality of EMC standardization (in relation with EMC essential requirements) reveals the fact that, in order to have a reliable certification, **the product EMC (and related topics) technical specifications must be elaborated by an independent body (like for example an EMC professional association)** with the participation of involved parties (regulatory authority, manufacturers, users, accredited laboratories, certification body).
- **The automatization of the calibration and the actual run procedures of the standards give a lot of advantages**, first to the design engineers who receive quick and very comprehensive test results, and also to the test engineers who can perform easily and with no errors the tests.
- It is very useful, that the standards describe test procedures that can be easily automatized.
- Analyzation of the test is necessary to find signals, affected from the RF signal, that can be easily measured.

## 5. REFERENCES


1. IEC Guide 107:1998, "Electromagnetic compatibility - Guide to the drafting of electromagnetic compatibility publications"
2. ETS 300386-1:1994, "Equipment Engineering (EE); Public telecommunication network equipment Electromagnetic Compatibility (EMC) requirements Part 1: Product family overview, compliance criteria and test levels"
3. EN 45001:1989, "General criteria for the operation of testing laboratories"
4. EN 61000-4-XX, "Electromagnetic compatibility (EMC) - Part 4: Testing and measurement techniques"
5. EN 55022:1998, "Information technology equipment - Radiodisturbance characteristics - Limits and methods of measurement"
6. EN 55024:1998, "Information technology equipment - Immunity characteristics - Limits and methods of measurement"
7. EN 300386-2:1997, "Electromagnetic compatibility and Radio spectrum Matters (ERM); Telecommunication network equipment Electromagnetic Compatibility (EMC) requirements; Part 2: Product family standard"
8. EN 50082-1:1997, "Electromagnetic compatibility - Generic immunity standard Part 1: Residential, commercial and light industry"
9. ITU-T Rec. K20:1996, "Resistibility of telecommunication switching equipment to overvoltages and overcurrents"
10. ITU-T Rec. K21:1996, " Resistibility of subscriber's terminal to overvoltages and overcurrents"


## BIOGRAPHICAL NOTES

**Marin Radulescu** Dipl. eng. degree in telecommunications from the Polytechnical University Bucharest in 1964. He firstly worked at "Electromagnetica" Factory, Development

Dept. After 1976 he is with "Research and Development Institute for Telecommunication Equipment". Since 1994 he is Senior Researcher at "National Communications Research Institute" in Bucharest, involved in elaborating of technical specifications for network components, also EMC specifications, test procedures and complying tests.

**Dan Cristian Rucinschi** He received the Dipl.eng. degree in Electrical Engineering at Polytechnical University of Bucharest in 1969. After that he worked in H.V. Laboratory and Quality Research Laboratory of Institute for Electrical Engineering (ICPE) Bucharest until 1994. Now he is Technical manager of National Interuniversity Research Center for H.V. Engineering and EMC at University "Politehnica" of Bucharest and also technical auditor of RENAR (National Certification Network) in the field of H.V. and EMC Laboratories

**Ioannis Charalampakis** - Electrical Engineering from Technical University of Hannover-Germany. Design Verification Laboratory of INTRACOM SA. Active as test engineer for various products of the company. Developing of test software .

**Annex 1: Test plan for telephone set**

| Functional states | Immunity | | | | | Emission | | Resistibility | | |
|---|---|---|---|---|---|---|---|---|---|---|
| | $H_{50}$ | $E_{rf}$ | $V_{rf}$ | ESD | EFT | $E_{rf}$ | $V_{rf}$ | V | $V_{50}$ | ESD |
| Quiescent state | | | | | | | | | | |
| Communication subscriber – exchange | | | | | | | | | | |
| Outgoing call | | | | | | | | | | |
| Dialling | | | | B | | | | | | R |
| Conversation | A | A | A | | B | CIS | CIS | | R | |
| Metering | | | | B | B | | | R | | R |
| Call clearing | | | | | | | | | | |
| Quiescent state | | | | | | | | | | |
| Communication exchange – subscriber | | | | | | | | | | |
| Ringing state | | | | | | CIS | CIS | | | |
| Incoming call | | | | | | | | | | |
| Conversation | (A) | (A) | (A) | | (B) | | | | (R) | |
| Call clearing | | | | | | | | | | |
| Quiescent state | | | | | | | | | | |
| Management | | | | | | | | | | |
| Modem transmission | | | | | B | | | | | |
| Data memories | | | | B | B | | | R | | R |

**Symbols:** $H_{50}$ – Power frequency magnetic test; $E_{rf}$ – Radiated RF electromagnetic field; $V_{rf}$ – Conducted RF disturbances; ESD – Electrostatic Discharges; EFT – Electrical Fast Transients; CIS – Limits acc. to [5]; $V_I$ – Induced voltage, LEMP (10/700 μs); $V_{50}$ – Induced voltage 50 Hz; 0.2 s [10]; A,B,C,R – Performance criteria, associated with functional state to validate; (A),(B),(C),(R) – Performance criteria, previous verified

EMC 2000 INTERNATIONAL WROCŁAW SYMPOSIUM ON ELECTROMAGNETIC COMPATIBILITY

# COMPUTER ANALYSIS OF THE PERFORMANCES OF ESSENTIAL MICROELECTRONIC CIRCUITS IN INTRICATE ELECTROMAGNETIC ENVIRONMENT

K.A. Bochkov and S.N. Kharlap
Belorussian State University of Transport
246653, Belarus, Gomel, Kirov Str., 34
Tel. (0232)553361, e-mail: bochkov1999@mail.ru

*The presentation deals with the problem of the EMC effect upon safe performance of microelectronic circuits. The authors propose to perform simulation of performance of the circuits responsible for safety, the effects o errors and failures of hardware and software. The principles are disclosed how to create simulation models together with the algorithms of their evaluation. Then the results of computer evaluation are taken into consideration for designing test of microelectronic systems controlling safety for EMC in order to identify the tacts in the operation of a system critical for safety. The advance methods promote the validity of tests of microelectronic systems controlling safety.*

## 1. INTRODUCTION

Many systems controlling essential processes (incumbent with risk for people, significant material losses and negative effect upon the environment) operate in the intricate electromagnetic environment. Their reliable and safe performance is strongly governed by solving the problems of their electromagnetic compatibility with the existing electromagnetic environment. At present microelectronic, microprocessor and computer means are employed intensively to design the systems controlling safety (SCS). Hence there are challenging problems of creating the microelectronic systems satisfying the required safety level. There are international requirements that the safety of such systems should be obligatorily certified.

Broad use of microelectronic equipment and systems controlling safety, specifically inn railway traffic, has highlighted the problem of their electromagnetic compatibility. It has been reflected in the European standards, national regulations. This problem is specifically acute in the systems of railway automatics and telemechanics (RATM) due to the following reasons:

1. Compared with relay systems the microelectronic RATM are much stronger affected by electromagnetic noise because they are much more intricate, compact, packed, their components are much faster and more vulnerable.

2. The systems of railway automatics operate in intricate electromagnetic environment. Errors in the microelectronic systems occur one order of magnitude more frequently than their failures. Yet the effect of noise is comparable with failures of hardware and errors in the software. Therefore, to test the microelectronic systems controlling safety for EMC puts into foreground the problems of evaluating the consequences of failures, their location when they upset safety in performance (risky errors).

3. High intricacy of these systems determines a great variety of states (operation tacts). Meanwhile, electromagnetic effects in various tacts of performance of the systems may produce different results.

4. Tough standards of reliable and safe performance of the systems (the rate of dangerous failure $\lambda_s = 10^{-11}$ 1/h in the European standards) require to analyze all the situations which are determined by the inequality

$$P_s \le P_c \cdot P_d ,$$

where $P_c$ is the probability of existence of a certain state in the system; $P_d$ is the probability of occurrence of electromagnetic noise of a certain type leading to error; $P_s$ is the probability of a dangerous failure of the system.

The authors study microelectronic SCS which are highly reliable devices. The rate of dangerous failures upsetting the conditions of safe performance of these systems (specifically the railway automatic systems) should be of the order $10^{-11} \div 10^{-13}$ 1/h or average service over 100 years until any dangerous failure. Therefore, it is impossible to collect comprehensive statistics of dangerous errors or failures. In order to achieve high standards of reliable and safe performance of these systems, special methods of designing are used based on reserving, diagnosing and using safe components [1]. These safe components imply the components with the rate of a certain type of failures below the permissible standard (in this case $\lambda_s = 10^{-11}$ 1/h). Special control circuits are used in these systems to maintain their safety with stricter requirements for their safety and EMC.

The basic method of validating stable performance of a system under the effect of electromagnetic noise are

tests of pilot specimens using noise simulators. The quality of a system is rated based on the output parameters characterizing its performance. Yet, in intricate systems the effects of electromagnetic noise are strongly governed by the fact at which operation tact an error occurs. During tests with the help of noise simulators it is impossible to cover each operation tact of the system. Also, the inertia of the system may delay an error for several operation tacts when noise does not affect the system already. Hence, physical modeling excludes a comprehensive evaluation due to a very great number of tests (the time and economic factors). Therefore tests of pilot specimens should be supplemented with computer modeling [2]. Compared with other types of tests the simulation modeling accelerates tests, in the process a variety of possible process situations can be created; a great number of failures and errors of hardware and software can be simulated which impossible when testing physical models; to accumulate the statistics how errors affect safety; to validate the lists of dangerous failures.

## 2. MODELING FAILURES AND ERRORS

What are general principles of constructing models reflecting failures and errors of components? When studying engineering objects two approaches are employed: a functional and a structural. The functional approach deals just with the algorithms of performance, i.e. what functions are accomplished. The structural approach investigates also the internal organization of the structure of an object in addition to the implemented functions.

The functional models are simpler, yet the disadvantage of the functional approach is that such parameters of diagnostics like the depth of search and full identification of defects are unachievable for more or less intricate objects. Hence structural mathematical models are needed to solve the formulated problem. Structural models show objects as an integrity of individual components arranged in a certain manner to achieve the required functional dependencies. Frequently a component of the object is a structurally and functionally integral part which is not to be decomposed further. Hence, a functional mathematical model is sufficient to describe the component. A structural finite automaton is used to describe the object in its integrity. The disadvantage of the structural model is that it is intricate to describe interactions between individual components.

The laboratory of safety and EMC of engineering means of the Belorussian State University of Transport developed a system of modeling discrete circuits as a structural automaton. Description of the scheme of the structural automaton is made as a generalized transitional system [3]. It has allowed to simplify significantly formal representation of interactions between the model's components. The components are represented by abstract finite automatons. Description of the components as finite automatons reflects all the failures and errors occurring in modeled devices.

Disorders of a discrete member when described by its finite automaton are interpreted [1,2] as distortions of output symbols of the automaton or transitions between its states. In this case it is impossible very frequently to indicate the location where physical defects appear in the object without ambiguity when this disorder of transitions between the states of the abstract automaton is induced. Also, since there is a variety of states, the number of possible false transitions multiplicates and significantly exceeds the number of possible disorders. It restricts application of the abstract automaton model.

The authors advance a new approach to the modeling of failures of discrete objects which implies the following.

A failure of the components implies the distortion of output information compared with the output information of a normal component. The distortion may result from the distortion of input signals, the distortion of a function performed by the component or the distortion of output signals. The distortion of input and output signals is easily achievable by applying a "mask" to certain inputs and outputs of the components. It is highly intricate to describe the distortion of performance of intricate components (for example a microprocessor) due to a great variety of failures and their effect upon the algorithm of performance. Still, it is always possible to select the input and output distortions of information with the manifestations equivalent to the failures in the internal structure of a component.

Consider the advanced method using an example of combination members. The combination members are characterized by the fact the values of their outputs are fully determined by the input values, they are independent of time or the sequence of input effects. The combination member can be interpreted as a finite automaton with a single state. For example, the member of conjunction "2&" is described in the following manner:

$$V_{\&} = (A_{\&}, S_{\&}, B_{\&}, \varphi_{\&}, \psi_{\&}), \qquad (1)$$

where $A_{\&} = \{0, 1\} \times \{0, 1\}$ is the input alphabet; $S_{\&} = \{0\}$ is the set of states; $B_{\&} = \{0, 1\}$ is the output alphabet; $\varphi_{\&}(s, a) \equiv 0$ is the function of transitions; $\psi_{\&}(s, (a_1, a_2)) = a_1 \,\&\, a_2$ is the function of outputs.

To describe the performance of combination members with possible failures it is enough to use the distortion of the output signals only (Fig. 1).

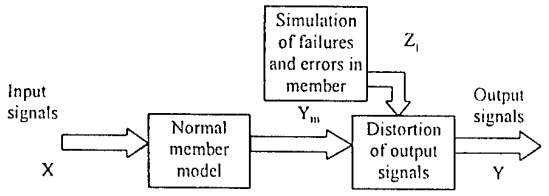



Fig. 1. Structure of combination device model

In this case the states of members are supplemented by the disordered state, the set of output signals is supplemented by an external disorder signal, correspondingly the functions of transitions and outputs change. The disordered state distorts the function of output in accordance with the type of a modeled disorder.

The analysis in [1,2] shows that constant failures are most common in microelectronic circuits when a constant potential appears at the output of a component as logic zero or one. In this case the model becomes still simpler. Description of the member "2&" with the account of the constant disorder "1→0" acquires the form:

$$V_{\&}^{*} = (A_{\&}^{*}, S_{\&}^{*}, B_{\&}^{*} \varphi_{\&}^{*}, \psi_{\&}^{*}), \qquad (2)$$

where $A_{\&}^{*} = \{0, 1\} \times \{0, 1\} \times \{0, 1\}$ is the input alphabet, $a_3 = 0$ is the disorder signal; $S_{\&}^{*} = \{0, 1\}$ is the set of states, "0" is the state of disorder; $B_{\&}^{*} = \{0, 1\}$ is the output alphabet; $\varphi_{\&}^{*}(s,a)=a_3$ is the function of transitions; $\psi_{\&}^{*}(s,(a_1,a_2,a_3)) = a_1 \,\&\, a_2 \,\&\, a_3 \,\&\, s$ is the function of outputs.

The behavior of discrete objects with memory is determined both by the output values and by its states. One and the same object may output different sequences in response to one and the same input sequence depending upon the original state of the object. Additional distortion of internal states of the object is required (Fig. 2).

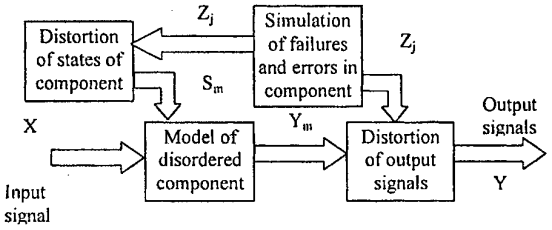



Fig. 2. Structural model of discrete object with memory

Microelectronic RATM may also fail in case components of the system output errors under the effect of all sorts of electromagnetic noise. Hence, models intended to evaluate safety of microelectronic RATM should include errors in addition to failures of components. Errors in performance are interpreted as a short-time failure [1]. The models of a component treat errors similarly to failures. The difference is in the algorithm of identification of failures and errors and in the method of reconstruction of the characteristics of the component after failure and error. The failure is specified before the first test sequence commences and is removed after the last test sequence. Error may be specified at any random moment of time and it is removed after a certain interval of time equal to the error duration.

## 3. METHODS OF TESTING MICROELECTRONIC MEANS FOR SAFETY

The model of performance of microelectronic RATM is used at the laboratory of safety and EMC for testing absence of dangerous failures and errors in essential microelectronic circuits (devices). Special methods and algorithms of validating the safety of microelectronic circuits by performing simulation tests. One of the key tests is to test for immunity against a dangerous failure (error). Target-oriented programming has been used to elaborate the software of the module of identification of dangerous sates of combination RATM devices and a memory device. Each standard component of the circuit for study is described as a separate class. Interrelations and interactions between the components of a circuit are described by two matrices: a bidimensional matrix of objects and a tridimensional matrix of relations.

Dangerous states are sought for by "direct" and "reverse" methods. It allows to move flexibly over the circuit (over matrices in fact) and to detect dangerous states with an accuracy down to each specific component. The sense of searching for dangerous states of a device is the following:

(1) A device is modeled.

(2) Criteria of dangerous failures and errors are formulated.

(3) The functions of dangerous failures and errors are described. The function of a dangerous failure implies the combination of the output effects of the system which result in dangerous failure at specified input effects and states of the system's components. For combination devices it may be a function determined by the functions of the logic algebra, for discrete memory devices and microprocessor systems it is to identify certain components of the model in one state of a given set.

(4) The circuit is checked in accordance with the algorithm in Fig. 3. Since the probability of any dangerous failure in any real railway automatic system is very small, it is necessary to analyze all possible states in order to determine the possibility of failures and errors of a certain type in order to search for possible dangerous states. All possible input effects are entered into the model for which dangerous failures and errors are specified. The output responses of the model are registered and compared with parameters of the dangerous failure function. In case the output responses coincide with the parameters of the dangerous failure function, the dangerous state of the circuit is registered and the information is outputted about the failure or error of which component results of dangerous failure.

(5) If the normal circuit is free of dangerous states, failures and errors of various components of this device are modeled. Validation is repeated until all registerable failures and errors are investigated. Failures and errors may occur once or they may repeat.

(6) A conclusion is made about absence of dangerous failures and errors in the circuit providing the results show not a single dangerous state.

Computer modeling identifies components and operation tacts of system which lack EMC. It allows to validate the results of modeling by testing the system using noise simulators in most vulnerable places and operation tacts. Thus the validity of tests for EMC of

intricate systems is promoted and the scope of tests is reduced.

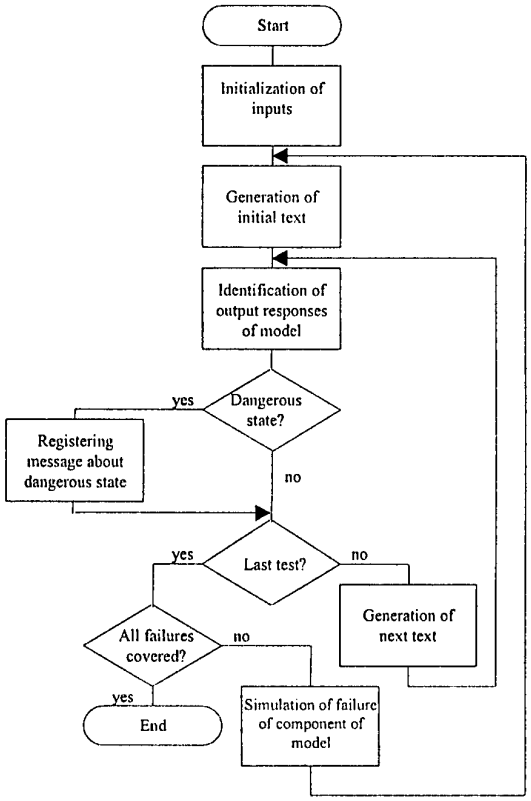



Fig. 3. Algorithm of identification of dangerous states

## 4. CONCLUSION

The laboratory of safety and EMC has elaborated software for checking microelectronic RATM for dangerous failures and errors. The package allows to create simulation models of microelectronic circuits controlling safety based on logic components and memory components, to enter constant failures and errors of the components, to identify the responses of the circuit and to compare them with the criteria of a dangerous failure or error. By analyzing the behavior of the system it is possible to prove whether the circuit is safe, to identify EMC-vulnerable components, to reduce significantly the cost of testing with noise simulators. The complex incorporates the state-of-the-art of programming, it has a convenient interface capable to image the results of experimentation , it is versatile and the component base of modeled devices is expandable.

The disclosed methods allow to achieve high validity (including the tests of large integrated circuits), to use a single algorithm for analyzing microelectronic RATM of various levels of complexity (including microprocessors), to register errors inducing dangerous failures, to check the states free of dangerous failures in ATM devices, including individual and repeating failures and errors.

The new method has been validated by detecting dangerous failures in a RATM device and has manifested its suitability for solving the problems of certifying engineering means at the laboratory of the University of transport. Experiments have manifested that the model and the elaborated algorithms are highly adequate for checking the immunity of circuits to dangerous failures and errors. At present studies continue with the objective to crate simulation models of microprocessor modules, multiprocessor systems and designing new types of tests, like analysis of the performance of a circuit in case of scatter of time parameters, distortion of input signals and some other procedures needed for promoting the adequacy of tests for safety.

## 5. REFERENCES

5.1 V.V. Sapozhnikov, Vl.V Sapozhnikov, H.A. Khristov, and D.V. Gavzov, "Methods of Designing Safe Microelectronic Systems for Railway Automatics", (in Russian), Moscow, 1995, 272 pp.

5.2 V.V. Sapozhnikov, Vl.V Sapozhnikov, T.I. Talalaev, et al., "Certification and Validation of Safety of Railway Automatic Systems", (in Russian), Moscow, 1997, 288 pp.

5.3 S.N. Kharlap, "Program Module to Detect and Register Errors and Failures of Microelectronic Devices" (in English), Proceedings of Int. Symp. on Electromagnetic Compatibility, Wroclaw, Poland, 1996, pp. 651-653

## BIOGRAFICAL NOTES

Konstantin A. Bochkov, Professor, Doctor of Engineering Sciences, born 1950, chief of the chair "Automatics and Telemechanics" and head of research laboratory "Safety and EMC of hardware" of the Belorussian State University of Transport. Specialist in EMC of microelectronic safety systems, over 100 publications. Graduate of the Belorussian State University of Transport (Dipl. Eng.), Post-graduate, Saint-Petersburg University of Transport, Ph.D. Dissertation, Saint-Petersburg University of Transport, D.Sc., Moscow State University of Transport Communications, IEEE member.

Sergey N. Kharlap , born 1967, Assistant Professor of the electrical Engineering Faculty of the Belorussian State University of Transport, Ph.D in Engineering in the same University. The field of scientific interest is EMC effect upon safe performance of microelectronic circuits.

**EMC 2000** INTERNATIONAL WROCŁAW SYMPOSIUM ON ELECTROMAGNETIC COMPATIBILITY

# IMMUNITY INVESTIGATION OF ELECTRONIC EQUIPMENT UNDER SIMULATION OF INDIRECT ELECTROSTATIC DISCHARGE

B.N. Faizoulaev, V.V. Logatchev, K.S. Oraevsky
EMC Scientific and Test Center "IMPULS"
Russia, Moscow, Varshawskoe shosse, 125, tel./fax: (095) 319-1645

*The transient analysis is carried out at effect of an indirect electroststic discharge (ESD) on a coupling plane at its standard connection to a Ground Reference Plane (GRP) via a cable with a 470 kΩ resistor located at each end (in accordance with the test methods of IEC 61000-4-2), and also at direct connection of coupling plane and GRP via a 2 m length cable that simulates grounding cable of object in the vicinity of the equipment on which ESD takes place from the operator. It is detected various character of transients from ESD at two methods of connection of coupling planes and GRP, that accordingly results in difference on immunity levels (in limits 30 % and more). In view of the carried out analysis with the purposes of the more exact immunity evaluation of technical equipment it is offered to supplement IEC 61000-4-2 standard by the test on effect indirect ESD at connection of coupling planes and GRP via a 2 m length cable.*

According to IEC 61000-4-2 requirements, application of indirect electrostatic discharge from ESD generator to Vertical Coupling Plane (VCP) and Horizontal Coupling Plane (HCP) performs when each of this planes connected to a Ground Reference Plane via a cable with a 470 kΩ resistor located at each end. Therefore it performs simulation of electromagnetic disturbance from personnel discharge current to ungrounding objects in the vicinity of the equipment under test (EUT) or to the object, on which EUT installed.

For purpose of safety, the cabinet of equipment as a rule shall be connected to the protective grounding system, and it is necessary to analyse transient phenomenon and to verify immunity level of EUT in its real installed conditions, that is VCP and HCP must connected to GRP via a 2 m length cable.

This work considers transient phenomenon of discharge current $I_{ESD}(t)$ at two cases of connecting VCP to GRP.

1. VCP is connected to GRP via a cable with a 470 kΩ resistor located at each end (in accordance with the test methods of IEC 61000-4-2).

Test network and appropriate equivalent scheme are given in fig. 1 a,b.

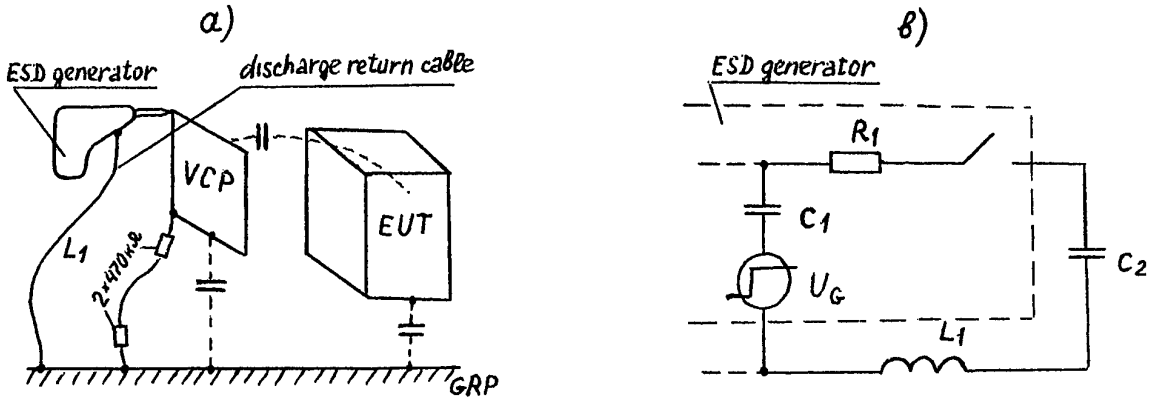



Fig. 1.

Using operational conversion (by Karson), we receive expressions for discharge current ($I_{ESD1}$) and voltage on VCP ($U_{ESD1}$):

$I_{ESD1}(p) = U_G \cdot p \cdot \tau_1 / A(p) \cdot R_1$ (1)

$U_{ESD1}(p) = U_G \cdot C_1 / A(p) \cdot (C_1 + C_2)$, (2)

where $A(p) = p^2 \cdot \tau_{L1}^2 + p \cdot \tau_1 + 1$,

$\tau_1 = R_1 \cdot C_1 \cdot C_2 / (C_1 + C_2)$,

$\tau_{L1}^2 = L_1 \cdot C_1 \cdot C_2 / (C_1 + C_2)$.

The account is carried out at present values of parameters:

$U_G$ =2kV, $C_1$=150 pF, $C_2$=50 pF, $R_1$=330Ω, $L_1$=1,5 μH, where $U_G$ -output voltage of ESD generator in the idle mode,

$C_1$ – energy storage capacitance of ESD generator;

R - discharge resistance of ESD generator;

$L_1$ – inductance of discharge return cable of ESD generator;

$C_2$ – equivalent capacitance between VCP and GRP.

In result is recieved expressions for transients of discharge current and discharge voltage:

$I_{ESD1}(t) = 17,7 \cdot \exp(-at) \cdot \sin bt$, (3)

$U_{ESD1}(t) = 1500 \cdot [1-1,77 \cdot \sin(bt + 0,6) \cdot \exp(-at)]$, (4)

where $a = 1,1 \cdot 10^8 \cdot c^{-1}$, $b = 0,754 \cdot 10^8 \cdot c^{-1}$.

Transients of discharge current $I_{ESD1}(t)$ and voltage $U_{ESD1}(t)$ are given in a fig. 3 (curve $I_1$) and in a fig. 4 (curve $U_1$).

2. VCP is connected to GRP via a 2 m length cable.

Test network and appropriate equivalent scheme are given in fig. 2 a,b.

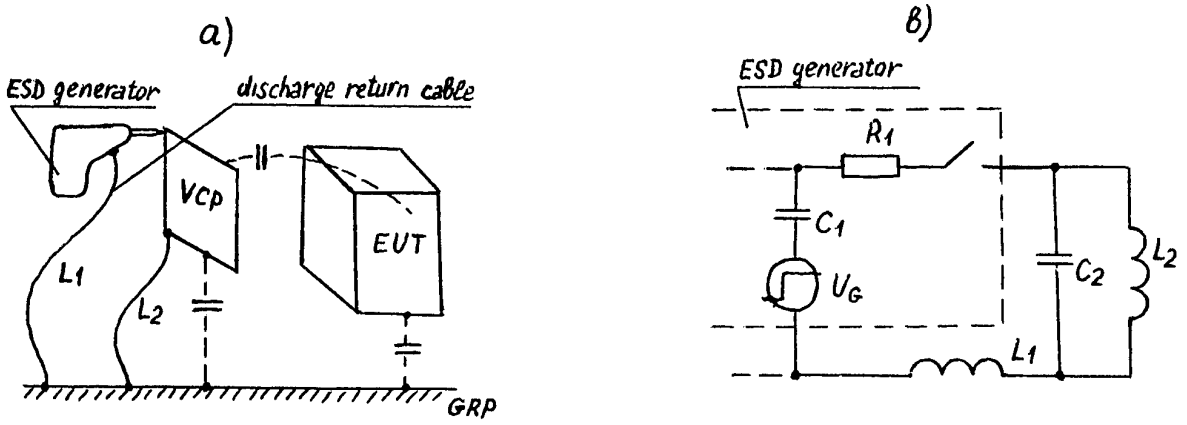



Fig. 2.

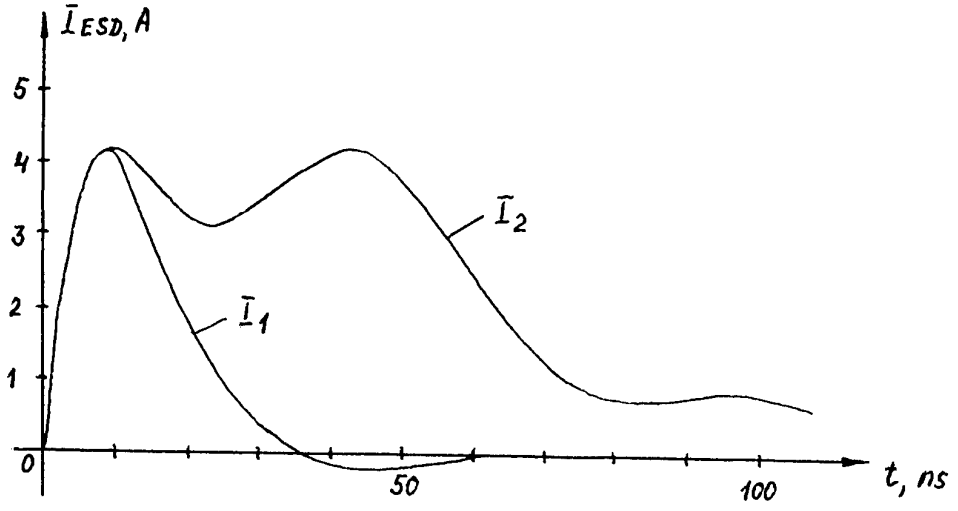



Fig. 3.

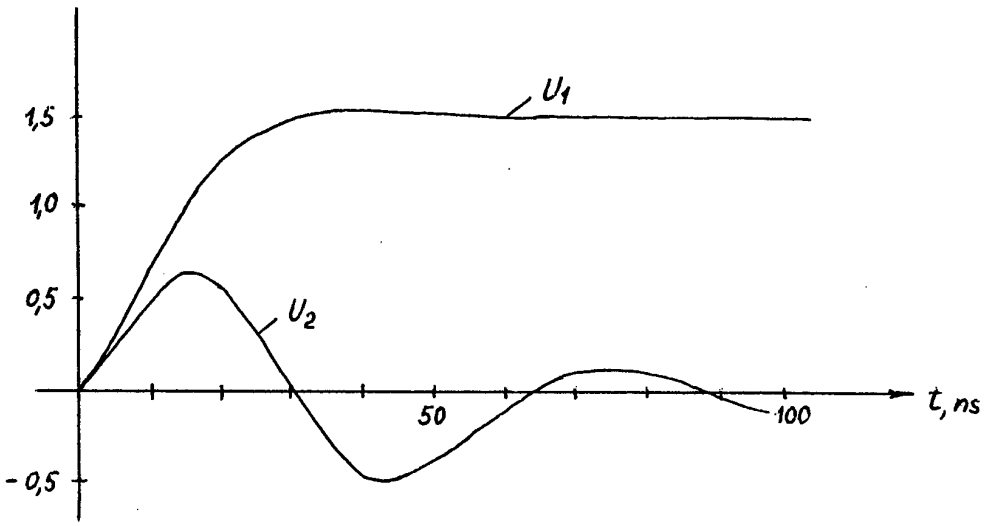



Fig. 4.

Operational expressions for discharge current ($I_{ESD2}$) and voltage on VCP ($U_{ESD2}$) have the following form:

$$I_{ESD2}(p) = U_G \cdot p \cdot \tau_1 \cdot (p^2 \cdot \tau_{L2}^2 + 1) / B(p) \cdot R_1 \quad (5)$$

$$U_{ESD2}(p) = U_G \cdot \tau_{L21}^2 \cdot p^2 / B(p), \quad (6)$$

where $B(p) = p^4 \cdot \tau_{L1}^2 \cdot \tau_{L2}^2 + p^3 \cdot \tau_1 \cdot \tau_{L2}^2 +$
$+ p^2 \cdot (\tau_{L1}^2 + \tau_{L21}^2 + \tau_{L2}^2) + p \cdot \tau_1 + 1,$
$\tau_{L1}^2 = L_1 \cdot C_1,$
$\tau_{L2}^2 = L_2 \cdot C_2,$
$\tau_1 = R_1 \cdot C_1,$
$\tau_{L21}^2 = L_2 \cdot C_1.$

The account is carried out at the values of parameters $U_G$, $C_1$, $R_1$, $L_1$, indicated in item 1. Capacitance $C_2$ has expanded by the distributed capacitance of cable, connecting VCP and GRP ($C_2$ = 60 pF). $L_2$ – inductance of cable, connecting VCP and GRP, is set equal 1,5 μH.

The following expressions for transients of discharge current and voltage are obtained at ESD on VCP, connecting to GRP via a 2 m length cable:

$$I_{ESD2}(t) = 3{,}84 \cdot \exp(-at) \cdot \sin(bt + 2{,}2) +$$
$$+ 10{,}44 \cdot \exp(-ct) - 13{,}54 \cdot \exp(-dt) \quad (7)$$

$$U_{ESD2}(t) = 1255{,}76 \cdot \exp(-at) \cdot \sin(bt - 0{,}55) -$$
$$- 394{,}4 \cdot \exp(-ct) + 1053{,}47 \cdot \exp(-dt), \quad (8)$$

where $a = 0{,}265 \cdot 10^8 \cdot c^{-1}$, $b = 1{,}13 \cdot 10^8 \cdot c^{-1}$,
$c = 0{,}26 \cdot 10^8 \cdot c^{-1}$, $b = 1{,}41 \cdot 10^8 \cdot c^{-1}$.

Transients of discharge current $I_{ESD2}(t)$ and voltage $U_{ESD2}(t)$ are given in a fig. 3 (curve $I_2$) and in a fig. 4 (curve $U_2$).

Comparing of transients of discharge current and voltage for the considered two methods (fig. 3 and fig. 4) points on their essential distinction at direct connection of a coupling plane with GRP consisting in expanding of discharge current pulse duration more than three times, and coupling plane voltage has oscillatory character with period about 60 ns.

Experimental research of immunity of the various PC configurations is carried out. The results are given in tables 1, 2. Threshold voltage (Uth) - minimum amplitude ESD voltage, causing failure in operation of test PC configuration.

Table 1

Result of measurments $U_{th}$ at effect ESD to Horizontal Coupling Plane

| ESD Polarity | Serial number of PC configuration | Method of connection HCP to ground reference plane | | Relative immunity distinction,* % |
|---|---|---|---|---|
| | | via 2x470kΩ ($U_{th.R}$, kV) | via a 2 m length cable ($U_{th.sh}$, kV) | |
| Plus | 1 | 0,6 | 0,8 | + 33 |
| | 2 | 1,0 | 1,2 | + 20 |
| | 3 | 0,65 | 0,6 | - 8 |
| | 4 | 2,7 | 2,7 | 0 |
| | 5 | 2,4 | 1,9 | - 21 |
| | 6 | 1,9 | 2,1 | + 10 |
| Minus | 1 | - 1,3 | - 0,9 | - 31 |
| | 2 | - 1,6 | - 1,0 | - 37 |
| | 3 | - 1,2 | - 1,3 | + 8 |
| | 4 | - 2,0 | - 1,9 | - 5 |
| | 5 | - 1,6 | - 1,9 | + 19 |
| | 6 | - 2,8 | - 2,1 | - 25 |

Table 2

Result of measurments $U_{th}$ at effect ESD to Vertical Coupling Plane

| ESD Polarity | Serial number of PC configuration | Method of connection VCP to ground reference plane | | Relative immunity distinction, * % |
|---|---|---|---|---|
| | | via 2x470kΩ ($U_{th.R}$, kV) | via a 2 m length cable ($U_{th.sh}$, kV) | |
| Plus | 1 | 0,85 | 1,0 | + 18 |
| | 2 | 1,6 | 1,8 | + 12 |
| | 3 | 1,05 | 0,95 | - 10 |
| | 4 | 6,5 | 6,3 | - 3 |
| | 5 | 3,3 | 3,3 | 0 |
| | 6 | 3,8 | 4,8 | + 26 |
| Minus | 1 | - 1,5 | - 1,1 | - 27 |
| | 2 | - 1,9 | -1,8 | - 5 |
| | 3 | - 1,4 | - 1,6 | + 14 |
| | 4 | - 5,8 | - 6,0 | + 3 |
| | 5 | - 3,2 | - 2,4 | - 25 |
| | 6 | - 5,3 | - 4,5 | - 15 |

* - relative immunity distinction (relative distinction of threshold voltage) at two methods of conntcting VCP (HCP) to GRP ($U_{th.R}$ - at connection via 2 x 470 kΩ, $U_{th.sh}$ - at connection via a 2 m length cable) is defined by a relation $(|U_{th.sh}| - |U_{th.R}| / |U_{th.R}|) \cdot 100$ %, and it also characterizes relative distinction in immunity levels at the indicated methods of connection.

The results of the given tests (table 1, 2) have shown:

1. When subjected indirect ESD on VCP and HCP, immunity of technical equipment depends on the method of connecting VCP and HCP to the grounding reference plane and is determined by features of element base, designing and mounting of technical equipment.
2. The experiments have shown, that at connection of coupling plane to grounding reference plane via a 2 m length cable immunity level differs from immunity level at connection of this plane to GRP via a cable with a 470 kΩ resistor located at each end in accordance with the test methods of IEC 61000-4-2. This distinction can exceed ± 30 %.
3. Taking into account, that both methods of connection VCP and HCP simulate actual conditions of maintenance of equipment, we consider expedient to supplement IEC 61000-4-2 standard by the test on effect indirect ESD on VCP and HCP at connection them to GRP via a 2 m length cable without resistors at its ends.

BIOGRAPHICAL NOTES

1. Boris N. Faizoulaev

He was born in Moscow, Russia, in 1930. He received Doctor of Science in Engineering degree in 1975 and Professor in 1980 at Scientific Reccarch Computer Center in Moscow. He is author of more than 200 scientific publications in the fields of digital microelectronics and electromagnetic compatibility. Now he is Director of EMC Scientific and Test Center in Moscow.

2. Valery V. Logatchev. Chief of test laboratory.
3. Konstantin S. Oraevsky. Scientist worker.

EMC 2000 INTERNATIONAL WROCŁAW SYMPOSIUM ON ELECTROMAGNETIC COMPATIBILITY

# MULTI-SIGNAL METHOD TO RECEIVER'S SELECTIVITY ESTIMATION

Vladimir B. Trigubovich

Belarusian State University of Informatics and Radioelectronics, Radio Systems Dept.,

220027, 6 P. Brovka str., Minsk, Belarus

Tel.: 00375-0172-398067; Fax.: 00375-0172 310914; E-mail: info@bsuir.edu.by

*In this paper a new method to multi-signal estimation of the receiver selectivity is discussed. Because analytical investigation and computer simulation of the receiver's selectivity in condition of massive and random interfering influence on it especially taking into account non-linear phenomena is very difficult, we suppose preferable to estimate receiver's selectivity by multi-signal test influence reproducing parameters of electromagnetic environment.*

## 1.PROBLEM FORMULATION

From point of view of electromagnetic compatibility (EMC) selectivity is the important radio receiver characteristic. Selective devices entering in structure of the receiver permit it to function in presence of natural and artificial radio interference (RI) sources.

In these devices differences in structures of RI and signals are used. So frequent and time filters, spatial and signal form filters and other filters are distinguished.

Frequent selectivity is widely used in radars, navigation and communication systems. Most fully frequent selection is realized in the frequency filter of the superheterodyne receiver. The simplified scheme of such filter is given in figure 1.

Here Ampl – amplifier, BPF – bandpass filter, LO - local oscillator, $f_S$ – incoming signal frequency, $f_{LO}$ - frequency of local oscillator, $f_I$ – intermediate frequency (IF).

In order to estimate receiver performance under conditions of interfering influence it is possible to use at least three following ways: analytical investigation, numerical simulation, measurement of the receiver's selectivity characteristics by test signals. All stated methods have the advantages and lacks.

In present paper we discuss a new method to estimation of frequent selectivity of the superheterodyne receiver under condition of massive and random interfering influence on it. In this method we suppose to utilize multi-

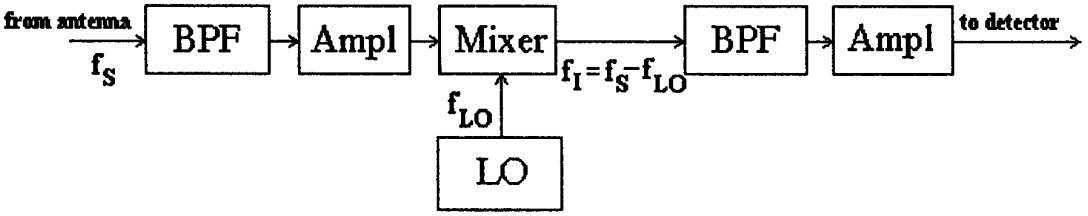



Fig. 1. Simplified scheme of the single-convertion superheterodyne receiver

signal test influence on receiver in order to simulate electromagnetic (EM) interfering environment. Parameters of signals to be used for estimation are frequency f, power P, duration T, time of incoming $\tau$. These parameters are according to EM environment model accepted.

The various ways to estimation of radio receiver susceptibility to interference's are known, look [1], [2]. The typical circuit of an estimation of susceptibility by a two-signal method is given in a figure2. Operating by generators $G_1$ and $G_2$, we can estimate receiver's susceptibility to intermodulation interferences (method CS03), on channels of secondary reception (method CS04), to cross modulation (method CS05) in accordance with MIL-STD-462 requirements.

Three-signal tests for receiver selectivity estimation exist as well. These and other ways allows to estimate a susceptibility of receivers to interferences of the certain types.

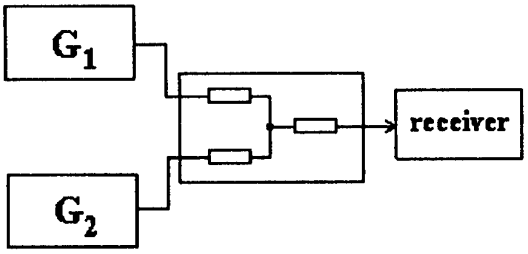



Fig. 2. Typical test configuration to receiver selectivity measurement.

But when real EM environment interfering signals, which can penetrate through receiver on main, secondary and intermodulation channels of reception may be simultaneously applied.

Therefore we offer to form a group test signal that is to determine number of generators and parameters of test signals to be generated, such as frequency, duration, power in accordance with the essential characteristics of EM environment.

## 2. EM ENVIRONMENT MODEL

To define number N generators and parameters of signals characterizing EM environment it is possible to utilize some of the following assumptions [3], [4]. Let EM environment is formed in general by L different RI sources. The first approximation to performance these sources in time domain is a stochastic process without aftereffect [5] known as Poisson process. Time interval $\theta$ between two occurrences of interfering signals has probability density function (PDF)

$$\omega_j(\theta)=\lambda_j \exp(-\lambda_j \theta),$$

where $\lambda_j$ is intensity of Poisson process, $\lambda_j=N_j'/T_0$, where $N_j'$ is number of occurrences in observation period $T_0$, j=1,...,L. As for PDF of RIs duration $\omega(\tau)$ it may be improved separately.

Utilizing methods given in [6], we can estimate coincidence probability of 2, 3,..., k RIs and mean duration of impulses of coincidence process, measure of after-effect in integral process.

By applying the queuing theory [7] and considering each interfering signal as the demand that should be servicing by the generators, we can define number of generators N necessary for adequate reproduction of EM environment.

For definition of number M of trials acceptable for adequate receiver's selectivity estimation we can use limit theorems of the probability theory [5].

As for PDF of radio interferences in frequent domain $\omega(f)$ as a first approach we suppose RI sources uniformly distributed, so

$$\omega(f)=1/Df,$$

where Df is frequent range into which interferences can penetrate through receiver. RI spectrum width is

$$\Delta f=k/\tau, \quad k\geq 1,$$

where $\tau$ is the RI duration.

The PDF of RIs in a point of receiver can be as postulated or that it is more preferable to be evaluated as a histogram for concrete region and time.

In analytical investigations in frame of statistical theory of EMC [3] a class of hyperbolic distribution functions is used. RI power has PDF

$$\omega(P)=\beta P^{-m}, \quad P_0\leq P\leq P_{max},$$

where $\beta$ is normalizing factor, m is distribution parameter, $m\geq 0$, $P_0$ is the receiver's threshold level. The amplitude range $D=P_{max}/P_0$ of interfering power is important parameters of EM environment as well.

Let's give statistical estimation of RI penetration through filter with transfer characteristic on parameter x selected in filter k(x), figure 3. Filter model includes receiver threshold level $P_0$ as well.

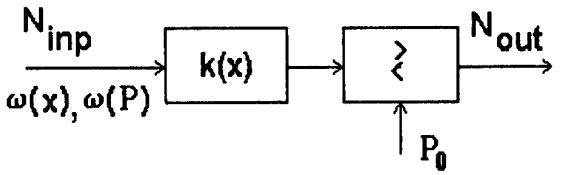



Fig. 3. Simplified mathematical model for computer simulation of one-dimensional filter

Electromagnetic environment is defined by mean of PDF of interfering power $\omega(P)$ in a point of receiver, by distribution of RI sources on selection parameter x $\omega(x)$, by number of interfering signals at the filter input $N_{inp}$. Utilizing direct Monte-Carlo simulation [8] and forming by random number generator sequences $x_i$ and $P_i$, i=1,...,M in accordance with PDFs $\omega(P)$ and $\omega(x)$, we can determine on M trials the probability of penetration of RI through filter as the ratio $N_{out}/M$, where $N_{out}$ – number of trials, in which interference overcomes a threshold level $P_0$, M – general number of tests [9]. If the bandpass $\Delta X$ of the researched filter is known, it is possible to define the attitude

$$\eta = N_{out}/N_{\Delta F}, \qquad (1)$$

where $N_{out}$ is general number of signals penetrated through filter when testing, $N_{\Delta F}$ is the number of signals,

penetrated through it in pass band $\Delta X$. By definition $\eta \geq 1$. For ideal filter with the rectangular selectivity characteristic $\eta=1$. It is true to say that the EM interfering environment is more difficult if filter is less perfect the $\eta$ is more.

Thus parameter $\eta$ allows to compare selective properties of filters in conditions of certain electromagnetic environment [3], [10].

## 3. FORMULATION OF THE METHOD

It is necessary to notice that the use of superheterodyne receiver selectivity estimations like as (1) at numerical simulation is complicated because the model of the receiver is rather complex as in view of the nonlinear phenomena as on conditions of a task assuming massive and random interfering influence on it. Therefore we consider that the most complete information on receiver selectivity can be received by testing it by signals reproducing the basic characteristics of interfering disturbance.

The block diagram of the device for receiver's frequent selectivity estimation is shown in figure 4.

A device for estimation of receiver's interference susceptibility, developed in the EMC for Radio Device laboratory in the staff of the Radio Systems Dept.,

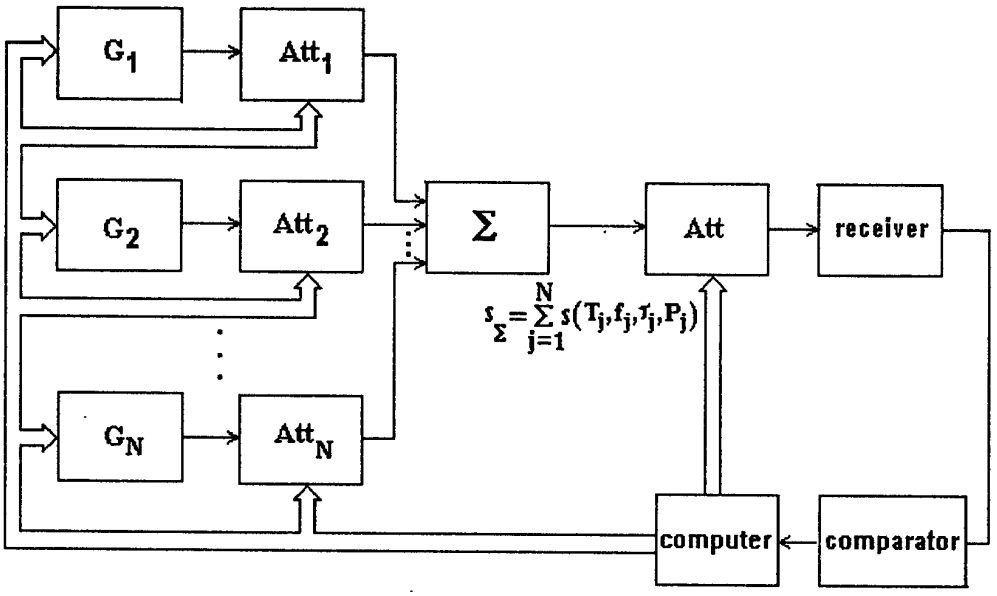



Fig. 4. Configuration for multi-signal estimation of receiver's selectivity

BSUIR [11] was used as a prototype.

The device implementing new way contains N generators $G_1,...,G_N$ controlled by computer, adjustable attenuator $Att_1...$, $Att_N$, matching device $\Sigma$ for adding together the signals from generators, controlled attenuator Att, comparator, computer. The receiver to be investigated is shown as well.

The device estimates selectivity of the receiver by criterion (1) and works as follows. Before the measurements by returning one of the generators in the receiver's band we define sensitivity $P_0$ and bandpass of the receiver $\Delta F$ at 3 dB level. After definition of the characteristics $\Delta F$ and $P_0$ the receiver is tested by signals reproducing EM interfering environment.

Signals formed by the test generators $G_1...$, $G_N$ with parameters (frequency f, duration $\tau$, time of generating t) to be determined in computer according to the accepted model of EM environment are transferred onto inputs of attenuators $Att_1,...$, $Att_N$ and then drive to the matching device. The level of the attenuation is operated by computer according to PDF of interfering power $\omega(P)$.

Radio signals from the output of matching device are applied onto controlled attenuator Att. So, the group signal reproducing accepted EM environment model in power, frequency and in time domain is formed on the controlled attenuator output.

Possible range of power of signals on an output of controlled attenuator Att D is equal to $P_{max}/P_0$, where $P_{max}$ - maximal power of RI in the point of receiver. Number of attenuation levels is determined by required discretization to exact reproduction of PDF of interfering signals $\omega(P)$.

The test signal from the attenuator Att output is applied onto the receiver input. The responses from the IF amplifier output are delivered first to comparator and then to computer. The computer counts up these.

The number $N_{\Delta F}$ of interfering signals penetrating through the receiver in bandpass $\Delta F$ in time $T_a$ of receiver testing by the signals reproducing EM environment is determined when level of test signals is 3 dB above than threshold level $P_0$.

At definition of number $N_{out}$ of signals penetrating through receiver during time of receiver estimation Ta as on major as on secondary and intermodulation reception channels, power of the test signals on the receiver input is changed by adjusting of controlled attenuator Att from $P_0$ up to $P_{max}$ with a step $\Delta P$.

The number of interference's $N_{\Delta F}$ penetrating into receiver in the bandpass $\Delta F$ and the number $N_{out}$ of the interference's passed onto output of the intermediate frequency amplifier through basic, secondary and intermodulation channels of reception are counted and the ratio $\eta = N_{out}/N_{\Delta F}$ that is numerical estimation of the receiver's frequent selectivity is determined.

The comparative analysis shows that the offered way differs from known ones that in it for the most complete estimation of the receiver to mass influence of radio interference's is used N-signal influence simulating electromagnetic environment on the input of the receiver. Parameters of the test signals f, P, T and $\tau$ are changing from trial to trial and are counted in accordance with EM environment parameters.

## 4. QUANTITATIVE DEFINITION OF THE METHOD

Characteristics of the interfering signals in time domain determine interfering influence on receiver in great measure. It is known that simultaneous influence of some interfering signals on receiver is one of the causes for non-linear phenomena, for example intermodulation. Therefore in order to estimate parameter of the test signals and number N of generators we must discuss more carefully EM environment model in time domain.

It is true to say that sequence of pulses and pauses may be used for determination of performance of different RI sources in time domain. For such sequence we have

$$T_i = t_{i+1} - t_i > \tau_i,$$

where $T_i$ is period of the pulse sequence, $t_i$ and $\tau_i$ are times of incoming and pulse duration correspondingly. All RI sources are characterized by mean of PDF $\omega(\tau)$ of pulse duration and PDF $\omega(\upsilon)$ of pauses between pulses. Average sequence period is equal to $T_\Sigma = \langle\tau\rangle + \langle\upsilon\rangle$, where $\langle\tau\rangle$ and $\langle\upsilon\rangle$ notes mean pulse and mean pause duration in accordance with PDF $\omega(\tau)$ and $\omega(\upsilon)$. Intensity of the random point flow which corresponds to the time of interferences incoming to the receiver input ($\lambda$) is equal to $L/(\langle\tau\rangle+\langle\upsilon\rangle)$, where L is general number of RI sources.

In order to simulate interfering influence on receiver from L independent RI sources we must in ideal to use L generators. But cost of such device is very high. It is obviously that the task of forming of group radio signal by some limited number N of generators, simulating RIs from L device is the task of queuing theory. In this case every of interfering signal parameters of which such as duration $\tau$, time of forming t, frequency f and power P are random and are determined from PDFs of interferences on corresponding parameters may be considered as a request for servicing by one of the limited number N generators. If all servers (generators) are busy, then demand is lost or is waiting when server is free.

Because we use Monte-Carlo scheme for estimation of the receiver's selectivity, which is based on repetition of trials, so loss of some demands may be cancelled by increasing of number of tests. It permits us to utilise scheme with losses [7] as a mathematical model for our system. Gain in decreasing number of servers from L to N is possible because of intensity of demands servicing $\mu = N/\langle\tau\rangle$ may be more than intensity of demands flow $\lambda = L/(\langle\tau\rangle+\langle\upsilon\rangle)$.

The formula for probability $P_N$ that all N from N servers are busy and hence next demand will be lost is known in queuing theory:

$$P_N = \frac{(1/N!)\rho^N}{\sum_{k=0}^{N}(1/k!)\rho^k},$$

where $\rho$ is

$$\rho = \lambda/\mu = \left(\frac{L}{\langle\tau\rangle+\langle\upsilon\rangle}\right)\Big/\left(\frac{N}{\langle\tau\rangle}\right) = \frac{L}{N}\,\frac{\langle\tau\rangle}{\langle\tau\rangle+\langle\upsilon\rangle}.$$

Figure 5 gives dependence's of loss demand probability on number N generators and ratio $\langle\tau\rangle/\langle\upsilon\rangle$. Scale on axis $P_N$ is logarithmical, sign E notes decimal order of number.

General number of RI sources L is equal 20. By fixing some value of $P_N$ we can estimate number N of servers (generators) for adequate reproduction of EM environment. If L is equal to 25—50 in some cases 3-4 servers can reproduce EM environment exactly. When L is 100 and more 5-7 server are desirable.

As shown in the figure, when ratio $\langle\tau\rangle/\langle\upsilon\rangle$ is increasing, probability $P_N$ is increasing as well. It may be explained by increasing of loading per server.

Because we count signals on the output of the receiver so probability **p** of penetration RIs trough it may be estimated. An adequate estimation of **p** is ratio K/M where K is the number of trials when interference penetrates through receiver and M is the general number of trials. Because number of trials M is limited some

value of error in probability p determination exists. The error is equal to ε =p-K/M.

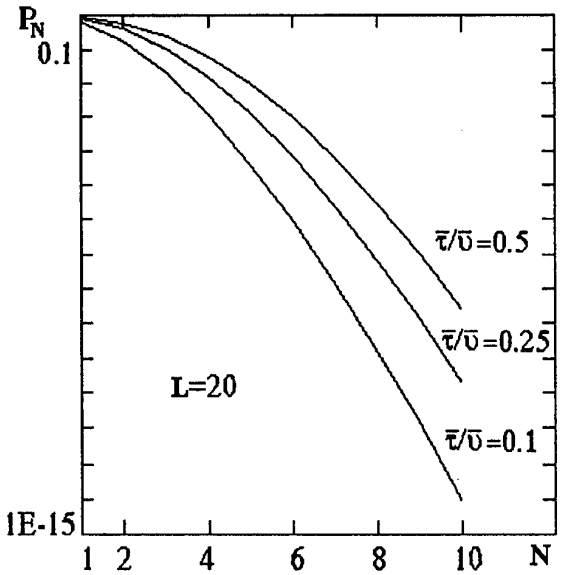



Fig. 5 Dependences of the demand loss in multi-signal testing.

Laplace theorem [5] gives us estimation of probability of inequality $|p\text{-}K/M| > \varepsilon$ as a function $\Phi(p,M,\varepsilon)$ where $\Phi(.)$ is Laplace integral. For example if p=0.5, ε=p/10=0.05 then number M of trial equal to $10^3$ is acceptable. If p=0.05, ε=p/100 then M counted in accordance with Laplace theorem is near $10^6$. The duration of the analysis $T_a$ depends on necessary number of tests M. Time of analysis $T_a$ may be estimated approximately as $T_a \approx M\langle T\rangle/N$, where $\langle T\rangle$ is the mean time for signal generation including retuning. As a first step to $\langle T\rangle$ determination we suppose it equal to mean RI duration $\langle\tau\rangle$. Let $M=10^5$, N=3, $\langle\tau\rangle=10^{-2}$ sec. Then $T_a=10^3/3\cong330$ sec.=5.5 min. In general case time of receiver estimation is depend on receiver characteristics. The receiver is more perfect the $T_a$ is lager. By this way different receivers may be estimated for some "fixed" EM environment.

In the device (11) that is the prototype are used controlled generators Г4-158. It has range in frequency 10KHz-99.9MHz. These generators also has inner attenuators for adjustments of output power level The. As a computer is used standard PC IBM compatible.

Now device for multi-signal estimation of the receiver selectivity by the offered way is designing.

## 5. CONCLUSION

The positive effect on definition of the receiver selectivity by the offered way in comparison with known ways is that the more exact imitation of interfering influence on receiver is reached. The method allows estimating receiver's selectivity in condition of massive and random RI influence on it when penetration on output of the receiver of RIs trough basic, secondary and intermodulation channels of reception is possible. The process of measurement is completely automated.

In general, method is based on statistical theory of EMC [3], queuing theory [7], Monte-Carlo method [8].

## 6. REFERENCES

1. A Handbook Series on EM Interference and Compatibility. By Donald R. J. White. Published by: D. White Consultants, Inc., Germantown, Maryland 1971-1973.

2. Mikhailov A. S., Measurement of EMC Parameters of Radio Devices, Moscow: Sviaz Publ., 1980. (*In Russian*).

3. Aporovich A. F., Statistical Theory of the Electromagnetic Compatibility of Radio Systems. Minsk: Nauka Publ., 1984. (*In Russian*).

4. Trigubovich V., On Some Characteristics of EM Environment, Proceedings of the International Conference on Mathematical Methods in Electromagnetic Theory "MMET-98", Ukraine, Kharkov, vol. 1, pp. 447-449.

5. Gnedenko B. V., The Theory of Probability. Moscow: Mir publisher, 1973.

6. Sediakin N. M., Elements of the Random Impulse Processes Theory. Moscow: Sov. radio Publ., 1965. (*In Russian*).

7. Bremaud P., Point processes and queues: martingale dynamics. — Heidelberg: Springer-Verlag, 1981.

8. Sobol I. M., Monte-Carlo Numerical Methods. Moscow: Nauka Publ., 1973. (*In Russian*).

9. Trigubovich V., Computer Simulation of EM Environment Parameters, Thesis of the III International Conference Theory and Technique of the Information Processing, Ukraine, Kharkov, pp. 160-161. (*In Russian*).

10. Trigubovich V., Statistical Estimation of Antenna's Selectivity, Proceedings of the International Conference on Microwaves & Radars "MIKON-98", Poland, Krakow, vol. 3, pp. 375-379.

11. Aporovich A. F. et al., Device for Receiver's Susceptibility to Interferences Estimation. Patent N2032272, Int. Cl. H04B 17/00, 1995, RU. (*In Russian*).

## BIOGRAPHICAL NOTE

Vladimir B. Trigubovich (b. 1973) graduated with distinction from Belarusian State University of Informatics and Radioelectronics (BSUIR). In 1995-1998 studied post-graduate course. Since November 1998 – assistant prof. of the Radio Systems dept., BSUIR. Has 17 publications in the fields of EMC of radar's, navigation and communication systems.

EMC 2000 INTERNATIONAL WROCŁAW SYMPOSIUM ON ELECTROMAGNETIC COMPATIBILITY

# REQUIREMENTS FOR MITIGATION IN INTENTIONAL ELECTROMAGNETIC INTERFERENCE

Robert L. Gardner, Consultant and David C. Stoudt
Joint Program Office for Special Technology Countermeasures (JPO/STC)
Mail Stop Code B20
NAVSURFWARCENDIV
17320 Dahlgren Road
Dahlgren, VA 22448-5100
540-653-2715, GardnerRL@nswc.navy.mil
540-653-8050, StoudtDC@nswc.navy.mil

*Intentional electromagnetic interference has become a very important topic for discussion in the scientific community. Terrorists or criminals could cause damage or confusion in society's infrastructure. A disruption could cause problems with records, electronic security, banking records or even navigation and communications systems. As a community, we must evaluate the threat to society and act accordingly to protect our critical systems. Quantitative evaluation of the threat requires execution of planned experiments and analysis to assure ourselves that we know the threat and we know how well we know the answers. HPM sources can appear in a variety of forms. They can be large or small or even be similar to common equipment. The sources can also radiate a large variety of waveforms that are, in turn lethal against a variety of electronic equipment. This variation allows a large number of parameters into the experiment space. To reach reasonable conclusions, all of these parameters must be explored in sufficient detail to reach statistically significant conclusions. That data will allow us to bound the work that must be done to protect the infrastructure.*

## 1. INTRODUCTION

At their General Assembly in August 1999, the 41 member nations of the International Union of Radio Science (URSI) issued a resolution to support research into the criminal uses of intentional electromagnetic interference (IEMI). The resolution stated that the illegal use of radio frequency (RF) devices against the civilian infrastructure was a potential problem and that the member nations should conduct research to quantify the problem. They further resolved that member nations should conduct research to uncover possible countermeasures. JPO-STC is studying the consequences of the resolution and the possible impact of RF devices on the U.S. high-technology infrastructure. This paper represents considerations by the JPO-STC on the requirements for a program to protect the infrastructure from RF attack.

Assessing the impact of the RF threat requires that we consider who might threaten the infrastructure, what tools they might use, how they might employ them, and finally how effective those tools might be [1]. People who might threaten the infrastructure considered here are normally not representatives of nations but are criminals, terrorists, or careless users of RF technology. Consideration of the nationally sponsored HPM weaponeers is beyond the scope of this study.

Finding the effectiveness of the various transmitters and antennas that make up an RF weapon requires that we evaluate the access the criminal has to the target and the size and power requirements of his RF weapon. The further the criminal can be kept from the target the more robust and therefore heavy and expensive his weapon must be. The required characteristics of the weapon can be compared to the RF weapons that are potentially available on the open market, and their overall effectiveness.

Judging the effectiveness of an RF weapon in this application requires the most careful experiment design. We must simulate each scenario and decide if the targeted system is vulnerable. The core, critical electronics of most businesses or similar organizations consists of computer networks and support systems. This paper will describe applied test and analysis methods used to draw conclusions about the potential RF threats.

Finally, we must take this data and draw conclusions about the protection of electronic systems. Protection may include additional isolation, changes in building parameters such as wall thickness or rebar content, as well as normal electronic hardening. We must contribute to the proper evaluation of risk versus cost equation. An EMP-like hardening program is very expensive and so it is difficult to convince a system builder of its value.

## 2. THE THREAT

High power microwave (HPM) weapons can be used in a variety of situations. They can be small and portable or they can tax the carrying capacity of a large truck. The variety of sizes allows a large variety of pulse shapes. Usually, as the power and energy requirements become larger, the physical size of the device becomes larger. With the variations associated with antenna gain the weapons themselves are available with a large variety of parameters [2]. These parameters, which include peak power, energy per pulse, pulse repetition rate, duration of pulsing, and others, vary the effectiveness of the source against different types of targets. Effects on the targets can include interference, interruption of function, or even damage. Our challenge is to balance this large number of parameters and make quantitative statements about the risk to society of certain types of RF weapons.

An HPM weapon usually consists of a prime power supply, a power conditioning system, a microwave source and an antenna. Power supplies and power conditioning for a number of sources of the few megawatt class are available commercially. Microwave tubes up to a few megawatts and having a variety of center frequencies and pulse shapes are also available on the surplus market. These sources are primarily based on World War II technology, but are effective even though their power is below that of modern laboratory tubes.

As noted in Benford and Swegle [2] HPM laboratory sources have been built that are much higher power than these commercial devices, but these laboratory devices are not as available and are more difficult to keep running than the surplus tubes.

The usual parameter used for specification of an RF source is its power density on target. Power density on target is a measure of the quotient of the weapon's effective radiated power (ERP) and the distance squared. Using that technique of systems analysis assumes that the failures in the systems are proportional to the power density at the target. That is one of the issues that must be established in our research program. Incident power density may or may not be the parameter of interest for digital electronics.

## 3. RF EFFECTS

RF weapons can cause damage, disruption or interference of electronic systems. The character of the electromagnetic waveforms that has a specified effect on a particular electronic system varies over a large range of the above stated parameters. This variability has a number of important consequences when they are injected into the analysis of an RF weapon design. These weapons can have this large variability when applied to electronics whether excited by intended weapons in the HPM environment or within the context of electromagnetic compatibility [3]. Variability in lethality, which can span many orders of magnitude, makes it very difficult to draw conclusions about the effectiveness of an RF weapon. If the tactical requirement is harassment or some other broad based threat then one should expect some disruption of the electronics. On the other hand, if the weapon has to have a designed effect on a target system almost every time, the requirements on the HPM source are severe.

Some electronic systems respond to power density and some to the incident energy. LoVetri, et al [4] describe a system that causes PCs to fail at levels as low as 30 V/m. The lethal waveform has a multi-gigahertz carrier that is modulated and has a high duty cycle. Surplus RF sources and antennas are available that will radiate 30 V/m fields at a kilometer range are easily available.

Another way to cause a system failure is to use in band transmission to prevent communication between different parts of the system. This failure mechanism is closer to problems that are observed in EMC than in HPM. An example of such a thing might be the in band jamming of a GPS receiver.

## 4. EXPERIMENT REQUIREMENTS

Our goal for an experimental program is to provide clear scientific guidance to the owners of infrastructure components on how to make a wise investment in the protection of those assets. Data required to support those conclusions must include evaluation of a number of HPM devices deployed against a variety of targets. These experiments must be done in such a way that the statistical confidence limits on the data are sufficiently tight to support the conclusions of the systems analysis.

If each of the parameters is varied "one variable at a time" the number of tests required is usually in excess of twenty for each parameter of interest. For our situations the number of parameters may vary from three to a dozen. Inefficient experiment planning then leads to thousands of experiments; well beyond the budget of most experimenters. Use of "design of experiment" [5] techniques greatly reduces the total number of experiments required and introduces a certain discipline in experiment planning.

While it is possible to estimate the output waveforms of the combinations of antennas and microwave sources [6], it is better to first prioritize the available sources and then experimentally characterize the most important threats. For our purposes availability of the source is as important as the source performance. That way information is available on the possible cost of the weapon system as well as its actual performance. The source is then available for experiments that will show the effectiveness of the device against specific targets of interest.

Fortov [7] described a number of RF sources that are commercially available from various Russian vendors. These sources are mostly compact and transmit powers above those of the WWII vintage tubes. These systems are available in a variety of waveforms and powers, but represent a number of other sources that might later be threats to the infrastructure.

## 5. PROTECTION OF THE INFRASTRUCTURE

This research program will lead to a large number of data points that will include various types of failure (including no failure) of an electronic target in response to a number of different types of illumination. The data will require careful statistical and analytical examination before using it to guide the owner of a component of the infrastructure on a smart protection strategy. The data will indicate failure levels and uncertainties. It is very important to carefully determine the uncertainties in the stated recommendations. The results can then be used to suggest system changes. One of the easiest changes might be to suggest a fence around the sensitive building to establish a keep-out zone. Other approaches to protection could follow along the lines of EMC hardening practices.

## 6. REFERENCES

6.1. R. L. Gardner, M. W. Wik, and D. C. Stoudt, "Intentional Electromagnetic Interference", *Review of Radio Science 1996-1999*, Oxford University Press, New York, 1999, Ch. 13, p. 349.

6.2. J. Benford and J. Swegle, *High-Power Microwaves*, Artech House, Boston, 1999.

6.3. R. L. Gardner and C. W. Jones, "System Lethality: Perspective on High Power Microwaves", *System Design and Assessment Notes*, Note 34, EMP Note Series, AFRL/DEPE, Air Force Research Laboratory, Kirtland AFB, NM, 1995.

6.4. J. LoVetri, A. T. M. Wilbers, A. P. M. Zwamborn, "Microwave Interaction With A Personal Computer: Experiment and Modeling", Proceedings of the13th International Zurich Symposium and Technical Exhibition on Electromagnetic Compatibility, 1999, p. 39G6.

6.5. W. J. Diamond, *Practical Experiment Design*, Wiley, New York, 1989.

6.6. C. D. Taylor and D. V. Giri, *High Power Microwave Systems and Effects*, Taylor & Francis, New York, 1995.

6.7. V. Ye Fortov, Undocumented Presentation to the Electromagnetic Terrorism Panel, 13th International Zurich Symposium and Technical Exhibition on Electromagnetic Compatibility, 1999.

Dr. Robert L. Gardner received his PhD from the University of Colorado in 1980. He has been active in High Power Electromagnetics since that time. He has worked in the EMP, lightning, and high power microwave communities in a variety of positions with the US Navy and the US Air Force. He has published widely in these areas. Dr. Gardner is currently a Consultant supporting the JPO-STC located in Dahlgren, VA.

Dr. David C. Stoudt's current research efforts include the effects of high-power microwaves on electronic equipment, the development of high-power photoconductive switches, and the development and evaluation of other high-power electromagnetic sources. He is currently the US Senior National Representative to the NATO SCI-019 Panel on "Tactical Implications of High Power Microwaves," and the Counter-RF Program Manager for the JPO-STC. In 1999 he was awarded the Navy's Meritorious Civilian Service Award. He is widely published with thirty-five refereed journal and conference papers, two book chapters, and has been awarded five patents.

EMC 2000 INTERNATIONAL WROCŁAW SYMPOSIUM ON ELECTROMAGNETIC COMPATIBILITY

# DESIGN OF ELECTRONIC SYSTEMS PROTECTED FROM ELECTROMAGNETIC TERRORISM

T.R.Gazizov

Tomsk State University of Control Systems and Radioelectronics,
Lenin Ave., 40, Tomsk, Russia, 634050,
phone/fax:+7 3822 223262, E-mail: talgat@tu.tusur.ru

*New requirement in design process to electronic system to be protected from electromagnetic terrorism is considered. Distinctions of interconnects suitable for intentional crosstalk are noted. A general "Guidance on the revealing and elimination of adverse and undesired effects and phenomena" is given. Using the theory of solving the invention problems (TRIZ) within the guidance is proposed for design of electronic systems protected from electromagnetic terrorism.*

## 1. INTRODUCTION

Electromagnetic terrorism treat becomes a problem which solving is impossible without active scientific investigations, particularly, by EMC community. The public discussions of the important topic have begun from plenary lecture of Prof. Loborev to the AMEREM conference in May 1996. At the Zurich EMC'97 Symposium the URSI Commission E formed a subcommittee on Electromagnetic Terrorism chaired by Dr. Wipf under the existing URSI Committee on EMP and Other Matters led by Dr. Wik. A review of the problem was published in plenary paper of Dr. Gardner at previous Wroclaw EMC Symposium [1]. Comprehensive workshop on Electromagnetic Terrorism and Adverse Effects of High Power Electromagnetic (HPE) Environments took place at recent Zurich EMC'99 Symposium [2]. Particularly, systematic and broad review of EM terrorism have been given and application of modeling and simulation methods to assess EM terrorism effects have been considered. It should be noted that some very interesting not published papers of the workshop have been reported also. Particularly, many photos and technical characteristics of marketable high power EM equipment have been presented in impressing report of vice-president of Russian Academy of Sciences academician Fortov. The report concluded convincingly (and this conclusion has been emphasized in concluding remark of Dr. Wik closing the workshop) that international cooperation in solving the problem of EM terrorism is necessary. At last, the fact that the "EM Terrorism Treat" appeared for the first time as a separate topic in call for papers of Wroclaw EMC'2000 shows the growing actuality and importance of the problem.

## 2. NEW REQUIREMENT IN DESIGN PROCESS

Thus, along with usual requirement to electronic system to function properly a new requirement to electronic system to be protected from electromagnetic terrorism arises. To comply with this requirement properly it must be considered as early as possible and guaranteed as much as possible by design process. The new requirement may be extremely important in case of critical electronic systems, for example, alarm, security and access systems, aircraft systems, vital medical electronics, control systems in atomic industry. The requirement is close to such well-known ones as reliability, protection from unintentional damage, and electromagnetic compatibility, of course. However, by author's opinion, it must be extracted as a separate item due to its specific properties.

The EM terrorism, in general, assumes some *intentional EM action (excitation, effect)* giving some result necessary for terrorist. However, the action may not be certainly the only action, but it may be one of the set of actions (EM, mechanical, thermal, chemical) related with each other to reach the final result. The actions may not be certainly the straightforward damaging actions giving the fault, but they may be hidden, while the relation of the actions may be very sophisticated. For example, in case of electronic system being a target of a terrorist, an example of mechanical action may consist in some mechanical change of electronic system's structure. The change may not influence on the main functioning of the system and therefore to be invisible. However some characteristics of the system (for example, vulnerability to external EMI) may change significantly or even new functions of the system may appear (for example, interconnect becomes effective antenna or resonator). Thus, the EM terrorism may be very close to electronic espionage and sabotage.

A main reason why similar possibilities becomes real consists in availability of *resources* understood in this text in broad sense as the any that may promote to reach the result desired. Clearly, that there are much resources where there is some *redundancy*. Moreover, clearly that the resources may be used more successfully if *access* to these resources is easy.

## 3. DISTINCTIONS OF INTERCONNECTS

It would be noted that various parts of an electronic system may comply with the two conditions: redundancy and access. However, a case of interconnects seems to be especial.

1. Indeed, as an example of redundant number of interconnects a usual case of unused wires in standard multiconductor cable is well known. Another examples of redundancy inherent in interconnects are the ability to be receiving or transmitting antenna and the electromagnetic coupling between interconnects.

2. Such usual properties of interconnects' structures as the long extension and complex networking promote easy access to contact with interconnects. Another example of easy access consists in direct conducting of possible EM excitation via a wire of unshielded part of a network to very responsible and properly shielded part of the network. The wire may not be a target wire. However, it may be one of unused (open or short circuit at the ends) or assumed by designer to be always grounded (but excited intentionally in reality by terrorist) wires in multiconductor cable.

3. Therefore, if the wire or a number of similar ones are electromagnetically coupled with a target wire, then an effective and hidden path for *intentional crosstalk* to possible victim part of electronic system may be constructed.

## 4. TRIZ CAN HELP

However, let's return to a designer, which must foresee all possible plans of EM terrorists and must design a system making any such plan to be doomed to failure. What level of the designer's experience is necessary for solving this problem, which may be difficult even for an EMC expert? Can we help to the designer by some way except the advice to grow to EMC expert's level? The answer is yes.

The theory of solving the invention problems (TRIZ, by Russian abbreviation) can help very effectively. Developed by G.S.Altshuller [3,4] the theory was extended widely by several of its developers. The author of this paper was studying the TRIZ at Kishinev (Moldova) in 1990 and now he is teaching the students to the TRIZ in Tomsk State University of Control Systems and Radioelectronics. Simultaneously the author is a lector on EMC and CAD courses. By author's opinion, a grate help for design of electronic systems protected from EM terrorism may be taken from using the TRIZ within the "Guidance on revealing and elimination of adverse and undesired effects and phenomena" composed by TRIZ developers. It would be noted that this approach is very general and may be used successfully for very wide range of research problems in various systems. Particularly, a human being as a part of the system is considered also. However, for effective use of this approach in practice the basic knowledge of TRIZ principles is necessary. Anyway, all steps of the guidance and its six appendixes are given here in detail.

## 5. GUIDANCE ON REVEALING AND ELIMINATION OF ADVERSE AND UNDESIRED EFFECTS AND PHENOMENA

1. Formulation of the original problem.

Write the original problem using the following template:

A. "There is a (specify, man-made or natural) system for (specify the main function). The system consists of (specify the main subsystems), the system is included in (specify the main supersystems), the system is interacted with (specify the main "neighboring" systems, including environment).

B. It is necessary to reveal and to eliminate the possibility of appearance of adverse and undesired effects and phenomena among the subsystems, among the system, "neighboring" systems and supersystems."

2. Formulation of the inverse problem.

Transform the original research problem into the invention problem by change the formulation of item 1B using the following template:

"It is necessary to make as much as possible adverse interactions among the subsystems, among the system, "neighboring" systems and supersystems."

3. The seeking for the known methods of making the adverse effects.

3.1. Consider the typical reasons for appearance of adverse effects (see Appendix 1) and determine the possibilities and conditions for its feasibility in the considered system.

3.2. Consider the adverse phenomena which are inherent in such and similar systems and determine the possibilities and conditions for its feasibility in the considered system.

3.3. Consider the typical ways of adverse effects on a human being: direct or indirect, through environment or through engineering systems, (see Appendix 2) and determine the possibilities and conditions for its feasibility in the considered system.

3.4. Consider the typical results of adverse influences on a human being (see Appendix 3) and determine the possibilities and conditions for its feasibility in the considered system.

4. Identification and utilizing the resources.

4.1. Consider the typical "ill points" and "vulnerable places" of a system (see Appendix 4) for the considered system and determine the possibility of appearance in these zones the adverse effects and conditions for its feasibility.

4.2. Consider the resources of the considered system, reveal such resources, which are able to afford the appearance of adverse effects (see Appendix 5), and determine the possibilities and conditions for feasibility of the adverse effects at the expense of the revealed resources.

5. The seeking for the adverse effects by TRIZ databases.

Consider the tables and indexes of physical, chemical and geometrical effects from TRIZ databases, select such effects, which have a chance to be feasible and to give adverse effect in the considered system. Determine the conditions for the feasibility of these effects.

6. The seeking for the new methods of making the adverse effects.

Use all TRIZ tools to reveal the adverse effects.

7. "Masking" the adverse phenomena.

Consider the possibility of adverse effects (revealed at previous steps) to be hidden from timely detection:
7.1. Consider the typical methods of "masking" the adverse phenomena (see Appendix 6) and determine the possibilities for the feasibility of these methods.
7.2. Consider the possibility to solve the problem of "masking" the adverse phenomena by means of TRIZ tools.

8. Analyzing of revealed adverse effects.

8.1. Determine such revealed effects, which take place really (use TRIZ tools to detect hidden effects, if necessary).
8.2. Determine for each of the effects the probability of appearance, the power of undesirability and/or danger.
8.3. Draw the cause-consequence diagram showing obviously for each of the effects the probability of appearance, the power of undesirability and/or danger.

9. Elimination of adverse effects.

Reveal the original (the very first) adverse effects, formulate and solve by means of TRIZ for the problems to avoid the appearance of these adverse effects or to eliminate their consequences.

## 6. APPENDIXES

Appendix 1.

Reasons of appearance of adverse effects.

1. The absence of knowledge about mechanisms of various mutual couplings, not accounting for the complex chains of the cause-consequence couplings, "solving by force" and so on.
2. Not understanding the relation between adverse and useful effects, the aspiration to get or to increase the useful effect at any price, the inability to solve the discrepancies and the invention problems.
3. Not understanding the nature of the "systems" effects and of the appearance of the new ("systems") properties of various systems during their mutual working.
4. The ability of adverse effects to be "useful" for aims of some people.
5. The mistakes in design, in manufacturing and in usage of the system or of the supersystem.

Appendix 2.

Typical ways of adverse effects to a human being.

1. Direct adverse effects on a human being.
1.1. Mechanical actions: a blow, a push, pressure difference, vibrations, acoustic actions and so on.
1.2. Thermal effects: heating (overheating), cooling (overcooling).
1.3. Chemical and biological effects: upsetting of the chemical balance of human organism (shortage or surplus of some compounds or substances), destructive actions, allergic or mutagenic effects, effects of living organisms (bacteria, fungus, parasites)
1.4. Electric effects: effects of electric voltage and current.
1.5. Electromagnetic effects: effect of light, effect of ionizing and non ionizing radiation.
2. Indirect adverse effects on a human being through environment.
2.1. Deterioration of natural systems guaranteeing the living of a human being: pollution of the water, air, soil by substances being adverse for a human being; the decreasing of the soil fertility; shrinkage of the space suitable for life and so on.
2.2. Upset of biological balance. Reproduction of adverse species and reduction of useful biological species. Evolution of some species in undesirable direction.
2.3. Creation in environment some processes stimulating the adverse effects.
2.4. Reduction of irreproducible natural resources being necessary for human life and development of engineering.
3. Indirect adverse effects on a human being through engineering systems.
3.1. By means of interaction of engineering system with a human being: incorrect direction of development of the engineering system, low quality of manufacture or utilizing, intentional or accidental damage and so on.
3.2. By means of interaction of engineering system with natural systems: environmental effects (atmospheric effects, corrosion, chemical and electrochemical processes, effect of light and so on), effect of biological factors (microorganisms, plants, animals), effects of natural cataclysms and so on.
3.3. By means of interaction of various engineering systems: accidents (collisions, intentional destruction by weapon), "systems" effects during interactions, effect of interference and wastes of some systems to others.

Appendix 3.

Results of adverse effects to a human being.

1. Physical disturbances: traumata, health disturbances, decreasing of immunity, professional illness, deterioration of state of health, decreasing of life deadline, damage of genetic fund and so on.
2. Psychical disturbances: psychical illnesses, hypochondria, depression, deformation of a set of moral valuables, conformism, morale disturbances and so on.
3. Emotional disturbances: creation of stresses, decreasing of satisfaction by life, disturbance of emotional balance and so on.

4. Social disturbances: destruction of various relations of people (cognate, friendly, professional and so on), disturbance of structure of society, creation of various kinds of discrimination (national, racial, religious, sexual, by age).
5. Intellectual disturbances: increase of psychological inertia, total decreasing of intellectual abilities (logical thought, memory, ability to the critical perception and so on), disturbance of ability and of need to create a new, distortion of information and of the ability to take up and to analyze the information and, as a result, to orient in life and so on.
Warning. It would be noted that the various kinds of adverse effects on a human being (Appendix 2) are closely coupled. The results of adverse effects to a human being (Appendix 3) are closely coupled too. For example, one effect may result in a number of disturbances.

Appendix 4.

Typical "ill points" and "vulnerable places" of systems.

1. Zones, where the flows of matter or energy, passing through the system are concentrated (for example, zones of concentration of mechanical forces, zones of electrical overvoltage and so on).
2. Zones, which are subject to the effect of high intensity fields (for example, of the vibrations, loads with alternating signs, "dry" friction, high temperature, active chemical matter and so on).
3. Zones and units, offering the big number of various services.
4. Zones of a junction of various systems and subsystems.
5. Zones, which the inconsistent requirements are specified to (i.e. there are unsolved discrepancies).

Appendix 5.

Resources promoting to appearance of adverse effects.

1. Material resources: materials being in system and subsystem, ancillary materials (for example, lubricant and so on), a raw material, products, waste, materials from environment.
2. Energy resources: the (mechanic, thermal, electromagnetic) energy flows being in system, subsystem and environment.
3. Space resources: free space or partly non-occupied space in system, subsystem and environment.
4. Time resources: the various periods during the preparation of system to function, during the functioning of system and after the functioning of system and supersystem.
5. Functional resources: the ability of system, subsystem or environment to execute unforeseen functions.
6. Systems resources: the effects appearing due to the mutual coupling of two or more systems (resonant phenomena, self-synchronization, synergism and so on).
7. Change resources: any changes occurring in the system, subsystem and environment (unforeseen effects appearing because of some intentional actions).

Appendix 6.

Typical means of "masking" the adverse phenomena.

1. Appearance of adverse effects in the course of time.
2. Appearance of adverse effects under extremal conditions.
3. Appearance of adverse effects under seldom occurring circumstances or under seldom combined conditions.
4. Appearance of adverse effects because of long consequence of interactions in the system.
5. Appearance of adverse effects because of qualitative steps (jumps) after some quantitative changes in system.
6. Appearance of adverse effects because of action of special mechanisms (for example, "releasing hook", "avalanche", chained reaction with positive feedback, catalyzed reactions and so on).
7. Appearance of adverse effects at the expense of "systems" interactions (because of unforeseen interactions of various systems).

## 7. ACKNOWLEDGMENT

T.R.Gazizov thanks N.I.Bazenkov for enthusiasm on scientific work and A.V.Gazizova for great support.

## 8. REFERENCES

8.1. R.L.Gardner, "Electromagnetic terrorism. A real danger", Proceedings of the 14-th Int. Wroclaw Symposium on EMC, Wroclaw, Poland, June 23-25, 1998, pp.10-14.

8.2. M.W.Wik, "Electromagnetic Terrorism and Adverse Effects of High Power Electromagnetic (HPE) Environments", papers of workshop, Supplement to Proc. of the 13-th Int. Zurich Symp. on EMC, Zurich, Switzerland, February 16-18, 1999, pp.179-200.

8.3. G.S.Altshuller, "Creativity as an exact science" (Russian), "Soviet radio", Moscow, 1979.

8.4. G.S.Altshuller, "To find an idea" (Russian), "Science", Novosibirsk, 1986

## BIOGRAFICAL NOTE



Gazizov Talgat Rashitovich was born in 1963. He got his higher professional education on radioengineering in 1985 in the Tomsk Institute of Automatic Control Systems and Radioelectronics and Ph.D degree in 1999. His research interest is signal integrity problem. Now he is working toward Doctor of Sciences degree.

**EMC 2000** INTERNATIONAL WROCŁAW SYMPOSIUM ON ELECTROMAGNETIC COMPATIBILITY

# THE HUMAN HEALTH DEPENDENCE ON THE GEOMAGNETIC ACTIVITY

V. P. Kuleshova and S. A. Pulinets
IZMIRAN, Troitsk Moscow Region, 142190, Russia, FAX:+7-095-3309607, E-mail: pulse@izmiran.rssi.ru

*It is shown and statistically confirmed the growth of daily trauma occurrence during global geomagnetic storm periods. The daily data do not permit to reveal the effects of short-time geomagnetic disturbances of natural or technogenic character on the acute mental and cardiovascular pathologies*

## 1. INTRODUCTION

One of the important factors of outer space origin having impact on biosystems is the variations of geomagnetic field. The complexity of the problem is connected, particularly, with the fact that the objects under study have their biophysical individuality changing during the object life under action of endogenic and exogenic factors. That's why the probability techniques are used to estimate the biotropic effects of the geophysical processes. It was shown in [1] the statistically confident with confidential probability P=0.95 the effect of the geomagnetic storms in the form of growth of daily number of heavy mental and cardiovascular diseases by factor 1.5-2 during the storm period in comparison with undisturbed periods.

## 2.THE SERIOUS TRAUMAS DURING GEOMAGNETIC STORM PERIOD

The present paper deals with the effect of planetary geomagnetic storms [2] on the daily occurrence of serious trauma fixed by Moscow ambulance with subsequent hospitalization (period of March 1983 – September 1984, 225 thousands cases totally). Accomplishment of random event criterion permits to estimate the event probability with the help of confidential interval, which was selected as 0.95. As well as in [1,3], the 7-day variation with maximum on Friday-Saturday, connected probably with the social causes, was excluded from the raw data. The amplitude of this variation was ~ 100 hospitalizations per day. The background of seasonal (yearly) variations was not excluded because it does not exceed the standard mean deviation. On the Fig. 1 are presented the

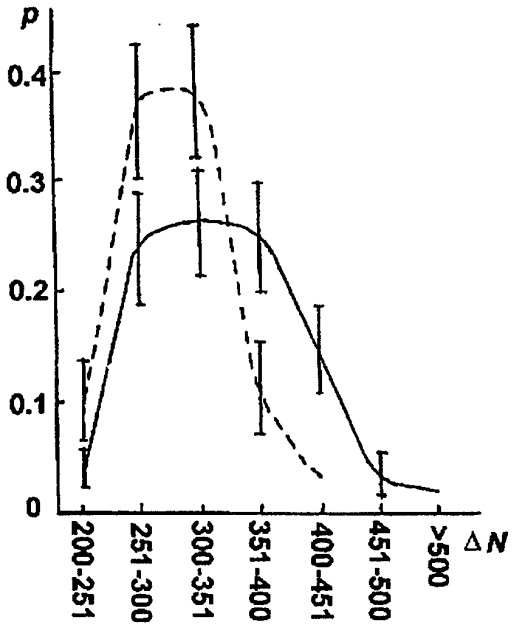



Fig.1 Distributions of daily occurrence of serious trauma for quiet conditions (dashed line) and for magnetic storm periods (solid line)

trauma ($p$) for quiet geomagnetic conditions and during geomagnetic storms. One can see that distribution for the geomagnetic storm period is shifted to the large number of hospitalizations. The confidential intervals are shown on the picture by vertical lines and they do not intersect for the quiet and disturbed conditions what means that the trauma occurrence growth is connected with the geomagnetic storms. It could be the attention weakness, de-coordination of movements and other malfunctions of human organism. The present analysis permits to make the quantitative estimation of the biotropic effect. The sum of hospitalizations for ranges which do not exceed the average daily occurrence ($\overline{\Delta N}$ = 330) during geomagnetic storms is 0.55 while for the quiet periods it equals 0.86. For the ranges higher than daily mean occurrence these numbers are 0.45 and 0.14 respectively. It means that low number of

hospitalizations happens 1.5 times (0.86:0.55) more during quiet periods that during the geomagnetic storms, and contrary, the high number of hospitalizations happens 3 times more frequently (0.45:01.4) during geomagnetic storm period. The seasonal variations of the biotropic effects for trauma events were not revealed.

## 3. ACUTE MENTAL AND CARDIOVASCULAR PATHOLOGIES DURING SORT-TIME GEOMAGNETIC DISTURBANCES

It was shown in [3] that biotropic effect in acute mental and cardiovascular pathologies does not depend on the intensity of the planetary geomagnetic storm. It is of interest to regard the dependence of the short-time geomagnetic disturbances representing the substorms effects or the local technogenic effects. The same database (March 1983 – October 1984) was used for the analysis. The periods without the magnetic storms analyzed in [1] were divided for the quiet intervals when during the whole day the K-index did not exceed 3, and intervals of the short-time geomagnetic disturbances with the duration no less than 12 hours when the K-index exceeded 3 at least for one 30hour interval. The total number of days under analysis was 352, form then there were 200 quiet and 152 with short-time disturbances. The IZMIRAN magnetic observatory data [2] were used for the K-index. The hospitalization occurrence data of Moscow ambulance for the suicide (2-23 cases per day), mental deceases (10-60 cases per day), myocardial infarction (5-70 cases per day) and brain vessels defeat (16-80 cases per day) were used. As in the previous analysis [1,3] the data were "cleaned" from the week variation. The background of seasonal (yearly) variations was not excluded because it does not exceed the standard mean deviation. The similar to Fig.1 distributions were built for every of pathologies for quiet and disturbed periods. The examples of distributions for suicides and myocardial infarction are shown in Fig.2. On can se that the curves practically coincide (the same effect is for other kinds of regarded pathologies). The absence of obvious effect does not mean the absence of the effect of sort-time geomagnetic disturbances. The biologic response probably exists but is within adaptation possibilities of organism [4] or the analysis needs more detail time scale, shorter than one day.

## 4. CONCLUSIONS

The statistical analysis of daily occurrence of hospitalization by Moscow ambulance for different deceases gave the following results:

1. with confidential probability P=0.95 the effect of the planetary geomagnetic storms on the heavy trauma occurrence is demonstrated. The trauma occurrence exceeding the mean daily number for the whole regarded period growth by 3 times during geomagnetic storms in comparison with the quiet period.
2. daily sampling does not permit to reveal the effect of the short-time geomagnetic disturbances of natural and technogenic nature on the occurrence of acute mental and cardiovascular deceases

The present paper was supported by the Russian Foundation of Basic Research, project 98-05-64286.

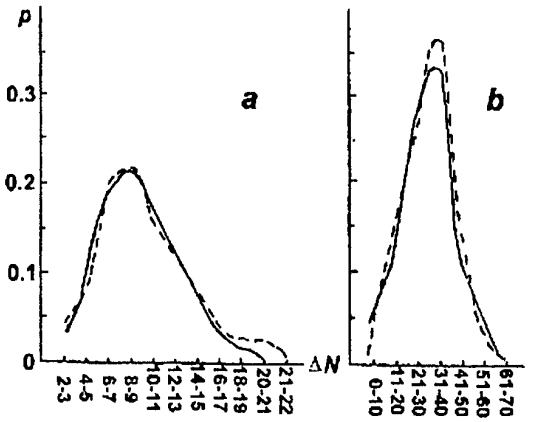



Fig.2 Daily occurrence distributions for suicides (a) and myocardial infarction (b) for quiet (dashed line) and disturbed (solid line) conditions

## 5. REFERENCES

1. Kuleshova V.P., Pulinets S.A., Sazanova E.A., Charchenko A.M., *Biophysics*, 1999, **44**, to be published
2. Cosmic data, Monthly review, 1983-1984, Moscow, Nauka
3. Oraevsky V.N., Kuleshova V.P., Gurfinkel Yu.I., Guseva A.V., Rapoport S.I., *Biophysics*, 1998, **43**, No.5, p.844
4. Chibisov S.M., Breus T.K., Levitin A.E., Dorogova G.M., *Biophysics*, 1995, **40**, No.5, p.959

## BIOGRAPHICAL NOTES

Valentina P. Kuleshova, graduated from Physical Faculty of the Leningrad State University. Is working at IZMIRAN more than 35 years. Main interests are: solar-terrestrial relations, development of forecast for planetary magnetosphere-ionosphere disturbances. Recently studied the biotropic effects of geomagnetic activity. Results are published in more than 60 papers.

Sergey A. Pulinets, graduated from Physical Faculty of the Moscow State University. Deputy director of IZMIRAN. One of the pioneers of ionosphere radiospectroscopy. Main interests: physics of the ionosphere, atmosphere-ionosphere-magnetosphere coupling, electromagnetic ecology, natural and technogenic disasters. Results are published in more than 150 papers.

EMC 2000 INTERNATIONAL WROCŁAW SYMPOSIUM ON ELECTROMAGNETIC COMPATIBILITY

# ELF EM RADIATIONS AND INTRINSIC EM PHENOMENA IN HUMAN ORGANISM. NEED FOR A CONVENTION

Mikołajczyk J.H.
Occupational Hygienist (emeritus)
90-136 Łódź, Narutowicza st. 56/15
Poland, tel. +4842 631-90-18

## 1. ABSTRACT

*The ELF magnetic pulses may penetrate tissues and cells interfering their functions by induction current. The magnetic pulses of 1.2 Hz, 3 Hz, 4 Hz, and 5 Hz of unknown origin were measured. Such pulses of peak B induction 50 μT to 1000 μT are able to induce behavioral, mental, mood, free will, and even fatal vital disorders. The International Convention is needed for: elaboration of the advanced instruments and methods to measure such pulses; identification and localization the sources of such pulses; cancellation and forbidding generation and emission of EM ELF waves, and pulses interfering IEMPh in human organism.*

## 2. INTRODUCTION

The knowledge concerning the intrinsic electro-magnetic phenomena (IEMPh) in human organism is so advanced that there are technical possibilities to inflence, at least, some its vital functions by determined electro-magnetic waves and/or pulses of external origin. Especially, the magnetic pulses of extremely low frequency (ELF) may penetrate tissues and cells interfering their functions by induction current (9.5).

IEMPh in the distinct regions of brain accompany the cognitive processes through the sensory system, the internal activities of the organism, motor activity, and mental activity. The heart action is accompanied by very regular IEMPh arising in the heart automacity centers.

The IEMPh from fraction of Hz to tens Hz in nervous system, heart, and muscles are targets for external intrusions which might be nonintentional or intentional, and beneficial or noncompatible. IEMPh in state of human health and diseases are vulnerable to well adjusted electromagnetic waves and/or pulses able to induce behavioral, mental, mood, free will, and even fatal vital disorders.

It is reasonable time to establish the international regulations for identification and localization of sources of such intentional or nonintentional ELF E-M waves and pulses interfering IEMPh in the human organism.

## 3. MATERIALS AND METHODS

During testing the simple measuring set, characterized below, it has been observed its indication magnetic field pulses having few Hz frequency. This observation was encouraging for further reading of such pulses. The set involved the selective nanovoltmeter switched to 25 dB octave selectivity and high time constant, and special coil receiver (styrophoam model of man covered by turns of copper foil belts (0.5 cm) spaced by 0.5 cm gapes). Each of output ends of this coil was loaded with 1 kΩ resistor (9.1).

Using this set the incident ELF magnetic pulses have been observed occasionally since 1991 in laboratory and domestic environments in big town.

## 4. RESULTS

Low, mild, and high repetition pulses with changing time course and peak induction values were observed in frequencies 1.2 Hz, 3 Hz, 4 Hz, and 5 Hz which denote pathological functions of the brain in the adult humans. At the time of all observations the switching on and of light in the laboratory and domestic rooms has been avoided.

In general, four time courses of the pulses were observed (fig. 1): 1) single pulse; 2) single pulse with two successive peaks; 3–4) pulses with two or three peaks with intervals. The first pulse in series started always from nul value.

At frequency 8 Hz, 10 Hz, and 20 Hz the pulses were regularly of low induction value. Moreover, at 20 Hz the pulses started from stable value of 10 μT. At 40 Hz and 50 Hz ther were indications of stable induction values (table 1).

Periodically the magnetic pulses were still more modulated in their time course. The pulses have been observed in various time of day and they were of higher repetition rate in time of regional political activity and tension, of some military events, and of some international conflicts. The pulses showed the peak induction B on average 50 μT to over 1000 μT, and time derivative of 0.1–10 mT/s. It has not been performed detailed analysis of observed magnetic pulses which were of unknown origin.

Table 1. B induction values of observed pulses at 6:45 p.m. on 2000-01-29

| Hz | Peaks, μT | | mT/s | |
|---|---|---|---|---|
| 1.2 | 120, | 1000 | 0.64, | 5.35 |
| 3 | 50, | 240 | 0.66, | 3.23 |
| 4 | 110, | 150 | 1.95, | 2.63 |
| 5 | 90, | 140 | 1.98, | 3.10 |
| 8 | 70, | 90 | 2.50, | 3.20 |
| 20 (stable) | 10 | | 0.9 | |
| 20 (peak) | 70 | | 6.3 | |
| 40 (stable) | 60 | | 10.5 | |
| 50 (stable) | 320 | | 71.0 | |

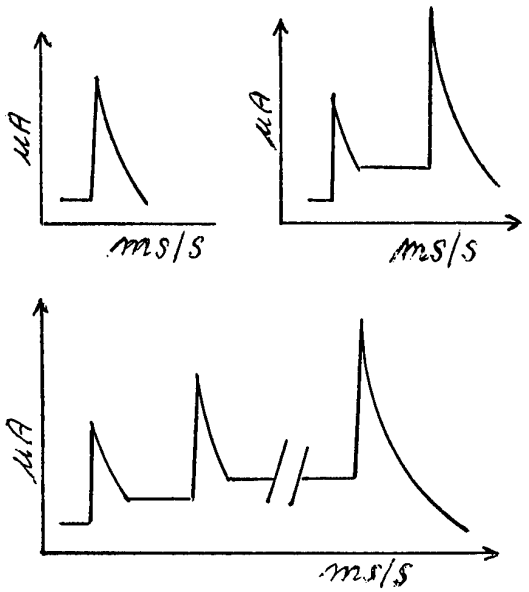



Fig. 1. The shapes of observed magnetic pulses

## 5. DISCUSSION

The neuron (nerve cell) with input dendrites and output axon is basic functional unit of nervous system. A typical neuron in the cerebral cortex receives inputs from thousands of similar neurons and transmits signal to thousands of other neurons. Such connections are made by synapses. Each functional unit exhibits resting potential of –70 mV (polarization) which after firing the unit changes to action potential of +40 mV (depolarization).

After receiving imput stimulus from outside or inside of the body the specific nerve cells are firing in response for appropriate time and then the firing potential decreases progressively but in case of stronger new stimulus the response of nerve cell may be increased again (fig. 2). Such processes in nerve cells follow the algorithm which is adequate to kind and strength of stimuli (9.2).

The observed magnetic pulses look to have inverse course in respect to courses of firing of nerve cells. The magnetic pulses penetrating tissues induce current responsible for tissue excitation. The threshold current density for brain excitation is about 0.1 μA/cm$^2$. Such current density in the brain tissue may be induced by magnetic pulse of 1–10 mT in the frequency range 1–40 Hz.

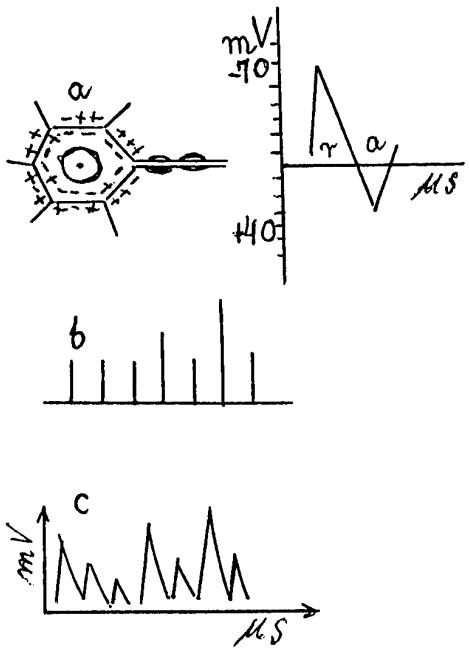



Fig. 2. a) resting (r) and action (a) potential of nerve cell; b) strength of input stimulus; c) response of nerve cell

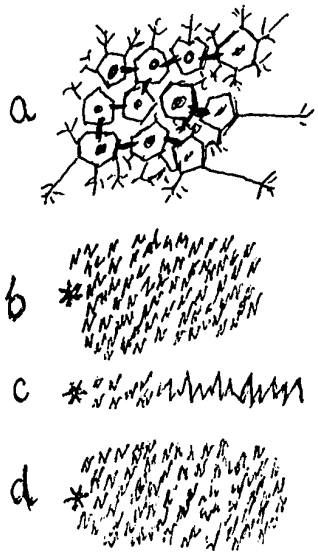



Fig. 3. a ) Group of nerve cells. Asterisk denotes natural stable periodic point susceptible for perturbation; b ) Chaos of potentials; c ) synchronization after application of small current; d ) desynchronization after application of another small current

Within the frequency range of brain potentials there have been distinguished, among others, the main alpha waves 8–12/13/ Hz, beta waves /13/14–40 Hz, theta waves 4–7 Hz, delta waves 0.5–3.5 Hz. During brain activity such oscillations of action potential of great number of individual nerve cells must be synchronized. This processe may be perturbed by relatively small current.

In respect to synchronization of action potentials within the brain the theory of chaos control has been applied (9.6). There is chaos in the action potentials of thousands of nerve cells engaged in any neural processe. Such chaotic potentials must be synchronized on synaptic and/or gape junction levels. However, in particular group of nerve cells there are determined natural stable periodic points responsible for initiation of potential synchronization after small perturbation e.g. by current of few to tens μA. In this way chaos of potential may be controlled. If such perturbation is apply to stable periodic point in state of potential synchronization the potentials become again chaotic (fig. 3) what is called anticontrol effect. The theory of chaos control is very promising for explanation of brain disorders under the influence of ELF magnetic pulses.

## 6. NEED FOR A CONVENTION

At International Wrocław Symposium on Electromagnetic Compatibility held in 1990 the attention has been called on the need to control the electromagnetic chaos in environment (9.4). Now aboves suggestion can be sustained and extended by the proposal to establish the International Convention for protection of the intrinsic electromagnetic phenomena in the human organism against the extremely low frequency electro-magnetic waves and pulses.

Such the convention should contain regulations as follows.

1. Professional elaboration of the advanced instruments for measurement of EM waves and pulses having physical characteristics comparable to IEMPh in human organism.

Identification of ELF EM waves and pulses from fraction of Hz to tens of Hz may be accomplished by simple and advanced instrumentation. The simple set including rod and coil antenna, and sensitive selective voltmeter makes possible identification frequency, amplitude, and time course of EM waves and pulses. The advanced instrumentation including above mentioned receiving antenna, frequency analyzer, and computer aided algorithm will be needed for spectral analysis of waves and pulses.

2. Institutional identification and localization of sources of intentional or nonintentional EM waves and pulses with potentional interference to IEMPh in human organism.

For localization of sources of ELF EM waves and pulses from fraction of Hz to tens of Hz the highly advanced instrumentation is needed.

3. Regulations of legal generation and emission of ELF EM waves and pulses interfering IEMPh in human organism. Restriction of cancellation and forbidding generation and emissions of such waves and pulses should be taken into power decision.

## 7. ACTUAL AND POSSIBLE APPLICATIONS OF ELF MAGNETIC PULSES

A. Applications of magnetic pulses from near distance (e.g. through coil electrode).

1. Low repetition rate of single magnetic pulses are applied for transcranial magnetic stimulation (TMS) or transmural magnetic stimulation for detection of motor and sensory dysfunction in central and peripheral nerve routes.

2. Rapid rate transcranial magnetic stimulation (rTMS) for treatment of schizophrenic depression and/or some other psychiatric disorders.

3. TMS and/or sTMS for scientific investigations, under allowance of ethic commission, for cognition of changes in association, mood, behavioral, free will, and other psychological phenomena in volunteers.

B. Some applications of magnetic pulses from remote transmitters.

1. Intrusions with magnetic pulses to single or to group of crimes or terrorists to make them susceptible for verbal persvassions to abandon illegal action.

2. Intrusions with modulated magnetic pulses to humans:

a) to suppress or to sustain the mass aggression after appropriate propaganda;

b) to make the people susceptible to illusive suggestion for political or military purposes;

c) to disable people for critical thinking.

## 8. CONCLUSIONS

1. The attention is called to ELF EM pulses possibly interfering intrinsic EM phenomena in human organism.

2. It is claimed to establish the International Convention for reasonable control of such interference.

## 8. REFERENCES

9.1. M. Kamedula, T. Kamedula, "Testing of EM energy in a specified volume of space". Proc. of the Eleventh International Wrocław Symposium on Electromagnetic Compatibility, Wrocław, Poland, Sept. 2–4, 1992, Part I, 80–81.

9.2. Ch. Koch, "Computation and the single neuron", Nature (London), 385, 1997, 207–210.

9.3. A. Kuład P. Mierzwa, "Measurement of ULF electromagnetic fields in the area of big town", Proc. of VIII Country Symposium U.R.S.I., Wrocław, Poland, Feb. 15–16, 1996, 229–231.

9.4. H. Mikołajczyk, "Electromagnetic hazards for biologicalsystems and strategy of electromagnetic compatibility control", Proc. of the Tenth International Wrocław Symposium on Electromagnetic Compatibility, Wrocław, Poland, June 26–29, 1990, 185–187.

9.5. J.M. Saypol, B.J. Roth, L.G. Cohen, M. Hallett, "A theoretical comparison of electric and magnetic stimulation of the brain", Ann. Biomed. Engn., 1991, 19, 317–328.

9.6. S.J. Schiff, K. Jerger, D.H. Duong, T. Chang, M.L. Spano, W.L. Ditto, "Controlling Chaos in the brain", Nature (London), 370, 1994, 615–620.

## BIOGRAPHICAL NOTE

Henryk MIKOŁAJCZYK was born in 1927 and received from the Univ. School of Medicine in Łódź the diploma of physician in 1953, the M.D. degree in experimental endocrinology in 1959, the second M.D. degree in environmental medicine in 1963. He worked in the Department of Endocrinology till the end on 1967. Since 1968 he moved to the Institute of Occupational Medicine where he has been head of the Department of Physical Hazards. He was promoted to professor in 1975. His research interests have been in the interaction of electromagnetic fields on the endocrine system. He retired in 1997.

# LIST OF EXHIBITORS

## AM Technologies Sp. z o.o.
Ochota Office Park, Al. Jerozolimskie 181, PL-02-222 Warszawa, Poland
Phone: +48 22 608 45 55, Fax: +48 22 608 45 54,
e-mail: info@am-tech.pl

## ASTAT Sp. z o.o.
Dabrowskiego 461, PL-60-451 Poznan, Poland
Phone: +48 61 848 88 71, Fax: +48 61 848 82 76,
e-mail: info@astat.com.pl

## ELSINCO POLSKA Sp. z o.o.
Gdanska 50, PL-01-691 Warsaw, Poland
Phone: +48 22 832 40 42, Fax: +48 22 832 22 38,
e-mail: elsinco.warsaw@it.com.pl

## NATIONAL INSTITUTE OF TELECOMMUNICATIONS
Wroclaw Branch
Swojczycka 38, PL-51-501 Wroclaw, Poland
Phone: +48 71 348 30 51, Fax: 48 71 372 88 78,
e-mail: hlug@il.wroc.pl

## ROHDE UND SCHWARZ OESTERREICH
Sonnleithnergasse 20, A-1100 Vienna, Austria
ODDZIAŁ W WARSZAWIE
Stawki 2, floor 28, PL-00-193 Warsaw, Poland
Phone: +48 22 860 6490 to 6498, Fax: +48 22 860 6499,
e-mail: rohdepl@rsoe.com

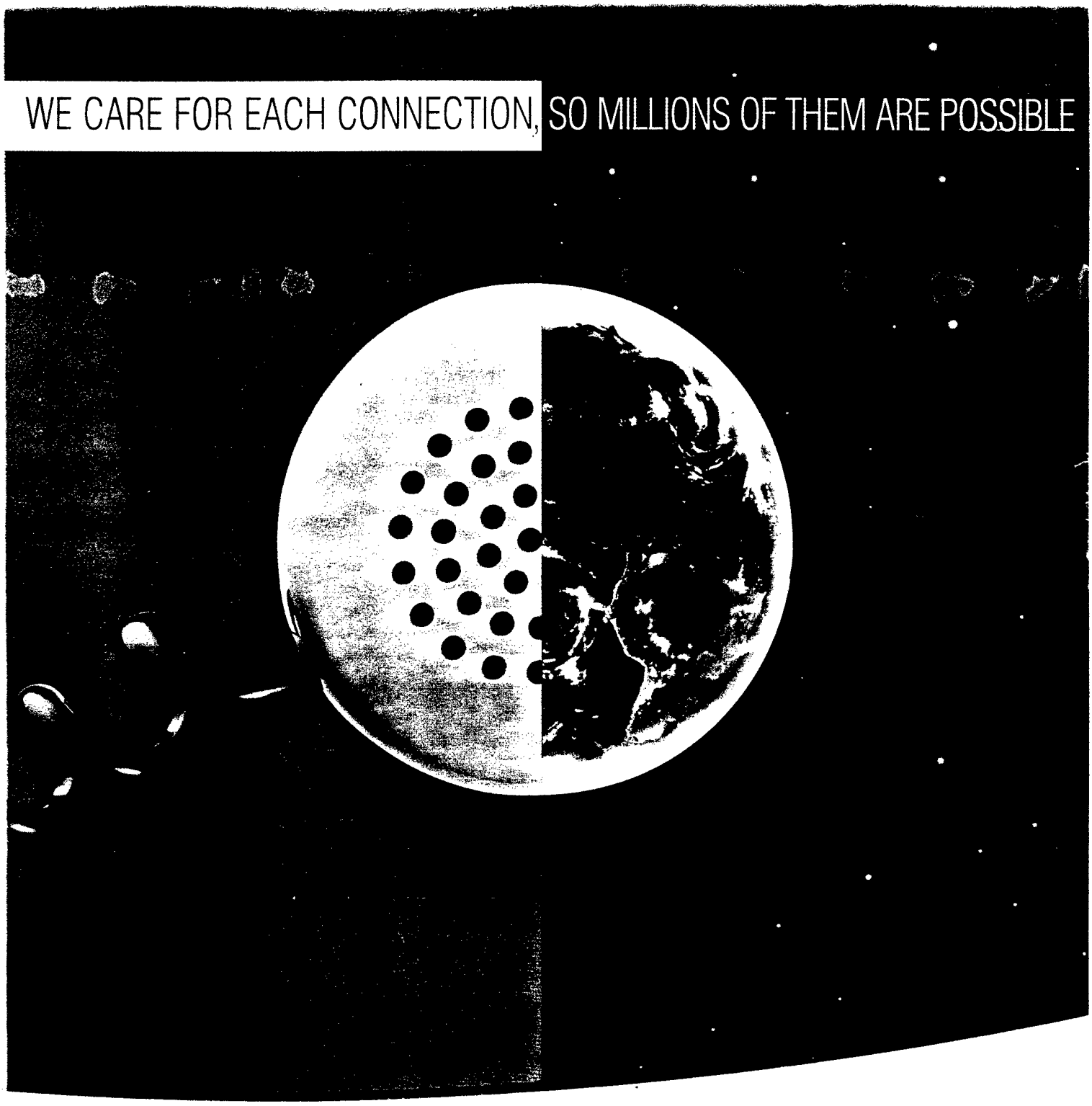
## SCHROFF GMBH
Feldrennach, Langenalberstr. 96-100, D-75334 Straubenhardt, Germany
Phone: +49 7082 794-0, Fax: +49 7082 794-2 00,
e-mail: info@schroff.de

## TECHTRONIC
Grabiszynska 85, PL-53-503 Wrocław, Poland
Phone: +48 71 342 5856, Fax: +48 71 342 0264,
e-mail: tom@techtronic.com.pl

## TEKTRONIX POLSKA Sp. z o.o.
Pulawska 15, PL-02-515 Warsaw, Poland
Phone: +48 22 521 53 40, Fax: +48 22 521 53 41,
e-mail: measurement.poland@tektronix.com

## UNITRONEX POLAND Sp. z o.o.
Grzybowska 87, PL-00-844 Warsaw, Poland
Phone: +48 22 631 26 43, Fax: +48 22 632 75 59,
e-mail: uwo@unitronex.com

# WE CARE FOR EACH CONNECTION, SO MILLIONS OF THEM ARE POSSIBLE



Telekomunikacja Polska S.A. enables you to make any call you want.
Reliability, experience, advanced technology and expertise
are the cornerstones of our growing success.
And as we enter the 21st century, its demands are not a mystery to us.
We have a digital network with fully integrated services.
A satellite communications system. Secure electronic mail.
A data transmission network. An Internet link with the entire world.
We have all that assures a constant, fast, and reliable flow of information.



# anex®

**ANDRZEJ POSTAWKA**
**Przedsiębiorstwo**
**Wielobranżowe**
**ul. Jerzmanowska 99**
**54-430 Wrocław**

Anex Multibranch Company manufactures, as one of its main fields of activity since 1989, broadcast **antennas, antenna systems**, and antenna equipment for **radio and television** networks. The Company has its own **development** and **design** division, its own measuring **equipment**, and means of transport, including the big **terrain trucks**.

We have set into operation over **150 antenna systems** of various size.

**e-mail: anex@k.pl**
**tel. (071) 349 30 80**
**(071) 349 31 32**
**(071) 349 32 16**
**(090) 664 154**
**(071) 349 31 77**









Plus GSM

# THE LEADER IN CORPORATE MOBILE MARKET

Plus GSM is the unquestionable leader in the supply of mobile telephone services to the corporate market. More than 66% of 500 largest Polish businesses have already chosen Plus GSM.
Why do these leading companies choose Plus GSM?

- we guarantee the highest quality of service
- we offer solutions adjusted to individual requirements
- we are constantly introducing new state of the art technologies

Our success is built on the trust of our clients. We would like to thank all our corporate clients and wish them many successful business conversations.

Internet: www.plusgsm.pl
Call free: 0 800 601 601

*Data based on "Gazeta Bankowa" report

# W@P

# Z Ideą po Internecie.

## W@P IDEA - WHAT IS IT?

W@P Idea is a new service offered by the Idea network. It opens a whole new world of web opportunities for mobile phone users. You can browse information resources and use various services offered on the Internet through your WAP (Wireless Application Protocol) compatibile phone.

## USING W@P IDEA

To access WAP services on the Idea network, you must have:

a) the Standard Data Transmission Service set up on your account (available with no additional connection charge and no mothly fee to all Idea users, i.e. Idea Optima and Meritum service plans plus POP pre-paid service users),

b) a WAP-enabled phone with appropriate settings programmed.

The Standard Data Transmission Service is available to all Idea network users from March 1, 2000.

All customers who signed a contract with PTK Centertel earlier and chose the Idea 50 or Idea 150 service plans can activate the Standard Data Transmission Service by sending an "AKT DATA" text message (SMS) to the 555 number *, or by ordering the service directly through the Customer Service Centre ( dial *22 from your handset ).

the SMSC Idea Messaging Centre number ( +48 501 200 777 ) must be set on your phone



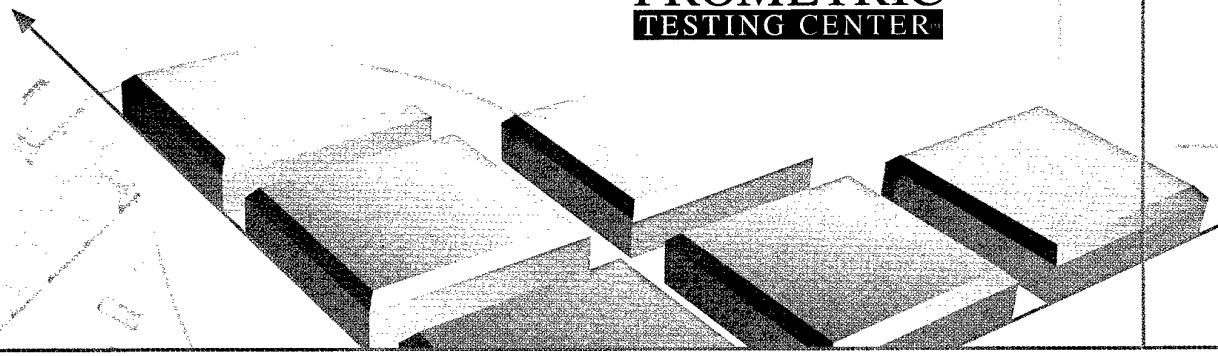
molex®

PREMISE NETWORKS
A Division of Molex

Authorized PROMETRIC TESTING CENTER

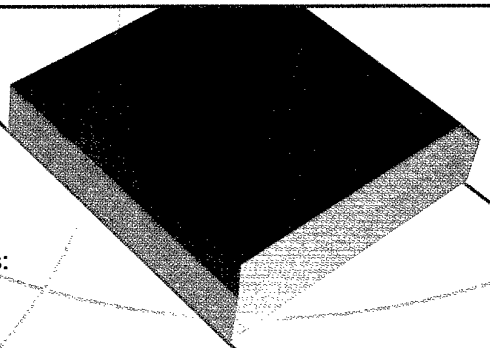
Microsoft Certified Technical Education Center

Microsoft Certified Solution Provider



# TECHTRONIC

RANGE OF TECHTRONIC SERVICES:
- comprehensive delivering of computers and computer equipment
- warranty and after-warranty computers and computer equipment service
- instalation of computer networks
- designs and installations of telecommunication networks
- designs and installations of dedicated supply systems for computer networks
- designs and installations of sprinkler systems
- designs and installations of emergency supply systems
- designs and installations of following telecommunication engineering systems:
  * structured cabling systems
  * fire alarm signaling
  * communication and security systems
  * presence control
  * providing sound
  * TV + TVSAT
  * industrial TV
- system integration
- computering training and courses



www.techtronic.com.pl
e-mail: system@techtronic.com.pl

# NATIONAL INSTITUTE OF TELECOMMUNICATIONS

WROCLAW BRANCH • ul. Swojczycka 38, 50-501 Wroclaw
tel. (+4871) 348-30-51 • fax (+4871) 3728878



## EMC MEASUREMENT DIVISION

**M.Pietranik@il.wroc.pl**

- EMC measurements according to IEC-61000-4--2/3/4/5/6/11, EN-55011/13/14/20/22, ISO-7637 standards
- Expert opinions, measurements in situ, advice on compliance with EMC Directive (89/336/EEC)
- Advice on, and organisation of measurement set-ups, test equipment completion,
- Design and delivery of specialised measuring equipment,
- Development of software for automatic EMC measurements
- Verification of parameters of EMC test equipment used for emission measurements; special laboratory certified b the Polish Central House of Measures (GUM)

## SPECTRUM MANAGEMENT DIVISION

**W.Sega@il.wroc.pl**

- Many years' experience in radio network planning and development of frequency management support systems for government and private sector
- Turn-key systems containing all you need to solve your frequency management problems
- Creation of planning tools, propagation models, and digital terrain models
- Seminars in network planning, network optimization, spectrum engineering, and spectrum management
- Evaluation of trends in spectrum management
- Strategic spectrum planning (evaluation of spectrum requirements and availability, and spectrum allocation plans)
- Studies on strategy for introducing the new radiocommuniaction services

## ANTENNA AND FIELD DIVISION

**M.Kaluski@il.wroc.pl**

- Spectrum monitoring systems in frequency range 0,1 MHz to 3 GHz. Design, turn-key delivery, installation, service
- EM fields measurements in the frequency range 0,1 MHz to 5 GHz
- Hazardous EM fields measurements in the frequency range 0,1 MHz to 6 GHz
- Computer modeling for the EM fields evaluation
- Antenna and antenna systems design, and parameters measurements
- Antenna measurements for certification and technical approval
- Adaptive antennas design and consulting, high frequency digital signal processing using DSP

**Visit our web site http://www.il.wroc.pl**

**The Symposium Organizers gratefully acknowledge the following organisations and companies for offering scholarships for participants from various countries**

**URSI INTERNATIONAL UNION OF RADIO SCIENCE**
c/o University of Gent
St.-Petersnieuwstraat, B-9000 Gent, Belgium

**DEPARTAMENT OF THE AIR FORCE**
**EUROPEAN OFFICE OF**
**AEROSPACE RESEARCH AND DEVELOPMENT**
223/231 Old Marylebone Road
London NW1 5TH, United Kingdom

**MTU INFORM Company**
27-28 Smolenskaya-Sennaya sq, bldg 2
Moscow, 119121, Russia

**SATCOM Commercial Office**
Wiertnicza 151, 02-952 Warsaw, Poland

**ANEX Multibranch Company**
Jerzmanowska 99, 54-530 Wroclaw, Poland

**ELTEST s.c., Electronic and Electrotechnical**
**Equipment Testing, Development**
**and Evaluation Center**
Ratuszowa 11, 03-450 Warsaw, Poland